ADVANCED TOPICS IN SCIENCE AND TECHNOLOGY IN CHINA

Tingyun Kuang
Congming Lu
Lixin Zhang *Editors*

Photosynthesis Research for Food, Fuel and the Future

15th International Conference on Photosynthesis

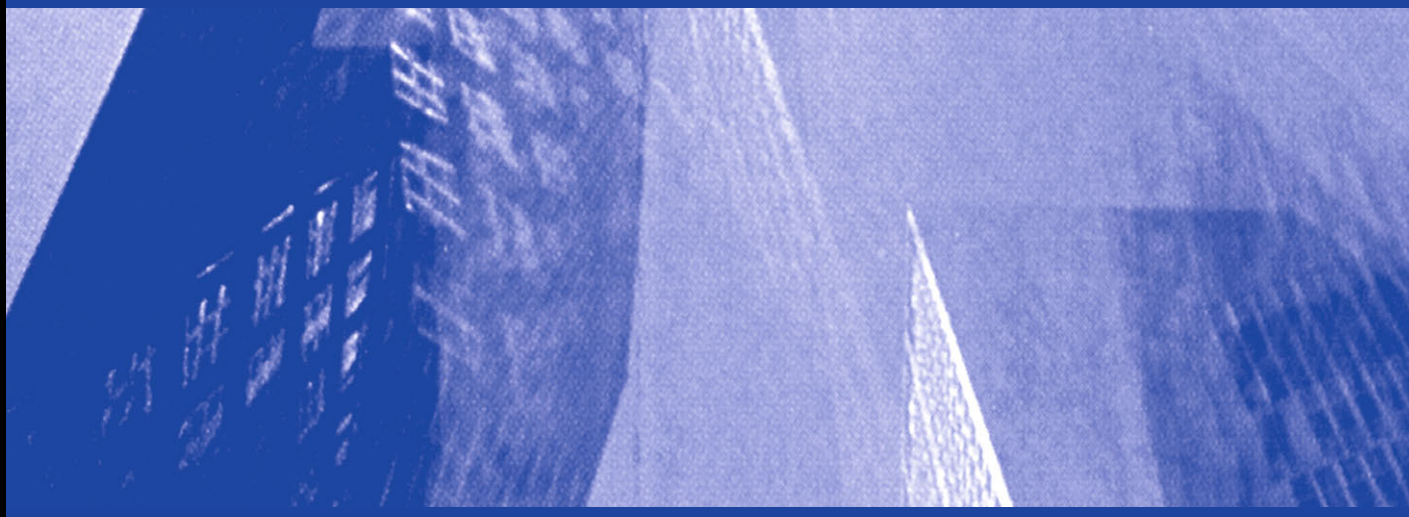

ZHEJIANG UNIVERSITY PRESS
浙江大学出版社

Springer

Tingyun Kuang
Congming Lu
Lixin Zhang

Photosynthesis Research for Food, Fuel and the Future

15th International Conference on Photosynthesis

Tingyun Kuang
Congming Lu
Lixin Zhang

Photosynthesis Research for Food, Fuel and the Future

15th International Conference on Photosynthesis

With 508 figures

ZHEJIANG UNIVERSITY PRESS
浙江大学出版社

Springer

Editors:
Prof. Tingyun Kuang
key Laboratory of Photobiology
Institute of Botany
Chinese Academy of Sciences
Beijing, China
Email: kuangty@ibcas.ac.cn

Prof. Congming Lu
Head, Photosynthesis Research Center
Institute of Botany
Chinese Academy of Sciences
Beijing, China
Email: lucm@ibcas.ac.cn

Prof. Lixin Zhang
key Laboratory of Photobiology
Institute of Botany
Chinese Academy of Sciences
Beijing, China
Email: zhanglixin@ibcas.ac.cn

ISBN 978-7-308-09694-2
Zhejiang University Press, Hangzhou

ISBN 978-3-642-32033-0
Springer Heidelberg New York Dordrecht London

ISBN 978-3-642-32034-7 (eBook)

Library of Congress Control Number: 2012943604

Preface

Photosynthesis is a natural process that converts solar energy to chemical energy. It is widely distributed in many different organisms, ranging from plants to bacteria. It provides all the food we eat and all the fossil fuel we use. Photosynthesis has long been studied in order to understand its underlying mechanisms and then to apply this knowledge to produce energy and food for the needs of our society.

The 15th international conference on photosynthesis was successfully held on 22–27 August 2010, in Beijing, China. The conference was organized by the Institute of Botany, Chinese Academy of Sciences and International Society of Photosynthesis Research. The conference had a fantastic scientific program and featured eminent speakers and state-of-the-art symposium speakers who are at the cutting edge of discovery in their field. These speakers provided an exciting scientific program which covered the breadth and depth of photosynthesis from molecular to global.

Under the conference theme, "photosynthesis research for food, fuel and the future", a total of 24 chapters were collected in this proceeding which contained twenty-three sections, each section representing one of the topics covered by plenary lectures and sessions at the conference. Therefore, the papers contained in this proceeding include all aspects of photosynthesis. We thank all conference participants and in particular those whose chapters are published here.

It is our belief that the Proceeding of the 15th International Conference on Photosynthesis will provide an opportunity for students, postdoctoral fellows and scientists from all over the world to enjoy the latest advanced developments on photosynthesis.

Tingyun Kuang
Chairman of Organizing Committee of
15th International Conference on
Photosynthesis, 2010, Beijing
10 January 2012

Contents

Symposium 01　Type I Reaction Centres

Symposium 02　Type II Reaction Centres

Symposium 03 Light Harvesting Anaerobic Systems

Symposium 04 Light Harvesting Aerobic Systems

Symposium 05 Bioenergetics of Photosynthetic Electron Flow

Symposium 06 Mechanisms of Water Oxidation

Symposium 07 Mimicking Photosynthetic Catalysis

Symposium 08 Regulation of Electron Transfer

Symposium 9 Control of the Calvin-Benson Cycle

Symposium 10 CO_2 Concentrating Mechanisms

Symposium 11 C_3, C_4 and CAM and Genetic Engineering

Symposium 12 Regulation of Photosynthetic Gene Expression

Symposium 13 Computational Systems Biology

Symposium 14 Biogenesis of Photosynthetic Apparatus

Symposium 15 Assembly of Photosynthetic Protein Complexes

Symposium 16 Photoprotection, Photoinhibition and Dynamics

Symposium 17 Perception of Environmental Stress and Acclimation

Symposium 18 Organelle Communication

Symposium 19 Marine Photosynthesis and Global Impact

Symposium 20 Crop Yield Improvement

Symposium 21 Microbial Derived Biofuels

Symposium 22 Photosynthesis and New Environmental Challenges

Symposium 23 Global Photosynthesis and Climate Change

Symposium 24 Photosynthesis Education

Symposium 01

Type I Reaction Centres

Deconvolution Analysis of Photoacoustic Waves of Electron Transfer in Photosystem I of *menG* Null Mutant of *Synechocystis* sp. PCC 6803

Xuejing Hou[a], Lien-Yang Chou[a], Harvey JM Hou[a,*]

[a]Department of Chemistry and Biochemistry, University of Massachusetts Dartmouth, North Dartmouth, massachusetts 02747, USA.
[*]Corresponding author. Tel. No. +01 508 999 8234; Fax No. +01 508 999 9167; E-mail: hhou@umassd.edu.

Abstract: Inactivating the *menG* gene causes 2-phytyl-1,4-naphthoquinone (Q) to be presented as a quinone acceptor in PSI of *Synechocystis* sp. PCC 6803. The electron transfer from Q^- to F_X is slowed to 600 ns in the *menG* null mutant [Sakuragi Y, B Zybailov G Shen, AD Jones, PR Chitnis, A van der Est, R Bittl, S Zech, D Stehlik, JH Golbeck, and DA Bryant. (2002) *Biochemistry* 41: 394-405]. Despite of the alternation of kinetics, the thermodynamics of electron transfer in the mutant is not known. In this work, we conducted deconvolution analysis on photoacoustic waves of the menG null mutants and the wild type strains of *Synechocystis* sp. PCC 6803 obtained by pulsed photoacoustics on the microsceond time scale. The fit by convolution of *menG* photoacoustic waves revealed a large volume contraction (-28 ± 2 Å^3) for the $P_{700}^* \rightarrow Q$ step and a positive volume change ($+5 \pm 2$ Å^3) for the $Q^- \rightarrow F_{A/B}$ step. The enthalpy changes were -0.7 ± 0.2 eV for the $P_{700}^* \rightarrow Q$ step and $+0.5 \pm 0.2$ eV for the $Q^- \rightarrow F_{A/B}$ step, respectively. Taking the free energy of –0.7 eV and –0.1 eV for these steps, the data presented here shows that the Q^- to $F_{A/B}$ electron transfer step in the *menG* null mutant is entropy driven.

Keywords: Enthalpy; Entropy; Volume change; Photoacoustics; Electron transfer; Photosystem I; *menG*

Introduction

Photosynthesis involves a series of light driven electron transfer steps in the reaction center to store the solar energy into the electrochemical energy. Photoacoustic method has been applied to gain new insights into enthalpy and volume changes associated with light driven reactions in photosynthesis (Delosme *et al*., 1994; Hou *et al*., 2001a; Hou *et al*., 2001b; Losi *et al*., 2003).

Application of photoacoustic signal deconvolution procedures is able to resolve the thermodynamic parameters of elemental steps (Small *et al*., 1992). The photoacoustic signal is the convolution between instrument response function and a time-dependent pressure evolution. The photoacoustic reference delivers all the absorbed energy into the medium as prompt heat. The singal of photoacoustic reference is thus the signal of the instrument response. After convolution, ther resulting simulated signal is compared to the measure photoascoustic waves of photoactive sample. The fit by convolution of photoacoustic waves on the nanosecond and microsecond time scales resolves two kinetic components in photosystem I from *Synechocystis* 6803 (Hou and Mauzerall, 2006).

Inactivating the *menG* gene causes 2-phytyl-1,4-naphthoquinone (Q) to be presented as a quinone acceptor in PSI of *Synechocystis* sp. PCC 6803. The electron transfer from Q^- to F_X is slowed to 600 ns in the *menG* null mutant (Sakuragi *et al*., 2002). Despite of the alternation of kinetics, the thermodynamics of electron transfer in the mutant is not known. In this work, we conducted deconvolution analysis on photoacoustic waves of the *menG* null mutants and the wild type strains of *Synechocystis* sp. PCC 6803 obtained by pulsed photoacoustics on the microsecond time scale.

Materials and Methods

Preparation of Purified PS I Trimers

PS I trimers were isolated from *Synechocystis* sp.

PCC 6803 and purified according to published methods (Sakuragi *et al*., 2002). For photoacoustic measurements, the sample buffer was replaced by ultrafiltration over a Centriprep YM-50 membrane with pH 8.0, 10 mmol N-[2-hydroxyethyl] piperazine-N'-2-ethanesulfonic acid (HEPES), and 0.03% dodecyl-R-D-maltoside (DM) without sucrose or glycerol.

Photoacoustic Measurements

The pulsed time resolved photoacoustic setup on the microsecond time scale. The light beam was produced by a Nd:YAG laser (Surelite) and an optical parametric oscillator (OPO, Surelite). An excitation wavelength of 680 nm was selected to excite the PS I centers.

Deconvolution Analysis of Photoacoustic Waves

The methodology and procedures of deconvolution of photoacoustics were similar to those described previously (Feitelson and Mauzerall, 2002; Hou and Mauzerall, 2006; Small *et al*., 1992). A deconvolution procedures of photoacoustic waves uses a commercial software Sound Analysis (Version 1.50 D) from Quantum Northwest, Inc. Assuming the photoacoustic wave represents a convolution between the photoacoustic reference and a sum of exponents (Small *et al*., 1992).

$$S(t) = R(t) * \sum_i \frac{\alpha_i}{\tau_i} e^{-\frac{t}{\tau_i}} \quad (1)$$

Where *R(t)* and *S(t)* are the photoacoustic reference and sample waves; α_i and τ_i are the photoacoustic intensity factor and deay lifetime for the ith component in the sum of exponentials. The asterisk (*) represents the convolution process. The analysis assumes that the noise on the photoacoustic waves is Gaussian.

Results and Discussion

Photoacoustics provides directly the volume and enthalpy change of photochemical reaction using calorimetry. We have previously reported the thermodynamic parameters of electron transfer in menA and menB null nutant PSI from *Synechocystis* sp. PCC 6803 on the microsecond time scale (Hou *et al*., 2009). However, our convolution analysis on *menA/B* PS I failed to resolve any convincing parameter for the plastoquinone anion to $F_{A/B}$ step. One main reason may be due to its long lifetime of 15 – 300 μs. In the *menG* null mutant, the electron transfer from Q^- to F_X is 600 ns (Sakuragi *et al*., 2002). The 600 ns time constant in *menG* null PS I is within the 1-μs time window and makes the extraction of its thermodynamic parameters possible.

Fig. 1 showed a typical fit by convolution of *menG* photoacoustic signal. The best simulation fit gave a prompt component less than 10 ns and a slow component with a lifetime of 600 ns. The prompt component is attributed to the charge separation to produce $P_{700}^+Q^-$; and the 600 ns component is attributed to the subsequent electron transfer from Q^- to $F_{A/B}$ step.

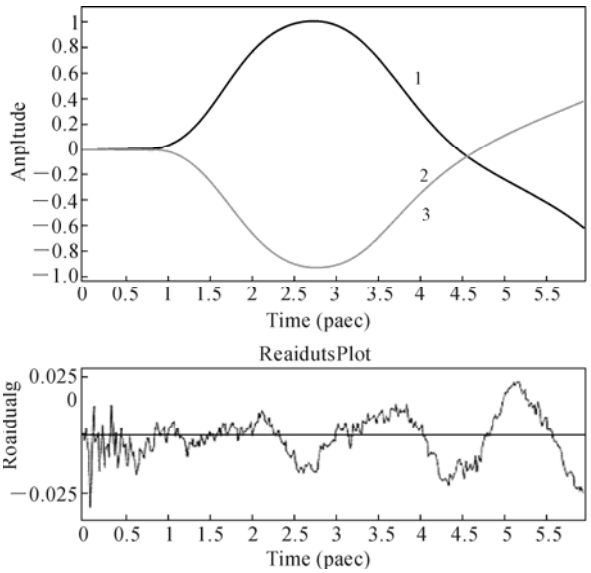

Fig. 1 Deconvolution of photoacoustic waves of PSI complexes from *menG* null mutant of *Synechocystis* sp. PCC 6803 at 25 °C. Upper panel: Curve 1 is the photoacoustic wave of the reference ink. Curve 2 is the photoacoustic signal of the *menG* null PS I complexes. Curve 3 is the simulation fit using convolution equation and gives prompt amplitude of –1.01 and a 600 ns component with amplitude of 0.19. Lower panel: The residue signal of the convolution fit.

The volume and enthalpy changes of electron transfer steps in *menG* null mutant can be obtained by plotting the amplitudes of deconvolution analysis multiplying the compressibility of water versus expansivity of water. The detailed description of photoacoustic data analysis to retrieve the thermodynamic parameters was reported previously (Hou *et al*., 2001b). As in Fig. 2, the charge separation and subsequent electron transfer in wild type photosystem I offer a large volume contraction and negative enthalpy change for the first step and a small volume contraction and positive enthalpy change for the second step. Similarly, the *menG* null mutant gave negative enthalpy change first and followed by a positive enthalpy change. In contrast, the volume change in the *menG* null mutant for the Q^- to $F_{A/B}$ step was a volume expansion and not volume contraction.

Table 1 Molecular volume change, enthalpy, free energy, and entropy change of electron transfer in PS I from the *menA/B null (Hou et al*., 2009*)*, *menG* null and wild type strains of *Synechocystis* sp. PCC 6803 (Hou and Mauzerall, 2006).

	ΔV, Å^3	ΔH, eV	ΔG, eV	–TΔS, eV
WT PSI (Hou *et al.*, 2006)				
$P_{700}^* \rightarrow A_1$	–21	–0.8	–0.7	+0.2
$A_1^- \rightarrow F_{A/B}$	–3	+0.4	–0.1	–0.5
*men*A/B PSI (Hou *et al*., 2009)				
$P_{700}^* \rightarrow A_P$	–17	–0.7	–0.7	0
$A_P^- \rightarrow F_{A/B}$	–9	+0.3	–0.1	–0.4
menG PSI (This work)				
$P_{700}^* \rightarrow Q$	–28	–0.7	–0.7	0
$Q^- \rightarrow F_{A/B}$	+5	+0.5	–0.1	–0.5

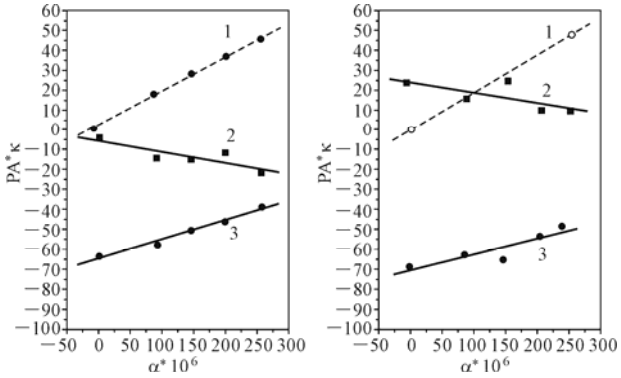

Fig. 2 Plots of amplitude times compressibility versus expansivity of the wild type PSI redraw from the ref (Hou and Mauzerall, 2006) with permission from the American Chemical Society and *menG* null PSI of *Synechocystis* sp. PCC 6803. Left panel: Curve 1 is the reference. Curve 2 is the 100 ns component. Curve 3 is the prompt component. Right panel: curve 1 is a photoacoustic reference signal. Curve 2 is the 600 ns component. Curve 3 is the prompt component. The enthalpies and volume changes are listed in Table 1.

Table 1 lists the thermodynamic parameters of charge separation and subsequent electron transfer in *menA/B*, *menG*, and wild type photosystem I of *Synechocystis* 6803. The *menG* null mutant revealed a large volume contraction (−28 ± 2 Å^3) for the $P_{700}^* \rightarrow$ Q step and a positive volume change (+5 ± 2 Å^3) for the $Q^- \rightarrow F_{A/B}$ step. These numbers are different from those in menA/B (–17 Å^3 and –9 Å^3) and wild type photosystem I (–21 Å^3 and –3 Å^3). This is largely due to the difference in the chemical structure of the quinone acceptors: A_1 (2-methyl-3-phytyl-1,4-naphthoquinone) in wild type, A_P (plastoquinone-9) in *menA/B*, and Q (2-phytyl-1,4-naphthoquinone) in *menG* photosystem I. As the quinone-binding pocket is naturally designed for the A_1, the foreign quinones (A_P and Q) would cause changes in the binding moiety of protein including compressibility and polarity of protein.

The volume contraction caused by electrostriction can be expressed using the equation:

$$\Delta V_{el} = \frac{\partial \Delta G_{el}}{\partial P} = \left(\frac{e^2 \cdot \kappa}{2 \cdot \varepsilon}\right) \times \left(\frac{\partial \ln \varepsilon}{\partial \ln V}\right) \times \left[\frac{z_+^2}{r_+} + \frac{z_-^2}{r_-} + \frac{2 z_+ z_-}{r_\pm}\right] \quad (2)$$

where ΔV_{el} is electrostriction, ΔG_{el} is the Born charging energy, P is pressure, z^+, z^- are the signed charge on the positive and negative ions, κ is compressibility of the protein, V its molar volume, ε its dielectric coefficient, r_+ and r_- the radii of the donor and acceptor (assumed previously neutral) and $r\pm$ is the distance between the two ions.

The large tail in plastoquinone (AP) may decrease the compressibility of protein. Additionally, the small size of plastoquinone may allow a water molecule to present in the pocket and increase the polarity of protein and effective dielectric coefficient (ε). These decease the volume change (ΔV_{el}). In the case of *menG* null mutant, the Q lacks the 2-methyl group and thus creates a looser and more polar quinone pocket. Similar effect of small size quinones on volume changes was reported previously in bacterial reaction centers with different quinones (Edens *et al*., 2000).

The enthalpy changes of charge separation and electron transfer in *menG* null mutant were –0.7 ± 0.2 eV for the $P_{700}^* \rightarrow$ Q step and +0.5 ± 0.2 eV for the $Q^- \rightarrow F_{A/B}$ step, respectively. Taking the free energy of –0.7 eV and –0.1 eV for these steps, the data presented here indicates a key role of the apparent entropy in the Q^- to $F_{A/B}$ electron transfer step in the *menG* null mutant.

In the *menA/B* null mutant, deconvolution analysis

failed to resolve the 15 μs component (Hou *et al*., 2009). Assume the overall reaction in *menA/B* photosystem I is similar to that of wild type photosystem I, we infer the electron transfer from A_P^- to $F_{A/B}$ step is entropy driven. In this work, we resolve the 600 ns component and demonstrated the Q^- to $F_{A/B}$ step is entropy driven. In addition, the entropy driven reaction for A_1^- to $F_{A/B}$ step in wild type photosystem I was reported. We concluded that the entropy driven reaction in *Synechocystis* photosystem I is not affect by recruitment of foreign quinone. The observation of entropy driven reaction in photosystem is explained as vibrational effect which is due to the loosening of protein structure and decrement of interaction in protein (Hou and Mauzerall, 2006). Recently, the significant entropy change was observed for charge separation in artificial photosynthesis (Rizzi *et al*., 2008). We believe that the driving force of electron trasfer is not only dependent on the bonding energy of cofactors (enthalpy) but also on the available states of interaction of proteins (entropy).

Acknowledgements

We thank Prof. Mauzerall for his continuous support. The photoacoustic measurements were conducted in Prof. Mauzerall laboratory. We thank Prof. Golbeck and Dr. Gaozhong Shen for providing the *menG* null samples. We also thank Fan Zhang for assistance in data analysis and Wanshu He for helpful discussions. This work is supported by the University of Massachusetts Dartmouth.

References

Delosme R, D Beal, P Joliot (1994) Photoacoustic Detection of Flash-Induced Charge Separation in Photosynthetic Systems. Spectral Dependence of the Quantum Yield. Biochim. Biophys. Acta. 1185: 56-64

Edens GJ, MR Gunner, Q Xu, D Mauzerall (2000). The Enthalpy and Entropy of Reaction for Formation of $P^+Q_A^-$ from Excited Reaction Centers of Rhodobacter Sphaeroides. J. Am. Chem. Soc. 122: 1479-1485

Feitelson JD Mauzerall (2002) Enthalpy and Electrostriction in the Electron-Transfer Reaction between Triplet Zinc Uroporphyrin and Ferricyanide. J. Phys. Chem. B. 106: 9674-9678

Hou HJM, D Mauzerall (2006) The A-FX to FA/B Step in Synechocystis 6803 Photosystem I is Entropy Driven. J. Am. Chem. Soc. 128: 1580-1586

Hou HJM, G Shen, VA Boichenko, JH Golbeck, D Mauzerall (2009) Thermodynamics of Charge Separation of Photosystem I in the MenA and MenB Null Mutants of Synechocystis sp. PCC 6803 Determined by Pulsed Photoacoustics. Biochemistry 48: 1829-1837

Hou JM, VA Boichenko, BA Diner, D Mauzerall (2001a) Volume Change, Enthalpy, and Entropy of Electron Transfer Reactions in Manganese-Depleted Photosystem II Core Complexes. Biochemistry 40: 7117-7125

Hou JM, VA Boichenko, YC Wang, PR Chitnis, D Mauzerall (2001b) A Pulsed Photoacoustic Study of Electron Transfer in Photosystem I Reveals a Similarity to Bacterial Reaction Centers in Both Volume Change and Entropy. Biochemistry 40: 7109-7116

Losi A, I Yruela, M Reus, AR Holzwarth, SE Braslavsky (2003) Structural Changes upon Excitation of D1-D2-Cyt b559 Photosystem II Reaction Centers Depend on the β-carotene Content. Photochem. Photobiol. Sci. 2: 722-729

Rizzi AC, M van Gastel, PA Liddell, RE Palacios, GF Moore, G Kodis, AL Moore, TA Moore, D Gust, SE Braslavsky (2008) Entropic Changes Control the Charge Separation Process in Triads Mimicking Photosynthetic Charge Separation. J. Phys. Chem. A. 112: 4215-4223

Sakuragi Y, B Zybailov, G Shen, AD Jones, PR Chitnis, A van der Est, R Bittl, S Zech, D Stehlik, JH Golbeck, DA Bryant (2002) Insertional Inactivation of the MenG Gene, Encoding 2-phytyl-1,4-naphthoquinone Methyltransferase of Synechocystis sp. PCC 6803, Results in the Incorporation of 2-phytyl-1,4-naphthoquinone into the A_1 Site and Alteration of the Equilibrium Constant between A_1 and F_X in Photosystem I. Biochemistry 41: 394-405

Small JR, LJ Libertini, EW Small (1992) Analysis of Photoacoustic Waveforms Using the Nonlinear Least Squares Method. Biophys. Chem. 42: 29-48

Towards Uncovering the Energetics of Secondary Electron Transfer Reactions in Photosystem I

Stefano Santabarbara[a,b*], Fabrice Rappaport[c], Kevin Redding[a]

[a]Department of Chemistry and Biochemistry, Arizona State University, Tempe, U.S.A.;
[b]Institute de Biologie Physico-Chimique, Paris, France;
[C]Instituto di Biofisica, Consiglio Nazionale delle Ricerche, Milano, Italy.
[*]Corresponding author. Tel. No. +39 2 503 14857; Fax No. +39 2 503 14815; E-mail: stefano.santabarbara@cnr.it.

Abstract: Phylloquinone (PhQ) acts as the secondary electron acceptor in the reaction centre of Photosystem I. At room temperature the semiquinone anion is oxidized with complex multiphasic kinetics by electron transfer to the iron-sulphur cluster F_X. The two principle phases of the oxidation kinetics are characterized by lifetimes of 20 ns and 250 ns. The 20-ns phase is associated primarily with the oxidation of PhQ_B, which is bound by the PsaB subunit, and the 250-ns phase is associated with oxidation of PhQ_A, which is bound by the PsaA subunit. The difference of about one order of magnitude between the two oxidation lifetimes can be explained by considering the difference in the driving force for oxidation of the PhQ_A ($\Delta G^0 > 0$) and PhQ_B ($\Delta G^0 < 0$) semiquinone forms. Such an energetic scenario also promotes a transient electron transfer from PhQ_A^- to PhQ_B, with F_X acting as an intermediary.

Keywords: Photosystem I (PS I); Electron Transfer (ET); Reaction centre (RC); Phylloquinone; Iron-sulphur clusters

Introduction

Photosystem I (PS I) is a large macromolecular chromophore-protein supercomplex serving as a fundamental component of the oxygenic photosynthesis. The core of PS I, which is well conserved in different organisms, harbours all the cofactors involved in light-induced electron transfer (ET) as well as about ~100 Chlorophyll (Chl) *a* and 30 β-carotene molecules, acting as the internal antenna. Crystallographic models have been solved for core complexes from cyanobacteria (Jordan *et al*., 2001) and core-light harvesting supercomplexes of higher plants (Ben-Shem *et al*., 2003). Both structures shows a symmetric arrangement of the cofactors involved in ET reactions, which are organized in two chains, each of which is coordinated primarily by either the PsaA or by the PsaB subunit of the reaction centre (RC), with the exception of the terminal electron acceptors, the iron-sulphur clusters F_A and F_B, which are bound to PsaC. Symmetric arrangement of ET cofactors is a common structural feature in photosynthetic RCs, and is also observed also in the structural models of Type II RCs (PS II and purple bacteria RCs). However, whereas in Type II RCs only one of the two chains is active in ET reactions (*i.e.*, asymmetric or unidirectional ET), there is a general consensus that both ET chains are functional in PS I, which operates according to a so-called bidirectional ET mechanism (Santabarbara *et al*., 2005a; Rappaport *et al*., 2006; Srinivasan and Golbeck, 2009). The functionality of both ET branches has been observed primarily by monitoring the effect of site-directed mutations of cofactor bound by primarily either by PsaA (ETC_A chain) or PsaB (ETC_B chain) on the kinetics of oxidation of the secondary electron acceptor, Phylloquinone (PhQ). At room temperature the oxidation of semiquinone form (PhQ^-) is described by a minimum of two exponential functions characterised by lifetimes of 15–25 ns and 200–300 ns (depending on the organism and preparation) (Santabarbara *et al*., 2005a; Rappaport *et al*., 2006). It was shown that mutations affecting the binding of PsaA-bound

phylloquinone (PhQ_A) altered the lifetime of the 250-ns phase only, whereas mutation of PhQ_B (PsaB-bound) affected the 20-ns lifetime only. At the same time, the amplitude of these phases, which in WT is ~1:2 (20-ns:250-ns) is not affected by the mutations (Guergova-Kuras *et al*., 2001; Byrdin *et al*., 2006). Altering the binding of the primary electron donor, Chl A_0, the cofactors located upstream to the PhQs, affected the amplitude (redistribution) without significant modification of the lifetimes (Li *et al*., 2006; Byrdin *et al*., 2006). More recently, the effect of mutating the A_0 binding site, on both subunits, was also monitored directly on the kinetics of primary charge separation (Müller *et al*., 2010). To a good approximation, it is also possible to assign, the 20-ns phase to PhQ_B^- oxidation and the 250-ns PhQ_A^- oxidation, whereas the amplitude of the two phases are determined at the level of primary charge separation. Still, the reason for the ~10-fold difference in PhQ_A^- and PhQ_B^- oxidation lifetimes remains unclear. Structurally the two PhQs are substantially equi-distant from the electron acceptor F_X, which is shared by both ET chains. Thus, it is likely that differences in lifetimes arises from different physical-chemical properties of PhQ_A and PhQ_B induced by the interaction with the respective protein host. The structures suggest two principal interactions PhQ-subunit interactions: (i) π-stacking between the naphthyl ring of PhQ and the indole of a nearby Trp residues, and (ii) asymmetric H-bonding to the C2-keto group of PhQ from the backbone amide of a specific Leu residue (PsaA-L722; PsaB-L708). Whereas the effect of mutating the conserved tryptophans (and other amino acids affecting the hydrophobicity of the binding site) have been already investigated, the impact of H-bonding on the energetics is less studied, also because it virtually impossible to suppress the bond. Here we discuss the effect of substituting the natural Leu residues with Threonine and Tyrosine, both of which possess larger side chain, hence potentially perturbing the interaction indirectly through steric hindrance effects. We also present a discussion of the effect of point mutations affecting PhQ binding, and their effect in controlling the redox properties of these cofactors.

Materials and Methods

Construction of point mutations of PsaA and PsaB subunits of PS I in *C. reinhardtii* was performed as described (Byrdin *et al*., 2006). For spectroscopic investigations, mutations were engineered in the P71-Fud7 genetic background, a strain lacking PS II and most of the external antenna complement. As the P71-Fud7 harbours a wild-type PS I, we refer hereafter to this strain simply as WT.

The kinetics of secondary ET in PS I was studied by time-resolved absorption difference spectroscopy, using a pump-probe set-up previously described in detail (Beal *et al*., 1999). In brief, actinic excitation (pump) is from a dye (LDS 698) laser pumped by a frequency-doubled ND-YAG laser. The excitation pulse is centred at 700 nm, has a duration of ~5 ns, and is attenuated to excite about 70% of the reaction centres. The measuring (probe) pulse is from the output of a tuneable OPO, pumped by a frequency-tripled Nd-Yag laser. For measurements in the UV, the output of the OPO is frequency doubled. The pump-probe delay is controlled by a home-built pulse programmer. The resolution of the instrumentation is ~ 5 ns, without deconvolution of the actinic pulse. The kinetics, acquired at several different wavelengths, are fitted globally to a sum of exponentials, yielding lifetimes (τ) and their decay associated spectra (DAS). Fitting is obtained by a non-linear least square Levernberg-Marquart algorithm that minimises χ^2.

Results

Fig. 1 shows the kinetics of transient absorption in the 10 ns to 20 μs time window, monitored at 390 nm, which is close to the maximal differential absorption difference of the PhQ^--PhQ spectrum, recorded in whole cells of the WT and two mutants of *C. reinhardtii* in which the π-stacking residue on the PsaA subunit (W697, numbering is that of *Synechococcus elongatus*) has been substituted with a phenylalanine (W697F, Fig. 1B) and leucine (W697L, Fig. 1C). Global fitting of the kinetics (not shown) yields three exponential lifetimes in all cases, plus a non-decaying component. The relative contributions of each lifetime to the total absorption transient are also shown in Figs. 1A, 1B and 1C. The slowest of these decay lifetimes (~6 μs) is assigned to the reduction of P_{700}^+ based on its DAS. As observed in previous studies, the value of this lifetime and its associated spectrum are not affected by mutations of PhQ binding site (*i.e.*, Rappaport *et al*., 2006). Hence, it will not be discussed further. The two remaining

lifetimes fall in the nanosecond regime, as also previously reported (reviewed in Rappaport *et al*., 2006) and are characterised by values of 24 and 256 ns: these lifetimes are assigned to PhQ^- oxidation.

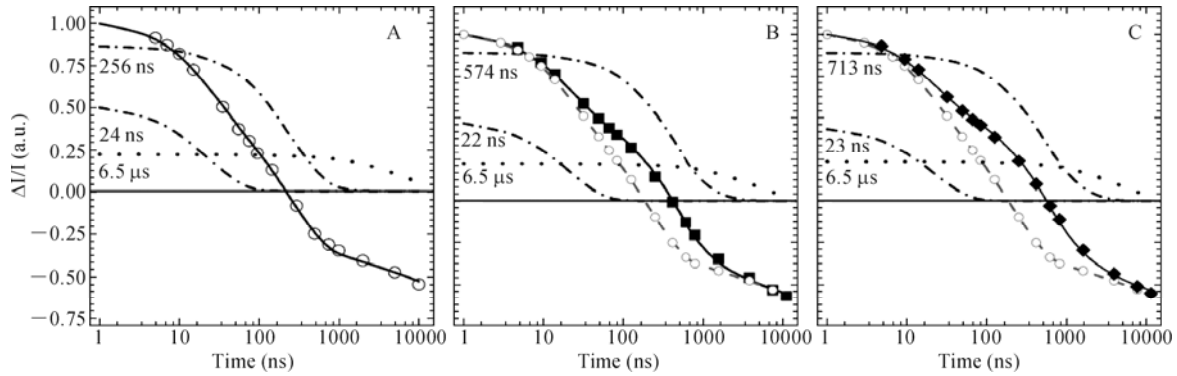

Fig. 1 Kinetics of ET monitored at 390 nm in WT (A) PsaA-W697F (B), and PsaA-W697L (C) mutants. Experimental: solid symbols: mutant, open symbols: WT. Solid line: fit to the kinetics. Dashed-dot line: contribution of "fast and slow" phase of PhQ^- oxidation, dotted line: P_{700}^+ reduction.

As commonly observed, in all three strains, the fastest lifetime is in the range of 22–24 ns; the differences fall in the margin of errors. In contrast, the slowest phase of PhQ^- oxidation is slowed to 574 ns in PsaA-W697F and 713 ns in PsaA-W697L.

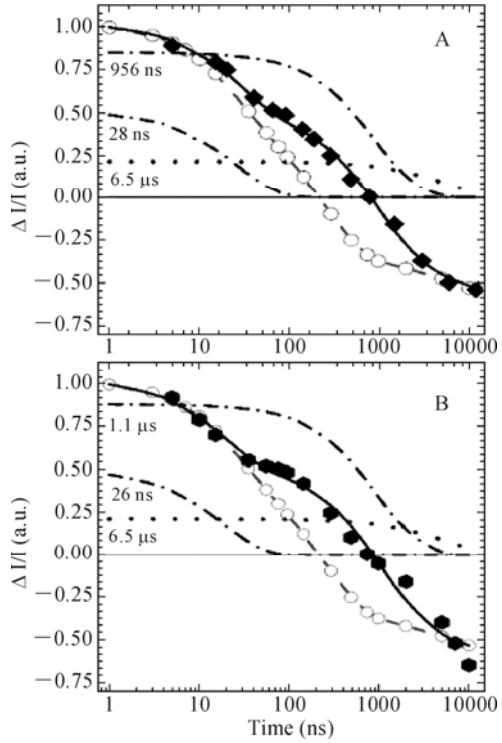

Fig. 2 Kinetics of ET monitored at 390 nm in PsaA-S692A (A) and PsaA-F689W (B) mutants. Line and symbols as in Fig.1.

Fig. 2 shows the kinetics of ET, also monitored at 390 nm, in mutants of two conserved residues, PsaA-S692A and PsaA-F689W. The latter residue contributes to the hydrophobic environment. As observed in the other PhQ_A site mutants, the lifetime of the 25 ns component is unchanged in the PsaA-S692A and PsaA-F689W mutants, whereas that of 250-ns phase is significantly slower, characterized by values of 956 ns (PsaA-S692A) and 1089 ns (PsaA-F689W). Another crucial feature is that in all these mutants, as well as in others already investigated but not presented here (*e.g.* Rappaport *et al.*, 2006), the relative amplitude of the 20 ns to 250 ns is not affected by the mutations; within the confidence interval it remains about 1:2, as measured by the PhQ difference absorption in the near UV.

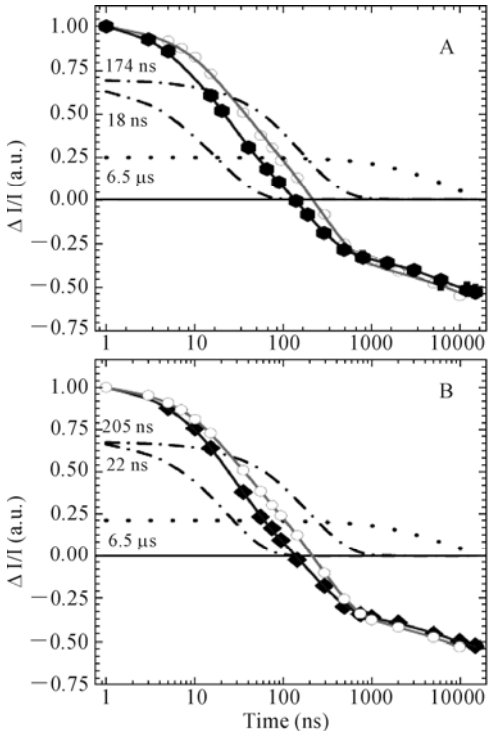

Fig. 3 Kinetics of ET monitored at 390 nm in PsaA-L722T (A) and PsaA-L722Y (B) mutants. Line and symbols as in Fig. 1.

Fig. 3 shows the kinetics of PhQ^- oxidation in two mutants designed to perturb the H-bonding between the protein backbone and the naphthoquinone moiety, by exchanging the conserved residue PsaA-L722, with a tyrosine and threonine (PsaA-L722Y/T). Both mutations designed to perturb H-bonding have little effect on the value of the fast PhQ^- oxidation phase (Fig. 3). Interestingly, both in PsaA-L722Y (205 ns) and PsaA-L722T (174 ns), the lifetime characterizing the slowest PhQ^- oxidation phase becomes faster than in WT (248 ns), whereas other mutations had the opposite kinetic effect (*i.e.* Figs. 1 and 2). Moreover, again in contrast to observation in other mutations of conserved residues, we observe a redistribution of the fast:slow phases of PhQ^- oxidation from 1:2 in WT to ~1:1 in PsaA-L722Y/T (Fig. 3). This redistribution of the amplitudes is observed not only at 390 nm, but throughout the most characteristic spectral features of the DAS (data not shown, but see Santabarbara *et al*., 2010a).

Hence, whereas these mutants provide further confirmation for the bidirectional model, as mutants of PsaA subunit affect essentially only the lifetime of the slowest phase of PhQ^- oxidation, which is therefore assignable primarily to PhQ_A^- kinetics, some peculiar effect of these mutation, such as acceleration of the kinetics and, especially, apparent redistribution of the amplitude of the oxidation phases require reconsidering the details of secondary ET kinetics in PS I.

Discussion

We have then sought a plausible explanation capable of accommodating observations gathered on all mutants affecting π-stacking interactions and H-bonding to PhQ, by implementing a kinetic model describing secondary ET reactions in PS I (Fig. 4). In this model we consider only the ET reactions, involving PhQ_A, PhQ_B and F_X, and the kinetics are obtained by the solution of a system of linear differential equations. The rate of electron transfer between couples of acceptors-donor cofactors can be described according to tunnelling formalism as:

$$k_{ET} = \frac{2\pi}{\hbar}\frac{|H_{DA}|^2}{\sqrt{4\pi\lambda_{tot}\mathrm{k}_b\mathrm{T}}}\exp\left[-\frac{(\lambda_{tot}+\Delta G^0)^2}{4\lambda_{tot}\mathrm{k}_b\mathrm{T}}\right] \qquad (1)$$

where $|H_{DA}|$ is the electronic element of the Hamiltonian, λ_{tot} is the total reorganization energy, ΔG^0 is the standard Gibbs free energy difference, and all the other terms have their usual physical meaning.

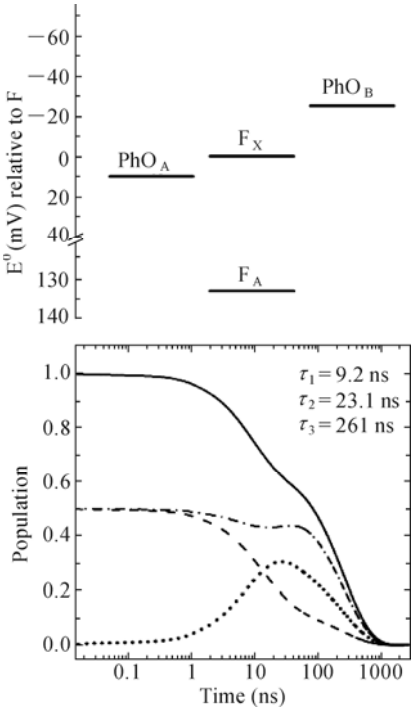

Fig. 4 Simulation of ET kinetics in WT PS I. Top: energetic scheme. Bottom: calculated population evolution of PhQ_B^- (dash), PhQ_A^- (dash-dot); F_X^{red} (dot). Total PhQ^- evolution, solid line.

To a good approximation, $|H_{DA}|$ depends exponentially on the donor-acceptor distance (r_{DA}), according to $|H_{DA}| = |H^0_{DA}|\exp[-\beta r_{DA}]$, where $|H^0_{DA}|$ is the is the value at contact and β is an attenuation factor, both of which are dependent on the tunnelling barrier. For ET in redox proteins it has been proposed that $|H^0_{DA}| = 4\times10^{-2}$ eV and β=0.7 $Å^{-1}$ (*e.g.* Moser *et al*., 1992). These values were used in our simulations. Moreover, it has been suggested that λ_{tot} displays a spread in redox-active protein, in the range of 0.6–1.0 eV. Hence, it is unlikely that there exist large differences in λ_{tot} for the reduction of F_X by $PhQ_{A/B}^-$ and we assumed that $\lambda_{tot} = 0.65$ eV for all the reactions considered; thus, only the values of ΔG^0 has to be tuned in order to simulate the experimental results. Finally, we consider $PhQ_A^-(0) = PhQ_B^-(0) = 0.5$, and $F_X^{red}(0) = 0$.

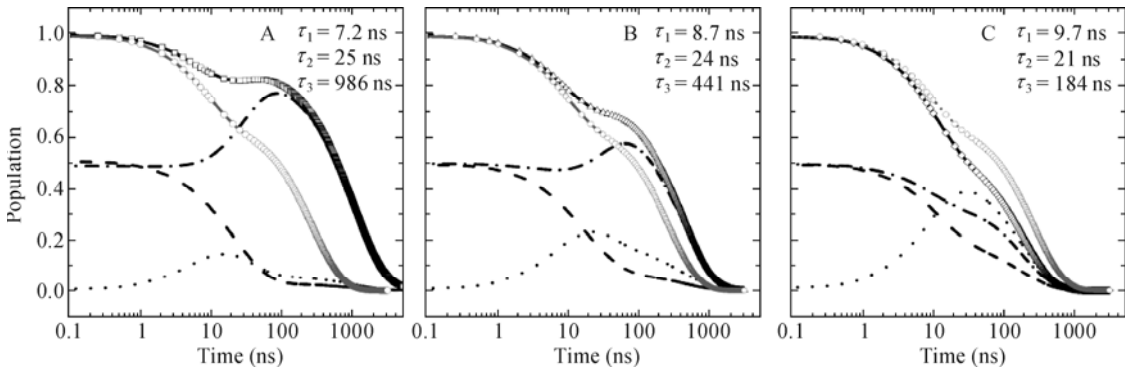

Fig. 5 Simulation of ET kinetics in PsaA-F689W (A), PsaA-W677F (B) and PsaA-L722T (C). Line and symbolds as in the legend of Fig. 4. Shown for comparison is the simulatuions in WT (grey lines and symbols).

The ET kinetics in the wild type can be satisfactorily simulated by assuming that $\Delta G^0_{PhQ_A \to F_X}$ = +10 meV and $\Delta G^0_{PhQ_B \to F_X}$ = –25 meV, *i.e.* the oxidation of PhQ_B^- is thermodynamically favourable and that of PhQ_A^- is unfavourable (Fig. 4). Similar suggestions have already been advanced and, as a corollary, they provide a simple explanation for the well-documented heterogeity of ET reactions at cryogenic temperatures (Santabarbara *et al*., 2005). It is worth noting that: (i) the kinetic model predicts three exponential lifetimes (as three stages are considered), and two of them are in the 5–30 ns interval, and describe the "fast" oxidation phase, while one is ~260 ns; (ii) the ratio of amplitudes of the fast:slow phases is 1:2, as in the experiments, starting from equal initial population of PhQ_A and PhQ_B; (iii) the calculated *rates* of PhQ_A (2.7×10^{-2} ns^{-1}) and PhQ_B (5.9×10^{-2} ns^{-1}) oxidation only differ by a factor of ~2, which is much less than the difference between lifetimes (~10).

Fig. 5 shows the simulations for the PsaA-W697F (A) and the PsaA-F695W (B) mutants. The effect of mutations affecting proximal and distal π-stacking, as well as change in hydrophobicity of the PhQ_A binding site, can be simulated satisfactorily by an increase $\Delta G^0_{PhQ_A \to F_X}$ of 25–60 meV, depending on the mutation (Fig. 6). Consistent with the experiments, the simulations predict a sizable effect only on the longer lifetimes, from 261 ns in ET to 441 (W697F) and 986 ns (F695W). We also predict a small redistribution of amplitudes (10%–15%) in favour of the slowest phase. This margin seems to exceed the experimental results. However, the predicted redistribution is relatively small, so that, considering the simplification employed in constructing the kinetic model, we consider this description overall satisfactorily.

In order to simulate H-bond (PsaA-L722 mutants) perturbation, (also shown in Fig. 5C), we need to decrease the value of $\Delta G^0_{PhQ_A \to F_X}$ by 10–20 meV (Fig. 6). This is consistent with a destabilization of semiquinone form of PhQ, making it a more reductive species, hence increasing the driving force for the reaction. Simulations of the PsaA-L718Y/T mutant's kinetics also predict a redistribution of (total) amplitudes for the fast and slow phases, which have almost identical amplitudes as observed in the experiments (Fig. 3). The macroscopic explanation for the observed amplitude redistribution is that the energetic configurations of WT, where PhQ_A represent a local thermodynamic minimum, favours transient electron transfer from PhQ_B to PhQ_A, via F_X in ns time scale. This transient electron transfer results in an enhancement of the total amplitude of 250 ns lifetime with respect to the initial population of PhQ_A (by A_{0A}^-). In the H-bond mutants, the driving force for $PhQ_B \to F_X \to PhQ_A$ transfer is dramatically reduced, so that the amplitude of this transfer process is decreased and the amplitude of fast and slow phases more closely resemble the initial populations (which were assumed identical). This type of kinetic modelling was extended to several other mutations, including those affecting PhQ_B binding, and a compilation of the estimated perturbations of $PhQ_{A/B}$ midpoint potential (determining ΔG^0) are presented in Fig. 6. It can be seen that, in all mutants examined so far, the perturbations ranges in $\pm 50 - 80$ mV. Whereas mutations that weaken the H-bond decrease the midpoint potential, those affecting hydrophobic interactions tend to increase its value. Surprisingly, the extent of the increase seems to be similar for residues that are located in proximity to the quinones (*e.g.* PsaA-W697/PsaB-W677) and residue that are more distal to them (*e.g.* PsaA-F689/PsaB-W673).

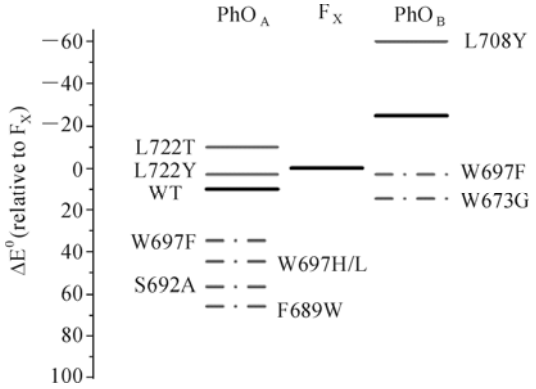

Fig. 6 Mutation-induced perturbation of redox potential of PhQ_A and PhQ_B derived from simulation of ET kinetics.

In conclusion, the difference in lifetimes describing PhQ oxidation in PS I RC can be rationalized assuming difference driving forces for PhQ_A and PhQ_B oxidation, with $\Delta G^0_{PhQ_A \to F_X} > 0$ and $\Delta G^0_{PhQ_B \to F_X} < 0$, respectively. This asymmetry in the energetic configurations of PhQ_A and PhQ_B promotes a transient inter-quinone electron transfer, mediated by F_X. Hydrophobic interactions play a central role in poising PhQ potential toward more reducing values, *i.e.* favouring rapid ET, whereas asymmetric H-bonding has the opposite effect. However, H-bonding might be required in order to stabilize the binding of quinone to the RC (Santabarbara *et al*., 2010).

Acknowledgements

Work in KR's laboratory was supported by Energy Biosciences grant DE-FG02-08ER15989 from the U.S. Dept. of Energy. FR acknowledges funding by CNRS and UPMC. SS thanks the CNR for funding.

References

Béal D, Rappaport F, Joliot P (1999) A New High-Sensitivity 10-ns Time-Resolution Spectrophotometric Technique Adapted to in Vivo Analysis of the Photosynthetic Apparatus. Rev. Sci. Instr. 70: 202-207

Ben-Shem A, Frolow F, Nelson N (2003) Crystal Structure of Plant Photosystem I. Nature 426: 630-635

Byrdin M, Santabarbara S, Gu F, Fairclough WV, Heathcote P, Redding K, Rappaport F (2006) Assignment of a Kinetic Component to Electron Transfer between Iron-Sulfur Clusters F_X and $F_{A/B}$ of Photosystem I. Biochim. Biophys. Acta. 1757: 1529-1538

Guergova-Kuras M, Boudreaux A, Joliot A, Joliot P, Redding K (2001) Evidence for two Active Branches for Electron Transfer in Photosystem I. Proc. Nat. Acad. USA 98: 4437-4442

Jordan P, Fromme P, Klukas O, Witt HT, Saenger W, Krauss N (2001) Three-dimensional Structure of Cyanobacterial Photosystem I at 2.5 Angstrom Resolution. Nature 411: 909-917

Li Y, van der Est A, Lucas MG, Ramesh VM, Gu F, Petrenko A, Lin S, Webber AN, Rappaport F, Redding K (2006) Directing Electron Transfer within Photosystem I by Breaking H-bonds in the Cofactor Branches. Proc. Natl. Acad. Sci. USA 103: 2144-2149

Moser CC, Keske JM, Warncke K, Farid RS, Dutton PL (1992) Nature of Biological Electron Transfer. Nature 355: 796-802

Müller MG, Slavov C, Luthra R, Redding KE, Holzwarth AR (2010) Independent Initiation of Primary Electron Transfer in the Two Branches of the Photosystem I Reaction Centre. Proc. Natl. Acad. Sci. USA 107: 4123-4128

Rappaport F, Diner BA, Redding K (2006) In Photosystem I: the Plastocyanin: Ferredoxin Oxidoreductase in Photosynthesis, Golbeck JH (ed.) Kluwer: Dordrecht, pp. 223-244

Santabarbara S, Heathcote P, Evans MCW (2005) Modelling of the Electron Transfer Reactions in Photosystem I by Electron Tunnelling Theory. Biochim. Biophys. Acta Bioenergetics 1708: 283-310

Santabarbara S, Reifschneider K, Jasaitis A, Gu F, Agostini G, Carbonera D, Rappaport F, Redding KE (2010a) Interquinone Electron Transfer in Photosystem I as Evidenced by Altering the Hydrogen Bond Strength to the Phylloquinone(s). J. Phys. Chem. B. 114: 9300-9312

Srinivasan N, Golbeck JH (2009) Protein-Cofactor Interactions in Bioenergetic Complexes: the Role of the A_{1A} and A_{1B} Phylloquinones in Photosystem I. Biochim. Biophys. Acta 1787: 1057-1088

Supercomplex Organizations and Evolution of Photosystems I and II (*Anabaena* sp. PCC 7120, *Cyanophora Paradoxa* and *Cyanidioschyzon Merolae*)

Mai Watanabe*, Hisako Kubota, Hajime Wada, Rei Narikawa, Masahiko Ikeuchi

Department of Life Sciences (Biology), Graduate School of Arts and Science, University of Tokyo, Komaba, Meguro, Japan.
*Corresponding author. Tel. No. +81 3 5454 4375; Fax No. +81 3 5454 4337; E-mail: MAIMAI@bio.c.u-tokyo.ac.jp.

Abstract: Supercomplex organization of photosystem complexes was studied in various cyanobacteria, a glaucocystophyte and a primitive rhodophyte by blue-native PAGE. As already shown in *Thermosynechococcus elongatus*, PSII complexes yielded the dimeric and monomeric forms. In any case, the recovery of the dimeric PSII was increased at high detergent concentrations. On the other hand, there were unexpected variations in the organization of the PSI supercomplexes depending on the species. In filamentous N_2-fixing cyanobacterium *Anabaena* sp. PCC 7120 and a glaucocystophyte *Cyanophora paradoxa* gave PSI tetramer and dimer but no trimer at all.

Keywords: *Anabaena*; Blue-native PAGE; *Cyanophora;* Photosystem; Supercomplex

Introduction

Functional photosystems I and II (PSI and PSII) have been isolated as a multisubunit membrane supercomplex from cyanobacteria, algae and land plants. It is known that the PSII complex functions as a dimer from cyanobacteria to land plants. On the other hand, it is generally accepted that the PSI complex functions as a trimer in cyanobacteria and as a monomer associated with light-harvesting chlorophyll complex (LHC) in algae and land plants. Crystal structures of the PSII dimer and PSI trimer from *Thermosynechococcus elongatus* and the PSI monomer from pea have been determined (Jordan *et al*., 2001; Ben-Shem *et al*., 2003; Guskov *et al*., 2009).

Previously, we reported the organization of PSII and PSI complexes of *T. elongatus* by blue-native PAGE (BN-PAGE) (Watanabe *et al*., 2009, 2011). The ratio of the PSII monomer to the dimer varied depending on the concentrations of with *n*-dodecyl-β-D-maltoside (DM). In contrast, the PSI complex was almost recovered as a trimer at wide concentrations of DM. Here we studied supercomplex organization of photosystems of various cyanobacteria, glaucocystophyte and primitive rhodophyte by BN-PAGE with wide range of detergent concentrations.

Materials and Methods

Thylakoid membranes of *Anabaena* sp. PCC 7120, *Synechocystis* sp. PCC 6803, *T. elongatus* and *Cyanidioschyzon merolae* 10D were isolated as described in Watanabe *et al*. (2009). Cyanelles from *Cyanophora paradoxa* strain NIES 547 were isolated as described in Koike *et al*. (2000). Isolated cyanelles were disrupted with zirconia beads as described in Watanabe *et al*. (2009). Thylakoid membranes [1 (mg Chl) ml^{-1}] were solubilized with DM on ice for 30 min, followed by centrifugation at 300,000 xg for 30 min at 4 ^{o}C. The solubilized supernatant was subjected to BN-PAGE and BN-PAGE gel was subjected to two-dimensional SDS-PAGE.

Results and Discussion

The thylakoid membranes from cyanobacteria, a glaucocystophyte and a primitive rhodophyte were solubilized with 1% DM and subjected to BN-PAGE

(Fig. 1a). In agreement with previous reports (Aro *et al*., 2005; Watanabe *et al*., 2009), four or three green bands were detected in *Synechocystis*, *Synechococcus* sp. PCC 7942 and *T. elongatus*. These bands corresponded to PSI trimer, PSII dimer, PSI monomer and PSII monomer (Fig. 1a, band 1–4). In contrast, the separation patterns of *Anabaena* and algae were distinctively different from *T. elongatus*, *Synechocystis* and *Synechococcus*. A PSI band was found at high-molecular-mass region but not at the PSI trimer region in *Anabaena* and *C. paradoxa*. PSI of *C. merolae* was resolved as two closely migrated bands near the dimeric PSII band. Sometimes an additional faint band of PSI was observed near the PSI trimer region.

In Anabaena, the high-molecular PSI band was abundantly recovered at 0.6%–2% DM, less abundantly at 3% and detected as a faint band at 5%. Conversely, a putative PSI dimer band was abundantly detected near the PSII dimer band at 3%–5% DM and slightly detected at 1%–2% DM (Fig. 2a). On the other hand, the PSI trimer band was not detected at all in Anabaena under any solubilization conditions. Two-dimensional PAGE confirmed that all the PSI bands consisted of identical at least 6 spots (Fig. 2b). Apparently, there were no differences in the subunit composition between these PSI bands. The PSII complexes of *Anabaena* were separated into the monomer and the dimer and their ratio was also dependent on the DM concentrations. The features of the *Anabaena* PSII were similar to the *T. elongatus* PSII (Watanabe *et al*., 2009).

The high molecular PSI complex was also observed in the glaucocystophyte *C. paradoxa* in addition to the dimer and the monomer (Fig. 1a, lane 4). The mobility of the high molecular PSI band and the dimer band were very close to that of *Anabaena*. And the PSI trimer was also absent in *C. paradoxa*. There were no differences in subunit composition between the high molecular, dimeric and monomeric PSI bands (data not shown). Notably, recovery of the dimeric and monomeric PSII also depended on the detergent concentration like in *Anabaena* and *T. elongatus*.

We plotted known PSI and PSII complexes of *T. elongatus* for estimation of the high molecular PSI complexes. The PSI dimer bands of *Anabaena* and *C. paradoxa* fit very well with the line of the known photosystems. By extrapolation, we obtained ca. 1387 kDa for the high molecular PSI bands. These results suggest that the high molecular PSI complex is the tetramer (Watanabe *et al*., 2011).

C. merolae produced bands of PSI between the typical monomer and dimer regions (Fig. 1a). 2D PAGE revealed that both bands consisted of the identical PSI subunits and two LHCI bands (Fig. 1b). Based on the molecular size relationship, these PSI-LHCI bands were monomeric PSI and LHCI supercomplex. The faint PSI band was detected near the PSI trimer region. 2D PAGE and molecular mass suggested the dimer of PSI-LHCI complex (Fig. 1b).

To date, the PSI trimer and monomer have been isolated from many cyanobacteria, for example *T. elongatus*, *Synechocystis*, *Synechococcus* sp. PCC 7002 and *Gloeobacter violaceus* (Tsiotis *et al*., 1995; Kruip *et al*., 1997; Mangels *et al*., 2002). On the other hand, a PSI complex of *Nostoc punctiforme* was assigned to the trimer according to BN-PAGE

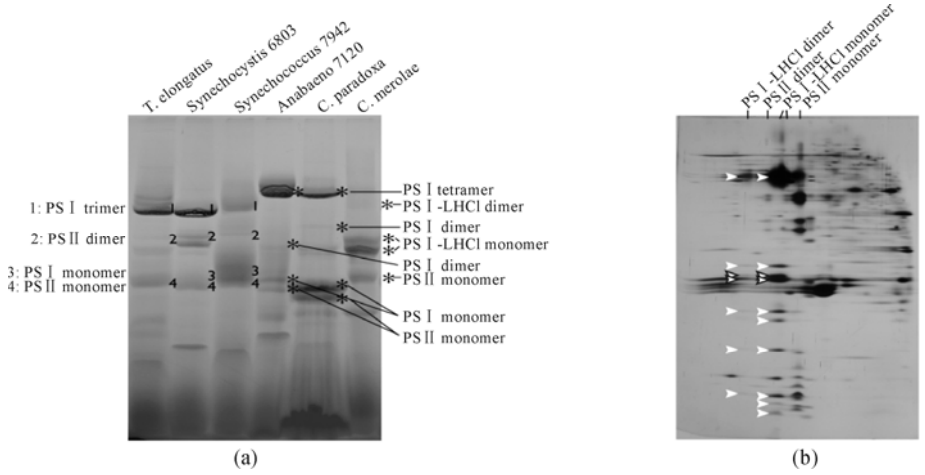

Fig. 1 BN-PAGE of thylakoid membranes from several species (a) and 2D PAGE of *C. merolae* (b) Thylakoid membranes were solubilized with 1% DM.

(Cardona *et al*., 2009) but it migrated near the PSII dimer, which resembles of the *Anabaena* PSI dimer in our study. Further, we can see another high molecular spot of PSI, which again resembles the tetramer of *Anabaena* PSI. These features seem to suggest that PSI of *N. punctiforme* can be fractionated as the dimer and the tetramer but not as the trimer. Since *N. punctiforme* is close in phylogeny to *Anabaena* sp. PCC 7120, heterocyst differentiation or some common features may be related to the unique PSI organization of the dimer and tetramer.

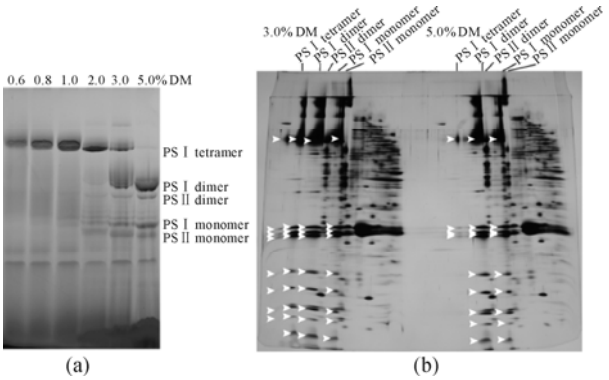

Fig. 2 BN-PAGE (a) and 2D-PAGE (b) of *Anabaena* Arrowheads indicate the PSI subunits.

In the structure of the PSI trimer of *T. elongatus*, PsaL subunit is important for trimeric organization. The assembly of the PSI trimer was prevented by mutagenesis of the PsaL subunit in *Synechocystis* (Chitnis and Chitnis, 1993). The phylogenetic tree of PsaL revealed that *Anabaena* and related heterocyst-forming cyanobacteria were clustered together into a clade distinct from the other cyanobacteria (Fig. 3a). Similar feature was also found in the tree of PsaI, which locates next to PsaL in the PSI complex (Fig. 3b). On the other hand, the tree of the other PSI subunits such as PsaF and PsaA showed that the heterocyst-forming cyanobacteria are positioned within the other cyanobacteria (Figs. 3c and 3d). The unique feature of PsaL might be required for specific function(s) in N_2-fixing heterocysts. The *Anabaena*-type PsaL extends in N-terminus, which locates at the acceptor side of PSI. The N-terminal extension of PsaL might be involved in interaction with other factor such as ferredoxin. Additionally, the *Anabaena*-type PsaL has a deletion in a part of C-terminal helix, which interacts each other among the trimer. These features might be responsible for the tetrameric

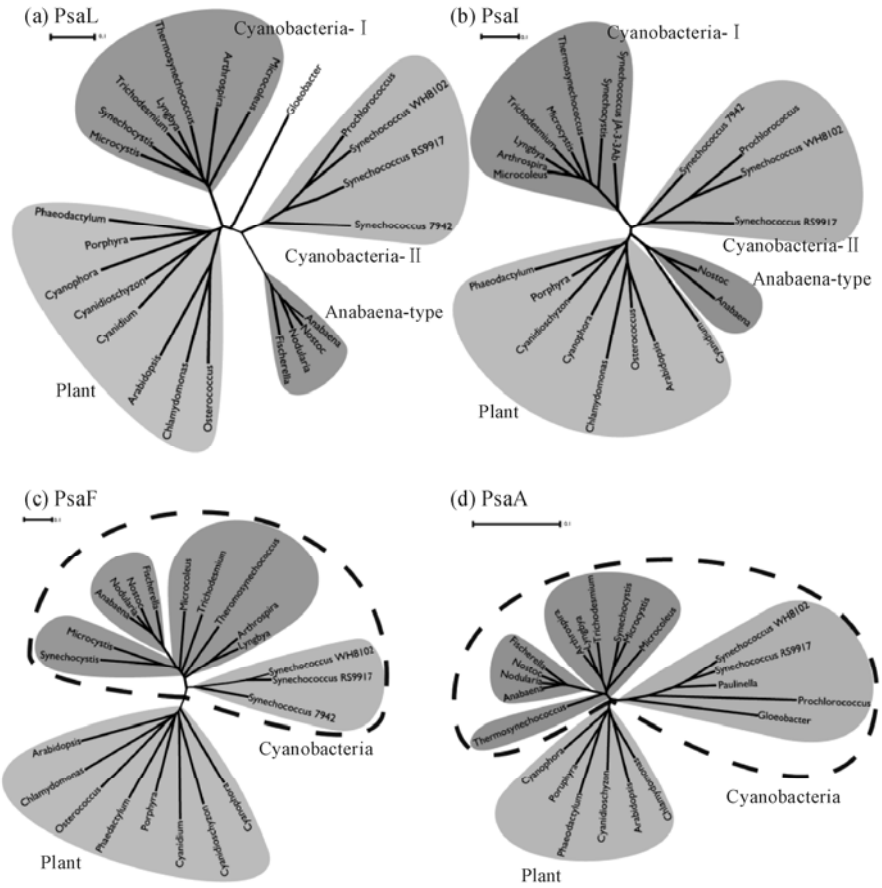

Fig. 3 Phylogenic trees of (a) PsaL, (b) PsaI, (c) PsaF and (d) PsaA.

assembly. The tetramer was also observed in *C. paradoxa*, where only C-terminal short truncation is found in PsaL. These results suggest that the chloroplast of eukaryotes might be derived from the *Anabaena*-type cyanobacteria. Further evolution of LHCI may have resulted in structural changes of the PSI complex, leading to monomerization (Fig. 4) (Watanabe *et al*., 2011).

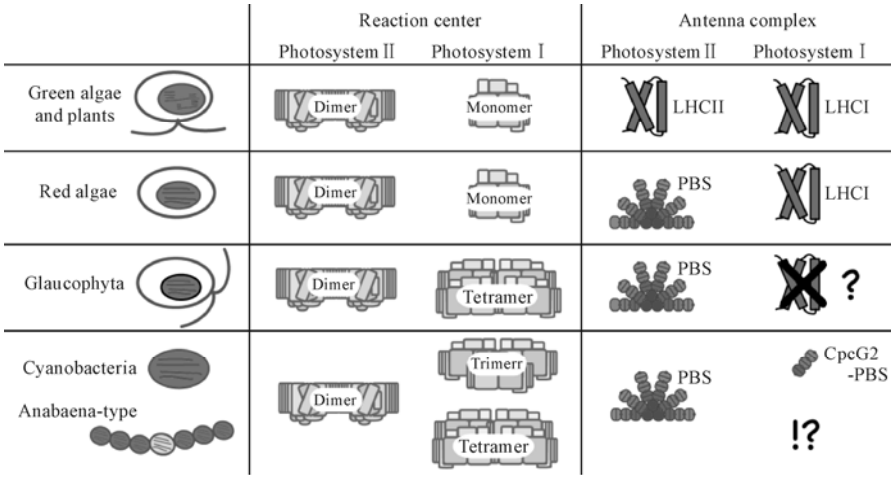

Fig. 4 Evolution of organization of photosystems and antenna complexes.

Acknowledgements

This work was supported by Grants-in-Aid for Young Scientists (to RN), Scientific Research and the GCOE program from the Ministry of Education, and Science (to MI).

References

Aro EM, Suorsa M, Rokka A, Allahverdiyeva Y, Paakkarinen V, Saleem A, Battchikova N, Rintamaki E (2005) Dynamics of Photosystem II: a Proteomic Approach to Thylakoid Protein Complexes. J Exp Bot 56: 347-356

Ben-Shem A, Nelson N, Frolow F (2003) Crystallization and Initial X-Ray Diffraction Studies of Higher Plant Photosystem I. Acta Crystallogr D Biol Crystallogr 59: 1824-1827

Cardona T, Battchikova N, Zhang P, Stensjo K, Aro EM, Lindblad P, Magnuson A (2009) Electron Transfer Protein Complexes in the Thylakoid Membranes of Heterocysts from the Cyanobacterium Nostoc Punctiforme. Biochim. Biophys. Acta 1787: 252-263

Chitnis VP, Chitnis PR (1993) PsaL Subunit is Required for the Formation of Photosystem I Trimers in the Cyanobacterium Synechocystis sp. PCC 6803. FEBS Lett. 336: 330-334

Guskov A, Kern J, Gabdulkhakov A, Broser M, Zouni A, Saenger W (2009) Cyanobacterial Photosystem II at 2.9-A Resolution and the Role of Quinones, Lipids, Channels and Chloride. Nat. Struct. Mol. Biol. 16: 334-342

Jordan P, Fromme P, Witt HT, Klukas O, Saenger W, Krauss N (2001) Three-Dimensional Structure of Cyanobacterial Photosystem I at 2.5 a Resolution. Nature 411: 909-917

Koike H, Shibata M, Yasutomi K, Kashino Y, Satoh K (2000) Identification of Photosystem I Components from a Glaucocystophyte, Cyanophora Paradoxa: the PsaD Protein Has an N-Terminal Stretch Homologous to Higher Plants. Photosynth. Res. 65: 207-217

Kruip J, Chitnis PR, Lagoutte B, Rogner M, Boekema EJ (1997) Structural Organization of the Major Subunits in Cyanobacterial Photosystem I. Localization of subunits PsaC, -D, -E, -F, and -J. J. Biol. Chem. 272: 17061-17069

Mangels D, Kruip J, Berry S, Rogner M, Boekema EJ, Koenig F (2002) Photosystem I from the Unusual Cyanobacterium Gloeobacter Violaceus. Photosynth. Res. 72: 307-319

Tsiotis G, Haase W, Engel A, Michel H (1995) Isolation and Structural Characterization of Trimeric Cyanobacterial Photosystem I Complex with the Help of Recombinant Antibody Fragments. Eur. J. Biochem. 231: 823-830

Watanabe M, Iwai M, Narikawa R, Ikeuchi M (2009) Is the Photosystem II Complex a Monomer or a Dimer? Plant Cell Physiol. 50: 1674-1680

Watanabe M, Kubota H, Wada H, Narikawa R, Ikeuchi M (2011) Novel Supercomplex Organization of Photosystem I in Anabaena and Cyanophora Paradoxa. Plant Cell Physiol. in press

3D Model of PSI-LHCI Supercomplexes from *Chlamydomonas Reinhardtii*

Venkateswarlu Yadavalli[a+], Chandramouli Malleda[a+], Rajagopal Subramanyam[a,b*]

[a]Department of Biochemistry, [b]Department of Plant Sciences, School of Life Sciences,
University of Hyderabad, Hyderabad (A.P), India 500046, [+]both authors contributed equally.
[*]Corresponding author. Tel. No. +91-40-2313 4572; Fax No. +91-40-2301 0120; E-mail: srgsl@uohyd.ernet.in.

Abstract: The function of Photosystem I (PSI) is catalyzing one of the initial steps in driving oxygenic photosynthesis in cyanobacteria, algae and higher plants. The recent crystallographic model at 3.3 Å resolution represents the most complete plant PSI structure. The *Chlamydomonas reinhardtii* PSI-LHCI supercomplex structure is not known since it contains a unique structure having additional subunits of light harvesting complex I (LHCI). We have modeled PSI core and LHCI in order to elucidate the structure of PSI-LHCI supercomplexes of *C. reinhardtii*. Most of the core subunits are homologous to the higher plants except PsaO and now it has been modeled based on threading. All core subunits were located similarly like pea structure however, PsaO, a new subunit is closely located to the PsaH, PsaI and PsaL subunits. The location of PsaO subunit at this position may suggest that it may be involved in state transition mechanism in *C. reinhardtii*. From our model, it indicates that there are non-covalent strong inter protein-protein relationship, especially from PSI core to LHCI. Our 3D model may give the structural information for better understanding of PSI-LHCI arrangement and its physiological role in *C. reinhardtii* as well as other algae, where it serves many biotechnological applications.

Keywords: *C. Reinhardtii*; 3D Model; PS I-LHCI; Supercomplex

Introduction

Photosynthesis occurs on thylakoid membranes catabolized by several multimeric membrane supercomplexes that include PSI, PSII, their associated light harvesting complexes, Cyt b_6f complex and ATP synthase (Jensen *et al.*, 2007; Scheller *et al.*, 2001). PSI catalyzes the light-driven electron transfer from the soluble electron carrier plastocyanin, located at the lumenal side (inside) of the thylakoid membrane, to ferredoxin, at the stromal side (outside) of the natural photosynthetic membrane. The structure of PSI supercomplex comprises of core subunits and light harvesting complexes, chlorophylls, phylloquinones and Fe_4S_4 clusters (Amunts *et al.*, 2007; Amunts *et al.*, 2010; Ben-Shem *et al.*, 2003; Jensen *et al.*, 2007). Also, the structure of PSI is highly conserved between cyanobacteria and higher plants which acts as a light driven plastocyanin-ferridoxin-oxidoreductase contained several nucleate and chloroplast encoded subunits (Fyfe *et al.*, 2002; Jordan *et al.*, 2001; Rochaix, 2002; Subramanyam *et al.*, 2006). However, the structure of PSI-LHCI supercomplexes of *C. reinhardtii* is unique as LHCI composition is different and so far there is no structure available to understand the function of PSI-LHCI integrity. By various biochemical and electron microscopy studies, it was revealed that there could be even more than 10 LHCI polypeptides (Hippler *et al.*, 1998; Mozzo *et al.*, 2010). Thus, in the present study, we build a model with 14 PSI core subunits and 9 LHCI subunits based on the crystallographic model of plant PS I at 3.3 Å (Amunts *et al.*, 2010) which contains 13 PSI core subunits and four Lhca polypeptides.

Materials and Methods

Protein sequences of *C. reinhardtii* PSI-LHCI was collected from expasy database. Target sequences were used for getting the template that has detectable similarity to the target sequence by using BLAST. All the sequences were taken as a single FASTA format

file where in each chain has been separated and scanned against a library of sequences extracted from known protein structures in the Protein Data Bank to find the templates. All the chains of both target and templates with their highest percentage of identity were individually aligned in CLUSTALW. The alignment of output file was set to PIR format of target and template sequence. Further, target sequences were aligned with template (2WSC) sequence (Amunts *et al.*, 2010). The output alignment of multiple sequences was exported to .ali and .pap of the previous PIR and PAP formats respectively. PsaO core subunit of *C. reinhardtii* was unique for which similarity was not found with any of the template sequences, was built by using threading server. Best aligned target sequences obtained from threading server were used for building the 3D model. 3D modeling of aligned file, which contains 5289 amino acid residues, was run on Modeller 9v7 version (Sali *et al.*, 1995). The geometrical parametersofthe created 3D model was evaluated using PROCHECK.

Results and Discussion

The sequence identity between target sequences and template sequences were from 36% to 85%. The arrangement of PS I core (14 subunits) and Lhca1 to Lhca9 subunits were shown in Fig. 1. We predicted the arrangement as *Lhca*5, Lhca1, Lhca6, Lhca4, Lhca2, Lhca7, Lhca8, Lhca9 and Lhca3 based on spatial restraints of modeller. However the higher plants PSI structural arrangements was entirely different, where Lhca 1 and 4 forms as one dimer and Lhca 2 and Lhca3 forms another dimer in a half moon shape surrounding PSI core (Amunts *et al.*, 2010). The presence of extra LHCI in *C. reinhardtii* may help in efficient light energy trapping mechanism and thus helps in maximum utilization of solar energy. LHCI proteins of *C. reinhardtii* have significant identity to the higher plants LHCI polypeptides. There are 14 PSI subunits exist in PSI core of *C. reinhardtii* and most of them are placed in similar positions as in higher plants except PsaO subunit (Amunts *et al.*, 2010). In addition, PsaO subunit of *C. reinhardtii* build by threading model has three transmembrane helices. PsaO was located at PsaH, PsaI and PsaL subunits. Since all these subunits are known to be involved in state transitions and thus PsaO subunit may play a major role in state transition mechanism in *C. reinhardtii*. It is not only involved in state transition mechanism, but also may involve in organization of PSI-LHCI supercomplexes of *C. reinhardtii.*

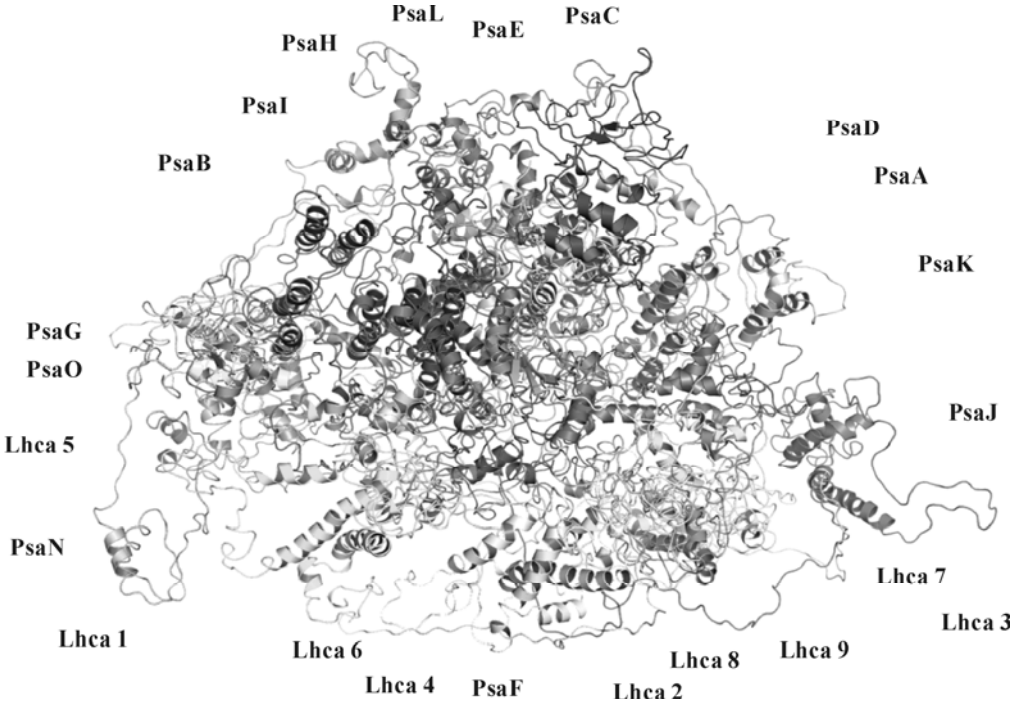

Fig. 1 3D model of PSI-LHCI supercomplex of *C.reinhardtii* build on Modeller 9v7 version.

The results of PROCHECK analysis shows that most of the amino acid residues lie in the allowed regions and was in better agreement in relation to the higher plants of 2WSC structure (Amunts *et al.*, 2010) (Table 1). The total number of amino acid residues fall in to four major regions. When coming to the case of R-factors most unusual value is –1.0, where the PSI-LHCI model stands at –0.8 Å deviation that is better in two folds from original structure (PDB:2WSC) which possess –0.9 Å deviation. Superimposed model with the template of higher plant (Amunts *et al.*, 2010) shared major part of co-ordinates and it was found that RMSD equals to 2.7, which was in a better state of existence and not deviating much from the main template. Thus, the model generated by Modeller 9v7 of PSI-LHCI supercomplexes of *C. reinhardtii* was the most reliable method for understanding the various structural domains.

Table 1 Statistical analysis of PSI-LHCI of *C. reinhardtii* and PSI-LHCI of higher plants (PDB: 2WSC) from using Ramachandran plot.

Important parameters	PSI-LHCI of *C. reinhardtii*		PSI-LHCI of higher plants (PDB: 2WSC)	
	Number of amino acid residues	Percentage (%)	Number of amino acid residues	Percentage (%)
Residues in most favoured regions [A,B,L]	3119	70.2	1170	43.7
Residues in additional allowed regions [a,b,l,p]	878	19.8	931	34.8
Residues in generously allowed regions [~a,~b,~l,~p]	258	5.8	353	13.2
Residues in disallowed regions	190	4.3	225	8.4
Number of non-glycine and non-proline residues	4445	100.0	2679	100.0
Number of end-residues (excl. Gly and Pro)	42		38	
Number of glycine residues (shown as triangles)	498		302	
Number of proline residues	304		170	
Total number of residues	5289		3189	

The 3D model which was shown here is mainly based on energy minimization approach. The evaluation of 3D model data by various methods such as PROCHECK and RMSD values suggests that this could be the most preferential arrangement of light harvesting complexes and PSI core subunits. Thus the 3D model of PSI-LHCI supercomplexes represented here, provides more detailed structural information for *C. reinhardtii* that could be useful for understanding the structural information and various biotechnological understanding applications. Further studies like crystallography and NMR studies may provide the exact location of these subunits.

Acknowledgments

RS thank DST-PURSE grant, UOH, Hyderabad, India for travel fellowship. Also thank DST (SR/SO/BB-34/2006, SR/FT/L-89/2006), DBT (BT/PR11277/GBD/27/152/2008), India for funding the infrastructure facilities and VY thanks CSIR, India for providing JRF/SRF.

References

Amunts A, Drory O, Nelson N (2007) The Structure of a Plant Photosystem I Supercomplex at 3.4 Å Resolution. Nature 447(7140): 58-63

Amunts A, Toporik H, Borovikova A, Nelson N (2010) Structure Determination and Improved Model of Plant Photosystem I. J. Biol. Chem. 285(5): 3478-3486

Ben-Shem A, Frolow F, Nelson N (2003) Crystal Structure of Plant Photosystem I. Nature 426(6967): 630-635

Fyfe PK, Jones MR, Heathcote P (2002) Insights into the Evolution of the Antenna Domains of Type-I and Type-II Photosynthetic Reaction Centres through Homology Modelling. FEBS Lett. 530(1-3): 117-123

Hippler M, Redding K, Rochaix JD (1998) Chlamydomonas Genetics, a Tool for the Study of Bioenergetic Pathways. Biochim. Biophys. Acta 1367(1-3): 1-62

Jensen PE, Bassi R, Boekema EJ, Dekker JP, Jansson S, Leister D, Robinson C, Scheller HV (2007)

Structure, Function and Regulation of Plant Photosystem I. Biochim. Biophys. Acta 1767(5): 335-352

Jordan P, Fromme P, Witt HT, Klukas O, Saenger W, Krauss N (2001) Three-Dimensional Structure of Cyanobacterial Photosystem I at 2.5Å Resolution. Nature 411(6840): 909-917

Mozzo M, Mantelli M, Passarini F, Caffarri S, Croce R, Bassi R (2010) Functional Analysis of Photosystem I Light-Harvesting Complexes (Lhca) Gene Products of Chlamydomonas Reinhardtii. Biochim. Biophys. Acta 1797(2): 212-221

Rochaix JD (2002) Chlamydomonas, a Model System for Studying the Assembly and Dynamics of Photosynthetic Complexes. FEBS Lett. 529(1): 34-38

Sali A, Potterton L, Yuan F, van Vlijmen H, Karplus M (1995) Evaluation of Comparative Protein Modeling by MODELLER. Proteins 23(3): 318-326

Scheller HV, Jensen PE, Haldrup A, Lunde C, Knoetzel J (2001) Role of Subunits in Eukaryotic Photosystem I. Biochim. Biophys. Acta 1507(1-3): 41-60

Subramanyam R, Jolley C, Brune DC, Fromme P, Webber AN (2006) Characterization of a Novel Photosystem I-LHCI Supercomplex Isolated from Chlamydomonas Reinhardtii under Anaerobic (State II) Conditions. FEBS Lett. 580(1): 233-238

Reaction of A_1-menaquinone in Type I Reaction Center of *Heliobacterium Modesticaldum* at Cryogenic Temperature

Toru Kondo[a], Masahiro Matsuoka[b], Chihiro Azai[b], Hiroyuki Mino[a], Hirozo Oh-oka[b], Shigeru Itoh[a*]

[a]Division of Material Science Physics, Graduate School of Science, Nagoya University, Japan;
[b]Department of Biological Sciences, Graduate School of Science, Osaka University, Japan.
[*]Corresponding author. Tel/Fax. No. +81-52-789-2883; E-mail: itoh@bio.phys.nagoya-u.ac.jp.

Abstract: Temperature dependence of electron transfer reaction via A_1-menaquinone in type I homodimeric reaction center of *Heliobacterium modesticaldum* (hRC) was observed by time-resolved electron paramagnetic resonance (EPR) spectroscopy. Flash excitation induced an electron spin polarization (ESP) signal due to $P800^+F_X^-$ radical pair at 14 K, exhibiting an E/A (E, emission; A, absorption) spectral pattern. After the hRC core complex was pre-illuminated at 210 K for 1 hour and subsequently cooled to 5 K during illumination, another ESP signal due to $P800^+A_1^-$, exhibiting an A/E pattern, was flash-induced at 14 K. The decay time was estimated to be 90 μs at 5 K and 25 μs at 20 K, respectively. The recombination of $P800^+A_1^-$ in hRC is significantly faster at all the temperatures, compared to that of $P700^+A_1^-$ in PS I, which occurs in around 100 μs with little temperature dependence. The recombination time of $P800^+F_X^-$ was a 4–11 ms at 5 K in contrast to the longer time than 100 ms in PSI. These results indicate that A_1^- menaquinone is involved in the rapid electron transfer between P700 and F_X in hRC, as phylloquinone in PSI, probably with unique energy gap or geometry.

Keywords: Heliobacteria; Type I RC; EPR; Quinone; Homodimer RC; Electron spin polarization

Introduction

Heliobacteria are strict anaerobe that have a type I reaction center (RC) complex essentially analogous to photosystem (PS) I of plant and cyanobacteria. The heliobacterial RC (hRC) has a homodimeric structure made of two identical polypeptides (PshA) in contrast to the heterodimer RCs of PS I and all the type-II RCs that are made of two different polypeptides. The 3D-structures of the hRC and green sulfur bacterial RC, which is also homodimeric type-I RC, have not been clarified yet although the structures of the multiple heterodimeric RCs have been resolved. The hRC contains one special pair bacteriochlorophyll *g* (P_{800}), two primary electron acceptor chlorophyll *a*-670 (A_0), and three 4Fe-4S iron sulfur centers ($F_X/F_A/F_B$) as the electron transfer components (Heinnickel and Golbeck, 2007; Oh-oka, 2007). Menaquinone-9 is present in hRC (Trost and Blankenship, 1989), while it has long been debated whether or not the quinone functions as an electron acceptor like phylloquinone (A_1) that is known to mediate the electron transfer from A_0 to F_X in PS I.

The re-oxidation of A_0^- in hRC occurs with a 500–600 ps time constant after the primary charge separation (Lin *et al*., 1995; Nuijs *et al*., 1985). The time constant is considerably longer than the 20–50 ps for electron transfer from A_0^- to A_1 in PSI (Hastings *et al*., 1994; Kumazaki *et al*., 1994). The slow decay of A_0^- in hRC, has been interpreted as the evidence for the direct electron transfer from A_0 to F_X with no participation of A_1. The electron paramagnetic resonance (EPR) and optical studies actually have not succeeded in detection of the $P^+A_1^-$ state signal under the same conditions as those for the detection of $P700^+A_1^-$ signal in PSI. Recently, we detected an electron spin poralization (ESP) EPR signal of $P800^+A_1^-$ radical pair in the purified hRC core complex (hRC_{core}) (Miyamoto *et al*., 2008).

In this study, we observed temperature dependence of the recombination rate of $P800^+A_1^-$ and $P800^+F_X^-$ in hRC_{core}. The results indicated the unique behavior of A_1-menaquinone in hRC.

Materials and Methods

The hRC_{core} was purified from *Heliobacterium modesticaldum* (*Hbt. modesticaldum*) cells as previously reported (Miyamoto *et al.*, 2008). Appropriate amounts of sodium dithionite were added to reduce cofactors in the RC.

EPR spectra were measured with a Bruker ESP-300E X-band spectrometer (Bruker Biospin, Germany) equipped with a liquid-helium flow cryostat and a temperature control system (CF935, Oxford Instruments, Oxford, U.K.). Continuous white light illumination was given from a 650 W tungsten lamp through heat cut glass filters and **cm water filter. Repetitive Xenon-flash excitation light with submicrosecond duration was given through a 1 m glass fiber light guide at 1 Hz for time-resolved EPR experiments. Transient signals were detected with the field modulation mode as a first-derivative signal.

Results and Discussion

Temperature dependence of ESP-EPR signals in hRC

Fig. 1 shows the transient ESP-EPR spectra at 5–50 K induced by a flash excitation in the hRCcore. The closed and open circles represent the signal intensities at 0 and 500 μs after the flash excitation, respectively. Panel A shows the ESP spectra at 5–50 K obtained in the dark-frozen hRCcore. All the spectra at 0 μs exhibited an E/A pattern (E, emission; A, absorption). The ESP signal was assigned to $P800^+F_X^-$ radical pair (van der Est *et al.*, 1998). The spectra at 500 μs can be attributed to the thermally equilibrated state signal due to $P800^+$. Similar E/A pattern signals were observed even at 200 K (data not shown). No temperature dependent change in the intensities of $P800^+F_X^-$ was detected at 5–50 K.

Panel B in Fig. 1 shows the ESP spectra detected at 5–50 K upon the flash excitation after hRCcore had been pre-illuminated at 210 K for 1 h and then cooled down to 5 K under illumination. The 5 K spectrum at 0 μs (closed circles) exhibits an A/E pattern, which is obviously different from the E/A pattern of $P800^+F_X^-$, and was assigned to $P800^+A_1^-$ state. The A/E pattern is slightly different from the previously reported A/E/A/E pattern in similar hRCcore preparation after pre-illumination in the presence of dithionite (Miyamoto *et al.*, 2008). Similar A/E/A/E pattern ESP signal was detected in the hRC_{core} pre-illuminated in the presence of ascorbate (data not shown). Therefore, we concluded that the A/E/A/E signal was due to the insufficient reduction of hRC_{core}. Some contribution of the E/A pattern of the $P800^+F_X^-$ ESP signal would have been involved in the previously reported ESP signal.

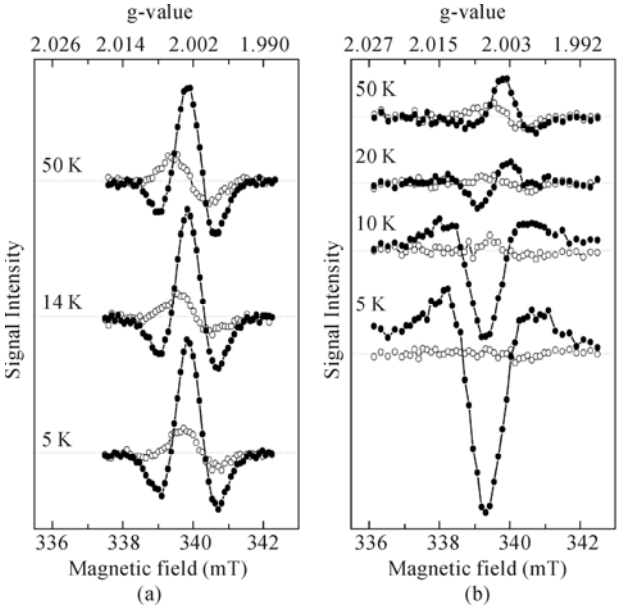

Fig. 1 Temperature dependence of ESP-EPR spectra (derivertive form) in (A) the dark-frozen and (B) the light-cooled hRC_{core} of *H. modesticaldum*. Closed and open circles represent transient spectra at 0 and 500 μs after flash excitation, respectively. Experimental conditions: microwave power, 1 mW; microwave frequency, (A) 9.527 and (B) 9.533 GHz; modulation amplitude, 4 G; modulation frequency, 100 kHz; time constant, 0.01 ms.

The spectra at 500 μs after flash excitation in pre-illuminated hRC_{core} (panel B, open circles) were almost negligible, which is significantly different from the case in the dark-frozen hRC_{core} (panel A, open circles). The result indicates that the $P800^+A_1^-$ radical pair is recombined more rapidly than the relaxation of the $P800^+A_1^-$ ESP spin state. Therefore, the decay kinetics of the ESP signal directly reflects the charge recombination between $P800^+$ and A_1^-.

The A/E pattern signal became smaller at high temperature and undetectable above 20 K, and the 50 K spectrum was consisted of only a small E/A pattern signal of $P800^+F_X^-$. If the sample was cooled down below 20 K again after heating to 50 K, the A/E signal could be observed again, indicating the reversible production of this signal.

Temperature dependent change of the charge recombination reactions in hRC

Fig. 2 shows the kinetics of (A) $P800^+F_X^-$ and (B) $P800^+A_1^-$ signals, and (C) *Arrhenius* plots of the decay rates. Panel A shows time courses of the $P800^+F_X^-$ ESP signal at 7 and 20 K in hRC_{core}. The magnetic field was fixed at 3389 G that corresponds to the negative peak of $P800^+F_X^-$ ESP signal. The decay kinetics at 7 K was fitted with two exponentially decaying components with time constants of 115 μs and longer than 1 ms at relative amplitudes of 87 and 13%, respectively. The decay kinetics at 20 K was fitted with two phases with time constants of 120 μs (83%) and > 1 ms (17%). The faster phases can be ascribed to the relaxation of the $P800^+F_X^-$ ESP state. There was no temperature dependence at 5–20 K (Fig. 2C, closed diamonds).

Inset (Fig. 2A) also shows kinetics of $P800^+$ signal at 7 and 20 K detected in the longer time range. The decay curve at 7 K was fitted with two time constants of 2.6 ms (81%) and 8.9 ms (19%), which seem to be corresponded to the charge recombination between $P800^+$ and F_X^-. The time constants of 2.2 ms (78%) and 7.4 ms (22%) were obtained at 20 K. Closed circles and triangles in Fig. 2C indicate *Arrhenius* plots for decay constants of the fast and slow phases, respectively. Linear plots (dotted lines with closed circles and triangles in Fig. 2C) gave activation energies of 0.3 meV for both phases. The very low activation energies suggest the charge recombination via electron tunneling process between $P800^+$ and F_X^- at the cryogenic temperature in hRC.

Panel B (Fig. 2) shows the kinetics at 5 and 20 K in the pre-illuminated hRC_{core} at 3393 G that corresponds to the negative peak of $P800^+A_1^-$ ESP signal. The decay kinetics at 5 K was fitted with two decay time constants of 90 μs (93%) and > 1 ms (7%). The faster phase was attributed to the charge recombination between $P800^+$ and A_1^-, assuming the decay rate of the charge recombination is faster than the relaxation rate of the $P800^+A_1^-$ ESP state. The signal decay with the time constant of 90 μs is comparable to the charge recombination of $P700^+A_1^-$ state with time constants of 15–150 μs at 10 K in PS I (Brettel and Golbeck, 1995), and obviously different from the decay of the $P800^+A_0^-$ state with a time constant of 55 ns at 5 K (Kleinherenbrink *et al*., 1991). The slow phase would occur due to a portion of insufficiently reduced hRC_{core}. The kinetics at 20 K was fitted with the two time constants of 25 μs (71%) and > 1 ms (29%). The temperature dependence is somewhat different from the corresponding one in PSI (Brettel and Golbeck, 1995).

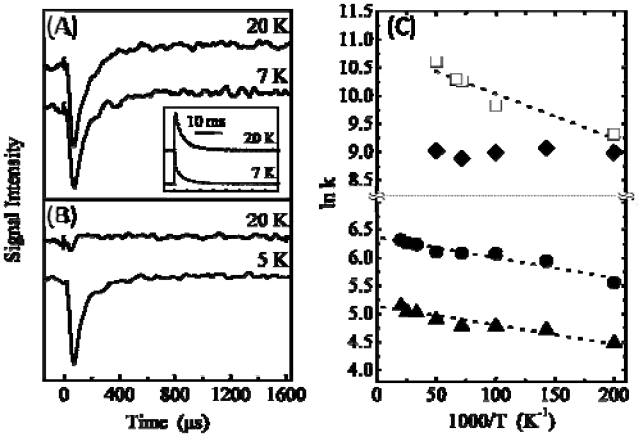

Fig. 2 Flash-induced ESP signals of (A) $P800^+F_X^-$ observed at 7 and 20 K, and (B) $P800^+A_1^-$ observed at 5 and 20 K. *Inset* show transient EPR signals of $P800^+$ measured in the range of 40 ms. (C) Arrhenius plots of the decay constant *k* of $P800^+F_X^-$ (closed symbols) and $P800^+A_1^-$ (open symbols). Closed diamonds indicate the relaxation rate of the spin polarization of $P800^+F_X^-$, and closed circles and triangles indicate the fast and slow components of the charge recombination of $P800^+F_X^-$. Open squares indicate charge recombination rate of $P800^+A_1^-$. Dotted lines represent linear plots. Experimental conditions: microwave power, 1 mW; microwave frequency, 9.533 GHz; modulation amplitude, 4 G; modulation frequency,100 KHz; time constant, 0.01 ms. Transient signals in the *inset* were observed with the same experimental conditions except microwave frequency of 9.527 GHz and modulation amplitude of 8 G.

Open squares in Fig. 2C indicate the *Arrhenius* plot of decay constants estimated for the fast phase of the $P800^+A_1^-$ ESP signal decay. The decay became faster as the increase of temperature. Linear plot (dotted line with open squares in Fig. 2C) gave an activation energy of 0.7 meV. Extrapolation of the plot to room temperature predicts the decay time constant of A_1^- to be faster than 20 μs, although there might be some other reaction paths neglected at cryogenic temperature due to the higher activation energy and they will make the rate to be faster.

The amplitude of the $P800^+A_1^-$ signal became smaller at higher temperature and almost negligible above 20 K (Fig. 2B) in contrast to the case of the $P800^+F_X^-$ signal, which was virtually temperature independent (Fig. 2A). It might reflect the situation that the $P800^+A_1^-$ signal decays more rapidly at higher temperature beyond the time resolution of 10 μs in the

present measurement. Direct measurement studies would be required to determine the decay rate of $P800^+A_1^-$ at the room temperature precisely.

Electron transfer via A_1-menaquinone in hRC

The ESP signals of $P800^+A_1^-$ and $P800^+F_X^-$ detected at 5 K suggest that the electron transfers from A_0 to A_1 as well as from A_1 to F_X are very fast (probably less than a few μs) even at the cryogenic temperature. When we assume an edge-to-edge distance between A_0 and F_X to be 16 Å as that in PS I RC, the empirical law concerning the electron transfer rate in a protein (Moser and Dutton, 2006) predicts several microseconds for the direct electron transfer from A_0 to F_X even at the maximum matching of the free energy gap. Our results based on the $P800^+A_1^-$ ESP signal show that the fast rate of the forward electron transfer from A_0 to F_X can be explained by the mediation of electron transfer reaction by A_1.

The charge recombination between $P800^+$ and F_X^- in hRC was independent of the temperature, in which the time constants were 2–11 ms at 5–50 K (Fig. 2) and 20 ms at room temperature (Kleinherenbrink *et al*., 1994). The situation is in contrast to that in PS I RC where time constant of reoxidation of F_X^- varies from 250 μs at room temperature to 130 ms at cryogenic temperature (Shuvalov *et al*., 1979). The fast rate of charge recombination from F_X^- at the cryogenic temperature, *i.e.*, almost activationless reaction, in hRC can also be explained by the mediation of electron transfer by A_1 as in PSI, but with different energy gaps and geometries of components. Further studies would reveal unique functional mechanism of A_1-menaquinone in hRC.

References

Brettel K, Golbeck JH (1995) Spectral and Kinetic Characterization of Electron Acceptor A_1 in a Photosystem I Core Devoid of Iron-Sulfur Centers F_X, F_B and F_A. Photosynth. Res. 45: 183-193

Hastings G, Kleinherenbrink FAM, Lin S, Mchugh TJ, Blankenship RE (1994) Observation of the Reduction and Reoxidation of the Primary Electron Acceptor in Photosystem I. Biochemistry 33: 3193-3200

Heinnickel M, Golbeck JH (2007) Heliobacterial Photosynthesis. Photosynth. Res. 92: 35-53

Kleinherenbrink FAM, Aartsma TJ, Amesz J (1991) Charge Separation and Formation of Bacteriochlorophyll Triplets in Heliobacterium Chlorum. Biochim. Biophys. Acta 1057: 346-352

Kleinherenbrink FAM, Chiou HC, Lobrutto R, Blankenship RE (1994) Spectroscopic Evidence for the Presence of an Iron-Sulfur Center Similar to F_X of Photosystem I in Heliobacillus Mobilis. Photosynth. Res. 41: 115-123

Kumazaki S, Iwaki M, Ikegami I, Kandori H, Yoshihara K, Itoh S (1994) Rates of Primary Electron Transfer Reactions in the Photosystem I Reaction-Center Reconstituted with Different Quinones as the Secondary Acceptor. J. Phys. Chem. 98: 11220-11225

Lin S, Chiou HC, Blankenship RE (1995) Secondary Electron Transfer Processes in Membranes of Heliobacillus Mobilis. Biochemistry 34: 12761-12767

Miyamoto R, Mino H, Kondo T, Itoh S, Oh-Oka H (2008) An Electron Spin-Polarized Signal of the $P800^+A_1(Q)^-$ State in the Homodimeric Reaction Center Core Complex of Heliobacterium Modesticaldum. Biochemistry 47: 4386-4393

Moser CC, Dutton PL (2006) Photosystem I, Springer: Dordrecht

Nuijs AM, Vandorssen RJ, Duysens LNM, Amesz J (1985) Excited States and Primary Photochemical Reactions in the Photosynthetic Bacterium Heliobacterium Chlorum. Proc. Natl. Acad. Sci. U. S. A. 82: 6865-6868

Oh-oka H (2007) Type I Reaction Center of Photosynthetic Heliobacteria. Photochem. Photobiol. 83: 177-186

Shuvalov VA, Dolan E, Ke B (1979) Spectral and Kinetic Evidence for Two Early Electron Acceptors in Photosystem I. Proc. Natl. Acad. Sci. USA 76: 770-773

Trost JT, Blankenship RE (1989) Isolation of a Photoactive Photosynthetic Reaction Center Core Antenna Complex from Heliobacillus Mobilis. Biochemistry 28: 9898-9904

van der Est A, Hager-Braun C, Leibl W, Hauska G, Stehlik D (1998) Transient Electron Paramagnetic Resonance Spectroscopy on Green Sulfur Bacteria and Heliobacteria at Two Microwave Frequencies. Biochim. Biophys. Acta 1409: 87-98

Symposium 02

Type II Reaction Centres

Calculation of Connectivity of Photosynthetic Units in Intact Cells of *Rhodobacter Sphaeroides*

Péter Maróti*, Emese Asztalos

Department of Medical Physics, University of Szeged, Hungary
*Corresponding author. Tel. No. 36-62-544-120; Fax No. 36-62-544-121; E-mail: pmaroti@sol.cc.u-szeged.hu.

Abstract: The kinetics of the bacteriochlorophyll fluorescence of intact cells of photosynthetic bacterium *Rhodobacter sphaeroides* was measured under rectangular shape of intense excitation in the microsecond time range. The interest was focused to the initial (sigmoidal) rise of the fluorescence to characterize the connectivity of the photosynthetic units. As the rate of the primary photochemistry (charge separation) was set to be much larger than that of the re-reduction of the oxidized dimer of the reaction center, there was reciprocity between light intensity and photochemical rise time, and therefore a simple model of single fluorescence (photochemical) quencher could be applied. By linearization of the fluorescence induction kinetics, the connectivity parameter p could be directly obtained ($p = 0.47 \pm 0.01$) and was independent on the intensity of the light excitation. The mean value of the number of steps (visits) in the antenna was calculated before an exciton is either trapped by an open reaction center (it is utilized by photochemistry) or dissipated in form of fluorescence emission. According to these calculations, the mean number of steps is less than 1 if $p < 0.5$, even if all of the reaction centers are closed. The observed small p value includes highly restricted mobility of excitions among the photosynthetic units.

Keywords: Bacterial photosynthesis; Fluorescence induction; Sigmoidal rise; Exciton migration; Coupling of PSUs

Introduction

The phenomenon of induction of chlorophyll fluorescence has become a routine tool in photosynthesis research as the parameters derived from the kinetics can be used to describe the photosynthetic activity (Papageorgiou and Govindjee, 2004). One of the essential characteristics is the initial curvature of the rise from which the excitonic coupling of the photosynthetic units (PSU) consisting of the reaction center protein (RC) surrounded by core (LH1) and peripheral (LH2) light harvesting antenna can be derived. The degree of the connectivity is usually characterized by the probability p ($0 \le p \le 1$) of the event that an exciton trapped in a closed PSU will visit the neighboring (either closed or open) PSU (Joliot and Joliot, 1964). As the difference between the exponential and sigmoidal rise is not very large (Kolber *et al*., 1998), precautions in experiments and evaluation should be taken to obtain the real value of the connectivity (Trissl, 1996). Although the tightness of the packing of the antenna system depends on the strains and physiological conditions, as rule of thumb, the bacteria have more tightly bound systems than the plants. In several approximations, the antenna systems of the bacteria are considered as a lake-type system where the excitons can visit all PSUs with no (or minor) restriction (Grondelle and Duysens, 1980; Kingma *et al*., 1983).

Recently, several papers questioned the theoretical background of the simple interpretation of the measured fluorescence induction curves (Lavergne and Trissl, 1995) or even denied the conventional elucidation of the lag phase of the kinetics (Vredenberg, 2008). We would not worry about the throw away of the method and apparatus for (bacterio) chlorophyll fluorescence induction (Holtzwarth, 1993) but these papers warn us against the formal analysis of the fluorescence induction curves.

In this work, the origin of the lag phase of the fluorescence induction kinetics of whole cells of bacteria is revisited under well defined experimental

conditions using rectangular shape of excitation (Maróti and Lavorel, 1979; Maróti, 2008). The double reciprocal plot of the variable fluorescence vs. complementary area enabled us to determine the connectivity parameter *p* directly. Smaller connectivity of the PSUs was obtained than reported earlier (Kingma *et al*., 1983; Lavergne and Trissl, 1995) which remained however independent on the intensity of light excitation (Vredenberg, 2008).

Materials and Methods

The cells of the wild type purple non-sulfur photosynthetic bacteria *Rhodobacter* (*Rba.*) *sphaeroides* (2.4.1) were cultivated anaerobically in Siström medium continuously stirred in 1 liter screw top flasks and illuminated by tungsten lamps. The light flux was 13 W m^{-2} on the surface of the vessel. The cytochrome c_2 deficient mutant of *Rba. sphaeroides* (generous gift from Dr. Wraight, University of Illinois, Urbana USA) was cultivated in the dark on a shaker (1 Hz) in the presence of antibiotic kanamycin. The bacteria were harvested in the late stationary phase of the cell growth.

The induction and subsequent relaxation of the yield of fluorescence were excited by rectangular shape of illumination of a high power laser diode (2 W at 808 nm, Kocsis *et al*., 2010). To correct for the minor deviation from the rectangular shape of the laser diode, the observed kinetics of fluorescence induction of intact cells was always referred to that of bacteriochlorophyll solution. All experiments were performed in the presence of 120 μM inhibitor terbutryn, although the induction curves were highly insensitive to the electron transfer on the acceptor side of the RC.

Results

The rising (induction) and subsequent relaxation phases of bacteriochlorophyll fluorescence (Fig. 1) are called variable fluorescence that is usually normalized to the maximum (F_{max}) and dead (F_0 = 1) fluorescence:

$$F_v(t) = \frac{F_{max} - F(t)}{F_{max} - F_0} \qquad (1)$$

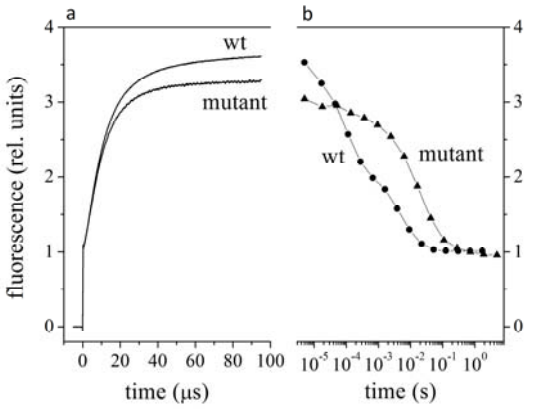

Fig. 1 Induction of fluorescence (λ > 850 nm) yield upon rectangular shape of laser diode excitation (λ = 808 nm) (a) and subsequent relaxation in the dark (b) in intact cells of *Rhodobacter sphaeroides* wild type and cytochrome c_2 deficient mutant. The fluorescence yield is related to that of the constant part (induction) or to the ratio of the area of the 2 μs wide monitoring flashes with and without actinic flashes (relaxation).

In the lack of fast native electron donor to the oxidized RC in cytochrome c_2-less mutant, the halftime of re-reduction of P^+ is large (> 10 ms), therefore the observed induction completed in the 100 μs time range reflects the light-induced transition from open (PQ_A) to closed ($P^+Q_A^-$) states of the RC. The validity of the reciprocity law between the exciting light intensity and the photochemical rate constant supports the action of single (photochemical) fluorescence quencher ($[PQ_A]= q$) on wide time scale (Fig. 2).

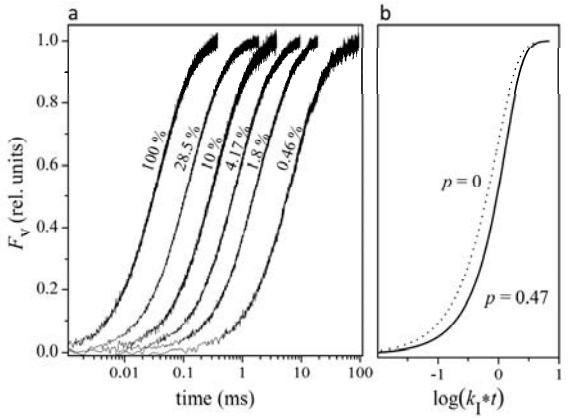

Fig. 2 Normalized variable fluorescence of intact mutant cells, F_v upon rectangular shape of excitation attenuated by a set of neutral density filters (a) and calculated from Eqs. (2) and (3) for p = 0 and 0.47 (b).

To treat the kinetics of the fluorescence induction quantitatively, we will return to Joliot's original idea of restricted motion of the excition among the PSUs (Joliot and Joliot, 1964). The exciton arriving at a

PSU with closed RC (fraction of (1-q) of all RCs), either visits a neighboring PSU with probability p or is dissipated (*e.g.* in form of fluorescence, Fig. 3).

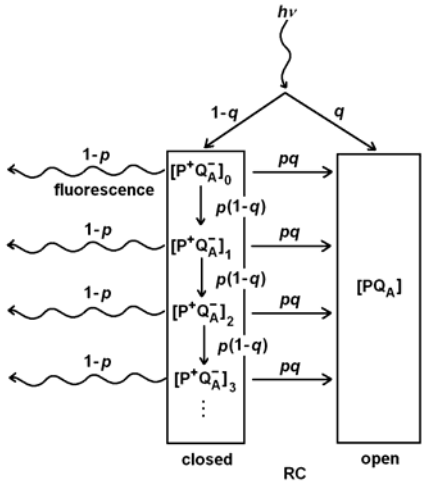

Fig. 3 Absorption of the incident photon (hv) by open (q) or closed ($1-q$) RCs. The excitons in the PSU with closed RCs can either visit a neighboring (open or closed) PSU with probability p or dissipate via fluorescence emission ($1-p$).

The observed variable fluorescence is given by the sum of an infinite geometrical series of quotient p ($1-q$):

$$F_v = \frac{(1-p)(1-q)}{1-p(1-q)} \qquad (2)$$

As the photon absorbed in the pigment bed will induce (either directly or indirectly) charge separation with a probability of ($1 - F_v$), the kinetic equation of the disappearance of the open RC (photochemistry) is

$$-\frac{dq}{dt} = k_I \cdot (1 - F_v). \qquad (3)$$

Where k_I denotes the photochemical rate constant. From Eqs. (2) and (3), the kinetics of the fluorescence induction can be calculated (Fig. 2b). As the connectivity parameter p does not influence the shape of the time-dependence of the fluorescence spectacularly, a more convenient (and sensitive) method is needed to derive p.

Let's express $q(t)$ from Eq (2) and (3), and set the two expressions equal:

$$(q =) \frac{1 - F_v(t)}{1 + \frac{p}{1-p} F_v(t)} = 1 - k_I \cdot \int_0^t (1 - F_v(\tau)) d\tau \qquad (4)$$

The right-hand-side of Eq. (4) is the integrated form of Eq. (3) that obeys the $q(t = 0) = 1$ initial condition and is expressed by the complementary area of the

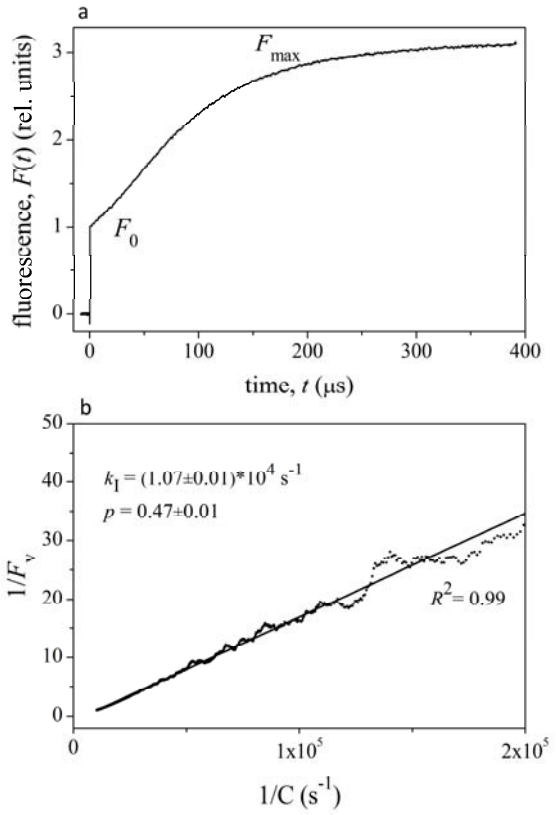

Fig. 4 Induction of fluorescence upon rectangular shape of excitation in intact cells of cytochrome c_2 deficient mutant (a) and its linearization in double reciprocal representation of the variable fluorescence (F_v) and the complementary area (C) with high correlation value (R^2).

fluorescence induction curve $C(t) = \int[1-F_v(\tau)]d\tau$. After rearrangements, we can get linear relationship between the reciprocal values of the normalized variable fluorescence $F_v(t)$ and the complementary area above the induction curve:

$$\frac{1}{F_v(t)} = \frac{1}{k_I(1-p)} \cdot \frac{1}{\int_0^t (1 - F_v(\tau))\, d\tau} - \frac{p}{1-p} \qquad (5)$$

The photochemical rate constant, k_I and the connectivity parameter, p can be obtained from the measured values of the slope and the interception of the straight line. The larger is the interception, the higher is p, the excitonic coupling among the PSUs. The slope of the straight line is inversely proportional to the photochemical rate constant. To demonstrate the effectiveness of the method, the induction kinetics is linearized according to Eq. (5) in Fig. 4. The 10^4 data points sit on a straight line of high correlation coefficient ($R^2 = 0.99$) that offers $k_I = 1.07 \cdot 10^4$ s^{-1} and $p = 0.47$ for the photochemical rate constant and the connectivity of the PSUs, respectively.

Based on the branching and random pathways of excitons in Fig. 3, the probability to make exactly s steps among the PSUs before dissipation or photochemistry can be calculated:

$$P_s = [(1-p)(1-q)+q]\cdot[p(1-q)]^s \qquad s = 0,1,2,3,... \qquad (6)$$

P_s is a random variable as $P_s \geq 0$ and $\sum P_s = 1$. The mean value of the number of steps (M) and the standard deviation (D) can be determined by

$$M = \sum_{s=0}^{\infty} s \cdot P_s, \quad D^2 = \sum_{s=0}^{\infty} s^2 \cdot P_s - \left(\sum_{s=0}^{\infty} s \cdot P_s \right)^2 \qquad (7a\text{-}b)$$

M is the function of p and q and covers large range (Fig. 5). At fixed p value, M is largest at $q = 0$ (no photo-chemical trap is available) and disappears ($M = 0$) at $q = 1$ (all photochemical traps are open). The mean number of visits will exceed 1 if $p > 0.5$ (at $q = 0$). Below this limit, the excitons will practically not migrate among the PSUs and is localized to the PSU where it is absorbed. The mobility of the excitons among the PSUs will sharply increase when p approaches to 1.

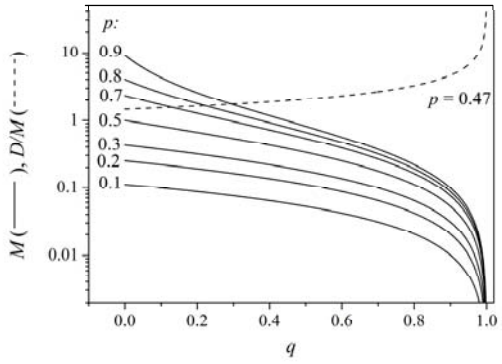

Fig. 5 The mean number of visits (M) of the exciton during migration among PSUs as a function of fraction of open RC (q) and connectivity parameter p calculated from Eq. (7). The relative deviation of the mean (D/M) is plotted for $p = 0.47$. Note the logarithmic scale.

The standard error of the mean is large and is comparable to the actual value of the mean: the deviation relative to the mean value (D/M) is always larger than 1. The number of visits show relatively large scattering, and therefore the mean number of steps is not very sharp.

Discussion

Earlier works reported relatively high connectivity values for whole cells (p = 0.5−0.7, Kingma *et al*., 1983; Lavergne and Trissl, 1995; Koblizek *et al*., 2005) and for chromatophores (p = 0.61−0.63, Trissl, 1996) of *Rhodo-spirillum rubrum* that supported the general view of lake-type organization of the light harvesting system (van Grondelle and Duysens, 1980). As relatively small mean numbers of steps correspond to these p values (Fig. 5), the PSUs are rather separated than fully connected in the antenna pigment bed. We measured even smaller connectivity (p = 0.47) in intact cells of cytochrome c_2 less mutant of *Rba. sphaeroides*, where the kinetics of the fluorescence induction demonstrated slight but recognizable initial sigmoidicity (Fig. 4a). Similar connectivity characterizes the thylakoids of higher plants (Joliot and Joliot, 1964). Other studies reported similarly small p values for wild type *Rba. sphaeroides* (Koblizek *et al*., 2005), *Rps. viridis* (Trissl, 1996) and *Rb. capsulatus* (0.49, Trissl, 1996). Although the exchange of excitons is very fast and effective within the PSU, it is highly restricted among the PSUs.

It was shown that he excitonic coupling among PSUs was weak in most of the bacterial antenna systems. In this work, a direct method of linearization of the fluorescence induction kinetics was elaborated to direct determination of the connectivity parameter if the photochemistry was the only fluorescence quencher in the system. The procedure is straightforward, simple and highly useful compared to computer (least-square) fitting processes of several variables whose ranges and mathematical behavior are difficult to predict and are usually beyond the capacity of the plant physiologist.

Acknowledgements

Thanks to NKTH-OTKA (K-67850) and COST (CM0902) for the support.

References

Joliot P, Joliot A (1964) Études Cinétique de la Réaction Photochimique Libérant L'Oxygène au Cours de la Photosynthèse. CR Acad Sci Paris 258: 4622-4625

Kingma H, Duysens LNM, Van Grondelle R (1983) Magnetic Field Stimulated Luminescence and a Matrix Model for Energy Transfer. A New Method for Determining the Redox State of the First Quinone Acceptor in the Reaction Center of

Whole Cells of Rhodospirillum Rubrum. Biochim Biophys Acta 725: 434-443

Kolber ZS, Prasil O, Falkowski PG (1998) Measurements of Variable Chlorophyll Fluorescence Using Fast Repetition Rate Techniques: Defining Methodology and Experimental Protocols. Biochim Biophys Acta 1367: 88-106

Holtzwarth A (1993) Is It Time to Throw Away Your Apparatus for Chlorophyll Fluorescence Induction? Biophys J 64: 1280-1281

Koblízek M, Shih JD, Breitbart SI, Ratcliffe EC, Kolber ZS, Hunter CN, Niederman RA (2005) Sequential Assembly of Photosynthetic Units in Rhodobacter Sphaeroides as Revealed by Fast Repetition Rate Analysis of Variable Bacteriochlorophyll a Fluorescence. Biochim Biophys Acta 1706: 220-231

Kocsis P, Asztalos E, Gingl Z, Maróti P (2010) Kinetic Bacteriochlorophyll Fluorometer. Photosynth Res 105: 73-82.

Lavergne J, Trissl HW (1995) Theory of Fluorescence Induction in Photosystem II: Derivation of Analytical Expressions in a Model Including Exciton-Radical-Pair Equilibrium and Restricted Energy Transfer between Photosynthetic Units. Biophys J 68: 2474-2492

Maróti P (2008) Kinetics and Yields of Bacterio-Chlorophyll Fluorescence: Redox and Conformation Changes in Reaction Center of Rhodobacter Sphaeroides. Eur Biophys J 37: 1175-1184

Maróti P, Lavorel J (1979) Intensity- and Time-Dependence of the Carotenoid Triplet Quenching under Rectangular Illumination in Chlorella. Photochem Photobiol 29: 1147-1151

Papageorgiou G, Govindjee (2004) Chlorophyll a Fluorescence: a Signature of Photosynthesis. Advan-ces in Photosynthesis and Respiration. Springer: Dordrecht, The Netherlands

Trissl H-W (1996) Antenna Organization in Purple Bacteria Investigated by Means of Fluorescence Induction Curves. Photosynth Res 47: 175-185

Van Grondelle R, Duysens LNM (1980) On the Quenching of the Fluorescence Yield in Photosynthetic Systems. Plant Physiol 65: 751-754

Vredenberg WJ (2008) Analysis of Initial Chlorophyll Fluorescence Induction Kinetics in Chloroplasts in Terms of Rate Constants of Donor Side Quenching Release and Electron Trapping in Photosystem II. Photosynth Res 96(1): 83-97

Oxygen-Dependent Production and Arrangements of the Photosynthetic Pigments in Intact Cells of *Rhodobacter Sphaeroides*

Emese Asztalos, Mariann Kis, Péter Maróti*

Department of Medical Physics, University of Szeged, Hungary.
*Corresponding author. Tel. No. +36 62 544 120, Fax No. +36 62 544 121; E-mail: pmaroti@sol.cc.u-szeged.hu.

Abstract: The development and re-arrangement of photosynthetic membrane of *Rhodobacter sphaeroides* were studied by absorption spectroscopy and fast induction of bacteriochlorophyll fluorescence when the cells grown under semiaerobic conditions were inoculated to aerobic medium and, after accommodation to aerobiosis, transferred to anaerobic conditions during constant illumination. After sudden transition from semiaerobic to aerobic cultures, the photochemical yield characterized by the relative variable fluorescence F_v/F_{max} decreased from 0.70 gradually to 0.30, the photochemical rate constant dropped from $5 \cdot 10^4$ s^{-1} to $1 \cdot 10^4$ s^{-1} and the contribution of the peripheral antenna (LH2) to the RC-LH1 core complex became less significant. The aerobic growth is characterized by bleaching of the pigment system. The transfer to anaerobiosis resulted in photosynthetic growth with opposite tendency of the parameters and the initial values were restored after a couple of cell cycling periods of doubling time of ~4 h. The LH2 to LH1 ratio increased by a factor of 5. It was demonstrated that the fast fluorescence induction is a sensitive and non-invasing method to monitor the physiological state of the photosynthetic apparatus upon variation of the oxygen concentration of the culture.

Keywords: Bacterial photosynthesis; Photosynthetic membrane; Harvesting the light; Pigment-protein complexes; Fluorescence induction

Introduction

The facultative photoheterotroph purple bacterium *Rhodobacter* (*Rba*.) *sphaeroides* is known about the metabolic versatility. It is able to grow under both aerobic and anaerobic conditions and is capable of anoxygenic photosynthesis in the absence of oxygen. The intracytoplasmic membrane (ICM) houses the photosynthetic apparatus. The ICM originates from the invagination of the cytoplasmic membrane (CM) that occurs at low (around 3%) oxygen concentration (Kiley and Kaplan, 1988). The photosynthetic apparatus consists of a pheophytin-quinone type reaction center (RC) surrounded by the internal light harvesting antenna (LH1) and the PufX protein (called core complex) and a peripheral light harvesting complex (LH2) in the outer sphere of the core complex. The RC-LH1-PufX complex is a dimer (Qian *et al.*, 2008) and participates in light-induced cyclic electron transfer (Asztalos and Maróti, 2009). The amount of LH2 relative to that of the LH1 is inversely proportional to the light intensity under otherwise constant (anaerobic) conditions. It is a challenge to study how the LH2/LH1 ratio is influenced by the oxygen content of the culture medium.

The photosynthetic bacterium *Rba. sphaeroides* has become the ideal target of studies of biogenesis and construction of photosynthetic membrane (Koblizek *et al.*, 2005). It was revealed that the photosynthetic units in the membrane were assembled in a sequential manner, *i.e.* the appearance of the core complex was followed by the accumulation of the peripheral complexes.

The oxygen and light are two essential environmental factors that influence the development and arrangement of the photosynthetic apparatus of the bacterium. In this work, the role of the oxygen

will be studied by steady-state and kinetic optical spectroscopy when the illumination is kept constant. Special attention will be devoted to detection of fast fluorescence induction of the intact cells which method is widely used in plants (Lazar, 1999; Papageorgiou and Govindjee, 2004; Vredenberg *et al.*, 2009) but much less often is applied for photosynthetic bacteria (Kocsis *et al.*, 2010; Asztalos *et al.*, 2010a, b; Bína *et al.*, 2010). The fast fluorescence induction kinetics of the cells provides information of the status of the photosynthetic apparatus with high sensitivity (the fluorescence can be detected right after the inoculation of the cells) and selectivity. It will be demonstrated that the adaptation of *Rba. sphaeroides* to different oxygen concentrations is nicely reflected by changes of the kinetic fluorescence properties of the cells.

Materials and Methods

Bacterial strain and growth conditions

Rba. sphaeroides 2.4.1 was grown in Siström's medium either in completely filled screw top vessels without oxygen (photoheterotrophic growth), or in half filled Erlenmeyer flasks with bubbling air by an air pump (aerobic growth). The cells were illuminated by tungsten lamps that assured 13 Wm^{-2} irradiance on the surface of the vessels. The number (concentration) of the cells was determined by calibrated Bürker chamber under light microscope.

Absorption measurements (Fig. 1)

The steady-state near infrared absorption spectra of the cells during the growth were recorded at room temperature by a single beam spectrophotometer (Thermo Spectronic Helios). After subtraction of the (hyperbolic) background, the spectra were peeled into 3 Gaussian components by least square Marquardt procedure (Asztalos *et al.*, 2010b).

Fluorescence measurements (Fig. 2)

The induction of the bacteriochlorophyll *a* fluorescence of intact cells was measured by a home built fluorometer (Maróti, 2008; Kocsis *et al.*, 2010). The light source was a laser diode (808 ± 5 nm wavelength and 2 W light power) that produced rectangular shape of illumination and the emission wavelength matched the 800 nm absorption band of the LH2 peripheral antenna of the cells. The

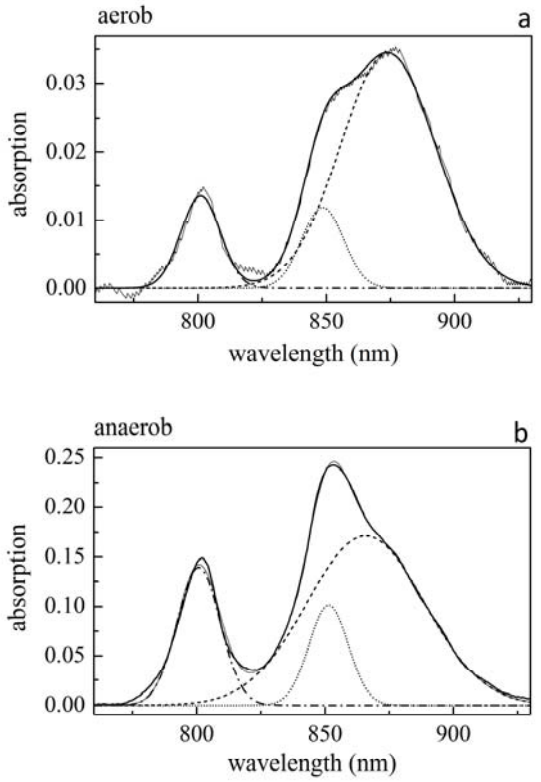

Fig. 1 Typical near infrared steady-state absorption spectra of *Rba. sphaeroides* cells grown under aerobic (a) and anaerobic (b) conditions at room temperature in 1 cm cuvette. The spectra were corrected for light scattering and decomposed into the sum of three Gaussian components centered at 800 nm and 850 nm (LH2) and at 875 nm (LH1).

bacteriochlorophyll *a* fluorescence (> 850 nm) was detected in the direction perpendicular to the actinic light beam, with a near infrared sensitive avalanche photodiode, protected with an 850 nm high-pass filter (RG-850) from the scattered light of the laser. The usually very small deviation of the kinetics of the excitation from the rectangular shape was corrected

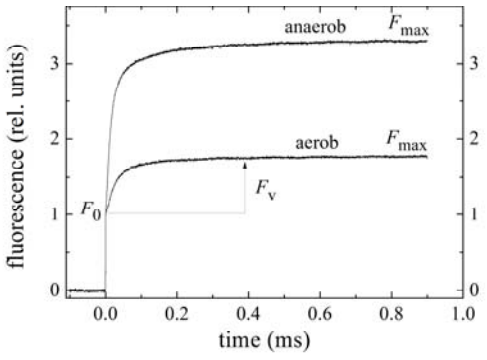

Fig. 2 Typical kinetics of fluorescence induction under rectangular shape of laser-diode excitation in *Rba. sphaeroides* intact cells grown under aerobic and anaerobic conditions at room temperature. The fluorescence is referred to the initial (dark or dead) fluorescence level F_0.

by detection of the kinetics of extracted bacteriochlorophyll *a* in organic solvent. The major quantities introduced into evaluation of the fluorescence induction kinetics of bacteria with single fluorescence quencher are F_0 (dark level of fluorescence, when all RCs are open), F_{max} (maximum level of fluorescence, when all RCs are closed and no photochemistry takes place), F_v (= F_{max}–F_0; variable fluorescence) and k_I (photochemical rate constant) (Asztalos *et al.*, 2010a).

Results and Discussion

The cells kept under semiaerobic conditions were inoculated into large volume of aerobic culture medium. After one day of cultivation in the light, they were transferred to anaerobic conditions. The physiological consequences of the two sudden changes of the oxygen concentration in the cell culture were monitored by comprehensive measurements of the absorption spectra, fluorescence kinetics and cell concentration (Fig. 3).

Aerobic growth (*"bleaching"*)

After transition of the inoculated cells from semiaerobic to aerobic conditions, the number of cells starts to increase exponentially (the doubling time is about 4 h) but soon saturates. The cell division, however, is not followed by production of new pigments (expressed by their absorption (OD_{850}) and fluorescence (F_{max}) in accordance with the expectations that the ICM formation and the pigment synthesis is repressed in aerobically grown cells. Not only the pigments are destructed ("bleached") but the membrane is re-arranged in a way that decreased the efficiency of the photochemical conversion of the light energy. All the physical quantities that monitor the function of the photosynthetic machinery indicate this tendency.

The peripheral antenna size (LH2) becomes smaller relative to that of the core antenna (LH1) during the aerobiosis while the ratio of the characteristic pigments centered at 800 nm and 850 nm of the LH2 remains constant. The aerobiosis does not influence the internal structure of the LH2 pigment-protein complex but decreases its relative weight in the light harvesting system.

The fluorescence induction kinetics is exceptionally sensitive on the aerobiosis. Both the relative variable fluorescence (F_v/F_{max}) and the photochemical rate constant (k_I) decrease upon transfer of the cells from semiaerobic to aerobic growth conditions. The F_v/F_{max} ratio drops from 0.7 to 0.4 and k_I from $5{\cdot}10^4$ s^{-1} to $3{\cdot}10^4$ s^{-1} with an apparent halftime of about 4–5 h that is close to the initial doubling time of the cell

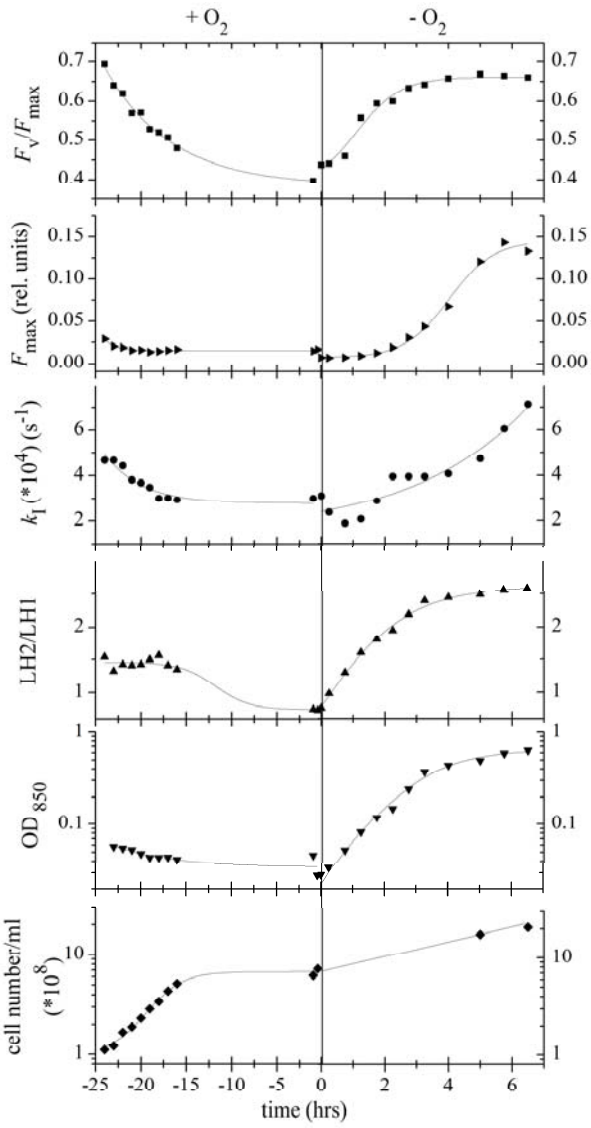

Fig. 3 Absorption and fluorescence changes of intact cells of *Rba. sphaeroides* under constant illumination upon transition (t = 0) from aerobic ($+O_2$) to anaerobic ($-O_2$) growing conditions at 30 °C temperature. Watch the different time scales for ± O_2! The cultivation started by inoculation of semiaerobically kept cells into aerobic culture at −25 h. The production of new pigments is reflected by increase of the absorption (OD_{850}), the maximum of fluorescence (F_{max}) and the number of cells (note the logarithmic scale) of the culture. The development or re-arrangement of the photosynthetic apparatus in the membrane is characterized by the relative variable fluorescence (F_v/F_{max}), the photochemical rate constant (k_I) and the ratio of the two light harvesting systems (OD_{850}/OD_{875} is identified as LH2/LH1).

population. The observed changes of the fluorescence parameters are in good correlation with the partial loss of the light harvesting capacity of the antenna. The variable fluorescence is a good indicator of the photochemical utilization (yield) of the absorbed light energy by the photosynthetic apparatus. Smaller variable fluorescence means smaller yield of photochemical conversion. The rate constant of the photochemistry, k_I depends on the exciting light intensity and on the absorption cross section of the antenna. As the excitation intensity was kept constant during the sampling of the cell culture, the observed change of the k_I was indicative to the changes of the composition, arrangement and coupling of the pigments in the antenna.

***Anaerobic growth* (*"greening"*)**

Turning the growth conditions from aerobic to anaerobic suddenly, all of the observed parameters undergo fast and significant changes. The adaptation of the bacteria to the oxygen-less condition occurs rapidly and the highly limited growth combined with relatively slow bleaching of the pigments will be switched to favored photosynthetic growth. The doubling time is ~4 h that corresponds to the initial doubling time of the cells when inoculated from semiaerobic to aerobic conditions. The major difference is the duration of the exponential phase of the growth curve or (equivalently) the steady-state cell concentration. Due to greening of the bacteria, the cell number in the stationary phase is much larger under anaerobic than under aerobic conditions.

The ignition of the greening process is visualized by rapid increase of the absorption attributed to the newly synthesized antenna pigments. The production, however, is not evenly distributed among the dyes. The 850 nm band that belongs to LH2 grows faster than the 875 nm band of the LH1, which means that the cells produce more pigments to the LH2 antenna than to the LH1. Consequently, the weight of the LH2 relative to the LH1 increases progressively from 0.6 to 2.6 within 5–6 h after the transition. The observation can be interpreted as the bacterium is primarily involved in production of the LH1 core complex and the operation of the peripheral complex is less preferred under not proper physiological circumstances. This view is in agreement with the results of similar work by Koblízek *et al.* (2005), who suggested that the photosynthetic units of *Rba. sphaeroides* were assembled not in a parallel (or in a more complicated branching) but in a sequential way: first the RC, the LH1 antenna and PufX protein were produced, assembled and activated to core complex in the photosynthetic membrane and subsequently it was surrounded by the LH2 peripheral antenna.

The characteristics of the fluorescence induction reflect also the tendency to improve the photosynthetic activity of the cells by pigment production and structural re-arrangements of the photosynthetic apparatus. Indeed, the relative variable fluorescence increases rapidly from 0.4 and reaches the level of 0.7 with a halftime of ~2 h. The photochemical rate constant shows larger increase with actually no saturation within the observed time range. These changes call for larger antenna size (absorption cross section) and stronger coupling of the photosynthetic units which result in faster and more efficient capture of light energy. It is worth to notice the different kinetics of the changes: the kinetics of F_{max} and k_I follow the prompt increase of the pigment absorption, which is tracked by the traces of LH2/LH1 and F_v/F_{max} with certain delay only. One can argue that, after the transition to anaerobiosis, the production of newly synthesized pigments and their transfer and construction into functional units might have different time regimes that can be made responsible for the observed difference of the kinetics.

The presence and absence of oxygen resulted in reversible changes of the photosynthetic apparatus with different rates. In our experiments, the bacteria could outgrow the oxygen-induced degradation of the pigment system after a couple of generations in anaerobic conditions. The recovery of the bacterial culture from oxygen shock can be treated in a similar way as the revitalization of photosynthetic bacteria after heavy metal pollution (Asztalos *et al*., 2010a). The experiences what we learn from laboratory system can be utilized to monitor and protect the aquatic environment (bioremediation).

Acknowledgements

Thanks to NKTH-OTKA (K-67850) and COST (CM0902) for the support.

References

Asztalos E, Maróti P (2009) Export or Recombination of Charges in Reaction Centers in Intact Cells of

Photosynthetic Bacteria. Biochim. Biophys. Acta 1787: 1444-1450

Asztalos E, Italiano F, Milano F, Maróti P, Trotta M (2010a) Early Detection of Mercury Contamination by Fluorescence Induction of Photosynthetic Bacteria. Photochem Photobiol Sci 9: 1218-1223

Asztalos E, Kis M, Maróti P (2010b) Aging of Photosynthetic Bacteria Monitored by Absorption and Fluorescence Changes. Acta Biologica Szegediensis (in press)

Bína D, Litvin R, Vácha F (2010) Absorption Changes Accompanying the Fast Fluorescence Induction in the Purple Bacterium Rhodobacter Sphaeroides. Photosynth Res 105: 115-121

Kiley PJ, Kaplan S (1988) Molecular Genetics of Photosynthetic Membrane Biosynthesis in Rhodobacter Sphaeroides. Microbiol Rev 52: 50-69

Koblízek M, Shih JD, Breitbart SI, Ratcliffe EC, Kolber ZS, Hunter CN, Niederman RA (2005) Sequential Assembly of Photosynthetic Units in Rhodobacter Sphaeroides as Revealed by Fast Repetition Rate Analysis of Variable Bacteriochloro phyll a Fluorescence. Biochim Biophys Acta 1706: 220-231

Lazar D (1999) Chlorophyll a Fluorescence Induction. Biochim Biophys Acta 1412: 1-28

Kocsis P, Asztalos E, Gingl Z, Maróti P (2010) Kinetic Bacteriochlorophyll Fluorometer. Photosynth Res 105: 73-82

Maróti P (2008) Kinetics and Yields of Bacteriochlorophyll Fluorescence: Redox and Conformation Changes in Reaction Center of Rhodobacter Sphaeroides. Eur Biophys J 37: 1175-1184

Papageorgiou G, Govindjee (2004) In Chlorophyll a Fluorescence: a Signature of Photosynthesis. Advances in Photosynthesis and Respiration, Springer: Dordrecht, The Netherlands

Qian P, Bullough PA, Hunter CN (2008) Three-Dimensional Reconstruction of a Membrane-bending Complex: The RC-LH1-PufX Core Dimer of Rhodobacter Sphaeroides. J Biol Chem; 283: 14002-14011

Vredenberg WJ, Durchan M, Prasil O (2009) Photochemical and Photoelectrochemical Quenching of Chlorophyll Fluorescence in Photosystem II. Biochim Biophys Acta 1787: 1468-147

Electronic Structure Studies of the Spin Density Distribution of the Q_A Plastosemiquinone Free Radical of Photosystem II

Tzu-Jen Lin , Patrick J O'Malley*

School of Chemistry, the University of Manchester, Manchester, M13 9PL, UK.
*Corresponding author. E-mail: Patrick.omalley@manchester.ac.uk.

Abstract: Density functional calculations are used to calculate the spin density distribution for the plastosemiquinone anion radical in the Q_A binding site of Photosystem II. A number of models are examined which explore the effect of iron depletion on the Q_A site semiquinone spin density distribution and resultant hyperfine couplings. For a model system with a divalent metal ion in the non-heme site the calculated spin density in the Q_A site model suggests that differential hydrogen-bonding strength to the O1 and O4 oxygen atoms of the radical results in an asymmetric spin density distribution in the semiquinone anion free radical form. The hydrogen bond to the proximal O1 atom is significantly stronger. This is similar to the situation shown to exist previously in the bacterial reaction centre of *Rba sphaeroides*. Various models of depleted non-heme site metal show the profound effect that the presence of a divalent ion in this site has on the spin density distribution of the Q_A site semiquinone. The variation in calculated spin density distribution of the Q_A site plastosemiquinone as a function of the occupancy of the non-heme site needs to be taken into account in the interpretation of experimental paramagnetic resonance data. For Type II reaction centres a major role for Fe^{2+} in the non-heme site may be the raising of the redox potential of the Q_A/Q_A^- couple to ensure that electron transfer from the (bacterio)pheophytin anion free radical occurs at a sufficient rate to compete with wasteful back-reactions.

Keywords: A DFT, density functional theory; B3LYP, Becke3 Lee Yang Parr; QM, Quantum Mechanics; MM Molecular Mechanics; PQ, Plastoquinone, PSQ, Plastosemiquinone; PS II, Photosystem II, ONIOM, Our Own N-layered Integrated Molecular Orbital and Molecular Mechanics; EPR, electron paramagnetic resonance; ENDOR, electron nuclear double resonance; ESEEM, electron spin echo envelope modulation

Introduction

Quinones are important cofactors for electron transfer in photosynthesis and respiration (Wraight, 2004; Kern and Renger, 2007). In photosynthesis, quinones act as electron acceptors in the initial charge separation. For type II reaction centres, two quinones termed Q_A and Q_B act in concert to enable efficient charge separation to take place (Diner, Petrouleas *et al.*, 1991; Lubitz and Feher, 1999). In the crucial initial charge-separation step, Q_A is one-electron reduced by a neighbouring (bacterio)pheophytin anion radical to form the semiquinone anion radical. This is then oxidized by electron transfer to Q_B forming the Q_B semiquinone anion radical. On further charge separation, Q_A accepts another electron to form the semiquinone anion radical again. This electron is then passed on to the already reduced Q_B which accepts two protons to form quinol, QH_2, and leaves the Q_B site to be replaced by another quinone molecule from a quinone pool nearby. Electron transfer from the primary donor, prior to the Q_A site, proceeds *perpendicular* to the membrane plane. At the Q_A site electron transfer direction switches and proceeds *parallel* to the membrane plane, towards the Q_B site. The Q_B site quinone appears to function in a similar fashion to quinones in protic solvents undergoing two-electron reduction to the hydroquinol form. In striking contrast, Q_A, however functions as a one-electron acceptor sequentially shuttling two electrons parallel to the membrane plane towards Q_B. This is of

course crucial to the efficient functioning of electron transfer in photosynthesis and the cause of this unique one electron shuttling at the Q_A site needs to be discerned. In the native protein, a non-heme Fe^{2+} ion lies midway between the Q_A and Q_B sites but is not implicated directly as an electron transfer agent – its exact function remaining unknown.

In purple bacterial reaction centres the Q_A and Q_B quinones are usually ubiquinones whereas in Photosystem II (PS II) the native quinones present in the Q_A and Q_B sites are both plastoquinone (PQ) molecules. X-ray crystal structure analysis of the Q_A site in PS II (Barber, 2003; Loll, Kern *et al.*, 2005) shows that the O1 atom of the Q_A site PQ is potentially hydrogen bonded to the peptide NH group of D2-Phe261 and the O4 atom is potentially hydrogen bonded to the δNH group of D2-His214, see Fig. 1. The D2-His214 residue is also a ligand to a non-heme Fe^{2+} ion. A similar hydrogen bonding arrangement is found for the Q_A site ubiquinone in *Rba sphaeroides*. At the current resolution, the X-ray data are not able to distinguish between the PQ and one-electron reduced plastosemiquinone (PSQ) forms which would allow one to assess any structural changes occurring on reduction of the quinone to the semiquinone form or any changes in hydrogen bonding interactions that occur on reduction. The number and strength of hydrogen bonds to the semiquinone form are believed to be a major factor in regulating the redox potential of the quinone and in determining its electron transfer characteristics (O'Malley, 1997; Wraight, 2004). Important information on the spin density distribution of semiquinones plus their hydrogen bonding interactions can be obtained using Electron Paramagnetic Resonance (EPR) and higher resolution variants thereof such as Electron Nuclear Double Resonance (ENDOR) and Electron Spin Echo Envelope Modulation (ESEEM) spectroscopies (Lubitz and Feher, 1999). In the native system however the presence of the nearby high spin S = 2, Fe^{2+} leads to severe spectral broadening of the semiquinone EPR signal. Experimental analysis of the Q_A PSQ by paramagnetic resonance methods requires decoupling of the high spin Fe^{2+} from the semiquinone. This has been carried out by a variety of means such as $LiClO_4$ treatment and substitution by Zn^{2+} (Astashkin, Kawamori *et al.*, 1995), high pH treatment (Deligiannakis, Jegerschold *et al.*, 1997; Deligiannakis, Hanley *et al.*, 1999) cyanide treatment (Koulougliotis, Kostopoulos *et al.*, 1993; Deligiannakis, Boussac *et al.*, 1995; Rigby, Heathcote *et al.*, 1995) and trypsinisation (Macmillan, Lendzian *et al.*, 1995). All allow the observation of the unperturbed PSQ EPR signal. All are believed to lead to removal of the Fe^{2+} ion from its binding site except treatment with the strong field ligand cyanide which under high pH conditions converts the high spin Fe^{2+}, to a low spin S = 0 form (Sanakis, Petrouleas *et al.*, 1994) A drawback to all of these methods is that they do not provide clear evidence for the state of the non-heme iron site after decoupling. In purple bacterial reaction centres Fe^{2+} substitution by Zn^{2+} is the preferred and most reproducible method for decoupling the Fe^{2+} from the Q_A ubisemiquinone signal and leads to no alteration in electron transfer ability (Lubitz and Feher, 1999). It is generally believed that direct substitution of the Fe^{2+} ion by Zn^{2+} occurs without any significant structural changes to the ligands. Although it has been reported in certain favourable cases (Astashkin, Kawamori *et al.*, 1995), similar substitution of the Fe^{2+} by Zn^{2+} in PS II is not as reproducible as it is for the purple bacterial reaction centres thereby leading to the other decoupling approaches mentioned above.

EPR, ENDOR and ESEEM spectroscopies have contributed greatly to the characterization of the semiquinone free radicals formed *in vitro* (Lubitz and Feher, 1999). In turn the interpretation of hyperfine couplings has been aided significantly in recent years by the prediction of accurate spin density distributions and hyperfine couplings using density functional theory (DFT) based electronic structure calculations. Since the first demonstration of this ability (O'Malley 1996; O'Malley and Collins, 1996) in the mid 1990s, DFT based calculations have been used successfully to model small isolated hydrogen bonded complexes mimicking the key interactions undergone in solution or in the *in vivo* protein environment. Many studies have demonstrated the ability of smaller hydrogen bonded models to mimic the solution state and this has been demonstrated explicitly for the PSQ anion free radical in (O'Malley, 1998). For the bacterial systems such as *Rba Sphaeroides*, the *in vivo* protein environment has been modelled using suitably terminated cluster models, and these have been successful in delineating trends in spin density distribution and resultant hyperfine couplings caused by direct hydrogen bonding between the semiquinone oxygen atoms and proton donors from neighbouring

amino acid residues(O'Malley, 1998). We recently extended these small models by extending the local environment using Quantum Mechanics/Molecular Mechanics (QM/MM) type calculations using the ONIOM method. (Lin and O'Malley, 2008). ONIOM (Our Own N-layered Integrated Molecular Orbital and Molecular Mechanics) is a hybrid method which allows the combination of two or more computational techniques in one calculation and makes it feasible to investigate the chemistry of very large systems with high precision. In this specific case it allows the effects of the specific quinone binding site up to a radius of 20 angstroms from the quinone to be taken into account. An overview of the ONIOM method is given in references (Vreven, Byun *et al*., 2006).

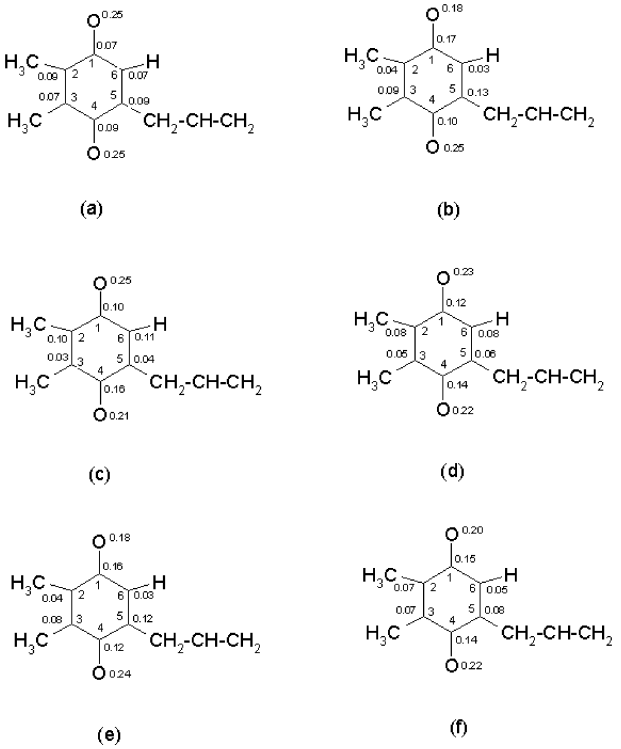

Fig. 1 Spin populations.

In this study we use ONIOM studies to model PQ and PSQ in the Q_A binding site of PS II. The PQ/PSQ and immediate hydrogen bonding ligand interactions are treated at the quantum mechanics (QM/DFT) level while the surrounding residues in the binding pocket are modeled in a molecular mechanics (MM) type framework. In this fashion we are able to model electronically the PSQ spin density and examine the influence of the neighbouring protein matrix on the spin density distribution. In particular we study various modifications of the Fe^{2+} non-heme site and calculate the predicted effects on the PSQ spin density distribution and hyperfine couplings. Comparison with experimentally observed hyperfine couplings allows us to assess the state of the non-heme site in different sample preparations.

Methods

Starting with the cyanobacterial PS II structure of Loll et al (Loll, Kern *et al*., 2005) (PDB file 2AXT) we created a subset of the Q_A site containing residues up to 20 angstroms from the centre of Q_A. For the present model this specifically consisted of D2 residues 244-263, 210-220, 264-270 and D1 residues 270-274 and 213 to 217. In addition the iron atom and its ligands including bicarbonate were included. Hydrogens were added and the native non-heme iron atom was replaced by zinc. This starting structure is called Model 1. For the ONIOM studies, two-layer calculations ONIOM(B3LYP/6-31G(d)):UFF were performed. The high layer contained the plastoquinone, D2-His 214, D2-Ala260, D2-Phe261 and D2-Ser262 plus Zn^{2+} and its ligands, all suitably truncated. The remaining atoms formed the lower layer, see Fig. 2. Keeping all atoms except all hydrogens and the heavy atoms of the quinone fixed we optimised the quinone/semiquinone geometry within the site. Charges for the MM layer were generated using the qEq method and electrostatic embedding *i.e.* ONIOM-EE was employed (Vreven, Byun *et al*., 2006). This geometry was then used in a further single point ONIOM(B3LYP/EPR-II:UFF) to calculate spin densities and hyperfine couplings. In addition, to enable us to gauge the influence of the divalent ion on the semiquinone's spin density distribution and resultant hyperfine couplings, we examined a number of models in which the non-heme site metal occupancy was varied.

In all five models were studied,

Model 1: Zn^{2+} in non-heme site.

Model 2: Model 1 with Zn^{2+} removed leaving the non-heme site vacant.

Model 3: Model 2 minus the bicarbonate ligand.

Model 4: Model 1 with Ca^{2+} replacing Zn^{2+}

Model 5: Model 1 with carbonate replacing the bicarbonate ligand.

All calculations were performed using Gaussian

09 (MJ Frisch, GW Trucks *et al*., 2009) software.

Results and Discussion

Spin Populations and Anisotropic Hyperfine Couplings for Q_A PSQ

We now focus our discussion on the changes to the spin density distribution of the PSQ free radical in the Q_A site proceeding from the isolated "gas phase" to insertion in the Q_A site as exemplified by the extended QM/MM models 1–4. Fig. 3 shows the Mülliken spin population changes occurring on going from the isolated radical to the protein binding site as represented by models 1–4. It has been found previously for simpler semiquinone models, that the primary effect of hydrogen bonding to the semiquinone carbonyl oxygen atom is a redistribution of spin density from the oxygen atom position to the carbon of the carbonyl group (O'Malley, 1997). In the Q_A site, Model 1, this redistribution is shown to occur mainly from O1 to C1 with a no redistribution occurring between C4 and O4. For Model 2 the opposite occurs with the redistribution now taking place between O4 and C4. For Model 3 a similar redistribution is observed for both carbonyl groups whereas for Model 4 the spin density redistribution is similar to that found for Mode 1. The differences can be explained by the differing strengths of hydrogen bond exhibited by the different models and the resultant polarization of spin density caused by this effect. In Models 1 and 4, a divalent ion is present in the non-heme site and this leads to strong hydrogen bond formation to the O1 atom of the semiquinone as reflected in the short hydrogen bond shown in Table 1. This strong hydrogen bond dominates over the weaker hydrogen bond to the O4 atom and leads to a significant polarization of the C1O1 spin density with a decrease on O1 and an increase on C1. The increased spin population at C1 will lead via spin polarization to a lower spin population at positions C2 and C6 which in turn lead to a higher spin population at positions C3 and C5. This "domino" spin polarization effect should lead to a lower spin population at C4 but this is offset by the presence of the weak hydrogen bond to the O4 atom which balances the spin polarization pattern somewhat. The spin populations obtained for Models 1 and 4 therefore can be explained by the presence of a strong hydrogen bond to the O1 atom of PSQ and a weaker hydrogen bond to the O4 atom. On removing the divalent ion from the site, Model 2, the polarization pattern of the spin density distribution of the Q_A PSQ is reversed. Now the spin density on O4 is decreased and C4 increases compared with the isolated model. The stronger hydrogen bond now occurs at the O4 atom and the polarization of the PSQ spin density is reversed compared with models 1 and 4. The negative charge around the vacant non-heme site leads to a significant weakening in the hydrogen bond strength of the δNH group of D2-His214 and leads to the altered spin density population shown in Fig. 1(c). In Model 3 we model the effect of removing the bicarbonate ligand in addition to the divalent ion. It is reasonable to expect that experimentally removal of the divalent ion will also result in loss of the bicarbonate ligand. Fig. 2(d) shows that for this model the spin population at the Q_A PSQ is symmetrical reflecting nearly equal hydrogen bond strength to both oxygen atoms and is similar to that found for hydrogen bonded models modeling the PSQ environment *in vitro* (O'Malley, 1998). The greater polarization of the C1O1 spin density in Model 1 can be attributed to the stronger hydrogen bond interaction at the O1 oxygen atom in the site. This is very similar to the situation observed for the Q_A site in *Rba sphaeroides* where the hydrogen bond to the analogous His M-215 residue was found to be stronger than to the peptide NH of Ala M- 260(Lubitz and Feher, 1999; Lin and O'Malley, 2008). As for the Q_A site in *Rba sphaeroides*, this enhanced polarization of the semiquinone spin density can be mainly attributed to the presence of the Zn^{2+} ion and its ligands. Replacement of the Zn^{2+} ion by another divalent ion such as Ca^{2+}, Model 4, results in an almost identical spin distribution on the Q_A PSQ. In both cases the presence of the divalent transition metal ion strengthens the hydrogen bond formed by the ligating histidine residue. The absence of a divalent ion in the non-heme site leads to a considerable weakening of the O1 hydrogen bond interaction and a significantly altered spin density distribution for the Q_A SQ.

Calculated ^1H and ^{14}N hyperfine couplings and comparison with experimental determinations

As mentioned in the introduction decoupling of the high spin Fe^{2+} from the semiquinone is necessary to permit analysis of the PSQ in the Q_A site of PS II

by paramagnetic resonance techniques. It has often been assumed in such studies that the different decoupling procedures should not unduly influence the semiquinone spectral characteristics. However our analysis of the calculated semiquinone spin density distribution in the previous section shows that this spin density distribution depends crucially on the state of the non-heme site. ^{1}H hyperfine couplings measured for ring positions on the PSQ are directly proportional to this spin density and therefore can be expected to vary considerably depending on the decoupling procedure used. The often different spectral characteristic reported (Macmillan, Lendzian *et al*., 1995; Rigby, Heathcote *et al*., 1995; Deligiannakis, Jegerschold *et al*., 1997) in the literature for different decoupling procedures is likely a reflection of this. Two proton ENDOR studies (Macmillan, Lendzian *et al*., 1995; Rigby, Heathcote *et al*., 1995) have been reported for the PSQ in the Q_A site of PSII. Because of the broad overlapping nature of the powder spectra observed, reliable assignments can only be attempted for methyl groups 1 and 2 and for exchangeable protons. In Table 1 we compare calculated hyperfine coupling tensors for models 1–3 with these experimental values. For Model 1 the ^{1}H CH_3 couplings for the 3 position are calculated to be the larger. This is due to the higher spin population calculated for C3 in Model 1. The opposite occurs for Model 2 where the larger methyl group coupling is now the 2 position. This again is due to the larger spin population at C2 for Model 2, Fig. 3 and Table 1, reflecting the significant change in spin density for the Q_A PSQ brought about by removal of the divalent ion from the non-heme site. For Model 3 the ^{1}H CH_3 coupling for position C2 is slightly larger than position 3 reflecting again the more symmetrical spin population of this model. The best agreement with experimental determinations is achieved for model 3. This is especially the case for the experimental data of reference (Macmillan, Lendzian *et al*., 1995). Both experimental studies used different decoupling procedures. In reference (Macmillan, Lendzian *et al*., 1995) the decoupling procedure used involved trypsinisation which has been shown conclusively to result in iron depletion from the non-heme site (Noguchi, Kurreck *et al*., 1999). Models 2 and 3 are therefore most relevant but as mentioned above agreement between experiment and theory is best for Model 3 where both the divalent ion and the bicarbonate are absent and a more symmetrical spin density distribution for the Q_A PSQ, similar to the isolated form, is observed. In reference (Rigby, Heathcote *et al*., 1995), cyanide treatment at high pH was used to decouple the Fe^{2+}. This is known to lead to a low spin form of the Fe^{2+} (Sanakis, Petrouleas *et al*., 1994). It is unclear however how many CN ligands bind to the Fe^{2+} and what native ligands are replaced by such binding. FTIR studies (Noguchi, Kurreck *et al*., 1999) indicate that the PSQ interaction with the D2-His214 residue is perturbed using such treatments. The experimental ENDOR data have been interpreted to indicate identical ^{1}H hyperfine couplings for both methyl groups of the PSQ indicating a symmetrical spin density distribution for the PSQ thereby suggesting that the interaction of the PSQ with the non-heme site is perturbed using such sample treatments. In the absence of specific structural information on the nature of the ligand structure to the non-heme iron after such cyanide treatment, it is difficult to model such effects with any confidence. Both ENDOR studies used incubation in D_2O to detect exchangeable protons in the Q_A site. The values for these are given in Table 2. In reference (Macmillan, Lendzian *et al*., 1995) the values observed are much smaller than those calculated for any of the Q_A site models. The calculated values are however similar to those calculated and observed experimentally for the Q_A site in the purple bacterium *Rba sphaeroides* (Lubitz and Feher, 1999). Based on comparison with the calculated values in Table 1 it is unlikely that the exchangeable protons observed in reference (Macmillan, Lendzian *et al*., 1995) correspond to the hydrogen bonds from D2-His214 or D2-Phe261. In reference (Rigby, Heathcote *et al*., 1995) on the other hand the significantly larger exchangeable proton couplings observed experimentally are in better agreement with the calculated values for the hydrogen bonding residues in Table 1. It is clear that further, better resolved, possibly single-crystal ENDOR studies of the Q_A PSQ are needed to provide more reliable data for comparison with the calculated hyperfine couplings of this study.

In addition to the PSQ ring nuclei directly interacting with the semiquinone spin density, the N_δ of D2-His214 and the peptide NH of D1-Phe261 are calculated to have a significant ^{14}N isotropic coupling value for all models, see Table 2. Delocalization of significant spin density along the hydrogen bond is evidenced by a significant calculated isotropic hyperfine coupling value for both residues, Table 4.

This is in agreement with experimental determinations, where ESEEM studies of the Q_A PSQ have revealed ^{14}N hyperfine couplings and these have been ascribed to nearby hydrogen bonding residues (Astashkin, Kawamori *et al*., 1995). A similar situation has been shown for the better characterized Q_A site in *Rba sphaeroides* where a recent ESEEM analysis (Martin E, Narasimhulu KV *et al*., 2010) has reported isotropic ^{14}N hyperfine coupling values of 2.5 and 1.9 MHz for the N_δ nitrogen atom of the M-His219 and the peptide NH of M-Ala260 respectively. As shown in reference (Martin E, Narasimhulu KV *et al*., 2010) the calculated values of 2.6 MHz and 1.5 MHz obtained from QM/MM studies on the *Rba sphaeroides* Q_A site are in good agreement with these values. Calculated ^{14}N isotropic hyperfine coupling values for the Q_B site ubisemiquinone in *Rba sphaeroides* also show excellent agreement with experimental determinations (Martin E, Narasimhulu KV *et al*., 2010). Table 4 shows that for the PS II Q_A site Models 1 and 4, similar values to the *Rba sphaeroides* site are obtained for the equivalent residues N_δ, D2-His214 (2.5 MHz) and NH, D1-Phe261 (1.9 MHz). Metal-depleted models 2 and 3 show a reduction in the N_δ, D2-His214 coupling to 1.7 MHz. From the purple bacterial studies reported in Martin *et al*. (2010), it is clear that the current modeling method is able to reproduce very accurately the experimentally determined hyperfine couplings for these nitrogens so we can expect a similar performance for the PS II model. Included in Table 2 are experimental ^{14}N nuclear Hyperfine tensor data observed using ESEEM/HYSCORE studies of the PSII Q_A site. Again different sample preparations have been used to decouple the high spin iron. In reference (Astashkin, Kawamori *et al*., 1995) Zn^{2+} ion has replaced the native Fe^{2+} whereas in reference (Deligiannakis, Jegerschold *et al*., 1997) treatment at high pH has been used to deplete the sample of Fe^{2+}. Model 1 is therefore appropriate for the Astashkin et al (Astashkin, Kawamori *et al*., 1995) study who estimated an approximate value of 1.9 MHz for both ^{14}N isotropic hyperfine couplings which are in reasonable agreement with the calculated values of 2.5 and 1.8 MHz, Table 4. In the iron depleted sample of reference (Deligiannakis, Jegerschold *et al*., 1997), the peptide NH, D2-Phe261 coupling was found to be the larger of the two having an isotropic hyperfine coupling value of 2.1 MHz with the D2-His214 coupling equal to 1.7 MHz. The calculated values for the metal-depleted models 2 and 3 of 1.9 and 1.7 MHz, Table 4, are in excellent agreement with the experimental determinations.

Table 1 Comparison of calculated ^1H Total (Isotropic + Anisotropic) Hyperfine Coupling Constants (A_{nn}) for Isolated and Models 1–3 with experimental determinations. All values in MHz.

Position	A_{nn}	Isolated	Model 1	Model 2	Model 3	Experimental [a]	
						Reference (Macmillan, Lendzian *et al*., 1995)	Reference (Rigby, Heathcote *et al*., 1995)
^1H, CH_3(2)	A_{11}	3.7	2.0	5.6	3.6	4.8	4.1
	A_{22}	4.6	2.8	6.4	4.6	4.8	4.1
	A_{33}	8.0	6.0	9.9	8.1	7.8	7.3
^1H, CH_3(3)	A_{11}	3.0	4.7	1.5	2.7	3.3	4.1
	A_{22}	3.3	5.6	2.3	3.6	3.3	4.1
	A_{33}	6.9	9.2	5.5	6.9	6.7	7.3
$^1HN_\delta$ D2- His214	A_{11}	-	−6.3	10.9	−10.2	−2.6	−5.6
	A_{22}	-	−5.7	−11.6	−9.6	−2.6	−5.6
	A_{33}	-	12.4	−12.3	11.4	5.3	13.1
N^1H D2- Phe 261	A_{11}	-	−7.8	−6.3	−6.8	−0.85	-
	A_{22}	-	−7.5	−5.9	−6.5	−0.85	-
	A_{33}	-	8.7	8.3	8.5	5.5	-

[a] Assignment of observed couplings to specific protons is not possible from experimental ENDOR data alone.

Table 2 Calculated and experimental ^{14}N isotropic hyperfine coupling, A_{iso} for Models 1–4. All values given in MHz.

						Experimental	
		Model 1	**Model 2**	**Model 3**	**Model 4**	Reference (Astashkin, Kawamori *et al.*, 1995)	Reference (Deligiannakis, Jegerschold *et al.*, 1997)
D2- Phe 261							
^{14}NH	**Aiso**	1.8	1.9	1.9	1.8	1.9	2.1
D2- His 214							
$^{14}N_{\delta}$	**Aiso**	2.5	1.7	1.7	2.4	1.9	1.7

Replacing bicarbonate ligand with carbonate

A recent study has proposed that carbonate as opposed to bicarbonate acts as the native ligand to the non-heme iron atom in PS II (Cox, Jin *et al*., 2009). Model 5 simulates the effect of this ligand change. The increase in hydrogen bond length to the proximal O1 atom 1.50 Å to 1.56 Å brought about by this change, Table 1, suggests a weaker hydrogen bond to the O1 atom is formed for the carbonate model. The spin density distribution, Fig. 3 and the ^{13}C and ^{17}O anisotropic hyperfine coupling tensors, Table 1, indicates that replacement of bicarbonate by carbonate leads to a more symmetrical spin density distribution for the PSQ. The calculated ^{1}H isotropic hyperfine coupling values for 2 and 3 methyl groups have the same value of 5.4 MHz. The additional negative charge of the carbonate ligand weakens the proximal O1 hydrogen bond leading to a more symmetrical spin density distribution for the PSQ. A drawback to the proposal in (Cox, Jin *et al*., 2009) is the high pK_a value for the carbonate/bicarbonate couple of 10.33 (Cox, Jin *et al*., 2009) which renders it unlikely that the carbonate form exists at the lower pH values in which paramagnetic measurements are usually carried out. It was proposed in (Cox, Jin *et al*., 2009) that iron ligation could reduce the pK_a value but no evidence was presented for this assumption.

Role of non-heme Fe^{2+} in Type II reaction centres

The role of the non-heme iron in Type II reaction centres is still not clear. The original "iron wire" hypothesis (Feher and Okamura, 1999) was rejected when it was found that in iron-depeleted reaction centres electron transfer from Q_A to Q_B still occurred albeit at a reduced rate and native kinetics could be fully restored by substitution with other divalent metals such as Cu^{2+}, Mn^{2+}, Ni^{2+}, Co^{2+} and Zn^{2+} (Debus, Feher *et al*., 1986; Kirmaier, Holten *et al*., 1986). The presence of a divalent metal ion in the site was shown to be the primary requirement for native electron transfer kinetics to be achieved. In the iron-depleted bacterial reaction centres the most significant kinetic change is a reduction in the electron transfer rate for the reduction of the Q_A quinone by the intermediate acceptor bacteriopheophytin anion radical (Feher and Okamura, 1999). Our current PS II study and our previous reports on the purple bacterial reaction centres (O' Malley, 1998; O' Malley, 2003; Lin and O' Malley, 2008) shows that the presence of a divalent metal ion in the non-heme site significantly strengthens the hydrogen bond to the proximal oxygen atom of the semiquinone present in the Q_A site, which additionally leads to an asymmetric spin density distribution with the largest spin density residing on the distal oxygen atom of the semiquinone. The increased hydrogen bonding strength will increase the electron affinity of the Q_A site quinone leading to an increase in its redox potential (O' Malley, 1997; Feldman, Hester *et al*., 2007). Detailed studies on bacterial reaction centres have shown the sensitivity of the initial quantum yield to the rate of Q_A reduction by the bacteriopheophytin anion radical (Kirmaier, Holten *et al*., 1986). The sensitivity of this reaction rate to the redox potential of the Q_A quinone has also been shown with the rate being directly proportional to the redox potential of the Q_A quinone (Gunner and Dutton, 1989). While it is difficult to estimate quantitatively the enhancement to the redox potential of the Q_A/Q_A^- couple brought about the divalent metal in the non-heme site this enhancement may be crucial to ensure that reduction of Q_A by pheophytin is favoured over wasteful back-reactions. This may be a major reason for the ubiquitous presence of the non-heme iron site in direct contact with quinone acceptors in Type II reaction centres.

Conclusions

In conclusion therefore, QM/MM studies of the

Q_A site in Photosystem II reveal that the spin density distribution of the PSQ formed there is very sensitive to the occupancy of the non-heme iron site. The presence of a divalent ion in the non-heme site results in a very strong hydrogen bond interaction with the O1 oxygen atom which leads to a polarization of the spin density on the Q_A PSQ. This results in a decreased spin density on the O1 oxygen atom proximal to the non-heme site. Removal of the divalent ion leads to an opposing spin polarization of the Q_A PSQ with the distal O4 oxygen atom now containing the reduced spin density. Removal of the bicarbonate ligand with the divalent ion leads to a more symmetrical spin density distribution for the Q_A PSQ. The state of the non-heme site also leads to changes in calculated ^{1}H methyl group and hydrogen bonded protons hyperfine couplings in addition to ^{14}N hyperfine couplings observed for hydrogen bonded amino acid residues D2-His214 and D2-Phe261. For Type II reaction centres a major role for Fe^{2+} in the non-heme site may be the raising of the redox potential of the Q_A/Q_A^- couple to ensure that electron transfer from the (bacterio)pheophytin anion free radical occurs at a sufficient rate to compete with wasteful back-reactions.

References

Astashkin AV, A Kawamori, *et al*. (1995) An Electron-Spin Echo Envelope Modulation Study of the Primary Acceptor Quinone in Zn-Substituted Plant Photosystem-Ii. Journal of Chemical Physics 102(14): 5583-5588

Barber J (2003) Photosystem II: the Engine of Life. Quarterly Reviews of Biophysics 36(1): 71-89

Cox N, L Jin, *et al*. (2009) The Semiquinone-Iron Complex of Photosystem II: Structural Insights from ESR and Theoretical Simulation; Evidence that the Native Ligand to the Non-Heme Iron Is Carbonate. Biophysical Journal 97(7): 2024-2033

Debus RJ, G Feher, *et al*. (1986) Iron-Depleted Reaction Centers from Rhodopseudomonas-Sphaeroides R-26.1 - Characterization and Reconstitution with Fe-2+, Mn-2+, Co-2+, Ni-2+, Cu-2+, and Zn-2+. Biochemistry 25(8): 2276-2287

Deligiannakis Y, A Boussac, *et al*. (1995) ESEEM Study of the Plastoquinone Anion Radical (Q(A)(Center Dot-)) in N-14- and N-15-Labeled Photosystem II Treated with CN. Biochemistry 34(49): 16030-16038

Deligiannakis Y, J Hanley, *et al*. (1999) 1D- and 2D-ESEEM Study of the Semiquinone Radical Q(A)(-) of Photosystem II. Journal of the American Chemical Society 121(33): 7653-7664

Deligiannakis Y, C Jegerschold, *et al*. (1997) EPR and ESEEM Study of the Plastoquinone Anion Radical Q(A)(-Center Dot) in Photosystem II Treated at High pH. Chemical Physics Letters 270(5-6): 564-572

Diner BA, V Petrouleas, *et al*. (1991) The Iron-Quinone Electron-Acceptor Complex of Photosystem-Ii. Physiologia Plantarum 81(3): 423-436

Feher G, MY Okamura (1999) The Primary and Secondary Acceptors in Bacterial Photosynthesis II. The Structure of the Fe2+-Q(-) Complex. Applied Magnetic Resonance 16(1): 63-100

Feldman KS, DK Hester, *et al*. (2007) A Relationship between Amide Hydrogen Bond Strength and Quinone Reduction Potential: Implications for Photosystem I and Bacterial Reaction Center Quinone Function. Bioorganic & Medicinal Chemistry Letters 17(17): 4891-4894

Gunner MR, PL Dutton (1989) Temperature and -Delta-G-Degrees Dependence of the Electron-Transfer from Bph.- to Qa in Reaction Center Protein from Rhodobacter-Sphaeroides with Different Quinones as Qa. Journal of the American Chemical Society 111(9): 3400-3412

Kern J, G Renger (2007) Photosystem II: Structure and Mechanism of the Water : Plastoquinone Oxidoreductase. Photosynthesis Research 94(2-3): 183-202

Kirmaier C, D Holten, *et al*. (1986) Primary Photochemistry of Iron-Depleted and Zinc-Reconstituted Reaction Centers from Rhodopseudomonas-Sphaeroides. Proceedings of the National Academy of Sciences of the United States of America 83(17): 6407-6411

Koulougliotis D, T Kostopoulos, *et al*. (1993) Evidence for Cn- Binding at the Ps-Ii Nonheme Fe2+ - Effects on the Epr Signal for Q(a)-Fe2+ and on Q(a)/Q(B) Electron-Transfer. Biochimica Et Biophysica Acta 1141(2-3): 275-282

Lin TJ, PJ O'Malley (2008) An ONIOM Study of the Q(A) Site Semiquinone in the Rhodobacter Sphaeroides Photosynthetic Reaction Centre. Journal of Molecular Structure-Theochem 870(1-3): 31-35

Loll B, J Kern, *et al*. (2005) Towards Complete Cofactor Arrangement in the 3.0 Angstrom Resolution Structure of Photosystem II. Nature 438(7070): 1040-1044

Lubitz W, G Feher (1999) The Primary and Secondary Accepters in Bacterial Photosynthesis III. Characterization of the Quinone Radicals QA(-)Center Dot and QB(-Center Dot) by EPR and ENDOR. Applied Magnetic Resonance 17(1): 1-48

MJ Frisch, GW Trucks, *et al*. (2009) Gaussian 09, Revision A.02. Wallingford CT, Gaussian, Inc

Macmillan F, F Lendzian, *et al*. (1995) Epr and Endor Investigation of the Primary Electron-Acceptor Radical-Anion Q(a)(Center-Dot-) in Iron-Depleted Photosystem-Ii Membrane-Fragments. Biochemistry 34(25): 8144-8156

Martin E, Narasimhulu KV, *et al*. (2010) Hydrogen Bonding to the QA and QB Site Semiquinones in Bacterial Reaction Centres. J. Amer. Chem. Soc. submitted for publication

Noguchi T, J Kurreck, *et al*. (1999) Comparative FTIR Analysis of the Microenvironment of Q(A)(-Center Dot) in Cyanide-Treated, High pH-Treated and Iron-Depleted Photosystem II Membrane Fragments. Biochemistry 38(15): 4846-4852

O'Malley PJ (1996) 1H, 13C and 17O Principal Hyperfine Tensor Determination for the p-Benzosemiquinone Anion Radical Using Hybrid Density Functional Methods. Chem. Phys. Lett. 262(6): 797-800

O'Malley PJ (1997) A Density Functional Study of the Effect of Reduction on the Geometry and Electron Affinity of Hydrogen Bonded 1,4-Benzoquinone. Implications for Quinone Reduction and Protonation in Photosynthetic Reaction Centers.. Chemical Physics Letters 274(1, 2, 3): 251-254

O'Malley PJ (1997) Effect of Hydrogen Bonding on the Spin Density Distribution and Hyperfine Couplings of the p-Benzosemiquinone Anion Radical in Alcohol Solvents: A Hybrid Density Functional Study. Journal of Physical Chemistry A 101(50): 9813-9817

O'Malley PJ (1997) A Hybrid Density Functional Study of the p-Benzosemiquinone Anion Radical: The Influence of Hydrogen Bonding on Geometry and Hyperfine Couplings. J. Phys. Chem. 101(35): 6334-6338

O'Malley PJ (1998) Density Functional Calculated C-13 and O-17 Hyperfine Couplings for the Ubisemiquinone Anion Radical in an Alcohol Solvent Model and in a Model of the Q(a) Binding Site of Rb-Sphaeroides. Chemical Physics Letters 285(1-2): 99-104

O'Malley PJ (1998) H-1, C-13, and O-17 Isotropic and Anisotropic Hyper-Fine Couplings for the Plastosemiquinone Anion Radical. Journal of the American Chemical Society 120(20): 5093-5097

O'Malley PJ (2003) The Origin of the Spin Density Asymmetry at the Q(A) Binding Site of Type II Photosynthetic Reaction Centres. Chemical Physics Letters 379(3-4): 277-281

O'Malley PJ, SJ Collins (1996) Density Functional Studies of Free Radicals: Accurate Geometry and Hyperfine Coupling Prediction for Semiquinone Anions. Chem. Phys. Lett. 259(3, 4): 296-300

Rigby SEJ., P Heathcote, *et al*. (1995) Endor and Special Triple-Resonance Spectroscopy of Qa(Center-Dot-) of Photosystem-2. Biochemistry 34(37): 12075-12081

Sanakis Y, V Petrouleas, *et al*. (1994) Cyanide Binding at the Nonheme Fe^{2+} of the Iron-Quinone Complex of Photosystem-Ii - at High-Concentrations, Cyanide Converts the Fe^{2+} from High (S = 2) to Low (S = 0) Spin. Biochemistry 33(33): 9922-9928

Vreven T, KS Byun, *et al*. (2006) Combining Quantum Mechanics Methods with Molecular Mechanics Methods in ONIOM. Journal of Chemical Theory and Computation 2(3): 815-826

Wraight CA (2004) Proton and Electron Transfer in the Acceptor Quinone Complex of Photosynthetic Reaction Centers from Rhodobacter Sphaeroides. Frontiers in Bioscience 9: 309-337

Spectral Properties of the *Rhodobacter Sphaeroides* Mutant Photo-Reaction Center with Double Amino Acid Substitution I(L177)H+H(L173)L

Tatiana Y Fufina*, Lyudmila G Vasilieva, Ravil A Khatypov, Vladimir A Shuvalov

Institute of Basic Biological Problems, Russian Academy of Sciences, Pushchino, Moscow region, Russia.
* Corresponding author: Tel. No. +7-496-773-2680; Fax No. +7-496-733-0532; E-mail: tat-fufina@yandex.ru.

Abstract: In the reaction center of purple bacterium *Rhodobacter sphaeroides* histidine L173 serves as the fifth ligand of Mg atom of the bacteriochlorophyll P_A. It is known that after substitution of this histidine by leucine the bacteriochlorophyll loses its central Mg atom and turns into bacteriopheophytin. Our data show that double mutation I(L177)H + H(L173)L results in considerable changes of spectral properties of the reaction center: distinct Q_Y absorption band of the dimer bacteriochlorophyll P disappears, and Q_Y bacteriochlorophyll band near 800 nm broadens and shifts by 6 nm to the red. The pigment content of the mutant RC and the value of E_m P/P^+ remain unaltered indicating secure P_A Mg atom coordination. Our data show that among other potential ligands located close enough to the center of the P_A macrocycle, histidine L177 seems to be the most probable. According to the obtained results the dislocation of the fifth ligand of the P_A Mg atom from L173 to L177 position has little effect on the stability and overall photochemistry of the mutant RC, changing mainly the excitonic interaction between P_A and P_B, which leads to a considerable blue shift of the P Q_Y band.

Keywords: Photosynthetic reaction center; Bacteriochlorophyll; Central Mg atom coordination; Site-directed mutagenesis; *Rhodobacter sphaeroides*

Introduction

The photosynthetic utilization of solar energy is most often associated with (bacterio)chlorophyll (BChls) pigments that take part both in the light-harvesting process and energy conversion. The photosynthetic reaction center (RC) of purple bacterium *Rhodobacter (Rba.) sphaeroides* is an integral membrane complex that performs the initial steps of light-induced trans-membrane charge separation. It consists of three polypeptides and several cofactors including four BChl and two bacteriopheophytin (BPheo) molecules (Ermler *et al*., 1994). The cofactors are arranged in two near-symmetrical branches of electron transfer, A and B, and only A-branch is photochemically active. Each trans-membrane branch is formed by two BChl molecules (P_A and P_B) serving as the primary electron donor P, monomeric BChls (B_A and B_B), BPhes (H_A and H_B) and quinones (Q_A and Q_B) (Ermler *et al*., 1994). Dimeric primary donor appears to be a universal part of all studied bacterial RCs, suggesting that the properties of this "special pair" should be important for efficient electron transfer and charge separation. As a rule, conserved histidines serve as ligands to the central Mg atom of P BChls in bacterial RCs. Properties of the primary electron donor can be dramatically altered upon substitution of these histidines by amino acids incapable of BChl Mg atom coordination. In the present report we describe spectral properties of a new *Rba. sphaeroides* mutant reaction center with histidine ligand to the central Mg atom of BChl P_A dislocated from the L173 to the L177 position.

Materials and Methods

Cell growth, procedure of site-directed mutagenesis and preparation of intracytoplasmic membranes, RC purification and pigment analysis were described previously (Khatypov *et al*., 2005). Absorption

spectra at room temperature were recorded on Shimadzu UV-1601PC spectrophotometer. Gaussian deconvolution of the spectra was performed using Sigma plot program. Light minus dark difference spectra were obtained as described earlier (Khatypov *et al*., 2005). Determination of E_m P/P^+ was described in detail elsewhere (Williams *et al*., 1992).

Results

A stable RC mutant of *Rba. sphaeroides* with double amino acid substitution I(L177)H + H(L173)L was constructed.

Fig. 1 shows room temperature absorption spectra of isolated wild type (spectrum 1) and the mutant RCs (spectrum 2) normalized at 535 nm which corresponds to the Q_X absorption band of BPhe.

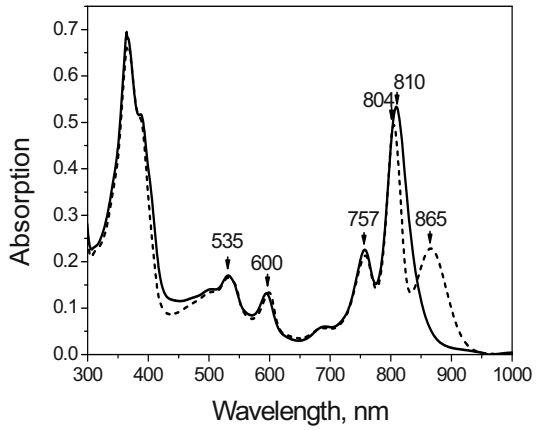

Fig. 1 Room temperature absorption spectra of the wild-type (dash line) and I(L177)H + H(L173)L (solid line) RCs normalized at 535 nm.

Three main bands were observed in the near infrared region of the wild type RCs absorption spectrum: the P Q_Y band at 865 nm, the B Q_Y band at 804 nm and the H Q_Y band at 757 nm. Besides, the spectrum shows Q_X BChl absorption bands at 600 nm, Q_X BPhe band at 535 nm, carotenoid absorption nearby 500 nm and the Soret band around 365 nm. The spectrum of the mutant RCs demonstrates major changes associated with Q_Y BChl absorption: (1) no distinct long-wavelength P band is observed, (2) the Q_Y band near 800 nm becomes broader, and (3) the maximum of this band shifts from 804 to 810 nm.

Parallel changes were found in the difference (light minus dark) absorption spectra corresponding to $P^+Q_A^-$ formation in the mutant and wild type RCs (Fig. 2). In the ΔA spectrum of the wild type RC the light–induced formation of the charge separated state $P^+Q_A^-$ results in the bleaching of the long-wavelength P band at 870 nm, in the short-wavelength shift of the monomer BChl band at 800 nm and in the long-wavelength shift of the 760 nm band (Fig. 2, spectrum 1). In the ΔA spectrum of the mutant RC changes characteristic of the $P^+Q_A^-$ state formation were also observed with the single bleaching maximum at 818 nm (Fig. 2, spectrum 2).

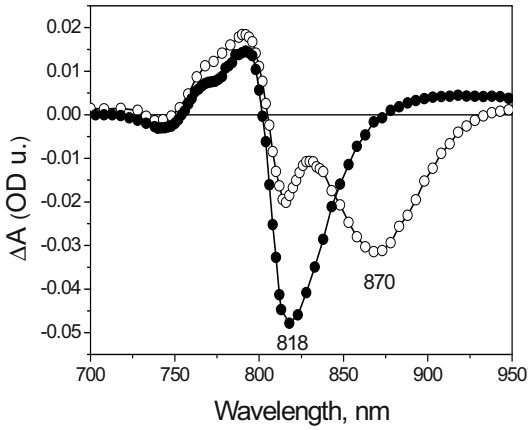

Fig. 2 The difference (light minus dark) absorption spectra of the wild-type (open symbol) and I(L177)H + H(L173)L (closed symbol) RCs.

Pigment analysis revealed that the molar ratio of BChl to BPhe in the wild type and the mutant RCs were similar, namely 2:1, indicating the presence of four BChl molecules and two BPhe molecules in each RC.

Gaussian deconvolution of the 810 nm band in the absorption spectrum of the mutant RC revealed that this band was composed of two bands, 808 nm and 820 nm (Fig. 3).

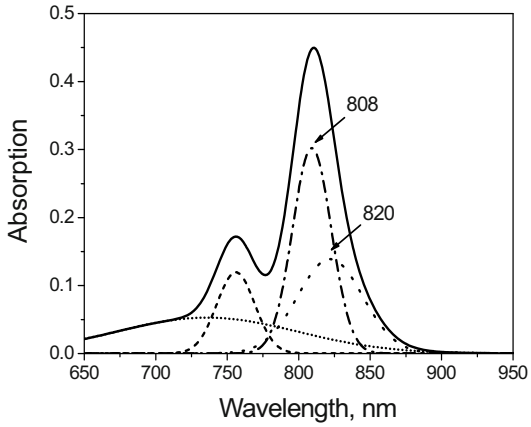

Fig. 3 Gaussian deconvolution of the 810 nm band in the absorption spectrum of the mutant RC.

The latter one, presumably attributed to the altered BChl dimer absorption, was used to determine the midpoint redox potential of the P/P^+ redox couple. The value of E_m P/P^+ in the mutant RC (485 ± 15 mV) was found to be close to that of the wild type RC (500 ± 10 mV).

Discussion

A large number of mutations has been constructed in the vicinity of the primary electron donor P in bacterial reaction centers to investigate how properties of this BChl pair are influenced by the surrounding protein (Williams *et al*., 2009). In particular, coordination of the BChl central Mg atoms strongly depends on the protein environment. In all known bacterial RCs conserved histidines serve as ligands to the Mg atoms of the P BChls. Substitution of these histidine ligands by non-polar side-chain amino acids incapable of BChl Mg atom coordination can greatly affect properties of the primary electron donor. For example, in *Rba. sphaeroides* mutant RC H(L173)L a BPhe is incorporated in the binding pocket of P_A, and the primary donor becomes a heterodimer (Nabedryk *et al*., 2000). Reversed heterodimer can be obtained after similar substitution of His M202. Inclusion of BPhe in the heterodimer results in considerable changes of the near infrared absorption spectrum of the RC and increases the redox potential of P by approximately 130 mV due to the higher oxidation potential of BPhe (Nabedryk *et al*., 2000)

In this report we have described the double mutant RC I(L177)H + H(L173)L in which substitution of His L173 by Leu was accompanied by placing of another His in the L177 position. The double mutation resulted in approximately 45 nm short-wavelength shift of the P near-infrared band. This blue shift, the largest among other known mutant RCs, completely masked P band in the room temperature absorption spectrum by overlapping it with the monomeric BChls absorption band at 804 nm. Lack of the spectral changes in the regions of bacteriopheophytin Q_X and Q_Y transitions, unaltered pigment content and the value of E_m P/P^+ indicated that in this mutant RCs the primary donor P remained a homodimer.

The next question that arises – what can serve as Mg ligand of P_A BChl in the absence of His L173? Histidines L177 and L168 as well as the conserved water molecule located in the RC structure relatively close to the center of P_A macrocycle plane can be considered as potential ligands. More distant His L168 is known to donate a hydrogen bond to the acetyl carbonyl group of the P_A BChl. Removing of this hydrogen bond by mutagenesis was shown to result in the decrease of midpoint redox potential of the P/P^+ redox couple by 60−123 mV depending on amino acid replacing His L168 (Spiedel *et al*., 2002). In *Rba. sphaeroides* RC the value of E_m P/P^+ is around 500 mV. The value of E_m P/P^+ in RC I(L177)H + H(L173)L was found to be practically unaltered (485 ± 1.5 mV) suggesting integrity of this hydrogen bond and indicating that His L168 is not the Mg ligand. It seems that the double mutation also gives no chance for the conserved water molecule located in the close vicinity of P_A and B_B BChls to be the Mg ligand, given that Leu is hydrophobic and has similar molecular volume with His. It is therefore most likely that His L177 serves as the fifth ligand to the central Mg atom of P_A BChl in the mutant RC, even though predictable position of this histidine is apparently not optimal for the coordination. Presumably the plane of His L177 imidazole ring forms acute angle with the plane of P_A macrocycle that might cause disturbance of the inter-dimer structure and interactions, and this might be the reason of unusually large short-wavelength spectral shift of the P absorption band. An example of the poorly positioned ligand donor, His L121, was described by Heller et al. when the active branch BPhe was replaced by BChl in a F(L97)V + F(L121)H double mutant (Heller *et al*., 1995). Interestingly that in spite of the considerable changes of the primary donor spectral properties the RC with double mutation I(L177)H + H(L173)L is found to have overall photochemical activity identical to that of the wild type RC. This finding is consistent with the opinion that P bacteriochlorophylls are tolerant to coordination changes, and that the energetics of the primary donor only weakly depends upon the nature of the coordination (Williams *et al*., 2009).

Acknowledgements

Authors thank Dr. Proskuryakov II for critical reading of the manuscript. This work was supported by MCB Grant from the Russian Academy of Sciences, by RFBR Grant 09-04-00109 and by the State contract No. 02.740.11.0293.

References

Ermler U, Fritzsch G, Buchanan SK, Michel H (1994) Structure of the Photosynthetic Reaction Centre from Rhodobacter Sphaeroides at 2.65 A Resolution: Cofactors and Protein-Cofactor Interactions. Structure 2: 925-936

Khatypov RA, Vasilieva LG, Fufina TY, Bolgarina TI, Shuvalov VA (2005) Substitution of Isoleucine L177 by Histidine Affects the Pigment Composition and Properties of the Reaction Center of the Purple Bacterium Rhodobacter Sphaeroides. Biochemistry (Moscow) 70: 1256-1261

Williams JC, Alden RG, Murchison HA, Peloquin JM, Woodbury NW, Allen JP (1992) Effect of Mutations Near the Bacteriochlorophylls in Reaction Centers from Rhodobacter Sphaeroides. Biochemistry 31: 11029-11037

Williams CJ, Allen JP (2009) In Directed Modification of Reaction Centers from Purple Bacteria: The Purple Phototrophic Bacteria, C Neil Hunter, Fevzi Daldal, Marion C, Thurnauer J, Thomas Beatty (eds.) Springer: The Netherlands, pp. 337-353

Nabedryk E, Schulz C, Mu F, Lubitz W, Breton J (2000) Heterodimeric Versus Homodimeric Structure of the Primary Electron Donor in Rhodobacter Sphaeroides Reaction Centers Genetically Modified at Position M202. Photochemistry and Photobiology 71: 582-588

Spiedel D, Roszak A, McKendrick K, McAuley KE, Fyfe PK, Nabedryk E, Breton J, Robert B, Cogdell RJ, Isaacs NW, Jones MR (2002)Tuning of the Optical and Electrochemical Properties of the Primary Donor Bacteriochlorophylls in the Reaction Centre from Rhodobacter Sphaeroides: Spectroscopy and Structure. Biochimica et Biophysica Acta 1554: 75- 93

Heller BA, Holten D, Kirmaier C (1995) Characterization of Bacterial Reaction Centers Having Mutations of Aromatic Residues in the Binding-Site of the Bacteriopheophytin Intermediary Electron Carrier. Biochemistry 34: 5294-5302

Spectroelectrochemical Determination of the Redox Potentials of Pheophytin *a* and Primary Quinone Q_A in Photosystem II from *Thermosynechococcus Elongatus*

Yuki Kato[a,*], Tadao Shibamoto[a], Akinori Oda[a], Miwa Sugiura[b], Tadashi Watanabe[a]

[a]Institute of Industrial Science, the University of Tokyo, Japan;
[b]Cell-Free Science and Technology Research Center, Ehime University, Japan.
*Corresponding author. Tel. No. +81 3 5452 6332; Fax No. +81 3 5452 6331; E-mail: yukikato@iis.u-tokyo.ac.jp.

Abstract: Thin-layer cell spectroelectrochemistry was applied for the first time to measure the redox potentials of pheophytin (Phe) *a* and the primary quinone Q_A in photosystem (PS) II core complexes from a thermophilic cyanobacterium *Thermosynechococcus elongatus*. The determined potentials for oxygen-evolving PS II from a *T. elongatus* wild type strain were –522 ± 3 mV and –140 ± 2 mV for Phe *a* and Q_A, respectively. Based on the determined values together with kinetic analytical data in literature, a renewed diagram is proposed for the energetics in PS II, and further, modification of the redox properties for acclimation to cultivate conditions is also discussed.

Keywords: Redox potential; Electron transfer; Charge separation; Spectroelectrochemistry

Introduction

Photosystem (PS) II drives photo-induced electron transfer from a Mn_4Ca cluster, catalyzing oxidative water cleavage, to plastoquinones, playing also a role in proton transfer (Renger, 2008). Redox potential of cofactors on the electron transfer chain is an essential physicochemical parameter for discussing the energetics within PS II. Not all the redox potentials of the cofactors, however, have been determined because of experimental difficulty; only the potentials of the primary electron acceptor pheophytin (Phe) *a* and the primary quinone electron acceptor Q_A have been measured. Unapproachable potentials of other cofactors, for example the primary electron donor P680 and the secondary quinone Q_B, have been estimated from the measured potentials together with free energy differences. Though the redox potentials of Phe *a* and Q_A are thus key points for discussing on PS II energetics, the estimated potential values from the measured potential of Phe *a* or Q_A are not necessarily consistent each other, and the potential difference between Phe *a* and Q_A often contradicts with values obtained by other techniques, such as time-resolved spectroscopic measurements.

As the redox potential of Phe *a*, E_m(Phe *a*/Phe a^-), Klimov *et al*. (1979) reported for the first time a value of –610 ± 30 mV. They also obtained a value of ca. 80 meV for the P680* - Phe *a* energy difference from delayed fluorescence measurements (Klimov *et al*., 1978), and thus estimated the E_m(P680/P680$^+$) to be +1,120 ± 50 mV. Rutherford *et al*. (1981) later reported a similar value (–604 mV) to that by Klimov et al. Since then, the values of ca. –600 mV and +1.1 V for E_m(Phe *a*/Phe a^-) and E_m(P680/P680$^+$), respectively, have been widely accepted in the discussion on the PS II energetics.

In contrast to only the above two works reporting E_m(Phe *a*/Phe a^-) values, there are many reports on E_m(Q_A/Q_A^-) in literature (as a review, see Krieger *et al*., 1995); however, the values exhibit scatters and seem to be summarized in a form of four clusters (ca. –300, –100, 0, and +100 mV). By a systematic evaluation of critical parameters for the scattering, Krieger *et al*. (1995) concluded that E_m of (Q_A/Q_A^-) in the oxygen evolving active PS II is –81 ± 16 mV, while in inactive PS II it is +64 ± 25 mV, suggesting possible factors on the change in E_m of Q_A from the

low-potential to the high-potential form as reasons for the scattering values in past reports.

The reported potential values of Phe *a* and Q_A yields simply ca. 520 meV as the Phe a^- Q_A energy difference. Johnson *et al*. (1995) noted, however, such a value is so large in view of physiological phenomena observed for PS II that the measured potentials might be invalid: Hardly a back reaction from $P680^+$ Q_A^- via $P680^+$ Phe a^- occur theoretically if the free energy difference is so large, though thermodynamic and kinetic analytical data suggest occurrence of the back reaction. Later, Rappaport *et al*. (2002) also pointed out the validity of the measured potentials, and then reported that the Phe a^- Q_A energy difference should be smaller by ca. 250 meV by analyzing the fluorescence decay. As a consequence, they estimated the E_m(P680/$P680^+$) value to be +1.26 V citing the E_m(Q_A/Q_A^-) value by Krieger *et al*. In a similar manner based on their delayed and prompt fluorescence data, Grabolle and Dau (2005) assessed the Phe a^- Q_A energy difference and E_m(P680/$P680^+$) to be 340 meV and +1.25 V, respectively.

We have considered that the above situations resulted at least partly from the limited accuracy of chemical titration employed traditionally for the measurements of redox potentials. Further, in the titrations of E_m(Phe *a*/Phe a^-), pH of sample solutions must be adjusted high values (pH 8–11) to achieve reductive power of titrants for potential regions sufficiently negative to reduce Phe *a* because an equilibrium redox reaction of $2H^+/H_2$ is thermodynamic restriction (Hawkridge and Ke, 1977). In view of this, by applying spectroelectrochemistry, we have tried to determine the redox potential values of Phe *a* and Q_A in PS II under a physiological condition (Kato *et al*., 2009; Shibamoto *et al*., 2009; Sugiura *et al*., 2010). Based on the determined potential values for PS II from a thermophilic cyanobacterium *Thermosynechococcus elongatus* together with the kinetic analytical data, a renewed diagram is proposed here for the energetics within PS II.

Materials and Methods

Oxygen-evolving PS II core complexes were purified from a *T. elongatus* 43H strain (WT'), in which the carboxyl terminus of the CP43 subunit was genetically His-tagged, using Ni^{2+}-affinity column chromatography (Sugiura and Inoue, 1999). Depletion of the Mn cluster from the PS II complexes was performed by NH_2OH washing; the water oxidation activity of Mn cluster depleted PS II complexes was practically negligible. In addition, PS II core complexes were prepared from *T. elongatus* WT*, in which only *psbA*$_3$ among three *psbA* genes encoding the D1 protein is genetically remained (Sugiura *et al*., 2010). The prepared PS II core complexes were suspended in a buffer containing 50 mmol MES-NaOH (pH 6.5), 0.2 mol KCl, 0.1% dodecyl-β-D-maltoside, 1 mol Glycine-betaine, and the following redox mediators: for the measurements of Phe *a* redox potentials, 500 μM anthraquinone (E_m = –225 mV), 500 μM methyl viologen (–443 mV), and 1,1'-propylene-2,2'-bypyridylium (Triquat, –556 mV); for Q_A, 100 μM anthraquinone, 100 μM 2-hydroxy-1,4-naphthoquinone (–100 mV), and 200 μM *N,N,N',N'*-tetramethyl- *p*-phenylenediamine (TMPD, +300 mV).

In spectroelectrochemical measurements for Phe *a*, the PS II sample solution was, after addition of 5 mg mL^{-1} sodium dithionite, transferred to an airtight optically transparent electrode (OTTLE) cell, employing a mercury-electroplated Au mesh as a working electrode, filled with Ar. The cell was set in a spctrophotometer modified for lateral illumination. In the case of Q_A, the sample solution was transferred into an OTTLE cell under nitrogen atmosphere, and the cell was arranged in a spectrofluorometer.

Results and Discussion

Presence of several *psbA* genes encoding the D1 protein (PsbA) is a common feature to cyanobacteria. *T. elongatus* has three genes, and their expression levels depend on cultivate conditions (Kos *et al*, 2008): Normally the *psbA*$_1$ gene is dominantly expressed, while high light and/or UV illumination expresses *psbA*$_3$. For more direct comparison of E_m(Phe *a*/Phe a^-) to be obtained in this work with those in the previous reports on higher plants (Klimov *et al*., 1979; Rutherford *et al*., 1981), we used PsbA3-PS II in addition to PsbA1-PS II (WT'), since PsbA3-PS II is similar to higher plant PS II in view of the residue at D1-130, which is within an H-bonding distance of the 9-keto carbonyl of Phe *a* in the D1 branch: The residue 130 is Gln in PsbA1, whereas it is Glu in PsbA3 as well as in PsbA of higher plants.

Fig. 1 shows the light-induced difference absorption spectra indicative of Phe *a* photoreduction in the PsbA1- and PsbA3-PS II core complexes. The spectral shapes of both PS II are essentially the same as those of previous reports; a red-shifted by 4 nm in the spectrum of PsbA3-PS II was observed at the spectral region of the Phe *a* Qx absorption (543 to 547 nm), agreeing well with the spectra found for the D1-Glu130Gln single site directed mutagenesis in *Synechocystis* PCC 6803 (Giorgi *et al*., 1996). This result implies that the H-bonding strengths between Phe *a* (or Phe a^-) and the 130th residues (Gln or Glu) are different. A recent FT-IR study revealed that Glu is the stronger H-bonding donor to the 9-keto carbonyl of Phe a^- (Shibuya *et al*., 2010).

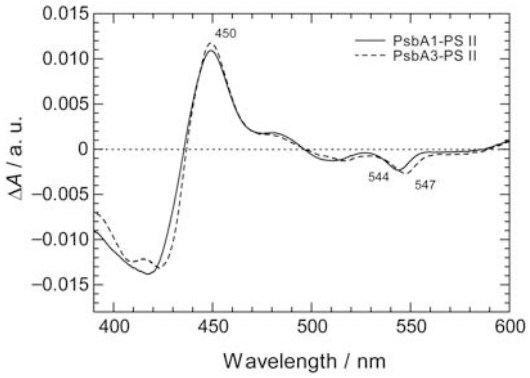

Fig. 1 Light-minus-dark difference spectra indicative of photoreduction of Phe *a* in the PS II core complexes in the OTTLE cell, where potential of the working electrode was set at –350 mV.

By investigating spectroelectrochemically absorbance changes at 450 nm due to the photoreduction of Phe *a* at various electrode potentials (data not shown), we determined the E_m(Phe *a*/Phe a^-) values in PsbA1- and PsbA3-PS II at a physiological pH of 6.5 to be –522 ± 3 mV (n = 3; Sugiura *et al*., 2010) and –505 ± 6 mV (n = 4; Kato *et al*., 2009), respectively.

In spectroelectrochemical measurements for Q_A, we monitored the fluorescence intensity at 681 nm, the peak wavelength of Chl *a* fluorescence, during a potential journey in a reductive direction for the PS II complexes. Based on the magnitude of the fluorescence intensity changes against the electrode potentials (data not shown), the $E_m(Q_A/Q_A^-)$ value in PsbA1-PS II was determined to be –140 ± 2 mV (n = 4; Shibamoto *et al*., 2009). By inactivating the PS II core complexes with NH_2OH, we confirmed that the $E_m(Q_A/Q_A^-)$ value shifted to +20 mV.

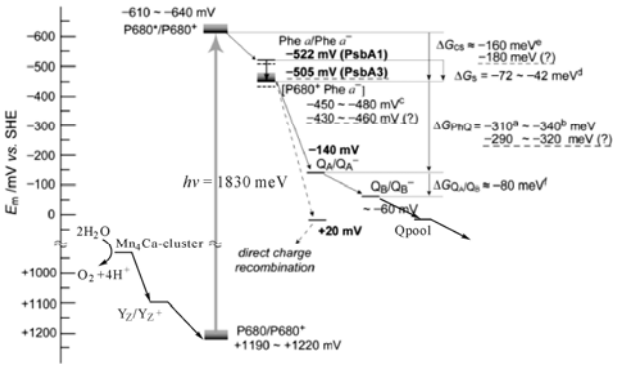

Fig. 2 Proposed diagram for the energetics within PS II from *T. elongatus* based on the determined redox potentials and the free energy differences cited from the literature: The values of ΔG_{PhQ} derive from the kinetic analytical data (a: Rappaport *et al*., 2002; b: Grabolle and Dau, 2005); the energy level for [$P680^+$ Phe a^-][c] is yielded by $E_m(Q_A/Q_A^-)$ and ΔG_{PhQ}; the values of ΔG_S[d] is calculated by subtracting the energy level for [$P680^+$ Phe a^-] from the E_m(Phe *a*/Phe a^-) value; for ΔG_{cs}[e] and $\Delta G(Q_A/Q_B)$[f], see Dau and Sauer (1996), and Minagawa *et al*. (1999), respectively.

An energetic diagram for the electron transfer within PS II from *T. elongatus* is summarized as Fig. 2 on the basis of the determined E_m(Phe *a*/Phe a^-) and $E_m(Q_A/Q_A^-)$ values for PsbA1-PS II together with kinetic analytical data in the literature. According to the Weller's equation (Weller, 1982), which describes an energetic relationship between an electron donor and an acceptor, the free energy correlation surrounding the P680* → Phe *a* electron transfer should obey the following formula:

$$\Delta G_{CS} = q[E_m(P680^*/P680^+) - E_m(\text{Phe } a/\text{Phe } a^-)] + \Delta G_S$$

where q is the elementary charge, ΔG_{CS} is the free energy difference for the charge separation, and ΔG_S is the stabilization energy induced by the separated ion pair formation. In the present context, ΔG_{CS} denotes the energy difference between [P680* Phe *a*] and [$P680^+$ Phe a^-], and have been scrutinized often by time-resolved fluorescence spectroscopy, yielding a typical value of ca. –160 meV (Dau and Sauer, 1996). ΔG_S is generally referred to as a static Coulombic interaction calculated as $-q^2/(4\pi\varepsilon r)$, where ε is the permittivity and r is the ionic center-to-center distance. Since the exact value of ε in matrix proteins of PS II is unknown and further electrostatic effects from other cofactors and/or charged amino acid residues should also be taken into account, we estimated –40 meV at most for ΔG_S by considering

that an electron transfer step from an entropic equilibrated state for excitation between P680 and antenna Chls ([AnChl P680]*) to Phe *a* should not be uphill at the beginning of the discussion on the energetics within PsbA3-PS II (Kato *et al*., 2009). However, it came to our attention that this consideration is not accurate on physical grounds, and therefore, we calculated here for ΔG_S from the E_m(Phe *a*/Phe a^-) and $E_m(Q_A/Q_A^-)$ values in PsbA1-PS II and values of ΔG_{PhQ}, the free energy difference from [$P680^+$ Phe a^- Q_A] to [$P680^+$ Phe *a* Q_A^-], found in the literature (–310 mV: Rappaport *et al*, 2002; –340 mV: Grabolle and Dau, 2005), yielding values of –72 — –42 meV. As a consequence, the $E_m(P680/P680^+)$ value is estimated to be +1190 — +1220 mV.

Assuming $E_m(P680/P680^+)$ remains in PsbA3-PS II, we reach a conclusion that the E_m(Phe *a*/Phe a^-) shift by +17 mV increases ΔG_{CS}, and this increase would be one of the reasons for the ~1.7 times higher oxygen-evolving activity in PsbA3-PS II (Sugiura *et al*., 2010), which is probably preferable for high light cultivate conditions compared with PsbA1-PS II. On the other hand, if $E_m(Q_A/Q_A^-)$ is also remained, the resultant decrease in ΔG_{PhQ} might not be preferable; however, kinetic/ thermodynamic studies implied that $E_m(Q_A/Q_A^-)$ is also modified (Sugiura *et al*., 2010), and now we are trying to measure $E_m(Q_A/Q_A^-)$ in PsbA3-PS II. In any case, redox properties of the cofactors would be modified by not only the amino acid substitution at D1-130 but also the other 20 substitutions in PsbA1- and PsbA3-PS II, and these multiple modifications would be adjusted to a more efficient forward electron transfer under high light conditions. As demonstrated here, the development of direct spectroelectrochemical measurements for E_m of Phe *a* and Q_A in the PS II complexes from *T. elongatus* allows us to depict the energetics in more detail and to discuss more quantitatively on the acclimation of the cofactors' redox properties to cultivate conditions.

Acknowledgements

We would like to thank Alain Boussac and Fabrice Rappaport for helpful discussion. This work was supported in part by a Grant-in-Aid for Scientific Research (No. 22550146 to TW and 21612007 to MS) from JSPS, a Grant-in-Aid (21750012 to YK) and a global COE program for "Chemistry Innovation through Cooperation of Science and Engineering" from MEXT of the Japanese Government.

References

Dau H, Sauer K (1996) Exciton Equilibration and Photosystem II Exciton Dynamics - a Fluorescence Study on Photosystem II Membrane Particles of Spinach. Biochim. Biophys. Acta 1273: 175-190

Giorgi LB, Nixon PJ, Merry SAP, Joseph DM, Durrant JR, Rivas JDL, Barber J, Porter G, Klug DR (1996) Comparison of Primary Charge Separation in the Photosystem II Reaction Center Complex Isolated from Wild-Type and D1-130 Mutants of the Cyanobacterium Synechocystis PCC 6803. J. Biol. Chem. 271: 2093-2101

Grabolle M, Dau H (2005) Energetics of Primary and Secondary Electron Transfer in Photosystem II Membrane Particles of Spinach Revisited on Basis of Recombination-Fluorescence Measurements. Biochim. Biophys. Acta 1708: 209-218

Hawkridge FM, Ke B (1977) An Electrochemical Thin-Layer Cell for Spectroscopic Studies of Photosynthetic Electron-Transport Components. Anal. Biochem. 78: 76-85

Johnson GN, Rutherford AW, Krieger A (1995) A Change in the Midpoint Potential of the Quinone Q_A in Photosystem II Associated with Photoactivation of Oxygen Evolution. Biochim. Biophys. Acta 1229: 202-207

Kato Y Sugiura, M Oda A, Watanabe T (2009) Spectroelectrochemical Determination of the Redox Potential of Pheophytin a, the Primary Electron Acceptor in Photosytem II. Proc. Natl. Acad. Sci. USA 106: 17365-17370

Klimov VV, Allakhverdiev SI, Pashchenko VZ (1978) Measurement of the Activation Energy and Lifetime of Fluorescence of Photosystem 2 Chlorophyll. Dokl. Akad. Nauk SSSR 242: 1204-1207

Klimov VV, Allakhverdiev SI, Demeter S, Krasnovskii AA (1979) Photoreduction of Pheophytin in the Photosystem 2 of Chloroplasts with Respect to the Redox Potential of the Medium. Dakl. Akad. Nauk SSSR 249: 227-30

Kos PB, Deak Z, Cheregi O, Vass I (2008) Differential Regulation of psbA and psbD Gene Expression, and the Role of the Different D1 Protein Copies in the Cyanobacterium Thermosynechococcus

Elongatus BP-1. Biochim. Biophys. Acta 1777: 74-83

Krieger A, Rutherford AW, Johnson GN (1995) On the Determination of Redox Midpoint Potential of the Primary Quinone Electron Acceptor, Q_A, in Photo-System II. Biochim. Biophys. Acta 1229: 193-201

Minagawa K, Narusaka Y, Inoue Y, Satoh K (1999) Electron Transfer between Q_A and Q_B in Photosystem II is Thermodynamically Perturbed in Phototolerant Mutants of Synechocystis sp. PCC 6803. Biochemistry 38: 770-775

Rappaport F, Guervova-Kuras M, Nixon PJ, Diner BA, Lavergne J (2002) Kinetics and Pathways of Charge Recombination in Photosystem II. Biochemistry 41: 8518-8527

Renger G (2008) Functional Patter of Photosystem II. In: Renger G (ed.), Primary Processes of Photosynthesis: Principles and Apparatus, Part II. Royal Society Chemistry: Cambridge, pp. 237-290

Rutherford AW, Mullet JE, Crofts AR (1981) Measurement of the Midpoint Potential of the Pheophytin Acceptor of Photosystem II. FEBS Lett. 123: 235-237

Shibamoto T, Kato Y, Sugiura M, Watanabe T (2009) Redox Potential of the Primary Plastoquinone Electron Acceptor Q_A in Photosystem II from Thermo-Synechococcus Elongatus Determined by Spectro-Electrochemistry. Biochemistry 48: 10682-10684

Shibuya Y, Takahashi R, Okubo T, Suzuki H, Sugiura M, Noguchi T (2010) Hydrogen Bond Interaction of the Pheophytin Electron Acceptor and Its Radical Anion in Photosystem II as Revealed by Fourier Transform Infrared Difference Spectroscopy. Biochemistry 49: 493-501

Sugiura M, Inoue Y (1999) Highly Purified Thermo-Stable Oxygen-Evolving Photosystem II Core Complex from the Thermophilic Cyanobacterium Synechococcus Elongatus Having His-Tagged CP43. Plant Cell Physiol. 40: 1219-1231

Sugiura M, Kato Y, Takahashi R, Suzuki H, Watanabe T, Noguchi T, Rappaport F, Boussac A (2010) Energetics in Photosystem II from Thermosynechococcus Elongatus with a D1 Protein Encoded by Either the $psbA_1$ or $psbA_3$ gene. Biochim. Biophys. Acta 1797: 1491-1499

Weller A (1982) Photoinduced Electron Transfer in Solution: Exciplex and Radical Ion Pair Formation Free Enthalpies and Their Solvent Dependence. Z. Phys. Chem. 133: 93-98

PsbP does Not Require LHCII to Bind the PSII Core

Cristina Pagliano[a,*], Fabiana Chimirri[a], Guido Saracco[a], James Barber[a, b]

[a]Department of Materials Science and Chemical Engineering - BioSolar Lab, Politecnico di Torino, Alessandria, Italy;
[b]Wolfsons Laboratories, Imperial College, London, United Kingdom.
[*]Corresponding author. Tel. No. +39 131 229301; Fax No. +39 131 229344; E-mail: cristina.pagliano@polito.it.

Abstract: Photosystem II of higher plants and green algae contains three extrinsic subunits PsbO, PsbP and PsbQ located on the lumenal surface where they stabilize the Mn-cluster of the oxygen evolving complex (OEC) and facilitate its catalytic activity.

To isolate active PSII complexes from higher plants several methods are available, which include sucrose density centrifugation and column chromatography. However, when isolating pure PSII cores, depleted of light-harvesting antennae (LHCII), a total loss of PsbP and PsbQ usually occurs. By direct solubilization of stacked thylakoids with low concentration of n-dodecyl-beta-D-maltoside in combination with sucrose density gradient centrifugation containing glycine-betaine we isolated PSII cores completely depleted of LHCII, but retaining an almost full complement of PsbO and significant amount of PsbP (30%). Along the sucrose gradient PsbQ was completely lost in the first fractions, while PsbO was present mainly in fractions containing PSII, indicating respectively a weak binding to the PSII core of the former and a strong binding of the latter. Although some PsbP was partially lost along the gradient, this OEC protein was present in appreciable amount in PSII containing fractions, ruling out the possibility of its nonspecific co-migration with PSII and confirming that LHCII proteins are not a strict requirement for its assembly to the PSII core.

Keywords: Photosystem II; Extrinsic polypeptides; PsbP protein

Introduction

Plants, algae and cyanobacteria contain Photosystem II (PSII), which is unique in its ability to catalyze the oxidation of water to molecular oxygen using light energy. Located on the thylakoid lumenal side of PSII is a cluster of three inorganic ions Mn, Ca and Cl (referred to hereafter as Mn-cluster) responsible for catalyzing water oxidation. The Mn-cluster is surrounded by several lumenal extrinsic protein subunits stabilizing these ionic components (OEC proteins). In higher plants and green algae the lumenal OEC proteins of PSII are PsbO, PsbP and PsbQ. An additional lumenally exposed protein is PsbR. The functional characteristics of each protein have been intensively analyzed by release-reconstitution experiments (Enami *et al*., 2000). PsbO is most strongly bound to PSII and stabilizes the Mn-cluster; PsbP is involved in Ca^{2+} and Cl^{-} retention in PSII, PsbQ participates primarily in Cl^{-} retention and PsbR is required for the optimization of electron transfer from the plastoquinone pool and for stable assembly of PsbP and PsbQ (Roose *et al*., 2007). PsbP is more crucial than PsbQ for PSII function in higher plants (Ifuku *et al*., 2005; Yi *et al*., 2007), playing structural roles in protecting the Mn-cluster from attack by exogenous reductants (Ghanotakis *et al*., 1984) and in the dynamic life cycle of PSII (Roose *et al*., 2007; Suorsa and Aro, 2007; Ido *et al*., 2008). Moreover, a substantial pool of unassembled OEC proteins exists in the thylakoid lumen and bound PsbP is in rapid binding equilibrium with free PsbP in the lumen (Hashimoto *et al.*, 1997). Its binding has been shown to relate with the morphology change of the grana, due to interactions between the lumenal cofactors of the PSII complexes in opposing thylakoid membranes

(Boekema *et al*., 2000). It has been proposed that the binding of PsbP requires the presence of light harvesting chlorophyll a/b complexes (LHC), particularly LHCII (Caffarri *et al*., 2009). Here we show that PsbP does bind to PSII cores isolated from peas completetly depleted of LHCII light-harvesting antennae.

Materials and Methods

Pea (*Pisum sativum* L., var. Palladio nano) seeds were grown hydroponically in Long Ashton nutrient solution (Hewitt, 1966) into a growth chamber with 8 h daylight, 60% humidity, 150 μmol m^{-2} s^{-1} photons.

Thylakoids membranes were isolated from 21 day-old pea leaves according to Eshaghi *et al*. (1999) and finally stored in 25 mmol MES pH 6.0, 10 mmol NaCl, 5 mmol $MgCl_2$ and 2 mol glycine betaine. Solubilization of stacked thylakoid membranes with 20 mmol n-dodecyl-beta-D-maltoside (β-DM) occurred at a chlorophyll concentration of 1 mg/ml for 1 minute at 4 °C in the dark in the presence of 500 μM phenylmethylsulphonylfluoride. After a short centrifugation at 21.000 x g for 10 minutes at 4 °C, 450 μl of the supernatant were added to the top of sucrose gradient, prepared by freezing and thawing ultracentrifuge tubes filled with a buffer made of 25 mmol MES, pH 5.7, 10 mmol NaCl, 5 mmol $CaCl_2$, 0.5 mol sucrose, 0.5 mol glycine betaine, 0.03% β-DM. Centrifugation was carried out at 39.000 rpm for 18 h at 4 °C (TH-641 rotor, Thermo Scientific). The third sucrose band, containing PSII particles, was carefully removed using a syringe and concentrated by membrane filtration with Amicon Ultra 100 kDa cut-off devices (Millipore). Chlorophyll concentration was determined according to Arnon (1949). Absorption spectra were recorded at 6 °C in the sucrose gradient buffer. Oxygen evolution measurements were performed at 20 °C using a Clark-type oxygen electrode (Hansatech) under saturating light intensities at a chlorophyll concentration of 5 μg/ml in 25 mmol MES pH 6.5, 2 mol glycine betaine, 10 mmol $NaHCO_3$, 10 mmol NaCl and 25 mmol $CaCl_2$ using as electron acceptor 2,6-dichlorobenzoquinone at a concentration of 500 μM. Electrophoresis was carried out using the Laemmli's system (Laemmli, 1970). Protein bands were resolved on 12.5% polyacrylamide gels in the presence of 5 mol urea and stained by Coomassie brilliant blue R-250 or transferred onto nitro-cellulose membrane and immunodetected with specific antisera against main PSII subunits by using 5-bromo-4-chloro-3-indolyl phosphate/nitro blue tetrazolium staining.

Results and Discussion

Pea thylakoids, usually characterized by a Chl a/b ratio of 3.20–3.30 and oxygen evolution rates around 190 μmol O_2 mg Chl^{-1} h^{-1}, were subjected to a brief solubilization with β-DM and separated on a sucrose gradient into 5 pigment binding complexes (Fig. 1a), from top to bottom of the gradient: LHCII monomers (B1), LHCII trimers (B2), PSII cores (B3), PSI (B4) and PSI-LHCI supercomplexes (B5) as assessed by SDS-PAGE (Fig. 1b). The PSII core is composed of the main PSII intrinsic subunits CP47, CP43, D2 and D1 and it is depleted of LHCII polypeptides as shown in the Comassie stained gel (Fig. 1b, lane B3).

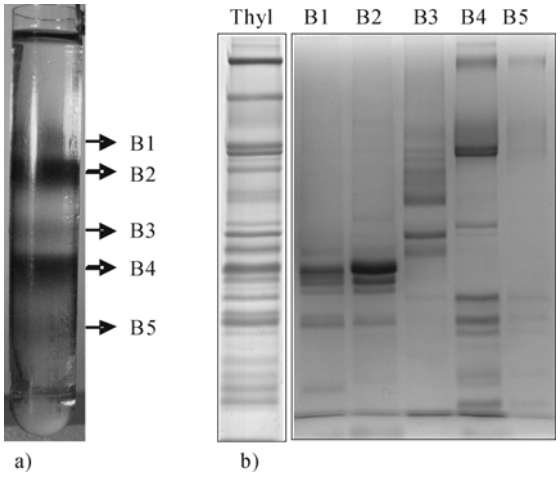

Fig. 1 (a) Sucrose density gradient of solubilized pea thylakoids. Chlorophyll containing fractions labeled B1–5. (b) Polypeptide composition of thylakoid membranes (Thyl) and sucrose gradient bands B1–5. Lane Thyl contains pea thylakoids (4 μg chlorophyll), lanes B1–5 contain a same volume (22 μl) of each sucrose band B1–5.

The absence of LHCII from the PSII core was further confirmed by the absorption spectrum reported in Fig. 2a, showing two peaks at 674 and 437 nm and absence of absorption in the region of 470 and 650 nm, typical of Chlb absorption whose intensity is proportional to the antenna content, and by immunoblotting with the antibody against LHCII (Fig. 2b).

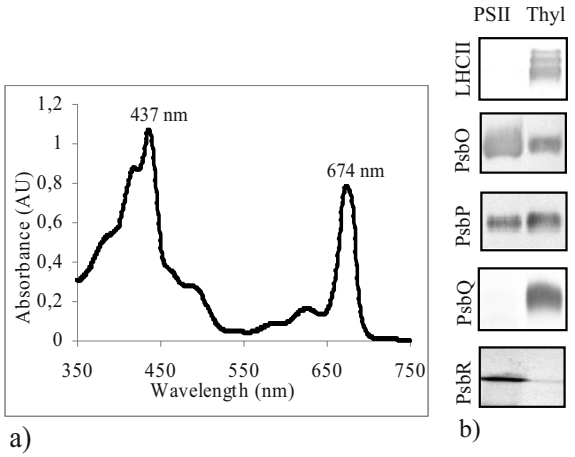

Fig. 2 a) Absorption spectrum profile of isolated PSII cores b) Western blots with antibodies against LHCII and extrinsic polypeptides. Lane PSII contains pea PSII (1 µg chlorophyll); lane Thyl contains pea thylakoids (1 µg chlorophyll).

If compared to other PSII cores depleted of LHCII and isolated by sucrose gradient (Hankamer *et al*., 1997; Wang *et al*., 2010), the pea PSII core complex reported here showed a high integrity in the polypeptide composition of its catalytic site: an almost stoichiometric presence of PsbO and PsbR was confirmed, as well as a significant amount of PsbP (Fig. 2b). On the other hand PsbQ was undetectable in the PSII core.

A quantification of the amount of the PsbP extrinsic subunit in the PSII core was attempted. Comparing the signal of PsbP in five independent western blots to the signal of the reaction centre subunits (assuming a constant ratio of 1:1 between reaction centre subunits and extrinsics), the amount of PsbP bound to the reaction centre was evaluated as 30% (data used for the calculations not shown), indicative of a retention of a significant quantity of this subunit during the isolation procedure. This probably contributes to the high oxygen evolution activity displayed by the isolated PSII core complex, reaching oxygen evolution rates of 1,000 µmol O_2 mg Chl^{-1} h^{-1} in the presence of an optimal concentration of Ca^{2+} and Cl^- in the measurement buffer.

To investigate the strength of the binding of the OEC proteins to the pea PSII core, a sucrose gradient tube was sampled from top to bottom into 33 fractions and equal volumes of each fraction were loaded on a gel. Immunoblottig analyses with antibodies towards the extrinsic subunits (not shown) revealed that PsbQ was located exclusively in top fractions, while PsbO was present mainly in fractions containing PSII, suggesting respectively a weak binding to the PSII core of the former and a strong binding of the latter. In the case of PsbP, it was detected both in fractions above the B3 band (but not in the very top fractions) and in the B3 band itself, suggesting that this subunit is partially lost from the PSII core during the first hours of ultracentrifugation, but still remains attached to it in line with the 30% level of binding estimated by comparison with intrinsic PSII proteins. Using the same fractions, western blot analyses were performed with antibodies towards the reaction centre subunit D1 and LHCII (Fig. 3) and emphasised that LHCII proteins are present in fractions (6–13) above the PSII complex (14–16).

The results presented above suggest that the PsbP extrinsic protein can bind to the PSII without the requirement for the presence of the LHCII antenna system, a conclusion which contrasts with that of Caffarri *et al*. (2009), where it was shown that in Lhcb3 knock out *Arabidopsis thaliana* mutants, PsbP is not able to bind the PSII core.

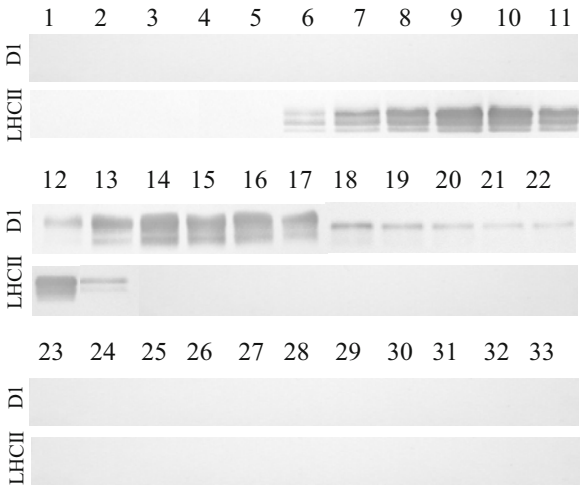

Fig. 3 Western blots of sucrose gradient fractions using antibodies against D1 and LHCII. Lanes 1–33 contain the same volume (22 µl) of each fraction in which the tube of sucrose gradient was fractionated from top to the bottom. Fractions 8–9 contain B1, fractions 10–12 B2, fractions 14–16 B3, fractions 18–20 B4, fractions 24–25 B5.

References

Arnon DJ (1949) Copper Enzymes in Isolated Chloroplast Polyphenoloxydase in Beta Vulgaris. Plant Physiol. 24: 1-14

Boekema EJ, Breemen JFL, van Roon H, Dekekr JP (2000) Conformational Changes in Photosystem II

Supercomplexes upon Removal of Extrinsic Subunits. Biochemistry 39: 12907-12915

Caffarri S, Kouril R, Kereiche S, Boekema EJ, Croce R (2009) Functional Architecture of Higher Plant Photosystem II Supercomplexes. EMBO J. 28: 3052-3063

Enami I, Yoshihara S, Tohri A, Okumura A, Ohta H, Shen JR (2000) Cross-Reconstitution of Various Extrinsic Proteins and Photosystem II Complexes from Cyanobacteria, Red Alga and Higher Plant. Plant Cell Physiol. 41: 1354-1364

Eshaghi S, Andersson B, Barber J (1999) Isolation of a Highly Active PSII-LHCII Supercomplex from Thylakoid Membranes by a Direct Method. FEBS Lett. 446: 23-26

Ghanotakis DF, Topper JN, Yocum CF (1984) Structural Organization of the Oxidizing Side of Photosystem II. Exogenous Reductants Reduce and Destroy the Mn-Complex in Photosystem II Membranes Depleted of the 17 and 23 kDa Polypeptides. Biochim. Biophys. Acta 767: 524-531

Hankamer B, Nield J, Zheleva D, Boekema E, Jansson S, Barber J (1997) Isolation and Biochemical Characterization of Monomeric and Dimeric PSII Complexes from Spinach and Their Relevance to the Organisation of Photosystem II in Vivo. Eur. J. Biochem. 243: 422-429

Hashimoto A, Ettinger WF, Yamamoto Y, Theg SM (1997) Assembly of Newly Imported Oxygen Evolving Complex Subunits in Isolated Chloroplasts: Sites of Assembly and Mechanisms of Binding. Plant Cell 9: 441-452

Hewitt EJ (1966) Sand and Water Culture Methods in the Study of Plant Nutrition. In Technical Communication, no. 22, second ed., rev commonwealth AGR, Bur. London

Ido K, Ifuku K, Ishihara S, Yamamoto Y, Miyake C, Sato F (2008) Effects of the PsbP Knock-Down on the Photosynthetic Electron Transfer in Nicotiana Tabacum. In: Allen JF, Gantt E, Golbeck JH, Osmond B (eds) Energy from the Sun: 14th International Congress on Photosynthesis. Springer: Heidelberg, pp. 609-612

Ifuku K, Yamamoto Y, Ono TA, Ishihara S, Sato F (2005) PsbP Protein, but not PsbQ Protein, Is Essential for the Regulation and Stabilization of Photosystem II in Higher Plants. Plant Physiol. 139: 1175-1184

Laemmli UK (1970) Cleavage of Structural Proteins during the Assembly of the Head of Bacteriophage T4. Nature 227: 680-685

Roose JL, Wegener KM, Pakrasi HB (2007) The Extrinsic Proteins of Photosystem II. Photosynth. Res. 92: 369-387

Suorsa M, Aro EM (2007) Expression, Assembly and Auxiliary Functions of Photosystem II Oxygen-Evolving Proteins in Higher Plants. Photosynth. Res. 93: 89-100

Wang ZG, Xu TH, Liu C, Yang CH (2010) Fast Isolation of Highly Active Photosystem II Core Complexes from Spinach. JIPB 52: 793-800

Yi X, Hargett SR, Liu H, Frankel LK, Bricker TM (2007) The PsbP Protein Is Required for Photosystem II Complex Assembly/Stability and Photoautotrophy in Arabidopsis Thaliana. J. Biol. Chem. 282: 24833-24841

Compositional and Structural Analyses of the Photosystem II Isolated from the Red Alga *Cyanidioschyzon Merolae*

Joanna Kargul[a], Marko Boehm[b], Nina Morgner[c], Carol V. Robinson[c], Peter J. Nixon[b], James Barber[a,*]

[a]Division of Molecular Biosciences, Faculty of Natural Sciences, Imperial College London, London, SW7 2AZ, UK;
[b]Division of Biology, Faculty of Natural Sciences, Imperial College London, London, SW7 2AZ, UK;
[c]Department of Chemistry, Physical and Theoretical Chemistry Laboratory, University of Oxford, Oxford OX1 3QZ, UK.
[*]Corresponding author. Tel. No. +44 2075945266; Fax No. +44 2075945267; E-mail: j.barber@imperial.ac.uk.

Abstract: Members of the rhodophytan order *Cyanidiales* are unique among phototrophs in their ability to live in extremely low pH levels and moderately high temperatures. The photosynthetic apparatus of the red alga *Cyanidioschyzon merolae* represents an intermediate type between cyanobacteria and higher plants, suggesting that this alga may provide the evolutionary link between prokaryotic and eukaryotic phototrophs. While red algal PSI resembles that of the higher plants, the PSII complex is more reminiscent of the cyanobacterial ancestor in that it contains phycobilisomes as the light-harvesting system instead of Chl*a*/*b* binding proteins of green algae and higher plants, as well as the PsbU and PsbV subunits stabilising the oxygen evolving complex (OEC). The most remarkable feature of the red algal PSII is the presence of the fourth extrinsic protein of 20 kDa (PsbQ′) which is not found in the cyanobacterial OEC and which is distantly related with the green algal PsbQ. This feature together with some differences in the structural cooperation between the OEC subunits suggests that the lumenal side of red algal PSII may vary from the prokaryotic ancestor. In order to elucidate the structural differences between cyanobacterial and eukaryotic PSII, we have isolated highly active and stable dimeric complexes of the *C. merolae* PSII and subjected them to high throughput crystallization and mass spectrometry analyses. Here we report the full subunit composition and preliminary results of 3D crystallization of the dimeric *C. merolae* PSII.

Keywords: PSII structure; *Cyanidioschyzon merolae*; X-ray diffraction; Mass spectrometry

Introduction

Recently, the crystal structure of photosystem II (PSII) isolated from the thermophilic cyanobacterium *Thermosynechococcus vulcanus* has been reported at a resolution of 1.9 Å (Shen *et al*., submitted). This atomic structure has confirmed a working model for understanding the water splitting reaction based on the previous crystallographic structures of cyanobacterial PSII obtained in our laboratory (Ferreira *et al.*, 2004; Kargul *et al*., 2007; Murray *et al*., 2008a; Murray *et al*., 2008b) and others (Kamiya and Shen, 2003; Loll *et al*., 2005; Guskov *et al*., 2009; Yano *et al*., 2006). The catalytic site is composed of a Mn_4Ca-cluster surrounded by a number of highly conserved amino acids. Although the precise arrangement of the metal ions was uncertain in the available crystallographic structures of PSII (due to the resolution limitation and possible radiation modification during diffraction data collection), the model which places three Mn ions and a Ca ion at the corner of a cubane with oxo-bridges and the forth Mn linked to the cubane via a bridging oxygen has gained support in the latest atomic structure of PSII (Shen *et al*., submitted), as well as from quantum mechanical considerations (Sproviero *et al*., 2008; Dau *et al*., 2008; Siegbahn, 2009).

Although we now have a detailed structural model of PSII from cyanobacteria at an atomic resolution, no corresponding structure of the eukaryotic PSII complex has been reported to date. To this end, we

isolated and characterized PSII from the extremophilic unicellular red alga *Cyanidioschyzon merolae* aiming at structural characterization of this eukaryotic PSII complex. *C. merolae* belongs to the rhodophytan order *Cyanidiales* whose members thrive in acidic hot springs (Ciniglia *et al*., 2004), and are unique among phototrophs in the ability to live in extremely low pH levels (pH 0.2–4) and moderately high temperatures (40–56 ºC). Furthermore, *C. merolae* is considered to be one of the most primitive photosynthetic prototrophs because it diverged near the root of the red algal lineage that forms a basal group within the photosynthetic eukaryotes (Nozaki *et al*., 2003). It is well established that the oxygen evolving complex (OEC) from *C. merolae* is stabilized by 4 extrinsic lumenal subunits: cyanobacterial-like PsbV and PsbU, the evolutionary conserved PsbO subunit, and an additional 20-kDa subunit PsbQ′ exhibiting low homology with the higher plant and green algal PsbQ polypeptides (Ohta *et al*., 2003). The precise localization of this subunit and its role in stabilization of the OEC are currently unknown, although low-resolution single particle analysis and reconstitution experiments suggested that red algal PsbQ′ directly binds to CP43 of the core complex independently of other extrinsic proteins and is required for effective binding of the PsbV and PsbU subunits (Gardian *et al*., 2007; Enami *et al*., 2008). In contrast, PsbQ in higher plants functionally associates with PSII via its direct interaction with both PsbO and PsbP (reviewed in Enami *et al*., 2008). Interestingly, PsbQ′ can functionally replace PsbQ in spinach during cross-reconstitution experiments despite their low amino acid sequence homology (Enami *et al*., 2008). Moreover, it has been shown that the binding mode of PsbV differs between cyanobacteria and red alga, in that the red algal PsbV binds via other extrinsic subunits, whereas its cyanobacterial counterpart binds directly with the PSII core (reviewed in Enami *et al*., 2008). All these observations point towards significant structural differences on the lumenal side of PSII at various evolutionary stages.

The logic of working with *C. merolae* was to obtain a crystal structure of a eukaryotic form of PSII using an organism which was likely to provide a very stable form of the enzyme. Here we describe the fist steps towards the ultimate goal of obtaining the first structure of eukaryotic PSII. We demonstrate that a highly active and robust preparation of the dimeric PSII from *C. merolae* can be used to obtain 3D crystals of this complex.

Materials and Methods

Functionally active Photosystem II (PSII) has been isolated from the red alga *Cyanidioschyzon merolae,* strain N1332 (obtained from the NIES microbial culture collection). Thylakoid membranes were prepared from late-log phase cells grown in the Allen 2 medium (OD_{682} 3.5), using a modified procedure of Adachi *et al*. (2009). The cells were collected by centrifugation at 4,000 x g, washed once with buffer A (40 mmol MES-NaOH, pH 6.1, 25% w/w) glycerol, 10 mmol $CaCl_2$, 5 mmol $MgCl_2$) and resuspended in buffer A supplemented with 50 µg/ml DNAse I and the Complete™ protease inhibitor cocktail (Roche Diagnostics GmbH). Cells were broken by passing through a French Press (≈ 2000 psi) twice. Thylakoids were pelleted by centrifugation at 104,200 x g for 30 minutes at 4 °C and washed once with buffer A. The thylakoid pellets were resuspended in buffer A at a chlorophyll (Chl) concentration of 2–3 mg/ml, snap-frozen in liquid N_2 and stored at −70 °C prior to use. The dimeric PSII has been isolated by two-step anion exchange chromatography according to the modified protocol of Adachi *et al*. (2009) using the DEAE ToyoPearl 650 mol followed by DEAE ToyoPearl 650 S chromatographic media. Thylakoids (1 mg/ml Chl) were solubilized with 1.2% (w/v) dodecyl-β-D-maltoside (DDM, Biomol) by stirring in the dark at 4 ºC for 40 min. Soluble fraction was collected by centrifugation at 100,000 g for 30 min, then loaded onto the DEAE ToyoPearl 650 mol column equilibrated with buffer B (40 mmol MES-NaOH, pH 6.1, 25% (w/w) glycerol, 3 mmol $CaCl_2$, 0.03% (w/w) DDM). The immoblized crude PSII was washed with the wash buffer (40 mmol MES-NaOH, pH 6.1, 25% (w/w) glycerol, 3 mmol $CaCl_2$, 0.09 mol NaCl, 0.03% (w/v) DDM), then eluted with Elution 1 buffer (40 mmol MES-NaOH, pH 6.1, 25% (w/w) glycerol, 3 mmol $CaCl_2$, 0.23 mol NaCl, 0.03% (w/v) DDM), and dialysed against buffer A supplemented with 0.03% DDM overnight at 4 ºC in the dark. Dialysed crude PSII was loaded onto the DEAE ToyoPearl 650 S column (equilibrated with buffer A + 0.03% (w/v) DDM) to separate the PSII monomers and dimers using a continuous gradient of 0.05–0.15 mol NaCl. The PSII dimer fractions were pooled and concentrated using the VivaSpin-20 (Sartorius Stedim

Biotech) concentrating devices to at least 3 mg/ml Chl. Functional activity of purified thylakoids and PSII dimers (5 µg Chl) was measured using a Clark-type electrode (Hansatech). Measurements were performed at 30 ºC in buffer A in the presence of 0.125 mmol 2,6-dichloro-*p*-benzoquinone (DCBQ) and 2.5 mmol potassium ferricyanide as the exogenous electron acceptors, using white light illumination intensity of 6,000 µE. In addition, samples have been biochemically analysed by size exclusion chromatography, SDS-PAGE, and mass spectrometry, using standard procedures. The highly active and pure dimeric PSII was subjected to extensive 3D crystallisation trials using a Mosquito nano-litre high throughput robot (TTP Labtech) and 14 commercially available screens pre-dispensed into 96 well MRC plates.

Results and Discussion

We set out to purify a highly active, intact and homogenous preparation of the *C. merolae* dimeric PSII that would be suitable for 3D crystallization trials. Following solubilisation of thylakoids with the detergent (dodecyl-β-D-maltoside, DDM) we separated PSII monomers and dimers using a 2-step anion exchange chromatography approach (see Fig. 1). In the second step, we purified a robust and highly active PSII dimer preparation (yield 3.5%) that was stable for up to 24 h of incubation at an ambient temperature (see Fig. 2b). The homogeneity of the sample was verified by size-exclusion chromatography which showed a single elution peak with the retention time corresponding to the PSII dimer (data not shown). The oxygen evolving activity varied between 3200–4300 µmoles O_2/mg Chl/h for different preparations tested. It was the highest recorded oxygen evolving activity obtained under our experimental conditions, and exceeded the activity of PSII isolated from the thermophilic cyanobacterium *Thermosynechococcus elongatus* used to obtain the X-ray structure of PSII (Ferreira *et al*., 2004). Moreover, this preparation retained its oxygen evolving activity when illuminated with high light intensities (up to 13,000 µE, see Fig. 2a), indicating that the oxygen evolving complex remained intact when subjected to a high light stress.

We analysed the subunit composition of the purified *C. merolae* PSII dimer by biochemical and mass spectromentry approaches. Table 1 and Fig. 3a show that the reaction centre subunits (D1, D2), inner antenna subunits (CP43, CP47), four extrinsic subunits stabilizing the OEC (PsbO, PsbU, PsbV, PsbQ′), and small intrinsic subunits were present in our preparation. Interestingly, our mass spectrometry analysis showed the presence of the PSII auxiliary subunits Psb27 and Psb28 implied in the regulation of the PSII repair cycle and biogenesis (Nowaczyk *et al.*, 2006; Dobáková *et al*., 2009). However, their stoichiometry of binding to PSII is presently unknown.

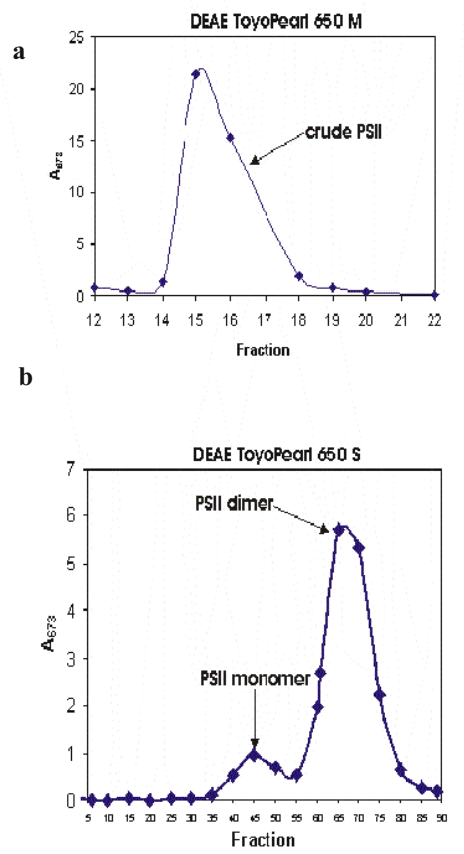

Fig. 1 Purification of the *C. merolae* PSII.
PSII was purified using two-step anion exchange chromatography. In the first step (a), crude PSII was purified which was subsequently separated into PSII monomer and dimer fractions (b).

Having obtained a highly robust and homogenous preparation of the *C. merolae* dimeric PSII we used it for extensive crystallization trials aiming at obtaining well-diffracting 3D crystals of this eukaryotic PSII. Initially, we tried to manually reproduce crystallization conditions that were successfully used to obtain crystals of PSII from *T. elongatus* (Ferreira *et al*., 2004) and a related red alga *Cyanidium caldarium* (Adachi *et al*., 2009). These conditions did not yield any crystals when the dimeric *C. merolae* PSII was used. To search for alternative

conditions, we have performed high throughput robot-based screening using 14 commercially available crystallizations screens. In this approach, we identified 9 conditions which yielded 3D crystals (see Fig. 3b) with some diffracting properties (data not shown). Work is under way to optimize these conditions in order to produce crystals with improved X-ray diffraction characteristics.

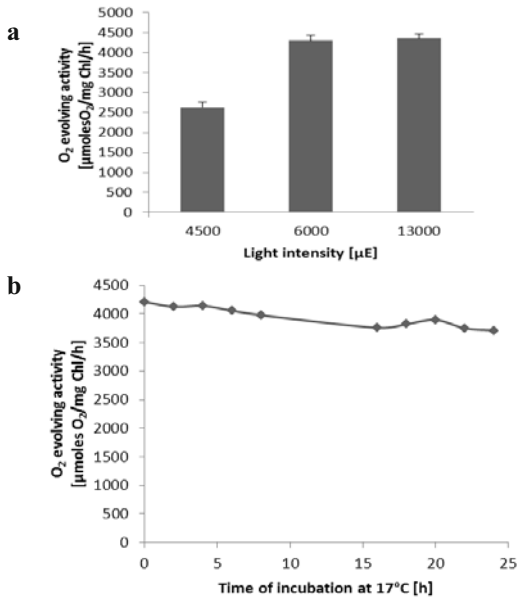

Fig. 2 Stability of purified *C. merolae* PSII.
Activity of PSII dimers was measured at various light intensities (a) or as a function of time over a 24 h period of incubation at 17 ºC in the dark (b). Oxygen evolving activity of PSII was measured at 30 ºC in the presence of 0.125 mmol DCBQ and 2.5 mmol ferricyanide as the exogenous electron acceptors.

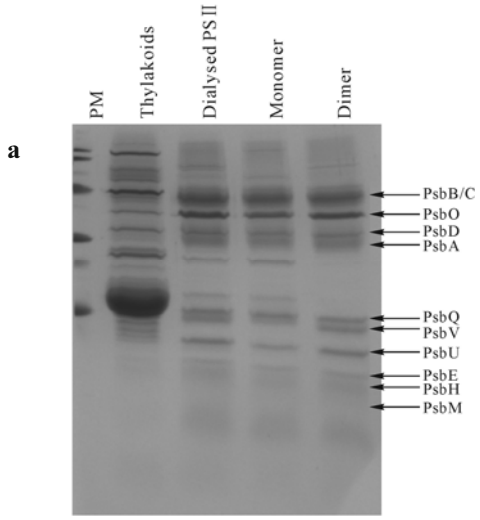

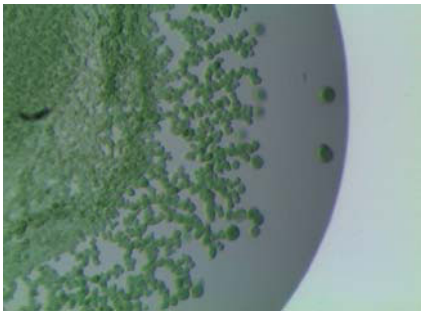

Fig. 3 High-throughput screening of crystal-forming conditions using the *C. merolae* PSII dimmer.
(a) Sitting drops of 200 nl were set up at 4 ºC or 20 ºC by mixing a PSII dimer sample (1.4 mg Chl/ml) and mother liquor of 14 various crystallization screening kits (96 conditions per kit). (b) SDS-PAGE analysis of the *C. merolae* PSII dimer subunits. Proteins (5 ug Chl/lane) were separated on a 15% polyacrylamide gel, then visualized by Coomassie staining. PM, prestained marker. The PSII subunits are arrowed on the right-hand side of panel a.

Table 1 LC/MS and MS/MS analysis of protein composition of the *C. merolae* dimeric PSII.

Protein subunit	Calculated mass from database	No. of peptides	Experimental mass
PsbA	39706	3	39218
PsbB	56300	6	56218
PsbC	51912	7	50410
PsbD	39290	3	37910
PsbE	9094	2	9084
PsbF	4706	2	4504
PsbH	7220	3	6644
PsbI	4475	3	4473
PsbJ	3991	2	3865
PsbK	4895	2	4867
PsbL	4382	1	4298
PsbM	16126	3	16054
PsbN	4725	1	4688
PsbO	35454	12	34757
PsbQ′	23622	5	23504
PsbT	3791	2	3769
PsbU	16847	6	16673
PsbV	16609	2	16350
Psb28	12580	2	12466
PsbX	4592	1	4376
PsbY	3926	2	3921
ycf12	3792	1	3732
PsbZ	6484	1	6396
Psb27	22017	3	21845

Acknowledgement

JK, MB, JB and PN acknowledge the support of EPSRC (grant EP/F00270X/1) to conduct this work.

References

Adachi H, Umena Y, Enami I, Henmi T, Kamiya N, Shen JR (2009) Towards Structural Elucidation of Eukaryotic Photosystem II: Purification, Crystallization and Preliminary X-Ray Diffraction Analysis of Photosystem II from a Red Alga. Biochim. Biophys. Acta 1787: 121-128

Ciniglia C, Yoon HS, Pollio A, Pinto G, Bhattacharya D (2004) Hidden Biodiversity of the Extremophilic Cyanidiales Red Algae. Mol. Ecol. 13: 1827-1838

Dau H, Grundmeier A, Loja P, Haumann M (2008) On the Structure of the Manganese Complex of Photosystem II: Extended-Range EXAFS Data and Specific Atomic-Resolution Models for Four S-States. Philos Trans R Soc Lond B Biol Sci. 363: 1237-1243

Dobáková M, Sobotka R, Tichý M, Komenda J (2009) Psb28 Protein Is Involved in the Biogenesis of the Photosystem II Inner Antenna CP47 (PsbB) in the Cyanobacterium Synechocystis sp. PCC 6803. Plant Physiol. 149: 1076-1086

Enami I, Okumura A, Nagao R, Suzuki T, Iwai M, Shen JR (2008) Structures and Functions of the Extrinsic Proteins of Photosystem II from Different Species. Photosynth. Res. 98: 349-363

Ferreira KN, Iverson TM, Maghlaoui K, Iwata S, Barber J (2004) Architecture of the Photosynthetic Oxygen-Evolving Center. Science 303: 1831-1838

Gardian Z, Bumba L, Schrofel A, Herbstova M, Nebesarova J, Vacha F (2007) Organisation of Photosystem I and Photosystem II in Red Alga Cyanidium Caldarium: Encounter of Cyanobacterial and Higher Plant Concepts. Biochim. Biophys. Acta 1767: 725-731

Guskov A, Kern J, Gabdulkhakov A, Broser M, Zouni A, Saenger W (2009) Cyanobacterial Photosystem II at 2.9-A Resolution and the Role of Quinones, Lipids, Channels and Chloride. Nat. Struct. Mol. Biol. 16: 334-342

Kamiya N, Shen JR (2003) Crystal Structure of Oxygen-Evolving Photosystem II from Thermosynechococcus Vulcanus at 3.7-A Resolution. Proc. Natl Acad. Sci. 100: 98-103

Kargul J, Maghlaoui K, Murray JW, Deak Z, Vass I, Boussac A, Rutherford AW, Barber J (2007) Purification, Crystallization and X-Ray Diffraction Analyses of the T. Elongatus PSII Core Dimer with Strontium Replacing Calcium in the Oxygen-Evolving Complex. Biochim. Biophys. Acta 1767: 404-413

Loll B, Kern J, Saenger W, Zouni A, Biesiadka J (2005) Towards Complete Cofactor Arrangement in the 3.0 A Resolution Structure of Photosystem II. Nature 438: 1040-1044

Murray JW, Maghlaoui K, Kargul J, Ishida N, Lai T-L, Rutherford AW, Sugiura M, Boussac A, Barber J (2008a) X-Ray Crystallography Identifies Two Chloride Binding Sites in the Oxygen Evolving Centre of Photosystem II. Energy Environ. Sci. I: 161-166

Murray JW, Maghlaoui K, Kargul J, Sugiura M, Barber J (2008b) Analysis of Xenon Binding to Photosystem II by X-ray Crystallography. Photosynth. Res. 98: 523-527

Nowaczyk MM, Hebeler R, Schlodder E, Meyer HE, Warscheid B, Rögner M (2006) Psb27, a Cyanobacterial Lipoprotein, Is Involved in the Repair Cycle of Photosystem II. Plant Cell 18: 3121-3131

Nozaki H, Matsuzaki M, Takahara M, Misumi O, Kuroiwa H, Hasegawa M, Shin-i T, Kohara Y, Ogasawara N, Kuroiwa T(2003) The Phylogenetic Position of Red Algae Revealed by Multiple Nuclear Genes from Mitochondria-Containing Eukaryotes and an Alternative Hypothesis on the Origin of Plastids. J. Mol. Evol. 56: 485-497

Ohta H, Suzuki T, Ueno M, Okumura A, Yoshihara S, Shen JR, Enami I (2003) Extrinsic Proteins of Photosystem II: an Intermediate Member of PsbQ Protein Family in Red Algal PSII. Eur. J. Biochem. 270: 4156-4163

Siegbahn PE (2009) Structures and Energetics for O_2 fFormation in Photosystem II. Acc Chem Res. 42: 1871-1880

Sproviero EM, Shinopoulos K, Gascón JA, McEvoy JP, Brudvig GW, Batista VS (2008) QM/MM Computational Studies of Substrate Water Binding to the Oxygen-Evolving Centre of Photosystem II. Philos. Trans. R Soc. Lond. B Biol. Sci. 363: 1149-1156

Yano J, Kern J, Sauer K, Latimer MJ, Pushkar Y, Biesiadka J, Loll B, Saenger W, Messinger J, Zouni A, Yachandra VK. (2006) Where Water Is Oxidized to Dioxygen: Structure of the Photosynthetic Mn_4Ca Cluster. Science 314: 821-825

The Position and Orientation of Active Carotenoid in Photosystem II

Asako Kawamori[a*], Hiroyuki Mino[b], Jianren Shen[c]

[a]AGAPE-Kabutoyama Institute of Medicine, [b]Department of Physics Nagoya University and
[c]Department of Biology Okayama University, Japan.
[*]Corresponding author. Tel./Fax No. +81 798 61 8402; E-mail: agape-kawa@nifty.com.

Abstract: The distances between Y_D and active carotenoid have been determined in cyanobacterium (*synecochoccus vulcanus*) and spinach PSII by pulsed electron double resonance (PELDOR). The observed spectra were analyzed taking into spin distribution of over 30 carbon atoms in the carotenoid molecule. The result of simulations based on the recent crystal structure fitted well with the spectra. The observed spectra for spinach PSII was different, showing the crystal structure of spinach PSII is slightly different from that of cyanobacteria. The ELDOR spectra of Y_D-Y_Z radical pair were observed in a cyanobacterium. The result showed the different distance from Spinach PSII.

Keywords: PSII; Carotenoide; Y_D; Y_Z; Structures; PELDOR

Introduction

Electron Transfer in Photosystem II is inhibited at the low temperatures below 250 K. In a normal photosystem water provides electrons to P680 via Mn_4 complex and tyrosine Z by illumination of PS II at physiological temperature. When cytochrome b559 is oxidized, Chlorophyll D and Z, one of the carotenoids provide an electron to oxidized P680 (Lakshmi *et al.*, 2003). There are the same chlorophyll and the carotenoid in D1 and D2 proteins. Which Chlorophyll or which Carotenoid worked as an electron donor has not yet been clarified. In this report we present the result of PELDOR (Pulsed ELectron DOuble Resonance) with Y_D to determine the active site of Carotenoid in Cyanobacterium and Spinach. To analyze the PELDOR spectra we use the derived distance between Y_D and Carotenoid from recently reported crystal data (Loll *et al.*, 2005).

ENDOR (Electron Nuclear DOuble Resonance) study of trapped carotenoid radical in Spinach showed hyperfine interaction over the carbon atoms (Fallers *et al*., 2001). From these data spin distribution on each carbon atom was determined (Guo *et al*., 2002) To compare the structure of PSII in spinaches PELDOR of Y_D and Y_Z was observed in a cyanobacterium.

Sample Preparation and Experiment

Cyanobacteria (*synecochoccus vulcanus*) PSII were prepared (Shen *et al.*, 1994). To remove Mn-cluster the particles were incubated with 0.5 mmol NH_2OH and then washed twice to remove remained NH_2OH. 1mmol ferricyanide is added to oxidize Cytochrome b559. The same treatment was applied to remove Mn-cluster in Spinach PSII. Light illumination were applied for both PSII samples for 1 minutes and dark adapted about 10 min. at 273 K to restore Y_D radical. To produce Carotenoid radical light illumination of PSII in the cavity was applied at 20 K about 5 min. Y_Z radical was trapped at 77 K soon after illumination at 253 K.

EPR and PELDOR of Y_D and Carotenoid radicals were observed at 10 K using Bruker ESP300E X-band spectrometer. Both spectra were overlapping. We observed Y_D radical, together with Carotenoid radical at 9.7 GHz and excited Carotenoid radical including

Y_D radical at 9.6 GHz. Principle of PELDOR is shown in Fig. 1 (a) for dipolar interacting radical pair and (b) applied pulse sequences. Fig. 2 shows the PELDOR signal first observed for Y_D and trapped Y_Z radicals in spinach PSII (Astashkin *et al.*, 1994). In this case the same frequency for ω_1 and ω_2 was applied (2+1 pulse method).

The observed PELDOR signal for YD and carotenoid in cyanobacterium and spinach are shown in Fig. 3 and in Fig. 4 respectively.

Results and Discussion

For analysis of PELDOR spectra simulation based on the following equations were applied

On the first time we estimated the distance by a point dipole approximation. The distance from Y_D to the center of carotenoid was 31 Å in cyanobacteria and 33 Å in Spinach PSII. The derived value was different from X-ray data of 28.5 Å. Then we applied distances and spin densities of 30 carbon atoms on Eqs. (1) and (2).

$$M_y(t) = \iint \sin\theta_B d\theta_B \phi_B \cos[\omega(\theta_B)t] \quad (1)$$

$$\hbar\omega(\theta_B) = \Sigma\gamma_1\gamma_2\beta^2 P_i(3\cos^2\theta_1 - 1)/r_1^3 \quad (2)$$

$$i = 1, 30$$

r_i Distance between tyrosine and i-th carbon atom.
P_i Spin projection (density) on the i-th carbon in carotenoid molecule shown in Fig. 4.

Table 1 The derived values of distances along crystalline axes (a, b, c) taken from Loll *et al.* (2005) and spin densities ρ of three carbon atoms No1, 15 and 1' taken from Guo *et al.*(2002).

Center of Y_D position				
a		b		c
3.7926		43.5974		50.0364
Y_D-Car(D2)$_i$				
a	b	c	r	ρ
C_1 -7.5756	24.9406	2.7786	26.2134	-0.05
C_{15} 8.0504	28.5396	7.1286	30.6298	0.04
$C_{1'}$ 5.1474	28.4306	8.0386	29.9902	-0.05

In Table 1 the center of Y_D molecule and the distances from both end and the center of carotenoid are shown based on Loll *et al.* (2005).

Fig. 7 shows PELDOR spectra for Y_D and Y_Z radical pair in a Cyanobacterium. The estimated distance using a point dipole approximation is 33 Å.

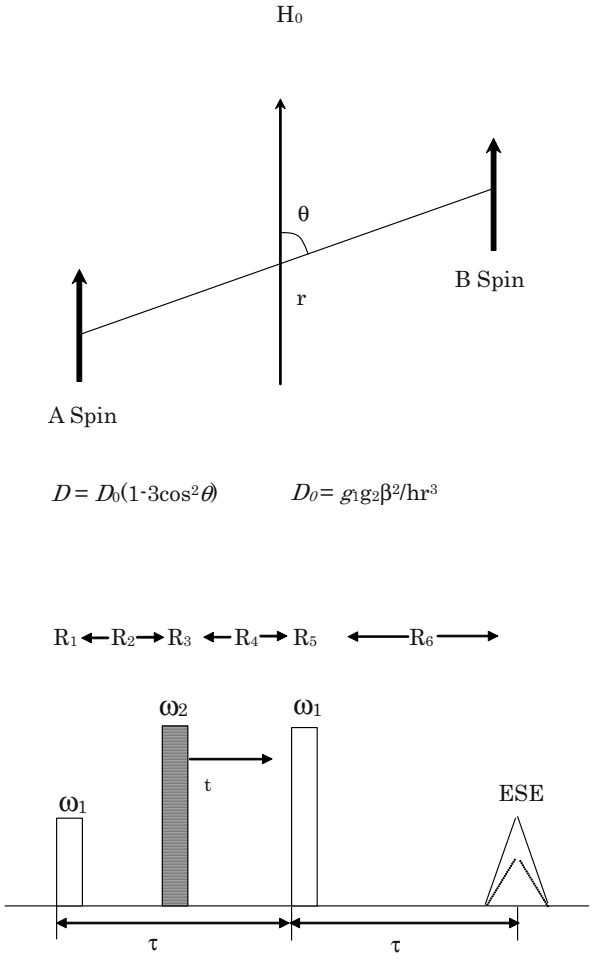

Fig. 1 Dipolar interaction between a radical pair A spin and B spin shown in the above. Pulse sequence shown below the first and the third pulses make up ESE (Electron Spin Echo) of A spin and the second pulse turns the direction of B spin, resulting a decrease of ESE intensity because of change of the local field at the A spin site. ω_1 is the resonance frequency of A spin and ω_2 is that of B spin.

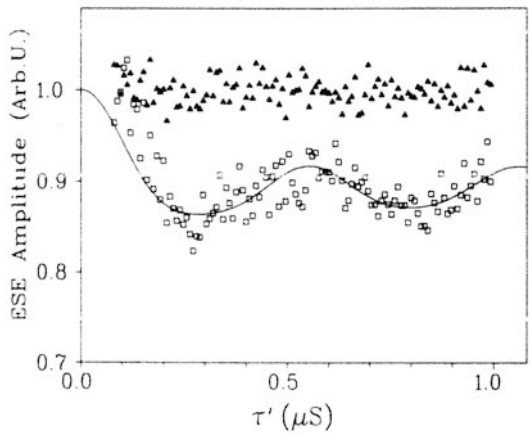

Fig. 2 The observed ESE signal intensity for change of τ'(the application time of the second pulse). Closed triangles show the intensity with no Y_Z radical, and open squares show that with Y_Z radical trapped in Spinach PSII.

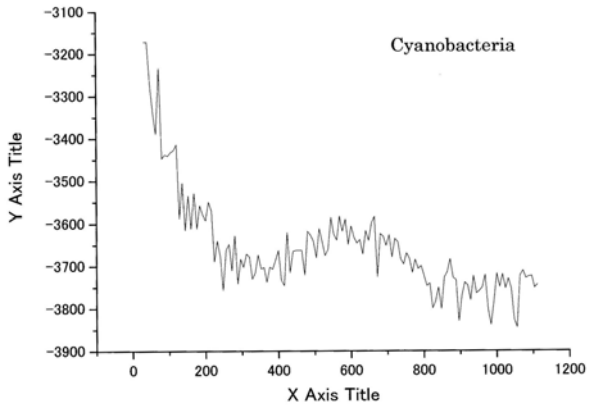

Fig. 3 PELDOR spectra of cyanobacterium. The derived frequency was 1.7 MHz.

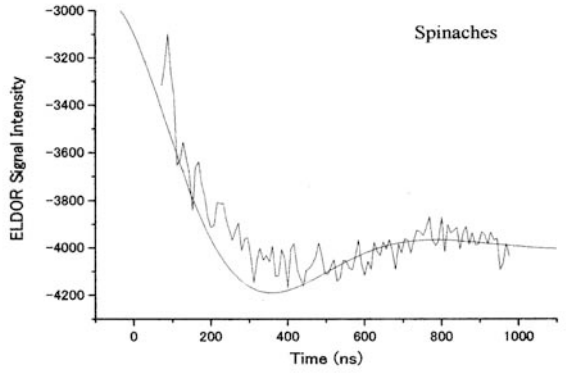

Fig. 4 PELDOR spectra of Spinaches. The derived frequency was 1.4 MHz.

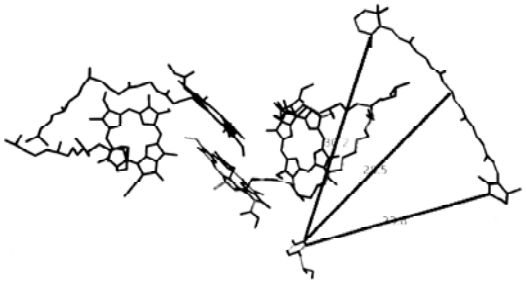

Fig. 5 A part of crystal structure showing Y_D and carotenoid in D2 protein taken from Loll *et al.* (2005).

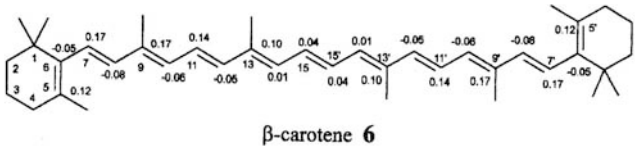

Fig. 6 The molecular structure of carotene with numbering carbon atoms and spin densities shown by Guo *et al.* (2002).

PELDOR for Spinaches PSII shown in Fig. 2 indicates about 30 Å distance.

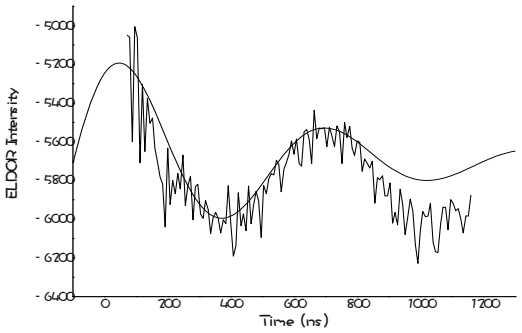

Fig. 7 PELDOR spectra obtained for Y_D and Y_Z radical in a cyanobacterium.

In conclusion the distances for Spinach PSII are not same as those for cyanobacteria.

References

Astashkin AV, Kodera Y, Kawamori A (1994) Distance between Tyrosine Z^+ and D^+ in Plant Photosystem II Biochim. Biophys. Acta 1187: 89-93

Guo JD, Luo Y, Himo F (2002) Density Functional Theory Study of the Canthaxanthin and Other Carotenoid Radical Cations. Chem. Phys. Lett. 366: 73-81

Fallers P, Maly T, Rutherford AW, MacMillan F (2001) Chlorophylls and Carotenoid Radicals in Photosystem II Studied by Pulsed ENDOR. Biochemistry 40: 320-326

Lakshmi KV, Poluektov OG, Reifler MJ, Wagner AM, Thurnauer MC, Brudvig GW (2003) Pulsed High-Frequency EPR Study on the Location of Carotenoidand Chlorophyll Cation Radicals in Photosystem II. J. Am. Chem. Soc. 125: 5005-5014

Loll B, Kern J, Saenger W, Zouni A, Biesiadka J (2005) Towards Complete Cofactor Arrangement in the 3.0 Å Resolution Structure of Photosystem II. Nature 438: 1040-1044

Shen JR, Inoue Y (1993) Binding and Functional Properties of Two New Intrinsic Components, Cytochrome c_{550} and as 12kDa Protein,in Cyanobacterial Photsystem II. Biochemistry 32: 1825-1832

Functional Roles of the Amino- and Carboxyl-Regions of PsbP Protein in Photosystem II

Shusuke Kakiuchi[a], Kentaro Ifuku[a, b,*], Megumi Tomita[c], Kunio Ido[a], Takumi Noguchi[c, d], Fumihiko Sato[a]

[a]Graduate School Biostudies, Kyoto University, Kyoto 606-8502, Japan;
[b]PRESTO, Japan Science and Technology Agency (JST), Saitama 332-0012, Japan;
[c]Institute of Materials Science, University of Tsukuba, Ibaragi 305-8573, Japan;
[d]Graduate School Science, Nagoya University, Aichi 464-8602, Japan.
[*]Corresponding author. Tel. No. +81-75-753-6381; Fax No. +81-75-753-6398; E-mail: ifuku@kais.kyoto-u.ac.jp.

Abstract: The PsbP protein of photosystem II (PSII) regulates the binding properties of Ca^{2+} and Cl^{-}, indispensable cofactors for water-splitting reaction, and stabilizes the Mn cluster. It was reported that amino (N)-terminal sequence of PsbP is important for the ion retention in PSII [Ifuku et al., Photosynth. Res. 2005, 84: 251-255], while molecular function of the carboxyl (C)-terminal domain of PsbP has not been characterized. In this study, we investigated function of the C-terminal domain of PsbP by site-directed mutagenesis based on the crystal structure. Among the mutated PsbP investigated, PsbP-H144A with the substitution of conserved His144 to Ala showed significantly lower ability to recover the activity of NaCl-treated PSII membranes, whereas PsbP-H144A could bind to PSII in a manner similar to wild-type protein. This His144 residue coordinates Zn^{2+} in the crystal structure of spinach PsbP (PDB ID: 2VU4), while exact functional role of His144 in PSII remains to be elucidated. Our results suggest that both of the amino- and the carboxyl-terminal regions of PsbP are important for ion-retention within PSII.

Keywords: Extrinsic protein; Oxygen-evolving complex; Photosystem II; PsbP

Introduction

The extrinsic subunits of photosystem II (PSII) in the lumenal side of thylakoids play crucial roles in optimizing the water-oxidizing activity. Green plants, such as higher plants, green algae, and euglena, have a set of three extrinsic proteins (PsbO (33 kD), PsbP (23 kD), and PsbQ (17 kD) (Bricker and Burnap, 2005). PsbO is responsible for the stable binding of the Mn cluster (Seidler, 1996), PsbP is involved in retention of Ca^{2+} and Cl^{-}, essential cofactors for PSII activity, and PsbQ mainly participates in Cl^{-} retention in PSII. However, molecular mechanisms behind their functions, particularly those of PsbP and PsbQ, were not clarified.

Recent light-induced Fourier transform infrared (FTIR) difference spectroscopy analysis demonstrates the relation between the protein conformation change around the Mn cluster and the PsbP binding (Tomita *et al*., 2009): Removal of PsbP causes the protein conformation change around the Mn cluster, and the PsbP reconstitution to PSII recover this conformational change. Furthermore, the N-terminal region of PsbP is required to induce the recovery of this change. Since the N-terminal truncated PsbP (Δ15) did not show the activation of oxygen evolution at all (Ifuku *et al*., 2005), the result in FTIR indicates that the interaction of N-terminal of PsbP with PS II induces the protein conformation change required for Ca^{2+} and Cl^{-} retention in PS II. The C-terminal structure of PsbP is also likely to interact with PSII; however, its functional role has not been characterized.

In this study, we characterized three PsbP mutants to investigate function of the C-terminal domain of PsbP: PsbP-H144A (H144A), PsbP-D165V (D165V), and PsbP-E177V (E177V) with the substitution of conserved His144 to Ala, Asp165 to Val, and Glu177 to Val, respectively. These residues are in the vicinity of the Zn^{2+} binding site in the spinach PsbP crystal structure (PDB-ID: 2VU4) and it is possible that these

residues might have function in ion retention in PSII. Finally, we conclude that His144 in PsbP is important for Ca^{2+} and Cl^- retention in PS II.

Materials and Methods

Spinach leaves used to prepare PSII membranes (BBY) were purchased at the local market. PSII membranes were prepared basically as reported previously (Berthold *et al*., 1981).

PsbP-WT, PsbQ, and Δ15 proteins were expressed in *E. coli* and purified as previously reported (Ifuku and Sato, 2001). The expression plasmids for the mutated PsbP proteins, H144A, D165V and E177V, were constructed by using a site-directed mutagenesis kit (Stratagene) with the designed primer 5′-GGTGATGAGGGTGGAAAAGCCCAAGTAATTG CAGCGACTG-3′, 5′-GCTCAAGCTGGAGTCAAG AGATGGTTC-3′, 5′- GCTAAGAAGTTTGTCGTG AGTGCTACCAGTTC-3′, and their complementary primers, respectively.

Reconstitution of the extrinsic proteins to the NaCl-washed PSII membranes and the measuring of O_2 evolution were performed basically by the procedure reported elsewhere (Ifuku and Sato, 2001) with slight modification: 1 mol betaine instead of 0.4 mol sucrose was added to the buffers for the reconstitution and the activity measurements in order to stabilize the interaction of the extrinsic proteins and the NaCl-washed PSII membranes.

The chlorophyll concentration was calculated from the equations reported in (Arnon, 1949). SDS-PAGE was done by the standard procedure and the gel was stained by Flamingo (Bio-Rad) and visualized by Fluoro image analyzer FLA-3000 (FUJIFILM). The protein amounts bound to PSII were determined by measuring the fluorescence intensity with the software, Multi Gauge Ver2.2 (FUJIFILM).

Results and Discussion

Functions of the mutated PsbP proteins were investigated by conventional release-reconstitution experiments (Fig. 1). The protein amounts bound to PSII were similar between the wild-type (WT) and the C-terminal mutated PsbP proteins. However, the H144A protein showed lower ability to support oxygen-evolution than WT, while other mutants, D165V and E177V, showed similar ability to support the oxygen-evolution when compared to WT. These data indicate that His144 in PsbP should have an important role for Ca^{2+} and Cl^- retention in PSII.

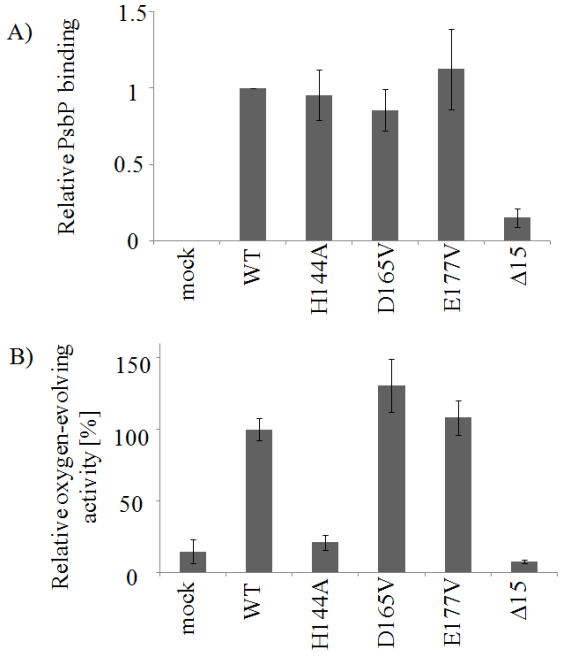

Fig. 1 (A) Relative binding of WT, H144A, D165V, E177V and Δ15 PsbP proteins to NaCl-washed PSII membranes. The amount of PsbP in WT sample was taken as 1. (B) Relative oxygen-evolving activities of NaCl-washed PSII membranes reconstituted with WT, H144A, D165V, E177V and Δ15. The oxygen-evolving activity in WT sample was taken as 100%. The PsbP proteins-to-PSII ratio was 2:1 in reconstitution experiments. The relative PsbP binding and the oxygen-evolving activity were analyzed in the buffer (25 mmol MES, pH 6.5, 1 mol betaine) without addition of Ca^{2+} and Cl^-.

Previous report suggested that 15 residues of the N-terminus of PsbP was important for Ca^{2+} and Cl^- retention in PS II, while these N-terminal residues were not essential for the binding of PsbP to PS II (Ifuku *et al*., 2005). However, In Fig. 1, both the amount of bound protein in PSII and the ability to support oxygen-evolution were significantly lower in a truncated PsbP lacking N-terminal 15 residues (Δ15) than in WT, indicating that the N-terminal of PsbP was essential for the binding of PsbP to PSII. This inconsistency is due to the difference in the amount of protein used for the reconstitution experiments; the PsbP-to-PSII ratio was 2:1 in this study, while 10:1 in the previous experiment. This suggests that the truncation of N-terminal residues of PsbP largely lowers the binding affinity of PsbP to PSII. In contrast, H144A protein had lower ability to support oxygen-

evolution even though the binding amount of H144A to PSII was equal to that of WT. This suggests that the effect of the H144A mutation on PsbP function is different from that caused by the N-terminal truncation.

Circular dichroism spectra and tryptophan fluorescence spectra of WT and H144A were analyzed and compared to detect the possible conformational change causing the functional defect of H144A. However, all parts of these spectra were similar between WT and H144A, indicating that the disruption of overall structure did not occur in H144A (data not shown). Therefore, the functional defect of H144A would be the result of missing crucial residue for ion retention or that of a minor change in a conformation that could not be detected by our spectrophotometry.

Recently, the Zn^{2+} binding site was found near His144 in C-terminal domain of spinach PsbP structure (PDB ID: 2VU4) (Kohoutová *et al*., 2009). It was suggested that PsbP might bind Mn^{2+} to act as a reservoir capable of binding and delivering manganese to the OEC (Bondarava *et al*., 2005, 2007). It was also speculated that the Zn^{2+} binding sites in the crystal structures might be physiological Mn^{2+} or Ca^{2+} binding site *in vivo*, and Zn^{2+} is present as an artifact of crystallizing condition. We then performed the ICP-MS analysis and confirmed that a recombinant PsbP was purified exclusively as metal-free from *E. coli*. (data not shown). Besides, Mn^{2+}-binding of PsbP was not detected by atomic absorption spectroscopy after gel-filtration of the PsbP/Mn^{2+} mixture (Kakiuchi, unpublished). Therefore, it is unlikely that PsbP by itself binds those metal ions with high affinity. We do not exclude the possibility that His144 is directly involved in the retention of Ca^{2+} in PSII. However, the D165V and E177V mutations near the Zn^{2+} binding site of PsbP do not affect the ion-retention activity of PsbP at all (Fig. 1). This suggests that His144 likely has a structural role and the H144A mutation may cause a minor structural change in PsbP and alter the interaction between PsbP and PSII. In fact, our preliminary FTIR analysis suggested that reconstitution of the H144A protein to NaCl-washed PSII did not recover of the conformational change around the Mn cluster as observed for Δ15 (data not shown).

In summary, our present study suggests that both of the N- and C-terminal regions of PsbP independently interact with other PSII subunits, and that both domains of PsbP are required to keep a proper protein conformation of PSII required for the stable Ca^{2+} and Cl^{-} retention for the water splitting reaction.

Acknowledgements

We thank Dr. K Ochiai and Dr. K Kuroda in Kyoto University. for their help in the metal analyses. This work was supported partially by the grant from JST PRESTO (to Ke I) and by Grant-in-Aid for Young Scientists (B) from JSPS (grant no. 18770032 to Ke.I.)

References

Arnon DI (1949) Copper Enzymes in Isolated Chloroplast. Polyphenol Oxidase in Beta Vulgaris. Plant Physiol. 24: 1-15

Berthold DA, Babcock GT, Yocum CF (1981) A Highly Resolved Oxygen-Evolving Preparation from Spinach Thylakoid Membranes. FEBS Lett. 134: 231-234

Bondarava N, Beyer P, Krieger-Liszkay A (2005) Function of the 23 kDa Extrinsic Protein of Photosystem II. Biochim. Biophys. Acta 1708: 63-70

Bondarava N, Un S, Krieger-Liszkay A (2007) Manganese Binding to the 23 kDa Extrinsic Protein of Photosystem II. Biochim. Biophys. Acta 1767: 583- 588

Bricker TM, Burnap RL (2005) The Extrinsic Proteins of Photosystem II. In: Wydrzynski T, Satoh K (eds), Photosystem II: the Light-Driven Water: Plastoquinone Oxidoreductase. Springer: Dordrecht, pp. 95-120

Ifuku K, Nakatsu T, Shimamoto R, Yamamoto Y, Ishihara S, Kato H, Sato F (2005) Structure and Function of the PsbP Protein of Photosystem II

Ifuku K, Sato F (2001) Importance of the N-Terminal Sequence of the Extrinsic 23 kDa Polypeptide in Photosystem II in Ion Retention in Oxygen Evolution. Biochim. Biophys. Acta 1546: 196-204

Ifuku K, Sato F (2002) A Truncated Mutant of the Extrinsic 23-kDa Protein that Absolutely Requires the Extrinsic 17-kDa Protein for Ca^{2+} Retention in Photosystem II. Plant Cell Physiol. 43: 1244-1249

Kohoutová J, Kutá Smatanová I, Brynda J, Lapkouski

M, Revuelta JL, Arellano JB, Ettrich R (2009) Crystallization and Preliminary Crystallographic Characterization of the Extrinsic PsbP Protein of Photosystem II from Spinacia Oleracea, Acta Crystallogr. Sect. F Struct. Biol. Cryst. Commun. 65: 111-115

Seidler A (1996) The Extrinsic Polypeptides of Photosystem II. Biochim. Biophys. Acta 1277: 35-60

Tomita M, Ifuku K, Sato F, Noguchi T (2009) FTIR Evidence that the PsbP Extrinsic Protein Induces Conformational Change around the Oxygen-Evolving Mn Cluster in Photosystem II. Biochemistry 48: 6318-6325

A New Value for the Redox Potential of Cytochrome *c*550 in Photosystem II from *Thermosynechococcus Elongatus*

Fernando Guerrero[a,b], Arezki Sedoud[b,c], Diana Kirilovsky[b,c], A William Rutherford[b,c], Mercedes Roncel[a], José M Ortega[a,*]

[a]Instituto de Bioquímica Vegetal y Fotosíntesis, Universidad de Sevilla-CSIC, Américo Vespucio 49, 41092 Sevilla, Spain; [b] Commissariat à l'Energie Atomique, Institut de Biologie et Technologies de Saclay (iBiTec-S), 91191 Gif-sur-Yvette, France and [c]Centre National de la Recherche Scientifique, URA 2096, 91191 Gif-sur-Yvette, France.
*Corresponding author: Tel. No. 34 954489573; Fax No. 34 954460065; E-mail: ortega@us.es.

Abstract: Cytochrome *c*550 (cyt *c*550), which is one of the extrinsic proteins of photosystem II (PSII), is only present in cyanobacteria and red algae. Although this cytochrome has been reported to stabilize the binding of Ca^{2+} and Cl^- ions, which are essential for activity of PSII, the specific function of heme is not yet clear. The reported negative values of the midpoint redox potential (E_m) of cyt *c*550 (–300 mV in the soluble state and –80 mV when associated with PSII) appear to be incompatible with a redox function in PSII. It has been reported that the E_m of Q_A in PSII-enriched membranes was affected by the presence of redox mediators at low ambient potentials. We have carried out new measurements of E_m of cyt *c*550 associated to PSII changing the type and number of redox mediators used. We have determined that the E_m of cyt *c*550 is about +200 mV in the absence of mediators or in the presence of a very limited number of mediators. Our results suggest that the highly reducing conditions reached in the presence of mediators, favor the reduction of a PSII component, most likely the Mn cluster, thereby inducing alterations in protein, the heme environment and consequently the E_m of the heme. The new value of E_m of cyt *c*550 opens the possibility of a redox function for this protein.

Keywords: Cytochrome *c*550; Photosystem II; Redox potential

Introduction

In green algae and higher plants, three extrinsic proteins are associated to reaction center (RC) in water-splitting active PSII complexes: 23–24 kDa, 16–18 kDa and 33 kDa proteins, while in cyanobacteria, red algae and some other eukaryotic algae, cyt *c*550, 12 kDa and 33 kDa proteins are found. The 3-D structure of PSII confirmed that cyt *c*550 binds on the lumenal membrane surface in the vicinity of the D1 and CP43 (Zouni *et al*., 2001; Kamiya *et al*., 2003; Biesiadka *et al*., 2004; Ferreira *et al*., 2004; Guskov *et al*., 2009).

Cyt *c*550 stabilize the binding of Cl^- and Ca^{2+} ions needed to the oxygen-evolving activity as the other extrinsic proteins (Shen *et al*., 1998; Kerfeld *et al*., 1998). However, the exact physiological role of the heme of cyt *c*550 is unclear. Extensive research has established that it does not participate in the main photosynthetic reactions. The fact that cyt *c*550 can be isolated as a soluble protein suggests that other functions not directly related to PSII are possible for this protein (Morand *et al*., 1994; Krogmann *et al*., 1991; Kang, 1994).

The E_m of cyt *c*550 is one of the key parameters for elucidating the biological role of this cytochrome. Values from –240 mV to –314 mV were obtained for the E_m of purified cyt *c*550 from some species of cyanobacteria (Hoganson *et al*., 1990; Navarro *et al*., 1995). The E_m for cyt *c*550 associated with PSII was not established until our group was able to measure it using intact PSII core complexes preparations from *T. elongatus*. Using potentiometric redox titrations, a significantly higher E_m value (E_{m6}= –80 mV) was obtained. (Roncel *et al*., 2003; Kirilovsky *et al*., 2004)

One of the most standard techniques for

determining redox potentials of proteins is the redox potentiometry. It involves measuring the ambient redox potential while simultaneously determining the concentration of the oxidized and reduced forms of the protein using a spectroscopic technique. In most redox titrations of proteins, equilibrium is ensured by the addition of a cocktail of redox mediators which establishes rapid (heterogeneous) electro-chemical equilibrium with the electrode and rapid (homogeneous) electron transfer with the protein without chemically modifying it in any way.

It has been reported that the E_m of Q_A in PSII-enriched membranes was affected by the presence of redox mediators at low ambient potentials. This effect was attributed to the loss of the very high potential Mn_4Ca cluster due to reductive attack by the mediators and the sodium dithionite itself under some conditions (Krieger *et al*., 1995). Based on these observations it seemed possible that E_m of cyt *c*550 when bound to PSII could suffer from this unexpected technical difficulty. The E_m value obtained for the E_m of cyt *c*550 may not reflect the fully intact form of the PSII-bound cytochrome. The main objective of this work has been to re-evaluate the E_m of cyt *c*550 associated with PSII considering the effect of redox mediators.

Materials and Methods

His-tag CP43 mutant *T. elongatus* cells were grown in a DTN-medium as described by Kirilovsky *et al*. (2004). PSII core complexes were prepared from cells as described by Kirilovsky *et al*. (2004).

Potentiometric redox titrations were carried out basically as described in Roncel *et al.* (2003). When indicated (mixture 1), a set of the following ten redox mediators was added: 10 μM *p*-benzoquinone (E_{m7} = +280 mV), 20 μM 2,3,5,6-tetramethyl-*p*-phenylendiamine (also called diaminodurol or DAD) (E_{m7} = +220 mV), 10 μM 2,5-dimethyl-*p*-benzoquinone (E_{m7} = +180 mV), 20 μM *o*-naphthoquinone (E_{m7} = +145 mV), 2.5 μM N-methylphenazonium methosulfate (E_{m7} = +80 mV), 10 μM N-methylphenazonium ethosulfate (E_{m7} = +55 mV), 20 μM duroquinone (E_{m7} = +10 mV), 30 μM 2-methyl-*p*-naphthoquinone (E_{m7} = 0 mV), 30 μM antraquinone (E_{m7} = –100 mV) and 30 μM 2-hidroxi-*p*-naftoquinone (E_{m7} = –145 mV). Some other redox titrations were carried out in the absence of the two last low potential redox mediators and with half concentration of the other redox mediators (mixture 2).

Results

Initially potentiometric redox titrations of the isolated PSII core complexes preparations in the presence of a mixture of ten redox mediators (mixture 1, see Materials and Methods), covering the potential range between +430 and –145 mV, were performed. Fig. 1 (curve 1) shows a representative potentiometric titration of PSII core complexes at pH 6.5 under these conditions. Differential spectra of cyt *c*550 (data not shown) were obtained by subtracting the spectrum recorded at +210 mV (cyt *c*550 almost fully oxidized and cyt *b*559 fully reduced) from each spectrum performed at different ambient redox potential (between +210 and –295 mV). The relative content of cyt *c*550 was calculated from the absorbance difference between 549 and 538 nm. Then, the percentages of reduced cyt *c*550 versus solution redox potential (E_h) were plotted and an E_m value of –100 mV was calculated by fitting the experimental points to the Nernst equation for one $n = 1$ component.

The E_m of cyt *c*550 was also measured in the absence of the two low potential redox mediators antraquinone and 2-hidroxi-*p*-naftoquinone and with half concentration of the other redox mediators of mixture 1 (mixture 2, see Materials and Methods). Fig. 1 (curve 2) shows a representative potentiometric titration of PSII core complexes at pH 6.5. This figure clearly shows that under these conditions PSII core complexes contain two different components with absorption maxima in the α-band at 549 nm, which are progressively reduced during the course of titration. The two components can be assigned to cyt *c*550. A plot of the percentages of reduced cyt *c*550, obtained from the difference spectra, versus E_h could be fitted to a Nernst equation for two $n = 1$ components. It clearly indicated the existence of two different cyt *c*550 components with E_m values of –10 mV (accounting for approximately 15% of the total amount of protein) and +185 mV (approximately 85% of the total amount of protein).

Finally the E_m of cyt *c*550 was measured in the absence of redox mediators other than sodium dithionite. The reductive potentiometric titration of PSII core complex was started from ambient redox potential of the reaction mixture without previous

addition of potassium ferricyanide (Fig. 1, curve 3). The figure shows the plot of percentages of reduced cyt *c*550 obtained from the difference absorption spectra of cyt *c*550 during the course of the redox titration versus E_h. It clearly showed that cyt *c*550 had a significant higher E_m value (+200 mV) than that obtained in the presence of low potential redox mediators (see curve 1).

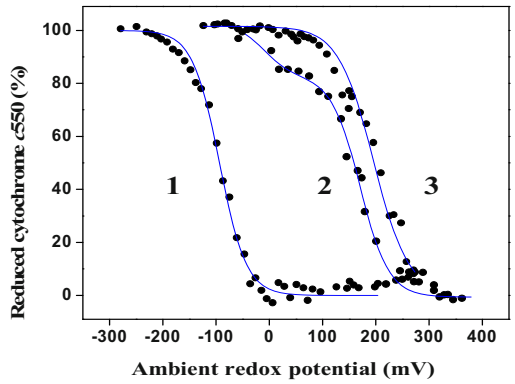

Fig. 1 Reductive potentiometric titrations of cyt *c*550 in PSII core complexes with different mixtures of redox mediators. *1*, mixture 1; *2*, mixture 2; *3*, without redox mediators (for details see Materials and Methods). Plot of the percentages of reduced cyt *c*550 obtained from the absorbance differences at 549–538 nm versus ambient redox potentials. The *solid curves* represent the best fit of the experimental data to the Nernst equation in accordance with one-electron processes ($n = 1$) for two components (2) and for one component (1, 3).

Discussion

Redox titrations of cyt *c*550 performed on PSII core complexes from *T. elongatus* in the absence of low potential redox mediators showed an E_m value for this heme protein that is higher than was obtained previously. This E_m value of +200 mV is about 300 mV more positive than the previously determined when low potential redox mediators were present (E_m= –80 mV) (Roncel *et al*., 2003; see also Fig. 1, curve 1). The redox potential shift induced by low potentials is reminiscent of earlier reports on the redox potential of Q_A that were reported by Krieger *et al.* (1995) and Johnson *et al*. (1995). The Mn_4Ca cluster has a very high potential even in the most reduced form of the enzyme cycle. It is protected from reductive attack from the medium by being buried inside a large protein complex, with access channels for substrate and products. However, reductants have access to the cluster when highly reducing conditions are used, when mediators are used or when extrinsic polypetides are removed. The reduction of the cluster leads to the weaker binding of the metal ions of the cluster to the site and eventually to their release (Tamura *et al*., 1985; Debus *et al*., 1992). We suggest that these conformational changes are responsible for the increased solvent access and weaker binding of the cyt *c*550 in the presence of mediators giving E_m values of about –100 mV.

The change in the PSII structure associated with the reduction of the Mn_4Ca cluster could lead to a greater accessibility of the heme to the aqueous medium and consequently to a total or partial release of cyt *c*550 from PSII. It seems likely that the increase in solvation energy that occurs when moving the heme out of the low dielectric of the protein environment into the high dielectric of water stabilizes the oxidized state more than the reduced state making the midpoint potential more negative (Mao *et al.*, 2003; Wirtz *et al*., 2000; Kassner *et al*., 1972).

These results lead us to suggest that the E_m of cyt *c*550 in PSII *"in vivo"* may be +200 mV, at least under certain conditions. This opens the possibility of a redox function for this protein in electron transfer in PSII. The nearest redox cofactor is the Mn_4Ca cluster (22 Å) (Guskov *et al.*, 2009). This long distance means that electron transfer would be slow (ms-s time scale) relative to the charge separation events in the RC. However, this rate remains potentially significant relative to the lifetime of the reversible charge accumulation states in the enzyme (tens of seconds to minutes) (Moser *et al*., 2005). Some kind of protective cycle involving a soluble redox component in the lumen may be envisioned.

Acknowledgements

This work was supported by grants from the Ministry of Education and Culture of Spain (BFU2007-68107-C02-01/BMC) and Andalusia Government (PAI CVI-261). The work done in France was supported by the EU/Energy Network project SOLAR-H2 (FP7 contract 212508).

References

Biesiadka J, Loll B, Kern J, Irrgang KD, Zouni A (2004) Cristal Structure of Cyanobacterial Photosystem II at 3.2 Angstrom Resolution: a

Closer Look at the Mn-Cluster. Phys. Chem. Chem. Phys. 6: 4733-4736

Debus RJ (1992) The Manganese and Calcium Ions of Photosynthetic Oxygen Evolution. Biochim. Biophys. Acta 1102: 269-352

Ferreira KN, Iverson TM, Maghlaoui K, Barber J, Iwata S (2004) Architecture of the Photosynthetic Oxygen-Evolving Center. Science 303: 1831-1838

Guskov A, Kern J, Gabdulkhakov A, Broser M, Zouni A, Saenger W (2009) Cyanobacterial Photosystem II at 2.9-A Resolution and the Role of Quinones, Lipids, Channels and Chloride. Nat. Str. Mol. Biol. 16: 334-342

Hoganson CW, Lagenfelt G, Andréasson LE (1990) EPR and Redox Potentiometric Studies of Cytochrome c-549 of Anacystis Nidulans. Biochim. Biophys. Acta 1016: 203-206

Johnson GN, Rutherford AW, Krieger A (1995) A Change in the Midpoint Potential of the Quinone Q_A in Photosystem II Is Associated with Photoactivation of the Primary Quinone Acceptor Q_A. Biochim. Biophys. Acta 1229: 202-207

Kamiya N, Shen JR (2003) Crystal Structure of Oxygen-Evolving Photosystem II from Thermosynechococcus Vulcanus at 3.7-A Resolution. Proc. Natl. Acad. Sci. USA 100: 98-103

Kang C, Chitnis RP, Smith S, Krogmann DW (1994) Cloning and Sequence Analysis of the Gene Encoding the Low Potential Cytochrome c of Synechocystis PCC 6803. FEBS Lett. 344: 5-9

Kerfeld CA, Krogmann DW (1998) Photosynthetic Cytochromes c in Cyanobacteria, Algae and Plants. Annu. Rev. Plant Physiol. Plant Mol. Biol. 49: 397-425

Kassner RJ (1972) Effects of Nonpolar Environments on the Redox Potentials of Heme Complexes. Proc. Natl. Acad. Sci. USA 69: 2263-2267

Kirilovsky D, Roncel M, Boussac A, Wilson A, Zurita, JL, Ducruet JM, Bottin H, Sugiura M, Ortega JM, Rutherford AW (2004) Cytochrome c550 in the Cyanobacterium Thermosynechococcus Elongatus: Study of Redox Mutants. J. Biol. Chem. 279: 52869-52880

Krieger A, Rutherford AW, Johnson GN (1995) On the Determination of the Redox Midpoint Potential of the Primary Quinone Acceptor, Q_A, in Photosystem II. Biochim. Biophys. Acta 1229: 193-201

Krogmann DW (1991) The Low-Potential Cytochrome c of Cyanobacteria and Algae. Biochim. Biophys. Acta 1058: 35-37

Mao J, Hauser K, Gunner MR (2003) How Cytochromes with Different Folds Control Heme Redox Potentials. Biochemistry 42: 9829-9840

Morand LZ, Cheng RH, Krogmann DW, Ho KK (1994) Soluble Electron Transfer Catalysts of Cyanobacteria. In: Bryant DA (ed), The Molecular Biology of Cyanobacteria. Kluwer Academic Publishers: Dordrecht, pp. 381-407

Moser CC, Page CC, Dutton PL (2005) Tunneling in PSII. Photochem. Phobiol. Sci. 4: 933-939

Navarro JA, Hervás M, De la Cerda B, De la Rosa MA (1995) Purification and Physicochemical Properties of the Low-Potential Cytochrome c549 from the Cyanobacterium Synechocystis sp. PCC 6803. Arch. Biochem. Biophys. 318: 46-52

Roncel M, Boussac A, Zurita JL, Bottin H, Sugiura M, Kirilovsky D, Ortega JM (2003) Redox Properties of the Photosystem II Cytochromes b559 and c550 in the Cyanobacterium Thermosynechococcus Elongatus. J. Biol. Inorg. Chem. 8: 206-216

Shen JR, Qian M, Inoue Y, Burnap RL (1998) Functional Characterization of Synechocystis sp. PCC 6803 Delta psbU and Delta psbV Mutants Reveals Important Roles of Cytochrome c-550 in Cyanobacterial Oxygen Evolution. Biochemistry 37: 1551-1558

Tamura N, Cheniae GM (1985) Effects of Photosystem II Extrinsic Proteins on Microstructure of the Oxygen-Evolving Complex and Its Reactivity to Water Analogs. Biochim. Biophys. Acta 809: 245-259

Wirtz M, Oganesyan V, Zhang X, Studer J, Rivera M (2000) Modulation of Redox Potential in Electron Transfer Proteins: Effects of Complex Formation on the Active Site Microenvironment of Cytochrome b5. Faraday Discuss. 116: 221-234

Zouni A, Witt HT, Kern J, Fromme P, Kraub N, Saenger W, Orth P (2001) Crystal Structure of Photosystem II from Synechococcus Elongatus at 3.8 A Resolution. Nature 409: 739-743

The Polyhydroxybutyrate Pathway Promoters Can Drive Foreign Gene Expression under Circadian Rhythm in *Synechocystis* sp. PCC 6803

Ryan E Hill, Julian J Eaton-Rye*

Department of Biochemistry, University of Otago, P.O. Box 56, Dunedin, 9054, New Zealand.
*Corresponding author. Tel. No. +64 3 479-7865; Fax No. +64 3 479-7866; E-mail: julian.eaton-rye@otago.ac.nz.

Abstract: This study investigated the use of promoters belonging to the *phaAB* and *phaEC* operons of the polyhydroxybutyrate (PHB) biosynthetic pathway to drive foreign expression of the *luxAB* operon, which encodes the reporter enzyme luciferase from *Vibrio harveyi*. Luciferase expression was successfully achieved under conditions previously reported for PHB production. Expression is controlled by circadian rhythm under growth conditions in BG-11. Under phosphate-limiting conditions luciferase exhibited a three-fold increase in expression levels and was constitutively expressed with circadian rhythm abolished. The PHB promoters for the *phaAB* and *phaEC* operons present a potentially useful set of promoters for introducing new metabolic pathways under the control of a circadian rhythm or phosphate availability.

Keywords: Circadian rhythm; Luciferase; Polyhydroxybutyrate (PHB); *Synechocystis* sp. PCC 6803

Introduction

The cyanobacterium *Synechocystis* sp. PCC 6803 (henceforth *Synechocystis* 6803) has been a model organism for photosynthesis research for many years. A key feature of *Synechocystis* 6803 is the ability to perform oxygenic photosynthesis using water as a source of electrons. This ability to fix carbon dioxide combined with the ease in which *Synechocystis* 6803 can be genetically modified, provides a unique platform for metabolic engineering and the synthesis of useful compounds in an environmentally sustainable manner.

The focus of this study is the modification of the polyhydroxybutyrate (PHB) metabolic pathway in *Synechocystis* 6803. PHB synthesis is achieved by three enzymes, acetoacetyl-CoA thiolase, 3-hydroxybutryl-CoA dehydrogenase and polyhydroxybutyrate synthase. These are encoded by the genes *phaA*, *phaB* and *phaE*/*phaC*, respectively, grouped into the two operons *phaAB* and *phaEC* (Hein *et al*., 1998; Taroncher-Oldenburg *et al*., 2000). PHB is produced in low amounts under normal conditions (4%–6% w/w dry mass) (Panda *et al*., 2006). However, when under conditions of high reducing power (high levels of NADPH) or nutrient limitation (phosphate or nitrogen) PHB production is up-regulated, reaching as high as 30% w/w (dry mass) (Panda and Mallick, 2007). In addition, PHB is only produced under a day/night cycle (Panda *et al*., 2006), subsequently the transcripts are sensitive to circadian rhythm (Kucho *et al*., 2005).

We have developed a number of integrative vectors that allow the insertion of genes under the control of *phaAB* or *phaEC* promoters in *Synechocystis* 6803. In addition usage of the *phaEC* integrative vector removes all of *phaE* and 60% of *phaC* open reading frames (ORFs), eliminating the ability for *Synechocystis* 6803 to produced PHB. A luciferase (*luxAB*) reporter system was used to demonstrate the ability for the integration and subsequent expression of foreign genes using the native promoters.

Materials and Methods

Strains of *Synechocystis* 6803 were routinely

grown in liquid culture of 150 mL BG-11 media with approximately 50–55 $\mu Em^{-2}s^{-1}$ light at 30 °C, and aerated through bubbling. Day/night cycled cultures were grown under 14 h light, 10 h complete darkness. Phosphate limited growth experiments used BG-11 with K_2HPO_4 substituted with equal molar KCl. Cell density was measured at 730 nm. All cloning work was conducted using *Escherichia coli* DH5α. Luciferase activity was assayed using a whole cell, 96-well microplate assay method. Cultures of *Synechocystis* 6803 harboring the *luxAB* operon were grown to late stationary phase (3.5–5 OD_{730}), samples of 1–2 mL were taken and assayed as follows. For each sample three 350 µL aliquots were assayed; the assay was started by addition of 7 µL of 50 mmol n-decanal (dissolved in 100% methanol) to each well, to give a final concentration of 1 mmol. Activity was monitored every 1.5–3 min for 15 s using a Polarstar Optima (BMG LABTECH GmbH, Germany) in luminescence detection mode at 30 °C for 20–30 min. After approximately 10 min the assay reached a steady state. Data from three measurements per well, in the steady-state region, were taken for further analysis to give a total of nine measurements per sample. The presence of PHB granules in *Synechocystis* 6803 were detected using a whole cell *in vivo* stain, Nile Blue A (Ostle and Holt, 1982; Tyo *et al*., 2006). In order for appreciable levels of PHB to accumulate, cultures of *Synechocystis* 6803 were grown under simulated day/night conditions. Initial cultures were grown to stationary phase in BG-11 supplemented with 5 mmol glucose. Upon reaching stationary phase the cultures were collected, washed and transferred to phosphate-limiting media (without glucose), supplemented with 0.4% (v/v) sodium acetate. After 3–4 days the samples were taken and stained for PHB, 10 µl of 1 mg/mL Nile Blue A solution (in DMSO) preheated to 65 °C was added to 1 mL of cells and heated for 10 min at 65 °C, followed by a wash with water and re-suspension in 1 mL water. 5 µL cells were fixed to microscope slides and observed under a fluorescence microscope using blue light (ca. 490 nm). PHB can be observed as small spherical inclusions that fluoresce orange-yellow.

Results and Discussion

Two plasmids were developed to modify the *phaAB* and *phaEC* operons on the *Synechocystis* 6803 genome, pRH-BT7b and pRH-ECT7, respectively. The plasmid pRH-BT7b, when integrated, appends an additional ORF to the end of the *phaAB* mRNA, essentially extending the operon by one ORF. This ORF utilizes an artificially added ribosomal binding site (RBS) from the *psbA2* gene to ensure translation. Integration of pRH-ECT7 removes *phaE* and 60% of *phaC* ORFs in *Synechocystis* 6803 with the consequence of removing the ability to produce PHB from the organism. In addition, foreign ORFs inserted between *Nco*I and *Bam*HI or *Hind*III sites of pRH-ECT7 will be inserted in-frame of the *phaE* RBS and promoters. Thus, pRH-ECT7 switches out the *phaEC* operon and replaces it with one or more ORF, retaining the *phaEC* promoter and RBS.

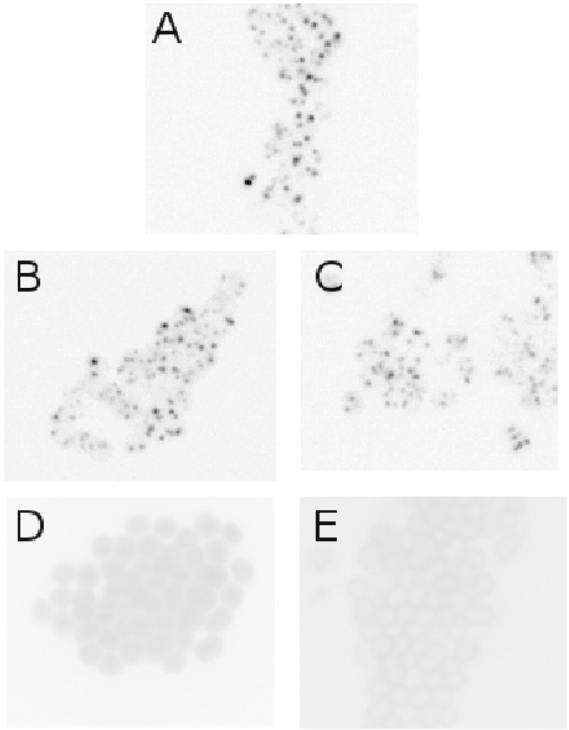

Fig. 1 Nile Blue A staining of PHB granules (black dots, (A) wild type) in *Synechocystis* 6803 strains. Cells of each strain were prepared as described in Materials and Methods. Images are inverted greyscale for clarity. Extension and modification of *phaAB* region does not inhibit PHB production (B) *phaB*:*cat* (C) *phaB*:*luxAB*, *cat*. Removal of *phaEC* from the genome removes the ability of the cells to produce PHB (D) Δ*phaEC*::*aph* (E) Δ*phaEC*::*luxAB*, *aph*.

Variants of the two plasmids were developed for further investigation of *phaAB* and *phaEC* promoter activity. Chloramphenicol resistance (*cat*) and kanamycin resistance (*aph*) were introduced into pRH-BT7b and pRH-ECT7, respectively. These

plasmids were used to determine if integration and disruption of the genome at *phaAB* and *phaEC* was detrimental to the organism. However, no change in growth was observed under any conditions tested, compared to wild type (data not shown). In addition, *phaB*:*cat* retained its ability to produce PHB, indicating that the *phaAB* operon was still functional whereas Δ*phaEC*::*aph* was unable to produce PHB as expected (Figs. 1B and 1D). Luciferase genes *luxAB* from *Vibrio harveyi* were added to the two plasmids and new strains developed. PHB production was identical to that of the antibiotic-resistance only strains (Figs. 1C and 1E).

Luciferase expression under control of either the *phaAB* or *phaEC* promoters was determined for standard and phosphate-depleted conditions (Fig. 2). Native *phaAB* and *phaEC* mRNA are known to be expressed under a circadian rhythm, with expression peaking at dusk and lowest at dawn. It was expected that luciferase activity should also follow a similar pattern in the constructed strains. Luciferase activity was observed peaking 2–4 h post dusk, dropping to almost undetectable levels by dawn (Fig. 2A). While the expression pattern observed between *phaAB* and *phaEC* was similar, *phaEC* exhibited approximately two- to three-fold greater activity at almost every time point assayed. This could be attributed to the difference in mRNA structure, as *phaAB* linked luciferase was part of a larger operonic structure with *phaA-phaB-luxA-luxB* where as *phaEC* linked mRNA was simply *luxA-luxB*. However, this remains to be investigated.

Under phosphate-limiting conditions *Synechocystis* 6803 accumulates approximately two-fold more PHB (11% w/w dry mass). Thus, luciferase activity was expected to increase under phosphate limitation. We observed a three-fold increase in activity compared to phosphate-replete conditions (Fig. 2B). In addition, the cyclic expression observed in phosphate-replete conditions was abolished, and constitutive expression was exhibited. Interestingly the same difference in activity between *phaAB* and *phaEC* linked activity was retained, with *phaEC* linked activity having approximately two-fold greater activity over *phaAB*.

Here we have shown that the promoters for PHB production can be utilized to drive expression of foreign ORFs with either a circadian rhythm or controlled by the availability of phosphate . We intend to use this system to introduce foreign pathways that use acetyl-CoA as a precurser such as alcohol biosynthesis (ethanol, butanol) to determine the usefulness of the PHB promoters for biotechnology applications.

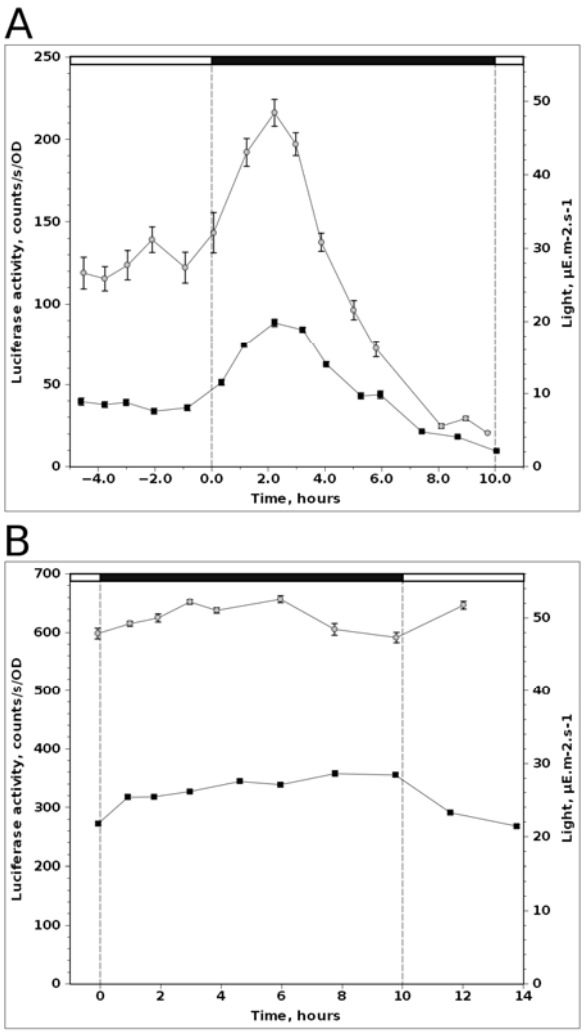

Fig. 2 Luciferase activity under control of promoters for *phaEC* (open circles) and *phaAB* (closed circles), over a 15 h period encompassing the light-dark transition. Cultures were grown for 9 days under a light-dark cycle of 14:10 h. Luciferase activity was measure on the 9th day. Time is relative to dusk (t = 0), black bars indicate dark phase (10 h), open bars indicate light phase at an illumination of 55 $\mu Em^{-2}s^{-1}$. Means of three cultures are shown, error is SEM (n = 27) (A) Luciferase activity over the course of the light-dark transition under photoautotrophic conditions (B) Luciferase activity over the course of the light-dark transition under photoautotrophic conditions in BG-11 media lacking phosphate.

References

Hein S, Tran H, Steinbüchel A (1998) Synechocystis sp. PCC6803 Possesses a Two-Component Polyhydroxyalkanoic Acid Synthase Similar to that of Anoxygenic Purple Sulfur Bacteria. Arch.

Microbiol. 170: 162-170

Kucho K, Okamoto K, Tsuchiya Y, *et al*. (2005) Global Analysis of Circadian Expression in the Cyanobacterium Synechocystis sp. Strain PCC 6803. J. Bacteriol. 187: 2190-2199

Ostle AG, Holt JG (1982) Nile blue A as a Fluorescent Stain for Poly-Beta-Hydroxybutyrate. Appl. Environ. Microbiol. 44: 238-241

Panda B, Mallick N (2007) Enhanced Poly-beta-Hydroxybutyrate Accumulation in a Unicellular Cyanobacterium, Synechocystis sp. PCC 6803. Lett. Appl. Microbiol. 44: 194-198

Panda B, Jain P, Sharma L, *et al*. (2006) Optimization of Cultural and Nutritional Conditions for Accumulation of Poly-Beta-Hydroxybutyrate in Synechocystis sp. PCC 6803. Bioresource Technol. 97: 1296-1301

Taroncher-Oldenburg G, Nishina K, Stephanopoulos G (2000) Identification and Analysis of the Polyhydroxyalkanoate-Specific Beta-Ketothiolase and Acetoacetyl Coenzyme A Reductase Genes in the Cyanobacterium Synechocystis sp. strain PCC6803. Appl. Environ. Microbiol. 66: 4440-4448

Tyo KE, Zhou H, Stephanopoulos GN (2006) High-throughput Screen for Poly-3-Hydroxybutyrate in Escherichia Coli and Synechocystis sp. Strain PCC6803. Appl. Environ. Microbiol. 72: 3412-3417

Removal of the PsbT Subunit of Photosystem II in *Synechocystis* sp. PCC 6803 Causes Q_A^- Oxidation to be Blocked by Dimethyl-*p*-Benzoquinone

Robert D Fagerlund, Roger Young, Hao Luo, Fiona K Bentley, Julian J Eaton-Rye*

Department of Biochemistry, University of Otago, P.O. Box 56, Dunedin 9054, New Zealand.
*Corresponding author. Tel. No. +64 3 479 7865; Fax No. +64 3 479 7866; E-mail: julian.eaton-rye@otago.ac.nz.

Abstract: The PsbT subunit of cyanobacterial photosystem II (PSII) is a membrane-spanning α-helix of ~3.5 kDa positioned at the PSII dimer interface with each monomer contributing a copy. Removal of PsbT, as a result of interrupting the *psbT* gene in *Synechocystis* sp. PCC 6803, reduced the rate of electron transfer between Q_A and Q_B and these ΔPsbT cells were susceptible to photodamage. However, the extent of photodamage depended upon the electron acceptor and was severe in the presence of the PSII-specific electron acceptor dimethyl-*p*-benzoquinone (DMBQ) but minimal when whole chain electron transport was measured in the presence of bicarbonate. Here we show formate and DMBQ cause a slowing of Q_A^- oxidation in ΔPsbT cells and this effect is reversed, in part, by the addition of bicarbonate. These results indicate that PsbT plays an important role in the architecture of the acceptor side of PSII and affects the ligand environment of the non-heme iron and the binding environment of DMBQ.

Keywords: Bicarbonate; DMBQ; Formate; Photosystem II (PSII); PsbT

Introduction

The crystal structures of cyanobactrial photosystem II (PSII) from *Thermosynechococcus vulcanus* and *T. elongatus* have shown PsbT to be a membrane-spanning α-helix with a stoichiometry of one copy per monomer. These structural studies have positioned the PsbT subunit at the monomer-monomer interface of the PSII dimer (Kamiya and Shen, 2003; Ferreira *et al*., 2004; Guskov *et al*., 2009).

Inactivation of *psbT* in *T. elongatus* revealed reduced levels of dimeric PSII but no difference in oxygen-evolving activity compared to wild-type cells, thylakoids and isolated PSII centers (Iwai *et al*., 2004; Watanabe *et al*., 2009). However, in *Synechocystis* sp. PCC 6803 (hereafter, *Synechocystis* 6803), ΔPsbT cells had impaired oxygen evolution and were rapidly photoinhibited (Bentley *et al.*, 2008). Furthermore, Q_A^- reoxidation studies following a single actinic flash indicated the ΔPsbT mutant had impaired electron flow between the primary and secondary plastoquinones electron acceptors Q_A and Q_B. However, recombination of Q_A^- with the S_2 state of the oxygen-evolving complex was similar in wild type and ΔPsbT cells. These results suggested the absence of PsbT in *Synechocystis* 6803 specifically perturbed electron transfer between Q_A and Q_B.

We recently noticed that the extent of photodamage to ΔPsbT cells depended upon the electron acceptor used to support oxygen evolution. In the presence of the PSII-specific electron acceptor dimethyl-*p*-benzoquinone (DMBQ) cells were susceptible to photodamge whereas in the presence of bicarbonate, which supports whole chain electron transfer, photodamage in ΔPsbT cells was similar to that observed in the wild type (Young, 2010).

The quinone-acceptor complex of PSII contains a non-heme iron coordinated by His residues supplied by the two reaction center proteins D1 and D2 and a fifth ligand is provided by a bicarbonate ion (Cox *et al*., 2009; Takahashi *et al*., 2009). Displacement of the bicarbonate ligand by formate slows electron transfer between Q_A and Q_B (Eaton-Rye and Govindjee, 1988a). We have therefore conducted a preliminary

study to investigate the role of bicarbonate in protecting PSII from photodamage in ΔPsbT cells by probing with formate in the presence and absence of DMBQ to determine if PsbT is important for the operation of the iron-quinone complex of PSII.

Materials and Methods

Synechocystis 6803 cultures were maintained on solid BG-11 media and liquid cultures were grown mixotrophically in unbuffered BG-11 media containing 5 mmol glucose and appropriate antibiotics as described by Eaton-Rye (2004). The construction of the ΔPsbT strain has been described in Bentley *et al*. (2008).

Oxygen evolution assays were carried out in BG-11 containing 25 mmol HEPES-NaOH (pH 7.5) at a chlorophyll concentration of 10 μgmL^{-1}, essentially as described in Bentley *et al.* (2008) but with 1 mmol $K_3Fe(CN)_6$ and 200 μM DMBQ as electron acceptors.

Decay kinetics of the variable chlorophyll *a* fluorescence yield following a single actinic flash were measured with a double modulation kinetic fluorometer (PSI Instruments, Brno, Czech Republic) using a blue 455 nm measuring light. Cells were dark adapted at 30 °C for 20 min and measurements were taken at a chlorophyll concentration of 5 μgmL^{-1}.

When present sodium formate was at 25 mmol and the concentration of sodium bicarbonate was 15 mmol.

Results and Discussion

The effect of the addition of formate on oxygen evolution in wild type and ΔPsbT cells is shown in Fig. 1. Formate had little effect on wild type (Fig. 1a) although the inclusion of bicarbonate stimulated the rate of oxygen evolution and the initial rate was sustained, with photodamage during the period of actinic illumination less evident. In contrast, the addition of formate to ΔPsbT cells reduced oxygen evolution essentially to zero but this inhibitory effect was prevented by the presence of bicarbonate (Fig. 1b). In fact addition of bicarbonate to formate-containing ΔPsbT cells reversed formate-induced inhibition (data not shown).

To investigate whether this striking difference was PSII specific, the decay of chlorophyll *a* variable fluorescence was measured to analyze Q_A^- reoxidation following a single turnover actinic flash (Fig. 2).

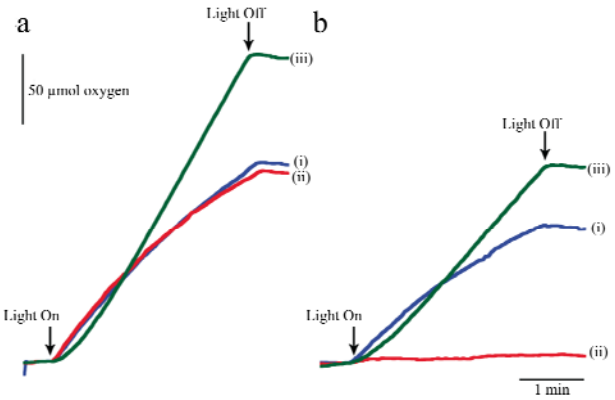

Fig. 1 Oxygen evolution traces of wild type (a) and ΔPsbT cells (b) performed with electron acceptors DMBQ and $K_3Fe(CN)_6$ and either no additional reagents (i), addition of formate (ii) or formate and bicarbonate (iii).

The decay of the variable chlorophyll *a* fluorescence yield is slowed in ΔPsbT cells relative to wild type (Bentley *et al*., 2008); however, addition of formate further impaired the fluorescence decay in ΔPsbT cells and this was reversed by bicarbonate (Fig. 2a). The decay of chlorphyll *a* fluorescence displays three phases (Vass *et al*., 1999): the initial fast component

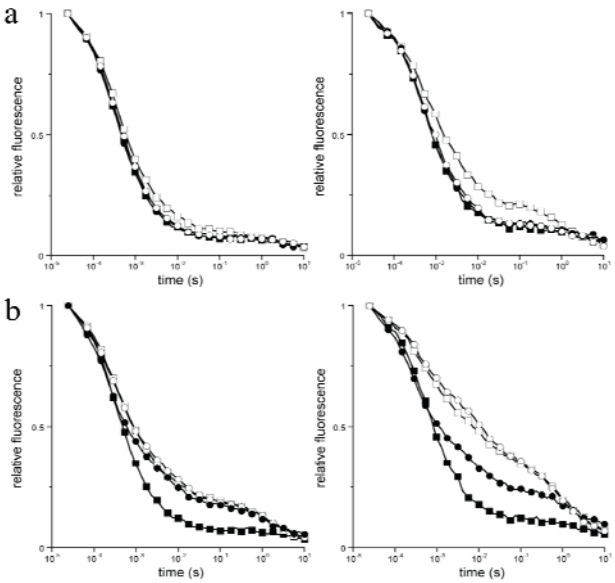

Fig. 2 Chlorophyll *a* fluorescence decay following a single turnover actinic flash. Effect of formate and bicarbonate on wild type (left) and the ΔPsbT mutant (right) either without (a) or with (b) DMBQ. Symbols in (a) are: no addition (closed squares); 25 mmol formate (open squares); 15 mmol bicarbonate (closed circles), and 25 mmol formate and 15 mmol bicarbonate (open circles). Symbols in (b) are: no addition (closed squares); 200 μM DMBQ (open squares); 200 μM DMBQ and 25 mmol formate (open circles), and 200 μM DMBQ, 25 mmol formate and 15 mmol bicarbonate (closed circles).

Table 1 Decay kinetics of chlorophyll *a* fluorescence. Analysis of half-times ($t_{1/2}$) and amplitudes (amp) from chlorophyll *a* fluorescence assays that correspond to Fig. 2. Values in parentheses refer to assays performed with 200 μM DMBQ.

		Fast phase		Intermediate phase		Slow phase	
Strain	Supplement	$t_{1/2}$ (μs)	amp (%)	$t_{1/2}$ (ms)	amp (%)	$t_{1/2}$ (s)	amp (%)
Wild Type	No addition	240	68	2.7	25	5.7	7.0
	(+DMBQ)	(190)	(57)	(3.5)	(27)	(3.5)	(16.0)
	Formate	260	64	3.8	26	3.2	10.0
	(+DMBQ)	(200)	(58)	(5.4)	(26)	(3.4)	(16.0)
	Formate + Bicarbonate	220	64	2.8	28	6.7	8.0
	(+DMBQ)	(160)	(61)	(4.8)	(25)	(4.8)	(14.0)
ΔPsbT	No addition	350	56	5.8	28	4.2	16.0
	(+DMBQ)	(330)	(37)	(9.6)	(27)	(1.6)	(36.0)
	Formate	380	42	6.9	32	1.4	26.0
	(+DMBQ)	(340)	(34)	(12.0)	(30)	(1.5)	(36.0)
	Formate + Bicarbonate	330	55	6.8	30	5.7	15.0
	(+DMBQ)	(250)	(50)	(11.0)	(27)	(6.2)	(23.0)

reflects electron transfer from Q_A^- to Q_B, the second intermediate component incorporates centers where plastoquinone is not bound in the Q_B pocket, and the third slow component indicates Q_A^- recombination with the donor side of PSII. Kinetic analysis revealed formate had little effect on the half-time of the fast component for both strains, although the corresponding amplitude in ΔPsbT cells was reduced (Table 1). Similarly, formate only exhibited a small effect on the intermediate phase for wild type and ΔPsbT cells; however, the half-time and amplitude for the slow component indicated an increased fraction of centers in ΔPsbT cells were recombining with the S_2 state of the donor side with a half-time of 1 to 2 s resembling recombination in the presence of diuron that blocks forward electron transfer to Q_B (*e.g.*, Eaton-Rye and Govindjee, 1988a).

These findings are therefore indicative of an increased population of Q_A^- in the ΔPsbT cells in the presence of formate — presumably due to impaired electron transfer to Q_B. However, the addition of bicarbonate countered the formate-induced inhibition (Table 1). This result supports the notion that removal of PsbT increases the accessibility of formate to the non-heme iron and/or reduces the binding affinity of bicarbonate.

Although formate impaired electron transfer between Q_A and Q_B in ΔPsbT cells the extent of the inhibition revealed in Fig. 2a and Table 1 is not enough to explain the level of formate-induced inhibition observed for the ΔPsbT mutant in the oxygen evolution assays presented in Fig. 1. To investigate this further, the effect of adding DMBQ in the presence or absence of formate on the decay of chlorophyll *a* fluorescence was studied (Fig. 2b). In wild type, DMBQ accelerated the fast phase and increased the fraction of centers undergoing a backreaction with the S_2 state (Table 1). In contrast, the rate of the fast phase was essentially unresponsive to the addition of DMBQ in the ΔPsbT mutant but the intermediate phase was considerably slowed and the kinetics of the back reaction were accelerated, again consistent with an increased population of centers undergoing a back rection between Q_A^- and the S_2 state in ΔPsbT cells. The inclusion of formate in addition to DMBQ did not exhibit any major additive effect. Nevertheless, the inclusion of bicarbonate with formate and DMBQ substantially restored the kinetics of the slow phase suggesting the population of Q_B^- was restored to the level observed in ΔPsbT cells when formate and DMBQ are not present. However, the intermediate component, potentially reflecting the affinity of plastoquinone for the Q_B site in the presence of DMBQ, was not restored.

The ability of formate to suppress DMBQ-supported oxygen evolution in ΔPsbT cells was unexpected since it is usually necessary to deplete the system of bicarbonate to observe a formate-induced "bicarbonate effect" (Van Resen, 2002). Because bicarbonate prevented formate inhibition, we examined the effect of formate on Q_A^- oxidation in ΔPsbT cells by measuring the decay of chlorophyll *a* fluorescence following a single actinic flash. While formate slowed this reaction in ΔPsbT cells the

impaired rate could not explain the complete block in oxygen evolution observed in Fig. 1. In part this may be due to the fact that a complete turnover of the two-electron gate may be necessary to observe the full effect of formate inhibition in these cells (Eaton-Rye and Govindjee, 1988b). Nevertheless, the inability of formate to completely block electron transfer between Q_A and Q_B prompted us to also determine the effect of DMBQ on the decay of chlorophyll *a* fluorescence. Intriguingly, DMBQ, a routinely used PSII-specific electron acceptor, inhibited forward electron transfer between Q_A and Q_B and increased the extent of the back reaction with the S_2 state of the oxygen-evolving complex in ΔPsbT cells. Our results therefore indicate that PsbT plays an important role in the structure of the iron-quinone complex of PSII and affects both the coordination of the non-heme iron by bicarbonate and the ability of DMBQ to act as an efficient electron acceptor.

Acknowledgement

This work was supported by a Marsden Grant 08-UOO-043 to J.J.E.-R.

References

Bentley FK, Luo H, Dilbeck P, Burnap RL, Eaton-Rye JJ (2008) Effects of Inactivating psbM and psbT on Photodamage and Assembly of Photosystem II in Synechocystis sp. PCC 6803. Biochemistry 47: 11637-11646

Cox N, Jin L, Jaszewski A, Smith PJ, Krausz E, Rutherford AW, Pace R (2009) The Semiquinone-Iron Complex of Photosystem II: Structural Insights from ESR and Theoretical Simulation. Evidence that the Native Ligand to the Non-Heme Iron Is Carbonate. Biophys. J. 97: 2024-2033

Eaton-Rye JJ (2004) The Construction of Gene Knockouts in the Cyanobacterium Synechocystis sp. PCC 6803. In: Carpentier R (ed.), Methods of Molecular Biology, Vol 274: Photosynthesis Research Protocols. Humana Press: Totowa, NJ, pp. 309-324

Eaton-Rye, Govindjee (1988a) Electron Transfer through the Quinone Acceptor Complex of Photosystem II after One or Two Actinic Flashes in Bicarbonate-Depleted Spinach Thylakoid Membranes. Biochim. Biophys. Acta 935: 248-257

Eaton-Rye, Govindjee (1988b) Electron Transfer through the Quinone Acceptor Complex of Photosystem II in Bicarbonate-Depleted Spinach Thylakoid Membranes as a Function of Actinic Flash Number and Frequency. Biochim. Biophys. Acta 935: 237-247

Ferreira KN, Iverson TM, Maghlaoui K, Barber J, Iwata S (2004) Architecture of the Photosynthetic Oxygen-Evolving Center. Science 303: 1831-1838

Guskov A, Kern J, Gabdulkhakov A, Broser M, Zouni A, Saenger W (2009) Cyanobacterial Photosystem II at 2.9-Å Resolution and the Role of Quinones, Lipids, Channels and Chloride. Nat. Struct. Mol. Biol. 16: 334-342

Iwai M, Katoh H, Katayama M, Ikeuchi M (2004) PSII-Tc Protein Plays an Important Role in Dimerization of Photosystem II. Plant Cell Physiol. 45: 1809-1816.

Kamiya N, Shen J-R (2003) Crystal Structure of Oxygen-Evolving Photosystem II from Thermosynechococcus Vulcanus at 3.7 Å Resolution. Proc. Natl. Acad. Sci. USA 100: 98-103

Takahashi R, Boussac A, Sugiura M, Noguchi T (2009) Structural Coupling of a Tyrosine Side Chain with the Non-Heme Iron Center in Photosystem II as Revealed by Light-Induced Fourier Transform Infrared Difference Spectroscopy. Biochemistry 48: 8994-9001

Van Rensen JJS (2002) Role of Bicarbonate at the Acceptor Side of Photosystem II. Photosynth. Res. 73: 185-192

Vass I, Kirilovsky D, Etienne A-L (1999) UV-B Radiation-Induced Donor- and Acceptor-Side Modifications of Photosystem II in the Cyanobacterium Synechocystis sp. PCC 6803. Biochemistry 38: 12784-12794

Watanabe M, Iwai M, Narikawa R, Ikeuchi M (2009) Is the Photosystem II Complex a Monomer or a Dimer? Plant Cell Physiol. 50: 1674-1680

Young R (2010) Characterisation of the Role of the PsbT Subunit of Photosystem II in Synechocystis sp. PCC 6803. MSc thesis. University of Otago, Dunedin

Metal and Serine Proteases in the Crude Photosystem II Particles from a Diatom, *Chaetoceros Gracilis*

Ryo Nagao[a], Eri Noguchi[b], Tatsuya Tomo[b], Isao Enami[b], Masahiko Ikeuchi[a,*]

[a]Department of Life Sciences (Biology), Graduate School of Art and Sciences, University of Tokyo, Japan;
[b]Department of Biology, Faculty of Science, Tokyo University of Science, Japan.
[*]Corresponding author. E-mail: mikeuchi@bio.c.u-tokyo.ac.jp.

Abstract: We found that most of subunits in crude Photosystem II particles (crude PSII) from a marine centric diatom, *Chaetoceros gracilis*, were degraded during incubation for 18 h at 25 ºC in the dark (Nagao *et al.*, 2010). In this study, we attempted to suppress the protein degradation by addition of protease inhibitors to the crude PSII during incubation for various times at 25 ºC in the dark. When no proteases inhibitor added to the crude PSII, fucoxanthin chlorophyll *a*/*c*-binding protein (FCP), especially upper subunits of FCP, were first degraded, followed by most of PSII subunits. The degradation was slightly suppressed by a metal protease inhibitor, EDTA, or a serine protease inhibitor, PMSF, and the proteolysis activity of metal protease is slightly stronger than that of serine protease. On the other hand, the significant suppression was observed only by both EDTA and PMSF. These results suggest that the metal and serine proteases are associated with the crude PSII and the primary target of the proteases is the upper subunits of FCP.

Keywords: *Chaetoceros gracilis*; Photosystem II; Protease; Proteolysis

Introduction

Diatoms are one of the most important constituents of phytoplankton in aquatic ecosystems and the global carbon cycle (Field *et al.*, 1998). Recently, we succeeded for the first time in isolation of crude PSII particles (crude PSII) retaining oxygen-evolving activities from a marine centric diatom, *Chaetoceros gracilis*, and the crude PSII contained PSII intrinsic proteins, five extrinsic proteins and a large number of fucoxanthin chlorophyll *a*/*c*-binding protein (FCP) (Nagao *et al.*, 2007). In our previous report, degradation of not only PSII subunits but also FCP subunits was observed in the crude PSII during incubation for 18 h at 25 ºC in the dark (Nagao *et al.*, 2010). In this study, we attempted to suppress the degradation by addition of protease inhibitors to the crude PSII during incubation for 1, 3, 6 and 18 h at 25 ºC in the dark, and determined types of the proteases and their primary target in the crude PSII.

Materials and Methods

Preparation of the crude PSII from C. gracilis. A marine centric diatom, *C. gracilis*, was grown in artificial seawater as described previously (Nagao *et al.*, 2007, 2010). Crude PSII of *C. gracilis* was prepared according to Nagao *et al.*, 2007 and 2010 without 1 mmol PMSF when disrupted the cells by freeze-thawing and not containing 1 mmol EDTA in a preparation buffer, and then suspended in a medium containing 0.4 mol sucrose and 40 mmol Mes-NaOH (pH 6.5).

SDS-PAGE. Protease inhibitors (final concentration of 1 mmol) were added to the crude PSII, and incubated at 25 ºC for 1, 3, 6 and 18 h in the dark. Then, treated crude PSII was solubilized with 5% lithium lauryl sulfate and 75 mmol dithiothreitol. The solubilized samples (3 μg chl) were applied to a gradient gel containing 16%–22% acrylamide and 7.5 mol urea (Ikeuchi and Inoue, 1988). After electrophoresis, gels were stained with Coomassie Brilliant Blue R-250 and photographed.

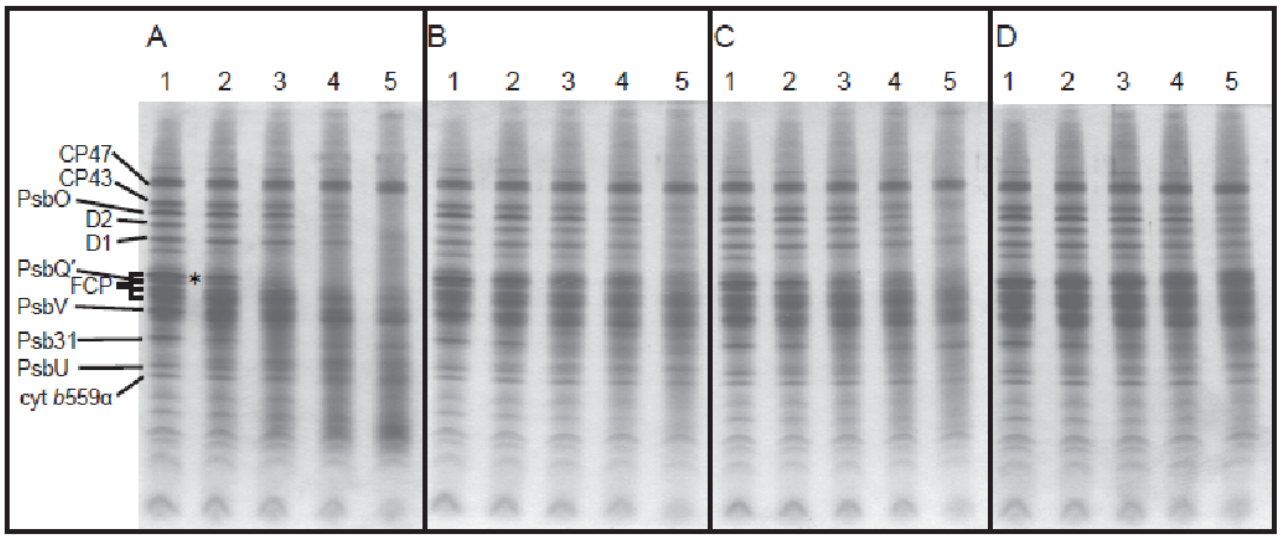

Fig. 1 Protein degradation of the crude PSII by addition of no protease inhibitors (A), 1 mmol EDTA (B), 1 mmol PMSF (C) and 1 mmol EDTA/1 mmol PMSF (D). Lanes 1–5, incubation for 0, 1, 3, 6 and 18 h, respectively, at 25 ºC in the dark.

Results

To examine what kind of proteases are present, the crude PSII was incubated at 25 ºC for 1, 3, 6, 18 h in the dark after addition of protease inhibitors, and then the treated crude PSII was subjected to SDS-PAGE (Fig. 1). In the absence of protease inhibitors (Fig. 1A), the upper subunits of FCP (marked as asterisk) were completely degraded during the dark incubation for 3 h (lane 3). After 18 h, most of subunits in the crude PSII disappeared and the low molecular weight region apparently became denser (lane 5). In the presence of a metal protease inhibitor, EDTA, the striking degradation of the upper subunits of FCP was suppressed at 3 and 6 h (Fig. 1B, lanes 3 and 4). Even at 18 h, PSII and FCP subunits were not completely degraded with concomitant suppression of the dense smear bands at the low molecular region (Fig. 1B, lane 5). Similar suppression was observed in the presence of the serine protease inhibitor, PMSF (Fig. 1C). However, proteolysis pattern in the presence of PMSF differed from that in the presence of EDTA. Degradation of PSII and FCP subunits was suppressed more efficiently by EDTA than PMSF. These results suggest that metal and serine proteases are active in the crude PSII preparation and the proteolysis activity of metal protease is stronger than that of serine protease. On the other hand, the degradation was largely, but not completely, suppressed by addition of both EDTA and PMSF (Fig. 1D), suggesting that another protease is present in the crude PSII preparation.

Discussion

Most subunits in the crude PSII were rapidly degraded during the dark incubation (Fig. 1A), but the degradation was more pronounced than that in our previous report (Nagao *et al.*, 2010). In the report, cells of *C. gracilis* were disrupted by freeze-thawing in presence of 1 mmol PMSF, and the isolation buffer included 1 mmol EDTA (Nagao *et al.*, 2010). These data suggest that the metal and serine proteases were, partially or completely, suppressed during the preparation with EDTA and PMSF. In photosystem II, FtsH and Deg proteases are well known as metal and serine proteases, respectively, and they preferentially attack the damaged D1 protein during photoinhibition (Sakamoto *et al.*, 2003; Kapri-Pardes *et al.*, 2007). Our findings suggest that the proteases in the crude PSII preparation may be different from FtsH and Deg proteases in term of their substrate specificity, because most subunits of PSII including D1 protein were more or less evenly degraded in the crude PSII. Interestingly, the degradation of the upper subunits of FCP (marked as asterisk in Fig. 1A) is more pronounced than that of PSII subunits. Therefore, it is likely that the primary target of the proteases is the upper subunits of FCP, implying that the proteases are

localized near FCP. In agreement with this finding, the purified PSII preparation from *C. gracilis* that lacked major FCP was hardly degraded during incubation for 18 h at 25 ºC in the dark (Nagao *et al.*, 2010). Furthermore, an FCP fraction obtained during fractionation of the purified PSII by anion exchange chromatography was degraded during the dark incubation, in our preliminary experiment. This supports the idea that the active proteases are associated with FCP in the crude PSII. To further confirm it, biochemical characterization of the FCP associated with PSII is now in progress.

Acknowledgements

This work was supported in part by Grants-in-aid for Scientific Research from the Ministry of Education of Japan 18570049 (to I. E.) and 21570038 and 22370017 (to T. T.), and Research Fellow (to R. N.) from the Japan Society for the Promotion of Science.

References

Field CB, Behrenfeld MJ, Randerson JT, Falkowski PG (1998) Primary Production of the Biosphere: Integrating Terrestrial and Oceanic Components. Science 281: 237-240

Kapri-Pardes E, Naveh L, Adam Z (2007) The Thylakoid Lumen Protease Deg1 Is Involved in the Repair of Photosystem II from Photoinhibition in Arabidopsis. Plant Cell 19: 1039-1047

Ikeuchi M, Inoue Y (1988) A New Photosystem II Reaction Center Component (4.8 kDa Protein) Encoded by Chloroplast Genome. FEBS Lett. 241: 99-104

Nagao R, Ishii A, Tada O, Suzuki T, Dohmae N, Okumura A, Iwai M, Takahashi T, Kashino Y, Enami I (2007) Isolation and Characterization of Oxygen-Evolving Thylakoid Membranes and Photosystem II Particles from a Marine Diatom Chaetoceros Gracilis. Biochim. Biophys. Acta 1767: 1353-1362

Nagao R, Tomo T, Noguchi E, Nakajima S, Suzuki T, Okumura A, Kashino Y, Mimuro M, Ikeuchi M, Enami I (2010) Purification and Characterization of a Stable Oxygen-Evolving Photosystem II Complex from a Marine Centric Diatom, Chaetoceros Gracilis. Biochim. Biophys. Acta 1797: 160-166

Sakamoto W, Zaltsman A, Adam Z, Takahashi Y (2003) Coordinated Regulation and Complex Formation of Yellow Variegated1 and Yellow Variegated 2, Chloroplastic FtsH Metalloproteases Involved in the Repair Cycle of Photosystem II in Arabidopsis Thylakoid Membranes. Plant Cell 15: 2843-2855

Structure-Function Studies of the Photosystem II Extrinsic Subunits PsbQ and PsbP from the Cyanobacterium *Synechocystis* sp. PCC 6803

Simon A Jackson [1], Robert D Fagerlund [1], Mark G Hinds[2], Sigurd M Wilbanks [1], Julian J Eaton-Rye [1,*]

[1]Department of Biochemistry, University of Otago, New Zealand;
[2] Walter and Eliza Hall Institute of Medical Research, Parkville 3052, Australia.
*Corresponding author. Tel. No. +64 3 479-7865; Fax No. +64 3 479-7866; E-mail: julian.eaton-rye@otago.ac.nz.

Abstract: The oxygen-evolving centre of Photosystem II (PS II) is located on the lumenal side of the PS II complex and is surrounded by a group of polypeptides known as the extrinsic proteins. In PS II of the cyanobacterium *Synechocystis* sp. PCC 6803 six extrinsic proteins have been identified: PsbO, PsbP, PsbQ, PsbU, PsbV and Psb27. We have obtained two X-ray crystallographic structures of PsbQ, from crystals grown in either the presence or absence of Zn^{2+} ions. The structures were solved by multiple wavelength anomalous dispersion phasing using data obtained from a selenomethionine derivative and have essentially identical structures. The protein was found to consist of a four-helix bundle with an up-down-up-down fold. His76 (present in a unique HisGlyPro motif which forms a kink in helix 2 of cyanobacterial PsbQ) together with Asp116 (helix 3), coordinates Zn adjacent to a hydrophobic cavity on the H2/H3 face. We hypothesize this metal binding site and cavity may play a role in a protein-protein interaction with another PS II subunit. Similar structure-function studies are underway for the PsbP subunit; to facilitate solving the structure of PsbP in solution we have determined the NMR backbone chemical shift values of isotopically labelled recombinant PsbP.

Keywords: CyanoP; CyanoQ; Extrinsic Proteins; Photosystem II; PsbP; PsbQ; *Synechocystis*

Introduction

The oxygen-evolving centre (OEC) of Photosystem II (PSII) consists of a tetra-manganese calcium chloride cluster and is located on the lumenal side of the PSII complex where it is surrounded by a group of polypeptides known as the extrinsic proteins. The complement of extrinsic subunits varies between phyla; of the six PSII lumen-localized extrinsic protein subunits that have been identified in cyanobacteria only PsbO, PsbU and PsbV are present in the current PSII crystal structures (Ferreira *et al.*, 2004; Guskov *et al.*, 2009). The missing extrinsic subunits PsbP, PsbQ and Psb27 are characterized in cyanobacteria by an N-terminal lipid attachment and thus form a unique group of PSII extrinsic lipo-proteins. These extrinsic lipoproteins appear to influence the assembly, stability, degradation and repair of PSII but specific roles have not yet been definitively linked to individual subunits. The order of assembly of the extrinsic subunits and the manganese cluster itself has not yet been resolved. It is currently theorized the Psb27 subunit binds the PSII complex and is exchanged for other extrinsic subunits as the D1 precursor is processed and the manganese cluster is sequentially assembled (Roose and Pakrasi, 2008).

The functional role of the cyanobacterial PsbQ subunit (CyanoQ) has yet to be fully defined. It is known to be required for photoautotrophic growth under calcium- and chloride-limiting conditions, suggesting its presence stabilizes these co-factors within the OEC cluster (Eaton-Rye, 2005). In *Synechocystis* sp. PCC 6803 (hereafter *Synechocystis* 6803) the PsbQ subunit is found at stoichiometric levels (to PSII) in combination with the PsbO, PsbU and PsbV subunits and appears to bind centres with higher than average rates of oxygen evolution, suggesting these subunits are associated with fully

mature PSII centres (Roose *et al.*, 2007a). In contrast the cyanobacterial PsbP subunit (CyanoP) appears sub-stoichiometric and is likely to be involved in biogenesis or repair of PSII (Thornton *et al.*, 2004; Summerfield *et al.*, 2005).

High resolution X-ray crystal structures for both higher plant PsbP and PsbQ are available and recently the solution structure of cyanobacterial Psb27 has been solved (Ifuku *et al*., 2004, 2005; Balsera *et al.*, 2005; Cormann *et al*., 2009; Mabbit *et al*., 2009). We have now determined the first structure of PsbQ from a cyanobacterial species in both the presence and absence of bound zinc (Jackson *et al*., 2010). A low resolution crystal structure of PsbP from *Thermosynechococcus elongatus* has recently been reported that contained a large number of bound zinc atoms, the biological significance of which remains unresolved (Michoux *et al.*, 2010). To more clearly explore structural similarities and differences between the higher plant and CyanoP, with a view to selecting targets for *in vivo* mutagenesis, we have progressed toward an NMR solution structure of the PsbP protein from *Synechocystis* 6803.

Methods and Materials

The nucleotide sequences of sll1638 and sll1418, corresponding to the regions encoding Cys22 and Cys24 to the C-termini of the *Synechocystis* 6803 homologues of PsbQ and PsbP, respectively, were cloned as glutathione S-transferase (GST) fusion constructs in the pGEX-6-P-3 vector. The resultant fusion proteins were overexpressed in *Escherichia coli* BL21(DE3) cells and purified by affinity chromatography followed by proteolytic cleavage of the GST tags with 3C protease. The liberated recombinant peptides included the entire predicted mature sequence of PsbQ (residues 22–149) or PsbP (residues 24–188) as well as a 5 residue N-terminal artefact (GPLGS) from the protease cleavage site.

Native recombinant PsbQ was expressed in rich media whilst selenomethionine (Se-Met) labelled PsbQ, used for phase determination, was produced similarly by expression in restricted media supplemented with Se-Met. Purified recombinant PsbQ was buffer exchanged with 10 mmol Tris-HCl (pH 7.0) with and without 5 mmol $ZnCl_2$ present and concentrated to between 14 and 18 mg mL^{-1}. Native crystals were formed via the hanging drop method with a 1:1 ratio of protein to reservoir solution containing 0.1 mol MES-NaOH (pH 6.5) and 25% PEG 1450. For the Se-Met crystals the reservoir contained 0.05 mol MES, 0.05 mol Tris-HCl (pH 7.0) and 25% PEG 1450.

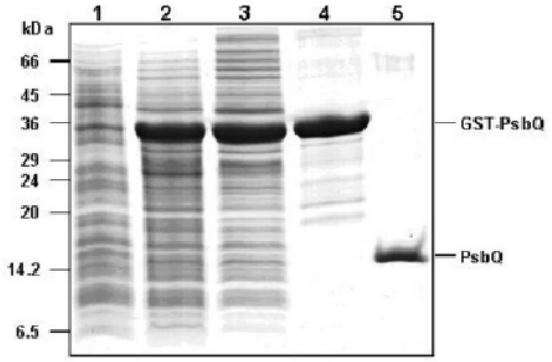

Fig. 1 Purification of PsbQ: (1) pre-induced cells; (2) induced cells after 3.5 h; (3) clarified lysate; (4) resin bound fusion protein; (5) liberated PsbQ.

Recombinant PsbP was overexpressed in minimal media supplemented with either ^{15}N labelled NH_4Cl or ^{15}N labelled NH_4Cl and ^{13}C labelled glucose. Labelled PsbP proteins were further purified by gel filtration with 25 mmol sodium phosphate (pH 6.7) buffer containing 10 mmol NaCl and 5 mmol TCEP before concentration to 0.4 mmol. Polydispersion, as measured by dynamic light scattering, was determined to be 12%–14%, indicating the samples were essentially monodisperse.

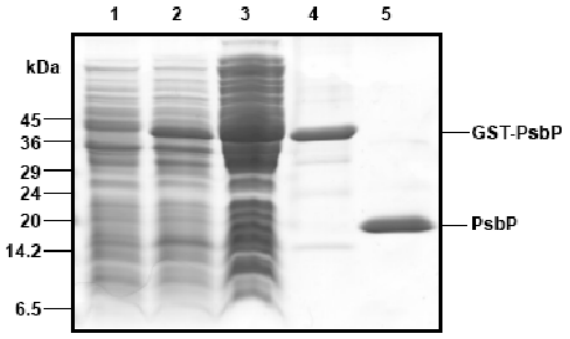

Fig. 2 Purification of ^{15}N labelled PsbP: (1) pre-induced cells; (2) induced cells after 4 h; (3) clarified lysate; (4) resin bound fusion protein; (5) liberated PsbP.

Results and discussion

PsbQ

The CyanoQ structures obtained in the presence and

absence of zinc appear highly similar and fold in an up-down-up-down helical bundle. Whilst the N-termini differ significantly the C-terminal helical bundle of CyanoQ appears similar to that of spinach PsbQ with the exception of a pronounced kink in helix 2 (H2) and different sites of zinc co-ordination (Fig. 3). Comparison of CyanoQ surface cavities and conserved residue analysis reveals the largest solvent accessible cavity is located on the H2/H3 face near a conserved GlyPro di-peptide which forms the kink in H2. The CyanoQ structure obtained in the presence of Zn^{2+} contains a zinc atom bound near this cavity coordinated by His76 and D116. Furthermore this cavity is also found in the spinach PsbQ structure along with the highly conserved ligand residues R79 and D119; although in the case of spinach they do not coordinate a zinc atom in the crystal structure. The conserved nature of these ligands and the proximity of the site to the large hydrophobic cavity suggests this site on the H2/H3 face might be functionally important for the role of PsbQ. A notable difference in the surface topology of PsbQ between the two species is the N-terminal extension of spinach PsbQ which extends out over the surface of H2 compared to the exposed split H2 of CyanoQ, furthermore the N-terminus of spinach PsbQ has been identified as required for binding to PSII (Balsera *et al.*, 2005). These observations together suggest the H2 helix of CyanoQ may be specifically involved in binding cyanobacterial PSII centres.

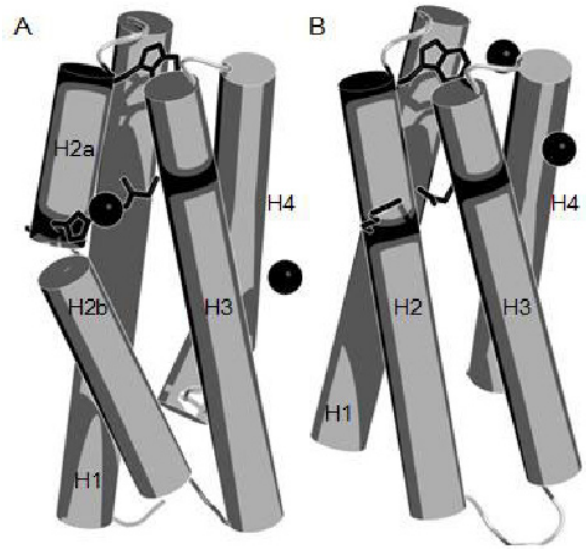

Fig. 3 Comparison of the C-terminal helical bundles of PsbQ from *Synechocystis* 6803 (A) and spinach (B). Zinc atoms are shown as black spheres, the side chains of H76, D116, the conserved Trp and their equivalent residues (H79, D119) in spinach are also shown.

PsbP

To facilitate structural analysis of the PsbP protein from *Synechocystis* 6803 in solution we have obtained the ^{1}H, ^{15}N and ^{13}C backbone chemical shifts (99% complete) by sequential assignment using $^{1}H^{15}N$-HSQC, HNCA, HNCACB, HNCO and HN(CA)CO spectra (Fig. 4). Spectra were collected on a 600 MHz spectrometer (HSQC - 800 Mhz) at the Walter and Eliza Hall Institute of Medical Research. The HN root resonances for Gly19 and Asp63 have not yet been identified. The backbone chemical shifts have been used to predict elements of secondary structure. This information combined with further NMR spectra, for sidechain assignment and NOE distance determination, can be used to solve the structure of the PsbP protein in solution.

Insights gained from analysis of the CyanoQ structure have been used to select residues with potential functional roles as targets for *in vivo* mutagenesis. Of particular significance are the conserved Trp and the H/RGP motif. Similarly, upon completion, the NMR solution structure of CyanoP may help to determine whether any of the proposed zinc binding sites observed in the crystal structure are of biological significance and to enable a more targeted approach to mutagenesis. Despite the apparent similarly between the structures of PsbP and PsbQ of cyanobacteria and their higher plant homologues there appears to be distinct evolutionary differences in the function of these subunits which may correlate with the loss of the PsbU and PsbV extrinsic subunits in higher plants. By mutation of specific residues with potential functional significance the roles of CyanoP and CyanoQ and their interaction with PSII may be further defined.

Acknowledgement

This work was supported by Marsden Grant 08-UOO-043 to J.J.E.-R.

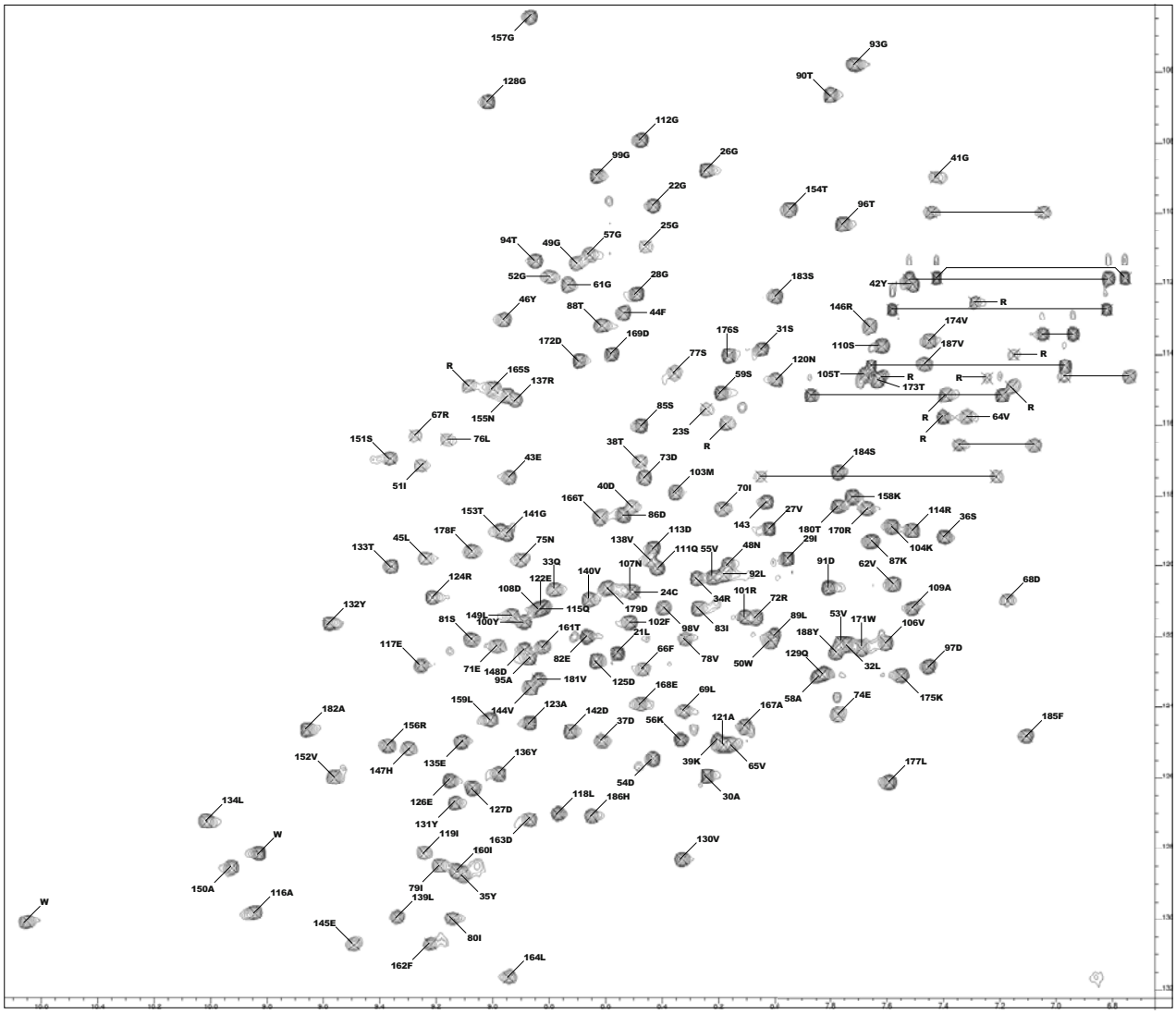

Fig. 4 Preliminary assignment of the ^{1}H ^{15}N HSQC of PsbP. Amide side chain NH_2 pairs are identified by solid lines, Arg Hε-Nε side chain groups (aliased 30 ppm in the nitrogen dimension) are labelled R and the two Trp Hε-Nε groups are indicated by W.

References

Balsera M, Arellano JB, Revuelta JL, de las Rivas J, Hermoso JA (2005) The 1.49 Å Resolution Crystal Structure of PsbQ from Photosystem II of Spinacia Oleracea Reveals a PPII Structure in the N-Terminal Region. J. Mol. Biol. 350: 1051-1060

Cormann KU, Bangert JA, Ikeuchi M, Rögner M, Stoll R, Nowaczyk MM (2009) Structure of Psb27 in Solution: Implications for Transient Binding to Photosystem II during Biogenesis and Repair. Biochemistry 48: 8768-8770

Eaton-Rye JJ (2005) Requirements for Different Combinations of the Extrinsic Proteins in Specific Cyanobacterial Photosystem II Mutants. Photosynth. Res. 84: 275-281

Ferreira KN, Iverson TM, Maghlaoui K, Barber J, Iwata S (2004) Architecture of the Photosynthetic Oxygen-Evolving Center. Science 303: 1831-1838

Guskov A, Kern J, Gabdulkhakov A, Broser M, Zouni A, Saenger W (2009) Cyanobacterial Photosystem II at 2.9-A Resolution and the Role of Quinones, Lipids, Channels and Chloride. Nat. Struct. Mol. Biol. 16: 334-342

Ifuku K, Nakatsu T, Kato H, Sato F (2004) Crystal Structure of the PsbP Protein of Photosystem II from Nicotiana Tabacum. EMBO Rep. 5: 362-367

Ifuku K, Nakatsu T, Shimamoto R, Yamamoto Y, Ishihara S, Kato H, Sato F (2005) Structure and Function of the PsbP Protein of Photosystem II from Higher Plants. Photosynth. Res. 84: 251-255

Jackson SA, Fagerlund RD, Wilbanks SM, Eaton-Rye JJ (2010) Crystal Structure of PsbQ from Synechocystis sp. PCC 6803 at 1.8 Å:

Implications for Binding and Function in Cyanobacterial Photosystem II. Biochemistry 49: 2765-2767

Mabbitt PD, Rautureau GJ, Day CL, Wilbanks SM, Eaton-Rye JJ, Hinds MG (2009) Solution Structure of Psb27 from Cyanobacterial Photosystem II. Biochemistry 48: 8771-8773

Michoux F, Takasaka K, Boehm M, Nixon PJ, Murray JW (2010) Structure of CyanoP at 2.8 Å: Implications for the Evolution and Function of the PsbP Subunit of Photosystem II. Biochemistry 49: 7411-7413

Roose JL, Kashino Y, Pakrasi HB (2007a) The PsbQ Protein Defines Cyanobacterial Photosystem II Complexes with Highest Activity and Stability. Proc. Natl. Acad. Sci. USA 104: 2548-2553

Roose JL, Wegener KM, Pakrasi HB (2007b) The Extrinsic Proteins of Photosystem II. Photosynth. Res. 92: 369-387

Roose JL, Pakrasi HB (2008) The Psb27 Protein Facilitates Manganese Cluster Assembly in Photosystem II. J Biol Chem. 283: 4044-4050

Summerfield TC, Winter RT, Eaton-Rye JJ (2005) Investigation of a Requirement for the PsbP-Like Protein in Synechocystis sp. PCC 6803. Photosynth. Res. 84: 263-268

Sveshnikov D, Funk C, Schröder WP (2007) The PsbP-Like Protein (sll1418) of Synechocystis sp. PCC 6803 Stabilizes the Donor Side of Photosystem II. Photosynth. Res. 93: 101-109

Thornton LE, Ohkawa H, Roose JL, Kashino Y, Keren N, Pakrasi HB (2004) Homologs of Plant PsbP and PsbQ Proteins Are Necessary for Regulation of Photosystem II Activity in the Cyanobacterium Synechocystis 6803. Plant Cell 16: 2164-2175

Coherent Electron Transfer in Reaction Centers of YM210L and YM210L/HL168L Mutants of *Rba. Sphaeroides*

Andrei G Yakovlev[a,*], Lyudmila G Vasilieva[b], Tatyana I Khmelnitskaya[b], Valentina A Shkuropatova[b], Anatoli Ya Shkuropatov[b], Vladimir A Shuvalov[a,b]

[a] A.N.Belozersky Institute of Chemical and Physical Biology, Moscow State University, Moscow 119991, Russian Federation;
[b] Institute of Basic Biological Problems, Russian Academy of Sciences, Pushchino, Moscow Region 142290, Russian Federation.
* Corresponding author. Tel. No. +7(495)939-5363; Fax No. +7(495)939-3181; E-mail: yakov@genebee.msu.su.

Abstract: A role of tyrosine M210 in the charge separation and stabilization of separated charges was studied by analyzing of the femtosecond oscillations in the kinetics of decay of stimulated emission from P* and of a population of the primary charge separated state $P^+B_A^-$ in the YM210L and YM210L/HL168L mutant reaction centers (RCs) of *Rhodobacter (Rba.) sphaeroides* in comparison with those in native RCs of *Rba. sphaeroides*. Kinetics of P* decay at 940 nm of the both mutants show a significant slowing-down of the primary charge separation reaction in comparison with native RCs. Distinct damped oscillations in these kinetics with main frequency bands in the range of 90–150 cm^{-1} reflect mostly nuclear motions inside the dimer P. Formation of a very small absorption band of B_A^- at 1020 nm is registered in RCs of both mutants. The formation of the B_A^- band is accompanied by damped oscillations with main frequencies from 10 to 150 cm^{-1}. Only a partial stabilization of the $P^+B_A^-$ state is seen in the YM210L/HL168L mutant in the form of a small non-oscillating background of the1020-nm kinetics. Similar charge stabilization is absent in the YM210L mutant. A model of oscillatory reorientation of the OH-group of TyrM210 in the electric fields of P^+ and B_A^- was proposed to explain a rapid stabilization of the $P^+B_A^-$ state in native RCs. A conclusion was done that, probably, the absence of TyrM210 can not be compensated by lowering of the $P^+B_A^-$ free energy that is expected for the double YM210L/HL168L mutant.

Keywords: Photosynthesis; Charge separation; Reaction center; Wave packet; Electron transfer

Introduction

The reaction center (RC) of photosynthetic bacteria and green plants is a pigment protein complex in which the light energy is conversed into the free energy of the charge-separated states. On the basis of time-resolved spectroscopic measurements, it has been suggested that B_A is the primary electron acceptor and the state $P^+B_A^-$ can be a first charge-separated state. The stabilization of the state $P^+B_A^-$ is completed within ~1,5 psec in Pheo-modified and native RCs of *Rba. sphaeroides* R-26 at 90 K (Yakovlev *et al*., 2002). The mechanism of the stabilization process is not yet completely clear. One possibility can be related to a reorientation of the polar groups of the amino acid residues located near P and B_A. For example, it may be the OH group of tyrosine located at the position M210 in the vicinity of P and B_A in *Rba. sphaeroides* RCs (Komiya *et al*., 1988). We found in the present work that the kinetics of P* decay at 940 nm of the YM210L and YM210L/HL168L mutant RCs of *Rba. sphaeroides* showed a significant slowing-down of the primary charge separation reaction in comparison with native RCs. The kinetics of the B_A^- absorption band at 1020 nm in the mutant YM210L/HL168L RCs show a weak stabilization of the $P^+B_A^-$ state accompanied by distinct oscillations. On the contrary, the analogous kinetics for the YM210L mutant shows the absence of $P^+B_A^-$ state stabilization. These data are discussed in

terms of dynamic stabilization of separated charges in the state $P^+B_A^-$ by reorientation of the OH group of tyrosine M210 and of the HOH55 molecule in *Rba. sphaeroides* RCs.

Materials and Methods

The mutations HL168L and YM210L were introduced in *puf*L gene encoding L protein subunit and *puf*M gene encoding M protein subunit of the reaction center of *Rba. sphaeroides* using bacterial strains and plasmids as described in (Vasilieva *et al*., 2001). Mutant and native RCs of *Rba. sphaeroides* were isolated by treatment of membranes with LDAO followed by DEAE-cellulose chromatography (Shuvalov *et al*., 1986). RCs were suspended in 10 mmol Tris-HCl, pH 8.0/0.1% Triton-X100 buffer. Low temperature (90 K) measurements were performed on the samples containing 65% glycerol (v/v). 5 mmol of sodium dithionite was added to keep RCs in the state $PB_AH_AQ_A^-$.

Femtosecond transient absorption measurements were carried out with a spectrometer based on Tsunami Ti:sapphire mode-locked laser (Spectra Physics, U.S.A.). The duration of pump and probe pulses was 16–18 fsec. Spectrally broadband pump pulses were centered at 870 nm. Transient absorption difference (light-minus-dark) spectra were obtained by averaging of 5000–10000 measurements at each time delay. The accuracy of absorbance measurements was $(1–2)\times10^{-5}$ units of optical density. The amplitude of the spectral band at 1,020 nm was taken at its maximum after subtraction of the superimposed broad background. The kinetics of absorbance changes (ΔA) at fixed wavelength were plotted using the measured difference spectra.

Results and Discussion

The kinetics of P* stimulated emission at 940 nm for the YM210L/ HL168L and YM210L mutants are similar to each other and show very slow P* decay whereas the P* decay in native RCs is much faster (Fig. 1). The remarkable damped oscillations reflecting a nuclear wavepacket motion (Vos *et al*., 1996) are seen in the kinetics of mutant and native RCs at 940 nm. The Fourier transformed (FT) spectra of the oscillations are similar for mutant and native

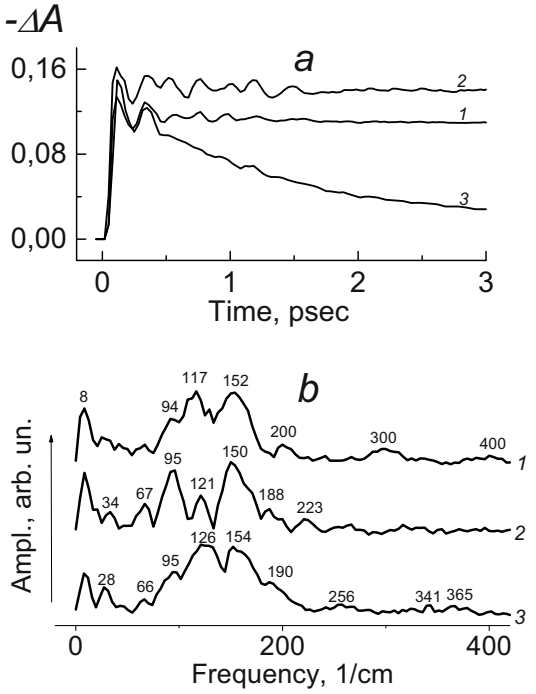

Fig. 1 Kinetics of ΔA (a) and FT spectra of its oscillatory parts (b) for the 940-nm band of P* stimulated emission in mutant YM210L/HL168L (curve 1), YM210L (curve 2) and native (curve 3) RCs of *Rba. sphaeroides* at 90 K.

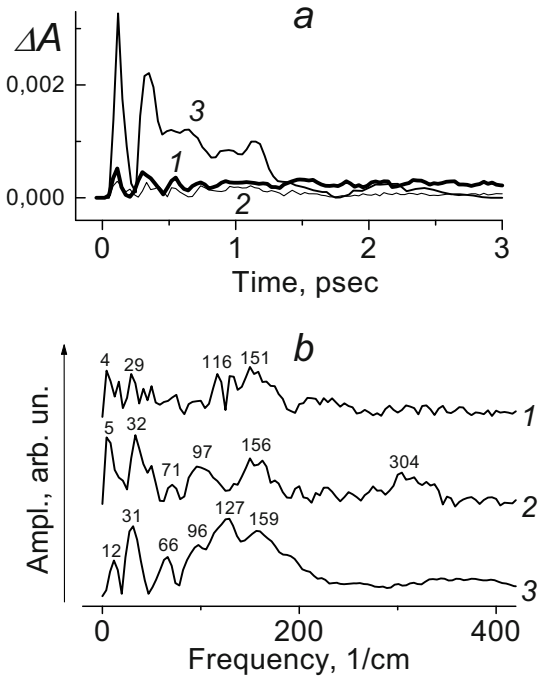

Fig. 2 Kinetics of ΔA (a) and FT spectra of its oscillatory parts (b) for the 1,020-nm band of B_A^- absorption in mutant YM210L/ HL168L (curve 1), YM210L (curve 2) and native (curve 3) RCs of *Rba. sphaeroides* at 90 K.

RCs with slight differences in the spectral position and amplitude of the peaks (Fig. 1b). The formation of the B_A^- absorption band centered at 1,020 nm is observed for RCs of both mutants. This absorption band is, however, much weaker than that found for native *Rba.* sphaeroides RCs (Yakovlev *et al.*, 2002). A reason for it can be related to rising the free energy of $P^+B_A^-$ in both mutant RCs, which energy may be higher than that of P* due to replacement of the tyrosine YM210 by apolar residue (leucine) (Nagarajan *et al*., 1993). The kinetics of ΔA at 1,020 nm for the YM210L/ HL168L and YM210L mutants, and for the native *Rba. sphaeroides* contains strong oscillations (Fig. 2). These oscillations reflect the reversible electron transfer from P* to B_A due to a nuclear wavepacket motion (Yakovlev *et al*., 2002). A small none-oscillating background of coherent oscillations in the 1,020-nm kinetics of YM210L/ HL168L mutant (Fig. 2a, curve 1) reflects a quasi-exponential stabilization of the $P^+B_A^-$ state. This stabilization is almost absent in YM210L mutant (Fig. 2a, curve 2). Stabilization of the separated charges in the state $P^+B_A^-$ is clearly observed in native RCs (Fig. 2a, curve 3). The main difference of the FT spectra of the oscillatory parts of the kinetics at 1,020 nm (Fig. 2b) from the analogous FT spectra at 940 nm (Fig. 1b) is the increased amplitudes of the low-frequency modes.

The double mutant YM210L/ HL168L of *Rba. sphaeroides* gives an opportunity to see a key role of TyrM210 in the stabilization of $P^+B_A^-$ state. The HL168L mutation put the redox potential of P^+/P by 123 mV below that of native RCs (Spiedel *et al*., 2002). It is much more than 30-mV increase of this potential caused by the YM210L mutation (Beekman *et al.*, 1996). The resulting ~90 mV decrease of P^+/P redox potential in the YM210L/HL168L mutant would provides a significant lowering of the $P^+B_A^-$ free energy level that would speed up the primary reaction $P^* \rightarrow P^+B_A^-$ and improve the stabilization of $P^+B_A^-$ state in comparison with the single YM210L mutant. However the experimentally observed effect of the addition of the HL168L mutation is much smaller than an expected one. The P* lifetime in YM210L/ HL168L mutant is much more than in native RCs (Fig. 1). The 1,020-nm kinetics of YM210L/ HL168L mutant shows only a slight accumulation of B_A^- (Fig. 2). These facts mean that the absence of TyrM210 can not be compensated by lowering of the $P^+B_A^-$ free energy.

Two possible mechanisms of the dynamic stabilization of $P^+B_A^-$ in native RCs can be considered. The first possibility is that electron can be transferred from P* to the higher vibrational level on the $P^+B_A^-$ potential energy surface with subsequent vibrational relaxation to the lowest level (Bixon *et al*., 1988). This possibility requires non-symmetrical arrangement of the potential energy surfaces of P* and $P^+B_A^-$. The second possibility is that dynamical stabilization of $P^+B_A^-$ can be due to a reorientation of surrounding groups when $P^+B_A^-$ state is formed. In native RCs, the nuclear position can be changed non-coherently by reorientation of the surrounding polar groups like $O^{\delta-}H^{\delta+}$ of TyrM210. The motion of $H^{\delta+}$ towards B_A^- could low down the energy of $P^+B_A^-$ with respect to that of P* and stabilize $P^+B_A^-$.

According to electrostatics and molecular-dynamics calculations (Alden *et al*., 1996), the presence of the polar OH-group of TyrM210 lowers down the energy level of $P^+B_A^-$ by ~1,500 cm^{-1} due to a static redistribution of charges in the near vicinity of B_A. The dynamic effect of reorientation of the OH-group due to charge separation was found to have an additive influence on the rate of primary reaction. Calculations of the reorientation of the OH-group in TyrM210 of *Rba. sphaeroides* RCs show that the spectrum of autocorrelation function of stochastic rotations of the OH-group consists of several narrow (~4 cm^{-1}) peaks in the range from 270 to 390 cm^{-1} with two main peaks at 356 and 368 cm^{-1}. Note that the spectrum of resonance Raman scattering of tyrosine does not contain any peaks in the range from 300 to 450 cm^{-1} (Nabiev *et al*., 1988). This proves the idea that the reorientation of the OH-group of TyrM210 appears only when charge separation between P and B_A takes place. The FT spectrum of the oscillations in the B_A^- band of native RCs of *Rba. sphaeroides* at 1,020 nm contains a small feature at 330–390 cm^{-1} (Fig. 2, curve 3). Two very small bands at 341 and 365 cm^{-1} are observed in the FT spectrum of oscillations in the P* stimulated emission band of native RCs of *Rba. sphaeroides* at 940 nm (Fig. 1, curve 3). These bands are absent in the analogous FT spectra of YM210L/HL168L and YM210L mutant RCs (Figs. 1 and 2). These observed bands may reflect the rotation of the OH-group of TyrM210.

Another possibility of the dynamical stabilization of the $P^+B_A^-$ state may be associated with

crystallographycally defined water molecule HOH55 located in the structure of purple bacteria RCs between P_B and B_A (Potter *et al*., 2005). A hydrogen bond interaction with the 13^1-keto carbonyl group of B_A would stabilize B_A^- in native RCs, particularly when P is oxidized during charge separation. Stochastically oriented water dipole can changes its orientation in the electric fields of P^+ and B_A^- during charge separation. In the final orientation, the $H^{\delta+}$ atom is closer to the 13^1-keto carbonyl group of B_A that makes easier the possible formation of H-bond.

Acknowledgements

Support by Russian Basic Research Foundation grants N 08-04-00888 and N 11-04-00312, and by a program of basic research of Presidium of RAS "Molecular and Cell Biology" N 10P is gratefully acknowledged.

References

Alden RG, Parson WW, Chu ZT, Warshel A (1996) Orientation of the OH Dipole of Tyrosine (M)210 and Its Effect on Electrostatic Energies in Photosynthetic Bacterial Reaction Centers. J. Phys. Chem. 100: 16761-16770

Beekman LMP, Van Stokkum IHM, Monshouwer R, Rijnders AJ, McGlynn P, Visschers RW, Jones MR, Van Grondelle R (1996) Primary Electron Transfer in Membrane-Bound Reaction Centers with Mutations at the M210 Position. J. Phys. Chem. 100: 7256-7268

Bixon M, Jortner J, Plato M, Michel-Beyerle ME (1988) Mechanism of the Primary Charge Separation in Bacterial Reaction Centers. In: Breton J, Vermeglio A (eds.), The Photosynthetic Bacterial Reaction Center: Structure and Dynamics. Plenum Press: NY, London, pp. 399-419

Komiya H, Yeates TO, Rees DC, Allen JP, Feher G (1988) Structure of the Reaction Center from Rhodobacter Sphaeroides R-26 and 2.4.1.: Symmetry Relations and Sequence Comparisons between Different Species. Proc. Natl. Acad. Sci. U.S.A. 85: 9012-9016

Nabiev IR, Efremov RG, Chumanov GD (1988) Gigantic Raman Scattering and Its Application in Study of Biology Molecules. Uspehi Fizicheskih Nauk 154**:** 459-496 (in Russian)

Nagarajan V, Parson WW, Davis D, Schenck C (1993) Kinetics and Free Energy Gaps of Electron-Transfer Reactions in Rhodobacter Sphaeroides Reaction Centers. Biochemistry 32**:** 12324-12336

Potter JA, Fyfe PK, Frolov D, Wakeham MC, Van Grondelle R, Robert B, Jones MR (2005) Strong Effects of an Individual Water Molecule on the Rate of Light-Driven Charge Separation in the Rhodobacter Sphaeroides Reaction Center. J. Biol. Chem. 280: 27155-27164

Shuvalov VA, Shkuropatov AY, Kulakova SM, Ismailov MA, Shkuropatova VA (1986) Photoreactions of Bacteriopheophytins and Bacteriochlorophylls in Reaction Centers of Rhodopseudomonas Sphaeroides and Chloroflexus Aurantiacus. Biochim. Biophys. Acta 849: 337-348

Spiedel D, Jones MR, Robert B (2002) Tuning of the Redox Potential of the Primary Electron Donor in Reaction Centres of Purple Bacteria: Effects of Amino Acid Polarity and Position. FEBS Letters 527: 171-175

Vasilieva LG, Bolgarina TI, Khatypov RA, Shkuropatov AYa, Shuvalov VA (2001) Substitution of Valine-157 Residue by Tyrosine in the L-Subunit of the Rhodobacter Sphaeroides Reaction Center. Dokl. Biochem. and Biophys. (Russian) 376: 46-49

Vos MH, Jones MR, Breton J, Lambry JC, Martin JL (1996) Vibrational Dephasing of Long- and Short-Lived Primary Donor Excited States in Mutant Reaction Centers of Rhodobacter Sphaeroides. Biochemistry, 35: 2686-2693

Yakovlev AG, Shkuropatov AYa, Shuvalov VA (2002) Nuclear Wavepacket Motion between P* and $P^+B_A^-$ Potential Surfaces with a Subsequent Electron Transfer to H_A in Bacterial Reaction Centers at 90 K. Electron Transfer Pathway. Biochemistry 41: 14019-14027

Coordination Changes of Carboxyl Ligands at the Q_AFeQ_B Triad in Photosynthetic Reaction Centers Studied by Density-Functional Theory

Petko Chernev, Ivelina Zaharieva, Holger Dau, Michael Haumann*

Freie Universität Berlin, Institut für Experimentalphysik, 14195 Berlin, Germany.
*Corresponding author. Tel. No. +49 30 8385 6101; Fax No. +49 30 8385 6299; E-mail: michael.haumann@fu-berlin.de.

Abstract: The electron exit pathway of photosystem II (PSII) in plants and cyanobacteria comprises two quinone molecules (Q_A and Q_B) working in a series and in between a non-heme iron atom with a carboxyl ligand. Currently, the role of the Fe atom and its ligand in the Q_A-Fe-Q_B triad is insufficiently understood. We investigated the changes in the oxidation state and the coordination environment of the Fe in PSII upon quinone reduction using density-functional theory calculations (DFT). The electron transfer from Q_A^- to Q_B in PSII was not accompanied by an oxidation state change of Fe(II), as previously also found for bacterial reaction center. Instead, DFT on large geometry-optimized cluster models of the Fe site and its surrounding environment based on the crystal structure suggested a transition from 6-coordinated Fe(II) to 5-coordinated Fe(II) due to a switch from bidentate to monodentate ligation (carboxylate shift) of bicarbonate at the Fe, which is induced by Q_A^- formation. We propose that the non-heme Fe serves an essential function in the $Q_A^-\rightarrow Q_B$ reaction: it steers charge densities and hydrogen-bonding within the iron-bicarbonate-quinone complex, facilitating rapid and high-yield Q_B reduction.

Keywords: Non-heme iron; Photosystem II; Electron transfer; Bicarbonate; Density-functional theory

Introduction

Currently, the high yield of the electron transfer (ET) reactions in photosynthetic reaction center (RC) proteins is in practice unparalleled in artificial systems. Understanding all aspects of these reactions is therefore of prime interest as it may lead to the development of technical devices for sunlight-powered sustainable production of fuels, *e.g.* molecular hydrogen (H_2), from inexhaustible resources (Barber, 2009).

In type-II RCs, the electron exit pathway consists of two chemically identical quinone molecules (Q_A and Q_B) working in series (Fig. 1). Upon light excitation of dark-adapted reaction centers, Q_A is reduced within < 1 ns (Diner *et al*., 2002). The electron is then transferred to Q_B in micro- to milliseconds (Parson, 2003). After a second excitation, the $Q_A^-Q_B^- + 2H^+ \rightarrow Q_AQ_BH_2$ reaction proceeds and the quinol is exchanged against an oxidized quinone molecule (Parson, 2003). The inter-quinone ET represents a striking example of a directed and efficient reaction between protein-bound cofactors of the same chemical type. The high efficiency of the reaction suggests that there must be mechanisms that provide sufficient thermodynamic driving force for the forward ET. Extensive experimental and theoretical investigations on the events associated with the inter-quinone ET reactions have disclosed a wealth of information, *e.g.*, on the ET kinetics and accompanying protonation reactions (reviewed in *e.g.* Nabedryk and Breton, 2008; Renger and Renger, 2008), mostly on bacterial reaction centers (BRC) for which high-resolution crystal data is available (Koepke *et al*., 2007; Li *et al*., 2006). Crystal structures of PSII so far were reported only at lower resolution (Ferreira *et al*., 2004; Guskov *et al*., 2009), but a structure at higher resolution may become available in the near future (Shen *et al*., 2011).

In between the two quinones, a non-heme iron atom with a carboxyl ligand (bicarbonate in photosystem II (PSII), glutamate in BRC) is located

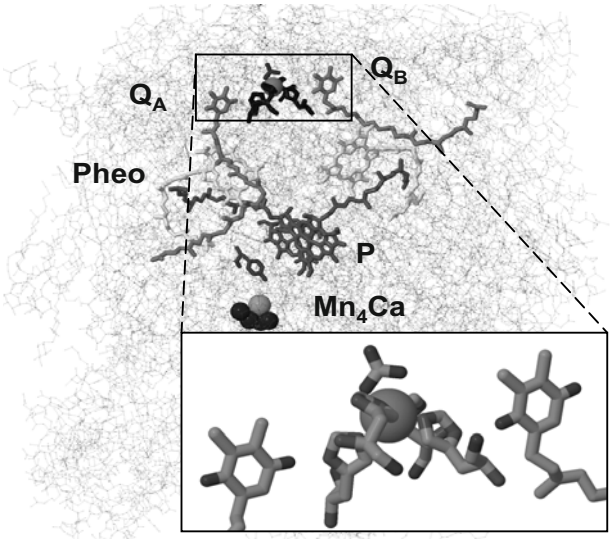

Fig. 1 Redox cofactors in photosystem II. Electrons are extracted from water at the Mn_4Ca cluster, and are transferred through a tyrosine residue, a special chlorophyll *a* pair (P), one pheophytin molecule (Pheo) and Q_A finally to Q_B. Between Q_A and Q_B, a non-heme iron atom is located, ligated to four histidine residues and bicarbonate. The scheme was based on the structure reported in (Guskov *et al*., 2009).

(Ferreira *et al*., 2004; Guskov *et al*., 2009). For decades, the functional role of this iron has remained enigmatic. Based on time-resolved FTIR and UV/vis absorption experiments on BRC, the transient oxidation of the Fe(II) to Fe(III) by Q_B after formation of Q_A^-, and the subsequent re-reduction of the iron by Q_A^- have been invoked (Remy and Gerwert, 2003). Later studies on BRC using time-resolved X-ray absorption spectroscopy (XAS) at the Fe K-edge provided no evidence for Fe(III) formation during the $Q_A^-\rightarrow Q_B$ ET. However, a kinetic XAS signal tentatively was assigned to structural changes of unclear origin (Hermes *et al*., 2006).

In the present study, we investigated the non-heme iron site using density-functional theory (DFT) on Q_AFeQ_B site models for PSII and BRC. The observed coordination changes at the iron imply an essential function of the Fe(II)-carboxyl complex in the inter-quinone ET (Chernev *et al*., 2010).

Materials and Methods

Spin-unrestricted DFT geometry optimizations were performed with the ORCA program package (Neese, 2007). The Becke-Perdew BP86 functional and a split-valence (SV) basis set were used for all atoms except for the Fe, for which the triple-zeta valence plus polarization (TZVP) basis set was used. The resolution of the identity (RI) approximation was used with the auxiliary SV/J and TZV/J Coulomb fitting basis sets. A conductor-like screening model (COSMO) for the solvation environment (Sinnecker *et al*., 2006) was applied using a dielectric constant of $\varepsilon = 4$. Tight self-consistent field (SCF) convergence criteria were employed. At the equilibrium geometries, single-point calculations were done with the B3LYP functional and TZVP basis set for all atoms.

Starting structures for the PSII, the Fe site, and its amino acid environment were derived from the 2.9 Å resolution structure ((Guskov *et al*., 2009), PDB code 3BZ1). Three models of different complexity were analyzed. The simplest model included only the non-heme iron, the bicarbonate, the four histidines ligands to Fe, and Q_A (Fig. 2a); a medium-size model included also Q_B (Fig. 2b); and the large model (Fig. 2c) comprised in addition eight amino acid residues and a water molecule near the bicarbonate.

For the oxidized state of the complex, the iron was assumed to formally carry a charge of +2; the bicarbonate anion HCO_3^- had a charge of –1. The four His ligands (D2H214, D2H268, D1H215, D1H272; represented by 4-methylimidazole in the model) were deprotonated and thus neutral. The isoprenoid tails of quinones were shortened to only two carbon atoms and the quinones were assumed to be neutral. In the largest version of the model the following amino acid residues were included: D1Glu244 (represented as acetic acid) was assumed to be protonated and thus neutral, D1Ser268 (represented as methanol), D1Tyr246 and D2Tyr244 (represented as two 4-methylphenols), D2Trp253 (represented as 3-methylindole), D1Ser264 (represented as methanol), D1His252 (represented as 4-methylimidazole) was deprotonated and thus neutral. The total charge of the oxidized state of the complex therefore was assumed to be equal to +1. The singly-reduced state, simulating the Q_A^- state, was achieved by the addition of one electron to the whole complex (an initial guess of the electron density was done using the PModel feature of ORCA) and had a total charge of zero. The Fe(II) atom was assumed to be high-spin (S = 2) (Petrouleas *et al*., 1982) and thus the spin multiplicity (M) of the complex in its oxidized state was set to 5. For the reduced state, M-values of both 4 and 6 were considered.

Initial coordinates for the model of the iron site in the bacterial reaction center were taken from the 1.87 Å

resolution structure of *Rhodobacter sphaeroides* ((Koepke *et al.*, 2007), PDB code 2J8C). The model included the iron, its four histidine and one glutamate ligands, a crystal water molecule near the iron, and Q_A (Fig. 2d).

During the geometry optimization procedure, for each amino acid residue the carbon atom that was closest to the protein backbone was constrained to its position in the crystal structure; for the quinones, the last remaining carbon atom of the isoprenoid tail was fixed. In the large PSII model, for all amino acid residues that were not ligated to the iron, the non-hydrogen atoms were fixed to their positions in the corresponding crystal structure.

Results and Discussion

Geometry-optimized structures with oxidized quinones (Fig. 2 left) consistently revealed a six-coordinated iron with bicarbonate that was only slightly asymmetrically chelating, *i.e.* a bidentate ligand (mean length difference between the two Fe-O bonds of 0.17 Å). Low Mayer bond-orders implied that both

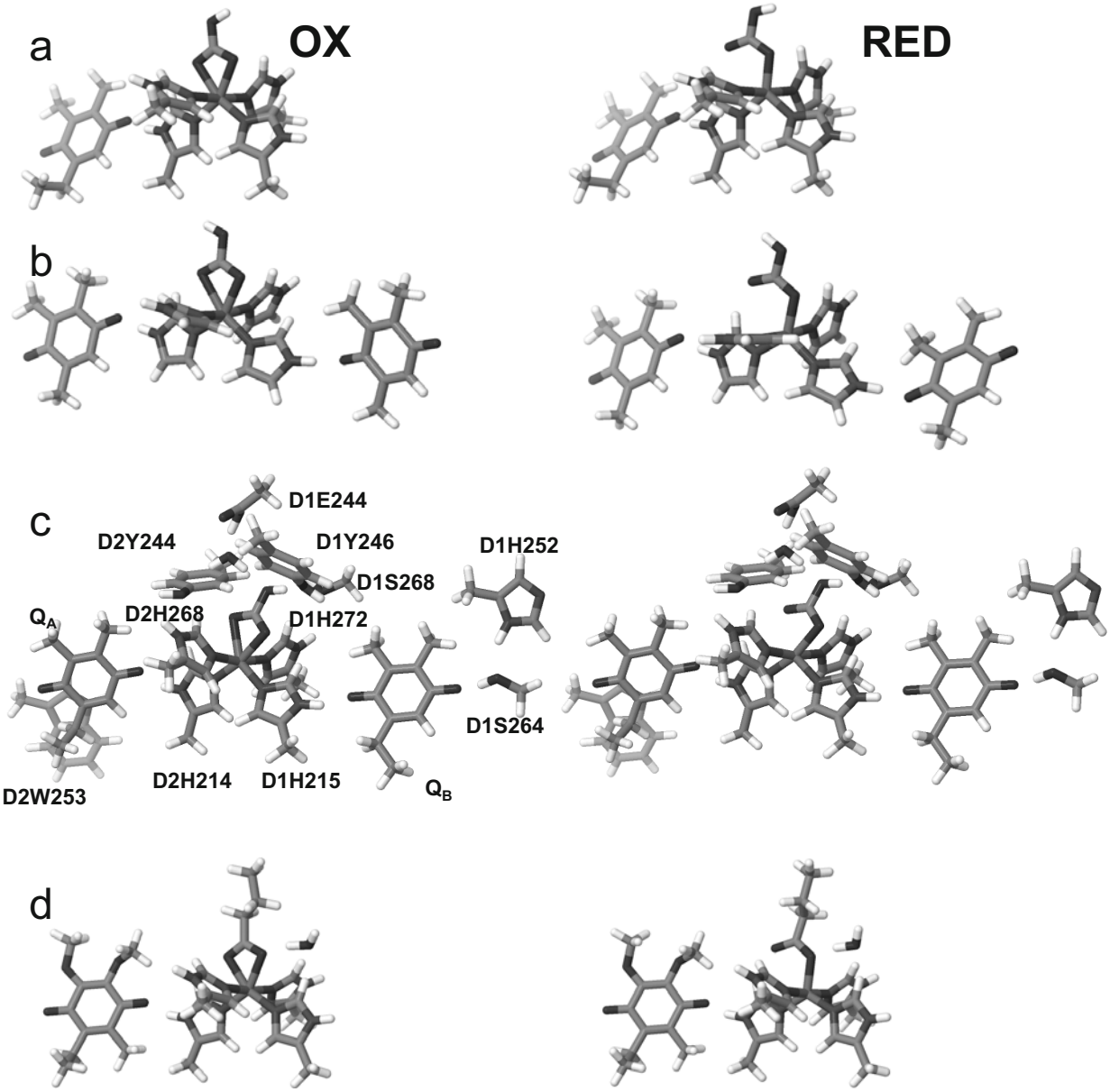

Fig. 2 Models of the Q_A-Fe-Q_B site derived by DFT calculations. (a) small model of the site in PSII, containing only the quinone ring of Q_A, the iron, its four histidine ligands and bicarbonate; (b) medium model, containing additionally Q_B; (c) large model that includes also several amino acid residues; (d) small model of the Q_A-Fe site in the bacterial reaction center from *Rhodobacter sphaeroides*. Left: geometry-optimized structures of the oxidized complexes; right: respective structures of the reduced (*i.e.*, Q_A^- containing) complexes.

Fe-O bonds were weak. In this state, the iron atom had a population of its d-orbitals close to 6 and a total spin close to 4 (see Table 1), which is what is formally expected for a high-spin iron with an oxidation state of +2. The occupied molecular orbital with strongest Fe-$d(z^2)$ character (Fig. 3a) was oriented approximately along the axis perpendicular to the Q_A-Fe-bicarbonate-Q_B plane (in PSII, this is the (histidine D2-268)N-Fe-N(histidine D1-272) axis). The molecular orbital with Fe–$d(x^2–y^2)$ character was roughly aligned with the basal Fe-N(histidine) and Fe-O(bicarbonate) bonds, indicating a distorted octahedral Fe(II).

When the structure was reduced by adding one electron, a pronounced elongation of the longer Fe-O bond (mean of about 0.8 Å) was observed, which corresponded to a change from 6-coordinated to 5-coordinated iron (Fig. 2, right).

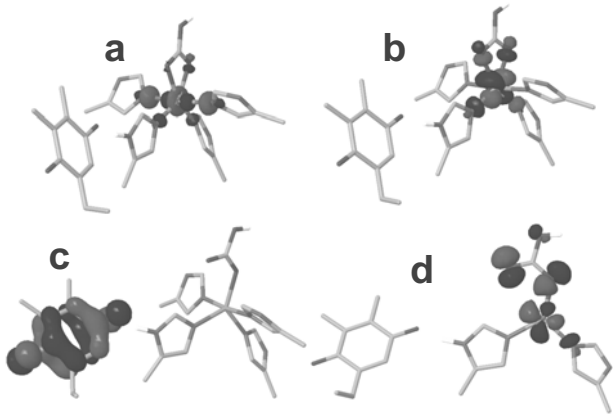

Fig. 3 Molecular orbital (MO) plots of the small PSII model. (a) MO with strongest Fe–$d(z^2)$ character in the oxidized state; (b) MO with strongest Fe–$d(x^2–y^2)$ character; (c) highest-occupied MO in the reduced state; (d) strongly anti-bonding MO for the bond between the iron and one of the oxygen atoms from the bicarbonate.

In the smallest reduced PSII model, the HOMO was entirely located on Q_A^- (Fig. 3c). The Fe *d*-orbital orientations were similar, *i.e.* the now trigonal-bipyramidal Fe(II) had a basal Fe-O bond. The Fe geometries were in good agreement with the calculated molecular orbital energies and Fe *d*-orbital occupancies (Fig. 4a). In particular, the Fe–$d(z^2)$ orbital had an increased energy, as expected for a trigonal-bipyramidal configuration (Fig. 4b), making a lower-spin state energetically possible. In most of the calculations for the reduced state, the iron remained high spin; only in the models that did not contain Q_B, reduced states calculated with total spin multiplicity M equal to 4 resulted in an intermediate-spin iron atom (S = 1). In the smallest PSII model, the high-spin structure (obtained with M = 6) had a slightly lower energy (by 0.4 eV) than the one with intermediate-spin; in both of these reduced structures, the iron was 5-coordinated. In the BRC model, however, a clear switch of the carboxylate to monodentate configuration occurred only in the intermediate-spin state. This monodentate structure had a lower energy (by 0.2 eV) than the M = 6 version, in which the bond elongation was smaller. These results suggest that a coordination change at the Fe may involve a transient spin state change, from high-spin Fe(II) to intermediate-spin Fe(II).

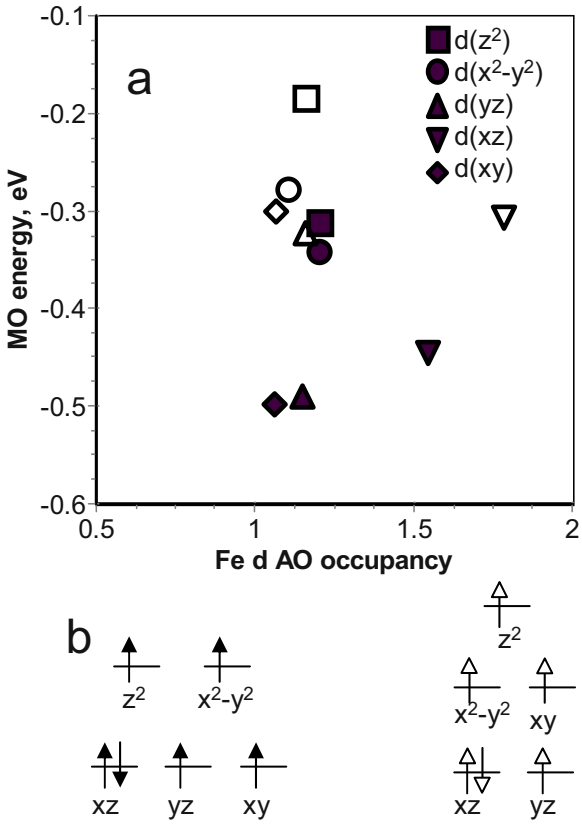

Fig. 4 (a) Plot of Fe-d atomic orbital (AO) occupancies versus averaged energies of the α- and ß-spin molecular orbitals with the highest respective Fe-d character for oxidized Q_A (solid symbols, spin multiplicity M = 5) and reduced Q_A (M = 6, open symbols; high-spin Fe(II)). Data for PSII are for the small model (Fig. 2a). (b) Idealized Fe-3d orbital energy levels and occupancies for octahedral high-spin Fe(II) (left) and trigonal-bipyramidal high-spin Fe(II) (right), in agreement with the coordination geometries shown in Fig. 2a and with Fe-d orientations and MO energies from the DFT calculations.

No indications for a change of the oxidation state of the iron were observed. The bond-valence sum (calculated according to (Liu *et al*., 1993)) for the

small model was 1.92 for the oxidized state, 1.89 for the reduced state with M = 6, and 2.34 for the reduced state with M = 4, *i.e.* compatible with Fe(II) within uncertainty limits.

In the model of the bacterial reaction center, when the water molecule near the glutamate (which is present in the 2J8C structure, see Fig. 2d) was not included in the calculation, the switch to a monodentate form was not observed, regardless of the total spin multiplicity. This may suggest that the carboxylate shift may also involve protein-bound water molecules.

The Fe-O bonds were already weak in the oxidized state. In the reduced state, the redistribution of electron density and the presence of molecular orbitals with strong anti-bonding character involving Fe and bicarbonate (Fig. 3d) additionally weakened one of the Fe-O bonds. As a result of the nuclear and electron redistribution, in the Q_A^- state, the Q_A···H-histidine bond was shortened by ~0.07 Å (Table 1); the proton of the histidine-H···Q_B also shifted towards Q_B, *i.e.* a partial protonation of Q_B prior to its reduction (Berthomieu *et al.*, 2001) was observed, which transiently may increase the redox potential of Q_B. We therefore suggest an active role of the Fe-carboxyl moiety in modulation of charge distribution and hydrogen bonding within the Q_AFeQ_B triad.

Time-resolved XAS data and K-edge spectral simulations (Chernev *et al.*, 2010) also suggested a coordination change of the bicarbonate from bidentate to monodentate ligation at the non-heme Fe(II) after the formation of Q_A^- in PSII. In this study direct experimental evidence indicated that the carboxylate shift occurred prior to the $Q_A^-\rightarrow Q_B$ reaction and was reverted concomitantly with the ET. The DFT data presented here and previous XAS and crystallography studies (Hermes *et al.*, 2006; Koepke *et al.*, 2007) favor a similar coordination change also in the BRC. Thus, we propose that a coordination change of the Fe(II)-bound carboxyl is a general feature of the type-II photosynthetic reaction centers.

Replacement of the bicarbonate by other carboxylic molecules can cause large changes in the E_m of the Fe(II)/Fe(III) pair and a drastic slowing down of the $Q_A^-\rightarrow Q_B^-$ET (Petrouleas *et al.*, 1994), these effects being most pronounced for the stronger bidentate ligands. Nitric oxide was found to bind to Fe(II) much more rapidly in the Q_A^- than in the Q_A state (Goussias *et al.*, 2002). These results circumstantially support our view that coordination flexibility of the ligand is essential for the function of the Fe(II)-carboxyl complex in the inter-quinone ET.

Table 1 Structural and electronic parameters of Q_AFeQ_B sites from DFT calculations. Values are for three PSII model structures of different size (see Figs. 2A, 2B and 2C) and for a model of BRC (Fig. 2D). For the reduced quinone complex, the total spin multiplicity M was set to 4, except for the small PSII model for which M was 6.

parameter	model	ox	red	Δ
shorter Fe-O [Å]	PSII small	2.19	2.02	–0.17
	PSII medium	2.16	2.00	–0.16
	PSII large	2.20	2.18	–0.02
	BRC	2.16	2.03	–0.13
longer Fe-O [Å]	PSII small	2.31	3.16	+0.85
	PSII medium	2.38	3.11	+0.73
	PSII large	2.37	2.51	+0.14
	BRC	2.29	3.21	+0.92
Mayer bond order of shorter Fe-O	PSII small	0.32	0.44	+0.12
	PSII medium	0.48	0.58	+0.10
	PSII large	0.39	0.39	0
	BRC	0.36	0.42	+0.06
Mayer bond order of longer Fe-O	PSII small	0.23	<0.10	<–0.13
	PSII medium	0.26	<0.10	<–0.16
	PSII large	0.29	0.21	–0.08
	BRC	0.31	<0.10	<–0.21
Q_A···· H(NHis) [Å]	PSII small	1.61	1.54	–0.07
	PSII medium	1.62	1.54	–0.08
	PSII large	1.68	1.63	–0.05
	BRC	1.66	1.53	–0.13
Q_B····H(NHis) [Å]	PSII medium	1.68	1.53	–0.15
	PSII large	1.71	1.59	–0.12
Fe-d population	PSII small	6.28	6.27	–0.01
	PSII medium	6.14	6.18	+0.06
	PSII large	6.11	6.16	+0.05
	BRC	6.16	6.82	+0.66
Fe spin population	PSII small	3.80	3.81	+0.01
	PSII medium	3.97	3.89	–0.08
	PSII large	4.00	3.93	–0.07
	BRC	3.93	1.99	–1.94
charge on Q_A	PSII small	+0.08	–0.83	–0.91
	PSII medium	–0.09	–0.44	–0.35
	PSII large	–0.05	–0.42	–0.37
	BRC	–0.19	–0.82	–0.63
charge on Q_B	PSII medium	–0.07	–0.47	–0.40
	PSII large	–0.12	–0.50	–0.38

Likely, there are further changes in the extended H-bonded network around the Q_AFeQ_B site (Berthomieu *et al.*, 2001; Iwata *et al.*, 2009), which could not be explicitly included in this investigation because of limited structural information from

crystallography. We conclude that the carboxylate shift and associated H-bonding changes lead to the formation of an intermediate with a nuclear geometry optimized for the subsequent ET (priming state).

This study shows that a change in the coordination of the non-heme iron during the $Q_A^- \rightarrow Q_B$ ET is possible. The state formed by the movement of a carboxylate group at the iron is likely an intermediate state in the biphasic reaction of the $Q_A^- \rightarrow Q_B$ ET (Chernev *et al*., 2010). This structural change prepares protein and cofactors for the subsequent ET reaction. The quinone reaction at the acceptor side of photosystems seems to be a further member of the growing family of cofactor processes in biology (Haumann *et al*., 2005; Wöhri *et al*., 2010), in which the initial formation of a "smart" intermediate by nuclear rearrangement prepares the system for subsequent electron transfer and chemistry.

Acknowledgements

Financial support by the Deutsche Forschungsgemeinschaft (grant Ha3265/3-1 to MH), Unicat (Berlin Cluster of Excellence), and the European Union (FP7 program, SolarH2 consortium) is gratefully acknowledged. MH thanks the Deutsche Forschungsgemeinschaft for a Heisenberg-Fellowship.

References

Barber J (2009) Photosynthetic Energy Conversion: Natural and Artificial. Chem. Soc. Rev. 38: 185-96

Berthomieu C, Hienerwadel R (2001) Iron Coordination in Photosystem II: Interaction between Bicarbonate and the Q_B Pocket Studied by Fourier Transform Infrared Spectroscopy. Biochemistry 40: 4044-4052

Chernev P, Zaharieva I, Dau H, Haumann M (2010) Carboxylate Shifts Steer Inter-Quinone Electron Transfer in Photosynthesis. J. Biol. Chem. (in press) doi: 10.1074/jbc.M110.202879

Diner BA, Rappaport F (2002) Structure, Dynamics, and Energetics of the Primary Photochemistry of Photosystem II of Oxygenic Photosynthesis. Annu. Rev. Plant Biol. 53: 551-80

Ferreira KN, Iverson TM, Maghlaoui K, Barber J, Iwata S (2004) Architecture of the Photosynthetic Oxygen-Evolving Center. Science 303: 1831-1838

Goussias C, Deligiannakis Y, Sanakis Y, Ioannidis N, Petrouleas V (2002) Probing Subtle Coordination Changes in the Iron-Quinone Complex of Photosystem II during Charge Separation, by the Use of NO. Biochemistry 41: 15212-15223

Guskov A, Kern J, Gabdulkhakov A, Broser M, Zouni A, Saenger W (2009) Cyanobacterial Photosystem II at 2.9-Å Resolution and the Role of Quinones, Lipids, Channels and Chloride. Nat. Struct. Mol. Biol. 16: 334-342

Haumann M, Liebisch P, Muller C, Barra M, Grabolle M, Dau H (2005) Photosynthetic O_2 Formation Tracked by Time-Resolved X-Ray Experiments. Science 310: 1019-1021

Hermes S, Bremm O, Garczarek F, Derrien V, Liebisch P, Loja P, Sebban P, Gerwert K, Haumann M (2006) A Time-Resolved Iron-Specific X-Ray Absorption Experiment Yields No Evidence for an Fe^{2+} —> Fe^{3+} Transition during Q_A^- —> Q_B Electron Transfer in the Photosynthetic Reaction Center. Biochemistry 45: 353-359

Iwata T, Paddock ML, Okamura MY, Kandori H (2009) Identification of FTIR Bands Due to Internal Water Molecules around the Quinone Binding Sites in the Reaction Center from Rhodobacter Sphaeroides. Biochemistry 48: 1220-1229

Koepke J, Krammer EM, Klingen AR, Sebban P, Ullmann GM, Fritzsch G (2007) pH Modulates the Quinone Position in the Photosynthetic Reaction Center from Rhodobacter Sphaeroides in the Neutral and Charge Separated States. J. Mol. Biol. 371: 396-409

Li L, Mustafi D, Fu Q, Tereshko V, Chen DL, Tice JD, Ismagilov RF (2006) Nanoliter Microfluidic Hybrid Method for Simultaneous Screening and Optimization Validated with Crystallization of Membrane Proteins. Proc. Natl. Acad. Sci. USA 103: 19243-19248

Liu W, Thorp HH (1993) Bond Valence Sum Analysis of Metal-Ligand Bond Lengths in Metalloenzymes and Model Complexes. 2. Refined Distances and Other Enzymes. Inorg. Chem. 32: 4102-4105

Nabedryk E, Breton J (2008) Coupling of Electron Transfer to Proton Uptake at the Q_B Site of the Bacterial Reaction Center: a Perspective from FTIR Difference Spectroscopy. Biochim. Biophys. Acta 1777: 1229-1248

Parson WW (2003) Bacterial Photosynthesis. Anu. Rev. Microbiol. 28: 41-58

Petrouleas V, Deligiannakis Y, Diner BA (1994) Binding of Carboxylate Anions at the Non-Heme Fe(II) of PS II. II. Competition with Bicarbonate and Effects on the Electron Transfer Rate. Biochim. Biophys. Acta 1188: 271-277

Petrouleas V, Diner BA (1982) Investigation of the Iron Components in Photosystem II by Mössbauer Spectroscopy. FEBS Lett. 147: 111-114

Remy A, Gerwert K (2003) Coupling of Light-Induced Electron Transfer to Proton Uptake in Photosynthesis. Nat. Struct. Biol. 10: 637-644

Renger G, Renger T (2008) Photosystem II: the Machinery of Photosynthetic Water Splitting. Photosynth. Res. 98: 53-80

Shen JR, Kawakami K, Koike H (2011) Purification and Crystallization of Oxygen-Evolving Photosystem II Core Complex from Thermophilic Cyanobacteria. Meth. Mol. Biol. 684: 41-51

Sinnecker S, Rajendran A, Klamt A, Diedenhofen M, Neese F (2006) Calculation of Solvent Shifts on Electronic G-Tensors with the Conductor-Like Screening Model (COSMO) and Its Self-Consistent Generalization to Real Solvents (Direct COSMO-RS). J. Phys. Chem. A 110: 2235-2245

Wöhri AB, Katona G, Johansson LC, Fritz E, Malmerberg E, Andersson M, Vincent J, Eklund M, Cammarata M, Wulff M, Davidsson J, Groenhof G, Neutze R (2010) Light-Induced Structural Changes in a Photosynthetic Reaction Center Caught by Laue Diffraction. Science 328: 630-633

Symposium 03

Light Harvesting Anaerobic Systems

Strontium Ions are Functionally Replaceable with Calcium Ions in the Light-Harvesting 1 Reaction Center Core Complex from Thermophilic Purple Sulfur Bacterium *Thermochromatium Tepidum*

Yukihiro Kimura[a,b,*], Yuta Inada[b], Longjiang Yu[c], Takashi Ohno[b], Zhengyu Wang[c]

[a]Organization of Advanced Science and Technology, Kobe University, Nada, Kobe 657-8501, Japan;
[b]Department of Agrobioscience, Graduate School of Agriculture, Kobe University, Nada, Kobe 657-8501, Japan;
[c]Faculty of Science, Ibaraki University, Bunkyo, Mito 310-8512, Japan.
[*]Corresponding author. Tel./Fax No. +81 78 803 5819; E-mail: ykimura@people.kobe-u.ac.jp.

Abstract: *Thermochromatium tepidum* (TTP) is a themophilic purple sulfur photosynthetic bacterium of which light-harvesting 1 reaction center (LH1RC) complexes exhibit an unusual LH1 Q_y absorption at 915 nm and thermal resistance relative to those of mesophilic counterparts. Recently, we demonstrated that these unique properties were regulated by an inorganic cofactor, Ca^{2+}. Wild-type TTP cells grew anaerobically at 50 °C in a culture medium containing a small amount of $CaCl_2$. When Ca^{2+} was removed from the medium or replaced with other metal cations, the photosynthetic growth was largely suppressed, however, only Sr^{2+} was biofunctionally replaceable with Ca^{2+}. The resulting Sr^{2+}-substituted TTP (Sr^{2+}-TTP) cells showed different spectral properties compared with the native ones in the LH1 Q_y region. The LH1RC complex purified from Sr^{2+}-TTP cells exhibited its Q_y maximum at 888 nm (B888). Depletion of Sr^{2+} from the B888 species induced a blue-shift of the LH1 Q_y peak and decreased the thermal stability. Upon the Sr^{2+}-reconstitution, the LH1-RC recovered its thermal stability and Q_y peak position depending on the Sr^{2+}-concentration with an approximately 10^4 M^{-1} of binding constant. This is the first evidence for a functional LH1-variant which was prepared by the biosynthetic metal substitution.

Keywords: Purple bacteria; Light-Harvesting complex; Thermostability; Calcium

Introduction

Photosynthetic purple bacteria convert light energies into chemical energies through a light-driven redox cycle (Cogdell *et al*., 2006). Purple bacteria have two types of light-harvesting complexes, LH1 and LH2. The reation center (RC) is surrounded by a cylindrical LH1 to form a core complex (LH1RC), and LH2 complexes locate in the periphery of the LH1RC complex. It is known that peripheral LH2 antenna complexes are adaptable for various light conditions and show a variety of spectral feature by modulating the ring antenna sizes (Scheuring *et al*., 2004), $\alpha\beta$-polypeptide composition (Tharia *et al*., 1999), or hydrogen-bonding interactions (Sturgis *et al*., 1995) in the LH2 complex. By contrast, structural and spectral properties of the LH1 complex associated with the RC are rather insensitive to the culture condition although RC-lacking mutants from *Rba. sphaeroides* indicated flexibility and size heterogeneity of the LH1 complex (Bahatyrova *et al*., 2004).

Tch. tepidum (TTP) is the unique photosynthetic purple bacteria in terms of the unusual LH1 Q_y band at 915 nm (B915), red-shifted by ~25 nm than that of mesophilic analogue, *Ach. vinosum* (AVN), and its thermophilic nature growing at temperatures up to 58 °C, the highest among purple bacteria. It has been demonstrated that these unique properties are regulated by an inorganic cofactor, Ca^{2+} (Kimura *et al*., 2008; Kimura *et al*., 2009). Upon the Ca^{2+}-depletion, the LH1 Q_y band was blue-shifted to 880 nm (B880) with a marked deterioration of the thermal stability. The

altered properties were almost completely recovered by the reconstitution with Ca^{2+}, or to a lesser extent by the biochemical substitution with Sr^{2+}. This indicated a possibility that Sr^{2+} ions are functionally replaceable with Ca^{2+} in this thermophilic organism.

In the present study, we report for the first time a spectroscopic variant of the LH1-RC complex from the Sr^{2+}-TTP which was biosynthetically substituted Sr^{2+} for Ca^{2+}. Based on the findings presented here, the structural and functional roles of inorganic cofactors in this thermophilic organism are discussed.

Materials and Methods

Wild-type TTP cells were cultivated as described previously (Suzuki *et al*., 2007). Sr^{2+}-TTP cells were obtained by repeated subculturing at 50 °C in a medium containing 0.34 mmol of $SrCl_2$, instead of $CaCl_2$, under an incandescent lamp for 7–10 days. Photosynthetic growth was monitored with the absorption intensities at 860 nm and 910 nm were monitored for the culture cultivated at 40, 45, or 50 °C under the light intensities of 10, 40, or 160 μmol m^2 s. BChl *a* contents were estimated from the extracts of the LH1-RC with acetone/methanol = 7/2 (v/v) using the molar extinction coefficient of BChl *a* ($\varepsilon_{770} = 76\ M^{-1}cm^{-1}$) as described previously (Suzuki et al. 2007). Preparation of the Sr^{2+}-LH1RC (B888) and depletion of Sr^{2+} from the B888 using metal chelator (EDTA) were conducted according to the procedures reported for the wild-type LH1RC (B915) with minor modifications (Kimura *et al*., 2008). The Sr^{2+}-depleted B888 with a Q_y peak at 873 nm (B873) was extensively washed with a buffer containing 20 mmol Tris-HCl (pH 7.5) and 0.08% DDPC using Amicon Ultra 100 K (Millipore) to remove the residual EDTA. Effects of metal cations were examined by adding 20 mmol of various metal cations to the B888 complex.

Raman spectra were collected by HoloProbe532 (Kaiser Optics) equipped with an optical microscope. The excitation light was provided from the frequency-doubled Nd-YAG laser. Circular dichroism (CD) and magnetic CD (MCD) spectra were recorded on a Jasco J-720w spectropolarimeter as described elsewhere (Suzuki *et al*., 2007). Differential Scanning Calorimetry (DSC) measurements were conducted on a nanoDSC II calorimeter (Model 6100, Calorimetry Science Co.) in the temperature range of 25–125 °C at a heating rate of 1.0 °C/min. The sample solution for the B888 and B915 included 20 mmol of $SrCl_2$ and $CaCl_2$, respectively, in a buffer containing 20 mmol Tris-HCl (pH 7.5) and 0.08% DDPC. The filtrate of each sample solution was used as the reference.

Results and Discussion

Growth and preparation in Sr^{2+}-TTP

First, we conducted screening of the growth condition for the Sr^{2+}-TTP cells. Absorption properties of the Sr^{2+}-TTP cells were largely dependent on the growth temperature and light intensity as shown in Table 1. The amounts of BChl *a* and ratios of LH1RC/LH2 increased under the cultivation at higher temperatures with lower light intensities. Such a growth condition is preferable to obtain LH1RC-rich TTP cells, which is a great advantage in preparation of the LH1RC complexes. Therefore, Sr^{2+}-TTP cells were cultured at 50 °C with the light intensity of 10–20 mmol/s/m^2.

Table 1 Effects of temperature and light intensity on the amounts of BChl *a* and ratios of LH1RC to LH2 in Sr^{2+}-TTP cells.

Light Intensity	BChl *a* [μM]			OD_{910}/OD_{860}		
μmol/s/m^2	40 °C	45 °C	50 °C	40 °C	45 °C	50 °C
10	15	18	19	0.46	0.47	0.47
40	14	15	17	0.39	0.36	0.34
160	13	14	13	0.37	0.34	0.34

Sr^{2+}-LH1RC complexes were purified by an anion-exchange chromatography with a linear gradient of $SrCl_2$. The LH1RC with a ratio of A_{888}/A_{280} over 1.7 was highly purified as revealed by typical SDS-PAGE profiles, where four bands for C, H, M, L-subunits from the RC and two bands for α, β-subunits from the LH1 complex were clearly separated (Fig. 1A). Fig. 1B shows absorption spectra of the LH1RC complexes from Sr^{2+}-TTP and wild-type TTP. The Q_y maximum appeared at 888 nm which was largely blue-shifted compared with that of the wild-type. The purified LH1-RC was also obtained by a sucrose density gradient ultracentrifugation and showed a Q_y peak at 890 nm (data not shown). The results strongly support that the Sr^{2+} was not originated from the exogenous Sr^{2+} contained in the elution buffer during the purification, but was biosynthetically incorporated into the LH1RC during the photosynthetic growth.

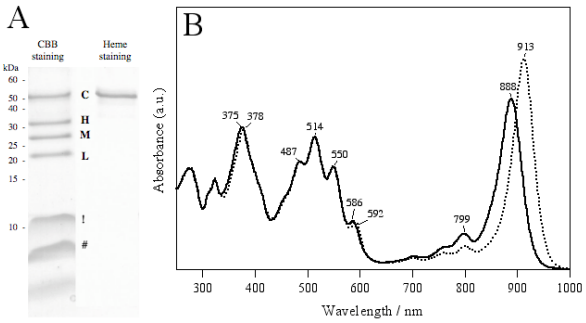

Fig. 1 (A) SDS-PAGE profiles of the purified LH1-RC complex from Sr^{2+}-TTP. (B) Absorption spectra of purified LH1RC from Sr^{2+}-TTP (solid line) and wild-type TTP (dotted line).

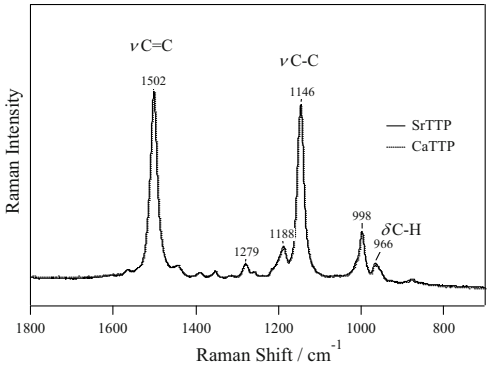

Fig. 2 Resonance Raman spectra of the LH1-RC complexes from Sr-TTP (solid line) and Ca-TTP (dotted line) obtained by an excitation of α–β region.

Fig. 2 shows resonance Raman spectra of the LH1-RC complexes from Sr^{2+}-TTP and Ca^{2+}-TTP obtained by laser excitation at 532 nm, which provides valuable information on the conformation of carotenoid molecules bound to the LH1RC complex. Intensive Raman bands at 1,502 cm^{-1} and 1,146 cm^{-1} were assigned to C = C and C–C stretching modes of all-*trans* spirilloxanthin, respectively. The spectral feature was almost identical between Sr^{2+}-TTP and Ca^{2+}-TTP in their peak position and band intensity, indicating that the molecular conformation and interaction modes of carotenoid molecules are largely similar between both species. In addition, the Sr^{2+}-substitution induced blue-shifts of CD signals for the Q_y and Q_x bands in response to the changes of electronic absorption bands, whereas other signals from RC and carotenoids remained to be unchanged (data not shown). These results suggest that inorganic cofactors are not related with the conformation and binding properties of carotenoid molecules (spirilloxanthin). Therefore, the spectral alterations induced by the substitution are originating from the changes in conformation and/or interaction modes of the BChl *a* molecules incorporated into the LH1 complex.

Binding affinity of Sr^{2+} in Sr^{2+}-TTP

The binding affinity of Sr^{2+} to the Sr^{2+}-depleted LH1RC complex was examined by a spectroscopic analysis. Fig. 3 shows absorption spectra of B873 after the addition of indicated concentration of $SrCl_2$. The Q_y peak at 873 nm was shifted to longer wavelength up to 888 nm with an isosbestic point at 871 nm, indicating that Sr^{2+} ions bind to the Sr^{2+}-depleted state to form B888 species with a one-to-one correspondence.

It is of note that the binding affinity of metal cations was different between Sr^{2+}-TTP and Ca^{2+}-TTP (wild-type) as clearly seen in the shift of sigmoid curves (Fig. 4, inset).

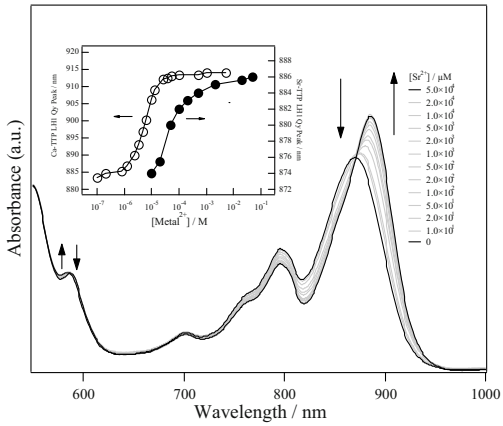

Fig. 3 Spectral changes of the B873 species upon the reconstitution with Sr^{2+}. The changes of the LH1 Q_y peak for Sr^{2+}-TTP (open) and Ca-TTP (closed) were shown in the inset.

Fig. 4 shows the plots of ΔA_{obs} at 900–930 nm as a function of the Sr^{2+} concentration. These wavelengths were selected as to minimize contribution from the RC. Assuming that an LH1 $\alpha\beta$-subunit of the B873 species binds to a Sr^{2+} at a 1:1 ratio to yield an LH1 subunit of the B888 species, the absorption changes ΔA observed can be expressed by the following equation,

$$\Delta A_{obs} = l \times (\varepsilon_{888} - \varepsilon_{873}) \times [(1 + C_0K + Kx) - \{(1 + C_0K + Kx)^2 - 4C_0K^2x\}^{0.5}]/2K \quad (1)$$

where l is a light-path length, ε_{888} and ε_{873} are molar extinction coefficients of the LH1 subunit in the B888

and B873 forms, respectively, C_0 is the initial concentration of subunit of the B873 species, K is the Sr^{2+}-binding constant, and x is the concentration of Sr^{2+}. The binding affinity of Sr^{2+} to B873 was evaluated by a non-linear least-square fitting of the spectroscopic data. The calculated and observed data showed a good agreement (Fig. 4) and Sr^{2+}-binding constant K was estimated to be approximately 1.7×10^4 M^{-1}. This value is 40 times lower than that of the wild-type ($K = 6.5 \times 10^5$ M^{-1}) (Kimura *et al.*, 2008). These results support that the binding affinity of metal cation in the LH1RC complex is lower in Sr-TTP than wild-type TTP.

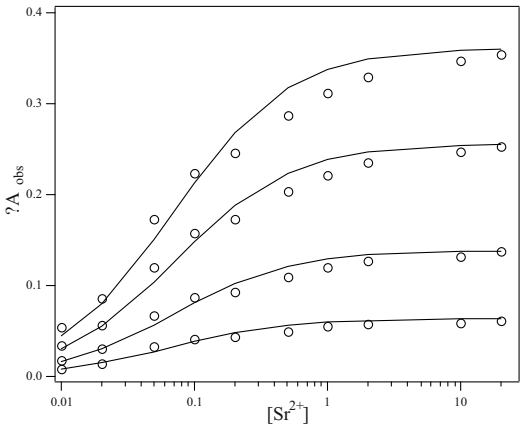

Fig. 4 Plots of absorption changes at 900, 910, 920, and 930 nm as a function of the Sr^{2+} concentration and the non-linear least square fitting (solid lines).

Thermal stability of Sr^{2+}-LH1RC complex Next, the thermal stability of the Sr^{2+}-variant was examined by using DSC analysis. Fig. 5 shows DSC profiles of the B888 and B915 species. An intensive DSC band of the Sr^{2+}-LH1RC complex appeared at 67.3 °C which was lower by 7.7 °C than that of Ca^{2+}-LH1RC, but was higher by 7.4 °C than that of Ca^{2+}-depleted LH1RC (B880) (Kimura *et al.*, 2009). The result demonstrated the thermal stability of these complexes to be in the following order: B915 > B888 > B880. Interestingly, the DSC bands of metal-bound species were sharpened and intensive in contrast to that of metal-depleted form. A possible explanation is that the metal-depleted forms are in an equilibrium of many different unstable states, resulting in a broad DSC band. By contrast, metal-bound forms acquired the tertiary structure tightly assembled by the metal cations, and therefore, showed the intensive band with a low FWHM value.

In the present study, we reported the functional spectroscopic variant of the LH1RC complex which was obtained by the biosynthetic metal substitution of Sr^{2+} for Ca^{2+}. The Sr^{2+}-LH1RC was purified and characterized. The spectral properties and thermal stability were compatible with the results reported previously (Kimura *et al.*, 2008; Kimura *et al.*, 2009). The present biosynthetic metal substitution is useful method for understanding roles of metal cations in this unique thermophilic organisms without possible modifications and/or contamination during the biochemical treatments. Further spectroscopic and thermodynamic analyses using the Sr^{2+}-variant are in progress.

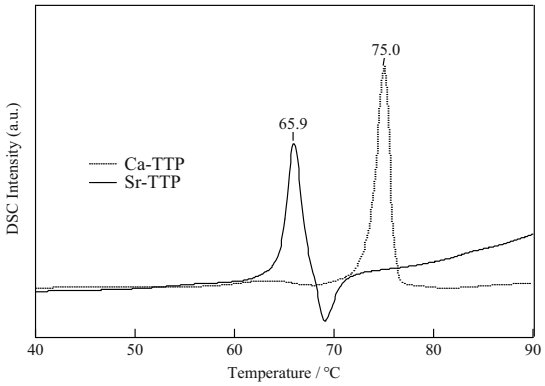

Fig. 5 DSC profiles of the LH1-RC complexes from Sr-TTP (solid line) and Ca-TTP (dotted line).

Acknowledgment

This work was supported by grant-in-Aid for Young Scientists (B) (20770102) (to Y.K.) from MEXT of Japan.

References

Bahatyrova S, Frese RN, van der Werf KO, Otto C, Hunter CN, Olsen JD (2004) Flexibility and Size Heterogeneity of the LH1 Light Harvesting Complex Revealed by Atomic Force Microscopy - Functional Significance for Bacterial Photosynthesis. J Biol Chem 279: 21327-21333

Cogdell RJ, Gall A, Kohler J (2006) The Architecture and Function of the Light-Harvesting Apparatus of Purple Bacteria: from Single Molecules to in Vivo Membranes. Q Rev Biophys 39: 227-324

Kimura Y, Hirano Y, Yu LJ, Suzuki H, Kobayashi M, Wang ZY (2008) Calcium Ions Are Involved in the Unusual Red Shift of the Light-Harvesting I Qy Transition of the Core Complex in Thermophilic

Purple Sulfur Bacterium Thermochromatium Tepidum. J Biol Chem 283: 13867-13873

Kimura Y, Yu LJ, Hirano Y, Suzuki H, Wang ZY (2009) Calcium Ions Are Required for the Enhanced Thermal Stability of the Light-Harvesting-Reaction Center Core Complex from Thermophilic Purple Sulfur Bacterium Thermochromatium Tepidum. J Biol Chem 284: 93-99

Scheuring S, Rigaud JL, Sturgis JN (2004) Variable LH2 Stoichiometry and Core Clustering in Native Membranes of Rhodospirillum Photometricum. EMBO J 23: 4127-4133

Sturgis JN, Jirsakova V, Reisshusson F, Cogdell RJ, Robert B (1995) Structure and Properties of the Bacteriochlorophyll Binding-Site in Peripheral Light-Harvesting Complexes of Purple Bacteria. Biochemistry (Mosc) 34: 517-523

Suzuki H, Hirano Y, Kimura Y, Takaichi S, Kobayashi M, Miki K, Wang ZY (2007) Purification, Characterization and Crystallization of the Core Complex from Thermophilic Purple Sulfur Bacterium Thermochromatium Tepidum. Biochim Biophys Acta 1767: 1057-1063

Tharia HA, Nightingale TD, Papiz MZ, Lawless AM (1999) Characterisation of Hydrophobic Peptides by RP-HPLC from Different Spectral Forms of LH2 Isolated from Rps. Palustris. Photosynthesis Research 61: 157-167

Cell-Free Expression of the Lhcb1 Protein of *Arabidopsis Thaliana*

Anjali Pandit[a,b*], Tineke de Ruijter[c], Riekje Brandsma[c], Jaap Brouwer[c],
Huub JM de Groot[a] , Willem J de Grip[a]

[a]Dept. of Solid-State NMR, Leiden Institute of Chemistry, Leiden University, Einsteinweg 55, 2300 RA Leiden, The Netherlands;
[b] Present address: Dept. of Biophysics, Fac. of Sciences, VU University Amsterdam, De Boelelaan 1081, 1081 HV Amsterdam, The Netherlands;
[c] Dept. of Molecular Genetics, Leiden Institute of Chemistry, Leiden University, Einsteinweg 55, 2300 RA Leiden, The Netherlands.
*Corresponding author. Tel. No. +31(0)20 5987937; Fax No. +31(0)205987899; Email a.pandit@vu.nl.

Abstract: We applied a cell-free expression system for *in-vitro* synthesis the Lhcb1 protein of *Arabidopsis thaliana* using a commercial in-vitro expression kit. The advantages of the cell-free system are that lipids or detergents can be added directly to the reaction mixture and that amino-acid residues can readily be substituted by isotope-labeled ones for studies by NMR. We carried out Lhcb1 batch-mode synthesis reactions in the presence of pigments and/or lipid nanodiscs. Interestingly, the Lhcb1 protein yield was significantly increased in the presence of lipid nanodiscs even though the majority of the synthesized proteins were obtained as precipitates. By optimizing the cell-free reaction mix parameters, we might eventually be able to refold and pigment-reconstitute the antenna complexes during the synthesis reaction.

Keywords: Light-harvesting complex II; *In-vitro* expression; Lipid nanodiscs

Introduction

The major antenna complex of higher-plant photosynthesis, LHCII, is composed by the products of Lhcb1 and two other genes, called Lhcb2 and Lhcb3 (Caffarri S *et al.*, 2004). The LHCII complex can be re-assembled by reconstituting Lhcb proteins overexpressed in *E. coli* bacteria, and refolding of the proteins in the present of pigments (Sandona D *et al.,* 1998). While this method is well-established for obtaining functional recombinant light-harvesting complexes, it is less suitable to produce high amounts of sample due to losses in the refolding and subsequent purification steps. On the other hand, cell-free protein expression is now an emerging technique for production and functional studies of a wide range of membrane proteins (Schwarz D *et al.*, 2008; Sobhanifar S *et al.*, 2010). By addition of detergents, liposomes or lipid nanodiscs to the reaction mixture, various membrane proteins could be correctly refolded *in vitro* during the synthesis reaction (Kai L *et al.*, 2010; Katzen F *et al.*, 2009; Schwarz D *et al.*, 2008). Upon addition of retinal and lipid nanodiscs to a cell-free reaction of the seven-helix transmembrane protein bacteriorhodopsin, soluble proteins were obtained inserted in lipid nanodiscs with characteristic absorption of the bound retinal chromophore (Katzen F *et al.*, 2008).

We show that the Lhcb1 protein of *Arabidopsis thaliana* can be synthesized in a commercial cell-free expression system. Lipid nanodiscs and pigment mixtures were added to the reaction mixture, in order to stimulate folding and pigment binding of the synthesized Lhcb1.

Materials and Methods

The sequence for the mature protein of Lhcb1.3 was cloned in a pExp5 vector and in a home modified pET vector derived from the pEt20. The cell-free synthesis reaction was carried out using a commercial cell-free expression kit (MembraneMax^{TM}, Invitrogen Life Technologies, Carlsbad CA). This kit contains a

control set including a pExp5 vector with the sequence for bacteriorhodopsin (Br), DMPC (dimyristoyl phosphatidylcholine) lipid nanodiscs and the chromophore retinal. The lipid nanodiscs are 10–12 nm diameter disc-shaped model membranes, consisting of a double layer of lipids surrounded by a membrane scaffold protein. For Lhcb1 synthesis reactions in the presence of its chromophore pigments, a crude extract of pigments was obtained from fresh spinach leaves by extraction with acetone. Batch-mode cell-free synthesis reactions for expression of the Lhcb1 and of bacteriorhodopsin as a control were initiated by mixing the *E. coli* lysate, amino acid mix, and energy components with the constructed plasmids in 20–50 µl reaction vessels. Substrate and energy components were supplied in two steps. The reactions were carried out at temperatures ranging from 20–35 ^{o}C and using a thermo shaker for constant stirring and the reaction incubation time was varied from 2–12 h. Afterwards, the reaction samples were spun for 5 min. at 10 rpm to separate the soluble and pellet fractions and were loaded on gel for analysis.

Results and Discussion

The Lhcb1 protein was synthesized using both the pExp5 and pEt constructs at reaction temperatures between 20 ^{o}C and 25 ^{o}C. Above 25 ^{o}C, no Lhcb1 protein was produced. In contrast, Br was synthesized over the whole temperature range, with optimal yields at 35 ^{o}C. For both the Lhcb1 and Br, reaction incubation times exceeding 4 h did not significantly improve the production yield.

After determining the optimal temperature and incubation time conditions (25 ^{o}C and ~4 h incubation time for Lhcb1), reactions were carried out in the presence of pigments and/or lipid nanodiscs. For Lhcb1 synthesis, the reaction mix included (1) the Lhcb1 pExp5 vector, (2) the Lhcb1 pExp5 vector and DMPC lipid nanodiscs or (3) the Lhcb1 pExp5 vector, DMPC lipid nanodiscs and pigment mixture extracted from spinach. For Br synthesis as a control (Br), the reaction mix contained the Br pExp5 vector, DMPC lipid nanodiscs and retinal. The pellets and soluble fractions of the reaction mixtures were loaded on gel afterwards (see Fig. 1). The membrane scaffold protein (disc protein) appears in the soluble fractions, confirming solubility of the lipid nanodiscs. Br also appears in the soluble fractions, indicating that the produced bacteriorhodopsin protein was incorporated in the discs. In contrast, the Lhcb1 protein was contained in the pellet fractions and apparently not incorporated in the discs. Interestingly, for reactions (2) and (3) in the presence of lipid nanodiscs, the protein yield is higher than for (1), thus protein synthesis was enhanced by the presence of the lipid nanodiscs in the reaction mix. The lower graph is an immunoblot of the same fractions. Very weak bands appear for the soluble fractions of (2) and (3), showing that a small fraction of the Lhcb1 is incorporated in the discs. The presence of pigments did not improve the synthesis yield nor the solubility of the synthesized Lhcb1 under conditions tested so far.

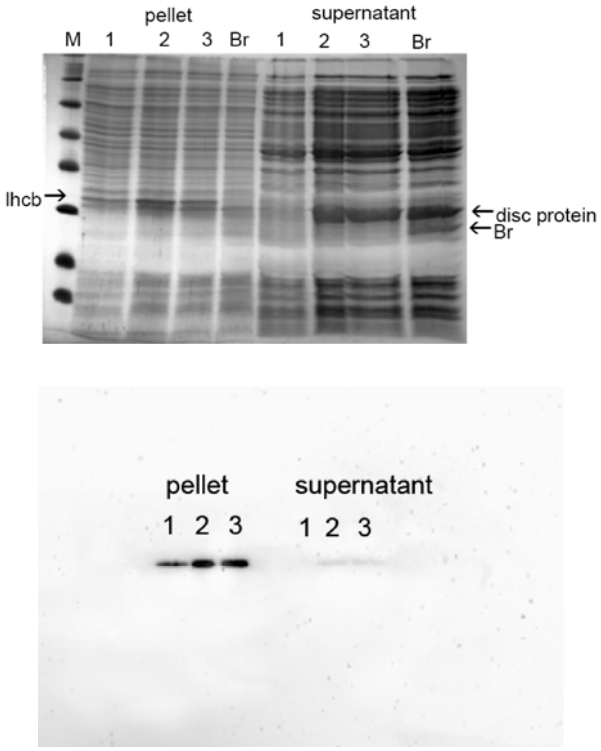

Fig. 1 Cell-free reactions of Lhcb1 (1-3) and Br as a control. Upper graph 1-3: *in vitro* expression of the Lhcb1, (1) without lipid nanodiscs and pigments, (2) in the presence of lipid nanodiscs without pigments and (3) in the presence of lipid nanodiscs and pigments. Br was expressed *in vitro* in the presence of lipid nanodiscs and retinal. Lower graph: immunoblot of the Lhcb1 fractions. A very small fraction of the Lhcb1 is incorporated in the lipid nanodiscs (supernatant). The presence of lipid nanodiscs in the reaction mixture (2 and 3) significantly increases the Lhcb1 expression yield.

In conclusion, we have demonstrated that the LHCII apoprotein can be expressed in an *in-vitro* synthesis expression system based on *E. coli*. The presence of lipid nanodiscs in the reaction mixture

supports *in vitro* synthesis of the Lhcb1 proteins, perhaps by providing a hydrophobic environment during the synthesis reaction, even though the majority of the proteins are not inserted in the discs.

Optimization of the reaction mix parameters, *i.e.* pigment and nanodisc ratios, or the addition of detergent could improve refolding of the synthesized Lhcb1 and reconstitution with pigments during the synthesis reaction. The protein synthesis yields will be significantly improved by using a dialysis system in which substrates and energy components are supplied by a way of continuous-exchange via a semi-permeable membrane (Jun SY *et al.,* 2008), at the same time diluting potentially inhibitory reaction by-products via diffusion through the membrane into a larger feeding compartment.

Acknowledgements

Prof. Roberta Croce and drs Francesca Passarini (Groningen University, The Netherlands) are kindly acknowledged for providing the Lhcb1.3 sequence. The Netherlands Organization of Scientific Research (NWO) is acknowledged for financial support of AP through a NWO-Veni grant.

References

Caffarri S, R Croce, L Cattivelli, R Bassi (2004) A Look within LHCII: Differential Analysis of the Lhcbl-3 Complexes Building the Major Trimeric Antenna Complex of Higher-Plant Photosynthesis. Biochemistry 43(29): 9467-9476

Jun SY, SH Kang, KH Lee (2008) Continuous-Exchange Cell-Free Protein Synthesis Using PCR-Generated DNA and an RNase E-Deficient Extract. Biotechniques 44(3): 387-391

Kai L, R Kaldenhoff, J Lian, X Zhu, V Dotsch, F Bernhard, P Cen, Z Xu (2010) Preparative Scale Production of Functional Mouse Aquaporin 4 Using Different Cell-Free Expression Modes. PLoS One 5(9): e12972

Katzen F, JE Fletcher, JP Yang, D Kang, TC Peterson, JA Cappuccio, CD Blanchette, T Sulchek, BA Chromy, PD Hoeprich, MA Coleman, W Kudlicki (2008) Insertion of Membrane Proteins into Discoidal Membranes Using a Cell-Free Protein Expression Approach. Journal of Proteome Research 7(8): 3535-3542

Katzen F, TC Peterson, W Kudlicki (2009) Membrane Protein Expression: No Cells Required. Trends in Biotechnology 27(8): 455-460

Sandona D, R Croce, A Pagano, M Crimi, R Bassi (1998) Higher Plants Light Harvesting Proteins. Structure and Function as Revealed by Mutation Analysis of Either Protein or Chromophore Moieties. Biochimica Et Biophysica Acta-Bioenergetics 1365(1-2): 207-214

Schwarz D, V Dotsch, F Bernhard (2008) Production of Membrane Proteins Using Cell-Free Expression Systems. Proteomics 8(19): 3933-3946

Sobhanifar S, S Reckel, F Junge, D Schwarz, L Kai, M Karbyshev, F Lohr, F Bernhard, V Dotsch (2010) Cell-free Expression and Stable Isotope Labelling Strategies for Membrane Proteins. Journal of Biomolecular Nmr 46(1): 33-43

Optimal Mutual Orientational Ordering of Q_Y Transition Dipoles of Adjacent Subantennae Pigments in the Superantenna of the Photosynthetic Green Bacterium *Chloroflexus Aurantiacus*. Theoretical and Experimental Studies

Andrey Yakovlev, Vladimir Novoderezhkin, Alexandra Taisova, Anastasiya Zobova, Zoya Fetisova*

A.N.Belozersky Institute of Physico-Chemical Biology, M.V. Lomonosov Moscow State University, Moscow, 119992, Russian Federation.
*Corresponding author. E-mail: Zfetisova@genebee.msu.ru.

Abstract: This work continues the series of our studies on the basic principles in the organization of natural light-harvesting antennae, which we theoretically predicted for the optimal model light-harvesting systems, initiated by our concept of the rigorous optimization of photosynthetic apparatus structure by functional criteria. This work deals with the problem of the structure optimization of *Cf.aurantiacus* heterogeneous superantenna, consisting of several uniform subantennae, which raises the problem of their optimal interfacing. Mathematical modeling of the functioning of this natural superantenna allowed us to consider possible optimization of this process via optimizing the mutual orientation of Q_y transition dipole moments vectors of the light-harvesting molecules in adjacent subantennae and, as a consequence, to suggest a model of optimal orientation of B798 BChl *a* Q_y transition dipoles within a single chlorosome. This model was confirmed by polarized difference absorption spectroscopy of isolated *Cf.aurantiacus* chlorosomes.

Keywords: Structure-function correlations; Green bacterium *Cf.aurantiacus*; Orientation of B798 pigments

Introduction

Several years ago we put forward the concept of strict functional optimization of light-harvesting antenna structure (Fetisova and Fok, 1984). Using simulations of excitation energy transfer (EET) from antenna to reaction center, one can identify the guiding principles for organization of an optimal antenna model. Targeted searches for theoretically identified structural optimization criteria have subsequently allowed us to recognize them in some natural antennae (Fetisova *et al*., 1984, 2004 (see the references); Mauring *et al*., 1996; Savikhin *et al*., 1998; Novoderezhkin *et al*., 1999, 2001; Yakovlev et al., 2002a, 2002b, 2004; Zobova *et al*., 2009, 2010). This approach to the study of the structure - function correlations in natural photosynthetic antennae is of great importance not only from the basic research standpoint; it also provides guidance for optimizing artificial light conversion systems in large-scale solar power engineering.

This work deals with the problem of the structure optimization of *Cf.aurantiacus* heterogeneous superantenna, consisting of several uniform subantennae, which raises the problem of their optimal interfacing. We used mathematical modeling of the functioning of this natural superantenna to consider possible optimization of this process via optimizing the mutual spatial orientation of Q_y transition dipole moments vectors of the light-harvesting molecules in adjacent subantennae.

In our model calculations (Zobova *et al*., 2009) we used infinite 3D antennae an elementary 1D fragment of which contained B740, B798 and B808 pigments (or their clusters). Orientations of the Q_y transition dipoles are known only for B740 and B808 pigments (Fetisova *et al*., 1986, 1988; Vasmel *et al*., 1986; Novoderezhkin and Fetisova, 1999). Orientations of B798 BChl *a* dipoles were determined by deviation from the B798 plane by φ angles, $\varphi \in [-\pi/2; +\pi/2]$.

Using the probability matrix approach, we computed the time (t, a.u.) of EET B740→B798→B808 as a function of mutual orientations of B740, B798 and B808 dipoles. Optimal orientations of B798 BChl *a* dipoles (φ_{opt}) were determined by the stable minima (t_{min}) of parametric curves $t(\varphi)$ if $t_{min} < t_r$, where t_r is the EET time for randomly oriented B798 BChl *a* dipoles. According to our computations, the optimal mutual orientation of B740, B798 and B808 dipoles leads to stable minimization of the EET time within the superantenna, thereby ensuring high efficiency and stability of the overall superantenna function.

Our findings conform to two models - triaxial and uniaxial - of optimal orientation distribution of B798 BChl *a* Q_y transition dipoles. The triaxial model implies that the BChl *a* dipoles orientations are strongly fixed in space with variable deviation from the B798 plane by φ_{opt} angles, and $\varphi_{opt} \in [37 ; 70]^o$ being governed by mutual orientations of B740, B798, and B808 dipoles. At the same time, the angle $\varphi_{opt} \approx 54^o$, corresponding to the center of the found φ_{opt} range $[37 ; 70]^o$, possesses the unique feature, notably**:** at the fixed value $\varphi_{opt} \approx 54^o$ and any mutual orientation of B740, B798, and B808 dipoles, the calculated efficiencies of EET showed practically the same values as those for the triaxial model described above. Thus, the uniaxial model implies random (*i.e.*, isotropic upon the average) orientation of BChl *a* dipoles around the normal to the B798 plane with a fixed deviation from this plane by the φ_{opt} angle, and $\varphi_{opt} \approx 54^o$ at that. Note that these conclusions were obtained by calculations for a single *Cf. aurantiacus* chlorosome. Recently, by using fluorescence polarization study of single chlorosomes, Shibata *et al*. (2007, 2009) observed uniaxial orientation distributions of BChl *a* emitting dipoles within single *Cf. aurantiacus* chlorosomes at 13 K. This allowed us to choose from two described above models the uniaxial one with the predicted by us value $\varphi_{opt} = 54 \pm 3^o$ to investigate this model *in vivo* by difference absorption spectroscopy with femtosecond resolution.

Materials and Methods

Chlorosomes from the filamentous nonsulfur thermophilic green bacterium *Cf. aurantiacus* strain Ok-70-fl, cultivated anaerobically in batch cultures at 55 °C (Pierson and Castenholz, 1974) were prepared in 2 mol NaSCN and 10 mmol sodium ascorbate by standard methods (Savikhin *et al*., 1998) with minor modifications.

Femtosecond/picosecond transient absorption spectra were measured using a setup based on a mode-locked Ti:sapphire femtosecond oscillator (Tsunami, Spectra Physics, U.S.A.) together with a home-built Ti:sapphire 8-pass amplifier producing pulses centered around 800 nm at a repetition rate of 15 Hz (Yakovlev *et al*., 2002). The output linear polarized pulses had a duration of ~50–100 fs and a spectral bandwidth of ~15–40 nm (full width at half maximum). The studies were carried out in the typical pump-probe setup. The output of the amplifier was split into the major part and the minor part with the energy ratio of ~100:1. The major part was passed through an interference filter centered at 800 nm with a 7 nm spectral bandwidth (Karl Zeiss, Germany) and was used after this as a pump pulse. The minor part was used as a probe pulse. The angle between the planes of polarization of the pump and the probe beams could be set equal to 0^o or 90^o. The delay of the probe pulse with respect to the pump pulse could be varied in the range of 0–2 ns with the accuracy of 1 fs. The difference (light – dark) time-resolved absorption spectra were registered by optical multi-channel analyzer based on CCD matrix detector coupled with spectrograph (InstaSpec, Oriel, France). Each spectrum was obtained by averaging of 50000 measurements and consisted of ~400 points. The typical values of ΔA were $\sim 10^{-4}$ OD. The optical density of the samples was 0.5–1.0 (1-mm thickness of cuvette). An estimation of excitation energy density in the samples gives a value $\sim 10^{12}$ photon/cm^2 per pulse. All measurements were carried out at room temperature.

Results and Discussion

Room temperature isotropic and anisotropic pump-probe spectra of *Cf.aurantiacus* chlorosomes were measured on femtosecond through picosecond time scales for the BChl *a* Q_y band upon direct excitation of this band. The anisotropy parameter value (Fig. 1)

$$r(\lambda) = (A_{II} - A_{\perp}) / (A_{II} + 2A_{\perp})$$

was constant within the whole B798 BChl *a* band and decayed from $r = 0.4$ (at $\Delta t = 200$ fs , not shown) to $r = 0.1$ (at $\Delta t = 30 \div 100$ ps) on the picosecond

timescale due to localized exciton migration between BChl *a* molecules (Fig. 1 shows the spectra only for Δt = 100 ps).

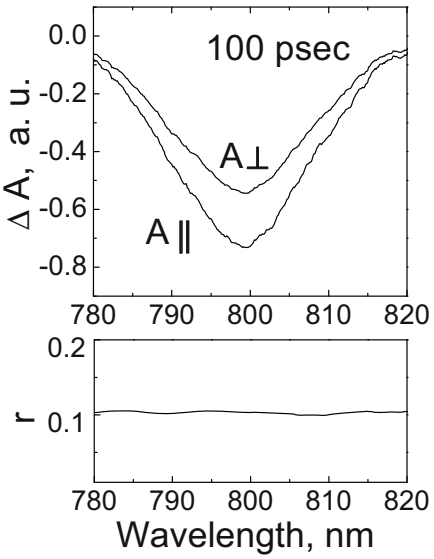

Fig. 1 Room temperature anisotropic pump-probe spectra of *Cf .aurantiacus* chlorosomes, measured at delay Δt = 100 ps for the chlorosome BChl *a* Q_y band upon direct excitation of the band (upper panel), and the anisotropy parameter value $r(\lambda)$ (lower panel).

We showed that the theoretical dependence of the steady state anisotropy parameter r on the sought angle φ for the examined model (at a random orientation of chlorosomes realized in our experiments) is described by the equation:

$$r(\varphi) = 0.1(3\cos^2\varphi - 2)^2.$$

According to this theoretical dependence $r(\varphi)$, the angle φ, corresponding to the experimental steady state value r = 0.1 at room temperature, was found to be equal to the magic angle φ = 54.7°. Thus, the findings are in complete agreement with our theoretically predicted model of optimal orientation of BChl *a* dipoles within the baseplate of *Cf. aurantiacus* chlorosomes, in which the B798 BChl *a* Q_y transition dipoles, randomly distributed around the normal to the baseplate plane, form the magic angle φ = 54.7° with the subantenna plane.

Acknowledgement

The work was supported by the Russian Foundation for Basic Research (Grant 08-04-01587a to Z.G.F.).

References

Fetisova ZG, Fok MV (1984) Optimization Routes for the Transformation of Light Energy in Primary Acts of Photosynthesis. I. The Necessity of Structure Optimization for Photosynthetic Unit and Method for the Calculation of Its Efficiency. Mol. Biol. (Moscow) 18: 1651-1656

Fetisova ZG, Fok MV, Shibaeva LV (1984/1985) Optimization Routes for the Transformation of Light Energy in Primary Acts of Photosynthesis. II. Mol. Biol. (Moscow) 18: 1657-1663; III. Mol. Biol. (Moscow) 19: 974-982; IV. Mol. Biol. (Moscow) 19: 983-991 V. Mol. Biol. (Moscow) 19: 1476-1488; VI. Mol. Biol. (Moscow) 19: 1489-1500

Fetisova ZG, Kharchenko SG, Abdourakhmanov IA (1986) Strong Orientational Ordering of the Near-Infrared Transition Moment Vectors of Light-Harvesting Antenna Bacterioviridin in Chroma-Tophores of the Green Photosynthetic Bacterium Chlorobium limi Cola. FEBS Lett. 199: 234-236

Fetisova ZG, Freiberg AM, Timpmann KE (1988) Long-Range Molecular Order as an Efficient Strategy for Light Harvesting in Photosynthesis. Nature 334: 633-634

Fetisova ZG, Shibaeva LV, Fok MV (1989) Biological Expedience of Oligomerization of Chlorophyllous Pigments in Natural Pho-tosynthetic systems. J. Theor. Biol. 140: 167-184

Fetisova ZG, Mauring K (1992) Experimental Evidence of Oligomeric Organization of Antenna Bacteriochlorophyll *c* in the Green Bacterium Chloroflexus Aurantiacus by Spectral Hole Burning. FEBS Lett. 307: 371-374

Fetisova ZG, Mauring K (1993) Spectral Hole Burning Study of Intact Cells of the Green Bacterium Chlorobium Limicola. FEBS Lett. 323: 159-162

Fetisova ZG, Mauring K, Taisova AS (1994) Strongly Coupled BChl *e* Chromophore System in Chlorosomal Antenna of Intact Cells of the Green Bacterium Chlorobium Phaeovibrioides: Spectral Hole Burning Study. Photosynth. Res. 41: 205-210

Fetisova ZG, Shibaeva LV, Taisova AS (1995) Oligomerization of Light-Harvesting Pigments as a Structural Factor Optimizing the Photosynthetic Antenna Function. I. Model Calculations Mol. Biol. (Moscow) 29: 1384-1390

Fetisova ZG, Freiberg AM, Mauring K, Novoderezhkin VI, Taisova AS, Timpmann KE (1996) Excitation Energy Transfer in Chlorosomes of Green Bacteria: Theoretical and Experimental Studies. Biophys. J. 71: 995-1010

Fetisova ZG (2004) Survival Strategy of Photosynthetic Organisms. I. Variability of the Extent of Light-Harvesting Pigment Aggregation as a Structural Factor Optimizing the Function of Oligomeric Photosynthetic Antenna. Model Calculations. Mol. Biol. (Moscow) 38: 434-440

Mauring K, Taisova AS, Novoderezhkin VI, Shibaeva LV, Fetisova ZG (1996) Oligomerization of Light-Harvesting Pigments as a Structural Factor Optimizing the Photosynthetic Antenna Function. 2. Experimental Proof of Oligomeric Organization of Pigments in Antenna of Green Bacteria. Mol. Biol. (Moscow) 30: 442-448

Novoderezhkin VI, Fetisova ZG (1999) Exciton Delocalization in the B808-866 Antenna of the Green Bacterium Chloroflexus Aurantiacus as Revealed by Ultrafast Pump-Probe Spectroscopy. Biophys. J. 77: 424-430

Novoderezhkin VI, Taisova AS, Fetisova ZG (2001) Unit Building Block of the Oligomeric Chlorosomal Antenna of the Green Photosynthetic Bacterium Chloroflexus Aurantiacus: Modeling of Nonlinear Optical Spectra. Chem. Phys. Lett. 335: 234-240

Pierson BK, Castenholz RW (1974) Studies of Pigments and Growth in Chloroflexus Aurantiacus, a Phototrophic Filamentous Bacterium. Arch. Microbiol. 100: 283-305

Savikhin S, Buck DR, Struve WS, Blankenship RE, Taisova AS, Novoderezhkin VI, Fetisova ZG (1998) Excitation Delocalization in the Bacteriochlorophyll c Antenna of the Green Bacterium Chloroflexus Aurantiacus as Revealed by Ultrafast Pump-Probe Spectroscopy. FEBS Lett. 430: 323-326

Shibata Y, Saga Y, Tamiaki H, Itoh S (2007) Polarized Fluorescence of Aggregated Bacterio-Chlorophyll c and Baseplate Bacteriochlorophyll a in Single Chlorosomes Isolated from Chloroflexus Aurantiacus. Biochem. 46: 7062-7068

Shibata Y, Saga Y, Tamiaki H, Itoh S (2009) Anisotropic Distribution of Emitting Transition Dipoles in Chlorosome from Chlorobium Tepidum: Fluorescence Polarization Anisotropy Study of Single Chlorosomes. Photosynth. Res. 100: 67-78

Vasmel H, van Dorssen RJ, de Vos GJ, Amesz J (1986) Pigment Organization and Energy Transfer in the Green Photosynthetic Bacterium Chloroflexus Aurantiacus. I. The Cytoplasmic Membrane. Photosynth. Res. 7: 281-294

Yakovlev AG, Taisova AS, Fetisova ZG (2002a) Light Control over the Size of an Antenna Unit Building Block as an Efficient Strategy for Light Harvesting in Photosynthesis. FEBS Lett. 512: 129-132

Yakovlev AG, Novoderezhkin VI, Taisova AS, Fetisova ZG (2002b) Exciton Dynamics in the Chlorosomal Antenna of the Green Bacterium Chloroflexus Aurantiacus: Experimental and Theoretical Studies of Femtosecond Pump-Probe Spectra. Photosynth. Res. 71: 19-32

Yakovlev AG, Taisova AS, Fetisova ZG (2004) Survival Strategy of Photosynthetic Organisms II. Experimental Proof of the Size Variability of the Unit Building Block of Light-Harvesting Oligomeric Antenna. Mol. Biol. (Moscow) 38: 441-446

Zobova AV, Yakovlev AG, Taisova AS, Fetisova ZG (2009) The Search for an Optimal Orientational Ordering of Qy- Transition Dipoles of Subantenna Molecules in the Superantenna of Photosynthetic Green Bacteria: Model Calculations. Mol. Biol. (Moscow) 43: 426-443

Zobova AV, Taisova AS, Fetisova ZG (2010) Search for an Optimal Interfacing of Subantennae in Superantenna of Photosynthetic Green Bacteria from Oscillochloridaceae Family: Model Calculations. Doklady Biochem.Biophys. 433: 148-151

CsmA Protein is Associated with BChl *a* in the Baseplate Subantenna of Chlorosomes of the Green Photosynthetic Bacterium *Oscillochloris Trichoides* Belonging to the Family *Oscillochloridaceae*

Alexandra S Taisova [a,*], Anastasiya V Zobova[a], Eugeney P Lukashev[b], Nataliya V Fedorova[a], Zoya G Fetisova [a]

[a]A.N. Belozersky Institute of Physico-Chemical Biology, M.V. Lomonosov Moscow State University; [b]Department of Biophysics, M.V. Lomonosov Moscow State University, Moscow 119991, Russian Federation.
[*]Corresponding author. Tel. No. +7 495 939 5413; Fax No. +7 495 939 3181;
E-mail: zoana@mail.ru, taisova@genebee.msu.ru.

Abstract: The idea of association of bacteriochlorophyll *a* (BChl *a*) with protein in chlorosomes of the photosynthetic green anoxygenic filamentous bacterium *Osc.trichoides*, member of the family *Oscillochloridaceae*, was probed by low-temperature fluorescence spectroscopy and sodium dodecyl sulfate polyacrylamide gel electrophoresis (SDS-PAGE) analysis of alkaline-treated and untreated chlorosomes. Alkaline treatment of *Osc.trichoides* chlorosomes resulted in disappearance of BChl *a* band in their fluorescence spectra. The determination of BChl *c* and BChl *a* content confirmed the removal of BChl *a* from *Osc.trichoides* chlorosomes upon alkaline treatment. Based on the data obtained, we concluded that alkaline treatment of chlorosomes destroys the BChl *a* in the baseplate while leaving BChl *c* in a form that is spectrally indistinguishable from that in untreated chlorosomes. It was shown that upon alkaline treatment, only the 5.7 kDa CsmA protein was removed from the chlorosomes among five proteins detected by SDS-PAGE analysis, concomitantly with the disappearance of BChl *a* fluorescence emission. Based on these results, we suggest that CsmA protein is associated with BChl *a* in the baseplate subantenna in the chlorosomes of the photosynthetic green bacterium *Osc. trichoides*. Comparison of the data for the three families of green photosynthetic bacteria is relevant to assessing the universal principles of optimal antenna organization preserved in evolution despite marked changes in antenna size and structure.

Keywords: *Oscillochloridaceae*; Chlorosome; Baseplate; Bacteriochlorophylls *a* and *c*; CsmA protein

Introduction

The photosynthetic apparatus of green anoxygenic bacteria has a particular molecular organization and contains chlorosomes, unique extra membrane light-harvesting antennae structures that are attached to the inner surface of the cell membrane (Bryant and Frigaard, 2006). Chlorosomes are ellipsoid bodies (70–260 nm long, 30–100 nm wide and 10–30 nm thick) that are surrounded by a monolayer lipid–protein envelope. The bulk of light-harvesting pigments, bacteriochlorophylls (BChl) *c*/*d e* and carotenoids, is located within chlorosomes. These BChl *c/d/e* oligomers form either rod-(with a diameter of 5–10 nm) (Staehelin *et al.*, 1978, 1980) or lamellar-like structures (Pšenčik *et al*., 2004, 2006, 2009), arranged parallel to the longer chlorosome axis. A minor amount of BChl *a* pigments, absorbing at 795–800 nm, is also present in the chlorosome. This BChl *a* is located in the baseplate, observed in freeze-fracture electron-micrographs of chlorosomes from *Chloroflexaceae* and *Chlorobiaceae* species as a 5–6 nm thick paracrystalline layer (Staehelin *et al*., 1978, 1980). This BChl *a* serve as an intermediate antenna component, transferring excitation energy from chlorosomal BChl *c/d/e* to membrane-bound BChl *a* (Blankenship, Matsuura *et al*., 2003).

The baseplate is believed to be a pigment-protein

complex that is located at the base of the chlorosome (Bryant and Frigaard, 2006). Chlorosomes from the green filamentous bacterium *Cf . aurantiacus* have been reported to contain three major proteins, CsmA, CsmM and CsmN, with molecular masses 5.7, 11 and 18 kDa (Sakuragi *et al*., 1999). CsmA is the smallest and most abundant of these proteins. In green sulfur bacteria (*Chl. tepidum*, *Chl. vibrioforme*, and *Chl. phaeobacteroides*) ten chlorosome proteins have been identified. The 6.2-kDa CsmA accounts for about half of the protein present in the chlorosome (Bryant and Frigaard, 2006).

In this work, the idea of association of BChl *a* with protein in chlorosomes of *Osc. trichoides* was probed by low-temperature fluorescence spectroscopy and SDS-PAGE analysis of alkaline-treated and untreated chlorosomes. We showed that the baseplate BChl *a* subantenna does exist in *Oscillochloridaceae* chlorosomes as a complex of BChl *a* with the 5.7 kDa CsmA protein.

Materials and Methods

Osc. trichoides DG-6, the type strain of the species *Osc. trichoides* (327 KM MGU), was grown as described earlier, in batch cultures with stirring under anaerobic conditions at 30 °C on a modified DGN medium at a moderate light intensity (50 μE m^{-2} s^{-1}) from incandescent lamps (Taisova *et al*., 2002).

Chlorosomes were isolated from *Osc. trichoides* cells through two successive continuous sucrose gradient (55%–20% and 45%–15%) in the presence of 10 mmol sodium ascorbate and 2 mol sodium thiocyanate as described earlier (Taisova *et al*., 2002).

Absorption spectra were recorded at room temperature with a Hitachi-557 spectrophotometer (Japan). Fluorescence emission spectra were measured at liquid nitrogen temperature (77 K) with a Hitachi-850 spectrometer. Excitation wavelength was 720 nm. The absorbance of the samples of chlorosomes was 0.2 at 750 nm. Before fluorescence measurements the chlorosomes were incubated 60 min with 20 mmol sodium dithionite at 4 °C to ensure strongly reduced conditions (up to −400 mV).

Quantitative BChl *a* and BChl *c* contents were determined according to the method developed by (Feick *et al.*, 1982).

Chlorosomes were treated with alkali according to the method developed by Van Walree *et al.* (1999).

Proteins from alkaline-treated and untreated chlorosomes were separated by SDS-PAGE analysis. Chlorosome samples were extracted with 1.4 ml of acetone at −20 °C overnight. Proteins were collected by centrifugation and dissolved in sample buffer [50 mmol Tris-HCl (pH 8.6), 24% (v/v) glycerol, 8% (w/v) SDS, 2% (v/v) 2-mercaptoethanol, and 0.1% (w/v) bromophenol blue]. The samples were boiled for 1 min before being loaded onto gels containing 16.5, 10 and 4% acrylamide as separating, spacer and stacking gel, respectively, as described by Schägger and van Jagow 1987. After electrophoresis, the gels were stained with Coomassie brilliant blue R-250 (CBB).

Results and Discussion

To degrade selectively the baseplate BChl *a* in *Osc. trichoides* chlorosomes we applied the method of alkaline treatment (Van Walree *et al*., 1999). Fig. 1 shows the effect of alkaline treatment (dotted line) on the absorption spectrum of the *Osc. trichoides* chlorosomes. Obviously, that the absorption bands of BChl *c*, the main light-harvesting pigment in *Osc. trichoides* chlorosomes, were not affected by alkaline treatment.

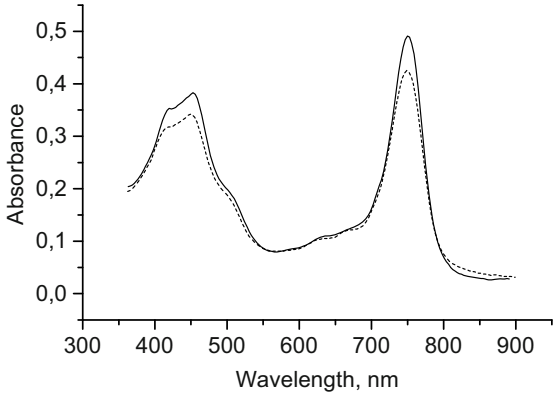

Fig. 1 Absorption spectra of untreated (solid line) and alkaline-treated (dotted line) *Osc. trichoides* chlorosomes in 50 mmol tris-buffer (pH 8.0).

In contrast to absorbance spectra, BChl *a* emission could be discerned in the fluorescence emission spectra of *Osc. trichoides* chlorosomes at 77 K (but not at room temperature) (Taisova *et al*., 2002). Additionally, it was shown by us that the light-harvesting *Osc. trichoides* chlorosome antenna exhibited a highly redox-dependent BChl *c* fluorescence similar to *Chlorobiaceae* species

(Taisova *et al*., 2002). For this reason, fluorescence emission spectra of untreated and alkaline-treated chlorosomes were measured at 77 K under reducing conditions (dithionite, 20 mmol) after excitation in the Q_y-band of BChl *c* at 720 nm.

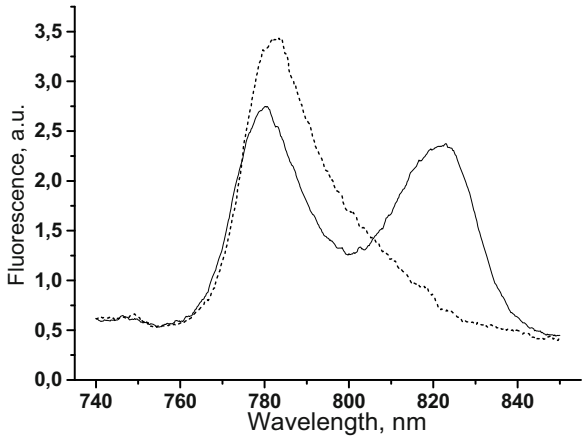

Fig. 2 Fluorescence emission spectra of untreated (solid line) and alkaline-treated (dotted line) *Osc. trichoides* chlorosomes at 77 K under reducing conditions.

Fig. 2 shows that alkaline treatment of *Osc. trichoides* chlorosomes resulted in disappearance of BChl *a* band in the 821 nm spectral region in their fluorescence spectra measured at 77 K (dotted line). The determination of BChl *c* and BChl *a* content confirmed the removal of BChl *a* from *Osc. trichoides* chlorosomes upon alkaline treatment (data not shawn). We conclude that alkaline treatment of chlorosomes destroys the BChl *a* in the baseplate while leaving BChl *c* in a form that is spectrally indistinguishable from that in untreated chlorosomes.

The effects of alkaline treatment on *Osc. trichoides* chlorosomal proteins were analyzed by SDS-PAGE analysis. Study of protein composition of *Osc. trichoides* chlorosomes were carried out in comparison with *Cfx .aurantiacus* chlorosomes. Five proteins (three major and two minor) were detected in native *Osc. trichoides* chlorosomes (Fig. 3A, lane 2). It was shown that upon alkaline treatment, only the 5.7 kDa CsmA protein was removed from the chlorosomes among five proteins detected by SDS-PAGE analysis (Fig. 3, lane 3), concomitantly with the disappearance of BChl *a* fluorescence (Fig. 2, dotted line), leaving BChl *c* unchanged spectrally. The protein composition of native *Cfx. aurantiacus* chlorosomes and its changes after alkaline treatment are shown in Fig. 3B. It is seen, that protein profiles of untreated and alkaline-treated *Osc. trichoides* and *Cfx. aurantiacus* chlorosomes were very much alike**.** In view of this, we designated the proteins of *Osc.trichoides* chlorosomes similarly to the proteins of *Cfx.aurantiacus* chlorosomes: CsmA (5.7 kDa), CsmM (11 kDa) and CsmN (18 kDa). Selective BChl *a* and 5,7 kDa protein disappearance should be expected only in case when both of them are located out of the BChl *c* body. Based on the results obtained, we suggest that CsmA is associated with BChl *a* in the baseplate subantenna in the chlorosomes of the green mesophilic filamentous photosynthetic bacterium *Osc. trichoides*, member of the new family *Oscillochloridaceae*.

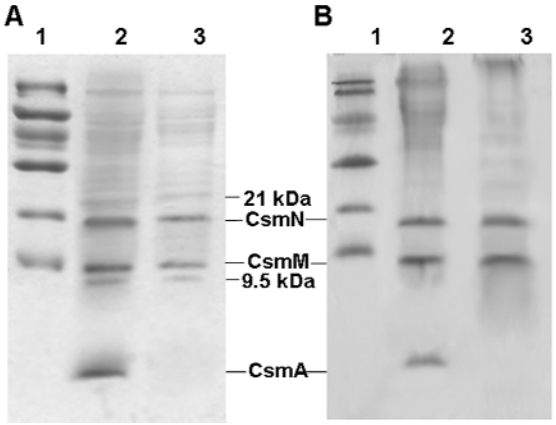

Fig. 3 CBB-stained SDS-PAGE of untreated and alkaline-treated *Osc. trichoides* (A) and *Cfx. aurantiacus* chlorosomes (B). A: Lane 1, molecular markers. Lane 2, untreated *Osc. trichoides* chlorosomes; Lane 3, alkaline-treated *Osc. trichoides* chlorosomes; B: Lane 1, molecular markers. Lane 2, untreated *Cfx. aurantiacus* chlorosomes; Lane 3, alkaline-treated *Cfx. aurantiacus* chlorosomes. All *Cfx. aurantiacus* samples were adjusted to contain 4.5 μg BChl *c*, while *Osc. trichoides* samples were adjusted to contain 18 μg BChl *c*.

The presented results support the idea that the baseplate subantenna, representing a complex of BChl *a* with a ~6 kDa CsmA protein, is a universal interface between the BChl *c* subantenna of chlorosomes and the light-harvesting BChl *a* subantenna of the cytoplasmic membrane in all three known families of green anoxygenic photosynthetic bacteria (*Chloroflexaceae*, *Oscillochloridaceae* and *Chlorobiaceae*). The group of chlorosome-containing bacteria with this type of baseplate organization was enlarged by the recently discovered new phototrophic chlorosome-containing organism *Candidatus* Chloracidobacterium thermophilum from the phylum *Acidobacteria* (Bryant *et al*., 2007).

Acknowledgement

This work was supported by grants No.10-04-01758 from the Russian Foundation for Basic Research.

References

Blankenship RE, Matsuura K (2003) Antenna Complexes from Green Photosynthetic Bacteria. In: Green BR, Parson WW (eds.), Light-Harvesting Antennas in Photosynthesis. Kluwer Academic Publishers: Dordrecht, pp. 195-217

Bryant DA, Costas AMG, Maresca JA, Chew AGM, Klatt CG, Bateson MM, Tallon LJ, Hostetler J, Nelson WC, Heidelberg JF, Ward DM (2007) Candidatus Chloracidobacterium Thermophilum: an Aerobic Phototrophic Acidobacterium. Science 31**7:** 523-526

Frigaard NU, Bryant DA (2006) Chlorosomes: Antenna Organelles in Photosynthetic Green Bacteria. In: Shively JM (ed.), Complex Intracellular Structures in Prokaryotes. Microbiology Monographs, Vol. 2. Springer: Berlin, Germany, pp. 79-114

Feick RG, Fitzpatrick M, Fuller RC (1982) Isolation and Characterization of Cytoplasmic Membranes and Chlorosomes from the Green Bacterium Chloroflexus Aurantiacus. J. Bacteriol. 150(2): 905-915

Oelze J, Golecki JR (1995) Membranes and Chlorosomes of Green Bacteria: Structure, Composition and Development. In: Blankenship RE, Madigan MT, Bauer CE (eds.), Anoxygenic photosynthetic bacteria. Kluwer Academic Publishers: Dordrecht, pp. 259-278

Pšenčik J, Arellano JB, Ikonen TP, Borrego CM, Laurinmäki P, Butcher SJ, Serimaa RE, Tuma R (2006) Internal Structure of Chlorosomes from Brown-Colored Chlorobium Species and the Role of Carotenoids in Their Assembly. Biophys. J. 91: 1433-1440

Pšenčik J, Ikonen TP, Laurinmäki P, Merckel MC, Butcher SJ, Serimaa RE, Tuma R (2004) Lamellar Organization of Pigments in Chlorosomes, the Light Harvesting System of Green Bacteria. Biophys. J. 87: 1165-1172

Psencík J, Collins AM, Liljeroos L, Torkkeli M, Laurinmäki P, Ansink HM, Ikonen TP, Serimaa RE, Blankenship RE, Tuma R, Butcher SJ (2009) Structure of chlorosomes from the Green Filamentous Bact Crium Chloroflexus Aurantiacus. J. Bacteriol. 191: 6701-6708

Sakuragi Y, Frigaard NU, Shimada K, Matsuura K (1999) Association of Bacteriochlorophyll a with the CsmA Protein in Chlorosomes of the Photosynthetic Green Filamentous Bacterium Chloroflexus Aurantiacus. Biochim. Biophys. Acta 1413: 172-180

Schägger H, van Jagow G (1987) Tricine-Sodium Dodecyl Sulfatepolyacrylamide Gel Electrophoresis for the Separation of Proteins in the Range from 1 to 100 kDa. Anal. Biochem. 166: 368-379

Staehelin LA, Golecki JR, Fuller RC, Drews G (1978) Visualization of the Supramolecular Architecture of Chlorosomes (Chlorobium Type Vesicles) in Freeze-Fractured Cells of Chloroflexus Aurantiacus. Arch. Microbiol. 119: 269-277

Staehelin LA, Golecki JR, Drews G (1980) Supramolecular Organization of Chlorosomes (Chlorobium Vesicles) and of Their Membrane Attachment Sites in Chlorobium Limicola. Biochim. Biophys. Acta 589: 30-45

Taisova AS, Keppen OI, Lukashev EP, Arutyunyan AM, Fetisova ZG (2002) Study of the Chlorosomal Antenna of the Green Mesophilic Filamentous Bacterium Oscillochloris Trichoides. Photosynth. Res. 74: 73-85

Van Walree CA, Sakuragi Y, Steensgaard DB, Bosinger CS, Frigaard NU, Cox RP, Holzwarth AR, Miller M (1999) Effect of Alkaline Treatment on Bacteriochlorophyll a, Quinones and Energy Transfer in Chlorosomes from Chlorobium Tepidum and Chlorobium Phaeobacteroides Photochem. Photobiol. 69: 322-328

Effects of Anaerobic Conditions on Photosynthetic Units of *Acaryochloris Marina*

Yuankui Lin[1], Ben Crossett[2] , Min Chen[1*]

[1]Biological School of University of Sydney, [2]School of Molecular Biosciences, University of Sydney, NSW 2006, Australia.
*Corresponding author. Tel. No. +61 2 9036 5006; Fax No. +61 2 9351 4119; E-mail: min.chen@sydney.edu.au.

Abstract: *Acaryochloris marina* is a unicellular oxygenic photosynthetic cyanobacteria. Its pigment composition (Chl *d* > 95%) and ability to adapt various environments (aerobic and anaerobic) make it a unique species. And from some aspects it is a candidature of evolution intermediate of non-oxygenic to oxygenic photosynthesis. Our experiment aims to study the relationship between anaerobic and aerobic metabolism of *Acaryochloris marina* and compare the photosynthetic apparatus under oxygen-stressed conditions. *Acaryochloris marina* MBIC 11017 was cultured in aerobic (normal cultural condition as control) and micro-anaerobic condition (achieved by constantly bubbling N_2). Growth rate and pigment composition have been monitored during the time. Treated cultures grew slower than control, but it showed an increase in cell density. Oxygen evolution was measured with Clark oxygen electrode. Cells were harvested in one week after inoculation then broken using vortex the mixture of cells with silicon beads. Proteins were extracted and then fractionated with SDS-PAGE. The bands with different abundances between each sample were picked and analyzed with Mass-fingerprint. Several proteins were identified with high scores. Two of them were phycobilisome rod-core linker polypeptides which were important to membrane binding and energy transfer. Their bands were removed in the micro-anaerobic samples while they are clear in aerobic samples. Low temperature fluorescence result agreed with the results from protein analysis: The phycobiliprotein may be uncoupled from photosynthetic membrane by losing its linker polypeptides under oxygen-stressed condition.

Keywords: *Acaryochloris marina*; Oxygenic photosynthesis; Non-oxygenic photosynthesis;Phycobiliprotein

Introduction

Acaryochloris marina is a unicellular oxygenic photosynthetic cyanobacterium that was first discovered and isolated by Japanese scientists from a colonial ascidian in Palau (Miyashita H, 1996). Instead of chlorophyll (Chl) *a* in most of oxygenic photoautotroph, *A. marina* contains Chl *d* as its major photosynthetic pigment (> 95%). Only about 3% of Chl *a* presents in its total photosynthetic pigments (Miyashita *et al*., 1997). Chl *d* (3-desvinyl-3-formyl Chl *a*) has a formyl group at the C-3 position in ring A of the structure, that induces a red-shift of the absorption spectrum (Miyashita *et al*., 1997). The absorption maximum of Chl *d* is approximately 700 nm in organic solvents and 720 nm in vivo (the range of cell absorption can reach to 740 nm) (Miyashita *et al*., 1997), which is larger than that of Chl *a*, beyond the range of any other oxygenic photosynthetic organisms (except the Chl *f* that was discovered very recently (Chen *et al*., 2010). Chl *d* absorption maximum falls between Chl *a* and Bacterio-Chls (BChls), which suggests *A. marina* may be a candidates of evolution intermediate of oxygenic photosynthesis and non-oxygenic photosynthesis (Blankenship and Hartman, 1998). Physiological and proteomics study were carried out to investigate the metabolic transitions in *A. marina* under various oxygen-stressed conditions.

Methodology

Two different cultural conditions were set up:

normal cultural condition (bubbling with air) as control and the micro-aerobic treatment condition.

All of them were inoculated with the same cell density (A_{750nm} = 0.2) in K+ES seawater medium with 25 mmol TES buffer pH = 8.0 and cultured in 27 °C, continuous white light 10–15 uE, constantly shaking at 90 rpm. 0.25 mmol $NaHCO_3$ was added daily to the enclosed culture systems as an extra carbon source.

Micro-aerobic environment was achieved by vacuuming and refilling a two necks round culture flask with pure nitrogen gas, repeat 5 times. The flask was sealed and continuously bubbled with a small stream of nitrogen gas through needle to evacuate the possible oxygen generated by oxygenic photosynthetic reactions. OD_{750nm} was monitored daily for growth rate. Pigments were extracted in pre-chilled 100% methanol and analyzed by HPLC using C_{18} reverse phase column (Phenomenex Synergi fusion-RP HPLC column 246218-1, 250×4.60 mm 4 micron). The flow rate was 0.8 ml/min. Column was run form 85%–100% methanol for 5 min, then in 100% methanol for 30 min.

Cells were harvested at the 7th day by centrifugation and broken by beads-vortex (with 0.1 mm silicon beads) in 50 mmol phosphate buffer. Phenylmethanesulfonyl fluoride was added prior the vortex. The mixtures were then centrifuged at top speed of micro-centrifuge for 5 min. Supernatant was collected as total soluble protein sample. The pellet was resuspended in 50 mmol phosphate buffer with 1% (w/v) dodecyl maltoside and kept rotating in dark for one hour followed by centrifugation (top speed of Micro-centrifuge for 5 min). The supernatant was collected as solubilized membrane bound protein samples.

Each sample was loaded on 10% SDS-gel with the same amount of protein (based on A_{280nm} reading). The bands that show different abundances between samples were picked and analyzed with protein mass-finger-printing technology.

To investigate the energy transfer, low temperature emission fluorescence was measured with excitation wavelength at 600 nm.

Result

The micro-aerobic cultural condition contains only about 1% of oxygen in normal air, *i.e.* lower than 0.21% oxygen in the gas phase. Normal cultural condition demonstrated a higher growth rate; doubling time is about 5 days based on $OD_{750\ nm}$. While the micro-aerobic culture show about 7 days in doubling time.

A SDS-PAGE gel is shown in Fig. 1. The numbered bands were picked and analyzed with mass-finger-printing technology according to the different abundances between two samples (micro-aerobic and aerobic cultural condition). The band 4 which was pointed out by an arrow in Fig. 1 is the phycobilisome rod-core linker polypeptide (cpcG). This band is missed in the micro-aerobic culture sample. As previous study this protein binds phycobilinprotein (alpha and beta subunits) to the photosynthetic membrane and involves in the energy transfer in photosynthesis (Chen *et al.*, 2008, 2009). The bands 10 and 11 are phycocyanin beta and alpha subunits. Phycocyanin alpha and beta subunits are visible through all samples (Fig. 1), which indicate that changes of oxygen concentration have no influences on the presentence of phycobliproteins, although the gene, *cpcG* was down-regulated under micro-aerobic culture condition (Lin *et al.*, 2010, unpublished data). The phycobiliprotein may loss its connection to photosynthetic units under micro-aerobic conditions and the functions of those uncoupled phycobiliproteins are uncertain.

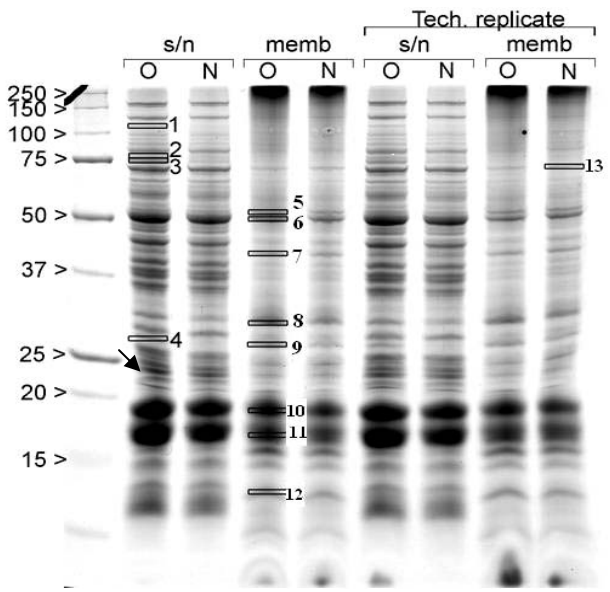

Fig. 1 The picture of protein SDS-PAGE of the micro-aerobic sample and the control. The numbered bands are the bands picked for mass finger printing. "O" represents control; "N" represents the micro-anaerobic culture. "s/n" represents the soluble and membrane attached proteins and the "memb" represents the membrane embedded proteins.

The ratio of Chl *a*/Chl *d* in *A. marina* cells was greatly impacted by the levels of oxygen in the cultural system. In the micro-aerobic condition concentration of Chl *a* reached up to 2.5% of total pigments and the highest Chl *a*/*d* ratio of 7%–8%. While the control cultures only had normal Chl *a* concentration of ~1.0% of totla pigments. It is known that the oxygen atom in the C_3^1-formyl group of Chl *d* is derived from dioxygen via an oxygenase-type reaction mechanism (Schliep *et al*., 2010). The result comfirms that the synthesize pathway of Chl *d* is suppressed under micro-aerboic condition.

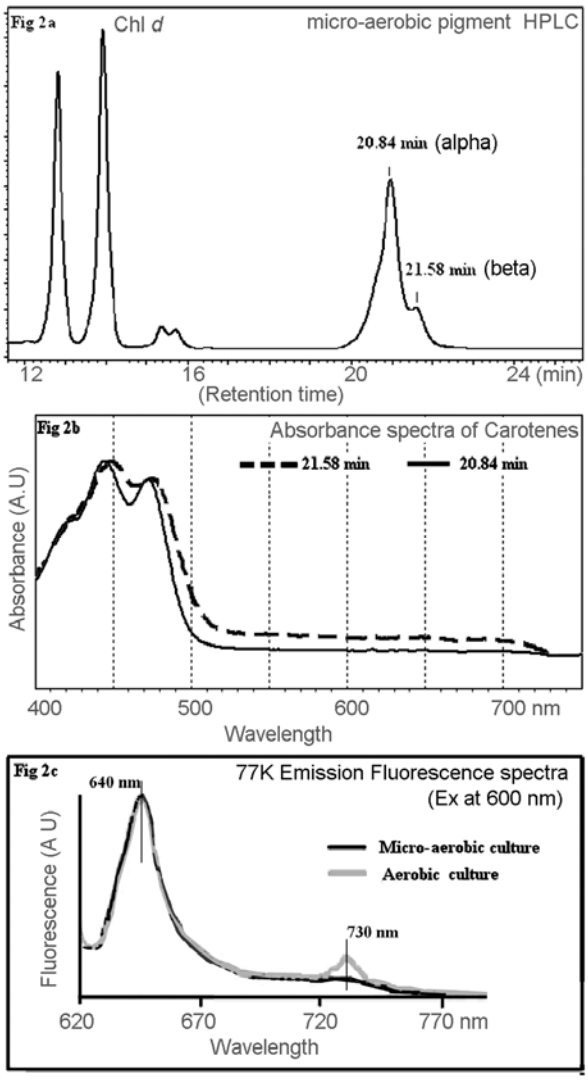

Fig. 2a A typical chromatogram of pigments sample of micro-aerobic culture recorded at 448 nm. Two peaks of carotene were labeled with their retention time.
Fig. 2b The absorbance spectral comparison of 20.84 min and 21.58 min of the sample in Fig. 2a.
Fig. 2c Low temperature emission fluorescence spectral comparison of two *A. marina* cultures (aerobic culture and micro-aerobic culture) using excitation wavelength of 600 nm (at 77 K).

It is noticed that *A. marina* produced both α-carotene and β-carotene under micro-aerobic condition (Figs. 2a and 2b), while under the normal cultural conditions, *A. marina* can only produce and use α-carotene (Miyashita *et al*., 1997).

To investigate the energy transfer, low temperature (77 K) emission fluorescence was measured using whole cells collected under various cultural conditions with excitation wavelength of 600 nm. Both cultural conditions showed phycobiliprotein fluorescence emission of 640 nm, but no 730 nm (generated from Chl *d*) fluorescence was observed in micro-aerobic cultural condition, which confirms the proteomic analysis: the phycobiliprotein linkers were lost, *i.e*. Phycobiliprotein complexes were disassembled, under oxygen-stressed condition (Fig. 2c).

Discussion and Conclusion

This study confirms that *A. marina* can grow in an extreme lower oxygen concentration (oxygen-stressed) environments, though the growth rate is slow-down. The pigment composition was impacted by the oxygen level, especially the ratio of Chl *a*/Chl *d*. The increased Chl *a* in micro-aerobic condition confirmed that oxygen is the essential molecules for biosynthesis of Chl *d* from Chl *a* (Schliep *et al.*, 2010). The normal *A. marina* cells contain only α-carotene (Miyachita *et al.*, 1997). It is surprised to detect β-carotene together with α-carotene from the cells under micro-aerobic condition. However the function of β-carotene in *A. maina* and the possible inferences to the photo-protection is still unknown. The phycobiliprotein lost its linker which is a step of energy transfer to the photosynthetic systems and Chl *d*-binding membrane protein complexes under micro-aerobic environment. In this case, the phycobiliprotein are no more functional in collecting energy for reaction centers. Whether uncoupled alpha and beta subunits of phycocyanin are functional is uncertain. Losing the linker proteins at the 7th days under the micro-aerobic condition may represent the beginning of disassembly process of phycobiliprotein. Alternatively there may be another energy transfer pathway not be identified yet.

Acknowledgements

The authors thank Anthony Larkum and Ritchie

for useful discussions. The project is supported by Australian Research Council (ARC). MC holds an Australian Queen Elizabeth Ⅱ Fellowship.

Reference

Blankenship, RE, Hartman, H (1998) The Origin and Evolution of Oxygenic Photosynthesis. Trends Biochem Sci 23(3): 94-97

Chen M, Donohoe K, Crossett B, Schliep M, Larkum T (2008) In 14th International Congress on Photosynthesis Research 2007

Chen M, Floetenmeyer M, Bibby TS (2009) Supramolecular Organization of Phycobiliproteins in the Chlorophyll d-Containing Cyanobacterium Acaryochloris Marina, FEBS Lett. 583: 2535-2539

Chen M, Schliep M, Willows RD, Cai ZL, Neilan BA, Scheer H (2010) A Red-Shifted Chlorophyll. Science 329(5997): 1318-1319

Miyashita HAK, Kurano N, Ikemoto H, Chihara M, Miyachi M (1997) Pigment Composition of a Novel Oxygenic Photosynthetic Prokaryote Containing Chlorophyll d as the Major Chlorophyll. Plant Cell Physiol 38: 274-281

Miyashita HIH, Kurano N, Adachi K, Chihara M, Miyachi S (1996) Chlorophyll d as a Major Pigment. Nature 383: 402

Schliep M, Crossett B, Willows RD, Chen M (2010) 18O Labeling of Chlorophyll d in Acaryochloris Marina Reveals that Chlorophyll a and Molecular Oxygen Are Precursors. J Biol Chem 285(37): 28450-28456

Symposium 04

Light Harvesting Aerobic Systems

Closed Reaction Centers of PS1 Still Can Perform the First Steps of Charge Separation. A Mid IR Pump Probe Study with fs Resolution

Andreas D Stahl[1*], Mariangela Di Donato[1,2], Ivo van Stokkum[1], Rienk van Grondelle[1] , Marie Louise Groot[1]

[1] Faculty of Sciences Department of Physics and Astronomy, VU University Amsterdam, Amsterdam, The Netherlands.
*E-mail: ad.stahl@few.vu.nl.
[2] Current address: LENS (European Laboratory for non linear spectroscopy) via N. Carrara 1 Sesto Fiorentino (FI)-Italy.

Abstract: Time resolved femtosecond Visible-pump/midIR-probe measurements on photosystem I with open and closed reaction centers are compared, and the formation of the first step of charge separation in the system, $A^+A_0^-$ is shown for both cases.

Keywords: PSI closed RC; FemtoIR; Radical Pair 1

Introduction

Photosystem I (PSI) is a membrane protein involved in the primary processes of oxygenic photosynthesis. The structure of both cyanobacterial and plant PSI have been resolved (Fromme, Jordan *et al*., 2001; Jordan, Fromme *et al*., 2001) showing that this complex consists of 11–13 protein subunits, binding approximately 90–100 chlorophyll pigments. The two largest subunits, denoted as PsaA and PsaB form a heterodimer which binds most of the core antenna pigments as well as the cofactors of its reaction center (RC). The latter binds six chlorophyll pigments and two phylloquinone molecules, arranged in a symmetric way along the two PsaA and PsaB branches. In contrast with bacterial and PSII reaction centers, a growing number of experiments suggest that charge separation in PSI can occur along both branches. (Brettel and Leibl, 2001; Guergova-Kuras, Boudreaux *et al*., 2001; Fairclough, Forsyth *et al*., 2003; Ivashin and Larsson, 2003; Xu, Chitnis *et al*., 2003; Dashdorj, Xu *et al*., 2005; Poluektov, Paschenko *et al*., 2005; Ali, Santabarbara *et al*., 2006; Muller, Slavov *et al*., 2010)

Furthermore, it has recently been proposed that the primary donor in PSI is not the chlorophyll dimer usually indicated as P_{700}, but the monomer chlorophyll located between P_{700} and the primary electron acceptor, the A_0 chlorophyll. (DiDonato *et al*., submitted) (Holzwarth, Müller *et al*., 2006; Giera, Ramesh *et al*., 2010) According with this interpretation, the initially formed radical pair $A^+A_0^-$ rapidly evolves into $P_{700}^+A_0^-$ and the electron then reaches the phylloquinone (A_1) on a 30–40 ps time scale.

One of the most counterintuitive and intriguing aspects of PSI is the fact, that features of the initial steps of charge separation can even be observed in closed RC's (Giera, Ramesh *et al*., 2010) .

Material and Methods

S*ynechococcus elongatus* trimers were isolated as previously described.(Fromme and Witt, 1998) For vis/mid-IR experiments the sample was concentrated at OD 0.2 at the excitation wavelength of 700 nm for a 20 μm optical path length. The particles were suspended in 10 mmol 2-(N-morpholino)ethane sulfonic acid (MES) buffer (pD 7) in D_2O containing 20 mmol NaCl, 20 mmol $MgCl_2$ and 0.05% β-DM. In order to keep the reaction center open during the measurements, 40 mmol sodium ascorbate and 60 μM phenazine methosulphate were added to the sample, while 3 mmol ferrycyanide was added to the sample in order to close the RCs.

The experimental setup consisted of an integrated

Ti:sapphire oscillator-regenerative amplifier laser system (Hurricane, SpectraPhysics) operating at 1 kHz and 800 nm, producing 85 fs pulses of 0.8 mJ. A portion of the 800 nm light was used to pump a non-collinear optical parametric amplifier to produce the excitation pulses, whose wavelength was selected by using an interference filter for the desired excitation wavelength. The filters full width half maximum (fwhm) was 5.6 nm (LOT-Oriel). The excitation pulses were focused on the sample with a 20 cm lens. A second part of the 800 nm light was used to pump an optical parametric generator and amplifier with a difference frequency generator (TOPAS, Light Conversion) to produce the mid-IR probe pulses, which were focused on the sample with a 6 cm lens.

The probe and pump pulses were spatially overlapped in the sample. After passing the sample the probe pulses were dispersed in a spectrograph, imaged on a 32-element MCT detector and fed into 32 home-built integrate and hold devices that were read out every shot with a National Instruments acquisition card.

To ensure a fresh spot for each laser shot, the sample was moved by a home-built Lissajous scanner. The polarization of the excitation pulse was set to the magic angle (54.7^{o}) with respect to the IR probe pulses. A phase locked chopper operating at 500 Hz was used to ensure that every other shot the sample was excited and that the change in transmission could be measured.

The instrument response function was about 120 fs. The excitation wavelength was 700 nm with a pulse energy of 100 nJ. All measurements were performed at room temperature (RT) and the data were subjected to global analysis (van Stokkum, Larsen *et al*., 2004).

Results

Fig. 1, panel A shows the evolution associated decay spectra (EADS) for closed RC's obtained from global analysis of the data. Four lifetimes were required for a satisfactory fit. For closed RC's the data were fitted with kinetic constants of 0.7 ps, 6.3 ps, 43 ps and a long living, > 2 ns and hence considered infinite with respect to the experiments' time frame.

The first spectra of closed RC's are dominated by a broad positive band in the 1660–1620 cm^{-1} region representing the fast decaying exited state absorption of the antenna chlorophylls (Gibasiewicz, Ramesh *et al*., 2001; Holzwarth, Muller *et al*., 2006) and furthermore two negative peaks at 1,690 and 1,670 cm^{-1} respectively are present. Beside that, 2 positive bands at 1,710 and 1,725 cm^{-1} are found. Negative bands in the region 1,750 down to 1,650 cm^{-1} have been previously assigned to 13^{1}-keto modes of chlorophyll. These modes are very sensitive to their surrounding and possible hydrogen bonds. *E.g.* downshifts up to 30 cm^{-1} in a polar environment compared to a no polar have been reported (Closs, Katz *et al*., 1963)

Their counterpart in the excited state downshifts by several wavenumbers (Groot, Breton *et al*., 2004; Groot, Pawlowicz *et al*., 2005; DiDonato, vanGrondelle *et al*., 2007; Stahl, Di Donato *et al*., 2009), and in this case are the positive peaks at 1,650 and 1,635 cm^{-1} in the broad 1660–1620 cm^{-1} positive feature.

After 1 ps the band at 1,708 cm^{-1} has gained in amplitude. The 1,725 cm^{-1} band follows the same trend. The negative doublet bleaching at 1670/1690 cm^{-1} has

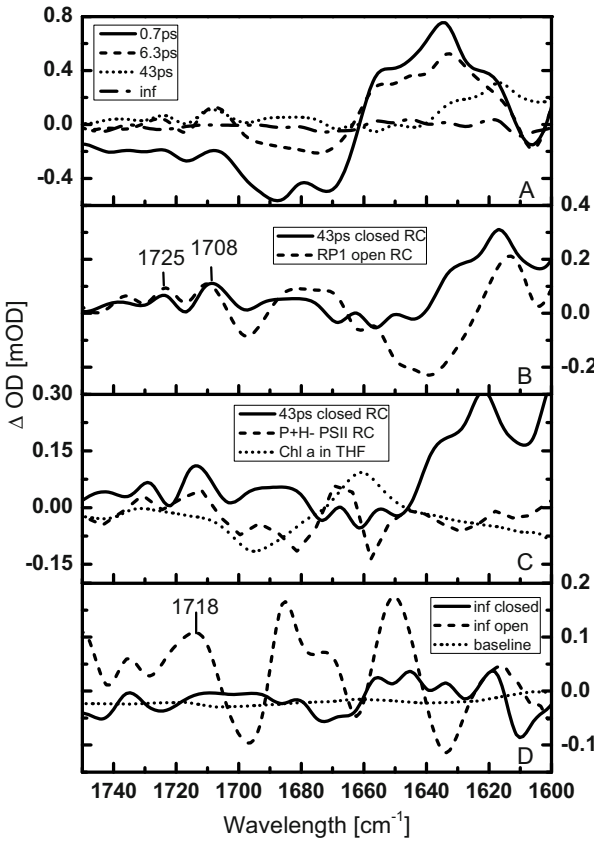

Fig. 1 EADS of PSI with closed (panel A) reaction centers after 700 nm excitation. Panel B; Comparison of 43 ps component with the literature radical pair (dashed) spectrum of PSI, and PSII $P^{+}H_{-}$ (dashed) and excited chlorophyll *a* (dotted) spectrum (panel C). Panel D; Infinite spectrum of open (dashed) and closed RC PSI (solid) and the baseline of the measurement (dotted).

broadened and resembles now as a single broad negative band. The main cause for this is a loss in amplitude at 1,690 cm^{-1}. The band at 1,610 cm^{-1} has gained in amplitude. The decay in excited state absorption observed here is indicative for energy transfer/equilibration to the RC. Additional losses may be explained by excition-exciton annihilation in the antenna pigments due to multiple excitations per complex.

6.3 ps later, the excited state absorption has decayed to about 20% of its initial amplitude. The band has narrowed somewhat and now shows a single feature peaking at 1,620 cm^{-1}. The 1725/1708 cm^{-1} bands in have further gained in amplitude (2x), the broad negative band stretching from 1700–1670 cm^{-1} (panel B) has downshifted 30 cm^{-1} and shows now three distinct negative peaks at 1,670, 1,655 and 1,645 cm^{-1}.

The final state is reached after 43 ps (dot dashed line, also panel D). Very little features are present in this state. Only a positive ester band at 1,735 cm^{-1} and a negative band at 1,610 cm^{-1}. No characteristics of P^+ formation (compare with the 1,718 cm^{-1} fingerprint of P^+ (panel D)) can be found, indicating that the RC's were completely closed.

Discussion

The shown EADS of closed RC's show distinct features, which were generally believed to be only observable in the open state. Below we will discuss these intriguing features in greater detail.

Primary step(s) of charge separation

Already the initial spectrum (Fig. 1, panel A) shows precursors to features previously assigned to cation formation; namely the 1725/1708 cm^{-1} band. This assignment is strongly supported by the comparison with the first radical pair spectrum of open RC PSI (panel B)(DiDonato et al, submitted), and the time resolved charge separated P^+H^- spectrum measured in PSII-RC's (panel C) (Groot, Pawlowicz *et al*., 2005), which shows a pronounced double peak feature with maxima at 1,715 and 1,730 cm^{-1}, and which have been attributed to the localization of a positive charge on a chlorophyll dimer (*48*).

The same double peaked band has also be found in the radical pair spectra measured for PSII core particles and bacterial reaction centers (panel C) (Pawlowicz, Groot *et al*., 2007; Di Donato, Cohen *et al*., 2008; Pawlowicz, van Grondelle *et al*., 2008).

Conclusion

In the framework of this article, we have shown that in PS1 the first step(s) of charge separation, the formation of $A^+A_0^-$ is possible, despite the fact that the RC is closed, and P^+ already pre-oxidized.

Acknowledgements

We thank Jos Thieme for technical support and H Fidder and K Heyne for providing the sample.

References

Ali K, S Santabarbara, *et al*. (2006) Bidirectional Electron Transfer in Photosystem I: Replacement of the Symmetry-Breaking Tryptophan Close to the PsaB-Bound Phylloquinone (A1B) with a Glycine Residue Alters the Redox Properties of A1B and Blocks Forward Electron Transfer at Cryogenic Temperatures. Biochimica et Biophysica Acta (BBA) - Bioenergetics 1757(12): 1623-1633

Brettel K, W Leibl (2001) Electron Transfer in Photosystem I. Biochimica et Biophysica Acta (BBA) - Bioenergetics 1507(1-3): 100-114

Closs GL, JJ Katz, *et al.* (1963) Nuclear Magnetic Resonance Spectra and Molecular Association of Chlorophylls a and b, Methyl Chlorophyllides, Pheophytins, and Methyl Pheophorbides. Journal of the American Chemical Society 85(23): 3809-3821

Dashdorj N, W Xu, *et al*. (2005) Asymmetric Electron Transfer in Cyanobacterial Photosystem I: Charge Separation and Secondary Electron Transfer Dynamics of Mutations Near the Primary Electron Acceptor A0. Biophysical Journal 88(2): 1238-1249

Di Donato M, RO Cohen, *et al*. (2008) Primary Charge Separation in the Photosystem II Core from Synechocystis: A Comparison of Femtosecond Visible/Midinfrared Pump-Probe Spectra of Wild-Type and Two P680 Mutants. Biophysical Journal 94(12): 4783-4795

Di Donato M, R van Grondelle, *et al*. (2007) Excitation

Energy Transfer in the Photosystem II Core Antenna Complex CP43 Studied by Femtosecond Visible/Visible and Visible/Mid-Infrared Pump Probe Spectroscopy. J. Phys. Chem. B 111(25): 7345-7352

Fairclough WV, A Forsyth, *et al.* (2003) Bidirectional Electron Transfer in Photosystem I: Electron Transfer on the PsaA Side Is Not Essential for Phototrophic Growth in Chlamydomonas. Biochimica et Biophysica Acta (BBA) - Bioenergetics 1606(1-3): 43-55

Fromme P, P Jordan, *et al*. (2001) Structure of Photosystem I. Biochim Biophys Acta 1507(1-3): 5-31

Fromme P, HT Witt (1998) Improved Isolation and Crystallization of Photosystem I for Structural Analysis. Biochimica et Biophysica Acta (BBA) - Bioenergetics 1365(1-2): 175-184

Gibasiewicz K, VM Ramesh, *et al*. (2001) Excitation Dynamics in the Core Antenna of PS I from Chlamydomonas Reinhardtii CC 2696 at Room Temperature. The Journal of Physical Chemistry B 105(46): 11498-11506

Giera W, VM Ramesh, *et al*. (2010) Effect of the P700 Pre-Oxidation and Point Mutations Near A0 on the Reversibility of the Primary Charge Separation in Photosystem I from Chlamydomonas Reinhardtii. Biochimica et Biophysica Acta (BBA) - Bioenergetics 1797(1): 106-112

Groot ML, J Breton, *et al*. (2004) Femtosecond Visible/Visible and Visible/Mid-IR Pump-Probe Study of the Photosystem II Core Antenna Complex CP47. J. Phys. Chem. B 108(23): 8001-8006

Groot ML, NP Pawlowicz, *et al*. (2005) Initial Electron Donor and Acceptor in Isolated Photosystem II Reaction Centers Identified with Femtosecond Mid-IR Spectroscopy. Proceedings of the National Academy of Sciences of the United States of America 102(37): 13087-13092

Groot ML, NP Pawlowicz, *et al*. (2005) Initial Electron Donor and Acceptor in Isolated Photosystem II Reaction Centers Identified with Femtosecond Mid-IR Spectroscopy. PNAS 102(37): 13087-13092

Guergova-Kuras M, B Boudreaux, *et al*. (2001) Evidence for Two Active Branches for Electron Transfer in Photosystem I. PNAS 98(8): 4437-4442.

Holzwarth AR, MG Muller, *et al*. (2006) Ultrafast Transient Absorption Studies on Photosystem I Reaction Centers from Chlamydomonas Reinhardtii. 2: Mutations Near the P700 Reaction Center Chlorophylls Provide New Insight into the Nature of the Primary Electron Donor. Biophys J 90(2): 552-65

Holzwarth AR, MG Müller, *et al*. (2006) Ultrafast Transient Absorption Studies on Photosystem I Reaction Centers from Chlamydomonas Reinhardtii. 2: Mutations Near the P700 Reaction Center Chlorophylls Provide New Insight into the Nature of the Primary Electron Donor. Biophysical Journal 90(2): 552-565

Ivashin N, S Larsson (2003) Electron Transfer Pathways in Photosystem I Reaction Centers. Chemical Physics Letters 375(3-4): 383-387

Jordan P, P Fromme, *et al.* (2001) Three-Dimensional Structure of Cyanobacterial Photosystem I at 2.5 A Resolution. Nature 411(6840): 909-17

Muller MG, C Slavov, *et al*. (2010) Independent Initiation of Primary Electron Transfer in the Two Branches of the Photosystem I Reaction Center.PNAS 107(9): 4123-4128

Pawlowicz NP, ML Groot, *et al*. (2007) Charge Separation and Energy Transfer in the Photosystem II Core Complex Studied by Femtosecond Midinfrared Spectroscopy. Biophysical Journal 93(8): 2732-2742

Pawlowicz NP, R van Grondelle, *et al*. (2008) Identification of the First Steps in Charge Separation in Bacterial Photosynthetic Reaction Centers of Rhodobacter Sphaeroides by Ultrafast Mid-Infrared Spectroscopy: Electron Transfer and Protein Dynamics. Biophysical Journal 95(3): 1268-1284

Poluektov OG, SV Paschenko, *et al*. (2005) Bidirectional Electron Transfer in Photosystem I: Direct Evidence from High-Frequency Time-Resolved EPR Spectroscopy. Journal of American Chemical Society 127(34): 11910-11911

Stahl AD, M Di Donato, *et al*. (2009) A Femtosecond Visible/Visible and Visible/Mid-Infrared Transient Absorption Study of the Light Harvesting Complex II. Biophys J 97(12): 3215-23

Modulation of Chlorophyll b Biosynthesis and Photosynthesis by Overexpression of Chlorophyllide a Oxygenase (CAO) in Tobacco[1]

Ajaya K Biswal[2,a], Gopal K Pattanayak[2,a], Sadhu Leelavathi[b], Vanga S Reddy[b], Govindjee[c] , Baishnab C Tripathy[a]*

[a]School of Life Sciences, Jawaharlal Nehru University, New Delhi 110067, India;
[b]International Center for Genetic Engineering and Biotechnology, New Delhi 110067, India; [2] AKB and GKP contributed equally to this article;
[c] Department of Plant Biology, University of Illinois, Urbana, IL 61801, USA.
*Corresponding author. E-mail: bctripathy@mail.jnu.ac.in.
[1] *A full length article will be published elsewhere*

Abstract: Chlorophyll (Chl) b is synthesized by oxidation of a methyl group on the B ring of the porphyrin molecule to a formyl group by chlorophyllide (Chlide) a oxygenase (CAO). The overexpression of *Arabidopsis thaliana* full length *CAO* (*AtCAO*) in tobacco (*Nicotiana tabacum*) resulted in an increased Chl synthesis and a decreased Chl a/b ratio in low-light-grown (LL) as well as in high-light-grown (HL) tobacco plants, where the effect was more pronounced. In HL-plants, increased [Chl b] resulted in efficient capture of solar energy and enhanced (40%–80%) electron transport rates at both limiting and saturating light intensities.

Keywords: Chlophyll b biosynthesis; Chlorophyllide a Oxygenase; *Nocotiana tabacum*; Photosynthesis

Introduction

Chlorophyll (Chl) b is a closed Mg-tetrapyrrole found in plants, green algae and some prochlorophytes. The main function of Chl b is to gather light energy and transfer it with 100% efficiency to Chl a. Chl b is synthesized from Chl a by oxidation of methyl group on the B ring to a formyl group at that position. The genes encoding chlorophyllide a oxygenase (CAO), responsible for Chl b synthesis, have been isolated from several different species (Tanaka *et al*., 1998; Espineda *et al*., 1999; Nagata *et al*., 2004). The CAO enzyme is localized in chloroplast envelope and thylakoid membranes and contains domains for a [2Fe-2S] Rieske center and for a mononuclear nonheme iron-binding site (Eggink *et al*., 2004). The conserved Rieske center and non-heme-iron binding motifs of CAO are likely to be involved in the electron transport from ferredoxin to moleclular oxygen. The recombinant CAO protein catalyzes the oxidation of Chlide *a* to Chlide *b* (Oster *et al*., 2000). We have previously reported that overexpression of full length *AtCAO* results in increased Chl b synthesis and decreased Chl a/b ratio in low-light, but more so in high-light-grown tobacco plants (Pattanayak *et al*., 2005). In the present study, we show that the overexpression of full length *AtCAO* modulates the flux of Chl biosynthesis pathway leading to increased Chl b synthesis both in low-light- and high-light-grown transgenic tobacco plants. We further show that increased Chl b biosynthesis in full-length CAO-overexpressing (CAOx) plants results in efficient capture of solar energy and increased electron transport mostly at limiting light intensities.

Materials and Methods

Plant Materials and Growth Conditions

Wild-type (WT) and CAO overexpressing (CAO_X) tobacco (*Nicotiana tabacum cv. Petit*

Havana) plants (Pattanayak *et al*., 2005) were grown in greenhouse in natural photoperiod for 25–30 days under light intensity of 200 μmol photons m^{-2} s^{-1} at 25 ± 2 °C. In our studies, these plants were transferred either to low light (LL) (70–80 μmol photons m^{-2} s^{-1}) or to high light (HL) (700–800 μmol photons m^{-2} s^{-1}) for additional 18–20 days in a greenhouse.

Chlorophyll a Fluorescence Measurements

Chl a fluorescence was measured with a PAM-2001 Chl fluorometer (Walz, Germany) at room temperature, from the front surface of leaves (see *e.g.*, Dutta *et al*., 2009). Before each measurement, the leaf was dark-adapted for 20 min.

Results

CAO Overexpressed (CAOx) Plants Grown in Low Light or High Light Regimes had Altered Chlorophyll a/b Ratio

The CAOx (CAOx1 and CAOx2) plants accumulated higher amounts of Chl in low light (LL; 70–80 μmol photons m^{-2} s^{-1}) as well as in high light (HL; 700–800 μmol photons m^{-2} s^{-1}) as compared to that in the wild-type (WT) plants grown under identical light regimes. As expected, WT-LL plants had higher Chl content and reduced Chl a/b ratio than the WT-HL plants (Fig. 1). The leaves of CAOx1-HL-plants were greener and accumulated 28% more Chl than WT-HL plants. The CAOx2-HL-plants accumulated 20% more Chl than the WT-HL plants (data not shown). Due to increased (70%) synthesis of Chl b in the CAOx plants grown in HL (CAOx1-HL), they showed an ~30% decline in Chl a/b ratio as compared to WT-HL plants. Similarly, CAOx2-HL-plants showed ~50% increase in Chl b synthesis as compared to WT-HL plants (data not shown). The CAOx plants grown in LL (CAOx1-LL) were greener than LL-grown WT plants (WT-LL) and had 15% lower Chl a/b ratio (Fig. 1). The Chl a/b ratio and Chl content of WT and transgenic plants showed some minor variations in different growth seasons. Since CAOx1 plants had high amount of Chl b and reduced Chl a/b ratio as compared to that of CAOx2, we characterized the CAOx1 plants in detail, henceforth referred simply as CAOx.

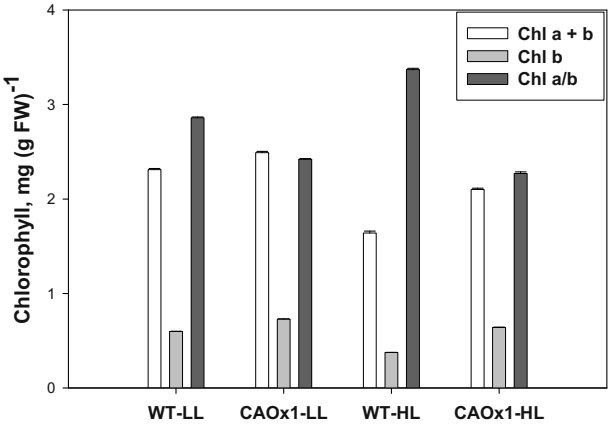

Fig. 1 Chlorophyll content and the leaf phenotype of wild-type (WT) and CAO overexpressing (CAOx1) tobacco plants grown under low-light (LL) and high-light (HL). Total chlorophyll (Chl a+b) content, chlorophyll b (Chl b) and chlorophyll a/b (Chl a/b) ratio of WT and CAOx1 plants grown in LL (WT-LL, CAOx1-LL) and HL (WT-HL, CAOx1-HL). Plants grown for up to 20–25 days under light intensity of 200 μmol photons m^{-2} s^{-1} were transferred to LL (70–80 μmol photons m^{-2} s^{-1}) and HL (700–800 μmol photons m^{-2} s^{-1}) for additional 18–20 days in the greenhouse. The 2nd leaf was harvested from each plant types for pigment analysis. Each data point is the average of five replicates.

Photosynthetic Responses of CAOx Plants Grown in Low Light and High Light Regimes

To ascertain if increased Chl b content had the expected effect on photosynthetic apparatus, Chl *a* fluorescence of leaves of both WT and CAOx tobacco plants grown in LL (70 μmol photons m^{-2} s^{-1}) or HL (700–800 μmol photons m^{-2} s^{-1}) was measured.

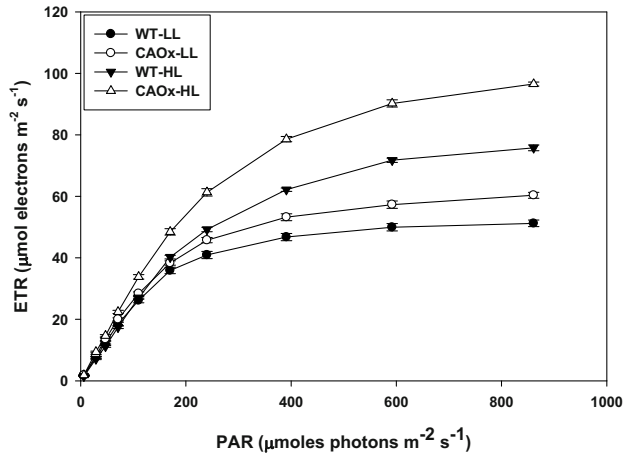

Fig. 2 Electron transport rate (ETR) of WT and CAOx plants. LL and HL-grown WT and CAOx plants were dark adapted for 20 min before readings were taken by PAM 2100 fluorometer. The ETR values were calculated from these fluorescence data (Table 1). The experiment was repeated thrice and each data point is the average of ten replicates.

Chl *a* fluorescence is used as a nondestructive and noninvasive signature of photosynthesis, particularly of Photosystem II (for reviews, see Papageorgiou and Govindjee, 2005). The minimal fluorescence (F_0), the maximum fluorescence (Fm) and the maximum photochemical efficiency of PSII in dark-adapted leaves, measured as Fv/Fm (where $F_v = F_m - F_o$), were not substantially affected in LL- or HL- grown WT or CAOx plants (Table 1). The electron transport rate (ETR, μmol electrons m^{-2} s^{-1}) was estimated from fluorescence parameters. The light-response curves of ETR suggest that in limiting (up to 70 µmol photons m^{-2} s^{-1}) as well as saturating light intensities, the ETR was higher in CAOx plants than that in WT plants grown in LL- or HL-regimes suggesting better light absorption and utilization, especially in Photosystem II, in the transgenic plants (Fig. 2). In WT, at limiting light intensities, the rate of increase in ETR in LL-grown plants was essentially the same as that in HL-grown plants (Fig. 2) even though the latter have less Chl (Fig. 1). The ETR in LL-grown WT and CAOx plants saturated at lower light intensity, around 400 µmol photons m^{-2} s^{-1} than HL-grown plants that saturated at around 800 µmol photons m^{-2} s^{-1} (Fig. 2). Both LL and HL CAOx plants had higher ETR at higher light intensities than equivalent WT plants since they have higher [Chl] and higher Chl b: Chl a ratio, the former being more in Photosystem II, and thus, the ratio of PSII : PSI is likely to be higher. Further, at limiting light intensities (Fig. 2), CAOx – HL had higher ETR than that in CAOx –LL as well as both LL- and HL- WT plants.

Table 1 Chlorophyll a fluorescence parameter of WT and CAOx plants grown under different light intensities. WT and CAOx plants were exposed to LL and HL conditions as mentioned under methods. Leaves were kept in dark for 20 min before the measurement of their minimal fluorescence (Fo), maximum fluorescence (Fm) and photosynthetic efficiency (Fv/Fm) by PAM 2100 fluorometer. The experiment was repeated 3 times and the values are mean ± SD (n = 10).

Plant lines	Chl a fluorescence		
	Fo	Fm	Fv/Fm
WT-LL	0.245 (± .003)	1.150 (± .003)	0.786 (± .003)
CAOx-LL	0.246 (± .006)	1.239 (± .028)	0.801 (± .0029)
WT-HL	0.253 (± .003)	0.885 (± .022)	0.714 (± .003)
CAOx-HL	0.257 (± .005)	1.254 (± .012)	0.794 (± .0028)

Discussion

Studies from other research groups and that of ours have demonstrated that high light decreases total Chl and Chl b content. Overexpression of *AtCAO* in tobacco or *Arabidopsis* results in increased total Chl and Chl b content, decreased Chl a/b ratio both in LL- and HL-grown plants (Fig. 1) (Pattanayak *et al.*, 2005; Tanaka and Tanaka, 2005). As expected from WT plants, the ETR values, calculated from yield parameters of PAM fluorometry (Schreiber, 2004), were higher in HL-grown plants than that in LL-grown plants (Fig. 2). As compared to that of HL-grown plants, the ETR saturated at a relatively lower light intensity (400 µmol photons m^{-2} s^{-1}) in LL-grown plants (Fig. 2). Due to increase in the antenna size, the ETR values at limiting light intensities of LL-grown WT-plants were higher than that of HL-grown WT plants (Fig. 2). At higher light intensities, the HL-grown CAOx plants had elevated ETR than that of HL-grown WT plants.

Our studies reveal that regulated increase in Chl b biosynthesis by over-expression of full length *CAO* increases the light-harvesting potential. Our results further demonstrate that controlled upregulation of endogenous Chl b biosynthesis, by genetic manipulation of full length *CAO*, partially increases photosynthesis.

References

Dutta S, Mohanty S, Tripathy BC (2009) Role of Temperature Stress on Chloroplast Biogenesis and Protein Import in Pea. Plant Physiology 150: 1050-1061

Eggink LL, LoBrutto R, Brune DC, Brusslan J, Yamasato A, Tanaka A, Hoober JK (2004) Synthesis of Chlorophyll b: Localization of Chlorophyllide a Oxygenase and Discovery of a Stable Radical in the Catalytic Subunit. BMC Plant Biol 4: 5

Espineda CE, Linford AS, Devine D, Brusslan JA (1999) The AtCAO Gene, Encoding Chlorophyll a Oxygenase, Is Required for Chlorophyll b Synthesis in Arabidopsis Thaliana. Proc Natl Acad Sci USA 96: 10507-10511

Nagata N, Satoh S, Tanaka R, Tanaka A (2004) Domain Structures of Chlorophyllide a Oxygenase of Green Plants and Prochlorothrix Hollandica in

Relation to Catalytic Functions. Planta 218: 1019-1025

Oster U, Tanaka R, Tanaka A, Rudiger W (2000) Cloning and Functional Expression of the Gene Encoding the Key Enzyme for Chlorophyll b Biosynthesis (CAO) from Arabidopsis Thaliana. Plant J 21: 305-310

Papageorgiou GC, Govindjee (2005) Chlorophyll a Fluorescence: A Signature of Phoosynthesis. In: Papageorgiou GC, Govindjee (eds.), Advances in Photosynthesis and Resiration, vol 19. Springer: Dordrecht

Pattanayak GK, Biswal AK, Reddy VS, Tripathy BC (2005) Light-Dependent Regulation of Chlorophyll b Biosynthesis in Chlorophyllide a Oxygenase Overexpressing Tobacco Plants. Biochim Biophys Res Com 326: 466-471

Schreiber U (2004) Pulse-Amplitude-Modulation (PAM) Fluorometry and Saturation Pulse Method: an Overview. In: Papageorgiou GC, Govindjee (eds.), Chlorophyll a Fluorescence: A Signature of Photosynthesis. Springer: Dordrecht, pp. 279-319

Tanaka A, Ito H, Tanaka R, Tanaka NK, Yoshida K, Okada K (1998) Chlorophyll a Oxygenase (CAO) Is Involved in Chlorophyll b Formation from Chlorophyll a. Proc Natl Acad Sci USA 95: 12719-12723

All of α-Carotene and Its Derivatives Have a Sole Chirality?

Shinichi Takaichi[a,*], Akio Murakami[b], Mari Mochimaru[c]

[a]Department of Bilogy, Nippon Medical School;
[b]Kobe University Research Center of Inland Seas;
[c]Department of Natural Science, Komazawa University.
Corresponding author. Tel. No. +81 44 733 3584; Fax No. +81 44 733 3584; E-Mail: takaichi@nms.ac.jp.

Abstract: Distribution of a-carotene and its derivatives is reported to be limited in some taxonomic groups of phototrophic organisms. In addition, C-6' in a-carotene between e-end group and conjugated double bonds is chiral, (6'*R*)- and (6'*S*)-types. The chirality was not systematically investigated, and the reported algae and land plants contained only (6'*R*)-type of a-carotene and/or its derivatives. To confirm the reliability of chirality, we re-examined distribution of a-carotene and its derivatives, and analyzed their C-6' chirality using circular dichroism or nuclear magnetic resonance spectra after purification of the carotenoids. We found a-carotene and/or its derivatives from Rhodophyceae (macrophytic type), Cryptophyceae, Euglenophyceae, Chlorarachniophyceae, Prasinophyceae, Chlorophyceae, Ulvophyceae, Charophyceae, and land plants, while we could not detected them from Glaucophyceae, Rhodophyceae (unicellular type), Chryosophyceae, Raphidophyceae, Bacillariophyceae, Phaeophyceae, Xanthophyceae, Eustigmatophyceae, Haptophyceae, and Dinophyceae. Further, loroxanthin, siphonaxanthin, and their fatty acid esters, which are synthesized from lutein, were found from Euglenophyceae, Chlorarachniophyceae, Prasinophyceae, Chlorophyceae, and Ulvophyceae. We analyzed chirality of a-carotene and/or its derivatives from around 40 species described above, and found they had only (6'*R*)-type.

Keywords: A-Carotene; Algae; Lutein; Lycopene e-cyclase

Introduction

Eukaryotic phototrophic organisms produce not only chlorophylls but also some carotenoids for photosynthesis. Carotenoids can be divided into two groups; b-carotene and its derivatives (zeaxanthin, violaxanthin, 9'-*cis* neoxanthin, diadinoxanthin, fucoxanthin, peridinin, etc.), and a-carotene and its derivatives (lutein, loroxanthin, siphonaxanthin, prasinoxanthin, etc.) (Fig. 1). All of Eukaryotic phototrophic organisms always contain b-carotene and its derivatives, while the distribution of a-carotene and its derivatives is limited in phototrophic organisms.

Some carotenoids have chiral carbon(s), but the chirality is investigated only limited species. In the case of a-carotene, its C-6' is chiral, and (6'*R*)- and (6'*S*)-types are possible (Fig. 2). The derivatives of a-carotene should hold the chirality. Their chiralities were also investigated only limited species, and not systematically.

In this study, we re-examined distribution of a-carotene and its derivatives, and analyzed their C-6' chirality.

Materials and Methods

Around 20 species, which were obtained from culture collections and cultivated, and collected at Seto Inland Seas (Japan), were used for this study (Table 1). Carotenoids and chlorophylls were extracted with acetone/methanol (7:2, v/v) containing 10 mmol Tris-HCl (pH 8.0) to prevent acidification. Pigments in crude extracts were analyzed with HPLC equipped with a m bondapak C_{18} column (Waters). Usually, a-carotene and its derivatives could be detected with their special absorption spectra in HPLC eluent (Takaichi and Shimada, 1992; Takaichi, 2000),

and their specific retention times on C_{18}-HPLC (Takaichi, 2000). When a-carotene and/or its derivatives were detected with C_{18}-HPLC, they were purified with combination of DEAE-Toyopearl column (Toso), silica gel column and TLC (Merck), and C_{18}-HPLC described above (Takaichi and Mimuro, 1998; Takaichi *et al*., 2010).

For chrality analysis, the circular dichroism (CD) spectra of the purified carotenoids in diethyl ether/2-pentane/ethanol (5:5:2, by vol.) at room temperature were measured using a J-820 spectropolarimeter (JASCO) (Takaichi *et al*., 2010).

Results

Around 20 species were analyzed for this study, and chirality data of around 20 species were obtained from our previous papers (Takaichi and Mimuro, 1998; Yoshii *et al*., 2005; etc.) and some acceptable papers (Fiksdahl *et al*., 1984; Partali *et al*., 1985; etc.) (Table 1). a-Carotene and/or lutein were found from Rhodophyceae (macrophytic type), Cryptophyceae, Euglenophyceae, Chlorarachniophyceae, Prasinophyceae, Chlorophyceae, Ulvophyceae, Charophyceae, and land plants. Further, loroxanthin, siphonaxanthin, and their fatty acid esters, which are synthesized from lutein (Fig. 1), were found from Euglenophyceae, Chlorarachniophyceae, Prasinophyceae, Chlorophyceae, and Ulvophyceae.

The only (6'*R*)-type chilarity of a-carotene and/or its derivatives were found, but (6'*S*)-type was not.

On the other hand, a-carotene and its derivatives were not detected from Glaucophyceae, Rhodophyceae (unicellular type), Chryosophyceae, Raphidophyceae, Bacillariophyceae, Phaeophyceae, Xanthophyceae, Eustigmatophyceae, Haptophyceae, and Dinophyceae.

Discussion

In biosynthesis of a-carotene in land plants, both lycopene b-cyclase and lycopene e-cyclase are needed to produce a-carotene from lycopene. They have high homology with each other, and therefore lycopene e-cyclase gene might be produced by duplication of lycopene -cyclase gene (Cunningham *et al*., 2007). Further, the organisms without a-carotene and its derivatives contain lycopene e-cyclase.

In enzymatic reaction of cyclization, the mechanisms of lycopene b-cyclase, lycopene (6'*R*)-e-cyclase, and lycopene (6'*S*)-e-cyclase are almost the same; the products are depending on the carbon number to eliminate H^+ and on the direction of elimination (Britton, 1998). Therefore, both lycopene e-cyclases could be exist, but only lycopene (6'*R*)-e-cyclase was found based on the presence of only (6'*R*)-type. Since the chirality of (6'*R*)- and (6'*S*)-a-carotenes are different for the direction of e-end groups, binding site on the protein should not be identical. Consequently, the binding protein moiety in pigment-protein complex in photosynthesis might restrict to one chirality of a-carotene, (6'*R*)-a-carotene.

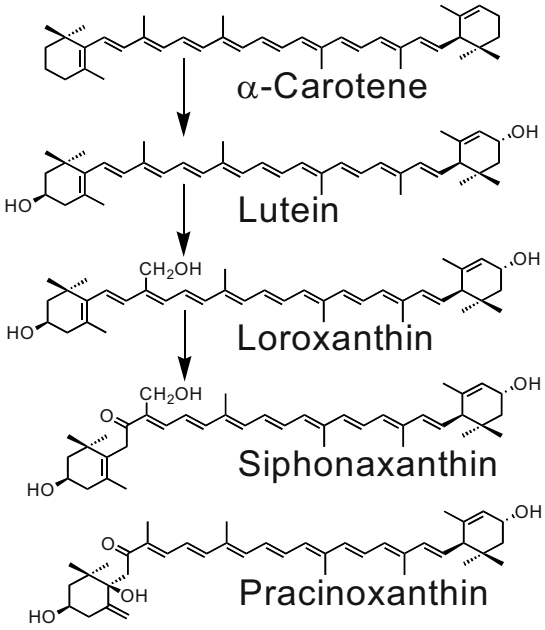

Fig. 1 Structures of (6'*R*)-type a-carotene and its derivatives usually found in nature.

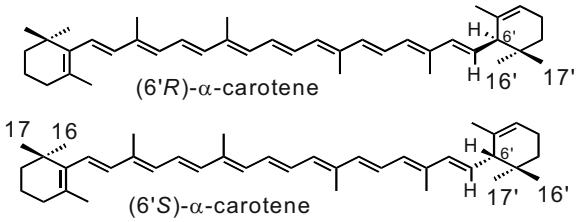

Fig. 2 Structures of (6'*R*)- and (6'*S*)-a-carotene.

Acknowledgements

The authors thank M Tanaka and K Sanji for CD measurement, and H Okuyama, J Minagawa, S Nishitani, T Maoka, and K Niwa for cultivation, collection or identification of biological materials.

Table 1 Distribution and chirarity of a-carotene and its derivatives.

Class Genus and species	Presence of a-carotene and its derivatives, or their absence [1]	References
Glaucophyceae		
Cyanophora paradoxa NIES-547	Absence	Reanalyzed[2]
Rhodophyceae		
Bangiophycidae		
Cyanidioschyzon merolae	Absence	Reanalyzed[2]
Cyanidium caldarium	Absence	Reanalyzed[2]
Porphyra yezoensis	a-Carotene, Lutein	This study
Florideophycidae		
Grateloupia lanceolata	a-Carotene, Lutein	This study
Chondrus giganteus	a-Carotene, Lutein	This study
Cryptophyceae		
Rhodomonas sp.strain D3	a-Carotene, Monodoxanthin	Pennington *et al*., 1985
Cryptomonas ovata	e-Carotene	Pennington *et al*., 1985
Chrysophyceae		
Ochromonas danica	Absence	This study
Raphidopheceae		
Heterosigma akashiwa	Absence	Reanalyzed[2]
Bacillariophyceae		
Phaeodactylum tricornutum	Absence	Reanalyzed[2]
Thallassiorsia sp.	Absence	This study
Phaeophyceae		
Undaria pinnatifida	Absence	This study
Petalonia fascia	Absence	Reanalyzed[2]
Xanhophyceae		
Vaucheria terrestiris	Absence	Reanalyzed[2]
Eustigmatophyceae		
Nannochloropsis oculata NIES-2145	Absence	This study
Haptophyceae		
Emiliania hyxleyi	Absence	Reanalyzed[2]
Calyptrosphaera sphaeroides	Absence	Reanalyzed[2]
Dinophyceae		
Alexandorium tamarense	Absence	Reanalyzed[2]
Symbiodinium sp. NBRC 104786	Absence	This study
Euglenophyceae		
Eutreptiella gymnastica	Siphonaxanthin	Fiksdahl *et al.*, 1984
Euglena sanguinea	Loroxanthin ester	Grung, Liaaen-Jensen 1993
Chlorarachniophyceae		
Chlorarachnion sp. NIES-254	Loroxanthin ester	Sasa *et al.*, 1992
Prasinophyceae		
Pterosperuma cristatum	Siphonaxanthin ester	Yoshii *et al.*, 2002
Nephroselmis sp. NIES 486	19-Methoxysiphonaxanthin	Yoshii *et al.*, 2005
Chlorophyceae		
Scenedesmus acutus	a-Carotene	Partali *et al.*, 1985
Chlamydomonas reinharditt	Lutein, Loroxanthin	This study
Ulvophyceae		
Ulva pertusa	a-Carotene, Lutein	This study
Monostroma nitidum	Lutein	This study
Charophyceae		
Spirogyra sp.	Lutein	This study
Land Plants		
Marchantia polymorpha	Lutein	This study
Daucus carota root	a-Carotene	This study
Oryza sativa	Lutein, Lutein 3-acetate	Kusaba *et al.*, 2009

[1]Chirality at C-6' of a-carotene and its derivatives was only (6'*R*)-type.

[2]Reanalyzed from the HPLC data of Takaichi and Mimuro (1998).

References

Britton G (1998) Overview of Carotenoid Biosynthesis. In: Britton G, Liaaen-Jensen S, Pfander H (eds.), Biosynthesis and Metabolism, Carotenoids Vol. 3. Birkhäuse: Basel, pp. 13-147

Cunningham Jr FX, Lee H, Gantt E (2007) Carotenoid Biosynthesis in the Primitive Red Alga Cyanidioshyzon Merolae. Eukaryo Cell 6: 533-545

Fiksdahl A, Bjørnland T, Liaaen-Jensen S (1984) Algal Carotenoids: Algal Carotenoids with Novel End Groups. Phytochemistry 23: 649-655

Grung M, Liaaen-Jensen S (1993) Algal Carotenoids: Secondary Carotenoids of Algae: Carotenoids in a Natural Bloom of Euglena Sanguinea. Biochem System Ecol 21: 757-763

Kusaba M, Maoka T, Morita R, Takaichi S (2009) A Novel Carotenoid Derivative, Lutein 3-Acetate, Accumulates in Senescent Leaves of Rice. Plant Cell Physiol 50: 1573-1577

Partali V, Olsen Y, Foss P, Liaaen-Jensen S (1985) Carotenoids in Food Chain Studies: Zooplankton (Daphnia Magna) Response to a Unialgal (Scenedesmus Acutus) Carotenoid Diet, to Spinach, and to Yeast Diets Supplemented with Individual Carotenoids. Comp Biochem Physiol 82B: 767-772

Pennington FC, Haxo FT, Borch G, Liaaen-Jensen S (1985) Algal Carotenoids: Carotenoids of Cryptophyceae. Biochem System Ecol 13: 215-219

Sasa T, Takaichi S, Hatakeyama N, Watanabe MM (1992) A Novel Carotenoid Ester, Loroxanthin Dodecenoate, from Pyramimonas Parkeae (Prasinophyceae) and a Chlorarachniophycean Alga. Plant Cell Physiol 33: 921-925

Takaichi S (2000) Characterization of Carotenes in a Combination of a C18 HPLC Column with Isocratic Elution and Absorption Spectra with a Photodiode-Array Detector. Photosynth Res 65: 93-99

Takaichi S, Mimuro M (1998) Distribution and Geometric Isomerism of Neoxanthin in Oxygenic Phototrophs: 9'-cis, a Sole Molecular Form. Plant Cell Physiol 39: 968-977

Takaichi S, Shimada K (1992) Characterization of Carotenoids in Photosynthetic Bacteria. Methods Enzymol 213: 374-385

Takaichi S, Maoka T, Takasaki K, Hanada S (2010) Carotenoids of Gemmatimonas Aurantiaca (Gemmatimonadetes): Identification of a Novel Carotenoid, Deoxyoscillol 2-Rhamnoside, and Proposed Biosynthetic Pathway of Oscillol 2,2'-Dirhamnoside. Microbiology 156: 757-763

Yoshii Y, Takaichi S, Maoka T, Hanada S, Inouye I (2005) Characterization of Two Unique Carotenoid Fatty Acid Esters from Pterosperma Cristatum (Prasinophyceae, Chlorophyta). J Phycol 38: 297-303

Yoshii Y, Takaichi S, Maoka T, Suda S, Sekiguchi H, Nakayama T, Inouye I (2005) Variation of Siphonaxanthin Series among the Genus Nephroselmis (Prasinophyceae, Chlorophyta), Including a Novel Primary Methoxy Carotenoid. J Phycol 41: 827-834

Fluorescence Lifetime Imaging Microscopy of *Synechocystis* WT Cells — Variation in Photosynthetic Performance of Individual Cells in Various Strains of *sp.* PCC 6803

Tünde Tóth[ab], Volha V Chukhutsina[a], Sashka B Krumova[c], Zoltan Gombos[b], Herbert van Amerongen[a,d,*]

[a]Wageningen University, Laboratory of Biophysics, Wageningen, The Netherlands;
[b]Institute of Plant Biology, Biological Research Center, Hungarian Academy of Sciences, Hungary;
[c]Institute of Biophysics, Bulgarian Academy of Sciences, Sofia, Bulgaria;
[d]MicroSpectroscopy Centre, Wageningen University, Wageningen, The Netherlands.
[*]Corresponding author. Tel. No. +31317482634; Fax No. +31317482725; E-mail: Herbert.vanAmerongen@wur.nl.

Abstract: The FLIM (fluorescence lifetime imaging microscopy) technique allows picosecond fluorescence measurements at the level of the individual cell. Using this technique we were able to observe heterogeneity of cyanobacterial cells in a culture grown under controlled conditions and we were able to resolve structural variations within individual cells. It can be concluded that on the one hand the inhomogeneous distribution of photosynthetic pigments within the cell leads to variation of the fluorescence intensity, whereas on the other hand it is impossible to detect variation in the relative amounts of photosystem I and II throughout the cell. Different *Synechocystis sp*. PCC 6803 strain lines were compared to each other and differences were observed in the average fluorescence lifetimes obtained for individual cells of the various cell lines. The differences can be traced back to variable efficiency of excitation energy transfer from the phycobilisome antenna to the photosystems. We could successfully demonstrate that there is heterogeneity inside individual cells, within individual cultures, and between various wild-type cell lines.

Keywords: Photosystem; FLIM; Light harvesting; Excitation energy transfer; Cyanobacteria

Introduction

In the present work we study cells of the cyanobacterium *Synechocystis sp*. PCC 6803 with the use of picosecond (ps) microscopy. In general, aerobic photosynthetic organisms contain pigments bound to proteins for light energy collection. Fluorescence that is emitted by these pigments can provide information about the rate and efficiency of the photosynthetic process. Recently it has become possible to detect time-resolved fluorescence on a ps time scale with sub- m spatial resolution with the use of FLIM (fluorescence lifetime imaging microscopy). Our FLIM setup combines ps TCSPC (time-correlated single-photon counting) with microscopy using two-photon excitation and allows measurements at the individual cell level, thereby outcompeting the commonly used bulk experiments at the ensemble level (Krumova *et al.*, 2010) As such, the technique can also provide information about heterogeneity of the system.

Currently, several cell lines of *Synechocystis sp*. PCC 6803 are being used world-wide and numerous mutants originate from these lines. For a good comparison of literature data it is important to know whether the various WT lines are indeed identical and the FLIM technique provides a way to detect both structural and functional differences. Here we compare cyanobacterial cells of various lines of *Synechocystis sp*. PCC 6803 originating from different laboratories using FLIM.

Materials and Methods

WT *Synechocystis* sp. PCC 6803 cell cultures were

grown in BG11 medium, on a rotary shaker and under continuous illumination with white light of 10 μmol photons m^{-2} s^{-1}. The cells used for the measurements were in the logarithmic growth phase and were measured between the 3rd and 6th day of cultivation, with the OD in the range of 0.1–0.2 measured at 679 nm.

Two-photon excitation (860 nm) FLIM was performed *in vivo*; cells were immobilized in 3% low gelling temperature agarose, type VII (Sigma-Aldrich) dissolved in BG11 and pressed between microscopy and cover glasses. The FLIM setup was described in (Borst *et al.*, 2005). Fluorescence was detected via non-descanned single photon counting detection, through two band-pass filters of 700 nm (75 nm bandwidth). To minimize photodamage, the lowest possible excitation power (of the order of 60 μW average power at 860 nm) in combination with long integration times (20–30 min) was used. The amplitude-weighted average lifetime was calculated via

$$\tau_{ave} = \sum_{i=1}^{n} \alpha_i . \tau_i \ .$$

The lifetime distribution for different cells (and inside individual cells) was found to be very reproducible in most cases.

FLIM images were analyzed with the TIMP package for R language and environment for statistical computing (Laptenok *et al.*, 2007). Only pixels with intensity above 50 cps were selected for global analysis resulting in a set of lifetimes that are the same for all pixels and amplitudes that can differ to some extent. For a good comparison in all cases, the shortest lifetime was fixed to 71 ps, whereas the corresponding amplitude could be either positive or negative (Krumova *et al.*, 2010). For calculating the average lifetimes only the slowest components with positive amplitude were used. Pinacyanol in methanol with a 6 ps lifetime was used as a reference for the time-resolved measurements (van Oort *et al.*, 2008). The fit quality was judged by singular value decomposition of the residual matrix associated with each FLIM image (Laptenok, 2009).

All measurements were performed at 22 °C.

Results and Discussion

Fluorescence kinetics of individual WT cells show a multi-exponential decay. The decay kinetics comprise several processes and this can make the analysis/ interpretation complicated. Phycobilisomes (PBS), Photosystem I (PSI) and Photosystem II (PSII) all have their own individual multi-exponential kinetics and energy transfer from PBSs to PSI and PSII complicates the kinetics even further (Krumova *et al.*, 2010). Moreover, it is well known that the pigment composition influencing fluorescence properties of the cyanobacterial cells varies, depending on the physiological state of the cells (Gombos *et al.*, 1987).

A typical FLIM intensity (time-integrated) image of WT cells with an average diameter of 2 μm is shown in Fig. 1A. Fluorescence decay kinetics were recorded in each individual pixel. Global analysis of the fluorescence kinetics of selected pixels was fitted with three exponential decay components. The comparison of the average lifetime of pixels belonging to individual cells demonstrates the heterogeneity of cells taken from the same culture (Fig. 1B).

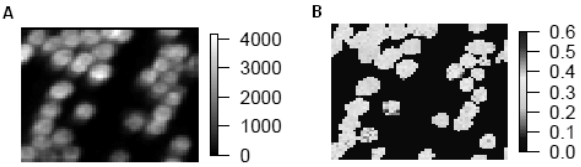

Fig. 1 Global analysis results of a representative FLIM image of *Synechocystis sp*. PCC 6803 WT cells detected with a 700-nm bandpass filter. Global analysis was performed with a 3-exponential model. (A) Fluorescence intensity image (B) Fluorescence lifetime image with color-coded average lifetimes (in ns).

We also addressed the question whether it is possible to resolve structural variations within individual *Synechocystis* cells and whether this is related to fluorescence lifetime variations. It should be realized that the excitation beam focuses into a voxel of 0.5 × 0.5 μm in the X-Y direction and 2 μm in the Z direction which is comparable to the total cell size. Nevertheless it is possible to observe clear intensity variations within the cells (Fig. 2) where the highest intensity is mainly present near the cell wall.

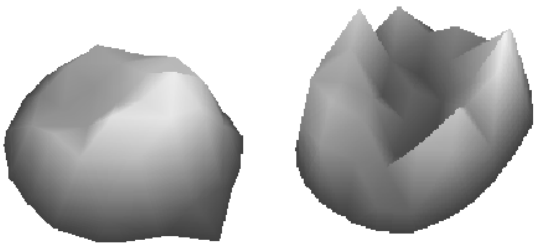

Fig. 2 3D Fluorescence intensity image of two *Synechocystis sp.* PCC 6803 WT cells (the grayscale colors represent relative intensities).

This intensity distribution can originate from different sources. It was reported before that PSII and PBSs are mainly localized close to the cell wall, whereas PSI is relatively more present in the middle part of the cell (Vermaas *et al.*, 2008). Because the fluorescence yield of PSI is far lower than that of PSII + PBS this would indeed lead to less fluorescence in the center of the cells. On the other hand, it is also possible that the reduced intensity in the center of the cells is due to the fact that the thylakoid membranes are mainly localized at the periphery of the cell. The first explanation would predict shorter fluorescence lifetimes in the center of the cells in contrast to the second one. Because we could not observe any systematic variation in the average lifetimes over the cell, we conclude that the intensity variation is mainly due to a denser packing of thylakoid membranes near the cell wall.

We also performed a comparison study of *Synechocystis sp* PCC 6803 stock cell cultures originating from different lines but grown under the same conditions.

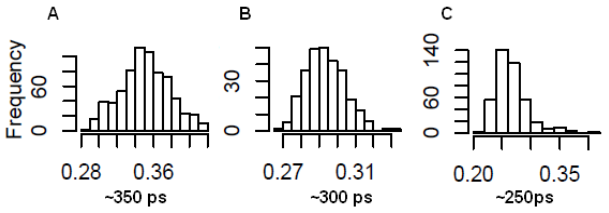

Fig. 3 Histogram of the avarege lifetime (in ns) of the different cell lines and their mean values obtained from three-exponential global analysis (A) represents values for cell line 1, (B) for line 2 and (C) for line 3.

The histogram of the average lifetimes of individual cells from the three different cell lines (lines 1, 2 and 3) that were studied are shown in Fig. 3. All tree lines show significantly different average fluorescence lifetimes. (The absorption spectra of the three cultures were rather similar.) In order to better understand the origin of the difference in average lifetimes, we looked in more detail at the values of the various lifetime components as obtained by global analysis and the corresponding normalized amplitudes. For the analysis we selected cells with an average lifetime that was characteristic for a certain line. The global analysis performed on different lines resulted in slightly different lifetime components but these differences were significant. Both the obtained lifetimes and the corresponding amplitudes contain information about energy transfer and utilization in the cells. In an earlier study on WT cells of *Synechocystis sp*. PCC 6803 (Krumova *et al.*, 2010) global analysis of the FLIM images showed 3 lifetimes: 71 ps, 246 ps and 842 ps. In most cases the 71 ps component had a positive amplitude but sometimes it was negative and this was ascribed to PBS that were disconnected from the photosystems. In general the occurrence of this negative component was accompanied by an increase of the amplitude of the slowest component, also due to disconnected PBSs. The long component is probably also partly due to the the presence of closed PSII reaction centers The middle (~250 ps) component is due to excitation trapping (mainly charge separation in PSII).

In Fig. 4 the global analysis results are presented for one characteristic cell from each culture (analyses were performed on several cells) and the lifetimes are given in the legend of the figure. It is clear that for line 1 the shortest component has a negative amplitude in many pixels and this is also accompanied by an increase of the amplitude of the longest component. As argued above, this is due a higher percentage of PBSs that are disconnected (or badly connected) to the photosystems. The middle component shows an increase in the amplitude while the lifetime decreases from 260 ps for line 1, 245 ps for line 2 to 205 ps for line 3.

The lifetime of the longest component does not significantly differ for the various cells and the main difference concerns the decrease of its contribution going from line 1 to line 3.

Based on the above observations we conclude that the main difference between the various lines concerns the efficiency of energy transfer from the PBS to PSII. The observations nicely demonstrate that the FLIM technique is suitable to detect differences in the functional properties within and between different cell lines.

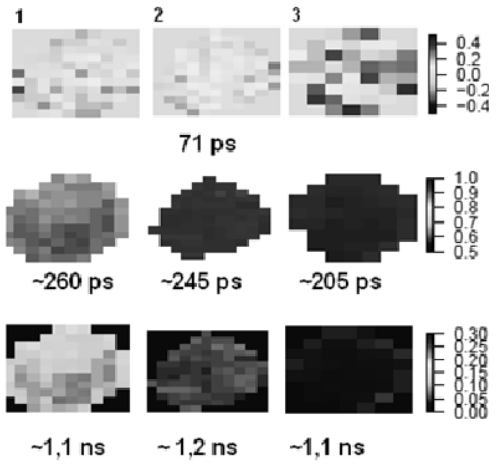

Fig. 4 Global analysis results of one representative cell of each *Synechocystis PCC* 6803 WT cell line (1) line 1, (2) line 2 and (3) line 3 are shown in different columns. For each pixel the relative amplitude of the corresponding lifetime (fast, middle, slow) are respresented in color-code.

Acknowledgements

Helpful discussions were kindly provided by László Kovács and Sergey Laptenok and the help of Lijin Tian is kindly acknowledged.

References

Borst JW, Hink MA, van Hoek A, Visser AJWG (2005) Effects of Refractive Index and Viscosity on Fluorescence and Anisotropy Decays of Enhanced Cyan and Yellow Fluorescent Proteins. J. Fluor. 15: 153-160

Csatorday K， Horváth G (1977) Synchronization of Anacystis Nidulans. Oxygen Evolution during the Cell Cycle. Arch Microbiol. 111: 245-246

Gombos Z, Szalontai B, Suranyi G (1987) Selective Alteration of the Pigment Composition of the Green-Alga, Anacystis Nidulans. Photochem. Photobiol. 45: 399-402

Krumova SB, Laptenok SP, Borst JW, Ughy B, Gombos Z, Ajlani G, van Amerongen H (2010) Monitoring Photosynthesis in Individual Cells of Synechocystis sp. PCC6803 on a Picosecond Timescale. Biophys J. 99: 2006-2015

Laptenok S, Mullen KM, Borst JW, van Stokkum IHM, Apanasovich VV, Visser AJWG (2007) Fluorescence Lifetime Imaging Microscopy (FLIM) Data Analysis with TIMP. J. Stat. Software. 18: 1-20

Laptenok S (2009) Global Analysis of Time-Resolved Fluorescence Microspectroscopy and Applications in Biomolecular Studies. PhD thesis. Wageningen University, The Netherlands

van Oort B, Amunts A, Borst JW, van Hoek A, Nelson N, van Amerongen H, Croce R (2008) Picosecond Fluorescence of Intact and Dissolved PSI-LHCI Crystals. Biophys. J. 95: 5851-5861

Vermaas, WFJ, Timlin JA, Jones HDT, Sinclair MB, Nieman LT, Hamad SW, Melgaard DK, Haaland DM (2008) In Vivo Hyperspectral Confocal Fluorescence Imaging to Determine Pigment Localization and Distribution in Cyanobacterial Cells. Proc. Natl. Acad. Sci. USA. 105: 4050-4055

Isolation of Intact Phycobilisomes in Low Salt: a Novel Method for Purifying Phycobilisomes by Mild Cross-Linking

Liron David , Noam Adir

Schulich Faculty of Chemistry, Technion-Israel Institute of Technology, Haifa, 32000 Israel.
Tel. No. 972-4-8292141; Fax No. 972-4-82925703; E-mail: nadir@tx.technion.ac.il.

Abstract: Photosynthesis is initiated by the capture of light energy, absorbed and transferred to photosynthetic reaction centers by light harvesting complexes. In cyanobacteria and red algae the major light harvesting complex is the Phycobilisome. The phycobilisome is a gigantic photosynthetic antenna with a molecular weight between 3–7 MDa and dimensions of 40–60 nm. The complex is assembled by two multi-subunit sub-complexes: a central core which is surrounded by rods in which the energy is transferred from the distal side of the rod to the core. In order to isolate the entire complex, the presence of high concentration of phosphate buffer (> 0.75 mol) is necessary, to prevent immediate complex disassemble into subunits. We have developed a mild procedure of cross-linking the phycobilisome from the thermophilic cyanobacterium *Thermosynechococcus vulcanus* that enables us to obtain an intact and functional complex under low ionic strength conditions. The cross-linked complex was examined by a spectroscopic analysis that confirmed that the isolated complex was indeed intact and continues to transfer energy from the rod to the core.

Keywords: Photosynthesis; Chemical cross-linking; Cyanobacteria; Fluorescence

Introduction

The phycobilisome (PBS) is an enormous light harvesting complex which is attached to the stromal side of the thylakoid membrane and is unique to cyanobacteria and red algae. In the initial step of the photosynthetic process, the PBS serves as an extremely efficient antenna complex that absorbs light energy and transfers it to the photosynthetic reaction centers (mostly to Photosystem II). The PBS is distinguished from other photosynthetic antennas found in plants and green algae both in size and pigment content. The molecular weight of the PBS range between 3–7 MDa, with dimensions of between 40 nm to 60 nm. The complex is built up from phycobiliproteins (PBP) which are pigmented proteins that covalently bind bilin cofactors and unpigmented proteins typically referred as linker proteins (David *et al*., 2010; Glazer, 1989; Liu *et al*., 2005). The PBS was visualized by electron microscopy (EM)(Gantt and Lipschultz, 1972; MacColl, 1998; Yamanaka *et al*., 1978; Yamanaka *et al*., 1982), as a complex constructed from two large sub-complexes, rods and core. The overall structure of the complex showed a central core build up from 2–5 core cylinders surrounded by 6–8 rods (Adir, 2005; Adir, 2008). The architectural structure of PBS is still unclear and based on those EM micrographs, since it has been suggested that the rods can be arranged in two possible manners around the core. The first model suggested that the rods arranged around the core in a radial fashion, while the second model proposed that the rods are arranged in pairs, in a way that two rod doublets are parallel to the thylakoid membrane and one rod doublet which is perpendicular to the membrane (Glazer, 1989). This model was also supported by cryo-EM micrographs (Yi *et al*., 2005) and is consistent with the crystal structures of phycocyanin (PC), which is one of the PBP components found in all rods. The PBS from the thermophilic cyanobacterium *Thermosynechococcus vulcanus* contains six rods arranged around three core

cylinders. Only two PBPs (from the four available PBP forms) are present in *T. vulcanus*, allophycocyanin (APC) located in the core and PC located in the rods. Energy is transferred by the PBS into the photosynthetic reaction centers via the specific arrangement of the cofactors within the complex. The PBS thus serves as a type of energy funnel, with the higher energy absorbed by PC (absorption maxima at 620 nm), transferred down through APC (absorption maxima at 652 nm) and specific minor APC forms have absorption maxima that overlap with the absorption of chlorophyll *a* (MacColl, 2004; McGregor *et al*., 2008). *In vitro*, an intact PBS can only be isolated in the presence of a high concentration of phosphate or citrate buffer (0.7–0.9 mol). The high phosphate increases the strength of hydrophobic interactions, and may mimic the crowded cytosolic environment in which the PBS is found *in vivo* (McGregor *et al*., 2008; Stagg *et al*., 2007; Zilinskas and Glick, 1981). In this report, we present a procedure developed to isolate an intact and functional PBS in low ionic strength conditions by minimal cross-linking of the complex.

Methods and Materials

T. vulcanus cells were grown in a 10 liter temperature-controlled growth chamber on BG11 medium supplemented with 5% CO_2 in air at 55 °C, with fluorescent lamp illumination. Cells were grown for 5 to 7 days before collection by centrifugation (Sorvall super T21 centrifuge). Harvested cells were resuspended in 0.9 mol phosphate buffer (pH 7.0) and disrupted by French Pressure cell treatment followed by centrifugation at 15,000 rpm. The pellet was resuspended with 0.9 mol phosphate buffer and incubated for 1 h with 2% Triton X-100 (w/v, sigma), followed by clarification by centrifugation. The resulting supernatant was centrifuged (Beckman Coulter, optima L-90K ultracentrifuge, Beckman Type T70.1 rotor) in 10 ml tubes for 2 h at 35,000 rpm and the resulting blue pellet was resuspended with 0.9 mol phosphate buffer and placed on a 0.8 mol sucrose cushion and centrifuged for 2 h at 40,000 rpm. The resulting pellet was resuspended with 0.9 mol phosphate buffer and placed on a four-step sucrose gradient built in the following fashion: 0.9 mol sucrose/0% GA; 1.0 mol sucrose/0.15% GA; 1.125 mol sucrose/0.25% GA; 1.25 mol sucrose/0.35% GA, all in 0.9 mol phosphate for 30 min, 50,000 rpm. The resulting pellet was then resuspended in 50mmol Tris buffer (pH = 8.0) and the PBS was further purified in two sequential sucrose step gradients. The first was 1.25–1.75 mol and the intact PBS pelleted. The pellet was resuspended in 50 mmol Tris buffer and applied to the second gradient of 2–2.25 mol sucrose. Both of the final gradients were ultracentrifuged for 1.5 h at 50,000 rpm and the cross-linked PBS (clPBS) was identified as a band at the interface between 2 and 2.25 mol sucrose. The isolated band was characterized by absorption (Varian spectrophotometer – Cary Bio 50) and fluorescence spectroscopy (Cary Eclipse spectro-fluorometer, excitation at 580 nm, 10 nm slit width).

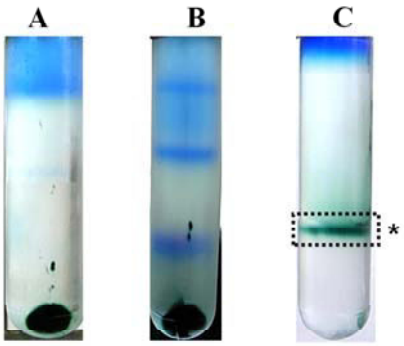

Fig. 1 Isolation of intact and functional PBS by cross-linking sucrose gradient centrifugation in comparison to hpPBS. A, sucrose step gradient (in the presence of 0.9 mol phosphate buffer) composed of the following steps: 0.9 mol Sucrose , 1 mol sucrose +0.15% GA, 1.125 mol sucrose +0.25% GA and 1.25 mol sucrose +0.35% GA. B, second sucrose step gradient (in the presence of 50 mmol Tris) with the following steps: 1.25 mol, 1.5 mol and 1.75 mol sucrose. C, the final sucrose step gradient made up of 2 mol and 2.25 mol sucrose in 50 mmol Tris. The asterisk indicates the isolated clPBS in 50 mmol tris buffer in the interface between the 2 mol and 2.25 mol sucrose steps.

Results and Discussion

Isolation of phycobilisomes in low salt

The PBS is a dynamic complex which has the ability to self-assemble and disassemble. In order to isolate and purify the complex *in vitro*, a stabilization buffer must be present. It has been shown that isolation of an intact and functional PBS was performed in the presence of high concentration of phosphate (0.75–0.9 mol) or citrate buffer, otherwise the complex immediately disassembles and degrades into trimers. The PBS is usually isolated by sucrose

gradient ultracentrifugation however, the presence of high phosphate buffer prevents the utilizing of additional purification steps such as ion exchange chromatography and therefore, obtaining a homogeneous PBS complex in solution is a challenging task. The PBS from *T. vulcanus* was also isolated by sucrose gradient ultracentrifugation, in the presence of 0.9 mol phosphate buffer (hpPBS), pH = 7.0 and three to four different fractions of intact and functional hpPBS were isolated from a 1–1.2 mol sucrose gradient. The isolated hpPBS expressed only small differences in their fluorescence and absorbance spectra and in their protein content as analyzed by SDS-PAGE. The different fractions may represent heterogeneities in the natural population of the PBS complex, or perhaps the isolation process induces such heterogeneities. Lack of homogeneity may negatively affect most physical methods that are used for investigation of the functionality of the complex, therefore, it was vital to develop a method which will allow us to obtain a single homogeneous fraction of the PBS in the absence of high phosphate buffer.

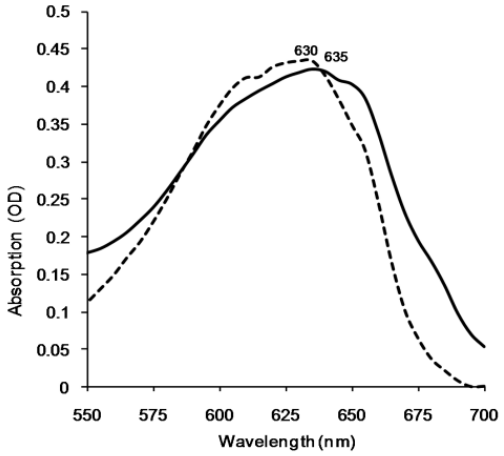

Fig. 2 Room temperature fluorescence emission spectrum of hpPBS in 0.9 mol phosphate buffer (thin line). and clPBS in 50 mmol Tris (bold line). Excitation was performed at 580 nm.

In order to isolate a low-phosphate stable PBS we performed mild crosslinking of the PBS by modifying the GraFix method for preparing cryoEM samples (Kastner *et al*., 2008). The resulting preparation led to an intact and functional cross linked PBS (clPBS). The procedure gently cross-links the PBS with glutaraldehyde (GA) during sucrose gradient ultracentrifugation by slowly increasing the concentration of GA, in order to create mostly intra-molecular contacts within the complex and prevent the formation of inter-molecular contacts between the complexes. The method is composed of several sucrose gradients during which the PBS is cross-linked and simultaneously transferred to a 50 mmol Tris buffer, pH 8.0 (for details see Methods and Materials section). As the PBS progressed along the gradient, the complex was introduced to a simutanously increasing sucrose and a GA concentration. The cross-linking gradient was centrifuged for short times at a high speed in order to prevent the PBS from being cross-linked to a higher degree. This ultracentrifugation process resulted in a turquoise pellet which contained a higher APC/PC ratio compared to hpPBS, indicating the loss of some PC hexamers. The turquoise pellet was solubilized in 50 mmol Tris which also immediately reacts with any remaining unreacted GA. This pellet was then submitted to further purification by sucrose gradients and additional, smaller crosslinked complexes of PC were obtained and removed in this fashion. Finally, a single soluble band of clPBS was obtained at the interface between 2 and 2.25 mol sucrose, in addition to a blue fraction of crosslinked PC, that did not enter the gradient (Fig. 1). We propose that following cross-linking (and in the presence of the Tris buffer), the PBS is assmbled in a tighter fashion which results in a higher density and the resulting migration to a higher concentratuion of sucrose.

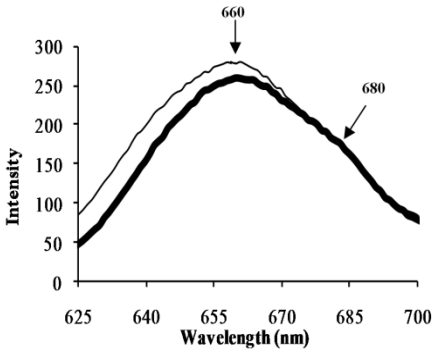

Fig. 3 Room temperature absorption spectrum of isolated hpPBS (broken line) and clPBS (continuous line).

Spectroscopic characterization of cross linked phycobilisome

The functional intactness of clPBS in 50 mmol Tris was confirmed by spectroscopic analysis. The fluorescence emission spectrum of the clPBS showed a maximum at 660 nm with a shoulder at 680 nm, when the sample was excited at 580 nm. Similar results were obtained for isolated hpPBS (Fig. 2). In addition, the absorption spectrum of the clPBS was

measured and exhibited maxima at 635 nm (due to rod-form phycocyanin) with a shoulder at 652 nm (due to allophycocyanin), as expected for intact PBS (Fig. 3). The absorption spectra indicated that the isolated clPBS was similar but not identical to the hpPBS and contained a higher APC/PC ratio with a more significant shoulder at 652 nm. Loss of loosely associated PC hexamers during the isolation proceedure may be the source of the small red shift in the absorption maxima we identiy as rod-PC (from 630 nm to 635 nm). Crosslinking of the phycobiliproteins prevents the quantitative assessment of the PC/APC ratio by either SDS-PAGE or absorption spectroscopy (since the extinction coefficients have been determined for isolated trimeric forms). Preliminary electron microscopic evaluation of the clPBS indicates that the PC trimer /APC trimer ratio is about 20/12, as opposed to 24/12 for hpPBS containing six rods (12 PC hexamers) and 3 core cylinders (12 APC trimers).

The spectroscopic analysis of the clPBS showed that the isolated complex in low ionic strength buffer was intact and functional and transfer energy from the rod to the core. We hope that this method for utilizing these stable PBS complexes will be an important tool for investigating the PBS energy transfer mechanism and arrangement.

Acknowledgements

This work was supported by the Israel Science Foundation founded by the Israel Academy of Sciences and Humanities (1045/06) and US-Israel Binational Science Foundation (2009406).

References

Adir N (2005) Elucidation of the Molecular Structures of Components of the Phycobilisome: Reconstructing a Giant. Photosynth Res, 85: 15-32

Adir N (2008) Structure of the Phycobilisome Antennae in Cyanobacteria and Red Algae. In: Fromme P (ed.), Photosynthetic Protein Complexes: A Structural Approach. WILEY-VCH Verlag GmbH & Co. KGaA: Weinheim, pp. 243-274

Adir N, Dines M, Klartag M, McGregor A, Melamed-Frank M (2006) Assembly and Disassembly of Phycobilisomes. In: Shively, JM (ed.), Microbiology Monographs: Inclusions in Prokaryotes, Vol. 2. Springer: Berlin/Heidelberg, pp. 47-77

Arteni AA, Ajlani G, Boekema EJ (2009) Structural Organisation of Phycobilisomes from Synechocystis sp. Strain PCC6803 and Their Interaction with the Membrane. Biochimica et Biophysica Acta 1787: 272-279

David L, Marx A, Adir N (2010) High-Resolution Crystal Structures of Trimeric and Rod Phycocyanin. J Mol Biol 405: 201-213

Dines M, Sendersky E, David L, Schwarz R, Adir N (2008) Structural, Functional, and Mutational Analysis of the NblA Protein Provides Insight into Possible Modes of Interaction with the Phycobilisome. Journal of Biological Chemistry 283: 30330-30340

Gantt E, Lipschultz CA (1972) Phycobilisomes of Porphyridium Cruentum. I. Isolation. J. Cell Biol. 54: 313-324

Glazer AN (1989) Light guides. Directional Energy Transfer in a Photosynthetic Antenna. J Biol Chem 264: 1-4

Kastner B, Fischer N, Golas MM, Sander B, Dube P, Boehringer D, Hartmuth K, Deckert J, Hauer F, Wolf E, Uchtenhagen H, Urlaub H, Herzog F, Peters JM, Poerschke D, x00Fc, hrmann R., Stark H (2008) GraFix: Sample Preparation for Single-Particle Electron Cryomicroscopy. Nature Methods 5: 53-55

Liu LN, Aartsma TJ, Thomas JC, Lamers GE, Zhou BC, Zhang YZ (2008) Watching the Native Supramolecular Architecture of Photosynthetic Membrane in Red Algae: Topography of Phycobilisomes and Their Crowding, Diverse Distribution Patterns. Journal of Biological Chemistry 283: 34946-34953

Liu LN, Chen XL, Zhang YZ, Zhou BC (2005) Characterization, Structure and Function of Linker Polypeptides in Phycobilisomes of Cyanobacteria and Red Algae: an Overview. Biochim Biophys Acta 1708: 133-142

MacColl R. (1998) Cyanobacterial Phycobilisomes. J Struct Biol 124: 311-334

MacColl R. (2004) Allophycocyanin and Energy Transfer. Biochim Biophys Acta 1657: 73-81

McGregor A, Klartag M, David L, Adir N (2008) Allophycocyanin Trimer Stability and Functionality Are Primarily Due to Polar Enhanced Hydrophobicity of the Phycocyanobilin Binding Pocket. Journal of Molecular Biology 384: 406-421

Stagg L, Zhang SQ, Cheung MS, Wittung-Stafshede P (2007) Molecular crowding enhances native structure and stability of alpha/beta protein flavodoxin. Proc Natl Acad Sci U S A, 104, 18976-18981

Yamanaka G, Glazer AN, Williams RC (1978) Cyanobacterial phycobilisomes. Characterization of the phycobilisomes of Synechococcus sp. 6301. J Biol Chem, 253, 8303-8310

Yamanaka G, Lundell DJ, Glazer AN (1982) Molecular architecture of a light-harvesting antenna. Isolation and characterization of phycobilisome subassembly particles. J Biol Chem, 257, 4077-4086

Yi ZW, Huang H, Kuang TY, Sui SF (2005) Three-dimensional architecture of phycobilisomes from Nostoc flagelliforme revealed by single particle electron microscopy. FEBS Lett, 579, 3569-3573

Zilinskas BA, Glick RE (1981) Noncovalent Intermolecular Forces in Phycobilisomes of Porphyridium cruentum. Plant Physiol, 68, 447-452

Differential Association of the Light-Harvesting Proteins (FCPs) with PSI and PSII in the Small Brown Tide Alga *Aureococcus Anophagefferens*

Meriem Alami, Beverley R Green

Department of Botany, University of British Columbia, Vancouver BC, V6T 1Z4 Canada.

Abstract: *Aureococcus anophagefferens* is a picoplanktonic microalga that is very well adapted to growth at low nutrient and low light levels, causing devastating blooms ("brown tides"). Its thylakoid membranes have a high content of FCPs (fucoxanthin/Chl a/c-binding proteins) belonging to the light harvesting complex (LHC) superfamily. Its genome sequence shows the presence of at least 64 genes for FCPs. To begin to understand the protein organization of the thylakoid, the membranes were solubilized with dodecyl maltoside and analyzed by sucrose gradients. Some of the FCPs appear to be organized in supercomplexes of 140 and 240 kDa where they are associated with PSII, while others might form independent supercomplexes. This protein organization probably reflects the ability of this alga to grow to very high cell densities in nature, with consequent limitation of incident light intensity due to shading.

Keywords: Alga; Fucoxanthin Chl *a/c* complexes; *Aureococcus anophagefferens*; Heterokont; Light-harvesting.

Introduction

Aureococcus anophagefferens is a small (2 μm diameter) picoplanktonic microalga that is very well adapted to growth at low nutrient and low light levels (Sieburth *et al*., 1988; Popels *et al*., 2002). It has caused massive harmful blooms ("brown tides") in U.S. waters in the past 25 years (Milligan and Cosper, 1997). It is a typical heterokont with thylakoids appressed in threes, Chl *a/c* light-harvesting complexes and a Chl *a/c* ratio of about 3, depending on the growth conditions. The major carotenoid is fucoxanthin, but there is also 19'-butanoyloxy-fucoxanthin, diatoxanthin and diadinoxanthin. Its genome sequence shows the presence of at least 64 genes for FCPs, belonging to several branches of the light harvesting complex (LHC) superfamily, approximately double the number found in two other diatoms. It also revealed the presence of LHC genes which are unique to *Aureococcus*.

However, little information is available concerning the characterization of the photosystems and the light harvesting complexes in this ecologically important alga. To gain some insight into what such a small cell is doing with so many FCP genes, we are beginning to characterize the association of the FCP proteins with photosynthetic super-complexes.

Materials and methods

An axenic *Aureococcus anophagefferens* strain 1984 (CCMP, Bigelow) was grown in artificial sea water medium at 18 °C at 60 μmol photons m^{-2} s^{-1} on a 12L:12D light cycle. Cells in late exponential phase were harvested at the beginning of the light phase. The cells were harvested by centrifugation at 6,000 g at 4 °C and washed once with buffer A (50 mmol Hepes pH 8, 10 mmol KCl, 50 mmol EDTA, 0.1% BSA, 0.6 mol sorbitol). The pellet was resuspended in the same buffer with β-glucuronidase (snail gut extract, Roche) and incubated 90 minutes at room temperature. This enzyme helps in digesting the copious extracellular exopolysaccharides. After a 10 minutes centrifugation step at 6,000 g at 4 °C, the cells were resuspended in buffer A then lysed with a Yeda Press at 350 psi. After a low speed

centrifugation step at 1,000 g at 4 °C to remove unbroken cells, the crude membrane fraction was pelleted at 10,000 g.

The membrane fraction was adjusted to a final concentration of 300 µg Chl/ml in buffer B (50 mmol Hepes pH 8, 5 mmol KCl, 2 mmol EDTA) and solubilized with n-docedyl β-D-maltoside (DDM) at chlorophyll: DDM of 1:30 for 40 minutes at 4 °C. Solubilized material was loaded onto a continuous sucrose gradient (10%–30%) in buffer B containing 0.03% DDM. After centrifugation at 200,000 x g for 24 h in a SW41 rotor, fractions were recovered and analyzed by SDS-PAGE, BN-PAGE, 2D BN/SDS-PAGE and immunoblotting. (Wittig *et al*., 2006). Two different antibodies were used to detect FCPs: α-HaFCP: raised to the 19 kDa FCP of *Heterosigma akashiwo* (another heterokont) in our laboratory, α -Lhcr: raised to the Chl *a* light-harvesting complex of the red alga *Porphyridium cruentum* (Agrisera). PSII was detected with an anti-D1 antibody (Agrisera) and PSI with an antibody raised to barley CPI.

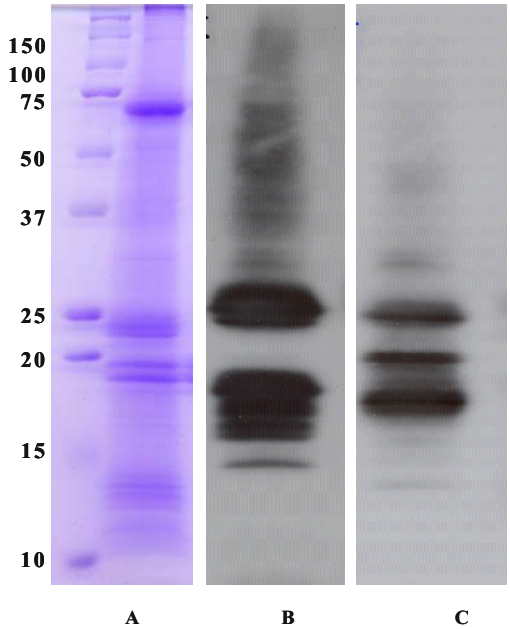

Fig. 1 Separation of *Aureococcus* thylakoid proteins on a 12-16% SDS-PAGE gel and visualisation by Coomassie staining (A) and by immunoblotting with anti-HaFCP (B) and with anti-Lhcr (C).

Results

The crude thylakoid pellet was solubilized with SDS and the proteins resolved on a 12%–16% SDS-PAGE gel (Fig. 1A). At least 11 separable polypeptides between 14 and 27 kDa can be detected by immunoblotting with two different antibodies that recognize members of the LHC superfamily (Figs. 1B and 1C). Polypeptides immunostained with the antibody raised to another heterokont (*Heterosigma akashiwo)* (Fig. 1B) fall into two molecular weight groups, one of about 24–27 kDa and the other ranging from 14–19 kDa. The major bands are not at the same position as the major bands detected by Coomassie staining (Fig. 1A). With the antibody raised to the red algal Lhcr (Fig. 1C), fewer bands are recognized, at least one of which was not detected by the other antibody.

Solubilized thylakoids were fractionated on a 10%–30% sucrose gradient on top of a 1.3 mol cushion. A broad dark brown band near the top of the gradient had a Chl *a/c* ratio of about 2 and contained most of the FCPs and PSII as detected by immunoblotting. It was well separated from a bright green fraction which was enriched in PSI complex and had a Chl *a/c* ratio of 4. Using the anti-HaFCP antibody, two major protein bands of about 20 and 25 kDa were visible (Fig. 2): the upper gradient fraction was enriched in the 25 kDa and the lower in the 20 kDa. According to the intensity of pigmentation, most of the FCPs are in the upper part of the gradient, but the antibodies showed that FCPs are also present in the lower band along with PSI.

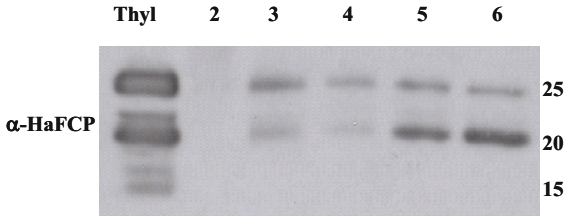

Fig. 2 Sucrose gradient fractions immunoblotted with anti-HaFCP. Fractions are numbered from the top of the gradient.

When the FCP-enriched fraction was analyzed by BN-PAGE, it showed the presence of several high molecular weight complexes of about 240, 140, and 67 kDa as well as a smaller band below 67 kDa (Fig. 3). To determine the association of FCPs with these complexes, the four major bands were cut out and the polypeptides denatured and separated in a second dimension on SDS-PAGE. Immunodetection with antibodies to D1 (PsbA) and HaFCP showed that D1 and the 25 kDa FCP polypeptide(s) are present in all four bands. This shows that FCPs are associated with D1 in several sizes of supercomplex.

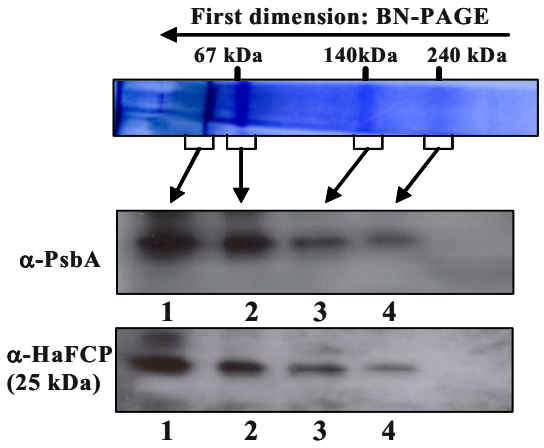

Fig. 3 Two dimensional separation of sucrose gradient fraction 3, first by BN-PAGE (top), followed by denaturing SDS-PAGE, and visualization by immunoblotting with anti-PsbA (D1) and anti-HaFCP.

On BN-PAGE, the green fraction enriched in PSI showed much larger complexes of about 440 kDa, as well as aggregates that did not enter the gel, indicating the presence of super-complexes (Fig. 4). When the gel strip was excised and subjected to a second denaturing dimension followed by immunostaining, it became clear that the FCP band of about 20 kDa was not associated with PS I, even though it was more pronounced in the sucrose gradient fraction. This suggests that PSI and the FCPs form separate supercomplexes that co-sediment on sucrose gradients. Size exclusion chromatography of solubilized thylakoids also showed that most of the FCPs are in high molecular weight fractions (data not shown).

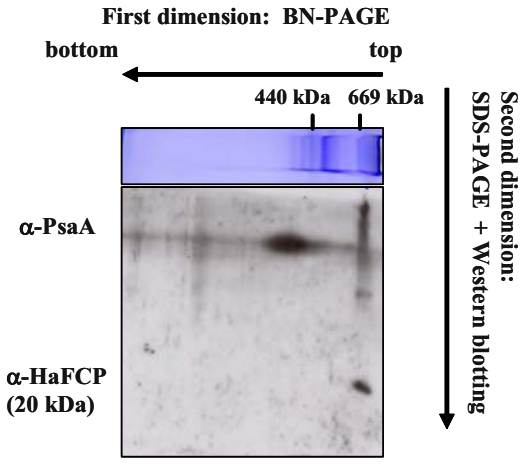

Fig. 4 Two dimensional separation of sucrose gradient fraction 6, first by BN-PAGE (top), followed by denaturing SDS-PAGE, and visualization by immunoblotting with anti-PsaA and anti-HaFCP.

Discussion

The *Aureococcus anophagefferens* genome (http://genome.jgi-psf.org/Auran1) has a large number of genes encoding Chl *a/c* FCPs. They fall into several clades on phylogenetic trees (Green, unpublished), and include 11 of the *Lhcx* genes that are involved in photoacclimation in diatoms (Nymark *et al*., 2009; Zhu and Green, 2010; Park *et al*., 2010). *Aureococcus* is also known to be able to grow efficiently under low light and fluctuating light levels (Milligan and Cosper, 1997).

Immunoblotting with two different antibodies showed that a significant number of polypeptides (15–27 kDa) could be separated on a high resolution SDS-PAGE gel. Furthermore, the two antibodies, both raised to polypeptides of the LHC superfamily, reacted differently to the different polypeptides, showing their diversity. There are clearly differences in the expression levels of these related proteins.

After DDM solubilization (DDM/Chl = 30), most of the FCPs are in large complexes, and some are associated with PS II, suggesting their involvement in different functions. Under these conditions, FCP supercomplexes were not associated with PSI.

We are currently investigating the contribution of these proteins to the acclimation of *Aureococcus* to a great variety of environmental conditions including changes in light intensity.

Acknowledgements

This work was supported a grant from the Natural Sciences and Engineering Research Council of Canada (NSERC) to BRG.

References

Milligan AJ, Cosper EM (1997) Growth and Photosynthesis of the Brown Tide Microalga Aureococcus Anophagefferens in Subsaturating Constant and Fluctuating Irradiance. Mar. Ecol. Prog. Ser. 153: 67-75

Nymark M, Valle KC, Brembu T, Hancke K, Winge P, Andresen K, Johnsen G, Bones AM (2009) An Integrated Analysis of Molecular Acclimation to High Light in the Marine Diatom Phaeodactylum Tricornutum. PloS ONE 4:

e7743

Park S, Jung G, Hwan YS, Jin E (2010) Dynamic Response of the Transcriptome of a Psychrophilic Diatom, Chaetoceros Neogracile, to High Irradiance. Planta 231: 249-360

Popels LC, Hutchins DA (2002) Factors Affecting Dark Survival of the Brown Tide Alga Aureococcus Anophagefferens (Pelagophyceae). J. Phycol. 38: 416-425

Sieburth J McN, Johnson PW, Hargraves PE (1988) Ultrastructure and Ecology of Aureococcus Anophagefferens Gen. et sp. nov. (Chrysophyceae): the Dominant Picoplankter during a Bloom in Narragansett Bay, Rhode Island, summer 1985. J. Phycol. 24: 416-425

Wittig I, Braun HP, Schaegger H (2006) Blue Native PAGE. Nature protocols 1: 418-428

Zhu SH, Green BR (2010) Photoprotection in the Diatom Thalassiosira Pseudonana: Role of LI818-Like Proteins in Response to High Light Stress. Biochim. Biophys. Acta 1797: 1449-1457

Non-Linear Spectroscopy of Carotenoid-Chlorophyll Interactions in Photosynthetic Light-Harvesting Complexes

Alexander Betke[a], Klaus Teuchner[a], Bernd Voigt[a], Heiko Lokstein[b,*]

[a]Institut für Physik und Astronomie/Photonik, Universität Potsdam, D-14476 Potsdam-Golm, Germany;
[b]Institut für Biochemie und Biologie/Pflanzenphysiologie, Universität Potsdam, D-14476 Potsdam-Golm, Germany.
[*]Corresponding author. Tel. No. +49 331 977 5491; Fax No. +49 331 977 2512; E-mail: lokstein@uni-potsdam.de.

Abstract: In addition to chlorophylls *a* and *b* light-harvesting complex (LHC II) binds xanthophylls. Nonlinear polarization spectroscopy in the frequency domain (NLPF) was used to investigate the changes in the interactions between xanthophylls and chlorophylls in LHC II upon alteration of its aggregation state. Additionally, two-photon excitation profiles in the xanthophylls presumed $1^1A_g^- \rightarrow 2^1A_g^-$ transition region were measured of LHC II samples containing different xanthophyll complements, as well as of chlorophylls *a* and *b* in solution. Implications of the results for recently proposed mechanism(s) of qE/NPQ will be discussed.

Keywords: Light-harvesting complex II (LHC II); Non-linear polarization spectroscopy in the frequency domain (NLPF); Optically "dark" states; Photoprotection; Two-photon fluorescence excitation (TPFE); Xanthophylls

Introduction

Plant major light-harvesting complex (LHC II) binds - in addition to chlorophylls (Chls) *a* and *b* - also xanthophylls: luteins, neoxanthin, violaxanthin (and/or its de-epoxidation products). Xanthophylls have pivotal functions in LHCs: in stabilization of the structure, in light-harvesting and photoprotection. LHC II can exist *in vitro* and *in vivo* in various states of aggregation (cf. *e.g.*, Voigt *et al*., 2008). Aggregation of LHC II profoundly alters interactions between various pigments. Aggregation of LHC II *in vitro* is thought to mimic structural changes that may be related to the energy-dependent component (qE) of non-photochemical quenching of Chl fluorescence (NPQ). The xanthophyll cycle appears to be crucial in this regard. The molecular mechanism(s) of xanthophyll involvement in qE/NPQ have not been established, yet.

Nonlinear polarization spectroscopy in the frequency domain (NLPF; for a recent review, see Lokstein *et al*., 2011) was used to investigate changes in the interactions between xanthophylls and Chls in LHC II upon aggregation.

Two-photon fluorescence excitation (TPFE) profiles of LHC II samples containing different xanthophyll complements were measured in the presumed $1^1A_g^- \rightarrow 2^1A_g^-$ ($S_0 \rightarrow S_1$) transition region of xanthophylls, too.

Materials and Methods

Principle and set-up for NLPF spectroscopy were described previously (cf. Lokstein *et al*., 2011). NLPF spectra of LHC II were measured over a wide concentration range of added n-dodecyl ß-D-maltoside (ß-DM). Additionally, conventional absorption, fluorescence and circular dichroism spectra were measured (cf. Voigt *et al*., 2008).

For TPFE measurements, a femtosecond near-infrared tunable laser system (Coherent OperASolo) was used. Samples in a rotating cuvette were excited with 100 fs pulses in a home-made set-up. TPFE was measured behind a monochromator at 685 nm using a photomultiplier. The fluorescence yield showed a quadratic dependence on laser intensity over the entire wavelength range. To obtain the TPE spectra the photon flux density was set to the same value for all

excitation wavelengths.

TPFE profiles of LHC II samples containing different xanthophyll complements (isolated from dark-adapted and zeaxanthin-enriched spinach thylakoids, as well as from the lutein-lacking *lut2*-mutant of *Arabidopsis thaliana*) were measured in the presumed xanthophyll $S_0 \rightarrow S_1$ absorption region. Additionally, Chls *a* and *b* in solution (freshly prepared by HPLC) were measured for comparison.

Results and Discussion

Xanthophylls (carotenoids in general) are thought to influence excited state properties of neighboring (bacterio-)Chls via different mechanisms (cf. also the discussion in Theiss *et al*., 2009). NLPF has been shown previously to be uniquely suited to investigate carotenoid-Chl interactions in the peridinin-Chl *a*-protein, PCP (Krikunova *et al*., 2006).

NLPF spectra of LHC II obtained by pumping in the Chl *a/b* Q_y region and probing at selected wavelengths (λ_t) in the xanthophyll S_2 ($2^1B_u^+$) absorption region clearly indicated dramatic changes in xanthophyll-Chl interactions upon altering the aggregation state (Voigt *et al*., 2008).

NLPF has been employed to further elucidate the changes in Chl-xanthophyll interaction that occur upon varying the aggregation state of LHC II (from monomers to trimers to small aggregates) by using a specific variant of NLPF spectroscopy called "inverse" NLPF: The "inverse" NLPF approach relies on pumping at specific λ_p in Chl *a/b* Q_y region and *continuously* probing in the (xanthophylls) absorption region to identify individual xanthophylls interacting with the Chls S_1 state, most probably via the energetically close S_1 ($2^1A_g^-$). An example of an "inverse" NLPF spectrum is shown in Fig. 1**:** Of note is the drastic reduction of a subband centered at about 505 nm upon aggregation (arrow) indicating altered xanthophyll-Chl *b*-interaction.

So far, the individual xanthophylls interacting with Chls *a* or *b* in different states of aggregation have not been definitely identified. However, a recent proposal that one of the two luteins in LHC II may be responsible for aggregation-induced fluorescence quenching (Yan *et al*., 2007; Ruban *et al*., 2007) seems unlikely: It has been shown by NPQ "light-activation" experiments - comparing lutein-deficient mutants and wild-type plants of *Arabidopsis thaliana* - that the luteins (or any other xanthophylls in the lutein binding sites, *e.g.*, zeaxanthin) are not quenching active (Lokstein *et al*., 2002). Global analyses of NLPF spectra obtained for different aggregation states of LHC II as well as for LHC II samples with different xanthophyll complements, to identify individual xanthophylls interactions with Chls are currently underway in our lab.

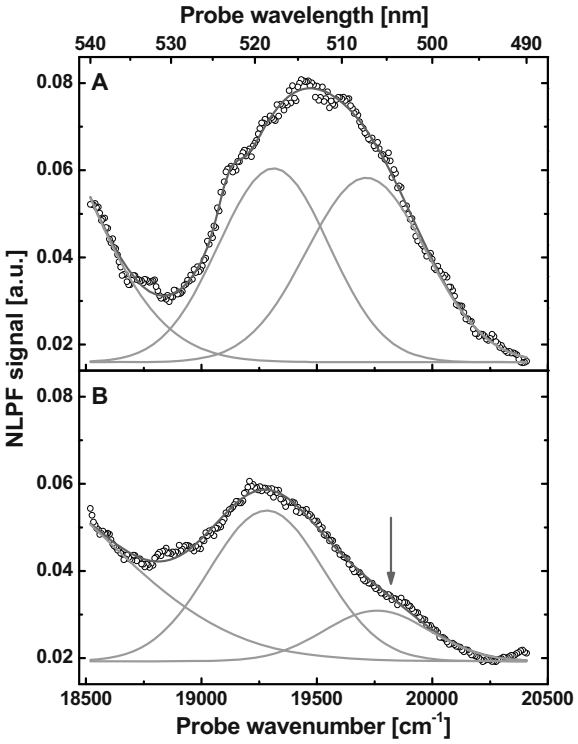

Fig. 1 "Inverse" NLPF spectra of trimeric (A) and slightly aggregated (B) LHC II, pumped at 650 nm and probed in the allowed xanthophyll S_2 ($2^1B_u^+$) region.

TPFE profiles of LHC II samples from dark-adapted and zeaxanthin-enriched spinach thylakoids, as well as LHC II from the *lut2*-mutant were measured in the presumed xanthophyll $S_0 \rightarrow S_1$ absorption region. Within the range of error the spectra are virtually indistinguishable (Fig. 2). Except for the somewhat better spectral resolution the present spectra resemble previously published ones (Walla *et al*., 2000).

To our best knowledge, no TPFE spectra of Chls *a* and *b* in solution have been published. To assess their contributions to TPFE in LHC II, Chls *a* and *b* in solution were measured (Fig. 3). The spectra are remarkable different to the Chls one-photon absorption spectra in the same region. Interestingly, a linear combination of the Chl *a* and *b* TPFE spectra in solution (together with a slight red shift) is apparently sufficient to explain the LHC II spectra (Fig. 3).

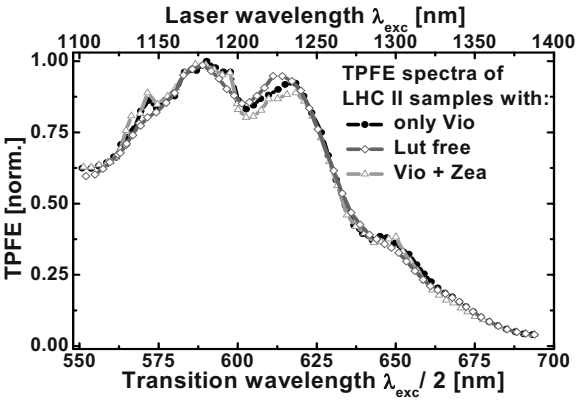

Fig. 2 TPFE spectra of LHC II. LHC II from dark-adapted spinach, zeaxanthin-enriched LHC II and LHC II from the *lut2*-mutant of *Arabidopsis thaliana*.

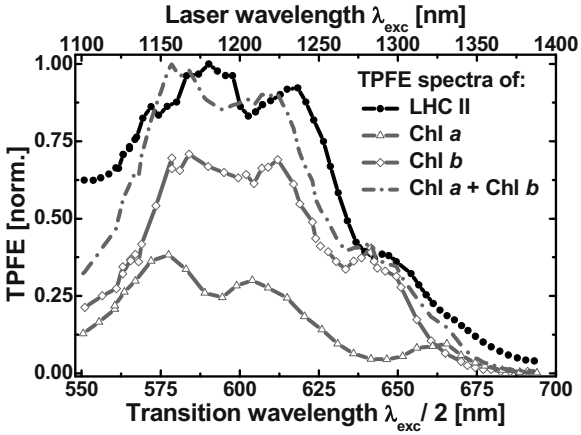

Fig. 3 TPFE spectrum of Chls *a* and *b* in acetonitrile/water and linear combination of the two spectra in comparison to the TPFE spectrum of LHC II.

These results would be consistent with previous TPFE experiments comparing carotenoid-containing and carotenoid-less LH2 samples from the purple bacterium *Allochromatium minutissimum* which suggested prevailing direct TPFE of bacteriochlorophyll itself in this spectral region (Krikunova *et al*., 2002). Moreover, the results also bear potentially important implications on the interpretation of previously published TPFE data (cf. Walla *et al*., 2000) as well as of recently proposed mechanism(s) of xanthophyll involvement in qE/NPQ (Bode *et al*., 2009) and excitation energy transfer between carotenoids and Chls.

Acknowledgements

Long-term (1999–2010) financial support by the Deutsche Forschungsgemeinschaft through SFB 429, TP A2, is gratefully acknowledged.

References

Bode S, Quentmeier CC, Liao PN, Hafi N, Barros T, Wilk L, Bittner F, Walla PJ (2009) On the Regulation of Photosynthesis by Excitonic Interactions between Carotenoids and Chlorophylls. Proc. Natl. Acad. Sci. USA 106: 12311-12316

Krikunova M, Kummrow A, Voigt B, Rini M, Lokstein H, Moskalenko A, Scheer H, Razjivin A, Leupold D (2002) Fluorescence of Native and Carotenoid-Depleted LH2 from Chromatium Minutissimum, Originating from Simultaneous Two-Photon Absorption in the Spectral Range of the Presumed (Opticall "Dark") S_1 State of Carotenoids. FEBS Lett. 528: 227-229

Krikunova M, Lokstein H, Leupold D, Hiller RG, Voigt B (2006) Pigment-Pigment Interactions in PCP Amphidinium Carterae by Non-Linear Polarization Spectroscopy in the Frequency Domain. Biophys. J. 90: 261-271

Lokstein H, Tian L, Polle J, DellaPenna D (2002) Xanthophyll Biosynthetic Mutants of Arabsidopsis Thaliana: Altered Nonphotochemical Quenching of Chlorophyll Fluorescence Is Due to Changes in Photosystem II Antenna Size and Stability. Biochim. Biophys. Acta 1553: 93-103

Lokstein H, Grimm B (2007) Chlorophyll Binding Proteins. In: K Roberts (ed.), Handbook of Plant Science Wiley, Vol. I. pp. 1180-1187

Lokstein H, Krikunova M, Teuchner K, Voigt B (2011) Elucidation of Structure-Function Relationships in Photosynthetic Light-Harvesting Antenna Complexes by Non-Linear Polarization Spectroscopy in the Frequency Domain (NLPF). J. Plant Physiol. in press

Ruban AV, Berera R, Ilioaia C, van Stokkum IHV, Kennis JTM, Pascal AA, van Amerongen H, Robert B, Horton P, van Grondelle R (2007) Identification of a Mechanism of Photoprotective Energy Dissipation in Higher Plants. Nature 450: 575-579

Theiss C, Leupold D, Moskalenko AA, Razjivin AP, Eichler HJ, Lokstein H (2008) Femtosecond Transient Absorption Spectroscopy of Native and Carotenoid-Less Purple Bacterial LH2 Clarifies Functions of Carotenoids. Biophys J. 94: 4808-4811

Voigt B, Krikunova M, Lokstein H (2008) Influence of Detergent Concentration on Aggregation and the Spectroscopic Properties of Light-Harvesting

Complex II. Photosynth. Res. 95: 317-325

Walla PJ, Yom J, Krueger BP, Fleming GR (2000) Two-Photon Excitation Spectrum of Light-Harvesting Complex II and Fluorescence Upconversion after One- and Two-Photon Excitation of the Carotenoids. J. Phys. Chem. B 104: 4799-4806

Yan H, Zhang P, Wang C, Liu Z, Chang W (2007) Two Lutein Molecules in LHCII Have Different Conformations and Functions: Insights into the Molecular Mechanism of Thermal Dissipation in Plants. Biochem. Biophys. Res. Commun. 355: 457-463

Three Step Dissociation and Covalent Stabilization of Phycobilisome

Qiang Wang*

Institute of Hydrobiology, Chinese Academy of Sciences, 7 South Donghu Rd., Wuhan, Hubei Province, 430072 China.
*Corresponding author. Tel. No. 86-027-68780790; E-mail: wangqiang@ihb.ac.cn.

Abstract: Phycobilisomes are large, light harvesting complexes that extend the spectral range of photosynthesis of cyanobacteria by capturing visible light (470–660 nm) and transfer the energy to Photosystem II and Photosystem I. These complexes are soluble complexes that attach to the thylakoid membrane and act as antennae for both PSII and PSI. Phycobilisomes utilize up to 1,500 linear tetrapyrrole chromophores or bilins that are covalently attached to the α and β subunits found in either the rod subunits or the core complexes. Within these enormous structures are pigment-containing linker proteins that facilitate the very rapid and efficient downhill energy transfer from PE → PC → APC → Chl. Interestingly, efficient energy transfer in vitro has been observed only in the presence of very high phosphate (0.7–1.0 mol). We have investigated the mechanism and kinetics of how these complexes dissociate during dilution from the high phosphate buffer. This disassembly process has been followed using fluorescence spectroscopy, differential scanning calorimetry, circular dichroism, density gradient centrifugation, and Western blotting. This analysis has lead to a 3-step model of how the PBS disassembles. To facilitate the use of these large light harvesting complexes in applied photosynthesis, we have also explored covalent method for stabilization of the phycobilisome subunit interactions in aqueous, low salt conditions. Using the stabilization condition we are now beginning to determine if the light harvesting capabilities can be used to drive charge separation in Photosystem I for either photovoltaic or hydrogen evolution.

Keywords: Phycobilisome; Dissociation; Stablization; Phycoerythrin; Phycocyanin; Allophycocyanin

Introduction

Phycobilisomes (PBS) function as light harvesting devices in cyanobacteria and red algae. These large pigment-protein complexes are capable of absorbing light over a broad range of the visible spectrum and efficiently delivering this captured energy to the photosynthetic reaction center (Glazer, 1985; MacColl, 1998). PBS exist as large macromolecular complexes attached to the thylakoid membrane and transfer absorbed energy to Photosystem II (or under certain circumstances to Photosystem I) (Capuano *et al*., 1991). Optimized over the last ~3.5 billion years, the PBS are able to transfer absorbed energy with near 100 percent efficiency(Porter *et al*., 1978).

The main components of PBS are the phycobiliproteins (PBP) which contain linear tetrapyrrole pigments, called bilins (Glazer, 1988). The total number of bilins per PBS is highly variable between different species and even within a species under different growth conditions (MacColl, 1998; Nomsawai *et al*., 1999; Ritz *et al*., 2000; Miskiewicz *et al*., 2002). In cyanobacterial, PBPs are considered the major proteins and could account for up to 24% of the dry weight, and well over 50% the total soluble proteins (Glazer, 1988). Although no high resolution structure exists for any intact PBS, low resolution structures based on EM and AFM, have shown a common structural organization, where the PBS is organized with a series of attached hexameric disks organized into several non-parallel rods, emanating from a core structure that contains two or more parallel cylinders, with a triangular arrangement being the most common (Glazer *et al*., 1979; MacColl, 1998). The PBS core contains allophycocyanin (APC) that of low energy, and the rods contain phycocyanin

(PC) that of intermediate energy, and some organisms may also contain phycoerythrin (PE) that of high energy (MacColl, 1998) at the distal ends of the rods (Ong and Glazer, 1991).

In general, non-marine cyanobacteria have PBS tuned to absorb more red light (*i.e.* PBS lacking PE) while marine cyanobacteria must absorb available blue-shifted light found deeper in the water column; this is accomplished by incorporating the blue absorbing PBP phycoerythrin-I, the bilin content of which is composed mostly of phycoerythrobilin, or a further blue-shifted absorbing PBP phycoeryhtrin-II, the bilin content of which is composed mostly of phycourobiliin, into the distal ends of the PBS rods (Wilbanks and Glazer, 1993). The PBPs have their bilins arranged in such a way that high energy radiation is captured at the outermost portion of the PBS and conducted through the PBS to the core (Glazer, 1989). PE, with an absorption maxima near 570 nm, forms the outermost portion of the rod, while PC, with an absorption maxima near 625 nm, forms the portion of rod adjacent to the core (Sidler, 1994). The PBS core itself, is formed almost entirely of APC which has an absorption maxima near 650 nm. This layout forms a complex in which absorbed energy is rapidly conducted downhill from PE $\rightarrow$ PC $\rightarrow$ APC $\rightarrow$ Chl where energy from absorbed photons is transduced to chemical energy through photosynthesis (Porter *et al*., 1978; Searle *et al*., 1978).

Linker proteins contribute 10%–15% of the mass to PBS and are necessary for the arrangement of PBPs into the PBS complex (de Marsac and Cohen-bazire, 1977; Lundell *et al*., 1981; Glick and Zilinskas, 1982). In assembling the PBPs into the PBS, linkers serve to direct efficient energy migration throughout the PBS by tuning the properties of the PBPs (Glazer, 1989). Four major types of linkers exist: The core membrane linker (L_{CM}) which anchors the core of the PBS to the thylakoid membrane and is the major terminal energy transmitter to PSII, small core linkers (L_C) which are associated with the periphery of the APC core, rod-core linkers (L_{RC}) which attach the rods to the core, and rod linkers (L_R) that associate the PBPs into rods (Glazer, 1989; Capuano *et al*., 1991; Sidler, 1994).

In vivo, organisms use several mechanisms to regulate the assembly, number, location, and even PBP composition of PBS (Swanson and Glazer, 1990; Kehoe and Grossman, 1994; Sidler, 1994; Piven *et al*., 2005). These mechanisms are necessary to adapt to changing environments and regulate the large biosynthetic commitment that the PBS represents. Under high light conditions or during nitrogen starvation, PBS may be remodeled and/or consumed by the organism as necessary (Piven *et al*., 2005; Everroad *et al*., 2006). It has been discussed that the process of the phosphorylation of the linker proteins could be instrumental in the regulation of assembly/disassembly of the PBS (Piven *et al*., 2005), however, no direct evidence were provided. Methylation of the PBPs also appears to contribute to stabilization of the PBS complex and significantly contributes to the efficient energy transfer of the PBS (Swanson and Glazer, 1990).

PBPs have been used for many years as fluorescent tags in cell labeling, fluorescence activated cell sorting, flow cytometry, immunoassay and histochemistry (Glazer and Stryer, 1983; Glazer, 1994). The properties of the PBPs that make them useful in these applications (large stokes shift, shielded location of bilins within PBP, large range of absorption, rapid and efficient energy transfer) is magnified when the PBPs are organized together in the PBS complex. *In vitro*, the high efficiency of energy transfer within the PBS has only been observed in high phosphate (0.7–1.0 mol) buffer (Gantt and Lipschultz, 1972; Gray and Gantt, 1975; Yamanaka *et al*., 1982; Glazer, 1988; Six *et al*., 2005). Although the individual PBPs themselves appear to be stable in aqueous solution, the quaternary organization of the PBS complex itself is labile. Upon dilution of the PBS into low ionic solutions, there is an uncoupling of energy transfer from PE $\rightarrow$ PC $\rightarrow$ APC, this uncoupling is the result of structural changes that lead to complex disassembly of the rods from the core complex (Gantt *et al*., 1976; Yamanaka *et al*., 1978; Gantt *et al*., 1979; Rigbi *et al*., 1980; Kume and Katoh, 1982).

Recently, interest has risen in the potential use of PBS in applied photosynthesis (Das *et al*., 2004) . In this application, the PBS must be able to maintain their highly efficient energy transfer outside of high phosphate buffer. In order to optimize mechanisms for keeping the PBS intact and functional outside of high phosphate buffer, it is necessary to understand the dynamics of PBS dissociation upon dilution from high phosphate buffer. In an effort to better understand the mechanism of PBS dissociation we have investigated the dissociation of PBS from two organisms, *Synechococcus sp. WH7803* and *Synechocystis sp. PCC6803*, using a variety of techniques. By analyzing

the kinetics, energy transfer properties and subunit size and composition, we have developed a model for how these large macromolecular complexes undergo disassembly. This information is useful for not only understanding the structure and assembly of the native PBS, but also is informative for future applied research which may utilize these complexes as highly efficient light harvesting complexes.

Materials and Methods

Organism and Culture Conditions

The fresh water strain *Synechocystis* strain sp. PCC6803 was grown in BG11 at room temperature (25 °C ± 2) under a light intensity of 50 μmol quanta m^{-2} s^{-1} with constant bubbling. The marine culture strain Synechococcus WH7803 was grown at room temperature (25 °C ± 2) in artificial seawater medium (ASM) (Rippka and Lester Packer, 1988), supplemented with 5 mmol $NaHCO_3$ and 10 mmol Tris (pH 8.0), and bubbled with air. The light intensity was 5–8 μmol quanta m^{-2} s^{-1}.

PBS Isolation PBSs from *Synechocystis* sp. PCC6803 and *Synechococcus* sp. WH7803 were isolated as described respectively (Glazer, 1988; Six *et al*., 2005). Cells were collected at 5,000 x g for 5 min, and resuspended at 0.12 g wet weight/ml in 750 mmol $NaKPO_4$ (pH 8.0), incubated with 1% TX100 for 45 min at room temperature. Cell were lysed by passing through the French Press at 20,000 PSI and repeated twice. The cell lysate of PCC6803 was clarified by centrifugation at 31,000 x g for 30 min. For WH7803 a similar treatment was performed yet at the lower value of 7,000 x g. In both cases, the middle phase containing PBSs were collected and loaded on sucrose step gradient. For PCC6803 the gradient was composed of 2 mol, 1 mol, 0.75 mol, 0.5 mol and 0.25 mol sucrose each density contained 750 mmol $NaKPO_4$ (pH 8.0). This was spun in a SW27 rotor at 98,000 x g 18 °C for 16 h. For WH7803 the gradient contained a 2 mol, 0.75 mol, 0.62 mol, 0.5 mol, 0.37 mol and 0.25 mol sucrose gradient was used and 40,000 x g 18 °C for 16 h. The intact PBS containing fractions (0.75 mol sucrose fraction) were carefully collected, diluted in 0.75 mol phosphate buffer and centrifuged at 80,000 g for 4 h at 4 °C. The PBS pellets were dissolved in 0.75 mol phosphate buffer, kept away from light and refrigerated until use. When using, phycobilisomes were diluted to desired concentration with either 750 mmol $NaKPO_4$ (pH 8.0) or de-ionized water (DIW), incubated in dark at room temperature for 2 h.

Differential Scanning Calorimetric

Differential scanning calorimetric (DSC) was done by using a MicroCal VP-DSC microcalorimeter with a scan rate of 60 °C/h, and a protein concentration of 1mg/ml was used, unless specified. A first run of the buffer *vs*. buffer as background scan every time and was subtracted by the sample scan.

Fluorescence Spectroscopy

Fluorescence emission was followed with a Photon Technology International fluorometer, an excitation wavelength at 375 nm which could excite PE, PC and APC almost equally was used, with a 1nm slit for both excitation and emission. Sample concentration was monitored to ~30μg/ml protein.

Circular Dichroism

A Circular dichroism (CD) spectrometer (Model 202, Instruments Inc.) was used, sample concentration was monitored to 0.6 mg protein/ml.

SDS-PAGE and Immunological Analysis

SDS-PAGE was run on a 12% gel, and PBSs were loaded with a total of 10 ug protein. Anti-phosphor-tyrosine, anti-phosphor-serine and anti-phosphor-threonine were purchased from Zymed Laboratories Inc. Immuno-blot results were viewed by chemiluminecence (LumiGen). Native gel was run on a 7% gel without SDS in either gel buffer or running buffer, and viewed directly by color or by fluorescence excited by a UV light.

Peak fitting and Data Analysis

Curve fitting and peak resolving was done by using the Origin 7.0 software (OriginLab Corporation). And the quantification of the western results was done by using ImageJ (National Institutes of Health, U.S.A.).

Crosslinking

Crosslinking reagents, with different spacer arm length (0–10Å), include homobifunctional (DST, DCC, DMA, GA) and heterobifunctional (SIA, EMCS and Sulfo-EMCS) crosslinkers were perchursed from Pierce. Crosslink reactions were done in 750 mmol phosphate with intact PBS.

Results and Discussion

Sucrose Gradient Centrifugation and SDS-PAGE

PBSs from both Synechocystis sp. PCC 6803 and Synechococcus sp. WH 7803 were purified by ultra speed step sucrose gradient centrifugation as described in "material and methods". The PBS of the PE-lacking strain *Synechocystis* sp. PCC 6803 appears to be blue (Fig. 1A) in color due to maximum absorption of PC at 625 nm, while the PE-containing strain *Synechococcus* sp. WH 7803 appears to be magenta (Fig. 1A) in color due to the maximum absorption of PE at 570 nm.

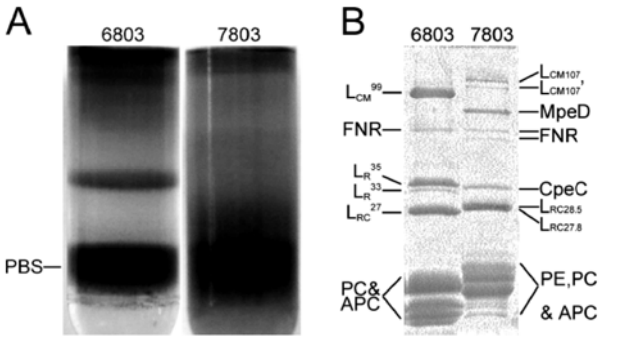

Fig. 1 Preparation of the PBSs. A, Photo of PBS gradients; B, SDS-PAGE of the PBS subunits. 6803 and 7803 stand for *Synechocystis* sp. PCC6803 and *Synechococcus* sp. WH7803, seperatly, same for the rest of the tables and figures.

When analyzed by Coomassie-stained SDS-PAGE (Fig. 1B), in addition to the PBPs in the 20 kDa range, both strains contain core membrane linker (L_{CM}), rod-core linkers (L_{RC}), rod linkers (L_R), and FNR (ferrodoxin-NADP-reductase), while the small core linkers (L_C) are too small in molecular weight to be resolved by the gel system.

Fluorescence Spectral Analysis of PBS Dissociation

Earlier research by various group (Gantt and Lipschultz, 1972; Gray and Gantt, 1975; Yamanaka *et al*., 1978; Yamanaka *et al*., 1982; Glazer, 1988; Six *et al*., 2005) have shown that, PBSs could be isolated structurally and functionally intact if the preparation procedures after the breakage of cells were done in concentrated phosphate at pH 7 or pH 8. The integrity of PBSs could be assessed by following their fluorescence emission spectra (Glazer, 1982). As shown in Fig. 2 (straight line), the fluorescence emission spectra of the intact PBS from *Synechocystis* sp. PCC6803 (Fig. 2A) shows a single fluorescence peak at 666 nm, and the spectra of the intact PBS from *Synechococcus* sp. WH7803 (Fig. 2B) shows three peaks at 677 nm, 652 nm and 565 nm region, indicate well performed energy transfer from PE (only in *Synechococcus* sp. WH7803) → PC → APC.

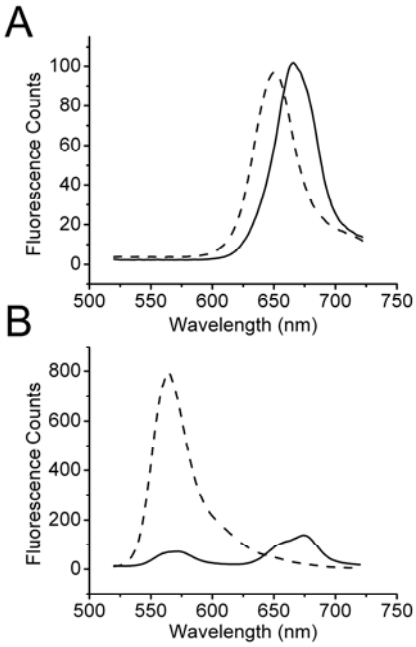

Fig. 2 PBS Fluorescence emission spectra of *Synechocystis* sp. PCC6803 (A) and *Synechococcus* sp. WH7803 (B) upon dilution into DIW. Solid lines, intact PBS in 750 mmol phosphate; dashed lines, dissociated PBS in DIW.

To investigate how PBSs act to low phosphate, intact PBSs in 750 mmol phosphate were diluted ten times with de-ionized water (DIW), kept at room temperature in dark for 2 h and the fluorescence spectra were followed again. Fig. 2 (dashed lines) shows that, when diluted with DIW, the PBSs experienced dissociation and significant blue-shifts were observed from the fluorescence emission. In *Synechocystis* sp. PCC6803 (Fig. 2A, dashed line), the 666 nm peak shifted to 652 nm, while in *Synechococcus* sp. WH7803 (Fig. 2B, dashed line), both the 677 nm and the 652 nm peak disappeared with the rising of a peak at 565 nm. These changes indicate the dissociation of the intact PBSs and the loss of functional energy transfer between the PBPs.

Kinetic Analysis of Fluorescence Changes associated with Dissociation

As demonstrated in Fig. 2, PBSs from both strains show APC fluorescence emission peaks at the 670 nm region, to make sure that no cross interaction of the PC emission peak, 680 nm was used to evaluate the

APC fluorescence emission, which could be used as an assessment of the integrity of the PBSs.

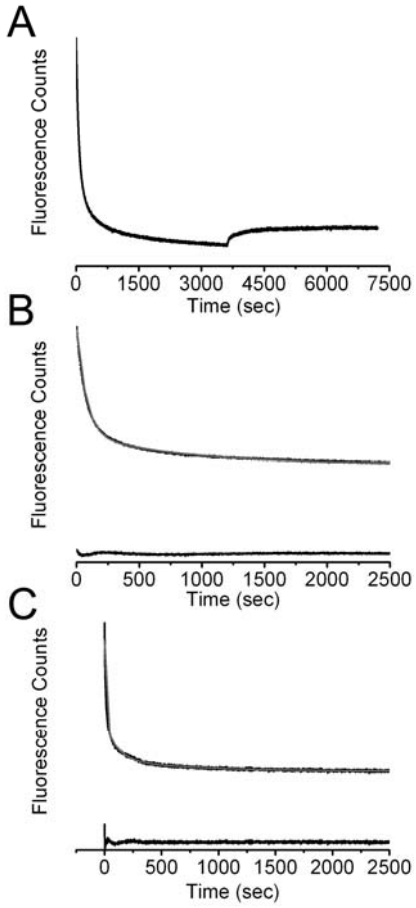

Fig. 3 PBS dissociation Kinetics. A, Dissociation of *Synechocystis* sp. PCC6803 in DIW and rebuilt of the high phosphate (indicated by arrow); B, *Synechocystis* sp. PCC6803; C, *Synechococcu*s sp. WH7803. In panel B and C, black lines, dissociation kinetics of the PBS; gray lines, non-linear curve fitting of the PBS dissociation kinetics; lines below the dissociation kinetics, residues of the curve fitting.

To understand the dynamic change of the PBS dissociation, fluorescence emission in DIW at 680 nm was followed as a function of time (Fig. 3). PBSs were first diluted with DIW, and fluorescence emission at 680 nm was followed until a plateau was reached, the system was then changed back to 750 mmol Phosphate (pH 8.0) by adding 1/5 volume of a 4.2 mol $NaKPO_4$ (pH 8.0) stock. The fluorescence was followed and normalized accordingly. Fig. 3A shows that when diluted with DIW, the fluorescence signal of the *Synechocystis* sp. PCC6803 PBS dropped immediately and dramatically, rebuilt the high phosphate environment only induced a minor restoration, indicated that the dissociation of the PBS are mostly irreversible, with a very small reversible portion.

Table 1 Dissociation rate constants and amplitudes (displayed as percentage of total).

	6803	*7803*
A1(%)	67±8	47±1
t1(sec)	79±1	4±0.4
A2(%)	33±7	30±0.7
t2(sec)	1041±94	37±2
A3(%)		23±2
t3(sec)		1271±29

To further investigate the kinetic of the dissociation, the fluorescence decay at 680 nm was fitted exponentially (Figs. 3B and 3C), the fitting amplitudes and constants were then calculated (Table 1). The *Synechocystis* sp. PCC6803 PBS dissociation pattern could be fitted in two components (Fig. 3B, black line; Table 1), a fast phase with a decay constant of 79 sec and amplitude of 67%, and a slow phase with a decay constant of 1041 sec and amplitude of 33% (Table 1). Comparing these results with Fig. 3A, it suggested that the fast phase was related to the detachment of the PC, while the reversible slow phase was related to APC, the reversible feature of the APC phase indicated that the core-complex was not completely dissociated.

Comparing with the *Synechocystis* sp. PCC6803 PBS, the *Synechococcus* sp. WH7803 PBS dissociation could be fitted in three decays (Fig. 3C, black line; Table 1). A fast (4 sec), a mid (30 sec) and a slow (1271 sec) phase. The fast phase here, which is much faster than the *Synechocystis* sp. PCC6803 fast phase, could be assigned to the detachment of PE, while the mid and slow phases were related to PC and APC, as in *Synechocystis* sp. PCC6803.

Dissociation demonstrated by differential scanning calorimetry

Differential scanning calorimetry (DSC) was used to study the thermo stability of the PBSs. The DSC profile of the *Synechocystis* sp. PCC6803 PBS in 750 mmol Phosphate shows an endothermic transition with a shoulder contributed by PBS dissociation, and an exothermic transition (Fig. 4A, dashed line) assigned as protein aggregation. The DSC signal could be further resolved (Fig. 4B, light gray long dashed lines) as two endothermic transitions at 61.1 °C and 62.8 °C, and one exothermic transition at 65.2 °C. These results indicate that there are two steps of dissociation followed by the exothermic

aggregation, which agrees with the two-component kinetic fluorescence fitting of the *Synechocystis* sp. PCC6803 (Fig. 3B).

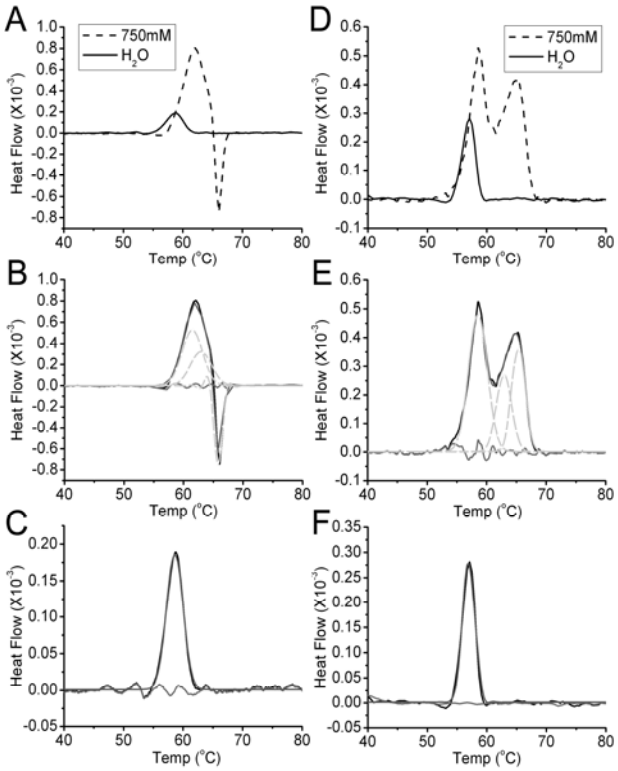

Fig. 4 PBS dissociation demonstrated by DSC. A and D, DSC of the intact and dissociate PBSs; B and E, nonlinear curve fitting of the intact PBS; C and F, nonlinear curve fitting of the dissocated PBSs of *Synechocystis* sp. PCC6803 and and *Synechococcu*s sp. WH7803. Black lines, DSC scan curves; dark gray lines, non-linear fitted DSC curves; light gray long dashed lines, fitted DSC peaks; gray lines below the curves, residues of the curve fitting.

The DSC profile of the *Synechococcus* sp. WH7803 PBS in 750 mmol phosphate shows two endothermic peaks (Fig. 4D, dashed line), and could be resolved (Fig. 4E, light gray long dashed lines) to three transitions at 59.0 °C, 62.5 °C and 66.0 °C (Table 2), which indicates a three-step dissociation, and fits well with its three-component kinetic fluorescence fitting results (Fig. 3C). However, no exothermic transitions were observed, indicated increased stability of the *Synechococcus* PBS.

Table 2 Non-linear curve fitting peaks of the DSC.

	Intact		Dissociated	
	6803	7803	6803	7803
1 (°C)	61.1±0.8	59.0±0.3	58.6±0.1	59.5±3.9
2 (°C)	62.8±1.6	62.5±1.5		
3 (°C)	65.2±0.8	66.0±0.6		

When diluted with DIW, PBSs from both strains show similar DSC profiles. Much smaller peaks (Figs. 4A and 4D, solid lines) were observed and could only be resolved to single transitions at 58.6 °C (*Synechocystis* sp. PCC6803, Fig. 4C) and 59.5 °C (*Synechococcus* sp. WH7803, Fig. 4F), respectively. Even a protein concentration of 3 mg/ml was used for the *Synechococcus* sp. WH7803 PBS to get a detectable signal. These results indicated that the DIW diluted PBSs were dissociated, and the detached small peptides went into the baseline, thus decreased the transition signal of the core-complex.

Dissociation demonstrated by Circular Dichroism

To gain structural information of the PBSs, Circular Dichroism (CD) spectrum of the intact/dissociated PBSs were monitored. Fig. 5A (solid line) shows that the CD spectrum of the intact *Synechocystis* sp. PCC6803 PBS has three bands, the 651 nm band contributed by PC, while the 680 nm and 696 nm bands were assigned to APC. The dissociated PBS had a CD peak at 647 nm and a shoulder at 596 nm (Fig. 5A, dashed line), which was similar to the reported trimeric PC of *Synechococcus* 6301 (Glazer and Fang, 1973) and its AN112 mutation strain (Yamanaka *et al*., 1982).

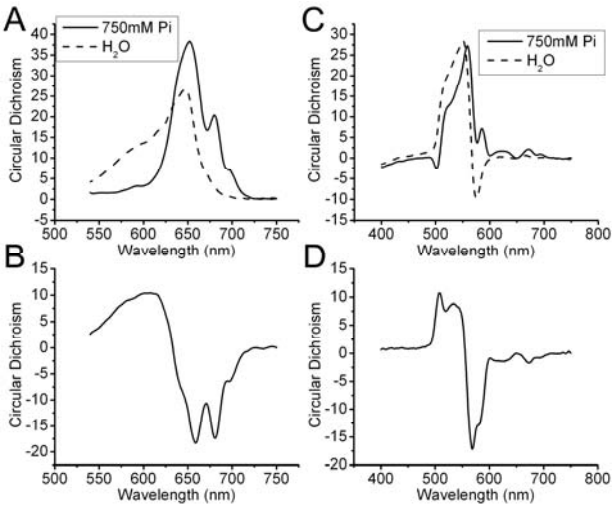

Fig. 5 PBS dissociation demonstrated by CD. A and C, CD spectra of intact (solid lines) and dissocitated (dashed lines) PBSs of *Synechocystis* sp. PCC6803 and *Synechococcu*s sp. WH7803; B and D, CD Difference spectra of *Synechocystis* sp. PCC6803 and *Synechococcu*s sp. WH7803.

The CD bands at 558 nm and 585 nm from intact *Synechococcus* sp. WH7803 PBS (Fig. 5C, solid line) were associated with PE, the band near 623 nm was

contributed by PC, and the band at 670 nm was assigned to APC (Rigbi *et al*., 1980). A paired bands, one positive at 551 nm, one negative at 575 nm, was detected from the CD spectrum of the dissociated *Synechococcus* sp. WH7803 PBS (Fig. 5C, dashed line). This resulted from the exciton splitting, which was considered the signature of free PE CD spectrum (MacColl *et al*., 1994).

To better interpret the changes in CD resulting from dissociation, CD difference spectra was done and plotted as Fig. 5B and Fig. 5D. From the difference spectra, it could be seen very clearly that the increased PC (Fig. 5B) and PE (Fig. 5D) with the decreased APC (Figs. 5B and 5D) and PC (Fig. 5D) CD signal in the dissociated PBSs.

Native Gel Electrophoresis of Subunit Association

PBPs are differently colored with strong fluorescence, this allows them to be easily recognized on native gel either by color or by fluorescence. Intact PBSs from both stains were diluted by DIW and treated for 2 h at room temperature, loaded and separated by a 7% native gel. Due to the mobility of the proteins (protein complexes) in this gel system, only relatively small proteins will enter the gel. The gel was then visualized simply by color (Fig. 6A) or by UV-fluorescence (Fig. 6B).

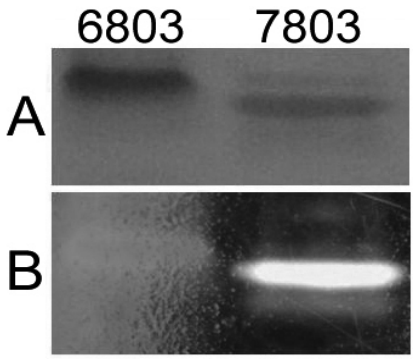

Fig. 6 Size Analysis of PBS dissociation. Native Gel-PAGE of dissociated PBSs of *Synechocystis* sp. PCC6803 and *Synechococcu*s sp. WH7803 displayed by color (A) and fluorescence (B).

The dissociated *Synechocystis* sp. PCC6803 PBS has a blue band (Fig. 6A) with strong red fluorescence (Fig. 6B) originated from PC, and no APC bands were detected. This suggests that when dissociation happened, only PC was detached, while the APC core complex remained intact and was too large in molecular weight to get into the gel.

The dissociated *Synechococcus* sp. WH7803 PBS (Fig. 6) shows two light blue bands (Fig. 6A) with red fluorescence (Fig. 6B) originated from PC and one magenta band with bright yellow fluorescence originated from PE, and no APC bands were detected, either. The native-PAGE results indicate that the dissociated PBSs contain APC core complex, free PC, and free PE, if presents. Which agree with the DSC and CD spectra analysis (Fig. 5).

Linker peptides (de)phosphorylation is involved in PBS dissociation

PBS linker proteins are phosphorylated (Piven *et al.*, 2005) and could be detected by phosphor-Ser, phosphor-Thr and phosphor-Tyr (Fig. 7A). To investigate if the dissociation of the PBS was affected by the phosphorylation status of the linker proteins, PBS was diluted in DIW, stayed at room temperature and kept away from light, samples were taken at various time intervals, and subjected to western analysis of the phosphorylated proteins. It could be seen from Fig. 7B that when diluted in DIW, the phosphorylation level of the 27 kDa linker dropped sharply, while that of the 99 kDa increased gradually.

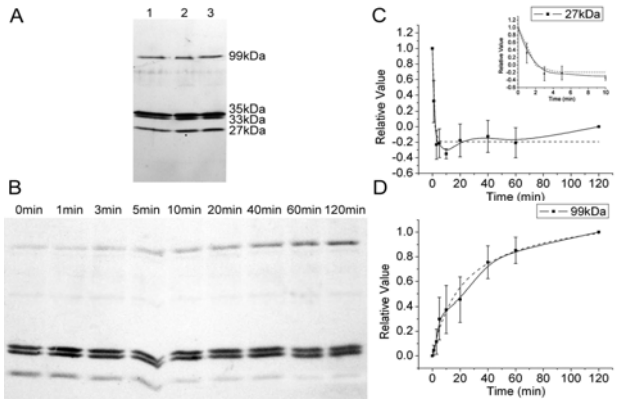

Fig. 7 Phosphorylation of PBS subunits in *Synechocystis* sp. PCC6803. A, Ser (lane 1), Thr (lane 2), Tyr (lane 3) phosphorylation of multiple PBS subunits. B, Phosphorylation kinetics of PBS subunits upon dilution to DIW. C and D, quantitation of phosphorylation of the 27 and 99 kDa linker proteins (solid lines), and the non-linear curve fitting of the kinetics (dashed lines).

To identify the changes more directly, particle counting was done by using the ImageJ software and plotted against the time scale. The 35 kDa and 33 kDa linker vary in a range of 5% during the treatment (data not shown), and could be taken as the inner quantity marker. The 27 kDa linker (Fig. 7C, solid line) shows

a sharply decrease and reach its plateau within 3min (Fig. 7C, small panel) in its phosphorylation level, which could be fitted exponentially with a decay constant of 1min (Fig. 7C, dashed line). While the 99 kDa linker shows a slow increase (Fig. 7D, solid line), and the exponential curve fitting gives a time constant of 41min (Fig. 7D, dashed line). Comparing these results with the fluorescence decay of the dissociation, it suggests that the dephosphorylation/ phosphorylation of the 27/99 kDa linker are responsible for the fast/slow phase of the dissociation, respectively.

Covalent stabilization

To be used as the light harvesting system to drive charge separation in Photosystem I for photovoltaic or hydrogen evolution, the first important feature of the PBSs should be the ability to keep functionally intact under low ionic conditions. For this purpose, various crosslinkers were used to investigate the possibilities to stabilize the PBS through covalent reaction, so that the PBS could maintain functionally intact under low phosphate conditions.

Various crosslinkers, with different spacer arm length (0–10Å), include homobifunctional (DST, DCC, DMA, GA) and heterobifunctional (SIA, EMCS and Sulfo-EMCS), were tested. Intact PBS was first incubated with crosslinkers in 750 mmol phosphate, and then pretested with fluorescence emission. Among those tested, only GA (glutaraldehyde) gave out positive result, possibly because all other reagents failed to survive the high phosphate condition and lost their activities.

The PBSs were incubated with GA for various time (0.5, 1, 2, 3, and 5 h), diluted in DIW for 2 h and re-purified by ultra sucrose gradient centrifugation. As shown in Fig. 8A, the un-treated intact PBS was observed at 0.75 mol sucrose, as expected; the GA treated PBSs were also observed at 0.75 mol sucrose, indicated effective cross-link reaction which resulted in intact PBSs. After recollected from sucrose gradient (Fig. 8A), the fluorescence emission spectra of the GA cross-linked PBSs (Fig. 8B, gray dotted line) shows that when diluted in DIW, unlike the untreated (Fig. 8B, gray dashed line), the GA cross-linked PBS (Fig. 8B, dash-dotted line) had similar fluorescence emission as the control, *i.e.* in 750 mmol phosphate (Fig. 8B, black solid line), except the rising of a 640 nm shoulder. These results indicate that the PBSs were well cross-linked, and even the cross-linked intact PBSs had certain extent of dissociation shown by the appearance of the 640 nm shoulder.

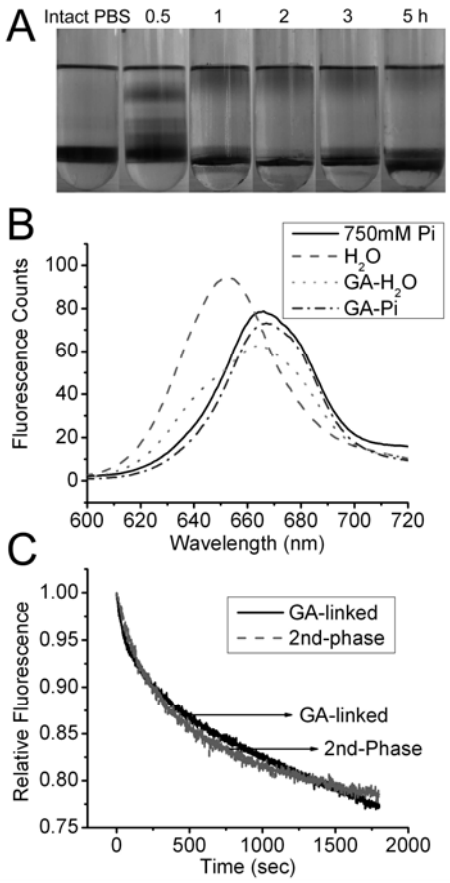

Fig. 8 Covalent stabilization of the *Synechocystis* sp. PCC6803 PBS. A, PBS recollected by sucrose gradient centrifugation. Tube 1, intact PBS; Tube 2–6, PBS crosslinked by GA for 0.5, 1, 1.5, 2 and 3 h, diluted with DIW and recollected by sucrose gradient. B, Fluorescence properties of the GA covalently stabilized PBS. Black solid line, PBS in 750 mmol phosphate; gray dashed line, PBS in DIW; dash-dotted line, GA stabilized in 750 mmol phosphate; gray dotted line, GA stabilized in DIW. C, Overlap of the PBS dissociation fluorescence of the slow phase and the GA cross-linked.

The 640 nm shoulder indicates a fluorescence decrease in APC and increase in PC. The APC fluorescence at 680 nm was tracked as a function of time to understand the kinetic of this change. As shown in Fig. 8C (black line), a slow decrease with a decay constant of 900 sec was detected. If plotted together with the the slow phase (Fig. 3B) of the fluorescence decay of the dissociated PBS (Fig. 8C, gray line), both traces look similar to one another and well overlapped (Fig. 8C). These results suggested that the 740 nm shoulder could be assigned to the slow phase of the PBS dissociation.

Discussion

The fluorescence study (Fig. 2) showed that when diluted from high phosphate to water, PBSs dissociated (Gray and Gantt, 1975; Gantt *et al*., 1979) and displayed a sequential release of PBPs, as conformed by curve fitting of the fluorescence emission at 680 nm (Fig. 3, Table 1).

The DSC signal of the intact PBSs (Fig. 4) could be resolved as 2 and 3 endothermic transitions for *Synechocystis* sp. PCC6803 and *Synechococcus* sp. WH7803, separately; which agree with their 2 and 3 components fluorescence fitting results (Fig. 3, Table 1). The greatly reduced single DSC peak of the DIW diluted PBSs (Fig. 4) indicated that the dissociated PBSs contain the core complex and the detached small proteins. Separation of the dissociated PBSs on native gel (Fig. 6) resolved magenta and/or blue bands with yellow and/or red fluorescence, which could be assigned for free PC and PE. The fact that no APC bands could be detected indicated that it is attached as a core complex and too large in molecular weight to be resolved by the gel system. Add up to the results of the increased PC and PE peak with the decreased APC peak of the CD spectra (Fig. 5) of the dissociated PBS, these results suggested that the dissociated PBS mixture contains the APC core complex, PC, and PE, if any.

The time resolved fluorescence emission of the DIW diluted PBSs at 680 nm stands for the kinetic of their integrity, exponential fitting of the fluorescence decay revealed a fast phase (for *Synechococcus* sp. WH7803 only), a mid phase, and a reversible slow phase (Fig. 3, table 1). The greatly decreased single transition signals of the DSC (Fig. 4) profiles of the dissociated PBSs, together with the native-PAGE (Fig. 6) results indicated that the fast phase could be assigned as the detachment of PE, the mid phase (fast phase, in case of the *Synechocystis*) could be assigned as the detachment of PC, while the slow phase was related to the APC core-complex.

When cross-linked by GA, the fast and mid phase disappeared, while the slow phase was still there, and a 740 nm shoulder possibly responsible for the slow phase was detected by fluorescence spectra (Fig. 8), indicated that even intact PBSs have some extent of dissociation. The reversible feature of the slow-phase-dissociation (Fig. 3) suggested that it may not be a complete detachment. Since it was cross-linked by GA, this slow reversible dissociation could not be a real dissociation, as has been shown by both sucrose gradient centrifugation (Fig. 8) and native-PAGE (Fig. 6); we speculated that it may probably be a loosen form of the core-complex. This agrees with the fact that the APC remains in the core-complex in dissociated PBSs (Figs. 4 and 6).

As have been shown in earlier study (Piven *et al*., 2005), the PBS linker proteins were found phosphorylated and could be detected by phosphor-Ser, phosphor-Thr and phosphor-Tyr (Fig. 7). Furthermore, exponential curve fitting of the kinetic of the phosphorylation level of the 27 kDa and 99 kDa linker proteins showed a nice match with the two phases of the PBS dissociation demonstrated by fluorescence emission (Fig. 3). This suggests that the phosphorylation statuses of the linker proteins are responsible for the PBS dissociation.

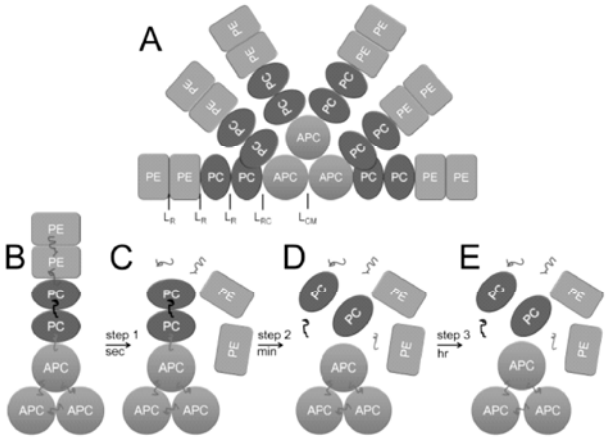

Fig. 9 Proposed 3-step PBS dissociation. A, Intact PBS. B-E, Different PBS dissociation status.

To summarize, the mechanism and kinetics of how the PBS complexes dissociate during dilution from the high phosphate buffer were investigated by using fluorescence spectroscopy, differential scanning calorimetry, circular dichroism, density gradient centrifugation, and Western blotting. These analyses have lead to a model of how the PBS disassembles (Fig. 9), and a three-step-dissociation was proposed: When diluted from high phosphate to DIW, intact PBS Figs. 9A and 9B), 1. Releases PE discs (Fig. 9C) within seconds - fast phase; 2. Releases PC discs (Fig. 9D) within minutes—mid phase; 3. Loosen the APC core-complex (Fig. 9E) within hours—slow phase. The dephosphorylation/phosphorylation of the L_{RC}/L_{CM} may play important roles in the mid and slow dissociation phase.

Acknowledgements

Supported jointly by the National Program on Key Basic Research Project (2011CB200902) and the 100 Talents Program of the Chinese Academy of Sciences (Y05101-1-601).

References

Capuano V, Braux AS, Tandeau de Marsac N, Houmard J (1991) The "Anchor Polypeptide" of Cyanobacterial Phycobilisomes. Molecular Characterization of the Synechococcus sp. PCC 6301 Apce Gene. J Biol Chem 266: 7239-7247

Das R, Kiley PJ, Segal M, Norville J, Yu AA, Wang LY, Trammell SA, Reddick LE, Kumar R, Stellacci F, Lebedev N, Schnur J, Bruce BD, Zhang SG, Baldo M (2004) Integration of Photosynthetic Protein Molecular Complexes in Solid-State Electronic Devices. Nano Letters 4: 1079-1083

De Marsac NT, Cohen-bazire G (1977) Molecular Composition of Cyanobacterial Phycobilisomes. Proc Natl Acad Sci U S A 74: 1635-1639

Everroad C, Six C, Partensky F, Thomas JC, Holtzendorff J, Wood AM (2006) Biochemical Bases of Type IV Chromatic Adaptation in Marine Synechococcus spp. J Bacteriol 188: 3345-3356

Gantt E, Lipschultz CA (1972) Phycobilisomes of Porphyridium Cruentum. The Journal of Cell Biology 54: 313-324

Gantt E, Lipschultz CA, Grabowski J, Zimmerman BK (1979) Phycobilisomes from Blue-Green and Red Algae: Isolation Criteria and Dissociation Characteristics. Plant Physiol. 63: 615-620

Gantt E, Lipschultz CA, Zilinskas B (1976) Further Evidence for a Phycobilisome Model from Selective Dissociation, Fluorescence Emission, Immunoprecipitation, and Electron Microscopy. Biochimica et Biophysica Acta (BBA) - Bioenergetics 430: 375-388

Glazer AN (1982) Phycobilisomes: Structure and Dynamics. Annu Rev Microbiol 36: 173-198

Glazer AN (1985) Light Harvesting by Phycobilisomes. Annu Rev Biophys Biophys Chem 14: 47-77

Glazer AN (1988) Phycobiliproteins. Methods Enzymol 167: 291-303

Glazer AN (1988) Phycobilisomes. Methods Enzymol 167: 304-312

Glazer AN (1989) Light Guides. Directional Energy Transfer in a Photosynthetic Antenna. J Biol Chem 264: 1-4

Glazer AN (1994) Phycobiliproteins - a Family of Valuable, Widely Used Fluorophores. Journal of Applied Phycology 6: 105-112

Glazer AN, Fang S (1973) Chromophore Content of Blue-Green Algal Phycobiliproteins. J Biol Chem 248: 659-662

Glazer AN, Stryer L (1983) Fluorescent Tandem Phycobiliprotein Conjugates. Emission Wavelength Shifting by Energy Transfer. Biophys J 43: 383-386

Glazer AN, Williams RC, Yamanaka G, Schachman HK (1979) Characterization of Cyanobacterial Phycobilisomes in Zwitterionic Detergents. Proc Natl Acad Sci U S A 76: 6162-6166

Glick RE, Zilinskas BA (1982) Role of the Colorless Polypeptides in Phycobilisome Reconstitution from Separated Phycobiliproteins. Plant Physiol 69: 991-997

Gray BH, Gantt E (1975) Spectral Properties of Phycobilisomes and Phycobiliproteins from the Bluegreen Alga-Nostoc SP.*. Photochemistry and Photobiology 21: 121-128

Kehoe DM, Grossman AR (1994) Complementary Chromatic Adaptation: Photoperception to Gene Regulation. Semin Cell Biol 5: 303-313

Kume N, Katoh T (1982) Dissociation Kinetics of Anabaena Phycobilisomes. Plant and Cell Physiology 23: 803-812

Lundell DJ, Williams RC, Glazer AN (1981) Molecular Architecture of a Light-Harvesting Antenna. In Vitro Assembly of the Rod Substructures of Synechococcus 6301 Phycobilisomes. J Biol Chem 256: 3580-3592

MacColl R (1998) Cyanobacterial Phycobilisomes. J Struct Biol 124: 311-334

MacColl R, Williams EC, Eisele LE, McNaughton P (1994) Chromophore Topography and Exciton Splitting in Phycocyanin 645. Biochemistry 33: 6418-6423

Miskiewicz E, Ivanov AG, Huner NPA (2002) Stoichiometry of the Photosynthetic Apparatus and Phycobilisome Structure of the Cyanobacterium Plectonema Boryanum UTEX 485 Are Regulated by Both Light and Temperature. Plant Physiol. 130: 1414-1425

Nomsawai P, De Marsac NT, Thomas JC, Tanticharoen M, Cheevadhanarak S (1999) Light

Regulation of Phycobilisome Structure and Gene Expression in Spirulina Platensis C1 (Arthrospira sp. PCC 9438). Plant and Cell Physiology 40: 1194-1202

Ong LJ, Glazer AN (1991) Phycoerythrins of Marine Unicellular Cyanobacteria. I. Bilin Types and Locations and Energy Transfer Pathways in Synechococcus spp. Phycoerythrins. J Biol Chem 266: 9515-9527

Piven I, Ajlani G, Sokolenko A (2005) Phycobilisome Linker Proteins Are Phosphorylated in Synechocystis sp. PCC 6803. J Biol Chem 280: 21667-21672

Porter G, Tredwell CJ, Searle GFW, Barber J (1978) Picosecond Time-Resolved Energy Transfer in Porphyridium Cruentum. Part I. In the Intact Alga. Biochimica et Biophysica Acta (BBA) - Bioenergetics 501: 232-245

Rigbi M, Rosinski J, Siegelman HW, Sutherland JC (1980) Cyanobacterial Phycobilisomes: Selective Dissociation Monitored by Fluorescence and Circular Dichroism. Proc Natl Acad Sci U S A 77: 1961-1965

Rippka R, Lester Packer ANG (1988) Isolation and Purification of Cyanobacteria. In Methods Enzymol, Vol Volume 167. Academic Press, pp. 3-27

Ritz M, Thomas JC, Spilar A, Etienne AL (2000) Kinetics of Photoacclimation in Response to a Shift to High Light of the Red Alga Rhodella Violacea Adapted to Low Irradiance. Plant Physiol. 123: 1415-1426

Searle GFW, Barber J, Porter G, Tredwell CJ (1978) Picosecond Time-Resolved Energy Transfer in Porphyridium Cruentum. Part II. In the Isolated Light Harvesting Complex (Phycobilisomes). Biochimica et Biophysica Acta (BBA) - Bioenergetics 501: 246-256

Sidler W (1994) Phycobilisome and Phycobiliprotein Structures. In: DA Bryant (ed.), The Biology of Cyanobacteria. Kluwer Academic Publishers: Dortrecht, Netherlands, pp. 139-216

Six C, Thomas JC, Thion L, Lemoine Y, Zal F, Partensky F (2005) Two Novel Phycoerythrin-Associated Linker Proteins in the Marine Cyanobacterium Synechococcus sp. Strain WH8102. J Bacteriol 187: 1685-1694

Swanson RV, Glazer AN (1990) Phycobiliprotein Methylation. Effect of the Gamma-N-Methylasparagine Residue on Energy Transfer in Phycocyanin and the Phycobilisome. J Mol Biol 214: 787-796

Wilbanks SM, Glazer AN (1993) Rod Structure of a Phycoerythrin II-Containing Phycobilisome. I. Organization and Sequence of the Gene Cluster Encoding the Major Phycobiliprotein Rod Components in the Genome of Marine Synechococcus sp. WH8020. J Biol Chem 268: 1226-1235

Yamanaka G, Glazer AN, Williams RC (1978) Cyanobacterial Phycobilisomes. Characterization of the Phycobilisomes of Synechococcus sp. 6301. Journal of Biological Chemistry 253: 8303-8310

Yamanaka G, Lundell DJ, Glazer AN (1982) Molecular Architecture of a Light-Harvesting Antenna. Isolation and Characterization of Phycobilisome Subassembly Particles. J Biol Chem 257: 4077-4086

Symposium 05

Bioenergetics of Photosynthetic Electron Flow

Ferredoxin:NADP$^+$ Oxidoreductase Associated with Cytochrome b_6f Complex is Highly Active in Plastoquinone Reduction

Renata Szymańska[a], Jolanta Pierścińska[a], Ireneusz Ślesak[b,c], Jerzy Kruk[a,*]

[a]Department of Plant Physiology and Biochemistry, Faculty of Biochemistry, Biophysics and Biotechnology, Jagiellonian University, ul. Gronostajowa 7, 30-387 Kraków, Poland;
[b]Institute of Plant Physiology, Polish Academy of Sciences, ul. Niezapominajek 21, 30-239 Kraków, Poland;
[c]Department of Plant Genetics, Breading and Biotechnology, Warsaw University of Life Sciences (SGGW), ul. Nowoursynowska 159, 02-776 Warszawa, Poland.
*Corresponding author. Tel. No. +48 12 664 6361; Fax No. +48 012 664 6902 E-mail: jerzy.kruk@uj.edu.pl.

Abstract: Three methods, differing in the preservation of the cytochrome b_6f-associated ferredoxin:NADP$^+$ oxidoreductase (FNR), have been applied for the isolation of the cytochrome b_6f complex from spinach. The complexes isolated by all three methods showed presence of FNR peptide(s), as revealed immunoblot analysis. However, when incorporated into liposome membranes, the NADPH-PQ (plastoquinone) oxidoreductase activity was not detected for the cytochrome b_6f complex isolated with the classical method including NaBr wash. Partial activity was found for the complex isolated with the omission of the wash, but the highest activity was detected for the complex isolated with the use of digitonin. The reaction rate was not significantly influenced by the addition of free FNR or ferredoxin. The reaction was neither affected by triphenyltin nor isobutyl cyanide. On the other hand, the reaction was severely inhibited by NQNO, an competitive inhibitor of PQ at the Q_i site. The obtained data indicate that FNR associated with the cytochrome b_6f complex can participate in the cyclic electron transport or chlororepiration as PSI-PQ or NADPH-PQ oxidoreductase, respectively. Moreover, we have shown that PQ in liposomes can be non-enzymatically reduced by ascorbate and this reaction might contribute to dark-reduction pathways of PQ-pool in chloroplasts.

Keywords: Ferredoxin:NADP$^+$ reductase; Cytochrome b_6f; Plastoquinone; Cyclic electron transport; Chlororespiration

Introduction

Cytochrom b_6f complex is one of the four major complexes of thylakoid membranes involved in photosynthesis. Recently, crystal structure of cytochrome b_6f complexes from two cyanobacteria (Kurisu *et al*., 2003; Baniulis *et al*., 2009) and *Chlamydomonas reinhardtii* (Stroebel *et al*., 2003) has been resolved showing, apart from the known cofactors, the presence of an additional heme c_n in all the structures which is located close to the Q_i site. The function of this heme remains unknown but it is suggested to take part in the cyclic electron transport.

Cyclic electron transport is known to occur in all the photosynthetic organisms from cyanobacteria to higher plants where electrons from photosystem I are transferred back to the PQ-pool, but there is no agreement on the proteins engaged in PQ reduction (Johnson, 2005; Joliot and Joliot, 2006).

It was already shown that ferredoxin:NADP$^+$ oxidoreductase (FNR) can be detected in the isolated spinach cytochrome b_6f complex but not in the cyanobacterial complex and that only the spinach complex had the diaphorase activity using dichloro-indophenol as an electron acceptor (Zhang *et al*., 2001). However, in these studies no evidence was presented for the FNR-PQ oxidoreductase activity of the isolated complexes.

In the present study, we used different methods of isolation of the cytochrome b_6f complex to obtain the highest NADPH-PQ activity of the purified complexes incorporated into liposome membranes and the presence of FNR in the investigated complexes was followed by different methods.

Materials and methods

Preparation of the cytochrome b_6f complex

The cytochrome b_6f complex was isolated from market spinach by three methods. The first two methods are modifications of the method described by Hurt and Hauska (1981), where thylakoid membranes are solubilized with octyl glucoside/cholate mixture. The first method included NaBr wash of thylakoid membranes before detergent treatment and it was modified as follows. After the precipitation between 45%–55% ammonium sulfate (AS) saturation and centrifugation, the pellet was suspended in 15 ml of the buffer (25 mmol Tris pH 7.8, 10 mmol NaCl, 2.5 mmol $MgCl_2$, 0.5% cholate) and fractionation between 20%–35% of AS saturation was performed. The obtained pellet was suspended again in 15 ml of the buffer. In the subsequent precipitation, the fractions between 20%–30% (cyt-NaBr-A) and 30%–35% (cyt-NaBr-B) of AS saturation were collected. The pellets from each fraction were suspended in 5 ml of the buffer each and dialyzed against the buffer overnight. After dialysis, the fractions were centrifuged at 100,000 *g* for 1 h and the supernatants were frozen until use.

In the second procedure, the NaBr wash was omitted and Tris (pH 7.8) was replaced by Hepes (pH 7.5) throughout the whole procedure. The other buffer components remained unchanged. After the precipitation between 45%–55% AS saturation and centrifugation, the pellet was suspended in 15 ml of the buffer and fractions between 20%–30% (cyt-FNR-A), 30%–35% (cyt-FNR-B) and 35%–40% (cyt-FNR-C) of AS saturation were collected. The pellets from each fraction were suspended in 5 ml of the buffer and after centrifugation at 100,000 *g* for 1 h the fractions were frozen until use.

In the third method, based on the procedure described by Nelson and Neumann (1972), the isolated thylakoids were adjusted to 1 mg/ml chlorophyll. Then, solid digitonin and NaCl were added up to concentrations of 1.25% and 0.1 mol, respectively. The suspension was stirred at cold overnight followed by centrifuged at 40,000 g for 10 min. To the obtained supernatant during stirring, 1.5 volumes of 2 mg/ml protamine sulfate was added per 10 volumes of the initial solution. After 1 h, the suspension was centrifuged 40,000 g for 10 min. The yellowish-green supernatant was loaded on a DEAE-Sephacel column (15 × 2 cm) and washed with 50 mmol Tris (pH 8.0)—0.5% cholate to remove the unbound proteins. Cytochrome b_6f was eluted with 0.1 mol Tris (pH 8.0)—1% cholate. The cytochrome fraction was brought to 55% saturation of AS and centrifuged. The pellet was suspended in 10 ml of 10 mmol Hepes (pH 7.5) buffer containing 0.5% cholate. Then, the fraction between 10%–20% (cyt-Dig) of AS saturation was collected and stored at –20 ºC.

The concentration of cytochrome b_6f complex in the obtained fractions was determined by spectrophotometric quantification of cytochrome *f*. The samples were first oxidized with 10 mmol ferricyanide and then reduced with solid ascorbate. The differential millimolar extinction coefficient of cytochrome *f* was taken as 17.7 at 554 nm.

Liposome preparation

Egg yolk phosphatidylcholine (PC), type V-E, was obtained from Sigma, while plant lipids were from Lipid Products (South Nutfield, Redhill, Surrey, U.K.). Liposomes with the incorporated cytochrome b_6f complex were prepared by the dialysis method. Appropriate volumes of lipid stock solutions in ethanol (PC or the chloroplast lipid mixture) and PQ were mixed in a glass vial and evaporated under stream of nitrogen and finally under vacuum. Then 3 ml of the buffer (50 mmol Hepes 7.5, 20 mmol NaCl, 5 mmol $MgCl_2$) were added, the mixture was shaken on a vortex to obtain homogeneous suspension, sodium cholate was added to give final concentration of 0.5% and then the cytochrome b_6f complex was added to the final concentration of 0.1 or 1 μM. The solution was dialyzed against 10 mmol Hepes 7.5 with 2 mmol NaCl overnight. After dialysis, the liposome suspension was centrifuged for 5 min at 3,000 *g* before further experiments. The reaction was started by the addition of NADPH from the concentrated stock solution (0.2 mol).

When reduction of PQ in liposomes by ascorbate was tested, liposomes were prepared by an injection

method. Appropriate volumes of the PQ and lipid mixture in ethanol were slowly injected into the buffer (50 mmol Hepes 7.5, 20 mmol NaCl, 5 mmol $MgCl_2$) with the syringe to obtain final lipid concentration of 1 mmol. The stock solutions of PC and the chloroplast lipid mixture (in the proportions as above) in ethanol were 40 mmol and 20 mmol, respectively. The reaction was started by the addition of ascorbate from the concentrated stock solution (2.5 mol) to give final concentration of 30 mmol.

Determiantion of the redox state of PQ in liposomes

Oxidized PQ-2 in extracts from liposomes was followed by HPLC using absorption detection at 255 nm and the reduced plastoquinones were monitored using fluorescence detection (excitation-emission at 290–330 nm) according to Kruk and Karpiński (2006).

Determination of FAD content in cytochrome b_6f fractions

FAD was released from the obtained cytochrome b_6f fractions or the FNR standard according to the modified procedure of Zanetti *et al*. (1982). The fractions in 50 mmol Hepes 7.5 with 0.5% cholate were treated with 1 mmol dithiothreitol, 0.1 mol guanidine-HCl and 2.5 mol $CaCl_2$ at room temperature for up to 1 h.

After 30 min and 1 h of the reaction, 60 µl of the reaction mixture was taken, mixed with 40 µl water, centrifuged shortly and analyzed by HPLC. The released FAD was analyzed by HPLC using C_{18} RP column (Nucleosil 100, 250 × 4 mm, 5 µm) in water/methanol (60/40, v/v) at the flow rate of 0.8 ml/min and fluorescence detection (excitation-emission at 450–530 nm). The retention time of FAD standard was 3.0 min.

Immunoblot analysis

Samples of denaturated proteins of cytochrome fractions and FNR standard (Sigma) were loaded on 12% (w/v) SDS containing PAM gels and electrophoresis was performed in a standard Laemmli membrane. Antibodies against commercial FNR were prepared by immunization of rabbits. A goat-anti-rabbit IgG-alkaline phosphatase conjugate was used as a secondary antibody. Immunostaining was performed using the NBT/BCIP protocol.

Results

Immunoblot analysis of all the cytochrome b_6f complex preparations showed the presence of one or two isoforms of FNR (Fig. 1) and other peptides characteristic for the complex, as revealed SDS electrophoresis (data not shown). FAD content varied considerably among the preparations (Table 1).

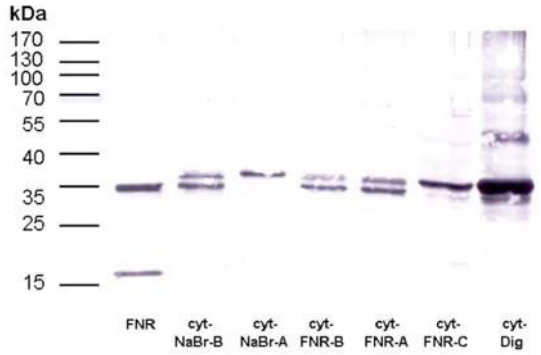

Fig. 1 Immunoblot of the FNR and of the different cytochrome b_6f preparations investigated. In the lower panel, 2.5 µl of each fraction was examined. FNR concentration was 2 µM and that of cytochrome b_6f fractions were as those given in the Table 1.

Table 1 Concentration of FAD and cyt *f* in the purified fractions of cytochrome b_6f complex. FAD was determined by HPLC and cyt *f* quantified spectrophotometrically as described in Materials and methods. FNR standard was also included for comparison. The error of FAD determination was ≤ 10%.

Fraction	FAD (µM)	Cyt *f* (µM)	Cyt f/FAD (mol/mol)
Cyt-NaBr-A	0.11	2.3	20.9
Cyt-NaBr-B	0.41	3.5	8.54
Cyt-FNR-A	0.94	3.2	3.4
Cyt-FNR-B	0.60	2.7	4.5
Cyt-FNR-C	5.36	3.0	0.56
Cyt-Dig	1.48	1.25	0.84
FNR (1µM)	0.89	-	-

The cyt-NaBr fractions showed the lowest FAD content, while cyt-Dig, as well as cyt FNR-C fraction had the highest FAD content. Neither of the cyt-NaBr fractions showed any reducing activity of PQ-2.

The addition of free FNR or ferredoxin (Fd) had no effect on the investigated reaction (not shown). The cyt-FNR-C fraction showed significant PQ-2 reduction and the addition of free FNR was slightly stimulatory (Fig. 2).

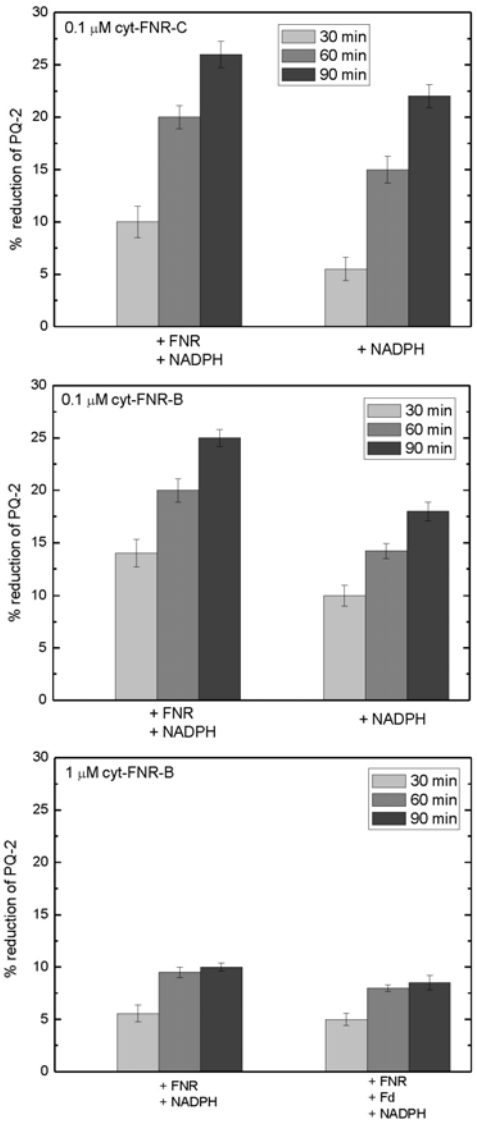

Fig. 2 Time course of PQ-2 reduction in PC liposomes with the incorporated cytochrome b_6f preparations. The medium was Hepes buffer (50 mmol Hepes, pH 7.5, 20 mmol NaCl, 5 mmol $MgCl_2$). Other conditions: 1 mmol PC, 20 μM PQ-2, 0.5 mmol NADPH. Where indicated, 0.1 μM FNR and 1 μM ferredoxin (Fd) was included. The data are means (n = 3) ± SE.

The cyt-FNR-B fraction showed faster initial reaction rate than cyt-FNR-C but the lower extend of the reaction after 90 min in the presence of NADPH only (Fig. 2). The higher concentration of FNR-B fraction turned out to be inhibitory. Digitionin-purifed cytochrome b_6f complex showed very high rate of PQ-2 reduction (Fig. 3) and the addition of free FNR was without further effect on the reaction. Isobutyl cyanide, inhibitor of the heme c_n, was without any effect on PQ-2 reduction by the cyt-Dig complex (not shown). On the other hand, NQNO, an inhibitor of the Q_i site that was recently shown to be a ligand of heme c_n (Yamashita *et al*., 2007), turned out to inhibit the investigated reaction by about 60% (not shown). Moreover, we have shown that PQ in liposomes can be slowly, non-enzymatically, reduced by ascorbate (not shown).

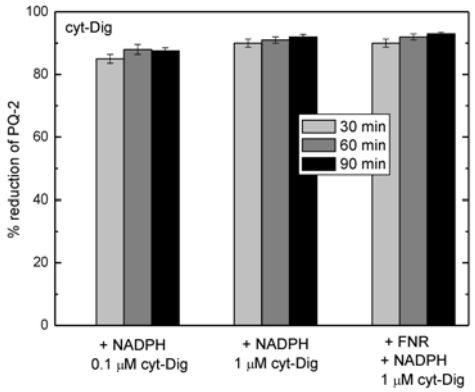

Fig. 3 Time course of PQ-2 reduction in PC liposomes with the incorporated cyt-Dig preparation. The medium was Hepes buffer (50 mmol Hepes, pH 7.5, 20 mmol NaCl, 5 mmol $MgCl_2$). Other conditions: 1 mmol PC, 20 μM PQ-2, 0.5 mmol NADPH. Where indicated, 0.1 μM FNR was included. The data are means (n = 3) ± SE.

Conclusions

All preparations of cytochrome b_6f complex obtained by three different isolation methods showed the presence of FNR polypeptide - one or two isoforms of the enzyme. Although all the obtained fractions showed the presence of FNR, their FAD content was different. The highest activity of the cyt-Dig fraction was surprising and indicates that not only the FNR peptide and FAD content is sufficient for the maxiamal activity, but also other factors like probably optimal FNR association with the complex. The effect of the inhibitors of the cytochrome b_6f complex on the PQ-2 reduction suggests that Q_i site is engaged in the reaction but rather not heme c_n. Ferredoxin had no effect on the investigated reaction in liposomes, which suggested that Fd is not directly required for PQ reduction, but rather for reduction of FNR under light conditions during operation of the cyclic electron transport. In our system, FNR was reduced by NADPH showing NADPH-PQ diaphorase activity. This light-independent reaction is characteristic for chlororespiratory pathway and our results support the idea that FNR participates not only in the cyclic electron transport but also in chlororespiration.

References

Baniulis D, Yamashita E, Whitelegge JP, Zatsman AI, Hendrich MP, Hasan SS, Ryan CM, Cramer WA (2009) Structure-Function, Stability, and Chemical Modification of the Cyanobacterial Cytochrome b_6f Complex from Nostoc sp. PCC 7120. J. Biol. Chem. 284**:** 9861-9869

Hurt E, Hauska G (1981) Cytochrome f/b_6 Complex of Five Polypeptides with Plastoquinol-Plastocyanin-Oxidoreductase Activity from Spinach Chloroplasts. Eur. J. Biochem. 117: 591-599

Johnson GN (2005) Cyclic Electron Transport in C_3 Plants: Fact or Artefact? J. Exp. Bot. 56: 407-416

Joliot P, Joliot A (2006) Cyclic Electron Flow in C_3 Plants. Biochim. Biophys. Acta 1757: 362-368

Kruk J, Karpiński S (2006) An HPLC-Based Method of Estimation of the Total Redox State of Plastoquinone in Chloroplasts, the Size of the Photochemically Active Plastoquinone Pool and Its Redox State in Thylakoids of Arabidopsis. Biochim. Biophys. Acta 1757: 1669-1675

Kurisu G, Zhang H, Smith JL, Cramer WA (2003) Structure of the Cytochrome b_6f Complex of Oxygenic Photosynthesis. Tuning the Cavity. Science 302: 1009-1014

Nelson N, Neumann J (1972) Isolation of a Cytochrome b_6-f Particle from Chloroplasts. J. Biol. Chem. 247: 1817-1824

Stroebel D, Choquet Y, Popot JL, Picot D (2003) An Atypical Heam in the Cytochrome b_6f Complex. Nature 426: 413-418

Yamashita E, Zhang H, Cramer WA (2007) Structure of the Cytochrome b_6f Complex: Quinone Analogue Inhibitors as Ligands of Heme c_n. J. Mol. Biol. 370: 39-52

Zanetti G, Cidaria D, Curti B (1982) Preparation of Apoprotein from Spinach Ferredoxin-$NADP^+$ Reductase. Studies on the Resolution Process and Characterization of the FAD Reconstituted Holoenzyme. Eur. J. Biochem. 126: 453-458

Zhang H, Whitelegge JP, Cramer WA (2001) Ferredoxin:$NADP^+$ Oxidoreductase Is a Subunit of the Chloroplast Cytochrome b_6f Complex. J. Biol. Chem. 276: 38159-38165

The Mutation E242K in the Chloroplast ATP Synthase Gamma Subunit Increases the Inhibitory Binding of the Epsilon Subunit without Changing the Apparent Redox Potential of the Regulatory Dithiol.

Kim K Colvert[a], Fei Gao[b], Daxin Zheng[c], Shyam Mehta[c], Mark L Richter[c]*

[a] Ferris State University, Michgan; [b] COBRE Protein Production Core Laboratory and [c]Department of Molecular Biosciences, The University of Kansas, Lawrence, KS, USA.

*Corresponding author. Tel. No. +1 785 864 3334; Fax No. +1 785 864 5321; E-mail: richter@ku.edu.

Abstract: A single point mutation in the gamma subunit of the ATP synthase, E244K, was recently shown to change the apparent redox potential of a critically placed, regulatory dithiol in the gamma subunit of the photosynthetic ATP synthase *in situ* in thyolakoid membranes of *Arabadopsis thaliana* (Wu *et al*., 2006). The mutation resulted in loss of light-dependent activation of the ATPase activity of the ATP synthase and decreased ATP synthesis. This identified, for the first time, that the redox state of the gamma dithiol is a strong determinant of photosynthetic efficiency in higher plants. To determine how the gamma dithiol modulates ATP synthesis the effect of the E244K mutation on the redox potential of the gamma dithiol was examined *in vitro* using an assembled recombinant hybrid CF_1 enzyme system previously described. The mutation did not significantly alter the redox potential of the gamma dithiol. It did, however, decrease the dilution-dependent activation of the ATP hydrolysis activity of the enzyme that results from release of the inhibitory epsilon subunit. This suggests that the mutation blocks the light-dependent change in epsilon conformation that leads to activation of the latent ATPase activity of CF_1 *in situ*.

Keywords: Chloroplast ATP synthase; E244K gamma mutation; Regulatory dithiol redox potential

Introduction

The catalytic F_1 segment of the chloroplast ATP synthase is a latent ATPase either when bound to the F_O portion of the enzyme on thylakoid membranes or when isolated from the membrane. Activation on the membrane requires the presence of a proton gradient together with the natural reductant thioredoxin or an artificial reductant such as dithiothreitol, which is required to reduce a critically placed dithiol in the gamma subunit of the enzyme (Dann and McCarty, 1992). Activation *in vitro* requires removal of the inhibitory epsilon subunit or reduction of the gamma disulfide by an added reducing agent. Maximum activation requires both treatments (Richter *et al*., 1985). The latency of the enzyme is considered necessary to prevent non-productive ATP hydrolysis in the dark that would deplete essential ATP pools (He *et al.*, 2000). The importance of this process for efficient photosynthesis was demonstrated recently when it was discovered that a point mutation in the gamma subunit (E244K) led to a negative shift in the apparent redox potential of the gamma dithiol. This resulted in loss of physiological ATPase activation and a severe reduction in ATP synthesis capacity (Wu *et al*., 2007). How this happens is not known although

[1]**Abbreviations Used:** *atpC*, the DNA sequence encoding the ATP synthase gamma subunit; DTT, dithiothreitol; F_1, the membrane-associated portion of the ATP synthase complex contains the catalytic domains; F_O the integral membrane proton transport component of the ATP synthase; PCR, polymerase chain reaction; Tris, tris(hydroxy methyl)amino-methane. SD, standard deviation.

it is assumed that the mutation alters the local environment in the vicinity of the dithiol thus altering its redox potential.

A molecular model of the spinach chloroplast gamma subunit (Richter *et al*., 2005) and comparison of the mode of binding of the epsilon subunits in the analogous mitochondrial and bacterial F_1 enzymes, suggest that the glutamate residue at position 244 may form part of a binding site for the inhibitory epsilon subunit. Further, molecular modeling predicts that changing the glutamate residue at position 244 to a lysine residue would not be likely to significantly affect the local environment of the gamma dithiol (Cys199 and Cys205) that is a considerable distance away.

To clarify the effect of the E244K mutation, recombinant spinach chloroplast gamma subunit containing the E244K mutation was assembled with alpha and beta subunits from the photosynthetic bacterium *Rhodospirillum rubrum* into a catalytically active hybrid enzyme. The hybrid enzyme is well characterized and been used extensively as a model system to examine the effects of mutations on CF_1 function (Du *et al*., 1999; Samra *et al*., 2006). These data indicate that the shift in redox potential of the gamma dithiol may result from a change in the binding affinity of the epsilon subunit.

Materials and Methods

Materials

CF_1 and CF_1 deficient in the delta and epsilon subunits, $CF_1(-\delta\varepsilon)$, were prepared from fresh market spinach (Richter *et al*., 1984; Gao *et al*., 1995). ATP (grade II) and antibiotics (ampicillin, tetracycline) were purchased from Sigma. Tryptone and yeast extract were from DIFCO. Urea (ultrapure) was from Fluka.

Generation of the E244K mutant

The E244K mutant gamma subunit was constructed by enzymatic amplification of the expression plasmid pET8c-gamma.BB1 (Gao *et al*., 1995; Samra *et al*., 2006) using a pair of "inverse" primers with abutting 5' ends. Primers were 24–31 nucleotides long and were chemically phosphorylated at the 5' termini. PCR was carried out as described in detail elsewhere (Sokolov *et al*., 1999). Cloned plasmid was isolated and transformed into the expression host *E.coli* BL21(DE3)/pLysS. The entire sequence of the mutant gamma gene was confirmed.

Production and assembly of F_1 subunits

The **r**ecombinant gamma subunit, which was expressed in the form of inclusion bodies, was solubilized with urea, folded and assembled with recombinant alpha and beta subunits from *Rhodospirillum rubrum* using a slow dialysis protocol (Du *et al*., 1999). Unreconstituted subunits were separated from the reconstituted enzyme by anion exchange chromatography (Gao *et al*., 1995).

Similarly, the epsilon protein was solubilized from inclusion bodies in 8 mol urea and folded by the dilution method of Cruz *et al*. (1995). The cloned epsilon subunit was reconstituted with the assembled enzyme complex using the same procedure for reconstituting the native epsilon subunit with $CF_1(-\varepsilon)$ (Richter *et al*., 1984).

Redox titrations

Oxidation-reduction titrations were performed using the ATP hydrolysis activity of native $CF_1(-\delta\varepsilon)$ and recombinant enzyme assemblies. Samples of 5 μg of protein were equilibrated at room temperature at potentials (*E*h) generated by ratios of reduced:oxidized DTT, for times and total DTT concentrations chosen as consistent with maximum activation for $CF_1(-\delta\varepsilon)$ (Richter *et al*., 1985). At the end of the equilibration period, pre-warmed CaATPase assay mix was added to yield incubation conditions of 50 mmol Tris-HCl (pH 7.9), 5 mmol ATP, and 5 mmol $CaCl_2$ then incubated for 2 min at 37 ^{o}C. The Nernst equation: $E_h = E_m + RT/nF \ln([DTTox]/[DTTred])$, was used to calculate redox potentials. The equilibrium redox potential for DTT at pH 7.9 ($E_{m,7.9}$) was calculated using the $E_{m,7}$ value of –327 mV at 25 ^{o}C (Lees *et al*., 1993). The redox potentials (*Eh*) were calculated using $n = 2$ for the two electrons transferred in thiol/disulfide exchange. A pH of 7.9 was chosen to simulate the pH of illuminated chloroplast stroma (Wu *et al*., 2007).

Other procedures

ATPase activities were determined by measuring phosphate release (Richter *et al*., 1984) for 1 to 5 minutes at 37 ^{o}C. The assay mixture for calcium-dependent ATPase activity contained 50 mmol Tris-

HCl (pH 8.0), 5 mmol ATP and 5 mmol $CaCl_2$. Protein concentrations were determined as in Richter *et al*. (2004). Sodium dodecylsulfate polyacrylamide gel electrophoresis was performed under reducing conditions on pre-cast 12% NOVEX gels.

Results and Discussion

The E244K mutant gamma subunit proved to be as competent as the wild type gamma subunit in assembling with the alpha and beta subunits as judged by the yield of the assembled enzyme (~8% in each case) and by the relative staining of bands following denaturing gel electrophoresis (data not shown). The response of the mutant to reductive activation by dithiothreitol (Fig. 1) was also identical to those of native $CF_1(-\delta\varepsilon)$ and the wild type assembly. Further, the kinetics of CaATP hydrolysis (Fig. 2) of the mutant were essentially identical to those of the assembly containing the wild type gamma subunit, indicating that the mutation had no discernable effect on the catalytic parameters.

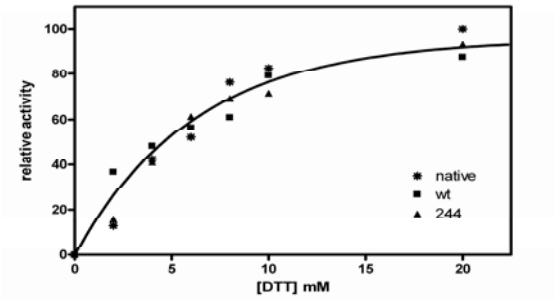

Fig. 1 Reductive activation of the CaATPase activity of native (stars), wild type (squares) and E244K mutant (triangles) enzymes. Each enzyme was pre-treated with 50 μM $CuCl_2$ for 30 min prior to addition of dithiothreitol. The relative activities are the percentage of the total increase in activity above that of the oxidized enzyme form which was approximately two-fold in each case. Error bars show SD for n = 3.

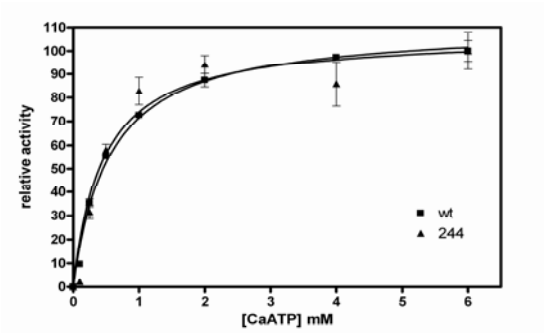

Fig. 2 Comparison of CaATPase activities of enzymes assembled with wild type (squares) and E244K mutant (triangles) gamma subunits. Error bars show SD for n = 3.

The redox potential of the dithiols of the native and recombinant enzymes were determined (Fig. 3) by titrating the enzymes with the [DTTox]/[DTTred] redox couple and monitoring the CaATPase activities of the enzymes as described elsewhere (Dann and McCarty, 1992). It must be stressed that the CaATPase activity has been used here to document the effects of the mutation but the MgATPase activity responded in an identical manner when measured either in the presence or absence of stimulatory oxyanions (data not shown).

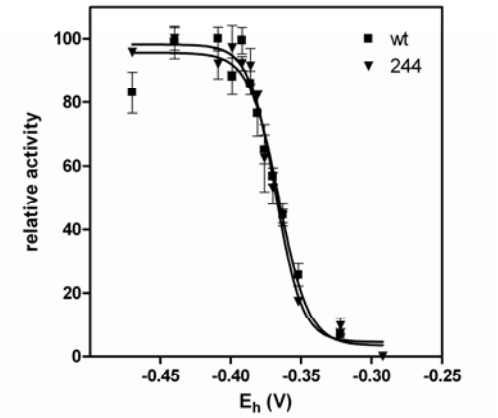

Fig. 3 CaATPase activities of enzymes assembled with wild type (squares) and E244K mutant (triangles) gamma subunits were titrated against the [DTTox]/[DTTred] redox couple. The redox potentials (E_h) were calculated using the Nernst equation as indicated in the *Materials and Methods*. Error bars show SD for n = 3.

The main point to note is that the midpoint redox potential of the gamma dithiol (–0.36 V) was the same for the mutant and the wild type assembly. The same value was also obtained for the native enzyme as reported previously (Dann and McCarty, 1992). The result strongly indicates that, contrary to expectation, replacing the glutamate residue with a lysine residue at position 244 did not directly affect the environment surrounding the gamma dithiol sufficiently to alter its redox potential. This implies that the E244K mutation indirectly affected the apparent redox potential of the gamma dithiol *in situ* (Wu *et al*., 2007).

Since E244 is predicted to lie at an interface between the epsilon and gamma subunits, the effect of replacing this residue with one of opposite charge on binding of the epsilon subunit was explored. The enzymes were first exposed to excess amounts of the epsilon subunit followed by gel filtration to remove any unbound epsilon. The enzymes were then diluted

and the release of bound epsilon monitored as increased CaATPase activity (Fig. 4). The observed difference in the release of the epsilon subunit and the corresponding activation of catalytic activity at high dilution between the oxidized and reduced forms has been documented elsewhere (Soteropoulis *et al*., 1992). The reduced amount of epsilon released at high dilution by the mutant enzyme was observed in several independent experiments suggesting that the E244K mutation increased the inhibitory binding affinity of the epsilon subunit.

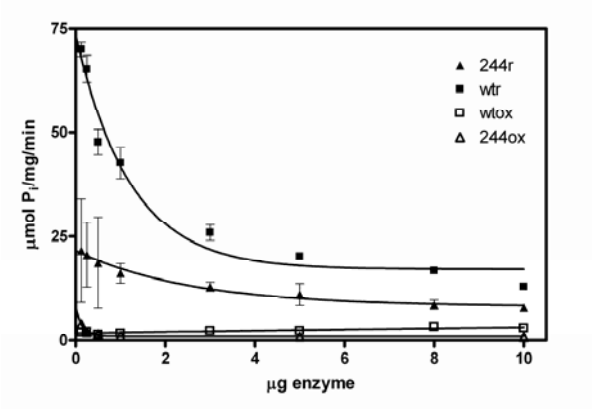

Fig. 4 Enzymes assembled with wild type (squares) and E244K mutant (triangles) gamma subunits were pretreated with $CuCl_2$ (oxidized, open symbols) or DTT (reduced, closed symbols) prior to dilution into the assay mixture as indicated for determination of CaATPase activity.

Inspection of the modeled structure of the CF_1 gamma subunit predicts that E244 lies near the tip of the twisted helical pair formed by N- and C-terminal helical elements within the gamma structure. The structure in this region of the protein is conserved in the bovine mitochondrial and *E.coli* F_1 gamma subunits and is predicted to be the same in the CF_1 gamma. By analogy to the *E.coli* and mitochondrial structures, E244 is positioned to form a salt bridge with a positively charged lysine residue on the beta sandwich portion of the epsilon subunit. If this is the case for CF_1, replacing the glutamate with lysine would prevent formation of the salt bridge and would be expected to at least partially disrupt the binding interaction between the beta sandwich domain of epsilon and the twisted helical element of gamma. However, it is known from mutational studies (Nowak and McCarty, 2004) that the C-terminal helix-turn-helix domain rather than the N-terminal beta sandwich domain of the epsilon subunit is primarily responsible for epsilon inhibition. Further, extensive mutational analysis of the dithiol-containing domain of the CF_1 gamma subunit indicated that the productive inhibitory binding interaction between the epsilon and gamma subunits involves an interaction between the C-terminal domain of epsilon and the regulatory, dithiol-containing domain of the gamma subunit (Samra *et al*., 2006).

While mutations in the N-terminal beta sandwich domain of the epsilon subunit have little or no effect on epsilon inhibition, they strongly affect proton-coupled ATP synthesis by the CF_1F_O complex (Cruz *et al*., 1995). These observations suggest that the E244K mutation could impair proton-driven conformational changes in the epsilon subunit that are required for activation of the latent ATPase activity (Richter and McCarty, 1987) and at the same time reducing ATP synthesis rates by reducing the proton coupling efficiency. This effect could also result in a decrease in access of the gamma dithiol to thioredoxin (or DTT) due to an enhanced interaction between the C-terminal domain of epsilon and the regulatory domain of gamma. An altered interaction could well result in a change in the local environment surrounding the gamma dithiol, explaining the observed increased redox potential of the dithiol (Wu *et al*., 2007). Further work is in progress to test this possibility.

Acknowledgements

This work was supported by NSF MCB-0818743 and Kansas EPSCoR grants.

References

Cruz JA, Harfe B, Radkowski CA, Dann MS, McCarty RE (1995) Molecular Dissection of the Epsilon Subunit of the Chloroplast ATP Synthase of Spinach. Plant Physiol. 109: 1379-1388

Dann MS, McCarty RE (1992) Characterization of the Activation of Membrane-Bound and Soluble CF(1) by Thioredoxin. Plant Physiol. 99: 153-160

Du Z, Gromet-Elhanan Z (1999) Refolding of Recombinant Alpha and Beta Subunits of the *R*.rubrum F(0)F(1) ATP Synthase into Functional Monomers that Reconstitute an Active Alpha(1) Beta(1)-Dimer. Eur.J.Biochem. 263: 430-437

Gao F, Lipscomb B, Wu I, Richter ML (1995). In

Vitro Assembly of the Core Catalytic Complex of the Chloro-Plast ATP Synthase. J.Biol.Chem 270: 9763-9769

He X, Miginiac-Maslow M, Sigalat C, Keryer E, Haraux F (2000) Mechanism of Activation of the Chloroplast ATP Synthase. A Kinetic Study of the Thiol Modulation of Isolated ATPase and Membrane-Bound ATP Synthase from Spinach by Eschericia Coli Thioredoxin. J.Biol.Chem. 275: 13250-13258

He F, Samra HS, Tucker WC, Mayans DR, Hoang E, Gromet-Elhanan Z, Berrie CL, Richter ML (2007) Mutations within the C-Terminus of the Gamma Subunit of the Photosynthetic F1-ATPase Activate MgATP Hydrolysis and Attenuate the Stimulatory Oxyanion Effect. Biochemistry 46: 2411-2418

Hightower KE, McCarty RE (1996) Proteolytic Cleavage within a Regulatory Region of the Gamma Subunit of Chloroplast Coupling Factor 1. Biochemistry 35: 4846-4851

Ketcham SR, Davenport JW, Warncke K, McCarty RE (1984) Role of the Gamma Subunit of Chloroplast Coupling Factor 1 in the Light-Dependent Activation of Photophosphorylation and ATPase Activity by Dithiothreitol. J.Biol.Chem. 259: 7286-7293

Lees WJ, WHitesides GM (1993) Equilibrium Constants for Thiol-Disulfide Interchange Reactions: a Coherent, Corrected set. J.Org.Chem. 58: 642-647

Nowak KF, McCarty RE (2004) Regulatory Role of the C-Terminus of the Epsilon Subunit from the Chloro-Plast ATP Synthase. Biochemistry 43: 3273-3279

Richter ML, Patrie WJ, McCarty RE (1984) Preparation of the Epsilon Subunit and Epsilon Subunit-Deficient Chloroplast Coupling Factor I in Reconstitutively Active Forms. J.Biol.Chem. 259: 7371-7373

Richter ML, Snyder B, McCarty RE, Hammes GG (1985) Binding Stoichiometry and Structural Mapping of the Epsilon Polypeptide of Chloroplast Coupling Factor I. Biochemistry 24: 5755-5763

Richter ML, Samra HS, He F, Giessel AJ, Kuczera KK (2005) Coupling Proton Movement to ATP Synthesis in the Chloroplast ATP Synthase. J.Bioenerg.Biomembr. 37: 467-473

Richter ML, McCarty RE (1987) Energy-Dependent Changes in the Conformation of the Epsilon Subunit of the Chloroplast ATP Synthase. J.Biol.Chem. 262: 15037-15040

Samra HS, Gao F, He F, Hoang E, Chen Z, Gegenheimer PA, Berrie CL, Richter ML (2006) Structural Analysis of the Regulatory Dithiol-Containing Domain of the Chloroplast ATP Synthase Gamma Subunit. J.Biol.Chem. 281: 31041-31049

Sokolov M, Lu L, Tucker W, Gao F, Gegenheimer PA, Richter ML (1999) The 20 C-Terminal Amino Acid Residues of the Chloroplast ATP Synthase Gamma Subunit Are Not Essential for Activity. J.Biol.Chem. 274: 13824-13829

Soteropoulos P, Suss KH, McCarty RE (1992) Modifications of the Gamma Subunit of Chloroplast Coupling Factor I Alter Interactions with the Inhibitory Epsilon Subunit. J.Biol.Chem. 267: 10348-10354

Wu G, Ortiz-Flores G, Ortiz-Lopez A, Ort DR (2007) A Point Mutation in AtpC1 Raises the Redox Potential of the Arabidopsis Chloroplast ATP Synthase Gamma-Subunit Regulatory Disulfide above the Range of Thio-Redoxin Modulation. J.Biol.Chem. 282: 36782-36789

Analysis of Dark Drops, Dark-Induced Changes in Chlorophyll Fluorescence during the Recording of the OJIP Transient

Vasilij Goltsev[1 *], Maria Gurmanova[1], Margarita Kouzmanova[1], Ivan Yordanov[1], Scheng Qiang[2], Alison Pentland[3], Neil Wilson[3], Shiguo Chen[2], Ivelina Zaharieva[4], Reto Jörg Strasser[2,5]

[1]Department of Biophysics and Radiobiology, Faculty of Biology, St. Kliment Ohridski University of Sofia, Sofia, Bulgaria;
[2]Weed Research Laboratory, Nanjing Agricultural University, Nanjing 210095, China;
[3]Hansatech Instruments Ltd, Narborough Road, Pentney, King's Lynn, Norfolk PE32 1JL, England;
[4]Freie Universität Berlin, FB Physik, Arnimallee 14, D-14195 Berlin, Germany;
[5]Bioenergetics Laboratory, University of Geneva, CH-1254 Jussy/Geneva, Switzerland.
[*]Corresponding author. E-mail: goltsev@biofac.uni-sofia.bg.

Abstract: In a search for a powerful and easy-to-handle instrument for investigation of photosynthetic energy and electron transfer reactions, the mPEA (Hansatech Instrument Ltd., King's Lynn, Norfolk, PE30 4NE, U.K.) was developed. The instrument can record simultaneously, *in vivo*, the photo-induced changes in prompt (PF) and delayed (DF) chlorophyll fluorescence and modulated infrared light reflection at 820 nm (MR_{820}) using a protocol of alternating periods of illumination and darkness. In this way the standard OJIP induction transient of PF is modified by the dark intervals causing a decrease of the PF intensity during the dark periods (so called dark fluorescence drops, DD). The dependence of the relative DD on the redox level of Q_A was analyzed for different initial states of bean leaves. A strong linear correlation was found between the relative dark drops and the fraction of oxidized Q_A for the phase starting before the J level and going up to the P level of the PF induction transient. We propose that the experimentally measurable DDs offer a tool for *in vivo* quantification of the redox reactions of Q_A and Q_B during the fluorescence rise from F_0 to F_M.

Keywords: Chlorophyll fluorescence; Delayed fluorescence; Dark drops; OJIP rise; Q_A/Q_B electron transfer

Introduction

The illumination of dark adapted plants by actinic light induces a cascade of electron-transport reactions that change the state of the photosynthetic apparatus and modify its ability to emit light. The principal scheme including functional components for energy transfer and electron transport during the light phase of photosynthesis is presented in Fig. 1. The variety of redox states of the electron carriers and the different redox reactions can be studied by the analysis of the shape of the light induced transients of chlorophyll fluorescence (PF) and its characteristic points (OJIP, see Fig. 2). As an informative approach for quantification of the OJIP transients the JIP-test was proposed by Strasser and his coworkers (Strasser *et al.*, 2004, 2010; Tsimilli-Michael *et al.*, 2008). It is a non-invasive method for studying the electron transport reactions in photosynthesis which is of particular importance as it can be applied for both fundamental studies of the photosynthesis reactions and for estimation of the crop production in the field in agriculture.

Simultaneously with PF the antennae complexes of the active reaction centers of Photosystem II, PSII, (Chl_2^*-RC_2^* in Fig. 1) emit delayed fluorescence, DF, which is a result of back reaction of electron transport within PSII (Goltsev *et al.*, 2009 and references therein). The DF intensity correlates with forward and backward reactions both in donor and acceptor sides of PSII as well as with the thylakoid membrane energization. Another informative signal which can be recorded from intact leaves is the modulated infrared

light reflection at 820 nm (MR_{820}). It gives information about the activity of the donor and acceptor side of Photosystem I (Strasser *et al.*, 2010).

The combination of these three non-invasive methods in a single instrument will result in a powerful tool for *in situ* studies of photosynthesis. The instrument mPEA (Multi-signal Plant Efficiency Analyzer) allows simultaneous recording of photo-induced changes in PF, DF and MR_{820} (Strasser *et al.*, 2010). As the DF can be separated from the PF only on the time base (DF has much longer lifetime that PF), the simultaneous measurement of induction curves of PF and DF requires alternation of periods of illumination during which PF is measured and dark periods during which DF is recorded. Due to re-oxidation of reduced PSII primary quinone acceptor, Q_A^-, the values of PF recorded after preceding darkness decrease in comparison to the values obtained before the dark period. We introduce a new term – dark fluorescence drops (DD) – to describe this phenomenon during the OJIP fluorescence rise.

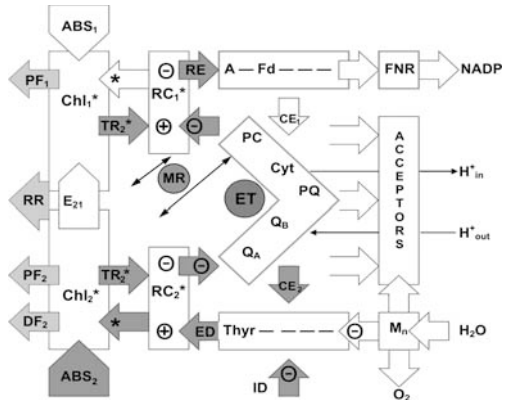

Fig. 1 Σ-Scheme explaining the sources of PF, DF and MR_{820} signals in photosynthetic electron transport chain. The boxes represent structural components. Light grey arrows present physical signals that can be measured and dark grey arrows – electron and energy flows recalculated from these signals. Signals: DF, delayed fluorescence; PF, prompt fluorescence; MR, modulated reflection; RR, far-red light (735 nm) reflection. Flows: TR, energy trapping; E_{21}, energy migration from PSII antennae to PSI (spillover); ED, electron donation toward PSII from water or ID, from internal donors; RE, electron flow through PSI to NADP; CE, cycle electron flow. RC_1^* and RC_2^* are the reaction center chlorophylls of PSI and PSII, respectively and the other abbreviations are the standard abbreviation used for the classical Z-scheme of the photosynthetic light reactions. (Redrawn from Strasser, 1978; with permission from Strasser.)

The main goal of this paper is to analyze the reactions in PSII during these short dark periods, which are necessary to record DF and to estimate to what extend they modify the PF and MR_{820} signals which became already standard techniques in the *in situ* characterization of the photosynthetic apparatus.

Materials and Methods

Bean plants (*Phaseolus vulgaris* L., var. "Cheren Starozagorski") were grown as water culture on Knop solution in climatic chamber at 24 °C, 50%–55% humidity and at luminescent light (250 μmol photons $s^{-1}m^{-2}$, day/night ratio 12:12). Before the experiments leaf discs from 20–25 days-old plants were cut and kept in darkness for 1 h on a wet filter paper. The kinetics of PF, DF and MR_{820} were simultaneously recorded with mPEA as described in Strasser *et al.* (2010).

Results and Discussion

A typical record of mPEA signals is presented in Fig. 2. In alternating periods of illumination and dark (duration ratio 3:1) we record PF and MR_{820} (during the light periods) and DF decays (in dark). The duration of one light/dark cycle increases logarithmically during the induction period. Recording the DF decays at different moments of the induction time we can reconstruct the induction curves of DF integrated at different dark intervals. The DF induction curves are described by specific points according the nomenclature of Goltsev and Yordanov (1997).

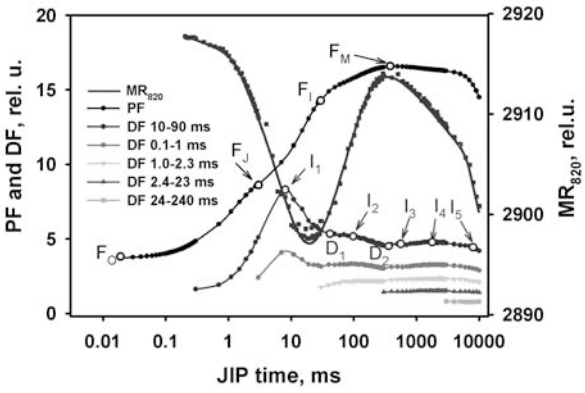

Fig. 2 Simultaneously recorded PF, DF and MR_{820} during dark to light transition in dark adapted bean leaves. The DF curves shown are recorded in 5 time intervals of DF decay curve. Actinic light intensity was 5,000 μmol m^{-2} s^{-1}. With open cycles the characteristic points of PF (F_O, F_J, F_I, F_M) and DF (I_1, I_2 ... I_5) are marked.

During recording of the DF the illumination of the sample is interrupted and Q_A in part of PSII reaction centers is re-oxidized. This results in a decrease of the PF yield measured just after dark interval. In Fig. 3 are presented the records of PF signal alone (at continuous illumination—open circles) or simultaneously with DF (closed symbols). The insertion of short dark intervals during actinic illumination does not modify significantly the shape of PF transients. The amplitude of the relative PF decrease (fluorescence "dark drop", DD) after dark application depends on the variable fluorescence values (Fig. 3, ▲).

To study the changes in the photosynthetic apparatus during the dark periods we recorded PF and DF after sudden switch of the actinic light intensity off in the three characteristic points during the induction kinetic (J, I and P).

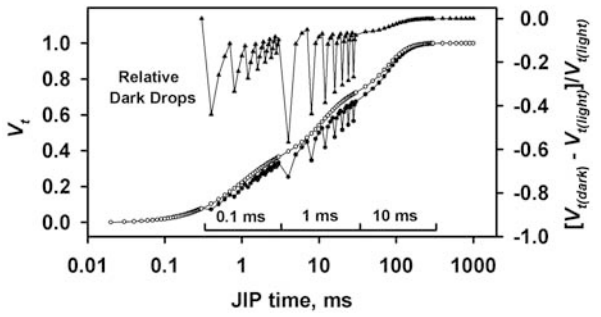

Fig. 3 Effect of insertion of dark intervals during OJIP transients. Open circles: relative values of variable chlorophyll fluorescence measured at continuous illumination. Closed circles: actinic light was interrupted by short dark intervals (0.1, 1 and 10 ms, see the bar above the time axes) with a 3:1 light/dark ratio. The relative values of dark drops of variable fluorescence were calculated as $[V_{t(dark)} - V_{t(light)}]/ V_{t(light)}$.

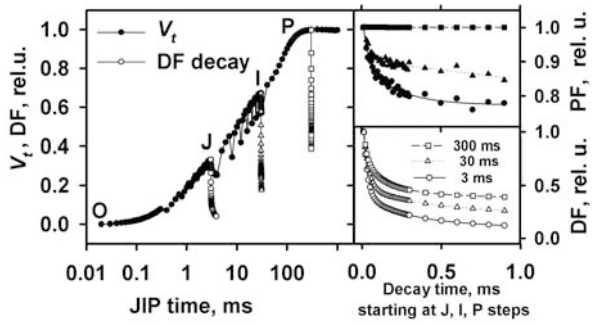

Fig. 4 Comparison of the dark decay kinetics for PF and DF signals after switch off of the actinic light at different moments during the OJIP transient. Black symbols represent the PF signal measured with light intensity 1 μmol m^{-2} s^{-1}; open symbols – DF measured in dark. The DF values are normalized to PF values at J, I and P levels. Insets: PF and DF decays normalized to the maximal value.

The PF decay curves under low excitation light monitor the reoxidation of the reduced primary electron acceptor of PSII, Q_A. The amplitude (Fig. 4) and the dynamics of the PF decay (Fig. 5a) depend on the moment of the OJIP-transition when the "dark pulse" is applied. For example the decay is very slow if the illumination is interrupted at the P level of the PF induction. Parameters of the best fit of PF decay data by two-exponential function are presented in Table 1. During the reduction of the electron-transport chain (transition from J to I to P) there is a slowdown of the fastest fluorescence decay phase. This means that it is determined by different reactions: at J phase $\tau = 0.12$ ms (the electron transfer reaction $Q_A^- \rightarrow Q_B$), at I phase 0.66 ms ($Q_A^- \rightarrow Q_B^-$) and at P phase – 4.56 ms ($Q_B^= \rightarrow PQ$).

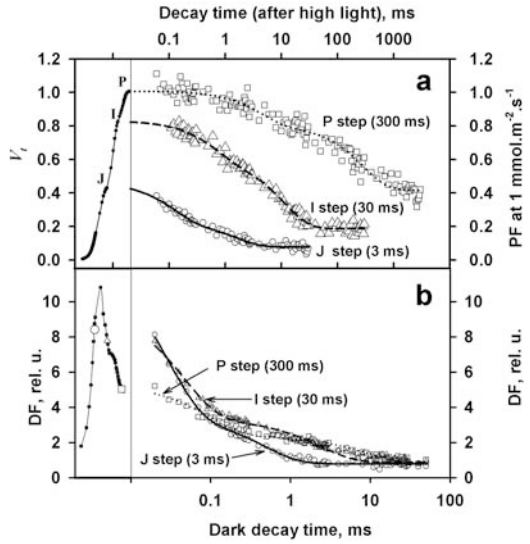

Fig. 5 Decay kinetics for PF (a) and DF (b) signals during actinic light switch off measured at different moments of JIP transient: ○ – 3 ms illumination (near J phase); △ – 30 ms illumination (I); □ – 300 ms illumination (near P).

Table 1 Fit results of PF decays (as 2-exponential function) and DF decays (as 4-exponential function) in bean leaves pre-illuminated with 5,000 μmol m^{-2} s^{-1} light for 3, 30 or 300 ms (see Figs. 4 and 5).

PF decay equations
$V_J = 0.08 + 0.24\,e^{-t/0.12} + 0.15\,e^{-t/1.6}$
$V_I = 0.19 + 0.23\,e^{-t/0.66} + 0.41\,e^{-t/11.4}$
$V_P = 0.42 + 0.21\,e^{-t/4.56} + 0.39\,e^{-t/291}$
DF decay equations
$DF_J = 7.7 + 9.1\,e^{-t/0.025} + 2.0\,e^{-t/0.22} + 13.6\,e^{-t/0.69} + 0.7\,e^{-t/9.2}$
$DF_I = 7.8 + 6.4\,e^{-t/0.035} + 1.7\,e^{-t/0.38} + 11.7\,e^{-t/2.72} + 5.9\,e^{-t/23.4}$
$DF_P = 8 + 2.5\,e^{-t/0.022} + 1.8\,e^{-t/0.14} + 9.3\,e^{-t/2.96} + 8.1\,e^{-t/19.7}$

The DF signal during dark periods decays quicker than the variable fluorescence (Figs. 4 and 5b). These DF decays can be fitted as sums of 4-exponentials (Table 1). In the sub-ms time interval DF decay is determined by electron transfer reactions in PSII donor side (Zaharieva *et al.*, 2010) but the slower ms-components correlate with PSII acceptor site redox reactions and in this way to PF dark relaxation kinetics (Table 1).

To analyze the relation between Q_A redox state and relative DD values, we compared the OJIP transients in dark adapted bean leaves and in samples pre-illuminated for 1 s with saturating actinic light (Fig. 6). One-second pre-illumination reduces the PSII quinine acceptors and as a result modifies the OJIP transients. In pre-illuminated samples the DDs are suppressed during J-I phase and appear again during I-P transition when the electron transport through PSI starts and the plastoquinone pool is re-oxidated (as judged from MR_{820} data, not shown). As seen in Fig. 6 the course of the absolute DDs values is reciprocal to OJIP-transients in J to P region for dark adapted leaves and from I to P only for the pre-illuminated leaves.

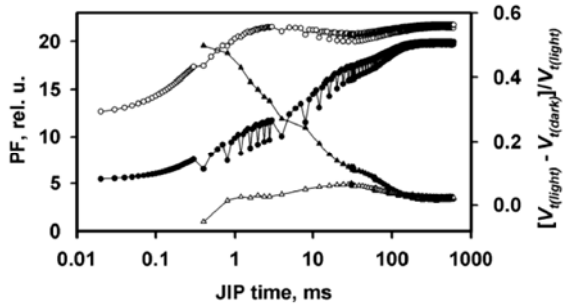

Fig. 6 Left scale: OJIP transients induced in dark adapted sample (closed circles) and again after 1 s in dark interval (open circles). Right scale: DD values for the first (closed triangles) and the second hit (open triangles). The DD values after 0.1 ms dark are normalized to DD after 1 ms dark pulse.

Using this data we can now follow the correlation between the redox level of the quinone acceptors and DD values by presentation of DD data as a function of (1-V_t) value (Fig. 7). Both for the dark-adapted and pre-illuminated samples the data show a good linear dependence, except for the points from the initial phase of the OJIP transients.

We can conclude that:

1. Application of short (0.1 or 1 ms) "dark pulses" during illumination of leaf discs does not change significantly the shape of chlorophyll fluorescence transient.

2. In dark adapted samples the relative value of amplitude of dark induced fluorescence drop is inversely proportional to concentration of the reduced states of the PSII quinone acceptor, Q_A^- in a wide region of values of relative variable fluorescence, V_t (from 0.3 to about 1.0).

3. PF dark relaxation is slower than DF dark relaxation and its kinetics is dependent on the initial level of oxidation of electron carriers in PSII acceptor side.

4. The DD analysis provides additional opportunities for evaluation of the photosynthetic electron transport chain in living plant tissues.

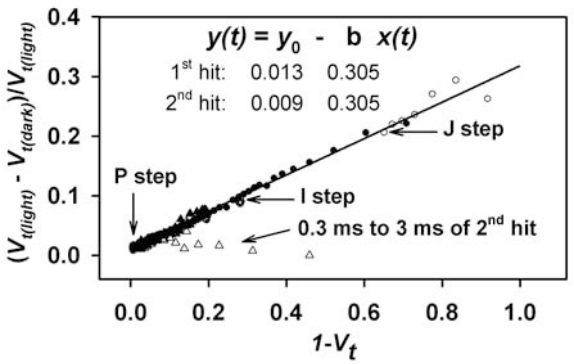

Fig. 7 Correlation between the relative DD and the relative variable fluorescence values ($1 - V_t$). The data is recalculated from Fig. 6. The DD values after short dark period (0.1 ms - open symbols) are normalized to 1 ms dark duration (closed symbols). The DD values for the first hit are shown with circles and for the second hit – with triangles.

Acknowledgements

VG, MG, MK and IZ thank the National Science Fund for the financial support (Project № DO 02-137 / 15.12.2008). RJS and SQ acknowledge support by China 863 Program (2006AA10A214) and 111 Program (B07030). R.J.S acknowledges support by the Swiss National Science Foundation, Project Nr: 200021-116765.

References

Goltsev V, Yordanov I (1997) Mathematical Model of Prompt and Delayed Chlorophyll Fluorescence Induction Kinetics. Photosynthetica 33: 571-586

Goltsev V, Zaharieva I, Chernev P, Strasser R (2009) Delayed Fluorescence in Photosynthesis. Photosynth.

Res. 101: 217-232

Strasser RJ (1978) The Grouping Model of Plant Photosynthesis In: Chloroplast Development, G Akoyunoglou, JH Argyroudi-Akoyunoglou (eds.), Elsevier/North-Holland Biomedical Press, pp. 513-524

Strasser RJ, Tsimilli-Michael M, Qiang S, Goltsev V (2010) Simultaneous in Vivo Recording of Prompt and Delayed Fluorescence and 820 nm Reflection Changes during Drying and after Rehydration of the Resurrection Plant Haberlea Rhodopensis. Biochim. Biophys. Acta 1797: 1313-1326

Zaharieva I, Grabolle M, Chernev P, Dau H (2010) Water Oxidation in Photosystem II: Energetics and Kinetics of Intermediates Formation in the $S_2 \rightarrow S_3$ and $S_3 \rightarrow S_0$ Transitions Monitored by Delayed Chlorophyll Fluorescence (this Issue)

Photosynthetic Measurements with the Idea Spec: an Integrated Diode Emitter Array Spectrophotometer/Fluorometer

Christopher C Hall, Jeffrey Cruz, Magnus Wood, Robert Zegarac, Dustin DeMars, Joel Carpenter, Atsuko Kanazawa, David Kramer

Washington State University, Institute of Biological Chemistry, Pullman, WA;
Michigan State University, Plant Research Lab, East Lansing, MI.

Abstract: In vivo spectrophotometry, a non-invasive, nondestructive technique that relies on the leaf's endogenous chromophores, has become an essential tool for understanding the photosynthetic response of plants to environmental stresses. Based on the pulsed-light spectrophotometer approach, and capitalizing on recent advances in optics and light emitting diode (LED) technology, we have developed an in vivo spectrophotometer capable of measuring absorbance changes of less than 3×10^{-5} absorption units and microsecond time resolution. The instrument can also simultaneously measure chlorophyll (or other) fluorescence signals with background or saturating actinic light, *e.g.* PAM fluorometry or induction curves, to give measurements of antenna and photosystem II efficiencies. We use a solid-state light source containing multiple LEDs for both measuring and actinic stimulation and direct the light to the leaf through non-focusing optics, allowing near-simultaneous multi-wavelength measurements useful for signal deconvolution.

Keywords: Spectrophotometry; Fluorometry; Spectroscopy; Electron transfer chain; Light reactions

Introduction

In vivo spectroscopy and fluorometry has been used to measure the photosynthetic light reactions in a broad variety of species (including plants, algae and photosynthetic bacteria) and under a wide range of environmental conditions. Numerous parameters can be probed without disturbing the sample, including: (1) electron flux rates through Photosystem (PS) 1, PS2, cytochrome (cyt) b_6f complex and plastocyanin, (2) proton flux rates through the chloroplast ATP-synthase, (3) proton motive force (*pmf*) storage, (4) xanthophyll cycle and 5) photoprotective exciton quenching (Cruz *et al*., 2001; Kramer *et al*., 2004; Baker, 2008). These measurements are made feasible by the presence of endogenous probes, whose absorbance or fluorescence spectra are sensitive to the specific photosynthetic states (for review see Kramer and Crofts, 1990).

Special challenges are posed by measuring photosynthetic systems by fluorometry and spectrophotometry: (1) Exceptional sensitivity is required to obtain sufficient signal-to-noise ratios. (2) The measuring and actinic lights must be evenly distributed across the surface of the leaf to avoid an orientation bias in the measurements. (3) Since light is a substrate for plant growth, the measuring light must be maintained at a low integrated intensity to avoid actinic effects (Joliot *et al*., 1980; Kramer *et al*., 1998). (4) To obtain useful information about the network of processes that contribute to the energy budget and regulation of photosynthesis, it is often necessary to measure multiple processes nearly simultaneously. (5) Measurements of many phenomena require deconvolution of multiple spectroscopic signals under essentially identical conditions. (6) Useful information can be obtained by comparing in vivo with well-controlled in vitro systems. (7) Important information can be gathers by observing phenomena over very wide range of time scales.

Some of these challenges have been addressed in previous spectrophotometric instruments. For example, short, high-intensity measuring pulses are used to achieve high signal to noise ratios without the

measuring beam itself becoming significantly actinic, and diffusing optics are used to deliver even illumination (Kramer *et al*., 1998; Sacksteder *et al*., 2001; Bína *et al*., 2006), while a multi-wavelength kinetic spectrophotometer was described by Klughammer and Schreiber (Klughammer *et al*., 1998). In this paper, we describe the development of a spectrophotometer design that incorporates non-focusing optics with an array of high flux LEDs to supply measuring pulses and actinic illumination that specifically address all of these issues.

Materials and Methods

Plants and growth conditions: *Arabidopsis thaliana* was grown under a photosynthetically-active photon flux density (PPFD) 80–100 μmol photons m^{-2} sec^{-1} white light with a 16:8 day:night cycle at 20 °C and 25% relative humidity. Tobacco was grown in a green-house under PPFD of 300–400 μmol photons m^{-2} sec^{-1}, 14:10 day night cycle with average temperature of 25 degrees Celsius and 40% humidity. For experiments, individual leaves on intact plants were gently clamped between 2 black foam rings with the upper surface of the leaf facing the dephasing/beam splitter light guide. Smaller leaves (~0.5 cm in diameter) required an alternative optical set-up (Fig. 1, small leaf adaptor).

The Integrated Diode Emitter Array spectrophotometer/fluorometer (IDEAspec) actinic illumination and intense, pulsed measuring lights were supplied by an array of light emitting diodes, incorporated into a single head. Measurements requiring pulses in the visible light spectrum used Luxeon III, high flux LEDs (Philips Lumileds, New York), with 6 degree collimating optics (Polymer Optics, UK) mounted on a custom printed circuit board. Narrow band interference filters (Omega Optical and Andover Optics) of the appropriate wavelengths were used to achieve more spectrally defined measuring pulses. In addition, up to six 5 mm LEDs could be fixed on the filter mount, for near IR measurements and/or for far red (740 nm) illumination (Roithner LaserTech, Austria). Actinic light was provided by red (Luxeon III) LEDs with intensity controlled by the computer.

A Compound Parabolic Concentrator (CPC) was fabricated from clear cast acrylic based using the principles described by Welford and Winston (1989) with a 50 mm entry aperture and 10 mm exit aperture. The CPC was used to combine, homogenize and concentrate light from the LEDs into a single spot. A modified acrylic light guide was added to the optical light path to act as a both a 'beam splitter' to divert light to the reference detector and a 'dephasing' element to minimize residual image formation or directional bias on the sample surface. Actinic light was optically filtered from measuring light using appropriate glass filters (*e.g.* Schott glass BG-18 filters for absorbance measurements between 460 and 572 nm; RG-9 for chlorophyll *a* fluorescence; and RG-780 for near IR absorbance measurements). A linear actuator was used to automate switching between 2 actinic filters and was controlled using by computer.

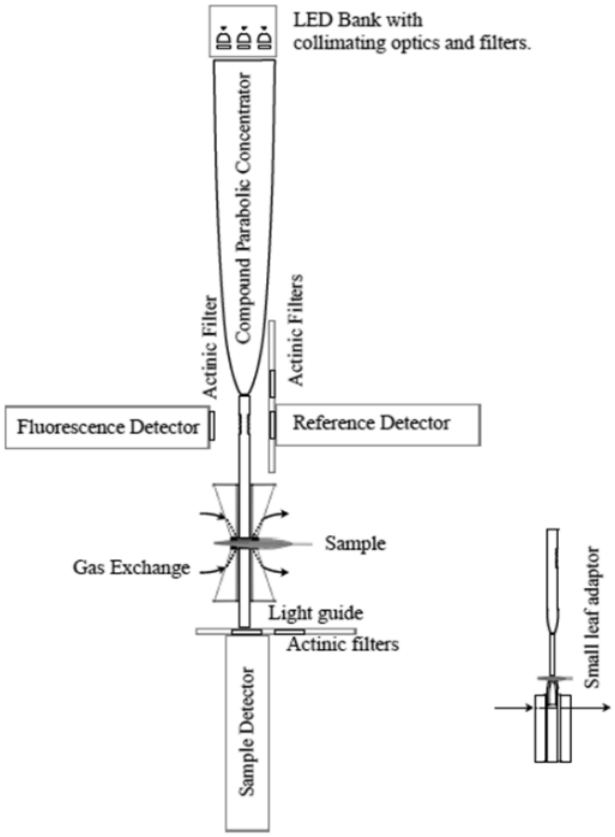

Fig. 1 Schematic of the optical layout of the IDEA spectrophotometer. Collimated light from high intensity LEDs are focused into the light guide by the compound parabolic concentrator. The light guide splits a fraction of this light to the reference detector and reflects some of the light emitted by the sample to the fluorescence detector. For small leaf measurements, the light guide is replaced with the small leaf adaptor.

Transmitted light/fluorescence was measured by 10 mm × 10 mm silicon PIN photodiodes (Hamamatsu), residual actinic and/or background light was electronically removed from the pulsed measuring light via AC filtering, as described previously.

Amplified analog signals were transiently stored on sample and hold amplifiers until digitally converted with 16-bit resolution. Actinic and measuring events were timed precisely using a high-resolution timing system developed in our laboratory.

The script-based UbiSpec software package was developed for the IDEAspec using Microsoft Visual Basic Express (2005, 2008, Microsoft, Redmond WA) and integrated with commercial and in-house device libraries.

Results and Discussion

Fluorescence measurements

Chlorophyll *a* fluorescence was measured in *Arabidopsis*. Fig. 2 shows a typical fluorescence induction experiment, a compilation of 13 individual fluorescence traces, using red (625 nm) light for actinic illumination and saturation pulses, and blue-green (505 nm) light for measuring pulses. Fluorescence yields were measured for the dark adapted state before (F_0) and during a saturating actinic flash (F_M), at steady state before (F_S), during (F_M') and after the saturating flash (without actinic light and in far red light to oxidize the electron transfer chain, (F_0') and recovery of the fluorescence maximum (F_M") in the dark. From these yields, photosynthetic parameters may be estimated including, quantum yield of photosynthesis (Φ_{II}), linear electron flux (LEF) through PSII, Non-photochemical quenching (NPQ), 'energy-dependent' quenching (q_E), photoinhibition (q_I) and reduction state of the plastoquinone pool (q_L).

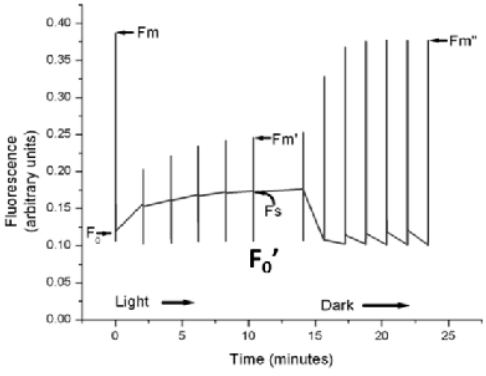

Fig. 2 Fluorescence induction of wild type *Arabidopsis thaliana*. Each vertical bar represents a fluorescence trace including measurements at background illumination (Fs), saturating illumination (Fm), and in the dark with far-red illumination (F_0').

The modular design of the IDEAspec allows fluorescence to be measured from either the incident surface or through the leaf, which provides important controls for experimental artifacts due to reabsorption (not shown), uneven light penetration and IR reflectance. Furthermore, the integrated LED head allows other measurements (*i.e.* absorption changes, as described below) to be made between fluorescence traces, without disturbing the sample. Since the same area on the leaf is surveyed under near identical conditions, correlations among fluorescence and absorbance data sets would be less subject to experimental error.

Absorbance change measurements

To demonstrate high-resolution absorbance measurements, proton flux and *pmf* were probed by measuring the using the electrochromic shift (ECS) signal at wavelengths around 520 nm. Fig. 3 shows dark interval relaxation kinetics (DIRK) collected in Arabidopsis, where steady state proton flux (v_H^+), *pmf* and thylakoid proton conductivity (g_H^+) are proportional to the initial rate of decay, the extent of decay and the inverse of the decay time, respectively. The ECS kinetics is highly resolved with millisecond time resolution and for changes ~3×10^{-5} absorption units (A) or less. Similar measurements are possible other photosynthetic reactions (not shown for brevity) including cytochrome b_6f (545, 554 and 572 nm) and photosystem I (810 and 900 nm). In addition, traces requiring time resolution as short as 10 microseconds, such as those arising from pulsed kinetics, are also possible.

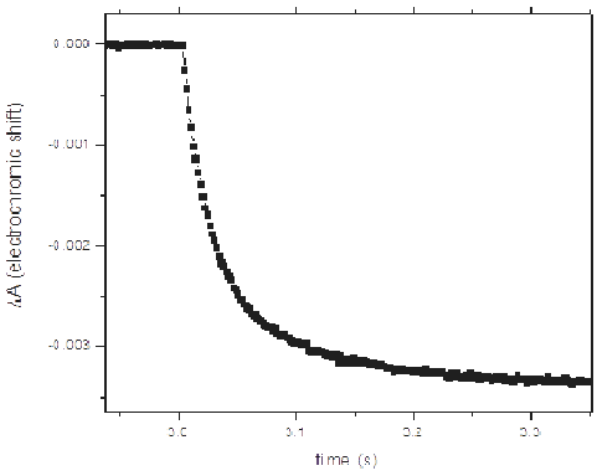

Fig. 3 Dark interval relaxation kinetic trace of the electrochromic shift signal in *Arabidopsis thaliana* from absorption of 520 nm measuring light. 16 traces were averaged to reduce noise.

Multi wavelength traces

Measurements of phenomena occurring over longer time scales require careful deconvolution from multiple signals with overlapping kinetics and spectral contributions. The data in Fig. 4 demonstrates the effective use of IDEAspec for such applications. A major advantage of the IDEAspec is that multiple LEDs may be pulsed in rapid succession for near simultaneous measurement of the corresponding wavelengths, minimizing deconvolution errors resulting from random drift in the contaminating signal. Shown in Fig. 4 (upper panel) is a long dark-interval relaxation kinetics (DIRK), experiment in which absorbance changes at 505, 520 and 535 nm were measured during a one minute dark interval and used to determine the partitioning of *pmf* into electric field (Δψ) and ΔpH components (Cruz *et al*., 2001). Deconvolution of the ECS signal using all three wavelengths yields the characteristic, multiphasic ECS decay and dark relaxation trace (Fig. 4, lower panel) which shows the collapse and inversion of Δψ during the initial decay and subsequent relaxation of the inverted Δψ to a dark steady state. In addition to *pmf* partitioning, multi-wavelength measurements are useful for probing induction of the xanthophyll cycle at 505 nm and induction of q_E at 535 nm (Zhang *et al*., 2010; Takizawa *et al*., 2007).

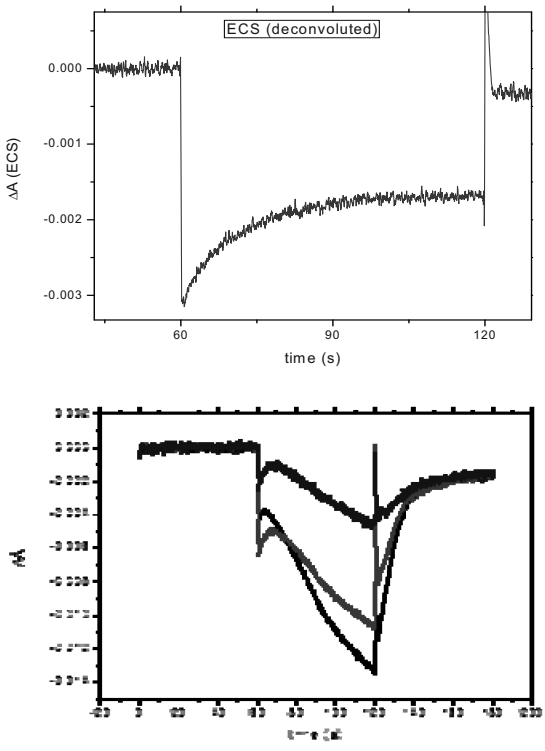

Fig. 4 Parsing the contributions of Δψ and ΔpH to the proton motive force (pmf) in *Arabidopsis thaliana*. The top panel shows the absorption signals at 505 nm, 520 nm, and 535 nm. The bottom panel shows the deconvoluted electrochromic shift (ECS) signal. During the dark period, the pmf collapses and then partially recovers. The fraction recovered is proportional to the ΔpH component of the pmf and the remainder is the Δψ component (Cruz *et al*., 2001).

Conclusions

The IDEAspec builds upon previous generations of essential photosynthesis instrumentation, combining fluorometry and absorbance spectrophotometry into a single flexible and modular instrument. The script based UbiSpec software allows the user to customize multiple measurement parameters as needed for any given experiment. The experiments presented here represent just a small fraction of all the experiments that we have performed on the IDEAspec and many more are feasible.

Acknowledgements

This work was supported by Division of Chemical Sciences, Geosciences and Biosciences, Office of Basic Energy Sciences of the U.S. Department of Energy, grant DE-FG02-04ERI5559.

References

Baker NR (2008) Chlorophyll Fluorescence: a Probe of Photosynthesis in Vivo. Annu. Rev. Plant Biol. 59: 89-113

Bína D, Litvín R, Vácha F, Šiffel P (2006) New Multichannel Kinetic Spectrophotometer–Fluorimeter with Pulsed Measuring Beam for Photosynthesis Research. Photosynthesis Res 88: 351-356

Cruz JA, Sacksteder CA, Kanazawa A, Kramer DM (2001) Contribution of Electric Field (Δψ) to Steady-State Transthylakoid Proton Motive Force (pmf) in Vitro and in Vivo. Control of pmf Parsing into Δψ and ΔpH by Ionic Strength. Biochemistry 40(5): 1226-1237

Joliot P, Beal D, Frilley B (1980) A New Spectrophotometric Method for the Study of Photosynthetic Reactions. J. de Chimie Physique et de Physico - Chimie Biologique 77(3): 209-216

Klughammer C, Schreiber U (1998) Measuring P700 Absorbance Changes in the Near Infrared Spectral Region with a Dual Wavelength Pulse Modulation System. Photosynthesis: Mechanisms and Effects, Vols I-V: 4357-4360

Kramer DM, Crofts AR (1990) Demonstration of a

Highly-Sensitive Portable Double-Flash Kinetic Spectrophotometer for Measurement of Electron Transfer Reactions in Intact Plants. Photosynthesis Res 23: 231-240

Kramer DM, Avenson TJ, Edwards GE (2004) Dynamic Flexibility in the Light Reactions of Photosynthesis Governed by Both Electron and Proton Transfer Reactions. Trends in Plant Science 9(7): 349-357

Kramer DM, Sacksteder CA (1998) A Diffused-Optics Flash Kinetic Spectrophotometer (DOFS) for Measurements of Absorbance Changes in Intact Plants in the Steady-State. Photosynthesis Res 56: 103-112

Sacksteder CA, Jacoby ME, Kramer DM (2001) A Portable, Non-Focusing Optics Spectrophotometer (NoFOSpec) for Measurements of Steady-State Absorbance Changes in Intact Plants. Photosynthesis Res 70: 231-240

Takizawa K, Cruz JA, Kanazawa A, Kramer DM (2007) The Thylakoid Proton Motive Force in Vivo. Biochimica et Biophysica Acta-Bioenergetics 1767(10): 1233-1244

Welford WT, Winston R (1989) High Collection Nonimaging Optics. Academic Press. San Diego: 53-95

Zhang R, Wise RR, Struck KR, Sharkey TD (2010) Moderate Heat Stress of Arabidopsis Thaliana Leaves Causes Chloroplast Swelling and Plastoglobule Formation. Photosynthesis Res 105(2): 123-134

Crystal Structure of Ferredoxin-NAD(P)$^+$ Reductase from the Green Sulfur Bacterium *Chlorobaculum Tepidum*

Daisuke Seo[1], Norifumi Muraki[2,3], Tomoo Shiba[2], Takeshi Sakurai[1], Genji Kurisu[3,4]

[1]Division of Material Science, Graduate School of Science and Technology, Kanazawa University, Kakuma, Kanazawa, Ishikawa 920-1192, Japan;
[2]Department of Life Sciences, University of Tokyo, Komaba, Meguro-ku, Tokyo 153-8902, Japan;
[3]Institute for Protein Research, Osaka University, Suita, Osaka 565-0871, Japan;
[4]Department of Macromolecular Science, Graduate School of Science, Osaka University, Toyonaka, Osaka 560-0043, Japan.

Abstract: Green sulfur bacterium *Chlorobaculum tepidum* contains a novel type of ferredoxin-NAD(P)$^+$ reductase (FNR) with high amino acid sequence homology to the NADPH-thioredoxin reductase (TdR) from prokaryotes. In this study, we determine the crystal structure of *C. tepidum* FNR by X-ray crystallography. *C. tepidum* FNR retains its structural topology with *E. coli* TdR but possesses several characteristic features that is absent in TdR. Each protomer is composed of two nucleotide binding domains, FAD-binding and NAD(P)$^+$-binding. The two domains are connected by a hinge region. Homo-dimeric *C. tepidum* FNR shows an asymmetric domain orientation between two protomers. The observed C-terminal sub-domain covers the re-face of the isoalloxazine ring of FAD prosthetic group. The C-terminal sub-domain includes the stacking Phe337 on the re-face of the isoalloxazine ring of the FAD. On the si-face, Tyr57 residue is stacked on. The two stacking ring systems are positioned almost parallel with respect to isoalloxazine ring at a distance of 3.5 Å. Such a configuration of stacking of two aromatic rings is absent in TdR but found in plastid-type FNRs, suggesting these structural characteristics are indispensable for the FNR reaction. To elucidate the function of these structural characteristics, mutational analysis was performed.

Keywords: Ferredoxin; Flavor protein; Electron transfer; Green sulfur bacteria

Introduction

Green sulfur bacterium *Chlorobaculum tepidum* is a moderate thermophilic anaerobe. The bacterium carries out a non-oxygenic photosynthesis with inorganic sulfur compounds as an electron donor. *C. tepidum* possesses a type I photoreaction center (RC) which can directly photoreduce ferredoxins (Fd) (Seo *et al*., 2001). The subsequent reduction of NAD(P)$^+$ to NAD(P)H is catalyzed by a Fd-NAD(P)$^+$ reductase ([EC 1.18.1.2], [EC 1.18.1.3], FNR) as found in chloroplast. Despite the physiological similarity, amino acid sequences of *C. tepidum* Fd and FNR are phylogenetically unrelated to those of their counterparts in chloroplast.

C. tepidum FNR (*Ct*FNR) exists as homo-dimer under physiological conditions and displays significant homology with NADPH-dependent thioredoxin reductase (TdR) from prokaryotes rather than conventional FNRs in amino acid sequence level (Seo and Sakurai, 2002). In this study, we have examined the crystal structure of *Ct*FNR by X-ray crystallography. Crystal structure analysis revealed several unique structural features. To elucidate the function of these structural characteristics, mutational analysis of Phe337 and residues in a hinge region has been performed.

Materials and Methods

*Ct*FNR was overexpressed, purified and crystallized as described previously (Muraki *et al*., 2008). Selenomethionine (SeMet)-substituted *Ct*FNR was obtained using the methionine auxotroph strain of *E. coli* B834(DE3) and LeMaster medium supplemented with *L*-SeMet (Wako Pure Chemical Industries,

Japan). Crystallization conditions for native and SeMet substituted *Ct*FNRs were screened with the hanging-drop vapor diffusion method at 293 K. The fine crystals of both FNRs were obtained using 0.1 mol MES buffer pH 6.0 containing 20% (w/v) PEG 4000 and 0.1 mol ammonium sulfate as precipitant. For data collection under cryogenic conditions, crystals were briefly soaked in a reservoir solution containing 15% (v/v) glycerol. Diffraction data from crystals of native and SeMet substituted *Ct*FNRs were collected by the oscillation method using synchrotron radiation at beamline NW-12 of the Photon Factory (Tsukuba, Japan). Diffraction images were collected at 100 K using an ADSC Quantum210 CCD detector and Rigaku GN2 cryosystem. The data were processed and scaled using the HKL2000 program package. Atomic coordinates and structure factors are deposited in the Protein Data Bank under the accession code 3AB1.

Replacement of Phe337 to Tyr, His and Ser was carried out with Quikchange methods using the pETBlue-1-CT1512 plasmid as a template (Muraki *et al*., 2008). Purification procedure of wild type (WT) and mutated FNRs were described in (Muraki *et al*., 2008). Diaphorase assay was performed with $K_3[Fe(CN)_6]$ as an electron acceptor (Seo *et al*., 2009).

Results

Crystal structure of CtFNR

The crystal structure of *Ct*FNR was determined by the single wavelength anomalous diffraction method with SeMet substituted recombinant protein. The final model of WT FNR was refined to a 2.4 Å resolution. In the crystal, two identical polypeptides exist in the crystallographic asymmetric unit forming a homo-dimer complex (Fig. 1). The N- and C-termini of each polypeptide chain (residues 1 to 12 of chain A and B, residues 349 to 360 of chain A and residues 331 to 360 of chain B) are disordered. Each protomer contains two Rossman-type nucleotide-binding folds building up domains for FAD- and $NAD(P)^+$-binding. The FAD-binding domain is composed of discontinuous regions of amino acid residues 13–131 and 262–329, whereas amino acid residues 134–258 form the NADPH-binding domain. These two domains are connected with a hinge region composed of two β-strands. The two protomers are attached at the surface of FAD-binding domain. The dimer interface of each protomer involves three α-helices α1, α3and α6, and one loop which are interacting to their counter-parts in the other protomer (Figs. 1and 2). At the surface of the cleft between the two domains, one FAD molecule is noncovalently bound in an extended form in each protomer.

Each nucleotide binding domains retain its structural topology with *E. coli* TdR (Lennon *et al*., 2000). In *Ct*FNR, an additional sub-domain is found at the C-terminal end region (Figs. 1 and 2). The observed C-terminal sub-domain is composed of the amino acid residues 329–348 comprising a helix α7. The C-terminal sub-domain covers the re-face of the isoalloxazine ring of FAD molecule of the opposite subunit (Figs. 1 and 3). An aromatic ring of the N-terminus residue Phe337 in the helix α7 formed strong π-π stacking on the re-face of the ring. Next Ser338 and Ser339 residues held hydrogen bonding to the O4 and N5 atoms of the ring. On the si-face of the ring, a phenol ring of Tyr57 residue stacks on. These two stacking aromatic-ring systems are positioned almost parallel orientation with respect to the isoalloxazine ring at a distance of 3.5 Å. Such a configuration is not found in TdR but found in plastid-type FNRs, suggesting these structural characteristics are indispensable for the FNR reaction. In order to elucidate the functional role of this FAD-stacking aromatic residue, we performed mutational analysis of the Phe337 residue.

Fig. 1 Ribbon representation of homo-dimeric *Chlorobaculum tepidum* ferredoxin $NAD(P)^+$ reductase. The FAD prosthetic group and side chains of Tyr57 and Phe337 residues are depicted in a stick representation.

A plausible complex of *Ct*FNR and $NADP^+$ based on TdR structure with $NADP^+$ suggests the distances between the nicotinamide C4 carbon and flavin N5 nitrogen are approximately 15 Å apart. Thus, a domain motion is required for catalysis as proposed in

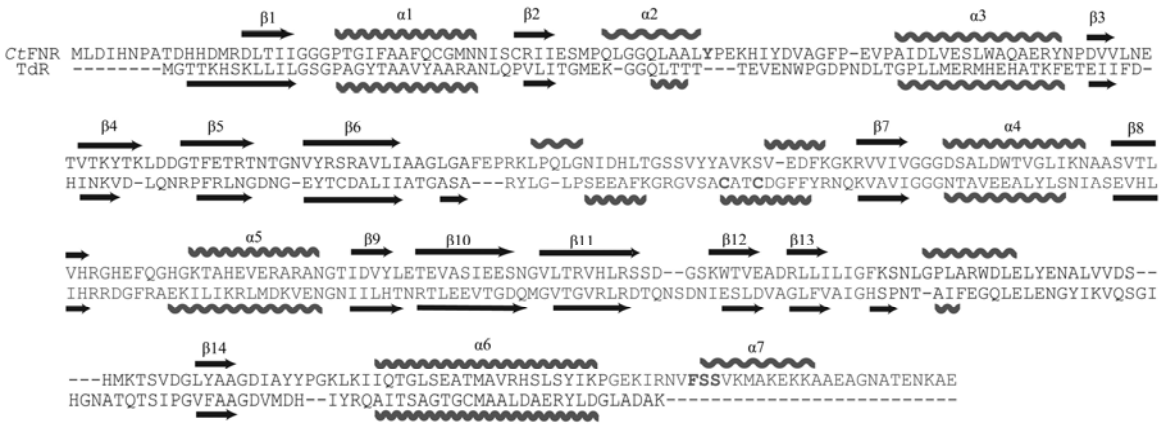

Fig. 2 Amino acid sequence alignment of *Ct*FNR and *E. coli* thioredoxin reductase.

E. coli TdR (Lennon *et al*., 2000). As no direct contact between the NAD(P)H- and FAD-binding domains has been observed and actually obtained crystal structure of homodimeric *C. tepidum* FNR shows an asymmetric domain orientation between two protomers, offering possibility for domain motion. In order to assess the importance of the flexible domain motion, we replaced the three conservative residues in hinge region, Phe132, Gly260 and Gly266, to Pro and tested their effects on the catalytic activities.

Spectral and Enzymatic properties of CtFNR and its variants

To investigate into the functional role of the Phe337 residue in the C-terminal subdomain and the hinge region, mutational analysis was performed. Effect of mutation on the reactivity with NADPH was evaluated by diaphorase assay with ferricyanide as an electron acceptor.

UV-visible spectra of the Phe337Ser, Phe337Tyr and Phe337His variants revealed that replacement of Phe337 in *Ct*FNR results blue shifts of transition bands of FAD prosthetic group by 5–7 nm against those of WT *Ct*FNR. These shifts presumably arise from alterations in the isoalloxazine ring environment upon replacement of Phe337. However, the replacements of Phe337 hardly affected on the reactivity with NADPH (k_{cat} values of ~ 300 s^{-1}).

Phe132Pro, Gly260Pro and Gly266Pro variants exhibited almost same UV-vis absorption properties for WT *Ct*FNR. However, diaphorase activities of Gly260Pro were drastically diminished (k_{obs} value of 4.5 s^{-1} at 1 mmol NADPH) while the Gly266Pro variant showed a considerable increase in K_m value (660 μM) and decrease of k_{cat} value (120 s^{-1}) for NADPH compared to the wild-type enzyme. Interestingly, the Phe132Pro mutant did not display any drastic change in kinetic parameters. Both Gly260 and Gly266 are present in the downstream β-strand of the anti-parallel β-sheet that comprises the hinge region connecting the two functional domains. The upstream β-strand is three residues longer and the downstream is one residue longer than those of *E. coli* TdR (Fig. 2). Differential hinge length between two homologous enzymes could explain this result.

Discussions

The FAD-stacking aromatic side chain is ubiquitously found among oxidoreductases of flavoenzyme family. In the case of *Ct*FNR homologues, the residue varies like Phe in *Ct*FNR, His in *Bacillus subtilis* FNR and Tyr in *Rhodopseudomonas palustris* FNR, while Tyr is conserved in almost all plant-type FNRs. In the case of *E. coli* TdR, the re-face of the isoalloxazine ring of FAD is always occupied by the redox-active functional groups; the loop containing the redox-active disulfide (Cys135–Cys138) in the FO state of TdR or the pyridine ring of bound $NADP^+$ analogue in the FR state of TdR (Lennon *et al*., 2000). Different configuration around the isoalloxazine ring suggests that stacking aromatic residues are functionally important in FNR reaction. In this study, site-directed mutagenesis of *Ct*FNR indicated that interaction with the FAD-stacking Phe337 influenced the microenvironment of isoalloxazine ring, but enzymatic activities of Phe337 variants of *Ct*FNR did not exhibit drastic changes as reported for the plant-type FNRs. This is probably due to hydrogen bondings from the adjacent Ser338 and Ser339 in *Ct*FNR to the isoalloxazine ring (Fig. 3), which helps maintain the interaction between the C-terminal sub-

domain and FAD. More precise studies on these homoplastic-like feature are required to understand its functional role in each NAD(P)H-dependent enzyme.

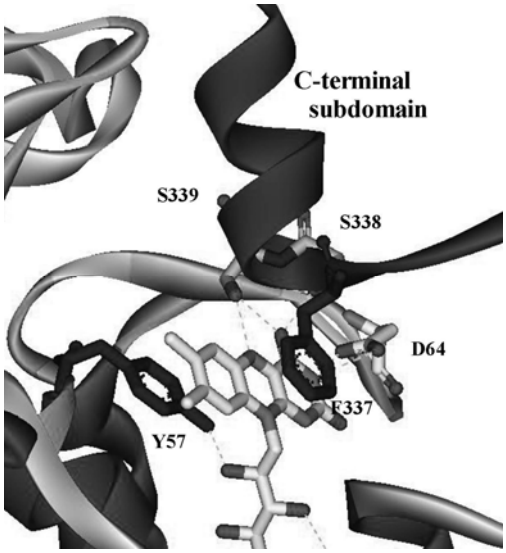

Fig. 3 Close-up view of the environment around the isoalloxazine ring of the FAD prosthetic group in *Ct*FNR.

Mutational analysis of the flexible hinge region with Gly260Pro and Gly266Pro variants confirmed that the flexibility of hinge region is catalytically indispensable. The hinge region of both *E. coli* TdR and *Ct*FNR is composed of a single anti-parallel β-sheet, but differed in the length. In addition, the NAD(P)H domain of *Ct*FNR did not contribute to dimerization, whereas that of *E. coli* TdR has some inter-subunit interactions. These distinctive structural features of the domain interface could be one reason for the different trajectories of the domain rotation between two structurally related enzymes. During the catalytic cycle of *E. coli* TdR, two cysteine residues located in the NAD(P)H domain mediate the redox reaction between the FAD and a thioredoxin molecule. In the case of *Ct*FNR, direct electron transfer between FAD and the FeS cluster of Fd occurs, requiring a productive docking of Fd to *Ct*FNR. Therefore, *Ct*FNR may adopt a domain motion distinct from that of TdR. Determination of a productive Fd-FNR complex structure is needed to clarify this issue.

In addition to the structural comparison with analogous plant-type FNR and homologous *E. coli* TdR, mutational analysis on the FAD stacking aromatic residue and potentially flexible hinge showed the unique structural basis for the substrate binding of TdR-like FNR. Recently, some *Ct*FNR homologues have been found and biochemically characterized (Seo *et al*., 2009, Mandai *et al*., 2009). Amino acid sequence alignments of these enzymes displayed that all homologous possess the C-terminal sub-domain and have the same length of hinge region connecting the two functional domains. In the dimeric *Ct*FNR structure, one of the two C-terminal sub-domains is mobile and could not be seen in the X-ray structure. Mobility of the C-terminal sub-domain might be important to make way for the nicotinamide ring stacking required for a hydride ion transfer and sometimes to shield the reduced FAD from the bulk solvent. It could be possible that the rotation of NAD(P)H domain is reciprocally correlated to the displacement of the mobile C-terminal sub-domain. This is an interesting matter to be examined.

References

Mandai T, Fujiwara S, Imaoka S (2009) A Novel Electron Transport System for Thermostable CYP175A1 from Thermus Thermophilus HB27. FEBS J. 276: 2416-2429

Muraki N, Seo D, Shiba T, Sakurai T, Kurisu G (2008) Crystallization and Preliminary X-Ray Studies of Ferredoxin-NAD(P)$^+$ Reductase from Chlorobium Tepidum. Acta Crystallogr Sect F Struct. Biol. Cryst. Commun. 64: 186-189

Seo D, Tomioka A, Kusumoto N, Kamo M, Enami I, Sakurai H (2001) Purification of Ferredoxins and Their Reaction with Purified Reaction Center Complex from the Green Sulfur Bacterium Chlorobium Tepidum. Biochim. Biophys. Acta 1503: 377-384

Seo D, Sakurai H (2002) Purification and Characterization of Ferredoxin-NAD(P)$^+$ Reductase from the Green Sulfur Bacterium Chlorobium Tepidum. Biochim. Biophys. Acta 1597: 123-132

Seo D, Okabe, Yanase K, Kataoka K, Sakurai T (2009) Studies of Interaction of Homo-Dimeric Ferredoxin-NAD(P)H Oxidoreductases of Bacillus Subtilis and Rhodopseudomonas Palustris, that Are Closely Related to Thioredoxin Reductases in Amino Acid Sequence, with Ferredoxins and Pyridine Nucleotide Coenzymes. Biochim. Biophys. Acta 1794: 594-601

Lennon BW, Williams CH Jr, Ludwig ML (2000) Twists in Catalysis: Alternating Conformations of Escherichia Coli Thioredoxin Reductase. Science 289: 1190-1194

A Potential Function for the γ2 Subunit (atpC2) of the Chloroplast ATP Synthase

Kaori Kohzuma[1,2], Cristina Dal Bosco[3], Atsuko Kanazawa[1,2], David M Kramer[1,2*] , Jörg Meurer[3]

[1]Plant Research Laboratory, S-222 Plant Biology Building, Michigan State University, East Lansing, MI 48824-1312;
[2]Institute of Biological Chemistry, 339 Clark Hall, Washington State University, Pullman, WA 99164-6340;
[3]Ludwig-Maximilians-Universitat, Department Biologie I, Botanik, Menzingerstrasse 67, 80638 Munchen,
[*]Corresponding author. Tel. No. +1 517-432-0072; Fax No. +1 517-432-0072; E-mail: kramerd8@msu.edu.

Abstract: Higher plants possess two, distinct genes for the ATP synthase γ subunit, atpC1 and atpC2. In *Arabidopsis*, atpC1 is the predominantly expressed form, while atpC2 is only weakly expressed in photosynthetic tissues. There is no evidence that atpC2 it plays any role in energy transudation. Indeed, mutants lacking atpC1 are incapable of photoautotrophic growth, while those lacking atpC2 have no noticeable phenotype. To elucidate the possible function of these orthologs, we analyzed mutants expressing exclusively atpC1 or atpC2 in *Arabidopsis thaliana. In vivo* chlorophyll fluorescence and electrochromic shift (ECS) analyses demonstrated that both atpC1 and atpC2 can function in ATP synthesis, though even under a strong promoter, the activity of atpC2-containing ATP synthase was low. However, we observed a striking difference in the regulation of ATP synthase containing the two orthologs. With atpC1, the ATP synthase was inactivated in the dark, likely via oxidation of the regulatory γ subunit thiols. ATP synthase containing exclusively atpC2 showed no decrease in activity even after extensive dark adaptation. We propose that atpC2 may function to catalyze low levels of ATP-driven proton translocation in the dark, when the bulk of ATP synthase is inactivated, maintaining sufficient transthylakoid proton gradient to drive protein translocation or other processes.

Keywords: ATP symthase; γ subunit; AtpC2; *In vivo* spectroscopy

Introduction

Arabidopsis thaliana genome contains the *atpC1* (At4G04640) gene encoding the plastid ATP synthase γ subunit, and an additional gene, *atpC2* (At1G15700), encoding a homologous protein of unknown function and localization (Inohara *et al*., 1991). Knocking out atpC1 results in complete loss of photosynthesis, whereas knocking out atpC2 has little effect on photosynthetic competence under studied conditions (Dal Bosco, 2006; Dal Bosco *et al*., 2004). It has been reported that the atpC2 protein is targeted to the chloroplast (Dal Bosco, 2006). In this report we suggest possible function for atpC2, based on *Arabidopsis* mutants lacking atpC2 (*atpC2*) mutants lacking atpC1 but with over-expression of atpC2 (C2II and C2III), total gene expression level of atpC in C2II is similar to wild type and whole atpC mRNA of C2III is about 5 fold higher than wild type (Dal and Bosco, 2006).

Materials and Methods

Plant Material and Growth Conditions

Wild-type Arabidopsis thaliana and mutants (*atpC2*, C2II and C2III) were grown on soil under continuous light under 20–30 μmol photons m^{-2} s^{-1} photosynthetically-active radiation at 22 °C for 4 weeks.

In vivo Spectroscopic Assays

Energy-dependent exciton quenching (q_E) was estimated as described Kanazawa and Kramer (2001), with F_M' measured after establishment of steady-state photosynthesis (30 min), and F_M'' measured after

10 min of dark relaxation. Steady state, light-induced protom motive forth; *pmf* (ECSt) and the conductivity of thylakoid membrane to protons (g_{H+}), attributable to activity of the ATP synthase, was estimated from dark-interval relaxation kinetic (DIRK) changes in absorbance associated with the electrochromic shift (ECS) at a 520 nm, as described in (Kanazawa and Kramer, 2002; Cruz *et al*., 2005). Flash-induced relaxation kinetics (FIRK) experiments were performed on intact leaves or infiltrated leaf disc described in Kohzuma *et al*. (2009).

Equilibrium Redox Titrations

Fully expanded detached leaves were vacuum-infiltrated with varying ratios of oxidized and reduced 20 mmol DTT solutions (Wu *et al*., 2007) for 30 min in darkness. ΔA_{520} FIRK measurements were carried out described as above. The equilibrium redox potential were calculated described as Wu *et al*. (2007).

Results and Discussion

Fig. 1 shows the light intensity responses of light-induced *pmf* (estimated by the ECSt parameter, top panel), 'energy-dependent' exciton quenching (q_E, middle panel) and thylakoid proton conductivity (estimated by the g_{H+} parameter) which reflects ATP synthase activity (bottom panel) (Kanazawa and Kramer, 2002; Avenson *et al*., 2005; Cruz *et al*., 2005). The responses of *pmf* and q_E were larger in the atpC2-expressed mutants increased significantly during actinic light intensity, compare to wild type and *atpC2.* The ATP synthase activity of atpC2-expressed mutants remained consistently lower than wild type and *atpC2*. However, western blot analysis showed that the overall ATP synthase protein levels were considerably lower in CII and CIII than in wild type or *atpC2* (data not shown). The ratios of g_{H+} / [ATP synthase] for wild type and the mutants were similar, within a factor of two, indicating that atpC2 (γ_2) can act as effectively as atpC1 (γ_1) in the ATP synthase.

We found dramatic differences in the regulation of ATP synthase containing the two orthologs. In wild type, ATP synthase is inactivated in the dark as the γ subunit regulatory thiol groups become oxidized (reviewed in Schwarz *et al*., 1997). This behavior is seen in the top panel of Fig. 2A, showing effects of dark adaptation on the decay of flash-induced ECS signals in wild type leaves, as previously described. In light-adapted leaves, the ECS decayed monotonically to baseline showing that with an active ATP synthase, protons pass rapidly through the ATP synthase even with a small *pmf*.

After dark-adaptation for 90 minutes, however, proton flux was dramatically slowed as the *pmf* decreased below a certain threshold level, as previously observed (Kramer and Crofts, 1989), reflecting the increased *pmf* activation threshold described by (Junesch and Grabber, 1985). The rate of ATP synthesis as a function of ΔpH in normal and dithiothreitol-modified chloroplasts.

A similar trend was observed in atpC2 (Fig. 2A, middle panel), indicating that eliminating atpC2 did not affect the regulation of ATP synthase activity. This result is consistent with the observed low expression level of atpC2 in photosynthetic tissues.

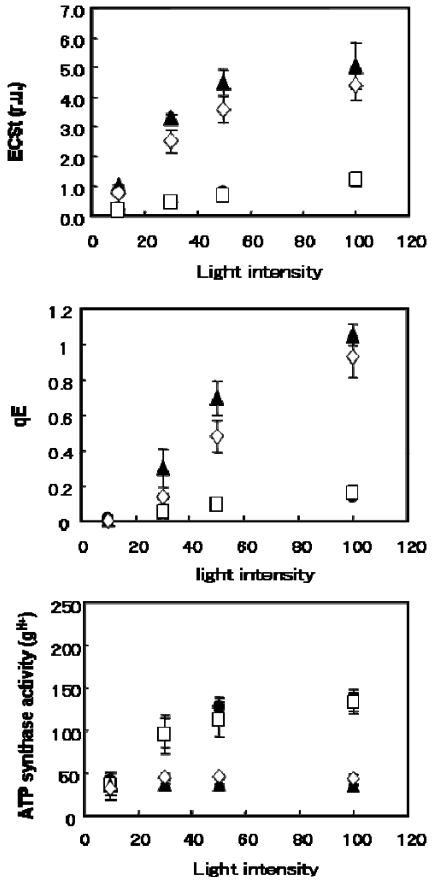

Fig. 1 Wild type (black circle), atpC2 (opened square), C2III (opened diamond) and C2II (closed triangle) are compared for difference in energy-dependent exciton quenching (q_E), light-induced *pmf* (ECSt) and proton conductivity across the thylakoid membrane (g_{H+}) versus light intensity. These parameters were estimated by chlorophyll fluorescence yield and ECS spectroscopy analysis.

In contrast, C2III, containing only γ_2, showed rapid, essentially monotonic ECS decay kinetics both in light- and dark-adapted leaves (Fig. 2A, lower panel), indicating that ATP synthase with γ_2 maintain ATP syntahse activation even after extensive dark acclimation.

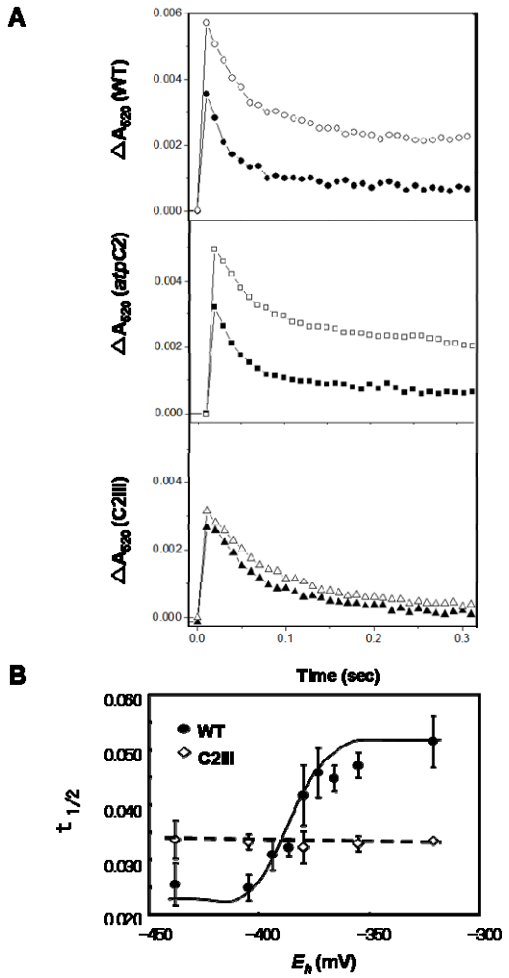

Fig. 2 A Trace of Flash induced relaxation kinetics (FIRK) in wild type (circles), *atpC2* (squares) and C2III (triangles). Two kinetic measurements were traced 10 sec later (black) and 90 minutes later (white) after pre-illumination for 2 minute. **B** Equilibrium redox titration (as in Wu *et al*., 2007) of thiol/disulfide regulatory groups in the γ-subunit of the chloroplast ATP synthase. The ΔA_{520} relaxation kinetics were measured and used to calculate the halftime of the kinetics.

To determine the cause of the altered light/dark regulation, we assayed the redox potential of ATP synthase γ-subunit S-S groups, in wild type and C2III mutant, via equilibrium redox titrations in situ, varying oxidized and reduced DTT at a combined total concentration of 20 mmol (Fig. 2). ATP synthase with atpC2 was not modulated by redox potential over the physiological range. In wild type, the ECS decay (reflecting ATP synthase activity) was fast with reduced dithiothrietol (DTT) but slow with oxidized DTT. The ECS decay of the mutant containing high atpC2 (C2III) was independent of DTT. We conclude that the ATP synthases containing atpC2 are not regulated by thiol/disulfide switching system because of altered thiol/disulfide redox potential. The *atpC2* protein (γ2) can functionally substitute for the atpC1 protein (γ1). However, γ2 appears to lack the thiol regulatory switch.

It is known that the ATP synthase is down-regulated in the dark, probably to prevent excessive ATP hydrolysis (Ort *et al*., 1990). However, some thylakoid proton gradient is maintained in the dark (Joliot and Joliot, 1989; Takizawa *et al*., 2007). In green algae, this gradient may be maintained by chlororespiration (Bennoun, 1982), but how this operates in higher plant chloroplasts is not clear.

We propose that atpC2 may function to catalyze low levels of ATP-driven proton translocation in the dark, (*i.e.* proton pumping into the lumen driven by ATP hydrolysis) when the bulk of ATP synthase is inactivated, possibly to maintain sufficient transthylakoid proton gradient to drive protein translocation via the TAT pathway or maintain ion gradients.

Acknowledgements

We are grateful to Dr. Alice Barkan (University of Oregon) for the CF_1-β antibodies. The work was supported by National Research Initiative competitive grant no. 2008-35318-04665 from the USDA National Institute of Food and Agriculture.

References

Avenson TJ, Kanazawa A, Cruz JA, Takizawa K, Ettinger WE, Kramer DM (2005) Plant Cell Environ 28: 97-109

Bennoun P (1982) Proc Natl Acad Sci 79: 4352-4356

Cruz JA, Avenson TJ, Kanazawa A, Takizawa K, Edwards GE, Kramer DM (2005) J Exp Bot 56: 395-406

Dal Bosco C, Lezhneva L, Biehl A, Leister D, Strotmann H, Wanner G, Meurer J (2004) J. Biol. Chem. 279: 1060-1069

Dal Bosco C (2006) Ph.D. Thesis, Universität München

Inohara N, Iwamoto A, Moriyama Y, Shimomura S, Maeda M, Futai M (1991) J. Biol. Chem. 266: 7333-7338

Joliot P, Joliot A (1989) Biochim. Biophys. Acta 975: 355-360

Junesch Grabber (1985) Biochim Biophys Acta 809: 429-434

Kanazawa A, Kramer DM (2002) Proc Natl Acad Sci USA 99: 12789-12794

Kohzuma K, Cruz JA, Akashi K, Hoshiyasu S, Munekage YN, Yokota A, Kramer DM (2009) Plant. Cell and Enviroment 32: 209-219

Kramer DM, Crofts AR (1989) Biochim Biophys Acta 976: 28-41

Ort DR, Grandoni P, Ortiz-Lopez A, Hangarter RP (1990) Perspectives in Biochemical and Genetic Regulation of Photosynthesis, pp. 159-173

Schwarz O, Schü"rmann P, Strotmann H (1997) J Biol Chem. 272: 16924-16927

Takizawa K, Kanazawa A, Cruz JA, Kramer DM (2007) Biochim Biophys Acta 1767: 1233-1244

Wu G, Ortiz-Flores G, Ortiz-Lopez A, Ort DR (2007) J. Biol. Chem. 282: 36782-36789

The Contribution of Light-Dependent Bicarbonate Uptake in Thylakoid Membrane Energization

*Zolotareva EK, Polishchuk OV, Semenikhin AV, Onoiko EB

M.G. Kholodny Institute of botany of the National Academy of Sciences of Ukraine Tereschenkivska str., 2, 01601, Kyiv-1, Ukraine.
*Corresponding author. E-mail: e.zolotareva@mail.ru.

Abstract: Illumination of the well stirred suspension of isolated spinach chloroplasts induced CO_2 uptake (up to 320 nmol CO_2/mg chlorophyll) from air phase over suspension. The process started immediately after onset of illumination, developed during 15–20 sec and completely reversed for the same time after switching off the light. Uncouplers (gramicidine D, NH_4Cl) inhibited the light-induced CO_2 uptake.

The value of light-induced CO_2 uptake was dependent on carbonic anhydrase (CA) activity and inhibited by CA inhibitors – lipophylic ethoxyzolamide (EZ) and water-soluble acetazolamide. The effect of exogenic bicarbonate and inhibitors of carbonic anhydrase on the rate of photophosphorylation was examined in the pH range 7.0–8.2. It was shown that exogenic bicarbonate (3–6 mmol) effectively stimulated photophosphorylation. The bicarbonate-induced enhancement of photophosphorylation showed a marked pH dependence, with the greatest response occurring at pH near 7.0. Both EZ and AZ reduced the stimulating effect of HCO_3^- on the rate of photophosphorylation. It is concluded that light-induced ATP synthesis depends not only on exogenic bicarbonate, but also on the activity of carbonic anhydrase that rapidly converts the forms of carbonic acid thereby facilitating protons removal from sites of their evolution.

Keywords: Proton transfer; Bicarbonate; Photophosphorylation; Carbonic anhydrase; Thylakoid membrane

Introduction

Thylakoid membranes contain a rather considerable amount (up to 1 μmol/mg Chl) of bicarbonate, bound with different affinity (Stemler, 1977; Klimov and Baranov, 2001). Tightly bound bicarbonate is absolutely necessary for retaining the functional activity of photosystem II (PS II), its removal leads to inhibiting the electron transfer reactions, as at the donor, as at the acceptor side of PS II. Localization point of the tightly bound bicarbonate, by a whole number of works, is PS II site between primary and secondary plastoquinone Q_A and Q_B acceptors. The functional role of the loosely bound HCO_3^- pool is not known.

The value of the proton motive force (PMF) in chloroplasts of higher plants under steady-state conditions is mainly determined by the difference of hydrogen ions concentration between the internal volume of thylakoids and the stromal space (Kramer *et al*., 1999; Dilley, 2000)

In the process of photosynthetic electron transport, protons are transferred inside thylakoids, and are also formed during the splitting of water molecules—directly in the intrathylakoid space (Kramer *et al*., 1999). It is known that illumination of dark-adapted chloroplasts leads to the alkalization of stroma and acidification of thylakoid lumen and it correlates with proton concentration and electrical potential differences across the thylakoid membrane. Massive transmembrane flow, in accordance with the electroneutrality principle, should be compensated by the transfer of other ions, different from H^+ ones. There are some experimental data (Hind *et al*., 1974) obtained by ion-specific electrodes and indicated that Cl^- and Mg^{2+} fluxes together compensate for most of the charge transferred as H^+.

Here, with the help of the infrared gas analysis we have demonstrated that the illumination of isolated chloroplasts leads to CO_2 uptake of up to 350 nmol/mg

Chl from the gas phase above the suspension, which is comparable with the number of protons uptaken during the illuminating of chloroplasts (ΔH^+) (Dilley, 2000) Results of present research showed bicarbonate transfer that can compensate light-induced proton uptake by isolated chloroplasts (so-called ΔH^+).

The aim of this work was investigation of possible role of light-induced CO_2 absorption in supporting the proton transport and thylakoid membrane energization.

Materials and Methods

Class C chloroplasts were prepared from market spinach (*Spinacea oleracea L.*) essentially as previously described (Zolotareva *et al*., 1997). The analyses were performed in the closed thermostated glass cell at 20 ^oC by help of infra red gas analyser (S151 type, Qubit Systems Inc., Canada) at the continuous air flow (350 ml/min), which held the 360–380 ppm CO_2. Reaction medium contained sorbitol (100 mmol), NaCl (10 mmol), tris-HCl (10 mol, pH 7.5) and chloroplasts equivalent to chlorophyll 10 μg/ml. Actinic light was 1,000 μmol quanta/m^2 s.

Photophosphorylation was carried out at room temperature in a mixture containing 20 mmol Tricine, 20 mol MES, 150 mmol KC1, 5 mmol MgCl, 30 mol glucose, 50 nmol phenazine methosulfate or 0.1 mmol methylviologen, 0.250 mmol ADP, 5 mmol Pi, and hexokinase (HK; 1 IU/ml). The mixture was illuminated for 2 min and the amount of ATP was determined enzymatically using glucose-6-phosphate dehydrogenase (G6PDH; 1.125 IU/ml) and NADP (0.5 mmol). The amount of NADPH formed is stoichiometrically equivalent with the amount of ATP and measured spectrophotometerically at 340 nm.

Results and Discussion

Fig. 1 shows, how the CO2 flow rate changes at illuminating the chloroplast suspension and after turning off the light. Light saturation of the process was achieved with the help of intensive stirring which was started concurrently with the light turn off.

In the absence of exogenic electron acceptor, the value of the light-induced CO_2 uptake is somewhat lower than in the presence of MV or PMS. After turning off the light, CO_2, in the amounts equivalent to the ones taken up in the light, was released into the gas phase. Total CO_2 uptake in different experiments varied from 0.1 to 0.35 μmol/mg Chl.

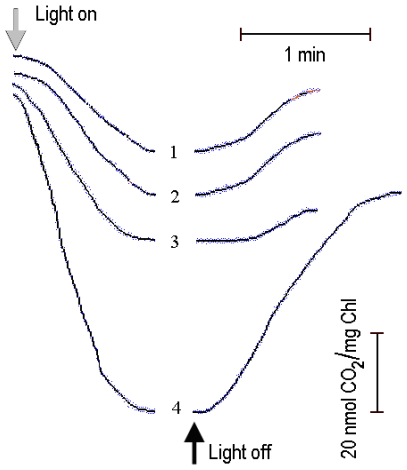

Fig. 1 Light-induced CO_2 uptake by isolated chloroplast suspension. Chlorophyll concentration was 1. 0.3 mg/ml; 2. 0.6 mg/ml; 3. 1.1 mg/ml; 4. 3.3 mg/ml.

The effect of CO_2 uptake by thylakoids was registered only in concentrated suspensions, the content of chorophyll in which constituted 2.5–3.5 mg Chl/ml. In more diluted suspensions CO_2 uptakes during illumination were not found. Data represented in Fig. 1 demonstrate how the level of light-dependent CO_2 uptake is decreasing in proportion to the suspension being diluted. These results might be explained by the fact that carbon dioxide invades the suspension in the process of simple diffusion, since, according to Fick's law, diffusion from the gas phase depends on the difference of concentrations between the solution and the ambient gas volume. It is evident that in the darkness, at the constant pH and temperature, carbon dioxide, diluted in the suspension, is in balance with CO_2 of the gas phase above the suspension. The illumination causes bicarbonate uptake from the solution, evidently, connected with transmembrane proton gradient formation.

Probable correlation of the light-induced uptake and the degree of energization of thylakoid membranes was checked in a series of experiments, the results of which are summed up in Table 1. In test experiments CO_2 uptake was registered in the presence of the PMS cyclic electron transport mediator. Injection of ionophore antibiotic gramicidin A, which was forming the channels and dissipating the transmembrane proton gradient, was also suppressing the light-induced CO_2, intake.

Table 1 The effect of uncouplers on light-dependent CO_2 (ΔCO_2) and H^+ (ΔH^+) uptake.
Chloroplast concentraton was equivalent to 2.7–2.9 mg Chl/ml. 0,1 mmol methylviologen was present as the electron acceptor.

Variant	Light-dependent CO_2 uptake (ΔCO_2), nmol CO_2/mg Chl	Light-dependent H^+ uptake (ΔH^+), nmol H^+/mg Chl
Control	140 ± 20	120 ± 15
+gramicidin A, 0.1 μmol	190 ± 22	80 ± 15
+gramicidin A, 1 μmol	0	0
NH_4Cl, 1 mmol	50 ± 12	70 ± 12
NH_4Cl, 5 mmol	0	0

Same results were also obtained during the experiments using protonophoric uncoupler NH_4Cl. The results allow to conclude that the integrity of the thylakoid membrane and forming a high level of transmembrane proton gradient represent the necessary conditions of the observed effect of CO_2 uptake during illumination of chloroplasts.

The effect of light-induced proton uptake developing at illumination of thylakoid membranes within the same time range was described about 50 years ago (Neumann and Jagendorf, 1964). This phenomenon, called ΔH^+ in the literature, is considered to be the integral part of thylakoids energization process. It is assumed that ΔH^+ value depends upon buffer capacity of thylakoid membranes (Walz *et al*., 1974). Comparison of the two processes—light-dependent proton and carbon dioxide uptakes—enables to detect their similarity. Isolated chloroplasts at illumination of slightly buffered suspension are uptaking 200–500 nmol H^+/mg Chl depending on the nature of electron acceptor. It was earlier noted not once that the number of thylakoid protein buffer groups, capable of binding protons in the physiological pH range, is not large; much smaller than the observed ΔH^+ value (Walz *et al*., 1974). In this respect, the probable role of light-dependent bicarbonate uptake by thylakoids is the increase of the system's buffer capacity necessary for the stabilization of the level of transmembrane proton gradient under conditions of active electron transport and release of a great number of protons inside thylakoids. The results of this work demonstrate that ΔH^+ and CO_2 uptakes during the illumination are interconnected processes. Nevertheless, it needs to point out that the experimental registration of CO_2 uptake, caused by chloroplasts energization, is possible only in very dense suspensions as distinguished from ΔH^+ which is easily registered in solutions of low buffer capacity and is disguised in solutions with a high content of buffer groups. Assuming that H^+ and CO_2 are uptaken simultaneously in parallel processes, it can be considered that CO_2 diffuses at that from the gas phase, while compensating the changes of soluble carbon dioxide forms in the suspension. In fact, the results of the work show that the light-induced CO_2 uptake is detected only under conditions of a low "CO_2-capacity".

Table 2 data demonstrate that the value of light-induced CO_2 uptake also depends upon carbonic anhydrase activity. Carbonic anhydrase inhibitors – lipophilic ethoxyzolamide (EZ) and hydrophilic acetazolamide (AZ)—have inhibited CO_2 uptake caused by illumination of the chloroplasts suspension. The degree of suppressing the reaction was dependent on the duration of the inhibitors activity: short incubation of reaction mixture after the injection of the inhibitor in the reaction medium was leading to partial inhibition, and the prolonged preincubation of thylakoids, that is during 3 h, in the presence of EZ or AZ—to the total inhibition of light-dependent CO_2 uptake by chloroplasts.

Table 2 The effect of carbonic anhydrase inhibitors on light-dependent CO_2 uptake in isolated chloroplast suspension.

	Light-dependent CO_2 uptake, nmol/mg Chl		
	Control	+ 0.4 mmol AZ	+ 0.4 mmol EZ
5 min incubation	260 ± 40	75 ± 10	81 ± 10
3 h incubation at 4 °C	230 ± 35	5 ± 2	4 ± 2

In the intact chloroplasts, capable of CO_2 photosynthetic uptake, the process of carbon dioxide fixation starts after 5–7 minutes of illumination. This phase of the process is called photosynthesis induction (Walker, 1973). It is shown in this work that class C chloroplasts, not capable of CO_2 fixation due to the absence of outer shells and loss of the necessary soluble components, also uptake a certain amount of CO_2 immediately after the illumination has started. The reaction develops during 30–40 s, and the amount of carbon dioxide uptaken by thylakoids reaches 320 mol CO_2/mg Chl.

The pool of CO_2 uptaken, evidently, remains bound with thylakoid membranes during the whole period of illumination and is released into the gas phase after the light has been turned off.

The process of light-induced CO_2 uptake is under control by carbonic anhydrase activity and its possible functional role consists in participation in forming of

the energized state of the thylakoid membrane and the stabilization of the pH level due to membrane buffer capacity increase. This conclusion is not in conflict with the assumption made earlier in a number of works about participation of CA thylakoids in the light-dependent replenishment of the stromal CO_2 fund, which provides for Rubisco activity (Raven, 1977).

As it well-known, light-dependent proton exchange supplies energy for photophosphorylation, forming transembrane proton gradient (ΔpH), which is converted in stationary conditions into ATP chemical energy in the process of photosynthetic photophosphorylation. The rate of photophosphorylation also depends on presence of bicarbonate in the medium, and accelerates at growing of its concentration in the suspension. (Cohen and MacPeek, 1980). The next part of the work was devoted to investigation of carbonic anhydrase role in stimulation of photosynthetic phosphorylation by exogenic bicardonate.

Data on the influence of 3–6 mmol $NaHCO_3$ upon non-cyclic photophosphorylation rate in the presence of MV, as electron acceptor, at different values of pH-media, are given in Table 3. In control conditions, non-cyclic ATP synthesis was registered at pH > 7.0, and maximum ATP synthesis rate was observed at pH .2, which corresponds with literary data. Dependency of photophosphorylation on pH substantially changed, where bicarbonate was added to the reaction medium. At that, maximum ATP synthesis rate did not differ from the control value, and was registered at same pH values, as at control one. In the presence of 6 mmol $NaHCO_3$ photophosphorylation rate significantly exceeded control values within the range of pH 6.5–8.0, and at medium pH < 7.7—by several times. Especially notably photophosphorylation was stimulated at pH .0 and lower. ATP synthesis rate at these pH values is very low in controlled conditions and grows by 4–8 imes after addition of $NaHCO_3$ to the concentration of 6 mol (Table 3). Stimulating influence of bicarbonate on photophosphorylation rate was diminishing in proportion to enhancement of reaction medium pH: at pH 7.6, addition of 6 mmol $NaHCO_3$ led to increase of ATP synthesis rate approximately by 2 times, and at pH 8.2—by 1.02–1.1 times. Stimulation of photophosphorylation with 3 mmol bicarbonate was less prominent, compared to the effect of 6 mmol bicarbonate. Photophosphorylation rate in the presence of 3 mmol bicarbonate constituted 130% and lowered to 106 and 109% against the control one with the addition of AZ and EZ, correspondingly.

Stimulation of photophosphorylation with exogenic added bicarbonate was effectively removed after a short-time (during 3 minutes) incubation of chloroplasts in the presence of carbonic anhydrase inhibitors—hydrophilic AZ or lipophilic EZ. Data given in Table 3 show that the effect of carbonic anhydrase inhibitors was most noticeable at pH 7.6. It is seen that in these conditions photophosphorylation rate, exceeding the control one by 2.3 times in the presence of 6 mmol bicarbonate, after addition of AZ or EZ decreased and amounted to 120% and 125% of the control value, correspondingly.

Table 3 Inhibition of pH-dependent bicarbonate stimulation of non-cyclic photophosphorylation by inhibitors of carbonic anhydrase acetazolamine (AA) and ethoxizolamide (EA).

Photophosphorylation rate, μmol/mg Chlh				
pH →		7.0 ± 0.05	7.6 ± 0.05	8.2 ± 0.05
Without added $NaHCO_3$	control	10 ± 1	90 ± 5	230 ± 11
	+ EA 0.5 mmol	12 ± 1	95 ± 5	225 ± 13
	+ AA 0.5 mmol	11 ± 1	89 ± 4	220 ± 12
+ 3 ммol $NaHCO_3$	control	16 ± 1	116 ± 6	250 ± 5
	+ EA 0.5 mmol	12 ± 1	98 ± 5	245 ± 5
	+ AA 0.5 mmol	13 ± 1	95 ± 5	240 ± 12
+ 6 ммol $NaHCO_3$	control	48 ± 3	210 ± 10	250 ± 12
	+ EA 0.5 mmol	20 ± 1	113 ± 6	228 ± 11
	+ AA 0.5 mmol	16 ± 1	108 ± 5	220 ± 11

Thus, carbonic anhydrase largely eliminated the stimulation of of photophosphorylation by exogenic bicarbonate.

The role of thylakoid carbonic anhydrase, removing the kinetic limitations connected with interconversion of carbon acid forms, in this case consists in retaining a sufficiently high concentration of free bicarbonate, which accepts protons, in the sites of their release. Apparently, binding and transfer of protons by HCO_3^-/H_2CO_3 pair are most effective when close to carbon acid ionization constant (pK ~ 6.36). Thus, if pH value greatly differs from pK, proton transfer with participation of bicarbonate ceases to be effective. Evidently, pH-dependence of carbonate stimulating the active effect on photophosphorylation, observed in this work, is connected with that.

As it well-known, light-dependent proton exchange supplies energy for photophosphorylation, forming trans-membrane proton gradient (ΔpH), which in stationary conditions, in the process of photosynthetic photophosphorylation, is converted into ATP chemical energy. It was possible to demonstrate in this study that photophosphorylation rate, stimulated in the presence of exogenic bicarbonate, depends on carbonic anhydrase activity. Early Shutova and co-authors (Villarejo *et al*., 2002; Shutova *et al*., 2008) supposed that thylakoid carbonic anhydrase Cah3 participates in proton transfer on the donor side of PS II, easing the removal of protons from water photo-oxidation sites. The data of present work suggest that the intrathylakoid bicarbonate pool is formed during thylakoid membrane light energization and takes part in photophosphorylation acceleration due to its participation in proton transfer from H^+-generating proton pumps to ATP synthase.

References

Cohen WS, MacPeek WA (1980) A Proposed Mechanism for the Stimulatory Effect of Bicarbonate Ions on ATP Synthesis in Isolated Chloroplasts. Plant Physiol. 66: 242-245

Dilley RA (2000) Distinguishing between Luminal and Localized Proton Buffering Pools in Thylakoid Membranes. Plant Physiol. 122: 583-596

Hind G, Nakatani HY, Izawa S (1974) Light-Dependent Redistribution of Ions in Suspensions of Chloroplast Thylakoid Membranes. Proc. Natl. Acad. Sci. USA 71: 1484-1488

Klimov VV, Baranov SV (2001) Bicarbonate Requirement for the Water-Oxidizing Complex of Photosystem II. Biochim. Biophys. Acta. 1503: 187-196

Kramer DM, Sacksteder CA, Cruz JA (1999) How Acidic Is the Lumen? Photosynth. Res. 60: 151-163

Neumann J, Jagendorf AT (1964) Dinitrophenol as an Uncoupler of Photosynthetic Phosphorylation. Biochem Biophys Res Commun. 16: 562-567

Raven JA (1997) CO_2-Concentrating Mechanism: a Direct Role for Thylakoid Lumen Acidification? Plant Cell Environ. 20: 147-154

Shutova T, Kenneweg H, Buchta J, Nikitina J, Terentyev V, Chernyshov S, Andersson B, Allakhverdiev SI, Klimov VV, Dau H, Junge W, Samuelsson G (2008) The Photosystem II-Associated Cah3 in Chlamydomonas Enhances the O_2 Evolution Rate by Proton Removal. EMBO J. 27: 782-791

Stemler AJ (1977) The Binding of Bicarbonate Ions to Washed Chloroplast Grana. Biochim. Biophys. Acta. 460: 511-522

Villarejo A, Shutova T, Moskvin O, Forssen M, Klimov VV, Samuelsson A (2002) Photosystem II-Associated Carbonic Anhydrase Regulates the Efficiency of Photosynthetic Oxygen Evolution EMBO J. 21: 1930-1938

Walker DA (1973) Photosynthetic Induction Phenomena and the Light Activation of Ribulose Diphosphate Carboxylase. New Phytologist. 72: 209-235

Walz D, Goldstein L, Avron M (1974) Determination and Analysis of the Buffer Capacity of Isolated Chloroplasts in the Light and in the Dark. Eur. J. Biochem. 47: 403-407

Zolotareva EK, Dovbysh EF, Tereshchenko AF (1997) Effect of Alcohols on Inhibition of Photophosphorylation and Electron Transport by N.N'-Dicyclohexylcarbodiimide in Pea Chloroplasts. Biochemistry (Moscow) 62: 631-635

Activation of Alternative Electron Transfer in PS II by Inhibition of Proton Transfer at the Acceptor Side

*Polishchuk OV, Topchiy NM, Podorvanov VV

M.G. Kholodny Institute of botany of the National Academy of Sciences of Ukraine Tereschenkivska str., 2, 01601, Kyiv-1, Ukraine.
E-mail: membrana@ukr.net.
*Corresponding author. E-mail: polishch@yandex.ru.

Abstract: Cd^{2+}, Zn^{2+} and Cu^{2+} have expressed effect on Q_B protonation and reduction in bacterial reaction centers (BRC) (Utschig *et al*., 2001). This work is dedicated to investigating influence of Cd^{2+}, Pb^{2+}, Hg^{2+}, Zn^{2+}, and Cu^{2+} at the level of acceptor side of photosystem II (PS II). Light-dependent proton uptake decreased in the presence of 80 μM Cu^{2+} by 90%, and of 200 μM Zn^{2+}—by 70%. At that, considerable reductions of electron transport rate were not observed. In the concentration range of 50–200 μM Cu^{2+} and Cd^{2+} caused an insignificant growth of $[PSII\text{-}Q_B\text{-non-reducing}]_{rel}$, whereas in the presence of Zn^{2+} and Pb^{2+} this value grew more than by 25%. At all concentrations of ions of heavy metals the $[PSII\text{-}Q_B\text{-non-reducing}]_{rel}$ value did not exceed 60%. By their effect on dark relaxation of variable chlorophyll fluorescence, heavy metals used might be divided in two groups: (1) Cu^{2+} Hg^{2+}, accelerating the fast and medium components of fluorescence decay; (2) Zn^{2+}, Pb^{2+} and Cd^{2+}, slowing down medium and fast components. An assumption was made that blocking the reaction of Q_B protonation by ions of heavy metals activates the alternative acceptor site in PS II.

Keywords: *Spinacia oleracea*; Electron transport; Proton transport; Photosystem II; Q_B-non-reducing PS II centers

Introduction

By the latest data, regulatory contribution of the mechanism regulating the input of the energy of light into the photosynthetic apparatus at photosystem II (PS II) level often reaches the maximum long before reaching the saturating light intensity (Oxborough and Baker, 1997). Thus, at the saturating light intensity, the regulation of plastoquinone reduction is decisive for protecting PS II from photodamage, which can be provided by the induction of cyclic and non-cyclic electron-transport chains in PS II. Whereas the importance of the cyclic electron transport in PS II is beyond any doubts (Arnon and Tang, 1988), and even its stimulating conditions were characterized (Miyake and Yokota, 2001; Laisk *et al.*, 2006), non-cyclic way, in which, instead of plastoquinone, an alternative acceptor participates, and, probably, an alternative PS II active center, was poorly investigated. In some works its existence is proven (Barr and Crane, 1981; Arnon, 1995), but the conditions of its induction are not specified.

The aim of this work: to track the connection between suppression of proton transport in isolated chloroplasts of spinach and activation of alternative non-cyclic electron transport in photosystem II, using ions of cuprum and zinc as inhibitors.

Materials and Methods

Class “C” chloroplasts were isolated by modified method of Avron. Reaction medium contained sorbitol (100 mmol), NaCl (10 mmol), tris-HCl (10 mmol, pH 7.5) and chloroplasts equivalent to chlorophyll 10 μg/ml. Samples were preincubated for 5 min in dark. Actinic light was 1,000 μmol quanta/m^2s. Q_B reduction/protonation was followed by light-dependent

proton uptake in unbuffered medium by glass pH electrode. Linear electron flow rate was estimated by light-dependent oxygen uptake in Mehler reaction with Clark type electrode. Estimation of ΔpH was conducted as in (Schuldiner *et al.*, 1972) by 9-aminoacridine fluorescence quenching analysis with the help of Xe-PAM fluorometer ("Walz", HmbH). $[PSII\text{-}Q_B\text{-non-reducing}]_{rel}$ was determined as in (Tomek *et al.*, 2003). Analysis of Q_A^- dark reoxidation was conducted according to (Bukhov *et al.*, 2001).

Results and Discussion

To research electron transport in PS II under conditions of proton transfer suppression, we investigated the effect of Cu^{2+} and Zn^{2+} on: (1) light-dependent reaction of proton uptake; (2) light-induced transmembrane proton gradient (ΔpH), and (3) electron transport. It was established that light-induced proton uptake in thylakoid suspension is characterized by a high sensitivity to Cu^{2+} and Zn^{2+} (Fig. 1).

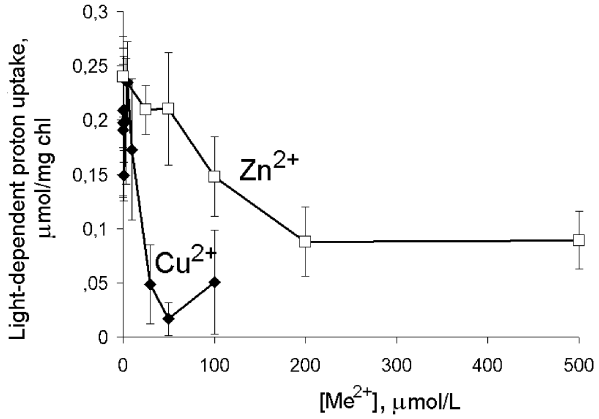

Fig. 1 The effect of Cu^{2+} and Zn^{2+} on light-dependent proton uptake.

Light-dependent proton uptake (ΔH^+) is associated with proton binding to the primary bound quinone Q_B, subsequent proton transfer into thylakoid membrane and protonation of membrane buffer groups with suitable pK values. Thus, the maximum value of light-induced proton uptake is determined by a number of intramembrane buffer groups (Walz *et al.*, 1974). Fig. 1 demonstrates that Cu^{2+} or Zn^{2+} addition results in ΔH^+ inhibition.

Zn^{2+} addition did not cause total suppression of proton uptake, which can be connected with the fact that a part of protons in Mehler's reaction is bound at reduction of molecules of oxygen, and not Q_B. In practice, almost total suppression of light-dependent proton uptake by Cu^{2+} can be explained, to our mind, by their competing with methyl viologen and/or oxygen for the PS II acceptor site. In the presence of ions of cuprum in the concentration of 50 μM and of zinc—in the concentration of 200 μM their inhibiting action was reaching maximum, saturating value. Cuprum maximally suppressed this reaction in average by 91%, and zinc—by 63% (Fig. 1).

The nature of ΔpH concentration dependence substantially differed from the previous value (Fig. 2). The calculated ΔpH value lowered at the increase of the concentration of Cu^{2+}, as of Zn^{2+}; at that, similar to light-dependent proton uptake, it was inhibited in a greater extent by Cu^{2+}, as compared to Zn^{2+}. The dependence was approaching the linear one. Relative changes of ΔpH value remained in much narrower limits than light-dependent proton uptake under similar conditions. Thus, adding of 100 μM Cu^{2+} caused the decrease of ΔpH approximately by 14%, and of 100 μM Zn^{2+} caused the reductions by only about 3% from the control value. Whereas 200 μM Zn^{2+}caused the saturating inhibition of light-dependent proton uptake value by 63%, reductions of ΔpH value did not exceed 8%.

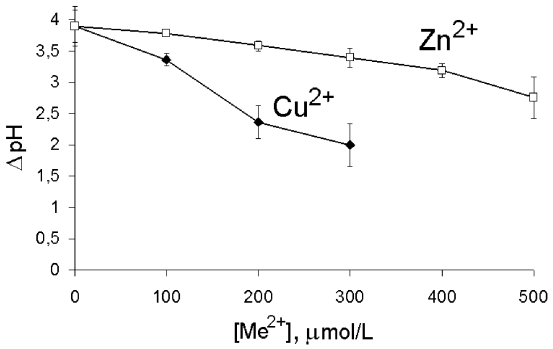

Fig. 2 The effect of Cu^{2+} and Zn^{2+} on light-induced ΔpH value.

Investigation results regarding the influence of growing concentrations of Zn^{2+} and Cu^{2+} on light-dependent oxygen uptake in Mehler's reaction, as in control, as in uncoupled thylakoid membranes, are given in Fig. 3. Gramicidin A was used as uncoupler in the concentration of 0.5 μM. The uncoupling was accompanied by the acceleration of light-dependent oxygen uptake (pH 7.8), more than by 77%. Addition of 25 μM Zn^{2+} and Cu^{2+} caused additional stimulation (mean value more than 2 times higher than the control

one), whereas in coupled chloroplasts such effect was not found.

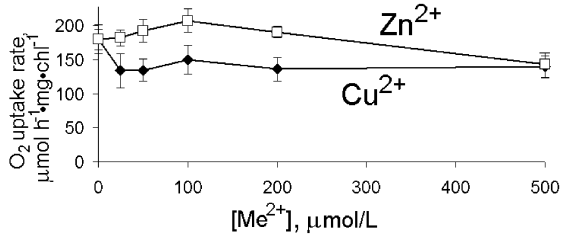

Fig. 3 The effect of Cu^{2+} and Zn^{2+}on light-dependent oxygen uptake rate in Mehler's reaction.

With the increase of concentration under conditions of uncoupling an increased inhibiting effect of these ions was observed. Lowering of the rate of light-dependent oxygen uptake at the increase of the concentration of these ions from 25 μM to 500 μM had quasi-exponential decay nature; at that, the action of ions of zinc was more expressed. At the concentration of 500 μM Zn^{2+} was suppressing this reaction by about 60% from the maximum value, and cuprum—only by 40%. Hence, Zn^{2+} affect the potential maximum rate of electron transport, not limited by ΔpH regulating influence, stronger than Cu^{2+}. These heavy metals represent effective inhibitors of electron transport under uncoupling conditions.

And in coupled chloroplasts, the activity of the abovementioned ions was quite different. Zn^{2+} in the concentration range of 50–200 μM manifested the tendency towards a weak stimulating influence. And Cu^{2+} effected inconsiderable inhibiting influence, starting from concentration of 25 μM. At the concentration of Cu^{2+} and Zn^{2+} of 500 μM , the rate of light-dependent oxygen uptake was decreased by 24% and 21%, correspondingly. At concentrations causing the saturating inhibition of light-dependent proton uptake—50 μM Cu^{2+} and 200 μM Zn^{2+}—light-dependent oxygen uptake in Mehler's reaction was suppressed only by 24% or was not reduced, correspondingly.

Thus, in the presence of 50 μM Cu^{2+} and 200 μM Zn^{2+} alternative electron transfer pathway at the level of PS II is induced which is accompanied by much lower proton uptake than the complete linear electron transfer.

The control value of $[PSII\text{-}Q_B\text{-non-reducing}]_{rel}$ in our investigations on isolated chloroplasts varied within rather wide limits – from 20% to 45%. Cu^{2+}, Cd^{2+} and Hg^{2+} caused an insignificant growth of the quantity $[PSII\text{-}Q_B\text{-non-reducing}]_{rel}$, whereas in the presence of Zn^{2+} and Pb^{2+} this value considerably increased (more than by 25%, Fig. 4).

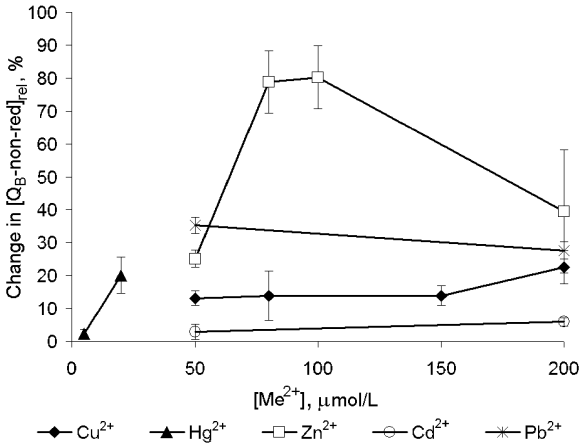

Fig. 4 Changes of the relative content of Q_B-non-reducing PS II centers after addition of ions of heavy metals.

Cd^{2+} caused the increase of $[PSII\text{-}Q_B\text{-non-reducing}]_{rel}$ value less than by 10%, their action in concentrations 50 and 200 μM did not differ. Cu^{2+} in concentration already of 50 μM caused the increase of the $[PSII\text{-}Q_B\text{-non-reducing}]_{rel}$ value approximately by 13%. At growing of concentration of ions of cuprum, the tendency towards a greater change of $[PSII\text{-}Q_B\text{-non-reducing}]_{rel}$ value was observed, which was clearly manifested in its proved growth by nearly 23% at the concentration of 200 μM.

Adding of only 20 μM Hg^{2+} caused a similar increase of $[PSII\text{-}Q_B\text{-non-reducing}]_{rel}$, as 200 μM of Cu^{2+}. Pb^{2+} more effectively, than Cu^{2+} and Cd^{2+}, increased $[PSII\text{-}Q_B\text{-non-reducing}]_{rel}$. At concentrations of 50 and 200 μM, they caused the increase of this value approximately by 35 and 28% against the control one, correspondingly. At the concentration of already 50 μM Zn^{2+} increased $[PSII\text{-}Q_B\text{-non-reducing}]_{rel}$ to 125% against the control value, at the concentration range of 80–100 μM—to 180%, and at the concentration of 200 μM this value was again decreased to 140% against the control one.

Results of the analyses of the decay of variable chlorophyll fluorescence are given in Fig. 5 in the form of relative changes of the time constants of each of three decay components, caused by the addition of ions of heavy metals, compared to the control one.

Zn^{2+} in the concentration of 50 μM slowed the first component more than by 20%, slowed the second

one by 8% and accelerated the first one nearly by 15%. At that, the amplitude of the third component significantly increased—more than by 20%. At the concentration of 200 μM action of Zn^{2+} practically did not change. The inhibition of the first component even diminished and amounted to 8%. At the same time, the amplitude changes of the first and the third components strengthened and constituted −5% and +50%, correspondingly.

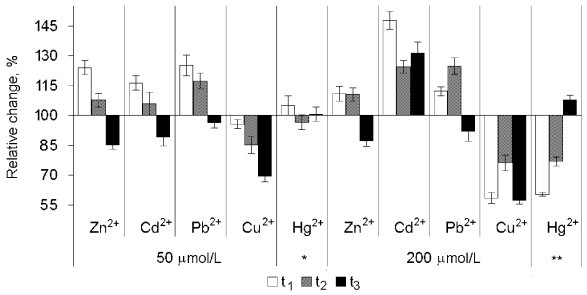

*- concentration 5 μM

** - concentration 20 μM

Fig. 5 Relative changes of the time constants of three fluorescence decay components (t_1, t_2 and t_3), caused by the addition of ions of heavy metals.

Cd^{2+} in the concentration of 50 μM caused the increase of decay time constant of the first component by 16% – and the decrease of decay time constant of the third component by 11%. At that, the amplitude of the third component increased by 15%. At the concentration of 200 μM Cd^{2+} caused the same amplitude changes of all three fluorescence decay components, just as Zn^{2+} at the similar concentration. At the same time, the increase of time constant of all three components was observed, the first—by 48%, the second—by 24% and the third—by 31%.

Pb^{2+} by their action also reminded the aforesaid heavy metals, and differed by a more expressed influence on the second fluorescence decay component. Thus, at the concentration of 50 μM they were increasing the time constant of the first component by 25%, the second—by 17%, diminishing the amplitude of the first component by 13% and increasing the third one by 80%. At the concentration of 200 μM Pb^{2+} were slowing the second component even by a greater measure (by 24%) as compared to the first one (by 12%). At that, the decrease of the second component amplitude by 27% was observed, and the increase of the third one by 123%. This way, Cd^{2+} and Pb^{2+} in the concentration of 200 μM effectively inhibited electron transfer at the acceptor side of PS II.

The action of Cu^{2+} and Hg^{2+} sharply differs from the action of the aforesaid heavy metals. Thus, Cu^{2+} in the concentration of 50 μM accelerated all the three decay components, at that, the third one—in the greatest measure (by 30%), the second one—by 15% and the first one—by 4%. At the concentration of 200 μM these ions accelerated the first and the third components by 42%, and the second – by 24%. The amplitude of the first, fastest components, which is the indicator of the electron transfer effectiveness, grew by 20% at the concentration of ions of cuprum 50 μM, and by 52%—at the concentration of 200 μM.

Hg^{2+} minutely influenced the rate parameters of fluorescence decay in the concentration of 5 μM, at that, they caused noticeable acceleration of the first (by 40%) and the second (by 23%) decay components at the concentration of 20 μM. The amplitude of the first component grew by 10% at the concentration of 5 μM, and by 44%—at the concentration of 20 μM. The second component, on the contrary, decreased by 16% at the concentration of 5 μM, and by 62%—at the concentration of 20 μM. Amplitude and rate changes of the third component under the influence of ions of mercury were insignificant.

By their influence, heavy metals used can be divided in two groups: (1) Cu^{2+} and Hg^{2+}, accelerating the fast and medium phases of fluorescence decay, increasing the amplitude of the fast phase at the cost of the medium and slow ones; (2) Zn^{2+}, Pb^{2+} and Cd^{2+}, which increase the amplitude of the slow phase and reduce the medium and fast ones.

These results suggest that alternative redox reactions in PS II are induced when Q_B reduction is suppressed by Cu^{2+} and Zn^{2+}. This effect may be caused by overreduction of the photosynthetic electron-transport chain, and may be one of the possible mechanisms that play an important role in photoprotection.

Acknowledgement

We are grateful to Prof. EK Zolotareva for her valuable advices and informal discussion of the results of our work.

References

Arnon DI, Tang GMS (1988) Cytochrome b-559 and Proton Conductance in Oxygenic Photosynthesis. Proc. Natl. Acad. Sci. USA 85: 9524-9528

Arnon DI (1995) Divergent Pathways of Photosynthetic Electron Transfer: The Autonomous Oxygenic and Anoxygenic Photosystems. Photosynth.Res. 46: 47-71

Barr R, Crane FL (1981) Ferricyanide Reduction in Photosystem II of Spinach Chloroplasts. Plant Physiol. 67: 1190-1194

Laisk A, Eichelmann H, Oja V, Rasulov B, Ramma H (2006) Photosystem II Cycle and Alternative Electron Flow in Leaves. Plant Cell Physiol. 47: 972-983

Lawson T, Oxborough K, Morison JIL, Baker NR (2002) Responses of Photosynthetic Electron Transport in Stomatal Guard Cells and Mesophyll Cells in Intact Leaves to Light, CO2 and Humidity. Plant Physiol. 128: 52-62

Miyake C, Yokota A (2001) Cyclic Flow of Electrons within PSII in Thylakoid Membranes. Plant and Cell Physiology 42: 508-515

Oxborough K, Baker NR (1997) Resolving Chlorophyll a Fluorescence Images of Photosynthetic Efficiency into Photochemical and Non-Photochemical Components – Calculation of qP and Fv/Fm without Measuring Fo. Photosynth. Res. 54: 135-142

Schuldiner S, Rottenberg H, Avron M (1972) Determination of DpH in Chloroplasts. 2. Fluorescent Amines as a Probe for Determination of DpH in Chloroplasts. Eur. J. Biochem. 25: 64-70

Utschig LM, Poluektov O, Schlesselman SL, Thurnauer MC, Tiede DM (2001) Cu^{2+} Site in Photosynthetic Bacterial Reaction Centers from Rhodobacter Sphaeroides, Rhodobacter Capsulatus, and Rhodopseudomonas Viridis. Biochemistry 40: 6132-6141

Walz D, Goldstein L, Avron M (1974) Determination and Analysis of the Buffer Capacity of Isolated Chloroplasts in the Light and in the Dark. Eur. J. Biochem. 47: 403-407

Bukhov NG, Egorova E, Krendeleva T (2001) Relaxation of Variable Chlorophyll Fluorescence after Illumination of Dark-Adapted Barley Leaves as Influenced by the Redox States of Electron Carriers. Photosynth. Res. 70: 155-166

Symposium 06

Mechanisms of Water Oxidation

Analysis of $S_{2,3}$-states Decay Processes: Focused on Cyanobacteria

Jiri Jablonsky[a,*] , Dusan Lazar[a]

[a]Palacky University, Faculty of Science, Department of Biophysics, Tr. Svobody 26, 771 46 Olomouc, Czech Republic.
[*]Corresponding author. Tel. No. +490 381 498 7683; Fax No. +490 381 498 7572; E-mail: jiri.jablonsky@gmail.com

Abstract: Decay processes of higher S-states occur in long time scale in the case of cyanobacteria. In order to examine these processes, we have tested the simplified and improved kinetic models of photosystem II (PSII). Either continuous or flash light regime was applied, followed by dark period where the $S_{2,3}$-states decay was analyzed. The simplified model matched the experimental data, however, this model disconnect the particular donor and acceptor sides of PSII, in comparison to the improved model. The simulations based on the improved PSII model showed that the charge recombination, even assuming reduced plastoquinone pool in the dark (due to respiration), cannot match the measured flash-induced S_3-state decay and the S_2-state is accumulated in the dark if the continuous light is applied. Our analysis indicated three options: (1) the simplified model is correct and the inter-monomer recombination occurs between PSIIs, or (2) the improved model is correct, part of the higher S-states is stable in the dark and the source of the faster S_3-state decay are impurities/chemicals in the experiments or (3) the improved model is correct and the cooperation between PSIIs in dimer is a partial source of the S_3-state decay.

Keywords: Cyanobacteria; Model; OEC; Water splitting; S-states decay; Cooperation

Introduction

Modeling of photosynthetic processes is a traditional field of computational biology and means, above all, kinetic modeling (Laisk *et al.*, 2009). One of the particularly interesting topic is modeling the water splitting and electron transport within the pigment-protein-complex photosystem II (PSII). There are several reasons why the study of PSII is interesting: (1) we can gather a great deal of information from oxygen evolution and variable chlorophyll fluorescence; both phenomena can be simulated, (2) the photolysis of water during photosynthesis in PSII is the renewable energy source, and (3) the PSII is the prime source of energy for all other processes in oxygenic photosynthesis but it is the most vulnerable part of the photosynthetic apparatus, threatened, for instance, by photoinhibition (Lazar *et al.*, 2005), heat degradation (Lipova *et al.*, 2010) or reactive oxygen species (Yamashita *et al.*, 2008).

Water splitting can be viewed as a simple four-step mechanism (Kok *et al.*, 1970), see Fig. 1-I; however, the influence of relaxation processes on electron transport is also known (Renger, 2004; Jablonsky and Lazar, 2008), see Fig. 1-II, and even deprotonation (Dau and Haumann, 2007), see Fig. 1-III, might be considered essential in the new generation of models if we want to understand the process of the water splitting entirely.

In this work, we have tested two kinetic models of cyanobacterial PSII. Both models were able to match the experiments but with different assumptions. Moreover, we also discuss the third option that the part of higher S-states is stable in the dark.

Methods

The PSII models were developed within GEPASI (Mendes, 1993) and exported as SBML (System Biology Markup Language) code through the

SimBiology Toolbox (MathWorks Inc.) in MATLAB (MathWorks Inc.), where all simulations were handled and executed. The simulations were based on the same conditions as the experiments (number of flashes and initial distribution of the S-states).

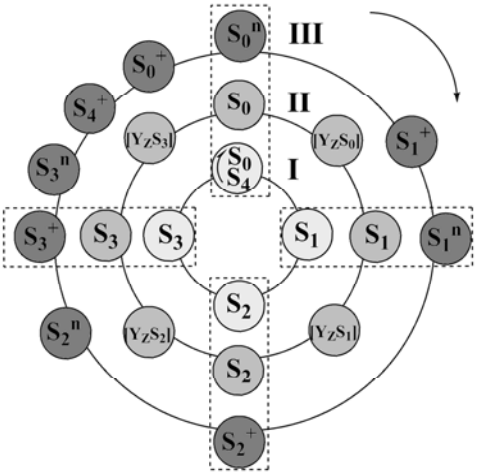

Fig. 1 Water splitting process: electron transport, regulation and deprotonation. The first level (I) shows the original Kok model of the S-states cycling (Kok *et al.*, 1970), the second level (II) shows the link between the electron transport (S-states advancement) and the relaxation process of the intermediate S-states ($[Y_zS_n]$, n = 0,1,2,3) formation (Jablonsky and Lazar, 2008). The third level (III) represents sequence of the deprotonation steps during the S-state cycle (Dau and Haumann, 2007). Superscript indicates the charge (positive or neutral) of the particular state.

Results and Discussion

Two Models - Two Interpretations

In order to simulate the changes in the S-states distribution from their steady states in the light to the decay of the higher S-states in the dark, we initially employed the simplified PSII model (Jablonsky and Lazar, 2008), modified by addition the charge recombination between S_3 and the Q_B^- (the secondary quinone electron acceptor); this reaction is usually omitted for its slowness. This approach succeeded in the expected stabilization of the S_1-state after several hours in the dark (99.3%), see Fig. 2a, and matched also the experimental decay of $S_{2,3}$-states (Fig. 2b).

Having successfully tested the previous PSII model in the description of oxygen evolution/ oscillation (Jablonsky and Lazar, 2008), it should be noted that the simplified model was not specially designed to investigate slow decay of the S-states. More significantly, this PSII model was, for simplicity, encoded in three modules (tyrosine D, acceptor and donor side of PSII) which could alter the interpretation of the decay processes. To examine any possible impact of used simplifications, we developed and employed an improved PSII model; the conceptual difference between the simplified and improved model is explained in Fig. 3.

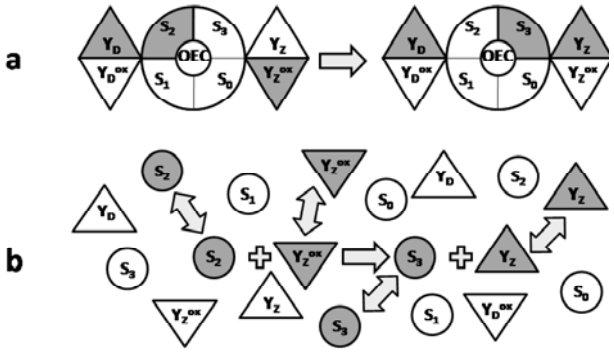

Fig. 2 Changes in the S-states distribution induced by different light conditions. Subplots a and c show the simulated changes of the S-states of OEC induced by 10 s of the light with the subsequent 3 hours in the dark based on the simplified and improved model, respectively; the same initial conditions and kinetic parameters for both models were applied, S_2* stands for simulation in the condition of reduced PQ pool. Subplots b and d show a comparison of the measured (cyanobacterium *S.elongatus*) and simulated decay of the $S_{2,3}$-states in the dark, after one or two flashes, based on the simplified and improved model (with considered cooperation), respectively. Experimental data for cyanobacterium were redrawn (Isgandarova *et al.*, 2003) and normalized to theoretical data (the experiments have provided only relative values). The initial conditions for simulations in subplots b and d are same as in the experiments (number of flashes, tyrosine D redox state).

The results based on the improved PSII model were too far from the expected pattern; see accumulation of the S_2-state, caused by S_3-Q_B^- recombination, in Fig. 2c. Our analysis of the model also clarified that there is no connection between the S_2-state accumulation and initial concentration of Q_B^- (data not shown). Taken together, these results indicate that either (1) the simplified model is valid, *i.e.*, in addition to the recombination between donor and acceptor side within one PSII, the inter-monomer recombination can also occur, or (2) the simplified concept used for previous model cannot be used for detailed analysis of water splitting and another decay mechanism must be taken in the account, *i.e.*, the improved model is incomplete.

Source of Electrons for Higher S-states Decay

Having established the gap between the known

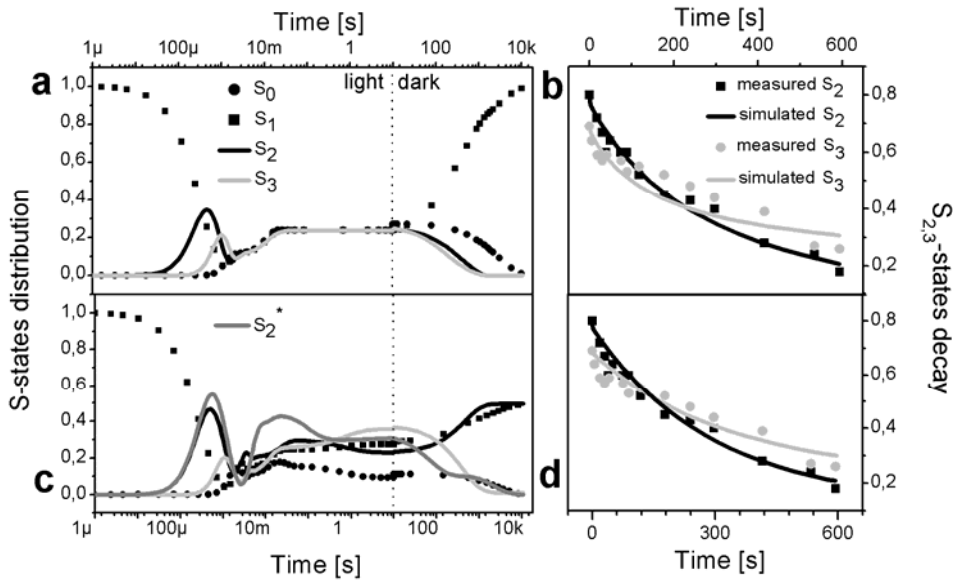

Fig. 3 A symbolic representation of the different approaches used in the donor side of tested PSII models. Schemes **a** and **b** represent the oxidation of OEC (oxygen evolving complex) in the S_2-state by the Y_Z^{ox} (D1-Y161) in the case of improved and simplified model, respectively. The gray color highlights the current redox state of the particular state variable (scheme **b**) or the current redox state of the multistate variable (scheme **a**). The one-side arrows indicate electron transport reactions and the two-side arrows indicate a possible involvement of several cofactors of the same type in the given reaction.

facts and our simulations, we started our search for the missing piece of the puzzle. The first step was to maximize the $S_{2,3}$-states decay by modification of the acceptor side of PSII. The aim was to address the following question: How the redox level of plastoquinone (PQ) pool influences the $S_{2,3}$-states decay?

Since the PQ pool is in cyanobacteria employed not only to photochemistry but also to respiration (Schultze *et al.*, 2009), we assumed for the following simulations that almost the entire PQ pool (92%) is initially reduced and almost the same amount is reached in the steady state in the dark after the exposure to the light. This modification significantly increased the occurrence of the recombination between the donor and acceptor sides, moreover, an accumulation of the S_2-state was not observed this time as it is shown in Fig. 2c (S_2*). This approach maximized the occurrence of recombination, however, still does not match (data not shown) the faster flash-induced decay of the higher S-states observed in the experiments (Isgandarova *et al.*, 2003). Finally, it was suggested that the acceptor side of *S. elongatus* PSII has been modified in a way that prevents too fast S_2 and S_3-states recombination (Isgandarova *et al.*, 2003). This suggestions is supported by our analysis and we therefore concluded that there is another source of electrons causing decay of the higher S-states.

If we exclude the acceptor side of PSII as the sole, besides tyrosine D, source of the higher S-stated decay, there are only two other options: (1) higher S-states are in the dark more stable than it was expected and discrepancies between observed results and simulations were caused by impurities, chemicals or imperfect experimental setup; non-zero concentration of the higher S-states in the dark was, for cyanobacteria, suggested before (Mauzerall and Dubinsky, 1993) or (2) there is another and yet unconsidered mechanism related to higher S-states decay. Since the model cannot tell us anything new about the first option we have focused on the last option.

We were therefore looking for a process within the PSII involving only water splitting itself, and the only known candidate fitting this criterion was the cooperation (Jablonsky *et al.*, 2008). The cooperation, electron transport through the chain of cofactors between two sequent S-states within the PSII dimer, was suggested as a mechanism necessary for explanation of the higher yield of the oxygen evolution after the second flash (Jablonsky *et al.*, 2008). Cooperation might be observed even in the long time scale if the formation of the intermediate S-states (Jablonsky and Lazar, 2008) is reversible or if another pathway of cooperation between the donor sides exists. We have analyzed only the simplest scenario: besides the charge recombination between the donor and acceptor sides of PSII, there is one

pathway of cooperation.

We have determined S_2-Q_A^- recombination (1/k = 1.5 s) to be the sole origin of S_2-state decay in the flash-induced decay, see Fig. 2d. In the case of S_3-state decay, the consideration of $S_3^{PSIIa} + S_3^{PSIIb} \rightarrow S_0^{PSIIa} + S_2^{PSIIb}$ (1 e^- oxidation and 1 e^- reduction) pathway of cooperation (1/k = 1052 s, *i.e.*, 526 s for each of the S_3-states) was able to simulate decay of the S_3-state in very good agreement with the experimental data, see Fig. 2d. Assumed pathways of cooperation in which one of the S_3-states is advanced to the S_0-state is supported by observation that the S_3-state does not always decay through the S_2-state, especially if the artificial electron acceptor is not present (Seibert and Lavorel, 1983).

Acknowledgements

This work was financially supported by the Grant Agency of Academy of Sciences of the Czech Republic grant No. KJB401370904 and by the Czech Science Foundation grant No. 522-08-H003.

References

Dau H, Haumann M (2007) Eight Steps Preceding O-O Bond Formation in Oxygenic Photosynthesis - A Basic Reaction Cycle of the Photosystem II Manganese Complex. Biochim. Biophys. Acta. 1767: 472-483

Isgandarova S, Renger G, Messinger J (2003) Functional Differences of Photosystem II from Synechococcus Elongatus and Spinach Characterized by Flash Induced Oxygen Evolution Patterns. Biochemistry 42: 8929-8938

Jablonsky J, Lazar D (2008) Evidence for Intermediate S-States as Initial Phase in the Process of Oxygen-Evolving Complex Oxidation. Biophys. J. 94: 2725-2736

Jablonsky Susila P, Lazar D (2008) Impact of Dimeric Organization of Enzyme and Its Function: the Case of Photosynthetic Water Splitting. Bioinformatics 24: 2755-2759

Kok B, Forbush B, McGloin M (1970) Cooperation of Charges in Photosynthetic O2 Evolution, I. A Linear Four-Step Mechanism. Photochem. Photobiol. 11: 457-475

Laisk A, Nedbal L, Govindjee (2009) Photosynthesis in Silico. Springer: Dordrecht

Lazar D, Ilik P, Kruk J, Strzalka K, Naus J (2005) A Theoretical Study on Effect of the Initial Redox State of Cytochrome b(559) on Maximal Chlorophyll Fluorescence Level (F-M) Implications for Photoinhibition of Photosystem II. J. theor. Biol. 233: 287-300

Lipova L, Krchnak P, Komenda J, Ilik P (2010) Heat-Induced Disassembly and Degradation of Chlorophyll-Containing Protein Complexes in Vivo. Biochim. Biophys. Acta 1797: 63-70

Mauzerall D, Dubinsky Z (1993) Interactions amongs the Photosystem II Oxygen-Forming Complex: a Novel Model for Damping of O_2 Oscillations. Biochim. Biophys. Acta 1183: 123-129

Mendes P (1993) GEPASI: a Software Package for Modeling the Dynamics, Steady States and Control of Biochemical and Other Systems. Bioinformatics 9: 563-571

Renger G (2004) Coupling of Electron and Proton Transfer in Oxidative Water Cleavage in Photosynthesis. Biochim. Biophys. Acta 1655: 195-204

Seibert M, Lavorel J (1983) Oxygen-Evolution Patterns from Spinach Photosystem II Preparations. Biochim. Biophys. Acta 723: 160-168

Schultze M, Forberich B, Rexroth S, Dyczmons NG, Roegner M, Appel J (2009) Localization of Cytochrome b6f Complexes Implies an Incomplete Respiratory Chain in Cytoplasmic Membranes of the Cyanobacterium Synechocystis sp. PCC 6803. Biochim. Biophys. Acta 1787: 1479-1485

Yamashita A, Nijo N, Pospisil P, Morita N, Takenaka D, Aminaka R, Yamamoto Y (2008) Quality Control of Photosystem II — Reactive Oxygen Species Are Responsible for the Damage to Photosystem II under Moderate Heat Stress. J. Biol. Chem. 283: 28380-28391

Energetics, Kinetics and Mechanism of Oxidative Water Splitting in Photosynthesis

G Renger

Max-Volmer-Laboratorium, Technical University Berlin, Straße des 17. Juni 135, Germany D 10623 Berlin.

Abstract: This short communication focuses on energetics, kinetics and mechanism of oxidative photosynthetic water splitting into molecular dioxyen and four protons. The process which takes place in the Photosystem II complex of all oxygen evolving organisms comprises three different types of reaction : i) light induced generation of the strongly oxidizing cation radical $P680^{+\bullet}$ ii) coupled proton and electron transfer leading to $P680^{+\bullet}$ reduction by Y_Z, and iii) sequence of redox steps within the WOC driven by Y_z^{ox}.

Keywords: Photosystem II; Tyrosine Y_z; Water oxidizing complex; "Complexed –peroxide" model

Introduction

The invention of a molecular machine for light induced oxidative water splitting into molecular oxygen and four protons was the bioenergetic "big bang" in the evolution of the biosphere (Renger, 2008). The key reactions that take place at a Mn_4O_xCa cluster within the water-oxidizing complex (WOC) are energetically driven by the strongly oxidizing cation radical $P680^{+\bullet}$ (formed as a result of photochemical charge separation in Photosystem II (PS II), Renger G and Renger T, 2008) and mediated by a special tyrosine residue Y_Z (Diner and Britt, 2005). The structure is known at 2.9 Å resolution from X ray diffraction crystallography (XRDC) of PS II core complexes from the thermophilic cyanobacterium *Thermosynechococcus* (*T.*) *elongatus* (Guskov *et al*., 2010) and the reaction pattern of oxidative water splitting has been analyzed in samples from both cyanobacteria and higher plants (Messinger and Renger, 2008).

$P680^{+\bullet}$ reduction by Y_Z

At physiological pH the OH group of Y_Z deprotonates upon its oxidation for energetic reasons (Sjödin *et al*., 2002), *i.e.* electron (ET) and proton transfer (PT) are coupled steps. The mode of this coupling is mechanistically very important, not only for this reaction, but it is of general relevance for many biological redox processes (Meyer *et al*., 2007).

The surprisingly complex kinetics of $P680^{+\bullet}$ reduction by Y_Z can be satisfactorily approximated by three distinct components with half lifetimes of 25–70 ns ("fast" ns kinetics), 300–600 ns ("slow" 1 ns kinetics), and 15–50 μs (μs kinetics).

This pattern, which is basically the same in all samples of different structural complexity (intact leaves, thylakoids, isolated PS II preparations) and of species from quite distinct evolutionary levels (cyanobacteria, higher plants) studied so far (for review, see Renger and Kühn, 2007), has been explained by the sequence of an ET step and subsequent relaxation processes. The bottom panel of Fig. 1 presents a reaction scheme.

Kinetic analyses (activation energies of about 10 kJ/mol, kinetic H/D exchange effects of < 1.05) revealed that the "fast" ns step requires a structurally well defined hydrogen bond between the OH group of Y_Z and His 190 and different orbitals participate in the coupled ET/PT reactions. This mode of coupling, illustrated in the top panel of Fig. 1, is referred to as multiple site electron proton transfer (MS-EPT) (Meyer *et al*., 2007). The "fast" ns reaction is slightly exergonic or even endergonic, depending on the redox state S_i of the WOC thus giving rise to only partial reduction of $P680^{+\bullet}$ (Kühn *et al*., 2004).

Progress in the extent of Y_Z oxidation at longer times ("slow" ns and μs kinetics) is assumed to

originate from thermodynamic shifts of the equilibrium $P680^{+\bullet}Y_Z \leftrightarrow P680Y_z^{ox}$ due to relaxation of the protein environment (local response) followed by proton rearrangement(s) within hydrogen bond network(s) that significantly contribute to the energetics of the overall reaction (Kühn *et al*., 2004).

The hydrogen bond of Y_z is disturbed by protonation of His 190. Accordingly the "fast" ns kinetics is expected to disappear at decreasing pH. A titration curve with a pK value of 4.6 was obtained for *T. elongatus* PS II core complexes with fully competent WOC (Renger and Kühn, 2007).

The reaction coordinate of $P680^{+\bullet}$ reduction by Y_z is drastically changed in samples deprived of the WOC (increase of activation energy by a factor of about 3 and significant kinetic H/D isotope effect of 2.7–3.3 which is completely absent for the "fast" and "slow" ns kinetics in intact PS II). Therefore sound conclusions on the mechanism and in particular on hydrogen bonding of Y_z *in vivo* cannot be drawn from results gathered from samples with a destroyed WOC (for details, see Renger, 2010).

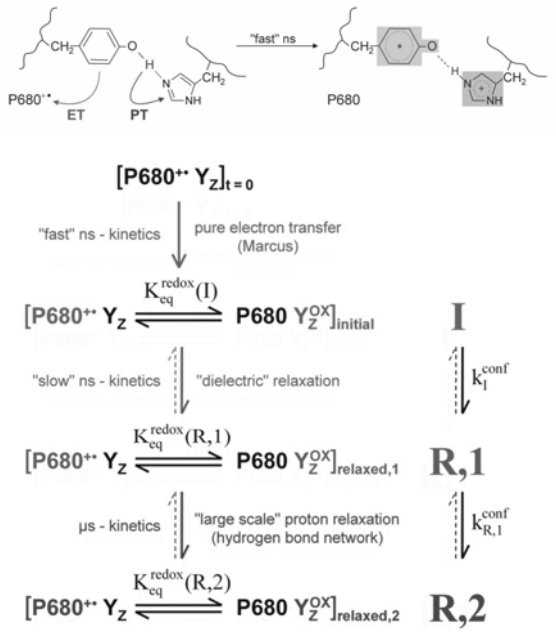

Fig. 1 MS-EPT scheme (top panel) and reaction sequence (bottom panel) of $P680^{+\bullet}$ reduction by Y_Z.

Energetics, kinetics and mechanism of the WOC reaction pattern

Our current knowledge on the energetics of the S_i state transitions has been described in a recent book chapter (Messinger and Renger, 2008). Conflicting results were reported on the last step of the sequence leading to O_2 release. This reaction was proposed to be highly exergonic (Renger, 1978) but later (on the basis O_2 back pressure effects) inferred to be only slightly exergonic (Clausen and Junge, 2004). Mass spectrometry measurements unambiguously showed that O_2 release is not suppressed at high O_2 pressure and therefore provide experimental evidence for a large energy gap of about 200 meV (Sheleva *et al*., 2011) thus confirming the original conclusion (Renger, 1978).

The sequence of oxidation steps in the WOC are characterized by comparatively small activation energies (5–35 kJ/mol) and kinetic H/D exchange effects (1.2–2.5). In order to gather information on the mechanism of these reactions, the experimental rate constants $k_{i+1,i}^{exp}$ of the S_i state transitions driven by Y_z^{ox} were compared with "theoretical" values $k_{i+1,i}^{NET}$ for nonadiabatic electron transfer (NET) calculated on the basis of an empirical rate constant-distance relationship (Page *et al*., 1999) and the structural model of 2.9 Å resolution (Guskov *et al*., 2010). Ratios of 10^5 and 10^2 are obtained for $k_{i+1,i}^{NET}/k_{i+1,i}^{exp}$ with i = (0)1 and 2, respectively, when using available data on Y_z·····Mn distances (Guskov *et al*., 2010) and experimental activation energies (Renger, 2001). These huge ratios clearly show that the redox steps in the WOC are triggered reactions, in striking contrast to Y_z reduction by $P680^{+\bullet}$ where the MS-EPT mechanism perfectly satisfies the empirical rate-constant relationship of NET (Renger *et al*., 1998). The trigger reactions of the redox steps in the WOC become blocked below characteristic threshold temperatures. The underlying mechanism of this triggering is not known but it seems most likely that proton shifts and/ or conformational changes are involved (Renger, 2011).

Marked differences exist between the stepwise 1-electron oxidation of the WOC up to the redox level S_3, characterized by a rate that is limited by the corresponding trigger reaction, and the sequence of steps leading to Y_z^{ox} reduction by the WOC in S_3 and the eventual release of O_2. The rate of the latter process is assumed to be limited by the overall MS-ETP step(s) which comprise(s) a redox equilibrium with a rather small constant for an endergonic reaction (Renger, 2011). All considerations on the

origin of this redox equilibrium depend on the nature of S_3. At present two alternative proposals are discussed for S_3: (i) single state redox level, or (ii) multiple state redox level comprising three distinct states with different electronic configuration and nuclear geometry that are connected via rapid redox isomerism and proton tautomerism equilibria. One of these states corresponds with a complexed peroxide and acts as the indispensable "entatic state" for the reduction of Y_z^{ox} (Renger, 2001; Renger G and Renger T, 2008). In the case of a single state S_3 it is not yet clarified as to whether the $S_2 \rightarrow S_3$ transition leads to oxidation of manganese or of an oxo-bridge thus giving rise to oxo-radical formation (for review, see Messinger and Renger, 2008). Regardless of this detail, in the single S_3 state model the essential O-O bond formation occurs only at the redox level S_4.

All currently discussed proposals can be summarized by the scheme presented in Fig. 2.

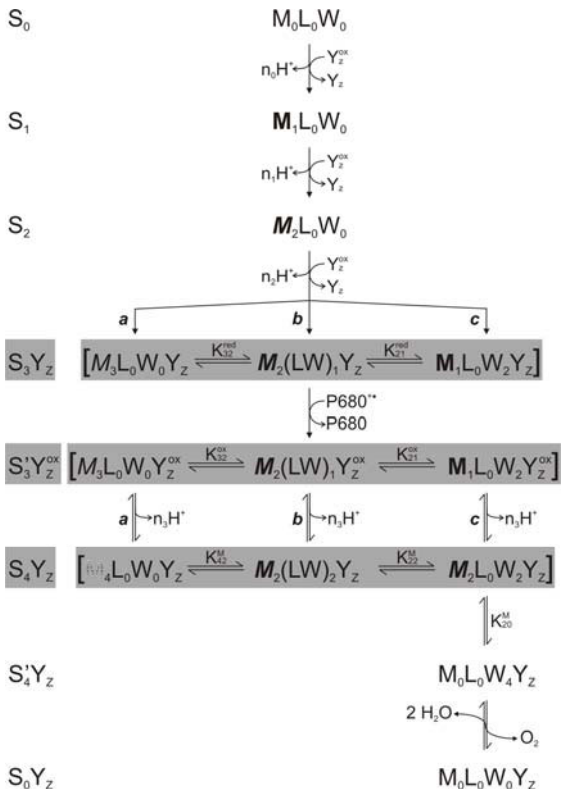

Fig. 2 Reaction scheme of oxidative water splitting (for details, see text).

The electronic configuration of the S_i states is characterized by the symbol $S_i = M_jL_kW_k$ (i = j + k + l) where indices j,k, and l symbolize formal oxidation states of manganese, ligand and substrate, respectively (see Messinger and Renger, 2008).

The redox steps $S_0 \rightarrow S_1$ and $S_1 \rightarrow S_2$ are accepted to be metal centered reactions leading to Mn(III) oxidation to Mn(IV) (for the sake of simplicity these redox states are single states, but see Renger, 2011). The pathway of S_3 oxidation depends on its nature (vide supra). In case of the dogma of O-O bond formation in S_4 the equilibrium constants are: $K_{21}^{red} = K_{21}^{ox} = 0$ and either $K_{32}^{red} = K_{32}^{ox} = 0$ for Mn oxidation during the $S_2 \rightarrow S_3$ transition or $K_{32}^{red} = K_{32}^{ox} \rightarrow \infty$ for oxo-radical formation. In the multiple state S_3 model the equilibrium constants are assumed to be dependent on the redox state of Y_z with $K_{32}^{red} K_{21}^{red} < K_{32}^{ox} K_{21}^{ox}$ and the peroxidic state $M_1L_0W_2$ is populated with a low probability (Renger, 2011). So far experimental evidence is lacking for the existence of the presumed multiple state equilibrium in redox state S_3. However, the pronounced heterogeneity of PS II with respect to the reactivity of S_3 in the CP43-E354 mutant of *Synechocystis* sp. PCC 6803 (Shimada *et al*., 2009; Service *et al*., 2011) might be a hint for a multiple state S_3 redox level of the WOC. A prevention of the population of the "entatic" state $M_1L_0W_2$ in the WOC of a large fraction of PS II complexes in the mutant would readily explain the blockage of Y_z^{ox} reduction by S_3. The formation of $M_1L_0W_2$ was inferred to be strictly dependent on a proton shift within the presumed tautomeric form (Renger G and Renger T, 2008). It is therefore reasonable to assume that the replacement of Glu by Gln at site 354 of CP43 interrupts in a large fraction of the PS II complexes the proton shift(s) that is(are) required for population of the S_3 form $M_1L_0W_2$ which acts as the indispensable reductant of Y_z^{ox}.

The crucial step of O_2 formation in the WOC is the linkage to the O-O bond of two oxygen atoms from the substrate. It is postulated that this reaction critically depends on the local proton-gradient $\nabla H^+(\vec{r})$ at the interacting oxygen atoms. This key parameter and its dynamics in S_3, *i.e.* $\nabla H^+(\vec{r}, t, S_3)$, are determined by the pK values and the time dependent spatial array of substrate molecules and protonatable groups within the protein matrix around the Mn_4O_xCa cluster. Therefore detailed mechanistic considerations are only reliable when based on a structural model of the WOC at atomic resolution with precise positions of the substrate molecules and

the network of hydrogen bonds. At present this information is not available. In spite of this lack, interesting suggestions have been recently reported, especially with respect to the "S_3 multistate hypothesis" where $S_3(P)$ is proposed to attain a Mn(III)-OOH configuration within the catalytic site (Meyer *et al*., 2007).

The oxidation of $S_3(P) = M_1L_0W_2$ by Y_Z^{ox} to complexed O_2 symbolized by $M_0L_0W_4$ is a 2-electron reaction. At present it is not clear if this process comprises the formation of a distinct superoxide intermediate $M_1L_0W_3$ (Meyer *et al*., 2007) or if a concerted reaction directly leads to $M_0L_0W_4$.

The postulated central role of $\nabla H^+(\vec{r}, t, S_3)$ for the oxidative O-O bond formation has its functional counterpart in the reductive O-O bond fission that is catalyzed by a large number of systems in oxygen enzymology. In this case the key function of local hydrogen bonding and directed protonation pathways has been demonstrated for different examples (Rinaldo *et al*., 2007; Rosenthal and Nocera, 2007).

In summary, the WOC has to be considered as a supermolecule which is especially tailored for the delicate process of oxidative water cleavage including definite pathways for substrate entry and product release (Renger G and Renger T, 2008).

Acknowledgments

I thank C Theiss for help in preparing the figures and DFG (Sfb 429) for financial support financial support.

References

Clausen J, Junge W (2004) Detection of an Intermediate of Photosynthetic Water Oxidation. Nature 430: 480-483

Diner BA, Britt RD (2005) The Redox-Active Tyrosines Y_Z and Y_D. In: Wydrzynski T, Satoh K (eds.), The Light-Driven Water: Plastoquinone Oxido-Reductase in Photosynthesis, Advances in Photosynthesis and Respiration, Vol. 22. Springer: Dordrecht, pp. 206-233

Kühn P, Eckert HJ, Eichler HJ, Renger G (2004) Analysis of the $P680^{+\cdot}$ Reduction Pattern and Its Temperature Dependence in Oxygen Evolving PS II Core Complexes from Thermophilic Cyanobacteria and Higher Plants. Phys Chem Chem Phys 6: 4838-4843

Guskov A, Gabdulkhakov A, Broser M, Glöckner C, Hellmich J, Kern J, , Frank J, Saenger W, Zouni A (2010) Recent Progress in the Crystallographic Studies of Photosystem II. Chem. Phys. Chem. 11: 1160-1171

Messinger J, Renger G (2008) Photosynthetic water splitting. In: Renger G (ed.), Primary Processes of Photosynthesis: Basic Priniciples and Apparatus, Part II. Royal Society Chemistry: Cambridge, pp. 295-353

Meyer TJ, Hang M, Huynh V, Thorp HH (2007) The Role of Proton Coupled Electron Transfer (PCET) in Water Oxidation by Photosystem II. Wiring for Protons. Angew Chem Int Ed 46: 5284-5304

Page CC, Moser CC, Chen X, Dutton PL (1999) Natural Engineering Principles of Electron Tunneling in Biological Oxidation-Reduction. Nature 402: 47-52

Renger G (1978) Theoretical Studies about the Functional and Structural Organization of the Photosynthetic Oxygen Evolution. In: H Metzner (ed.), Photosynthetic Oxygen Evolution Academic Press: London, pp. 229-248

Renger G (2001) Photosynthetic Water Oxidation to Molecular Oxygen: Apparatus and Mechanism. Biochim Biophys Acta 150(3): 210-228

Renger G (2008) Overview on Primary Processes of Photosynthesis. In: Renger G (ed.), Primary Processes of Photosynthesis: Basic Principles and Apparatus, Part I. Royal Society of Chemistry: Cambridge, pp. 7-35

Renger G (2010) Role of Hydrogen Bonds in Photosynthetic Water Splitting. In: KL Han, GJ Zhao (eds.), Excited State Hydrogen Bonding and Hydrogen Transfer. Wiley, 2010, pp. 433-461

Renger G (2011) Light Induced Oxidative Water Splitting in Photosynthesis: Energetics, Kinetics and Mechanism. J Photochem. Photobiol. B Biology (in press)

Renger G, Kühn P (2007) Reaction Pattern and Mechanism of Light Induced Oxidative Water Splitting in Photosynthesis. Biochim Biophys Acta 1767: 458-471

Renger G, Renger T (2008) Photosystem II: the Machinery of Photosynthetic Water Splitting. Photosynth. Res. 98: 53-812

Renger G, Christen G, Karge M, Eckert HJ, Irrgang KD (1998) Application of the Marcus Theory for

Analysis of the Temperature Dependence of the Reactions Leading to Photosynthetic Water Oxidation – Results and Implications. J Bioinorg Chem 3: 360-366

Rinaldo D, Philipp DM, Lippard SJ, Friesner RA (2007) Intermediates in Dioxygen Activation by Methane Monooxygenase: A QM/MM Study. J Am Chem Soc 129: 3135 -3147

Rosenthal J, Nocera DG (2007) Role of Proton-Coupled Electron Transfer in O–O Bond Activation. Acc Chem Res 40: 543-553

Service RJ, Yano J, McConnell I, Hwang HJ, Niks D, Hille R, Wydrzynski T, Burnap RL, Hillier W, Debus RJ (2011) Participation of Glutamate-354 of the CP43 Polypeptide in the Ligation of Manganese and the Binding of Substrate Water in Photosystem II. Biochemistry 50: 63-81

Sjödin M, Styring S, Åkermark B, Sun L, Hammarström L (2002) The Mechanism for Proton Coupled Electron Transfer from Tyrosine in a Model Complex and Comparison with Tyrosine Z Oxidation in Photosystem II. Phil. Trans. B 357: 1471-1478

Shimada Y, Suzuki H, Tsuchiya T, Tomo T, Noguchi T, Mimuro M (2009) Effect of a Single-Amino Acid Substitution of the 43 kDa Chlorophyll Protein on the Oxygen-Evolving Reaction of the Cyanobacterium Synechocystis sp. PCC 6803: Analysis of the Glu354Gln Mutation. Biochemistry 48: 6095-6103

Sheleva D, Beckmann K, Clausen J, Junge W, Messinger J (2011) Photosynthetic Oxygen-Evolution at Elevated Oxygen Pressure: Direct Detection by Membrane Inlet Mass Spectrometry. Proc. Nat. Acad. Sci. 108 (in press)

Charge Equilibrium Reactions S_2 and S_3 States of Photosystem II with Cyt b_{559} and Tyrosine Y_D

Yashar Feyziyev[a*], Stenbjörn Styring[b]

[a]Institute of Botany, 40 Patamdar Shosse, Az 1073 Baku, Azerbaijan; [b]Department of Photochemistry and Molecular Science, Uppsala University, Box 523, S-75120 Uppsala, Sweden.
[*]Corresponding author. Tel. No. +994 12 4381164; Fax No. +994 12 5102433; E-mail: feyziyev-y@botany-az.org.

Abstract: Electron transfer from the reduced tyrosine Y_D and cytochrome b_{559} (Cyt b_{559}) to the S_2 and S_3 states of photosystem II was investigated at the temperature of 195 K. Electron transfer reactions were followed by measuring EPR signals of tyrosine $Y_D^{\bullet}$, oxidized Cyt b_{559} and the S_2-state multiline signal. Long term incubation (~90 days) at 195 K causes decay of the majority of S_2 centers up to ~40% of initial value, while in this time scale the intensity of $Y_D^{\bullet}$ radical increases less than 10%. Samples advanced to S_3 state demonstrates an increasing behavior of the S_2-state multiline signal intensity in the beginning of incubation (~20 days) and slow decay up to 40% of maximal amplitude during further incubation of the samples. Similarly to the S_2 sample, small increase in $Y_D^{\bullet}$ radical signal was observed during the S_3 decay. However, in both types of samples prepared in S_2 and S_3 states after 90 days of incubation the signal of oxidized Cyt b_{559} is increased from 45%–50% up to 100% maximal intensity. The results obtained in this study support the conclusion of our early investigations which claimed the reduced Cyt b_{559} as electron source for the S_2 and S_3 states.

Keywords: Photosystem II; S-cycle; Tyrosine; Cytochrome b_{559}; Electron transfer

Introduction

Photosystem II (PSII) of oxygenic species catalyzes water oxidation reactions utilizing power of sunlight in light-induced electron transfer reactions (Barber, 2003). High potential produced in PSII reaction center and required for water oxidation chemistry accumulates through the catalytic S-cycle driven by (Ca-4Mn)-Y_Z-P_{680}-Phe-Q_AQ_B redox sequence. Electron transfer in photosystem II starts with excitation of P_{680} (chlorophyll) resulting in sequential reduction of pheophytin (Phe) and plastoquinone electron acceptors (Q_A, Q_B), and oxidation of tyrosine Y_Z and Ca-4Mn cluster. S-cycle involves five intermediate redox states: S_0-S_4. S_0 is the most reduced state. The S_2 and S_3 states are unstable and decays to the stable S_1 state in the dark. The S_4 state is a transient intermediate between S_3 and S_0 (Debus, 1992; Diner and Babcock, 1996).

In certain circumstances two other inner components of PSII, the redox active tyrosine Y_D and cytochrome b_{559}, may also interfere and support water oxidation reactions by electrons (Buser *et al.*, 1990; Styring and Rutherford, 1988; Vass and Styring, 1991; Stewart and Brudvig, 1998; Hanley *et al.*, 1999; Tompson and Brudvig, 1988; Faller *et al.*, 2001). Electron transfer from tyrosine Y_D and Cyt b_{559} to the S_2 and S_3 states of PSII above 245 K were investigated in previous studies (Styring and Rutherford, 1987, 1988; Feyziyev *et al.*, 2003). The subject of present work is the study of electron transfer reactions between tyrosine Y_D, Cyt b_{559} and S-state cycles (S_2 and S_3 states).

Materials and Methods

BBY-type PSII enriched membrane fragments (Berthold *et al.*, 1984) were prepared from hydroponically grown greenhouse spinach with modifications, described in (Völker *et al.*, 1985). The isolated membranes were resuspended in 50 mmol MES-NaOH buffer pH 6.2, contained 35 mmol NaCl and 300 mmol sucrose at a chlorophyll concentration of 4 mg/ml and stored at liquid nitrogen until use. In the presence of 200 μM PPBQ as an electron acceptor

the rate of oxygen evolution was ~450 μmol of O_2 (mg Chl)$^{-1}$h^{-1}.

Tyrosine $Y_D^{\bullet}$ and Cyt b_{559} were reduced chemically by an ascorbate and 3.6-diaminodurene (DAD) treatment in complete darkness. The PSII membranes at a chlorophyll concentration of 1 mg/ml were dark adapted for 30 min in complete darkness at room temperature. 5 mmol sodium ascorbate and 1 mmol DAD were added and the suspension was incubated for an additional 30 min. After incubation, the suspension was diluted about 8–10 times and the PSII membranes were precipitated at 30,000 g for 20 min, and thereafter the membranes were washed two times. Last pellet was resuspended in the storage buffer to get the chlorophyll concentration of 4 mg/ml. The treated PSII membranes were transferred into the calibrated EPR tubes. PPBQ (0.5 mmol, dissolved in DMSO, final DMSO concentration of 2% v/v) was added and the samples were illuminated with short (7 ns) light flashes from a Nd:YAG laser (400 mJ/pulse, 532 nm) to advance PSII to the $Y_D^{red}S_2$ (1 flash) or $Y_D^{red}S_3$ (2 flashes, 0.5 Hz) states. After laser flashes, the samples were frozen within 1 s in an ethanol-solid CO_2 bath, and then rapidly transferred into liquid nitrogen where they were stored until used. The dark (non-illuminated) samples were used to study PSII in the S_1 state.

EPR measurements were performed using a Bruker ESR-500 spectrometer and ST4102 standard cavity, equipped with an Oxford-900 cryostat and ITC-503 temperature controller. The S_2 state multiline signal was measured at 7 K with a microwave power of 13.1 mW and field modulation amplitude 20 G. The EPR signal from tyrosine $Y_D^{\bullet}$ and oxidized Cyt b_{559} was measured at 15 K. The $Y_D^{\bullet}$ radical was detected at microwave power of 1 μW and field modulation amplitude 3.2 G, and 5.3 mW microwave power and 16 G field modulation amplitude used for detection of oxidized Cyt b_{559}.

Results and Discussion

In the presence of reduced tyrosine (Y_D^{red}), the flash-induced turnover of S-cycle is rapidly desynchronized due to misses, the presence of Y_D^{red}, and the lack of a synchronized preflash (Styring and Rutherford, 1987; Feyziyev *et al*., 2003). The EPR signal (Fig. 1A) of oxidized tyrosine was absent in the dark sample (spectrum a) which shows that ascorbate-DAD treatment efficiently reduce tyrosine Y_D. The first flash resulted in appearance of small (~10%–14% of Y_D) tyrosine $Y_D^{\bullet}$ radical signal (spectrum b, state $Y_D^{red}S_2$). After the second flash further increase of the tyrosine $Y_D^{\bullet}$ signal (15%–16% of $Y_D^{\bullet}$, spectrum c) is occurred. Oxidation of the tyrosine results from electron transfer between Y_D^{red} and the oxidized species (preferable S_2 and S_3 states) of PSII prior freezing. Complete oxidation of tyrosine was achieved by room light / dark treatment (30 s vs. 5 min) of the reduced sample at room temperature (spectrum "max"). The registered spectrum of $Y_D^{\bullet}$ was identical with the signal of fully oxidized tyrosine Y_D obtained from the non-treated sample.

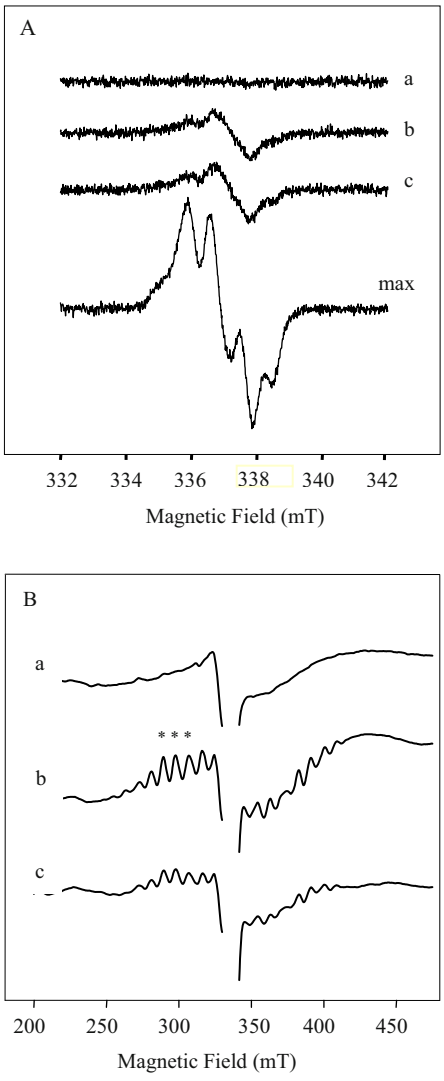

Fig. 1 EPR spectra of tyrosine $Y_D^{\bullet}$ (A) and S_2 state multiline signal (B) from $Y_D^{red}S_1$ (a), $Y_D^{red}S_2$ (b) and $Y_D^{red}S_3$ (c) states. Curve "max" (A) represent the maximal signal from $Y_D^{\bullet}$ registered in chemically reduced samples. The stars indicate the three lines used for the estimation o the multiline signal amplitude. EPR conditions are described in the section of Material and Methods.

Fig.1B demonstrates the EPP spectra of the S_2 state multiline signal. In the dark sample there was no observable multiline signal (spectrum a) indicating that nearly all centers were in the dark stable S_1 state. Illumination of the dark sample at 195 K rises the multiline spectrum (don't shown). The intensity of the signal was taken as maximal and used for estimation of the S_2 and S_3 population in the $Y_D^{red}S_2$ and $Y_D^{red}S_3$ centers. One-flash sample prepared with this reduction and illumination protocol was dominated by the S_2 state (spectrum b), although it also contained a considerable fraction of centers in the S_1 state. The amplitude of S_2 state multiline signal was further increased nearly 10%–20% in such samples. Similarly, a two-flash sample (S_3 state) prepared with our experimental protocol (spectrum c) also contained a large fraction of S_2 centers. Further illumination of the two-flash sample at 195 K hasn't increased the S_2 state of multiline signal indicating that virtually no centers remained in S_1 state. Thus, we can assume that about 80%–90% of PSII was found in the $Y_D^{red}S_2$ state after the first flash and 50%–60% in the $Y_D^{red}S_3$-state after the second flash.

The reduced PSII membranes illuminated with one or two flashes were stored at 195 K in total darkness and EPR spectra of the tyrosine $Y_D^{\bullet}$, multiline signal and Cyt b_{559} were registered at different time interval of the incubation.

In 1-flash sample (Fig. 2) which populated by the $Y_D^{red}S_2$ centers, the amplitude of the S_2-state multiline signal demonstrate an exponential decay up to 40% its maximal intensity during long term (~170 days) incubation at 195 K. The decrease of the S_2 multiline signal was concomitant with the oxidation of Cyt b_{559}. During incubation the signal of oxidized Cyt b_{559} rise up to 85% its maximal intensity (determined as a result of 77 K illumination of the sample). Signal of tyrosine $Y_D^{\bullet}$ radical also increased during the incubation; however tyrosine oxidation was significantly slower than oxidation of Cyt b_{559}.

The intensity of S_2 multiline signal registered from 2-flash sample ($Y_D^{red}S_3$ centers) incubated at 195 K shows (Fig. 3) quite different behavior than observed in $Y_D^{red}S_2$ centers: during the first 10–15 days of incubation the signal demonstrates an increasing behavior, and slow decrease followed after more than 200 days of incubation. Signal of oxidized Cyt b_{559} in 2-flash samples rise up to 88%–90% its maximal intensity. Again, the signal of $Y_D^{\bullet}$ radical demonstrate an increasing behavior during the incubation, however similar to the $Y_D^{red}S_2$ samples this process was less manifested than oxidation of Cyt b_{559}. The complex behavior of the S_2 state multiline signal in the $Y_D^{red}S_3$ samples can be explained by the increase of S_2 population in the initial step of the S_3-S_1 decay.

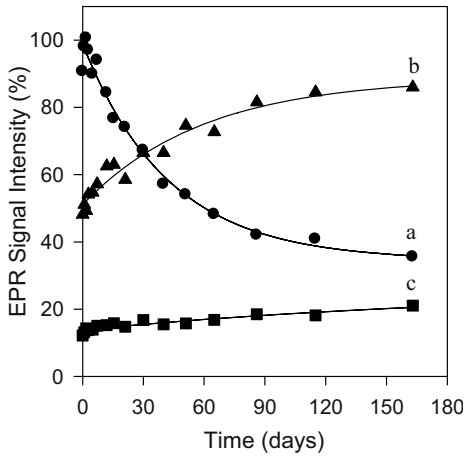

Fig. 2 The amplitudes of S_2 state multiline signal (a), cytochrome b_{559} (b) and tyrosine $Y_D^{\bullet}$ radical (c) registered during incubation of 1-flash sample (initial state was $Y_D^{red}S_2$) at the temperature of 195 K.

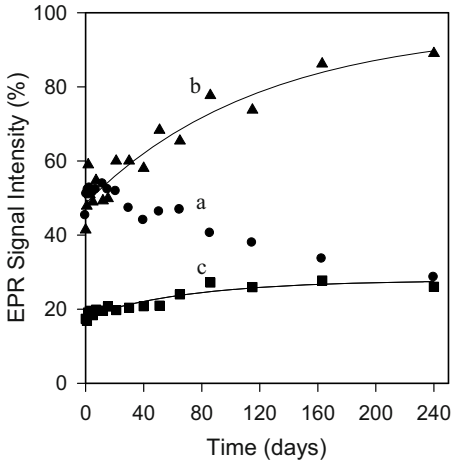

Fig. 3 The amplitudes of S_2 state multiline signal (a), cytochrome b_{559} (b) and tyrosine $Y_D^{\bullet}$ radical (c) registered during incubation of 2-flash sample (initial state was $Y_D^{red}S_3$) at the temperature of 195 K.

In ours previous study (Feyziyev *et al*., 2003) we show that both reduced tyrosine Y_D and Cyt b_{559} becomes oxidized in significant extent during the dark storage of the S_2 and S_3 samples at 245 K which was nterpreted as a capability of Cyt b_{559} to compete with tyrosine Y_D for electron donation to the highest S-states through the redox equilibrium with other cofactors situated in PSII (for example Car/Chl_Z-P_{680}-Y_Z pathway) or in direct reactions. The results of present investigation demonstrate that during the

decay of both S_2 and S_3 states to S_1 at temperature 195 K significant oxidation of the Cyt b_{559} take place while tyrosine oxidation was negligible. Thus the results of present study may confirm the early interpretation. Apparently very low temperature, as it was shown, blocks the tyrosine Y_D oxidation in both the S_2 and S_3 samples which was manifested by a little increase of $Y_D^{\bullet}$ radical signal. The obtained results show that in the situation when tyrosine Y_D cannot compete for electron donation, is suitable for reduced Cyt b_{559} become a favorable candidate as an electron donor to higher S-states. However either the electron transfer from Cyt b_{559} to the S_2 and S_3 states of PSII is a result of direct reaction or this process occurs through the equilibrium with other components still is not clear.

Acknowledgements

We are very appreciative for the kind discussion provided by Dr. G Bernat, Plant Biochemistry, Ruhr University Bochum, and Z Deák, Institute of Plant Biology, Szeged, Hungary.

References

Barber J (2003) Photosystem II: The Engine of Life. Quart. Rev. Biophys. 36: 71-89

Berthold DA, Babcock GT, Yocum CF (1981) A Highly Resolved, Oxygen-Evolving Photosystem II Preparation from Spinach Thylakoid Membranes. FEBS Lett. 134: 231-234

Buser CA, Thompson LK, Diner BA, Brudvig GW (1990) Electron-Transfer Reactions in Manganese-Depleted Photosystem II. Biochemistry 29: 8977-8985

Debus RJ (1992) The Manganese and Calcium Ions of Photosynthetic Oxygen Evolution. Biochim. Biophys. Acta 1102: 269-352

Diner BA, Babcock GT (1996) Structure, Dynamics, and Energy Conversion Efficiency in Photosystem II. In: Ort DR, Yocum CF (eds.), Oxygenic Photosynthesis: The Light Reactions. Kluwer Acad. Publ.: Dordrecht, pp. 213-247

Faller P, Maly T, Rutherford AW, MacMillan F (2001) Chlorophyll and Carotenoid Radicals in Photosystem II Studied by Pulsed ENDOR. Biochemistry 40: 320-326

Feyziyev Y, Van Rotterdam BJ, Bernat G, Styring S (2003) Electron Transfer from Cytochrome b_{559} and $Tyrosine_D$ to the S_2 and S_3 States of the Water Oxidizing Complex in Photosystem II. Chemical Physics 294: 415-431

Hanley J, Deligiannakis Y, Pascal A, Faller P, Rutherford AW (1999) Carotenoid Oxidation in Photosystem II. Biochemistry 38: 8189-8195

Stewart DH, Brudvig GW (1998) Cytochrome b_{559} of Photosystem II. Biochim. Biophys. Acta 1367: 63-87

Styring S, Rutherford AW (1987) In the Oxygen-Evolving Complex of Photosystem II the S_0 State Is Oxidized to the S_1 State by Y_D^+ (Signal II_{slow}). Biochemistry 26: 2401-2405

Styring S, Rutherford AW (1988) Deactivation Kinetics and Temperature Dependence of the S-State Transitions in the Oxygen-Evolving System of Photosystem II Measured by EPR Spectroscopy. Biochim. Biophys. Acta 933: 378-387

Thompson L, Brudvig G (1988) Cytochrome-b559 May Function to Protect Photosystem II from Photoinhibition. Biochemistry 27: 6653-6658

Vass I, Styring S (1991) pH Dependent Charge Equilibria between Tyrosine-D and the S-States in Photosystem II. Estimation of Relative Midpoint Redox Potentials. Biochemistry 30: 830-839

Völker M, Ono T, Inoue Y, Renger G (1985) Effect of Trypsin on the PSII Particles. Correlation between Hill Activity, Mn-Abundance and Peptide Pattern. Biochim. Biophys. Acta 806: 25-34

Molecular Dynamics Simulations of a Putative H^+ Pathway in Photosystem II

Felix M Ho[a,*]

[a]Department of Photochemistry & Molecular Science, The Ångström Laboratory, Uppsala University, 751 20 Uppsala, Sweden.
[*]Corresponding author. Tel. No. +46 18 471 6584; Fax No. +46 18 471 6844; E-mail: Felix.Ho@fotomol.uu.se.

Abstract: A putative H^+ exit pathway consisting of residues surrounding a dynamically stable water chain leading from the $CaMn_4$ cluster towards the lumen was studied using molecular dynamics (MD) simulations. A number of residues that were previously shown to be important for H^+ transport *in vivo* were found to interact with this water chain, consistent with the Grotthuss mechanism. Furthermore, MD data from PSII mutated *in silico* elucidated possible structural and electrostatic roles of other residues not previously regarded as directly involved in H^+ transport. These results could be correlated with literature data of *in vivo* mutants, and an earlier proposal of certain residues acting as a localised buffer for receiving released H^+. Overall, comparisons of our MD results of *in silico* mutants with *in vivo* mutagenesis data have revealed some unifying themes in the roles played by different residues involved in H^+ transport.

Keywords: Photosystem II; proton transport; molecular dynamics

Introduction

Considering the tightly-packed protein environment of PSII, it has been proposed that specific pathways may exist to facilitate the passage of substrate water molecules to the $CaMn_4$ cluster, and the exit of the O_2 and H^+ produced as a result of water oxidation. Such pathways may also help to control and tune the flow of these molecules through the protein matrix to optimise the function of PSII (reviewed in Ho, 2008).

Since "naked" H^+ do not exist in an aqueous environment, H^+ has to be transferred via water and/or amino acid residues, with the Grotthuss mechanism being generally accepted as a model for H^+ transport. Site-directed mutagenesis studies have shown the importance of a number of residues in this regard (Chu *et al.*, 1994, 1995a, 1995b). Based on the static crystal structure of PSII and literature biochemical studies, recent computation and crystallographic studies have proposed such a number of such pathways (see Ho, 2008). In the present study, the dynamic PSII was studied using molecular dynamics (MD) simulations, focusing on a putative H^+ transport pathway. Data from both the wild-type (WT) PSII and PSII mutated *in silico* were analysed and compared with each other to investigate the behaviour and roles of residues involved. These results were also compared with literature *in vivo* data to correlate the observations with experimental data. In this way, insights could be obtained into the roles the residues play and their interactions with water molecules at a molecular level.

Materials and Methods

10.0 ns MD trajectories (1 fs steps) were calculated for each of the WT and mutant PSII systems using the CHARMM forcefield, sampling every 5 ps. The coordinates from the crystal structure by Loll *et al*. (2005, 2AXT) was used as the starting point. As the focus was the putative H^+ pathway, a truncated spherical system 35 Å in radius was studied, with the centre of the sphere near the end of the pathway. Harmonic restraints were placed on atoms at the boundary layer to account for the truncation. The system was soaked with explicit solvent water molecules (TIP3 type), then first relaxed with a fixed protein environment, before being equilibrated (1 ns) through a series of steps with protein constraints being released gradually. The simulations were performed on resources provided by the Swedish

National Infrastructure for Computing (SNIC) at UPPMAX, Uppsala.

Results and Discussions

The putative H^+ transport pathway

The putative H^+ transport pathway that was studied is shown in Fig. 1. The pathway leads from the $CaMn_4$ cluster to the lumen, ending at a crevice between the D1, D2 and PsbO subunits. A dynamically stable chain of water molecules was found within a channel in the protein, and it was found that they interacted with a number of residues that have been shown by *in vivo* site-directed mutagenesis to be important for H^+ transport. In particular, the D1-D61 and -E65 were found to be critical for maintaining O_2 evolution activity, and mutations to non-protonatable or apolar residues were extremely detrimental to PSII activity (Chu *et al*., 1995a). Similar effects were also reported for D1-170 and -E333 (Chu *et al*, 1994; Chu *et al*., 1995b), though these may also involve direct interference with $CaMn_4$ stability. Interestingly, mutation of D1-R334 was also found to cause impairment of PSII activity (Li and Burnap, 2002), though the cause was less clear, since the already protonated R334 cannot act as a H^+ conduit.

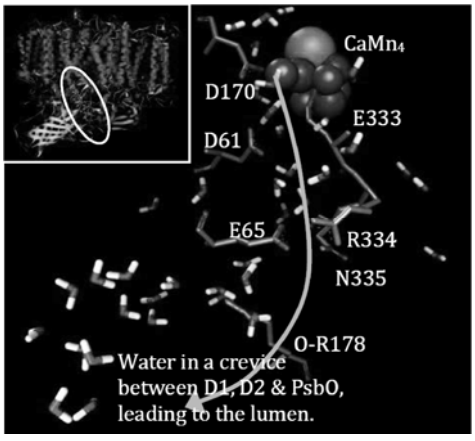

Fig. 1 The putative H^+ pathway studied by MD. All residues in the D1 subunit unless otherwise stated. Other residues in the vicinity completing the protein matrix omitted for clarity. Inset: the position of the chain in the PSII complex.

A "hot-spot" in the H^+ transport pathway

The analysis of the MD trajectory of WT PSII revealed a "hot-spot" around D1-D61, -E65, -R334, -N335 and PsbO-R178, where a highly interconnected hydrogen-bonding network was found. Several positions were highly occupied by water molecules that bridged between the surrounding residues (Fig. 2).

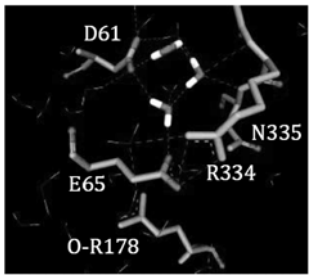

Fig. 2 The "hot-spot" in the putative H^+ pathway.

Consistent with their proposed roles in facilitating/enabling H^+ transport, D61 and E65 were found to be highly connected through water bridging. By analyzing the MD data, these residues were found to be bridged 98% of the time (93% via a 2-water bridge, 41% via a 1-water bridge; note that both motifs were sometimes present at the same time). This is consistent with their being protonable residues capable of passing H^+ towards the lumen. Literature *in vivo* studies have shown replacements of these residues with isosteric but non-protonatable residues, or with apolar residues dramatically reduced O_2 evolution activity (17%–21% of WT).

The next point of interest is the region around D1-E65 and R334. These residues were found to be connected 100% of the simulation time (95% direct hydrogen-bonding/salt-bridging, 7% via a 1-water bridge). In addition, it was found that E65 was connected to the adjacent N335 86% of the simulation time (36% direct, 53% via 1-water bridging). Together these three residues formed a steric block that prevented the exit of water molecules towards the lumen, but according to the Grotthuss mechanism, E65 could clearly pass H^+ to water molecules on the luminal side. Another residue with which E65 showed extensive interaction was PsbO-R178, found luminal to E65. These residues were connected 94% of the time (29% direct, 67% via 2-water bridging).

Additionally, a high degree of interaction between N335 and the surround residues were found. Apart from being connected to E65, N335 was also connected via its backbone N atom to the sidechain of D61 through 1- or 2-water bridges 82% of the time. As can be seen in Fig. 2, these are also the water molecules that are involved in the bridging between D61 and E65. Furthermore, even the sidechain of N335 was found to be connected via 1- or 2-water

bridges to the sidechain of D61 51% of time. Again, these water molecules were involved in D61-E65 bridging. Overall, both R334 and N335 may have a role in keeping these bridging water molecules in place and help maintain a stable connection between D61 and E65.

From the above analysis, it can be seen that there is extensive interconnections via hydrogen bonding between the residues and water molecules involved in this putative H^+ pathway. It seemed likely that this helps to keep the different components in the correct relative orientations and conformations for H^+ transport. In particular, E65 appears to be kept in place through a balance of numerous interactions with surround residues and water molecules, and that these contribute to the maintenance of a stable connection between D61 and E65. These points are clearly demonstrated in the simulations of mutant PSII.

Disrupting the pathway: R334 mutants

It was reported that *in vivo* PSII mutants at D1-R334 led to significant reduction of O_2 evolution activity, changes in the S-cycle oscillation pattern and flash-O_2 release kinetics (Li and Burnap, 2002). The reasons for this have not been entirely clear. Given the involvement of R334 in the "hot-spot" and the analyses above, the literature mutants (R334V, R334E) were constructed and simulated *in silico*, and their MD data compared with WT.

Very significant disruptions of the putative H^+ pathway were found in both cases (Fig. 3). Most clearly, the E65 rotated away from D61, due to the loss of salt-bridging to R334, thereby changing the balance of interactions around E65. Bridging between E65 and N335 was also thereby abolished. Instead, salt bridging between E65 and PsbO-R178 was established 100% of the simulation time. The "hot-spot" opened up as a result, and the distance between D61 and E65 increased. Instead of the stable and tight 1- or 2-water connection in WT, analysis of the positions occupied by water molecules showed that these residues were connected by longer chains of water (examples in Fig. 4), and the channel became open to the lumen. Furthermore, the conformation of D61 became more variable (Fig. 5), which may also contribute to reduced H^+ transport efficiency. Interestingly, in the R334E mutant, a new connection was established between D61 and R334E (Fig. 4b), which were 1- or 2-water bridged 94% of the time. This may contribute to the lesser disruption in PSII activity in this mutant compared to R334V (Li and Burnap, 2002). In addition, although it was found that D61 and E65 were generally connected by a shorter chain of water in the R334V mutant than in the R334E mutant (not shown), the chain of water in the former mutant was more frequently broken. In such instances, D2-E312 was found to interact with the water molecules in such a disrupted chain.

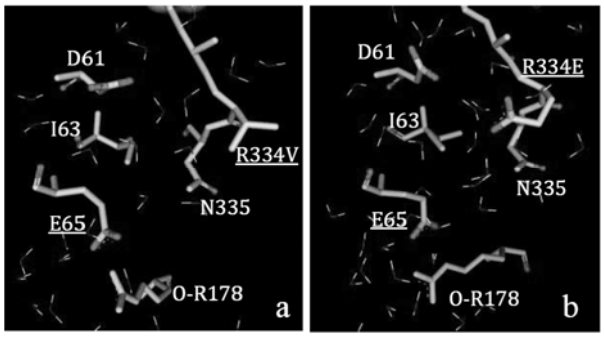

Fig. 3 The region around the "hot-spot" in the (a) R334V and (b) R334E mutant PSII.

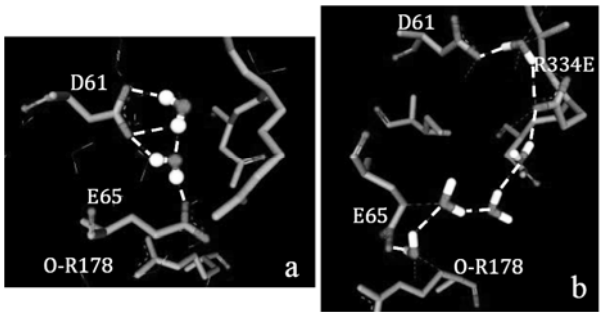

Fig. 4 Examples of the connections between D61 and E65 in (a) WT and (b) R334E mutant PSII.

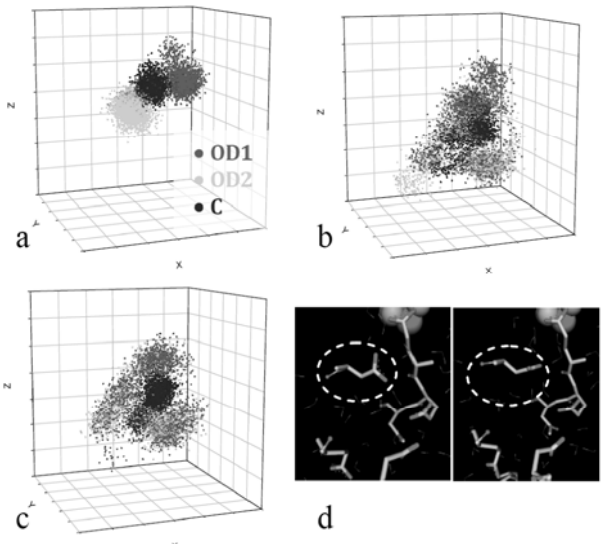

Fig. 5 3D-coordinate plots of the positions of the sidechain O (OD1, OD2) and carbon (C) atom of D61 in (a) WT (b) R334E and (c) R334V PSII during the course of the simulations. (d) Examples of D61 conformations in the R334E mutant.

Other indications of H^+ pathway involvement

The MD results gives strong indication that R334 plays an important role in keeping the conformations of residues at the "hot-spot" optimal for H^+ transfer. Apart from the reduction in O_2 evolution activity as a result of the mutations at R334, a number of other indications suggest that this residue is important to the proper function of a H^+ pathway. It has been found *in vivo* that R334E and R334V mutants exhibit slow flash-O_2 release (Li and Burnap, 2002). This has also been observed in the mutants D61E, -D61N, -D61A and PsbO-deletion mutants (Hundelt *et al*., 1998; Qian *et al*., 1999). Slow flash-O_2 release has also been observed in a carbonic anhydrase (Cah3)-deficient mutant of *Chlamydomonas reinhardtii*. This effect that has been attributed to inefficient H^+ removal, which could be reversed by the reconstitution with Cah3 and bicarbonate (Shutova *et al*., 2008). The observation that R334 mutations also lead to a similar O_2-release retardation, as well as the MD data above showing the disruptions to the region around E65 strongly suggest that the R334 mutations effects are related to H^+ transport efficiency.

Furthermore, it can be noted that the putative H^+ pathway studied here dovetails very well with the a cluster of carboxylic groups (CCG) located in the PsbO subunit that has been proposed to act as a buffer to accept H^+ released during water oxidation (Shutova *et al*. 2007; Fig. 6). The retarded flash-O_2 release in the PsbO-deletion mutant mentioned above gives further support for this proposal.

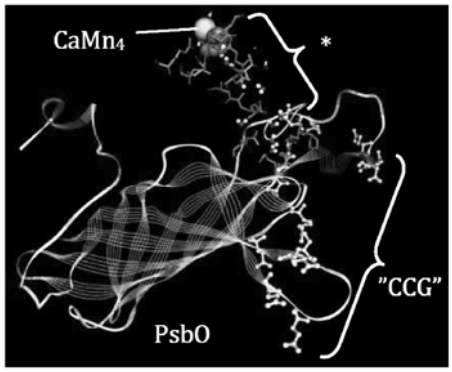

Fig. 6 The connection between the putative H^+ channel studied here (*) and the cluster of carboxylic groups (CCG) in the PsbO subunit.

Conclusions

Taken together, the present MD results in conjunction with the literature biochemical data strongly suggest that the chain of amino acid residues studied here are responsible for H^+ transport. The highly interconnected hydrogen bonding network at a "hot-spot" around D1-D61, -E65, -R334 and -N335 appears to be extremely important for maintaining efficient H^+ transfer to the lumen. In particular, through analysing the MD data for WT and mutant PSII, it could be demonstrated that R334 and N335 play an important structural and possibly also electrostatic role in maintaining this "hot-spot". Further clarity is thereby shed on the nature of the H^+ pathway in PSII.

Acknowledgements

I would like to thank Prof. Lennart Nilsson and Dr. Clyde Cady for valuable help and discussions. The financial support of the Carl Tryggers Foundation for Scientific Research, the Knut and Alice Wallenberg Foundation, the Solar-H2 program of the European Community, the Swedish Energy Agency and the Swedish Research Council is gratefully acknowledged.

References

Chu HA, Nguyen AP, Debus RJ (1994) Site-Directed Photosystem II Mutants with Perturbed Oxygen-Evolving Properties. Instability or Inefficient Assembly of Manganses Cluster in Vivo. Biochemistry 33: 6137-6149

Chu HA, Nguyen AP, Debus RJ (1995a) Amino Acid Residues that Influence the Binding of Manganese or Calcium to Photosystem II. The Luminal Interhelical Domains of the D1 Polypeptide. Biochemistry 34: 5839-5858

Chu HA, Nguyen AP, Debus RJ (1995b) Amino Acid Residues that Influence the Binding of Manganese or Calcium to Photosystem II. The Carboxyl-Terminal Domain of the D1 Polypeptide. Biochemistry 34: 5859-5882

Ho F (2008) Uncovering Channels in Photosystem II by Computer Modeling: Current Progress, Future Prospects, and Lessons from Analogous Systems. Photosyn. Res. 98: 503-522

Hundelt M, Hays AMA, Debus R, Junge W (1998) Oxygenic Photosystem II: the Mutation D1-D61N in Synechocystis sp. PCC 6803 Retards S-State Transitions without Affecting Electron Transfer

from Y_Z to P_{680}^+. Biochemistry 37: 14450-14456

Li Z, Burnap RL (2002) Mutations of Basic Arginine Residue 334 in the D1 Protein of Photosytem II Lead to Unusual S_2 State Properties in Synechocystis sp. PCC 6803. Photosyn. Res. 72: 191-201.

Loll B, Kern J, Saenger W, Zouni A, Biesiadka J (2005) Towards Complete Cofactor Arrangement in the 3.0Å Resolution Structure of Photosystem II. Nature 438: 1040-1044

Qian M, Dao L, Debus R, Burnap RL (1999) Impact of Mutations within the Putative Ca^{2+}-Binding Luminal Interhelical a-b Loop of the Photosystem II D1 Protein on the Kinetics of Photoactivation and H_2O Oxidation in Synechocystis sp. PCC6803. Biochemsitry 38: 6070-6081

Shutova T, Klimov VV, Andersson B, Samuelsson G (2007) A Cluster of Carboxylic Groups in PsbO Protein Is Involved in Proton Transfer from the Water Oxidizing Complex of Photosystem II. Biochim. Biophys. Acta 1767: 434-440

Shutova T, Kenneweg H, Buchta J, Nikitina J, Terentyev V, Chernyshov S, Andersson B, Allakhverdiev SI, Limov VV, Dau H, Junge W, Samuelsson G (2008) The Photosystem II-Associated Cah3 in Chlamydomonas Enhances the O_2 Evolution Rate by Proton Removal. EMBO J 27: 782-791

Catalytic Cooperativity of Mono-Manganese and Tri-Manganese Clusters for Water-Splitting and Oxygen-Evolving Reaction in Photosystem II: Chemical Mechanistic Insight

Masami Kusunoki[a]

[a]Department of Physics, School of Science & Technology, Meiji University, Kawasaki, 214-8571, Japan.
[*]Corresponding author. Tel. No. +81 44 934 7433; Fax No. +81 44 934 7911; E-mail: kusunoki@isc.meiji.ac.jp.

Abstract: Applying the UDFT/B3LYP/(lacvp**, lacv3p**) geometry optimization method together with a Poisson-Boltsman equation solver in the e = 4 dielectric medium to a version-upped "truncated-OEC-cluster" model of MT-type, we found that (1) Upon the S_i-state transitions (I = 0 – 4) in a cyclic change of the most-stable tautomer(s), a proton release pattern of 1:0:1:2 has been derived with use of calculated exothermic vs endothermic energies, to yield the oxidation states: $S_0\{Mn_a^{III}; Mn_b^{III}, Mn_c^{III}, Mn_d^{IV}\}$, $S_1\{Mn_a^{III}; Mn_b^{IV}, Mn_c^{III}, Mn_d^{IV}\}$, $S_2^+\{Mn_a^{IV}; Mn_b^{IV}, Mn_c^{III}, Mn_d^{IV}\}$, $S_3^+\{Mn_a^{IV}; Mn_b^{IV}, Mn_c^{IV}, Mn_d^{IV}\}$ and $S_{4a}\{Mn_a^{IV}; Mn_b^{IV}, Mn_c^{IV}, Mn_d^{IV}\}$, (2) The redox potential for the last S_3/S_{4a}^+ oxidation step has been evaluated to be ca.1.07 V, a significantly-reduced value due to the H-bonding network between Y_Z, H190 and Ca^{2+}-binding site in the Mn_4Ca cluster, (3) The S_{4a}-intermediate contains the catalytic Mn_a^{IV} ion binding two adjoining substrate derivatives, a hydroxyl anion (W1 = HO^-) and an oxo radical (W2 = $O^{-\bullet}$), and (4) The O-O bond formation is thermally induceable by a proton-coupled electron transfer (PCET) via a transition state with an activation energy of ca. 11.2 kcal/mol and a small exothermicity of ca. –4.5 kcal/mol, to yield a *side-on* superoxo anion radial bound to the Mn_a^{III} ion in the second intermediate, formulated as $S_{4b}\{Mn_a^{III}:O_2^{-\bullet}(W1 = W2); Mn_b^{IV}, Mn_c^{III}, Mn_d^{IV}\}$, where the third Mn_c^{III} ion is in a low-spin state of S_c=1.

Keywords: UDFT B3LYP method; Photosystem II; Oxygen evolving complex; Mn_4Ca cluster; O-O bond formation; Redox potential; Proton release pattern

Introduction

The molecular mechanism of the water-splitting and oxygen-evolving reaction in photosystem II (PSII) has been a subject of considerable studies since B. Kok proposed a phenomenological linear four-step mechanism (Kok *et al*., 1970). This reaction takes place in an oxygen evolving complex (OEC), which essentially incorporates four Mn, one Ca and one Cl ions, to cycle five intermediates, Si (i = 0 – 4). Recent remarkable improvements in X-ray diffraction data of PSII structure have established the existence of a catalytic Mn_4Ca core ligated by six polypeptide carboxylates (Asp and Glu) and one His, (Ferreira *et al*., 2004; Loll *et al*., 2005), and the essential cofactor Cl^- ion (Murray *et al*., 2008; Guskov *et al*., 2009; Kawakami *et al*., 2009). Then, some DFT-theoretical models for catalytic Mn_4Ca clusters were proposed (Kusunoki, 2007; Sproviero *et al*., 2008; Siegbahn, 2009). Here, we do version-up our previous model to a chemically more complete model for the Mn_4Ca cluster of the MT-5J type, one of the most-likely tautomers through out the S_i-state cycle, and show that it can cycle going over the last oxidation process during $S_3 \rightarrow S_4^+$ transition and lastly forming the O-O bond on the monomeric (M) Mn ion in the late-limiting process with a time constant of order ~0.1 msec.

Model and Methods

The present model in the S_1-state consists of the monomeric (M) and hetero-tetrameric (T: Mn_3CaO_4H) Mn clusters connected by mono-μ-oxo-mono-μ-

carboxylato bridge between Mn_a^{III} and Mn_b^{IV} ions, including 5 bidentate carboxylate bridge ligands (D170, E189, E333, D342, A344, CP43-E354), 2 mono-dentate ligands (E189, H332) to Mn_c^{III}, and 9 hydrated water molecules in an improved enzymatic field ($D61^{=}$, Cl^{-}, D2-$K317^{+}$, CP43-$R357^{+}$, and dielectric medium with $\varepsilon = 4$). Mn_a binds two *current-substrate* (W1/W2) and the third water molecule (W3) and Ca^{2+} ion does two water molecules (W5, W6). Only H332-E333 and Yz-H191 are full amino acids, but the others were truncated. This OEC-cluster model includes some fixed atoms in the geometry optimization by the following method.

The molecular structures of model Mn_4Ca clusters have been optimized by the standard UDFT/B3LYP/lacvp** method, which can predict the geometries of multinuclear manganese complexes within an accuracy of ~0.02 Å, but, the SCF energies were calculated for the high-spin states with use of a triple-ζ quality basis set, lavc3p**. All the possible tautomers in the S_i-state define the S_{ij}-substates, and their electron-abstracted and proton-released states were also investigated.

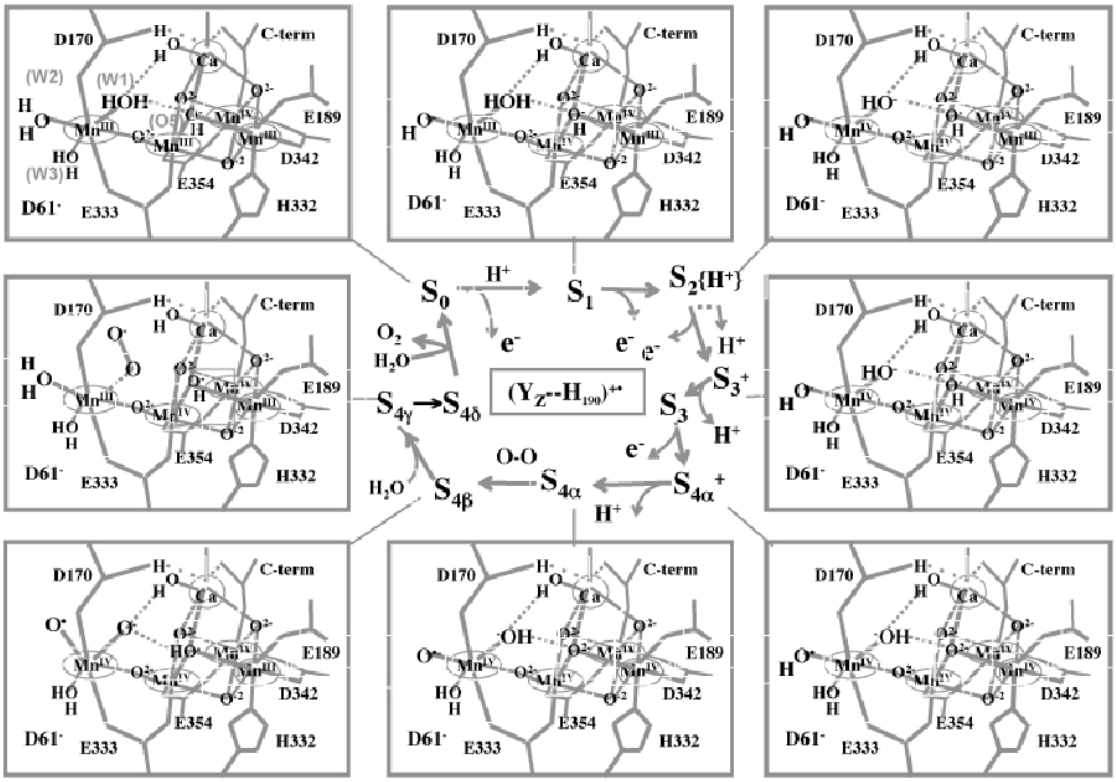

Fig. 1 The mechanism of water-splitting and oxygen-evolving reaction via the most-likely tautomers in PSII.

Results and Discussion

In Fig. 1, we have summarized the results of our DFT-geometry optimizations with use of *truncated-OEC-cluster model* of the MT-5J type to show the mechanism of water oxidation reactions via the most-likely Mn_4Ca complex tautomers in PSII. Notably, this OEC-cluster is neutral at pH 7 in the dark stable S_1-state involving $2Mn^{III}$ and $2Mn^{IV}$ ions. Hence, S_0-state can be generated by adding one hydrogen atom to this S_1-state. We found: **(1)** the positive electron-holes are accumulated as a cyclic change of four Mn-valencies, $S_{0a}(3334) \rightarrow S_{1a}(3434) \rightarrow S_{2a}(4434) \rightarrow S_{3a}^{+}(4444) \rightarrow S_{4a}(4444)$; **(2)** the 1st and 2nd electron-holes have been created in the Mn_a^{IV} ion upon the first two S_i-state transitions, while the 3rd electron-hole is created in Mn_c^{IV} ion upon $S_{2a} \rightarrow S_{3a}^{+}$ transition; **(3)** the proton release pattern around pH 7 is {1,0,1,2}, because the work to remove the 1st proton from W2 upon $S_{0a}^{+} \rightarrow S_{1a}$ transition (~255 kcal/mol in gas phase) is slightly less than the proton solvation energy (261 kcal/mol), but in S_{2a} the 2nd proton released from W1(= H_2O) can be trapped by a nearby H337 in the $S_{2a}\{H^{+}\}$-state until it will be released upon $S_{2a} \rightarrow S_{3a}^{+}$ oxidation step, while the last oxidation reaction must be preceeded by the 3rd proton release from a μ_3-oxo bridge, O5(= HO^{-}),

connecting Mn_b^{IV}, Mn_c^{IV} and Ca^{2+} ions so as to be able to oxidize W2(= HO^-) to form Mn_a^{IV}-($HO^\bullet$) species in $S_{4\alpha}^+$, which will immediately release the 4th proton to form Mn_a^{IV}-$O^{\bullet-}$ species in $S_{4\alpha}$-state; **(4)** the midpoint redox potentials (E_m) for one-electron oxidation upon $S_{0j}\rightarrow S_{1j}^+$, $S_{1j}\rightarrow S_{2j}^+$, $S_{2j}\rightarrow S_{3j}^+$ and $S_{3j}\rightarrow S_{4j}^+$ transitions, which may sensitively depend on the model OEC-cluster, their H-bond interactions with Y_Z and H190 and their electrostatic interactions with the far-distant surrounding proteinaceous charges, were calculated to be $E_{mi}^{(0)}$= 0.79, 0.86, 1.16, and 1.96 V, respectively, for the basic QM model of our OEC-cluster embedded in the ε = 4 dielectric medium.

Thus, the first three $E_{mi}^{(0)}$-values (i = 0-2) are smaller than the recent E_m value (≈ 1.26 V) for the $P680^+$/P680 couple (Rapaport *et al*., 2002) and hence may be acceptible, but the last $E_{m3}^{(0)}$-value much larger than 1.26 V points out the absolute necessity to account for the effect of H-bonding water network between Y_Z (Y161), H190 and Ca^{2+} ion binding two water molecules. Therefore, we prepared four coupled systems as depicted in Fig. 2 based on 2.9 Å XRD model (Guskov, 2009), which are named **1**=[S_{3b}-Y_ZOH••H_{190}], **2**=[S_{3b}-$Y_ZOH^{+\bullet}$-H_{190}], **3**=[S_{3b}-$Y_ZO^\bullet$-H^+-H_{190}], and **4**=[S_{4b}^+-Y_ZOH••H_{190}]. In DFT-gemetry optimizations, we fixed all the atoms except for all the ligands (including W5 and W6) coordinating to Ca^{2+} ion and two amino acid residues of Y_Z (= Y_ZOH) and H190. The H-bond distances between W6-O and Yz-O and between Y_Z-O and H190-N_ε atoms, designated R^k_{YW} and R^k_{YH}, respectively (k = 1 – 4) are filled in Fig. 2. Initial state **1** is stabilized by forming H-bonds with R^1_{YW} = 2.87Å and R^1_{YH} = 2.76Å. As Y_Z was oxidized by $P680^+$, the Y_Z-proton in **2**-state is localized near a center of the significantly shortened H-bond with H190 (R^2_{YH} = 2.54Å) and then transferred to N_ε-H190 with a relaxed bond length of R^3_{YH} = 2.78Å in **3**-state. This **3**-state can change its energy depending on the structure of H-bond network, hence only suggesting the E_m for **3**/**1** (*i.e.* Y_Z^{OX}/Y_Z) couple lying around 0.91~1.51 V. However, the final state **4** was more definitely stabilized due to stronger H-bonds with R^4_{YW} = 2.81Å and R^4_{YH} = 2.73Å than the **3**-state, yielding the key E_m for S_4^+/S_3 (*i.e.* **4**/**3**) couple at 1.07 V. The resultant $S_{4\alpha}^+$-state is illustrated in Fig. 1.

In Fig. 3, we have proposed a new mechanism of the O-O bond formation in PSII. This key step can occur via a transition state, $T_{4\alpha\beta}$, at the activation energy of ca. $\Delta E^\# \approx$ 11.2 kcal/mol, where a hydrated water molecule W4 catalizes the O-O bond formation between a hydroxo anion, HO^-(= W1) and an oxo radical $O^{\bullet-}$ (= W2) at cis-positions so as to bring an activated bond length, d(O-O)* = 2.30Å. Then, after the W1-proton came back to O5-bridge, an intra-cluster ET simultaneously takes place to produce the 3rd S_4-intermediate, $S_{4\beta}$(4434), where a superoxo ion, O_2^-, formed as a side-on ligand to Mn_a^{III} specified by a typical bond length, d(O-O) = 1.32Å. This step is rate-limiting and slightly exothermic ($\Delta E_{4\alpha\beta} \approx$ –4.5 kcal/mol).

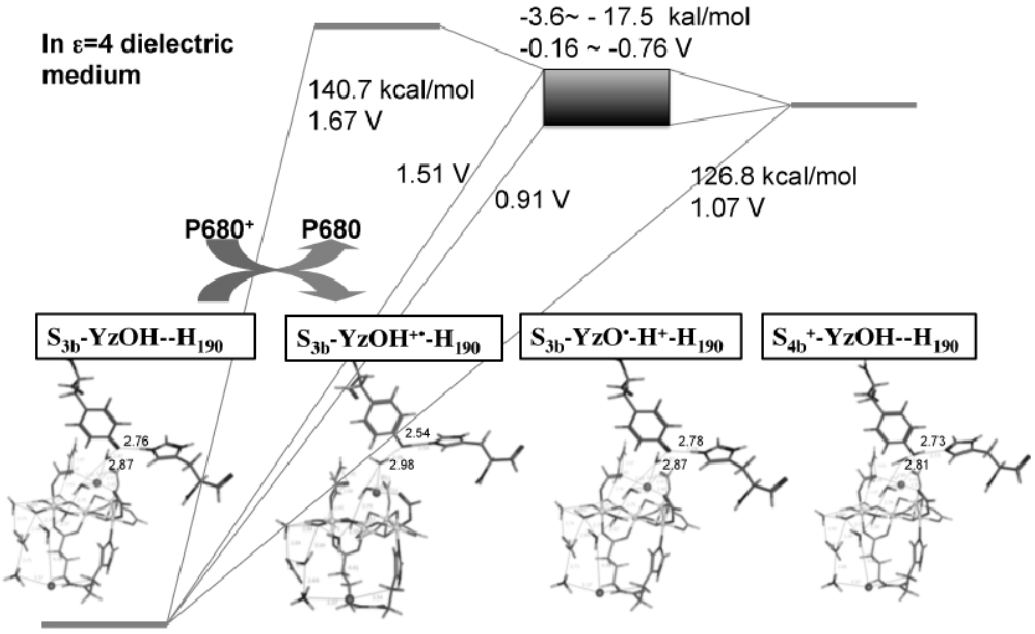

Fig. 2 Four coupled systems to evaluate the midpoint redox potential for the fourth oxidation step of S_{3b}-to-S_{4b}^+ transition in PSII.

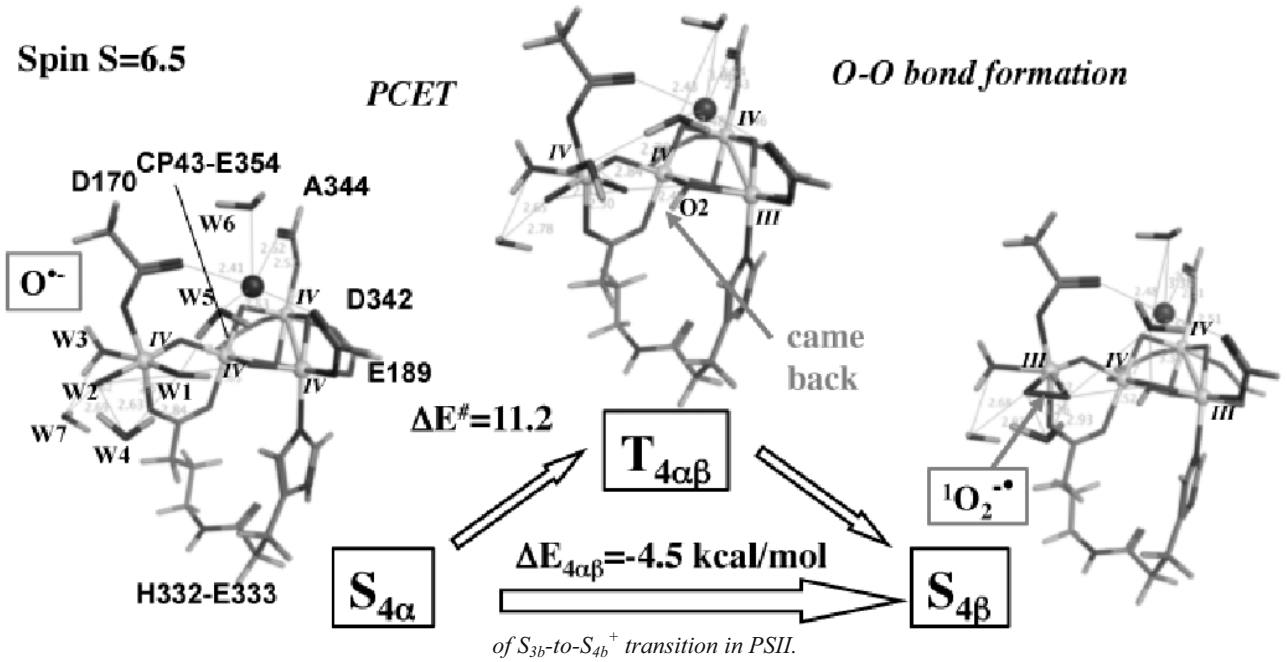

Fig. 3 A new mechanism of O-O bond formation on the monomeric Mn_a site induced by PCET between monomeric and trimeric Mn clusters as well as the catalytic hydrated water molecules in PSII.

Concluding Remark

The XRD model of the S_1-state OEC at 1.9Å resolution reported by Shen's group at this congress is reconcilable with our present model if a suitable tautomeric equilibrium can exist.

References

KN Ferreira, TM Iverson, K Maghlaoui, J Barber, S Iwata (2004) Architecture of the Photosynthetic Oxygen-Evolving Center, Science 303: 1831-1838

B Loll, J Kern, W Saenger, A Zouni, J Biesiadka (2005) Towards Complete Cofactor Arrangement in the 3.0 A Resolution Structure of Photosystem II. Nature 438: 1040-1044

A Guskov, J Kern, A Gabdulkhakov, M Broser, A Zouni, W Saenger (2009) Cyanobacterial Photosystem II at 2.9-A Resolution and the Role of Quinones, Lipids, Channels and Chloride. Nat Struct Mol Biol 16: 334-342

JW Murray, K Maghlaoui, J Kargul, N Ishida, TL Lai, AW Rutherford, M Sugiura, A Boussac, J Barber (2008) X-Ray Crystallography Identifies Two Chloride Binding Sites in the Oxygen Evolving Centre of Photosystem II. Energy Environ. Sci. 1: 161-165

K Kawakami, Y Umena, N Kamiya, JR Shen (2009) Location of Chloride and Its Possible Functions in Oxygen-Evolving Photosystem II Revealed by X-Ray Crystallography. Proc Natl Acad Sci USA 106: 8567-72

M Kusunoki (2007/2008) Mono-Manganese Mechanism of the Photosytem II Water Splitting Reaction by a Unique Mn_4Ca Cluster. Biochim Biophys Acta 1767: 484-92; Corregendom ibid 1777: 477

PE Siegbahn (2009) An Energetic Comparison of Different Models for the Oxygen Evolving Complex of Photosystem II. J Am Chem Soc 131: 18238-18239

EM Sproviero, JA Gascon, JP McEvoy, GW Brudvig, VS Batista (2008) Computational Studies of the O(2)-Evolving Complex of Photosystem II and Biomimetic Oxomanganese Complexes. Coord Chem Rev 252: 395-415

F Rappaport, M Guergova-Kuras, PJ Nixon, BA Diner, J Lavergne (2002) Kinetics and Pathways of Charge Recombination in Photosystem II. Biochemistry 41: 8518-8527

Direct Detection of Oxygen Ligands to the Mn_4Ca Complex in Photosystem II by X-ray Emission Spectroscopy

Jan Kern[a*], Henning Schroeder[a], Megan Shelby[a], Yulia Pushkar[a], Benedikt Lasalle[a], Pieter Glatzel[c], Vittal K Yachandra[a], Uwe Bergmann[b], Junko Yano[a]

[a]Lawrence Berkeley National Laboratory, Berkeley, CA 94720, USA;
[b]SLAC National Accelerator Laboratory, Menlo Park, CA 94025, USA;
[c]European Synchrotron Radiation Facility, Grenoble, France.
[*]Corresponding author. Tel. No. +1 510 486 4330; Fax No. +1 510 486 7768; E-mail: jfkern@lbl.gov.

Abstract: The Mn_4CaO_X cluster catalyzes the light driven oxidation of water in Photosystem II. To understand the mechanistic details of this intriguing machine it is necessary to unravel not only the geometric but also the electronic structure of this complex. X-ray emission spectroscopy can be one important tool in this endeavour due to its unique sensitivity towards light atoms ligated to a metal center. In addition X-ray emission spectroscopy provides information of the charge density distribution over the metal centers in the complex and is sensitive to protonation changes of bridging oxygens, both important questions in the light of different proposed mechanisms for water oxidation in PSII. Here we show that X-ray emission spectra of PSII can be collected with sufficient S/N from PSII samples and can yield insights into the mechanism of water oxidation.

Keywords: Photosystem II; Water oxidation; X-ray spectroscopy; X-ray emission spectroscopy

Introduction

Despite the availability of medium resolved crystal structures of Photosystem II (PSII) (Zouni *et al.*, 2001; Kamiya and Shen, 2003; Ferreira *et al.*, 2004; Loll *et al.*, 2005; Guskov *et al.*, 2009) some of the key questions related to the mechanism and structure of the OEC can not be answered yet. One of these questions is the involvement of oxygen atoms acting as ligands to Mn of the OEC in the reaction cycle. Another one is the change in charge density distribution over the Mn ions in the OEC during the catalytic cycle. X-ray emission spectroscopy (XES) is a highly specific technique allowing to probe both, the charge density at the metal and the interaction between the metal and its direct ligands (Glatzel and Bergmann, 2005). In XES the transitions (Fig. 1) probed are from the metal 3p into the metal 1s level ($K\beta_{1,3}$, Kβ') and from the metal-ligand 2s and 2p level into the metal 1s level ('cross over' transitions, Kβ", $K\beta_{2,5}$).

Due to the differences of the 2s binding energies the energy position for the Kβ" peak is different for each ligand element. Therefore this method - which is only sensitive to directly bound ligand atoms - allows to distinguish O, C and N ligands. In addition the peak intensity for the Kβ" transition is dependent on the metal-ligand distance and the spread of the molecular wavefunction over 2nd shell neighbours. Due to this XES can describe the first ligand sphere of Mn in the OEC in a detail that is not available by other methods.

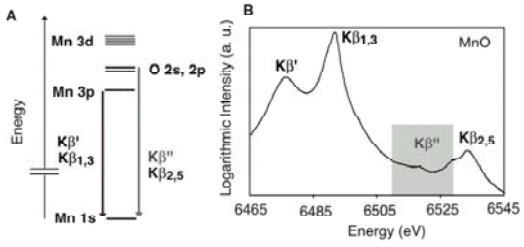

Fig. 1 Energy level scheme for transitions observed in the Mn XES experiment (left) and XES spectrum for MnO (right), showing the different energy regions for the various transitions.

Here we summarize recent results from XES studies on inorganic Mn model compounds and the first measurements on PSII together with recent approaches on the theoretical interpretation of these spectra.

Materials and Methods

PSII enriched membrane fragments were prepared from fresh market spinach following the protocol described by (Berthold *et al.*, 1981). Samples were painted on the back of a lexan sample holders and dark adapted for 1 hour to achieve > 95% population of the S_1 state. After laser flashes, the samples were frozen and stored in liquid nitrogen until use.

For recording XES spectra the samples were kept at 10 K in an Oxford cryostat, and a 14 crystal analyzer (Si 440 spherical crystals, 10 cm diameter, 1 m radius of curvature) and a Vortex energy resolving Si drift detector were arranged on a Roland circle (Fig. 2). Incident beam energy was 10.4 keV and the flux was ~ 2×10^{12} photons/(sec mm^2)**.**

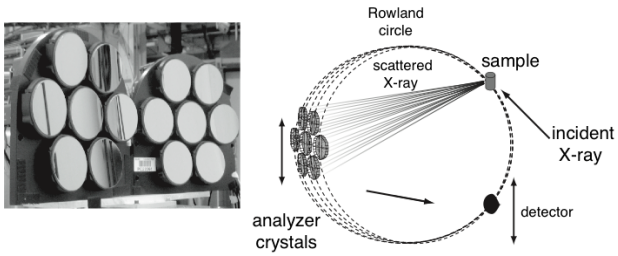

Fig. 2 Experimental setup for XES measurement showing the array of 14 analyzer crystals (left) and the arrangement of sample, analyzer and detector (right).

Results and Discussion

We used Mn XES to probe changes in the electron density distribution around Mn in the OEC and at the same time to selectively obtain information about oxygen bound to Mn against the large background of oxygen present in the entire protein complex. In addition we recorded spectra from a large set of inorganic Mn model compounds containing different modes of oxygen ligation and Mn oxidation states which allowed us to understand the different trends for changes in the XES by oxidation state, ligand type, etc.

$K\beta_{1,3}$ spectra (sensitive to charge density distribution at Mn) were collected from PSII predominantly in the S_1 state (dark adapted samples) as well as after continuous illumination at 200 K (predominantly in the S_2 state) and after giving two or three laser flashes (2F samples, predominantly in the S_3 state, or 3F samples, about 50% in the S_0 state). The $K\beta_{1,3}$ spectra show a different change in peak energy for the S_1-S_2 transition compared to the S_2-S_3 (2 flash) transition (Fig. 3), indicating a different change of the charge density distribution in the OEC for the two transitions, as observed previously (Messinger *et al*., 2001).

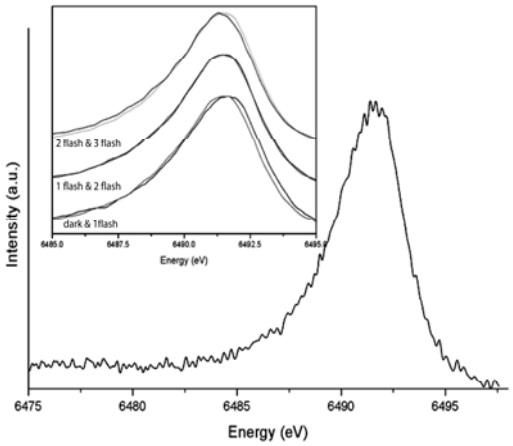

Fig. 3 $K\beta_{1,3}$ spectrum of PSII in the S_1 state and in higher flash states (inset).

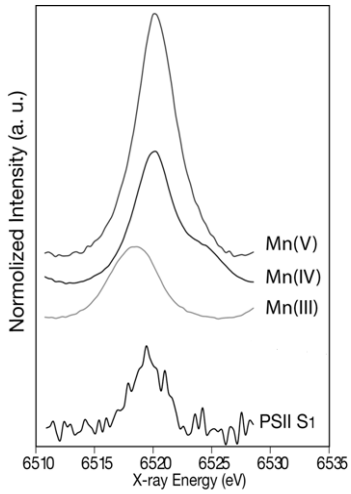

Fig. 4 Kβ" spectrum of PSII in the S_1 state with Mn(III) and Mn(IV) oxides and a Mn(V) coordination compound.

In addition spectra of the so called 'cross over' region containing the $K\beta_{2,5}$ and the Kβ" peak were collected from PSII predominantly in the S_1 state (Pushkar *et al*., 2010). In Fig. 4 the Kβ" region of PSII in comparison to three Mn oxides is shown.

The cross over region in our PSII spectra provides the first direct spectroscopic characterization of the oxygen bound to the Mn cluster. The Kβ"-spectrum of the S_1 state shows a peak between the peak positions obtained for Mn(III) and Mn(IV) in oxides. By comparing the peak intensity and position with several Mn model compounds it becomes evident that the predominant contribution to this peak comes from highly localized orbitals of metal ligands and that

contributions for example from carboxylate oxygens are weak, due to the delocalization of their 2s orbitals. The high intensity of the Kβ" peak compared to some of the model complexes indicated that there is a high number of μ-oxo bridged Mn-O bonds present in the OEC (Pushkar *et al.*, 2010).

Initial attempts to theoretically model such spectra have been undertaken recently (see *e.g.* Smolentsev *et al*., 2009). By these calculations the complementarity of XES and X-ray absorption spectroscopy (XANES, EXAFS) becomes evident (Fig. 5). In addition the high sensitivity of the XES spectra towards changes in the protonation state of the ligand bound to the metal could be demonstrated. For example the XANES and XES spectrum for hexaqua Mn(II) and the theoretical singly deprotonated complex were calculated, showing a big change in the Kβ" region but virtually no change in the absorption edge (Fig. 5) (Smolentsev *et al*., 2009).

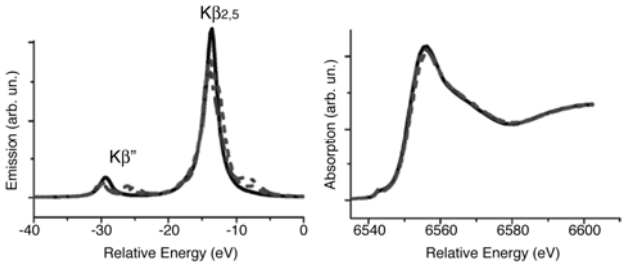

Fig. 5 Calculated spectra for XES (left) and XANES (right) of $[Mn(H_2O)_6]^{2+}$ (black line), $[Mn(H_2O)_5OH]^{+}$ (blue dashed line) and $[Mn(H_2O)_5NH_3]^{2+}$ (red dashed line) (after Smolentsev *et al.*, 2009).

Furthermore it became evident that it is important to not only focus on the Kβ" transition itself but that the $K\beta_{2,5}$ region contains a number of transitions sensitive to the nature of the ligand. Therefore it is necessary in the future to collect full spectra over the $K\beta_{1,3}$, Kβ" and $K\beta_{2,5}$ region for all S-states to facilitate a meaningful interpretation of the changes in the electronic structure of the OEC during the reaction of water oxidation in PSII.

Acknowledgements

This work was supported by the NIH grant (GM 55302), and the DOE, Director, Office of Science, Office of Basic Energy Sciences (OBES), Chemical Sciences, Geosciences, and Biosciences Division, under Contract DE-AC02-05CH11231. Portions of this research were carried out at SSRL, operated by Stanford University for DOE, OBES. The SSRL SMB Program is supported by the DOE, OBER and by the NIH, NCRR. We thank Prof. Ken Sauer for many useful discussions.

References

Berthold D, *et al*. (1981) A Highly Resolved, Oxygen-Evolving Photosystem II Preparation from Spinach Thylakoid Membranes. Febs Letters 134: 231-234

Ferreira KN, *et al*. (2004) Architecture of the Photosynthetic Oxygen-Evolving Center. Science 303: 1831-1838

Glatzel P, Bergmann U (2005) High Resolution 1s Core Hole X-Ray Spectroscopy in 3d Transition Metal Complexes—Electronic and Structural Information. Coord Chem Rev 249: 65-95

Guskov A, *et al*. (2009) Cyanobacterial Photosystem II at 2.9-Angstrom Resolution and the Role of Quinones, Lipids, Channels and Chloride. Nature Struct Mol Biol 16: 334-342

Kamiya N, Shen JR (2003) Crystal Structure of Oxygen-Evolving Photosystem II from Thermosynechococcus Vulcanus at 3.7-Å Resolution. Proc Natl Acad Sci USA 100: 98-103

Loll B, *et al*. (2005) Towards Complete Cofactor Arrangement in the 3.0 Å Resolution Structure of Photosystem II. Nature 438: 1040-1044

Messinger J, *et al*. (2001) Absence of Mn-Centered Oxidation in the S_2 -> S_3 Transition: Implications for the Mechanism of Photosynthetic Water Oxidation. J Am Chem Soc 123: 7804-7820

Pushkar Y, *et al*. (2010) Direct Detection of Oxygen Ligation to the Mn_4Ca Cluster of Photosystem II by X-Ray Emission Spectroscopy. Ang Chem Int Ed 49: 800-803

Smolentsev G, *et al*. (2009) X-Ray Emission Spectroscopy to Study Ligand Valence Orbitals in Mn Coordination Complexes. J Am Chem Soc 131: 13161-13167

Zouni A, *et al*. (2001) Crystal Structure of Photosystem II from Synechococcus Elongatus at 3.8 Å Resolution. Nature 409: 739-743

Water Oxidation in Photosystem II: Energetics and Kinetics of Intermediates Formation in the $S_2 \rightarrow S_3$ and $S_3 \rightarrow S_0$ Transitions Monitored by Delayed Chlorophyll Fluorescence

Ivelina Zaharieva*, Markus Grabolle, Petko Chernev, Holger Dau*

Freie Universität Berlin, FB Physik, Arnimallee 14, D-14195 Berlin, Germany.
*Corresponding authors. E-mail:ivelina.zaharieva@fu-berlin.de, holger.dau@fu-berlin.de.

Abstract: Water oxidation by Photosystem II (PSII) is a process of fundamental importance for atmosphere (O_2 production) and biosphere (primary biomass formation). In order to understand this basic biological process and to promote the rationale designs of artificial systems that mimic photosynthetic water oxidation, it is important to understand the energetic and kinetic parameters of intermediates formed in the course of the reaction cycle (S-state cycle). In the present study, we use time-resolved measurements of the delayed chlorophyll fluorescence to estimate rate constants, activation energies, free energy differences, and to discriminate between the enthalpic and the entropic contributions. Using a novel joint-fit simulation approach, kinetic parameters are determined for intermediates in the $S_2 \rightarrow S_3$ and in the $S_3 \rightarrow S_0 + O_2$ transitions. The estimated parameters provide evidence for intermediate formation by deprotonation processes that take place already before the electron transfer from the tetra-manganese complex to the light-oxidized Tyr_Z, in both of the above S-state transitions.

Keywords: Oxygen evolution; Delayed chlorophyll fluorescence; Proton release; S-state cycle; Thermodynamics

Introduction

As discovered by Bessel Kok and his coworkers (Kok *et al.*, 1970), in photosynthesis water is oxidized in a cyclic process involving four light-driven transitions from states denoted as S_0 to S_4. The S_4 spontaneously decays into S_0, coupled to the release of dioxygen. During one turnover of the S-state cycle, four oxidizing equivalents need to be accumulated by a tetra-manganese complex bound to the proteins of photosystem II (PSII) and this requires removal not only of electrons, but also of protons (Hoganson *et al.*, 1997; Dau *et al.*, 2008). A reaction cycle of photosynthetic dioxygen formation involving strictly alternate removal of four electron and four protons from the Mn complex has been proposed (Dau *et al.*, 2006, 2007a). The $S_1 \rightarrow S_2$ transition likely is solely an oxidation step, whereas the other classical S-state transitions involve both electron and proton removal from the Mn complex (meaning oxidation as well as deprotonation) (Dau *et al.*, 2007a). The proposed extension of Kok's classical cycle implies that some electron transfer steps (oxidation of the Mn complex) are preceded by formation of a deprotonated state, specifically in the $S_2 \rightarrow S_3$ and $S_3 \rightarrow S_4 \Rightarrow S_0 + O_2$ transitions (Haumann *et al.*, 2005; Dau *et al.*, 2006, 2007a, b). Studying the intermediate formation during the individual S-state transitions at the donor side of PSII is of clear importance for understanding of the mechanism of photosynthetic oxygen evolution.

In Haumann *et al.* (2005) and Dau *et al.* (2007b), the $S_3 \rightarrow S_4$ transition has been assigned to a deprotonation of the Mn complex or its immediate ligand environment that is electrostatically driven by the positive charge at or close to the $Y_Z^{\bullet}$ radical. The intermediate state in the $S_3 \rightarrow S_4 \Rightarrow S_0 + O_2$ transition has been identified using time-resolved X-ray measurements (Haumann *et al.*, 2005). It has been shown that dioxygen formation is preceded by a process that is completed within about 200 μs. This process has been assigned to the formation of an S_4-state by a deprotonation process. It also was demonstrated that this formation of an intermediate state prior to the onset of dioxygen formation is

clearly visible in the delayed fluorescence (DF) transients (Buchta *et al.*, 2007), as a drop in the intensity of the DF by a factor of almost hundred. This finding and the rationale developed for determination of free-energy changes using time-resolved DF measurements (Buchta *et al.*, 2007) renders DF a useful tool to study quantitatively the reactions of light-induced electron transfer at the donor side of PSII.

Here we use DF technique to study the energetics and kinetics of intermediates formation during the $S_2 \rightarrow S_3$ and $S_3 \rightarrow S_0$ transitions at the donor side of PSII. We extend the evaluation approach of the DF data proposed in an earlier publication (Buchta *et al.*, 2007) using a novel joint-fit procedure for more precise parameter estimations.

Materials and Methods

Highly active PSII membrane particles were prepared from spinach as described in Schiller *et al.* (2000). Time-resolved measurements of delayed chlorophyll fluorescence were performed at 7 different temperatures between 0 and 30 °C (step of 5 °C, pH 6.4) as described elsewhere (Buchta *et al.*, 2007), applying logarithmic averaging along the time axis. As the DF intensity decreases due to the decay of both [$P680^+$] and, to less extent, of [Q_A^-], we correct the recorded decays for the acceptor-side contribution using the time courses of the yield of the prompt chlorophyll fluorescence, as has been described before (Buchta *et al.*, 2007).

The corrected time courses of DF were simulated using a sum of exponential functions:

$$F(t) = \left(\sum_{i=1}^{4} a_i \exp\left(-t/\tau_i\right) \right) + c \qquad (1)$$

The parameters a_i, τ_i, and c (9 parameters in total for each DF decay) were determined by minimization of the error sum. For curve-fitting of the logarithmically averaged delayed fluorescence decays, the error sum was calculated according to:

$$\varepsilon^2 = \sum_N \left(\log \frac{F_{sim}}{F_{\exp}} \right)^2 . \qquad (2)$$

In a free-parameter fit for 7 different temperatures, we would have $7 \times 9 = 63$ adjustable parameter, which cannot be determined using the available experimental data, that is the 7 DF decays. To avoid overparametrisation we used a joint-fit approach where the rate constants at different temperatures were interrelated by the Arrhenius equation:

$$k_i = 1/\tau_i = k_{0_i} \exp\left(-E_{a_i}/k_B T\right) \qquad (3)$$

In this way instead of four rate constants for each of the 7 different temperatures, we have only 4 pre-exponential (frequency) factors and 4 activation energies which stay the same for all temperatures, thus reducing the overall number of the free parameters to 43 for the joint simulation of 7 DF transients.

To model the formation of an intermediate state before the ET step, two exponentials were used for the $S_2 \rightarrow S_3$ transition and three exponentials for $S_3 \rightarrow S_0$ transition. The mean time constant (τ_{relax}) and the Gibbs free-energy (ΔG_{relax}) of intermediate formation were calculated according to:

$$\tau_{relax} = \frac{\sum_i a_i \tau_i}{\sum_i a_i} \qquad (4)$$

and

$$\Delta G_{relax} = -k_B T \ln \frac{\sum_i a_i + c}{a_{slow} + c} , \qquad (5)$$

respectively, where the sum includes all exponential components used to model the multiphasic process of intermediate formation.

We note that at all times, the DF induced by the second flash is clearly stronger than the first-flash signal, and that the DF induced by the third flash is also stronger than that after the second flash. Therefore it is not required to correct the recorded signals for the contribution of the minority fraction of PSII (around 10%) that are not synchronized (due to 'misses' on the first or second flash).

Results and Discussion

The delayed fluorescence decays after the second and the third saturating Laser flash (5 ns, 532 nm) exhibit strong temperature dependence (Fig. 1).

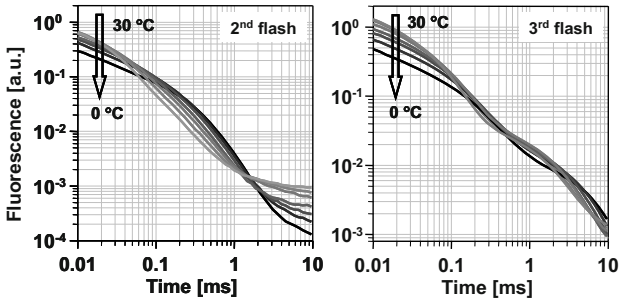

Fig. 1 Delayed fluorescence decay after the 2nd and the 3rd Laser flash at different temperatures (pH 6.4).

We simulated the DF decays by a sum of exponential functions. As shown in Buchta *et al.* (2007), excellent agreement was obtained only for simulation by a sum of four exponentials. For the $S_3 \rightarrow S_0$ transition, the slowest millisecond phase, which corresponds to the electron transfer step, is kinetically well resolved and very well described by a single exponential whereas the process of intermediate formation clearly is multiphasic (Figs. 1 and 2). On the basis of comparison of the DF transients and the time courses of X-ray signals that reflect the Mn oxidation state (Haumann *et al.*, 2005), it was assumed that three sequential reaction steps precede the onset of Mn reduction in the dioxygen-formation step (Dau *et al.*, 2007b). For the $S_2 \rightarrow S_3$ transition a similarly clear separation of phases assignable to intermediate formation and ET step is not observed and the quantitative analysis is clearly more demanding (Fig. 2).

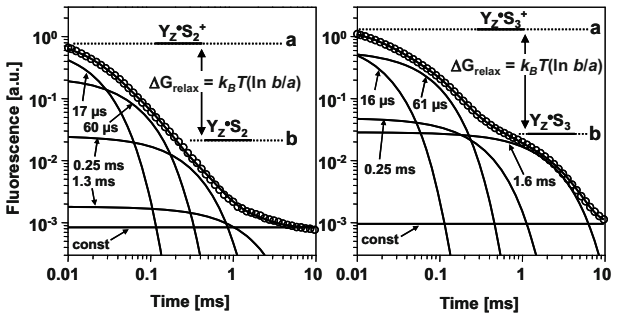

Fig. 2 Simulation of the delayed chlorophyll fluorescence decay after the 2nd (left) and the 3rd (right) saturating Laser flash (25 °C) simulated by a sum of four exponentials plus an additive constant. The dotted lines labeled by 'a' and 'b' indicate the levels used for calculation of ΔG_{relax} of the reactions that take place before the respective electron transfer step.

To account for all processes taking place during the intermediate formation and to avoid any underdetermined fits, we used a joint-fit approach where the rate constants for the individual exponentials are connected by the Arrhenius equation. The fit results for the third flash obtained using this restriction (Fig. 2) agree well with the previously determined rate constants (Buchta *et al.*, 2007; Dau *et al.*, 2007b), with the 1.6 ms rate constant assigned to the electron-transfer step. For the second flash the rate of the electron-transfer step was estimated to be around 250 µs (Haumann *et al.*, 1997) which agrees with the time constant of the third exponential in our fit results. The millisecond component obtained in this case has extremely low amplitude (Figs. 2 and 3) and its presence is probably explainable by a residual S_2 state population in dark-adapted PSII samples.

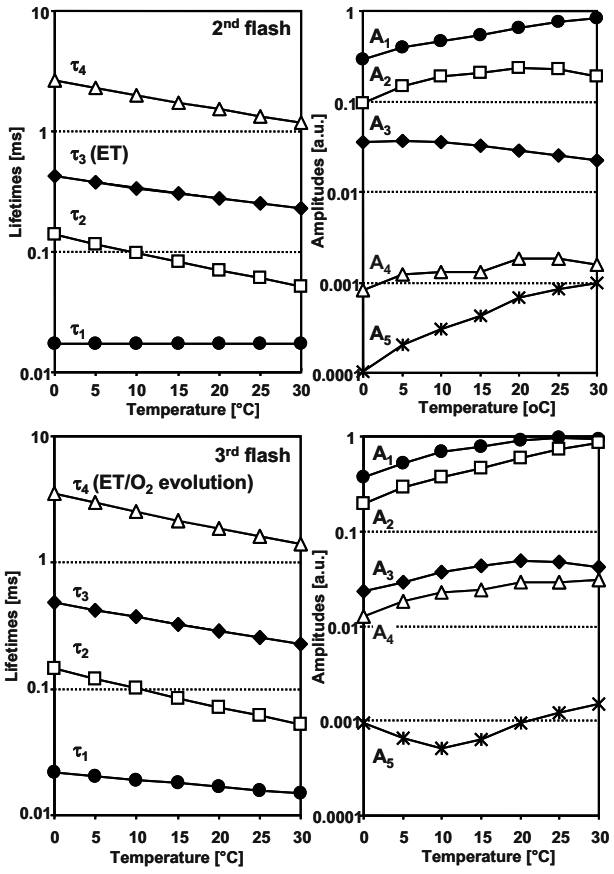

Fig. 3 Time constants and amplitudes of the DF decay after 2nd and 3rd flash.

The joint-fit results were used to determine kinetic and thermodynamic parameters of the $S_2 \rightarrow S_3$ and $S_3 \rightarrow S_0$ transitions. The rates of the intermediate formation and of the electron transfer steps were determined from the fit results as described in Materials and Methods. They are plotted in Fig. 4 (left). The rate constants of intermediate formation

imply activation energies of about 175 meV (~17 kJ/mol) for the intermediates formed before the ET steps in the $S_2 \rightarrow S_3$ and $S_3 \rightarrow S_0$ transition. The activation energy of the electron transfer step in $S_2 \rightarrow S_3$ transition was 140 meV (13.5 kJ/mol) and clearly higher 220 meV (21.4 kJ/mol) in the $S_3 \rightarrow S_0$ transition. The value obtained for the dioxygen formation step agrees well with the previously determined value of 231 meV (Buchta *et al.*, 2007) but, for still unclear reasons, is significantly lower than previously determined activation energies of 340 meV (near-UV data in (Clausen *et al.*, 2004)), 420 meV (polarographic data (Clausen *et al.*, 2004)), and 380 meV (Haumann *et al.*, 1994). The activation energies, the pre-exponential factors and the enthalpic and entropic contributions are summarized in Table 1. The free-energy difference, ΔG_{relax}, for the deprotonation step determined as described in eq. 5 shows a pronounced decrease with increasing temperature (Fig. 4, right). This suggests a sizable entropic contribution to the free energy, which is especially high in the $S_2 \rightarrow S_3$ transition.

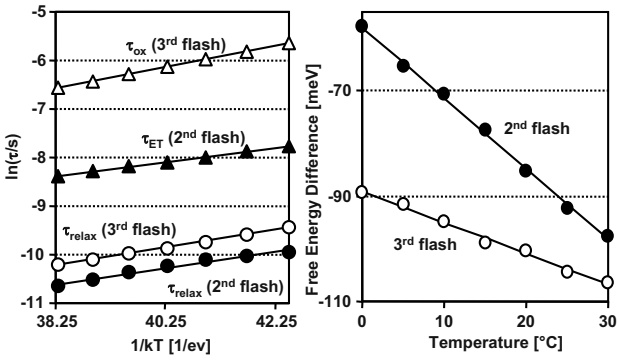

Fig. 4 Left: Arrhenius plot of the time constants of intermediate formation (τ_{relax}) and electron transfer (τ_{ox}, τ_{ET}). Right: Temperature dependence of the Gibbs energy, ΔG_{relax}, assignable to formation of a reaction intermediate after Y_Z oxidation but before ET.

Table 1 The Arrhenius activation parameters of the formation of the intermediate state and of the subsequent ET step, after the 2nd and 3rd Laser flash applied to dark-adapted PSII membrane particles. The uncertainties in the activation energies are of the order of ± 20 meV. The values for the individual rate constants at 25 °C are shown in Fig. 2.

	E_a [meV]				k_{i0} [μs^{-1}]				τ_{relax} #	$E_{a\ relax}$	$E_{a\ O2/ET}$	ΔG_{relax} #	ΔH_{relax}	$T\Delta S_{relax}$
	1st	2nd	3rd	4th	1st	2nd	3rd	4th	[μs]	[meV]	[meV]	[meV]	[meV]	[meV]
2nd	2.4	230	140	190	0.1	150	1.0	1.3	27	170	140	−92	308	−400
3rd	91	240	180	220	2.2	190	4.4	3.6	41	180	220	−104	72	−176

Values for data collected at 25 °C.

Simulation of the temperature dependence (according to $\Delta G = \Delta H - T\Delta S$) results in the straight lines shown in the Fig. 4 and the values for ΔH and $T\Delta S$ given in Table 1. For both, the $S_2 \rightarrow S_3$ and the $S_3 \rightarrow S_0$ transition, the positive enthalpy ΔH (endergonic process) and specifically the high entropic contribution (expected for proton release) provide evidence that a reaction intermediate is formed by proton removal from the Mn complex (deprotonation) and proton release to the lumenal bulk phase. Future work on the pH influence as well as H_2O/D_2O isotope effects will provide more information about these deprotonation steps.

Acknowledgements

Financial support by the Berlin cluster of excellence on Unifying Concepts in Catalysis (UniCat), the European Union (7th Framework Program, SOLAR-H2, #212508), and the Bundesministerium für Bildung und Forschung (BMBF consortium "H_2 Design Cell") is gratefully acknowledged. IZ thanks the DAAD for the travel grant to Beijing.

References

Kok B, Forbush B, McGloin M (1970) Cooperation of Charges in Photosynthetic O2 Evolution - I. A linear Four-Step Mechanism. Photochem. Photobiol. 11: 457-475

Haumann M, Junge W (1994) Extent and Rate of Proton Release by Photosynthetic Water Oxidation in Thylakoids: Electrostatic Relaxation Versus Chemical Production. Biochemistry 33: 864-72

Haumann M, Bögershausen O, Cherepanov D, Ahlbrink R, Junge W (1997) Photosynthetic Oxygen Evolution: H/D Isotope Effects and the Coupling between Electron and Proton Transfer during the Redox Reactions at the Oxidizing Side of Photosystem II. Photosynth. Res. 51: 193-208

Hoganson CW, Babcock GT (1997) A Metalloradical Mechanism for the Generation of Oxygen from Water in Photosynthesis. Science 277: 1953-1956

Schiller H, Dau H (2000) Preparation Protocols for High-Activity Photosystem II Membrane Particles of Green Algae and Higher Plants, pH Dependence of Oxygen Evolution and Comparison of the S_2-State Multiline Signal by X-Band EPR Spectroscopy. J. Photochem. Photobiol. B 55: 138-144

Clausen J, Debus RJ, Junge W (2004) Time-Resolved Oxygen Production by PSII: Chasing Chemical Intermediates. Biochim. Biophys. Acta 1655: 184-194

Haumann M, Liebisch P, Muller C, Barra M, Grabolle M, Dau H (2005) Photosynthetic O_2 Formation Tracked by Time-Resolved X-Ray Experiments. Science 310: 1019-1021

Dau H, Haumann M (2006) Reaction Cycle of Photosynthetic Water Oxidation in Plants and Cyanobacteria (Response Letter). Science 312: 1471-1472

Buchta J, Grabolle M, Dau H (2007) Photosynthetic Dioxygen Formation Studied by Time-Resolved Delayed Fluorescence Measurements - Method, Rationale, and Results on the Activation Energy of Dioxygen Formation. Biochim. Biophys. Acta 1767: 565-574

Dau H, Haumann M (2007a) Eight Steps Preceding O-O Bond Formation in Oxygenic Photosynthesis - a Basic Reaction Cycle of the Photosystem II Manganese Complex. Biochim. Biophys. Acta 1767: 472-483

Dau H, Haumann M (2007b) Time-Resolved X-Ray Spectroscopy Leads to an Extension of the Classical S-State Cycle Model of Photosynthetic Oxygen Evolution. Photosynth. Res. 92: 327-343

Dau H, Haumann M (2008) The Manganese Complex of Photosystem II in Its Reaction Cycle - Basic Framework and Possible Realization at the Atomic Level. Coord. Chem. Rev. 252: 273-295

An EPR and ENDOR Spectroscopic Investigation of the Ca^{2+}-Depleted Oxygen-Evolving Complex of Photosystem II

Thomas Lohmiller[a], Nicholas Cox[a], Jihu Su[a, b], Johannes Messinger[c], Wolfgang Lubitz[a,*]

[a]Max-Planck-Institut für Bioanorganische Chemie, Mülheim an der Ruhr, Germany;
[b]Department of Modern Physics, University of Science and Technology of China, Hefei, Anhui, China;
[c]Department of Chemistry, Umeå University, Umeå, Sweden.
[*]Corresponding author. Tel. No. +49 (0)208 306 3611; Fax No. +49 (0)208 306 3955; E-mail: lubitz@mpi-muelheim.mpg.de.

Abstract: Multifrequency EPR and ^{55}Mn ENDOR spectroscopy were used to characterize the S_2' state of the Ca^{2+}-depleted oxygen-evolving complex. The ^{55}Mn ENDOR spectrum of the S_2' state is broader than that of the native S_2 state. Simulations of the data were performed using the spin Hamiltonian formalism. It was observed that the magnitudes of the four ^{55}Mn hyperfine tensors ($A_{1,\ iso} \approx$ 300 MHz; $A_{2,\ iso}$, $A_{3,\ iso}$, $A_{4,\ iso} \approx$ 200 MHz) are approximately the same as in the native S_2 state. In addition, the geometries of the anisotropic hyperfine tensors are not changed. Thus, the same oxidation states are assigned to the Mn ions both in S_2 and S_2' (Mn_A, Mn_B, Mn_C: IV, Mn_D: III). The isotropic hyperfine values of the individual Mn ions, especially $A_{2,\ iso}$ and $A_{4,\ iso}$, do change upon Ca^{2+} depletion, indicating that, nonetheless, the electronic spin coupling scheme of the cluster is affected by Ca^{2+} removal.

Keywords: Oxygen-evolving complex; Calcium; EPR; ^{55}Mn ENDOR; Electronic structure; Zero-field splitting

Introduction

The oxygen-evolving complex (OEC) of photosystem II (PS II) —a Mn_4O_XCa inorganic cluster —catalyzes light-driven water oxidation (Lubitz *et al.*, 2008). It cycles through five different redox states, S_0 to S_4, in which the subscript denotes the number of stored oxidizing equivalents in the cluster. The S_4 state is catalytically active, spontaneously returning to the reduced S_0 state upon the release of dioxygen. The resting state of the enzyme is S_1. The Ca^{2+} ion of the cluster is essential for this reaction, and is thought to be involved in the binding and/or the deprotonation of substrate water.

S state advancement is driven by light excitation of the PS II reaction center and charge separation. Single photon excitation leads to the one step progression of the S state cycle at ambient temperature. At lower temperatures (~200 K), illumination only advances the OEC to the S_2 state. In this state, the oxidation numbers of the Mn ions are assigned as (III, IV, IV, IV) (Kulik *et al.*, 2007). The S_2 state displays a highly structured multiline EPR signal. It is centered at $g \approx 2$ and contains up to 18–20 spectral lines with a peak-to-peak (p-p) spacing of ~80 G (Dismukes and Siderer, 1981).

The Ca^{2+} ion can be removed from the OEC by salt washing (Boussac *et al.*, 1989) or in the presence of chelators at pH 3 (Ono and Inoue, 1988). The Ca^{2+}-depleted OEC cannot complete the enzymatic cycle. From the modified S_1' state, it can advance only to S_2' Both the Ca^{2+}-depleted states S_1' and S_2' have the same net oxidation states as the corresponding native S states. As seen from higher "half-inhibition" temperatures and the slower decay of the S_2' state, the transition between the Ca^{2+}-depleted states is impaired compared to the native $S_1{-}S_2$ transition. EXAFS measurements have demonstrated that Ca^{2+} removal does not lead to a fundamental spatial reorganization of the Mn_4O_x cluster (Latimer *et al.*, 1998).

Ca^{2+} removal is known to alter the multiline EPR signal (Boussac *et al.*, 1989; Sivaraja *et al.*, 1989).

The modified multiline signal has a larger number of spectral lines with smaller average p-p line spacing of 55–60 G as compared to 80 G in the Ca^{2+}-containing S_2 state. This suggests that the electronic structure of the Ca^{2+}-depleted Mn_4O_x cluster is in some way perturbed.

In this work, the Ca^{2+}-depleted Mn_4O_x cluster in the S_2' state was studied by EPR and, for the first time, by ^{55}Mn ENDOR spectroscopy at X- and Q-band frequencies. The results from the Ca^{2+}-depleted system provide new information about the Ca^{2+} binding site of the OEC.

Materials and Methods

Sample preparation and characterization

Ca^{2+}-depleted PS II spinach membrane samples were prepared using the low pH/citrate method (Ono and Inoue, 1988), by which the Ca^{2+} ion is removed during incubation at pH 3 for 5 min. The final buffer was 50 mmol MES, 15 mmol NaCl, 0.4 mol sucrose, 1 mmol EDTA, pH 6.5. The O_2 evolution rates of native PS II were ~400 μmol O_2/mg chlorophyll/h. O_2 evolution rates dropped to 5%–10% in Ca^{2+}-depleted and were reactivated to > 80% in Ca^{2+}-reconstituted samples. Ca^{2+} removal and, as a proof for the integrity of the OEC, Ca^{2+} rebinding was confirmed by CW X-band EPR. Similar percentages of the S_2 multiline signal were observed after continuous illumination of the respective samples at 200 K for 5 min. EPR samples were advanced to the S_2' state in the presence of 125 μM 3-(3,4-dichlorophenyl)-1,1-dimethylurea (DCMU) (10 mmol in dimethyl sulfoxide (DMSO)) by illumination at 0 °C for 3 min (Sivaraja *et al.*, 1989).

EPR and ENDOR spectroscopy

X-band CW EPR spectra were recorded on a Bruker ELEXSYS E500 spectrometer, equipped with an Oxford-900 liquid helium cryostat and an ITC-503 helium flow-temperature controller (Oxford Instruments Ltd.). Q-band pulse experiments were performed using a Bruker Elexsys-580 EPR spectrometer, which was equipped with a home-built cylindrical resonator and an Oxford ITC-5025 temperature controller and CF935 cryostat. X-band pulse experiments were performed with a Bruker ESP-380E spectrometer equipped with a dielectric ring resonator, temperature controller and an Oxford ITC liquid helium flow system.

Simulations of the EPR spectra were made based on the spin Hamiltonian formalism. Simulations were performed using the EasySpin software package (Stoll and Schweiger, 2006). For simulations of the ENDOR spectra, a separate script was written, which in part makes use of EasySpin functions. The fitting procedures employed a least squares minimization routine.

Results

The Ca^{2+}-depleted S_2' state showed the characteristic modified multiline CW-EPR signal (Fig. 1a) (Boussac *et al.*, 1989; Sivaraja *et al.*, 1989). This signal centered around $g \approx 2$ has a minimum of 27 hyperfine lines with an average p-p spacing of ~6 mT. The reduced $Q_A^{\bullet-}Fe^{2+}$ complex (Rutherford and Zimmerman, 1984) contributes broad underlying derivative signals in the 350–375 mT range.

Corresponding X- and Q-band ^{55}Mn ENDOR spectra of the Ca^{2+}-depleted S_2' state were measured. For measurements performed at Q-band, an additional signal was observed that superimposed the signal from the Mn_4O_x cluster. This additional signal was assigned to a Mn^{2+} ion specifically bound to the protein complex (not shown). It is not observed in the CW EPR spectrum (Fig. 1a) since its six-line Mn^{2+} spectrum is broadened beyond detection (Booth *et al.*, 1996). Subtraction of the Mn^{2+} signal was achieved by using the $m_S = -3/2$ Mn^{2+} line, occurring around 370 MHz, for normalization of the spectrum. The corrected ENDOR spectrum of the Mn_4O_x cluster in the S_2' state is observed over the range of ~60 to ~190 MHz (Fig. 1c). This spectral width is broader than in the native S_2 state. At Q-band, the S_2' state also exhibits five instead of the four major peaks observed in S_2. This extra peak is not due to an additional ENDOR transition, but rather due to a change in how the transitions of the individual Mn nuclei overlap.

A simultaneous least squares fitting of the EPR and ENDOR spectra was performed (Fig. 1, dashed traces). The effective Spin Hamiltonian used was:

$$H = \beta_e B_0 \cdot G \cdot S + \sum_i \left(- g_n \beta_n B_0 I_i + S \cdot A_i \cdot I_i \right). \quad (1)$$

It includes the electronic and nuclear Zeeman terms and the ^{55}Mn hyperfine terms. The *G*-tensor and

the four effective ^{55}Mn hyperfine tensors A_i (i = 1..4) were assumed to be collinear. The A_i tensors were constrained to be axially symmetric. This model represents the same approach as used by Kulik *et al.* (2007). The optimized parameters are given in Table 1.

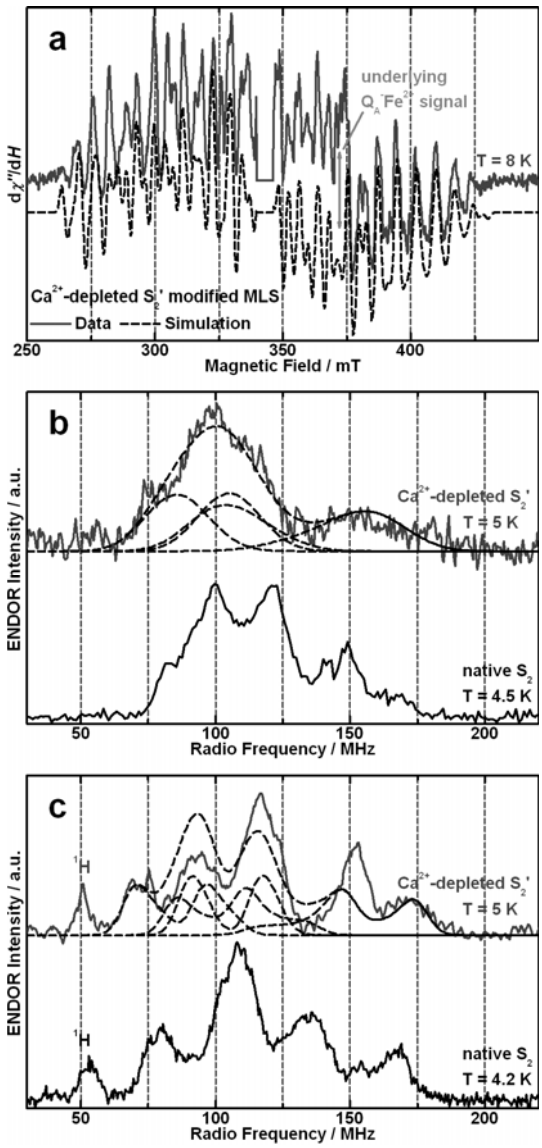

Fig. 1 (a): X-band CW EPR, (b) X-band Davies ENDOR and (c) Q-band Davies ENDOR spectra of the Ca^{2+}-depleted S_2' (grey solid lines) and the native S_2 state (black solid lines, Kulik *et al.*, 2007) from spinach PS II. The black dashed lines represent a least squares fitting based on the spin Hamiltonian formalism (eq. (1) and Table 1). The contributions of the individual Mn ions to the ENDOR spectra are also shown. In panel (a), the region of the overlapping $Y_D^\bullet$ signal ($g \approx 2$) was omitted for clarity. Experimental parameters: (a) CW EPR: microwave frequency: 9.634 GHz; microwave power: 0.5 mW; modulation amplitude: 7.5 G; (b), (c) S_2' Davies ENDOR: microwave frequencies: 9.717 GHz (b), 34.033 GHz (c); shot repetition rate: 5 µs; microwave pulse length (π): 12 ns (b), 72 ns (c); τ: 248 ns (b), 480 ns (c); magnetic fields (B_0): 380 mT (b), 1208 mT (c); radio frequency pulse length (π_{RF}): 4 µs. For the experimental parameters of the native S_2 state spectra, see Kulik *et al.* (2007).

Table 1 The principal values of the effective G- and ^{55}Mn hyperfine tensors of the Mn_4O_x cluster in the Ca^{2+}-depleted S_2' state and the Mn_4O_5Ca cluster in the native S_2 state (Kulik *et al.*, 2007) from spinach PSII membrane preparations.

		G	A_1	A_2	A_3	A_4
Ca^{2+}-depleted S_2', spinach	x	1.991	325	194	205	163
	y	1.986	325	194	205	163
	z	1.975	251	249	224	192
	*iso**	1.984	300	213	211	173
	*aniso***	–0.014	74	–55	-19	–29
Native S_2, spinach	x	1.997	310	235	185	170
	y	1.970	310	235	185	170
	z	1.965	275	275	245	240
	*iso**	1.977	298	248	205	193
	*aniso***	–0.023	35	–40	–60	–70

*The isotropic G and A_i values are the averages of the individual tensor components (x, y, z). **The anisotropy of the G and A_i tensors is expressed as the differences between the equatorial (x, y) and axial (z) component of the tensors.

The simulations reproduce the breadth and the key features of the spectra. The CW EPR peak positions are matched even in the range of the underlying $Q_A^\bullet Fe^{2+}$ signal, which demonstrates the quality of the fit. Subtraction errors in the Q-band ENDOR, as well as simplifications made in the simulations, such as exclusion of the nuclear electric quadrupole interaction and of line shape effects in pulse experiments, may explain the small discrepancies between the data and the simulation, especially in the 130–160 MHz region.

The fitted ^{55}Mn hyperfine tensors demonstrate that the basic arrangement of the manganese cluster remains intact upon Ca^{2+} removal, as seen in earlier XAS experiments (Latimer *et al.*, 1998), except for a minor fraction of damaged clusters, responsible for the Mn^{2+} signal observed. As for the native S_2 state, four hyperfine tensors of approximately the same magnitude are required to simultaneously simulate the EPR and ENDOR spectra. Since the isotropic component of the hyperfine tensor $A_{1,\,iso}$ is by far the largest (1.4–1.7 times $A_{i,\,iso}$ (i = 2..4), it is readily assigned to the only Mn^{3+} ion in the S_2' state.

The basic geometries of the hyperfine tensors, represented by the "signs of their anisotropies", are the same both for the Ca^{2+}-depleted S_2' state and the native S_2 state. Apart from A_1, all axial components are larger than the equatorial components.

Discussion

The effective ^{55}Mn hyperfine tensors (eq. (1)) can

be used to determine the overall spin coupling scheme of the Mn_4 cluster. In particular, the isotropic component of each hyperfine tensor is dependent on the exchange coupling topology of the Mn cluster. A simultaneous fitting of both the EPR and ENDOR data requires that all four hyperfine tensors are included in the simulation and that they all have approximately the same magnitude. As such, all four Mn contribute about equally to the electronic ground state of the complex. The magnitude of the hyperfine tenors is similar to that seen for monomeric Mn^{3+} and Mn^{4+} ions (Dismukes and Siderer, 1981). Thus, formally, all Mn have a spin projection coefficient ρ of ~1. The only OEC models consistent with this description are tetramer models. Peloquin *et al.* (2000) and Kulik *et al.* (2007) favored a topology in which three strongly coupled Mn ions (Mn_B, Mn_C, Mn_D) form a core structure to which the fourth Mn (Mn_A) is coupled. Theoretical model structures based on DFT are consistent with this basic scheme. By a combined EPR, ENDOR and DFT study, we recently assigned the Mn^{3+} ion to Mn_D within the trinuclear core (Cox *et al.*, *submitted*). The Ca^{2+} ion is bridged to this core structure (Mn^{IV}–($Mn^{IV}{}_2Mn^{III}$)Ca).

From the comparison of the isotropic ^{55}Mn hyperfine components, it is inferred that the electronic couplings between the four Mn ions *change* when Ca^{2+} is removed from the OEC. For the Ca^{2+}-depleted S_2' state, changes in excess of 10% are seen for two hyperfine tensors ($A_{2,\,iso}$ and $A_{4,\,iso}$) as compared to the native S_2 state from spinach (Table 1). Thus, the Ca^{2+}-depleted S_2' state represents a perturbation of the electronic structure of the native system and may (in part) explain the inactivity of the Ca^{2+} depleted OEC.

The anisotropy of the effective hyperfine tensors $A_{i,\,aniso}$ ($i = 2..4$) of the Mn^{4+} ions is larger than typically observed for monomeric Mn^{4+} complexes. It was shown by Peloquin *et al.* (2000) that the effective hyperfine tensor anisotropy of Mn^{4+} is not a measure of the intrinsic anisotropy of the Mn^{4+} ions of the cluster but instead is a measure of the onsite zero-field splitting (ZFS) d of the Mn^{3+} ion. This is due to the inherent differences between the d^4 ($S = 2$) Mn^{3+} ion and the d^3 ($S = 3/2$) Mn^{4+} ion. The Mn^{4+} ion in an octahedral ligand field is expected to have a small onsite ZFS (and hyperfine anisotropy) as its $^3T_{2g}$ levels are half filled. This is in contrast to the Mn^{3+} ion, which is a non-Kramers ion and often displays large spin-orbit coupling. As such, the onsite ZFS of Mn^{3+} provides a significant contribution to the ZFS of the whole cluster, whereas the three Mn^{4+} ions do not. The sign of d (Mn^{3+}) provides information on the ligand environment of the Mn^{3+}. As the signs of the anisotropy of each of the four hyperfine tensors do not change upon Ca^{2+} removal, it can be inferred that the basic coordination scheme of the Mn^{3+} and its position within the cluster does not change.

However, the changes in the magnitude of the anisotropy of the four hyperfine tensors, especially that of the $A_{1,\,aniso}$ (74 *vs.* 35 MHz), $A_{3,\,aniso}$ (–19 *vs.* –60 MHz) and $A_{4,\,aniso}$ (–29 *vs.* –70 MHz), does suggest that the contribution of the onsite ZFS d of the Mn^{3+} to the overall ZFS of the cluster is altered. This may also be linked to the non-functionality of the Ca^{2+}-depleted OEC.

Conclusions

We have characterized the Ca^{2+}-depleted Mn_4O_x cluster of spinach PS II poised in the S_2' state. Simulation of the X-band EPR and X- and Q-band ^{55}Mn ENDOR spectra shows that Ca^{2+} removal leads to a perturbation of the electronic structure, such that the exchange coupling pathways within the cluster are altered. The results refine the electronic constraints of the cluster that confer catalytic water oxidation. They also provide a more detailed picture of the role of the Ca^{2+} ion and the impact of its removal. Importantly, it is shown that the inactivity of the S_2' state may not simply be attributed to the inability of the cluster to bind the substrate.

A further characterization of the electronic structure of the Ca^{2+}-free Mn_4O_x cluster, as well as an investigation of the observed specific Mn^{2+} binding in Ca^{2+}-depleted PS II, will be addressed in an upcoming manuscript (Lohmiller *et al.*, in preparation).

References

Booth PJ, Rutherford AW, Boussac A (1996) Location of the Calcium Binding Site in Photosystem II: a Mn^{2+} Substitution Study. Biochim. Biophys. Acta, Bioenerg 1277: 127-134

Boussac A, Zimmermann JL, Rutherford AW (1989) EPR Signals from Modified Charge Accumulation States of the Oxygen-Evolving Enzyme in Calcium-Deficient Photosystem II. Biochemistry 28: 8984-8989

Dismukes GC, Siderer Y (1981) Intermediates of a Polynuclear Manganese Center Involved in Photosynthetic Oxidation of Water. Proc. Natl. Acad. Sci. USA 78: 247-278

Kulik LV, Epel B, Lubitz W, Messinger J (2007) Electronic Structure of the Mn_4O_xCa Cluster in the S_0 and S_2 States of the Oxygen-Evolving Complex of Photosystem II Based on Pulse ^{55}Mn-ENDOR and EPR Spectroscopy. J. Am. Chem. Soc. 129: 13421-13435

Latimer MJ, DeRose VJ, Yachandra VK, Sauer K, Klein MP (1998) Structural Effects of Calcium Depletion on the Manganese Cluster of Photosystem II: Determination by X-Ray Absorption Spectroscopy. J. Phys. Chem. B 102: 8257-8265

Lubitz W, Reijerse EJ, Messinger J (2008) Solar Water-Splitting into H_2 and O_2: Design Principles of Photosystem II and Hydrogenases. Energy Environ. Sci. 1: 15-31

Ono T, Inoue Y (1988) Discrete Extraction of the Ca Atom Functional for O_2 Evolution in Higher Plant Photosystem II by a Simple Low pH Treatment. FEBS Lett. 227: 147-152

Peloquin JM, Campbell KA, Randall DW, Evanchik MA, Pecoraro VL, Armstrong WH, Britt RD (2000) ^{55}Mn ENDOR of the S_2-State Multiline EPR Signal of Photosystem II: Implications on the Structure of the Tetranuclear Mn Cluster. J. Am. Chem. Soc. 122: 10926-10942

Rutherford AW, Zimmermann JL (1984) A New EPR Signal Attributed to the Primary Plastosemiquinone Acceptor in Photosystem II. Biochim. Biophys. Acta 767: 768-775

Sivaraja M, Tso J, Dismukes GC (1989) A Calcium-Specific Site Influences the Structure and Activity of the Manganese Cluster Responsible for Photosynthetic Water Oxidation. Biochemistry 28: 9459-9464

Stoll S, Schweiger A (2006) Easy Spin, a Comprehensive Software Package for Spectral Simulation and Analysis in EPR. J. Magn. Reson. 178: 42-55

Role of Protons in Photosynthetic Water Oxidation: pH Influence on the Rate Constants of the S-state Transitions and Hypotheses on the $S_2 \rightarrow S_3$ Transition

László Gerencsér* , Holger Dau*

Fachbereich Physik, Freie Universität Berlin, Arnimallee 14., Berlin, Germany.
* Corresponding authors. Tel. No. +49 30 838 53583; Fax No. +49 30 838 56299;
E-mail: laszlo.gerencser@fu-berlin.de, holger.dau@fu-berlin.de.

Abstract: The mode of proton relocation from the water-oxidizing Mn complex of photosystem II (PSII) toward the aqueous phase is of key importance in photosynthetic water oxidation. An adequate description of the interrelation of proton and electron removal from the Mn complex is still lacking. We reinvestigate the influence of the pH on the rate constants of the redox transitions of the Mn complex (S-state transitions). For high-activity PSII membrane particles from spinach, near-UV absorption transients (at 360 nm) induced by trains of ns-Laser flashes were analyzed. To obtain the rate constants of the 'pure' S-state transitions, a stringent deconvolution of the raw transients was carried out. The transients of the $S_1 \rightarrow S_2$ and $S_2 \rightarrow S_3$ transitions exhibit mono-exponential behavior whereas the transients of the '$S_3 \rightarrow S_0 + O_2$' transition display a lag-phase behavior that is assignable to formation of a reaction intermediate by deprotonation. The rate constants of the electron transfer (ET) in the $S_1 \rightarrow S_2$ and $S_3 \rightarrow S_0$ transitions exhibit a negligible pH-dependence only. The rate constant of the $S_2 \rightarrow S_3$ transition decreases below pH 6 significantly, but clearly less than those of the lag-phase in the $S_3 \rightarrow S_0$ transition. Two models for the coupling of electron and proton transfer in the $S_2 \rightarrow S_3$ transition are discussed.

Keywords: Electron transfer; Oxygen evolution; Photosystem II; Proton transfer

Introduction

The photosynthetic water oxidation takes place in the oxygen-evolving complex (OEC) of photosystem II (PSII) of higher plants and cyanobacteria. The core of the OEC is a Mn complex involving four Mn and one Ca atom that are interconnected by several di-μ-oxo-bridges (Dau and Haumann, 2008; McEvoy and Brudvig, 2006). The exact structure of the metal complex is still under debate.

After absorption of a photon by the chlorophyll pigment of PSII, a charge separated state is formed and a cation radical, P_{680}^{+}, is stabilized at the so-called donor side of PSII. The P_{680}^{+} is reduced by a redox-active tyrosine (Y_Z, Tyr-161 of the D1 subunit), which subsequently oxidizes the Mn complex. Absorbance of four photons and accumulation of four oxidizing equivalents by the Mn complex is required for the oxidation of two substrate water molecules and O_2 formation. The accumulation of oxidizing equivalents by the Mn complex is discussed in terms of the S-state cycle proposed by Kok and coworkers (Kok *et al*., 1970). To To address explicitly the essential removal of four protons from the Mn complex or its ligand environment, recently an extension of Kok's classical S-State cycle has been proposed (Dau and Haumann, 2006, 2007; see Fig. 1). Several aspects of the reaction cycle shown in Fig. 1 are supported by experimental finding whereas others have been largely hypothetical (Dau and Haumann, 2007; Dau and Haumann, 2008). We believe that any in-depth understanding of photosynthetic water oxidation will require specific insights in the interrelation between electron transfer and proton relocation.

Although the pH influence on the rate constants of the S-state transitions represents a straightforward approach for assessment of the role of protons in PSII water oxidation, only a relatively limited number of pH studies have been carried out before. Many of the previous investigations suffered from a low number of data points (low number of investigated pH values)

and noise problems. Moreover, frequently the raw absorption transients were not corrected stringently for the mixture of S states resulting from so-called miss and double-hit events. In this study we reinvestigate the effect of the pH on the rate constants of the individual S-state transitions by avoiding some pitfalls of earlier investigations.

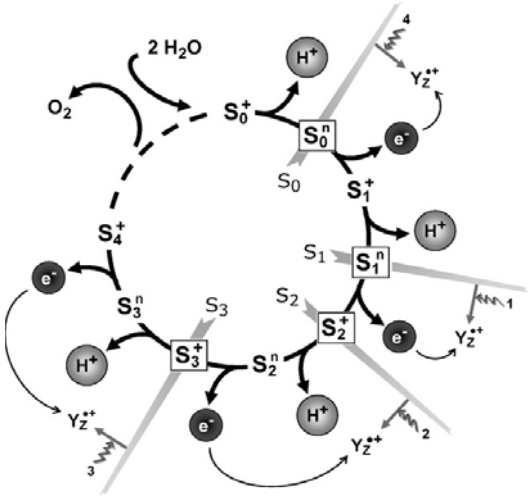

Fig. 1 Extended S-state cycle describing removal of electrons and protons from the Mn complex (from (Dau and Haumann, 2008)). The protons and electrons are removed from the Mn complex (or its immediate ligand environment) in a strictly alternating pattern so that the overall charge of the Mn complex oscillates between +1 and zero. There are nine intermediate states denoted as S_i^j, where subscript and superscript indicate the number of accumulated oxidation equivalents and the net charge of the Mn complex, respectively (positive (+) or neutral (n)). The semi-stable S-states of Kok's classical cycle are enclosed in a square. The reaction cycle has been proposed first in 2006 (Dau and Haumann, 2006); the scheme shown above involves the naming of intermediate states proposed later (Dau and Haumann, 2008).

Materials and Methods

PSII membrane particles (BBY membrane) were prepared from spinach according to the protocol described elsewhere (Schiller and Dau, 2000). The oxygen evolution activity (1200–1400 μM O_2 per mg of chlorophyll and h, at 28 °C) was measured under actinic continuous illumination in presence of 0.3 mmol 2,6-dichloro-*p*-benzoquinone (2,6-DCBQ) and 5 mmol $K_3[Fe(CN)_6]$.

The flash-induced absorption changes of the PSII particles were measured at 360 nm as described elsewhere (Gerencsér and Dau, 2010). The sample were centrifuged and resuspended carefully in puffer D (1 mol glycine betaine, 25 mmol buffer (Na-citrate at pH < 5.5, 2-(*N*-Morpholino)ethanesulphonic acid (MES) 5.5 < pH < 6.5, and 3-(*N*-Morpholino)propane-sulphonic acid (MOPS) pH > 6.5), 10 mmol NaCl, 5 mmol $CaCl_2$, and 5 mmol $MgCl_2$) before each measurement. Binary oscillations in the UV transients relating to the two-electron chemistry of the secondary quinone (Q_B) were eliminated by addition of electron acceptors of 100 μM 2,6-DCBQ and 0.5 mmol $K_3[Fe(CN)_6]$ to PSII membrane particles equivalent of 15 μM chlorophyll concentrations. The flash spacing was 1.4 s to allow for the complete reoxidation of Q_B^- between flashes. The electrical bandwidth of the absorption measurement was 1 MHz, and the here presented transients were smoothed further to 2.5 μs/point resolution. All measurements were carried out at 23 °C.

Results and Discussion

The flash-induced absorption transients (360 nm) of PSII membrane particles were measured at eight pH-values ranging from pH 5.0 to 7.0. The absorption transients were corrected for S-state mixing as described elsewhere in full detail (see deconvolution approach in Gerencsér and Dau (2010) and the accompanying supporting online material). After the deconvolution of the raw absorption transient, the signal represents the time course of the individual S-state transition. The signal can be described by a monoexponential function (in the $S_1 \rightarrow S_2$ and $S_2 \rightarrow S_3$ transitions) or a consecutive reaction scheme (in the $S_3 \rightarrow S_0 + O_2$ transition). In our study, an analysis of the $S_0 \rightarrow S_1$ transition is not included because the noise level of the corresponding transient was too large for a sufficiently reliable data analysis.

$S_1 \rightarrow S_2$ transition

The absorption transients of the $S_1 \rightarrow S_2$ transition measured at 360 nm are shown, in Fig. 2A, for three different pH values (pH 5.3, 6.2 and 7.0). Visual inspection does not reveal any pH dependence. This is confirmed by monoexponential simulations yielding essentially pH-independent time constant values (around 100 μs, Fig. 2B). Similar time constants were reported in former studies pursued in the neutral pH range (Dekker *et al*., 1984; Saygin and Witt, 1987; Rappaport *et al*., 1994; Karge *et al*., 1997; Haumann *et al*., 2005). The pH dependence has been studied in

more detail by Junge and coworkers (Haumann *et al*., 1997). The results shown in Fig. 2B are in line with their results for PSII core particles isolated from pea seedlings. Slightly greater rate-constant values were reported in the same study for data collected on thylakoid membranes, but the extent of the pH dependence was similar (Haumann *et al*., 1997).

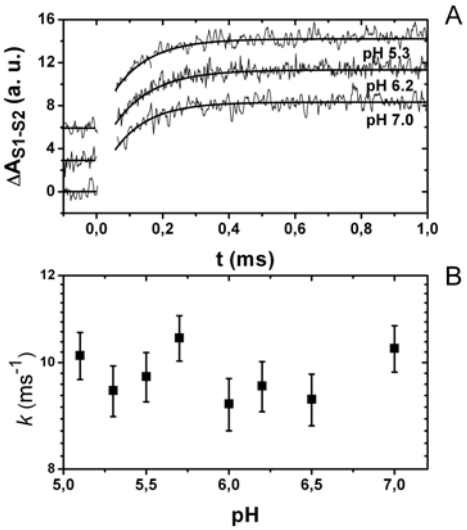

Fig. 2 Flash-induced absorption changes (at 360 nm) of PSII membrane particles: $S_1 \rightarrow S_2$ transition. In A, the transients are presented for three pH values (pH 5.3, pH 6.2 and pH 7.0). The absorption traces were normalized to equal amplitude and shifted vertically for better visualization. The time constant of the $S_1 \rightarrow S_2$ transition obtained from simulation of the absorption trace with a exponential function was independent of the pH (around 100 μs). In B, the rate constants (that is, the reciprocal values of the time constants) are plotted as a function of the pH.

The pH independence of the rate constant of the $S_1 \rightarrow S_2$ transition supports the absence of proton release during this redox transition, as has been concluded before (Damoder and Dismukes, 1984; Schlodder and Witt, 1999; Bernát *et al*., 2002; Junge *et al*., 2002; Suzuki *et al*., 2005). The rate of formation of the S_2-state multiline signal was monitored with electron paramagnetic resonance (EPR) spectroscopy on PSII membrane excited by a single flash at room temperature followed by a rapid cooling to 200 K (Damoder and Dismukes, 1984). The rate of formation of the multiline signal did not show any difference between measurements at pH 5.5, 6.5 and 7.5. The transition efficiency of $S_1 \rightarrow S_2$ did not change between pH 4 and 8.5 (Bernát *et al*., 2002; Suzuki *et al*., 2005). We note that the $S_1 \rightarrow S_2$ transition has been found to be accompanied by a pH-dependent proton release (Rappaport and Lavergne, 1991; Schlodder and Witt, 1999; Junge *et al*., 2002). However, the proton is not released from the Mn complex and assumed to be functionally of little relevance (Schlodder and Witt, 1999; Junge *et al*., 2002).

$S_2 \rightarrow S_3$ transition

Absorption transients of the $S_2 \rightarrow S_3$ transition are shown in Fig. 3A. Visual inspection reveals that the transition is slowed down at low pH, as confirmed by monoexponential simulation yielding time constant values of 350 μs (pH 5.3), 280 μs (pH 6.2), and 265 μs (pH 7.0).

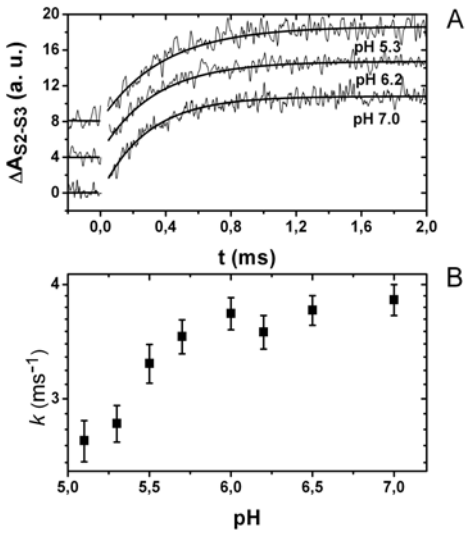

Fig. 3 Flash-induced absorption changes (at 360 nm) of PSII membrane particles: $S_2 \rightarrow S_3$ transition. The absorption traces were obtained by correction for miss and double-hit events. In A, the transients are presented for three pH values (pH 5.3, pH 6.2 and pH 7.0); they are normalized to equal amplitude and shifted vertically for better visualization. In B, the rate constants (reciprocal values of the time constants) are plotted as a function of the pH.

These time constants are in accordance with values of some previous studies: 275 μs at pH 6.2 (Haumann *et al*., 2005), 290 μs at pH 6.5 and 215 μs at pH 7.5 (Rappaport *et al*., 1994), 350 μs and 325 μs at pH 6.5 for PSII core particles and for PSII membranes, respectively (Karge *et al*., 1997). They deviate from the values of other studies: 500 μs at pH 6.0 (Dekker *et al*., 1984), 145 μs at pH 6.5, and 320 μs at pH 5.5 (Saygin and Witt, 1987). The here determined pH-dependence of the rate constant of the $S_2 \rightarrow S_3$ transition is shown in Fig. 3B. The rate constant decreases at pH values below 6. The relative change of the rate between pH 5.1 and 7.0 amounts to

about 40%, which is roughly in line with results reported previously for PSII core particles and thylakoid membranes (Haumann *et al*., 1997; 350 μs at pH 5; 150–200 μs at pH 7.5).

$S_3 \rightarrow S_0 + O_2$ transition

Analysis of the absorption transients of the oxygen-evolution transition suggests that proton relocation from the Mn complex toward the aqueous phase precedes ET and O-O bond formation (Rappaport *et al*., 1994; Haumann *et al*., 2005). Recently the 'lag phase' duration assignable to proton removal from the Mn complex was found to be strongly pH dependent whereas the rate constant of the ET step is almost pH independent (see Fig. 4), as discussed in more detail elsewhere (Gerencsér and Dau, 2010).

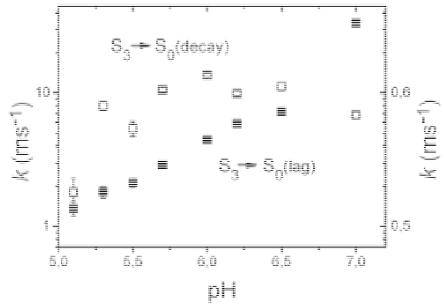

Fig. 4 pH dependence of the rate constants resolved in the oxygen-evolution transition ($S_3 \rightarrow S_0 + O_2$). The left axis relates to the lag phase duration (closed squares); the right axis to the rate constant of the ET step and the concomitant O_2 formation (open squares). The lag phase has been assigned to proton relocation from the Mn complex to the aqueous phase before electron transfer from Y_Z^{ox} to the Mn complex. For a detailed discussion, see Gerencsér and Dau (2010).

Hypothesis on the interrelation of proton and electron transfer in the $S_2 \rightarrow S_3$ transition

Aside from the moderate but still significant pH dependence of the rate constant of the $S_2 \rightarrow S_3$ transition presented in this work, several former results support the assumption that this redox transition is accompanied by proton release. A significantly larger activation energy (35 kJ/mol) than being typical for a mere ET step has been observed (15 kJ/mol; Haumann *et al*., 1997). More important, there is a sizeable kinetic isotope effect ($k_H/k_D = 1.7$, Gerencsér and Dau, 2010; $k_H/k_D = 2.1–2.4$ in Haumann *et al*., 1997). Moreover, the transition is blocked at low temperatures, as opposed to the $S_1 \rightarrow S_2$ transition (de Paula *et al*., 1985). What kind of mechanism of proton and electron removal from the Mn complex could match these and other results on the $S_2 \rightarrow S_3$ transition? Clearly, the available experimental data is insufficient for any definitive conclusions. However, some scenarios can be discussed.

The sequence of events from absorption of a light quantum by one of the PSII pigments to formation of the oxidized Y_Z is relatively well understood. The light excitation of PSII produces an oxidized P_{680} that is reduced by the Y_Z, mostly within 1 μs. The oxidation of Y_Z likely is coupled to the shift of the hydroxyl proton of Y_Z to the neighboring His190 of the D1 protein. There are no clear indications that the hydroxyl proton of Y_Z is transferred later to the lumenal bulk phase. This means that by Y_Z oxidation a positive charge is created at the Y_Z^{ox}/His190 pair. This positive charge induces a fast proton release, likely electrostatically by decreasing the p*K* values of protonatable groups (Junge *et al*., 2002). Accordingly a proton is released to the aqueous phase before electron transfer in the $S_2 \rightarrow S_3$ transition. However, presently it cannot be decided whether the 'fast proton' comes from the Mn complex itself (including the Mn ligands and nearby amino acid residues) or merely from peripheral amino acid side chains located close to the protein-water interface of PSII. In the oxygen-evolution transition ($S_3 \rightarrow S_0 + O_2$), proton removal from the Mn complex is relatively slow (~200 μs, Fig. 4) and precedes the even slower ET step. Similarly slow proton removal preceding a slow ET step (~300 μs) in the $S_2 \rightarrow S_3$ transition should result in an clear lag-phase behavior in the $S_2 \rightarrow S_3$ transition, which is not observed and thus can be excluded (Fig. 3A). Two alternative scenarios of proton and electron removal during $S_2 \rightarrow S_3$ transition are outlined in the following. We emphasize that both scenarios are in agreement with the extended Kok cycle of Fig. 1. In both suggested scenarios, proton removal from the Mn complex precedes the electron transfer from the Mn complex to the Y_Z radical (proton-first ET).

(i) *Fast electron transfer follows slow proton relocation in the $S_2 \rightarrow S_3$ transition*

In this scenario, the positive charge of the Y_Z^{ox}/His190 pair induces the proton relocation from the catalytic site to the aqueous bulk (at the lumen side of PSII). The involved processes, namely deprotonation (of the Mn complex), proton transfer

within the protein and release into the aqueous phase, are characterized by a time constant of about 300 µs ($S_2^+ \rightarrow S_2^n$ transition of Fig. 1). This slow proton release is followed by fast ET ($\tau_{ET} < 30$ µs) from the Mn complex to the oxidized Y_Z ($S_2^n \rightarrow S_3^n$ transition of Fig. 1). Therefore the absorption transients recorded at 360 nm reflect the kinetics of the rate-limiting proton release. The observed monophasic kinetics (Fig. 3) implies that there is a single rate-limiting step in the cascade of elementary proton-transfer steps that facilitate the long-distance proton relocation from the Mn complex to the aqueous phase. However, if this scenario described the real situation, it would be surprising that the pH dependence of the rate constant detected for the $S_2 \rightarrow S_3$ transition exhibited a weak pH dependence only (Fig. 3B), as opposed to the strong pH dependence of the lag-phase in the $S_3 \rightarrow S_0 + O_2$ transition (Fig. 4, closed circles).

(ii) *Concerted electron-proton transfer in the $S_2 \rightarrow S_3$ transition* (CEPT) *is preceded by formation of a proton-acceptor base*

In this scenario, a still unknown group in the vicinity of the Mn complex (which we call B) is deprotonated within less than 30 µs after absorption of a photon, driven by the positive charge on the Y_Z/His190 pair. This deprotonation involves the proton relocation from the Mn complex (or its immediate vicinity) toward a group at the protein periphery of the lumen side of PSII and the release of the protons into the aqueous phase. We assume that all these processes are so fast (< 30 µs) that they do not give rise to a discernible lag-phase behavior in the transients of the $S_2 \rightarrow S_3$ transition. The deprotonated group (B^-) is located in hydrogen-bonding distance to a protonated group of the Mn complex (denoted as {Mn}G-H). Not only the identity of B, but also the identity of G-H is unclear; options for the latter include hydroxides in bridging position between metal ions (G-H corresponds to µ-OH) and water molecules terminally coordinated to Mn or Ca ions. Subsequent to B^- formation, the ET from the Mn complex to Y_Z^{ox} proceeds. This ET is directly coupled to the shift of a proton from {Mn}G-H to B^-. The simultaneous ET and proton shift represents a concerted multi-site electron-proton transfer (CEPT,Hammes-Schiffer, 2009; Sjödin *et al*., 2002). The above sequence of events is summarized by Equ. 1 and 2.

$$Y_Z^{ox(+)} + \{Mn\}G\text{-}H \quad B\text{-}H \rightarrow Y_Z^{ox(+)} + \{Mn\}G\text{-}H\cdot\cdot B^{(-)} + \{H^+\}_{Lumen} \quad (1)$$

$$Y_Z^{ox(+)} + \{Mn\}G\text{-}H\cdot\cdot B^{(-)} \rightarrow Y_Z^{0} + \{Mn^{ox}\}G\cdot\cdot H\text{-}B \quad (2)$$

In terms of the extended S-state cycle of Fig. 1, Equ. 1 describes the $S_2^+ \rightarrow S_2^n$ transition, a proton relocation from the Mn complex to the aqueous phase, whereas Equ. 2 describes the $S_2^n \rightarrow S_3^n$ transition, which in scenario (ii) is a CEPT process. In the CEPT step (Equ. 2), the ET from the Mn complex to Y_Z^{ox} and the shift of a proton from G to B are assumed to proceed simultaneously in form of a concerted process. In addition, the ET from the Mn complex to Y_Z^{ox} may be coupled to the shift of a proton from His190 to Y_Z (the latter proton shift is not indicated in Equ. 2). The proposed CEPT of Equ. 2 could explain straightforwardly the existence of a clear kinetic isotope effect. The here observed weak pH dependence of the rate constant of the $S_2 \rightarrow S_3$ transition may result from a slight pH dependence of the driving force of the CEPT step or from fractional protonation of B^- at low pH values.

Further investigations are required to elucidate whether option (i) or option (ii) or yet another mechanism provides an adequate description of the interrelation of electron and proton transfer in the $S_2 \rightarrow S_3$ transition of photosynthetic water oxidation.

Acknowledgements

We thank Dr. M Haumann for valuable discussion and M Fünning for the preparation of PSII membrane particles. This work was supported by the European Union (7th FP, SOLAR-H2 consortium), the Federal Ministry of Education and Research of Germany (BMBF, H_2 Design cell, 03SF0355D), and the Berlin cluster of excellence on Unifying Concept in Catalysis (UniCat).

References

Bernát G, Morvaridi F, Feyziyev Y, Styring S (2002) pH Dependence of the Four Individual Transitions in the Catalytic S-cCycle during Photosynthetic Oxygen Evolution. Biochemistry 41: 5830-5843

Damoder R, Dismukes GC (1984) pH Dependence of the Multiline, Manganese EPR Signal for the ´S_2´ State in PSII Particles; Absence of Proton Release during of $S_1 \rightarrow S_2$ Electron Transfer Step of the Oxygen Evolving System. FEBS Lett. 174: 157-161

Dau H, Haumann M (2006) Reaction Cycle of Photosynthetic Water Oxidation in Plants and Cyanobacteria (Response Letter). Science 312: 1471-1472

Dau H, Haumann M (2007) Eight Steps Preceding O-O Bond Formation in Oxygenic Photosynthesis: a Basic Reaction Cycle of the Photosystem II Manganese Complex. Biochim. Biophys. Acta 1767: 472-483

Dau H, Haumann M (2008) The Manganese Complex of Photosystem II in Its Reaction Cycle: Basic Framework and Possible Realization at the Atomic Level. Coord. Chem. Rev. 252: 273-295

Dekker JP, Plijter JJ, Ouwehand L, van Gorkom HJ (1984) Kinetics of Manganese Redox Transitions in the Oxygen Evolving Apparatus of Photosynthesis. Biochim. Biophys. Acta 767: 176-179

Gerencsér L, Dau H (2010) Water Oxidation by Photosystem II: H_2O-D_2O Exchange and the Influence of pH Support Formation of an Intermediate by Removal of a Proton before Dioxygen Creation. Biochemistry 49: 10098-10106

Hammes-Schiffer S (2009) Theory of Proton-Coupled Electron Transfer in Energy Conversion Processes. Acc. Chem. Res. 42: 1881-1889

Haumann M, Bögershausen O, Cherepanov D, Ahlbrink R, Junge W (1997) Photosynthetic Oxygen Evolution: H/D Isotope Effects and the Coupling between Electron and Proton Transfer during the Redox Reactions at the Oxidizing Site of Photosystem II. Photosynth. Res. 51: 193-208

Haumann M, Liebisch P, Muller C, Barra M, Grabolle M, Dau H (2005) Photosynthetic O_2 Formation Tracked by Time-Resolved X-Ray Experiments. Science 310: 1019-1021

Junge W, Haumann M, Ahlbrink R, Mulkidjanian A, Clausen J (2002) Electrostatics and Proton Transfer in Photosynthetic Water Oxidation. Phil. Trans. R. Soc. Lond. B 357: 1407-1418

Karge M, Irrgang KD, Renger G (1997) Analysis of the Reaction Coordinate of Photosynthetic Water Oxidation by Kinetic Measurements of 355 nm Absorption Changes at Different Temperatures in Photosystem II Preparations Suspended in Either H_2O or D_2O. Biochemistry 36: 8904-8913

Kok B, Forbush B, McGloin M (1970) Cooperation of Charges in Photosynthetic O_2 Evolution. A Linear Four-Step Mechanism. Photochem. Photobiol. 11: 457-475

McEvoy JP, Brudvig GW (2006) Water – Splitting Chemistry of Photosystem II. Chem. Rev. 106: 4455-4483

De Paula JC, Innes JB, Brudvig GW (1985) Electron Transfer in Photosystem II at Cryogenic Temperatures. Biochemistry 24: 8114-8120

Rappaport F, Lavergne J (1991) Proton Release during Successive Oxidation Steps of the Photosynthetic Water Oxidation Process: Stoichiometries and pH Dependence. Biochemistry 30: 10004-10012

Rappaport F, Blanchard-Desce M, Lavergne J (1994) Kinetics of Electron Transfer and Electrochromic Change during the Redox Transition of the Photosynthetic Oxygen-Evolving Complex. Biochim. Biophys. Acta 1184: 178-192

Saygin Ö, Witt HT (1987) Optical Characterization of Intermediates in the Water-Splitting Enzyme System of Photosynthesis – Possible States and Configurations of Manganese and Water. Biochim. Biophys. Acta 893: 452-469

Schiller H, Dau H (2000) Preparation Protocols for High-Activity Photosystem II Membrane Particles of Green Algae and Higher Plants, pH Dependence of Oxygen Evolution and Comparison of the S_2-State Multiline Signal by X-Band EPR Spectroscopy. J. Photochem. Photobiol. B 55: 138-144

Schlodder E, Witt HT (1999) Stoichiometry of Proton Release from the Catalytic Center in Photosynthetic Water Oxidation. Reexamination by a Glass Electrode Study at pH 5.5-7.2. J. Biol. Chem. 274: 30387-30392

Sjödin M, Styring S, Åkermark B, Sun L, Hammarström L (2002) The Mechanism for Proton-Coupled Electron Transfer from Tyrosine in a Model Complex and Comparisons with Y_Z Oxidation in Photosystem II. Phil. Trans. R. Soc. Lond. B 357: 1471-1479

Suzuki H, Sugiura M, Noguchi T (2005) pH Dependence of the Flash-Induced S-State Transitions in the Oxygen-Evolving Center of Photosystem II from Thermosynechoccocus Elongatus as Revealed by Fourier Transform Infrared Spectroscopy. Biochemistry 44: 1708-1718

Electronic Structure of the $CaMn_4O_5$ Cluster in the PSII System Refined to the 1.9 Å X-ray Resolution. Possible Mechanisms of Photosynthetic Water Splitting

S Yamanaka[1], K Kanda[1], H Isobe[1], K Nakata[1], Y Umena[2], K Kawakami[3], JR Shen[4], N Kamiya[3], M Okumura[1], T Takada[5], H Nakamura[2], K Yamaguchi[6]

[1]Graduate School of Science, Osaka University, Toyonaka, 560-0043, Japan;
[2]Protein Institute, Osaka University, Suita, 560-0871, Japan ;
[3]Graduate School of Science, Osaka City University, 3-3-138 Sugimoto, Sumiyoshi, Osaka, 558-8585, Japan;
[4]Graduate School of Natural Science and Technology, Okayama University, Okayama 700-8530, Japan;
[5]RIKEN, Next-Generation Supercomputer R&D Center, Chiyodaku, Tokyo 100-0005, Japan;
[6]TOYOTA Physical & Chemical Research Institute, Nagakute, Aichi, 480-1192, Japan.

Abstract: Broken-symmetry (BS) UB3LYP calculations have been performed for the $CaMn_4O_5$ cluster (**1**) in the oxygen-evolving complex (OEC) of the PSII system refined to 1.9 Å resolution by Umena, Kawakami, Kamiya, Shen to elucidate its electronic structure that is crucial for consideration of possible mechanisms of photosynthetic water splitting. Our UB3LYP computations have elucidated the position of protonated oxygen of the $CaMn(III)_2Mn(IV)_2O_4(OH)$ cluster (**1a**) at the S_1 stage of Kok cycle. Starting from the newly elucidated S_1 structure of **1a**, we have calculated the electronic structure of proton and electron released $CaMn(IV)_4O_5$ cluster (**1b**) that mimics the S_4 stage of the cycle. The LUMOs of **1b** are depicted for pictorial understanding of electrophilic oxygen sites that are responsible for nucleophilic attack of hydroxide anion (or water) for the O-O bond formation. Implications of present computational results are discussed in relation to possible mechanisms of photosynthetic water splitting.

Keywords: Electrophilic mechanism; LUMO,; Protonated structure; Ab initio DFT calculation

Introduction

Oxygenic photosynthesis involves several protein-cofactor complexes embedded in the photosynthetic thylakoid membranes of plants, green algae and cyanobacteria such as Thermosynechococcus vulcanus. Among these complexes, PSII has a prominent role because it catalyzes the oxidation of water that is the prerequisite for all aerobic life. The oxygen-evolving complex (OEC) in Photosystem II (PSII) contains an inorganic cluster consisted of four manganese ions and one calcium ion that are bridged by at least five oxygens: the active site is therefore expressed by $CaMn_4O_5$ cluster (**1**). Past decades, molecular structures of the cluster have been investigated by the extended X-ray absorption fine structure (EXAFS), X-ray diffraction (XRD) (Zouni *et al*., 2001; Kamiya and Shen, 2003; Ferreira *et al*., 2004; Loll *et al*., 2005; Guskov *et al*., 2009; Kawakami *et al*., 2009) and ENDOR studies of PSII. Despite these efforts, it has been still not possible to derive an common atomic model of **1**. In this conference, Umena, Kawakami, Shen, Kamiya (Umena *et al*., to be published) have reported the XRD structure of the OEC complex refined to the 1.9 Å resolution. Their XRD results have indeed revealed the precise structure of the $CaMn_4O_5$ cluster (**1**) at the S_1-state of the catalytic cycle (the S_0-S_4 states of the Kok cycle) (Kok *et al*., 1970) as illustrated in Fig. 1.

However, the XRD experiment even at this resolution does not reveal the position of protonated oxygen of **1** of OEC at PSII. The DFT computations are therefore needed as a complementary and efficient procedure for the elucidation of its protonated

structure. Using this newest XRD structure, we also performed the spin unrestricted B3LYP calculations to investigate the electronic structure of the OEC complex for several oxidation states we assumed. The computational results are discussed in relation the fundamental features inherent in this native structure.

DFT calculations of protonated $CaMn_4O_4(OH)$ cluster

The molecular skeleton of **1** is given in Fig. 1, where we assume that all oxygen atoms are oxygen dianion as a first step of theoretical investigation of charge and spin fluctuated states. For surrounding proteins and ligands, we take all amino acid residues within the first coordination sphere of the X-ray structure refined to 1.9 Å resolution by Shen and Kamiya's group (Umena *et al*., to be published). We here fixed all heavy atoms in the XRD structure, but to reduce the computational complexity, Ala344, Asp342, Asp170, Glu333, Glu189, Glu354, Glu189, Glu333 and Glu354 residues were modeled by acetate ions, and His332 residue by an imidazole that ligates to a manganese ion, which are the same manner to those of the precursors (Sproviero *et al*., 2006; Pantazis *et al*., 2009; Siegbahn, 2009) of this system. Hydrogen atoms of these modeled amino acid residues are generated by the UCSF Chimera ver. 1.5 (Petterse *et al*., 2004). Two oxygen atoms ligated to the calcium ion and two oxygen atoms to the dangling manganese ion are assumed to be H_2O molecules, for which positions of hydrogen atoms are optimized using UB3LYP (Becke, 1993) calculation with employing STO-3G basis set for the highest spin states of **1** with the Mn(III)Mn(III)Mn(IV)Mn(IV) charged structure for Mn(1)Mn(2)Mn(3)Mn(4) (see Fig. 1) that is abbreviated as (3344). As a result, the water molecules, reasonably, coordinated to the calcium ion and the manganese ion via lone pairs of electrons, and therefore alignments of water molecules are fixed for further calculations presented below.

Fig. 1 shows only the core part of the OEC cluster, but the detailed structure of the OEC cluster, together with the amino residues and waters that are omitted in Fig. 1 will be published by the Shen and Kamiya's group (Umena *et al*., to be published).

DFT calculations are done using a modified version of GAMESS (Schmit *et al*., 1993) with employing UB3LYP functional (Becke, 1993). The basis set used is the LACVP* basis, which is a hybrid basis set optimized for investigation of manganese polynuclear systems using UB3LYP functional. Five different protonated structures as shown in Fig. 1 (A)-(E) are examined to elucidate their relative stability. UB3LYP calculations have elucidated that the O(57) protonated structure with vertical hydrogen: $C(OH_{57}V)$ is the most stable among them: the other (O57) protonated structure with horizontal hydrogen: $B(OH_{57}H)$ is less stable only by about 3 kcal/mol than $C(OH_{57}V)$. On the other hand, the O(56) protonated structure: $A(OH_{56})$ is unstable over 40 kcal/mol than $C(OH_{57}V)$. Moreover, the $CaMn_4O_5$ structures with deprotonated water (OH anion) at Ca(II) site: D(Ca-OH) and Mn(4) site: E(Mn-OH) are far more unstable than $C(OH_{57}V)$. Thus UB3LYP calculations concluded that O(57) site is protonated at the S_1 stage of the Kok cycle.

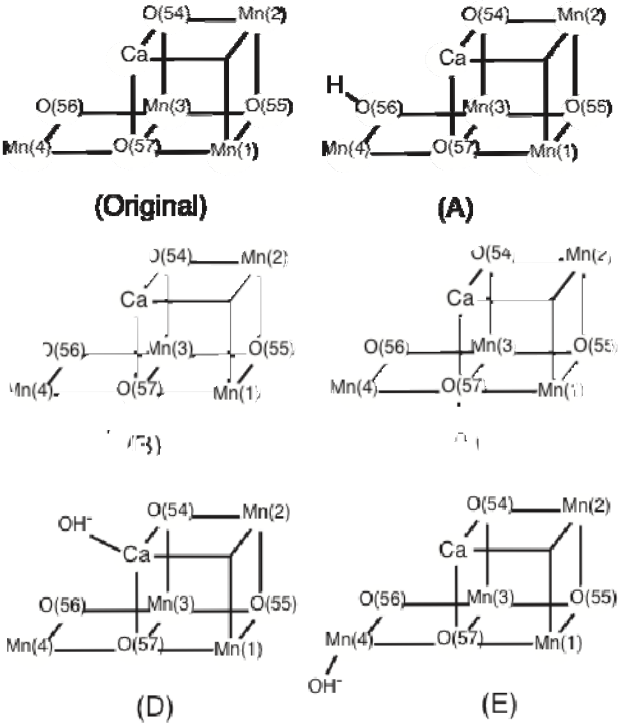

Fig. 1 The core of the OEC cluster. (Original) the fundamental structure of the XRD structure given by Umena *et al.* (A) $O_{56}H$ model, (B) $O_{57}H$ model. (C) $O_{57}H_V$ model. (D) $CaOH^-$ model. (E) $MnOH^-$ model.

Electrophilic oxygen revealed by the natural orbital analysis of UB3LYP solution

In order to elucidate the fundamental feature of the electronic structure of **1**, we performed the natural orbital (NO) analysis using the UB3LYP computational

results. Hereafter, we use the familiar terms, HOMO and LUMO, instead of HONO and LUMO.

Electron and proton releases occur starting from S_1 stage to S_4 stage in Kok cycle. We have examined the $CaMn(IV)_4O_5$ structure (**1b**) that undergoes the electrophilic addition reaction for the O-O bond formation. LUMOs are very useful for MO-theoretical explanation of the electrophilic reactivity.

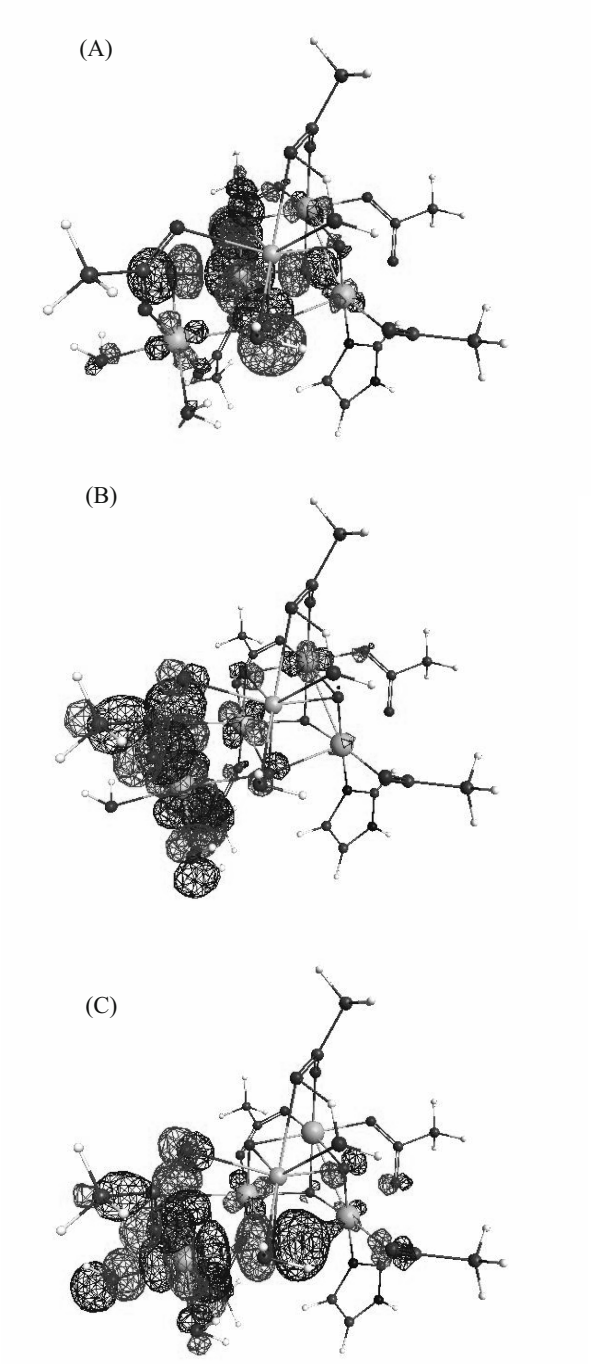

Fig. 2 The Natural orbitals of the UB3LYP solution of $CaMn(IV)_4O_5$ (**1b**) (isosurface level = 0.02 for the absolute value of probability amplitudes). (A) The third LUMO (LUMO+2). (B) The second LUMO (LUMO+1). (C) The LUMO.

Fig. 2 shows the σ-type, p-type and the other σ -type d-π conjugated LUMOs for **1b**. The σ -type LUMO of **1b** in Fig. 2(A) has large robes over the Mn(3) -O(57) region, indicating the electrophilic property of O(57). On the other hand, the π-type LUMO of **1b** in Fig. 2(B) has large robes over the Mn(4)-O(56) region, indicating the electrophilic property of O(56). On the other hand, the other σ-type d-π conjugated LUMO in Fig. 2(C) is delocalized over the O(56)-Mn(4)-O(57) region. Thus, judging from the shapes of LUMOs, it is clear that external O(56) and/or internal O(57) sites play an important role in the electrophilic reactivity (Umena *et al*., to be published; Isobe *et al*., 2005; Yamaguchi *et al*., 2007) of the $CaMn_4O_5$ cluster of OEC of PSII refined to 1.9 A resolution. In fact, the hydroxy anion or water of Mn(4) or Ca(II) can undergo the nucleophilic attack to the O(56) and/or O(57) site as illustrated in Fig. 3.

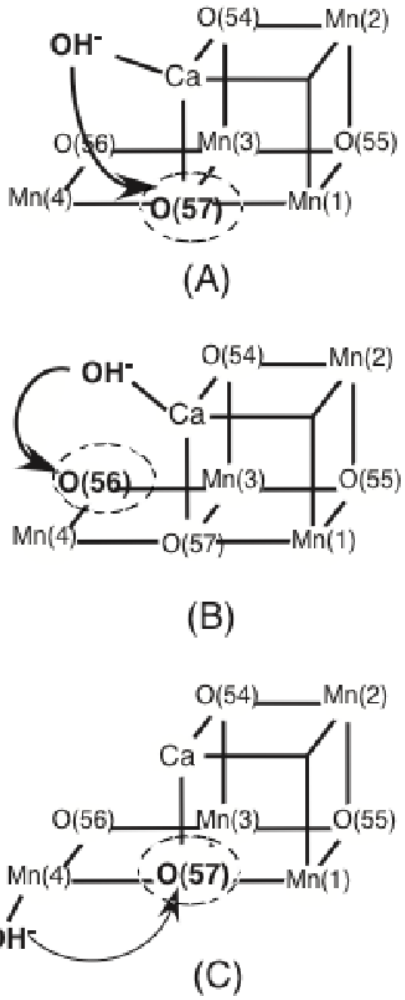

Fig. 3 Possible nucleophilic attacks (A) From the Ca site to the oxygen (57) site. (B) From the Ca site to the oxygen (58) site. (C) From the dangling Mn site to the oxygen (57) site.

Concluding Remarks

The present UB3LYP calculations have elucidated that O(57) site is protonated at the S1 stage of **1a** in the Kok cycle of photosynthetic water splitting. LUMOs of the proton and electron released structure **1b** are delocalized over Mn_4-O(56) and Mn_3-O(57), and O(56)-Mn_3-O(57), regions. Therefore electrophilic O(56) and/or O(57) play an important role for the nonradical O-O bond formation reaction in the water-oxidation process at OEC of PSII. In the present model calculations, we have neglected many water molecules existing near the cluster and second coordination sphere of protein amino acid residues (Umena, *et al.*) that may modify the shapes of LUMOs. Such computations are really desirable in future for further refinements of the present results.

Acknowledgements

This work has been supported by Grants-in-Aid for Scientific Research (Nos. 19750046, 19350070, 18350008) and for Research and Development of the Next-Generation Integrated Simulation of Living Matter, as a part of the Development and Use of the Next-Generation Supercomputer Project.

References

Zouni A, Witt HT, Kern J, Fromme P, Kraub N, Saenger W, Orth P (2001) Crystal Structure of Photosystem II from Synechococcus Elongatus at 3.8 Å. Nature 409: 739-743

Kamiya N, Shen JR (2003) Crystal Structure of Oxygen-Evolving Photosystem II from Thermosynechococcus Vulcanus at 3.7-Å Resolution. Proc Natl Acad Sci USA 100: 98-103

Ferreira KN, Iverson TM, Maghlaoui K, Barber J, Iwata S (2004) Architecture of the Photosynthetic Oxygen-Evolving center. Science 303: 1831-1838

Loll B, Kern J, Saenger W, Zouni A, Biesiadka J (2005) Towards Complete Cofactor Arrangement in the 3.0 Å Resolution Structure of Photosystem II. Nature 438: 1040-1044

Guskov A, Kern J, Gabdulkhakov A, Broser M, Zouni A, Saenger W (2009) Cyanobacterial Photosystem II at 2.9 Å Resolution and the Role of Quinones, Lipids, Channels, and Chloride. Nature Struct Mol Bio 16: 334-342

Kawakami K, Umena Y, Kamiya N, Shen JR (2009) Location of Chloride and Its Possible Functions in Oxygen-Evolving Photosystem II Revealed by X-Ray Crystallography. Proc Natl Acad Sci USA 106: 8567-8572

Umena Y, Kawakami K, Shen JR, Kamiya N to be published

Kok B, Forbush B, McGloin M (1970) Cooperation of Charges in Photosynthetic O_2 Evolution-I. A linear Four Step Mechanism. Photochem Photobiol 11: 457-475

Pantazis D, Orio M, Petrenko T, Zein S, Lubitz W, Messinger J, Neese F (2009) Structure of the Oxygen-Evolving Complex of Photosystem II: Information on the S_2 State through Quantum Chemical Calculation of Its Magnetic Properties. Phys Chem Chem Phys 11: 6788-6798

Siegbahn PM (2009) An Energetic Comparison of Different Models for the Oxygen Evolving Complex of Photosystem II. J. Am. Chem. Soc. 131: 18238-18239

Sproviero EM, Gascon JA, McEvoy JP, Brudvig GW, Batista VS (2008) Quantum Mechanics/Molecular Mechanics Study of the Catalytic Cycle of Water Splitting in Photosystem II. J Am Chem Soc. 130: 3428-3442

Pettersen EF, Goddard TD, Huang CC, Couch GCD, Greenblatt M, Meng EC, Ferrin TE (2004) UCSF Chimera – a Visualization System for Exploratory Research and Analysis. J Comput Chem25: 1605-1612

Sproviero EM, Gascon JA, McEvoy JP, Brudvig GW, Batista VS (2006) Characterization of Synthetic Oxomanganese Complexes and the Inorganic Core of the O2-Evolving Complex in Photosystem II: Evaluation of the DFT/B3LYP Level of Theory. J. Inorg. Biochem 100: 786-800

Becke AD (1993) Density-Functional Thermochemistry. III. The Role of Exact Exchange. J Chem Phys 98: 5648-5652

Schmidt MW, Baldridge KK, Boatz JA, Elbert ST, Gordon MS, Jensen JH, Koseki S, Matsunaga N, Nguyen KA, Su S, Windus LT, Dupuis M, Montgomery JA (1993) General Atomic and Molecular Electronic Structure System. J Comput Chem 14: 1347-1363

Isobe H, Shoji M, Koizumi K, Kitagawa Y,

Yamanaka S, Kuramitsu S, Yamaguchi K (2005) Electronic and Spin Structures of Manganese Clusters in the Photosynthesis II System. Polyhedron 24: 2767-2777

K Yamaguchi, S Yamanaka, H Isobe, K Koizumi, Y Kitagawa, T Kawakami, M Okumura (2007) Theory of Chemical Bonds in Metalloenzymes VI: Manganese-Oxo. Bonds in the Photosynthesis II System. Polyhedron, 26: 2216-2224

Symposium 07

Mimicking Photosynthetic Catalysis

The Structure of a Water-oxidizing Cobalt Oxide Film and Comparison to the Photosynthetic Manganese Complex

Marcel Risch[a], Katharina Klingan[a], Anna Fischer[b], Holger Dau[a,*]

[a] Freie Universität Berlin, FB Physik, Arnimallee 14, 14195 Berlin, Germany;
[b] Technische Universität Berlin, Institut für Chemie, Straße des 17. Juni 135, 10623 Berlin, Germany.
[*]Corresponding author. Tel. No. +49 30 838 53583; Fax No. +49 30 838 56299; E-mail: holger.dau@fu-berlin.de.

Abstract: In photosynthesis, water is oxidized at a protein-bound Mn_4Ca complex. Artificial water-oxidation catalysts that are similarly efficient and based on inexpensive and abundant materials are of great interest. A recently reported inorganic cobalt catalyst (CoCat) forms by electrodeposition as an amorphous layer on inert anodes, starting from an aqueous solution of cobalt ions and buffered salts such as potassium phosphate (KP_i). X-ray absorption spectroscopy (XAS) indicates that the central unit of the CoCat is a cluster of edge-sharing $Co^{III}(\mu\text{-}O)_6$ octahedra. We find that the apparent cluster nuclearity is higher for film formation at anode voltages below the water-oxidation threshold. These films exhibit only minimally lower cobalt oxidation states than the films of the same thickness but deposited at voltages supporting water-oxidation. The similarities in structure, function, and oxidative self-assembly of the all-inorganic CoCat and the photosynthetic Mn_4Ca complex are striking, despite stark differences in the chemical environment.

Keywords: Artificial photosynthesis; Biomimetic chemistry; Oxygen evolution; X-ray absorption spectroscopy

Introduction

Photosynthetic water oxidation is crucial for life on earth. It is efficiently catalyzed by a pentanuclear Mn_4Ca complex bound to the proteins of photosystem II (PSII) (Dau and Haumann, 2008; Dau and Zaharieva, 2009; Dau *et al.*, 2010). For large-scale technological production of molecular hydrogen (or other fuels) from water, synthetic water-oxidation catalysts are needed that are (i) similarly efficient as the photosynthetic Mn complex and; (ii) based on inexpensive and abundant materials. A cobalt catalyst for water-oxidation reported by (Kanan and Nocera, 2008) has attracted much interest because of its efficiency at neutral pH and self-assembly from low-cost materials. This catalyst (CoCat) assembles as an amorphous layer on inert anodes, by electrodeposition starting from aqueous solutions of cobalt and buffered salts, *e.g.* KP_i. For the amorphous CoCat, diffraction techniques are not applicable, whereas X-ray absorption spectroscopy (XAS) is well suited to analyze the local structure of the cobalt metal sites in the disordered material (Risch *et al.*, 2009a). Herein, new XAS data on oxidation state and structure of this cobalt catalyst (CoCat) deposited at two anode voltages is presented. Recent results on structure and function of the CoCat will be compared to the Mn_4Ca complex in PS II.

Methods, Results and Discussion

XAS measurements at cryogenic temperatures (20 K) were performed at the Helmholtz-Zentrum Berlin (BESSY, beamline KMC-1) using a 13-element fluorescence detector manufactured by Canberra. Details on sample preparation and the XAS setup may be found elsewhere (Risch *et al.*, 2009a). Total-reflection X-ray fluorescence (TXRF) analysis yields that approximately 50 nmol of Co was deposited on the samples discussed herein. $Co^{III}OOH$ was prepared by annealing (120 °C) of $Co^{II}(OH)_2$ in

air flow for 48 h. The transformation to Co^{III} was verified by X-ray powder diffraction.

In Fig. 1, the X-ray absorption near-edge structure (XANES) spectra of the CoCat films and reference materials are compared. The edge position of XANES spectra reflects the Co oxidation state, but is also sensitive to the Co ligand environment. In the absence of major modifications of the Co ligands, the latter influence is expected to be weak. Higher oxidation states cause the edge position to shift to higher energies. In Table 1, we present the edge positions as defined by the half-height of the normalized edge jump as well as by the integral method (Dittmer *et al.*, 1998), where the latter scales most linearly with the oxidation state (Dau *et al.*, 2003).

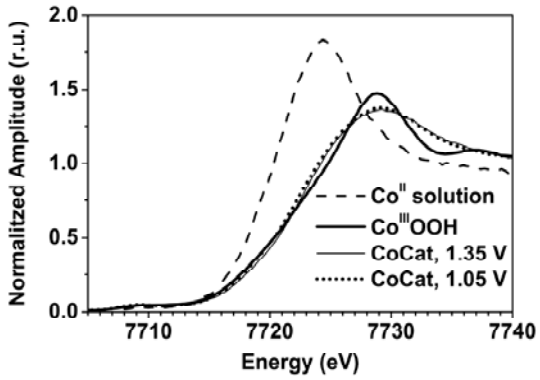

Fig. 1 Co *K*-edge XANES spectra of cobalt catalyst (CoCat) samples grown at 1.05 V and 1.35 V vs. NHE, and reference samples with oxidation state 3+ (CoOOH; thick line) and 2+ (0.5 mmol Co^{2+} solution; dashed line).

Table 1 Edge positions of selected XANES spectra

Compound	Half-height (eV)	Integral (eV)
$LiCo^{III}O$	7720.5 ± 0.2	7721.2 ± 0.1
$Co^{III}OOH$	7720.4 ± 0.1	7721.0 ± 0.1
CoCat, 1.35 V	7720.7 ± 0.1	7721.0 ± 0.1
CoCat, 1.05 V	7720.4 ± 0.1	7720.7 ± 0.1
Co^{II} solution	7718.3 ± 0.1	7718.4 ± 0.1

The integral method (Dittmer *et al.*, 1998) was used with limits of $0.15 < \mu < 1.0$. All error estimations from experimental scatter.

The edge position of CoCat samples deposited under conditions which support catalytic activity (1.35 V) is slightly higher than that of a CoCat sample deposited at anode voltages below the threshold for catalytic activity (1.05 V), see Table 1. Qualitatively, the same dependence of the edge position on the voltage during deposition was observed by Kanan *et al.* (2010). Nonetheless, the two edge positions of the CoCat are close to that of the Co^{III} references, from which we conclude that the Co oxidation state of the resting catalyst (open-circuit condition, no voltage applied) is close to 3+.

The high-resolution (data collection up to 16 $Å^{-1}$) Fourier-transformed EXAFS spectra of the CoCat and $Co^{III}OOH$ shown in Fig. 2 corroborate the absence of crystallinity. The x-axis shows reduced distances between the absorbing cobalt atoms and neighboring 'shells' of atoms that are about 0.3 Å shorter than the true nucleus-nucleus distance; precise distances are accessible through EXAFS simulations (Table 2). The amplitude of the peaks in the FT is a rough measure of the average number of the atoms at the respective distance. The peaks assigned to Co-Co vectors of the CoCat deposited at 1.05 V (Fig. 2, circles) are slightly higher than for a CoCat film of comparable thickness which was deposited at 1.35 V (Fig. 2, triangles), indicating a slightly stronger long-range order in the former. The FT of crystalline $Co^{III}OOH$ is shown for comparison. The minor but clearly resolved difference in the order at the atomic level suggests that the CoCat in general cannot be viewed as an aggregate of a multinuclear cobalt complex of a distinct size. Presently, we cannot exclude that clusters closer to the surface have lower nuclearity, as suggested by Kanan *et al.* (2010).

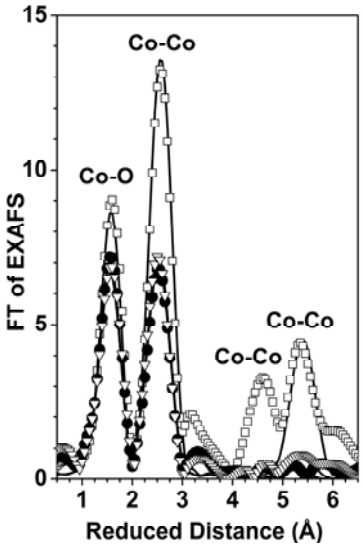

Fig. 2 Fourier-transform (FT) of an EXAFS spectrum of the cobalt catalyst (CoCat) for growth at a voltage not supporting water oxidation (1.05 V versus NHE; circles) and in the catalytic regime (1.35 V; triangles) compared to crystalline CoOOH (squares). CoOOH and CoCat are characterized by the same octahedral Co building blocks, but in CoOOH those blocks are arranged in an extended layer of side-sharing $Co^{III}O_6$ octahedra, which can be viewed also as a layer of side-sharing, incomplete Co-oxo cubanes $Co_3(\mu\text{-}O)_4$, see Fig. 3. EXAFS simulations are shown as solid lines.

We simulated the EXAFS with the in-house software 'SimX lite' (of Dr. P Chernev), to address both the questions of nuclearity and that of a suitable structural model of the CoCat film; see Table 2 for simulation results. We used the same phase functions and simulation approaches as described in Risch *et al.* (2009a). The known coordination numbers of CoOOH were fixed, in order to obtain estimates of the Debye-Waller parameter, σ.

Table 2 Parameters for the EXAFS simulation in Fig. 2.

CoOOH

Interaction	N	R (Å)	σ (10^{-3} Å)
Co-O	6*	1.90	43
Co-Co	6*	2.85	49
Co-Co	6*	5.69	58

CoCat, 1.05 V

Interaction	N	R (Å)	σ (10^{-3} Å)
Co-O	6.0	1.89	64
Co-Co	4.3	2.81	68
Co-Co	1.0	5.6	58*

CoCat, 1.35 V

Interaction	N	R (Å)	σ (10^{-3} Å)
Co-O	6.0	1.89	61
Co-Co	3.9	2.81	65
Co-Co	0.5	5.6	58*

The parameters marked by an asterisk were fixed; all other parameters were determined by curve-fitting of the data (*k*-range of 3–16 $Å^{-1}$). In all simulations, the amplitude reduction factor, S_0^2, was 0.75 and the energy axis of the fit was shifted by +1.5 eV relative to the initially selected E_0 of 7710 eV.

Two arrangements of the octahedral $Co^{III}O_6$ units have been proposed; one involving interconnected $Co_3K(\mu\text{-}O)_4$ or $Co_4(\mu\text{-}O)_4$ cubane units (Risch *et al.*, 2009a, 2009b) and one based on edge-sharing $Co^{III}O_6$ octahedra such as the $Co_{10}O_{32}$ cluster shown in Fig. 3, which represents a fragment of the CoO_2 layers found in $Co^{III}OOH$, $LiCoO_2$ and other metal oxides (tile model; Risch *et al.*, 2009b; Dau *et al.*, 2010; Kanan *et al.*, 2010). Both models are equally well compatible with the EXAFS of the CoCat. In the light of the remarkable Co_4-oxo water-oxidation catalyst reported by Yin *et al.* (2010), we focus our discussion on the tile model.

A planar $Co_{10}O_{32}$ unit composed of edge-sharing octahedra (Fig. 3) was derived from the simulation results in (Risch *et al.*, 2009a). The macroscopic CoCat would be composed of a large number of these tiles; the space between them is likely filled with cations (*e.g.* K^+), anions (*e.g.* HPO_4^{2-}), and water, in analogy to more-ordered layered structures, such as $LiCoO_2$. We emphasize that it would be not at all in conflict with the EXAFS data if some of the tiles were interconnected by bridging oxygen. Each CoCat film is likely composed of molecular clusters (tiles) of various sizes. Films deposited at lower voltages (slower growth) exhibit, on average, slightly larger clusters, as suggested by an increase in the EXAFS coordination number of both Co-Co interactions in Table 2. Our new data clearly indicates that the voltage during deposition determines the cluster size if the amount of deposited Co is kept constant. A decrease of the cluster size with lower voltage reported by (Kanan *et al.*, 2010) may be explained by dissolution of very thin films in Co-free electrolyte as reported by (Lutterman *et al.*, 2009).

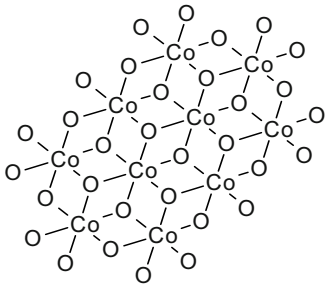

Fig. 3 Structure of μ-oxo-bridged cobalt atoms that is compatible with EXAFS data first reported elsewhere (Risch *et al.*, 2009a). In this $Co_{10}O_{32}$ unit, there are, on average, 3.8 Co-Co vectors of 2.8 Å length and 1.6 Co-Co vectors of 5.6 Å (no. per Co atom). Thus the structure satisfies the constraints resulting from EXAFS simulations. It is conceivable that several of these 'tiles' are interconnected to form an extended network or porous sheet. Layers of water molecules and cations may separate the Co-μ-oxo sheets, in analogy to layered Mn or Co dioxides.

A comparison of the structural motifs supposedly present in the CoCat, on the one hand, and the water-oxidizing Mn_4Ca complex of PSII (Haumann *et al.*, 2005), on the other hand, reveals similarities. Both metal catalysts involve extensive di-μ-oxo bridging between the transition-metal ions (Co in the CoCat, Mn in PSII) and additional redox-inert cations (K or others in the CoCat, Ca in PSII). However, the CoCat is assembled as an extended network of Co-oxo clusters whereas the active site of PSII water oxidation is a single metal-oxo complex bound to the proteins of PSII.

Light-driven assembly and operation of the CoCat was reported (Steinmiller and Choi, 2009; Zhong *et al.*, 2009), but the investigations relate to electrochemical assembly and self-repair of the films.

The lowest pH condition for efficient oxygen evolution of the CoCat and PSII are nearly identical: ~pH 6 for the CoCat (Surendranath *et al.*, 2010) and ~pH 5.5 for PSII (Dau and Zaharieva, 2009). Overpotential and turnover frequency (TOF) of the natural paragon are still unmatched by the inorganic CoCat. Table 3 summarizes the above discussion and updates similar comparisons (Kanan *et al.*, 2009; Nocera, 2009).

In conclusion, the Co/P/K/oxide based water-oxidation catalyst (CoCat) discussed herein shares properties with the Mn complex of PSII. It may serve as an easily accessible all-inorganic model for some aspects of the active site in PSII (Table 3), for example changes of the metal-oxygen distances and the μ-oxo bridging type upon oxidation of the catalyst film (unpublished results). However, the CoCat is not a close 'mimic' of the biological catalyst.

Table 3 Comparison between properties of the bulk oxide of the water-oxidizing CoCat and the natural paragon, the photosynthetic Mn_4Ca complex in PSII. For references, see text; still unpublished results are marked by a double-cross. This table updates and expands similar comparisons presented elsewhere (Kanan *et al.*, 2009; Nocera, 2009).

Property	CoCat	Mn_4Ca in PSII
Self-assembly	Electrodeposition from dissolved Co^{2+} ions; Co oxidation to the $Co^{3+/4+}$ level	Light-driven oxidative self-assembly from dissolved Mn^{2+}, Mn oxidation to the $Mn^{3+/4+}$ level
Self-repair	Electrochemical	Light-driven
Atomic distances	Co-μO: 1.9 Å Co-Co: 2.8 Å	Mn-μO: 1.8 – 2.0 Å Mn-Mn: 2.7 Å
Metals of proposed active site	*n* × Co, K, Na or Ca[#]	4 Mn, 1 Ca
Efficient O_2 production	pH > 6 in KP_i, at 23 °C, 1 bar	pH > 5.5, at 23 °C, 1 bar
Overpotential at 1 mA/cm^2	0.4 V in KP_i at pH 7	0.3 V at pH 5.5
TOF (per O_2 and Co/Mn ion)	< 1 s^{-1}, depending on thickness of CoCat film[#]	~100 s^{-1}

Acknowledgements

We thank F Schäfers and M Mertin (beamline KMC-1, BESSY, Berlin) for excellent technical support, M Haumann and I Zaharieva for valuable discussions, and P Chernev (all FU Berlin) for the development of EXAFS data analysis and simulation methods. Financial support by the UniCat cluster of excellence (Unifying Concepts in Catalysis, Berlin) and the European Union (7th FP program, SOLAR-H2 consortium) is gratefully acknowledged.

References

Dau H, Liebisch P, Haumann M (2003) X-Ray Absorption Spectroscopy to Analyze Nuclear Geometry and Electronic Structure of Biological Metal Centers - Potential and Questions Examined with Special Focus on theTetra-Nuclear Manganese Complex of Oxygenic Photosynthesis. Anal. Bioanal. Chem. 376(5): 562-583

Dau H, Haumann M (2008) The Manganese Complex of Photosystem II in Its Reaction Cycle - Basic Framework and Possible Realization at the Atomic Level. Coordin. Chem. Rev. 252: 273-295

Dau H, Limberg C, Reier T, Risch M, Roggan S, Strasser P (2010) The Mechanism of Water Oxidation: from Electrolysis Via Homogeneous to Biological Catalysis. Chemcatchem 2(7): 724-761

Dau H, Zaharieva I (2009) Principles, Efficiency, and Blueprint Character of Solar-Energy Conversion in Photosynthetic Water Oxidation. Acc. Chem. Res. 42(12): 1861-1870

Dittmer J, Iuzzolino L, Dörner W, Nolting HF, Meyer-Klaucke W, Dau H (1998) A New Method for Determination of the Edge Position of X-Ray Absorption Spectra. In: G Garab (ed.), Photosynthesis: Mechanisms and Effects. Kluwer Academic Publishers: Dortrecht. 2: 1339-1342

Haumann M, Muller C, Liebisch P, Iuzzolino L, Dittmer J, Grabolle M, Neisius T, Meyer-Klaucke W, Dau H (2005) Structural and Oxidation State Changes of the Photosystem II Manganese Complex in Four Transitions of the Water Oxidation Cycle (S0 --> S1, S1 --> S2, S2 --> S3, and S3,4 --> S0) Characterized by X-Ray Absorption Spectroscopy at 20 K and Room Temperature. Biochemistry 44(6): 1894-1908

Kanan MW, Nocera DG (2008) In Situ fFormation of an Oxygen-Evolving Catalyst in Neutral Water Containing Phosphate and Co^{2+}. Science 321(5892): 1072-1075

Kanan MW, Surendranath Y, Nocera DG (2009) Cobalt-Phosphate Oxygen-Evolving Compound. Chem. Soc. Rev. 38(1): 109-114

Kanan MW, Yano J, Surendranath Y, Dinca M, Yachandra VK, Nocera DG (2010) Structure and Valency of a Cobalt-Phosphate Water Oxidation Catalyst Determined by in Situ X-Ray Spectroscopy. J. Am. Chem. Soc. 132(39): 13692-13701

Lutterman DA, Surendranath Y, Nocera DG (2009) A Self-Healing Oxygen-Evolving Catalyst. J. Am. Chem. Soc. 131(11): 3838-3839

Nocera DG (2009) Chemistry of Personalized Solar Energy. Inorg. Chem. 48(21): 10001-10017

Risch M, Khare V, Zaharieva I, Gerencser L, Chernev P, Dau H (2009a) Cobalt-Oxo Core of a Water-Oxidizing Catalyst Film. J. Am. Chem. Soc. 131(20): 6936-6937

Risch, M, Ringleb F, Khare V, Chernev P, Zaharieva I, Dau H (2009b) Characterisation of a Water-Oxidizing Co-Film by XAFS. J. Physics Conf. Series 190(1-4): 012167

Steinmiller EMP, Choi KS (2009) Photochemical Deposition of Cobalt-Based Oxygen Evolving Catalyst on a Semiconductor Photoanode for Solar Oxygen Production. P. Natl. Acad. Sci. USA 106(49): 20633-20636

Surendranath Y, Kanan MW, Nocera DG (2010) Mechanistic Studies of the Oxygen Evolution Reaction by a Cobalt-Phosphate Catalyst at Neutral pH. J. Am. Chem. Soc. 132(46): 16501-16509

Yin Q, Tan JM, Besson C Geletii YV, Musaev DG, Kuznetsov AE, Luo Z, Hardcastle KI, Hill CL (2010) A Fast Soluble Carbon-Free Molecular Water Oxidation Catalyst Based on Abundant Metals. Science 328(5976): 342-345

Zhong DK, Sun JW, Inumaru H, Gamelin, DR (2009) Solar Water Oxidation by Composite Catalyst/ Alpha-Fe_2O_3 Photoanodes. J. Am. Chem. Soc. 131(17): 6086-6088

Catalytic Mechanism of a Bioinspired Mn-oxo Olgomer/Tungston Oxide System in Water Splitting and Its Relevance to PS II Water Oxidation

Wanshu He[a], Lien-Yang Chou[a], Ndi Geh[a], Robert Mulkern[a], Harvey JM Hou[a,*]

[a]Department of Chemistry and Biochemistry, University of Massachusetts Dartmouth, North Dartmouth, massachusetts 02747, USA.
[*]Corresponding author. Tel. No. +01 508 999 8234; Fax No. +01 508 999 9167; E-mail: hhou@umassd.edu.

Abstract: Solar energy is the most promising energy source as example to utilize solar energy on the large scale via natural and artificial photosynthesis. The decomposition of a synthetic Mn-oxo mix-valence dimeric complex, $[OH_2(terpy)Mn(O)_2Mn(terpy)OH_2](NO_3)_3 \cdot 6H_2O$, generated a highly active catalytic material, Mn-oxo oligomer. In this work we fabricated a Mn-oxo oligomer/WO_3 system to mimick the PS II water oxidation. The bioinspired Mn-oxo nanocatalysts described here take advantage of catalytic activity of PS II and exceedingly efficient holes production by n-type semiconductor such as WO_3. Based on experimental results, the hypothesis of our working cell is that the n-type semiconductor cooperates with Mn-oxo complex to efficiently split water by light driven. This unique Mn-oxo oligomer/WO_3 herterostructure was able to generate oxygen by photolysis of water, judged by capillary GC and GCMS analysis. Our design will not only produce new materials for efficient water splitting, but also establish new material design methodologies that can be extended to a wide range of combinations.

Keywords: Mn-oxo complex; Tungston oxide; Water oxidation, Water splitting, Photosystem II, Artificial photosynthesis; Catalysis

Introduction

Clean and renewable energy source is the key to resolve energy crisis in the 21st century. Solar energy is the most promising energy source as example to utilize solar energy (Hou and Harvey, 2010; Nocera, 2009). Photosynthesis provides an excellent example to utilize solar energy on the large scale (McConnell *et al*.). Solar energy conversion occurs in the reaction center of photosystem II (PSII) in cyanobacteria, algae, and green plants. The three-dimensional structures of PSII with oxygen-evolving activity were determined at the molecular level (Loll *et al*., 2005). However, due to the photosensitivity of PSII to X-ray radiation, the details of Mn_4Ca cluster in the PSII oxygen-evolving complex remains to be clarified.

The design of functional oxygen evolving catalysts was successfully achieved in synthesizing Mn-containing compounds. One such example is Mn-oxo cubic structure developed by Dismukes and co-workers (Ruettinger *et al*., 2000). Another excellent example is Brudivig Mn-oxo dimer, ($[OH_2(terpy)Mn(O)_2Mn(terpy)OH_2](NO_3)_3 \cdot 6H_2O$) (Limburg *et al*., 1999). The Mn-oxo dimer is able to evolve oxygen in the presence of chemical oxidants such as oxone or Ce^{4+} ion as a PS II functional model. The discovered provide significant insights into the mechanisms of water oxidation in PSII OEC complex (Cady *et al*., 2008; Limburg *et al*., 2001). It is generally established the active catalytic species is Mn(V) = O or Mn(V)-oxo radical, which is capable of releasing oxygen and closes the Sstate cycle (Brudvig, 2008).

However the Mn-oxo dimer is unstable under elevated temperature. The decomposition of the Mn(III/IV)-oxo dimer in aqueous solution at ~60 °C occurred involving a change in Mn valence (Zhang, 2010). We speculate that the thermal inactivation of PS II may also be associated with a Mn valence change in the Mn_4Ca cluster. Unexpectedly, the thermal decomposition of the Mn(III/IV)-oxo dimer was found to generate a Mn-containing precipitate that retained catalytic oxygen-evolution activity. The

solid Mn-containing material is not manganese dioxide as judged by EPR, FTIR, elemental analysis, and atomic absorption spectroscopy. The novel Mncontaining precipitate, tentatively assigned as a Mn-oxo oligomer, is thermally stable and may be a unique material for fabricating catalytic materials in solar fuel production.

In this work we fabricated a novel Mn-oxo oligomer/WO_3 nanocatalyst to mimick the PS II oxygen-evolving complex for efficient water photo-splitting. The design described here takes advantage of highly catalytic activity of Mn-oxo compound and exceedingly efficient holes production by n-type semiconductor such as WO_3.

Materials and Methods

Synthesis of Mn(III/IV)-oxo Dimer

The Mn(III/IV)-oxo mix-valence dimeric compound, $[Mn(III)(O)_2Mn(IV)(H_2O)_2(Terpy)_2](NO_3)_3$, was synthesized according the procedures reported previously (Chen *et al*., 2007). Oxone (potassium peroxymonosulfate, $KHSO_5$) solutions were made in acetate buffer (pH 4.50, 0.23 mol HAc/Ac-).

Preparation of the Mn-oxo oligomer/WO_3 catalyst

At room temperature, the Mn-oxo dimer was re-dissolved in H_2O to make a 1 mmol solution. When heated to 75 °C, the Mn-oxo dimer underwent thermal decomposition to yield the Mn-catalyst, which was received 4 by the WO_3 film.

GC and GCMS analysis

The gas phase sample was injected to an HP 5890 gas chromatography equipped with an HP-PLOT MoleSeive column. The temperatures of the injector and the detector were set at 100 °C. GC-MS analysis was performed in a Thermo Fisher Scientific ITQ 700 with Focus GC, which was equipped with Thermo TR-5MS SQC 30 m × 0.25 mm ID × 0.25 μm fused silica capillary column. The samples of 5.0 μL headspace gas were injected, and the amount of 18O-labeled O_2 was quantified using the peak height in the resulting mass spectra by averaging three independent measurements.

Results and Discussion

The working model of Mn-oxo oligomer/WO_3 is analogous to the mechanism of water oxidation in PS II as shown in Fig. 1. In PS II, sunlight energy is absorbed and induced charge separation through the primary donor P_{680}. The electron is delivered to Q_A and transferred to PS I to generate H_2 equivalent ($NADPH^+$). The positive charge at P^{680+} is neutralized by receiving electrons from water via Mn_4Ca cluster as a water oxidant. In the Mn-oxo oligomer/WO_3 system, WO_3 absorbe light photon and generate electron and hole in a similar way as P_{680} in PS II. The electron is transferred to the cathod for H_2 production. The Mn-oxo oligomer catalyzes the water oxidation via a Mn(V) intermediate species by shuttle the electron to WO_3 from water. The Mn-oxo oligomer/WO_3 nanocatalyst for efficient water photo-splitting takes advantage of highly catalytic activity of Mn-oxo compound and exceedingly efficient holes production by n-type semiconductor such as WO_3.

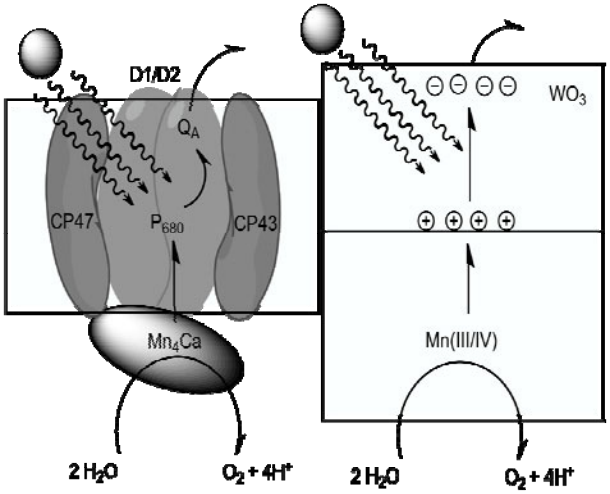

Fig. 1 Working model of Mn-oxo oligomer/WO_3 catalytic system (right panel) and simplified photochemical reaction in PS II water oxidation (left panel). Half black arrors represent the electron transfer steps.

The resulting photoelectrode was studied in an electrochemical cell using a two-electrode configuration for O_2 generation activity measurements and a three-electrode configuration for the photocurrent characterizations (Lin *et al*., 2009). Although an increase in the photocurrent was measured when Mn-oxo oligomer was present, the difference is insignificant. In contrast, the difference of O_2 generation as measured by GC was striking. This result is consistent with our design principles as illustrated in Fig. 1. The photo-to-electron conversion is performed by the semiconductor where a band-gap and a built-in field are present for light absorption and

charge separation, respectively. The primary role of Mn-oxo oligomer is to facilitate charge transfer to the solution and to catalyze H_2O oxidation. The photocurrent is limited by the ability of WO_3 to harvest light and to convert photons to charges, whereas the measurable O_2 generation depends on the catalytic activities of the electrode to fully oxidize H_2O. We noticed that there was an induction period for O_2 evolution over the sample with Mn-oligomer. This may be due to the optimization of O_2 evolution over time by the following reasons: formation of Mn-oxo olgomer on the optimized active catalytic sites on the Mn-oxo oligomer/WO_3 interface or rearrangement of W atom in WO_3 to eliminate the defect of WO_3 crystalline.

Alternatively, it may be caused by the unstability of WO_3 over prolong periodic time of water splitting. In this scenario, the role of Mn-oligomer may play protective role. This is supported by the observation that unstability of WO_3 material was tested in less acidic solutions (Liu, 2010). At pH = 7, WO_3 without the Mn-catalyst decayed more quickly than at pH = 4 (60% for 1 h), whereas approximately 4% performance degradation was observed when the Mn-catalyst was present for up to 2 h.

The photoelectrochemical setup permitted us to measure the photocurrent density, which was 0.807 mA/cm^2. In 7 h, this current density corresponds to a charge density of 6.98 C/cm^2-h and O_2 evolution rate of 18.1 μmol/cm^2-h. It is in excellent agreement with the measured O_2 generation rate 18.6 μmol/cm^2-h. In addition to O_2, the amount of H_2 generated by the photoelectrochemical setup was also measured. The 2:1 ratio of H_2 and O_2 generation rate confirms the complete decomposition of H_2O by the photogenerated charges unambiguously. The third piece of evidence is the ^{18}O isotope experiments. $H_2{}^{18}O$ was used in water splitting experiment. A significant amount of $^{16,18}O_2$ in the headspace gas sample was detected in addition to a small amount of $^{18,18}O_2$.

To understand the mechanism of water oxidation by the Mn-oxo-complex coated WO_3, we performed XPS analysis of the electrode surfaces before and after the water splitting experiments. The amount of Mn on the surface of WO_3 decreased significantly after the water oxidation process suggesting the complex catalytic cycle includes the formation of Mn(II)-species, which are subsequently dissolved in the solution. Notwithstanding this dissolution the catalytic activity of the Mn-oxo-complex coated WO_3 was maintained after 7 h of testing. This is because the dissolved Mn(II) remains in the near vicinity of the electrode and is readily regenerated by WO_3. When Mn(II) was intentionally added to the solution, the dissolution of Mn on the surface of WO_3 became negligible, supporting our hypothesis that Mn(II) is involved in the catalytic mechanism.

We suggest a possible mechanism of Mn-oxo oligomer/WO_3 system in water oxidation (Fig. 2). Four light photons are required to oxidize the Mn-oxo species accompanying four proton-coupled steps. Each step, the photon causes charge separation in WO_3. The hole generated in WO_3 receives electron from Mn-oxo complex and oxidizes the Mn ion via Mn valence changes. The Mn(V) intermediate species is generated by the fourth photon driven electron transfer reaction and splits water to dioxygen and regenerate active Mn-oxo catalyst.

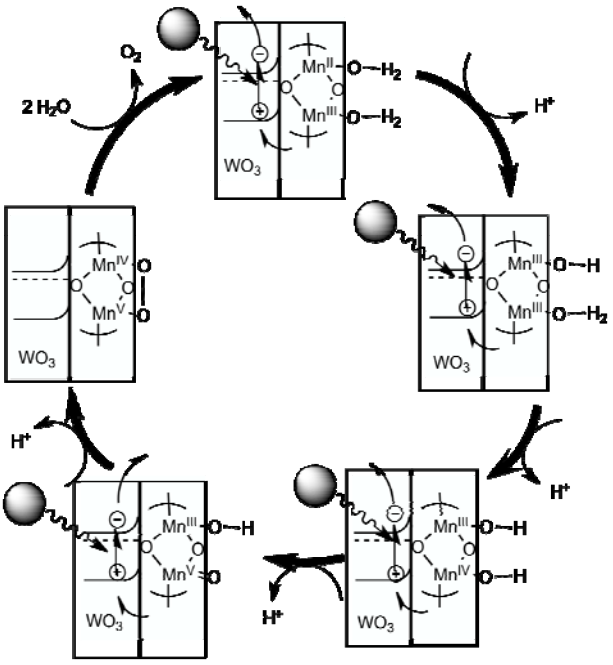

Fig. 2 Proposed mechanisms of Mn-oxo oligomer/WO_3 catalytic system in water oxidation. Full arrors indicate the proton transfer reaction; half arrors represent the electron transfer steps. Mn-oxo oligomer oxidizes H_2O by receiving photogenerated holes from WO_3 and undergoing a catalytic cycle, in which Mn valance change is a proton-coupled electron transfer in a similar way to PS II oxygen-evolvng complex.

In summary, we demonstrated that a Mn-oxo dimer-based complex can be readily deposited on the surface of WO_3 for complete H_2O oxidation. The semiconductor absorbs light, separates charges and

transfers holes to the Mn-oxo oligomer catalyst. The latter oxidizes H_2O and is regenerated subsequently by the photogenerated holes. In effect, the reaction may also be regarded as the Mn-oxo oligomer catalyst extracts electrons from H_2O to produce O_2, and then transfers the electrons to WO_3, where they are excited by incident photons and transported to the cathode for H_2O reduction to produce H_2. This approach combines more than one component to form a single material. Each component participates in one or more aspects of the H_2O photoelectrolysis process. New opportunities are opened up to the development of electrodes to directly utilize solar light for solar fuel generation. The wealth of knowledge of H_2O splitting catalyst and semiconductors and the ease to interface them makes this approach highly appealing.

Acknowledgements

We thank Professor Dunwei Wang for fruitful collaboration and support, Rui Liu for conducting structural and GC analysis, and Yongjing Lin for providing WO_3 material at Boston College. We also thank Fan Zhang for synthesizing Mn-oxo mix-valent dimeric compound. This work is supported by the University of Massachusetts Dartmouth.

References

Brudvig GW (2008) Water Oxidation Chemistry of Photosystem II. Philos. Trans. R. Soc., B. 363: 1211-1219

Cady CW, RH Crabtree, GW Brudvig (2008) Functional Models for the Oxygen-Evolving Complex of Photosystem II. Coord. Chem. Rev. 252: 444-455

Chen H, R Tagore, G Olack, JS Vrettos, TC Weng, J Penner-Hahn, RH Crabtree, GW Brudvig (2007) Speciation of the Catalytic Oxygen Evolution System:[MnIII/IV$_2$(mO)$_2$(terpy)$_2$(H_2O)$_2$](NO_3)$_3$+ HSO_5. Inorg Chem. 46: 34-43

Hou HJM Hou (2010) Structural and Mechanistic Aspects of Mn-Oxo and Co-Based Compounds in Water Oxidation Catalysis and Potential Application in Solar Fuel Production. J. Integr. Plant Biol. 52: 704-711

Limburg J, JS Vrettos, H Chen, JC de Paula, RH Crabtree, GW Brudvig (2001) Characterization of the O(2)-Evolving Reaction Catalyzed by [(terpy)(H_2O)Mn(III)(O)$_2$Mn(IV)(OH_2)(terpy)](N O_3)$_3$ (terpy = 2,2':6,2"-terpyridine). J Am Chem Soc. 123: 423-430

Limburg J, JS Vrettos, LM Liable-Sands, AL Rheingold, RH Crabtree, GW Brudvig (1999) A Functional Model for O-O Bond Formation by the O_2-Evolving Complex in Photosystem II. Science 283: 1524-1527

Lin Y, S Zhou, X Liu, S Sheehan, D Wang (2009) TiO2/TiSi2 Heterostructures for High-Efficiency Photoelectrochemical H_2O Splitting. J. Am. Chem. Soc. 131: 2772-2773

Liu R, Lin Y, Chou LY, Sheehan SW, He W, Zhang F, Hou HJM, D Wang (2010) Water Splitting Using Tungsten Oxide Prepared by Atomic Layer Deposition and Stabilized by Oxygen-Evolving Catalyst. Angew. Chem. Int. Ed., online 9 December 2010

Loll B, J Kern, W Saenger, A Zouni, J Biesiadka (2005) Towards Complete Cofactor Arrangement in the 3.0 A Resolution Structure of Photosystem II. Nature 438: 1040-1044

McConnell I, G Li, GW Brudvig. Energy Conversion in Natural and Artificial Photosynthesis. Chem. Biol. (Cambridge, MA, US) 17: 434-447

Nocera DG (2009) Personalized Energy: the Home as a Solar Power Station and Solar Gas Station. Chem Sus Chem 2: 387-390

Ruettinger W, M Yagi, K Wolf, S Bernasek, GC Dismukes (2000) O_2 Evolution from the Manganese-Oxo Cubane Core $Mn_4O_4^{6+}$: a Molecular Mimic of the Photosynthetic Water Oxidation Enzyme? J Am Chem Soc. 122: 10353-10357

Zhang F, Cady CW, Brudvig GW, HJM Hou* (2010) Thermal Stability of [Mn(III)(O)$_2$Mn(IV)(H_2O)$_2$ (Terpy)$_2$](NO_3)$_3$ (Terpy = 2,2':6',2"-terpyridine) in Aqueous Solution. Inorg. Chim. Acta, online 26 October 2010

An Artificial Water-Oxidizing Co Electro-Catalyst: Structure and Mechanism by *in Situ* X-Ray Absorption Spectroscopy

Junko Yano[a], Vittal K Yachandra[a,*], Matthew W Kanan[b], Yogesh Surendranath[b], Mirca Dinca[b], Daniel G Nocera[b,*]

[a]Physical Biosciences Division, Lawrence Berkeley National Laboratory, University of California, Berkeley, CA 94720, USA;
[b]Department of Chemistry, Massachusetts Institute of Technology, Cambridge, MA 02139, USA.
[*]Corresponding author. Tel. No. 1 510 486 4963; Fax No. 1 510 486 7668; E-mail: VKYachandra@lbl.gov.

Abstract: *In situ* X-ray absorption spectra (XANES and EXAFS) were obtained for a water-oxidizing Co electrocatalyst while operating at a potential that sustains water-oxidation and at open potential. Spectra were also collected at two different thicknesses of Co deposition, one which is extremely thin and almost a monolayer and the other which is thicker. *In situ* XANES spectra show that the Co valency is greater than 3+ for both samples during water oxidation at 1.25 V vs NHE. *In situ* EXAFS results indicate that a minimal bis-oxo/hydroxo-bridged Co multinuclear structure cluster, deposited at 1.1 V, grows into a higher nuclearity structure in the thicker films deposited at 1.25 V. On the basis of the growth pattern, and the structural parameters from both the thin and thick electrodes, we have proposed a structural model where the Co forms edge sharing CoO_6 oxo/hydroxo octahedra. In the thin layer electrode, the Co cluster has molecular dimensions, that increases in nuclearity to grow into a larger structure in the thicker layer electrode, while maintaining the same basic structural motif.

Keywords: Cobalt phosphate; Oxygen evolution; Water oxidation; X-ray spectroscopy

Introduction

Inorganic catalysts that contain cobalt, manganese, nickel, and other transition metals have been shown to work effectively as water-splitting catalysts (Kanan and Nocera, 2008; Dinca *et al*., 2010). However, there are not many detailed structural and mechanistic studies of such systems (McAlpin *et al*., 2010). Among the many such reported catalysts, one that is very promising is a cobalt oxide catalyst, which is generated via electro-deposition from aqueous solutions of Co^{2+} at neutral pH conditions.

The Co catalyst forms upon the oxidative polarization of an inert indium tin oxide electrode in phosphate-buffered water containing Co^{2+}. Electrolysis at ~1.29 V exhibits a rising current density that reaches a peak after 7 to 8 h. During this time, a dark coating forms on the ITO surface, presumably Co^{3+}. Co K-edge XANES and EXAFS studies have been carried out to determine the structural motifs of the Co catalyst on the electrode. We have used *in situ* XAS/electrochemistry to study the changes in the Co XANES and EXAFS as a function of the applied potential (Kanan *et al*., 2010).

Materials and Methods

Co-Pi catalyst samples were electrodeposited from freshly prepared 0.5 mmol $Co(NO_3)_2$ solutions in either 0.1 mol potassium phosphate buffer, pH 7.0 (KPi) or 0.1 mol sodium phosphate buffer, pH 7.0 (NaPi) just prior to collection of XAS spectra. An ITO layer (~0.15 μm) served as the working electrode upon which the catalyst was deposited.

The "bulk" and "surface" Co-Pi catalyst samples were electrodeposited from freshly prepared 0.5 mmol $Co(NO_3)_2$ solutions in 0.1 mol potassium phosphate buffer, pH 7.0 (KPi). Deposition of bulk Co-Pi was carried out at 1.25 V (all voltages are reported with

respect to the Normal Hydrogen Electrode, NHE) until 60 mC/cm^2 charge (0.26 C) was passed. Surface Co-Pi was electrodeposited at 1.1 V (NHE) until 1.6 mC of charge was passed (300 μC/cm^2).

X-ray absorption spectra were collected at the Stanford Synchrotron Radiation Lightsource (SSRL, Stanford)) on beamlines 7-3 and 9-3, and at the Advanced Light Source (ALS, Berkeley) on the micro-XAS beamline 10.3.2. The data were collected as fluorescence excitation spectra with a Ge detector (Canberra). Energy was calibrated by the rising edge position of Co foil (7709.5 eV) for Co XAS. Spectra were measured at room temperature. Data reduction of the EXAFS spectra was performed using EXAFSPAK (Drs. Graham George and Ingrid Pickering, SSRL). Curve fitting was performed with Artemis and IFEFFIT software using *ab initio*-calculated phases and amplitudes from the program FEFF 8.2.

Results and Discussion

X-ray absorption spectra (XANES and EXAFS) were obtained for the Co electrode (CoPi) while operating at a potential that sustains water-oxidation and at open potential. Spectra were also collected at two different thicknesses of Co deposition, one which is extremely thin and almost a monolayer (*surface CoPi*) and the other which is thicker (*bulk CoPi*).

In situ XANES spectra (Fig. 1) show that the Co valency is greater than 3+ for both samples during water oxidation at 1.25 V vs NHE.

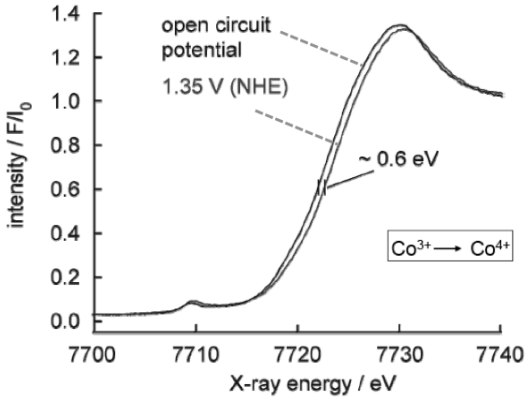

Fig. 1 Co XANES at 1.35 V (NHE) and at open circuit. There is a shift in the Co XANES of the CoPi electrode (bulk CoPi) to higher energy (~0.6 eV) between applied potentials of 0 V and 1.35 V, suggesting that there is an increase in the population of the higher oxidation states of Co (Co^{3+} to Co^{4+}) during the water-splitting reaction.

The Fourier transforms (FTs) of the EXAFS of the Co electrode are shown in Fig. 2. Peak I is from Co-O distances, peak II is from Co-Co distances and peaks III and IV are from shells at longer distances and multiple scattering contributions.

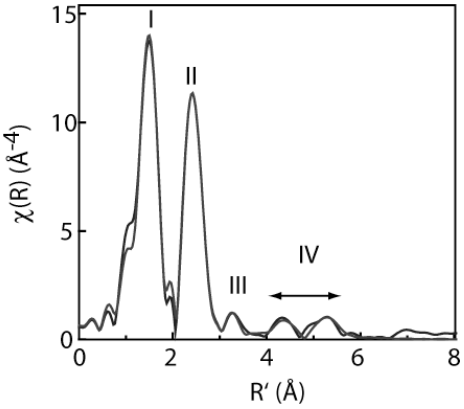

Fig. 2 FT of Co EXAFS of at 1.35 V (NHE) of bulk Co-Pi (black) and fit (grey). Peaks I and II are from Co-O and Co-Co distances. Region IV peaks are from more distant atoms that are not present in surface Co-Pi samples. The experimental data is in black and the fit is in grey.

EXAFS fitting results show that there are ~3.4 Co-Co interactions in the surface CoPi. However, in situ EXAFS shows that the CoPi increases in nuclearity to grow into a larger structure in the thicker layer electrode (bulk CoPi), depending on the condition (time, potential, etc.). On the basis of the growth pattern, and the structural parameters from both the thin and thick electrodes, we have proposed a model (Fig. 3) where the Co forms edge sharing CoO_6 oxo/hydroxo octahedra. This structure is very similar to that seen in CoO(OH).

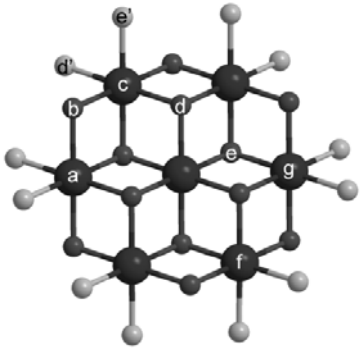

Fig. 3 The Structure of the surface Co electrocatalyst. Co, bridging O, and terminal O. Co (black circle), bridging O (small black circle), and terminal O (gray circle).

A proposed model for the larger nuclearity structure on the basis of the fits to the EXAFS data are

shown in Fig. 4. The fit parameters for the bulk electrode and growth preclude other structures based on a cubane-like structure that have been proposed (Risch *et al*., 2009).

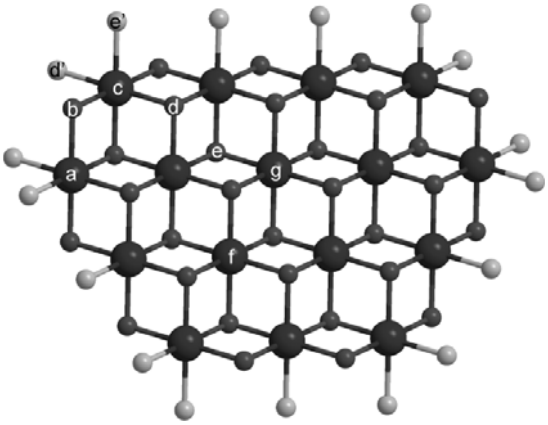

Fig. 4 The Structure of the bulk Co electrocatalyst. Co (black circle), bridging O (small black circle), and terminal O (gray circle).

Elemental analysis of CoPi films indicate ~1:1 ratio of K^+ ions to phosphate ions. To see if K^+ ion is a part of the CoPi structure, K^+ was substituted with Na^+ and Co EXAFS spectra were compared. The substitution of Na^+ for K^+ does not have a significant effect on Co-Pi activity. Although weak coordination of K^+ to the CoPi cluster cannot be ruled out, there is no evidence that Co-K interaction makes a substantial contribution to the EXAFS spectrum. Additionally, we also do not have any evidence that HPO_4^{2-} is strongly bound to the CoPi cluster.

Acknowledgements

We thank the Chesonis Foundation for generous financial support. MWK was supported by a Ruth L Kirschstein NIH Postdoctoral Fellowship. YS is supported by a NSF predoctoral fellowship. JY and VK Y were supported by the Director, Office of Science, Office of Basic Energy Sciences (OBES), Division of Chemical Sciences, Geosciences, and Biosciences of the Department of Energy (DOE) under Contract DE-AC02-05CH11231. Part of this work was funded by the Helios Solar Energy Research Center supported by OBES, DOE, under Contract DE-AC02-05CH11231. Synchrotron facilities were provided by the Stanford Synchrotron Radiation Laboratory (SSRL, Stanford), and the Advanced Light Source (ALS, Berkeley) funded by the DOE OBES. The SSRL Biomedical Technology program is supported by NIH, the National Center for Research Resources, and the DOE Office of Biological and Environmental Research.

References

Dinca M, Surendranath Y, Nocera DG (2010) Nickel-Borate Oxygen-Evolving Catalyst that Functions under Benign Conditions. Proc Natl Acad Sci USA 107: 10337-10341

Kanan MW, Nocera DG (2008) In Situ Formation of an Oxygen-Evolving Catalyst in Neutral Water Containing Phosphate and Co^{2+}. Science 321: 1072-1075

Kanan MW, Yano J, Surendranath Y, Dinca M, Yachandra VK, Nocera DG (2010) Structure and Valency of a Cobalt-Phosphate Water Oxidation Catalyst Determined by in Situ X-Ray Spectroscopy. J Am Chem Soc 132: 13692-13701

McAlpin JG, Surendranath Y, Dinca M, Stich TA, Stoian SA, Casey WH, Nocera DG, Britt RD (2010) Epr Evidence for Co(IV) Species Produced during Water Oxidation at Neutral pH. J Am Chem Soc 132: 6882-6883

Risch M, Khare V, Zaharieva I, Gerencser L, Chernev P, Dau H (2009) Cobalt-Oxo Core of a Water-Oxidizing Catalyst Film. J Am Chem Soc 131: 6936-6937

Symposium 08

Regulation of Electron Transfer

Quantification of Cyclic Electron Flow in Spinach Leaf Discs

Jiancun Kou[a,b], Shunichi Takahashi[b], Riichi Oguchi[b], Murray R Badger[b], Wah Soon Chow[b,*]

[a] North-West Agricultural & Forestry University, Yangling, Shaanxi 712100, China;
[b] Division of Plant Science, Research School of Biology, College of Medicine, Biology and Environment, The Australian National University, Canberra, ACT 0200, Australia.
[*]Corresponding author. Tel. No. +61 2 6125 3980; Fax No. +61 2 6125 8056; E-mail: Fred.Chow@anu.edu.au.

Abstract: We quantified the photosynthetic cyclic electron flux (CEF) around Photosystem I as the difference between the total electron flux through PS I (ETR1) and the linear electron flux through both photosystems. Both measurements were made in the whole tissue of spinach leaf discs illuminated in the same geometry and in CO_2-enriched air to suppress photorespiration. (1) CEF was negligibly small below 300 μmol photons m^{-2} s^{-1}. Above this irradiance, CEF increased approximately linearly up to the highest irradiance used (1,900 μmol photons $m^{-2}s^{-1}$). (2) CEF at a fixed irradiance of 980 μmol m^{-2} s^{-1} increased by a factor of almost 3 as the temperature was increased from 5 °C to 40 °C. It did not decline, even when the linear electron flux decreased at high temperatures. (3) Antimycin A, at a high concentration, decreased CEF to about 10% of the control value without affecting the linear electron flux. This method appears to be reliable for quantifying CEF non-intrusively. By contrast, estimation of the linear electron flux from chlorophyll fluorescence over-estimated CEF in the above treatments.

Keywords: Antimycin A; Cyclic electron flow; Linear electron flow; P700; Photosystem I

Introduction

The significance, mechanisms and roles of the photosynthetic cyclic electron flux (CEF) have been intensely studied (for reviews, see Bendall and Manasse, 1995; Allen, 2003; Johnson, 2005; Joliot and Joliot, 2006). Unfortunately, efforts to elucidate the importance of CEF have been hampered by the difficulty of quantifying CEF due to the absence of a net product of cyclic electron flow.

In this study we sought to quantify CEF by devising a method that is simple to apply routinely, that uses white light to simulate sunlight and that is relatively non-intrusive. Our approach was to measure the total electron flux (ETR1) through Photosystem I (PSI) and the linear electron flux (LINEAR) through PSII and PSI in series. Crucially, we ensured that both ETR 1 and LINEAR were measured in the whole tissue of a leaf disc illuminated in the same geometry in 1% CO_2. CEF was then calculated as CEF = ETR1 – LINEAR.

Materials and Methods

Spinacea oleracea L. (cv. Yates hybrid 102) plants were grown in a glasshouse at approximately 30/15 ºC (day/night) under natural light in autumn and winter. The plants were provided with a nutrient solution, supplemented by a slow release fertilizer.

When required, leaf discs (1.5 cm^2) were immersed in water, or a selected concentration of antimycin A, vacuum infiltrated using a water-driven pump for about 30 s, blotted with absorbent paper, and allowed to evaporate off the excess intercellular water in darkness for ~ 30 min before measurement.

LINEAR was determined by measurement of O_2 evolution by a leaf disc placed in a gas-phase Hansatech O_2 electrode equipped with an adaptor that accepts a multifurcated light guide. The electrode chamber contained 1% CO_2. White projector light filtered by a Calflex C heat-reflecting filter and neutral-density filter(s) was passed through one branch of the light guide. O_2 evolution was measured

over several minutes until a steady rate was reached. The post-illumination drift was added algebraically to the oxygen evolution rate during illumination, and the sum was multiplied by four to obtain LINEAR.

ETR1 was determined by redox changes of P700, the special chlorophyll (Chl) pair in PSI, with an ED-P700DW unit attached to a PAM fluorometer (Walz, Germany) (time constant = 95 μs). Prior to P700 measurements, a leaf disc had been brought to a steady photosynthetic state by illumination with white actinic light of a selected irradiance (I) for > 10 min during which O_2 evolution and light-acclimated Chl fluorescence yields were obtained. To ensure retention of the steady state after the earlier measurements, each leaf disc was immediately re-illuminated with the same actinic light for 9 s, defined by a shutter controlled by a pulse generator (Model 565, Berkeley Nucleonics Corporation, U.S.A.).

During each 9-s interval, at time = 8.80 s (corresponding to the time point −50 ms in Fig. 1A), data acquisition was started by a trigger from a second terminal of the pulse generator. At 8.85 s, a strong far-red light (FR, ~ 2,000 μmol photons m^{-2} s^{-1}) from a light-emitting diode array (emission peak 741 nm, LED735-66-60, Roithner LaserTechnik, Austria) was triggered on for 100 ms using a trigger from a third terminal of the pulse generator. The strong FR light further oxidized a fraction of the P700 even in the presence of white actinic light, depleting electrons from the inter-system chain, so that the subsequent saturating pulse (see immediately below) oxidizes P700 maximally in the light-acclimated state (Siebke *et al*., 1997). While the strong FR light was still on, at time = 8.90 s, a saturating light pulse (~9,000 μmol photons m^{-2} s^{-1}) was turned on by an electronic shutter for 10 ms, triggered by a fourth terminal of the pulse generator. Finally, the actinic light was turned off at 9.0 s. Data acquisition continued for a further 85 ms to obtain the baseline corresponding to zero $P700^+$. On completion of data acquisition, another 9-s sequence of illumination operations was started, thereby maintaining steady-state photosynthesis. Nine traces were averaged by software (written by the late A. B. Hope) to improve signal:noise.

Next, we determined the maximum extent of P700 oxidation under conditions with no limitation on the acceptor side of PS I. First, we established a steady state by illumination with weak far-red light (~12 μmol photons m^{-2} s^{-1} at 723 nm, from an LED) for > 10 s (Fig. 1B). Then we superimposed a saturating single-turnover flash on the weak far-red light. Flashes were given at 0.2 Hz, and 9 consecutive signals were averaged. The maximum signal immediately after the flash, $[P700^+]_{max}$, was taken as the total photo-oxidizable P700. The photochemical yield of PS I is given by $Y(I) = b/[P700^+]_{max}$, where b is the signal interval b in Fig. 1A (Klughammer and Schreiber, 2007). ETR1 was calculated as $Y(I) \times I \times 0.85 \times 0.5$ for the white actinic light used.

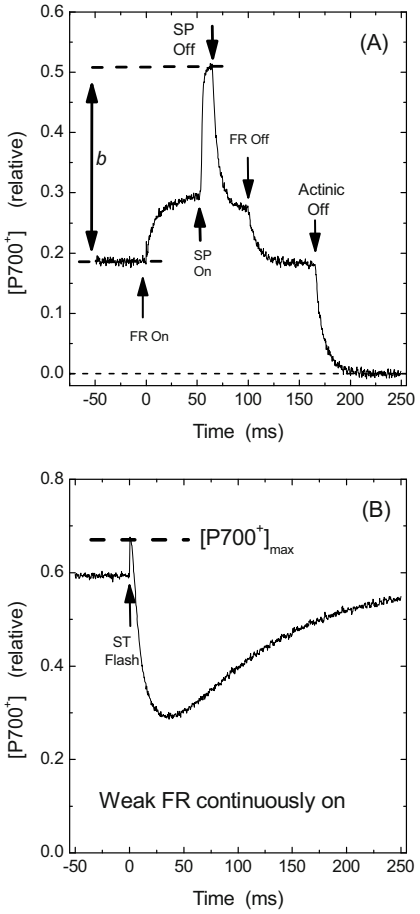

Fig. 1 Measurement of the photochemical yield of PS I in two steps. (A) When steady-state photosynthesis was occurring at 980 μmol m^{-2} s^{-1} with a steady $[P700^+]$, strong far-red light (FR) was turned on at t = 0 for 100 ms to further photo-oxidize P700. At t = 50 ms, a 10-ms saturating light pulse (SP) photo-oxidized P700 fully. Actinic illumination ended at t = 166 ms. The signal interval b represents the P700 still available for photo-oxidation. (B) Maximum photo-oxidizable P700 was obtained by illuminating a leaf disc with weak continuous far-red light to attain ~88% oxidation in the steady state. Then a single-turnover saturating flash photo-oxidized the remaining P700. The peak immediately after the flash is $[P700^+]_{max}$, the ratio $b/[P700^+]_{max}$ being the photochemical yield of PS I as defined by Klughammer and Schreiber (2007).

We also measured the quantum yield of PSII photochemistry averaged over open and closed traps

(Genty *et al*., 1989), *viz.* $\phi_{PS\ II} = (1 - F_s'/F_m')$, where F_s' is the fluorescence yield at steady state and F_m' the maximum fluorescence yield in the light-acclimated state. ETR2, the electron flux through PSII, was calculated as $(1 - F_s'/F_m') \times I \times 0.85 \times 0.5$, for comparison with LINEAR.

Results and Discussion

Electron Fluxes in Response to Irradiance

ETR1, the total electron flux through PS I, increased with irradiance, showing no saturation even at the highest irradiance (Fig. 2). By contrast, LINEAR peaked at about 1500 µmol e^- m^{-2} s^{-1}. The maximum LINEAR was ~188 µmol electrons m^{-2} s^{-1} (≡ 47 µmol O_2 m^{-2} s^{-1}). CEF = ERT1 – LINEAR was very small below 300 µmol m^{-2} s^{-1}, above which it increased approximately linearly with irradiance (Fig. 2). At the highest *I*, CEF almost equalled the linear rate. ETR2, assayed by Chl *a* fluorescence, underestimated the whole-tissue linear rate measured by O_2 evolution, the discrepancy increasing with irradiance.

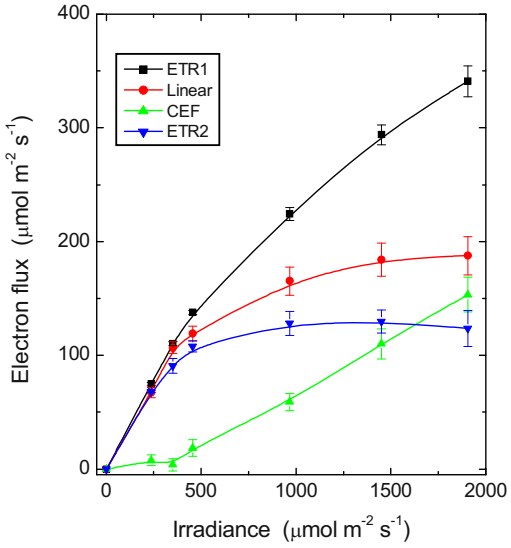

Fig. 2 Response of steady-state electron fluxes to irradiance. ETR1 is the total electron flux through PS I, and LINEAR the linear electron flux through both photosystems, both being whole-tissue measurements. CEF = ETR1 – LINEAR. ETR2 is the electron flux through PS II based on Chl fluorescence measurements. Values are means ± SE (n = 14 leaf discs).

The negligibly small CEF at $I < 300$ µmol m^{-2} s^{-1} (Fig. 2) is expected since the Calvin-Benson cycle was able to use the majority of NADPH at low irradiance, leaving little spare reduced ferredoxin for cyclic electron flow. When the linear electron flow reached a saturated rate at high irradiance, however, reduced ferredoxin accumulated, and CEF approached the linear electron flux.

Electron Fluxes in Response to Temperature

At a fixed irradiance of 980 µmol m^{-2} s^{-1}, ETR1 increased steadily with temperature until it peaked at about 32 °C, and then decreased above this temperature (Fig. 3). LINEAR, assayed by O_2 evolution, followed a similar pattern, but it peaked at a temperature slightly below 30 °C. The difference, representing CEF, increased steadily with temperature.

It has been suggested that cyclic electron flow is activated by high temperature (Bukhov *et al*., 1999; Clarke and Johnson, 2001). In our study, cyclic electron flow increased by a factor of almost 3 when the temperature was raised from 5 °C to 40 °C (Fig. 2). Liner declined between 32.5 °C and 40 °C, perhaps because of down-stream limitation in carbon assimilation. By contrast, CEF did not decrease at 40 °C (Fig. 3). If carbon assimilation decreased at high temperatures, reduced ferredoxin would accumulate, favouring cyclic electron flow, particularly if the warm temperature facilitated the diffusion of ferredoxin or accelerated enzymatic reactions involved in cyclic electron flow.

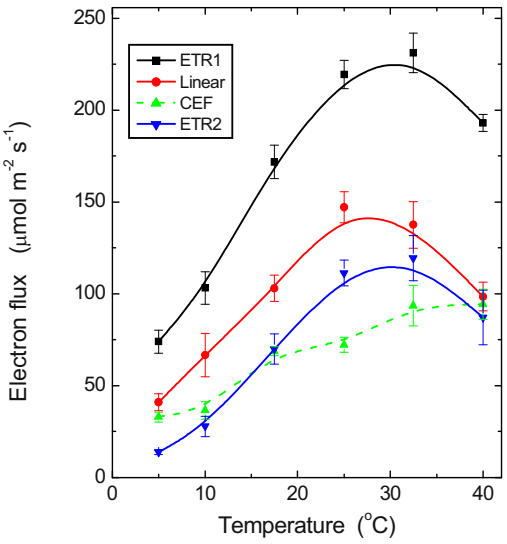

Fig. 3 Variation of steady-state electron fluxes with temperature. A fixed irradiance of 980 µmol m^{-2} s^{-1} was used. Values are means ± SE (n = 14 leaf discs).

Inhibition of CEF by Antimycin A

Antimycin A inhibits the ferredoxin-dependent cyclic electron flux. In Fig. 4A, ETR1 decreased

towards an asymptotic value. However, the inhibitor had no effect on the linear flux assayed by O_2 evolution. The difference between the two fluxes indicates that CEF decreased steadily with increase in [antimycin A], reaching a value of about 10% of that of control leaf tissue. With the loss of CEF, the fraction of excitation energy dissipated non-photochemically in a light-regulated manner (ϕ_{NPQ}) decreased by about 34% (Fig. 4B), *despite* the constancy of linear electron flow. That is, CEF contributed to ϕ_{NPQ} by producing a ΔpH.

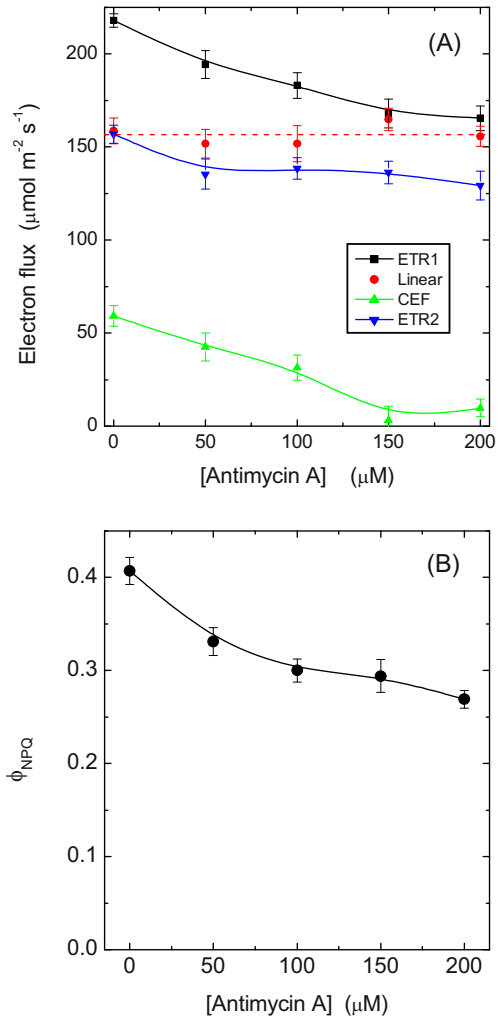

Fig. 4 (A) Variation of steady-state electron fluxes with [antimycin A] used to infiltrate leaf discs, at a fixed irradiance of 980 μmol m^{-2} s^{-1}. Values are means ± SE (n = 15 leaf discs). (B) ϕ_{NPQ}, the fraction of light absorbed by the PS II antennae that is dissipated as heat via ΔpH- and xanthophylls-regulated processes is plotted against [antimycin A].

Our observation that antimycin A largely abolished CEF suggests that (1) a cyclic path involving the NAD(P)H dehydrogenase may be a minor pathway, and (2) charge recombination in PSI (which would not contribute to ϕ_{NPQ}) might have only a small role in determining Y(I) under the experimental conditions.

Acknowledgements

A China Scholarship Council fellowship (to JK) and grants from the Australian Research Council to WSC (DP1093827) and MRB (Centre of Excellence in Plant Energy Biology) supported this work.

References

Allen JF (2003) Cyclic, Pseudocyclic and Noncyclic Photophosphorylation: New Links in the Chain. Trends Plant Sci 8: 15-19

Bendall DS, Manasse R (1995) Cyclic Photophosphorylation and Electron Transport. Biochim Biophys Acta 1229: 23-38

Bukhov NG, Wiese C, Neimanis S, Heber U (1999) Heat Sensitivity of Chloroplasts and Leaves: Leakage of Protons from Thylakoids and Reversible Activation of Cyclic Electron Transport. Photosynth Res 59: 81-93

Clarke JE, Johnson GN (2001) In Vivo Temperature Dependence of Cyclic and Pseudocyclic Electron Transport inBarley. Planta 212: 808-816

Genty B, Briantais JM, Baker NR (1989) The Relationship between the Quantum Yield of Photosynthetic Electron Transport and Quenching of Chlorophyll Fluorescence. Biochim Biophys Acta 990: 87-92

Johnson GN (2005) Cyclic Electron Transport in C_3 Plants: Fact or Artefact? J Exp Bot 56: 407-416

Joliot P, Joliot A (2006) Cyclic Electron Flow in C3 Plants. Biochim Biophys Acta 1757: 362-368

Klughammer C, Schreiber U (2007) Saturation Pulse Method for Assessment of Energy Conversion in PSI http://www.walz.com/e_journal/pdfs/PAN07002.pdf

Siebke K, Caemmerer S von, Badger M, Furbank RT (1997) Expressing an RbcS Antisense Gene in Transgenic Flaveria Bidentis Leads to an Increased Quantum Requirement for CO_2 Fixed in Photosystems I and II. Plant Physiol 115: 1163-1174

The Ancient Cyanobacterium *Gloeobacter Violaceus* PCC 7421 is Capable of State Transitions and Blue-Light Induced Fluorescence Quenching

Gábor Bernát[a,*], Ulrich Schreiber[b], Igor N Stadnichuk[c], Matthias Rögner[a], Friederike Koenig[d]

[a]Plant Biochemistry, Ruhr-University Bochum, D-44801 Bochum, Germany;
[b]University of Würzburg, Julius-von-Sachs-Institute for Biosciences, D-97070 Würzburg, Germany;
[c]A. N. Bakh Institute of Biochemitry, Russian Academy of Sciences, 119071 Moscow, Russia;
[d]Molecular Plant Physiology, University of Bremen, D-28359 Bremen, Germany.
[*]Corresponding author. Tel. No. +49 234 3225814; Fax No. +49 234 3214322; E-mail: gabor.bernat@rub.de.

Abstract: The atypical unicellular cyanobacterium *Gloeobacter violaceus* PCC 7421, diverged very early during the evolution of cyanobacteria, can be regarded as a key organism for understanding many structural, functional, regulatory, and evolutionary aspects of oxygenic photosynthesis. In our current study we investigated whether this ancient cyanobacterium lacking thylakoid membranes is capable of two basic phenomena common to all other photoautrophs: state transitions and non-photochemical fluorescence quenching. Our results clearly indicate dynamic changes in light energy distribution between the two photosystems. Similar to "modern" cyanobacteria *G. violaceus* is in state II in darkness and in state I upon illumination with weak blue- or far red light. Compared to state II, state I is characterized by an increased functional absorption cross-section of PS2. Furthermore, in contrast to weak blue light, strong blue light reversibly quenches chlorophyll fluorescence in *G. violaceus*, which suggests the existence of regulated heat dissipation triggered by the orange carotenoid protein in this primordial cyanobacterium.

Keywords: Cyanobacteria; Phylogeny; Fluorescence quenching; Light adaptation; State transitions

Introduction

The unicellular cyanobacterium *Gloeobacter violaceus* PCC 7421 (Rippka *et al*., 1974) is the only known oxygenic photoautotroph which does not contain thylakoid membranes (TM); therefore, all membrane-bound bioenergetic processes take place in the green plasma membrane (PM) of this organism. The PM of *G. violaceus* shows lateral heterogeneity: photosynthetic and respiratory protein complexes are localized together in functionally distinct membrane domains which are probably the evolutionary precursors of TM (Rexroth *et al*., unpublished). Structure and composition of phycobilisome (PBS) antennae (Bryant *et al*., 1981) as well as spectral properties of *G. violaceus* are also quite unique. The latter include an extreme blue-shift of the major low temperature fluorescence emission band of photosystem (PS) 1 (Mangels *et al*., 2002; Mimuro *et al*., 2010). These and other atypical features of *G. violaceus* are in accordance with the fact that this lineage diverged very early during the evolution of oxygenic photosynthesis (Falcón *et al*., 2010) and may represent an ancient stage of it. Investigation of *G. violaceus* could therefore provide valuable information for understanding many structural, functional, regulatory, and evolutionary aspects of photosynthesis. Here, we address two of these questions: whether *G. violaceus* is capable of (i) state transitions, the dominant short-term changes in light energy distribution between photosystems, depending on light regime, and, in turn, PQ redox state, and (ii) regulated thermal dissipation (non-photochemical fluorescence quenching) which protects photosynthetic organisms from damage upon exposure to intense light. Although the molecular mechanisms of these

processes are quite different in eukaryotes from those in higher plants (Mullineaux and Emlyn-Jones, 2005; Kirilovsky, 2010), both phenomena are common to (almost) all oxygenic photoautotrophs.

Materials and Methods

Growth conditions

G. violaceus cells were grown photoautotrophically in Allen's medium at 20 °C under continuous white light (4 μmol photons m^{-2} s^{-1}) and ambient air. Six month old cultures at a Chl concentration of 5 μg/ml were used in all spectroscopic experiments.

Low-temperature fluorescence measurements

Low temperature fluorescence emission spectra were recorded using an Aminco-Bowman Series 2 luminescence spectrometer (SLM Spectronic Instruments). All samples were first dark adapted for 1 h to induce state II as an initial state. State I was induced by a subsequent 15 min exposure to FR light (200 μmol photon m^{-2} s^{-1}) defined by an Omega BP700 filter. Samples in state I and II were frozen in liquid nitrogen.

Chlorophyll fluorescence transients

Chlorophyll fluorescence transients were measured by a Dual-PAM-100 measuring system (Walz). State II to state I and state I to state II transitions were induced by switching on/off either FR light (735 nm, 75 W/m^2) or weak blue light (BL, 440 nm, 11 μmol photons m^{-2} s^{-1}). OCP- quenching was induced by switching on strong (200 μmol photons m^{-2} s^{-1}) BL. 300-ms saturating pulses (1000 μmol photons m^{-2} s^{-1}) were applied at 1 min intervals to probe the maximal fluorescence yields.

Results

Changes in light energy distribution between the two photosystems can be followed by low temperature fluorescence spectroscopy (Murata, 1969). The main advantage of this method is that the fluorescence emission from PS2 and PS1 is usually manifested as distinct emission peaks at 685/695 nm and 725 nm, respectively, as illustrated by fluorescence spectra (PBS excitation; λ_{ex} = 580 nm) of dark-adapted (state II) and FR illuminated (state I) *Synechocystis* PCC6803 cells (Fig. 1a). The emission band and shoulder at 665 nm and 650 nm indicate allophycocyanin (APC) and phycocyanin (PC) emission, respectively, while the peaks at 685/695 nm and 725 nm reflect excitation energy transfer from PBS to PS2 and PS1, respectively. The increase in the intensity of 685/695 nm emission (as compared to that of 730 nm) upon illumination of dark-adapted samples with FR light indicates state II to state I transition.

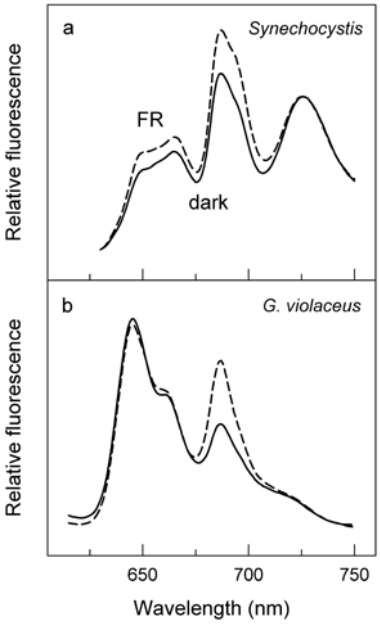

Fig. 1 Low temperature (77 K) fluorescence emission spectra of *Synechocystis* and *G. violaceus* cells with PBS excitation at 580 and 565 nm, respectively. (Different wavelengths were used due to different terminal acceptors.) Samples were frozen either after 1 h of dark incubation (solid lines) or after a subsequent 15 min FR illumination (dashed lines). The spectra were normalized to the 725 nm (*Synechocystis*) and 645/660 nm (*G. violaceus*) emission peak(s).

PBS excitation of dark adapted *G. violaceus* cells (λ_{ex} = 565 nm) induces intense PC emission at 645 nm with an APC shoulder at 660 nm and less intense chlorophyll fluorescence at 687 nm (Fig. 1b). FR illumination induces a 60% increase in the amplitude of the 687 nm peak. This shows a more efficient PBS to PS energy transfer in FR illuminated as compared to dark adapted cells, which may indicate that *G. violaceus* is capable of state transitions. However, due to the spectral properties of *G. violaceus* it is impossible to decide whether the energy transfer to PS2 or to PS1 is increased by FR illumination. To address this question we have performed room temperature fluorescence measurements in addition.

Fig. 2 shows chlorophyll fluorescence transients of dark-adapted *G. violaceus* induced upon switching on/off FR and BL. Saturation pulses are applied

repetitively for Fm determination. Dark incubation induces minimal Fo and Fm fluorescence yields, indicating that dark-adapted *G. violaceus* cells really are in state II. Exposure of cells to strong FR induces an increase in Fm which is a clear indication for state II to state I transition, *i.e.* light energy distribution between photosystems is changed in favor of PS2. The large increase of Fm is accompanied by only a small increase of Fo, which means an increase of the effective quantum yield, Φ(II) = (Fm–Fo)/Fm. State II to state I transition can be induced not only by FR light but also by weak BL (Fig. 2) which in cyanobacteria is a more efficient PS1 light than FR (Schreiber *et al*., 1995). These changes are reversible upon re-darkening of the sample (Fig. 2). Analysis of the photochemical phase of the Fo to Fm fluorescence rise in state I and state II revealed that state I (as compared to state II) is characterized by an increased functional absorption cross-section of PS2 (data not shown).

While *weak* BL in cyanobacteria is equivalent to strong FR light in inducing the high-fluorescent state I (Fig. 2), *strong* blue light provokes non-photochemical quenching (Schreiber *et al*., 1995; El Bissati *et al*., 2000), which reflects enhanced heat dissipation and plays an important role in photoprotection. This type of quenching probably is triggered by a conformational change of the orange carotenoid protein (OCP) upon exposure to strong BL (Wilson *et al*., 2008). The impact of strong BL on *G. violaceus* is shown in Fig. 3 (thick upward arrow). First, a small increase of Ft is induced which is followed by a robust gradual decrease of Ft and Fm'. Switching off the actinic light (downward arrow) induces a recovery from the quenched state. When subsequently *weak* BL is switched on (thin upward arrow) a state II to state I transition is induced.

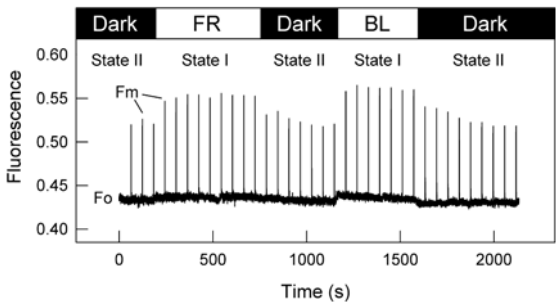

Fig. 2 Effect of FR and weak (11 µmol photons m^{-2} s^{-1}) BL on the chlorophyll fluorescence yield of dark-adapted *G. violaceus*. Saturation pulses were given to probe Fm every 1 min.

Discussion

Photosynthetic organisms have developed several molecular mechanisms to respond to changes in light intensities and/or qualities. State transitions and non-photochemical fluorescence quenching are the two most important balancing/protective short-term processes. *G. violaceus* is capable of both state transitions and non-photochemical fluorescence quenching. Phenomenologically these features are quite similar to those observed in other cyanobacteria: While in darkness *G. violaceus* is in state II (low energy transfer from PBS to PS2), illumination by FR or weak BL induces a transition to state I which is characterized by modified energy distribution between the two photosystems in favor of PS2 (Figs. 1 and 2). The BL-induced fluorescence quenching (Fig. 3) indicates the presence of regulated heat dissipation in this ancient organism. In good accordance with these observations, the genome of *G. violaceus* contains orthologs of cyanobacterial genes which encode proteins thought to play a role in these processes in other cyanobacteria: RpaC in state transitions and OCP in blue-light induced fluorescence quenching.

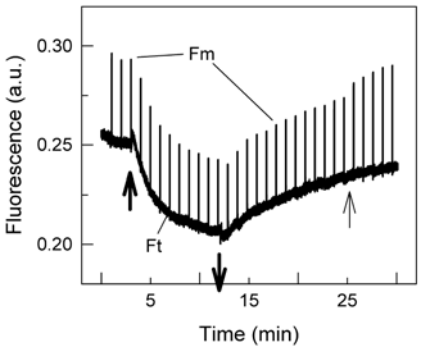

Fig. 3 Effect of strong (thick arrows) and weak BL (thin arrow) on chlorophyll fluorescence yield of *G. violaceus*. Saturation pulses were given to probe Fm every 1 min.

In evolutionary timescale, formation of modern photoautotrophs from two bacterial ancestors coincided with the introduction of water as terminal electron donor of photosynthesis. This transformation was one of the most important events during the history of life on Earth. As no intermediate organisms between anoxygenic and oxygenic photosynthetic bacteria are known, these events are considered to be "discontinuous" (Mimuro *et al*., 2008); however, an increasing number of molecular genetic and bioinformatic data sheds light on cyanobacterial evolution. All current phylogenetic trees of

cyanobacteria (*e.g.* Mimuro *et al*., 2008; Falcón *et al*., 2010) clearly show that the lineage of *G. violaceus* branched off the earliest from other extant cyanobacteria. As *G. violaceus* is capable of state transitions and non-photochemical fluorescence quenching, these mechanisms must be rather old. The branching of *G. violaceus* from other cyanobacteria is dated to approximately 2.7 Ga ago (Falcón *et al*., 2010), shortly after the formation of oxygenic photosynthesis. While at that time the Earth's atmosphere was still anoxygenic, oxygen producing organisms (*i.e.* cyanobacteria) must have already experienced potentially harmful intracellular oxygen levels. This could have meant strong selection pressure to induce the development of protective mechanisms to prevent the formation of reactive singlet oxygen which can be formed by photosynthesis when more light is absorbed by the photosynthetic antennae than can be utilized in CO_2 fixation. In addition, emergence of two photosystems must have entailed a tool to regulate light energy distribution between PS1 and PS2 effectively which also helps to avoid the overreduction of the intersystem electron transport chain and, thus, prevents the formation of singlet oxygen.

In summary, though the morphology and composition of the PBS antenna of *G. violaceus* as well as the membrane architecture of this primordial cyanobacterium is rather atypical, the molecular processes of state transitions and non-photochemical fluorescence quenching are apparently very similar to those in other classes of cyanobacteria.

Acknowledgements

The stimulating discussions with Navassard Karapetyan (Moscow) are much appreciated. This work was supported by BMBF (project Bio-H_2; G.B./M.R.), and DFG (SFB 480, project C1; M.R.).

References

Bryant DA, Cohen-Bazire G, Glazer AN (1981) Characterization of the Biliproteins of Gloeobacter Violaceus. Chromophore Content of a Cyanobacterial Phycoerythrin Carrying Phycourobilin Chromophore. Arch. Microbiol. 129: 190-198

El Bissati K, Delphin E, Murata N, Etienne AL, Kirilovsky D (2000) Photosystem II Fluorescence Quenching in the Cyanobacterium Synechocystis PCC 6803: Involvement of Two Different Mechanisms. Biochim. Biophys. Acta 1457: 229-242

Falcón LI, Magallón S, Castillo A (2010) Dating the Cyanobacterial Ancestor of the Chloroplast. ISME J. 4: 777-783

Kirilovsky D (2010) The Photoactive Orange Carotenoid Protein and Photoprotection in Cyanobacteria. Adv. Exp. Med. Biol. 675: 139-159

Mangels D, Kruip J, Berry S, Rögner M, Boekema EJ, Koenig F (2002) Photosytem I from the Unusual Cyanobacterium Gloeobacter Violaceus. Photosynth. Res. 72: 307-319

Mimuro M, Tomo T, Tsuchiya T (2008) Two Unique Cyanobacteria Lead to Traceable Approach of the First Appearance of Oxygenic Photosynthesis. Photosynth. Res. 97: 167-176

Mimuro M, Yokono M, Akimoto S (2010) Variations in Photosystem I Properties in the Primordial Cyanobacterium Gloeobacter Violaceus PCC 7421. Photochem. Photobiol. 86: 62-69

Mullineaux CW, Emlyn-Jones D (2005) State Transition: an Example of Acclimation to Low-Light Stress. J. Exp. Bot. 56: 389-393

Murata N (1969) Control of Excitation Transfer in Photosynthesis. I. Light-Induced Change of Chlorophyll a Fluorescence in Porphyridium Cruentum. Biochim. Biophys. Acta 172: 242-251

Rippka R, Waterbury J, Cohen-Bazire G (1974) A Cyanobacterium Which Lacks Thylakoids. Arch. Microbiol. 100: 419-436

Schreiber U, Endo T, Mi H, Asada K (1995) Quenching Analysis of Chlorophyll Fluorescence by the Saturation Pulse Method: Particular Aspects Relating to the Study of Eukaryotic Algae and Cyanobacteria. Plant Cell Physiol. 36: 873-882

Wilson A, Punginelli C, Gall A, Bonetti C, Alexandre M, Routaboul JM, Kerfeld CA, van Grondelle R, Robert B, Kennis JTM, Kirilovsky D (2008) A Photoactive Carotenoid Protein Acting as Light Intensity Sensor. Proc. Natl. Acad. Sci. USA 105: 12075-12080

Screening of Novel Subunits of Chloroplastic NAD(P)H Dehydrogenase in Arabidopsis

Noriko Ishikawa[a], Atsushi Takabayashi[a,b], Satoshi Ishida[a], Yasushi Hano[a], Kentaro Ifuku[a], Fumihiko Sato[a] , Tsuyoshi Endo[a, *]

[a] Graduate School of Biostudies, Kyoto University, Japan;
[b] Present address: Institute of Low Temperature Science, Hokkaido University, Japan.
*Corresponding author. Tel. No. +81 075 753 6381; Fax No. +81 075 753 6398; E-mail: tuendo@kais.kyoto-u.ac.jp.

Abstract: Chloroplastic NAD(P)H dehydrogenase is a homolog of respiratory complex I and involved in cyclic electron flow around photosystem I. Recent studies have revealed the difference in subunit constitution between chloroplastic and respiratory complex. Our *in silico* screening of subunits in chloroplastic NDH based on co-expression analysis identified several novel subunits including NDF6 which has a trans-membrane domain and would be specific to terrestrial plants. We discuss the efficiency of combining screening methods of novel subunits in chloroplastic NDH using the co-expression and phylogenic analysis.

Keywords: Co-expression; Cyclic electron flow around photosystem I; NAD(P)H dehydrogenase; Terrestrial plants

Introduction

Chloroplastic NAD(P)H dehydrogenase (NDH) is a homolog of respiratory complex I and involved in cyclic electron flow around photosystem I by transporting electrons from the acceptor side of photosystem I to plastoquinone. Although NDH and respiratory complex I have the common origin and share 11 homologous subunits, recent studies revealed that there are quite a few subunits of cloroplastic NDH which are not found in its respiratory counterpart (Rumeau *et al*., 2005; Majeran *et al*., 2008; Shimizu *et al*., 2008; Sripiö *et al*., 2009a, 2009b; Peng *et al*., 2009). This suggests that chloroplastic NDH has its own subunits which are specialized to photosynthesis and our *in silico* screening method based on co-expression analysis efficiently identified such unique subunits in chloroplastic NDH (Takabayashi *et al*., 2009).

In this report, we review our general strategy to find novel NDH subunits and focus on a subunit, NDF6. Further, the usefulness of combining screening of co-expression and phylogenic analysis is discussed.

Co-expression analysis to screen novel *ndh* genes

Biel *et al*. (2005) reported that Arabidopsis nuclear-encoded genes involved in light reaction are transcribed coordinately. Based on this finding, we examined the co-expression of the known nuclear-encoded *ndh* genes *ndhL*, *ndhN* and *ndhO* (Shimizu *et al*., 2008; Rumeau *et al*., 2005) and screened unidentified nuclear genes of NDH subunits. The degree of co-expression between a pair of genes was estimated based on Pearson's correlation coefficients (*r*) which were calculated by the "gene correlation table version 1" in the *Arabidopsis thaliana* trans-factor and cis-element prediction database (ATTED-II; http://atted.jp/ Ohbayashi *et al*., 2007).

As the results, three known *ndh* genes (*ndhL*, *ndhN* and *ndhO*) revealed to highly co-express each other with quite high *r* values: 0.944 between *ndhL* and *ndhN*, 0.940 between *ndhL* and *ndhO* and 0.901 between *ndhN* and *ndhO* (Takabayashi *et al*., 2009), and 33 candidates which had high *r* values (≥ 0.86) with all of three query *ndh* genes were screened. Among them, 6 genes, *NDF1*, *NDF2*, *NDF4*, *PPL2*, *PQL1* and *PQL2* were identified to encode NDH

subunits with analysis of T-DNA inserted mutants (Takabayashi *et al*., 2009; Ishihara *et al*., 2007; Yabuta *et al*., 2009). Further analysis of Arabidopsis T-DNA inserted mutant of a homologous gene of the novel identified *ndh* gene, *NDF2*, *NDF5* revealed that is essential for NDH activity, although its expression pattern is not so tightly co-related with other nuclear encoded *ndh* genes (Ishida *et al*., 2009).

Identification of NDF6 with improved co-expression analysis

Whereas first screening with co-expression analysis was done by the criterion that all queries, *ndhL*, *ndhN* and *ndhO* should show the high co-expression ($r \geq 0.86$), we re-examined the method to get more *ndh* candidate genes. We calculated the average of Pearson's correlation coefficient (average *r*) with the query genes *ndhL*, *ndhN* and *ndhO* and screened the candidate genes with average *r*. Using this modified screening, we identified *NDF6* which is essential for NDH activity and normal accumulation of NDH complex in Arabidopsis. Vice versa, NDH complex is required for the stable accumulation of NDF6 in Arabidopsis and tobacco. NDF6 is localized in the thylakoid membrane and would be specific to terrestrial plants with a putative trans-membrane domain (Ishikawa *et al*., 2008).

Integral membrane nature of NDF6 was examined in wild-type Arabidopsis thylakoid membrane by washing with either a moderate (2 mol NaBr) or a strong (2 mol KSCN) chaotropic salt. The finding that NDF6 was retained in thylakoid membrane with 2 mol KCN, with which treatment a stromal peripheral membrane protein (NDF1) and a lumenal peripheral membrane protein (PsbQ) were released, indicates the integrated membrane property of NDF6 (Yabuta *et al*., 2010).

Recent proteomics study of the thylakoid membrane of higher plants also showed that NDF6 is a component of NDH-PS I super-complex (Peng *et al*., 2009; Friso *et al*., 2010).

The effect of combining co-expression screening with phylogenic analysis

Besides the co-expression screening we examined another *in silico* screening method using phylogenic analysis (Takabayashi *et al*., 2009). Based on the fact that Chlamydomonas lost *ndh* genes in their genome during the evolution (Rumeau *et al*., 2005), we screened the *ndh* candidate genes which are conserved in cyanobacteria and Arabidopsis but not in Chlamydomonas. Among 34 candidates, 2 genes, *NDF1* and *NDF3* were identified to be essential for chloroplastic NDH. *NDF1* was also identified by co-expression analysis and *NDF3* was independently identified as *CRR*6 which functions in NDH complex assembly (Munshi *et al*., 2006; Peng *et al*., 2010). Less efficiency of the screening of novel *ndh* genes by phylogenic analysis than by co-expression analysis would be due to the fact that many chloroplastic NDH subunits such as NDF6 were acquired after terrestrial photosynthetic organisms emerged.

We analyzed the conservation of 33 candidate genes which were screened by co-expression analysis in Takabayashi *et al*. (2009) in Chlamydomonas. Analysis indicated that 8 genes among the 33 candidates were not found in Chlamydomonas genome and 7 of them were *ndh* genes *NDF1*, *NDF2*, *NDF4*, *PPL2*, *PQL1*, *PQL2* and *NDH18* (Takabayashi *et al*, 2009; Ishihara *et al*., 2007; Yabuta *et al*., 2010; Peng *et al*., 2009). This result indicates that the combination of the two screening methods improved the screening efficiency. However, two genes, *LHCA*6 and *HCEF*1, which were identified by Peng *et al*. (2009) and Livingston *et al*. (2010) to be involved in NDH complex but not the subunits of the complex, were omitted from the candidate list.

These results suggest that our *in silico* based screening analysis would be useful tools for the characterization of novel chloroplastic NDH subunits.

Acknowledgements

We are grateful to the Salk Institute Genomic Analysis Laboratory for providing the sequence-indexed Arabidopsis T-DNA insertion mutants and also the ABRC for providing seeds of the T-DNA insertion mutants. We are grateful to Dr. T Nakagawa of Shimane University and Dr. T Shikanai of Kyoto University for their kind gift of pGWB1 vector and Arabidopsis seeds, (Col-*gl*1 and *crr*2-2), respectively. This work was in-part supported by a grant from the Japan Society for the Promotion of Science Research Fellowship for Young Scientists to N.I.

References

Biel A, Richly E, Noutsos C, Salamini F, Leister D (2005) Analysis of 101 Nuclear Transcriptomes Reveals 23 Distinct Regulons and Relationship to Metabolism, Chromosomal Gene Distribution and Co-Ordination of Nuclear and Plastid Gene Expression. Gene. 344: 33-41

Friso G, Majeran W, Huand M, Sun Q, Wijk KJ (2010) Reconstruction of Metabolic Pathways, Protein Expression and Homeostasis Machinereies Across Maize Bundle Sheath and Mesophyll Chloroplasts; Large Scale Quantitative Proteomics Using the First Maize Genome Assembly. Plant Physiol. 152: 1219-1250

Ishida S, Takabayashi A, Ishikawa N, Hano Y, Endo T, Sato F (2009) A Novel Nuclear-Encoded Protein NDH-Dependent Cyclic Electron Flow 5, Is Essential for the Accumulation of Chloroplast NAD(P)H Dehydrogenase Complexes. Plant Cell Physiol. 50: 383-393

Ishihara S, Takabayashi A, Ido K, Endo T, Ifuku K, Sato F (2007) Distinct Functions for the Two PsbP-Like Proteins PPL1 and PPL2 in the Chloroplast Thylakoid Lumen of Arabidopsis. Plant Physiol. 145: 668-679

Ishikawa N, Takabayashi A, Ishida S, Hano Y, Endo T, Sato F (2008) NDF6: A Thylakoid Protein Specific to Terrestrial Plants Is Essential for Activity of Chloroplastic NAD(P)H Dehydrogenase in Arabidopsis. Plant Cell Physiol. 49: 1066-1073

Livingston AK, Cruz JA, Kohzuma K, Dhingra A, Kramer DM (2010) An Arabidopsis with High Cyclic Electron Flow around Photosystem I (hcef) Involving the NADPH Dehydrogenase Complex. Plant Cell 22: 221-233

Majeran W, Zybailov B, Ytterberg AJ, Dunsmore J, Sun Q, Wijk KJ (2008) Cunsequences of C4 Differentiation for Chloroplast Membrane Proteomes in Maize Mesophyll and Bundle Sheath Cells. Mol. Cell Proteomics 7: 1609-1638

Munshi MK, Kobayashi Y, Shikanai T (2006) Chlororespiratory Reduction 6 Is a Novel Factor Required for Accumulation of the Chloroplast NAD(P)H Dehydrogenase Complex in Arabidopsis. Plant Physiol. 141: 737-744

Ohbayashi T, Kinoshita K, NAkai K, Shibaoka M, Hayashi S, *et al*. (2007) ATTED-II: a Database of Co-Expressed Genes and Cis Elements for Identifying Co-Regulated Gene Groups in Arabidopsis. Nucleic Acids Res. 35D: 864-869

Peng L, Fukao Y, Fujiwara M, Takami T, Shikanai T (2009) Efficient Operation of NAD(P)H Dehydrogenase Requires Wuper Complex Formation with Photosystem I Via Minor LHCI in Arabidopsis. Plant Cell 21: 3623-3640

Peng L, Cai W, Shikanai T (2010) Chloroplast Stromal Protein CRR6 and CRR7 Are Required for Assembly of the NAD(P)H Dehydrogenase Subcomplex A in Arabidopsis. Plant J. 63: 203-211

Rumeau D, Becuwe-Linka N, Beyly A, Louwagie M, Garin J, Peltier G (2005) New Subunits NDH-M, -N, and -O, Encoded by Nuclear Genes, Are Essential for Plastid Ndh Complex Functioning in Higher Plants. Plant Cell 17: 219-232

Shimizu H, Peng L, Myoga F, Motohashi R, Shinozaki K, Shikanai T (2008) CRR23/NdhL Is a Subunit of the Chloroplast NAD(P)H Dehydrogenase Complex in Arabidopsis. Plant Cell Physiol. 49: 835-842

Sripiö S, Allahverdiyeva Y, Holmström M, Khrouchtchova A, Haldrup A, Battchikova N *et al*. (2009a) Novel Nuclear-Encoded Subunits of the Chloroplast NAD(P)H Dehydogenase Complex. J.Biol. Chem. 284: 905-912

Sripiö S, Holmström M, Battchikova N, Aro EM (2009b) AtCYP20-2 Is an Auxiliary Protein of the Chloroplast NAD(P)H Dehydrogenase Complex. FEBS Lett. 583: 2355-2358

Takabayashi A, Ishikawa N, Ohbayashi T, Ishida S, Obokata J, Endo T, Sato F (2009) Three Novel Subunits of Arabidopsis Chloroplastic NAD(P)H Dehydrogenase Identified by Bioinformatics and Reverse Genetic Approach. Plant J. 57: 207-219

Yabuta S, Ifuku K, Takabayashi A, Ishihara S, Ido K, Ishikawa N, *et al*. (2010) Three PsbQ-Like Proteins Are Required Fir the Function of the Chloroplast NAD(P)H Dehydrogenase Complex in Arabidopsis. Plant Cell Physiol. 51: 866-876

Regulatory Systems that Quantitatively Alter Two Anionic Lipids of Chloroplasts in *Chlamydomonas Reinhardtii* upon Sulfur-Starvation

Koichi Sugimoto, Mikio Tsuzuki, Norihiro Sato*

School of Life Sciences, Tokyo University of Pharmacy and Life Sciences.
*Corresponding author. Tel. No. +81 42 676 6716; Fax No. +81 42 676 6721; E-mail: nsato@ls.toyaku.ac.jp.

Abstract: Sulfoquinovosyl diacylglycerol (SQDG) and phosphatidylglycerol (PG) are commonly anionic membrane lipids of chloroplasts. *Chlamydomonas reinhardtii* starved for sulfur (S) degrades SQDG to ensure a sulfur-source, simultaneously elevating the PG content as if to compensate for the loss of SQDG. Similar compensation is observed even under normal growth conditions in a mutant (*hf-2*) of *C. reinhardtii* deficient in SQDG, which shows a higher content of PG than the wild type. We here investigated signaling mechanisms by which these two lipids alter in *C. reinhardtii* during S-starvation, with the use of two mutants (*sac1* and *sac3*) defective in normal responses to ambient S-status, and *hf-2*. Compared with the wild type, both *sac* mutants were largely repressed in the induction of SQDG degradation, indicating involvement of *SAC1* and *SAC3* genes in the induction. On the other hand, the wild type increased the PG synthesis by 3.5-fold after S-starvation of 3 h whereas *hf-2* has already been 2.8-fold higher in the PG synthesis than the wild type under S-replete conditions to maintain the level after the shift to S-sarved conditions. Therefore, in *C. reinhardtii* under S-starved conditions, the loss of SQDG seems to stimulate PG synthesis to up-regulate the PG content.

Keywords: *Chlamydomonas reinhardtii*;Phosphatidylglycerol; Sulfur starvation; Sulfoquinovosyl diacylglycerol; Thylakoid membranes

Introduction

SQDG and PG are found in plastids of plants and their postulated ancestor cyanobacteria, as part of lipid components that mainly construct thylakoid membranes (Sato and Wada, 2009; Shimojima *et al*., 2009). They possess negatively charged polar head groups, shown in several photosynthetic organisms to quantitatively change in opposite directions in response to some environmental stimuli or to some genetic defect in the synthesis of either anionic lipid. Resultantly, the summed contents of these two anionic lipids are maintained at a certain level. This metabolic regulation seems critical for the charge balance of thylakoid membranes, and thus for acclimation of photosynthetic organisms to these stressed conditions (Sato, 2004). Exposure of *Chlamydomonas reinhardtii* cells to S-starvation is one of well-defined ways to induce this kind of regulation: SQDG is almost completely degraded in 24 h after onset of sulfur (S)-starvation to provide a major intracellular S-source for protein synthesis whereas PG is quantitatively increased up to 2-fold the initial level (Sugimoto *et al*., 2007; Sugimoto *et al*., 2008). We here report regulatory systems of *C. reinhardtii* by which degradation of SQDG or elevation in the PG content is induced upon S-starvation, through metabolic characterization of SQDG or PG in mutants defective in signaling pathway for sulfur-availability, or SQDG synthesis.

Materials and Methods

The strains used were *C. reinhardtii* CC125 as the wild type, *hf-2*, an SQDG-deficient mutant that has been backcrossed five times with the wild type (Sato *et al*., 2003), two mutants of *sac1* and *sac3* that are

unable to normally respond to the ambient S-status, and their complemented strains through introduction of the wild-type *SAC1* and *SAC3* genes (Davies *et al*., 1996, 1999). The *sac* mutants and complemented strains were obtained from the *Chlamydomonas* Genetics Center (Duke University, Durham, NC, U.S.A.).

The cells were grown for 2–3 d in TAP medium containing 37 kBq mL^{-1} of [^{35}S]sulfate (55.28 MBq $nmol^{-1}$) for universal labeling of S compounds. After three washings of the cells by centrifugation with a fresh medium, they were shifted to non-radiolabeled TAP or S-free TAP medium for further growth. The cell suspension was centrifuged, and used for extraction of lipids and subsequent separation into individual lipid classes on a thin-layer chromatography (TLC) plate, as Sugimoto *et al*. described (2007). The radioactivity of the sulfolipid was quantified with a BAS imaging analyser (BAS2000; Fuji Film, Tokyo, Japan) on a TLC plate.

Otherwise, the cells were grown in TAP medium, and then were transferred to TAP-S medium. The activity of PG synthesis was estimated by measurement of the incorporation of ^{32}P into PG after incubation of the cells in medium containing 1.11 kBq mL^{-1} of [^{32}P] phosphate (PerkinElmer, equivalent to 1 fmol) for 15, 30, 45, and 60 min. The radioactivity of PG separated on a TLC-plate was measured with a liquid scintillation counter (LSC-6100; ALOKA, Tokyo, Japan).

Results and Discussion

In *C. reinhardtii*, *SAC1* and *SAC3* genes encode regulatory proteins for physiological processes related with the ambient S-status. We first labeled SQDG with ^{35}S in *sac1* and *sac3* mutants and also in their complemented strains by culturing these strains in the presence of [^{35}S]sulfate. The strains were thereafter transferred to [^{32}S]sulfate-replete or S-starved conditions for chasing of the radioactivity of SQDG (Fig. 1). All strains, similar to the WT (data not shown), demonstrated high stability of SQDG when grown under S-replete conditions. The complemented strains rapidly decreased the radioactivity of SQDG after the onset of S-starvation, as was previously reported for the wild type (Sugimoto *et al*., 2007). However, *sac1* and *sac3* mutants were largely repressed in the decrease. These results demonstrated that both *SAC1* and *SAC3* genes are responsible for induction of SQDG degradation under S-starved conditions.

The SAC1 protein, which is a homologue of the Na^+/SO_4^{2-} transporter, would sense the environmental S-deficiency to positively upregulate the levels of expression of a particular set of nuclear genes (Davies *et al*., 1996; Zhang *et al*., 2004). Meanwhile, SAC3, a putative serine/threonine kinase, could either positively or negatively regulate the physiological processes concerning the environmental S-status (Davies *et al*., 1999). SAC1 might be involved in upregulation of the levels of mRNA of genes responsible for SQDG degradation, in view of requirement of transcription for induction of the SQDG degradation in *C. reinhardtii* (Sugimoto *et al*., 2010). SAC3 does not seem to negatively regulate SQDG degradation, since the *sac3* mutant exhibited no more significant activity than the complemented strain under S-replete conditions (data not shown).

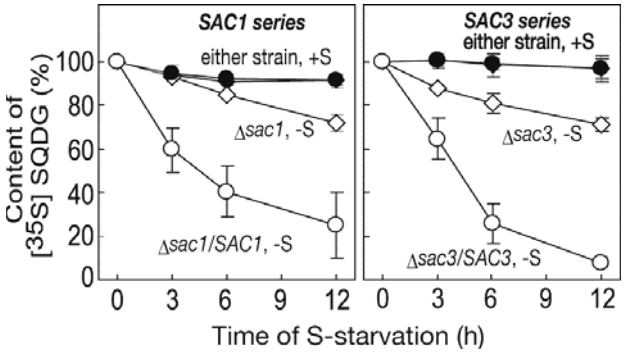

Fig. 1 Effects of *sac1* or *sac3* mutation on induction of SQDG degaradtion in *C. reinhardtii* after onset of S-starvation. Δ*sac1* and *3* indicate *sac1* and *3* mutants, respectively. Δ*sac1/SAC1* and Δ*sac3/SAC3* were strains complemented through introduction of the wild-type genes.

It is noted that neither *sac1* nor *sac3* mutation brought about complete repression in SQDG degradation, but allowed a low level of induction of SQDG degradation (Fig. 1). Some signaling pathway other than that SAC1 participates in may also contribute to induction of the gene expression for SQDG degradation. SAC3 may participate in this pathway. *C. reinhardtii* cells utilize an S-pool originated from SQDG degradation during S-starvation for the synthesis of proteins, which are involved in the proper functioning of photosynthesis and acquisition of external S-source, and thus seem critical for adaptation of the cells to the S-deficient stress (Sugimoto *et al*., 2010). In sum, we identified

both SAC proteins as positive regulators for induction of SQDG degradation, and could provide a basis for elucidation of the molecular mechanism in detail for this induction and therefore of survival strategy of the cells during S-starvation.

As was previously shown by Sugimoto *et al*. (2007), the PG content was elevated by 2-fold during S-starvation of 6 h (Fig. 2, left). We then investigated effects of S-starvation on an incorporation rate of [^{32}P]phosphate into PG in the wild type cells (Fig. 2, right). The results showed that the rate, as compared with the initial rate before the shift, became 3.5-fold higher after S-starvation of 3 h, thereafter kept > 2.2-fold higher for the next 9 h.

Thus, the elevation in the content of PG during S-starvation could be explained by activation of PG synthesis. This active response of *C. reinhardtii* to enhance PG synthesis seems responsible for the PSI complex, since Sugimoto *et al*. (2008) found that thylakoid membranes isolated from S-sarved cells of *C. reinhardtii* where the PG content had increased were lowered in the PSI activity by *in vitro* degradation of PG with phospholipase A_2. PG may be associated with the PSI complex for its proper conformation and functioning. In cyanobacterium, *Synechocystis* sp. PCC 6803, PG was shown to contribute to the structural integrity of the PSI complex (Sato *et al*., 2000). We then investigated effects of SQDG-deficient mutation on synthetic activity of PG under S-replete and -starved conditions (Fig. 2, right). An SQDG-deficient mutant, *hf-2*, showed a two-fold higher level of PG than the wild type under S-replete conditions (Sato *et al*., 1994). In accordance with the observation, the activity of PG synthesis in *hf-2* was 2.8-fold higher than in the wild type before onset of S-starvation whereas that stayed at the enhanced level during S-starvation for 12 h. We could thus attribute the higher content of PG in *hf-2* to its instinctively activated synthesis of PG. In *C. reinhardtii*, the up-regulation of synthetic activity of PG might take place directly by sensing of the decrease in SQDG content.

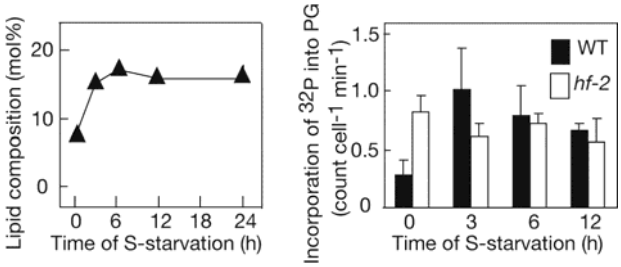

Fig. 2 Effects of S-starvation on the content and synthesis of PG in *C. reinhardtii*. Left, PG content in the wild type; right, PG synthesis in the wild type and *hf-2*.

In conclusion, SQDG degradation seems to be regulated by the signaling pathway for ambient S-status that involves *SAC1* and *SAC3* whereas the concomitant increase in PG synthesis would be triggered by the loss of SQDG that results from S-starvation (Fig. 3).

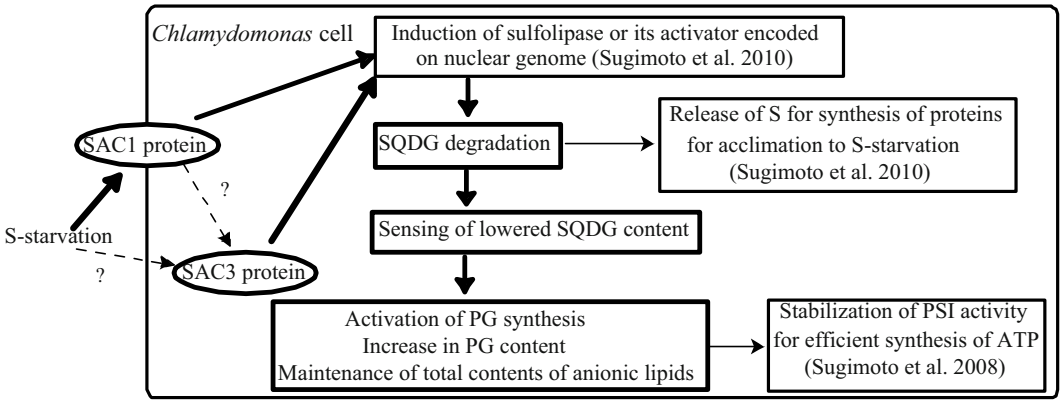

Fig. 3 Schematic diagram of mechanisms by which contents of anionic lipids change in *C. reinhardtii* cells starved for S.

Acknowledgements

This work was supported in part by Grants-in-Aid from the Ministry of Education, Culture, Sports, Science, and Technology of Japan (MEXT), the Promotion and Mutual Aid Corporation for Private Schools of Japan, Scientific Research for Plant Graduate Students from the Nara Institute of Science and Technology supported by MEXT, and a Sasakawa Scientific Research Grant from the Japan Science Society.

References

Davies JP, Yildiz FH, Grossman AR (1996) Sac1, a Putative Regulator that Is Critical for Survival of Chlamydomonas Reinhardtii during Sulfur Deprivation. The EMBO Journal 15: 2150-2159

Davies JP, Yildiz FH, Grossman AR (1999) Sac3, an Snf1-Like Serine/Threonine Kinase that Positively and Negatively Regulates the Responses of Chlamydomonas to Sulfur Limitation. Plant Cell 11: 1179-1190

Sato N, Tsuzuki M, Matsuda Y, Ehara T, Osafune T, Kawaguchi A (1994) Isolation and Characterization of Mutants Affected in Lipid Metabolism of Chlamydomonas Reinhardtii. Eur. J. Biochem. 230: 987-993

Sato N, Hagio M, Wada H, Tsuzuk M (2000) Requirement of Phosphatidylglycerol for Photosynthetic Function in Thylakoid Membranes. Proc. Nat. Acad. Sci. USA 97: 10655-10660

Sato N (2004) Roles of the Acidic Lipids Sulfoquinovosyl Diacylglycerol and Phosphatidylglycerol in Photosynthesis: Their Specificity and Evolution. J. Plant Res. 117: 495-505

Sato N, Aoki M, Maru Y, Sonoike K, Minoda A, Tsuzuki M (2003) Involvement of Sulfoquinovosyl Diacylglycerol in the Structural Integrity and Heat-Tolerance of Photosystem II. Planta 217: 245-251

Sato N, Wada H (2009) Lipid Biosynthesis and Its Regulation in Cyanobacteria. In: Wada H, Murata N (eds.), Lipids in Photosynthesis: Essential and Regulatory Functions. Springer, pp. 157-177

Shimojima M, Ohta H, Nakamura Y (2009) Biosynthesis and Function of Chloroplast Lipids. In: Wada H, Murata N (eds.), Lipids in Photosynthesis: Essential and Regulatory Functions. Springer, pp. 35-55

Sugimoto K, Midorikawa T, Tsuzuki M, Sato N (2008) Upregulation of PG Synthesis on Sulfur-Starvation for PS I in Chlamydomonas. Biochem. Biophys. Res. Commun. 369: 660-665

Sugimoto K, Tsuzuki M, Sato N (2009) Utilization of a Chloroplast Membrane Sulfolipid as a Major Internal Sulfur Source for Protein Synthesis in the Early Phase of Sulfur Starvation in Chlamydomonas Reinhardtii. FEBS Lett. 581: 4519-4522

Sugimoto K, Tsuzuki M, Sato N (2010) Regulation of Synthesis and Degradation of a Sulfolipid under Sulfur-Starved Conditions and Its Physiological Significance in Chlamydomonas Reinhardtii. New Phytol. 185: 676-686

Zhang Z, Shrager J, Jain M, Chang CW, Vallon O, Grossman AR (2004) Insights into the Survival of Chlamydomonas Reinhardtii during Sulfur Starvation Based on Microarray Analysis of Gene Expression. Eukaryotic Cell 3: 1331-1348

Do State Transitions Control CEF1 in Higher Plants?

Deserah D Strand[a,b], Aaron K Livingston[b], David M Kramer[a,b,*]

[a]Plant Research Laboratory and Department of Plant Biology, Michigan State University, East Lansing, MI and
[b]Institute of Biological Chemistry, Washington State University, Pullman, WA.
[*]Corresponding author. Tel. No. +01 517 4320072 ; E-mail: kramerd8@msu.edu.

Abstract: Cyclic electron flow around photosystem I (CEF1) in oxygenic photosynthesis is thought to augment the production of ATP/NADPH to balance the chloroplast energy budget. In the green alga *Chlamydomonas,* CEF1 has been shown to be regulated by the so-called state transitions, which involve reversible phosphorylation of antenna and other complexes in response to changes in plastoquinone redox state (Allen, 1981). Whether this regulatory system operates in C_3 plants, which have much less robust state transitions, have been unclear. Moreover, recent works by Iwai *et al*. (2010) and Livingston *et al*. (2010) suggest that CEF1 in *Chlamydomonas* and *Arabidopsis* may operate through different pathways, with the later involving the NDH complex. In this work, we test for the involvement of state transitions in CEF1 using a newly isolated mutant, *hcef2*, with constitutively high CEF1. We find that the high CEF1 mutant is predominantly in state II. We also find that the mutants *stn7* and *tap38*, locked in state I and state II (Bellafiore *et al*., 2004; Pribil *et al*., 2010), respectively, show elevated CEF1. This indicates STN7 is not necessary for activation of CEF1. We suggest a role of CEF1 as a compensatory mechanism to balance the redox state of the chloroplast when the state transition response is impaired.

Keywords: *Arabidopsis thaliana*; CEF1; Regulation; State transitions

Introduction

Plants must maintain a fine balance of the photosynthetic machinery in order to maximize efficiency and minimize photoinhibition and the generation of destructive reactive oxygen species. In order to do this they utilize several mechanisms, including state transitions and cyclic electron flow around photosystem I (CEF1). State transitions are a way to balance the excitation of photosystem II (PSII) and photosystem I (PSI). Under normal condition the PSII antenna is in state I where it is associated with PSII and linear electron flow is operating (Depège *et al*., 2003). Under conditions where PSII is preferentially excited LHCII may be reversibly phosphorylated in response to the redox state of the plastoquinone pool (Allen *et al*., 1981). This phosphorylation signals a transition to state II, where LHCII associates with PSI (Bellafiore *et al*., 2004). In addition to balancing excitation of the two photosystems, the transition to state II is also thought to be signal induction of CEF1 due to strong correlation of the two processes in algal systems (Finazzi *et al*., 2002; Iwai *et al*., 2010). CEF1 is thought to operate to balance the chloroplast energy budget by providing additional light-driven proton translocation into the lumen and therefore additional ATP to augment the ATP deficit of linear electron flow (reviewed in Kramer *et al*., 2003). The relationship between CEF1 and state transitions are well documented in algal systems, but still not clearly understood in C_3 plants due to the low level of both in higher plants.

In order to delineate the relationship of these processes in C_3 plants we used a recently characterized *Arabidopsis* mutant displaying high CEF1), *hcef2* (Livingston *et al.*, in preparation), as well as two Arabidopsis mutants *stn7* and *tap38*, which are locked in state I and state II respectively (Bellafiore *et al*., 2004; Pribil *et al*., 2010). The use of these mutants allows us to probe whether CEF1 and state transitions correlate as strongly in C_3 plants as they do in algae. We are able to answer several questions: (1) Does the activation of CEF1 correlate

with accumulation of the transition to state II? (2) Does the accumulation of state II induce CEF1 as seen in algae, or alternatively, is it possible this is an independent process?

Materials and Methods

Plant material and growth conditions

T-DNA insertion lines *stn7* (SALK 073254) and *tap38* (SAIL 514 C03) were obtained from ABRC (Alonso *et al*., 2003; Sessions *et al*., 2002). Lines were genotyped via PCR with insertion specific primers. The *hcef2* line was isolated as described in Livingston *et al*. (2010a). Plants were grown at 80uE light at a 16:8 light:dark photoperiod. Wildtype and T-DNA insertion lines were fully mature at 3 weeks. Mutant *hcef2* lines reached wildtype size at 7 weeks.

In vivo spectroscopic assays

Fully mature leaves were placed in the leaf chamber of an in-house constructed non-focusing optics spectrophotometer (Sacksteder and Kramer, 2000) modified to allow continually flowing humidified air. Both actinic light and saturation pulses were supplied by 3 red (635 nm) light emitting diodes (LEDs, Philips LumiLed) and measuring pulses were supplied by LEDs in the green region for both the fluorescence measurements and ECS, with the latter filtered at to allow specifically 520 nm to pass through (BG18; Schott). Fluorescence was detected by a photodiode protected by at filter at 730 nm to remove interference from the actinic and measuring light (RG9; Schott). The signal was captured and converted electronically (Kramer and Crofts, 1996).

After 10 min linear electron flow values were calculated from the quantum efficiency of photosystem II (**Φ**) calculated from steady state fluorescence and maximal fluorescence in the steady state during a saturation flash (Baker *et al*., 2008).

Proton flux (v_H^+) was calculated as α to the initial slope of the decay during a 300 ms dark interval in the steady state. This dark interval relaxation kinetics (DIRK) change in absorbance at 520 nm associated with the electrochromic shift (Sacksteder and Kramer, 2000).

77 K fluorescence

77 K fluorescence measurements on intact leaf tissue were performed as described in Weiss (1985). Samples were excited at 475 nm and the emission was recorded from 600–800 nm on a commercially available fluorimeter and liquid nitrogen dewer assembly (Horiba Jobin Yvon). Results are averages of 10 measurements and performed in triplicate. Emission spectra were normalized to the 685 nm peak for comparison.

Results

This lab has previously described two mutants with constitutively high levels of CEF1, one in *Arabidopsis*, *hcef1* (Livingston *et al*., 2010a) and one in tobacco GAPR (Livingston *et al*., 2010b). For this experiment we used another high CEF1 mutant isolated in this lab, *hcef2*, an *Arabidopsis* mutant constitutively high CEF1 (Livingston *et al*., in preparation).

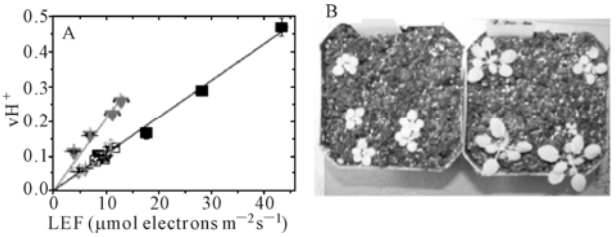

Fig. 1 (A) The *hcef2* mutant has high CEF1. LEF vs. v_H+ in the wild type (closed squares) and *hcef2* (closed triangles) and methyl viologen controls (open squares and triangles). (B) The hcef2 mutant is light sensitive. *hcef2* (left) and wildtype (right) ~ 3 weeks old. *hcef2* is slow growing and light sensitive in comparison to the wildtype.

The *hcef2* mutant is slow growing and light sensitive in comparison to the wildtype but robust compared to *hcef1*. Due to the high level of CEF1 this mutant accumulates, it was a good choice to probe the relationship between CEF1 and state transitions. We also looked at two other mutants, *stn7*, which is locked in state I, and a recently published mutant *tap38*, which is unable to make the transition back to state I, and therefore accumulates state II.

Fig. 1 shows the 77 K emission spectrum from plants grown under our growth conditions. The wildtype antennae system, in black, is shifted to state II in comparison to *stn7* in red which remains in state I. In green, *tap38* is shifted to state II at a level comparable to the wildtype. The extent of this shift agrees with the extent of state II accumulation as

described for this mutant. The high CEF1 mutant, *hcef2*, in blue, is strongly shifted to state II.

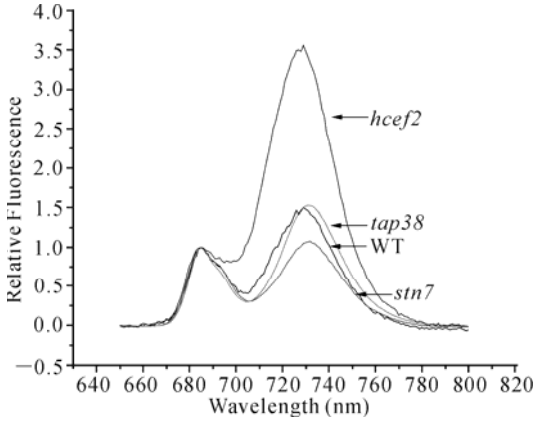

Fig. 2 The antenna system in the *hcef2* mutant is strongly shifted to state 2. The *stn7* and *tap38* mutants appear shifted into states 1 and 2, respectively.

Since CEF1 increases proton translocation into the lumen above that produced via LEF, an increase in the slope of v_H+ in the steady state vs. LEF, plotted in comparison with the wildtype, can be attributed to an increase in CEF1 over wildtype levels. Fig. 3 shows the large increase in CEF1 in *hcef2* in blue, as expected in this mutant. There is also a significant increase in CEF1 in both *tap38*, which is in state II, and *stn7*, which is in state I.

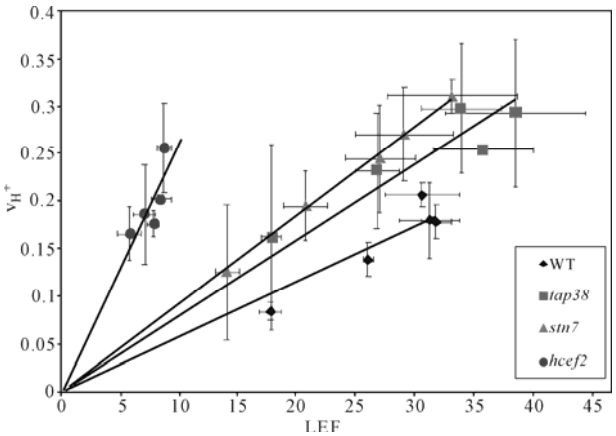

Fig. 3 CEF1 is strongly elevated in *hcef2* but surprisingly; it is also increased in *stn7* and *tap38*. This indicates that state 2 does not correlate with CEF1 activation.

Discussion

In some cases, such as *hcef2*, but not all, such as *tap38* vs. *stn7*, CEF1 is correlated with STN7 activity and state transitions. Therefore, STN7 does not appear to be sufficient for CEF1 activation. Additionally, knocking out either STN7 or TAP38 appears to *increase* CEF1, at least based on the v_H+ measurements. These results suggest that, in contrast to algal systems, the higher plant chloroplast can activate CEF1 in both state I and state II. We propose that in C_3 plants, the loss of one balancing mechanism can be compensated by modulation of others. This modulation may be in response to the redox state of the chloroplast. This would be in agreement with findings indicating activation of the NDH complex in response to reactive oxygen species (Casano *et al*., 2001)

Both high levels of CEF1 and a strong shift of the antenna complex to state II are seen in *hcef2*. We propose this mutation imposes a requirement for strong downregulation of PSII. Alternatively, the large quenching of PSII in this mutant (data not shown) could directly decrease the 685 nm peak in the 77 K spectra and therefore may reflect photoinhibition rather than state transitions. Further investigation is required to clarify these findings.

Acknowledgements

The authors thank Heather Enlow, Amelia Barhanovich, Dr. Helmut Kirchhoff, Stefanie Tietz, and Dr. Jeff Cruz for helpful discussions. This work was supported by Division of Chemical Sciences, Geosciences and Biosciences, Office of Basic Energy Sciences of the U.S. Department of Energy, grant DE-FG02-04ERI5559.

References

Allen, JF, Bennett J, Steinback KE, Arntzen CJ (1981) Chloroplast Protein Phosphorylation Couples Plastoquinone Redox State to Distribution of Excitation Energy between Photosystems. Nature 291: 25-29

Alonso JM, Stepanova AN, Leisse TJ, Kim CJ, Chen H, Shinn P, Stevenson DK, Zimmerman J, Barajas P, Cheuk R, Gadrinab C, Heller C, Jeske A, Koesema E, Meyers CC, Parker H, Prednis L, Ansari Y, Choy N, Deen H, Geralt M, Hazari N, Hom E, Karnes M, Mulholland C, Ndubaku R, Schmidt I, Guzman P, Aguilar-Henonin L, Schmid M, Weigel D, Carter DE, Marchand T,

Risseeuw E, Brogden D, Zeko A, Crosby WL, Berry CC, Ecker JR (2003) Genome-Wide Insertional Mutagenesis of Arabidopsis Thaliana. Science 301: 653-657

Avenson TJ, Kanazawa A, Cruz JA, Takizawa K, Ettinger WE, Kramer DM (2005) Integrating the Proton Circuit into Photosynthesis: Progress and Challenges. Plant, Cell & Environment 28: 97-109

Baker NR (2008) Chlorophyll Fluorescence: a Probe of Photosynthesis in Vivo. Annu. Rev. Plant Biol. 59: 89-113

Bellafiore S, Barnech F, Peltier G, Rochaix JD (2005) State Transitions and Light Adaptation Require Chloroplast Thylakoid Protein Kinase STN7. Nature 433: 892-895

Casano LM, Martin M, Sabater B (2001) Hydrogen Peroxide Mediated the Induction of Chloroplastic NDH Complex under Photooxidative Stress in Bareley. Plant Physiol 125: 1450-1458

Depege N, Bellafiore S, Rochaix JS (2003) Role of Chloroplast Protein Kinase Stt7 in LHCII Phosphorylation and State Transition in Chlamydomonas. Science 299: 1572-1575

Finazzi G, Rappaport F, Furia A, Fleischmann M, Rochaix JD, Zito F, Forti G (2002) Involvement of State Transitions in the Switch between Linear and Cyclic Electron Flow in Chlamydomonas Reinhardtii. EMBO Reports 3: 280-285

Iwai M, Takizawa K, Tokutsu R, Okamuro A, Takahashi Y, Minagawa J (2010) Isolation of the Elusive Supercomplex that Drives Cyclic Electron Flow in Photosynthesis. Nature 464: 1210-1213

Kramer DM, Cruz JA, Kanazawa A (2003) Balencing the Central Roles of the Thylakoid Proton Gradient. Trends in plant Science 8: 27-32

Kramer DM, Krofts AR (1996) Control of Photosynthesis and Measurement of Photosynthetic Reactions in Intact Plants. In: Baker N (ed.), Photosynthesis and the Environment Advances in Photosyntheis. Kluwer Academic Press: Dordrecht, the Netherlands, pp. 25-66

Livingston AK, Cruz, JA, Kohzuma K, Dhingra A, Kramer DM (2010) An Arabidopsis Mutant with High Cyclic Electron Flow around Photosystem I (hcef) Involving the NADPH Dehydrogenase Complex. Plant Cell 22: 221-233

Livingston AK, Kanazawa A, Cruz JA, Kramer DM (2010) Regulation of Cyclic Electron Flow in C_3 Plants: Differential Effects of Limiting Photosynthesis at Ribulose-1, 5-Bisphosphate Carboxylase/Oxygenase and Glyceraldehyde-3-Phosphate Dehydrogenase. Plant, Cell & Environment 33: 1779-1788

Pribil M, Oesaresi P, Hertle A, Barbato R, Leister D (2010) Role of Plastid Protein Phosphatase TAP38 in LHCII Dephosphorylation and Thylakoid Electron Flow. PLoS Biol 8(1): e1000288. doi:10.1371/journal.pbio.1000288

Sacksteder CA, Kramer DM (2000) Dark Interval Relaxation Kinetics of Absorbance Changes as a Quantitative Probe of Steady-State Electron Transfer. Photosynth. Res 66: 145-158

Sessions A, Burke E, Presting G, Aux G, McElver J, Patton D, Dietrich B, Ho P, Bacwaden J, Ko C, Clarke JD, Cotton D, Bullis D, Snell J, Miguel T, Hutchinson D, Kimmerly B, Mitzel T, Katagiri F, Glazebrook J, Law M, Goff SA (2002) A High-Throughput Arabidopsis Reverse Genetics System. Plant Cell 14: 2985-2994

Weiss E (1985) Chlorophyll Fluorescence at 77 K in Intact Leaves: Characterization of a Technique to Eliminate Artifacts Related to Self-Absorption. Photosynthesis Research 6: 73-86

Study on Post-Steady-State Chlorophyll a Fluorescence Kinetics of Plants

Chuanfei Zhong[a], Xiaoying Wu[b], Zhikui Gao[c], Yuntao Zhang[a], Guixia Wang[a], Jing Dong[a], Lina Wang[a], Linlin Chang[a], Rongfu Gao[d]*

[a]Institute of Forestry and Pomology, Beijing Academy of Agriculture and Forestry Sciences;
[b]Institute of Zoology, Chinese Academy of Sciences;
[c]College of Horticulture of Hebei Agriculture University;
[d]College of Biology Science and Technology of Beijing Forestry University.
*Corresponding author. Tel. No. +8610 6233 8647; Fax No. +8610 8259 8882; E-mail: gaorf@bjfu.edu.cn.

Abstract: The study uses Fo' model of PAM 2100 to measure the Chlorophyll a Fluorescence Kinetics of O'-P'-F-C-S multi-stage change in plants leaves under steady state of photosynthesis which is induced through alternation of far-red light, darkness, and actinic light. We call it "Post-Steady-State Chlorophyll a Fluorescence Kinetics" (PSF). The results have demonstrated that the above process has gradually evolved into the steady-state with the light induction process moving on. It is closely related with the redox state of the photosynthetic electron chain and the activation of the carbon assimilation. At the same time, this method has provided an effective means of research into the electronic transfer of photosynthesis and the dynamic change process of the carbon assimilation when the stomata of the CAM plants closes in light.

Keywords: Post-Steady-State Chlorophyll a Fluoresce; PS II-PS I-Carbon Assimilation; Far Red Light

Introduction

In the two books Papageargiou and Govindjee (edi, 2004) and DeEll and Toivonen (edi, 2003), the authors have summarized the research advances in the theory and practice of the Chlorophyll a Fluorescence Kinetics. In the modulated saturated pulse and OJIP research, they have brought out relative theories which facilitate the fast development of applicable research. Before, the Chlorophyll Fluorescence Kinetics mainly focused on the kinetics process which featured that the leaf dark adaptation had reached steady-state fluorescence under light induction. Relevant parameters can be calculated without paying too much attention to the development in the Chlorophyll a Fluorescence Kinetics under the steady-state carbon assimilation and the possible change in the electron transporter during this process(Schreiber, 1986). Because PAM 2100 had added far-red light and darkness between every two pulses, under 730 nm far-red light, Photosystem I (PS I) could be oxidized under the steady-state. Photosystem II (PS II) was temporarily suspended when the actinic light was turned off. Under the far-red light, the redox state of the photosynthetic electron transport chain had changed. When the actinic light was re-activated, the induction process of the Fluorescence Kinetics was initiated again and reached the steady-state.

When we look at the Fluorescence Induction Curve (FI) with or without far-red light, you can get the value of Fo' without any change in other parameters. If the time coordinate on the horizontal axis can be enlarged, another fluorescence kinetics process could be observed between every two saturated pulses. The above process can repeat itself if other conditions remain the same. However, the FI will change when we change the light conditions. Therefore, we can explore the inter-relationships between the steady-state electron transport between PS II and PS I and the change in Fluorescence Kinetics. We can then explore even further the relationships between the change in steady-state Fluorescence Kinetics and the carbon assimilation.

Materials and Methods

Peas and Jonquil, cultured by the cold light source (Dysprosium Lamp), the light intensity is 100 μmol proton m^{-2} s^{-1}, the light and dark cycle is 10/14 h, selecting the mature leaves for experiment. After a whole night of darkness, the Jonquil was treated by lighting from 0 h to 8 h, light intensity 600 μmol proton m^{-2} s^{-1}, using water insulation, the temperature of the leaves is controlled at 25 °C.

Fo' Saturated Pulse model: Using PAM 2100 (Walz, German)'s Fo' Saturated Pulse model to identify the FI. As in Fig. 1, during the testing process, there are 5 types of light sources which illuminate the plant alternatively: ML, AL, SP, FrL and Darkness. (ML: Measuring Light, Red LED, 650 nm, 0.1 μmol m^{-2} s^{-1}; AL: Actinic Light, Red LED, 665 nm, 149 μmol s^{-1} m^{-2}; SP: Saturated Pulse Light, halogen, white light, 8,000 μmol s^{-1} m^{-2}; FrL: Far-red Light, LED, 730 nm, 10.201 W m^{-2}). Among them, ML has been on from the beginning to stimulate the fluorescence. After we measure and test Fo and Fm, AL (31 s) and SP (0.8 s, before AL finishes 1 s is opened)—FrL (4 s)-Darkness (5 s) form a Saturated Pulse Induction Cycle. During a series of induction cycles, the plant was induced to the light steady-state. The whole process lasted 540 s. When identifying the FI, we can get the results of a series of fluorescence parameters of Saturated Pulse model (Schreiber U, 1986, 1995). The sampling frequency has increased to 20 ms/point.

Besides, we have used Daul-PAM 100 (Walz, German)'s Fo' Saturated Pulse model, the light induction process is similar to PAM 2100. The difference is that Daul-PAM 100 has an extra function of testing the redox state of P700 and it's sampling frequency has increased to 2 ms/point.

Results and Discussion

Comparisons between Classical and Fo' Saturated Pulse (SP) models

In Fig. 1, you can see the difference between "with far-red light" and "without far-red light": Fig. 1B show that after FI reaches gradually the light steady-state, each time the change in the FI curve of each induction cycle is almost identical, indicating that the steady-state plant can be converted between several fixed state of dynamic equilibrium after the alternation of AL, SL, Far-red Light and darkness. And when a single cycle of amplification, we found that after "far-red light and darkness", and then turn on the actinic light to form a multi-stage induction process from Fo' to Fs. We call this process PSF.

Obviously, this process (PSF) is closely related with the redox state of the photosynthetic electron chain, the re-oxidation of the far-red light, the de-activation of the enzymes due to the turn-off of the actinic light and the later re-activation. In order to identify this multi-stage process in a better way, we have converted the abscissa into logarithmic coordinates and put all the PSF together in each induction cycle from the dark adaptation to the light steady-state process (Fig. 2). We can see that under

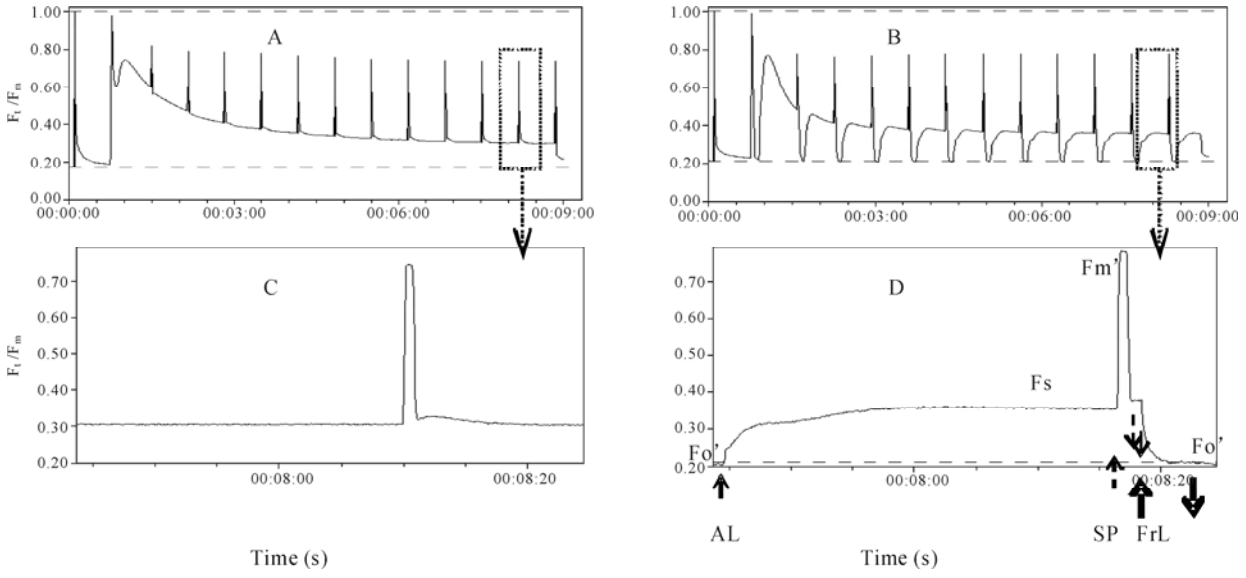

Fig. 1 Classical and Fo' Pulse-Amplitude-Modulated FI.

the light steady-state (463–494 s), PSF includes Fo' (named O'), the inflection point between 0 and 0.1 s (named p'), the crest between 0.1 and 3 s (named F), the crest after 3 s (named C) and the Steady-State Fs (referred to as S). The reason to name the above process O'P'FCS is that our later research has shown the change in PSⅡ, FNR and enzyme of CO_2 assimilation attributes to the change in the above multi-stage process.

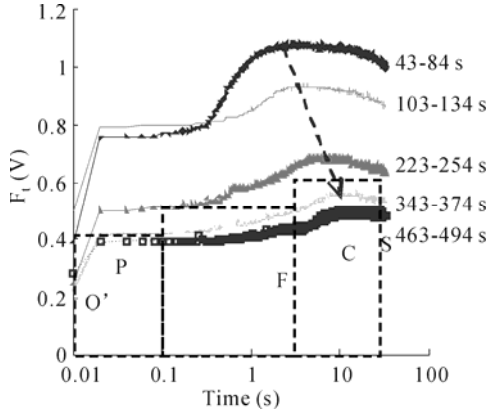

Fig. 2 Induction of steady state fluorescence kinetic curve.

The FI without the far-red light does not have the multi-stage rising process from Fo' to Fs (Fig. 1C). However, the two types of FI curve with and without the far-red light do not have significant difference in the Chlorophyll a Fluorescence intensity at Fo, Fm, Fs and Fm'. Therefore, the FI curve with the far-red light does not affect the calculation of all the regular Chlorophyll a Fluorescence parameters.

In Fig. 2, with the light induction process moving on, (during the induction process of PSF), the Chlorophyll a Fluorescence intensity was diminishing in every induction cycle and reached the steady-state at 300s. This is the result of the re-activation of different types of enzymes during the Calvin cycle (Govindjee, 1995). The steady-state multi-stage change in the light induction process of PSF is a gradual process. At the initial stage of PSF, F and C were overlapping with each other. The chlorophyll a fluorescence was rising very fast from O' to P' (0–0.1 s). Then, the FI curve was rising dramatically again, formed another inflection point and reached its peak of PSF value (3–10 s). At this stage, there was no clear dividing line between F and C. With the light induction process moving on, the rate of slope was gradually declining (0.1–3 s), the time when the peak value appeared was gradually delayed.

When the duration of the induction process reached about 223 s, the dip between F and C was beginning to appear. That is the O'P'FCS multi-stage process. When the light induction process reached 300 s, the light intensity of different peaks of O'P'FCS and the time of happening reached a steady-state which was the typical PSF.

After the plant was light induced to the steady-state, proton gradient, the change in state, stomatal conditions were relatively stable, while PS II- PS I-carbon assimilation reached dynamic equilibrium. This equilibrium depended on the lighting conditions, CO_2 supply and other factors (water supply, temperature, etc). Therefore, the cyclical alternation of the far-red light and the actinic light under the light steady-state can bring about change in the dynamic equilibrium between PS II-PS I-carbon assimilation: the turn-off of the actinic light and the turn-on of the far-red light can make the electron transporter under the redox state become re-oxidized, eventually Q_A was oxidized and the carbon assimilation was temporarily stopped. The turn-on of the actinic light again would start the redox reaction of the electron transporter between PS II and PS I and the re-activation of the carbon assimilation.

Because of the time differences in the rates of change between electron transporter and carbon assimilation to the photosynthetic reactions, the Fluorescence level has increased in multi-stages from Fo' to Fs. With this approach, we can explore the dynamic change process in the photosynthetic electron transport and carbon assimilation. It can also be used to study the process of stomatal closure of photosynthesis, such as CAM plants.

CAM plant Photosynthesis research

During the regular lighting conditions, the stomata of the CAM plant will be closed. Therefore, it is extremely difficult to conduct the photosynthetic mechanism research. So far, we have not been able to test live how long the CO_2 the CAM plant absorbed during the night can sustain the photosynthetic process during the day. Neither can we test the dynamic change of PS II-PS I-carbon assimilation during the above process. Although the air exchange mechanism is widely used in the plant photosynthetic rate research, it cannot do anything with the CAM plant with stomatal closure during the regular light. The Chlorophyll a Fluorescence Kinetics of plants is the only research method to monitor live CAM plants photosynthesis at the present time. (Rosenqvist and

Kooten, 2003) The traditional Chlorophyll a Fluorescence Kinetics research has to go through dark adaptation. After dark adaptation, the stomata will open up again to absorb CO_2, to what extent will the stomata open up? How much CO_2 will the stomata absorb? It's also unknown. Therefore, this approach is still unable to disclose the real photosynthetic state. The steady-state Chlorophyll a Fluorescence Kinetics theoretical study doesn't need dark adaptation, and can also indicate the dynamic change of PS II-PS I-carbon assimilation under the light adaptation of the plant.

Fig. 3 shows that at the initial stage of illumination, the bioactive activity of CAM plant (jonquil)'s steady-state chlorophyll a fluorescence kinetics is very high, especially around 1 s ,the amplitude of rise and fall of PSF curve is huge, indicating that CO_2 concentration in the chloroplast is very high, the carbon assimilation rate is relatively high.

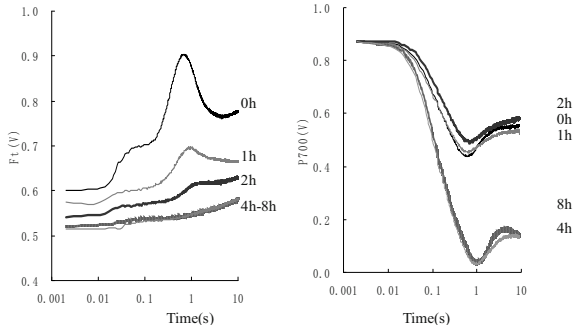

Fig. 3 PSFs and steady-state P700 of CAM plant (jonquil) leaves as illuminating.

With the illumination process moving on, the amplitude of PSF is diminishing, showing that CO_2 is being gradually consumed. After 4 hours of illumination, the steady-state multi-stage change has almost disappeared, showing that CO_2 concentration in the chloroplast is very low. The simultaneous testing results of the P700 Redox Kinetics show that the possibility of the P700 Redox has dramatically increased. It can be concluded that it is caused by the great reduction in the terminal electron receptor NADP + provided to PS I through carbon assimilation; 1 s after AL was opened, the re-oxidation increased gradually, indicating the circular electron transport, Mehlar Reaction and other non-linear electron transport rate increased.

After 8 h of illumination, the Redox rate of PSF and P700 were equivalent to that after 4 h of illumination, indicating further the CO_2 CAM plants (jonquil) absorbed during the night was consumed within a maximum of 4 h, and then entered the low CO_2 photosynthesis. After 8 h of illumination, P700's re-oxidation increased even further 1 s after AL was opened. Then, the second Redox reaction occurred after re-oxidation, indicating the further consumption of CO_2 which caused non-linear electron transport rate to increase again.

In summary, post-steady-state Fluorescence Kinetics theory provides a research methodology to explore the steady-state PS II- PS I electron transport kinetics and carbon assimilation dynamic cycle of Plants, especially provides an effective means to the photosynthetic mechanism research under the state of stomatal closure.

Acknowledgements

National Science and Technology Pillar Program (No. 2009BADB8B04-5).

References

Papageorgiou GC, Govindjee (2004) Chlorophyll a Fluorescence: a Signature of Photosynthesis. Springer: Dordrecht, pp. 819

DeEll JR, Toivonen PMA (2003) Practical Applications of Chlorophyll Fluorescence in Plant Biology[M]. Kluwer Academic Publishers

Rosenqvist E, Kooten O (2003) Chlorphyll Fluorescence: a General Description and Nomenclature. In Practical Applications of Chlorophyll Fluorescence in Plant Biology. Kluwer Academic Publishers: Dordrecht, The Netherlands, pp. 31-77

Schreiber U (1986) Detection of Rapid Induction Kinetics with a New Type of High-Frequency Modulated Chlo-Rophyll Fluorometer. Photosynth Res 9: 261-272

Govindjee (1995) Sixty-Three Years Since Kautsky: Chlorophyll a Fluorescence. Aust. J. Plant Physiol 22: 131-160

The Ancient Cyanobacterium *Gloeobacter Violaceus* PCC 7421 is Capable of State Transitions and Blue-Light Induced Fluorescence Quenching

Gábor Bernát[a,*], Ulrich Schreiber[b], Igor N Stadnichuk[c], Matthias Rögner[a], Friederike Koenig[d]

[a]Plant Biochemistry, Ruhr-University Bochum, D-44801 Bochum, Germany;
[b]University of Würzburg, Julius-von-Sachs-Institute for Biosciences, D-97070 Würzburg, Germany;
[c]A. N. Bakh Institute of Biochemitry, Russian Academy of Sciences, 119071 Moscow, Russia;
[d]Molecular Plant Physiology, University of Bremen, D-28359 Bremen, Germany.
[*]Corresponding author. Tel. No. +49 234 3225814; Fax No. +49 234 3214322; E-mail: gabor.bernat@rub.de

Abstract: The atypical unicellular cyanobacterium *Gloeobacter violaceus* PCC 7421, diverged very early during the evolution of cyanobacteria, can be regarded as a key organism for understanding many structural, functional, regulatory, and evolutionary aspects of oxygenic photosynthesis. In our current study we investigated whether this ancient cyanobacterium lacking thylakoid membranes is capable of two basic phenomena common to all other photoautrophs: state transitions and non-photochemical fluorescence quenching. Our results clearly indicate dynamic changes in light energy distribution between the two photosystems. Similar to "modern" cyanobacteria *G. violaceus* is in state II in darkness and in state I upon illumination with weak blue- or far red light. Compared to state II, state I is characterized by an increased functional absorption cross-section of PS2. Furthermore, in contrast to weak blue light, strong blue light reversibly quenches chlorophyll fluorescence in *G. violaceus*, which suggests the existence of regulated heat dissipation triggered by the orange carotenoid protein in this primordial cyanobacterium.

Keywords: Cyanobacteria; Phylogeny; Fluorescence quenching; Light adaptation; State transitions

Introduction

The unicellular cyanobacterium *Gloeobacter violaceus* PCC 7421 (Rippka *et al*., 1974) is the only known oxygenic photoautotroph which does not contain thylakoid membranes (TM); therefore, all membrane-bound bioenergetic processes take place in the green plasma membrane (PM) of this organism. The PM of *G. violaceus* shows lateral heterogeneity: photosynthetic and respiratory protein complexes are localized together in functionally distinct membrane domains which are probably the evolutionary precursors of TM (Rexroth *et al*., unpublished). Structure and composition of phycobilisome (PBS) antennae (Bryant *et al*., 1981) as well as spectral properties of *G. violaceus* are also quite unique. The latter include an extreme blue-shift of the major low temperature fluorescence emission band of photosystem (PS) 1 (Mangels *et al*., 2002; Mimuro *et al*., 2010). These and other atypical features of *G. violaceus* are in accordance with the fact that this lineage diverged very early during the evolution of oxygenic photosynthesis (Falcón *et al*., 2010) and may represent an ancient stage of it. Investigation of *G. violaceus* could therefore provide valuable information for understanding many structural, functional, regulatory, and evolutionary aspects of photosynthesis. Here, we address two of these questions: whether *G. violaceus* is capable of (i) state transitions, the dominant short-term changes in light energy distribution between photosystems, depending on light regime, and, in turn, PQ redox state, and (ii) regulated thermal dissipation (non-photochemical fluorescence quenching) which protects photosynthetic organisms from damage upon exposure to intense light. Although the molecular

mechanisms of these processes are quite different in eukaryotes from those in higher plants (Mullineaux and Emlyn-Jones, 2005; Kirilovsky, 2010), both phenomena are common to (almost) all oxygenic photoautotrophs.

Materials and Methods

Growth conditions

G. violaceus cells were grown photoautotrophically in Allen's medium at 20 °C under continuous white light (4 µmol photons m^{-2} s^{-1}) and ambient air. Six month old cultures at a Chl concentration of 5 µg/ml were used in all spectroscopic experiments.

Low-temperature fluorescence measurements

Low temperature fluorescence emission spectra were recorded using an Aminco-Bowman Series 2 luminescence spectrometer (SLM Spectronic Instruments). All samples were first dark adapted for 1 h to induce state II as an initial state. State I was induced by a subsequent 15 min exposure to FR light (200 µmol photon m^{-2} s^{-1}) defined by an Omega BP700 filter. Samples in state I and II were frozen in liquid nitrogen.

Chlorophyll fluorescence transients

Chlorophyll fluorescence transients were measured by a Dual-PAM-100 measuring system (Walz). State II to state I and state I to state II transitions were induced by switching on/off either FR light (735 nm, 75 W/m^{-2}) or weak blue light (BL, 440 nm, 11 µmol photons m^{-2} s^{-1}). OCP- quenching was induced by switching on strong (200 µmol photon m^{-2} s^{-1}) BL. 300-ms saturating pulses (1,000 µmol photon m^{-2} s^{-1}) were applied at 1 min intervals to probe the maximal fluorescence yields.

Results

Changes in light energy distribution between the two photosystems can be followed by low temperature fluorescence spectroscopy (Murata, 1969). The main advantage of this method is that the fluorescence emission from PS2 and PS1 is usually manifested as distinct emission peaks at 685/695 nm and 725 nm, respectively, as illustrated by fluorescence spectra (λ_{ex} = 580 nm) of dark-adapted (state II) and FR illuminated (state I) *Synechocystis* PCC6803 cells (Fig. 1a). The emission band and shoulder at 665 nm and 650 nm indicate allophycocyanin (APC) and phycocyanin (PC) emission, respectively, while the peaks at 685/695 nm and 725 nm reflect excitation energy transfer from PBS to PS2 and PS1, respectively. The increase in the intensity of 685/695 nm emission (as compared to that of 730 nm) upon illumination of dark-adapted samples with FR light indicates state II to state I transition.

PBS excitation of dark adapted *G. violaceus* cells (λ_{ex} = 565 nm) induces intense PC emission at 645 nm with an APC shoulder at 660 nm and less intense chlorophyll fluorescence at 687 nm (Fig. 1b). FR illumination induces a 60% increase in the amplitude of the 687 nm peak. This shows a more efficient PBS to PS energy transfer in FR illuminated as compared to dark adapted cells, which may indicate that *G. violaceus* is capable of state transitions. However, due to the spectral properties of *G. violaceus* it is impossible to decide whether the energy transfer to PS2 or to PS1 is increased by FR illumination. To address this question we have performed room temperature fluorescence measurements in addition.

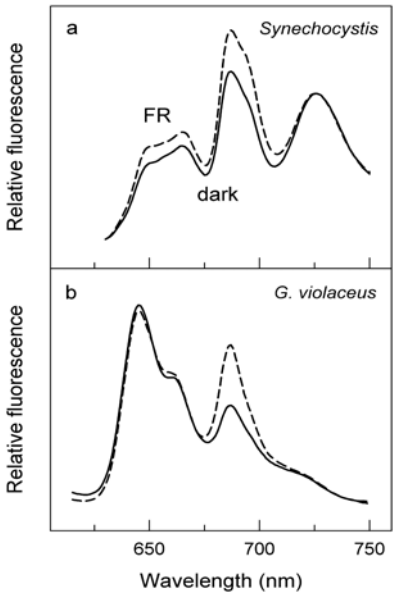

Fig. 1 Low temperature (77 K) fluorescence emission spectra of *Synechocystis* and *G. violaceus* cells with PBS excitation at 580 and 565 nm, respectively. Samples were frozen either after 1 h of dark incubation (solid lines) or after a subsequent 15 min FR illumination (dashed lines). The spectra were normalized to the 725 nm (*Synechocystis*) and 645/660 nm (*G. violaceus*) emission peak(s).

Fig. 2 shows chlorophyll fluorescence transients of dark-adapted *G. violaceus* induced upon switching on/off FR and BL. Saturation pulses are applied repetitively for Fm determination. Dark incubation induces minimal Fo and Fm fluorescence yields, indicating that dark-adapted *G. violaceus* cells really are in state II. Exposure of cells to strong FR induces an increase in Fm which is a clear indication for state II to state I transition, *i.e.* light energy distribution between photosystems is changed in favor of PS2. The large increase of Fm is accompanied by only a small increase of Fo, which means an increase of the effective quantum yield, Φ(II) = (Fm–Fo)/Fm. State II to state I transition can be induced not only by FR light but also by weak BL (Fig. 2) which in cyanobacteria is a more efficient PS1 light than FR (Schreiber *et al*., 1995). These changes are reversible upon re-darkening of the sample (Fig. 2). Analysis of the photochemical phase of the Fo to Fm fluorescence rise in state I and state II revealed that state I (as compared to state II) is characterized by an increased functional absorption cross-section of PS2 (data not shown).

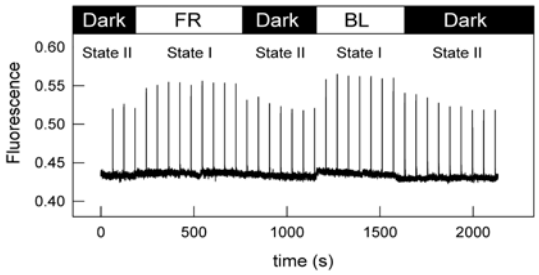

Fig. 2 Effect of FR and weak (11 µmol photon m^{-2} s^{-1}) BL on the chlorophyll fluorescence yield of dark-adapted *G. violaceus*. Saturation pulses were given to probe Fm every 1 min.

While *weak* BL in cyanobacteria is equivalent to strong FR light in inducing the high-fluorescent state I (Fig. 2), *strong* blue light provokes non-photochemical quenching (Schreiber *et al*., 1995, El Bissati *et al*., 2000), which reflects enhanced heat dissipation and plays an important role in photoprotection. This type of quenching probably is triggered by a conformational change of the orange carotenoid protein (OCP) upon exposure to strong BL (Wilson *et al*., 2008). The impact of strong BL on *G. violaceus* is shown in Fig. 3 (thick upward arrow). First, a small increase of Ft is induced which is followed by a robust gradual decrease of Ft and Fm'. Switching off the actinic light (downward arrow) induces a recovery from the quenched state. When subsequently *weak* BL is switched on (thin upward arrow) a state II to state I transition is induced.

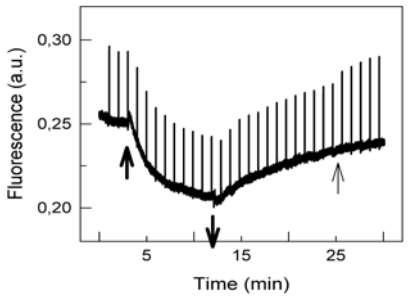

Fig. 3 Effect of strong (thick arrows) and weak BL (thin arrow) on chlorophyll fluorescence yield of *G. violaceus*. Saturation pulses were given to probe Fm every 1 min.

Discussion

Photosynthetic organisms have developed several molecular mechanisms to respond to changes in light intensities and/or qualities. State transitions and non-photochemical fluorescence quenching are the two most important balancing/protective short-term processes. *G. violaceus* is capable of both state transitions and non-photochemical fluorescence quenching. Phenomenologically these features are quite similar to those observed in other cyanobacteria: While in darkness *G. violaceus* is in state II (low energy transfer from PBS to PS2), illumination by FR or weak BL induces a transition to state I which is characterized by modified energy distribution between the two photosystems in favor of PS2 (Figs. 1 and 2). The BL-induced fluorescence quenching (Fig. 3) indicates the presence of regulated heat dissipation in this ancient organism. In good accordance with these observations, the genome of *G. violaceus* contains orthologs of cyanobacterial genes which encode proteins thought to play a role in these processes in other cyanobacteria: RpaC in state transitions and OCP in blue-light induced fluorescence quenching.

In evolutionary timescale, formation of modern photoautotrophs from two bacterial ancestors coincided with the introduction of water as terminal electron donor of photosynthesis. This transformation was one of the most important events during the history of life on Earth. As no intermediate organisms between anoxygenic and oxygenic photosynthetic bacteria are known, these events are considered to be "discontinuous" (Mimuro *et al*., 2008); however, an increasing number of molecular genetic and

bioinformatic data sheds light on cyanobacterial evolution. All current phylogenetic trees of cyanobacteria (*e.g.* Mimuro *et al*., 2008; Falcón *et al*., 2010) clearly show that the lineage of *G. violaceus* branched off the earliest from other extant cyanobacteria. As *G. violaceus* is capable of state transitions and non-photochemical fluorescence quenching, these mechanisms must be rather old. The branching of *G.violaceus* from other cyanobacteria is dated to approximately 2.7 Ga ago (Falcón *et al*., 2010), shortly after the formation of oxygenic photosynthesis. While at that time the Earth's atmosphere was still anoxygenic, oxygen producing organisms (*i.e.* cyanobacteria) must have already experienced potentially harmful intracellular oxygen levels. This could have meant strong selection pressure to induce the development of protective mechanisms to prevent the formation of reactive singlet oxygen which can be formed by photosynthesis when more light is absorbed by the photosynthetic antennae than can be utilized in CO_2 fixation. In addition, emergence of two photosystems must have entailed a tool to regulate light energy distribution between PS1 and PS2 effectively which also helps to avoid the overreduction of the intersystem electron transport chain and, thus, prevents the formation of singlet oxygen.

In summary, though the morphology and composition of the PBS antenna of *G. violaceus* as well as the membrane architecture of this primordial cyanobacterium is rather atypical, the molecular processes of state transitions and non-photochemical fluorescence quenching are apparently very similar to those in other classes of cyanobacteria.

Acknowledgements

The stimulating discussions with Navassard Karapetyan are much appreciated. This work was supported by BMBF (project Bio-H_2; GB/MR), and DFG (SFB 480, project C1; MR).

References

Bryant DA, Cohen-Bazire G, Glazer AN (1981) Characterization of the Biliproteins of Gloeobacter Violaceus. Chromophore Content of a Cyanobacterial Phycoerythrin Carrying Phycourobilin Chromophore. Arch. Microbiol. 129: 190-198

El Bissati K, Delphin E, Murata N, Etienne AL, Kirilovsky D (2000) Photosystem II Fluorescence Quenching in the Cyanobacterium Synechocystis PCC 6803: Involvement of Two Different Mechanisms. Biochim. Biophys. Acta 1457: 229-242

Falcón LI, Magallón S, Castillo A (2010) Dating the Cyanobacterial Ancestor of the Chloroplast. ISME J. 4: 777-783

Kirilovsky D (2010) The Photoactive Orange Carotenoid Protein and Photoprotection in Cyanobacteria. Adv. Exp. Med. Biol. 675: 139-159

Mangels D, Kruip J, Berry S, Rögner M, Boekema EJ, Koenig F (2002) Photosytem I from the Unusual Cyanobacterium Gloeobacter Violaceus. Photosynth. Res. 72: 307-319

Mimuro M, Tomo T, Tsuchiya T (2008) Two Unique Cyanobacteria Lead to Traceable Approach of the First Appearance of Oxygenic Photosynthesis. Photosynth. Res. 97: 167-176

Mimuro M, Yokono M, Akimoto S (2010) Variations in Photosystem I Properties in the Primordial Cyanobacterium Gloeobacter Violaceus PCC 7421. Photochem. Photobiol. 86: 62-69

Mullineaux CW, Emlyn-Jones D (2005) State Transition: an Example of Acclimation to Low-Light Stress. J. Exp. Bot. 56: 389-393

Murata N (1969) Control of Excitation Transfer in Photosynthesis. I. Light-Induced Change of Chlorophyll a Fluorescence in Porphyridium Cruentum. Biochim. Biophys. Acta 172: 242-251

Rippka R, Waterbury J, Cohen-Bazire G (1974) A Cyanobacterium Which Lacks Thylakoids. Arch. Microbiol. 100: 419-436

Schreiber U, Endo T, Mi H, Asada K (1995) Quenching Analysis of Chlorophyll Fluorescence by the Saturation Pulse Method: Particular Aspects Relating to the Study of Eukaryotic Algae and Cyanobacteria. Plant Cell Physiol. 36: 873-882

Wilson A, Punginelli C, Gall A, Bonetti C, Alexandre M, Routaboul JM, *et al*. (2008) A Photoactive Carotenoid Protein Acting as Light Intensity Sensor. Proc. Natl. Acad. Sci. U.S.A. 105: 12075-12080

Symposium 09

Control of the Calvin-Benson Cycle

Relationship Between Photosynthesis and Respiration in Leaves Using $^{13}C/^{12}C$ Isotope Labelling

Salvador Nogués

Departament de Biologia Vegetal, Universitat de Barcelona, Barcelona, Catalonia, Spain.
Corresponding author. Tel. No. +34 93 4037243; Fax No. +34 93 4112842; E-mail: Salvador.nogues@ub.edu.

Abstract: The relationship between photosynthesis and respiration was studied in four plant species (*Ranunculus glacialis*, *Chamaerops humilis*, *Phaseolus vulgaris* and *Fagus sylvatica*) using $^{13}C/^{12}C$ stable isotopes. This study was conducted using an open gas-exchange system coupled to an elemental analyzer and linked to an isotope ratio mass spectrometer (IRMS). We showed that the carbon recently assimilated during photosynthesis accounts for ca. 50% of the carbon in the CO_2 lost by dark respiration after illumination in *Phaseolus vulgaris* and *Fagus sylvatica*, and less than 10% in *Ranunculus glacialis* and *Chamaerops humilis*. Therefore, most of the carbon released by dark respiration after illumination in leaves does not come from 'new' photosynthates.

Keywords: Carbon; Stable Isotopes; Photosynthesis; Respiration

Introduction

Whereas photosynthesis provides the carbohydrate substrate upon which plants depend, glycolysis and respiration are the processes whereby the energy stored in carbohydrates is released. However, the amount of carbon assimilated during photosynthesis and immediately respired in plants is not well known.

The $^{13}C/^{12}C$ isotope labeling technique was used to study the respiratory metabolism of recently fixed carbon in leaves of four plant species (*Ranunculus glacialis*, *Chamaerops humilis*, *Phaseolus vulgaris* and *Fagus sylvatica*). We have used a system that consists of a LI-6400 open gas-exchange system directly coupled to an elemental analyzer (EA) and to an isotope ratio mass spectrometer (IRMS). This system takes advantage of the difference in $\delta^{13}C$ between atmospheric CO_2 (ca. –9.5‰) and commercially available (^{12}C-enriched) CO_2 (for example ca. –51.2‰). This allows one to pick up the contribution of stored carbon *vs.* current photosynthates to CO_2 production by respiration. Noteworthy, this would not have been possible if heavily labeled carbon was used (*i.e.* several percent in ^{13}C would have blurred the contribution of non-labeled carbon). The ^{13}C abundance in the CO_2 used for the labeling is in the same order of magnitude of that found in nature, thereby allowing us to calculate proportions of "new" (*i.e*. recently fixed) carbon in CO_2 respired in the dark (Nogués *et al*., 2004). Furthermore, this system also allowed estimations of leaf metabolic fluxes *in vivo*.

The aim of this study was to determine the origin of the carbon atoms in the CO_2 respired by leaves of four plant species (*Ranunculus glacialis*, *Chamaerops humilis*, *Phaseolus vulgaris* and *Fagus sylvatica*). We showed that the carbon recently assimilated during photosynthesis accounts for less than 50% of the carbon in the CO_2 lost by dark respiration in all four species. Therefore, most of the carbon released by dark respiration after illumination comes from 'old' carbohydrates.

Materials and Methods

Ranunculus glacialis were collected in the French Alps as described in Nogués *et al*. (2006b). *Chamaerops humilis* were grown in a greenhouse as described in Aranjuelo *et al*. (2009). *Phaseolus*

vulgaris were also grown in a greenhouse as previously described by Nogués *et al*. (2004). *Fagus sylvatica*) trees were grown in the campus of the *Université de Paris Sud* as previously described (Nogués *et al*., 2006a).

After the initial measurement of dark-respired CO_2, leaves were placed in a specially designed gas-exchange chamber for isotope labeling, as described by Nogués *et al*. (2004). The chamber was connected in parallel to the sample air hose of the LI-6400. This aluminum chamber ($20\times12\times6\times10^{-6}$ m^3), fitted with a clear plastic lid, holds two to four leaves (total leaf surface *ca*. 0.005 m^2). Two fans were enclosed in the chamber and gave a boundary layer conductance to water of *ca*. 6.7 mol m^{-2} s^{-1}. Leaf temperature in the chamber was maintained at *ca*. 20 ^oC by cool watering the jacket around the leaf chamber, and was measured with a cooper-constantan thermocouple plugged into the thermocouple sensor connector of the LI-6400 chamber/IRGA. Ingoing air was passed through the chamber at a rate of 1 L min^{-1}, monitored by the LI-6400. Molar fractions of CO_2 and humidity were measured with the infrared gas analyzer (IRGA) of the LI-6400. The PPFD inside the chamber was maintained at 500 μmol m^{-2} s^{-1}. For labeling, CO_2 was obtained from a bottle (Air Liquide, Grigny, France) with $\delta^{13}C$ value of for example *ca.* –51.2‰ ± 0.1‰. After photosynthetic measurements, the outgoing air of the chamber was flushed and the air at CO_2 *ca.* 300 μL L^{-1} was accumulated in 50-mL glass balloons or in 10-mL vacutainers and analyzed for the measurement of photosynthetic carbon isotopic discrimination ($\Delta^{13}C$). The $\Delta^{13}C$ measured ranked between *ca*. 15.5‰ was *ca*. 20.4‰.

After labeling, leaves were removed from the labeling chamber and replaced in the respiration chamber for measurements of dark-respired CO_2 (labeled).

Gas samples for analysis were collected in 50-mL glass balloons (Scott Glass, Mainz, Germany) or in 10-mL vacutainers (BD vacutainers, Plymouth, U.K.).

The gas inside the balloon was introduced into an elemental analyzer (EA) NA-1500 (Carlo-Erba, Milan), using a pump, through a 15-mL loop, as described by Tcherkez *et al*. (2003). The gas inside the vacutainers was directly injected in a gas chromatography-combustion-isotope ratio mass spectrometer (GC-C-IRMS) as previously described (Nogués *et al*., 2008).

Results and Discussion

The present study shows that most of the carbon released by dark respiration after illumination (between 50%–90%) does not come from newly assimilated C in these plants species (Table 1). Similarly, most of the carbon in sucrose is not inherited from newly fixed carbon atoms (data not shown).

The increase in the respiratory rate as a function of assimilated C (data not shown) shows that there is a tight link between photosynthetic and respiration. We argue that this increase could result from an increase in the availability of substrate fed directly from photosynthesis and also from one or more non-labeled pools.

The carbon recently assimilated during photosynthesis accounts for ca. 50% of the carbon in the CO_2 lost by dark respiration after illumination in *Phaseolus vulgaris* and *Fagus sylvatica*, and less than 10% in *Ranunculus glacialis* and *Chamaerops humilis* (Table 1; Nogués *et al*., 2004, 2006a, 2006b; Aranjuelo *et al*., 2009). These contrasting values indicate that in nature there might be two distinct "respiratory physiotypes": for a given amount of assimilated carbon, parsimonious

Table 1 The $\delta^{13}C$ of the CO_2 respired before and after labeling (‰), $\delta^{13}C$ of the CO_2 used during the labeling (‰), the $\Delta^{13}C$ measured during the labeling period (‰) and the % of new carbon in the CO_2 respired after the labeling are shown for four C3 plant species. All the species assimilated the same amount of labeled CO_2 from the bottle (*i.e. ca*. 350 mmol C m^{-2}). *Ranunculus glacialis* data is from Nogués *et al*. (2006b). *Chamaerops humilis* data is from Aranjuelo *et al*. (2009). *Phaseolus vulgaris* data is from Nogués *et al*. (2004). *Fagus sylvatica* data is from Nogués *et al*. (2006a).

Type of plants	Plant species	$\delta^{13}C$ before (‰)	$\delta^{13}C$ after (‰)	$\delta^{13}C$ labeling (‰)	$\Delta^{13}C$ (‰)	New C in CO_2 (%)
Slow-growing plants	*Ranunculus glacialis*	–23.4 ± 0.7	–28.0 ± 0.8	–51.2 ± 0.1	20.4 ± 0.7	9.6 ± 1.1
	Chamaerops humilis	–21.8 ± 0.5	–23.2 ± 0.3	–22.9 ± 0.1	15.5 ± 0.3	6.7 ± 0.7
Fast-growing plants	*Phaseolus vulgaris*	–22.0 ± 0.6	–44.8 ± 0.8	–51.2 ± 0.1	20.1 ± 0.2	50.3 ± 0.9
	Fagus sylvatica	–18.8 ± 0.7	–44.5 ± 0.9	–51.2 ± 0.1	17.0 ± 0.6	56.8 ± 1.0

plants have a slow turn-over of the respiratory pool, maybe favoring recycling of reserves (*i.e. Ranunculus glacialis* and *Chamaerops humilis*) and also have a small proportion of 'new' carbon after illumination (Table 1). Meanwhile others invest more recent carbon in respiration (*i.e. Phaseolus vulgaris* and *Fagus sylvatica*). Presumably, the respiratory strategy may be related to the biological constraints of the environment. Interestedly, Atkin and Tjoelker (2003) have identified two types of respiratory acclimation to temperature in plants, one of which is underpinned by adjustments in the Q_{10} (called Type I) and the other by changes in the enzymatic capacity of the respiratory system (called Type II); Type I acclimation enables rapid changes in respiratory flux at high temperatures to occur following changes in thermal environment, meanwhile Type II acclimation is likely to be maximal upon the development of new leaves and roots following a change in temperature.

For plants growing slowly in harsh environment, like *Ranunculus glacialis* (alpine conditions) and *Chamaerops humilis* (hot and dry conditions), most of the new assimilated carbon is not respired, and these species may be called "low respiratory turn-over plants". In fast-growing and cultivated plants and trees, like *Phaseolus vulgaris* and *Fagus sylvatica*, nearly 50% of the respiratory CO_2 comes from recently assimilated carbon; these may be called "high respiratory turn-over plants". However, further studies on the biodiversity of the leaf respiratory response are required to check the validity of this hypothesis and to relate it to the Atkin and Tjoelker' model.

Acknowledgements

This study was supported in part by *Ministerio de Educación y Ciencia* research project AGL2009-13539-C02-01 and the EC research project BIODIVERSA-VITAL. The author likes to thank G Tcherkez, G Cornic and J Ghashghaie (Université Paris Sud) and I Aranjuelo, Ll Cabrera and G Molero (Universitat de Barcelona) for early discussion on the study.

References

Aranjuelo I, Pardo A, Biel C, Save R, Azcón-Bieto J, Nogués S (2009) Leaf Carbon Management in Slow-Growing Plans Exposed to Elevated CO_2. Global Change Biology 15: 97-109

Atkin OK, Tjoelker MG (2003) Thermal Acclimation and the Dynamics Response of Plant Respiration to Temperature. Trends in Plant Science 8: 343-351

Nogués S, Tcherkez G, Cornic G, Ghashghaie J (2004) Respiratory Carbon Metabolism Following Illumination in Intact French Bean Leaves Using $^{13}C/^{12}C$ Isotope Labeling. Plant Physiology 136: 3245-3254

Nogués S, Damesin C, Tcherkez G, Maunoury F, Cornic G, Ghashghaie J (2006a) ^{13}C Isotope Labeling to Study Leaf Carbon Respiration and Allocation in Twigs of Field-Grown Beech Trees. Rapid Communications in Mass Spectrometry 20: 219-226

Nogués S, Tcherkez G, Streb P, Pardo A, Baptist F, Bligny R, Ghashghaie J, Cornic G (2006b) Respiratory Carbon Metabolism in the High Mountain Plant Species Ranunculus Glacialis. Journal of Experimental Botany 14: 3837-3845

Nogués S, Aranjuelo I, Pardo A, Azcón-Bieto J (2008) Assessing the Stable Carbon Isotopic Composition of Intercellular CO_2 in a CAM Plant Using Gas Chromatography-Combustion-isotope Ratio Mass Spectrometry. Rapid Communications in Mass Spectrometry 22: 1017-1022

Tcherkez G, Nogués S, Bleton J, Cornic G, Badeck F, Ghashghaie J (2003) Metabolic Origin of Carbon Isotope Composition of Leaf Dark-Respired CO_2 in French Bean. Plant Physiology 131: 237-244

Photosynthetic Labeling and Partitioning of Major Sugars and Monoterpenes in Leaves of *Plantago Lanceolata* L

Ildiko Szucs*, Mayhery Escobar, Demos Leonardos, Sarah Crain, Bernard Grodzinski

Department of Plant Agriculture, University of Guelph, Guelph, Ontario, Canada.
*Corresponding author. Tel. No. +519-824-4120 ext58271; E-mail: iszucs@uoguelph.ca.

Abstract: Steady-state $^{14}CO_2$ labeling was used to compare photosynthesis, C-partitioning, and export of greenhouse and field grown ribwort (*Plantago lanceolata* L.). In addition, to labeling starch and sucrose, ribwort produces a prominent alcohol sugar during photosynthesis and monoterpenes (iridoids). In *P. lanceolata,* the alcohol sugar, sorbitol, was heavily labeled relative to sucrose during $^{14}CO_2$ feeding and appeared to be exported to sink tissues for both growth methods, but more label was partitioned to sorbitol in field grown plants. Ribwort synthesizes the iridoid glycosides (IGs), catalpol and aucubin, the ^{14}C-labeling was primarily into sucrose and sorbitol that were readily exported with less than 1% partitioned into the iridoid fraction during steady-state $^{14}CO_2$ feeding conditions for both greenhouse and field grown plants.

Keywords: *Plantago lanceolata*; Iridoid Glycoside (IG); Catalpol; Aucubin; Plantaginaceae; ^{14}C-partitioining

Introduction

Labeling and carbon partitioning studies have shown that two snapdragon (*Antirrhinum majus* L.) cut flower cultivars (Protomac Ivory White and Maryland Ivory White) have a significant amount (30%) of ^{14}C of the soluble fraction portioned into two iridoid glycosides (IGs), antirrhinoside and antirrhide (Beninger *et al.*, 2007; Szucs *et al.*, unpublished). Plantaginaceae have undergone major reclassification due to molecular systematics (Albach *et al.*, 2005). The genera, *Antirrhinum* now belong to the enlarged Plantaginaceae family. Morphology and phytochemistry of the Plantaginaceae is variable but IGs are common (Beninger *et al*., 2007). Therefore, the distribution and function of the IGs in other members of this family deserve attention.

Ribwort plantain (*Plantago lanceolata* L.) is a common perennial weed, belonging to the Plantaginaceae, which produces two IGs, acubin and catalpol (Szucs *et al.*, in press). Ribwort has been extensively studied for host plant-herbivory interactions and may serve as an important model species for studying IGs within the Plantaginaceae. A preliminary study was conducted to compare the newly fixed ^{14}C-partitioing into metabolites, of greenhouse and field grown ribwort.

Materials and Methods

Plantago lanceolata L. seeds were collected from the University of Guelph grounds and sowed in "128 cavity plug trays" (Landmark Co. Plastic, Akron, OH, U.S.A.) and placed on a misting bench in a glass greenhouse in Guelph, ON, Canada (43° and 15' L.N.). Germination took place at 22/15 °C day/night temperatures, under natural light conditions. After three weeks seedlings were transplanted into 1 L pots and grown in a research greenhouse. Day/night temperatures were approximately 25/18 °C, under natural light conditions. *P. lanceolata* plants were also collected from Simcoe Research station and were transplanted into 1 L plots and placed outside at the Edmond Bovey Building on the main campus of the University of Guelph, Guelph, ON Canada. Gas exchange and ^{14}C-export studies were conducted on 6–8 week old greenhouse, and field grown *P. lanceolata.* Eight plants were selected from both growth methods and studies were done on one leaf randomly chosen from the inner or mid-rosette of each plant. Plants were acclimated to growth chamber conditions: CO_2 was kept constant in the chamber and the cuvette at ambient (approximately 400 ppm); O_2 was maintained at 21%; light levels were set at 1000 ± 50 μmol m^{-2} s^{-1} PPFD at the plant height, the

air and cuvette temperatures were maintained at 25 °C; the relative humidity was maintained at 50%. $^{14}CO_2$ steady-state labeling was measured by an open-flow system described previously (Jiao and Grodzinski, 1996). The $^{14}CO_2$ specific activity was kept constant by a precision syringe pump throughout the set time feeds. Following each labeling feed, leaves were cut at the petiole and areas of the leaf inside the cuvette were traced. The petiole and leaf were separated and were frozen in liquid nitrogen and stored in a −80 °C freezer. Frozen samples were rapidly extracted in 80% boiling ethanol as described by Jiao and Grodzinski (1996). Individual sugars and the iridoid glycosides from the ethanol-soluble fraction were separated using two HPLC (Beckman Instrument Inc. 119 solvent module with a refractive index detector and a fraction collector, LKB Broma 2111) columns: Alltech (4.6 × 300 mm; Alltech Associates, Mandel Scientific, Guelph, ON, Canada) to separate the glucose fraction from sorbitol and RP Amide column (4.6 × 250 mm; Sigma-Aldrich, Canada Inc.) to separate the iridoid glycosides, catalpol and aucubin from the glucose fraction. Effluent was collected in scintillation vials and was dissolved in 2.3 mL ES Cyto cocktail and radioactivity was determined by liquid scintillation counting (LSC) (LS-6800, Beckman). Chloroform and ethanol-soluble fractions were counted by LSC to quantify ^{14}C in each fraction. The radioactivity remaining in the ethanol-insoluble (95% starch) was counted by LSC after samples were combusted in a biological oxidizer (Model OX300, RJ Harvey Instrument Corp. Hillside, NJ, U.S.A.). SAS Statistical analysis was carried out using statistical Analysis Software, version 9.1 (SAS Institute Inc., NC, U.S.A.). Parameters for greenhouse and field grown plants were compared by one-way analysis of variance (ANOVA) using a general linear model (PROC GLM). To ensure assumptions for the one-way ANOVA were met, a test of residuals was performed using PROC UNIVARIATE). The Shapiro Wilkes test of residuals was computed to determine if the distributions were normal. To verify if outliers were present, standardized residuals were calculated and assessed against Lund's critical value. Results were considered significant at the $P \leq 0.05$ level.

Results and Discussion

Leaf net carbon exchange rate (NCER) was constant for both greenhouse and field grown ribwort over the whole day (11.5 h) $^{14}CO_2$-labelling feed (Fig. 1a). Mean NCER for greenhouse grown plant was 12.52 (± 0.75) and 11.36 (± 0.76) respectively. Export expressed as % of NCER (%-Export) was also constant throughout the whole day feed for both growth conditions with the exception of the first half hour of the green house grown plants (Fig. 1b). The average rate of %-Export was 64.04 (± 4.65) and 68.41 (± 5.11). NCER and %-Export were not significantly different between growth methods. There were no significant differences for % newly fixed ^{14}C-partioned into the starch, sugar, and chloroform ($CHCl_3$) fractions between the two growth methods (Fig. 2a). Over the whole day feed almost half of the ^{14}C accumulated in the starch fraction, whereas the other half into the sugar fraction. A small percentage of ^{14}C, 2.24 (± 0.64) and 1.78 (± 0.35) accumulated into the $CHCl_3$ fraction for greenhouse and field grown plants. Partitioning of % newly fixed ^{14}C into pools of the soluble sugar fraction had the highest accumulation in the alcohol sugar, sorbitol and then sucrose over the whole day feed for both growth methods, with sucrose to sorbitol ratio of 0.71 in greenhouse grown ribwort and 0.55 in field grown ribwort. Partitioning into sorbitol and fructose was significantly different between greenhouse and field grown ribwort (Fig. 2b). In greenhouse grown plants, 37.29 (±4.55) and 8.99 (± 3.39)% of the ^{14}C label was partitioned into sorbitol and fructose respectively, while 43.66 (± 3.54) and 5.43 (± 2.21)% was partitioned in the field grown plants. ^{14}C partitioned in the iridoid glycoside pools of greenhouse and field grown plants were at background counts of the LSC, indicating that less than 1% of ^{14}C was partitioned to the IG pools, catalpol and acubin.

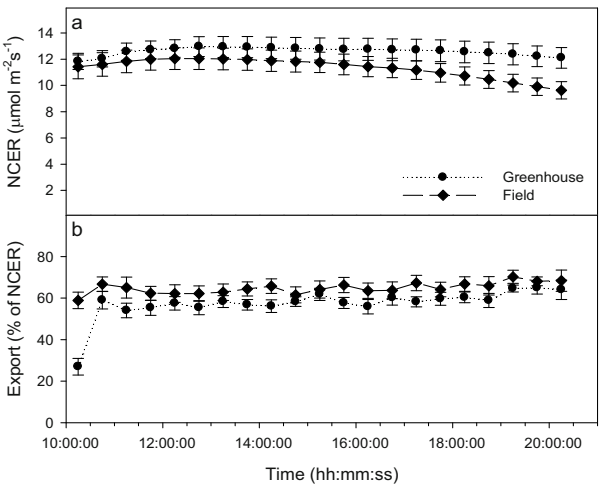

Fig. 1 (a) NCER and (b) %-Export for 11.5 h ^{14}C-steady state feed of greenhouse and field grown ribwort. Each point represents a mean±SE of 8 plants.

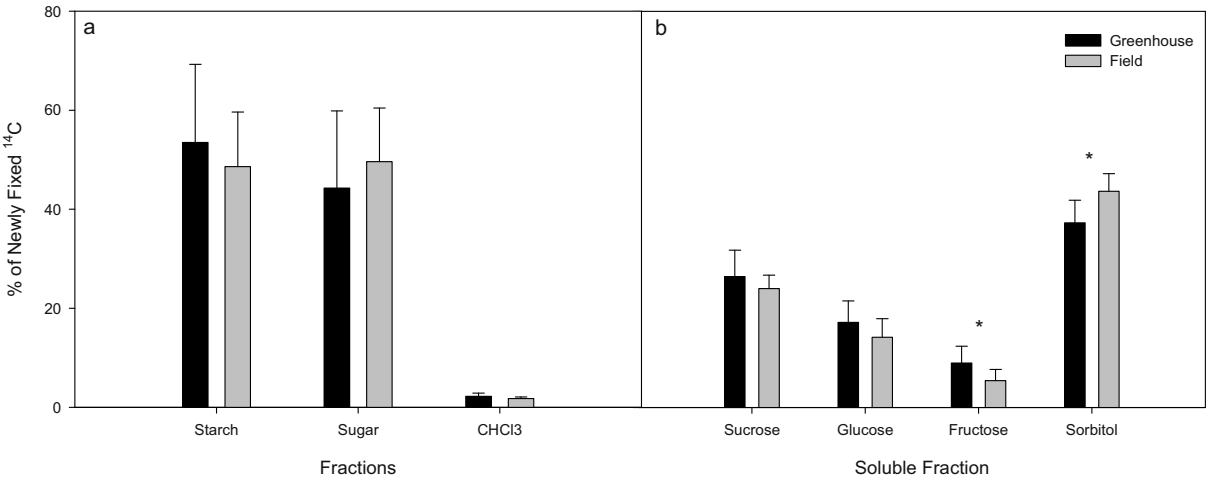

Fig. 2 (a) Percent newly fixed ^{14}C partitioned into the starch, sugar, and chloroform ($CHCl_3$) fractions for greenhouse and field grown plants over 11.5 h ^{14}C steady-state feed. (b) Percent newly fixed ^{14}C partitioned into the ethanol-soluble sugar fraction, including, sucrose, glucose, fructose, and sorbitol for greenhouse and field grown plants over 11.5 h ^{14}C steady-state feed.

Studies have found great variability in IG content in ribwort, especially, genetic and morphological differences, that influence IG content between and within populations (Bowers *et al*., 1992). In two main populations of ribwort, varieties from both hayfield and pasture exhibited canopy differences (Marak *et al.*, 2000). Selection studies within high and low IG lines were undertaken. High IG selection lines were characteristic of populations in hayfield, whereas low IG selection lines were associated with pasture populations (Marak *et al*., 2000). Among the two lines a 3 to 4-fold difference of IG content was found. Taken together, in low selection lines IGs can be undetectable, but IGs can still comprise 10% of the total dry weight in high selection lines (Marak *et al.*, 2000). Plants that were examined in this study were characteristic of pasture varieties, since they had small prostate rosettes with small leaves and inflorescences with small roundish spikes (Marak *et al.*, 2000). In addition seeds and plants that were taken from the University of Guelph grounds and Simcoe satellite station were in open vegetation, which is also characteristic of pasture varieties (Marak *et al*., 2000). IG content in ribwort is significantly influenced by leaf and plant age. Mature leaves can have little or no IGs whereas in young leaves IGs can make up 20% of the dry weight (Bowers *et al.*, 1992). Leaves that were ^{14}C labeled in this study were randomly chosen, however the age of leaves that were grown in the field cannot be confirmed. Other factors, such as, herbivory, neighboring plants, arbuscular mycorrhizal fungi (AMF) associations, and environmental conditions can also influence IG content (Bowers *et al.*, 1992; Fuches and Bowers, 2004). Studies have found that herbivory can induce production of IGs, especially catalpol, but it is limited and may also depend on the ontogenic stage of the plant as well as the type of herbivore (Fuches and Bowers, 2004). Bennett and Bever (2007) studied three distinct AMF associations and provided evidence that AMF type can influence plant-herbivory interactions and can effect production of IGs. In this study the field grown plant may have been exposed to herbivory and could have had AMF associations, but this was not examined. It can be concluded that due to the amount of variability within and between ribwort populations, ribwort is not a good model species to study IGs.

Many genera within the Plantaginaceae produce IGs, thus other species may prove to be better models for studying these compounds (Table 1). *Asarina scandens* and *Asarina barclaiana* both partition newly assimilated ^{14}C into the IG, antirrhinoside that was recovered in the phloem sap (Gowan *et al.*, 1995; Voitsekhovskaja *et al.*, 2006). Antirrhinoside comprised 39% of the total carbon transported in *A. barclaiana* (Voitsekhovakaja *et al.*, 2006) (Table 1). The invasive species toadflax (*Linaria dalmatica*) was also found to have high IG content. Concentrations up to 16.5 and 6.7% of the total dry weight of antirrhinoside and linarioside have been measured, respectively (Jamieson and Bowers, 2010). However, there is variability within this species and ^{14}C labeling studies have not yet been conducted. Snapdragon (*Antirrhinum majus* L.) that has also been placed into the family produces the IGs, antirrhinoside and

antirrhide (Table 1). ^{14}C-Steady state labeling studies of two cut flower cultivars show that antirrhide and especially antirrhinoside are predominantly labeled in the laminar tissue. In addition, antirrhinoside is also labeled in petioles indicating that it is phloem mobile (Beninger *et al.*, 2007) (Table 1). Preliminary studies also indicate that during a full day (11.5 h) ^{14}C-steady state feed sucrose to antirrhinoside ratios are close to 1 (Szucs and Grodzinski, unpublished). Since snapdragon is a model species relating gene regulation with shoot architecture and floral development it serves as a good model species to study carbon partitioning of major metabolites, such as IGs, that may be involved in source to sink relations. An examination of IG synthesis pathways may provide insight into stress responses involving osmoregulation and why some species synthesize and transport sorbitol over IGs like ribwort, while others like snapdragon synthesize and transport the IG, antirrhinoside over mannitol (Table 1).

Table 1 Summary of iridoid production in relation to major sugars in four species belonging to the new Plantaginaceae. Data adapted from *A. majus*, *A. barclaiana*, and *scandens* (Beninger *et al.,* 2007; Gowan *et al.,* 1995; Voitsekhovskaja *et al*., 2006).

	% ^{14}C Label Relative to Soluble Fraction							
Major Water Soluble	*Antirrhinum majus*		*Asarina scandens*		*Asarina barclaiana*		*Plantago lanceolata*	
Photoassimilates	Leaf	Petiole	Leaf	Petiole	Leaf	Petiole	Leaf	Petiole
Antirrhinoside	22.1	14.5	25.0	18.5	53.2	39.1	-	-
Antirrhide	8.0	< 0.01	-	-	-	-	-	-
Linarioside	-	-	-	-	-	-	-	-
Catalpol	-	-	-	-	-	-	< 1.0	< 1.0
Aucubin	-	-	-	-	-	-	< 1.0	< 1.0
Mannitol or Sorbitol*	< 1.2	0.0	nd	nd	9.1	6.8	37.8*	18.59*

Acknowledgements

Funding was provided by the Natural Sciences and Engineering Science Council of Canada (NSERC), Canada Foundation for Innovation/Ontario Innovation Trust, and the Ontario Ministry of Agriculture, Food and Rural Affairs (Bernard Grodzinski), and, various University Guelph Scholarships (*e.g.*, Vitamin Fellowship) plus NSERC-GreenCrop Network awards to Ildiko Szucs.

References

Albach DC, Meudt HM, Oxleman B (2005) Piecing Together the "New Plantaginaceae". Am. J. of Bot. 92(2): 297-315

Beninger CW, Cloutier RR, Monterio MA, Grodzinski, B (2007) The Distribution o Two Major Iridoids in Different Organs of Antirrhinum Majus L. at Selected Stages of Development. J. Chem. Ecol. 33: 731-747

Bennet AE, Bever JD (2007) Mycorrhizal Species Differentially Alter Plant Growth and Response to Herbivory. Ecology 88(1): 210-218

Bowers MD, Collinge SK, Gamble SE, Schmitt J (1992) Effects of Genotype, Habitat and Seasonal Variation on Iridoid Glycoside Content on Plantago Lanceolata (Plantaginaceae) and the Implications for Insect Herbivores. Oecologia 91(2): 201-207

Fuches A, Bowers MD (2004) Patterns of Iridoid Glycoside Production and Induction in Plantago Lanceolata and the Importance of Plant Age. J of Chem. Ecol. 30(9): 1723-1741

Gowan E, Lewis BA, Turgeon R (1995) Phloem Transport of Antirrhinoside, an Iridoid Glycoside, in Asarina Scandens (Scrophulariceae). J. of Chem. Ecol. 21(11): 1781-1778

Jamieson MA, Bowers MD (2010) Iridoid Glycoside Variation in the Invasive Plant Dalmatian Toadflax, Linaria Dalmatica (Plantaginaceae), and Sequestration by Biological Control Agent, Calophasia Lunula. J. of Chem. Ecol. 36: 70-79

Jiao J, Grodzinski B (1996) The Effect of Leaf Temperature and Photorespiratory Conditions on Export of Sugars during Steady-state Photosynthesis in Salvia Splendens. Plant Phys. 111(1): 169-178

Marak HB, Biere A, van Damme JMM (2000) Direct and Correlated Responses to Selection on Iridoid Glycosides in Plantago Lanceolata L. J. of Evol. Bio. 13: 985-996

Voitsekhovskaja OV, Koroleva OA, Batashev DR, Knop C, Tomos AD, Gamalei YV, Heldt H, Lohas G (2006) Phloem Loading in Two Scrophulariaceae Species that Can Drive Symplastic Flow Via Plasmodesmata? Plant Phys. 140(1): 383-395

Symposium 10

CO_2 Concentrating Mechanisms

The Periplasmic Carbonic Anhydrase, CAH1, is Absent in the Sequenced *Chlamydomonas Reinhardtii* Strain, CC-503

Bratati Mukherjee, Trang T Pham, Yunbing Ma ,Tiffany A Simms, James V Moroney*

Department of Biological Sciences, Louisiana State University, Baton Rouge, USA.
*Corresponding author. Tel. No.1225-578-8215; E-mail:btmoro@lsu.edu.

Abstract: The *Chlamydomonas reinhardtii* strain CC-503 (*cw-92*, mt^+), is a cell wall deficient strain that was used in the *C. reinhardtii* genome sequencing project. During the course of working with this strain, it was discovered that it lacks the periplasmic carbonic anhydrase, CAH1. The protein is undetectable on immunoblots probed with a polyclonal CAH1 antibody although other Carbon Concentrating Mechanism (CCM) proteins are found to be present in the expected amounts. However, the amount of *CAH1* mRNA in CC-503, analyzed by quantitative RT-PCR (qRT-PCR), shows no significant difference when compared to other wild-type strains, both walled and cell wall deficient. CC-503 shows reduced growth at lower pH conditions but no significant deficiency in the induction of the CCM. By serving as a natural *CAH1* mutant, this strain could be used in experiments investigating the importance of this carbonic anhydrase in *C. reinhardtii*.

Keywords: *Chlamydomonas reinhardtii*; CCM; Periplasmic carbonic anhydrase; CAH1; CC-503; Cell-wall deficient

Introduction

The photosynthetic green alga, *Chlamydomonas reinhardtii*, can successfully acclimate to fluctuating levels of external C_i, without compromising its photosynthetic efficiency. It does so by the induction of an efficient C_i uptake and utilization process that elevates the CO_2 levels around Rubisco, better known as the Carbon Concentrating Mechanism or CCM (Badger *et al*., 1980). Key components of this mechanism are carbonic anhydrases (CAs), nine of which have been identified in *C. reinhardtii* so far (Moroney and Ynalvez, 2007). A periplasmic CA, CAH1, like many other key CCM proteins, is highly induced under limiting CO_2 conditions (Coleman and Grossman, 1984). Many studies have focused on the role of this CA in the *C. reinhardtii* CCM (Fukuzawa *et al*., 1990; Ishida *et al*., 1993) and some *CAH1* mutants have been successfully generated and characterized (Van and Spalding, 1999).

The cell wall deficient strain CC-503 (*cw-92*, mt^+), is a fully sequenced *C. reinhardtii* strain. In addition, this strain also provides a background for the efficient generation of nuclear transformants mainly due to its cell wall deficiency. This led to its use as an alternate wild-type strain for many of our experiments. However, it was soon discovered that CC-503 was missing CAH1, unlike the other commonly used wild-type laboratory strains, both walled (C9) or cell wall deficient (D66, *cw15* mt^+). This report highlights the fact that the sequenced strain CC-503 is a natural mutant for the periplasmic CA, CAH1.

Materials and Methods

Cell strains and growth conditions: Cells from *C. reinhardtii* strains CC-503, D66, C9 and the CAH1 mutant, *cah1*, were grown mixotrophically on Tris-Acetate-Phosphate (TAP) medium and then transferred to minimal medium (without acetate) for phototrophic growth and bubbled with either 0.01% (v/v) CO_2 for low CO_2 condition, or air containing 5% CO_2 (v/v), for high CO_2 conditions. For testing the

growth phenotype, equal numbers of cells from each strain were spotted on agar plates containing minimal medium maintained at different pH levels with the help of the following buffers; 25 mmol MES-KOH (for pH 5.8 and 6.2), 25 mmol MOPS-KOH (pH 7.2) and 25 mmol HEPES-KOH (pH 8.2). The plates were then exposed to high CO_2 and low CO_2 conditions for 7 days under constant illumination of 100 µmol photon m^{-2} s^{-1}.

RNA extraction and qRT-PCR analysis: Total RNA was extracted from log phase high CO_2 grown cells that were switched to low CO_2 for 4 h, using the Trizol extraction method (Invitrogen, U.S.A.). cDNA synthesized after reverse transcription was used for quantitative RT-PCR (qRT-PCR) analysis as described previously (Ynalvez *et al.*, 2008). The relative quantification of qRT-PCR transcript amounts was performed according to the mathematical model of Plaffl (2001).

Protein extraction and Western blots: Protein extraction and western blot analyses with CAH1 and other antibodies were carried out as described previously (Ynalvez *et al.*, 2008). LCI1, CCP1, CAH4 and α-Tubulin (Sigma, U.S.A) were used as positive controls. The primary antibody serum dilution of 1:4000 was used for CAH1, LCI1, CCP1 and CAH4 antibodies and a dilution of 1:50000 used for α-Tubulin. Appropriate horseradish peroxidase conjugated secondary antibodies were used at a dilution of 1:10000. The chemiluminescent signals were used as a visible measure of protein presence.

Measurement of photosynthetic rate: Cell cultures grown autotrophically on minimal medium were acclimated to low CO_2 for one day and then harvested and resuspended to a concentration of 25 µg chlorophyll/mL in each of the following buffers, 25 mmol MES-KOH for pH 6.2, 25 mmol MOPS-KOH for pH 7.2 and 25 mmol Bicine-KOH for pH 8.2. Photosynthetic rates were then measured with a Clark-type Oxygen electrode (Rank Brothers) as a function of dissolved inorganic carbon concentration provided by $NaHCO_3^-$ solutions of varying molarities.

Results and Discussion

The *CAH1* gene is known to be highly transcribed upon induction of the *C. reinhardtii* CCM. However, in the course of CCM related experiments done with CC-503 as a wild-type strain, it was found that the CAH1 protein could not be detected in the low CO_2 induced cells of this strain (Fig. 1). The first possibility considered, to account for this absence, was a change in the gene sequence. The *CAH1* sequence available from the *C. reinhardtii* genome database (Version 4.0) was compared with the published sequence from another wild-type strain, C9, (Kucho *et al*., 1999).

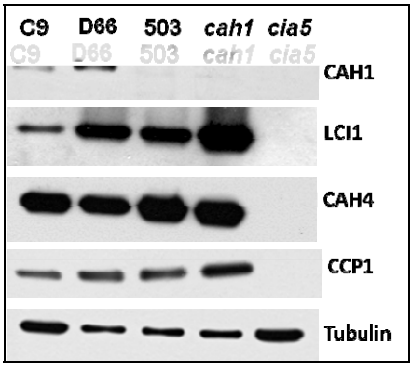

Fig. 1 Western blot analysis using a CAH1 specific antibody shows the absence of CAH1 in CC-503. LCI1, CAH4 and CCP1 are CCM proteins that are induced under low CO_2 conditions. *cah1*: CAH1 mutant strain; *cia5*: CCM mutant strain.

In the characterization of the *CAH1* promoter in the strain C9 (Kucho *et al*., 1999), a 543 base pair (bp) region had been identified upstream of the transcriptional start site that was sufficient for the CO_2 responsive transcription of the *CAH1* gene (Fig. 2). This region was found to consist of two parts, a 358 bp silencer region from −651 to −294 and a 185 bp enhancer element from −293 to −109 with respect to the transcriptional start site. The silencer region was shown to repress gene expression under high CO_2 conditions whereas the enhancer region induced gene expression under low CO_2 conditions.

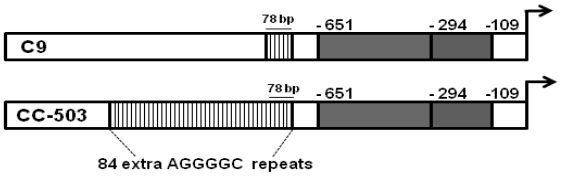

Fig. 2 A schematic diagram of the region upstream of the CAH1 transcriptional start site, from the two strains CC-503 and C9. There are 84 extra AGGGGC repeats upstream of the (−651 to −294) silencer region in CC-503. The region extending from −109 to −294 is the CO2-responsive enhancer element.

Both these regions as well as the DNA sequence downstream were found to be identical in both CC-

503 and C9. However, there was one difference in the sequence upstream from the 358 bp transcription regulatory region. In C9, a 78 bp region was reported, consisting of about 13 tandem repeats of the sequence AGGGGC, whereas in CC-503, this repeat region appears to be about 582 bp long, with 97 tandem repeats (Fig. 2). Attempts to verify the presence of the repeat region by PCR amplification using primers spanning the repeat region failed in case of CC-503 and revealed a slightly longer fragment than expected in case of C9 (data not shown). It is possible that this large tandem repeat region poses a difficulty in the amplification from the CC-503 genomic DNA. The presence of these repeats might also have interfered with the proper sequencing of this region which would mean that the actual number of AGGGGC repeats might vary from the values inferred from the sequences available from CC-503 and C9.

The presence of the extra 84 repeats was initially suspected to be a possible contributing factor to the absence of the protein by reducing the level of transcription of the *CAH1* gene, due to its close proximity to the transcription suppressor region. To test this hypothesis an attempt was made to see if the gene was transcribed at the expected levels in CC-503.

CAH1 transcript levels measured by qRT-PCR, revealed that there was no significant difference in the CC-503 strain in comparison to the cells of the other wild-type strains, both the cell wall deficient strain D66, and the cell walled C9 (Fig. 3). The presence of the whole transcript was also confirmed with PCR, using primers covering all exons and the 5' and 3' UTRs (data not shown). As mentioned earlier, the CAH1 protein could not be detected when total protein from low CO_2 grown unwashed CC-503 cells was probed with a polyclonal antibody made against CAH1 (Fig. 1). This was similar to the mutant, *cah1*, which is known to lack this protein (Fig. 1). However, most of the other prominent proteins of the CCM seem to be present in CC-503 (Fig. 1). Since the absence of the protein cannot be accounted for by a reduction in transcript levels, determining the cause for the absence of CAH1 will remain a focal point for future investigations.

The absence of CAH1 in *C. reinhardtii* cells fails to produce any significant differences in either the growth phenotype or the ability to induce a fully functional CCM, even when pH levels are varied. This is consistent with previous studies (Van and Spalding, 1999). When the growth phenotype of CC-503 was studied under different pH levels, it was noticed that the cells showed reduced growth at lower pH levels (pH 6.2) and a somewhat lesser reduction in growth at a high pH level of 8.2. This growth phenotype was often more severe when compared to the *cah1* mutant. While the *cah1* mutant cells could still grow at a low pH of 5.8, most of the CC-503 cells died at this low pH (Fig. 4).

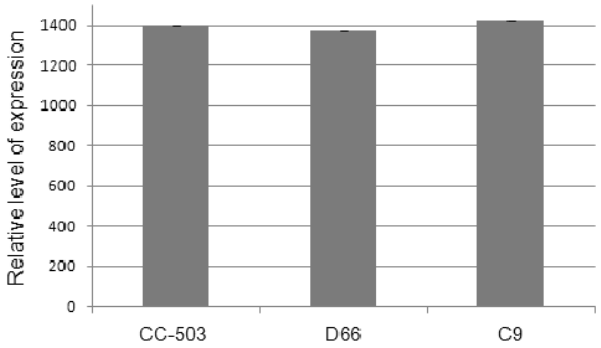

Fig. 3 qRT-PCR measurements of the relative abundance of the *CAH1* transcript in CC-503, in D66 and C9. The transcript levels shown are relative to transcript levels under high CO_2 conditions. The *CBLP* gene was used as an internal reference gene as it is of high abundance and its expression remains unchanged under varying CO_2 conditions.

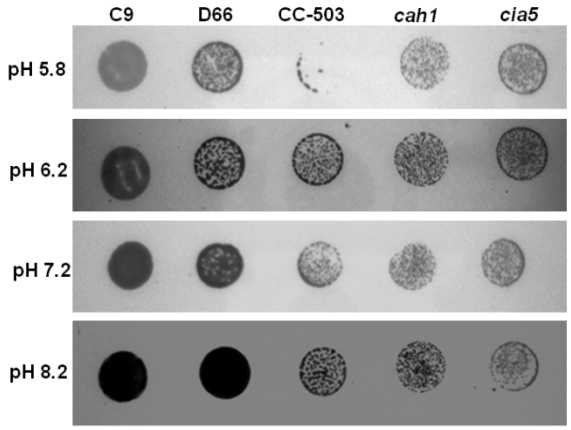

Fig. 4 Growth phenotype of CC-503, compared to other wild-type cells C9 and D66, when grown under low CO_2 conditions at different pH levels; *cah1*: CAH1 mutant, *cia5*: CCM mutant.

The ability of the CC-503 strain to induce an otherwise normal CCM was revealed by the presence of other key CCM proteins at levels comparable to other wild-type strains (Fig. 1), a trend shown by all laboratory generated *CAH1* mutant strains. The *CAH1* transcriptional regulator LCR1, (Yoshioka *et al*., 2004), is presumably functional in CC-503 as evident by the normal levels of LCI1, another protein that is

regulated by the same gene. The photosynthetic efficiency of CC-503 as measured by O_2 evolution assays at different pH levels showed that this strain does not deviate much from the other cell wall deficient wild-type strain D66. At a low pH level of 6.2, CC-503 cells showed a photosynthetic response similar to the mutant *cah1* (Fig. 5). The relative photosynthetic affinity for C_i in CC-503 cells was slightly lower than that of the other cell wall-less wild-type, D66, at pH 6.2. This trend was consistent at pH levels of 7.2 and 8.2 (data not shown).

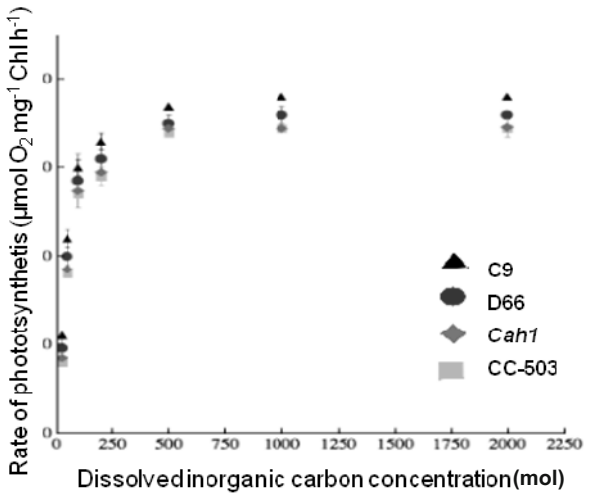

Fig. 5 The rate of photosynthesis in low CO_2 grown cells of D66 (●), CC-503 (□), cah1 (◆) and C9 (▲) measured as a function of the dissolved inorganic carbon concentration (provided by solutions of $NaHCO_3$ ranging from 25 μmol to 2 mmol). Experiments were carried out an external pH of 6.2 and each point represents the mean and standard deviation of three replicates.

Given the normal levels of photosynthesis and CCM induction in CC-503, it could be speculated that the growth phenotypes seen at lower pH values could be a result of the extreme cell wall deficiency shown in this strain due to the *cw-92* mutation that it carries. It is worthwhile to investigate whether other strains that carry this mutation are equally susceptible to low external pH levels. This report highlights the fact that CC-503 is a unique natural mutant for CAH1 as it lacks the protein despite normal levels of transcription, when compared to other wild-type strains. Hence, it could prove valuable in further elucidation of CAH1 regulation and function in *C. reinhardtii*.

References

Badger MR, Kaplan A, Berry JA (1980) Internal Inorganic Carbon Pool of Chlamydomonas Reinhardtii. Evidence for a CO_2 Concentration Mechanism. Plant Physiol 66: 407-413

Coleman JR, Grossman AR (1984) Biosynthesis of Carbonic Anhydrase in Chlamydomonas Reinhardtii during Adaptation to Low CO_2. Proc Natl Acad Sci USA 81: 6049-6053

Fukuzawa H, Fujiwara S, Yamamoto Y, Dionoso-Sere ML, Miyachi S (1990) cDNA Cloning, Sequence, and Expression of Carbonic Anhydrase in Chlamydomonas Reinhardtii: Regulation by Environmental CO_2 Concentration. Proc Natl Acad Sci USA 87: 4383-4387

Ishida S, Muto S, Miyachi S (1993) Structural Analysis of Periplasmic Carbonic Anhydrase 1 of Chlamydomonas Reinhardtii. Eur J Biochem 214: 9-16

Kucho K, Ohyama K, Fukuzawa H (1999) CO_2-Responsive Transcriptional Regulation of CAH1 Encoding Carbonic Anhydrase Is Mediated by Enhancer and Silencer Regions in Chlamydomonas Reinhardtii. Plant Physiol 121: 1329-1337

Moroney JV, Ynalvez RA (2007) A Proposed Carbon Dioxide Concentrating Mechanism. Eukaryot Cell 6: 1251-1259

Plaffl MW (2001) A New Mathematical Model for Relative Quantification in Real-Time PCR. Nucleic Acids Res 29: e45

Van K, Spalding MH (1999) Periplasmic Carbonic Anhydrase Structural Gene (Cah1) Mutant in Chlamydomonas Reinhardtii. Plant Physiol 120: 757-764

Ynalvez RA, Xiao Y, Ward AS, Cunnusamy K, Moroney JV (2008) Identification and Characterisation of Two Closely Related Beta-Carbonic Anhydrases from Chlamydomonas Reinhardtii. Physiol Plant 133: 15-26

Yoshioka S, Taniguchi F, Miura K, Inoue T, Yamano T, Fukuzawa H (2004) The Novel Myb Transcription Factor LCR1 Regulates the CO_2-Responsive Gene Cah1, Encoding a Periplasmic Anhydrase in Chlamydomonas Reinhardtii. Plant Cell 16: 1466-1477

Transcriptional Analysis of the Three Phosphoglycolate Phosphatase Genes in Wild Type and the *pgp1* Mutant of *Chlamydomonas Reinhardtii*

Yunbing Ma, Megan M Hartman, James V Moroney*

Department of Biological Sciences, Louisiana State University, Baton Rouge, USA, 70803.
*Corresponding author. Tel. No. +01 225 578 7152; E-mail: btmoro@lsu.edu.

Abstract: Phosphoglycolate phosphatase (PGPase) is an essential enzyme in the photorespiration pathway in plants and photosynthetic algae. In *Chlamydomonas reinhardtii*, mutants deficient in phosphoglycolate phosphatase (PGPase-1) were reported to require elevated levels of CO_2 for growth in the light. Here we described that this *pgp1* mutant reverted naturally and regained the ability to survive under low CO_2 conditions. Quantitative RT-PCR analysis demonstrated that the upregulation of *PGP2* in the *pgp1* revertants might contribute to this reversion in the growth phenotype.

Keywords: *Chlamydomonas reinhardtii*; Phosphoglycolate phosphatase; *Pgp1-1* mutation; PGPase isozyme

Introduction

In *Chlamydomonas reinhardtii*, chloroplast localized phosphoglycolate phosphatase (PGPase, EC 3.1.3.18), catalyzes the first reaction of the photorespiratory C2 cycle by dephosphorylating phosphoglycolate to glycolate (Husic and Tolbert, 1985). The glycolate formed can then either be oxidized to glyoxylate, a reaction catalyzed by glycolate dehydrogenase or be excreted to the surrounding medium (Moroney *et al*., 1986). Three putative PGPase genes, *PGP1*, *PGP2*, and *PGP3* have been identified in the JGI Chlamydomonas genome database (http://genome.jgi-psf.org/Chlre4/Chlre4.home.html). One mutant (18-7F) with a mutated *PGP1* isolated from *C. reinhardtii* has been identified, and this strain was reported to have a conditional lethal growth phenotype that required elevated concentrations of CO_2 for growth (Suzuki, 1995; Suzuki *et al*., 1990). The conditional lethal growth phenotype is presumably due to the lack of PGPase activity, resulting in the accumulation of phosphoglycolate which inhibits the Calvin Cycle (Anderson, 1971). In this mutant, a G to A point mutation created by EMS (ethylmethane sulfonate) at the beginning of the first intron destroyed the "GT" splice donor site, thus resulting in the fusion of the first exon, the first intron, and the second exon in the transcript, which eventually results in a nonfunctional PGPase. However, when the *pgp1* mutant was obtained from the Duke University Stock Center twenty years after its first characterization, it was found that its conditional lethal phenotype could no longer be observed. Even though the growth phenotype was lost during the prolonged storage of the mutant, the original splice mutation was still present. To explain this observation, a hypothesis was proposed that the other two PGPase isozymes (PGP2 and PGP3) might be up-regulated to compensate for the loss of the PGP1 function. Using Quantitative-RT PCR, this hypothesis was tested and revealed that the *PGP2* gene was upregulated and might be the factor that contributes to the phenotypic reversion in the *pgp1* mutant.

Materials and Methods

Cell Cultures and Growth

C. reinhardtii culture conditions were similar to those described previously (Rawat and Moroney, 1991). The *pgp1* mutant strain CC-2648 pgp1-18-7F, wild-type strains 2137, 137, and CC-503, were obtained from the Duke University Stock Center (http://www.chlamy.org). Strain D66 (nit2$^-$, cw15,

mt$^+$) was obtained from Rogene Schnell (University of Arkansas, Little Rock). Wild-type strain C9 was kindly provided by Dr. Hideya Fukuzawa (Kyoto University, Japan). To induce the CCM, cultures were switched to minimum liquid in low CO_2 for 3 h.

Quantitative RT-PCR analysis

RNA extraction and cDNA synthesis was performed as described previously (Ynalvez *et al*., 2008). Q-RT PCR primers used for this study were designed according to the following guidelines: (1) similar distance towards the 3' Poly (A) tail (approximate 150 bp); (2) Similar amplicon size (approximate 150 bp); (3) Tm around 60 °C and (4) GC% content around 50%. Considering the three PGPase genes all have relatively long 3'UTR, primers were chosen at the end of the 3'UTR instead of at the exon junction as is the normal procedure. The specificity of each primer is checked among the three PGPase genes. Primer sequences used for Q-RT PCR analysis are listed in Table 1.

Table 1 Primer sequences used in this study.

Q-RT PCR Primers	PGP1	5' GCAGAGTGTGTATCGGGTGTCG 3'
		5' TGGCCTTTGCACGCTTAAACCA 3'
	PGP2	5' TTTGTGTGGAGGCTGCGTCA 3'
		5' ACATGGTGCAACTTGTGGCGT 3'
	PGP3	5' TCTTGTTGTAGCGGCTCAGCTT 3'
		5' ATCTACAAGGTGCTCAAGCAGGTG 3'
	CBLP	5' ATTGCCATGCTGTGGGACC 3'
		5' CCACGATGCTCTTGCTCTCC 3'
	CAH4	5' TCTACTACAGCATCAGCCCG 3'
		5' ACGATCTTGAGCTTGCCCTCC 3'
PGP1Splice Mutation Test Primers		5' GTTCGCAGGATGGTTGCT 3'
		5' CAGGGACTGGAACTTGGA 3'

Results and Discussion

As its name indicates, the primary CO_2 fixation enzyme, ribulose 1.5-bisphosphate carboxylase-oxygenase (Rubisco) catalyzes not only the carboxylation but also the oxygenation of ribulose 1,5-bisphosphate. The potentially harmful product phosphoglycolate produced by oxygenase activity must be recycled through the photorespiratory pathway (Tolbert, 1997), otherwise the building-up of the phosphoglycolate would exert a potent inhibitory effect on triose phosphate isomerase and carbon recycling in the Calvin Cycle (Anderson, 1971). A mutant lacking a functional PGP1 was reported not able to grow under low CO_2 conditions (Suzuki *et al*., 1990). However, we found that this strain, maintained in our lab (refer to *pgp1-1-old*) had regained the ability to grow under low CO_2 conditions. This was perhaps not surprising as Suzuki (1995) was able to obtain a number of revertants in a screen and many of these were second-site suppressor mutations. We also ordered a new culture of the *pgp1* strain from the stock center (Refer to *pgp1-1-new*). However, both the one maintained in our laboratory and the one newly ordered from the Duke Chlamy center showed the reverted phenotype and could survive as well as its parental strain 2137, under low CO_2 on minimum medium (Fig. 1). Efforts were made to isolate single colonies which might still lack the ability to grow under low CO_2 conditions. One of the isolates named *pgp1-1-18* showed a little reduction in growth, but for the most part the cultures had regained the ability to grow under low CO_2 conditions.

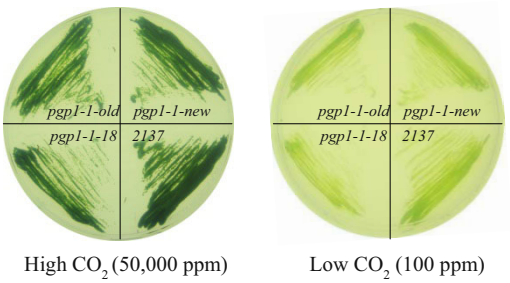

Fig. 1 Growth phenotype of the *pgp1* mutants under high (left panel) and low CO_2 (right panel) conditions. Although the three *pgp1-1* mutants exhibited relatively lower growth compared to the parent strain 2137, they could still survive under low CO_2 conditions, as opposed to "lethal phenotype" reported originally (Suzuki *et al*., 1990; with permission from Suzuki *et al.*).

One possible explanation for this observation was that the G to A mutation has reverted, resulting in the normal full length *PGP1* message. However, PCR amplification from the cDNA from all the *pgp1* mutants demonstrated that the original mutation was still present as evidenced by the extended exon size in the mutants (Fig. 2). The positions of the primers used for this analysis were indicated in Fig. 3, spanning the 2nd, 3rd and the 4th exons. The addition of the 1st intron in the mutant cDNA added an extra 81 bp to the wild-type cDNA. Since the original *PGP1* mutation was still present, it is worth noting that *C. reinhardtii* has multiple putative PGPase genes in its genome (Fig. 3). Comparison of the predicted amino acid sequences of the *PGP2* and *PGP3* with that of *PGP1* showed that they were similar and all consensus motifs of *p*-nitrophenyl phosphatases were present (Suzuki *et al*., 2005).

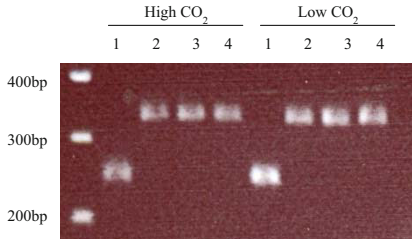

Fig. 2 The extended 1st exon caused by the point mutation at the splice donor site was present in all the *pgp1-1* mutants investigated. 1: wild-type strain 2137; 2: *pgp1-1-old*; 3: *pgp1-1-new*; 4: *pgp1-1-old-18*.

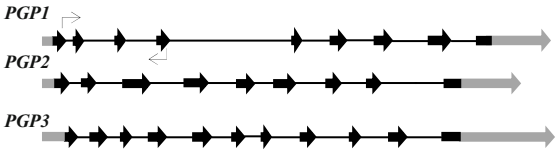

Fig. 3 Gene model of the three *PGPase* in *C. reinhardtii*. Exons are depicted with black arrows and introns are depicted with small black solid lines. Grey regions represent the UTRs. Primers used to differentiate the mutant and wild-type cDNA are displayed.

A second possible explanation is that *PGP2* or *PGP3*, or both were compensating for the loss of *PGP1*. To test this hypothesis, Q-RT-PCR was performed to determine the relative expression level of the three PGPase isozymes among five wild-type strains (including the parental strain 2137; D66, a strain often used in our laboratory; CC-503, the genome sequence reference strain; and two other wild-type strains C9, and 137), as well as three *pgp1* mutant strains (*pgp1-1-old*, *pgp1-1-new* and *pgp1-1-18*). The CCM transcriptional regulator deficient strain *cia5* was used as a negative control, since genes of the photorespritory pathways would not be expected to be induced in this mutant background.

The Q-RT PCR results (Fig. 4) revealed that in all the wild-type strains tested, *PGP1* was the most highly expressed of the *PGP* genes. In addition, *PGP1* expression was significantly upregulated under low CO_2 conditions, typically about 2 fold on average. The increased expression of *PGP1* under low CO_2 conditions is consistent with the earlier report of Marek and Spalding (1991), and of Tural and Moroney (2005). In the CCM mutant, *cia5*, the up-regulation of *PGP1* is not seen. This was also observed by Tural and Moroney (2005) that the expression of the many photorespiratory genes under low CO_2 was apparently under the control of the CIA5 transcriptional regulator. All strains with the exception of *cia5* showed a strong induction of the CCM under low CO_2 conditions as judged by the induction of expression of the carbonic anhydrase gene *CAH4*. In contrast, the expression pattern of the *PGP* genes in all the isolates of the *pgp1* mutants was different from wild-type strains (Fig. 5). In all three isolates tested, the expression of *PGP2* was significantly higher than the expression of *PGP1*. In addition, the expression of *PGP2* did not change appreciably under low CO_2 conditions. In these isolates, *PGP2* expression remained relatively high under both high and low CO_2 growth conditions.

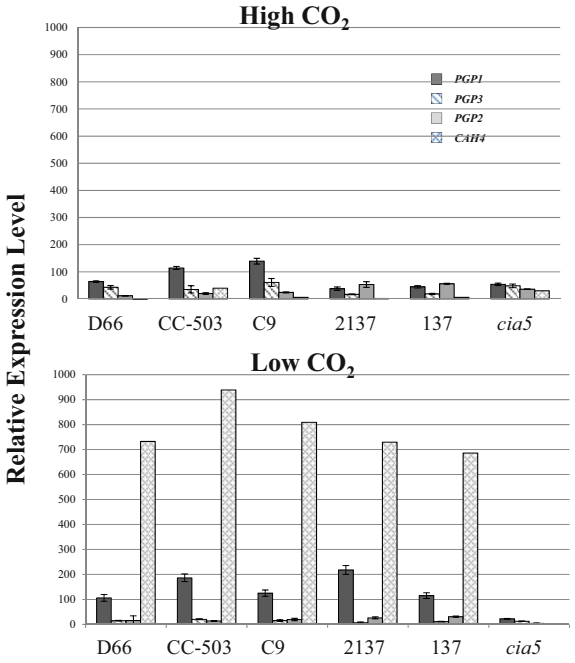

Fig. 4 Quantitative RT-PCR results for phosphoglycolate phosphatase genes under high (upper panel) and low CO_2 (lower panel) conditions in a variety of wild-type strains listed. The carbonic anhydrase *CAH4* was used as a positive control for effective CCM induction.

Originally characterized by Suzuki *et al*. (1990), the *pgp1-1* mutant was reported to have a defect in growth when under low CO_2 conditions. The G to A mutation on the splice donor site created an extended exon and an early translation stop, which resulted in a non-functional truncated PGPase Suzuki *et al*. (1990). However, after twenty years since its first discovery, this mutant was observed to regain the ability to grow under limited CO_2, although the original splice mutation was still present in all the isolates tested.

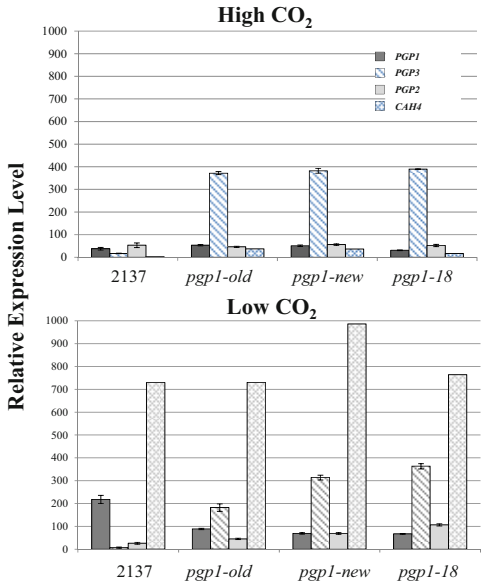

Fig. 5 Q-RT-PCR results for phosphoglycolate phosphatase genes under high (upper panel) and low CO_2 (lower panel) conditions in *pgp1* mutants and the parental strain 2137.

In an attempt to explain this observation, a hypothesis was proposed that the other two PGP isozymes might be compensating for the loss of PGP1. Q-RT PCR analysis revealed that, in contrast to the upregulation of *PGP1* in the wild-type strains under low CO_2 conditions, the *PGP1* message was relatively unchanged in all three *pgp1* isolates. This was unexpected since the *PGP1* mutation was found on the splice donor site of the coding region, unless this part of the *PGP1* DNA is involved in CCM transcriptional regulation under low CO_2 conditions. However, this observation could also be explained with the accumulation of the nonfunctional PGPase, or the accumulation of the phosphoglycolate or other Calvin Cycle intermediates could serve as a feedback signal that inhibits the induction of the *PGP1* gene in the mutants.

More importantly, despite the minimal level of *PGP1*, the *PGP2* message was significantly upregulated in all three *pgp1* isolates. This upregulation, although present in both high and low CO_2, could likely be regarded as a compensation mechanism for the loss of the PGPase activity in the mutants. The current method for maintaining most of the strains, including the *pgp1* mutants is to keep on tris-acetate plates in the light in room air. In this situation, most of the time cells are growing mixotrophically, especially considering the acetate in the plates can be depleted over time. Without the functioning of the phosphoglycolate phosphatases, the phosphoglycolate produced from Rubisco oxygenation would have accumulated to an extent that *pgp1* mutants could not survive under routine laboratory maintenance conditions. Under this pressure, it could be speculated that the *PGP2* was upregulated through unknown mechanism to serve as a back-up enzyme to recycle the phosphoglycolate and complement the *pgp1* mutation.

Acknowledgment

This work was supported by NSF grant IOS-0816957.

References

Anderson LE (1971) Chloroplast and Cytoplasmic Enzymes. Ii. Pea Leaf Triose Phosphate Isomerases. Biochim Biophys Acta 235: 237-244

Husic HD, Tolbert NE (1985) Properties of Phosphoglycolate Phosphatase from Chlamydomonas Reinhardtii and Anacystis Nidulans. Plant Physiol 79: 394-399

Moroney JV, Wilson BJ, Tolbert NE (1986) Glycolate Metabolism and Excretion by Chlamydomonas Reinhardtii. Plant Physiol 82: 821-826

Rawat M, Moroney JV (1991) Partial Characterization of a New Isoenzyme of Carbonic Anhydrase Isolated from Chlamydomonas Reinhardtii. J Biol Chem 266: 9719-9723

Suzuki K (1995) Phosphoglycolate Phosphatase-Defident Mutants of Chlamydomonas Reinhardtii Capable of Growth under Air. Plant And Cell Physiology 36: 95-100

Suzuki K, Marek LF, Spalding MH (1990) A Photorespiratory Mutant of Chlamydomonas Reinhardtii. Plant Physiol 93: 231-237

Suzuki K, Uchida H, Mamedov TG (2005) The Phosphoglycolate Phosphatase Gene and the Mutation in the Phosphoglycolate Phosphatase-Deficient Mutant (Pgp1-1) of Chlamydomonas Reinhardtii. Canadian Journal Of Botany 83: 842-849

Tolbert NE (1997) The C2 Oxidative Photosynthetic Carbon Cycle. Annu Rev Plant Physiol Plant Mol Biol 48: 1-25. Doi:10.1146/Annurev.Arplant.48.1.1

Ynalvez RA, Xiao Y, Ward AS, Cunnusamy K, Moroney JV (2008) Identification and Characterization of Two Closely Related B-Carbonic Anhydrases from Chlamydomonas Reinhardtii. Physiologia Plantarum 133: 15-26

Symposium 11

C_3, C_4 and CAM and Genetic Engineering

Effects of 1-butanol, Neomycin, and Calcium on the Photosynthetic Characteristics of *pepc* Transgenic Rice

Xia Li*, Chao Wang, Chenggang Ren

Institute of Food Crops, Jiangsu High Quality Rice R&D Center, Jiangsu Academy of Agricultural Sciences, Nanjing, Jiangsu Province, 210014, China.
*Corresponding author. Tel. No. 00862584390361; Fax No. 00862584390322; E-mail: jspplx@jaas.ac.cn.

Abstract: The effects of 1-butanol, neomycin, and calcium on the photosynthesis of *pepc* transgenic rice were studied with over-expressed *pepc* transgenic rice (PC) of the 8th generation as study materials and with non-transgenic wild type (WT) rice and maize, a typical C_4 plant, as control. The results indicated that 0.04% 1-butanol, 0.1 mmol L^{-1} neomycin, and 0.05 mmol L^{-1} calcium ions had not a significant effect on the net photosynthetic rate (P_n) of the three tested materials. The stepwise multiple linear regression analysis showed that the *pepc* transgenic rice maintained its relative high net photosynthesis rate through increasing stomatal conductance. It was proved by the scanning electron microscope (SEM) that compared with the WT, the stomatal density of PC leaves increased while the stomatal aperture also increased under the 1-butanol treatment. The separate1-butanol treatment significantly inhibited the PEPC activity of PC and maize leaves, while neomycin treatment alone had no significant effects on the PC and maize. However, the combined treatment with 1-butanol and neomycin evidently promoted the PEPC activity of PC and WT. Moreover, exogenous calcium significantly promoted the PEPC activity of the three materials. It is clear that the exogenous regulation on PEPC enzyme of *pepc* transgenic rice is different from both C_4 and C_3 plants.

Keywords: PEPC; 1-butanol; Neomycin; Photosynthesis; Stomatal

Introduction

The successful transfer of the phosphoenolpyruvate carboxylase (*pepc*) from C_4 maize into rice and its over-expression clearly promote rice photosynthesis, which has triggered an upsurge of strengthening C_4 photosynthetic characteristics in C_3 plants in order to enhance its photosynthetic efficiency. This is of great significance to raise rice production by increasing the photosynthetic capacity (Ku *et al.*, 1999; Fukayama *et al.*, 2002). In recent years, with the stable breeding of the transgenic rice over-expressing maize *pepc*, an increasing number of studies have demonstrated that it has a high photosynthetic efficiency and various stress resistances against oxidation and drought, etc(Jiao *et al*., 2001; Huang *et al*., 2002; Jiao *et al*., 2003; Li *et al*., 2005). The way that a single transferred C_4 *pepc* gene drives this complex photosynthesis of C_3 rice is an interesting scientific topic. When studying phosphatidic acid (PA) in plants, Christa Testerink (2004) found that PEPC could act as the target of PA and take precedence over other phospholipids in combination with PA. PA, as an inositol-dependent metabolism regulator, has certain functions in the signaling transduction pathway (Loewen *et al.*, 2004). PA is an important lipid signal molecule which can be produced by two different pathways, namely, phospholipase D (PLD) and phospholipase C (PLC) pathways. These two pathways may exist in different subcellular sites and start from different phosphate precursors, showing different specific activity towards downstream targets (Munnik *et al.*, 2004; Testerink *et al.*, 2005). Moreover, the Phosphoinositide pathway and intracellular calcium may play an important regulatory role in the light-dependent phosphorylation of C_4 PEPC (Coursol *et al.*, 2000; Giglioli *et al.*, 1996; Gousset *et al.*, 2005; Jose *et al.*, 2007; Li *et al.*, 2010).

PA can regulate cell processes in different modes

and perform various biological functions at different times, spaces, and concentrations (Wang *et al.*, 2006). Although PEPC has been proved to act as a target of PA, its mechanism remains unclear. With *pepc* transgenic rice as a unique material, the study of impact of PA on its photosynthetic characteristics may be helpful to reveal the regulatory characteristics of PA signaling pathway towards the exogenous PEPC of *pepc* transgenic rice. In this paper, PLD specific inhibitor, 1-butanol (Munnik *et al.*, 2001), and PLC specific inhibitor, neomycin (Van *et al.*, 1988), were used to inhibit respectively the production of PA from different sources, while calcium was applied to regulate the PEPC phosphorylation state in hope of finding the way to regulate the C_4 *pepc* transgenic rice to enhance the photosynthetic rate via the PA signaling pathway.

Materials and methods

Experimental Materials: A stable pepc transgenic rice (PC) of the 8th generation (*Oryza sativa* L.), wild type rice, Kitaake (WT) (*Oryza sativa* L.), and maize, Nongda 108 (*Zea mays* L.), was used in this study. The PC with 4–7 d after blossom, the flag leaf of WT and the last first leaf under tassel of maize were collected for indices measurement during 9:00–11:00 am on a sunny summer day in Nanjing, with the light intensity of (1200 ± 100) μmol m^{-2} s^{-1} and temperature (33 ± 2) °C. The treatment solutions containing 1-butanol, neomycin, and calcium chloride were absorbed by the leaf sheath with the concentration 0.04%, 0.1 mmol L^{-1} and 0.05 mmol L^{-1}, respectively. Net Photosynthetic Rate, Chlorophyll fluorescence parameters, PEPC Enzyme Activity, Protein extraction and electrophoresis, Western blot analysis, Gene Transcription of PEPC andScanning Electron Microscopy (SEM) were all measured in the leaves of different treatments.The disparity analysis was conducted with statistical software SPSS13.0; the stepwise multiple linear regression analysis of the material photosynthetic parameters was carried out with DPS statistical software; the quantitative analysis of the SDS-PAGE and RT-PCR bands was obtained via Band Scan5.0 and Band leader, respectively; data were processed and mapped with Excel 2003.

Results and Discussion

Fig. 1 indicates that the net photosynthetic rate (Pn) of PC flag leaf was significantly higher than that of WT with a significant difference ($P < 0.05$). Furthermore, there was a significant difference ($P > 0.05$) in terms of Pn between three materials treated with 1-butanol, neomycin, and calcium ions and the untreated control group. With 1-butanol, the percentages of Pn between before and after treatments were 54.90% of PC, 97.96% of WT and 72.26% of maize; with neomycin, those were 95.23% of PC, 91.13% of WT and 98.30% of maize with ; with calcium ions, those were 84.92% of PC, 112.44.96% of WT and 102.30% of maize At the same time, the treatment solutions had no evident effects on stomatal conductance (Fig. 1) and intercellular CO_2 concentration (data not shown). However, through the SEM observation, the average stomatal density was 225 mm^{-2} on the back of PC leaves, significantly higher than that of WT with 185 mm^{-2} (data not shown), showing that the high photosynthetic capacity of PC was not only related to CO_2 concentrating mechanism in PC (Jiao *et al.*, 2003), but also to its stomatal density,

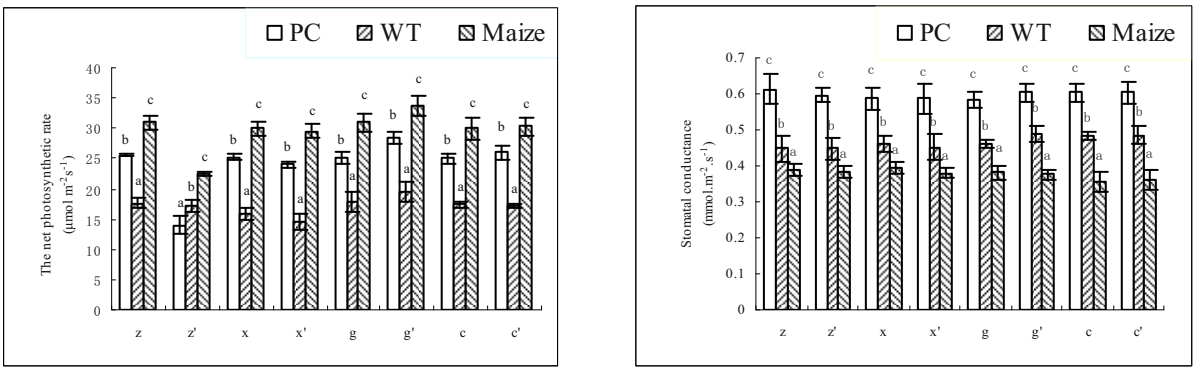

Fig. 1 Effects of 1-butanol, neomycin and calcium on photosynthesis and stomata conductance of the PC, WT and maize. Values followed by a different letter are significantly different at the 0.05 probability level. z: before 1-butanol treatment; z': after 1-butanol treatment; x: before neomycin treatment; x': after neomycin treatment; g: before calcium treatment; g': after calcium treatment; c: before control treatment; c': after control treatment.

which was different from the previous studies (Huang *et al.*, 2002). It seems that the regulation of high photosynthetic efficiency in PC may be involved in the inositol phosphate signaling pathways of phospholipase D (PLD) mediated by PA so as to regulate stomatal movement.

The effects of 1-butanol, neomycin, and calcium on the PEPC activity of the tested materials showed (Fig. 2) that 1-butanol inhibited the PEPC activity of PC and maize by 25.7% and 10.2%, respectively (Figs. 2A and 2C), but promoted PEPC activity of WT by 16.8% (Fig. 2B), all in significant differences ($P < 0.05$); neomycin had no significant effect on PC and maize, but it resulted in an increase of 17.9% in PEPC activity of WT ($P < 0.05$); calcium cleared with EGTA in cells significantly inhibited the PEPC activity of the three materials, among which the effect on PC was the most significant with a percentage of 22.9%. Calcium could also clearly promote PEPC activity of the three materials when added alone. The PEPC activity of PC was promoted by 66.8%, the most significant among the three materials ($P < 0.05$). The results indicated that the trend of the effects on the exogenous PEPC activity of PC was similar to that of maize when 1-butanol and neomycin were added separately, but the effect on PC was significantly stronger than that of maize. At the same time, calcium also promoted the PEPC activity of PC and WT after they had been treated by the combined solution of 1-butanol and neomycin, registering an increase of 32.4% in PEPC activity of PC, higher than the result of the treatment with calcium. This treatment also offset the 1-butanol inhibition of PEPC activity. However, the PEPC activity of maize under this treatment was decreased, showing that change of exogenous PEPC enzyme in PC was markedly different from that of maize under this condition. The statistical analysis of western blot and RT-PCR bands showed that PEPC protein and gene expression did not change significantly after the 1-butanol, neomycin, and calcium treatments of the three materials (data not shown). Structurally, *pepc* transgenic rice enhances stomatal conductance by increasing the leaf stomatal density, thus affecting its photosynthetic characteristics.

Acknowledgement

The authors are grateful to the National Natural Science Foundation of China (NSFC, No. 30871459) for their financial support.

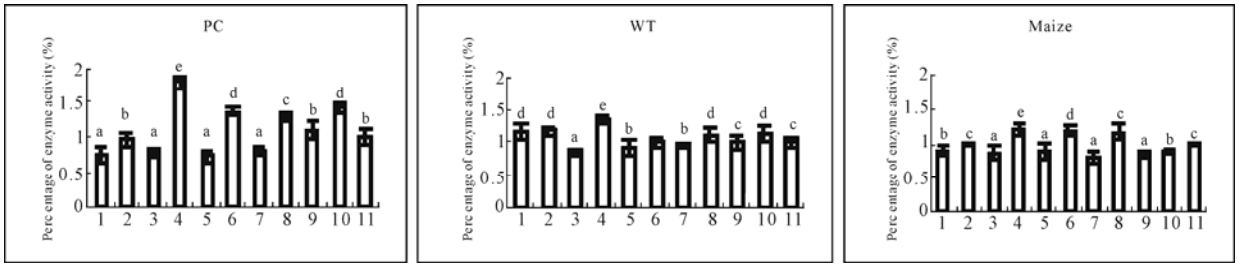

Fig. 2 Effects of 1-butanol, neomycin and calcium ions on the activity of PEPC of the PC, WT and maize.
Values followed by a different letter are significantly different at the 0.05 probability level. 1:the treatment of 1-butanol; 2; the treatment of neomycin;3: the treatment of EGTA;4: the treatment of calcium; 5: the treatment of 1-butanol after treatment of EGTA;6: the treatment of 1-butanol after treatment of EGTA and then treatment with calcium;7: the treatment of neomycin after treatment of EGTA;8: the treatment of neomycin after treatment of EGTA and then treatment with calcium; 9:the treatment of neomycin and 1-butanol after treatment of EGTA;10: the treatment of neomycin and 1-butanol after treatment of EGTA and then treatment with calcium;11:control.

References

Jiao DM, Kuang TY, Li X, Ge QY, Huang XQ (2003) Physiological Characteristics of the Primitive CO_2 Concentrating Mechanism in PEPC Transgenic Rice. Science in China 46: 438-446

Testerink C, Dekker HL, Lim ZY, Johns MK, Holmes AB, Koster CG, Ktistakis NT, Munnik T (2004) Isolation and Identification of Phosphatidic Acid Targets from Plant. Plant J. 39(4): 527-536

Li X, Wang C, Ren C, Cong W, Jin L, Guo S (2010) Change of Micro-Structure in Transgenic Rice of Pepc Gene from Maize with High Photo-Efficiency under the Strong Light with 1-Butanol Treatment. Acta Bot. Boreal. Occodemt. Sin. 30: 1614-1621

Some Physicochemical Properties of Carbonic Anhydrase in *Mesembryanthemum Crystallinum* Leaves

Bayramov Sh*, Orujova T, Babayev H, Guliyev N

Institute of Botany, Padamdar shosse 40, AZ-1073, Baku, Azerbaijan.
*E-mail: sbayramov@hotmail.com.

Abstract: CA extracted from the leaves of C_3 plants as well as CAM mode *M.crystallinum* plants which had been watering with 0.4 mol NaCl for a week manifested a wide range of the pH optimum. The extractable activity of CA from *M. crystallinum* was similar to that of C_3 and C_4 higher plants. Subcellular localization of CA from C_3 plants and leaves of the CAM mode *M. crystallinum* has been investigated using percoll gradient. There were not distinct differences in the subcellular localization of CA activity between C_3 and CAM mode plants. We have investigated an influence of 1,10-phenenthroline on the CA activity from *M.crystallinum* leaves, depending on pH and temperature of the medium. In neutral and weak alkaline medium (pH 7.0–7.4), at temperatures above 30 °C 1,10- phenanthroline completely inactivated the enzyme for 2 h. At the low concentrations DTNB (0.5–1.5 mmol) inhibited 40% of the enzyme activity for 30 min, whereas 3.0–4.0 mmol DTNB at pH 7.8-8.3 eliminated the activity of the enzyme for 60 min. CA was no sensitive to H_2O_2. Oxidased glutation and sodium- nitroprusside on CA from *M. crystallinum* leaves did not effect on the enzyme activity.

Keywords: Carbonic anhydrase; *M. crystallinum*; Localization; Zinc; SH-group

Introduction

Carbonic anhydrase (EC 4.2.1.1) (CA) is a zinc-containing enzyme that catalyzes the reversible dehydration of HCO_3 to CO_2. In photosynthetic organisms, the carbonic anhydrases are involved in diverse physiological processes such as ion exchange, acid/base balance, carboxylation/decarboxylation reactions and inorganic carbon diffusion between the cell and its environment as well as within the cell. Our understanding of the role that CA plays in the functioning of CAM photosynthesis is very limited. With the exception of one study by Tsuzuki *et al*.(1982) on activities and localization of CA in a variety of CAM species, little has been done on this group of plants. CAM is a relatively widespread adaptation to drought stress which has evolved in up to 7% of higher plants and permits the uptake of CO_2 at night. CAM plants can take up CO_2 at night when CA is the first enzyme required for the fixation of inorganic carbon (as is the case in C4 plants). Currently there are very rare data available on CA in CAM, although on theoretical grounds it must be expected that CA is very important in CAM (Luttge, 2002). However, during the day in CAM plants, CO_2 is fixed via the C_3 pathway. Although there have been few studies on the catalytic properties of CA in CAM plants, observations on the variation in intracellular localization of this enzyme between different CAM species have remained an enigma for over 25 years.

Materials and Methods

Plant Material

Common ice plant (*Mesembryanthemum crystallinum*) seeds were grown in a greenhouse under natural daylight supplemented with high-pressure sodium lamps providing a photon flux density of 350 μmol m^{-2} s^{-1} on a 12-h light (26 °C)/12-h dark (18 °C) cycle. Five-week-old plants were irrigated with 0.5x Hoagland solution containing 0.3 mol NaCl for 14 day. This treatment was found to give uniform and adequate stress to fully induce CAM. to a neutral

endpoint, as indicated by phenolphthalein or direct measure with a pH meter, and leaf titratable acidities were expressed as μmol H^+ g^- fresh weight.

Carbonic Anhydrase Assay

CA activity was determined with the the electrmetrically method of Wilbur and Anderson (1948).

Results and Discussion

Optimum conditions for the determination of this enzyme in some CAM plants have been established. CA extracted from the leaves of C_3 plants as well as CAM mode *M. crystallinum* plants which had been watering with 0.4 mol NaCl for a week manifested a wide range of the pH optimum. pH optimum of this enzyme was found to be pH 7.0 to 8.3, irrespective of the preincubation condition.The extractable activity of carbonic anhydrase from *M. crystallinum* was similar to that of C_3 and C_4 mode plants. Subcellular localization of CA from C_3 plants and leaves of the CAM mode *M. crystallinum* has been investigated using percoll gradient. There were not distinct differences in the subcellular localization of CA activity between C_3 and CAM mode plants. In both types 60% of the total activity was localized in the chloroplast fraction while 40% in cytosole. (Table 1) The activity of the carbonic anhydrase from *M. crystallinum* was not inhibited by different concentrations (50–500 mmol) of NaCl (Table 2).

Table 1 Distribution carbonic of carbonic anhydrase activity of *M. crystallinum* leaves.

M. crystallinum	% distribution	
	cytosol	chloroplast
C_3 mode	37,8	62,2
CAM mode	40,0	60,0

Table 2 Effects of NaCl on the carbonic anhydrase activity activity of *M.crystallinum* leaves.

Consentration NaCl (mmol)	CA activity mL WA/unit
0	135
50	135
100	135
150	135
200	135
400	135

We have also investigated an influence of 1,10-phenenthroline, forming metal complex with Zn atoms, on the CA activity from *M. crystallinum* leaves, depending on pH and temperature of the medium (Figs. 1 and 2). In neutral and weak alkaline medium (pH 7.0–7.4), at temperatures above 30 °C 1,10-phenanthroline completely inactivated the enzyme for 2 h. However at pH 7.6–8.3 for the complete loss of the enzyme activity under the agent influence a long period was required.

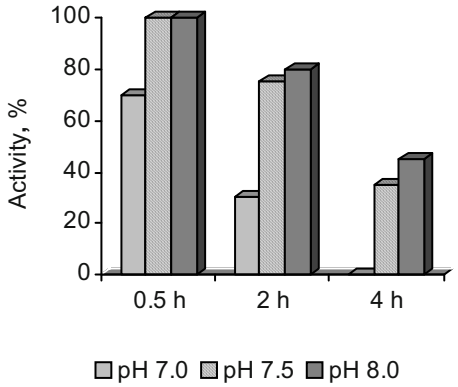

Fig. 1 Effects of 1,10-phenanthroline (2 mmol) on the carbonic anhydrase activity of *M. crystallinum* leaves (30 °C).

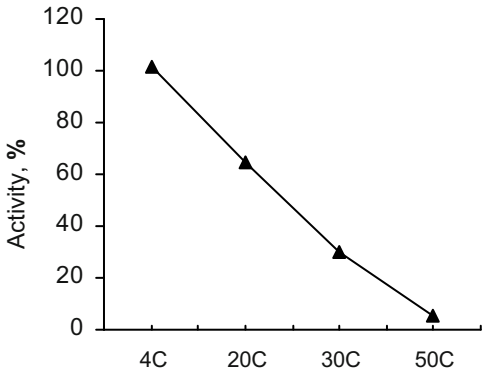

Fig. 2 Effects of temperature on the inactivation carbonic anhydrase activity by 2 mmol 1,10-phenanthroline during 2 h *M. crystallinum leaves*.

Unlike animal CAs, the plant enzyme was sensitive to oxidation, and reducing conditions in vitro were required to maintain the enzyme in its most active form (Guliyev *et al*., 2003). In assay medium lacking reducing agents the enzyme looses its activity quickly. Higher plants carbonic anhydrase gene expression and activity is regulated by light Since, thiol oxidation was shown to inhibit C_3 and C_4 higher plant carbonic anhydrase activities, we examined the

effects of the following two types of oxidizing agents on the carbonic anhydrase in *M. crystallinum*. First oxidant may form intermolecular mixed disulfide bonds, including 5,5-dithiobis (2 nitro-benzoic acid) (DTNB) and peroxide that produces a disulfide bond which may be oxidized further to sulfenate, sulfinate or sulfonate derivatives of cysteine. The time-dependent inactivation of CA by the different thiol-modifying agents was performed at room temperature. At the low concentrations DTNB (0.5–1.5 mmol) inhibited 40% of the enzyme activity for 30 min, whereas 3.0–4.0 mmol DTNB at pH 7.8–8.3 eliminated the activity of the enzyme for 60 min (Fig. 3).

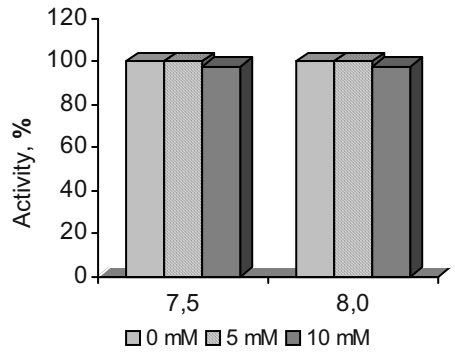

Fig. 3 Effects of DTNB on the carbonic anhydrase activity of *M.crystallinum* leaves.

Carbonic anhydrase was no sensitive to H_2O_2. Incubation of carbonic anhydrase in different concentrations of H_2O_2 (10–50 mmol) did not inactivate the enzyme activity (Fig. 4).

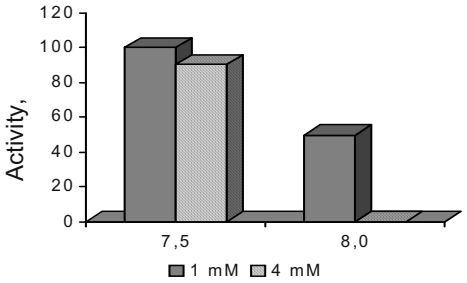

Fig. 4 Effects of H_2O_2 on the carbonic anhydrase ac activity of *M. crystallinum* leaves.

The addition of the monothiol reducing agent 2-mercaptoethanol and dithiol reducing agent DTT did not increase the *M. crystallinum* carbonic anhydrase activity. Obtained results indicate the enzyme insensitivity to redox state confirming that CA isolated from *M. crystallinum* leaves in the contrary to other CAs from higher plants maintains its catalytic activity for a long time in the absence of SH-group reducing agents. A recent work has established glutathiolation (Dalle-Donne *et al*., 2007) and nitrosothiolation of protein thiols (Lindermayr *et al*., 2005) as two other highly important thiol modification reactions affecting many cell protein functions also in plant cells. To study the effect of S-glutathionylation on CA from *M. crystallinum* leaves 5 to 10 mmol concentrations of the oxidized glutathione were used. There was no effect on the enzyme activity independently on the medium pH or the duration of the interaction (Fig. 5).

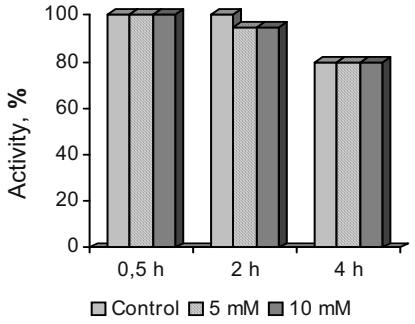

Fig. 5 Effects of oxidized glutathione on the carbonic anhydrase activity of *M. crystallinum* leaves.

S-nitrosylation of the enzyme was also investigated using sodium nitroprusside (nitric oxide donor) as the S-nitrosylation agent. As oxidized glutathione, sodium nitroprusside in 1–2 mmol concentrations had also no effect on the enzyme activity (Fig. 6).

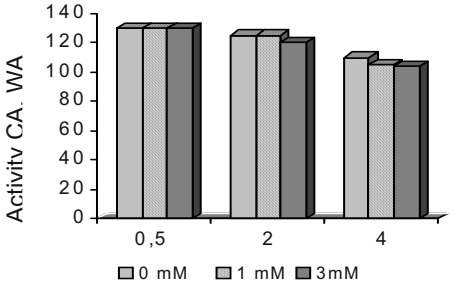

Fig. 6 Effects of sodium nitroprusside on the carbonic anhydrase activity of *M. crystallinum* leaves.

Some researchers propose that activation of higher plant carbonic anhydrase occurs via ferredoxin-thioredoxin system. In addition, in thioredoxin trapping approaches, where the resolving cysteinyl group was changed for serine, carbon anhydrase was identified as target of thioredoxin (Buchanan and

Balmer, 2005). Impact of reagents of carbonic anhydrase enzyme extracted from *M. crystallinum* leaves that oxidize SH groups on activity of carbonic anhydrase enzyme extracted from C_3 plants wheat and chickpea, as well as extracted from C_4 plants amaranth and millet is similar. It gives a ground to put forward a conception that redox regulation of carbonic anhydrase which have diverse of photosynthetic carbon assimilation pathways is undertaken in similar way.

References

Buchanan BB, Balmer Y (2005) Redox Regulation: a Broadening Horizon. Ann Rev Plant Biol 56: 187-220

Dalle-Donne I, Rossi R, Colombo G, Giustarini D, Milzani A (2009) Protein Sglutathionylation: a Regulatory Device from Bacteria to Humans. Trends Biochem Sci 34: 85-96

Guliev NM, Babayev HG, Bayramov ShM, Aliev JA (2003) Purification, Properties, and Localization of Two Carbonic Anhydrases from Amaranthus Cruentus. Russian Journal of Plant Physiology 50(2): 213-219

Lindermayr C, Saalbach G, Durner J (2005) Proteomic Identification of S-Nitrosylated Proteins in Arabidopsis. Plant Physiol. 137: 921-930

Luttge U (2002) CO_2-Consentrating: Consequences in Crassulacean Acid Metabolism. J.Exp.Botany. 53: 2131-2142

Tsuzuki M, Miyachi S, Winter K, Edwards GE (1982) Localization of Carbonic Anhydrase in CAM Plants. Plant Science Letters 24: 211-218

Wilbur KM, Anderson NG (1948) Electrometrik and Colorimetric Determination of Carbonic Anhydrase. J Biol Chem 179: 147-154

Symposium 12

T Regulation of Photosynthetic Gene Expression

GTP-Binding Proteins are Potential Messengers for Photosygnal Transduction in High Plants

Karim Gasimov

Institute of Botany, ANAS, 40 PatamdarShosse, Baku AZ1073, Azerbaijan.
Tel. No. 994 12 438 11 64; E-mail: gasimov-k@botany-az.org.

Abstract: The effect of special analog of GTP – Gpp(NH)p (Guanylyl(βγ-imido)diphosphate) on the activities of adenylylcyclase (AC) and guanylylcyclase (GC) isolated from etiolated sorghum seedlings was studied. The investigation revealed that Gpp(NH)p activates only that adenylylcyclase which isolated from irradiated by red light seedlings, but adenylylcyclase isolated from etiolated seedlings hasn't reacted on the action of Gpp(NH)p. In contrast to adenylylcyclase the guanylylcyclase isolated from irradiated by red light sorghum seedlings negatively reacted to the action of Gpp(NH)p. Obtained results supports the idea that G-proteins are potential transducers for transduction of photosygnals downstream of plant photoreceptors phytochromes.

Keywords: Signal transduction; Phytochrome; G-proteins; Cyclases

Introduction

G-proteins are involved in a wide range of processes which control important cell activities like cell sensory transduction, cell division, differentiation etc (Mello *et al*., 2002). A variety of investigations have shown that in high plants heterotrimer G-proteins are involved in transduction of photosignals initiated by red (R) and far red (FR) lights (Jones *et al*., 2003). The classic example of the molecular mechanism of photosignal transduction by heterotrimeric G protein to a downstream effector is vision in animals (Baylor, 1996) where the alpha subunit of the cognate heterotrimeric complex, transducin, couples the activated heptahelical membrane receptor rhodopsin to its cGMP phosphodiesterase effector in rod photoreceptor cells (Morris and Malbon, 1999). Plant cells are also light sensitive, especially in the red (R)/far-red (FR) light spectral region due to its highly light-sensitive family of photoreceptors called phytochrome. Therefore, an obvious question has been whether phytochrome light perception is similarly coupled by a heterotrimeric G protein to an unidentified downstream effector, whether cyclic-AMP an/or cyclic-GMP systems can be effector(s) for transduction of light signals transduced by G-proteins. Initially printed two articles in western journals (Neuhaus *et al*., 1993; Bowler *et al*., 1994) and the same time our paper (Fedenko and Kasumov, 1993) positively answered to these questions.

The studies have shown that the special analog of GTP – Gpp(NH)p increase the activity of phosphodiesterase (PDE) which isolated from etiolated maize seedlings irradiated by red light (Fedenko and Kasumov, 1993), but did not affect on the activity of PDE isolated from nonirradiated seedlings. The investigations have also revealed that some phenotypes of a tomato (*Lycopersicon esculentum*) phytochrome mutant could be rescued to wild type by pertussis and cholera toxins, agents that stabilize the activated form of the G protein subunit by different means (Neuhaus *et al*., 1993; Bowler *et al*., 1994). Microinjection of cGMP into aurea cells restored phytochrome mediated effects in darkness. Injection of Pertussis toxin or GDP S (which keep the G-proteins in their trimeric inactive form) with phytochrome-A blocked the response. Injection of high GTP S concentrations (30–100 mmol) or coinjection of cholera toxin and low GTP S concentrations (1 mmol) produced an intracellular response indistinguishable from that mediated by phytochrome-A. These observations led to conclude that a heterotrimeric G protein was positioned downstream of phytochrome (very likely phytochrome-

B) in the light signal transduction pathway and upstream of a cNMP mediated step, in analogy to light perception in visual cascade.

This data set provides an opportunity to test a new approach and to investigate the potential existence of cNMPs and G-proteins in photransduction pathways downstream of plant photoreceptor phytochrome.

Materials and Methods

Plant materials

In experiments five days old sorghum seedlings (Sorghum bicolor Moench, cv. Acme Broomcorn) were used. The seedlings were grown in absolute darkness at 20 ºC for 5 days.

Light source and irradiation of seedlings

As a light source the xenon lamps were used. To obtain red light the white light was separated into specters on monochromators MDR-23 LOMO (Russia) and HRS2 JOBIN YVON (France).

Etiolated seedlings were irradiated according to Shichijo *et al*. (1993, 1996) by R in the intensity of 100 mmol m^{-2} s^{-1} × 200 s (20,000 mmol m^{-2}) and FR 400 mmol m^{-2} s^{-1} × 30 s (12,000 mmol m^{-2}) (14). All processes of irradiation were carried out under deem green safelight.

Preparation of cyclases

For preparation of adenylyl- and guanylycyclases samples etiolated seedlings were homogenized in 25 mmol tris-HCl buffer, pH 7.4 containing 5 mmol $MgCl_2$, 0.25 mmol NaEDTA and 1 mmol Dithiothreitol (*threo*-1, 4 Dimercapto-2, 3-butanediol). Homogenization was done in 3 mL of buffer per gram of fresh weight seedlings on ice.

The homogenate was filtered through four layer cheesecloth and centrifuged at 1,000 g for 10 min at 4 °C. The pellet was discarded. The supernatant was re-centrifuged at 30,000 g for 40 min at 2–3 °C. The pellet (membrane fraction, enriched with cyclases activity) resuspended in 2 mL of the same buffer and was dialyzed against 4 L of it for 18–20 h. All the processes were carried out at 2–4 °C, under green safe light.

For separation of soluble fraction of adenylyl cyclase the supernatant from 30,000 g is subjected for precipitation in 50% saturation of $(NH_4)_2SO_4$. Precipitate centrifuged at 20,000 g for 20 min, pellet dissolved in 0.01 mol Tris-HCl buffer, pH 7.4, (containing: 2 mmol $MgCl_2$ and 2mmol DTT) and dialyzed against 4 L of Tris-HCl buffer, pH 7.4 (containing 2 mmol $MgCl_2$ and 2 mmol, β-mercaptoethanol) for 18–20 h. All processes of irradiation and protein isolation were carried out under deem green safelight.

Cyclase activity assay

The adenylylcyclase activity assay was performed by Cohen *et al*. (1980) with minor modifications based on formation of [^{32}P]-cAMP from [- ^{32}P]-ATP.

The guanylylcyclase activity assay was performed with minor modification of Kojda *et al*. (1999) and Schultz and Bohme (1984) based on formation of [^{32}P]-cGMP from [- ^{32}P]-GTP.

Protein concentration was measured by Loury.

Results and Discussion

It was previously shown that two forms—soluble and membrane attached forms of adenylylcyclase were fractionated from sorghum seedlings. These forms are differed by their reaction to the influence of red—far red light irradiation of etiolated seedlings (Gasimov, 2002). In this research the possibility of the regulation of adenylylcyclase by G-proteins was studied. To detect the G-protein effects on AC activity in experiments specific analog of GTP - Gpp(NH)p was used.

On the AC activity assay 10^{-5} mol of Gpp(NH) was added in reaction mixture. Gpp(NH)p has not affected on AC activity prepared from etiolated sorghum seedlings (Fig. 1), while the red light irradiation of seedlings did not have considerable effect on AC activity. But the enzyme (AC) isolated from irradiated by monochromatic red light seedlings has positively reacted to the action of Gpp(NH)p, it was activated by Gpp(NH)p for 60% in comparing with AC prepared from etiolated seedlings.

Since Gpp(NH)p had no effect on the activity of the enzyme (AC) isolated from etiolated seedlings (dark fraction) apparently ether G-protein is not included in the dark fraction, or it is included together with “dark” AC, but it can not be activated without receptor(s). We know that in animal organisms all heterotrimeric G-proteins in the initial state are non-integral bound to the membrane (Morris and Malbon, 1999), and for the activation they need the effect of the receptors. In plants the G-proteins are also in the heterotrimeric state

and associated with the membranes (Jones, 2002). It follows from this thinking about that G-proteins are together with "dark" adenylyl cyclase, but it is inactive in the absence of active receptor. And in the event of activation of AC isolated from red light irradiated seedlings, it seems like the red like excited plant photoreceptor phytochrome promotes the activation of G-protein that leads to the release of active alpha subunit from heterotrimer. And activated G-protein in its turn influences the activity of adenylylcyclase.

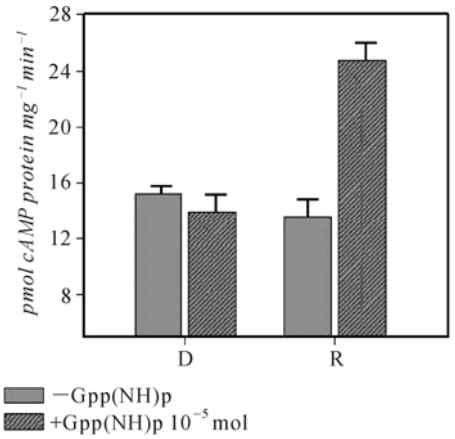

Fig. 1 Influence of Gpp(NH)p on the activity of adenylylcyclase isolated from 5 days old sorghum seedlings. D – adenylylcyclase isolated from etiolated seedlings; R – adenylylcyclase isolated from seedlings irradiated by monochromatic red light (660 nm).

The influence of Gpp (NH)p on the activity of the guanylate cyclase, an enzyme that synthesizes cGMP from GTP, was also examined. Similar to adenylyl cyclase, the addition of 10^{-5} mol Gpp(NH)p into reaction mixture did not affect on the activity of "dark" guanylate cyclase (Fig. 2). But unlike adenylylcyclase 10^{-5} mol of Gpp(NH)p has strongly inhibited guanylilcyclase (GC) isolated from seedlings irradiated by red light.

The inhibition of red GC by Gpp(NH)p is evidenced the existence of multiple forms of G-proteins in sorghum seedlings. Apparently these different forms of G-proteins in sorghum seedlings behave similar way as in animal organisms (Morris and Malbon, 1999), at the adrenergic receptor linked signal transduction pathway in vertebrate Gαs activates adenylylcyclase and Gαi inhibit it.

Another explanation for the inhibition of guanylylcyclase may be the possibility of competitive binding of GTP substrate to the G-protein. High GTPase activity and GTP binding affinity make the G-protein a potential competitor for guanylylcyclase.

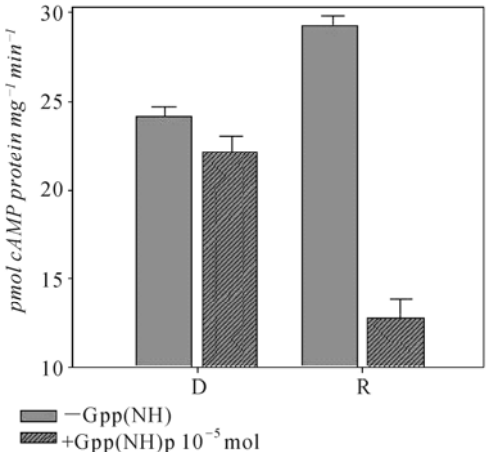

Fig. 2 Influence of Gpp(NH)p on the activity of guanylylcyclase isolated from 5 days old sorghum seedlings. D – guanylylcyclase isolated from etiolated seedlings; R – guanylylcyclase isolated from seedlings irradiated by monochromatic red light (660 nm).

Thus, it is possible that two types of heterotrimeric G-proteins associated in plant signal transduction. This fiorms of G-proteins being affected by photoreceptor phytochromes (perhaps with different forms), excited byred light, and activated G-proteins further affect the activity of specific cyclases. Activation of adenylylcyclase with Gpp(NH)p under irradiation with red light indicates that the analogue of Gαs in vertebrate exists in sorghum plants, and it is being activated byphotoreceptor phytochrome, excited with red light, involved in transduction of photosignals from the receptor to the effector - cAMP.

References

Fedenko EP, Gasumov KG (1993) Effect of Gpp[NH]p on Basal and Photoinduced Activities of Cyclic AMP and Phosphodiesterase in Maiza Sprouts. Reports of Russian Academy of Science, Biological Sciences 1: 131-137

Baylor D (1996) How Photons Start Vision. Proc Natl Acad Sci USA 93: 560-565

Bowler C, Neuhaus G, Yamagata H, Chua NH (1994) Cyclic GMP and Calcium Mediated Phytochrome Phototransduction. Cell 77: 73-81

Cohen RJ, Ness JL, Whiddon SM (1980) Adenylate Cycalse from Phycomyces Sporangiophore. Phytochemistry 19: 1913-1918

Gasimov KG (2002) Participation of Multiple Forms of Light Regulated Adenylyl Cyclase from S.Bicolor Seedlings in Plant Photosygnal Transduction Chain. Proc. of Azerbaijan Nat. Acad. Biological Sciences 1(6): 253-263

Jones AM (2002) G-Protein-Coupled Signaling in Arabidopsis. Current Opinion in Plant Biology 5: 402-407

Jones AM, Joseph R Ecker, Jin-Gui Chen A (2003) Reevaluation of the Role of the Heterotrimeric G-Protein in Coupling Light Responses in Arabidopsis. Plant Physiology 131: 1623-1627

Kojda G, Laursena JB, Ramasamya S, Kenta JD, Kurza S, Burchfield J, Shesely EG, Harrison DG (1999) Protein Expression, Vascular Reactivity and Soluble Guanylate Cyclase Activity in Mice Lacking the Endothelial Cell Nitric Oxide Synthase: Contributions of NOS Isoforms to Blood Pressure and Heart Rate Control. Cardiovascular Research 42: 206-213

Mello LV, Millner PA, Findlay JBC (2002) Biochemical Characteristics of Guanine Nucleotide Binding Protein A-Subunit Recombinant Protein and Three Mutants: Investigation of a Domain Motion Involved in GDP-GTP Exchange. Journal of Protein Chemistry 21(1): 29-31

Morris AJ, Malbon CC (1999) Physiological Regulation of G Protein-Linked Signaling. Physiological Reviews 79(4): 1373-1430

Neuhaus G, Bowler C, Kern R, Chua NH (1993) Calcium/Calmodulindependent and -Independent Phytochrome Signal Transduction Pathways. Cell 73: 937-952

Shichijo C, Hamada T, Hiraoka M, Johnson C, Hashimoto T, (1993) Enhancement of Red-Light-Induced Anthocyanin Synthesis in Sorghum First Internodes by Moderate Low Temperature Given in the Pre-Irradiation Culture Period. Planta 191: 238-245

Shichijo C, Hamada T, Johnson C, Hashimoto T (1996) Effects of Moderately Low Temperature (20 ^{o}C) on Phytochrome Responces during Preirradiation: Anthocyanin Synthesis in Sorghum Bicolor at High- and Low-Pfr/Ptot Ratios. Photochem.and Photobiol 63, pp. 328-335

Schultz G, Bohme E (1984) Guanylate Cyclase. In: Bergmeyer Hu (ed.), Methods of Enzymatic Analysis. FRG: Verlag Chemie: Weinheim, pp. 379-389

Expression of PEPC Gene, Lipid Content and Photosynthesis in *Anabaena* 7120

Lijun Hou[1], Xiaohui Jia[1], Dingji Shi[1,2,*], Xuekui Wang[1]

[1]School of Marine Sciences & Engineering, Tianjin University of Sciences & Technology, Tianjin 300457, China;
[2] Institute of Botany, Chinese Academy of Sciences, Beijing 100093, China.
* Corresponding author. E-mail: cyano.shi@yahoo.com.cn.

Abstract: The aim of this work was to prepare a material for biodiesel. Filamentous cyanobacterium *Anabaena* 7120 was mutated by DNA recombination technique. Anti and sense vectors, harbering phosphoenolpyruvate carboxylase (PEPC) gene fragment *pepcA*, were constructed and transformed *Anabaena* 7120. The down-regulating mutant decreased PEPC activity to 12.9% of that in wild type cells, and its lipid content elevated 54.7% of that in wild type cells. The lipid content may increase to 54.15% of dry weigh. The mutant elevated net photosynthetic activity 51%–77% higher than that in wild type cells, and the activity in BG11(-N) medium was higher than in BG11(+N) medium. Also, its tolerance to higher light intensity and temperature was enhanced. From these data, the mutant contained more lipid, grew fast, tolerated high light intensity and temperature, harvested easily and the species of cyanobacterium was no toxic. So, using the mutant as a feedstock for biodiesel production may reduce the cost.

Keywords: PEPC (phosphoenolpyruvate carboxylase); Gene expression; Lipid content; Photosynthesis; *Anabaena* (*Nostoc*) 7120; Biodiesel

Introduction

Microalgae have been demonstrated the only source of the renewable biodiesel that is capable of meeting the global demand for transport fuels (Chisti, 2007; Hu *et al*., 2008). To reduce the production cost of the biodiesel from microalgae lipid content and photosynthesis in microalgae have to increase (Sheehan *et al*., 1998). Although overexpression of acelyl-CoA carboxylase (ACCase) was not successful (Dunahay *et al*., 1996), genetic engineering attempt is worth to search for elevating lipid productivity in microalgae.

Anabaena (*Nostoc*) sp. PCC 7120 (*Anabaena* 7120) is a model prokaryotic alga, which is a heterocystous, filamentous cyanobacterium possessing nitrogen fixation capability and was easy to harvest, grew in a medium without combined nitrogen avoiding contamination of other microbial and algae, and contained no toxin. Fourteen foreign genes have been expressed and four inner genes have been down-regulated at our group (Shi, 2011). PEPC (EC4.1.1.31) is one of the CO_2-fixing enzymes, which yields oxaloacetate from phosphoenolpyruvate (PEP) and bicarbonate (HCO_3^-), which may play a key role in metabolic engineering (Izui *et al*., 2004; Peterhansel *et al*., 2008; Zhu *et al*., 2010).

Now, up- or down-regulating expression of phosphoenolpyruvate carboxylase (PEPC) in *Anabaena* 7120 has been tried in this work.

Materials and Methods

Strains. *Anabaena* (*Nostoc*) sp. PCC 7120 was from Pasteur Institute (Paris). *Escherichia coli* DH-5α was from Takara Co. Ltd. Plasmid pRL-489 was from MSU-DOE (U.S.A.).

Cultivating. *Anabaena* 7120 was cultivated under illumination (Shi *et al*., 1987) and *E. coli* was cultivated in LB medium (Sambrook *et al*., 2001).

Targeting gene fragment (*pepcA*). PEPC gene sequence was consulted and compared, and a primer

was designed and the gene fragment was cloned (Hou *et al.*, 2008 a, b).

Construction of vectors and transformation. pRL-489 was used to construct Antisense- or Sense-vectors (Qin *et al*., 1998, 1999), and transformation of both *E.coli* and *Anabaena* 7120 by the vectors was carried on (Hou *et al*., 2008b; Qin *et al*., 1998).

Measurements of PEPC activities. See Canovas *et al*. (1996).

Measurements of total lipids and proteins. See Bligh and Dyer (1959) and Bradford (1976).

Measurements of photosynthesis. See Shi (1987).

Result and Discussion

Shuttle expression vectors in forward or reverse orientative

For up- or down-regulating expression of PEPC, two vectors were constructed as showed in Fig. 1 and were transferred into *E .coli* and amplificated. Fig. 2 indicated PCR amplication and restriction pattern of these two vectors isolated from *E. coli*. These data demonstrated that antisense and sense vectors had been constructed.

Total lipids and PEPC activities in wild type and mutants of Anabaena 7120

Table 1 showed that PEPC activities in negative expression strain decreased to 12.9% of that in the wild type cells, and total lipids in the mutant transformed by Antisense *pepcA* increased 54.7% of that in the wild type cells.

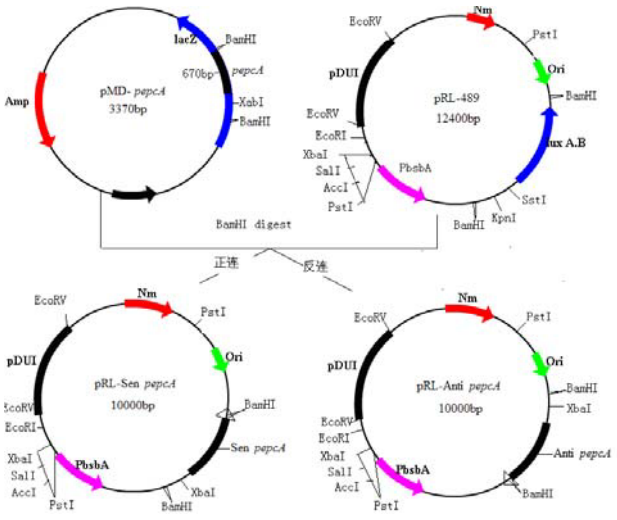

Fig. 1 Construction of shuttle vectors pRL-Antisense *pepcA* and pRL-Sense *pepcA*.

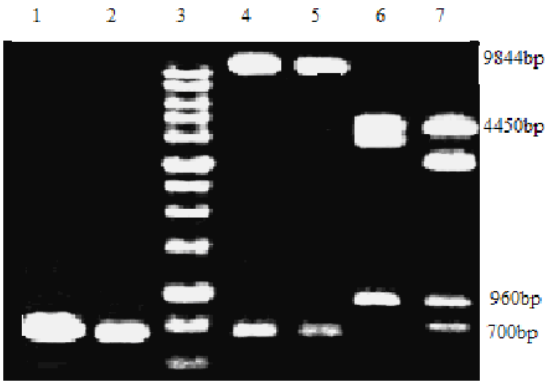

Fig. 2 Recombinant identification of the vectors pRL-Antisense *pepcA* and pRL-Sense *pepcA*.

It was interesting that the mutant of negative expression of *pepcA* in *Anabaena* 7120 was treated by a simple way and its lipid content elevated to 54.15% of dry weight while that in wild type cells was 21.36%.

Table 1 Total lipids and PEPC activities in wild type and mutants of *Anabaena* 7120.

Anabaena Strains	PEPC specific activities (U/mg)	Lipids (g/g)
Wide type 7120	0.132±0.003 (100%)	15.9% (100%)
pRL-489	0.116±0.002 (87.8%)	11.9% (74.84%)
pRL-Sense *pepcA*	0.239±0.004 (181.1%)	6.62% (41.63%)
pRL-Antisense *pepcA*	0.017±0.0008 (12.9%)	24.6% (154.7%)

Effects of light intensities on photosynthesis in wild type and mutant of Anabaena 7120

Figs. 3A and 3B showed their light intensity curves in BG11(-N) and BG11(+N) media. Tables 2 and 3 indicated their photosynthetic parameters responding to Fig. 3A or Fig. 3B, respectively.

From these data, net photosynthesis activities of all strains in BG11(-N) medium were higher than in BG11(+N) medium. When the cyanobacterium was cultivated in a medium without combined nitrogen, there may be less contamination of other species of algae.

In both of BG11 media the activities of the mutant strains expressed *pepcA* negatively were higher than that in wild type cells about 51%–77%. When down-regulated strain was cultivated in BG11(-N) medium its photoinhibition light intensity was about 400 μmol/m^{-2} s^{-1}, and that of wild type cells was about 200 μmol/ $m^{-2}s^{-1}$.

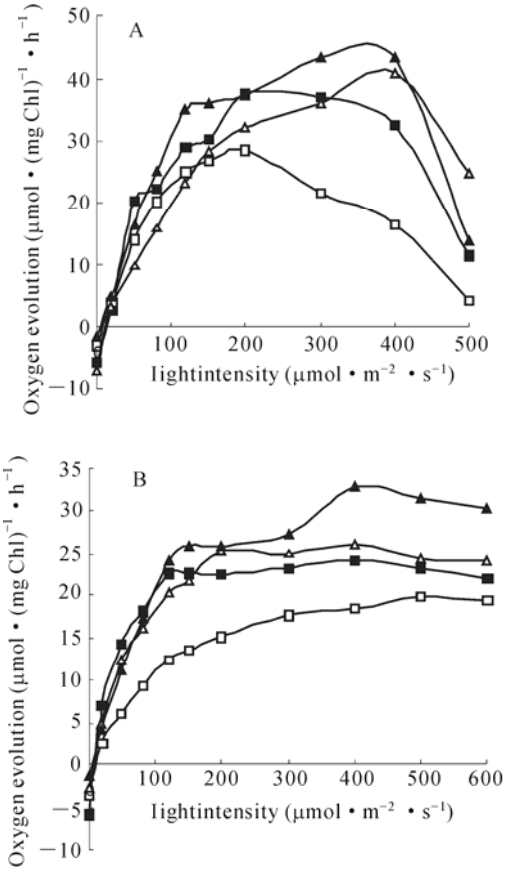

Fig. 3 Light intensity curves of net photosynthesis in wild type and mutants of *Anabaena* 7120 in (A) BG11(-N) and (B) BG11(+N) media. Wide type 7120(□), pRL-489(■), pRL-Sense *pepcA* (△), pRL-Antisense *pepcA*(▲).

Table 2 Photosynthesis parameters responsible to Fig. 3A.

Anabaena Strains	Pm (μmol O_2(mg Chl)$^{-1}$h^{-1})	Ik (μmol/m^{-2}s^{-1})	Ic (μmol/m^{-2}s^{-1})
Wide type 7120	28.561±7.822 (100%)	53.58	10.181
pRL-489	36.882±7.760	67.66	11.768
pRL-Sense *pepcA*	40.912±7.019	84.53	11.570
pRL-Antisense *pepcA*	43.207±7.583 (151.3%)	86.414	7.141

Table 3 Photosynthesis parameters responsible to Fig. 3B.

Anabaena Strains	Pm (μmol O_2(mg Chl)$^{-1}$h^{-1})	Ik (μmol/m^{-2}s^{-1})	Ic (μmol/m^{-2}s^{-1})
Wide type 7120	18.508±1.233 (100%)	125.054	13.340
pRL-489	24.149±1.341	62.724	8.938
pRL-Sense *pepcA*	26.42297±1.284	93.397	5.519
pRL-Antisense *pepcA*	32.918±1.248 (177.8%)	125.978	3.901

Effects of temperatures on photosynthesis of wild type and mutants of Anabaena 7120

Figs. 4A and 4B showed their temperature curves in BG11(-N) and BG11(+N) media, respectively. The figures indicated in both of media all of mutants increased their tolerance to higher temperature. The optimum temperature in BG11(-N) was about 32 °C for wild type and all mutants, however, the strain with negatively expressed *pepcA* kept higher net photosynthetic activities from 34 °C to 40 °C. In BG11(+N) the optimum temperature of down-regulating mutant extended the range from 28 °C to 36 °C.

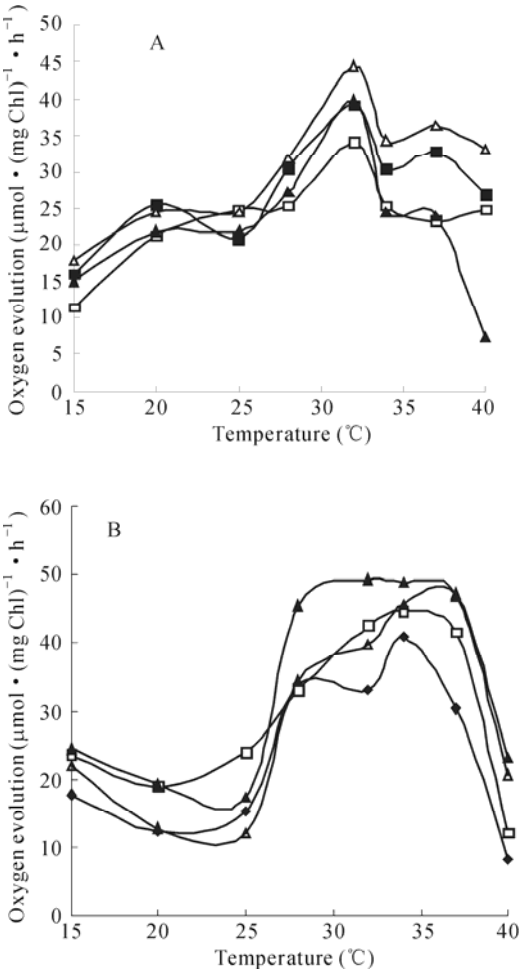

Fig. 4 Temperature curves of net photosynthesis in wild type and mutants of *Anabaena* 7120 in (A) BG11 (-N) and (B) BG11 (+N) media. Wide type 7120 (□), pRL-489(■), pRL-Sense *pepcA*(△), pRL-Antisense *pepcA*(▲).

Conclusion

Ntisense and Sense vectors were constructed, and down-regulating and up-regulating expressions of

PEPC in *Anabaena* 7120 were obtained by DNA recombination technique. The aim of this work was a preparation for a high quality feedstock for biodiesel.

The mutant with negatively expressed *pepcA* showed that PEPC activities reduced to 12.9% in wild type cells, and increased 54.7% of lipid content in wild type cells. When the mutant was treated by a simple way and its lipid content may elevate to 54.15% of dry weigh, while 21.36% in the wild type cells.

The mutant transformed by Antisense-*pepcA* vector performed net photosynthetic activity 51%–77% higher than that in the wild type cells, and the activity in BG11(-N) medium was higher than in BG11(+N) medium, and its tolerance to higher light intensity and temperature was increased.

References

Bligh EG, Dyer WJ (1959) A Rapid Method of Total Lipid Extraction and Purification. Canadian Journal of Physiology and Pharmacology 37: 911-917

Bradford MM (1976) A Rapid and Sensitive Method for the Quantification of Microgram Uantities of Protein Utilizing the Principle of Protein Dye Binding. Ann. Biochem 72: 248 − 254

Canovas JL, Kornberg HL (1996) Proc. Roy. Soc. Ser. B Biol. Sci. 165: 189-205

Chisti Y (2007) Biodiesel from Microalgae. Biotechnology Advances 25: 294-306

Dunahay TG, Jarvis EE, Dais SS, Roessler PG (1996) Manipulation of Microalgal Lipid Production Using Genetic Engineering. Applied Biochemistry and Biotechnology-Part A Enzyme Engineering and Biotechnology 57: 223-231

Hou LJ, Wang XK, Shi DJ (2008a) Bioinformatical Analysis of Phosphoenol-Pyruvate Carboxylase in Cyanobacteria. Biotech. Bull (in Chinese) 4: 149-154

Hou LJ, Shi DJ, Cai ZF, Song DH, Wang XK (2008b) Regulation of Lipid Synthesis in Escherichia Coli by Cyanobacterial pepcA. J. Chinese Biotech 28(5): 52-58

Hu Q, Sommerfeld M, Jarvis E, Ghirardi M, Posewitz M, Seribert M, Darzins A (2008) Microalgal Triacylglycerols as Feedstocks for Biofuel Production: Perspectives and Advances. Plant Journal 54: 621-639

Izui I, Matzumura H, Furumoto T, Kai Y (2004) Phosphoenolpyruvate Carboxylase: a New Era of Structural Biology. Annu. Rev. Plant Bio 55: 69-84

Peterhansei C, Niessen M, Kebeish RM (2008) Metabolic Engineering Towards the Enhancement of Photosynthesis. Photochem and Photobiol 84: 1317-1323

Qing JD, Shi DJ, Xu XD, Zhang JD, Guo PZ, Tang PS (1998) Construction of Antisense glnA Expression System in Anabaena 7120. Acta phytophysiol. Sini 24(3): 225-232

Qing JD, Shao N, Shi DJ, Xu XD, Zhang JD, Guo PZ, Wang WQ, Tang PS (1999) Construction of Secreting Ammonium Mutant from Synechococcus 7942 and Its Glutamine Synthetase Activity, Photosynthesis and Growth. Acta Bot. Sini 41(1): 65-70

Sambrook J, Fritsch EF, Maniatis T (2001) Molecular Cloning. A Laboratory Manual 3rd edition, Cold Spring Harbor Laboratory Press

Sheehan J, Dunahay T, Benemann J, Roessler P (1998) A Look Back at the US Department of Energy's Aquatic Species Program-Biodiesel from Algae. National Renewable Energy Laborattory, Golden, Colorado

Shi DJ (1987) Energy Metabolism and Structure of Immobilized Cyanobacterium Anabaena Azollae. Ph.D thesis, King's College London

Shi DJ, Brouers M, Hall DO, Robins RJ (1987) The Effects of Immobilization on the Biochemical, Physiological and Morphological Features of Anabaena azollae. Planta 172: 298-308

Shi DJ (2011) Construction of Cyanobacterial Cell Factories. Science & Technology Stimulating Development (in press). (in Chinese)

Zhu XG, Long SP, Ort DR (2010) Improving Photosynthetic Efficiency for Greater Yield. Annu Rev. Plant Biol 61: 235-261

Unique Central Carbon Metabolic Pathways and Novel Enzymes in Phototrophic Bacteria Revealed by Integrative Genomics, ^{13}C-based Metabolomics and Fluxomics

Kuo-Hsiang Tang[a, b], Xueyang Feng[c], Anindita Bandyopadhyay[a],
Himadri B Pakrasi[a, c], Yinjie J Tang[c], Robert E Blankenship[a, b,*]

Departments of [a]Biology, [b]Chemistry, [c]Energy, Environment, and Chemical Engineering,
Washington University in St. Louis, St. Louis, Missouri 63130, USA.
[*]Corresponding author. Tel. No. 1-314-935-7971; Fax No. 1-314-935-4432; E-mail: Blankenship@wustl.edu.

Abstract: Photosynthesis is the process to convert solar energy to biomass and biofuels, which are the only major solar energy storage means on Earth. To satisfy the increased demand for sustainable energy sources, it is essential to understand the process of solar energy storage, that is, the carbon metabolism in photosynthetic organisms. It has been well-recognized that one bottleneck of photosynthesis is carbon assimilation. In this report, we summarize our recent studies on the carbon metabolism pathways of several types of photosynthetic bacteria, including aerobic anoxygenic phototrophic proteobacteria, green sulfur bacteria, heliobacteria and cyanobacteria, using physiological studies, transcriptomics, enzyme assays, ^{13}C-based metabolomics and fluxomics. Our studies have revealed several unique and/or significant central carbon metabolic pathways and novel enzymes that operate in these phototrophs, quantified CO_2 assimilation pathways operative during mixotrophic cultivation conditions, and also suggested evolutionary links between photosynthetic and non-photosynthetic organisms.

Keywords: CO_2 fixation; Citramalate pathway; Entner-Doudoroff pathway; Metabolomics; Reductive TCA cycle; (*Re*)-citrate synthase

Introduction

Solar energy is the most abundant, albeit dilute, sustainable energy source on Earth, and photosynthesis is a process that converts solar energy into biofuels and biomass (Blankenship, 2002). However, the photosynthetic efficiency for bimass production in higher plants is at maximum only 4%–6% (Zhu *et al*., 2010). As the demand for sustainable energy has expanded significantly, it is important to improve the efficiency of photosynthesis. It has been determined that carbon assimilation is one important bottleneck of photosynthesis, so it is necessary to understand carbon metabolism pathways in photosynthetic organisms. In contrast to the rich information reported for biomedically relevant microbes, much less knowledge has been obtained for the metabolism of photosynthetic bacteria. Many photosynthetic microorgnisms live in environments that higher plants cannot survive in, so an understanding of the metabolism of these microorganisms is of substantial interest. In this review, we briefly summarize our recent studies on the carbon metabolism mechanisms of aerobic anoxygenic phototrophic proteobacteria, green sulfur bacteria, heliobacteria and cyanobacteria using physiological studies, transcriptomics, enzyme assays, ^{13}C-based metabolomics and fluxomics. Our studies have revealed several unique carbon metabolic pathways and enzymes that operate in these phototrophs. Possible evolutionary links between photosynthetic and non-photosynthetic organisms are suggested.

Materials and Methods

Physiological studies and integrative genomics

The methods for bacterial growth, physiological studies, gene expression profiles via quantitative real-time PCR (QRT-PCR) (Tang *et al*., 2009b) and enzyme assays of *Roseobacter denitrificans* (Tang *et*

al., 2009a), *Chlorobaculum tepidum* (Tang and Blankenship, 2010; Tang *et al*., 2010a), *Heliobacterium modesticaldum* (Tang *et al*., 2010b) and *Cyanothece* sp. ATCC 51142 (Feng *et al*., 2010a; Wu *et al*., 2010) are described elsewhere.

^{13}C-isotopic labeling and flux analysis

^{13}C-labeled glucose, pyruvate, acetate or bicarbonate was used as the sole carbon source in cell cultures, and the labeled protein-based amino acids were extracted from cell pellets, hydrolyzed, derivatized and analyzed by GC/MS (Fig. 1). For flux analysis, fluxes cannot be calculated directly from labeling data, but their accurate determination was achieved through a heuristic recursive procedure: the known metabolic reactions, atomic transitions, metabolite labeling, and extracellular fluxes are combined to produce an error function ε (the difference between the measured isotopomer data and the predicted isotopomer data from assumed fluxes), and then a search algorithm is applied to determine the actual fluxes by minimizing the error function (equation 1):

$$\varepsilon(v_n) = \sqrt{\sum_{i=1}^{k_j} \left(\frac{M_i - N_i(v_n)}{\delta_i} \right)^2} \qquad \text{(Eq. 1)}$$

$$\text{Subject to: } \boldsymbol{S} \bullet V_n = 0$$

where S is the stoichiometry matrix for all unknown fluxes, V_n are the unknown fluxes to be optimized in the program, M_i is the measured isotopomer data, N_i is the corresponding model-predicted isotopomer data, and δ_i is the corresponding standard deviation of the measured isotopomer data. The unknown metabolic fluxes are calculated to minimize ε (Feng *et al*., 2010b; Pingitore *et al*., 2007; Wahl *et al*., 2004).

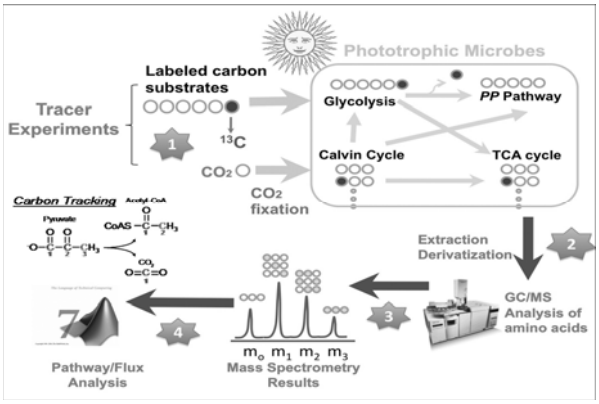

Fig. 1 ^{13}C-based metabolomics and fluxomics.

Results and Discussion

Using multiple approaches, we have identified several unique pathways and novel enzymes in several photosynthetic bacteria. Here we report some unique and/or significant central carbon metabolic pathways and novel enzymes; details can be found in our recent published studies (Feng *et al*., 2010a; Feng *et al*., 2010b; Tang and Blankenship, 2010; Tang *et al*., 2009a; Tang *et al*., 2010a; Tang *et al*., 2010b; Wu *et al*., 2010).

The Entner-Doudoroff pathway

The Embden-Meyerhof-Parnas (EMP) pathway (glycolysis), Entner-Doudoroff (ED) pathway and pentose phosphate pathway are three major carbohydrate metabolic pathways. While the majority of organisms use the EMP pathway for digesting glucose, some microorganisms, most of which are aerobes, have been reported to use the ED pathway (Conway, 1992; Fuhrer *et al*., 2005). Our studies indicate that the aerobic anoxygenic phototrophic (AAP) proteobacterium *Roseobacter denitrificans* predominantly uses the ED pathway for metabolizing sugars (Fig. 2), and that their EMP pathway is inactive (Tang *et al*., 2009a). Similar results were also reported in two other AAP bacteria using ^{13}C-metabolomics and fluxomics (Furch *et al*., 2009) as well as some purple bacteria (such as *Rhodobacter capsulatus* and *Rhodobacter sphaeroides*) under certain growth conditions (Conrad and Schlegel, 1977; Fuhrer *et al*., 2005). All of the cultured AAPs are photoheterotrophs and require organic carbon for growth. It has not been established if the ED pathway is active in all of the purple bacteria, and is also not entirely clear why those bacteria use the ED pathway, which has a lower thermodynamic efficiency compared to the EMP pathway. It is possible that those bacteria may use a high glucose metabolic rate to compensate the thermodynamic inefficiency of the ED pathway (Molenaar *et al*., 2009).

(Re)-citrate synthase

The majority of studied organisms synthesize citrate from acetyl-CoA and oxaloacetate by (*Si*)-citrate synthase ((*Si*)-CS) for initiating the TCA cycle. Our studies showed that the anoxygenic heliobacterium *Heliobacterium modesticaldum* uses (*Re*)-citrate synthase ((*Re*)-CS), an alternative biosynthetic pathway, to produce citrate (Tang *et al*.,

2010a). Activity of (*Si*)-CS has not been detected (Tang *et al*., 2010b) and the gene encoding (*Si*)-CS has not been annotated in the *H. modesticaldum* genome (Sattley and Blankenship, 2009; Sattley *et al*., 2008). As indicated in Fig. 3, the acetyl group from acetyl-CoA is attached to the *pro-S* or *pro-R* arm of citrate by (*Si*)-CS or (*Re*)-CS, respectively.

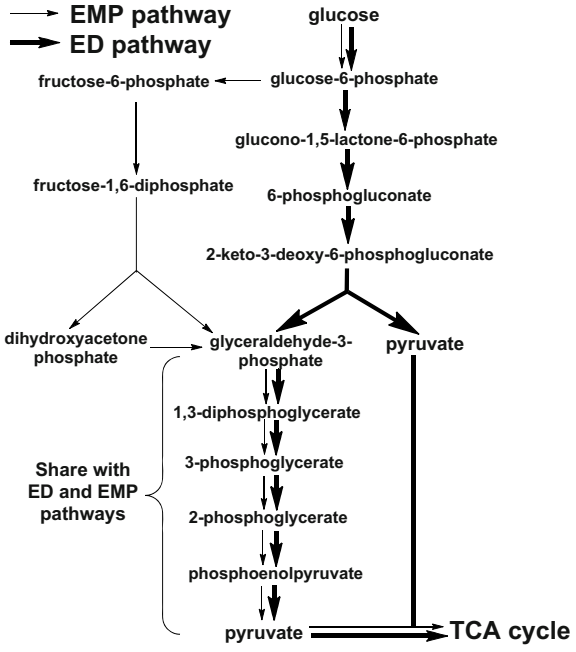

Fig. 2 The EMP pathway versus the ED pathway.

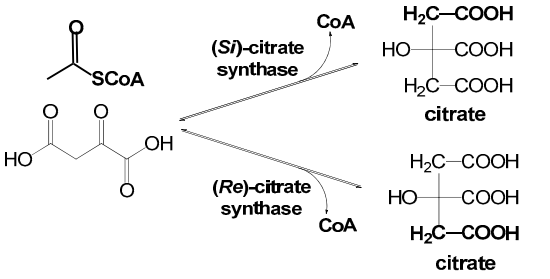

Fig. 3 The reactions catalyzed by (*Si*)- versus (*Re*)-CS.

Previous studies indicate that several *Clostridia* species exclusively use (*Re*)-CS to synthesize citrate (Li *et al*., 2007). These reports, together with our work on heliobacteria, suggest a possible evolutionary link between heliobacteria and *Clostridia*, both of which are anaerobic gram-(+) bacteria. Also, our studies on *H. modesticaldum* and a previous report on *Heliobacterium* strain HY-3 (Pickett *et al*., 1994) indicate that both heliobacteria use the oxidative (forward) TCA cycle to synthesize glutamate. Additionally, our studies demonstrate that the carbon flux is mostly carried out through the incomplete oxidative TCA cycle, in which the reducing equivalents (*i.e.* NADH) are generated (Fig. 4), although all of the genes, except one, in the reductive TCA cycle have been annotated in *H. modesticaldum* genome (Sattley *et al*., 2008) and the enzymatic activity of encoded proteins in the TCA cycle have been detected in *H. modesticaldum* (Tang *et al*., 2010b). Our studies may shed light on the proposed photosynthetic cyclic electron transport pathway in the heliobacteria (Kramer *et al*., 1997).

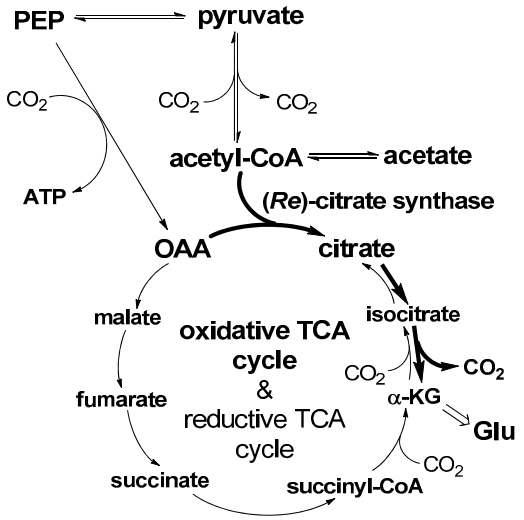

Fig. 4 The proposed central carbon flow in heliobacteria.

Citramalate pathway

Many organisms synthesize isoleucine through the threonine-deaminase dependent pathway, whereas we discovered that several photosynthetic bacteria, including *R. denitrificans* (Tang *et al*., 2009a), *Chlorobaculum tepidum* (Feng *et al*., 2010b), *H. modesticaldum* (Tang *et al*., 2010a) and *Cyanothece* sp. ATCC 51142 (Wu *et al.*, 2010), use the citramalate-dependent pathway to synthesize isoleucine (Fig. 5). Together with an active citramalate pathway reported in several non-photosynthetic bacteria (Feng *et al*., 2009; Risso *et al*., 2008), it is suggested that the citramalate-dependent pathway is much more widespread than previously recognized (Howell *et al*., 1999). Compared to the threonine-dependent pathway, it is more efficient to produce 2-ketobutyrate through the citramalate pathway. 2-ketobutyrate is an intermediate in the isoleucine biosynthesis pathway, for butanol and propanol production (Fig. 5) (Atsumi and Liao, 2008).

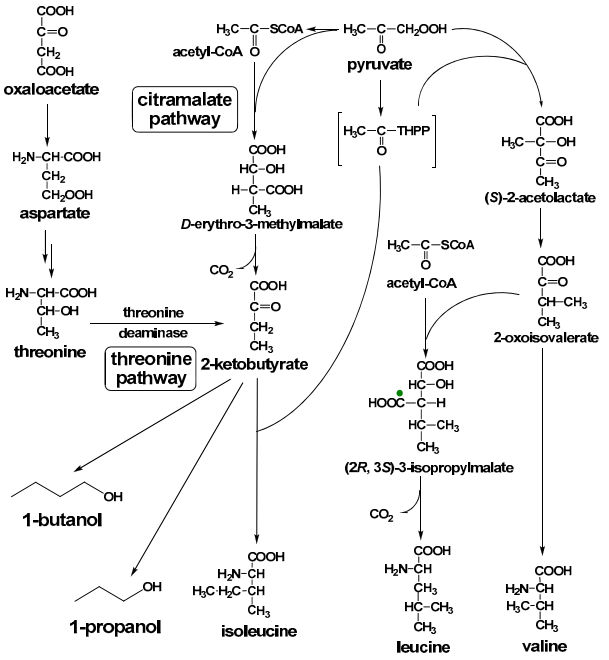

Fig. 5 The Val, Ile and Leu biosynthetic pathways.

Alternative CO_2-assimilation pathways

Several autotrophic CO_2-assimilation pathways have been identified in microorganisms, including the Calvin-Benson-Bassham (CBB) cycle, the reductive TCA cycle (Arnon-Buchanan-Evans cycle), the reductive acetyl-CoA pathway (Wood-Ljungdahl pathway), the 3-hydroxy-propionate cycle and the 3-hydroxypropionate/4-hydroxy-butyrate cycle (Thauer, 2007). Some photosynthetic bacteria are known to employ the CBB cycle (purple non-sulfur bacteria and cyanobacteria), the reductive TCA cycle (the green sulfur bacteria, GSBs) and the 3-hydroxypropionate cycle (*Chloroflexus aurantiacus*). Our studies indicate that the cyanobacterium *Cyanothece* 51142 grows photoautotrophically in the presence of glucose or pyruvate, and photoheterotrophically with minimal CO_2 assimilation when nitrate and glycerol are supplied (Feng *et al*., 2010a). Furthermore, our flux analysis show that *C. tepidum* can fix about ~3.6 (or ~6.0) mole CO_2 per mole acetate (or pyruvate) under mixotrophic conditions (Feng *et al*., 2010b). Alternatively, the CO_2-anaplerotic pathway is known to be essential in the energy metabolism of many chemoheterotrophic organisms, and the deficiency of enzymes in the anaplerotic pathways leads to accumulation of lipids, lack of gluconeogenesis, and other effects. Our studies demonstrate that the CO_2-anaplerotic pathways are active in *R. denitrificans*, *H. modesticaldum* and *C. tepidum*. The first two bacteria are obligate photoheterotrophs and our studies suggest strong carbon flow in their oxidative TCA cycle (Tang *et al*., 2009a; Tang *et al*., 2010a; Tang *et al*., 2010b), so the production of oxaloacetate (OAA) from carboxylation of pyruvate and of phosphoenolpyruvate (PEP) is essential for the oxidative TCA cycle when it is running low. Also, while CO_2-enhanced phototrophic growth of *H. modesticaldum* has not been detected using pyruvate as the sole organic carbon source, CO_2-enhanced growth has been observed in acetate-grown cultures (Tang *et al*., 2010b). The CO_2-enhanced phototrophic growth is most likely due to conversion of acetyl-CoA to pyruvate (Fig. 4). Further, an active anaplerotic pathway in *C. tepidum* confirmed by us is essential for efficient assimilation of pyruvate (mainly via the reductive TCA cycle) and acetate (via both oxidative and reductive TCA cycles) during mixotrophic growth of GSBs (Feng *et al*., 2010b; Tang and Blankenship, 2010), although GSBs require the autotrophic reductive TCA cycle for growth.

Acknowledgements

This work was supported by Exobiology Program of NASA Grant NNX08AP62G (REB), National Science Foundation Career Grant MCB0954016 (YJT) and Department of Energy Grant DE-FC02-07ER64694 (HBP and YJT).

References

Atsumi S, Liao JC (2008) Directed Evolution of Methanococcus Jannaschii Citramalate Synthase for Biosynthesis of 1-Propanol and 1-Butanol by Escherichia Coli. Appl Environ Microbiol 74: 7802-7808

Blankenship RE (2002) Molecular Mechanisms of Photosynthesis. Blackwell Science Ltd, Oxford

Conrad R, Schlegel HG (1977) Different Degradation Pathways for Glucose and Fructose in Rhodopseudomonas Capsulata. Arch Microbiol 112: 39-48

Conway T (1992) The Entner-Doudoroff Pathway: History, Physiology and Molecular Biology. FEMS Microbiol Rev 9: 1-27

Feng X, Bandyopadhyay A, Berla B, Page L, Wu B, Pakrasi HB, Tang YJ (2010a) Mixotrophic and Photoheterotrophic Metabolism in Cyanothece sp.

ATCC 51142 under Continuous Light. Microbiology 156: 2566-2574

Feng X, Mouttaki H, Lin L, Huang R, Wu B, Hemme CL, He Z, Zhang B, Hicks LM, Xu J, Zhou J, Tang YJ (2009) Characterization of the Central Metabolic Pathways in Thermoanaerobacter sp. X514 Via Isotopomer-Assisted Metabolite Analysis. Appl. Environ. Microbiol. 75: 5001-5008

Feng X, Tang KH, Blankenship RE, Tang YJ (2010b) Metabolic Flux Analysis of the Mixotrophic Metabolisms in the Green Sulfur Bacterium Chlorobaculum Tepidum. J Biol Chem 285: 39544-39550

Fuhrer T, Fischer E, Sauer U (2005) Experimental Identification and Quantification of Glucose Metabolism in Seven Bacterial Species. J Bacteriol 187: 1581-1590

Furch T, Preusse M, Tomasch J, Zech H, Wagner-Dobler I, Rabus R, Wittmann C (2009) Metabolic Fluxes in the Central Carbon Metabolism of Dinoroseobacter Shibae and Phaeobacter Gallaeciensis, Two Members of the Marine Roseobacter clade. BMC Microbiol 9: 209

Howell DM, Xu H, White RH (1999) (R)-Citramalate Synthase in Methanogenic Archaea. J Bacteriol 181: 331-333

Kramer DM, Schoepp B, Liebl U, Nitschke W (1997) Cyclic Electron Transfer in Heliobacillus Mobilis Involving a Menaquinol-Oxidizing Cytochrome bc Complex and an RCI-Type Reaction Center. Biochemistry 36: 4203-4211

Li F, Hagemeier CH, Seedorf H, Gottschalk G, Thauer RK (2007) Re-Citrate Synthase from Clostridium Kluyveri Is Phylogenetically Related to Homocitrate Synthase and Isopropylmalate Synthase Rather than to Si-Citrate Synthase. J Bacteriol 189: 4299-4304

Molenaar D, van Berlo R, de Ridder D, Teusink B (2009) Shifts in Growth Strategies Reflect Tradeoffs in Cellular Economics. Mol Syst Biol 5: 323

Pickett MW, Williamson MP, Kelly DJ (1994) An Enzyme and ^{13}C-NMR of Carbon Metabolism in Heliobacteria. Photosynth. Res. 41: 75-88

Pingitore F, Tang Y, Kruppa GH, Keasling JD (2007) Analysis of Amino Acid Isotopomers Using FT-ICR MS. Anal Chem 79: 2483-2490

Risso C, Van Dien SJ, Orloff A, Lovley DR, Coppi MV (2008) Elucidation of an Alternate Isoleucine Biosynthesis Pathway in Geobacter Sulfurreducens. J Bacteriol 190: 2266-2274

Sattley WM, Blankenship RE (2009) Insights into Heliobacterial Photosynthesis and Physiology from the Genome of Heliobacterium Modesticaldum. Photosynth. Res

Sattley WM, Madigan MT, Swingley WD, Cheung PC, Clocksin KM, Conrad AL, Dejesa LC, Honchak BM, Jung DO, Karbach LE, Kurdoglu A, Lahiri S, Mastrian SD, Page LE, Taylor HL, Wang ZT, Raymond J, Chen M, Blankenship RE, Touchman JW (2008) The Genome of Heliobacterium Modesticaldum, a Phototrophic Representative of the Firmicutes Containing the Simplest Photosynthetic Apparatus. J Bacteriol 190: 4687-4696

Tang KH, Blankenship RE (2010) Both Forward and Reverse TCA Cycles Operate in Green Sulfur Bacteria. J Biol Chem 285: 35848-35854

Tang KH, Feng X, Tang YJ, Blankenship RE (2009a) Carbohydrate Metabolism and Carbon Fixation in Roseobacter Denitrificans OCh114. PLoS One 4: e7233

Tang KH, Feng X, Zhuang WQ, Alvarez-Cohen L, Blankenship RE, Tang YJ (2010a) Carbon Flow of Heliobacteria Is Related More to Clostridia than to the Green Sulfur Bacteria. J Biol Chem 285: 35104-35112

Tang KH, Wen J, Li X, Blankenship RE (2009b) Role of the AcsF Protein in Chloroflexus Aurantiacus. J Bacteriol 191: 3580-3587

Tang KH, Yue H, Blankenship RE (2010b) Energy Metabolism of Heliobacterium Modesticaldum during Phototrophic and Chemotrophic Growth. BMC Microbiol 10: 150

Thauer RK (2007) Microbiology. A Fifth Pathway of Carbon Fixation. Science 318: 1732-1733

Wahl SA, Dauner M, Wiechert W (2004) New Tools for Mass Isotopomer Data Evaluation in (13)C Flux Analysis: Mass Isotope Correction, Data Consistency Checking, and Precursor Relationships. Biotechnol Bioeng 85: 259-268

Wu B, Zhang B, Feng X, Rubens JR, Huang R, Hicks LM, Pakrasi HB, Tang YJ (2010) Alternative Isoleucine Synthesis Pathway in Cyanobacterial Species. Microbiology 156: 596-602

Zhu XG, Long SP, Ort DR (2010) Improving Photosynthetic Efficiency for Greater Yield. Annu Rev Plant Biol 61: 235-261

Regulation of the Carbon and Nitrogen Balance by a Plastidic Invertase in *Arabidopsis*

Takanori Maruta[a], Kumi Otori[a], Tomoki Tabuchi[a], Noriaki Tanabe[a], Masahiro Tamoi[a,b], Shigeru Shigeoka[a,b,*]

[a]Japan Science and Technology Agency (JST), Core Research for Evolutional Science and Technology (CREST), Japan;
[b]Department of Advanced Bioscience, Faculty of Agriculture, Kinki University, Japan.
[*]Corresponding author. Tel./Fax No. +81 742 43 8083; E-mail: shigeoka@nara.kindai.ac.jp.

Abstract: Since the photosynthetic apparatus contains a massive amount of nitrogen in plants, the regulation of its development by sugar signals is important to the maintenance of the carbon-nitrogen balance. Here, we isolated an *Arabidopsis* mutant (*sicy-192*) whose cotyledon greening was inhibited by treatments with sugars, such as sucrose, glucose, and fructose. In the mutant, the gene encoding plastidic alkaline/neutral (A/N) invertase (INV-E) was point-mutated at codon 294, with Tyr substituted for Cys (C294Y). Interestingly, the greening of cotyledons in the knockout-INV-E lines was not inhibited by treatment with the sugars. The mutant INV-E was more stable than the wild-type INV-E. On treatment with sucrose, the expression of photosynthesis-related genes was weaker in seedlings of mutant plants than wild-type seedlings, while the activity of nitrate reductase was stronger in the mutant plants than wild-type plants. These findings suggest that Cys294 of INV-E is associated with the development of the photosynthetic apparatus and the assimilation of nitrogen in *Arabidopsis* seedlings to control the ratio of sucrose content to hexose content. The transcript and protein levels of plastid-encoded genes were lower in the *sicy-192* mutants than the wild-type plants, suggesting that sugar metabolism through INV-E promotes plastid signaling to regulate the carbon-nitrogen balance.

Keywords: Invertase; Carbon/nitrogen (C/N) balance; Greening; *Arabidopsis*

Introduction

The photosynthetic apparatus contains a massive amount of nitrogen and so its development closely depends on the distribution of nitrogen in plants. The system for regulating the distribution of nitrogen via sugar signaling appears to be important for the adjustment of primary metabolism to ensure growth, survival, and completion of the life cycle in plants. Therefore, the isolation of sugar-sensitive and -insensitive mutants should provide important clues to how the regulatory mechanism for the carbon-nitrogen balance in plants works (Castle *et al*., 1994; Hauser *et al*., 1995; Mita *et al*., 1997; Nemeth *et al*., 1998; Sato *et al*., 2009; Sheen *et al*., 1999).

We have recently isolated an *Arabidopsis* mutant, *sicy* (sugar-inducible cotyledon yellow)-*192*, that is a gain-of-function mutant of a plastidic invertase (INV-E). The cotyledon greening of the mutants was inhibited by treatments with sugars (Tamoi *et al*., 2010). Here we analyzed the expression of photosynthesis-related and nitrogen assimilation-related genes in the mutants. Moreover, we describe the effects of treatment with sucrose and plant hormones on the greening of *sicy-192* mutants in detail, and discuss how INV-E is involved in the regulation of plant development and carbon-nitrogen balance in plastids.

Materials and Methods

Sterilized *Arabidopsis* seeds were placed on 0.8% agar containing MS inorganic salt with or without sugar, incubated in a cold room (4 °C) for three days, and moved to a growth chamber (14 h-light, 25 °C/10 h-dark, 22 °C). Quantitative PCR analysis was performed as followings: total RNA was extracted

from whole seedlings grown for five days using QuickGene RNA cultured cell kit S (Fujifilm). To eliminate any DNA, the RNA was treated with DNase I (Takara) and converted into cDNA using the ReverTra Ace (Toyobo) with the oligo(dT)$_{20}$ primer. Primer pairs for quantitative RT-PCR were designed using Primer Express software (Applied Biosystems), and the gene-specific primers are shown in Tamoi *et al*. (2010). Quantitative PCR was performed with an Applied Biosystems 7300 Real Time PCR System, using the SYBR Premix Ex Taq (Takara). The transcript of *eIF4A-1* was used as an internal standard in all experiments.

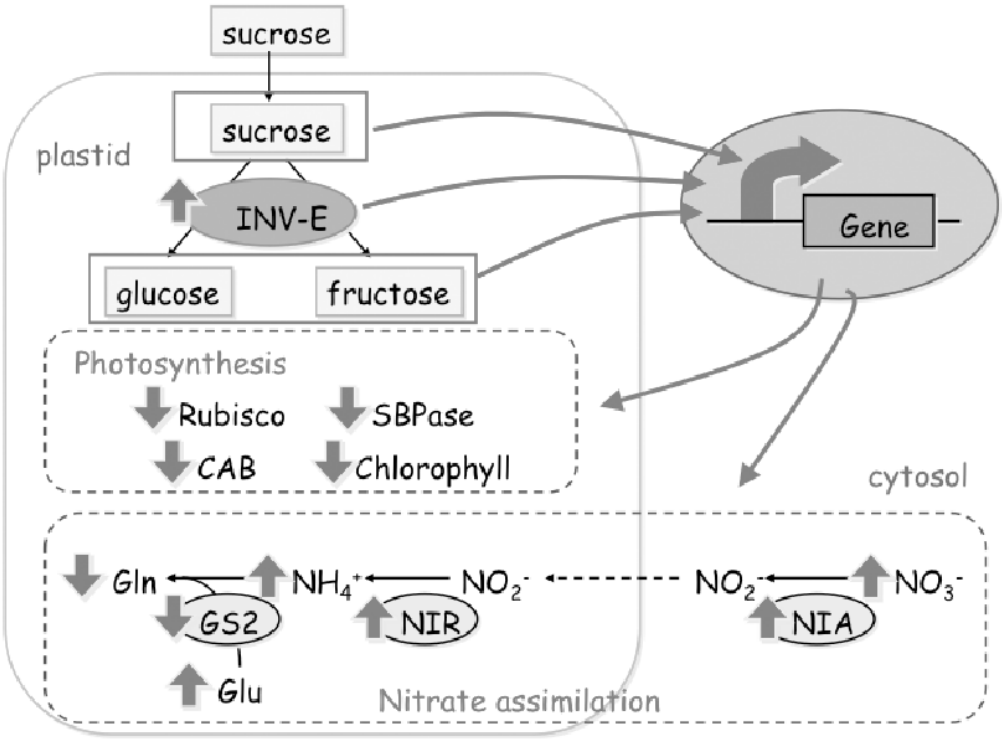

Fig. 1 Regulation of the carbon and nitrogen balance by INV-E.

Results and Discussion

In the *sicy-192* mutant, the gene encoding plastidic alkaline/neutral (A/N) invertase (INV-E) was point-mutated at codon 294, with Tyr substituted for Cys (C294Y). The Cys residue of INV-E was conserved in all A/N invertase proteins in plants including *Arabidopsis* and rice, suggesting that it has an important role in this family. A recombinant INV-E:C294Y protein had the same enzymatic activity and substrate specificity as a recombinant INV-E protein. Moreover, some putative A/N invertases in cyanobacteria, for example *Synechocystis* sp. PCC 6803, do not contain the Cys residue. These facts indicated that the Cys294 in A/N invertase is not necessary for its catalytic activity. Interestingly, the greening of cotyledons in the knockout-INV-E lines was not inhibited by treatment with the sugars. In addition, the knockout-INV-E lines expressing an *INV-E:C294Y* or *INV-E:C294A* gene had the same phenotype as *sicy-192* mutants, while the lines expressing a wild-type *INV-E* gene had the same phenotype as wild-type plants (Tamoi *et al*., 2010). Moreover, transgenic lines overexpressing the cyanobacterial invertase gene (*INV-A*: AJ489527) lacking the Cys residue corresponding to Cys-294 in INV-E showed inhibition of greening in the SUC$^+$ medium similar to the *sicy-192* mutants. Though the transcriptional level of *INV-E* was not altered, the protein and activity levels of INV-E were higher in the mutants than in the wild-type plants. These findings indicated that the mutant INV-E is more stable than the wild-type INV-E and Cys294 is necessary to regulate the stability of INV-E *in vivo* during greening.

To clarify the involvement of INV-E in the development of photosynthetic appartus, the transcript levels of the photosynthesis-related chlorophyll a/b

binding protein (*CAB*), sedoheptulose-1,7-bisphosphatase (*SBPase*), and plastidic fructose-1,6-bisphosphatase (*FBPase*) genes were lower in the five-day-old *sicy-192* plants than wild-type plants in the SUC^+ medium (Fig. 1; Tamoi *et al*., 2010). The protein levels of Rubisco large subunit (rbcL) and SBPase were also lower in the *sicy-192* seedlings. However, these decreases were not observed in the SUC^- medium. These data indicated that INV-E is associated with expression of photosynthesis-related genes and the development of the photosynthetic apparatus in *Arabidopsis* seedlings depends on the carbohydrate status of medium.

The photosynthetic apparatus contains a massive amount of nitrogen and thus its development is closely associated with the distribution of nitrogen in plants. To investigate the balance between the demand for nitrogen for the development of the photosynthetic apparatus and the supply of utilizable nitrogen to the cell by nitrate assimilation in sugar-treated *sicy-192* mutant plants, the transcript levels of nitrate assimilation-related genes and the activity of NR were analyzed. In the SUC^+ medium, transcript levels of the NR gene (*NIA1*) and nitrite reductase gene (*NIR1*) were higher in the *sicy-192* plants than wild-type plants. But there were no changes in the transcript levels of another NR gene (NIA2) in normal or SUC^+ medium (Fig. 1; Tamoi *et al*., 2010). The activities of total and active NR were higher in *sicy-192* mutants than wild-type plants in the SUC^+ medium. In *sicy-192* mutants in the SUC^+ medium, the NR activity state, which accounted for the NR activity of the active types as a percentage of total NR activity, was higher than that in the wild-type plants (Tamoi *et al*., 2010). It has been reported that NR activity was regulated not only at the transcriptional level, but also at the posttranslational level via phosphorylation and subsequent binding to 14-3-3 protein, leading to its degradation (40). Thus the suppression of NR activity at the posttranslational level may be affected by the change of sucrose-hydrolytic activity via the mutation of INV-E in plastids.

In *sicy-192* mutants, the development of the photosynthetic apparatus was inhibited in the Suc^+ medium, while the assimilation of nitrate was enhanced. These phenotypes of *sicy-192* were observed only during the greening of seedlings. Accordingly, INV-E is regulated for maintenance of the level of sucrose or its metabolites in plastids, preventing an imbalance between the supply of nitrogen to cells via nitrate assimilation and the demand for nitrogen for development of the photosynthetic apparatus. Thus, Cys-294 is necessary to regulate the activity of INV-E under conditions where the balance of carbon and nitrogen sources is disrupted.

Plant hormones such as abscisic acid (ABA) and ethylene are associated with sugar signaling (Smeekens 2000; Gazzarrini and McCourt, 2001). Additionally, ABA may be involved in plastid signaling (Koussevitzky *et al*., 2007; Kleine *et al*., 2007). Therefore, we studied the effects of such hormones on the greening inhibition in the sucrose-treated *sicy-192* mutants. However, ABA had no effect on the greening of *sicy-192* mutants grown on the Suc^+ medium. Moreover, the *sicy-192* and *abi4* (*abscisic acid insensitive 4*) double mutants, in which the transcription factor ABI4 involved in ABA signaling as well as sugar and plastid signaling is disrupted (Koussevitzky *et al*., 2007), showed the same sugar-sensitivity as the *sicy-192* mutants (Tamoi *et al*., 2010), indicating that the greening inhibition in *sicy-192* mutants was ABA-independent. Interestingly, co-treatment with sucrose and 1-amino cyclopropane-1-carbonic acid (ACC), a precursor of ethylene, markedly enhanced the greening inhibition in *sicy-192* mutants compared to sucrose alone (Maruta *et al*., 2010), suggesting the sugar signaling derived from plastids was related to ethylene signaling in *sicy-192* mutants to regulate greening and the carbon-nitrogen balance.

At present, we cannot explain how the sugar metabolism in plastids is associated with greening and the carbon-nitrogen balance in the *sicy-192* mutants. However, we have speculation that sugar metabolism through INV-E promotes plastid and/or hormone, such as ethylene, signaling to regulate both greening and the carbon-nitrogen balance (Maruta *et al*., 2010). These findings provide new insights into the regulation of greening and carbon-nitrogen balance by sugar metabolism through INV-E in plastids.

Acknowledgements

This work was supported by CREST, JST (SS: 2005–2010).

References

Castle LA, Meinke DW (1994) A FUSCA Gene of Arabidopsis Encodes a Novel Protein Essential for Plant Development. Plant Cell 6: 25-41

Gazzarrini S, McCourt P (2001) Genetic Interactions between ABA, Ethylene and Sugar Signaling Pathways. Curr. Opin. Plant Biol. 4: 387-391

Hauser MT, Morikami A, Benfey PN (1995) Conditional Root Expansion Mutants of Arabidopsis. Development 121: 1237-1252

Kleine T, Voigt C, Leister D (2009) Plastid Signalling to the Nucleus: Messengers Still Lost in the Mists? Trends. Genet. 25: 185-192

Koussevitzky S, Nott A, Mockler TC, Hong F, Sachetto-Martins G, Surpin M, Lim J, Mittler R, Chory J (2007) Signals from Chloroplasts Converge to Regulate Nuclear Gene Expression. Science 316: 715-719

Maruta T, Otori K, Tabuchi T, Tanabe N, Tamoi M, Shigeoka S (2010) New Insights into the Regulation of Greening and Carbon-Nitrogen Balance by Sugar Metabolism through a Plastidic Invertase. Plant Signal. Behav. 5: 1131-1133

Mita S, Hirano H, Nakamura K (1997) Negative Regulation in the Expression of a Sugar-Inducible Gene in Arabidopsis Thaliana. A Recessive Mutation Causing Enhanced Expression of a Gene for Beta-Amylase. Plant Physiol. 114: 575-582

Németh K, Salchert K, Putnoky P, Bhalerao R, Koncz-Kálmán Z, Stankovic-Stangeland B, Bakó L, Mathur J, Okrész L, Stabel S, Geigenberger P, Stitt M, Rédei GP, Schell J, Koncz C (1998) Pleiotropic Control of Glucose and Hormone Responses by PRL1, a Nuclear WD Protein, in Arabidopsis. Genes Dev. 12: 3059-3073

Sato T, Maekawa S, Yasuda S, Sonoda Y, Katoh E, Ichikawa T, Nakazawa M, Seki M, Shinozaki K, Matsui M, Goto DB, Ikeda A, Yamaguchi J (2009) CNI1/ATL31, a RING-type Ubiquitin Ligase that Functions in the Carbon/Nitrogen Response for Growth Phase Transition in Arabidopsis seedlings. Plant J. 60: 852-864

Sheen J, Zhou L, Jang JC (1999) Sugars as Signaling Molecules. Curr. Opon. Plant Biol. 2: 410-418

Smeekens S (2000) Sugar-Induced Signal Transduction in Plants. Annu. Rev. Plant Physiol. Plant Mol. Biol. 51: 49-81

Tamoi M, Tabuchi T, Demuratani M, Otori K, Tanabe N, Maruta T, Shigeoka S (2010) Point Mutation of a Plastidic Invertase Inhibits Development of the Photosynthetic Apparatus and Enhances Nitrate Assimilation in Sugar-Treated Arabidopsis Seedlings. J. Biol. Chem. 285: 15399-15407

Characterization of a pH-Sensitive Photosystem II Mutant in the Cyanobacterium *Synechocystis* sp. PCC 6803

Tina C Summerfield[a*], Roger Young[a], Louis A Sherman[b], Julian J Eaton-Rye[c]

[a]Department of Botany, University of Otago, P. O. Box 56, Dunedin, New Zealand;
[b]Department of Biological Sciences, Purdue University, West Lafayette, IN 47907, USA;
[c]Department of Biochemistry, University of Otago, P. O. Box 56, Dunedin, New Zealand.
[*]Corresponding author. Tel. No. +64 3 479 7875; Fax No. +64 3 479 7583; E-mail: tina.summerfield@otago.ac.nz.

Abstract: A number of photosystem II (PSII) mutants have been shown to grow photoautotrophically in media at pH 10.0 but not pH 7.5 [Eaton-Rye JJ, Shand JA, Nicoll WS (2003) FEBS Letters 543: 148-153]. These strains contain two or three mutations, including the absence of at least one of the extrinsic proteins associated with the lumenal face of PSII. However, these strains do not all lack the same extrinsic protein and some also contain mutations in a hydrophilic loop of the chlorophyll *a*-binding core antenna protein CP47. In pH 10.0 media, the different strains exhibited variation in photoautotrophic growth, oxygen evolution and PSII assembly. At pH 10.0 a strain lacking the two extrinsic proteins PsbO and PsbU assembled the highest number of PSII centres compared to other pH-sensitive mutants. To investigate the mechanisms enabling growth at elevated pH, we have used microarray analyses to determine the gene expression changes associated with the pH dependent recovery of the ΔPsbO:ΔPsbU mutant. We have compared the impact of the transition from pH 10.0 to pH 7.5 on gene expression in the wild type and in the ΔPsbO:ΔPsbU strain.

Keywords: Extrinsic proteins; Gene expression; Microarray; Photosystem II; pH; *Synechocystis*

Introduction

The crystallographic structures for Photosystem II (PSII) in *Thermosynechococcus vulcanus* at 3.7 Å and *Thermosynechococcus elongatus* at 3.5 Å (Kamiya and Shen, 2003; Ferreira *et al*., 2004) contain the PsbO, PsbU and PsbV extrinsic polypeptides associated with the lumenal face of the oxygen evolving complex. Cyanobacterial PsbQ and PsbP proteins have not been identified in the crystal structures but were identified in isolated PSII preparations from *Synechocystis* sp. PCC 6803 (hereafter *Synechocystis*) (Kashino *et al*., 2002; Thornton *et al*., 2004), indicating a role for five extrinsic proteins in *Synechocystis* (Thornton *et al*., 2004).

Synechocystis mutants lacking any one of these five proteins are able to grow photoautotrophically. However, strains lacking PsbO or PsbV, and to a lesser extent PsbU, show increased susceptibility to photoinactivation (Mayes *et al*., 1991; Morgan *et al*., 1998; Clarke and Eaton-Rye, 1999) and the PsbQ protein was shown to be required for optimal PSII activity (Roose *et al*., 2007).

The production of double mutants lacking more than one extrinsic protein identified a requirement for PsbQ in the absence of PsbV (Summerfield *et al*., 2005). This approach also showed the removal of both PsbO and PsbU produced a strain that was not photoautotrophic in unbuffered BG-11 (Eaton-Rye *et al*., 2003). However, photoautotrophic growth of both these double mutants could be recovered in BG-11 medium buffered at pH 10.0. Similar restoration of photoautotrophic growth at pH 10.0 was demonstrated in two mutants lacking PsbV and carrying a point mutation (E364Q) or short deletion Δ(R384-V392) in loop E of CP47 (Eaton-Rye *et al*., 2003). Photosynthetic performance of these mutants has been characterized but mechanisms enabling photoautotrophic growth at pH 10.0 but not at pH 7.5 or in unbuffered BG-11 have not been established.

Cyanobacteria are alkalitolerant and many thrive in environments with elevated pH. Adaptation to alkaline environments is associated with genome wide changes in gene expression in *Synechocystis*, including increased transcript abundance of a number genes encoding PSII proteins (Summerfield and Sherman, 2008). We have used DNA microarrays to investigate cellular adaptations that occur during changes in external pH associated with the differential growth of the pH-sensitive PSII mutants. We present preliminary data examing gene expression changes in the wild type (WT) and a ΔPsbO:ΔPsbU strain following transition from pH 10.0 to pH 7.5.

Materials and Methods

Culture maintenance and characterization were carried out according to Morgan *et al*. (1998) and Summerfield *et al*. (2005). Total RNA was extracted and purified using phenol-chloroform extraction and CsCl gradient purification as previously described (Reddy *et al*., 1990; Singh and Sherman, 2002). The microarray platform and construction was as described in Postier *et al*. (2003) and the cDNA labeling, prehybridization and hybridization protocols are described in detail in Singh *et al.* (2003). The microarray experiment involved a loop design that compared the WT and the ΔPsbO:ΔPsbU strain grown in BG-11 medium at pH 10.0 and 2 h following a transition to BG-11 medium at pH 7.5. Data acquisition and analysis was as described in Singh *et al*. (2003), the effects of interrupting *psbO* and *psbU* and the transition from pH 10.0 to pH 7.5 conditions were examined in an analysis of variance (ANOVA) essentially as described in Kerr and Churchill (2001a); Kerr and Churchill (2001b); Singh *et al.* (2003). We used the false discovery rate (FDR) of 5% to control the proportion of significant results that are Type I errors (false rejection of the null hypothesis) as described in (Summerfield and Sherman, 2007). Genes with an FDR = 0.05 (corresponding to 5% expected false positives) and that exhibited a change of at least 1.5-fold were considered interesting and retained for further analysis. The microarray experiment that examined the transition of WT *Synechocystis* from pH 7.5 to pH 10.0 (Summerfield and Sherman, 2008) was used to identify genes that were differentially regulated independent of the pH.

Results and Discussion

Five PSII mutant strains have been shown to grow photoautotrophically at pH 10.0 but not at pH 7.5. Each strain contains at least two mutations; two strains lacked two of the lumenal proteins of PSII, one strain lacked three PSII lumenal proteins and two strains lacked the PsbV lumenal protein and carried mutations in loop E of CP47. Physiological characterization of these mutants is summarized in Table 1 and was described in Eaton-Rye *et al.* (2003) and Summerfield *et al.* (2005). At pH 10.0, photoautotrophic doubling times were between 5 h and 20 h slower than the WT (Table 1).

Table 1 Photoautotrophic growth and relative rates of oxygen evolution and PSII assembly at pH 7.5 and 10.0 in *Synechocystis* sp. PCC 6803 strains lacking the extrinsic proteins and/or carrying mutations in loop E of CP47[a].

Strain	Photoautotrophic doubling time[b] (h)		Rate of oxygen evolution[c]				Chlorophyll/PSII ratio[f]	
			HCO_3^-[d]		$K_3Fe(CN)_6$[e]			
	pH 7.5	pH 10.0	pH 7.5	pH 10.0	pH 7.5	pH 10.0	pH 7.5	pH 10.0
WT	~13	~13	1.00	0.92	1.00	0.97	1.00	1.01
ΔPsbQ:ΔPsbV	ng[g]	~18	0.58	0.60	0.24	0.42	0.45	0.37
ΔPsbO:ΔPsbU	ng	~24	0.59	0.69	0.31	0.36	0.52	1.03
ΔPsbO:ΔPsbU:ΔPsbQ	ng	~33	0.54	0.65	0.33	0.36	0.40	0.67
E364Q:ΔPsbV	ng	~21	0.63	0.70	0.36	0.45	0.35	0.57
Δ(R384-V392):ΔPsbV	ng	~26	0.29	0.45	0.19	0.19	0.37	0.36

[a]Data from Summerfield *et al*., 2005. [b]The estimated doubling time used for this calculation was based on initial growth. [c]The rate of oxygen evolution was stable for at least 2 min of illumination. [d]Oxygen evolution supported by HCO_3^- was normalized to wild-type rate of 390 μmol O_2 (mg chlorophyll)$^{-1}$ h^{-1} at pH 7.5. [e]Oxygen evolution was supported by 1.0 mmol $K_3Fe(CN)_6$ and 0.2 mmol 2,5-dimethyl-*p*-benzoquinone and normalized to a wild type rate at pH 7.5 of 435 μmol O_2 (mg chlorophyll)$^{-1}$ h^{-1}. [f]as determined by [^{14}C]-atrazine binding and normalized to a wild type at pH 7.5 chlorophyll/PSII ratio of 460. [g]ng = no growth.

These strains evolved oxygen at pH 7.5 and most exhibited increased rate of oxygen evolution at pH 10.0 (Table 1). However, variation was observed in the rates of oxygen evolution at pH 7.5 and the increase at pH 10.0. For example in a Δ(R384-V392):ΔPsbV strain, the rate of oxygen evolution at pH 10.0 supported by bicarbonate was 1.5 times the rate at pH 7.5 but the PSII-specific rate was not altered by pH. Conversely, the ΔPsbQ:ΔPsbV strain exhibited similar whole chain oxygen evolution rates at pH 7.5 and pH 10.0 but PSII-specific rates were 1.75 times higher at pH 10.0 than pH 7.5. Three of the five strains exhibited increased numbers of PSII centres at pH 10.0. The ΔPsbO:ΔPsbU strain showed the largest increase in PSII centres at pH 10.0 having a similar number of centres to WT, although the rate of oxygen evolution remained lower in the mutant. These data show the relationship between photoautotrophic growth at pH 10.0, oxygen evolution and number of PSII centres is complex.

The WT strain showed similar doubling time, oxygen evolution and number of PSII centres at pH 10.0 compared to pH 7.5 (Table 1). Although initial doubling times were similar at both pHs, at elevated pH the WT grew to an $OD_{730\ nm}$ ~3, compared to $OD_{730\ nm} < 2$ when grown at pH 7.5 (Fig. 1).

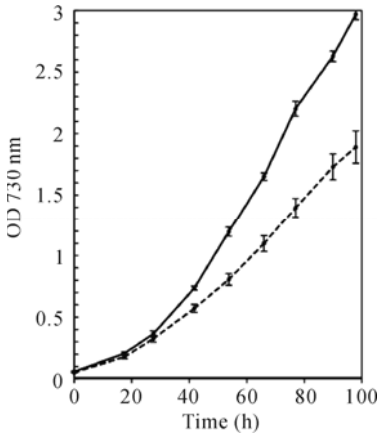

Fig. 1 Photoautotrophic growth curve of *Synechocystis* sp. PCC 6803 wild type in BG-11 at pH 7.5 (dashed line) and BG-11 at pH 10 (solid line). The data are the average ± standard error of three to five independent experiments. Error bars not visible are smaller than the symbols.

Previous microarray data indicated many genes (~12%) exhibited altered transcript levels in the WT at 2 h following transition from pH 7.5 to pH 10.0 (Summerfield and Sherman, 2008). To investigate the cellular changes enabling prolonged growth of the WT at pH 10.0, and to examine whether this is associated with recovery of the PSII mutants at pH 10.0, we determined gene expression changes in the WT and the ΔPsbO:ΔPsbU strain following the transition from pH 10.0 to pH 7.5. The strain ΔPsbO:ΔPsbU was selected as it exhibits the greatest recovery of PSII centres at pH 10.0 compared to pH 7.5.

The WT and ΔPsbO:ΔPsbU strain were grown photoautrotrophically at pH 10.0, transferred to pH 7.5, cells were harvested at 0 h and after 2 h at pH 7.5. The microarray design enabled comparison of both the WT and ΔPsbO:ΔPsbU strain at pH pH 10 vs pH 7.5. Genes with altered transcript abundance at 2 h following the transition from pH 10.0 to pH 7.5 represented 13% and 12% of the genome for the WT and ΔPsbO:ΔPsbU strain, respectively. In the WT more genes showed decreased than increased transcript abundance at pH 7.5, in contrast in the ΔPsbO:ΔPsbU strain more genes exhibited increased than decreased mRNA levels at pH 7.5.

Genes exhibiting altered mRNA levels were divided into functional categories according to Cyanobase (http://bacteria.kazusa.or.jp/cyanobase). For both strains more than half the genes with altered transcript abundance were hypothetical, other and unknown genes, of these more than two thirds exhibited decreased abundance in WT and approximately half were decreased in the ΔPsbO:ΔPsbU strain. The proportion of the differentially expressed genes (excluding hypothetical, other and unknown genes), belonging to each functional category is shown in Fig. 2.

The strains exhibited similar responses for a number of categories including: amino acid biosynthesis, biosynthesis of cofactors, prosthetic groups, and carriers, cellular processes, regulatory functions and transcription. In the WT, the category with the largest number of differentially abundant transcripts following transfer to pH 7.5 was the transport and binding proteins and mRNA levels of many of these genes were increased. These included many cation transporters that may be required to maintain cellular homeostasis at lower pH. These genes did not exhibit increased transcript abundance in the ΔPsbO:ΔPsbU strain.

Another category that exhibited a different response in the WT and ΔPsbO:ΔPsbU strain after transfer to pH 7.5 was cell envelope. Transcript levels of a number of cell envelope genes were increased in the mutant at pH 7.5 compared to pH 10. This included several pilin encoding genes that did not

show altered expression in the WT. In the mutant, photosynthesis and respiration genes showed the largest change on transfer to pH 7.5 and the majority of these genes exhibited increased transcript levels at pH 7.5, these genes were not altered in the WT. Gene expression data has identified a number of candidate genes for further investigation of the recovery of pH-sensitive PSII mutants.

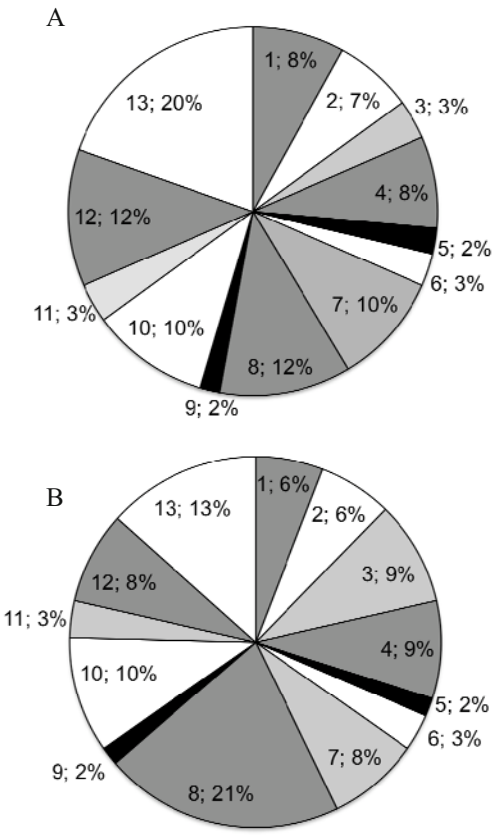

Fig. 2 Proportion of gene differentially expressed genes belonging to different functional categories, following the transition from pH 10.0 to pH 7.5. Functional categories are: 1, Amino acid biosynthesis; 2, Biosynthesis of cofactors, prosthetic groups, and carriers; 3, Cell envelope; 4, Cellular processes; 5, Central intermediary metabolism; 6, DNA replication, restriction, modification, recombination, and repair; 7, Energy metabolism; 8, Photosynthesis and respiration; 9, Purines, pyrimidines, nucleosides, and nucleotides; 10, Regulatory functions; 11, Transcription; 12, Translation; 13, Transport and binding proteins. A. wild type *Synechocystis* sp. PCC 6803. B. ΔPsbO:ΔPsbU strain. Genes exhibiting ≥ 1.5-fold change were considered differentially expressed. The functional categories: hypothetical, unknown and other were not included.

References

Clarke SM, Eaton-Rye JJ (1999) Mutation of Phe-363 in the Photosystem II Protein CP47 Impairs Photoautotrophic Growth, Alters the Chloride Requirement, and Prevents Photosynthesis in the Absence of either PSII-O or PSII-V in Synechocystis sp. PCC 6803. Biochemistry 38: 2707-2715

Eaton-Rye JJ, Shand JA, Nicoll WS (2003) pH-Dependent Photoautotrophic Growth of Specific Photosystem II Mutants Lacking Lumenal Extrinsic Polypeptides in Synechocystis PCC 6803. FEBS Lett 543: 148-153

Ferreira KN, Iverson TM, Maghlaoui K, Barber J, Iwata S (2004) Architecture of the Photosynthetic Oxygen-Evolving center. Science 303: 1831-1838

Kamiya N SJR (2003) Crystal Structure of Oxygen-Evolving Photosystem II from Thermosynechococcus Vulcanus at 3.7-Å Resolution. Proc Natl Acad Sci USA 100: 98-103

Kashino Y, Lauber WM, Carroll JA, Wang Q, Whitmarsh J, Satoh K, Pakrasi HB (2002) Proteomic Analysis of a Highly Active Photosystem II Preparation from the Cyanobacterium Synechocystis sp. PCC 6803 Reveals the Presence of Novel Polypeptides. Biochemistry 41: 8004-8012

Kerr MK, Churchill GA (2001a) Experimental Design for Gene Expression Microarrays. Biostatistics 2: 183-201

Kerr MK, Churchill GA (2001b) Statistical Design and the Analysis of Gene Expression Microarray Data. Genet Res 77: 123-128

Mayes SR, Cook KM, Self SJ, Zhang Z, Barber J (1991) Deletion of the Gene Encoding the Photosystem II 33 kDa Protein from Synechocystis sp. PCC 6803 Does Not Inactivate Water-Splitting but Increases Vulnerability to Photoinhibition. Biochim Biophys Acta - Bioenergetics 1060: 1-12

Morgan TR, Shand JA, Clarke SM, Eaton-Rye JJ (1998) Specific Requirements for Cytochrome C-550 and the Manganese-Stabilizing Protein in Photoautotrophic Strains of Synechocystis sp. PCC 6803 with Mutations in the Domain Gly-351 to Thr-436 of the Chlorophyll-Binding Protein CP47. Biochemistry 37: 14437-14449

Postier BL, Wang HL, Singh A, Impson L, Andrews HL, Klahn J, Li H, Risinger G, Pesta D, Deyholos M, Galbraith DW, Sherman LA, Burnap RL (2003) The Construction and Use of Bacterial DNA Microarrays Based on an Optimized Two-

Stage PCR Strategy. BMC Genomics 4: 23

Reddy KJ, Webb R, Sherman LA (1990) Bacterial RNA Isolation with One Hour Centrifugation in a Table-Top Ultracentrifuge. Biotechniques 8: 250-251

Roose JL, Kashino Y, Pakrasi HB (2007) The PsbQ Protein Defines Cyanobacterial Photosystem II Complexes with Highest Activity and Stability. Proc Natl Acad Sci USA 104: 2548-2553

Singh AK, McIntyre LM, Sherman LA (2003) Microarray Analysis of the Genome-Wide Response to Iron Deficiency and Iron Reconstitution in the Cyanobacterium Synechocystis sp. PCC 6803. Plant Physiol 132: 1825-1839

Singh AK, Sherman LA (2002) Characterization of a Stress-Responsive Operon in the Cyanobacterium Synechocystis sp. Strain PCC 6803. Gene 297: 11-19

Summerfield TC, Shand JA, Bentley FK, Eaton-Rye JJ (2005) PsbQ (Sll1638) in Synechocystis sp. PCC 6803 Is Required for Photosystem II Activity in Specific Mutants and in Nutrient-Limiting Conditions. Biochemistry 44: 805-815

Summerfield TC, Sherman LA (2007) Role of Sigma Factors in Controlling Global Gene Expression in Light/Dark Transitions in the Cyanobacterium Synechocystis sp. Strain PCC 6803. J Bacteriol 189: 7829-7840

Summerfield TC, Sherman LA (2008) Global Transcriptional Response of the Alkali-Tolerant Cyanobacterium Synechocystis sp. Strain PCC 6803 to a pH 10 Environment. Appl Environ Microbiol 74: 5276-5284

Thornton LE, Ohkawa H, Roose JL, Kashino Y, Keren N, Pakrasi HB (2004) Homologs of Plant PsbP and PsbQ Proteins Are Necessary for Regulation of Photosystem II Activity in the Cyanobacterium Synechocystis 6803. Plant Cell 16: 2164-2175

Solar-Powered Production of Biofuels and Other Petroleum Substitutes by Cyanobacteria: Stoichiometries of Reducing Equivalents and Chemical Energy, and Energy Conversion Efficiency

Wim Vermaas

School of Life Sciences and Center for Bioenergy and Photosynthesis, Arizona State University,
Box 874501, Tempe, AZ 85287-4501, USA.
Tel. No. +1 480 965 6250; Fax No. +1 480 965 6899; E-mail: wim@asu.edu.

Abstract: Cyanobacteria are a promising platform for solar-powered, CO_2-consuming production of biofuels, petroleum substitutes, and other useful products using photosynthesis. Efficient production of such compounds requires that the stoichiometry of reducing equivalents (NADPH) and chemical energy (ATP) produced as a result of photosynthetic electron transport is well-matched by the stoichiometry of reducing equivalents and chemical energy required for production of the desired compounds. Here it is shown that stoichiometry requirements are met when producing compounds generated via the fatty acid or isoprenoid biosynthesis pathways. In the case of fatty acid production, the amount of energy stored in the fatty acid can be up to 28% of the energy of the light if one were to excite with 680 nm light and all absorbed light was used for fatty acid production. Making adjustments for solar illumination (only ~50% of the energy can be used for photosynthesis), blue-photon utilization, and losses due to non-photochemical quenching and the requirements for maintenance energy, the solar energy conversion efficiency may still be in the range of ~7%, which is superior to most other bio-based approaches. However, photohydrogen production that directly uses reducing equivalents from photosynthetic electron transfer for H_2 production does not require ATP and thereby is not properly stoichiometrically balanced. An additional complexity of H_2 production in relatively small cyanobacterial cells at somewhat alkaline pH is that the number of free protons in a cell is extremely limited (a few protons per cyanobacterial cell of 1 fL at pH 8.0). However, regardless the inherent difficulties of light-driven H_2 production in cyanobacteria, the utilization of cyanobacteria for light-driven generation of carbon-based biofuels and related products can be efficient and is very promising.

Keywords: Cyanobacteria; Solar-to-Fuel conversion; Stoichiometry; Energy conversion efficiency

Introduction

Solar energy is the largest under-utilized energy source that may be tapped in our search for scalable alternative energy approaches as the amount of CO_2 in the atmosphere continues to rise and the amount of available fossil fuel is finite. Whereas reasonably efficient solar energy conversion to electricity is now feasible by means of photovoltaics, scalable and efficient generation of transportation fuels from renewable sources is more problematic. Terrestrial biomass can be converted to alcohols, but the efficiency of the overall process (energy of transportation fuel generated per amount of solar energy that hit the field used for biomass production) is relatively poor, particularly when considering the energy needed for transportation and biomass-to-fuel conversion processes.

Aquatic organisms that perform oxygenic photosynthesis provide an avenue to enhance the overall efficiency of solar energy conversion for production of fuels and other products currently coming from oil. Particularly photosynthetic microbes that can grow under relatively alkaline conditions,

such as cyanobacteria, offer major advantages with respect to efficiency of energy conversion. There are several reasons: (1) At alkaline pH, CO_2 is slowly hydrated and carbonic acid is readily converted to bicarbonate (pK_A~6.4). (2) CO_2 is more than an order of magnitude more soluble in water than N_2 or O_2. (3) Aquatic cultures can be maintained throughout the year in warmer parts of the world, and solar energy can be used productively at all times. (4) Photosynthetic microbes do not need to maintain an extensive infrastructure of stems and roots; in particular, cyanobacteria do not need to maintain organelles that are not central to photosynthesis, and essentially are free-living chloroplasts.

With the advent of metabolic engineering approaches, it has become possible to greatly alter the scope of products that can be made. Selected cyanobacteria such as *Synechocystis* sp. PCC 6803 are transformable, and their metabolism can be readily modified to produce significant levels of biofuels or related compounds (Atsumi *et al*., 2009). However, when significantly altering metabolic fluxes in an organism, it is important to keep in mind that for efficient solar-powered production of biofuels and other petroleum substitutes by cyanobacteria a balanced stoichiometry of generation and utilization of reducing equivalents and chemical energy is required. This balancing act, together with substrate concentration considerations, will be covered in some detail in the following sections.

Stoichiometry of Reducing Power and Energy

It is important that pathways to produce biofuels or related compounds utilize reducing equivalents (NADPH) and chemical energy (ATP) in a stoichiometry that corresponds to what is provided by photosynthesis. The reason for this is that the pools of NADP/NADPH and ATP/ADP/AMP are of rather limited size in cells and each must be regenerated quickly. If the stoichiometry of NADPH and ATP utilization would not be in line with the stoichiometry of production, then either reducing power or chemical energy would impose a rate limitation and the overall productivity would be reduced.

Linear photosynthetic electron transfer through photosystems II and I provides 2 or 3 protons per electron transported. One proton per electron is secreted into the thylakoid lumen upon water splitting, one proton per electron is translocated across the thylakoid membrane through plastoquinone, and a third proton may be translocated if the Q cycle around the cytochrome b_6f complex is operational. Based on results with chloroplasts, this stoichiometry is closer to 3 under unstressed conditions as the Q cycle is thought to be continually engaged then (Sacksteder *et al*., 2000). The number of protons to be translocated per ATP synthesized is now generally accepted to be four (Kobayashi *et al*., 1995; van Walraven *et al*., 1996). Per two electrons transported and per one NADPH formed, 1.5 molecules of ATP can be synthesized if the Q cycle is operational, and 1 ATP molecule if the Q cycle does not work. Cyclic electron transfer around photosystem I can provide additional proton translocation and ATP synthesis, at the expense of photons that otherwise could have been used for linear electron transport. Many cyanobacteria have a high ratio of photosystem I to photosystem II, suggesting a significant potential for cyclic electron flow around photosystem I, but rates of cyclic electron flow in cyanobacteria appear to be sluggish as reduction of $P700^+$ in the absence of photosystem II activity is on the order of hundreds of ms (Yeremenko *et al*., 2005).

For optimal light-driven production of desired compounds, the cell should invest its photosynthate into synthesis of bioproducts rather than growth and maintenance of the photosynthetic microbe. Therefore, it is important that the ratio by which NADPH and ATP are used for the combined reactions of CO_2 fixation (if applicable) and generation of the desired product is close to that of generation of NADPH and ATP (1:1 to 1:1.5) by linear photosynthetic electron flow.

As shown in Fig. 1, the NADPH and ATP requirement for generation of fatty acids from photosynthate generally fits very well with the stoichiometry of NADPH and ATP generation by photosynthesis. Actually, if assuming a stoichiometry value of NADPH and ATP generation of 3:4 (or 1:1.33, meaning that the Q cycle is active most of the time but not all the time), linear photosynthetic electron transport provides essentially the ratio of reducing power and energy that is required for fatty acid biosynthesis. Note that this reaction scheme allows for a direct conversion of fixed CO_2 into fatty acid via reactions of glycolysis, acetyl-CoA generation, and fatty acid biosynthesis. In contrast to what is generally done for biomass-based approaches,

the cyanobacterial platform allows for direct conversion of photosynthate to fatty acids, thus saving a significant number of biochemical steps and greatly boosting the degree of energy conservation.

As shown in Fig. 1, the theoretical maximum of the amount of energy stored in fatty acids relative to the amount of light energy absorbed to produce these fatty acids by means of photosynthesis is over 28%. This is a theoretical maximum calculated for illumination with 680 nm light. When illuminating with sunlight, this energy conversion efficiency will be at least a factor of two lower as about half of the energy in sunlight is in the infrared part of the spectrum that is not used for photosynthesis by cyanobacteria. Moreover, in practice this percentage will also be lower as (1) cells will need to use some energy for maintenance and repair, (2) non-photochemical quenching (NPQ) may occur resulting in the energy of some absorbed photons to be converted fully to heat, and (3) all absorbed photons in the visible range (400–700 nm) will be converted to the energy equivalent of 680–700 nm photons used for chlorophyll-driven photosynthesis in the two photosystems; therefore, a blue photon with about 70% more energy than a red photon drives the same photosynthesis process as a red photon.

However, even with these cautionary notes a conversion of photosynthate directly to fatty acids can have a significantly higher energy conversion efficiency than is seen with energy conversion pathways that have carbohydrates or other storage metabolites as intermediates. A reasonable estimate of the energy conversion efficiency that can be obtained under practical conditions can be derived as follows: (1) The theoretical conversion efficiency is 28% (Fig. 1); (2) correction for non-PAR (photosynthetically active radiation) in sunlight: 28% is halved to 14%; (3) blue photons have about 70% more energy than red ones, and on average about one third of the absorbed energy in the visible light spectrum is converted to heat: 14% is reduced to about 10%. Losses due to NPQ and requirements for biomass synthesis and maintenance depend on the specific conditions and are difficult to quantify, but obviously should be minimized.

In view of these considerations, a maximum energy conversion effiency (sunlight to fatty acid) of around 7%, allowing some loss for culture growth and maintenance as well as NPQ, should be a reasonable target if the amount of biomass generation can be minimized.

Fig. 2 illustrates another scenario, namely that of isoprene production. Lindberg *et al.* (2010) have demonstrated the production of isoprene (C_5H_8) by the cyanobacterium *Synechocystis* equipped with an isoprene synthase enzyme modified from that of kudzu. Cyanobacteria and chloroplasts employ the MEP (methyl erythritol phosphate or, more precisely, 2-C-methyl-D-erythritol-4-phosphate) pathway for isoprenoid biosynthesis (see Eisenreich *et al.* (2004) for a review). The canonical scheme of this pathway starts from pyruvate and glyceraldehyde-3-phosphate (G3P) but in *Synechocystis* other inputs are possibly present (Ershov *et al*., 2004).

The stoichiometry of the use of reducing equivalents (simplified to NADPH here, even though other forms of reducing equivalents may be used in the pathway) and chemical energy (ATP or equivalent converted to ADP) is 14:19 in the MEP pathway (see Fig. 2). The conversion of CTP to CMP in the pathway is counted as two ATP-to-ADP equivalents. This ratio is very close to the 1:1.3 ratio required for fatty acid biosynthesis (Fig. 1) and falls well within the range of the 1:1 to 1:1.5 ratios that linear photosynthetic electron transport can ideally provide.

A second pathway for the biosynthesis of isoprene precursors is the mevalonate pathway (see Kuzuyama (2002) for a review). This pathway is present in some bacteria, archaea and most eukaryotes, and plants use this pathway for cytoplasmic isoprenoid production; in plants the MEP pathway is used for isoprenoid production in the plastid (see Eisenreich *et al*. (2004) for a review). Importantly, introduction of the mevalonate pathway into *E. coli*, an organism that naturally employs only the MEP pathway for isoprenoid biosynthesis, has led to greatly increased isoprenoid biosynthesis rates (Martin *et al*., 2003; Yoon *et al*., 2009). Moreover, optimization of the mevalonate pathway has led to major improvements in the flux through the pathway in yeast (Ro *et al*., 2006) and *E. coli* (reviewed in Keasling (2008)).

If one would introduce the mevalonate pathway into cyanobacteria in order to boost the capacity of isoprenoid production, then the calculated NADPH/ATP utilization ratio is 14:24. This ratio is not within the range between 1:1 and 1:1.5, but cyclic electron flow around photosystem I can help to further enhance ATP supply.

Carbon fixation:

24 CO_2 + 64 ATP + 40 NADPH	→ 8 PGA + 64 ADP + 40 NADP + 64 P_i
8 PGA + 8 ADP + 8 P_i + 8 NAD + 8 CoA	→ 8 acetyl-CoA + 8 CO_2 + 8 NADH + 8 ATP
8 Acetyl-CoA + 7 ATP + 16 NADPH	→ 8 CoA + C16 fatty acid + 7ADP + 7P_i + 16 NADP
Net: 16 CO_2 + 63 ATP + 48 NADPH	**→ C16 fatty acid + 63 ADP + 63 P_i + 48 NADP**

Light reactions (linear electron flow):

48 H_2O + 48 NADP + 192 hν + 64 ADP/P_i	→ 48 NADPH + 24 O_2 + 64 ATP
A mole of quanta of 680 nm light:	177 kJ
A mole of C_{16} fatty acid:	9800 kJ
Maximum energy efficiency (680 nm illumination):	9800x100%/(177x192) = **28.8%**

Fig. 1 Summary of the "gold standard" reactions to photosynthetically generate fatty acids, and of the maximum energy efficiency of the reactions. PGA: 3-phosphoglycerate, the product of the RuBisCO-catalyzed reaction. Note that the efficiency calculation uses 680 nm monochromatic light.

Carbon fixation and mevalonate pathway:

9 CO_2 + 24 ATP + 15 NADPH	→ 3 PGA + 24 ADP + 15 NADP + 24 P_i
3 PGA + 3 ADP + 3 P_i + 3 NAD + 3 CoA	→ 3 acetyl-CoA + 3 CO_2 + 3 NADH + 3 ATP
3 Acetyl-CoA + 3 ATP + 2 NADPH	→ Isoprene + CO_2 + 3 CoA + 3 ADP + P_i + PP_i + 2 NADP
Net: 5 CO_2 + 24 ATP + 14 NADPH	**→ Isoprene + 24 ADP + 22 P_i + PP_i + 14 NADP**

Carbon fixation and MEP pathway:

6 CO_2 + 16 ATP + 10 NADPH	→ 2 PGA + 16 ADP + 10 NADP + 16 P_i
2 PGA + NADPH	→ G3P + pyruvate + NADP
G3P + pyruvate + ATP + CTP + 3 NADPH	→ isoprene + CO_2 + ADP + CMP + P_i +PP_i + 3 NADP
Net: 5 CO_2 + 17 ATP + CTP + 14 NADPH	**→ Isoprene + 17 ADP + CMP + 17 P_i + PP_i + 14 NADP**

Light reactions (linear electron flow):

14 H_2O + 14 NADP + 56 hν + 19 ADP/P_i → 14 NADPH + 7 O_2 + 19 ATP

Fig. 2 Summary of the "gold standard" reactions to photosynthetically generate isoprene. For simplicity, all reducing equivalents have been represented as NADPH/NADP. Note that the MEP pathway requires somewhat less energy (ATP/CTP) than the mevalonate pathway.

Hydrogen Production

As indicated above, the stoichiometry of NADPH and ATP utilization for CO_2 fixation and production of petroleum substitutes via the fatty acid or isoprenoid biosynthesis pathways is in line with the stoichiometry of NADPH and ATP generation via linear photosynthetic electron transport. However, this is not necessarily the case for H_2 production, if H_2 is to be produced directly from reducing equivalents generated by linear photosynthetic electron flow: reducing equivalents are required for hydrogen production, but ATP is not. Therefore, even if an O_2-tolerant hydrogenase were to be introduced into a cyanobacterium and most photosynthetically generated electrons were used for H_2 production, pathways to utilize ATP will need to be introduced as well in order to reduce the buildup of a very large proton gradient across the thylakoid membrane that cannot be dissipated due to the lack of ADP and that inhibits photosynthetic electron transfer. Options include to add an uncoupler or to grow under conditions where there is a large ATP requirement for, for example, ion pumping; the latter may be achieved by growing under conditions of high salt concentration in the medium.

Cellular Substrate Concentrations

Another important criterion is the substrate concentration required for generation of the desired product. As cyanobacteria are relatively small, with a cell diameter of typically 1 or 2 μm, the volume of a cell is only a few fL. If one molecule is present in 1 fL (one cell), the corresponding concentration is 1.7 nmol. This concentration is very low relative to the actual concentration of most metabolites, and therefore generally thousands if not millions of molecules are present if the internal concentration of a particular metabolite or building block (such as CO_2 or bicarbonate) is in the μM or mmol range. However, the concentration of protons, the substrate for hydrogenase if H_2 production is envisioned, is very low at physiological pH. For example, at pH 8.0,

which is realistic for cyanobacteria that are somewhat alkalinophilic, only about 6 free protons are expected per cell if the cell volume is 1 fL.

In hydrogenases, amino acid residues shuttle protons between the surface of the enzyme and the active site (for example, Dementin *et al*., 2004). This provides a buffer between the bulk medium inside the cell and the active site of the enzyme. Whereas very few free protons are available in small cells under somewhat alkaline conditions, "stored" protons are available at high concentration as parts of buffering groups of proteins and metabolites and presumably offer the great majority of protons used by hydrogenase. Nonetheless, the low number of free protons inside the cell may present challenges to obtain optimal rates of hydrogen production.

These considerations illustrate the excellent suitability of cyanobacteria for light-energy-driven metabolic engineering purposes, particularly to fix CO_2 and produce compounds generated via, for example, the fatty acid and isoprenoid biosynthesis pathways.

Acknowledgements

Biofuels-related research in my group is funded by the US Department of Energy's ARPA-E Program (DE-AR0000011) and by the ASU Intellectual Fusion Fund.

References

Atsumi S, Higashide W, Liao JC (2009) Direct Photosynthetic Recycling of Carbon Dioxide to Isobutyraldehyde. Nature Biotechnol. 27: 1177-1142

Dementin S, Burlat B, de Lacey AL, Pardo A, Adryanczyk-Perrier G, Giugliarelli B, Fernandez VM, Rousset M (2004) A Glutamate Is the Essential Proton Transfer Gate during the Catalytic Cycle of the [NiFe] Hydrogenase. J. Biol. Chem. 279: 10508-10513

Eisenreich W, Bacher A, Arigoni D, Rohdich F (2004) Biosynthesis of Isoprenoids Via the Non-Mevalonate Pathway. Cell Mol. Life Sci. 61: 1401-1426

Ershov YV, Gantt RR, Cunningham FX, Gantt E (2002) Isoprenoid Biosynthesis in Synechocystis sp Strain PCC6803 Is Stimulated by Compounds of the Pentose Phosphate Cycle but Not by Pyruvate or Deoxyxylulose-5-Phosphate. J. Bacteriol. 184: 5045-5051

Keasling JD (2008) Synthetic Biology for Synthetic Chemistry. ACS Chem. Biol. 3: 64-76

Kobayashi Y, Kaiser W, Heber U (1995) Bioenergetics of Carbon Assimilation in Intact Chloroplasts: Coupling of Proton to Electron Transport at the Ratio H^+/e^- =3 Is Incompatible with H^+/ATP=3 in ATP Synthesis. Plant Cell Physiol 36: 1629-1637

Kuzuyama T (2002) Mevalonate and Nonmevalonate Pathways for the Biosynthesis of Isoprene Units. Biosci. Biotechnol. Biochem. 66: 1619-1627

Lindberg P, Park S, Melis A (2010) Engineering a Platform for Photosynthetic Isoprene Production in Cyanobacteria, Using Synechocystis as the Model Organism. Metabolic Eng. 12: 70-79

Martin VJ, Pitera DJ, Withers ST, Newman JD, Keasling JD (2003) Engineering a Mevalonate Pathway in Escherichia Coli for Production of Terpenoids. Nature Biotechnol. 21: 796-802

Ro DK, Paradise EM, Ouellet M, Fisher KJ, Newman KL, Ndungu JM, Ho KA, Eachus RA, Ham TS, Kirby J, Chang MC, Withers ST, Shiba Y, Sarpong R, Keasling JD (2006) Production of the Antimalarial Drug Precursor Artemisinic Acid in Engineered Yeast. Nature 440: 940-943

Sacksteder CA, Kanazawa A, Jacoby ME, Kramer DM (2000) The Proton to Electron Stoichiometry of Steady-State Photosynthesis in Living Plants: a Proton-Pumping Q Cycle Is Continuously Engaged. Proc. Natl Acad. Sci. USA 97: 14283-14288

van Walraven HS, Strotmann H, Schwarz O, Rumberg B (1996) The H^+/ATP Coupling Ratio of the ATP Synthase from Thiol-Unmodulated Chloroplasts and Two Cyanobacterial Strains Is Four. FEBS Lett. 379: 309-313

Yeremenko N, Jeanjean R, Prommeenate P, Krasikov V, Nixon PJ, Vermaas WFJ, Haxaux M, Matthijs HCP (2005) Open Reading Frame ssr2016 Is required for antimycin A-sensitive photosystem I-Driven Cyclic Electron Flow in the Cyanobacterium Synechocystis sp. PCC 6803. Plant Cell Physiol. 46: 1433-1436

Yoon SH, Lee SH, Das A, Ryu HK, Jang HJ, Kim JY, Oh DK, Keasling JD, Kim SW (2009) Combinatorial Expression of Bacterial Whole Mevalonate Pathway for the Production of -Carotene in E coli. J. Biotechnol. 140: 218-226

D1′—a New Member of D1 Protein Family in Cyanobacteria

Ciprian Chis[a,c], Abdulah Mahboob[b], Sergey Vassilieev[b], Adriana Bica[c], Loredana Peca[c], Doug Brouce[b], Eva-Mari Aro[d] , Cosmin Ionel Sicora[ac*]

[a]Biological Research Center Jibou, Romania;
[b]Department of Biological Sciences, Brock University, St. Catharines, Ontario, Canada;
[c]Biological Research Institute Cluj-Napoca,Romania;
[d]Department of Biology, Plant Physiology and Molecular Biology, University of Turku, Finland.
[*]Corresponding author. Tel. No. +40732002251; Fax No. +40260644950; E-mail: cosmin.sicora@gmail.com.

Abstract: The D1 protein of Photosystem II (PSII), encoded by the *psbA* genes, is an indispensable component of oxygenic photosynthesis. Due to strongly oxidative chemistry of PSII water splitting, the D1 protein is prone to constant photodamage requiring its replacement, whereas most of the other PSII subunits remain ordinarily undamaged. In cyanobacteria, the D1 protein is encoded by a *psbA* gene family, whose members are differentially expressed according to environmental cues. In the recent years many cyanobacterial genomes have been sequenced and are available on the Internet. We have constructed a database of the D1 protein sequences and run several phylogenetic studies in an effort to elucidate the structure of the *psbA* gene families for those species where the functional studies are missing. Also, we present data regarding the change in *psbA* gene family expression under environmental stress. A general classification of cyanobacterial D1 isoforms in various cyanobacterial species into D1m, D1:1, D1:2, and D10 forms depending on their expression pattern under acclimated growth conditions and upon stress is discussed, taking into consideration the phototolerance of different D1 forms and the expression conditions of respective members of the *psbA* gene family.

Keywords: D1; Photosystem II; Cyanobacteria

Introduction

D1 protein is part of the multi-subunit protein complex of photosystem II (PSII) at the core of the photosynthetic electron transport chain and is encoded by the gene *psbA* (Vass *et al*., 2005; Aro *et al*., 1993). While higher plants have only one *psbA* gene, cyanobacteria generally display a small *psbA* gene family (http://www.kazusa.or.jp/cyano/, http://genome.jgi-psf.org/mic_home.html). The different *psbA* genes in cyanobacteria encode more than one type of D1 protein. Transcriptional regulation studies have proven the presence of two distinct regulation strategies of the cell to cope with stress conditions. One strategy is to enhance the production of the same type of D1 protein in order to compensate the higher rate of damage caused by stress conditions (Sicora *et al*., 2008), and the other strategy is to use two distinct types of the D1 protein, D1:1 and D1:2, where the former is present under normal growth conditions, to be replaced by the latter under stress conditions. This second type of response was documented initially in *Synechococcus* sp. PCC7942 and more recently also in *Anabaena* sp. PCC7120 (Sicora *et al.*, 2006) and *Thermosynechococcus elongatus* BP-1 (Kos *et al*., 2008).

A divergent *psbA* sequence (*psbA1*) encoding a different D1 protein has been found in *Synechocystis* 6803 (Mohamed and Janssen). While the expression of this gene could theoretically be relevant to stress response as outlined above, this gene has to date been considered to be silent and functionally a mystery, as it has not been possible to induce it under any conditions. Artificial induction of this gene through site-directed mutagenesis upstream of the gene produces a functional, albeit aberrant D1 protein called D1′.

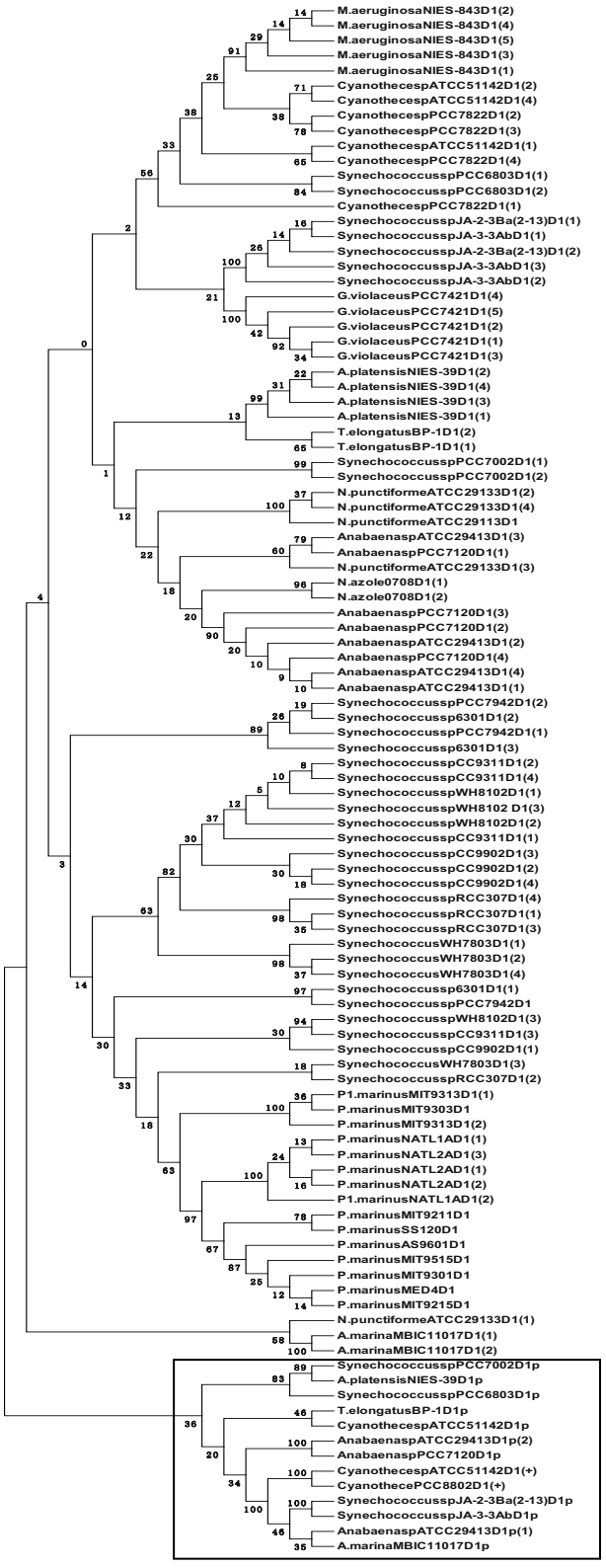

Fig. 1 Maximum parsimony phylogenetic tree generated from 103 D1 protein sequeces of fully sequenced cyanobacterial genomes. Bootstrap values correspond to 500 replicates. The rectangle at the bottom marks the clade of D1′ .

Other similar, divergent, low-expressed and non-responsive *psbA* genes have also recently been found in *Anabanena* 7120 (*psbA0*), *Thermosynechococcus elongatus* BP-1 (*psbA2*) and possibly *Gloeobacter violaceus* PCC7421. In fact, out of the five cyanobacteria species where the expression of the *psbA* gene family has been characterized, only *Synechococcus* PCC7942 does not contain such a gene (Kulkarni and Golden, 1994).

Here we present data supporting the hypothesis that a distinct type of D1 protein is present in several cyanobacteria strains and the structural characteristics of this protein could have implications on PSII functionality.

Materials and Methods

Phylogenetic analysis. A database of 103 D1 protein sequences was created from the fully sequenced cyanobacterial genomes available on various databases. These sequences were aligned using CLC Sequence Viewer 6.4. The phylogenetic trees were created using MEGA 4.1 software on regions of high similarity of the alignment.

Protein modeling and oxidation potential calculations. We calculated midpoint oxidation potentials of 4 RC Chls for wild-type, and 4 D1 mutants: S153- > A, F158- > L, F186- > L, T286- > A. Calculations were done using D1 and D2 proteins (3BZ1.pdb) embedded in a membrane slab.

Redox titration at pH 6 was carried out using Multi-Conformer Continuum Electrostatics (MCCE) program (Song *et al*., 2009). Determination of redox potentials in this program is broken into 3 steps: (1) Using simplified energy function ensemble of energetically favorable rotamers is generated, and acid/base and redox degrees of freedom are added. (2) Energy look-up tables are calculated for pairwise interactions between all conformers. (3) The probability of finding every conformer of each residue in a Boltzmann distribution is determined by Monte-Carlo sampling at different values of redox potential.

Results and Discussion

Phylogenetic analysis of the D1 protein sequences. The 103 sequences database was used to generate a multiple sequence alignment based upon which a phylogenetic tree has been generated (Fig. 1). A high degree of similarity is visible between the sequences, which can be explained due to the very specific

function of this important protein, and the little room for random sequence variations. However it if visible within the tree distinct clade of more divergent sequences (marked by a rectangle at the bottom of the tree in Fig. 1) that belong to several different strains of cyanobacteria. Interestingly all these sequences present the three specific point mutations (discussed below) presented as a possible marker for the presence of the microaerobically inducible D1 form (D1′).

Modeling of D1 protein modifications characteristic for the microaerobically induced form and calculations of the redox potential of key chlorophyll molecules. Out of 4 RC Chls only PD2 and ChlD1 were affected by point mutations. Three out of 4 mutations upshifted Em of PD2 (F186- > L, T286- > A by about 74 mV, F158- > L by 61 mV) (Fig. 2). This trend caused the difference between PD1 and PD2 to be higher. Em of ChlD1 on the other hand was downshifted by 56 mV in S153- > A mutant (Fig. 2). These results indicate that energetics of charge separation step as well as electron donation from Y_Z may be affected by these mutations. It can also affect pathways of Chl cation migration in the RC centers in conditions when donor side is blocked. At this time it is difficult to link these changes to the physiological response of the organism to specific stress conditions.

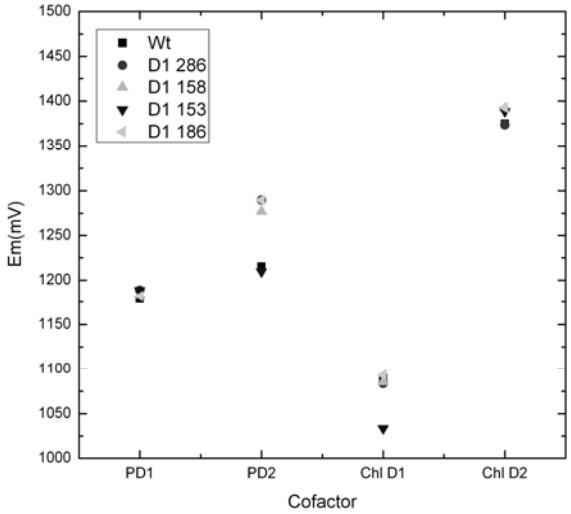

Fig. 2 Change in redox potentials of four Reaction Center chlorophills caused by point mutations in D1 protein.

While more functional studies need to be done we present here for the first time indications that D1′ protein isoform could be more generally present among cyanobacteria than previously believed. Also its key identification features, the three specific changes of aminoacids could impact in a pronounced way the electron flow in the electron transport chain and hence give specific functional characteristics to the new D1 form.

Acknowledgements

Part of this project was financed from a POS CCE Operation 2.1.2, Project number 236 grant, offered by Romanian Government and European Union.

References

Aro EM, Virgin I, Andersson B Photoinhibition of Photosystem II. Inactivation, Protein Damage and Turnover Biochim. Biophys. Acta 1143: 113-134

Kos PB, Deak Z, Cheregi O, Vass I (2008) Differential Regulation of psbA and psbD Gene Expression, and the Role of the Different D1 Protein Copies in the Cyanobacterium Thermosynechococcus Elongatus BP-1. Biochim. Biophys. Acta 1777: 74-83

Kulkarni RD, Golden SS (1994) Adaptation to High Light-Intensity in Synechococcus sp. Strain PCC-7942 - Regulation of 3 psbA Genes and 2 Forms of the D1 Protein. J. Bact. 176: 959-965

Sicora CI, Appleton SE, Brown CM, Chung J, Chandler J, Cockshutt AM, Vass I, Campbell DA (2006) Cyanobacterial psbA Families in Anabaena and Synechocystis Encode Trace, Constitutive and UVB-Induced D1 Isoforms. Biochim. Biophys. Acta 1757: 47-56

Sicora CI, Brown CM, Cheregi O, Vass I, Campbell DA (2008) The psbA Gene Family Responds Differentially to Light and UVB Stress in Gloeobacter Violaceus PCC 7421, a Deeply Divergent Cyanobacterium. Biochim. Biophys. Acta 1777: 130-139

Vass I, Szilard A, Sicora C (2005) Adverse Effects of UV-B Light on the Structure and Function of the Photosynthetic Apparatus. In: M Pessarakli (ed.), Handbook of Photosynthesis, 2nd ed., Marcel Dekker, Inc.: New York, pp. 827-843

Photosynthesis and Expression of Circadium Gene *KaiC* in *Synechococcus*

Xiaohui Jia[1, 2], Carl H Johnson[3], Dingji Shi[2,4*], Xiaoyan Wang[2], Guisen Du[1]

[1] College of Life Sciences, Capital Normal University, Beijing 100048, China;
[2] School of Marine Sciences & Engineering, Tianjin University of Sciences & Technology, Tianjin 300457, China;
[3] Department of Biological Sciences, Vanderbilt University, Nashville, TN37235, USA;
[4] Institute of Botany, Chinese Academy of Sciences, Beijing 100093, China.
* Corresponding author. E-mail: cyano.shi@yahoo.com.cn.

Abstract: This paper provided some evidences that there was a relationship between photosynthesis and circadian gene expression in unicellular cyanobacterium *Synechococcus elongates* PCC 7942. The gene *KaiC* was cloned by PCR technique and sense- or antisense-vectors were constructed. The cyanobacterium was transformed with two vectors, and up- or down-regulated mutants of *Synechococcus* were identified. Their photosynthesis and respiration was measured using oxygen electrode with wild type and mutants transformed by pRL-489, pRL-sense-*kaiC* and pRL-antisense-*kaiC*. The data showed that net photosynthesis in all mutants was lower than that in wild type cells, and dark respiration in all mutants was higher than that in wild type cells. When *Synechococcus* cells were cultivated in the filtrate of *Scenedesmus obliquus* medium the growth of both up- and down-regulated mutants were inhibited more than that of wild type cells. These data demonstrated that the expression of circadian gene *KaiC* affected cyanobacterial fitness, and the possible mechanism may be related to their photosynthesis.

Keywords: Photosynthesis; Fitness; Circadian gene *KaiC*; Cyanobacteria; *Synechococcus elongates* PCC 7942 (*Synechococcus* 7942)

Introduction

Photosynthesis, as a physiological process, may be affected by various external and internal factors. There has been a great deal of literatures on environmental regulation of photosynthesis and the study of internal effects on photosynthesis have not been enough. Thirty years ago our group reported that the daily changes of the photosynthetic capacity (based on DCMU induced chlorophyll fluorescence increase) was regulated by nitrogen fixing activity in unicellular cyanobacterium *Gloeocapsa* (Tang *et al*., 1981). Now this integration of temporal separation between photosynthesis and nitrogen fixation can be understood as a circadian rhythmic phenomenon.

Franz Halberg in 1959 first termed the daily clock phenomena as “circadium” (Halberg *et al*., 1977). The daily cycle of light, temperature and humidity presenting in the natural environment is a selective force which drove organisms to evolve endogenous timing mechanisms that allow them to temporally regulate biological activity as a function of the 24h per day (Johnson *et al*., 2008). This regulation of behaviors and metabolic events was interpreted to enhance fitness (Ouyang *et al*., 1998; Woelfle *et al*., 2004).

How the fitness is enhanced by the clock system in cyanobacteria? There have been three models presented (Woelfle and Johnson, 2009): (1) the Limiting Resource Model; (2) the Diffusible Factor Model; (3) the Cell to Cell Communication Model. Based on our understanding, all these Models may be related to photosynthesis.

The cyanobacterial circadian clock system consists of three conceptual designations (input, oscillator and output), and oscillator is the core part which contains three proteins KaiA, KaiB and KaiC encoded by genes *KaiA*, *KaiB* and *KaiC* (Ishiura *et al*.,

1998; Oysma and Kondo, 2009). Among them KaiC is an autokinase, autophosphatase and ATPase, and plays more important role (Xu *et al*., 2004; Dong *et al*., 2010).

In this work, *KaiC* gene was cloned and up- or down-regulated mutants of *Synechococcus* were transformed by two types of vectors. Then, photosynthesis and respiration in wild type and mutants were measured. Inhibited growth of wild type and mutants by *Scenedesmus obliquus* was compared as well.

Materials and Methods

Strains and plasmids

Synechococcus sp. PCC 7942 was from Prof CH Johnson's Lab (Vanderbilt University, U.S.A). *Escherichia coli* DH-5α was from Takara Co.Ltd. Plasmid pRL-489 was from Prof. P Wolk's Lab (MSU-DOE U.S.A). pUC-19 vector was bought from Takaba Bio Company.

Cultivating

Synechococcus sp. PCC 7942 was cultivated in autoclaved BG-11 medium. The cultivation

conditions were as follows: light intensity = about 100 μmol photon m^{-2} s^{-1}, light/dark ratio = 14:10 and temperature = 30 °C (Shi, 1987). *Escherichia. coli* was cultivated in LB medium (Sambrook *et al*., 2001). Wild type cells and mutants of *Synechococcus* sp. PCC 7942 was cultivated in the cell-free filtrated medium of the *S.obliquus* (Jia, 2010).

Targeting gene fragment (kaiC)

The full-length *kaiC* gene was amplified using a 5' primer (5' 5'CGGGATCCTTCCGACGACTTCTAAC) and a 3' primer(5'CTGGATCCTCTCGGTGCTCGG GTTG) with BamHI restriction sites. The PCR product was gel purified, digested with BamHI, and ligated into pUC-19 vector.

Construction of vectors and transformation

pRL- 489-*kaiC* was constructed by insertion of an BamHI *kaiC* gene from pUC-*kaiC* into the BamHI site of pRL-489 from positive and negative directions and obtained pRL-sense-*kaiC* and pRL-antisense-*kaiC* vector (Qin *et al*., 1998, 1999). Competent cells of *E. coli* and *Synechococcus* sp. PCC 7942 were prepared and transformed as described by Qin *et al*. (1998).

Measurements of photosynthetic O_2 evolution

Wild type and mutants of *Synechococcus* sp. PCC 7942 were measured by O_2 electrode (Shi, 1987).

Chlorophyll a determination

(Shi, 1987).

Results

Cloning KaiC gene and constructing sense- or antisense-vectors

After designing and synthesizing the primer, *KaiC* gene was cloned from the genome DNA of *Synechococcus* 7942 by PCR technique (Fig. 1). Fig. 2 showed the construction of two types of vectors. Sense vector may up-regulate and antisense vector may down-regulate the expression of circadian gene *KaiC*.

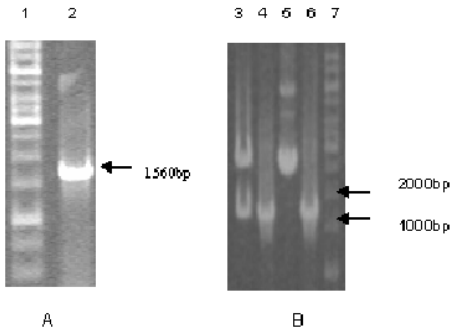

Fig. 1 *KaiC* of *Synechococcus* sp. PCC 7942 by PCR and restriction identification of pUC-*KaiC*. A: *KaiC* of PCR product; B: Restriction identification of pUC –*KaiC*. Lane 1, 7: 1kb DNA marker; Lane 2, 6: PCR product of *KaiC*; Lane 3: pUC -*KaiC*/BamHI; Lane 4: pUC-*KaiC* PCR product; Lane 5: pUC-*KaiC*.

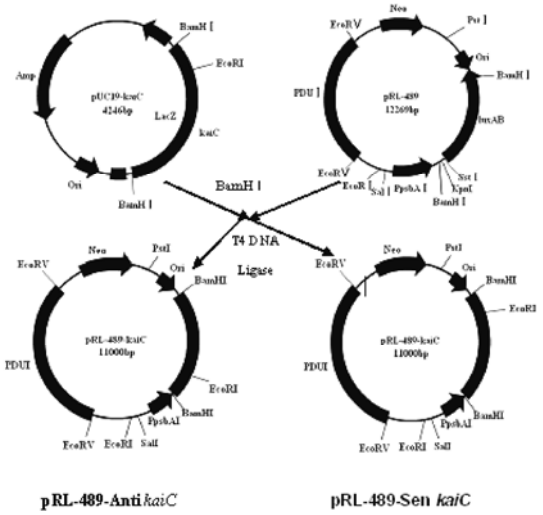

Fig. 2 Construction of recombinant shuttle vectors pRL-489-sense *kaiC* and pRL-489-antisense *kaiC*.

Molecular manipulation of Synechococcus 7942

Sense- and antisense-vectors harbering circadian gene *KaiC* were used to transform *Synechococcus* 7942, and mutants with up- or down-regulated expression of *KaiC* gene were constructed (Fig. 3).

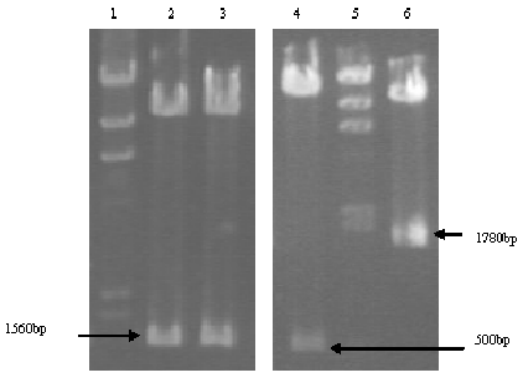

Fig. 3 Restriction pattern in two types of vectors form up- or down regulated mutants of *Synechococcus* sp. PCC 7942.
Lane 1,5: λHindⅢ Marker; lane 2: pRL-sense-*KaiC*/*Bam*HI; Lane 3: pRL-antisense-*KaiC*/BamHI; Lane 4: pRL-antisense-*KaiC*/EcoRI; Lane 6: pRL-sense-*KaiC*/EcoRI.

Photosynthesis and respiration in mutants and wild type cells of Synechococcus 7942

The data from oxygen electrode measurements showed that net photosynthesis in all mutants was lower than that in wild type cells, and photosynthetic activity in up-regulated mutant was the lowest. The dark respiration in all mutants was higher than that in wild type cells and respiration activity in down-regulated mutant was the highest (Fig. 4).

Regulation of relationship between Synechococcus 7942 and Scenedesmus obliquus

Cyanobacterial fitness may include species competition. Allelopathic inhibition of *S.obliquus* on *Microcystis aeruginosa* has been observed (Jia *et al*., 2008), and also played a role on *Synechococcus* 7942. When the cyanobacterium was cultivated in the filtrate of *S.obliquus* medium, their growth was inhibited (Fig. 5).

Fig. 5A showed that the growth inhibition of wild type cells and the transformant by pRL-489 in photoperiods 24 and 8 h was less than that of in 14 or 18 h. When *KaiC* gene was up-regulated (Fig. 5B) or down-regulated (Fig. 5C) the inhibition of *S.obliquus* over the mutants in all photoperiods were elevated. Comparing the data of different mutants, the growth of up-regulated mutant was inhibited more than that in down-regulated mutant.

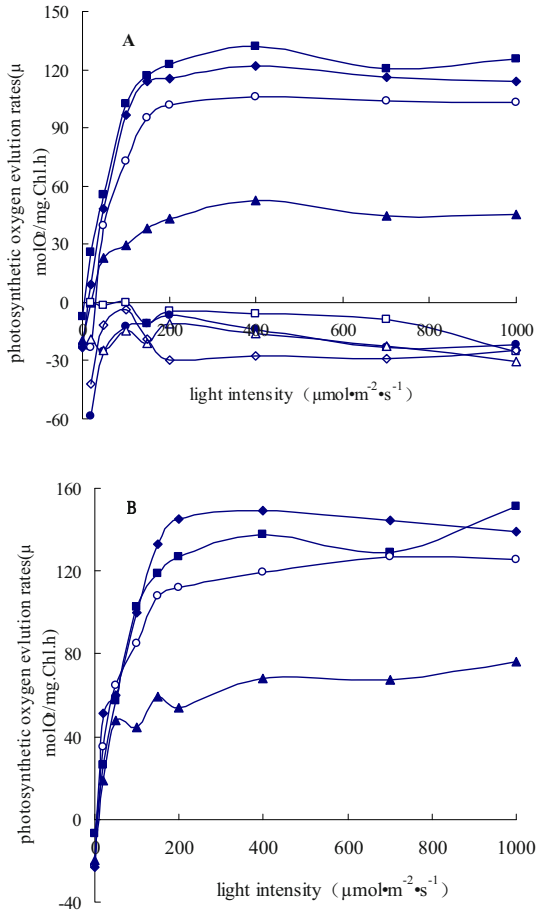

Fig. 4 Photosynthesis and respiration in wild type and mutants of *Synechococcus* sp. PCC 7942. A. Net photosynthesis of Wide type 7942 (■), pRL-489(○), pRL-Sense-*KaiC* (▲), pRL-antisense-*KaiC* (◆) and Respiration of Wide type 7942 (□), pRL-489(●), pRL-Sense-*KaiC* (△), pRL-antisense-*KaiC* (◇); B. Total photosynthesis.

Discussion

All cyanobacteria, algae and higher plants grow under sunlight and rhythmic environments, and all of their genes may be regulated by the circadian system. Photosynthesis is the most important physiological process and performs daily variation. When the frequency of internal biological oscillator of higher plants is resonate d with the environmental cycle, their photosynthesis operates most effectively (Dodd *et al*., 2005). This work proved when the circadian system was disrupted by up- or down-regulated expression of *KaiC* gene in *Synechococcus* 7942 cultivated in rhythmic illumination, the photosynthesis activity of the unicellular cyanobacterium was declined, phycobiliprotein content was decreased

(data unpublished), also their growth was decreased (data unpublished), and cell division was affected (data unpublished) as well.

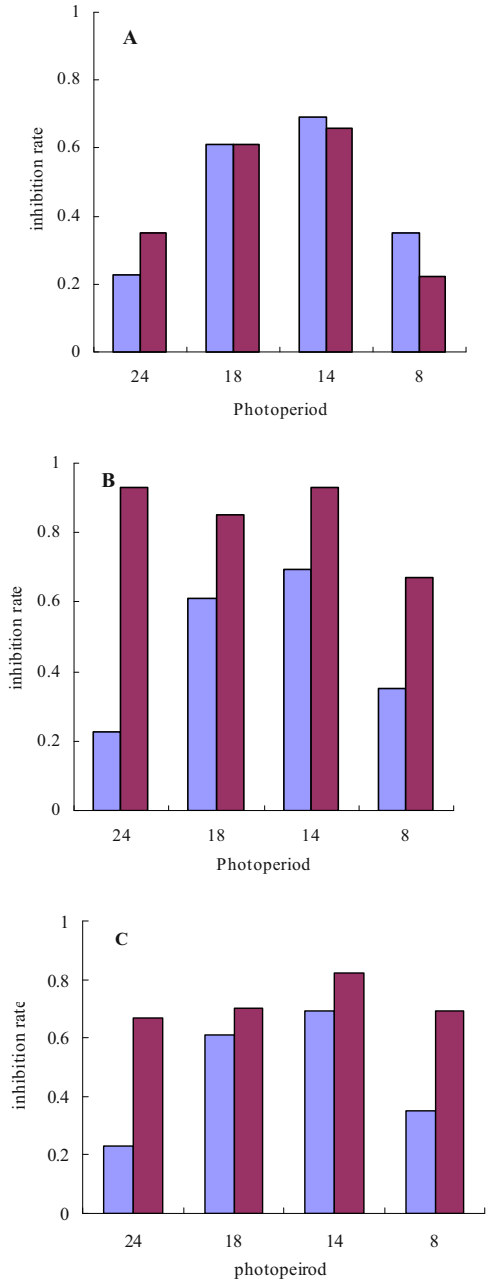

Fig. 5 Effects of allelopathic inhibition from the filtrate of *Scenedesmus obliquus* medium over the growth of wild type cells (■) and (■) mutants transformed by pRL-489 plasmid (A), pRL-Sense-*KaiC* (B) and pRL-antisense-*KaiC* (C) in *Synechococcus elongates* PCC 7942.

Relationship between species is an important aspect of cyanobacterial fitness, which has been tested with different circadian phenotypes (Ouyang *et al*., 1998; Woelfle *et al*., 2004). This work measured the inhibition of *S.obliquus* over *Synechococcus* 7942. When clock system was disrupted by regulating *KaiC* gene expressions, the inhibition rates was changed. It has been expounded that this inhibition was due to allelochemicals secreting and diffusing from *S.obliquus*, and the photosynthesis of *Synechococcus* cells was dropped, particularly that of photosystem II (Jia, 2010). The fitness mainly means reproductive fitness per se. Cyanobacteria is a group of asexutial microbiels and its propagation depend on photosynthesis. Higher plants have phytochrome to make response to photoperiods, which has not been found in cyanobacteria. Is it possible to be responsible to rhythmic environments by photosynthetic mechanism in cyanobacreria, such as, photosynthetic pigments, photophosphorylation, electron transfer, carbon dioxide fixation etc?

References

Dodd AN, Salathia N, Hall A, Kevei E, Toth R, Nagy F, Hibberd JM, Millar A, Webb AAR (2005) Plant Circadian Clocks Increase Photosynthesis, Growth, Survival, and Competitive Advantage. Science 309: 630-633

Dong G, Yang Q, Kim YI, Wood TL, Osteryoung KW, Van Oudenaarden A, Golden SS (2010) Elevated ATPase Activity of KaiC Applies a Circadian Checkpoint on Cell Division in Synechococcus Elongates. Cell 140: 529-539

Halberg F, Carandente F, Cornelissen G, Katinas GS (1997) Glossary of Chronobiology. Chronobiologica 4: 1-189

Ouyang Y, Andersson CR, Kondo T, Golden SS, Johnson CH (1998) Resonating Circadian Clocks Enhance Fitness in Cyanobacteria. Proc. Natl. Acad. Sci. USA 95: 8660-8664

Ishiura M, Kutsuna S, Aoki S, Iwasaki H, Andersson CR, Tanabe A, Golden SS, Johnson CH, Kondo T (1998) Expression of a Gene Cluster KaiABC as a Circadian Feedback Process in Cyanobacteria. Science 281: 1519-23

Jia XH, Shi DJ, Kang RJ, Liu Y, An ZZ, Wang SS, Song DH, Du GS (2008) Allelopathic Inhibition by Scenedesmus Obliquus over Photosynthesis and Growth of Microcystis Aeruginosa. In Photosynthesis. Energy from the Sun. pp. 1339-1342

Jia XH (2010) Studies on Ecology, Physiology and Molecular Biology of Blooms-Forming Cyanobacteria.

Ph.D Thesis, Capital Normal University: Beijing, China (in Chinese, English abstract) pp. 1-178

Johnson CH, Mori T, Xu Y (2008) A Cyanobacterial Circadian Clockwork. Current Biology 18: R816-825

Oyama T, Kondo T (2009) The Kai Oscillator. In: Ditty JL, Mackey SR, Johnson CH (eds.), Springer-Verlag: Berlin, pp. 87-101

Qing JD, Shi DJ, Xu XD, Zhang JD, Guo PZ, Tang PS (1998) Construction of Antisense glnA Expression System in Anabaena 7120. Acta phytophysiol. Sini 24(3): 225-232

Qing JD, Shao N, Shi DJ, Xu XD, Zhang JD, Guo PZ, Wang WQ, Tang PS (1999) Construction of Secreting Ammonium Mutant from Synechococcus 7942 and Its Glutamine Synthetase Activity, Photosynthesis and Growth. Acta Bot. Sini 41(1): 65-70

Sambrook J, Fritsch EF, Maniatis T (2001) Molecular Cloning. A Laboratory Manual 3rd edition, Cold Spring Harbor Laboratory Press

Shi DJ (1987) Energy Metabolism and Structure of Immobilized Cyanobacterium Anabaena Azollae. Ph.D thesis, King's College London

Tang PS, Shi DJ, Hu CZ, Wang FZ, Zhong ZP (1981) Regulation of Energy Metabolism (Photosynthesis and Nitrogen Fixation) in Blue-Green Algae. In "Proceedings of the Joint China-U.S. Phycology Symposium". pp. 339-363

Woelfle MA, Johnson CH (2009) The Adaptive Value of the Circadian Clock System in Cyanobacteria. In: Ditty JL, Mackey SR, Johnson CH (eds.), Springer-Verlag: Berlin, pp. 205-222

Woelfle MA, Ouyang Y, Phanvijhitsiri K, Johnson CH (2004) The Adaptive Value of Circadian Clocks: an Experimental Assessment in cyanobacteria. Curr Biol, 14: 1481-1486

Xu Y, Mori T, Pattanayek R, Pattanayek S, Egli M, Johnson CH (2004) Identification of Key Phosphorylation Sites in the Circadian Clock Protein KaiC by Crystallographic and Mutagenetic Analyses. Proc.Natl.Acad.Sci USA 101: 13933-13938

Symposium 13

Type I Reaction Centres

Prediction of *Cis* Regulatory Elements in the Genome of *Synechococcus Elongatus* PCC 6301

P Parvati Sai Arun, M Subhashini, CH Santhosh, P Sankara Krishna, Jogadhenu SS Prakash*

Laboratory of Functional Genomics and Regulatory Networks, Department of Plant Sciences, University of Hyderabad, India.
*Corresponding author. Tel. No. +91 40 66794505; E-mail: jsspsl@uohyd.ernet.in.

Abstract: Identification of putative *cis* regulatory elements by comparative analysis of genomes helps us to understand mechanism of global gene expression. Many approaches were previously used for identification of *cis* regulatory elements. Here we use phylogenetic foot-printing analysis and MEME suite for predicting *cis* regulatory elements in the genome of *Synechococcus elongatus sp.* PCC6301. We have identified total 102 putative *cis* regulatory elements, in which several of them were previously described, experimentally, while several motifs were new. As many motifs which were identified in the current computational predictions were previously reported, it is highly likely that the new ones would act as *cis* regulatory elements. The newly identified ones are target for experimental validation and to build gene regulatory network in the genome of *Synechococcus elongatus*.

Keywords: *Cis* regulatory elements; Phylogenetic foot printing: MEME; MAST; Gene expression

Introduction

DNA microarray-based studies of gene expression have indicated that the bacterial cell responds to any kind of environmental alterations by regulating the expression of large number of genes (Polissi *et al.*, 2003; Prakash *et al.*, 2009; Mostertz *et al.*, 2004). These findings have suggested that large number of transcription factors, by interacting with various *cis* regulatory elements, regulate the expression of majority of genes, and such regulation is a result of complicated networks of interactions. Genome sequencing and functional annotation of *Synechococcus elongatus* sp. PCC6301 (here after *S. elongatui*) indicates that this organism has 49 transcription factors probably involved in regulation of most of its genes (http://dbd.mrc-lmb.cam.ac.uk/DBD/index.cgi?Home). However, in this organism, the target *cis* regulatory elements for many of these putative transcription factors are not identified yet. Lack of information on regulation of gene expression by most of the putative transcription factors prompted us to look for regulatory elements by computational methods. Several algorithms to identify the *cis* regulatory motif have been developed over the past few years, Gibbs sampling (Thompson *et al*., 2003); an expectation maximization (Bailey and Elkan, 1994); and AlignACE and compare ACE (Roth*, et al.,* 1998). We used comparative genome analysis and MEME (Multiple Expectation maximum for Motif Elicitation) for predicting the *Cis-regulatory* elements in the genome of *S.* elongatus. We present a few predicted *cis-regulatory* elements and the co-regulated genes of *S. elongatus*.

Methods

The genome sequence and annotation files of the sequenced cyanobacteria were retrieved from NCBI at ftp://ftp.ncbi.nih.nih.gov/genomes/bacteria/. The genomes considered for our analysis were *Synechocystis PCC 6803, Thermosynechococcus elongatus BP1, Gloeobacter violaceus PCC7421, Anabaena variabilis ATCC29413, Trichodesmium erythraeum IMS101, Synechococcus sp. CC9311, Prochlorococcus marinus str. MIT9303, Acaryochloris marina MBIC11017, Microcystis aeruginosa NIES843, Synechococcus sp. PCC7002,*

Nostoc punctiforme PCC73102, Cyanothece sp. PCC7424. We created separate protein database and intergenic sequence databases for each selected cyanobacterial species. We have performed bi-directional best hit method of selection (BDBH) to identify the orthologs for each protein of *Synechococcus elongatus.* Orthologs of each protein of *S.elongatus* against the cyanobacteria were identified by reciprocal BLASTP with E-value of 10^{-10} in both directions.

Transcriptional Unit

Database of transcriptional units generated for all the selected cyanobacteria were obtained from Dr. Sarath Chandra Janga at MRC-LMB lab, University of Cambridge, U.K. (unpublished data). Transcription units and ortholog-clusters were combined to predict clusters of orthologous transcription units (COTs).

Retrieval of non-coding upstream sequences

We have retrieved a maximum of 500 nucleotides upstream of each transcriptional unit or the actual intergenic DNA regions, if the distance between the two transcriptional units is less than 500 nucleotides. Intergenic DNA sequences were retrieved from the sequence and the annotation file taken from NCBI using a Perl script.

Identification of cis-regulatory elements and co-regulated genes

The upstream DNA sequence of each COT was taken as input to Motif extraction by multiple expectation maximization (MEME ver. 4.3.0) using a Perl script. MEME was run using the parameters minw = 20, maxw = 30, zoops, revcomp. Conserved regulatory motifs thus identified were further filtered using MEME parser program. If the identified conserved motif is located in the upstream of at least ≥ 5 orthologs in a COT is considered for further analysis. The results were manually examined to pick candidate *cis*-regulatory elements. The candidate regulatory motifs thus picked up were subjected to MAST for identification of the co-regulated genes (Bailey *et al.*, 1998). The newly identified genes with common *cis*-regulatory element having *p*-value less than 10^{-4} were considered as co-regulated genes.

Results and Discussion

Identification of orthologs in other cyanobacteria for S.elongatus proteins

The genome of *Synechococcus* was sequenced and annotated in 2007 (Sugita C *et al.*, 2007). It includes 2,527 open reading frames that code for proteins involved in various cellular processes and proteins with unknown function. Out of these, 49 genes code for DNA binding proteins. The target DNA-binding site of only a few transcription factors has been identified by gel mobility shift assay coupled with DNase foot printing (Ramasubramanian *et al.*, 1996; Patterson *et al.*, 2008; Wang *et al.*, 2004). It is widely accepted that the orthologs from closely related organisms may be regulated by similar regulatory mechanism that involve the homologous DNA-binding protein. Hence similar regulatory binding element may be identified for that DNA binding protein in the upstreams of genes coding for protein orthologs. Therefore, similar DNA motifs located in the upstream of DNA regions of genes coding for orthologs are assumed to be a possible transcription factor-binding element (*Cis-regualtory* element).

Comparison of DNA binding proteins among cyanobacteria

Conservation of a DNA-binding protein among cyanobacterial genomes would reflect the conservation of its binding site. Thus, comparison of conservation of DNA-binding proteins would give us information about the extent of binding site conservation. Comparison of DNA binding proteins among the selected cyanobacteria indicates that the cyanobacterial species related closely to the *S.elongatus* have orthologs for most of the DNA binding proteins. Out of 49 transcription factors of *S.elongatus,* 37 (75%) have 5 or more than 5 orthologs in other selected cyanobacteria (Fig. 1). Orthologs for most response regulators of *S.elongatus* are present in one or the other selected cyanobacterial species. Out of the selected cyanobacterial species, *Prochlorococcus marinus* and *Synechococcus PCC9311* has very few orthologs for *S.elongatus* DNA binding proteins (Fig. 1). It is interesting to note that *Synechococcus PCC9311*, though it is closely related to *S.elongatus*, orthologs for less number of *S.elongatus* DNA binding proteins are present in it.

Identification of cis-regulatory elements in the upstream of COTs

The upstream sequences of all COTs were subjected

to find conserved regulatory elements using MEME standalone version. With the given parameters as described in Materials and Methods, MEME generated the consensus of the over represented (conserved) DNA sequence in the upstream of each COT. Thus MEME generated a number of putative *cis*-regulatory elements for submitted COTs. The full set of predicted *cis*-regulatory elements can be found at http://uohbif. in/jssp/. A *cis*-regulatory element, which is conserved at least in 60% of the total number of orthologs in a COT with 60% identity when the conserved sequences were aligned by pair wise alignment, was considered as a putative *cis*-regulatory element.

Several DNA binding *cis*-regulatory elements predicted using computation method were previously reported in the literature, such as DNA binding elements of *HrcA, psaA, SufR. Fur,* while the other *cis*-regulatory elements are found to be novel. The novel DNA binding elements predicted can be target for experimental validation. Thus a total 102 putative *cis*-regulatory elements were identified. The *Cis*-regulatory elements and co-regulated genes of S.*elongatus* are available at http://uohbif.in/jssp/.

Cis-regulatory element involved in Suf Regulon

An inverted repeat CAAC-N6-GTTG (Gaozhong S *et al.*, 2007) was identified in the upstream of open reading frame *syc2358_d* and is highly conserved in the upstreams of its orthologs (Table 1). S*ufR* of *Synechocystis* sp. PCC6803 is the ortholog of this gene. According to Wang *et al.* (2004), *sufBCDS* regulon is negatively regulated by *SufR* and is highly conserved in cyanobacteria. In *S. elongatus* we identified similar *Suf* regulon (*syc2356_d, syc2355_d, syc2354_d, syc2353_d*) with repressor binding site in the upstream of this operon. Thus the open reading frame syc2358_d might be a probable negative regulator of *Suf* operon in *S. elongatus*.

Cis-regulatory elements for ribosomal genes

We have identified GC rich *cis*-regulatory element in the upstream of *rplU, rplJ, rpsJ, prfB* encoding genes and AT rich *cis*-regulatory element upstream of genes syc0073_d, *rplS, rpsN, rpmG, fus* coding for proteins involved in translation. Previous studies have suggested that the genes for ribosomal proteins are under autogenous in control. That is, for a given ribosomal operon, a specific ribosomal protein has evolved to function not only as a component of the ribosome, but also as a regulatory protein responsible for coordinating expression of its operon (Zengel and Lindahl, 1994; Allen *et al.*, 2004). The identified motifs are likely to regulate the expression of the above mentioned genes. In Table 1, the GC rich *cis* regulatory element, in the upstream of *rplU* along with its co-regulated genes was shown.

Cis regulatory element of light regulated genes

In *Synechocystis, RpaB* is a response regulator recognize an AT rich region located in the upstream of genes encoding proteins of Photosystem complexes (Seino *et al.*, 2009). In our study, we have identified this *cis*-regulatory element in the upstream of *psbAII, psbF, psbB, psbO* and *psbH* of *S.elongatus* (data not shown).

Cis-regulatory element in the upstream of transcriptional regulator

A putative *cis*-regulatory element, GTA(N4)TAC was identified and is highly conserved in the upstreams of genes coding for orthologs of a transcriptional regulator, *syc1834_d* (Table 1). This DNA binding element was previously reported to be the binding site of a transcriptional regulator, NtcA, known to regulate the expression of genes involved in nitrogen metabolism. However, the NtcA binding motif has a spacer of N8 between GTA and TAC repeat (Zhengchang Su *et al.*, 2005). NtcA may regulator the expression of *syn1834_d* coding for *narL* type transcriptional regulator, in addition to genes involved in nitrogen metabolism in *S. elongatus.*

HrcA binding element

Our computational predictions identified a 9 bp inverted repeat, TTAGCACTC (N9)GAGTGCTAA in the upstream of *groES* and *groESL* genes (Table 1). The same was previously reported to be the binding site for a transcriptional repressor *HrcA,* which is known to negatively regulate the expression of *groESL* genes (Nakamoto *et al.*, 2003). Thus, the motifs identified by us using computational methods were matching with the previously reported ones and the data is consistent.

An highly conserved inverted repeat with no spacer has been identified in the upstream of *syc1362_d* (*PdhB*) and its orthologs. This *cis*-regulatory element is 100% conserved in the upstream of several other genes of *S. elongatus*, indicating that all these genes may be regulated by a common regulatory mechanism. This is one of the new *cis*

regulatory elements predicted in this study (Table 1).

As many *cis* regulatory elements which were identified using the computational predictions were previously reported in the literature, it is highly likely that the new ones would act as *cis* regulatory elements for the regulation of corresponding genes. The newly identified ones are target for experimental validation and to build gene regulatory network in the genome of *S. elongatus.*

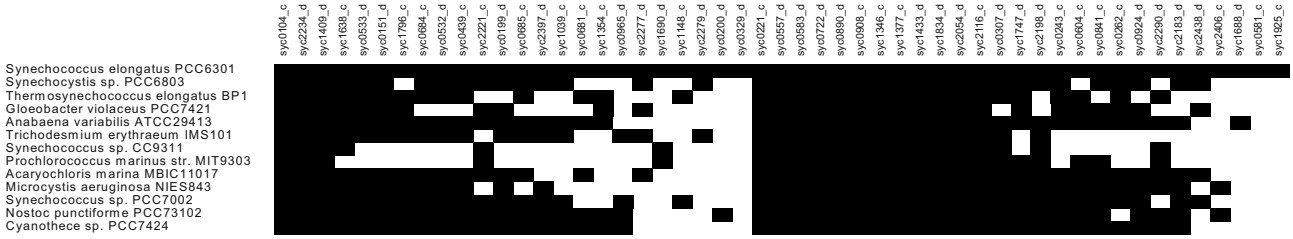

Fig. 1 Conservation of transcription factors and response regulators among the selected cyanobacterial species.
Comparison of conservation of transcription factors and response regulators of *S. elongatus* with other cyanobacterial genomes. Black box represents presence of orthologs for a given transcription factor or response regulator of *S. elongatus.* White box represent the lack of orthologs. Cells in the top row contain ORF numbers corresponding to *S. elongatus* transcription factors and response regulators.

Table 1 List of selected *cis*-regulatory elements in the genome of *S. elongatus*. ORFs containing similar motifs with p value ≤ 10^{-7} were identified as co-regulated genes using MAST tool.

ORF no.	Putative *cis*-regulatory element	Conservation *Cis*-regulatory elements in the upstreams of ortholog genes	Co-regulated genes
syc2358_d	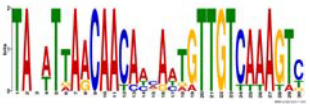	Ava_0423 TAGATTAACAACAACAATGTTGTCAAAGTC Npun_R4821 TAAATTAACAACAACAATGTTGTCAAAGTC MAE_23100 TAGATTAACAACAAAGCTGTTGTCAAAGTC syc2358_d TATTTCAACAACATCAATGTTGTCAAAGTC PCC7424_3070 TATATAAACAACATCATTGTTGTCAAAGTT sll0088 TAGATTAGCAACCCGATTGTTGTCAAAGTG Tery_4354 TACATTAACAATACTAATATTGTCAAAGTC PCC7002_A1815 TACTTTAACAACAAAAAAGTTGTCAAATAT tlr0491 TAATTTAGCAACAAAACGGTTGTTTTAGTC	*syc2357_c* (*ftrC* operon)
syc0331_c (*rplU*)		PCC7002_A0490 ATATCCTGCTCGGATCAGGT PCC7424_3466 AATTCCTGCTCGGATCAGGT Npun_R6114 AATTCCTGCTCGGATCAGGT MAE_08010 AATTCCTGCTCGGATCAGGT Tery_3243 AAATCCTGCTCGGACCAGGT Ava_1516 ATTACCTGCTCGGATCAGGT slr1678 CTATCCCGCTCGGATCAGGT AM1_3632 TTGTTCAGCTCGGATCAGGT syc0331_c AAAGGCGGCTCGGAACAGGT tll0167 TGAGTTTGCACGGAACAGGT gvip095 TGATTTCGCTCGAACCAGGT P9303_05411 TAGAACGGCTCTGATCAGCT sync_2223 CGAGCCTGTTCGCGTCCAGT	*syc0332_d (kaiA)*
syc1834_d		MAE_54580 TAAGTAAATATACGAGAGGA ssl0564 TGAGTAAATATACCTGAGGA Npun_F4241 TAAGTAGATATACCAAAGGA Ava_0483 TAAGTACATATACCAACGGA syc1834_d TAAGTACAAATACTTGAGGT PCC7424_3672 TGAGTAATTTTGCTAAGGGA Tery_2735 TAAGTGCTAAAACGACAGGA AM1_3844 TGAGTATTTATGCAGGGGTA tsl1865 TAAGTAATTATACGGATTTA	*Not identified*
syc1788_d (*groES*)	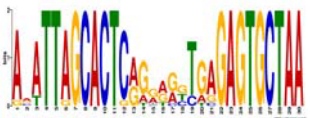	Npun_R0830 AAATTAGCACTCAGGGGTTGAGAGTGCTAA Ava_3627 AGATTAGCACTCAGGAGTTGAGAGTGCTAA PCC7002_A2457 AAATTAGCACTCAGAGATTGAGAGTGCTAA AM1_4412 AGATTAGCACTCGGGAGTCGAGAGTGCTAA PCC7424_1789 ACATTAGCACTCGGTAGGTGAGAGTGCTAA MAE_46070 AAATTAGCACTCGGAAGGTAAGAGTGCTAA tll0186 ACATTAGCACTCGAAGGGTGAGAGTGCTAA slr2075 AAATTAGCACTCGTGAGGTGGGAGTGCTAA syc1788_d ACATTAGCACTCAGGTACTGCGAGTGCTAA Tery_4326 AAATTAGCACTCAGATAGTAAGAGTGCTAA gvip139 AGTTTAGCACTGAAGACCCGAGAGTGCTAA sync_2283 GTTTTGGCACTCAGCGACTTCGAGTGCTAA	*syc1787_c*
Syc1362_d (*pdhB*)	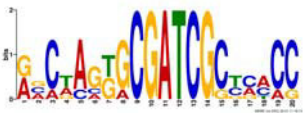	pun_F3849 AACTAGTGCGATCGCTCACC Ava_1491 AACTAGTGCGATCGCTCACC syc1362_d GGCTAGGACGATCGCTATCC tll0204 GCCGCCTGCGATCGCCCACC sll1721 AGCAAGGGCGATCGGGGCAC SYNPCC7002_A0655 GCAAAAGGCGATCGCCACCG	*syc1361_c* *syc0034_c*

Acknowledgements

We thank Mr. Anil Kumar and Mr. Mohit Midda for helpful discussion on automation of the computer programs and their maintenance.

References

Allen TD, Watkins T, Lindahl L, Zengel JM (2004) Regualtion of Ribosomal Protein Synthesis in Vibrio Cholerae. J. Bacteriol. 186: 5933-5937

Bailey, Charles E (1994) Fitting a Mixture Model by Expectation Maximization to Discover Motifs in Biopolymers, Proceedings of the Second International Conference on Intelligent Systems for Molecular Biology, pp. 28-36

Bailey, Michael G (1998) Combining Evidence Using P-Values: Application to Sequence Homology Searches. Bioinformatics, Vol. 14, pp. 48-54

Gaozhong S, Ramakrishnan B, Tao W, Yingxian W, Lee MH, Carsten K, Donald AB, John HG (2007) SufR Coordinates Two [4Fe-4S]2_,1_ Clusters and Functions as a Transcriptional Repressor of the sufBCDS Operon and an Autoregulator of sufR in Cyanobacteria. JBC. 282: 31909-31919

Mostertz J, Scharf C, Hecker M, Homuth G (2004) Transcriptome and Proteome Analysis of Bacillus Subtilis Gene Expression in Response to Superoxide and Peroxide Stress. Microbiology 150: 497-512

Nakamoto H, Michiru S, Kouji K (2003) Targeted Inactivation of the hrcA Repressor Gene in Cyanobacteria. FEBS Lett Volume 549, Issues 1-3

Patterson-Fortin LM, Owttrim GW (2008) A Synechocystis LexA-Orthologue Binds Direct Repeats in Target Genes. FEBS Lett. 582: 2424-2430

Polissi A, De Laurentis W, Zangrossi S, Briani F, Longhi V, Pesole G, Deho G (2003) Changes in Escherichia Coli Transcriptome during Acclimatization at Low Temperature. Res. in Microbiol. 154: 573-580

Prakash JSS, Sinetova M, Zorina A, Kupriyanova E, Suzuki I, Murata N, Los DA. (2009) DNA Supercoling Regulates the Stress-Inducible Expression of Genes in the Cyanobacterium Synechocystis. Mol. BioSyst. 5: 1904-1912

Ramasubramanian TS, Wei TF, Oldham AK, Golden JW (1996) Transcription of the Anabaena sp. Strain PCC7120 ntcA Gene: Multiple Transcripts and NtcA Binding. J. Bacteriol. 178: 922-926

Roth FP, Hughes JD, Estep PW, Church GM (1998) Finding DNA Regulatory Motifs within Unaligned Noncoding Sequences Clustered by Whole Genome mRNA Quantification. Nat. Biotechnol. 16: 939-945

Seino Y, Tomoko T, Yukako H (2009) The Response Regulator RpaB Binds to the Upstream Element of Photosystem I Genes to Work for Positive Regulation under Low-Light Conditions in Synechocystis sp. Strain PCC 680. JB vol. 191: 1581-1586

Sugita C, Ogata K, Shikata M, Jikuya H, Takano J, Furumichi M, Kanehisa M, Omata T, Sugiura M, Sugita M (2007) Complete Nucleotide Sequence of the Freshwater Unicellular Cyanobacterium Synechococcus Elongatus PCC 6301 Chromosome: Gene Content and Organization. Photosynth Res. 93: 55-67

Thompson W, Rouchka EC, Lawrence CE (2003) Gibbs Recursive Sampler: Finding Transcription Factor Binding Sites. Nucleic Acids Res. 31: 3580-3585

Wang T, Shen G, Ramakrishnan B, Lee M, Donald AB, John HG (2004) The sufR Gene (sll0088 in Synechocystis sp. Strain PCC 6803) Functions as a Repressor of the sufBCDS Operon in Iron-Sulfur Cluster Biogenesis in Cyanobacteria. Journal of Bacteriology 186: 956-967

Zengel JM, Lindahl L (1994) Diverse Mechanisms for Regulating Ribosomal Protein Synthesis in Escherichia Coli. Nucleic Acid Res. Mol. Biol. 47: 331-370

Zhengchang Su, Victor O, Fenglou M, Ying X (2005) Comparative Genomics Analysis of NtcA Regulons in Cyanobacteria: Regulation of Nitrogen Assimilation and Its Coupling to Photosynthesis. Nucleic Acids Res. 33(16): 5156-5171

Symposium 14

Biogenesis of Photosynthetic Apparatus

Chloroplast Biogenesis — Preliminary Structural and Proteomic Study

Lucja Rudowska[a*], Radoslaw Mazur[b], Maciej Garstka[b], Agnieszka Mostowska[a]

[a]Department of Plant Anatomy and Cytology, Faculty of Biology, University of Warsaw, Poland;
[b]Department of Metabolic Regulation, Faculty of Biology, University of Warsaw, Poland.
[*]Corresponding author. Tel. No. +48 502 133 959; E-mail: lucja.rudo@biol.uw.edu.pl.

Abstract: Chloroplast Biogenesis is a multistage process that can be observed on ultrastructural and molecular levels. The correlation between structural and proteomic changes during the chloroplast biogenesis is crucial to elucidate the role of particular proteins in stabilization and transformation of prolamellar body (PLB) and prothylakoids (PT) into characteristic arrangements of thylakoid membranes. The model used in our studies of chloroplast biogenesis represents the differentiation of mature chloroplast from etioplast. This model reflects the initial seedling growth occurring beneath the earth surface. To select the key stages of chloroplast differentiation we performed a quantitative and qualitative analysis of changes in protein composition in the extract from leaves of developing seedlings (Western-blot) simultaneously with studies of the plastid ultrastructure (TEM). We studied and examined the main protein components: of chloroplast stroma (Rubisco subunits), thylakoid membranes (proteins of photosynthetic complexes) and of prolamellar body characteristic of etioplasts (protochlorophyllide oxidoreductase, POR).

Keywords: Chloroplast Biogenesis; *Pisum sativum*; Prolamellar Body (PLB)

Introduction

Chloroplast Biogenesis consists of many correlated stages, which can be studied on ultrastructure and molecular levels. At the ultrastructural level this process can be observed as a transformation of prothylakoids (flat porous membranes, PT) and prolamellar bodies (paracrystalic tubular membrane structures, PLB) into grana and stroma thylakoids (Mostowska, 1986a, b). It has been already shown that expression of different chloroplast thylakoid proteins takes place during the chloroplast development (Kleffmann *et al*., 2007). Moreover, correlation between structure and function of fully developed chloroplast has been already investigated (Rumak *et al*., 2010; Garstka *et al*., 2007). What remains unknown is the correlation between structural and proteomic changes at given times of biogenesis of chloroplast and the role of particular proteins in stabilization and transformation of PLB and PT into thylakoid membranes with characteristic arrangements.

The aim of this study was to find relations between the ultrastructure of developing chloroplast and the level of selected proteins, which are the main protein components of chloroplast stroma, thylakoid membranes and PLB.

Materials and Methods

Pea plants (*Pisum sativum* L. cv. Demon from PlantiCo Zielonki, 05-082 Babice Stare, Poland) were grown in 3 L perlite-containing pots in a climate controlled room. For the first 8 days plants were grown in dark conditions at 18 °C. Then growing conditions were changed into a controlled environment at 21/18 °C (day/night) at photosynthetic active radiation (PAR) of 50 μmol photons m^{-2} s^{-1} during 16 h photoperiod and relative humidity of 60%–70%. Plants were fertilized with full Knop's nutrient solution. Samples were collected in selected times during 3 days of experiment after 8 days of

etiolation (Fig. 1). Specimens for TEM from the collected samples were prepared simultaneously with cell protein extracts used later for Western-blot analysis.

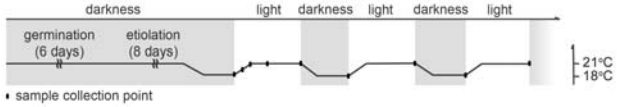

Fig. 1 Scheme of the experiment showing sample collection points.

Samples for TEM were prepared by cutting of about 3 mm^2 area from the middle part of the leaves. The material was fixed in 2.5% (w:v) glutaraldehyde in 5 mmol cacodylate buffer (pH 7.4) for 2 h, washed in the buffer and placed in a 2% (w:v) OsO4 at 4 °C in 50 mmol cacodylate buffer (pH 7.4) for about 12 h. The specimens, dehydrated in a graded acetone series, were embedded in a low viscosity epoxy resin and cut on a Leica UCT ultramicrotome. Sections stained with uranyl acetate were examined with a JEM 1400 electron microscope (Jeol, Japan).

Cell protein extracts were prepared using standard protein extraction buffer. Frozen in liquid nitrogen material was grid to a powder and transfer to buffer. After freezing and subsequent sonication the sample was centrifuged at 10,000 g to remove unbroken cells an insoluble material. Proteins in extracts were separated by standard SDS-PAGE electrophoresis and subsequently put to immunoblotting procedure against selected proteins. Immunoblot signals were visualized using secondary antibody conjugated with alkaline phosphatase and BCIP/NBT Color Development Solution (Bio Rad).

Results and Discussion

The first sample was collected on the 8th day of etiolation directly before the light was switched on (0.1). We observed regular paracrystalic structure of the PLB, the presence of plastoglobules at the margins of the PLB and few PT dispersed in the stroma (Fig. 3a). In cell extracts we detected the presence of proteins characteristic of chloroplast stroma (Rubisco subunits), etioplast PLB (POR) and LHC I complex (Lhca2 - one of the main proteins) (Fig. 2a). Then we collected samples after subsequent hours of light. After 2 h of light (2.1) paracrystalic structure gradually transformed into irregular one and more PT appeared in the stroma (Fig. 3b). Apart of all proteins recognized in the previous stage we observed the presence of Lhca1, and one of the LHC II complex protein, Lhcb5; the level of these proteins rise in subsequent hours of the experiment (Fig. 2b). Similarly to our results, Kleffmann and coworkers (2007) detected early light-induced changes in proteome during chloroplast development, especially of LHC II complex. After 4 h (4.1) further degradation of paracrystalic structure occurred (Fig. 3c). Groups of plastoglobules appeared in the margins of the PLB. Lhcb2 and D2 - the protein of PSII reaction center were newly localized proteins (Fig. 2c). The first

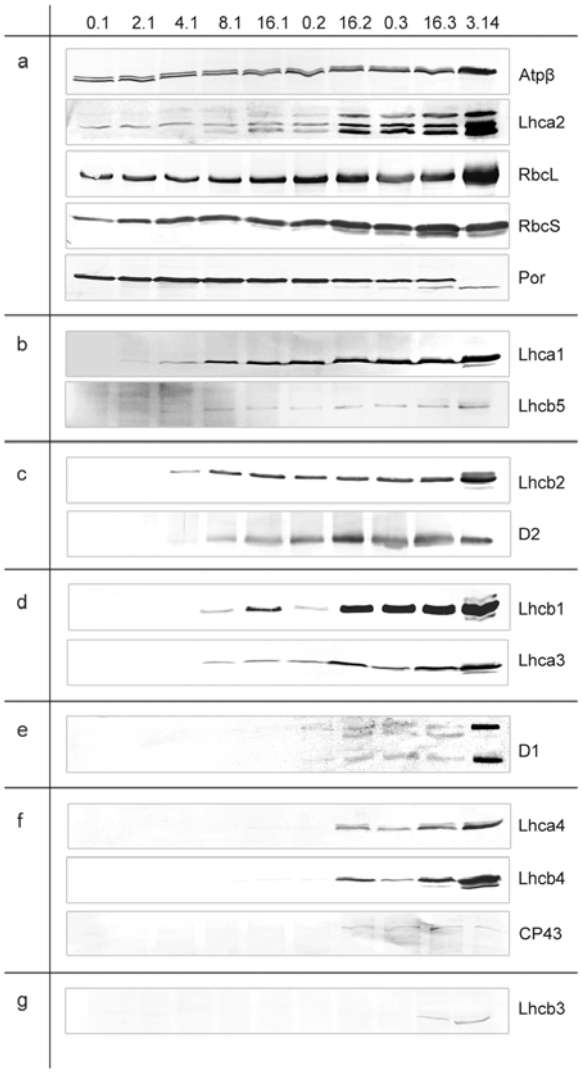

Fig. 2 Western-blot analysis of protein extracts from subsequent hours of day-night growth (ex. 2.1.–2 h, 1st day of experiment). Sections a –g show collection points when groups of proteins were localized for the first time: a- 8 days of darkness before the light was switched on; b- 2 h of light, 1st day of the experiment; c- 4 h of light, 1st day; d- 8 hours of light, 1st day; e- 8 h of darkness, 2nd day; f- 16 h of light, 2nd day; g- 16 h of light, 3rd day.

thylakoids forming unextended grana, mainly in proximity of the degrading PLB (Fig. 3d), Lhca3 and Lhcb1 proteins (Fig. 2d), were observed after 8 hours of light (8.1). Before the light was switched off it means 16 h of light (16.1), we observed: more extended grana formed also in the area abundant in PT, plastoglobules in the margins of newly-formed grana and large starch granules (Fig. 3e). Among the examined proteins no new proteins were detected. The next sample was collected after the first night of

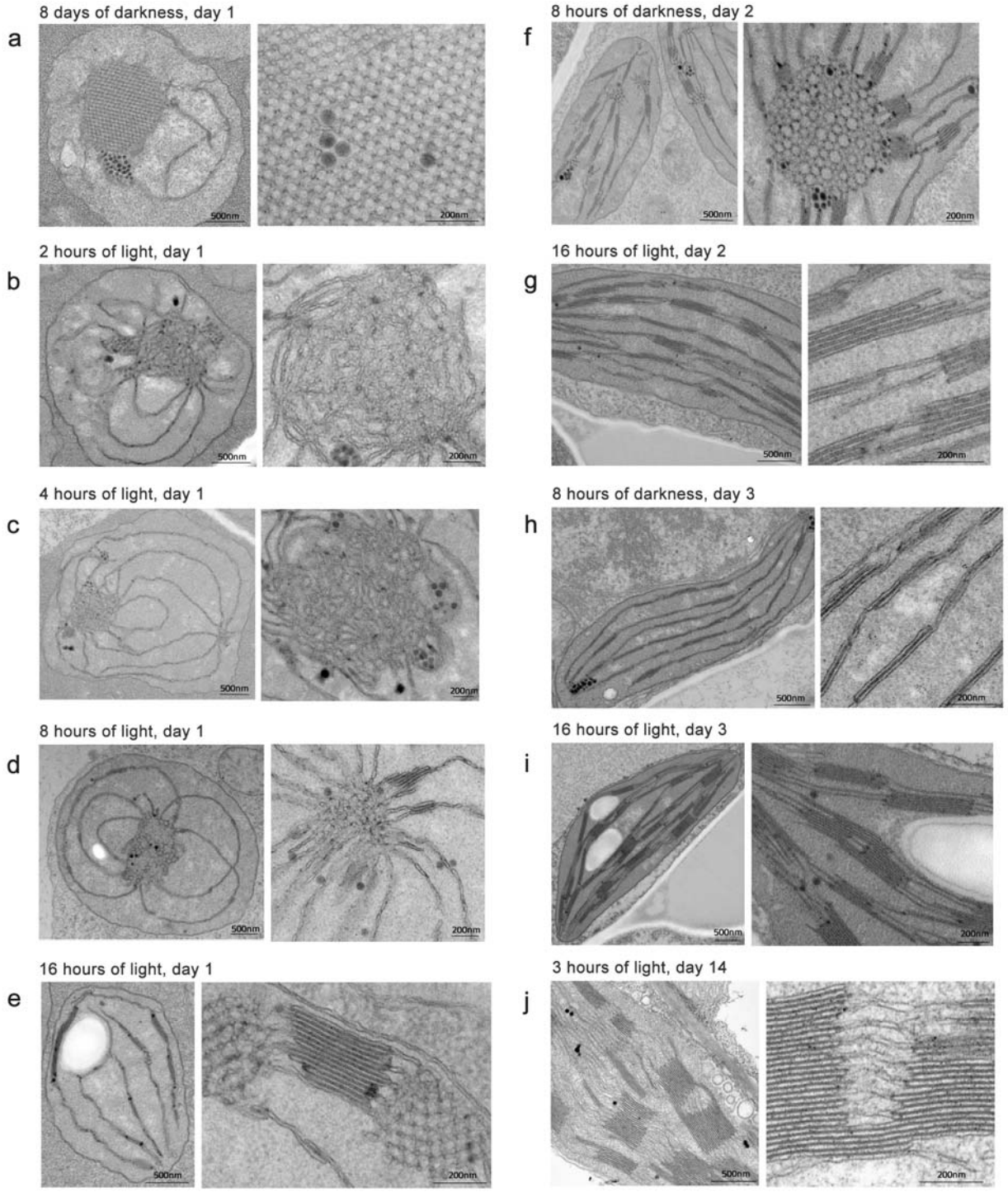

Fig. 3 Electronograms showing changes in mesophyll plastids during development of pea seedlings in a 16-h photoperiod. a - sample collected after 8 days of etiolation just before the light was switched on; b-e - samples collected in the subsequent hours of seedling light growth, day 1; f - sample collected after 8 hours of darkness, day 2; g - sample collected after 16 hours of light, day 2; h - similar to f, day 3; i similar to g, day 3; j - sample collected from a pea leaf at the 3rd h of light, day 14.

the experiment before the light was switched on (0.2). Electronograms showed partial recrystalization of PLB and the presence of numerous unextended grana (Fig. 3f). Additionally, Western-blot analysis revealed the presence of D1, the main PSII reaction center protein (Fig. 2e). After 16 hours of light (16.2) we could not found any PLB and PT, however well developed grana appeared (Fig. 3g). The following proteins were detected in the cell extract: Lhca4, Lhcb4, CP43 (Fig. 2f). After the second night of the experiment (0.3) no reconstruction of PLB occurred,only groups of plastoglobules were found in the place of degraded PLB. In stroma we observed grana stacks with a smaller than before number of thylakoids (Fig. 3h). Fully developed grana and starch granules were visible after the next 16 hours of the experiment (16.3) (Fig. 3i). At this stage all of examined proteins were already detected (Fig. 2g). As a control of the experiment we used a sample collected from fully expanded third leaves of 14 days old pea (3.14). The ultrastructure of control fully developed chloroplast was similar to one observed in the last hour of the third day of the experiment, except of larger grana (Fig. 3j). Moreover, in the cell extract we detected higher levels of examined proteins.

Summarizing, three days of pea seedlings growth were sufficient for the ultrastructure transformation of etioplast into mature chloroplast. Level of all major photosynthetic proteins although not as high as in fully developed chloroplast was sufficient to maintain the structure of the mature chloroplast. It means that forming of grana does not require all the main proteins of the photosystem II and the light harvesting complexes.

Detailed correlation of ultrastructure, level of main photosynthetic proteins and photosynthetic efficiency allow to distinguish the key stages of functionally developed chloroplast.

Acknowledgements

This work is supported by Polish Ministry of Science and Higher Education Grant N N303 530438.

TEM images were performed in the Laboratory of Electron Microscopy, Nencki Institute of Experimental Biology on JEM 1400 (JEOL Co. Japan) electron microscope. This equipment was installed within the project sponsored by the EU Structural Funds: Centre of Advanced Technology BIM – Equipment purchase for the Laboratory of Biological and Medical Imaging.

References

Kleffmann T, Zychlinski A, Russenberger D, Hirsch-Hoffmann M, Gehrig P, Gruissem W, Baginsky S (2007) Proteome Dynamics during Plastid Differentiation in Rice. Plant Physiol 143: 912-923

Garstka M, Venema JH, Rumak I, Gieczewska K, Rosiak M, Kozioł-Lipińska J, Kierdaszuk B, Vredenberg WJ, Mostowska A (2007) Contrasting Effect of Dark-Chilling on Chloroplast Structure and Arrangement of Chlorophyll-Protein Complexes in Pea and Tomato: Plants with a Different Susceptibility to Non-Freezing Temperature. Planta 226: 1165-1181

Mostowska A (1986a) Changes Induced on the Prolamellar Body of Pea Seedlings by White, Red and Blue Low Intensity Light. Protoplasma 131: 166-173

Mostowska A (1986b) Thylakoid and Grana Formation During the Development of Pea Chloroplasts, Illuminated by White, Red, and Blue Low Intensity Light. Protoplasma 134: 88-94

Rumak I, Gieczewska K, Kierdaszuk B, Gruszecki WI, Mostowska A, Mazur R, Garstka M (2010) 3-D Modelling of Chloroplast Structure under (Mg^{2+}) Magnesium Ion Treatment. Relationship between Thylakoid Membrane Arrangement and Stacking. Biochim Biophys Acta 1797: 1736-1748

Protochlorophyllide Forms in Etiolated Seedlings of Photoreceptor Mutants of *Arabidopsis Thaliana* — Is Chlorophyll Biosynthesis Controlled by Cooperation between Phytochromes and Phototropins?

Beata Myśliwa-Kurdziel*, Elżbieta Turek, Przemysław Malec

Department of Plant Physiology and Biochemistry, Faculty of Biochemistry, Biophysics and Biotechnology, Jagiellonian University, ul. Gronostajowa 7, 30-387 Kraków, Poland.
*Corresponding author. Tel. No. +48 12 664 6372; Fax No. +48 126646902; E-mail: b.mysliwa-kurdziel@uj.edu.pl.

Abstract: The accumulation of protochlorophyllide and the relative content of long-wavelength protochlorophyllide spectral form, *i.e.* having fluorescence maximum at 655 nm ($Pchlide_{655}$), were studied in etiolated seedlings of different ecotypes of *Arabidopsis* as well as in several photoreceptor mutants. The latter parameter provides information on the capability for protochlorophyllide photoreduction upon the first exposure of emergent seedlings to light. The capacity of Pchlide biosynthesis and its subsequent accumulation in the dark has been found to be dependent on the genetic background (ecotype). The Pchlide accumulation and the formation of $Pchlide_{655}$ have been found to be reduced in seedlings of both phytochrome-deficient (*phyA*, *phyB*) and phototropin 2-deficient (*phot2*) mutants. In contrast, cryptochrome-deficient mutants (*cry1*, *cry2*) showed no significant differences of both total Pchlide and $Pchlide_{655}$ contents in comparison to their respective background ecotypes. The results presented in this work indicate that the equilibrium between Pchlide accumulation and the formation of $Pchlide_{655}$ in etiolated seedlings of angiosperms, is dependent both on plant ecotype and on light conditions in the environment during seed germination and/or seedlings formation. Mutant analysis points to the role of both phytochromes and phototropin 2 in the regulation of the formation of different Pchlide forms in *Arabidopsis*.

Keywords: *Arabidopsis thaliana*; Chlorophyll biosynthesis; Light-dependent protochlorophyllide oxidoreductase; Photoreceptor mutants; Protochlorophyllide

Introduction

Chlorophyll (Chl) biosynthesis in angiosperms is light-dependent at the stage of protochlorophyllide (Pchlide) to chlorophyllide (Chlide) reduction. This reaction is catalyzed by a photoenzyme Pchlide oxidoreductase (LPOR) (see Bollivar, 2006; Masuda, 2008 for reviews).

In the dark, angiosperm seedlings accomplish a developmental program known as skotomorphogenesis. Etiolated seedlings are delicate, yellowish, with long hypocotyls, small closed cotyledons and an apical hook (Fig. 1). The first exposure of emergent dark-grown seedlings of angiosperms to light starts a deetiolation, *i.e.* the transition from heterotrophic to photoautotrophic growth. The deetiolation is a complex process comprising profound changes in seedling morphology and physiology caused by light-regulated

Fig. 1 Five-days old etiolated seedlings of *A. thaliana.*

expression of nuclear- and chloroplast encoded genes (von Arnim and Deng, 1996). This process is controlled by an interaction network of multiple photoreceptors (predominantly phytochromes and cryptochromes) and their downstream signaling elements (Casal, 2006).

Successful transition of etiolated angiosperm seedlings to photoautotrophy strongly depends on the accumulation of the initial pool of Pchlide. The accumulation of Pchlide in the dark ensures fast and effective Chl biosynthesis upon illumination, and in consequence, determines the assembly of the photosynthetic apparatus (Schoefs and Franck, 2003; Schoefs, 2005). On the other hand, bulk amounts of free Pchlide accumulated in cells may cause lethal damage upon light exposure due to photooxidation (Erdei *et al*., 2005). Therefore, in etiolated seedlings the significant level of Pchlide is attached to POR and localized in prolamellar bodies, which are highly organized lipid structures that play a protective role during the Pchlide to Chlide photoreduction (reviewed by Solymosi and Schoefs, 2010).

Using etiolated seedlings of *A. thaliana* mutants deficient in photoreceptors involved in the deetiolation transition, we have investigated how plants regulate the balance between the Pchlide biosynthesis and the capacity of its photoreduction.

Material and Methods

Plant material and seedling culture. *Arabidopsis thaliana* wild-type and mutant seeds were sterilized for 20 min with 3% of hypochlorite with addition of 0.1% of Triton X-100 (Serva, Germany), washed extensively with sterile deionized water and sown on Petri dishes containing Murashige and Skoog medium (Sigma -Aldrich Chem. Co., St. Louis, U.S.A.) with 1% agar, as described by Malec *et al*. (2002). The seeds were kept in darkness after sowing at 4 ^{o}C for 48 h and subsequently grown in darkness at 22 ± 2 ^{o}C for 5 days. All handling of the seedlings was done under dim green light, that did not induced any detectable Pchlide photoreduction. The wild-type seeds—ecotypes *Columbia* (Col-0), *Landsberg erecta* (Ler) and *Wassiliewskaja* (Ws) were from Arabidopsis Biological Resource Center, Ohio State University, Ohio, USA. The following mutant lines were used in this work: *phyA* (Reed *et al*., 1993), *phyB* (Koornneef *et al*., 1980), cry*1-304* (Ahmad and Cashmore, 1993), c*ry2-1* (Guo *et al*., 1998), *phot2 npl1*; (Jarillo *et al*., 2001). At least two independent seed batches were used for a single experiment. Experiments were repeated 3–5 times.

Relative Pchlide content in etiolated seedlings was calculated from the maximal fluorescence intensity read from the fluorescence spectrum as measured for acetone extract of pigments at room temperature. The fluorescence intensity at 633 nm (*i.e.* at the maximum) per gram of the fresh weight of the plant tissue has been taken as a measure of the Pchlide accumulation.

Relative amount of the photoactive Pchlide was estimated based on the fluorescence emission spectra measured at 77 K for homogenate of etiolated seedlings. A ratio of fluorescence intensity at 655 nm (F655) to the intensity at 633 nm (F633) was calculated from all recorded spectra and averaged for multiple repetitions of the experiment (at least 30). Statistical significance of experimental data was evaluated by using t-test.

Fluorescence spectra were measured with Perkin-Elmer LS-50 spectrofluorometer for the excitation at 440 nm.

Results and Discussion

Fluorescence emission spectra measured at 77 K for the wild type of *A. thaliana* in the dark (Fig. 2) have a shape typical for etiolated leaves (see *e.g.* Belyaeva and Litvin, 2007 for a review).

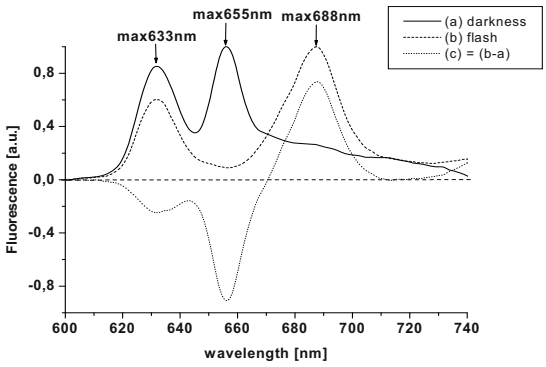

Fig. 2 Fluorescence emission spectra, measured at 77 K, of homogenate from 5 days-old etiolated seedlings of wild-type *Arabidopsis*, ecotype Columbia, in darkness (solid line), after flash of strong light (dashed line) and differential spectrum obtained by a subsequent subtraction (dotted line). Emission maxima of non-photoactive Pchlide (633 nm), photoactive Pchlide (655 nm) and chlorophyllide (688 nm) are indicated by arrows. Excitation wavelength - 440 nm.

Two emission bands, having maxima at 633 and 655 nm, were clearly seen. The observed bands are attributable to a non-photoactive ($Pchlide_{633}$) and photoactive ($Pchlide_{655}$), Pchlide pools respectively. The photoactivity of the band at 655 nm was proven upon an illumination with a flash of white light, which triggered the Pchlide photoreduction observed as a disappearance of this band and the appearance of a new band with a maximum at 688 nm (originating from newly formed Chlide). A differential spectrum shows a direct correlation between $Pchlide_{655}$ reduction and Chlide formation (dotted line in Fig. 2).

The accumulation of Pchlide in wild-type *Arabidopsis* seedlings grown in the dark under controlled conditions varied significantly between ecotypes. The preirradiation of imbibed seeds with white light (80 μmol m^2 s^{-1}, for 5 h) resulted in a significant increase of the total Pchlide accumulation in etiolated seedlings (data not shown). 77 K fluorescence emission spectra revealed differences in the ratio of photoactive to non-photoactive Pchlide as measured by intensity of 655 nm and 633 nm bands, among investigated photoreceptor mutants. The relative reduction of Pchlide content and the ratio of photoactive to non-photoactive Pchlide in selected mutants calculated with respect to their background ecotypes are presented in Table 1.

Table 1 Reduction of Pchlide content (1) and the ratio of fluorescence intensity at 655 nm to that at 633 nm (F_{655}/F_{633}) from low temperature spectra (2) for the investigated mutants of *A. thaliana* as compared with respective wild type. The mutants - p*hyA, phyB, cry2* were compared with *Columbia* (Col-0) while *cry1* and *phot2* with *Landsberg erecta* (Ler) *Arabidopsis* ecotypes. The calculated error in (1) stayed at the level of 10%, whereas in (2) is given in the table.

	Mutants	*phyA*	*phyB*	*cry2*	*cry1*	*phot2*
(1)	Reduction of Pchlide content	13%	41%	7%	6%	18%
(2)	F_{655}/F_{633}	0.91±0.06	0.74±0.2	0.88±0.14	0.94±0.10	0.77±0.08

In the phytochrome deficient (*phy*) and phototropin deficient (*phot2*) mutants, a significantly lower Pchlide content calculated per gram of fresh weight compared to the respective wild type was noticed (Table 1). The strongest effect was observed for *phyB* mutants, for which the Pchlide content was reduced by 41% as compared with that measured for Col-0. Formation of $Pchlide_{655}$ was considerably reduced in *phyB* and in *phot2* seedlings. In contrast, in cryptochrome-deficient mutants (*cry1*, *cry2*) neither Pchlide content nor the formation of $Pchlide_{655}$ were appreciably altered in comparison to their respective background ecotypes.

Our results show that the equilibrium between Pchlide accumulation and the formation of $Pchlide_{655}$, in etiolated seedlings of *A. thaliana*, is dependent on (a) the genetic background of plants and (b) light conditions in the environment during the seed germination and seedling formation. We propose that both the accumulation of Pchlide and the formation of its photoactive complexes are regulated on different ways and both phytochrome and phototropin photoreceptors might be involved into this regulation.

Processes leading to balance different forms of chlorophyll precursors in etiolated seedlings of angiosperms could be under control of a regulatory network involving phytochromes (mainly phytochrome B) and phototropins, as proposed in the scheme (Fig. 3). This regulatory network, which probably involves a cooperative action of the above mentioned photoreceptors, includes the activation of enzymes involved in Pchlide biosynthesis pathway (1), the expression of POR-encoding genes (2) and/or proteins participating in the formation of $Pchlide_{655}$ – an immediate precursor of chlorophyllide (3). The

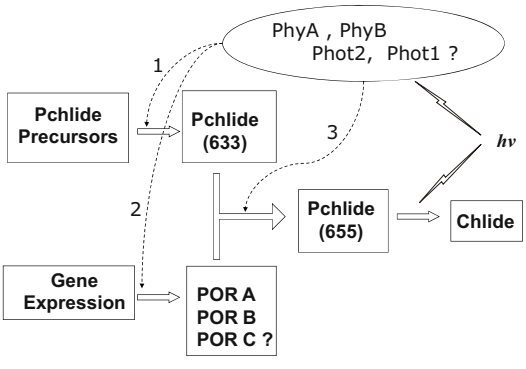

Fig. 3 A diagram presenting key processes of chlorophyll biosynthesis pathway in *Arabidopsis*, potentially regulated by a cooperative action of phytochromes and phototropins: (1) the activation of enzymes involved in Pchlide biosynthesis pathway, (2) the expression of POR-encoding genes, (3) the formation of $Pchlide_{655}$ complex.

detailed molecular mechanisms of the regulation of final steps of chlorophyll biosynthesis in angiosperms by environmental stimuli via phytochromes and phototropins remain to be characterized. In particular, the role of photoreceptors in the regulation of three isoforms of a light dependent protochlorophyllide oxidoreductase found in *A. thaliana*, known as PORA, PORB and PORC, needs elucidation.

Acknowledgements

We thank Prof. DA Chamovitz (Tel Aviv University, Israel) and Prof. JA Jarillo (INIA, Madrid, Spain) for providing seeds of mutant lines used in this work.

This work was supported by a grant N 303 498 438 from the Ministry of Science and Higher Education of The Republic of Poland (P.M.).

The Faculty of Biochemistry, Biophysics and Biotechnology of the Jagiellonian University is a beneficiary of the structural funds from the European Union (grant No: POIG.02.01.00-12-064/08 – "Molecular Biotechnology for Health").

References

Ahmad M, Cashmore AR (1993) HY4 Gene of Arabidopsis Thaliana Encodes a Protein with Characteristics of a Blue-Light Photoreceptor. Nature 366: 162-166

Belyaeva OB, Litvin FF (2007) Photoactive Pigment-Enzyme Complexes of Chlorophyll Precursor in Plant Leaves. Biochemistry (Moscow) 72: 1458-1477

Bollivar DW (2006) Recent Advances in Chlorophyll Biosynthesis. Photosynth. Res. 90: 173-194

Casal JJ (2006) The Photoreceptor Interaction Network. In: Schafer E, Nagy F (eds.), Photomorphogenesis in Plants and Bacteria 3rd ed. Springer: Netherlands, pp. 407-437

Erdei N, Barta C, Hideg E, Böddi B (2005) Light-Induced Wilting and Its Molecular Mechanism in Epicotyls of Dark-Germinated Pea (Pisum Sativum L.) Seedlings. Plant Cell Physiol. 46: 185-191

Guo H, Yang H, Mockler TC, Lin C (1998) Regulation of Flowering Time by Arabidopsis Photoreceptors. Science 279: 1360-1363

Jarillo JA, Gabryś H, Capel J, Alonso JM, Ecker JR, Cashmore AR (2001) Phototropin-Related NPL Controls Chloroplast Relocation Induced by Blue Light. Nature 410: 952-954

Koornneef M, Rolf E, Spruit CJP (1980) Genetic Control of Light-Inhibited Hypocotyl Elongation in Arabidopsis Thaliana (L.) Heynh. Z. Pflanzenphysiol. 100: 147-160

Malec P, Yahalom A, Chamovitz DA (2002) Identification of a Light-Regulared Protein Kinase Activity from Seedlings of Arabidopsis Thaliana. Photochem. Photobiol. 75: 178-183

Masuda T (2008) Recent Overview of the Mg Branch of the Tetrapyrrole Biosynthesis Leading to Chlorophylls. Photosynth. Res. 96: 121-143

Reed JW, Nagpal P, Poole DS, Furuya M, Chory J (1993) Mutations in the Gene for the Red/Far Red Light Receptor Phytochrome B Alter Cell Elongation and Physiological Responses Throughout Arabidopsis Development. Plant Cell 5: 147-157

Schoefs B (2005) Protochlorophyllide Photoreduction – What Is New in 2005? Photosynthetica 43: 329-343

Schoefs B, Franck F (2003) Protochlorophyllide Reduction: Mechanisms and Evolution. Photochem. Photobiol. 78: 543-557

Solymosi K, Schoefs B (2010) Etioplast and Etio-Chloroplast Formation under Natural Conditions: the Dark Side of Chlorophyll Biosynthesis in Angiosperms. Photosynth. Res. 105: 143-166

von Arnim A, Deng XW (1996) Light Control of Seedling Development. Annu. Rev. Plant Physiol. Plant Mol. Biol. 47: 215-43

Blue-Native Page Analysis Validates Heterogeneity in the Thylakoids of *Synechocystis 6803*

Rachna Agarwal[a], Andrea Matros[b], Michael Melzer[b], Hans-Peter Mock[b], Jayashree Krishna Sainis[a*]

[a]Molecular Biology Division, Bhabha Atomic Research Centre, Mumbai, India;
[b]Leibniz Institute of Plant Genetics and Crop Plant Research, Gatersleben (IPK), Germany.
[*]Corresponding author. Tel. No. +91-22-25595079; Fax No. +91-22-25505326; E-mail: jksainis@barc.gov.in.

Abstract: Thylakoids from mature chloroplasts of higher plants show distinct ultra structural differentiation into grana and stroma lamellae where the photosystems, PSII and PSI, are differentially distributed. The thylakoids from cyanobacteria do not show such differentiation, even if they have both PSII and PSI as components of electron transport like higher plants. Recently we have demonstrated that the thylakoids from cell free extracts of *Synechocystis* 6803 can be fractionated using differential ultra-centrifugation at 40,000 x g (40 k), 90,000 x g (90 k) and 150,000 x g (150 k). These native thylakoid fractions showed biochemical as well as proteomic heterogeneity. We have analyzed these fractions using Blue-Native (BN) PAGE followed by ESI-MS/MS or MALDI-MS. The 1-D BN gels showed protein super-complexes bands ranging from ~200~900 kDa. The protein super-complexes from 1-D gels were further separated into individual subunits in second dimension on the denaturing tricine SDS-PAGE. 44 differing bands from 1-D gels and 38 differing protein spots form 2-D gels were selected for identification. Our results showed that there were qualitative and quantitative differences in the pigment-protein complexes among the three fractions validating the hypothesis of heterogeneity in thylakoids of *Synechocystis* 6803.

Keywords: Blue-Native PAGE; Heterogeneity; *Synechocystis* 6803; Thylakoid membranes

Introduction

Lateral heterogeneity refers to non-homogeneous distribution of different photosynthetic complexes in the thylakoids of higher plant chloroplasts with grana stacks harboring PSII, interconnected with single membranes called stroma lamellae harboring preferentially PSI. The heterogeneity is an adaptation for "minimization of excitonic contact" between kinetically slow PSII and fast PSI favoring the resonance energy transfer from PSII to PSI, and to resist the degradation of labile PSII proteins under high light (Trissl and Wilheim, 1993; Staehelin and Arntzen, 1983; Anderson and Aro, 1994)

However Cyanobacteria, the photosynthetic prokaryotes, do not show any visible lateral heterogeneity into grana and stroma lamallae. There are only a few reports indicating heterogeneity in the thylakoids of these organisms. Sherman *et al*. (1994) have reported localization of PSI in the outer thylakoids and PSII in the inner thylakoids of *Synechococcus* 7942 by immuno-gold transmission electron microscopy. In contrast recently Vermaas *et al*. (2008) have shown preferential location of PSI in the inner thylakoids by employing *in vivo* hyperspectral confocal fluorescence imaging (Vermaas *et al.*, 2008).

The present study shows that the thylakoids of cyanobacteria can be fractionated using differential ultracentrifugation. These thylakoid membrane fractions show heterogeneity in various protein super-complexes on BN-PAGE and proteome analysis.

Materials and Methods

Culture conditions

Culture of *Synechocystis* 6803 was grown in BG-

11 medium (Rippka *et al.*, 1979) under continuous fluorescent white light of intensity 21 W/m^2 at 30 °C in static non-aerated conditions.

Preparation of membrane fractions

The three thylakoid membrane fractions were isolated as described previously (Agarwal *et al.*, 2010).

1-D Blue-Native (BN) PAGE and 2-D Tricine SDS-PAGE

For BN-PAGE, thylakoid membranes were resuspended in solubilisation buffer (50 mmol NaCl; 50 mmol Imidazole/HCl; 2 mmol 6-Aminohexanoic acid; 1 mmol EDTA, pH 7.0) and stored at −70 °C until further use. Thylakoid membranes equivalent to 250 µg protein were solubilized with dodecyl-β-D maltozide at a detergent to protein ratio 1:1 for 30 min at 4 °C followed by 10min at RT with continuous shaking. Un-dissolved membranes were removed by centrifuging at 18,000 rpm for 2 min at 4 °C. 5% v/v glycerol and 5% Coomassie blue G-250 from Serva were added to the solubilized membranes to give a detergent to dye ratio of 8 and the membranes were resolved on 20%–24% continuous gradient polyacrylamide gel with 3.5% stacking gel at 4 °C. Rest of the procedure was followed essentially according to Wittig *et al*. (2006).

For second dimension tricine SDS-PAGE, 1cm wide strips from 1-D BN-PAGE were incubated with 1% SDS and 1% ß-mercaptoethanol for 1h at room temperature for protein denaturation and rinsed briefly with DDW. The strip was mounted between clean glass plates of Hoefer SE 600 vertical electrophoresis unit. A 10% acrylamide resolving gel followed by 3.5% stacking gel holding the 1-D gel strip was cast. The gel was subjected to electrophoresis and silver stained essentially according to Schagger (2006).

ESI-MS on super complexes separated on BN-PAGE and MALDI-MS of proteins from 2-D tricine SDS-PAGE

Gel spots (1 mm^3) were cut from both 1-D BN gels and 2-D tricine SDS gels with a clean scalpel and washed with 400 µl of 10 mmol ammonium bicarbonate in 50% acetonitrile at RT for 30 min. The gel pieces were processed for proteome analysis according to Witzel *et al*. (2007). ESI-MS based identification was carried out as described previously (Agarwal *et al.*, 2010) MALDI-MS based identification was outsourced to TCGA, New Delhi, India.

Results and Discussion

Fig. 1 shows the representative 1-D BN gel pattern for the 40 k, 90 k, 150 k thylakoid membranes and the supernatant fractions. A total of 44 differing bands were observed and identified among these fractions. The band pattern showed qualitative (presence or absence of unique bands in a fraction) and quantitative differences among the three fractions. For example band 3 is present only in the 150 k fraction whereas band 6 and 8 appear in 40 k fraction. Band 5 is absent from 40 k fraction whereas band 7 is absent in the 150 k fraction. Important observations include the association of RuBisCO and GAPDH with

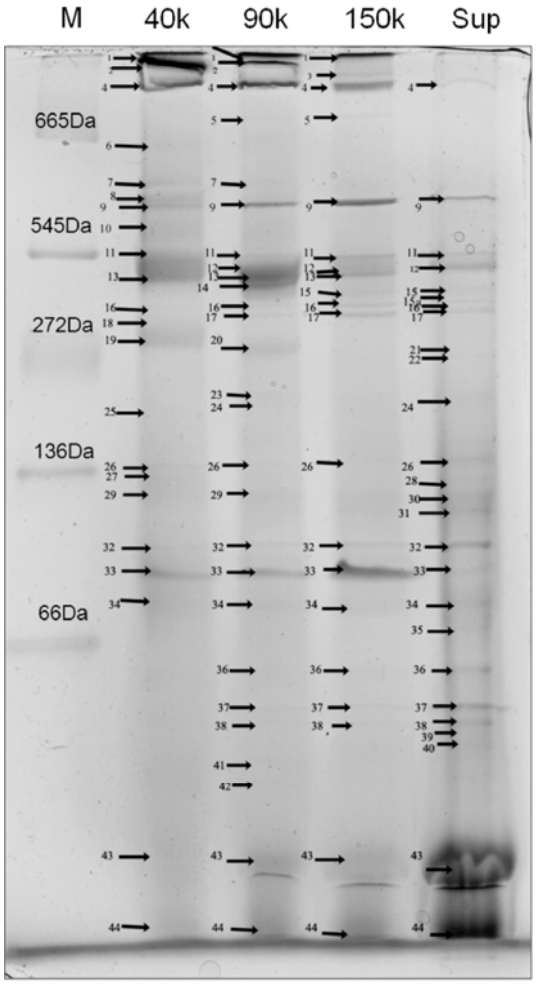

Fig. 1 1-D BN-PAGE of the three thylakoid fractions and supernatant. The arrows indicate the Super-complexes which were subjected to ESI-MS/MS analysis.

PSI in 150 k fraction (bands 1, 3 and 4 in the 150 k fraction), increasing association of glutamine ammonia ligase with thylakoids from 40 k to 150 k fraction (band 9), and presence of only dimeric form of PSII in 150k fraction (band 15 and 16 in 150 k fraction). These results corroborate our previous reports about association of soluble Calvin cycle enzymes (RuBisCO and GAPDH) with thylakoids and also predict PSI as a possible association site for them (Agarwal *et al.*, 2009, 2010).

The strips from the 1-D BN gels were cut and subjected to electrophoresis in second dimension using denaturing tricine SDS gels as described in materials and methods. Fig. 2 shows the comparative 2-D gel pictures of the 40 k, 90 k, 150 k and supernatant fractions on equal protein basis.

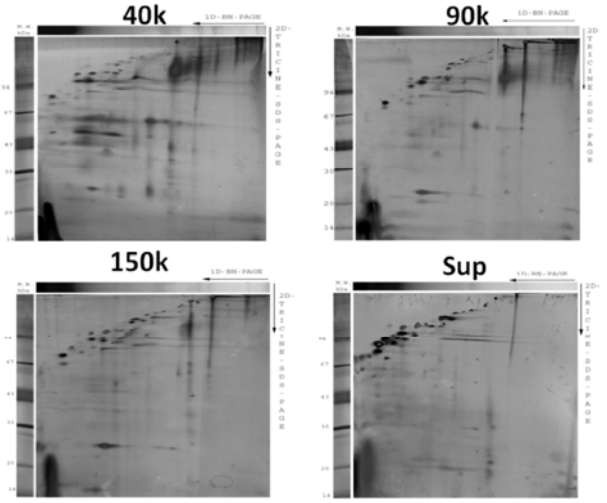

Fig. 2 Tricine SDS-PAGE gels of the 1-D BN-PAGE strips of the three thylakoid membrane fractions and supernatant fraction.

The results showed that there were many protein spots common between the membrane fractions and the supernatant fraction with equal intensity on equal protein basis which again suggest the possibility of association of soluble enzymes with thylakoid membranes.

Fig. 3 shows a representative 2-D gel of the fractions. More than 100 protein spots were observed after silver staining of the gels of which 38 could be identified successfully.

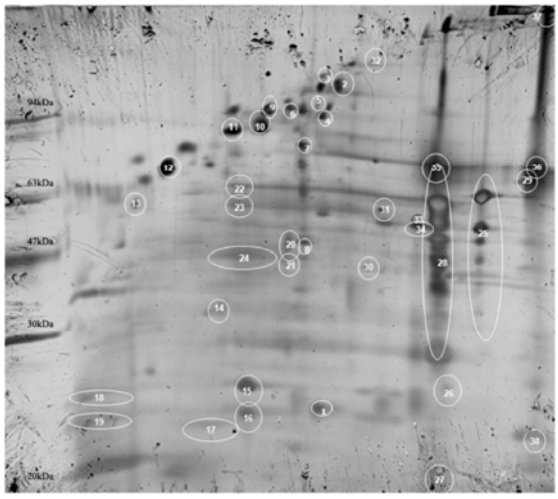

Fig. 3 A representative 2-D tricine SDS-PAGE silver stained gel of one of the thylakoid fractions. The labeled spots were cut, digested and identified using MS.

Table 1 List of proteins identified in the representative 2-D Tricine SDS Gel with the corresponding spot numbers.

Spot No.	Protein	Spot No.	Protein
1	C-phycocyanin alpha chain	20	IMP dehydrogenase homolog
2	Ribulose phosphate epimerase	21	Hypothetical protein
3	Adenosyl-homocysteinase	22	RuBisCO LSU
4	Hypothetical protein	23	RuBisCO LSU
5	slr7016	24	Hypothetical protein
6	Hypothetical protein	25	Glutamine ammonia ligase
7	Phosphoketolase	26	Keto acid reductoisomerase
8	Soluble dehydogenase	27	RuBisCO SSU
9	slr1855	28	RuBisCO LSU
10	Dihydrolipoyl dehydogenase	29	cpn60
11	Hypothetical protein	30	porphobillinogen synthase
12	slr1852	31	Glutamate decarboxylase
13	slr1853	32	porphobillinogen synthase
14	protein glpX	33	Phosphopyruvate hydratase
15	Phycocyanin alpha chain	34	PsbB
16	Phycocyanin alpha chain	35	PsaA
17	sll1130	36	PsaA
18	Phycocyanin beta chain	37	PsbB
19	Phycocyanin beta chain	38	PSI chain three precursor

MALDI-MS showed that the subunits of a super-complex were seen to be separating on the 2-D gels Table1). Out of these 38 proteins, some were soluble proteins besides sub-units of membrane located PSI and PSII. Some new proteins like Ribulose-5-phosphate-3- epimerase, slr 1852, slr 1853 and slr 1855 were identified, which were not observed in our previous study conducted through in-solution digestion of proteins from the thylakoids (Agarwal *et al.*, 2010).

BN-PAGE is known to be an effective technique in understanding the differences in the multisubunit protein super-complexes and has been mainly employed for understanding respiratory OXPHOS complexes. In comparison, the reports on use of this technique for photosynthetic super-complexes are relatively less. The current study has successfully reiterated the efficiency of BN PAGE in resolving large membrane located pigment protein complexes of photosynthesis. The results have also reconfirmed the existence of heterogeneity in the distribution of pigment-protein complexes in different thylakoid fractions of *Synechocystis* 6803. On the basis of the results, it can be concluded that the 40 k and 90 k fractions are closer to the stroma lamellae of higher plant chloroplast because of preponderance of PSI as seen on the 1-D gels. Similarly, the 150 k fraction can be the progenitor of the grana region due to higher proportion of dimeric PSII.

This primitive lateral heterogeneity may have functional significance as this can provide micro-compartmentation in these organelle-less prokaryotes thus leading to higher efficiency of various physiological processes.

References

Agarwal R, Ortleb S, Sainis JK, Melzer M (2009) Immunoelectron Microscopy for Locating Calvin Cycle Enzymes in the Thylakoids of Synechocystis 6803. Molecular Plant 2(1): 32-42

Agarwal R, Matros A, Melzer M, Mock HP, Sainis JK (2010) Heterogeneity in Thylakoid Membrane Proteome of Synechocystis 6803. J Proteomics 73: 976-991

Anderson JM, Aro EM (1994) Grana Stacking and Protection of Photosystem II in Thylakoid Membranes of Higher Plant Leaves under Sustained Irradiance: a Hypothesis. Photosynth. Res. 41: 315-326

Rippka R, Deruelles J, Waterbury J, Herdman M, Stanier R (1979) Generic Assignments Strain Histories and Properties of Pure Cultures of Cyanobacteria. J Gen Microbiol. 111: 1-61

Schagger H (2006) Tricine-SDS-PAGE. Nature Protocols 1: 16-22

Sherman DM, Troyan TA, Sherman LA (1994) Localisation of Membrane Proteins in the Cyanobacterium Synechococcus 7942: Radial Asymmetry in the Photosynthetic Complexes. Plant Physiol. 138: 1577-1585

Staehelin LA, Arntzen CJ (1983) Regulation of Chloroplast Membrane Function: Protein Phosphorylation Changes the Spatial Organization of Membrane Components. J Cell Biol. 97: 1327-1337

Trissl HW, Wilheim C (1993) Why Do Thylakoid Membranes from Higher Plants Form Grana Stacks? Trends Biochem. Sci. 18: 415-419

Vermaas WFJ, Timlin JA, Jones HDT, Sinclair MB, Lieman LT, Hamad SW, Melgaard DK, Haaland DM (2008) In Vivo Hyperspectral Confocal Fluorescence Imaging to Determine Pigment Localization and Distribution in Cyanobacterial Cells. Proceedings Natl Acad Sci. 105(10): 4050-4055

Wittig I, Braun HP, Schagger H (2006) Blue Native Page. Nature Protocols 1: 418-428

Witzel K, Surabhi GK, Jyothsnakumari G, Sudhakar C, Matros A, Mock HP (2007) Quantitative Proteome Analysis of Barley Seeds Using Ruthenium(II)-Tris-(Bathophenanthroline-Disulphonate) Staining. J Proteome Res. 6: 1325-1333

Spatial and Temporal Regulation of Chloroplast Development in Arabidopsis Root

Koichi Kobayashi[1,2], Tatsuru Masuda[2*]

[1]RIKEN Plant Science Center, Yokohama, Japan;
[2]Graduate School of Arts and Sciences, The University of Tokyo, Tokyo, Japan.
[*]Corresponding author. Tel. No. +81 3 5454 6627; Fax No. +81 3 5454 4321; E-mail: ctmasuda@mail.ecc.u-tokyo.ac.jp.

Abstract: In higher plants, heterotrophic organs develop non-green plastids whereas photosynthetic organs develop chloroplasts within the cells. In Arabidopsis, roots grow underground as heterotrophic organs with developing non-green plastids. Although the roots have a potential to develop chloroplasts, it may be usually repressed through the COP1/DET1-mediating degradation of HY5 even in the presence of light. On the other hand, our recent data demonstrate that the roots detached from the shoot develop chloroplasts through a modification of auxin/cytokinin signaling. To reveal the regulatory system of chloroplast biogenesis, in this study we investigated spatial and temporal patterns of chlorophyll accumulation, HY5 protein accumulation, and *CHLH* expression in Arabidopsis roots. While the patterns of chlorophyll accumulation and *CHLH* expression in roots were very similar, the distribution pattern of HY5 was largely different from those, suggesting that the accumulation of HY5 is not a rate-limiting factor for chlorophyll synthesis in roots. Meanwhile, overexpression of GOLDEN2-LIKE (GLK) 1 and GLK2 transcription factors resulted in an ectopic accumulation of chlorophyll in roots. Because GLKs are strong upregulators of genes associated with chlorophyll biosynthesis and light harvesting, the expression rate of *GLK1* and *GLK2* is likely one of limiting factors for chloroplast biogenesis in roots.

Keywords: Arabidopsis; Chlorophyll; Chloroplast; Root greening

Introduction

In higher plants, plastids undergo profound morphological changes into different plastid types depending on organ type development. Photosynthetic organs such as leaves develop chloroplasts from proplastids or other non-green plastids and perform photosynthesis. In contrast, non-photosynthetic organs like flowers and roots develop non-green plastids such as chromoplasts and amyloplasts. In general, roots grow underground as heterotrophic organs depending on leaves for their energy source. However, root cultures derived from an evolutionarily distant taxa (*Asteraceae*, *Solanaceae*, etc.) exhibit the ability to develop chloroplasts and to grow photoautotrophically (Flores *et al*., 1993). In extreme cases, photosynthesis by roots does contribute to the carbon economy of the whole plant of the epiphytic *Orchidaceae* (Benzing *et al*., 1983) and of mangroves (Gill and Tomlinson, 1977). Therefore, several plant species can develop chloroplasts in roots and perform photosynthesis when exposed to light, reflecting the plasticity of plant tissues. The regulation system of chloroplast biogenesis in roots, which still remains unclear at the molecular level, is one of important control mechanisms for plastid development upon differentiation of plant organs.

In *Arabidopsis thaliana*, roots are also heterotrophic organs growing underground. Even in the light, they predominantly develop non-photosynthetic plastids and receive energy supply from the shoots, suggesting that chloroplast development is essentially repressed in the root as heterotrophic organs. However, greening of the roots was clearly observed in *det1* (Chory and Peto, 1990) and *cop1* mutants (Deng and Quail, 1992), while it is absent in the *hy5* mutant (Oyama *et al*., 1997; Usami *et al*., 2004), showing a potential of Arabidopsis roots to develop chloroplasts. The data

also indicate that chloroplast development in the root is dependent on HY5 function and that is, however, usually repressed by the COP1/DET1-mediating signaling pathway. Recently we revealed that chlorophyll biosynthesis in Arabidopsis roots is positively regulated by cytokinin and negatively regulated by auxin at transcriptional level (Kobayashi *et al*., submitted). Such opposite effects of these phytohormones are dependent on a transcription factor HY5, which is indispensable for the expression of key chlorophyll biosynthesis genes in roots. The gene expression of yet another root greening transcription factor GOLDEN2-LIKE (GLK) 2 was also found to be regulated in opposite ways by auxin and cytokinin. Our current data suggest that the combination of HY5 and GLKs, located down-stream of light and auxin/cytokinin signaling pathways, is responsible for coordinated expression of the key genes in chloroplast biogenesis in Arabidopsis roots (Kobayashi *et al*., submitted).

In this study, we investigated spatial and temporal patterns of chlorophyll accumulation, HY5 protein accumulation, and *CHLH* expression in Arabidopsis roots. We also evaluated the effect of GLK1 and GLK2 on regulation of chloroplast biogenesis in roots.

Materials and Methods

Plants used here are all *Arabidopsis thaliana* grown vertically on solid medium (1× Murashige and Skoog medium, 1% [w/v] sucrose, and 0.8% [w/v] agar, pH 5.7) at 23 °C under continuous light. A transgenic line *hy5-1/Pro$_{HY5}$:HY5-YFP* was provided by Dr. Roman Ulm (Oravecz *et al*., 2006). *GLK1$_{OX}$* (*35S:GLK1*) and *GLK2$_{OX}$* (*35S:GLK2*) were provided from Dr. Jane A. Langdale (Waters *et al*., 2008). To produce transgenic plants expressing a *GUS* gene under the control of the *CHLH* promoter, the 5'-upstream region of *CHLH* between –1200 to +155 bp from the transcription initiation site (*CHLH$_{pro}$*) was cloned into pGEM-T Easy vector (Promega) according to the manufacturer's instructions. A plasmid fragment lacking G-box sequences in the *CHLH* promoter region (*CHLH$_{ProΔG\text{-}box}$*) was amplified from the *CHLH$_{pro}$* vector and self-ligated into a circular plasmid. These promoter sequences were fused to the *GUS* gene in a pBI101 vector. T-DNA regions carrying these constructs were introduced into Arabidopsis Col-0 genome using *Agrobacterium tumefaciens* strain GV3101:pMP90.

To detect fluorescence from chlorophyll and the HY5-YFP protein, *hy5-1/Pro$_{HY5}$:HY5-YFP* roots detached just from the hypocotyl were examined using a confocal laser scanning microscope (FV-1000, Olympus). For observation of chlorophyll fluorescence in lateral roots, third lateral roots from the root-hypocotyl junction were examined in 21-day-old wild type and the GLK overexpressors using FV-1000.

For histochemical GUS staining, seedlings or roots containing the hypocotyl region were incubated in 90% (v/v) acetone for 2 h and then treated with the GUS solution (1 mmol 5-bromo-4-chloro-3-indolylglucuronide, 2 mmol $K_3Fe(CN)_6$, 50 mmol NaCl, 20% [v/v] methanol, and 100 mmol Tris-HCl, pH 7.5) for 4 h. After removing pigments by 70% (v/v) ethanol, samples were treated with a clearing solution (Chloral hydrate, water, glycerol, 8:2:1 [v/v]) for 3 h.

Results and Discussion

To reveal the controlling mechanisms of chloroplast biogenesis in roots, we investigated a relationship between chlorophyll accumulation and HY5 protein accumulation in roots by using the *hy5-1/HY5$_{pro}$:HY5-YFP* transgenic line, which expresses the HY5-YFP fusion protein through HY5 native promoter in the *hy5-1* mutant (Oravecz *et al*., 2006). As reported previously (Usami *et al*., 2004), Arabidopsis roots partially accumulate chlorophyll in the presence of light. In the root of young seedlings, very weak chlorophyll fluorescence was observed only near the root-hypocotyl junction (Fig. 1). Then, chlorophyll fluorescence in the root became stronger and broader as plant grew, but was still restricted in the primary root. These data suggest that chlorophyll accumulation and also chloroplast biogenesis in the root is strictly regulated in a development- and region-dependent manner. By contrast, fluorescence from the HY5-YFP fusion protein was observed widely in the root of 4-day-old plants. Thereafter, HY5-YFP fluorescence was observed constantly and thoroughly in the root region. These large differences in accumulation patterns between chlorophyll and the HY5 protein demonstrate that the accumulation level of HY5 is not a rate-limiting factor for chlorophyll biosynthesis in roots.

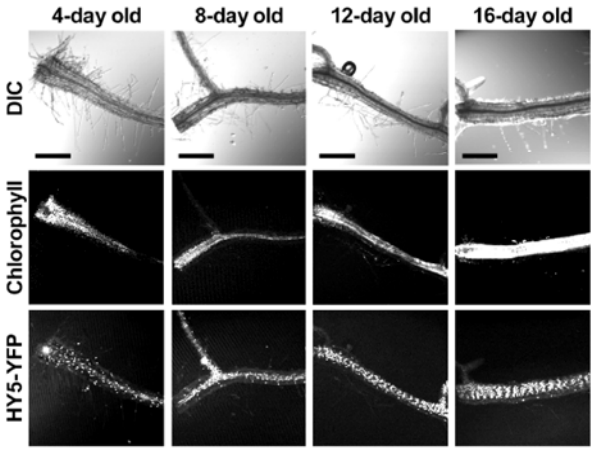

Fig. 1 Development- and region-specific accumulation of chlorophyll and the HY5-YFP protein in the *hy5-1/Pro$_{HY5}$:HY5-YFP* transgenic line. Fluorescence from chlorophyll and the HY5-YFP protein was observed around the hypocotyl junction of the primary root. DIC; differential interference contrast images. Bars = 0.2 mm.

One of the most important events during greening is the biosynthesis of chlorophyll which functions as a pigment for light energy harvesting and charge separation in photosystem I and II. Because chlorophyll and its intermediates are strong photosensitizers, plant cells must regulate strictly their metabolism in concert with the construction of the photosynthetic machinery. In fact, the expression of key genes involved in chlorophyll biosynthesis is highly co-regulated with nuclear-encoded photosynthesis-related genes (Masuda and Fujita, 2008). To assess whether gene expression is associated with chlorophyll accumulation in the root, we performed a GUS reporter analysis using a promoter region of the *CHLH* gene, which is a key coexpressed gene encoding the H subunit of Mg-chelatase. In 4- and 8-day-old young seedlings, while intense GUS staining was observed in the hypocotyl, it was undetectable in the root. In 12-day-old seedlings, weak GUS staining was observed in the primary root near the junction to hypocotyl. In 16-day-old seedlings, the staining in the root became stronger and broader but it was still restricted in the primary root. This GUS staining pattern was very similar to the accumulation pattern of chlorophyll in roots. Considering the fact that *CHLH* forms a highly-coexpressed gene network with other key chlorophyll synthesis genes and nuclear-encoded photosynthetic genes (Masuda and Fujita, 2008), it is likely that the expression of these key genes is a determinant step for chlorophyll synthesis in the root.

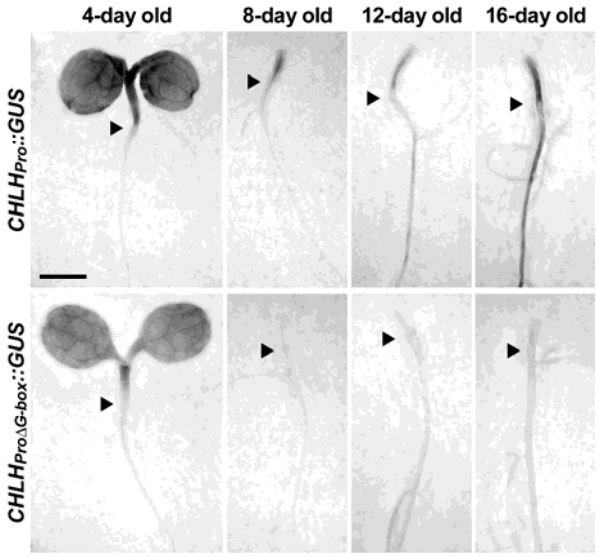

Fig. 2 Histochemical GUS staining derived from the native (*CHLH$_{Pro}$*) or G-box-lacking (*CHLH$_{Pro\Delta G\text{-}box}$*) *CHLH* promoter in roots. Whole GUS staining was shown in 4-day-old seedlings whereas staining in roots was displayed in more developed plants. Triangles indicate the root-hypocotyl junction. Bars = 2.0 mm.

The strong correlation between the *CHLH* expression and chlorophyll accumulation in the root suggests that the regulation at the transcript level is important for the control of chlorophyll synthesis in the root. Because the *CHLH* promoter region contains a potent cis-element so-called G-box (CACGTG) between −54 bp and −59 bp from the transcription initiation site, we also investigated the GUS activity derived from the *CHLH* promoter lacking the G-box element. As shown in Fig. 2, the GUS activity from this mutant promoter was consistently undetectable in the root through the development. Because chlorophyll accumulation in the root absolutely requires the G-box binding transcription factor HY5 (Usami *et al*., 2004; Kobayashi *et al*., submitted), the binding of HY5 to the G-box element on the *CHLH* promoter may be essential for its expression in the root. This hypothesis is supported by the evidence that the *CHLH* promoter is one of the *in vivo* binding targets of HY5 (Lee *et al*., 2007). On the other hand, because the accumulation pattern of the HY5 protein was largely different from the patterns of the *CHLH* expression and chlorophyll accumulation, other factors may be required for development- and region-dependent regulation of the *CHLH* expression and chlorophyll accumulation in the root.

While HY5 acts at the downstream of phytochrome signaling, GARP nuclear transcription

factors GLK1 and GLK2 positively influence the expression of nuclear-encoded photosynthetic genes, especially those associated with chlorophyll biosynthesis and light harvesting, independently of the phyB signaling pathway (Waters *et al*., 2009). The positive effect of these transcription factors on chloroplast biogenesis is more obvious in the root (Nakamura *et al*., 2009; Kobayashi *et al*., submitted). To address the relationship between regulation of chloroplast development and GLK functions, we analyzed the chlorophyll accumulation patterns in the root of *GLK1* and *GLK2* overexpression lines. As shown in Figure 3, each overexpression line showed prominent fluorescence from chlorophyll in the root. Furthermore, while chlorophyll fluorescence was only detectable in the primary roots in wild type, that in both overexpression lines was also observed in the lateral roots in addition to the primary roots. Because in these lines GLK factors are artificially over-expressed by the cauliflower mosaic virus 35S promoter in a *glk1 glk2* double mutant (Waters *et al*., 2008), it is likely that the strong ectopic expression of GLK factors in lateral roots induces chloroplast biogenesis there. The intensity and the tissue specificity of the expression of *GLK1* and *GLK2* may be one of limiting factors for chloroplast biogenesis in the root.

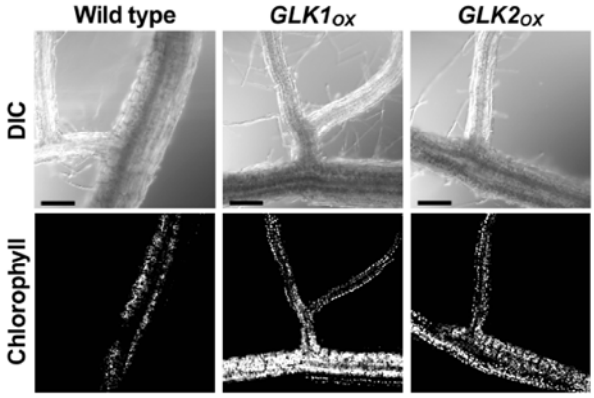

Fig. 3 Chlorophyll fluorescence detected in the primary root and lateral roots of wild type and *GLK* overexpressors. DIC; Differential interference contrast images. Bars = 0.2 mm.

Although Arabidopsis roots are heterotrophic organs depending on the shoot for their energy source, we recently revealed that the roots detached from the shoots activated greening in the presence of light by modulating phytohormone signaling (Kobayashi *et al*., submitted). This data imply that Arabidopsis roots can activate chloroplast biogenesis in response to the environmental changes probably to generate energy partly from the sun. GLK factors are likely to contribute to the plastic chloroplast development according to their surrounding environments whereas HY5 supports the basal potency of chloroplast biogenesis.

Acknowledgements

For the supply of Arabidopsis lines, we thank Roman Ulm, University of Freiburg (*hy5-1/HY5$_{pro}$:HY5-YFP*), and Jane A Langdale, Oxford University (*GLK1$_{OX}$* and *GLK2$_{OX}$*). This work was supported by grants for Grants-in-Aid for Scientific Research (No. 21570035 to TM) and in part by the Global Center of Excellence Program (K03) from the Ministry of Education, Culture, Sports and Technology, Japan. Supports by Research Fellowship for Young Scientists from the Japanese Society for the Promotion of Science and by RIKEN grants to KK are also acknowledged.

References

Benzing DH, Friedman WE, Peterson G, Renfrow A (1983) Shootlessness, Velamentous Roots, and the Pre-Eminence of Orchidaceae in the Epiphytic Biotope. Am. J. Bot. 70: 121-133

Chory J, Peto CA (1990) Mutations in the DET1 Gene Affect Cell-Type-Specific Expression of Light-Regulated Genes and Chloroplast Development in Arabidopsis. Proc. Natl. Acad. Sci. USA 87: 8776-8780

Flores HE, Dai Y, Cuello JL, Maldonado-Mendoza IE, Loyola-Vargas VM (1993) Green Roots: Photosynthesis and Photoautotrophy in an Underground Plant Organ. Plant Physiol. 101: 363-371

Gill AM, Tomlinson PB (1977) Studies of the Growth of Red Mangrove (Rhizophora Mangle L) 4: the Adult Root System. Biotropica 9: 145-155

Masuda T, Fujita Y (2008) Regulation and Evolution of Chlorophyll Metabolism. Photochem. Photobiol. Sci. 7: 1131-1149

Nakamura H, Muramatsu M, Hakata M, Ueno O, Nagamura Y, Hirochika H, Takano M, Ichikawa H (2009) Ectopic Overexpression of the Transcription Factor OsGLK1 Induces Chloroplast Development

in Non-Green Rice Cells. Plant Cell Physiol. 50: 1933-1949

Oravecz A, Baumann A, Máté Z, Brzezinska A, Molinier J, Oakeley EJ, Adám E, Schäfer E, Nagy F, Ulm R (2006) Constitutively Photomorphogenicl Is Required for the UV-B Response in Arabidopsis. Plant Cell 18: 1975-1990

Oyama T, Shimura Y, Okada K (1997) The Arabidopsis HY5 Gene Encodes a bZIP Protein that Regulates Stimulus-Induced Development of Root and Hypocotyl. Genes Dev. 11: 2983-2995

Usami T, Mochizuki N, Kondo M, Nishimura M, Nagatani A (2004) Cryptochromes and Phytochromes synergistically Regulate Arabidopsis Root Greening under Blue Light. Plant Cell Physiol. 45: 1798-1808

Waters MT, Moylan EC, Langdale JA (2008) GLK Transcription Factors Regulate Chloroplast Development in a Cell-Autonomous Manner. Plant J. 56: 432-444

Waters MT, Wang P, Korkaric M, Capper RG, Saunders NJ, Langdale JA (2009) GLK Transcription Factors Coordinate Expression of the Photosynthetic Apparatus in Arabidopsis. Plant Cell 21: 1109-1128

The Lattice-Like Structure Observed by Vipp1-GFP in Arabidopsis Chloroplasts

Lingang Zhang, [a] Yusuke Kato, [a] Koji Saigo, [a] Ute C Vothknecht, [b] Wataru Sakamoto [a]

[a]Institute of Plant Science and Resources, Okayama University, Kurashiki, Okayama 710-0046, Japan;
[b]Department of Biology I, Ludwig-Maximilians-Universität München, Menzinger Strasse 67, München D-80638, Germany.

Abstract: Vipp1 (vesicle inducing protein in plastids 1) is proposed to play a role in thylakoid biogenesis. It is closely related to PspA (phage shock protein A), a bacterial protein that is induced under stress conditions. Despite its discovery a decade ago and extensive analysis in cyanobacteria, green algae and higher plants, the precise role of Vipp1 in the process of chloroplast development remains unclear. In this research, we expressed Vipp1 C-terminally fused to GFP (Vipp1-GFP) in Arabidopsis and found that Vipp1 is able to assemble into rod-shaped supercomplexes. Vipp1-GFP can rescue heterotrophic growth of a *vipp1* knock-down mutant, suggesting that it complements Vipp1 function. Interestingly, Vipp1-GFP rods always appeared to cross with each other to form a lattice-like structure, which is similar to a scaffold structure formed by PspA in *Escherichia coli*. Based on these results, we infer that Vipp1 is involved in not only thylakoid biogenesis but chloroplast envelope integrity.

Keywords: Vipp1; PspA; Chloroplast; Lattice-like structure; Arabidopsis

Vipp1 (vesicle inducing protein in plastids 1) has been suggested to play a role in thylakoid biogenesis in photosynthetic organisms. Kroll *et al*. (2001) reported that a *vipp1* knock-down mutant (*vipp1-kd*), in which an insertion of T-DNA into the promoter region of *VIPP1* induced reduction of Vipp1 protein to about 20% of wild-type levels. Thylakoid membranes are diminished in *vipp1-kd*. They also proposed that Vipp1 is involved in vesicle trafficking between inner envelopes and thylakoid membranes in chloroplasts. However, evidence supporting this proposition is circumstantial, and the precise function of Vipp1 in vesicle budding, migration and fusion is still unclear. A recent study in cyanobacteria showed that initial detriment induced by *VIPP1* deletion was not the damage of thylakoid formation (Gao and Xu, 2009). They used copper-inducible expression of P*petE-VIPP1* in *Synechocystis* sp. PCC 6803 to promote different levels of Vipp1 *in vivo*. The results indicated that inhibition of photosynthetic activity in these strains was not directly attributable to the loss of thylakoid membranes, but rather to the loss of Vipp1 itself.

Consistent with its function in thylakoid biogenesis, Vipp1 was found to be associated with both thylakoid membranes and envelopes in Arabidopsis (Kroll *et al*., 2001). In *Synechocystis*, Vipp1 was also localized in thylakoid and plasma membranes (Srivastava *et al*., 2005). In contrast, there are two reports demonstrating that Vipp1 was localized only in inner envelope/plasma membrane but not in thylakoid membranes in the same organisms (Aseeva *et al*., 2004; Westphal *et al*., 2001). Inconsistent results of Vipp1 localization might result from different methods used in different experimental conditions. Nevertheless, all of these studies implicate that a large portion of Vipp1 is actually attached to envelopes or plasma membranes.

Vipp1 shares a high degree of sequence similarity with phage shock protein (PspA) from *Escherichia coli*. PspA is rapidly induced in *E. coli* upon stress conditions that perturb the membrane integrity, such as infection by filamentous phage, heat shock, and ethanol treatment (Brissette *et al*., 1990). Under these stress conditions, homo-oligomers of PspA are formed and bind to the inside surface of damaged plasma membranes to engender ‘lattice-like’ scaffolds, which can stabilize damaged membranes (Standar *et al*., 2008). As consequence of PspA expression, proton leakage through plasma membranes can be blocked.

Similarly to PspA, Vipp1 appear to form a large complex. In Arabidopsis, Vipp1 has been shown to form ring-like homo-oligomers of > 1000 kDa (Aseeva *et al*., 2004). In a green alga *Chlamydomonas reinhardtii*, the ring particles of Vipp1 adhered each other to form very long rod-like structure *in vitro* (>1000 kDa) have been observed (Liu *et al*., 2007). In line with the similarity of structure between Vipp1 and PspA, Vipp1 can functionally complement PspA in *E. coli* (DeLisa *et al*, 2004).

Structural and functional similarity between Vipp1 in chloroplasts and PspA in *E. coli* thus prompted us to characterize the possible role of Vipp1 in chloroplast envelopes. To this end, we generated transgenic Arabidopsis plants expressing Vipp1 C-terminally fused to GFP (Vipp1-GFP).

Materials and Methods

Arabidopsis thaliana (ecotype Columbia, Col) was used as wild type. Detail of *vipp1-kd* mutant was described in Kroll *et al*. (2001). Because *vipp1-kd* is semi-lethal, plants were grown on MS agar plates and maintained as heterozygotes. The chimeric construct *VIPP1-GFP* was prepared as described in Aseeva *et al*. (2004) and was under the control of CaMV *35S* promoter. The *VIPP1-GFP* fusion construct was cloned into the plant expression vector pGreen 0029, and was transformed into Col by *Agrobacterium* (GV3101) through the flower-dip method (Clough and Bent, 1998). Transgenic plants that expressed GFP signals were selected and crossed with heterozygous *vipp1-kd* to obtain Vipp1-GFP/*vipp1-kd* plants that expressed Vipp1-GFP and were homozygous for *vipp1-kd* mutation. Surface-sterilized seeds were sown onto 0.7% MS agar plates supplemented with 1.5% (w/v) sucrose. Plants were maintained under light (approximately 60 μmol m^{-2} s^{-1}) with 12/12 light/dark cycles at a constant temperature of 22 ^{o}C.

Total proteins were extracted following the protocol described in Kato *et al*. (2007). The leaflets were frozen in liquid nitrogen and grinded in extraction buffer (125 mmol Tris-HCl pH 6.8, 2% [w/v] SDS, 5% [v/v] glycerol, 5% [v/v] 2-mercaptoethanol, 0.05% [w/v] bromo phenol blue). Protein concentration was determined by Bio-Rad protein assay kit (Bio-Rad) following supplier's instructions. Equal amount of proteins were loaded on each lane and separated by 15% SDS-PAGE, and then transferred to Hybond-ECL nitrocellulose membrane (Amersham Biosciences) for immunoblotting with anti-Vipp1 (Aseeva *et al*., 2004).

Mature leaves from VIPP1-GFP/*vipp1-kd* were used to detect GFP signals with fluorescent microscopy equipped with a Disk Scanning Unit (DSU-BX61, Olympus, Tokyo, Japan) using a GFP filter set (U-MGFPHQ, Olympus), an excitation filter (460–480 nm), a dichroic mirror (DM485) and a barrier filter (495–540 nm).

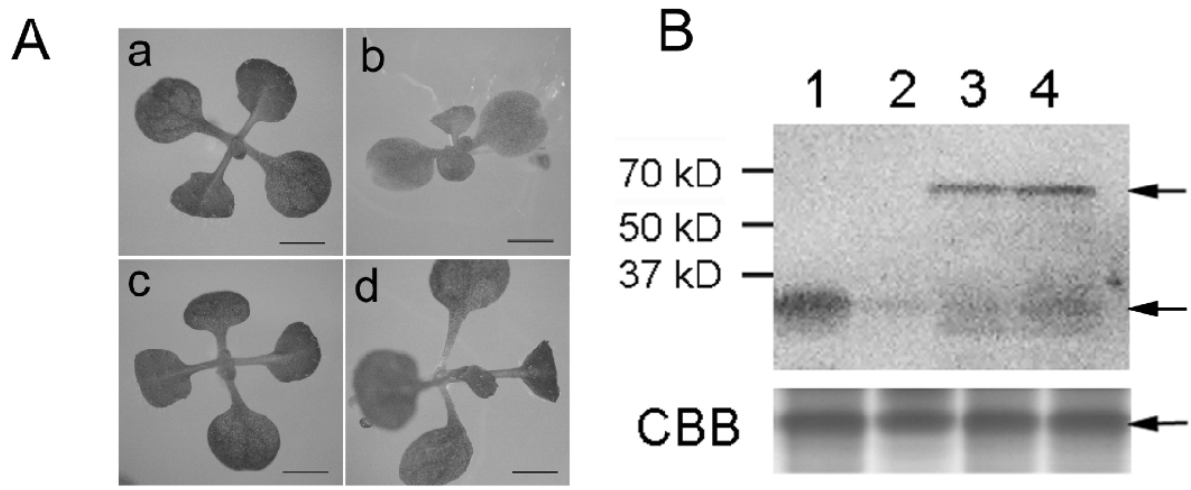

Fig. 1 Complementation of *vipp1-kd* with VIPP1-GFP. A, Representative photographs of 2-week-old Col (a), *vipp1-kd* (b), and two individual VIPP1-GFP/*vipp1-kd* plants (c and d). Bar = 2.5 mm. B, Immunoblot analysis against Vipp1 antibodies: 1, WT; 2, *vipp1-kd*; 3 and 4, two individual VIPP1-GFP/*vipp1-kd* plants. The gel stained with Coomassie blue (lower panel) is shown as a loading control. Arrows indicate Vipp1-GFP (upper), endogenous Vipp1 (middle) and Rubisco large subunit (lower), respectively.

Results and Discussion

In *vipp1-kd*, a T-DNA insertion disrupts the promoter region of At1g65260 (*VIPP1*), which engenders a limited amount of Vipp1 (about 20% of wild type content) and impaired formation of thylakoid membranes (Kroll *et al*., 2001). The mutant plant has lost the capability of photoautotrophic growth and developed a pale-green phenotype at an early developmental stage when grown on MS medium. This phenotype was shown to be rescued by over-expressing Vipp1-GFP (Fig. 1A). Under normal light conditions, the transgenic plant, showing *vipp1-kd/vipp1-kd* genotype and designated as Vipp1-GFP/*vipp1-kd*, looked like wild type and was able to grow photoautotrophically. Thus, we conclude that Vipp1-GFP can substitute for Vipp1 function. To examine accumulation of Vipp1-GFP protein in this transgenic plant, total proteins were subjected to immunoblot analysis. When the blot was probed with Vipp1-speicific antibodies, we detected a band of 60 kDa, which was not present in either Col or *vipp1-kd* (Fig. 1B). This band corresponded to the expected size of Vipp1-GFP fusion protein and indicated that the construct was expressed in Vipp1-GFP/*vipp1-kd*. In addition to this band, the Vipp1 antibody detected endogenous Vipp1 at 33 kDa. As expected, Col has a substantial level of Vipp1, whereas both *vipp1-kd* and Vipp1-GFP/*vipp1-kd* plants had limited amount of endogenous Vipp1 (~20%).

Microscopic observation of GFP signals in Vipp1-GFP/*vipp1-kd* revealed that, similar to the observation of PapA in *E. coli*, Vipp1-GFP was assembled into rod-shaped supercomplexes. We considered that although Vipp1-GFP complemented heterotrophic growth of *vipp1-kd*, Vipp1-GFP accumulation was not remarkably over-expressed and rather appeared to less than that of native Vipp1 in Col (Fig. 1B). Therefore, rod-like structures observed as GFP signals were unlikely to be induced by excessive expression of Vipp1-GFP. The similar macromolecular structure of Vipp1 has also been reported in *Chlamydomonas* cell extracts (Fuhrmann *et al*., 2009), which suggested that the internal α-helical domain of Vipp1 is responsible for its aggregation. In our experiment, the Vipp1-GFP rods appeared to cross with each other to form a lattice-like structure around chloroplasts (Fig. 2B). Given the fact that a majority of Vipp1 was localized at the inner envelope of Arabidopsis chloroplasts, we inferred that the scaffold structure made up with Vipp1 rods is attached to the inner membrane. Further study is currently underway to confirm that Vipp1-GFP is localized in chloroplast envelopes.

In *E. coli*, all individual particles aggregated with PspA showed a distinct ‘clathrin-like’ surface pattern. Subsequently, a large scaffold was formed by these basic units (Standar *et al*., 2008). In this scaffold, globular masses were often linearly aligned with a line spacing of about 6 nm. The structural data support the idea that PspA scaffolds may physically stabilize stressed plasma membranes by multiple interactions over large surface areas. Such large scaffolds could support membrane integrity and

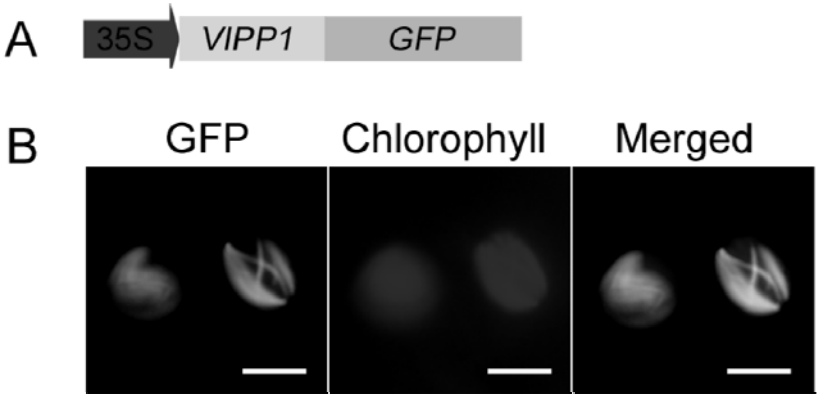

Fig. 2 Microscopic observation of lattice-like structures in Vipp1-GFP/*vipp1-kd* transgenic plants.
A, Schematic representation of the chimeric *VIPP1-GFP* gene introduced into *vipp1-kd* mutant. B, Images of Vipp1-GFP fusion proteins in Vipp1-GFP/*vipp1-kd*. Bar = 5.0 μm.

promote the closure of transient 'holes' or leaks by preventing their extension (Standar *et al*., 2008). By analogy with PspA, it is possible that the scaffold formed with Vipp1 exerts similar function in protecting chloroplast envelope against stresses. Substitution of Vipp1 to PsaA in *E. coli* can be partly explained by our finding here that macromolecular structures of Vipp1 and PspA are similar (DeLisa *et al*., 2004). Increased membrane permeability of oat chloroplasts induced by a herbicide (difenzoquat) has been implicated to induce fusion of grana thylakoids (Thai *et al*., 1989). Collectively, our data suggest that Vipp1 deletion in *vipp1-kd* affects thylakoid membrane biogenesis indirectly, and that Vipp1 plays a role in protecting chloroplast envelopes as scaffolds. Given the photoautotrophic growth of Vipp1-GFP/*vipp1-kd*, we consider that this transgenic plant is useful to study the possible role of Vipp1 in chloroplast envelopes in higher plants.

References

Aseeva E, Ossenbühl F, Eichacker LA, Wanner G, Soll J, Vothknecht UC (2004) Complex Formation of Vipp1 Depends on Its α-Helical PspA-Like Domain. J. Biol. Chem. 279: 35535-35541

Brissette JL, Russel M, Weiner L, Model P (1990) Phage Shock Protein, a Stress Protein of Escherichia Coli. Proc. Natl. Acad. Sci. USA 87: 862-866

Clough SJ, Bent AF (1998) Floral Dip: a Simplified Method for Agrobacterium-Mediated Transformation of Arabidopsis Thaliana. Plant J. 16: 735-743

DeLisa MP, Lee P, Palmer T, Georgiou G (2004) Phage Shock Protein PspA of Escherichia Coli Relieves Saturation of Protein Export Via the Tat Pathway. J. Bacteriol. 186: 366-373

Fuhrmann E, Bultema JB, Kahmann U, Rupprecht E, Boekema EJ, Schneider D (2009) The Vesicle-Inducing Protein 1 from Synechocystis sp. PCC 6803 Organizes into Diverse Higher-Ordered Ring Structures. Mol. Biol. Cell. 20: 4620-4628

Gao H, Xu XD (2009) Depletion of Vipp1 in Synechocystis sp. PCC 6803 Affects Photosynthetic Activity before the Loss of Thylakoid Membranes. FEMS Microbiol. Lett. 292: 63-70

Kato Y, Miura E, Matsushima R, Sakamoto W (2007) White Leaf Sectors in Yellow Variegated2 Are Formed by Viable Cells with Undifferentiated Plastids. Plant Physiol. 144: 952-960

Kroll D, Meierhoff K, Bechtold N, Kinoshita M, Westphal S, Vothknecht UC, Soll J, Westhoff P (2001) VIPP1, a Nuclear Gene of Arabidopsis Thaliana Essential for Thylakoid Membrane Formation. Proc. Natl. Acad. Sci. USA 98: 4238- 4242

Liu C, Willmund F, Golecki JR, Cacace S, Hess B, Markert C, Schroda M (2007) The Chloroplast HSP70B-CDJ2-CGE1 Chaperones Catalyse Assembly and Disassembly of VIPP1 Oligomers in Chlamydomonas. Plant J. 50: 265-277

Srivastava R, Pisareva T, Norling B (2005) Proteomic Studies of the Thylakoid Membrane of Synechocystis sp. PCC 6803. Proteomics 5: 4905-4916

Standar K, Mehner D, Osadnik H, Berthelmann F, Hause G, Lünsdorf H, Brüser T (2008) PspA Can Form Large Scaffolds in Escherichia Coli. FEBS Lett. 582: 3585-3589

Thai KM, Sakti J, Fowke LC (1989) Cell Membrane Permeability and Ultrastructural Effects of Difenzoquat on Wild Oats. Weed Sci. 37: 98-106

Westphal S, Heins L, Soll J, Vothknecht UC (2001) Vipp1 Deletion Mutant of Synechocystis: a Connection between Bacterial Phage Shock and Thylakoid Biogenesis? Proc. Natl. Acad. Sci. USA 98: 4243-4248

State Transition Mechanism in *Arabidopsis Thaliana*: Biophysical and Proteomic Studies

Sreedhar Nellaepalli[a], Ottó Zsiros[c], László Kovács[c],Yadavalli Venkateswarlu, Mekala Nageswara Rao[a], Prasanna Mohanty[b,d], Rajagopal Subramanyam[a,b*]

[a]Department of Biochemistry, [b]Department of Plant Sciences, School of Life Sciences, University of Hyderabad, Hyderabad, 500046 India;
[c]Institute of Plant Biology, Biological Research Center, Hungarian Academy of Sciences, Szeged, Hungary;
[d]College of Agriculture, Orissa University of Agriculture and Technology (OUAT), Bhubaneswar, India.
[*]Corresponding author. Tel. No. +91-40-2313 4572; Fax No. +91-40-2301 0120; E-mail: srgsl@uohyd.ernet.in.

Abstract: The redox state of plastoquinone (PQ) pool is the incipient signal in the signal transduction pathway of state transition mechanism, shifting from state I to state II and *vice versa*. The redox state of the Q_A, the primary acceptor of photosystem II (PSII) and the PQ pool are easily monitored by the OJIP fast fluorescence transients. The OJIP fast Chl *a* fluorescence transient studies revealed that in state II, there was reduction in maximal fluorescence which could be due to decreased antennae size of PSII. The same changes were not observed in *Stn7* mutant lacking thylakoid kinase which phosphorylates light harvesting complex (LHC) II. The phosphorylated LHCII is associated with PSI under state II condition. The redox state of PQ pool is signal for the kinase to phosphorylate/dephosphorylate major LHCII of PSII. The 2-D electrophoresis results showed that LHCII is resolved into 3 spots in state I. However, in state II this has been resolved into 4 spots. However, *Stn7* mutant there was no change of 2D spots in state II. The additional spot is yet to be investigated.

Keywords: 2D electrophoresis; *Arabidopsis thaliana*; Chl *a* fluorescence; Photosystems; State transition

Introduction

In oxygenic photosynthetic organisms the light conversion into chemical energy, involving photo oxidation of water and reduction of CO_2 to carbohydrates is mediated by two interactive photochemical reactions namely photosystem I (PSI) and photosystem II (PSII) (Blankenship, 2008). The two photosystems absorb solar radiation differentially resulting in unbalanced energy which requires a mechanism by which the energy can be balanced for optimal photosynthesis. This mechanism is known as state transition (Allen and Mullineaux, 2009).

The preferential excitation of PSII makes PQ pool more reduced. The reduced PQ pool tends to associate with cytochrome b6/f and activates thylakoid kinase (stn7/stt7 kinase) that mediates phosphorylation of light harvesting complex II (LHCII) (Gal *et al*., 1990). The phosphorylated LHCII migrates from PSII to PSI thereby increasing absorption cross-section of PSI, distributing the energy to PSI leading to state II (Murata, 1969; Bonaventura and Myers, 1969). When PSI gets preferentially excited, the reduced PQ pool starts oxidizing and if it reaches below the saturation level of oxidation of PQ pool, it in turn activates an enzyme called thylakoid phosphatase (TAP38) which dephosphorylates the phosphorylated LHCII (Pribil *et al*., 2010). The dephosphorylated LHCII undocks from PSI and reassociates with PSII, enhancing absorption cross-section of PSII, thereby leading to state I. The transition from state I to state II and state II to state I is termed as state transition. State transition occurs in natural environments, where light quality and quantity fluctuate with the time (Iwai *et al*., 2008).

In our study, we have induced state transitions by using red and far red filters for the expression of state II and state I, respectively in wt and mutant (*stn7*) plants of *Arabidopsis thaliana.* Full expression of state transitions has been confirmed by using PAM

and 77 K fluorescence emission spectroscopy (data not shown) and phosphoproteins were studies by 2D gel electrophoresis and western blotting.

Materials and methods

A. thaliana and its mutant *stn7* were grown in controlled environment chambers at 100–120 μmol $m^{-2} s^{-1}$, with 8 h light/16 h dark periods. Plants were pre-illuminated with either state I or state II light by using far red light filters or red filters respectively for 45 min, to achieve state shifts efficiently. Light intensity was adjusted to 35 μmol $m^{-2} s^{-1}$. OJIP measurements were carried out by using Handy PEA (Hansatech instrument Ltd). Leaves were dark adapted for at least 30 sec before measurements of fluorescence transients. Thylakoid membranes were isolated according to Subramanyam *et al*. (2006). Chlorophyll concentrations were determined spectroscopically after extraction with absolute methanol (Porra *et al*., 1998).

SDS-PAGE was carried out by using Tricine system described. Proteins were separated on 15% resolving gel (Subramanyam, 2006). Proteins were transferred on to polyvinyldenedifluoride (PVDF) membrane. Blots were probed with Rabbit Anti-phosphothreonine polyclonal antibodies (1/2500 dilution) from Cell Signaling Technologies to detect phosphorylated proteins at threonine site. To identify LHCII proteins, blots were probed with Anti Lhcb2 polyclonal antibodies (1/3000 dilutions) from Agrisera Pvt ltd. For 2D electrophoresis, thylakoid membranes were solubilized and isoelectric focusing and 2D gels were done according to Yadavalli *et al*. (2011).

Results and discussion

The growth of *Arabidopsis thaliana* wt and *stn7* mutant does not have significant morphological differences; however, *stn7* plant grows quite slowly compared to wt plants (Fig. 1).

Fig. 1 week old Arabidopsis and its mutant *stn7*.

The light required to reduce PQ pool is higher for state II than state I light condition because of differences in light absorption. Thus the fluorescence transient of state II is lower than state I (Fig. 2), because under state II, LHCII is associated with PSI. In *stn7* mutant no such changes were observed.

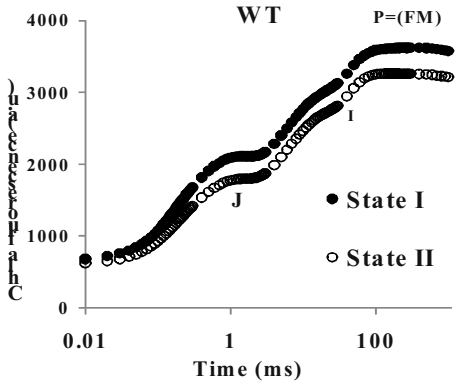

Fig. 2 Chl *a* fluorescence transients of state I and state II of *A. thaliana* leaves.

Isolated thylakoids from preilluminated plants with either state I or state II have shown signals for phospho thylakoid proteins when blotted with antiphospho threonine antibody (from Cell Signaling Technology, U.K.). We have observed three major signals which might correspond to phospho proteins of thylakoid membranes (Fig. 3) which corresponding to CP43, D1/D2 and LHCII. Similar pattern were observed when plants were preilluminated with low intensity light (30 μm m^{-2} s^{-1}) for different time periods (Tikkanen *et al*., 2010). In our study, LHCII underwent phosphorylation under state II and not in state I. However, CP43 and D2 proteins were phosphorylated under both state I and state II, however, strong signal phosphorylation were observed in state II conditions. At the same time *stn7* plants exposed to either state I light or state II light, did not show any signal for phosphorylated LHCII, but showed signals for CP43 and D2 proteins. Later the blots were also probed with Lhcb2 antibody, it was exactly matching with the lowest band which previously recognized as P-LHCII. The phosphorylation status of Lhcb1 and Lhcb3 is yet to be elucidated in our study. Based on these studies it is clear that Lhcb2 were one of the major antennae proteins which undergo phosphorylation under state transitions. Similar observation was noticed in the plants exposed to white light conditions (30 μm m^{-2} s^{-1}). It is clear that the mechanism of state transition is a natural

phenomenon generally which occurs at low light intensities.

2D electrophoresis has revealed changes in the thyalkoid proteins under state I and state II light exposed conditions. Thylakoids isolated from wt and *stn7* mutant plants preilluminated with either state I or state II light condition, have shown very similar pattern of 2D spots. However, in the range of 25–27 kDa, we have observed three major spots in state I preilliminated wt plants, where as in state II exposed condition, an additional spot was resolved as fourth spot. In *stn7* plants this was not observed. 2D gels were probed with antiphospho threonine antibody where 27 KDa protein spots were phosphorylated, however, this observation was seen in state I. We presume that the 4 spots in state II may correspond to major P-LHCII which tend to migrate to PSI and this P-LHCII distribute the energy between photosystems. The differential expression of P-LHCII antennae (resoled in to four spots) under state II exposed light conditions are yet to be studied.The redox status of PQ pool was analyzed by fast Chl *a* fluorescence transients. Plants adapted to state II light conditions have shown relatively less fluorescence in OJIP fluorescence transients. We have noticed that major LHCII is getting phosphorylated in state II and it is presumed that P-LHCII is migrating to PSI. Also observed four distinct 2D spots of LHCII in 2D electrophoresis in state II adapted light condition.

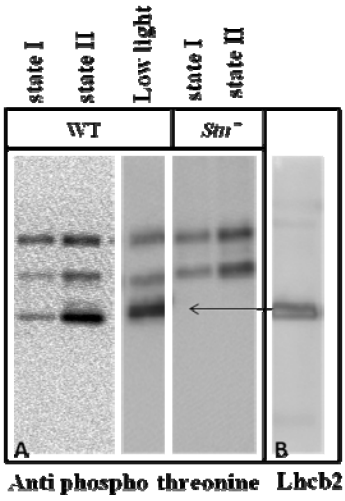

Fig. 3 Western blot analysis of thylakoid proteins under state I, state II and low white light conditions in wt and *stn7* mutant plants.

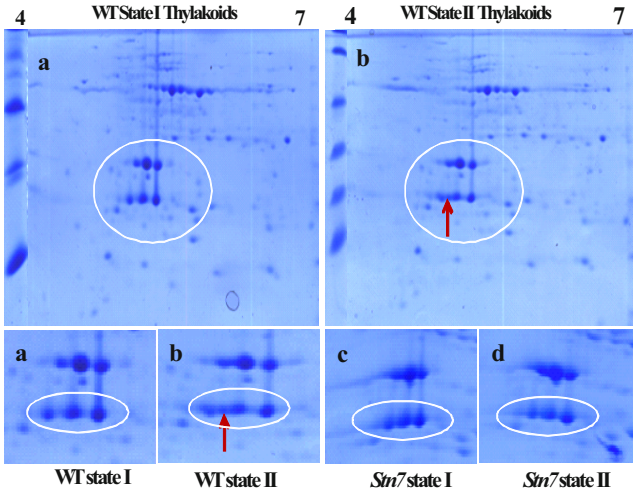

Fig. 4 2D gels (PI of 4–7) of thylakoid membrane proteins isolated from state I and state II preilluminated plants of wt and mutant *stn7*. a. wt thylakoid proteins preillumated with state I light; b. wt thylakoid proteins preilluminated with state II light; a' and b' are zoomed LHCII and its isoforms obtained from Figs. 4a and 4b; c and d are the zoomed areas of *stn7* mutant thylakoid proteins (Original 2D gels of *stn7* thylakoid membrane proteins were not shown).

Acknowledgments

RS thank DST (SR/SO/BB-34/2006, SR/FT/L-89/2006), DST Indo-Hungarian project (DST/INT/HVW/P-08/06) for financial support. SN thanks CSIR-UGC for JRF and SRF. We also thank Prof. A S Raghavendra, Dept. of Plant Sciences, UOH for providing plant growth chamber. SN thank G Mahesh and K Sireesha for comments and suggestions.

References

Allen JF, Mullineaux C (eds) (2009) State Transitions. Photosynthesis Research 99: 155-255

Blankenship RE (2008) Molecular Mechanisms of Photosynthesis (2nd ed.). John Wiley & Sons Inc

Bonaventura C, Myers J (1969) Fluorescence and Oxygen Evolution from Chlorella Pyrenoidosa. Biochim Biophys Acta 189 (3): 366-383

Gal A, Hauska G, Herrmann R, Ohad I (1990) Interaction between Light Harvesting Chlorophyll-a/b Protein (LHCII) Kinase and Cytochrome be/f Complex; In Vitro Control of Kinase Activity. J Biol Chem 265, 32: 19742-19749

Iwai M, Yuichiro T, Jun M (2008) Molecular

Remodeling of Photosystem II during State Transitions in Chlamydomonas Reinhardtii. The Plant Cell 20: 2177-2189

Murata N (1969b) Control of Excitation Transfer in Photosynthesis. I. Light-Induced Change of Chlorophyll a Fluorescence in Porphyridium Cruentum. Biochim Biophys Acta 172(2): 242

Porra RJ, Thompson WA, Kriedemann PE (1989) Determination of Accurate Extinction Coefficients and Simultaneous Equations for Assaying Chlorophylls a and b Extracted with Four Different Solvents: Verification of the Concentration of Chlorophyll Standards by Atomic Absorption Spectroscopy. Biochim Biophys Acta 975: 384-394

Pribil M, Pesaresi P, Hertle A, Barbato R, D Leister (2010) Role of Plastid Protein Phosphatase TAP38 in LHCII Dephosphorylation and Thylakoid Electron Flow. PLoS Biology 8(1): e1000288

Subramanyam R, Jolley C, Brune DC, Fromme P, Webber AN (2006) Characterization of a Novel Photosystem I–LHCI Supercomplex Isolated from Chlamydomonas Reinhardtii under Anaerobic (State II) Conditions. FEBS Lett 580: 233-238

Yadavalli V, Sreedhar N, Subramanyam R (2011) Proteomic Analysis of Thylakoid Membranes. Methods Mol Biol. 684: 159-170

Tikkanen M, Michele G, S Kangasjarvi, Aro EV (2010) Thylakoid Protein Phosphorylation in Higher Plant Chloroplasts Optimizes Electron Transfer under Fluctuating Light. Plant Physiol 2010 152: 723-735

Symposium 15

Assembly of Photosynthetic Protein Complexes

On the Localization of the Synthesis of Photosynthetic Proteins

James Uniacke, Oussama Rifai, Matthew Peters, Marco Schottkowski, William Zerges*

Biology Department, Concordia University, Montreal, Quebec, Canada.
*Corresponding author. Tel. No. +1 514 848 2424 ext 3416; Fax No. +1 514 848 2881; E-mail: Zerges@alcor.concordia.ca.

Abstract: Thylakoid membrane biogenesis requires polypeptides subunits of the photosynthesis complexes, their cofactors and pigments, and the galactolipids of the membrane bilayer. Although the pathways that synthesize and assemble these components are known or being elucidated, much less is known about the cytological organization of these pathways. Results of fluorescence confocal microscopy support the existence of a novel chloroplast compartment that is specialized in photosystem II biogenesis and possibly the synthesis of other components of thylakoid membranes. We are substantiating these findings with results of cellular subfractionation experiments, which reveal a that a minor class of chloroplast membranes has markers of a thylakoid biogenesis compartment and are distinct from the membranes of thylakoids or the chloroplast envelope (unpublished data). The characterization of these "thylakoid biogenesis membranes" could help reconcile the contradictions in the available evidence regarding where thylakoid membrane components are synthesized and how they are transported. For example, not much is known about how the thylakoid proteins encoded by the chloroplast genome are targeted for thylakoid membrane biogenesis. Our results reveal that mRNA-based localization of protein synthesis localizes PS II subunits and may be a prevalent targeting mechanism in chloroplasts.

Keywords: Thylakoid; Ribosome; Fluorescence in situ hybridization; Spinach; *Chlamydomonas*

Introduction

This presentation reviews where and how protein synthesis is localized for the biogensis of the photosynthesis machinery in thylakoid membranes. Many intracellular compartments and developmental patterns are established, in part, by the localized synthesis of proteins that function therein (reviewed by (St Johnston, 2005). The traditional and long-standing model is that the thylakoid membrane proteins that are encoded by chloroplast mRNAs are co-translationally inserted into thylakoid membranes. This is based on the following evidence. Chloroplast polyribosomes translating these mRNAs co-fractionated with thylakoid membranes on sucrose density gradients (Chua, Blobel *et al*., 1973; Margulies and Michaels 1974; Margulies, Tiffany *et al*., 1975; Chua, Blobel *et al*., 1976; Margulies and Weistrop 1980; Yamamoto, Burke *et al*., 1981; Margulies, 1983; Herrin and Michaels, 1985; Margulies, Tiffany *et al*., 1987; Breidenbach, Jenni *et al*., 1988; Klein, Mason *et al*., 1988; Muhlbauer and Eichacker 1999; Zhang, Paakkarinen *et al*., 1999). At least one chloroplast mRNA encoding a non-membrane protein, the *rbcL* mRNA, also is translated by thylakoid membrane-bound polyribosomes in Chlamydomonas, barley and spinach (Hattori and Margulies, 1986; Breidenbach, Jenni *et al*., 1988; Muhlbauer and Eichacker, 1999). This may reflect the localization of translational regulators to thylakoid membranes where so that they can respond to the electrochemical proton gradient (Muhlbauer and Eichacker, 1999). At least 50% of these polysomes are tethered to the membrane by a nascent polypeptide because this fraction could only be released by the dissociation of ribosomes with puromycin, which induces premature ribosome dissociation (Chua, Blobel *et al*., 1973; Margulies and Michaels, 1974). The other ribosomes (possibly those translating the *rbcL* mRNA) were bound by electrostatic interactions

because they could be dissociated by high ionic strength (0.5 mol KCl) washing step. The latter associations may be physiologically relevant (and not due to non-specific associations formed *in vitro*) because they could not be re-established when the ionic strength was restored (Chua, Blobel *et al*., 1973; Margulies and Michaels, 1974).

Translation of the chloroplast mRNAs that encode the major PS II core subunits (*e.g.* of *psbA*, *psbB*, *psbC*, *psbD*, *psbE*) may be colocalized with PS II assembly because only 2–5 minutes are required for the synthesis and assembly of these subunits into reaction center cores (Ossenbuhl, Gohre *et al*., 2004; Rokka, Suorsa *et al*., 2005). Translation is believed to occur at the end membranes of grana or membranes defining the highly elongated vesicles of stroma thylakoids. Chloroplast ribosomes and polyribomes were observed on, or near, them in EM images of cells (Bourque, Boynton *et al*., 1971) and isolated thylakoid membranes (Margulies and Michaels 1974; Chua, Blobel *et al*., 1976). Also, chloroplast sub-fractions with stroma thylakoid membranes were enriched over grana membranes in the precursor of the D1 subunit, which is converted to mature D1 by C-terminal proteolytic processing very soon after its synthesis (Adir, Shochat *et al*., 1990). Finally chlorophyll fluorescence from the earliest assembled PSII complexes in greening *y-1* cells (see below) indicated that these complexes are juxtaposed with newly synthesized PSI complexes, *e.g.* in non-appressed membranes, before PSI and PSII segregate to non-appressed and appressed thylakoid membranes, respectively (Hoober, White *et al*., 1994; White and Hoober, 1994).

Materials and Methods; The methods have been reported previously (Uniacke and Zerges, 2007; Uniacke and Zerges, 2009).

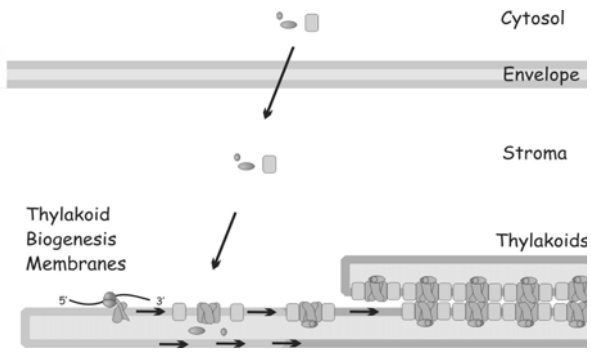

Fig. 1 Our data support a model in which photosystem II subunit synthesis and assembly occurs in specialized membranes.

Results

However, this traditional model is being challenged by evidence for a specialized compartment for the synthesis and assembly of photosystem II subunits. Some results suggest that the inner membrane of the chloroplast envelope, or another type of membrane that resembles it, has a direct role in the synthesis of chloroplast proteins (reviewed by (Hoober, White *et al*., 1994; Sato, Rolland *et al*., 1999; Zerges, 2000). Chloroplast membranes resembling the inner envelope membrane in buoyant density and chlorophyll level have been proposed to have a role in protein synthesis because they are associated with RNA-binding proteins, including RB47 (Zerges and Rochaix, 1998; Zerges, Wang *et al*., 2002) and a splicing factor (Perron, Goldschmidt-Clermont *et al*., 1999) or c.a. 50% of chloroplast ribosomes (Margulies and Weistrop, 1980). Alternatively, the association of these membranes with thylakoid membranes suggests they may be part of an unknown intra-chloroplast compartment. However, evidence presented here and published previously argues against the envelope as the site of thylakoid biogenesis.

To address this question we characterized the locations of the components in PSII subunit synthesis in the chloroplast of *C. reinhardtii* with fluorescence *in situ* hybridization (FISH), immunofluorescence (IF) staining, and confocal microscopy (Uniacke and Zerges, 2007; Uniacke and Zerges, 2009). This eukaryotic green alga is widely used as a model system for studies of chloroplast biogenesis (Rochaix *et al*., 1998). While exploring the aforementioned problems, we found that *C. reinhardtii* is ideally suited for characterizations of the distributions of specific chloroplast mRNAs and proteins by these techniques because its single chloroplast has a definite anatomy that is easily recognizable in every cell examined. Our results provide the first *in situ* evidence for the current model that D1 synthesis for PSII repair occurs in stroma thylakoid membranes throughout the chloroplast (Uniacke and Zerges, 2007; Uniacke and Zerges, 2009; Adir *et al*., 1990). They also contribute to the emergent realization that the processes underlying chloroplast biogenesis are highly compartmentalized by providing three lines of evidence showing that PSII subunit synthesis and assembly occur in a specific region of the chloroplast. First, during the rapid induction of PSII assembly, we

observed in punctate regions lateral to the pyrenoid, termed T-zones, the colocalization of multiple components of PSII subunit synthesis; the *psbC* and *psbA* mRNAs, chloroplast r-proteins, and RB38. Weaker colocalized signals from these mRNAs and translation proteins were localized with stroma and thylakoids around the pyrenoid, specifically in ML5' cells. The T-zones were typically within this region. Second, in the *psbC* translation-deficient mutant *FUD34*, ongoing *psbA* translation for attempted PSII assembly correlated with the translation-dependent localization of the *psbA* mRNA around the pyrenoid. Third, in two PSII assembly mutants, unassembled D1 and a partially assembled PSII subcomplex accumulate around the pyrenoid where we propose they mark a compartment of PSII subunit assembly (Uniacke and Zerges, 2007; Uniacke and Zerges, 2009). In work that is in progress and not reported here, we have recently fractionated chloroplasts of Chlamydomonas and spinach and identified membrane fractions with the properties expected of a thylakoid biogenesis compartment (Zerges, unpublished data). Additional work is required to characterize these membranes to determine whether or not they are involved in thylakoid membrane biogenesis.

Acknowledgements

We thank Prof. Francis-Andre Wollman for this invitation and Prof. Zhang and the other members of the committee for organizing this outstanding conference.

References

Adir N, S Shochat, *et al*. (1990) "Light-Dependent D1 Protein Synthesis and Translocation Is Regulated by Reaction Center II. Reaction Center II Serves as an Acceptor for the D1 Precursor." J Biol Chem 265(21): 12563-12568

Bourque DP, JE Boynton, *et al*. (1971) "Studies on the Structure and Cellular Location of Various Ribosome and Ribosomal RNA Species in the Green Alga Chlamydomonas Reinhardi." J Cell Sci 8(1): 153-183

Breidenbach E, E Jenni, *et al*. (1988) "Synthesis of Two Proteins in Chloroplasts and mRNA Distribution between Thylakoids and Stroma during the Cell Cycle of Chlamydomonas Reinhardii." Eur J Biochem 177(1): 225-232

Chua NH, G Blobel, *et al*. (1976) "Periodic Variations in the Ratio of Free to Thylakoid-Bound Chloroplast Ribosomes during the Cell Cycle of Chlamydomonas Reinhardtii." J Cell Biol 71(2): 497-514

Chua NH, G Blobel, *et al*. (1973) "Attachment of Chloroplast Polysomes to Thylakoid Membranes in Chlamydomonas Reinhardtii." PNAS 70(5): 1554-1558

Hattori T, MM Margulies (1986) "Synthesis of Large Subunit of Ribulosebisphosphate Carboxylase by Thylakoid-Bound Polyribosomes from Spinach Chloroplasts." Arch Biochem Biophys 244(2): 630-640

Herrin D, A Michaels (1985) "The Chloroplast 32 kDa Protein Is Synthesized on Thylakoid-Bound Ribosomes in Chlamydomonas Reinhardtii." FEBS Letters 184(1): 90-95

Hoober JK, R White, *et al*. (1994) "Biogenesis of Thylakoid Membranes with Emphasis on the Process in Chlamydomonas." Photosynthesis Research 39(1): 15-31

Klein RR, HS Mason, *et al*. (1988) "Light-Regulated Translation of Chloroplast Proteins. I. Transcripts of psaA-psaB, psbA, and rbcL Are Associated with Polysomes in Dark-Grown and Illuminated Barley Seedlings." J Cell Biol 106(2): 289-301

Margulies MM (1983) "Synthesis of Photosynthetic Membrane Proteins Directed by RNA from Rough Thylakoids of Chlamydomonas Reinhardtii." Eur J Biochem 137(1-2): 241-8

Margulies MM, A Michaels (1974) "Ribosomes Bound to Chloroplast Membranes in Chlamydomonas Reinhardtii." J Cell Biol 60(1): 65-77

Margulies MM, HL Tiffany, *et al.* (1987) "Photosystem I Reaction Center Polypeptides of Spinach Are Synthesized on Thylakoid-Bound Ribosomes." Arch Biochem Biophys 254(2): 454-461

Margulies MM, HL Tiffany, *et al*. (1975) "Vectorial Discharge of Nascent Polypeptides Attached to Chloroplast Thylakoid Membranes." Biochem Biophys Res Commun 64(2): 735-739

Margulies MM, JS Weistrop (1980) "Sub-Thylakoid Fractions Containing Ribosomes." Biochim Biophys Acta 606(1): 20-33

Muhlbauer SK, LA Eichacker (1999) "The Stromal Protein Large Subunit of Ribulose-1,5-Bisphosphate Carboxylase Is Translated by Membrane-Bound Ribosomes." Eur J Biochem 261(3): 784-788

Ossenbuhl F, V Gohre, *et al.* (2004) "Efficient Assembly of Photosystem II in Chlamydomonas Reinhardtii Requires Alb3.1p, a Homolog of Arabidopsis ALBINO3." Plant Cell 16(7): 1790-1800

Perron K, M Goldschmidt-Clermont, *et al.* (1999) "A Factor Related to Pseudouridine Synthases Is Required for Chloroplast Group II Intron Trans-Splicing in Chlamydomonas Reinhardtii." Embo J 18(22): 6481-6490

Rokka A, M Suorsa, *et al*. (2005) "Synthesis and Assembly of Thylakoid Protein Complexes: Multiple Assembly Steps of Photosystem II." Biochem J 388(Pt 1): 159-168

Sato N, N Rolland, *et al.* (1999). "Do Plastid Envelope Membranes Play a Role in the Expression of the Plastid Genome?" Biochimie 81(6): 619-629

St Johnston D (2005) "Moving Messages: the Intracellular Localization of mRNAs." Nat Rev Mol Cell Biol 6(5): 363-375

Uniacke J, W Zerges (2007) "Photosystem II Assembly and Repair Are Differentially Localized in Chlamydomonas." Plant Cell 19(11): 3640-3654

Uniacke J, W Zerges (2009) "Chloroplast Protein Targeting Involves Localized Translation in Chlamydomonas." Proc Natl Acad Sci USA 106(5): 1439-1444

White RA, JK Hoober (1994) "Biogenesis of Thylakoid Membranes in Chlamydomonas Reinhardtii y1 (A Kinetic Study of Initial Greening)." Plant Physiol 106(2): 583-590

Yamamoto T, J Burke, *et al*. (1981) "Bound Ribosomes of Pea Chloroplast Thylakoid Membranes: Location and Release in Vitro by High Salt, Puromycin, and RNase" Plant Physiol. 67(5): 940-949

Zerges W (2000) "Translation in Chloroplasts." Biochimie 82(6-7): 583-601

Zerges W, JD Rochaix (1998) "Low Density Membranes Are Associated with RNA-Binding Proteins and Thylakoids in the Chloroplast of Chlamydomonas Reinhardtii." J Cell Biol 140(1): 101-110

Zerges W, S Wang, *et al*. (2002) "Light Activates Binding of Membrane Proteins Tochloroplast RNAs in Chlamydomonas Reinhardtii." Plant Mol Biol 50: 573-585

Zhang L, V Paakkarinen, *et al.* (1999) "Co-Translational Assembly of the D1 Protein into Photosystem II." J Biol Chem 274(23): 16062-16067

Function of *sll1906*, a Member of the Bacteriochlorophyll Delivery Family, in the Cyanobacterium *Synechocystis* sp. PCC 6803

Cheng-I Daniel Yao, Wim Vermaas*

From the School of Life Sciences and Center for Bioenergy and Photosynthesis, Arizona State University, Tempe, AZ 85287-4501. Corresponding author. Tel. No. +1 480 965 6250; E-mail: wim@asu.edu.

Abstract: A deletion mutation was introduced into the *sll1906* gene in the cyanobacterium *Synechocystis* sp. PCC 6803 to examine the function of Sll1906, a member of the putative "bacteriochlorophyll delivery" protein family. The Sll1906 sequence contains possible chlorophyll-binding sites. The pigment profile indicated that the chlorophyll and carotenoids contents were not altered in the mutant, and no chlorophyll precursors accumulated. According to the oxygen evolution and 77 K fluorescence emission spectra, the PSII activity and PSII/PSI ratio remained the same upon deletion of the gene. The *sll1906* deletion was also introduced into the *chlL*$^-$ background mutant strain, in which chlorophyll is synthesized in the light only. When grown in light-activated heterotrophic growth (LAHG) conditions, the rate of chlorophyll degradation in the *chlL*$^-$/*sll1906*$^-$ mutant was similar to that in the *chlL*$^-$ background strain. When cells were returned to continuous illumination after a week of growth under LAHG conditions, both the rate of chlorophyll synthesis and chlorophyll-dependent photosystem biogenesis were monitored. The deletion of the *sll1906* gene affected neither. Although the *sll1906* deletion did not affect chlorophyll degradation/biosynthesis and photosystem assembly, Sll1906 could still be involved in these processes as other pathways may compensate for the absence of Sll1906.

Keywords: *Synechocystis*; PucC; *sll1906*; Chlorophyll

Introduction

Chlorophyll is a key pigment in the process of photosynthesis and chlorophyll *a* is present in all oxygenic phototrophs. However, in the light chlorophyll may give rise to harmful reactive oxygen species if chlorophyll excitation would not be quenched efficiently. Therefore, the concentration of free chlorophyll (not bound to proteins and not close to carotenoids) is minimized in the cell. This is achieved by highly regulating chlorophyll synthesis in conjunction with synthesis of photosynthetic proteins. However, even though chlorophyll biosynthesis has been well studied, it is unknown how, for example, chlorophyll delivery from chlorophyll synthase to chlorophyll-binding proteins occurs. The existence of chlorophyll transfer proteins in oxygenic phototrophs may be expected but has not been demonstrated. However, members of a putative bacteriochlorophyll delivery (BCD) family have been identified in purple bacteria (Saier *et al.*, 1999). The BCD proteins have 12 putative transmembrane segments and exhibit similar topological features. The topology of the PucC protein with 12 membrane-spanning segments has been examined in *Rhodobacter capsulatus*; both the N and C termini of the protein are located in the cytoplasm (LeBlanc and Beatty, 1996). The function of PucC is thought to be a shepherding activity that allows the light-harvesting complex (LH) 1 and 2 to assemble properly; the N terminus of the protein is important for its function (Jaschke *et al.*, 2008; LeBlanc and Beatty, 1996). In the cyanobacterium *Synechocystis* sp. PCC 6803, a PucC homolog is found. This homolog, Sll1906, is also a member of the BCD family. In this work, the *sll1906*$^-$ mutant was created and analyzed in terms of chlorophyll transfer potential.

Materials and Methods

Growth conditions

Synechocystis sp. PCC 6803 wild type and mutant strains were grown photoautotrophically with air bubbling at 30 °C in BG-11 medium at a light intensity of 40 μmol photons m^{-2} s^{-1}. When the strains were grown in liquid culture under light-activated heterotrophic growth (LAHG) conditions, cells were kept in complete darkness except for one 15 min light period (white light at 20 μmol photons m^{-2} s^{-1}) every 24 h, and the cultures were supplemented with 5 mmol glucose. Cell growth was monitored by measuring the optical density at 730 nm in a 1 cm cuvette using a Shimadzu UV-160 spectrophotometer.

Construction of mutants and transformation of Synechocystis sp. PCC 6803

Synechocystis sp. PCC 6803 *sll1906*$^-$ mutants were generated by transformation of *Synechocystis* cells with a plasmid containing the *sll1906* gene with the section from 25 bp (*Bam*HI) downstream of the start codon to 306 bp (*Bcl*I) upstream of the stop codon replaced by a kanamycin (Km) resistance cassette from pUC4K. Transformants were selected by screening for kanamycin resistance and subcultured at increasing concentrations of antibiotics to allow segregation of wild-type and mutant genome copies to occur, thus leading to homozygous strains. Segregation was confirmed by PCR using *Synechocystis* sp. PCC 6803 DNA from transformants as a template and one forward primer (CTTACAACAGGCCCTACAAG) and two reverse primers: one is CATCGGATACGTC CACCAAG that hybridizes to the *sll1906* gene, and the other is CATGAGTGACGACTGAATCC that is used to check insertion of the Km^r gene. Construction of the *chlL*$^-$ mutant was described earlier (Wu and Vermaas, 1995).

Pigments analysis

Pigments were extracted from *Synechocystis* cells with 100% methanol with 0.1% NH_4OH. Chlorophyll content of the cells was measured by a Shimadzu UV-160 spectrophotometer. Total pigment content was analyzed by HPLC using a Waters Spherisorb S10ODS2 (250 mm × 10 mm) Semi-Prep column. The column was eluted with H_2O, methanol, and acetone at a flow rate of 2.0 mL/min using the following gradient program: 0 to 1 min, 90% of methanol in water; 1 to 6 min, 90% to 100% of methanol in water; 6 to 10 min, 0 to 25% of acetone in methanol; 10–12 min, 25% to 60% of acetone in methanol; 12 to 21 min, 60% to 100% of acetone in methanol; and 21 to 25 min, 100% acetone.

Oxygen evolution

Oxygen evolution measurements were performed at 30 °C using a Clark-type electrode (Hansatech, Cambridge, U.K.). Intact cells were used, and 2.0 mmol $K_3Fe(CN)_6$ and 0.4 mmol 2,5-dimethyl-*p*-benzoquinone were used as electron acceptors. The light intensity (after filtering through a water filter and a filter transmitting > 550 nm light) was saturating (2,500 μmol photons m^{-2} s^{-1}).

Fluorescence spectroscopy

Fluorescence emission spectra of intact cells were measured at 77 K using a SPEX Fluorolog 2 instrument (SPEX Industries, Edison, NJ). Measurements were carried out with excitation and emission slit widths of 1 and 0.25 mm, respectively, which correspond to bandwidths of 4 and 1 nm. The excitation wavelength was 435 nm.

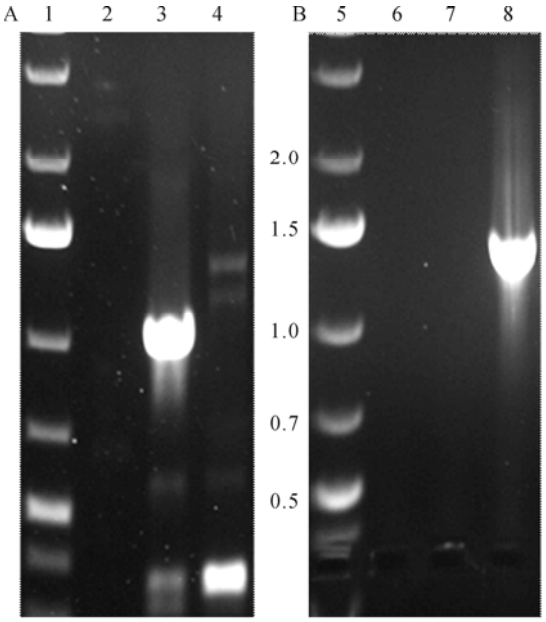

Fig. 1 Segregation of the *sll1906*$^-$ strain of *Synechocystis* sp. PCC 6803. PCR samples applied in A were amplified from the primers for confirmation of the existence of the native *sll1906* gene (PCR product of about 1 kbp), and those in B were amplified from the primers indicating the insertion of the kanamycin cassette. PCR products from wild type are in lanes 3 and 7, and from the *sll1906*$^-$ strain in lanes 4 and 8. The results indicate complete segregation of the *sll1906*$^-$ strain. Lanes 1 and 5 are DNA ladders (sizes in kbp are indicated), and 2 and 6 are negative controls where no DNA was added to the PCR.

Results

Construction and characteristics of sll1906⁻ deletion mutants

In order to examine the function of Sll1906, a *sll1906⁻* mutant was generated with an insertional deletion in the *sll1906* open reading frame. A kanamycin cassette was inserted in the *sll1906* gene, and 77% of *sll1906* was replaced with the antibiotic resistance cassette. Complete segregation of the *sll1906⁻* mutant was achieved and was verified by PCR. Fig. 1 illustrates the results for the *sll1906⁻* strain in comparison with the wild type.

Deletion of Sll1906 was found to have no significant impact on photoautotrophic growth, the amount of chlorophyll per cell, and photosystem II (PSII)-driven oxygen evolution (Table 1). This lack of a significant difference between strains with or without the *sll1906* gene was found also at a higher light intensity (110 μmol photons m^{-2} s^{-1}) (data not shown) and in *chlL⁻* background (*chlL⁻*) strains.

Table 1 Effects of the *sll1906* deletion mutation on doubling time, chlorophyll content, and oxygen evolution rates of wild type and *chlL⁻* cells. Listed are the average results of two or three independent experiments ± S.D.

Strain	Cell doubling time (h)	Chlorophyll content (μg chl/ ($mlOD_{730}$))	Oxygen evolution (μmol O_2/ (mg chlh)
Wild type	12 ± 2	3.55 ± 0.21	424 ± 36
sll1906⁻	13 ± 2	3.63 ± 0.25	442 ± 31
chlL⁻	12 ± 1	2.60 ± 0.14	ND
chlL⁻ /sll1906⁻	13 ± 1	2.65 ± 0.21	ND

Pigment composition of the mutants

To determine the effect of deletion of Sll1906 in wild-type strains in terms of their content of pigments such as chlorophyll, chlorophyll precursors, and carotenoids, cells were extracted with 100% methanol, and the extracts were subjected to HPLC analysis. Chlorophyll and chlorophyll precursors such as Mg-protoporphyrin IX, Mg-protoporphyrin 13-monomethyl ester, and protochlorophyllide would have been detected by HPLC by means of 410 nm absorbance if such precursors accumulated (Fig. 2A). However, no chlorophyll precursors accumulated in either strain. The chlorophyll (C) content was similar in the wild type and *sll1906⁻* mutant, consistent with the results reported in Table 1. Pheophytin *a* (P) was found in both strains at equally low levels. As shown in Fig. 2B, there is no change in the composition of carotenoids either. The amount of all four major carotenoids zeaxanthin (Z), echinenone (E), β-carotene (β), and myxoxanthophyll (M) were within 10% between the wild-type and *sll1906⁻* strains.

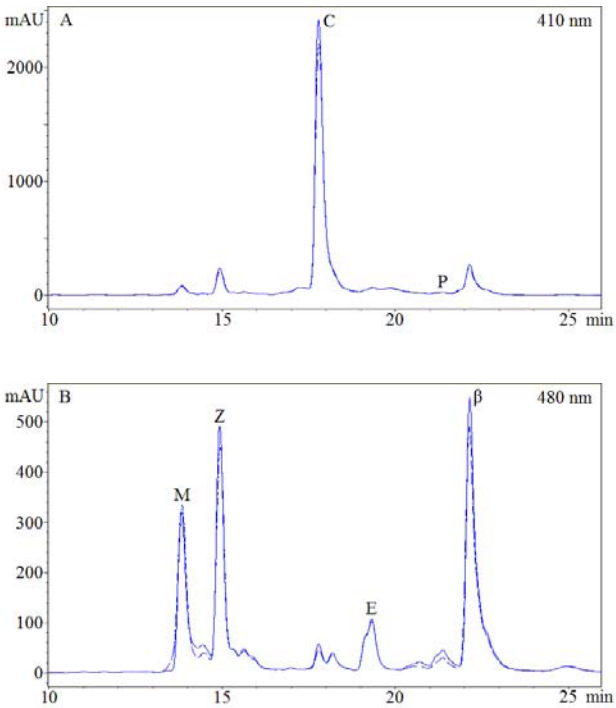

Fig. 2 HPLC spectra of cyanobacterial pigments. Each spectrum showed both wild type (solid line) and *sll1906⁻* (dashed line) samples that were extracted by 100% methanol from an equal amount of cells. Spectra were essentially overlapping. The absorption was monitored at 410 nm (A) and 480 nm (B) to indicate the presence and amount of chlorophyll (C), myxoxanthophyll (M), zeaxanthin (Z), echinenone (E), β-carotene (β), and pheophytin (P).

Chlorophyll degradation and synthesis

In cyanobacteria, both light-dependent protochlorophyllide reductase (LPOR) and light-independent protochlorophyllide reductase (DPOR) are present that convert protochlorophyllide to chlorophyllide, an immediate precursor of chlorophyll. When *chlL⁻* cells that have lost DPOR function were grown in darkness or under LAHG conditions, chlorophyll synthesis was inhibited, and existing chlorophyll was degraded or diluted by growth of the culture. Fig. 3A shows the chlorophyll content in the *chlL⁻* strains with and without the *sll1906* gene upon growth in LAHG conditions for 6 days. No significant difference in chlorophyll degradation was observed. To examine whether the chlorophyll biosynthesis rate

was affected by Sll1906, the cells were grown in LAHG conditions for at least about a week until the amount of chlorophyll was minimal, and subsequently the rate of synthesis of chlorophyll was determined upon continuous illumination at 40 μmol photons m^{-2} s^{-1}. As shown in Fig. 3B, the *sll1906*$^-$ mutant exhibited the same rate of chlorophyll synthesis as the wild type. Therefore, deletion of Sll1906 did not affect the process of chlorophyll degradation and synthesis.

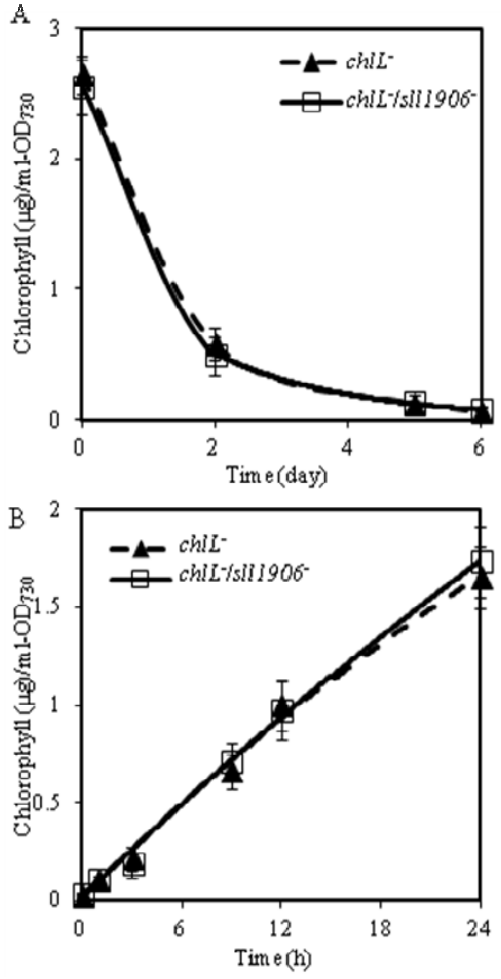

Fig. 3 Chlorophyll degradation and light-dependent chlorophyll synthesis. Chlorophyll levels (μg/ml-OD_{730}) were monitored in the *chlL*$^-$ (triangle with dashed line) and *chlL*$^-$*/sll1906*$^-$ (open square with solid line) strains upon transfer to LAHG conditions at time 0 (A) or upon transfer to continuous illumination (40 μmol photons m^{-2} s^{-1}) at time 0 after cells had been grown under LAHG conditions for 2 weeks (B).

Photosystem biogenesis

In order to study the effects of deletion of Sll1906 on photosystem I (PSI) and PSII, 77 K fluorescence emission spectra of whole cells were measured upon excitation at 435 nm. A major peak at 725 nm is characteristic for PSI-associated chlorophyll, and two smaller peaks at 685 and 695 nm correspond to phycobilisomes and chlorophylls, and CP47-associated chlorophyll, respectively (Fig. 4). Deletion of Sll1906 did not change the PSII/PSI ratio regardless of wild-type or *chlL*$^-$ backgrounds (Fig. 4A). However, the PSII/PSI ratio increased in the *chlL*$^-$ mutants. According to Table 1, the chlorophyll content was reduced about 25% upon deletion of *chlL*$^-$. Therefore, it most likely is a decrease in amount of PSI that caused the increase of the PSII/PSI ratio.

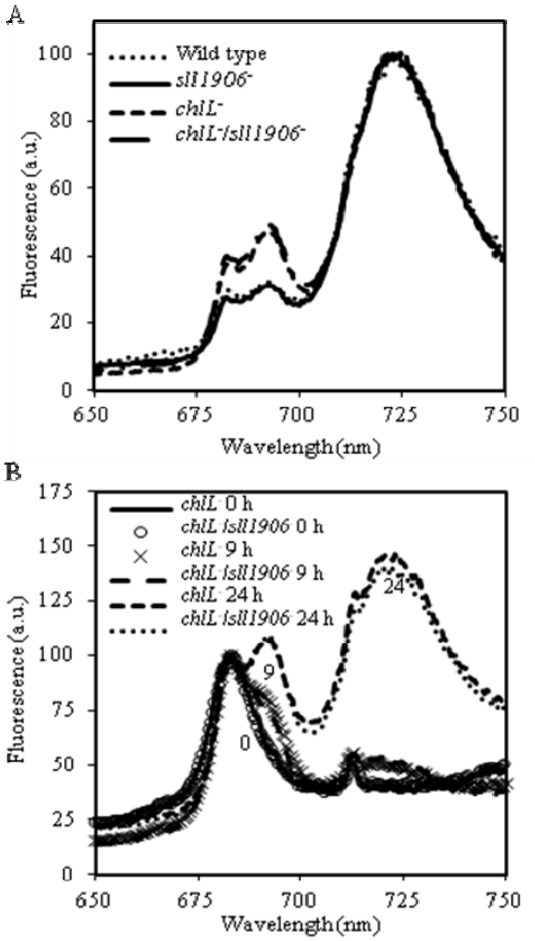

Fig. 4 77 K fluorescence emission spectra of *Synechocystis* sp. PCC 6803 cells. A. Spectra were recorded for the wild type (dotted line), *sll1906*$^-$ (solid line), *chlL*$^-$ (dashed line), and *chlL*$^-$*/sll1906*$^-$ (dashed and dotted line) strains grown at a light intensity of 40 μmol photons m^{-2} s^{-1}. The spectra were normalized to 100 at 725 nm, where PSI emits maximally. B. Spectra were recorded for the *chlL*$^-$ strain after growth at 40 μmol photons m^{-2} s^{-1} for 0 h (solid line), 9 h (X), and 24 h (short dashed line), and for the *chlL*$^-$*/sll1906*$^-$ strain after growth at this light intensity for 0 h (○), 9 h (long dashed line), and 24 h (dotted line) after a week of culturing under LAHG conditions. The spectra were normalized to 100 at 683 nm, where phycobilisomes and some chlorophylls emit maximally. The excitation wavelength was 435 nm. a.u., arbitrary units.

Table 2 Protein sequence alignments and possible chlorophyll-binding amino acid residues in Sll1906 relative to PucC from *Rhodobacter capsulatus* and *Synechocystis psbB*. Underlined residues represent possible chlorophyll binding sites. Sll1906 protein sequences 1 and 2 represent residues 22–49 and 76–87, respectively. CP47 protein sequence 2 represents residues 13–25.

Organisms	Protein sequence 1	Protein sequence 2
Rb capsulatus PucC	RLSLFQITVGMTLTLLAGTLNRVMIVEL	KSDTHKSALGLRR
Syn 6803 Sll1906	RLGLFQMGLGIMSLLTLGVLNRVLIDEL	LSDSQRLWGYH-R
PsbB (CP47)		LNDPGRLISVHLM

To see whether the absence of Sll1906 affected the biogenesis of PSII and PSI upon chlorophyll synthesis, the *chlL*$^-$ and *chlL*$^-$/*sll1906*$^-$ strains were monitored by 77 K fluorescence emission spectra at different stages of greening after a week of culturing under LAHG conditions. At time 0, there were no peaks at 695 and 725 nm, which means that very little or no PSII and PSI was present (Fig. 4B). During 24 h of illumination, deletion of Sll1906 did not have an impact on the rate of PSII and PSI biogenesis upon chlorophyll synthesis. The results show that deletion of Sll1906 did not appear to alter the delivery of chlorophyll to chlorophyll-binding proteins or to aid in photosystem assembly.

Discussion

The putative bacteriochlorophyll delivery (BCD) family was introduced in an earlier study (Saier *et al.*, 1999), and the BCD proteins in different organisms have been named as PucC or bacteriochlorophyll synthase. The function of the BCD family has been examined in *Rhodobacter capsulatus*, which contains three members of the BCD family, PucC, LhaA, and ORF428. The LhaA and PucC proteins were reported to enhance correct LH complex assembly (Young *et al.*, 1998; Jaschke *et al*., 2008). The Sll1906 protein in *Synechocystis* has a 24%–27% amino acid sequence identity with *Rhodobacter* BCD members and has a hydropathy profile similar to that of the LhaA/PucC proteins. The BCD family proteins sequences of purple bacteria (*Rhodobacter capsulatus* and *Rhodopseudomonas palustris*) and cyanobacteria (*Synechocystis* sp. PCC 6803, *Prochlorococcus marinus* 9211, and *Synechococcus* sp. CC9902) were analyzed. Transmembrane segments (TMSs) 1 and 2, and TMSs 7 and 8 as well as their connecting loop regions are well conserved, and the loop region between TMSs 4 and 5 as well as TMS5 is also well conserved. These results are consistent with an earlier study (Saier *et al.*, 1999). Interestingly, the rest of the protein sequence (over 50%) has low or no similarity between BCD family of purple bacteria and cyanobacteria but is highly conserved within purple bacteria and moderately conserved within cyanobacteria.

Sll1906 was suggested to be involved in tetrapyrrole delivery for assembly of chlorophyll-binding complexes (Young and Beatty, 1998). However, *Synechocystis* cells lacking *sll1906* have normal chlorophyll content and chlorophyll synthesis (Table 1 and Fig. 3), whereas also the tetrapyrrole biosynthesis pathway was not disrupted in the mutant (no accumulation in chlorophyll precursors) (Fig. 2A). Also, judging from the 77 K fluorescence emission spectra, lack of Sll1906 did not impair PSII and PSI assembly (Fig. 4).

In order to examine if Sll1906 possibly binds chlorophyll, Table 2 shows examples of the Sll1906 protein sequences that contain possible chlorophyll-binding amino acid residues (underlined). Protein sequence 1 is highly conserved in all organisms possessing BCD proteins and contain a few amino acid residues that could bind chlorophyll. Protein sequence 2 is conserved in cyanobacteria only but aligns well with part of PsbB containing a histidine that binds chlorophyll (Muh *et al.*, 2008). Therefore, Sll1906 may have chlorophyll-binding ability.

In conclusion, the *sll1906*$^-$ mutant did not show significant effects on pigment content and photosystem assembly. However, this does not necessarily mean that Sll1906 is not involved in these processes as other (parallel) pathways may exist that may fully compensate for the lack of Sll1906.

Acknowledgements

This research was supported by Energy Biosciences Program of the U.S. Department of Energy (DE-FG02-08ER15543).

References

Jaschke P, LeBlanc H, Lang A, Beatty J (2008) The PucC Protein of Rhodobacter Capsulatus Mitigates an Inhibitory Effect of Light-Harvesting 2 α and β Proteins on Light-Harvesting Complex I. Photosynth. Res. 95: 279-284

LeBlanc HN, Beatty, JT (1996) Topological Analysis of the Rhodobacter Capsulatus PucC Protein and Effects of C-Terminal Deletions on Light-Harvesting Complex II. J. Bacteriol. 178: 4801-4806

Muh F, Renger T, Zouni A (2008) Crystal Structure of Cyanobacterial Photosystem II at 3.0 Å Resolution: a Closer Look at the Antenna System and the Small Membrane-Intrinsic Subunits. Plant Physiol. Biochem. 46: 238-264

Saier M, Beatty J, Goffeau A, Harley K, Heijne W, Huang S, Jack D, Jahn P, Lew K, Liu J, Pao S, Paulsen I, Tseng T, Virk P (1999) The Major Facilitator Superfamily. J. Mol. Microbiol. Biotechnol. 1: 257-279

Wu Q, Vermaas WFJ (1995) Light-Dependent Chlorophyll a Biosynthesis upon chlL Deletion in Wild-Type and Photosystem I-Less Strains of the Cyanobacterium Synechocystis sp PCC 6803. Plant Mol. Biol. 29: 933-945

Young CS, Beatty JT (1998) Topological Model of the Rhodobacter Capsulatus Light-Harvesting Complex I Assembly Protein LhaA. J. Bacteriol. 180: 4742-4745

Young CS, Reyes RC, Beatty JT (1998) Genetic Complementation and Kinetic Analyses of Rhodobacter Capsulatus ORF1696 Mutants Indicate that the ORF1696 Protein Enhances Assembly of the Light-Harvesting I complex. J. Bacteriol. 180: 1759-1765

Functional Analysis of PsbP-Like Protein 1 (PPL1) in Arabidopsis

Shintaro Matsui[1], Seiko Ishihara[1], Kunio Ido[1], Kentaro Ifuku[1, 2*], Fumihiko Sato[1]

[1]Graduate School of Biostudies, Kyoto University, Sakyo-ku, Kyoto 606-8502, Japan;
[2]PRESTO, Japan Science and Technology Agency (JST), Saitama 322-0012, Japan.
[*]Corresponding author. Tel. No. +81-75-753-6381; Fax No. +81-75-753-6398; E-mail: ifuku@kais.kyoto-u.ac.jp.

Abstract: Higher plants have a number of PsbP homologs (PsbP-like proteins: PPLs, PsbP-domain proteins: PPDs) in addition to the authentic PsbP in the oxygen-evolving complex of photosystem II (PSII). Among the PsbP homologs, the PPL1 protein is most homologous to a cyanobacterial PsbP (cyanoP), and we previously reported that PPL1 is required for the efficient repair of photo-damaged PSII under high light conditions [Ishihara *et al*. (2007) Plant Physiol. 145: 668-679]. However, functional role of PPL1 in the PSII repair cycle has not been clarified yet. In this study, we further investigated molecular function of PPL1 by characterizing the phenotypes of the PPL1 knockdown plants (*ppl1i*) in which PPL1 expressions were differently suppressed. Although growth of the *ppl1i* mutants under low intensity light was comparable with that of wild type plants, PSII activity of the *ppl1i* mutants was more sensitive to high intensity light and the extent of photoinhibition was correlated with the levels of the knocked-down *PPL1*. The possible functional role of PPL1 in PSII repair is discussed.

Keywords: Photosystem II; Photoinhibition; PsbP homolog; PSII repair cycle; Thylakoid lumen

Introduction

It is known that the composition of the extrinsic subunits of photosystem II (PSII) in the lumenal side of thylakoids are significantly different among the photo-oxygenic organisms (Seidler, 1996): higher plants and green algae have a set of three extrinsic proteins [PsbO (33 kD), PsbP (23 kD), and PsbQ (17 kD)], whereas cyanobacteria have a different set of proteins [PsbO, PsbU (12 kD), and PsbV (cytcrome *c*550)] (Enami *et al*., 2008). In addition, recent genomic and proteomic studies have demonstrated that prokaryotic cyanobacteria have a homolog of PsbP (cyanoP) and PsbQ (cyanoQ). Furthermore, it turns out that higher plants have a number of PsbP and PsbQ homologs (PsbP-like proteins, PPL; PsbP-domain proteins, PPD; PsbQ-like protein, PQL) in thylakoid lumen (Roose *et al*., 2007). Significant progresses have been made to understand the functions of PsbP and PsbQ homologs in higher plants (Ifuku *et al*., 2008, 2010). However, further research is still needed to elucidate their molecular function fully.

Among the PsbP homologs, PPL1 is most homologous to cyanoP. We previously reported that PPL1 seems to express under stress conditions (Ishihara *et al*., 2007). In fact, PSII activity in an Arabidopsis mutant lacking PPL1 (*ppl1*) was more sensitive to high-intensity light than wild type, and the recovery of photoinhibited PSII activity was delayed in *ppl1* mutants. Therefore, we conclude that PPL1 is required for efficient repair of photodamaged PSII. However, the protein-protein interaction between PPL1 and PSII was not detected, so that functional role of PPL1 in the PSII repair cycle has not been clarified yet.

In this study, we characterized phenotypes of the RNAi mutants (*ppl1i*) in which PPL1 expressions are differently suppressed. Preliminary results of biochemical studies about PPL1 are also introduced.

Materials and Methods

Growth conditions

Arabidopsis wild-type (ecotype Columbia-0, Col-0),

and the *ppl1i* plants were grown in soil under growth chamber conditions (10/14 h light-dark photoperiod at 50 µmol photons m^{-2} s^{-1}, 21 °C).

Production of the ppl1i transgenic line

The following PCR primers were used to amplify the 408 bp fragment of *PPL1* cDNA: 5'-CACCTGCT CCTTGGATCTCATTGC-3', 5'-AACCGTGATGGTA CCCAGAG-3'. The PCR products were cloned into pENTR/D-TOPO vector and then transferred into pHellsgate8 vector by a LR recombination reaction (Gateway, Invitrogen). The plasmids pHellsgate8-PPL1 was used to transform Col-0 via *Agrobacterium tumefaciens* strain GV3101 by floral dip method. Seeds were collected and the transformants were selected on the medium containing Murashige and Skoog salt mix, 50 µg ml^{-1} kanamycin, and 0.8% agar.

SDS-PAGE and Immunoblotting

Total proteins extracted from 5-week-old leaves were solubilized and separated on 12.5% SDS-polyacrylamide gels including 6 mol urea. Separated proteins were transferred to a PVDF membrane using a semidry blotting system (Bio-Rad). Detection was performed with ECL-plus reagent (GE Healthcare).

RT-PCR Analysis

Total RNA was extracted from 3-week-old leaves and cDNA was reverse transcribed using Super Script III reverse transcriptase (Invitorogen). The *PPL1* cDNA was then amplified using following primers: *PPL1* (5′-CACCATGGCTTCTCTGAAGCTTTCAC-3′ and 5′-TCAAACAGTGATCTTGAAGGAATCT-3′). The products were visualized by ethidium bromide staining after agarose gel electrophoresis.

Photoinhibition Assay

Detached leaves from 5 weeks-old plants were placed adaxial side up on the filter papers steeped with water and illuminated at 650 µmol photons m^{-2} s^{-1}. Maximum efficiency of PSII (F_v/F_m) was monitored during exposure to an irradiance of high-intensity light. The measurements were done after 10 min dark-adaptation with Mini-PAM chlorophyll fluorometer (Walz, Germany).

Result and Discussion

Our previous report showed that PSII activity in an Arabidopsis mutant lacking PPL1 (*ppl1*) was more sensitive to high-intensity light than wild type. However, this *ppl1* mutant (Salk_014843) has a T-DNA insertion in the intron of the *PPL1* gene and residual *PPL1* expression was expected (Ishihara *et al.*, 2007). Therefore, we tried to establish the RNAi transgenic lines (*ppl1i*) in which *PPL1* expressions are severely suppressed. In addition, we expected to analyze whether *PPL1* knockdown affects PSII activity in a dose-dependent manner.

When three independent transgenic lines (*ppl1i-1*, *ppl1i-2*, *ppl1i-3*) were analyzed, all transgenic lines showed the severe suppression of the expressions of the *PPL1* gene (At3g55330) in both transcript (Fig. 1B) and protein (Fig. 1C) levels. Among the *ppl1i* transgenic lines, the *ppl1-2* plants showed the lowest accumulation of PPL1 protein (Fig. 1C). Growth of *ppl1i* transgenic plants under 50 µmol photons m^{-2} s^{-1} (moderate light condition) was comparable with that of wild type, which is consistent with the previous observation using the *ppl1* mutant (Fig. 1D).

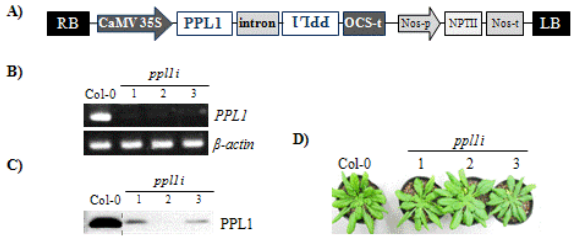

Fig. 1 Production of the *ppl1i* transgenic line A) RNAi construct. A 408bp fragment of the *PPL1* gene was amplified by RT-PCR and cloned into pHELLSGATE8 vector. B) The mRNA expression level of *PPL1* was determined by RT-PCR. *β-actin* was analyzed as control. C) Immunodetection of PPL1. Total protein (30 µg) was used for the SDS-PAGE / Immuno-blot analysis D) Visible phenotypes of Arabidopsis wild-type (Col-0) and the *ppl1i* plants grown in soil for 5 weeks under moderate light condition (~50 µmol photons m^{-2} s^{-1}).

To examine the performance of PSII in wild type and *ppl1i* leaves, detached leaves were irradiated with high-intensity light, and the changes in the F_v/F_m value were monitored by a PAM fluorometer. Wild type leaves showed little decline in F_v/F_m even under high-intensity light condition (650 µmol photons m^{-2} s^{-1}). On the other hand, the F_v/F_m value in the *ppl1i* leaves was decreased to 60%–70% of the initial value within 360 minutes of illumination. Among the *ppl1i* transgenic lines, *ppl1i-2*, in which the expression level of PPL1 protein was most severely reduced, showed

greatest reduction in F_v/F_m (Fig. 2). This suggests that the *PPL1* knockdown affects PSII activity in dose-dependent manner. In the presence of chloramphenicol that inhibits plastid protein synthesis, F_v/F_m decreased similarly in both wild type and the *ppl1i* leaves to ~40% within 360 minutes of illumination (data not shown). These data are fully consistent with our previous observation (Ishihara *et al*., 2007), and demonstrate that *PPL1* knockdown slows the rate of PSII repair but does not accelerate the rate of the PSII photodamage.

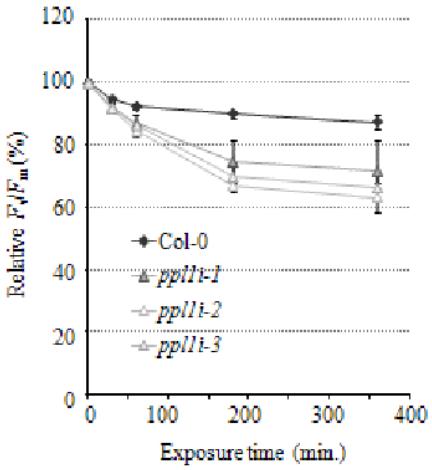

Fig. 2 Time course of photoinhibition under high-intensity light condition Detached leaves were illuminated at 650 µmol photons m^{-2} s^{-1}. Maximum efficiency of PSII (F_v/F_m) was measured during exposure to an irradiance of high-intensity light after 10 minutes of dark-adaptation. Values were averages ±SD (n = 3).

Recently, we observed that PPL1 was mainly localized in the stroma-exposed (unstacked) thylakoid regions where the PSII repair is thought to be conducted (Mulo *et al*., 2008) (data not shown). This is compatible with the results showing that PPL1 is involved in PSII repair. Furthermore, PPL1 was fractionated in relatively high-density fractions in a sucrose density gradient ultracentrifuge analysis (data not shown), suggesting that PPL1 should interact with some protein complexes. Because PPL1 knockdown affected PSII repair in dose-dependent manner (Fig. 2), it is possible that PPL1 may interact with and stabilize the PSII assemblies during the repair of photo-damaged PSII in stroma-exposed thylakoid regions. Further biochemical analyses to identify proteins or protein complexes interacting with PPL1 will clarify functional roles of PPL1 in the PSII repair cycle.

Acknowledgements

This work was supported partially by the grant from JST PRESTO (to Ke.I.), and by Grant-in-Aid for Young Scientists (B) (grant no. 18770032 to Ke.I.) from JSPS.

References

Enami I, Okumura A, Nagao R, Suzuki T, Iwai M, Shen JR (2008) Structures and Functions of the Extrinsic Proteins of Photosystem II from Different Species. Photosynth Res. 98(1-3): 349-363

Ifuku K, Ishihara S, Shimamoto R, Ido K, Sato F (2008) Structure, Function, and Evolution of the PsbP Protein Family in Higher Plants. Photosynth Res 98: 427-437

Ifuku K, Ishihara S, Sato F (2010) Molecular Functions of Oxygen-Evolving Complex Family Proteins in Photosynthetic Electron Flow. J Integr Plant Biol. 52(8): 723-34

Ishihara S, Takabayashi A, Ido K, Endo T, Ifuku K, Sato F (2007) Distinct Functions for the Two PsbP-Like Proteins PPL1 and PPL2 in the Chloroplast Thylakoid Lumen of Arabidopsis. Plant Physiol 145: 668-679

Mulo P, Sirpiö S, Aro EM (2008) Auxiliary Proteins Involved in the Assembly and Sustenance of Photosystem II. Photosynth Res. 98: 489-501

Roose JL, Wegener KM, Pakrasi HB (2007) The Extrinsic Proteins of Photosystem II. Photosynth Res. 92(3): 369-387

Seidler A (1996) The Extrinsic Polypeptides of Photosystem II. Biochim. Biophys. Acta 1277: 35-60

Insertion of a Rigid Structural Element into the Regulatory Domain of the Chloroplast F1-ATPase Gamma Subunit for Rotational Studies.

Stephanie C Bishop[a], Shyam Mehta[a], Kim K Colvert[d], Daxin Zheng[a], Mark L Richter[a], Cindy L Berrie[b], Fei Gao[c]*

Departments of Molecular Biosciences[a], Chemistry[b], and COBRE Protein Production Core Lab[c], The University of Kansas, Lawrence, KS, USA; [d]Ferris State University, Michgan.
*Corresponding author. Tel. No. +1 785 864 1825; Fax No. +1 785 864 8141; E-mail: gao@ku.edu.

Abstract: A two-step PCR approach was developed to insert the repressor of primer (Rop) DNA sequence into the ATP synthase gamma subunit DNA sequence that encodes a regulatory dithiol-containing domain. The construct was intended to lengthen the rotational arm of the gamma subunit for detailed studies of the rotational kinetics of attached nanoparticles. The PCR utilized unusually long (> 100 base pairs each) primers encoding a single site within a pACYC multiple cloning host vector. This approach avoided shortcomings such as inclusion or omission of base pairs associated with traditional sub-cloning methods by direct insertion of large pieces of DNA into a host DNA molecule without introducing restriction enzyme sites. The rigid helical structure of the Rop protein is expected to extend the regulatory domain of the gamma subunit by approximately 60 Ångstroms beyond the rotational axis of the hexameric F_1 to afford a more detailed study of the rotational process. The gamma construct was expressed and assembled with recombinant alpha and beta subunits into a core F_1-ATPase that exhibited wild type catalytic activity, normal sensitivity to the redox state of the regulatory dithiol of the gamma subunit, but loss of sensitivity to the inhibitory epsilon subunit.

Keywords: Chloroplast F_1-ATPase; Rotating arm; Gamma regulatory domain

Introduction

The goal of this study was to insert the 63 amino acid long repressor of primer (Rop) protein into the rotating spindle element (the gamma subunit) of the chloroplast F_1-ATPase. The insertion is intended to extend the rotational radius of the rotating spindle by 60 Å, beyond the enzyme periphery. The monomeric, twisted helical structure of Rop is expected to be rigid and highly stable, facilitating analysis of the rotational mechanism through attachment of metallic beads (Noji *et al*., 1997; Yasuda *et al*., 2001).

Of the several possible methods that were explored to insert the 189 nt long Rop gene, the successful one utilized a long primer approach in which two inverse PCR primers of approximately 100 nt each were designed to include the desired protein extension.

[1]**Abbreviations Used:** *atpC*, the DNA sequence encoding the ATP synthase gamma subunit; F_1, the membrane-associated portion of the ATP synthase complex that contains the catalytic domains; PCR, polymerase chain reaction; Rop, repressor of primer; Tricine, N-(2-hydroxy-1-bis(hydroxymethyl)ethyl)glycine; Tris, tris(hydroxy methyl)amino-methane.

The chosen site of Rop insertion is within a special regulatory dithiol-containing domain of approximately 40 amino acids long within the gamma subunit of the higher plant F_1-ATPase (Samra *et al*., 2006). The dithiol domain can be extensively modified or even deleted altogether without loss of catalytic function (Samra *et al*., 2006), making it a logical place for Rop insertion.

Materials and Methods

Materials

DEAE cellulose, antibiotics (ampicillin and chloramphenicol), Sephadex G-50 resin, and Ni-NTA

resin were purchased from Sigma-Aldrich. Tryptone and yeast extract were obtained from DIFCO. ATP (grade II) was purchased from Midwest Scientific and urea (ultra pure) was purchased from ICN Biomedicals Inc. *PfuUltra* DNA Polymerase was purchased from Stratagene and GoTaq® Flexi DNA Polymerase, BamH1, Nco1 and dNTPs were purchased from Promega. T4 Polynucleotide Kinase, pACYC Duet Coexpression Vector and BL21DE3pLys competent cells were from Novagen; T4 DNA Ligase and 5-αF'I^q competent cells were from New England Biolabs. The primers were obtained from Integrated DNA Technologies and a 10 kilobase DNA hyperladder was provided by Bioline. All other chemicals were of the highest quality reagent grade available.

Sub-cloning

The DNA encoding the chloroplast ATP synthase gamma subunit (*atpC*) was previously sub-cloned into the pET8cgam bb1 vector (Sokolov *et al*., 1999). The pACYCatpC vector (Fig. 1) was prepared by removing *atpC* from the pET8cgam bb1 vector and inserting it into the NcoI multiple cloning site of the pACYC Duet Co-expression Vector. This insertion was accomplished by restriction digestion of the gamma subunit N-terminus with NcoI and of the C-terminus with BamHI and a simultaneous restriction digestion of the pACYC Duet Co-expression Vector. The insert sequence was confirmed by DNA sequencing.

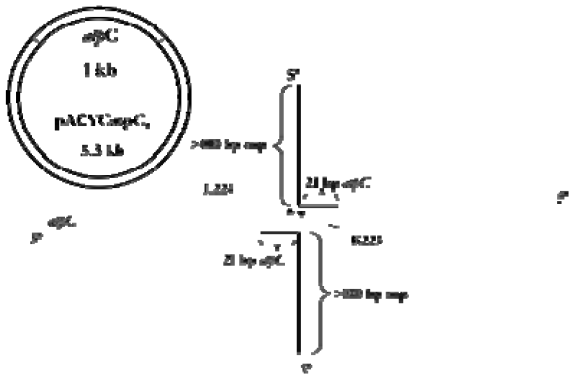

Fig. 1 Construction of the pACYCatpC gamma-Rop plasmid by insertion of the full-length Rop gene into the gamma (atpC) regulatory domain between residues 223 and 224 as indicated. Bi-directional primers, each containing about half of the Rop sequence, were used to insert the Rop gene.

Primer Extension

Primers were designed to insert the entire Rop DNA sequence (NCBI J01749; 189 bases) (Eberle *et al*., 1991) between the gammąsubunit amino acids 223 (lysine) and 224 (leucine) in the pACYCatoC vector as indicated in Fig. 1. Two unphosphorylated long primers contained (1) the DNA sequence for the N-terminal half of Rop in addition to 21 bases of the ATP synthase gamma subunit DNA sequence, and (2) the DNA sequence for the C-terminal half of Rop in addition to 21 bases of the ATP synthase gamma subunit DNA sequence. The primers contained no known restriction enzyme digestion sites.

Both *PfuUltra* High-fidelity DNA Polymerase and GoTaq® Flexi DNA Polymerase, were employed together in the inverse polymerase chain reaction using two annealing temperatures and durations (57 °C for 30 seconds; 68 °C for 10 minutes). Gel purification was performed using the Qiaquick® Gel Extraction kit (Qiagen). The gel-purified, linear, 5.5 kilobase PCR product was treated with T4 Polynucleotide Kinase at a final concentration of 1 U/μL according to the manufacturer's specifications. After treatment, the kinase was inactivated by incubation at 70 °C for 10 minutes. T4 DNA Ligase, at a final concentration of 2×10^6 mU/μL, was added for blunt-end ligation of the linear PCR products. T4 Polynucleotide Kinase was added during ligation.

Transformation

The recombinant pACYCatpC plasmid containing the Rop sequence was transformed first into *E.coli* XL1 blue then into *E.coli* BL21DE3pLys competent cells for protein over-expression (Gao *et al.*, 1995; He *et al*., 2008). The gamma subunit containing the Rop insert was solubilized from inclusion bodies, folded and assembled with recombinant F_1 alpha and beta subunits as described in detail elsewhere (Tucker *et al*., 2001; Samra *et al*., 2006; He *et al*., 2008).

ATPase Assay

ATPase activities were determined by measuring phosphate release (Taussky and Schorr, 1953; He *et al*., 2008) for 2–5 minutes at 37 °C. The assay mixture for Ca^{2+}-dependent ATPase activity contained 50 mmol Tricine-NaOH (pH 8.0), 5 mmol ATP and 5 mmol $CaCl_2$. That for Mg^{2+}-dependent ATPase activity contained 40 mmol Tricine-NaOH (pH 8), 4 mmol ATP, 2 mmol $MgCl_2$ and 50 mmol Na_2SO_2.

Results and Discussion

PCR Extension of Long Primers

Inverse PCR was employed to generate a plasmid

containing the Rop DNA inserted into the *atpC* gene (Fig. 1) at a position within the dithiol domain of the F_1-ATPase gamma subunit predicted from modeling studies (Richter *et al*., 2005) to extend the domain roughly horizontally with respect to the symmetry axis of the αβ hexamer. This was achieved using 105 and 123 nucleotide long primers, each containing about half of the DNA sequence of the fragment being inserted.

The inverse PCR extension method is commonly used for the introduction of nucleotide changes, for the insertion of small lengths of exogenous DNA into a gene or vector (*e.g.* Uccelli *et al*., 1997; Ochman *et al*., 1988), or in the deletion of base pairs of a gene of interest with higher deletion efficiency than the overlapping primer method (Williams *et al*., 2007). The insertion of the *rop* DNA into the *gamma* gene, an insert of 189 base pairs of foreign DNA, represents a novel application of this method, made possible using a multi-step PCR approach. Optimal long primer inverse PCR required an initial round (step one) with low annealing temperature and short annealing duration because primers were required to anneal to approximately 21 bases of the gamma subunit sequence. During the second PCR step, the annealing temperature and duration were increased significantly because the primers were annealing to a DNA sequence that was complementary to the entire primer length (> 100 base pairs). This two-step inverse PCR method resulted in a linear product.

One highly advantageous property of this inverse PCR technique was that it avoided inadvertent inclusion or omission of base pairs associated with restriction digestion methods, therefore reducing the incidence of missense mutations. Also, the inverse PCR approach inserted the DNA sequence of interest in a single orientation, unlike traditional restriction digestion and ligation methods, where varying ratios and orientations of products are possible. The inverse PCR technique also avoided other problems associated with traditional cloning approaches, including difficulty digesting DNA using restriction digestion enzymes, ligating insert DNA into a template, and ensuring that the ligated product contains the sequence of interest in the proper insert:vector ratio.

The inverse PCR conditions generated a single 5.5 kb product. The product was gel-extracted and treated with T4 polynucleotide kinase. Blunt-end ligation of the linear PCR products was achieved using T4 DNA Ligase. T4 Polynucleotide Kinase was present during ligation which was carried out at room temperature for 4 h then at 16 °C overnight. Ligation was confirmed by PCR.

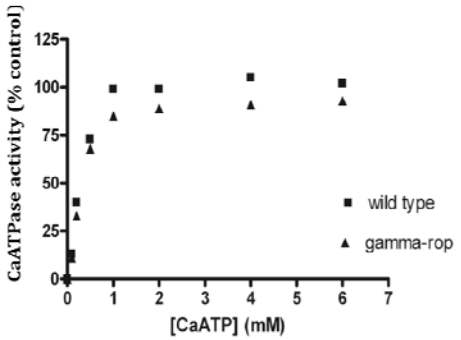

Fig. 2 CaATPase activity of core enzyme assemblies containing the wild type gamma and gamma with the Rop insert. The 100% (control) value in this experiment was 52 μmol min^{-1} mg $protein^{-1}$.

Over-expression and Assembly of the Gamma-Rop Construct

The *atpC*-Rop construct was transformed first into *E.coli* XL1 blue to increase plasmid copy number then into *E.coli* BL21DE3(pLys) cells for over-expression. Following induction, the gamma-Rop protein was produced in high yield (> 100 mg per liter of bacterial cells) in inclusion bodies. The protein was solubilized from inclusion bodies in urea, folded and assembled with recombinant alpha and beta subunits into a core F_1-ATPase as previously described (Gao *et al*., 1995; He *et al*., 2008; Tucker *et al*., 2001). The electrophoretic mobility of the mutant gamma was compared to that of the wild type gamma as shown in Fig. 3. The mutant form exhibited the expected increase in molecular weight resulting from the presence of the Rop insert.

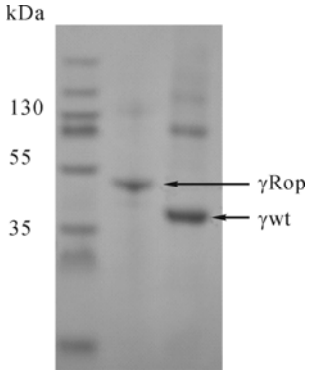

Fig. 3 Sodium dodecyl polyacrylamide gel comparing the gamma-Rop and wild type gamma subunits solubilized from inclusion bodies in urea.

The recombinant gamma-Rop was assembled with the alpha and beta subunits of the photosynthetic

bacterium *Rhodospirillum rubrum* using methods described in detail previously (Tucker *et al.*, 2001). The mutant was as effective as the wild type gamma subunit in assembling with the alpha and beta subunits as judged by the recovery of protein from assembly mixtures (~10%) and by the relative catalytic activity as shown in Fig. 2 for CaATP hydrolysis. The enzyme containing the mutant also exhibited normal sensitivity to the redox state of the gamma dithiol; exposure to the reducing agent dithiothreitol (10 mmol for 15 min st 37 ^{o}C) resulted in an increase in CaATPase activity of 45% over that of the enzyme exposed to $CuCl_2$ (50 μmol for 15 min at 37 ^{o}C), conditions known to result in oxidation of the gamma dithiol (Samra *et al*., 2007).

In contrast, the mutant enzyme containing the gamma-Rop was no longer inhibited by the epsilon subunit as shown in Fig. 4. This is consistent with previous observations (Samra *et al*., 2006) that even modest changes in the structure of the regulatory dithiol domain of the gamma subunit result in loss of epsilon inhibition.

The new assembly will be of considerable value in the analysis of gamma subunit rotation and in the construction of nanodevices that are based on the rotational capability of the F_1 molecule. The next step in this process is to engineer a site for attachment of metallic beads to the extended Rop armature within the gamma subunit for dark-field microscopic studies of the rotational kinetics (Yasuda *et al*., 2001).

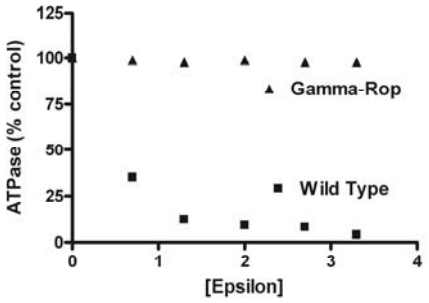

Fig. 4 Titration of wild type and mutant enzymes with the recombinant inhibitory epsilon subunit as per Samra *et al*., 2006. Normalized CaATPase activities are shown.

In conclusion, a novel method has been described for the direct incorporation of 189 bases of exogenous DNA into a specific location within the gene encoding the gamma subunit of the chloroplast ATP synthase using a simple two-step PCR extension procedure. Because of its ease of use and advantages over traditional cloning techniques, we anticipate that the method will be valuable for a variety of applications.

Acknowledgements

This work was supported by a grant from the Department of Defense (ARO #W911NF0810303) to MLR and CB, and a grant from the National Institute of Health (#RR-017708) to KU COBRE Center in Protein Structure and Function.

References

Eberle W, Pastore A, Sander C, Rösch P (1991) The Structure of ColE1 Rop in Solution. Journal of Biomolecular NMR. 1: 71-82

Gao F, Lipscomb B, Wu I, Richter ML (1995) In Vitro Assembly of the Core Catalytic Complex of the Chloroplast ATP Synthase. J.Biol.Chem. 270: 9763-9769

He F, Samra HS, Johnson EA, Degner NR, McCarty RE, Richter ML (2008) C-Terminal Mutations in the Chloroplast ATP Synthase Gamma Subunit Impair ATP Synthesis and Stimulate ATP Hydrolysis. Biochemistry 47: 836-844

Noji H, Yasuda R, Yoshida M, Kinosita Jr K (1997) Direct Observation of the Rotation of F_1-ATPase. Nature 386: 299-302

Ochman H, Gerber AS, Hartl DL (1988) Genetic Applications of an Inverse Polymerase Chain Reaction. Genetics. 120: 621-623

Richter. ML, Samra H, He F, Giessel A, Kuczera K (2005) Coupling Proton Movement to ATP Synthesis in the Chloroplast ATP Synthase. Bioenerg. and Biomemb. 37: 467-473

Samra HS, Gao F, He F, Hoang E, Chen A, Gegenheimer PA, Berrie CL, Richter ML (2006) Structural Analysis of the Regulatory Dithiol-Containing Domain of the Chloroplast ATP Synthase. J.Biol.Chem. 281: 31041-31049

Sokolov M, Lu L, Tucker W, Gao F, Gegenheimer PA, Richter ML (1999) The 20 C-Terminal Amino Acid Residues of the Chloroplast ATP Synthase γ Subunit Are Not Essential for Activity. J.Biol.Chem. 274: 13824-13829

Taussky HH, Schorr A (1953) Microcolorimetric Method for the Determination of Inorganic Phosphorus. J.Biol.Chem. 202: 675-685

Tucker WC, Du Z, Hein R, Gromet-Elhanan Z,

Richter ML (2001) The Role of the ATP Synthase Alpha Subunit in Conferring Sensitivity to Tentoxin. Biochemistry 40: 7542-7548

Uccelli A, Oksenberg JR, Jeong MC, Genain CP,Tombos T, Jaeger EEM, Giunti D, Lanchbury JS, Hauser S (1997) Characterization of the TCRB Chain Repertoire in the New World Monkey Callithrix jacchus. J.Immunology. 158: 1201-1207

Williams M, Louw AI, Birkholtz LM (2007) Deletion Mutagenesis of Large Areas in Plasmodium Falciparum Genes: a Comparative Study. Malaria Journal 6: 64-72

Yasuda R, Noji H, Yoshida M, Kinosita Jr K, Itoh H (2001) Resolution of Distinct Rotational Substeps by Submillisecond Kinetic Analysis of F_1-ATPase. Nature 401: 898-904

Functional Analysis of PsbR in PsbP Binding to Photosystem II

Kunio Ido[a], Kentaro Ifuku[a,b,*], Fumihiko Sato[a]

[a]Graduate School of Biostudies, Kyoto University, Kyoto 606-8502, Japan;
[b]PRESTO, Japan Science and Technology Agency (JST), Saitama 332-0012, Japan.
[*]Corresponding author. Tel. No. +81 75 753 6381; Fax No. +81 75 753 6398; E-mail: Ifuku@kais.kyoto-u.ac.jp.

Abstract: The PsbP protein is a thylakoid lumenal extrinsic subunit of photosystem II (PSII) specifically found in green plants, such as higher plants and green algae. The binding site of PsbP in PSII has not been determined because of the lack of the high-resolution 3D structure of green plant PSII. Recent studies indicate that the PsbR protein, which is specific to higher plants, is involved in the PsbP binding to PSII; however, the role of PsbR has not been clarified yet. In this study, we showed that PsbR was fractionated differently from PsbP when thylakoid protein complexes were solubilized and separated by sucrose density gradient ultracentrifugation. On the other hand, PsbP was dissociated more easily from the thylakoid membranes in Arabidopsis mutant lacking PsbR than in the wild type, when thylakoid membranes were washed by low-pH buffers or high-NaCl containing buffers. These results suggest that PsbR is not essential but has an auxiliary role for the PsbP binding to PSII.

Keywords: Extrinsic proteins; Oxygen evolving complex; Photosystem II; PsbP; PsbR

Introduction

Photosystem II (PSII), the water/plastoquinone oxidoreductase, is the supramolecular pigment-protein complex that consists of membrane intrinsic and extrinsic proteins (Nelson and Yocum, 2006). In addition to the major intrinsic subunits that bind pigments and/or cofactors involved in photochemical reaction, PSII has extrinsic subunits on the thylakoid lumenal side (Bricker and Burnap, 2005). These extrinsic proteins are called oxygen evolving complex (OEC) proteins, and the PsbO, PsbP, and PsbQ proteins are the OEC proteins in green plants, such as higher plants and green algae. Among those OEC subunits, PsbP and PsbQ are specific to green plants, and facilitate the retention of Ca^{2+} and Cl^{-}, essential cofactors for water-splitting reaction in PSII (Seidler, 1996). Because high-resolution 3D structure of green plant PSII has not been obtained so far, binding sites of PsbP and PsbQ in PSII still remain to be elucidated.

The PsbR protein is a nuclear-encoded PSII subunit specifically found in higher plants. PsbR is predicted to have one transmembrane domain and reported to be involved in the binding of PsbP to PSII (Suorsa *et al*., 2006; Liu *et al*., 2009), but the exact role of PsbR in the PsbP binding has been unclear.

In this study, we analyzed the function of PsbR in the PsbP binding to PSII. The analysis using sucrose density gradient ultracentrifugation suggests that PsbP can bind to PSII without PsbR when thylakoid protein complexes were solubilized and separated in the presence of 2 mol betaine. However, the treatment with low-pH or high-NaCl buffers dissociated PsbP from thylakoid membranes more easily in the absence of PsbR than in its presence. These data suggest that PsbR is not essential but has an auxiliary role for the PsbP binding to PSII.

Materials and Methods

Tobacco plants grown on agar solidified 0.5xLinsmaier-Skoog (LS) medium supplemented with 1.5% sucrose were transplanted into soil and grown under continuous light (50 μmol photons m^{-2} s^{-1}) at 28 °C. Fully developed leaves (the fourth-sixth

leaves from the top) were used in all experiments. Arabidopsis wild-type (ecotype Columbia-0, Col-0) and *psbr* T-DNA insertion mutant (Salk_114469) were grown in soil under growth chamber conditions (10/14-h light-dark photoperiod at 100 μmol photons m^{-2} s^{-1}, 21 °C).

Isolation of thylakoid membranes was basically done by the protocol as described (Ido *et al*., 2009): Leaves were homogenized in a blender with the ice-cold buffer 1 (50 mmol Hepes-KOH, pH 7.5, 330 mmol sorbitol, 1 mmol $MgCl_2$, 2 mmol EDTA, 0.05% BSA, 5 mmol sodium ascorbate). The mixture was filtered and centrifuged (2,500 x g, 5 min), and the pellet was resuspended in the buffer 2 (50 mmol Hepes-KOH, pH 7.5, 5 mmol sorbitol). The solution was centrifuged (2,500 x g, 5 min) and the pellet was resuspended in the buffer 3 (50 mmol Hepes-KOH, pH 7.5, 100 mmol sorbitol, 10 mmol $MgCl_2$). The chlorophyll concentration was determined as described by Arnon (1949).

To separate the thylakoid membrane protein complexes, isolated thylakoid membranes were solubilized with MNMβ buffer (25 mmol MES-NaOH, pH 6.0, 10 mmol NaCl, 5 mmol $MgCl_2$, 2 mol betaine, 1% (w/v) *n*-dodecyl-*β*-D-maltoside) and proteins corresponding to 100 μg chlorophyll were loaded on 0.1–1.0 mol sucrose density gradient in MNCβ buffer (25 mmol MES-NaOH, pH 5.7, 10 mmol NaCl, 5 mmol $CaCl_2$, 2 mol betaine, 0.03% (w/v) *n*-dodecyl-*β*-D-maltoside), and ultracentrifuged at 4 °C, 200,000 x g for 28 h. The sucrose density gradient was fractionated, and proteins were separated by SDS-PAGE, transferred to PVDF membranes and immunodetected with anti-D1, plastocyanine, PsbO, PsbP and PsbR antisera, respectively.

To analyze effects of the low-pH and high-NaCl treatment on the PsbP binding, thylakoid membranes were mildly solubilized with 0.05% Triton X-100 and washed with the buffers with various pH (25 mmol MES-NaOH or citrate-NaOH, pH 3.5–6.5, 300 mmol sucrose, 10 mmol NaCl, 5 mmol $MgCl_2$) or the high-NaCl containing buffers (25 mmol MES-NaOH, pH 6.5, 300 mmol sucrose, 0.2–1 mol NaCl, 5 mmol $MgCl_2$), respectively.

Results

Thylakoid protein complexes in wild-type tobacco leaves were solubilized with 1% *n*-dodecyl-*β*-D-maltoside and separated by sucrose density gradient ultracentrifugation in the presence of 2 mol betaine. Betaine was reported to stabilize the association of PsbP and PSII during the solubilization and centrifugation (Eshaghi *et al*., 1999). The gradient was subsequently fractionated and used for SDS-PAGE and immunoblot analysis (Fig. 1).

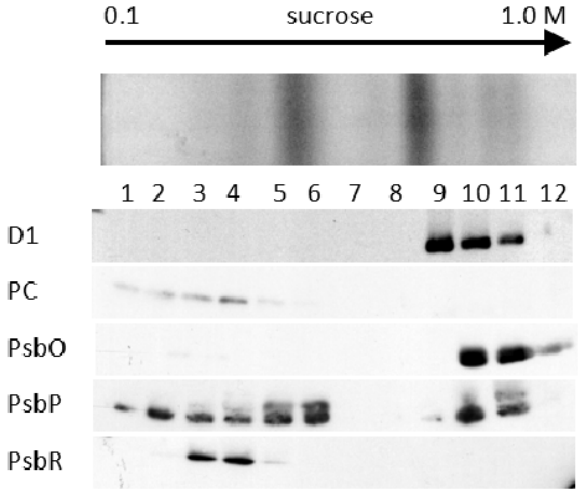

Fig. 1 Analysis of protein complexes in tobacco wild-type thylakoids. Thylakoids of wild-type tobacco leaves were solubilized with 1% *n*-dodecyl-*β*-D-maltoside and protein complexes were separated in 0.1–1.0 mol sucrose density gradient containing 2 mol betaine.

The D1 protein in PSII reaction center was detected mainly in the bottom fractions No. 9–11 that included the PSII core dimer and the PSII-light harvesting complex (LHC) II supercomplexes. The plastocyanine (PC) is a marker for free proteins that are not associated or weakly associated with the protein complexes and was detected in the upper fractions, No. 1–5. The PsbO protein was detected in the fractions No. 10–12, suggesting that most PsbO were associated to the PSII-LHCII supercomplexes in our experimental condition. PsbP was detected both in the upper fractions No. 1–6 and in the bottom fractions No. 10 and 11. PsbP in the bottom fractions was presumably associated with PSII-LHCII supercomplexes, while PsbP in the upper fractions would be a free PsbP pool existing in thylakoid lumen (Hashimoto *et al*., 1996). Some PsbP could be dissociated from PSII during the thylakoid membrane solubilization and centrifugation procedures. Interestingly, PsbR was detected only in the upper fractions No. 3–5, and not detected in the heavier fractions at all. This suggests that the binding of PsbR to PSII was very sensitive to this solubilization and separation procedure and that PsbP can be associated

with the PSII-LHCII supercomplexes without PsbR.

To further analyze the role of PsbR in PsbP binding, thylakoid membranes isolated from Arabidopsis wild-type (Col-0) and Salk T-DNA insertion mutant lacking *PsbR* gene expression (*psbr*) were washed with the buffers with various pH or the buffers containing various concentration of NaCl. It was reported that low-pH and high-NaCl treatments weaken the binding of PsbP and PsbQ to PSII (Kuwabara and Murata, 1983; Ono and Inoue, 1988). When the thylakoids were treated with acidic buffers (pH < 4.5), severer decrease in the amount of PsbP was detected in the *psbr* thylakoid membranes when compared with Col-0 thylakoids (data not shown). Similar observation was obtained when thylakoid membranes were washed by high-NaCl containing buffers (> 0.6 mol). These results suggest that PsbR is not essential for PsbP binding but has a role to stabilize its stable binding to PSII.

Discussion

The sucrose density gradient ultracentrifuge has been widely used to separate the thylakoid membrane protein complexes, while, as far as we know, this is the first report investigating the localization of PsbR in this technique. Although we could not detect PsbR in any PSII complexes, our data clearly suggest that PsbR is not prerequisite for PsbP binding to PSII, at least in the presence of 2 mol betaine. It was reported that PsbR was comigrated with PSII core monomer and CP43 less monomer in blue-native/ SDS 2D-PAGE analysis (Rokka *et al*., 2005). This indicates that PsbR may have an auxiliary role to help the assembly of PsbP during the biogenesis or the repair of the PSII complexes.

The localization of PsbR in the PSII supercomplex is still unknown. PsbR can be detected in PSII-enriched membranes (BBY membranes), but the exact stoichiometry of PsbR in PSII has not been determined. It was reported that tobacco PsbJ knockout plants completely misses PsbP and PsbR, although it accumulates considerable amounts of the PsbO and D1 proteins (Suorsa *et al*., 2006). In cyanobacterial PSII structures, the PsbJ protein is in contact with the cytochrome (Cyt) *b*559 and Cyt *b*559 interacts with the D2 protein (for review, Guskov *et al*., 2010). Therefore, it is probable that PsbR should be located in the D2/Cyt *b*559 side of PSII, and that PsbP may be localized on the lumenal side of those membrane subunits. In consistent with this assumption, recent crosslinking study suggests that PsbP is crosslinked with the Cyt *b*559 ˛ subunit in *Chlamydomonas* PSII (Nagao *et al*., 2010). Further biochemical research to identify the protein that directly interacts with PsbR is required to elucidate the molecular mechanism by which PsbR stabilizes the PsbP binding to PSII.

Acknowledgements

This work was supported partially by the grant from JST PRESTO (to Ke.I.), and by Grant-in-Aid for Young Scientists (B) (grant No. 18770032 to Ke.I.) and by a Research Fellowship for Young Students (Ku I) from JSPS.

References

Arnon DI (1949) Copper Enzymes in Isolated Chloroplast. Polyphenol Oxidase in Beta Vulgaris. Plant Physiol. 24: 1-15

Eshaghi S, Andersson B, Barber J (1999) Isolation of a Highly Active PSII-LHCII Supercomplex from Thylakoid Membranes by a Direct Method. FEBS Lett. 446: 23-26

Guskov A, Gabdulkhakov A, Broser M, Glöckner C, Hellmich J, Kern J, Frank J, Müh F, Saenger W, Zouni A (2010) Recent Progress in the Crystallographic Studies of Photosystem II. Chemphyschem. 11: 1160-1171

Hashimoto A, Yamamoto Y, Theg SM (1996) Unassembled Subunits of the Photosynthetic Oxygen-Evolving Complex Present in the Thylakoid Lumen Are Long-Lived and Assembly-Competent. FEBS Lett. 391: 29-34

Ido K, Ifuku K, Yamamoto Y, Ishihara S, Murakami A, Takabe K, Miyake C, Sato F (2009) Knockdown of the PsbP Protein Does Not Prevent Assembly of the Dimeric PSII Core Complex but Impairs Accumulation of Photosystem II Supercomplexes in Tobacco. Biochim. Biophys. Acta 1787: 873-881

Kuwabara T, Murata N (1983) Quantitative Analysis of the Inactivation of Photosynthetic Oxygen Evolution and the Release of Polypeptide and Manganese in the Photosystem II Particles of

Spinach Chloroplasts. Plant Cell Physiol. 24: 741-747

Liu H, Frankel LK, Bricker TM (2009) Characterization and Complementation of a psbR Mutant in Arabidopsis Thaliana. Arch. Biochem. Biophys. 489: 34-40

Nagao R, Suzuki T, Okumura A, Niikura A, Iwai M, Dohmae N, Tomo T, Shen JR, Ikeuchi M, Enami I (2010) Topological Analysis of the Extrinsic PsbO, PsbP and PsbQ Proteins in a Green Algal PSII Complex by Cross-Linking with a Water-Soluble Carbodiimide. Plant Cell Physiol. 51: 718-727

Nelson N, Yocum CF (2006) Structure and Function of Photosystems I and II. Annu.Rev.Plant.Biol. 57: 521-565

Ono TA, Inoue Y (1988) Discrete Extraction of the Ca Atom Functional for O_2 Evolution in Higher Plant Photosystem II by a Simple Low pH Treatment. FEBS Lett. 277: 146-152

Rokka A, Suorsa M, Saleem A, Battchikova N, Aro EM (2005) Synthesis and Assembly of Thylakoid Protein Complexes: Multiple Assembly Steps of Photosystem II. Biochem.J. 388: 159-168

Seidler A (1996) The Extrinsic Polypeptides of Photosystem II. Biochim.Biophys.Acta 1277: 35-60

Suorsa M, Sirpio S, Allahverdiyeva Y, Paakkarinen V, Mamedov F, Styring S, Aro EM (2006) PsbR, a Missing Link in the Assembly of the Oxygen-Evolving Complex of Plant Photosystem II. J. Biol. Chem. 281: 145-150

Functional Analysis of the Nitrogenase-Like Protochlorophyllide Reductase Encoded in Chloroplast Genome Using Cyanobacterium *Leptolyngbya Boryana*

Haruki Yamamoto[a], Shohei Kurumiya[a], Rie Ohashi[a], Yuichi Fujita[a,b*]

[a]Graduate School of Bioagricultural Sciences, Nagoya University, Nagoya, Japan;
[b]PRESTO, Japan Science and Technology Agency, Saitama, Japan.
[*]Corresponding author. Tel. No. +81 52 789 4105; Fax No. +81 52 789 4107; E-mail: fujita@agr.nagoya-u.ac.jp.

Abstract: Dark-operative protochlorophyllide (Pchlide) reductase (DPOR) is a nitrogenase-like enzyme consisting of two separable components, L-protein (a ChlL dimer) and NB-protein (a ChlN-ChlB heterotetramer), which are structural counterparts of Fe protein and MoFe protein of nitrogenase, respectively. In contrast to the limited distribution of nitrogenase only among prokaryotes, DPOR is distributed among not only photosynthetic prokaryotes but also eukaryotic phototrophs such as green algae, moss, ferns and gymnosperms. While prokaryotic DPORs have been characterized, there has very little study on eukaryotic DPOR functioning in the chloroplast. The three structural genes of DPOR, *chlL*, *chlN* and *chlB*, are encoded by the chloroplast DNA. Recently we have established an *in-vivo* complementation system using mutants lacking DPOR genes of the cyanobacterium *Leptolyngbya boryana* to examine whether DPOR genes are functional. We applied this system to evaluate the probable DPOR genes encoded by the chloroplast DNAs from the moss *Physcomitrella patens* and black pine *Pinus thunbergii*. We discuss the functional operation of DPOR in the chloroplasts of these photosynthetic eukaryotes.

Keywords: Chlorophyll biosynthesis; Dark-operative protochlorophyllide reductase; Chloroplast DNA; *Leptolyngbya boryana*; *Physcomitrella patens*; *Pinus thunbergii*

Introduction

Chlorophyll (Chl) biosynthesis consists of at least 15 enzymatic steps. Protochlorophyllide (Pchlide) reductase catalyzes the stereo-specific reduction of C17 = C18 double bond of Pchlide to produce chlorophyllide *a*, the direct precursor of Chl *a*. There are two structurally unrelated Pchlide reductases; one is light-dependent Pchlide reductase (LPOR) and the other is dark-operative Pchlide reductase (DPOR) (Reinbothe *et al.*, 2010). LPOR is a single polypeptide enzyme belonging short-chain alcohol dehydrogenase/ reductase family and light is required for the catalysis. DPOR is a nitrogenase-like enzyme consisting two separable components, L-protein (a ChlL dimer) and NB-protein (a ChlN-ChlB heterotetramer), which are structural homlogues of Fe protein and MoFe protein of nitrogenase, respectively. DPOR has been characterized in photosynthetic bacteria *Rhodobacter capsulatus* (Fujita and Bauer, 2000; Nomata *et al*., 2005, 2006, 2008) and some cyanobacteria (Yamazaki *et al*., 2006; Yamamoto *et al.*, 2009). The X-ray crystal structures of L-protein (Sarma *et al.*, 2008) and NB-protein (Muraki *et al.*, 2010; Bröcker *et al.*, 2010) have been recently solved. There is a structural framework common between DPOR and nitrogenase (Muraki *et al.*, 2010). Nitrogenase is distributed only among some prokaryotes. In contrast, the distribution of DPOR is wider than nitrogenase from photosynthetic prokaryotes to eukaryotes such as green algae, mosses, ferns and gymnosperms, in which the DPOR genes are encoded in chloroplast DNA (Fujita and Bauer, 2003). Though there have been some papers reporting the greening ability of some gymnosperms by the determination of Chl contents of seedlings grown in the dark (Mariani *et al.*,

1990; Mukai *et al.*, 1991; Kusumi *et al.*, 2006), very little information on the functional operation of chloroplast DPOR has been available so far. Recently we have established an *in-vivo* complementation system using mutants lacking DPOR genes of the cyanobacterium *Leptolyngbya boryana* to examine whether exogenously derived genes encode functional DPOR components (Yamamoto *et al*., 2009). Here we applied this system to evaluate probable DPOR genes encoded by chloroplast DNA from the moss *Physcomitrella patens* and the black pine *Pinus thunbergii*, and we discuss the functional operation of DPOR in the chloroplasts of these photosynthetic eukaryotes.

Materials and Methods

The mutants YFC2 (Δ*chlL*) and YFB14 (Δ*chlB*) of the cyanobacterium *Leptolyngbya boryana* (formerly *Plectonema boryanum*) IAM-M101 strain dg5 were cultivated in BG-11 medium with 15 μg ml^{-1} kanamycin. For transformants with shuttle vectors 10 μg ml^{-1} chloramphenicol was supplemented to the medium. When they were cultivated in the dark, glucose (30 mmol) was supplemented.

To construct L_{Pp}-protein expression vector, the coding region of *chlL* amplified from a PCR fragment LA4 (Sugiura *et al.*, 2003) from the *Physcomitrella patens* chloroplast genome was introduced into the *Sph*I-*Bam*HI sites of pPBHLI18 (Yamamoto *et al.*, 2009) to yield pHBLc3.

To construct NB_{Pp}-protein expression vector, two coding regions of *chlN* and *chlB* were amplified DNA fragment LA4 and LA6 (Sugiura *et al.*, 2003) from the *P. patens* chloroplast genome, respectively. These two amplified fragments were connected by an overlapping sequence of the primers in the second PCR. The amplified *chlN-chlB* fragment was cloned into *Sph*I-*Bam*HI sites of pPBHLI18 (Yamamoto *et al.*, 2009) to yield pHBNB3.

To construct L_{Pt}-protein expression vector, the coding region of *chlL* was amplified from a cDNA clone, which was prepared from total RNA in dark-grown seedlings of *Pinus thubnergii*. The *chlL* gene was introduced into the *Sph*I-*Bam*HI sites of pPBHLI18 (Yamamoto *et al.*, 2009) to yield pHBLc7.

To construct NB_{Pt}-protein expression vector, two coding regions of *chlN* and *chlB* were amplified from cDNA clones as well as *chlL*. The two fragments were connected by the overlapping sequence of the primers in the second PCR. The amplified *chlN-chlB* fragment was cloned into *Sph*I-*Bam*HI sites of pPBHLI18 (Yamamoto *et al.*, 2009) to yield pHBNB7.

In pHBNB3 and pHBNB7 *chlN* and *chlB* were artificially connected to form a small operon for co-expression as described (Yamamoto *et al.*, 2009). All nucleotide sequences of the vectors were verified by sequencing. As positive controls, we used pHBLc2 and pHBNB2, which carry the endogenous cyanobacterial *chlL* and *chlN-chlB*, respectively (Yamamoto *et al.*, 2009).

These plasmids were introduced into the cyanobacterial cells by electroporation (Fujita *et al.*, 1992), and transformants were selected on BG-11 plates containing 30 mmol glucose and 10 μg ml^{-1} chloramphenicol.

Pigments were extracted in 90% methanol from the dark-grown cells of the transformants. Aliquots of the methanol extracts were loaded onto an HPLC column (4.6 × 150 mm Symmetry C8 3.5 μm column; Waters) and separated as described (Zapata *et al.*, 2000). Chl and Pchlide were eluted at 7.9 min and 22.2 min, respectively, and their contents were determined by standard pigments.

Results and Discussion

To clarify the origin of the DPOR components, we designate them with a subscript of the organism, such as L_{Pp}-protein (from *P. patens*) and L_{Pt}-protein (from *P. thunbergii*), adopted in the previous report (Yamamoto *et al.*, 2009). We applied the *in-vivo* complementation system using the cyanobacterial mutants (Yamamoto *et al.*, 2009) to evaluate whether the chloroplast genome-encoded DPOR components from the moss *Physcomitrella patens* and black pine *Pinus thunbergii* are active. Shuttle vectors were constructed to express *chlL* and *chlN-chlB* from *P. patens* and *P. thunbergii* chloroplast DNAs. We constructed four shuttle vectors, pHBLc3, pHBLc7, pHBNB3 and pHBNB7, to express L_{Pp}-protein, L_{Pt}-protein, NB_{Pp}-protein and NB_{Pt}-protein, respectively. The two vectors for L-protein, pHBLc3 and pHBLc7, were introduced into YFC2 resulting in the transformants YFC2/Lc3 and YFC2/Lc7, respectively. The other two vectors for NB-protein, pHBNB3 and pHBNB7, were introduced into YFB14, giving rise to the transformants YFB14/NB3 and YFB14/NB7,

respectively (Table 1).

Table 1 Transformants of *L. boryana* used in this work.

Transformant	Host	Vector	Expressing protein	References
YFC2/H202	YFC2	pPBH202	- [a]	Yamamoto *et al*., 2009
YFC2/Lc2	YFC2	pHBLc2	L_{Lb}-protein	Yamamoto *et al*., 2009
YFC2/Lc3	YFC2	pHBLc3	L_{Pp}-protein	this work
YFC2/Lc7	YFC2	pHBLc7	L_{Pt}-protein	this work
YFB14/H202	YFB14	pPBH202	- [a]	Yamamoto *et al*., 2009
YFB14/NB2	YFB14	pHBNB2	NB_{Lb}-protein	Yamamoto *et al*., 2009
YFB14/NB3	YFB14	pHBNB3	NB_{Pp}-protein	this work
YFB14/NB7	YFB14	pHBNB7	NB_{Pt}-protein	this work

[a] empty vector.

These transformants were cultivated heterotrophically in the dark to examine how much amounts of Chl is produced by DPOR (Fig. 1). As previously shown (Yamamoto *et al.*, 2009), the transformants YFC2/Lc2 and YFB14/NB2, expressing the endogenous cyanobacterial L_{Lb}-protein and NB_{Lb}-protein (from *L. boryana*), respectively, restored the ability to produce Chl in the dark (Fig. 1, columns 2 and 5). Significant amounts of Chl were contained in both transformants, YFC2/Lc3 and YFB14/NB3, expressing L_{Pp}-protein and NB_{Pp}-protein from *P. patens* (Fig. 1, columns 3 and 6), suggesting that both components of *P. patens* have the ability to form active DPOR complexes with the endogenous complements. Since *P. patens* does not have the ability to grow heterotrophically in the dark, it is difficult to examine whether DPOR of *P. patens* is active from Chl content. This heterologous *in-vivo* complementation system provided firm evidence for the functionality of DPOR of *P. patens*.

The transformant YFC2/Lc7 also contained significant amount of Chl though the Pchlide content was still as high as the control YFC2/H202 (Fig. 1, column 4). This partial complementation would result from low content of L_{Pt}-protein. The codon usage of the chloroplast DNAs of *P. thubergii* is highly AT-rich, which would not be suitable for efficient expression of the *chlL* gene in the cyanobacterium cells. This result suggested that the L_{Pt}-protein is functional to form an active heterologous complex with the NB_{Lb}-protein.

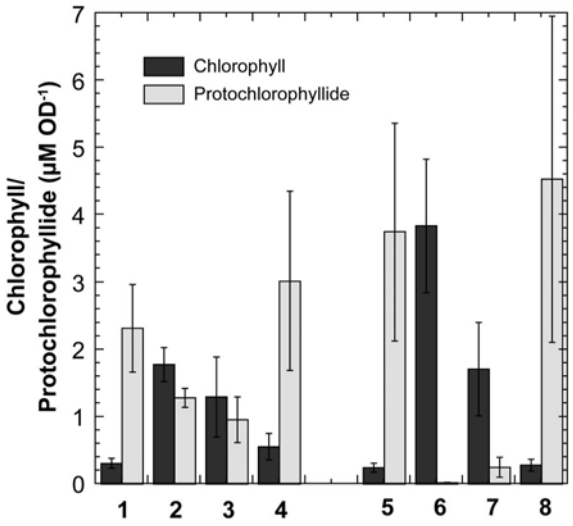

Fig. 1 Chl and Pchlide contents of the dark-grown transformants. The transformants, YFC2/H202 (column 1), YFC2/Lc2 (column 2), YFC2/Lc3 (column 3), YFC2/Lc7 (column 4), YFB14/H202 (column 5), YFB14/NB2 (column 6), YFB14/NB3 (column 7) and YFB14/NB7 (column 8). Chl (dark gray) and Pchlide (light gray) were determined by HPLC analysis of the methanol extracts.

In contrast, YFB14/NB7 accumulated Chl as little as the control YFB14/H202 (Fig. 1, column 8). The ChlB protein from *P. thunbergii* was detected by the anti-ChlB antiserum as well as the ChlB protein from *P. patens* in Western blot analysis (data not shown). This result is apparently inconsistent with the observation that seedlings of *P. thunbergii* produce Chl in the dark (Mariani *et al.*, 1990). There are two probable reasons. One is that NB_{Pt}-protein does not form an active complex with L_{Lb}-protein, though the sequence identities between ChlNs and ChlBs in the two organisms are considerably high (69% in ChlN and 65% in ChlB; Fujita, 1996). In nitrogenase complex, most heterologous combinations between Fe protein and MoFe protein are catalytically active. However, Fe protein from *Clostridium pasteurianum* forms an inactive tight complex with MoFe protein from *Azotobacter vinelandii* (Jacobson *et al*., 1990). It would be probable that NB_{Pt}-protein form an inactive complex with the cyanobacterial L_{Lb}-protein.

The other reason is the involvement of RNA editing in the *chlB* mRNA. In *P. sylvestris*, two cytosines of the two codons, CCA and CGG, in the *chlB* mRNA are converted to urasils (CUA and UGG) by RNA editing, altering the amino acid residues from Pro and Arg to Leu and Trp, respectively (Karpinska *et al.*, 1997). These codons CCA (Pro207) and CGG (Arg214) are also conserved in *P. thunbergii*. Even though the *chlB* gene was amplified from a cDNA

clone, the nucleotide sequence of *chlB* in pHBNB7 was confirmed to be remained unedited. The two amino acid residues, Leu and Trp, are conserved among all ChlBs encoded by chloroplast DNA except for those from coniferous plants. Demko *et al*. (2009) demonstrated that RNA editing in *chlB* plays an important role for DPOR activity in dark-grown seedlings in *Larix decidua* and *Picea abies*. Thus, such RNA editing would occur in the chloroplast of *P. thunbergii* to convert the *chlB* mRNA to encode an active ChlB protein and both amino acid residues Leu207 and Trp214 in ChlB would be critical for the DPOR activity. To confirm this hypothesis, we are now in progress to examine whether transformants with shuttle vectors expressing site-directed mutants ChlB of Pro207Leu and Arg214Trp restore the Chl biosynthesis in the dark of YFB14.

In this work we confirmed the activity of a nitrogenase-like enzyme encoded by chloroplast DNA from *P. patens* for the first time using the cyanobacterial *in-vivo* complementation system. Both components of *P. patens* form active DPOR complexes with the cyanobacterial complements. Though the NB_{Pt}-protein from *P. thubergii* and the cyanobacterial L_{Lb}-protein seems not to form an active DPOR complex, this observation would lead us further experiments for deeper understanding of chloroplast DPOR.

Acknowledgements

We thank Mamoru Sugita (Nagoya University) and Junko Kusumi (Kyushu University) for kindly donating the PCR fragments carrying the *chlL*, *chlN* and *chlB* genes from *P. patens* and cDNA clones of *chlL*, *chlN* and *chlB* from *P. thubergii*, respectively.

References

Bröcker MJ, Schomburg S, Heinz DW, Jahn D, Schubert WD, Moser J (2010) Crystal Structure of the Nitrogenase-Like Dark Operative Protochlorophyllide Oxidoreductase Catalytic Complex $(ChlN/ChlB)_2$. J. Biol. Chem. 285: 27336-27345

Demko V, Pavlovic A, Valková D, Slováková L, Grimm B, Hudák J (2009) A Novel Insight into the Regulation of Light-Independent Chlorophyll Biosynthesis in Larix Decidua and Picea Abies Seedlings. Planta 230: 165-176

Fujita Y (1996) Protochlorophyllide Reduction: a Key Step in the Greening of Plants. Plant Cell Physiol. 37: 411-421

Fujita Y, Bauer CE (2000) Reconstitution of Light-Independent Protochlorophyllide Reductase from Purified BchL and BchN-BchB Subunits: in Vitro Confirmation of Nitrogenase-Like Features of a Bacteriochlorophyll Biosynthesis enzyme. J. Biol. Chem. 275: 23583-23588

Fujita Y, Bauer CE (2003) The Light-Independent Protochlorophyllide Reductase: A Nitrogenase-Like Enzyme Catalyzing a Key Reaction for Greening in the Dark. In: Kadish KM, Smith KM, Guillard R (eds.), Porphyrin Handbook, Vol. 13. Academic Press: Oxford, UK, pp. 109-156

Fujita Y, Takahashi Y, Chuganji M, Matsubara H (1992) The nifH-Like (frxC) Gene Is Involved in the Biosynthesis of Chlorophyll in the Filamentous Cyanobacterium Plectonema Boryanum. Plant Cell Physiol. 33: 81-92

Karpinska B, Karpinski S, Hällgren J (1997) The chlB Gene Encoding a Subunit of Light-Independent Protochlorophyllide Reductase Is Edited in Chloroplasts of Conifers. Curr. Genet. 31: 343-347

Kusumi J, Sato A, Tachida H (2006) Relaxation of Functional Constraint on Light-Independent Protochlorophyllide Oxidoreductase in Thuja. Mol. Biol. Evol. 23: 941-948

Mariani P, Carli M, Rascio N, Baldan B, Casadoro G, Gennari G, Bodner M, Larcher W (1990) Synthesis of Chlorophyll and Photosynthetic Competence in Etiolated and Greening Seedlings of Larix Decidua as Compared with Picea Abies. J. Plant Physiol. 137: 5-14

Mukai Y, Yamamoto N, Koshiba T (1991) Light-Independent and Tissue-Specific Accumulation of Light-Harvesting Chlorophyll a/b Binding Protein and Ribulose Bisphosphate Carboxylase in Dark-Grown Pine Seedlings. Plant Cell Physiol. 32: 1303-1306

Nomata J, Kitashima M, Inoue K, Fujita Y (2006) Nitrogenase Fe-protein-Like Fe-S Cluster Is Conserved in L-Protein (BchL) of Dark-Operative Protochlorophyllide Reductase from Rhodobacter Capsulatus. FEBS Lett. 580: 6151-6154

Nomata J, Ogawa T, Kitashima M, Inoue K, Fujita Y (2008) NB-Protein (BchN-BchB) of Dark-

Operative Protochlorophyllide Reductase Is the Catalytic Component Containing Oxygen-Tolerant Fe-S Clusters. FEBS Lett. 582: 1346-1350

Nomata J, Swem LR, Bauer CE, Fujita Y (2005) Overexpression and Characterization of Dark-Operative Protochlorophyllide Reductase from Rhodobacter Capsulatus. Biochim. Biophys. Acta 1708: 229-237

Reinbothe C, El Bakkouri M, Buhr F, Muraki N, Nomata J, Kurisu G, Fujita Y, Reinbothe S (2010) Chlorophyll Biosynthesis: Spotlight on Protochlorophyllide Reduction. Trends Plant Sci. 15: 614-624

Sarma R, Barney B, Hamilton T, Jones A, Seefeldt L, Peters J (2008) Crystal Structure of the L Protein of Rhodobacter Sphaeroides Light-Independent Protochlorophyllide Reductase with MgADP Bound: a Homologue of the Nitrogenase Fe Protein. Biochemistry 47: 13004-13015

Sugiura C, Kobayashi Y, Aoki S, Sugita C, Sugita M (2003) Complete Chloroplast DNA Sequence of the Moss Physcomitrella Patens: Evidence for the Loss and Relocation of rpoA from the Chloroplast to the Nucleus. Nucleic Acids Res. 31: 5324-5331

Yamamoto H, Kurumiya S, Ohashi R, Fujita Y (2009) Oxygen Sensitivity of a Nitrogenase-Like Protochlorophyllide Reductase from the Cyanobacterium Leptolyngbya Boryana. Plant Cell Physiol. 50: 1663-1673

Yamazaki S, Nomata J, Fujita Y (2006) Differential Operation of Dual Protochlorophyllide Reductases for Chlorophyll Biosynthesis in Response to Environmental Oxygen Levels in the Cyanobacterium Leptolyngbya Boryana. Plant Physiol. 142: 911-922

Zapata M, Rodoriguez R, Garrido JL (2000) Separation of Chlorophylls and Carotenoids from Marine Phytoplankton:a New HPLC Method Using a Reversed Phase C8 Column and Pyridine-Containing Mobile Phases. Mari.-Ecol.-Prog. Ser. 195: 29-45

Solution Structure and Physiological Requirements for Psb27 in *Synechocystis* sp. PCC 6803

Peter D Mabbitt [1], Gilles J Rautureau [2], Catherine L Day[1], Mark G Hinds[2],
Sigurd M Wilbanks[1], Julian J Eaton-Rye[1,*]

[1] Department of Biochemistry, University of Otago, Dunedin 9054, New Zealand;
[2] Walter and Eliza Hall Institute of Medical Research, Parkville 3052, Australia.
*Corresponding author. Tel. No. +64 3 479-7865; Fax No. +64 3 479-7866; E-mail: julian.eaton-rye@otago.ac.nz.

Abstract: Photosystem II (PS II) is a membrane-embedded protein complex that has a highly regulated assembly pathway. A number of proteins that interact transiently with PS II have been identified. One of these proteins, Psb27, is a cyanobacterial lipoprotein that binds to inactive PS II monomers and is involved in the biogenesis of the active PS II dimer. We have solved the solution structure of Psb27 and have identified a group of conserved residues that potentially form an interaction with PS II [Mabbitt PD, Rautureau GJP, Day CL, Wilbanks SM, Eaton-Rye JJ, Hinds MG (2009) Biochemistry 48: 8771-8773]. Despite the conservation of Psb27 across plants and cyanobacteria, ΔPsb27 *Synechocystis* sp. PCC 6803 cells lack a phenotype when grown under standard laboratory conditions. To assess Psb27 function, we have identified conditions where the ΔPsb27 mutant cannot grow photoautotrophically.

Keywords: Assembly; Biogenesis; Photosystem II; Psb27; Structure; Photoinactivation

Introduction

Photosystem II (PS II) is a multiprotein, membrane-embedded complex that catalyses water oxidation. Many proteins bind transiently to the lumen exposed regions of PS II and enhance its function. In cyanobacteria the PsbO, U and V proteins bind to the lumenal side of PS II and to varying degrees enhance the oxygen-evolving activity of PS II. The core D1 protein of PS II is subject to damage and repair. During the repair cycle, the PsbO, U and V proteins are released whilst a new D1 peptide is co-translationally incorporated into the PS II complex (reviewed in Nixon *et al*., 2010). The Psb27 protein binds to PS II complexes containing newly formed D1 protein (Roose and Pakrasi, 2004; Nowaczyk *et al*., 2006). Although not active in photosynthesis, this Psb27-bound complex is a key intermediate in the PS II assembly cycle. Deletion of *psb27* in *Synechocystis* sp. PCC 6803 has been shown to impair manganese cluster assembly, further supporting a role for Psb27 in PS II biogenesis (Roose and Pakrasi, 2007). Two Psb27 homologues have been identified in the higher plant *Arabidopsis thaliana.* The first homologue (Psb27-H1) was shown to be involved in PS II's recovery from photodamage (Chen *et al*., 2006), whilst removal of the second homologue (Psb27-H2) resulted in a marked reduction in PS II abundance (Wei *et al*., 2010).

We have solved the solution structure of cyanobacterial Psb27 and identified conserved features on the surface of the protein that may be important for its interaction with PS II (Mabbitt *et al*., 2009). These residues represent initial targets for site-directed mutagenesis designed to elucidate the mechanistic role of Psb27 in PS II turnover. To assess Psb27's function, we have identified growth conditions where our ΔPsb27 strain of *Synechocystis* sp. PCC 6803 cannot support photoautotrophic growth.

Materials and Methods

Synechocystis sp. PCC 6803 cultures were maintained

on BG-11 plates containing 5 mmol glucose, 20 μM atrazine, 10 mmol TES-NaOH (pH 8.2), 0.3% (w/v) sodium thiosulfate and appropriate antibiotics. Chloramphenicol was present at 15 μg/mL in both solid and liquid culture. Liquid cultures were grown photoautotrophically in BG-11 or calcium-limiting BG-11. In the case of calcium-limiting BG-11, 0.24 nmol $CaCl_2$ was replaced by 0.48 nmol NaCl. Cultures were maintained at 30 °C at light intensities of 40 or 150 μE m^{-2} s^{-1}. The glucose tolerant strain of *Synechocystis* sp. PCC 6803 (Williams, 1988) is referred to as wild type and the *psb27* interruption strain is referred to as ΔPsb27 (Bentley *et al*., 2008).

For multiple sequence alignments, sequences were accessed from the NCBI database and aligned using Clustal-W (Larkin *et al*., 2007). Signal sequences were identified using DOLOP (Madan Babu and Sankaran, 2002; Madan Babu *et al*., 2006); for *A. thaliana* Psb27-H1 the signal sequence was identified experimentally by Peltier *et al.* (2002). For the *A. thaliana* H-2 Psb27, residues 92 to 199 were aligned as no signal sequence has been identified.

Results and Discussion

The photautotrophic growth of wild type and ΔPsb27 *Synechocystis* sp. PCC 6803 in calcium-limiting BG-11 was compared under conditions of constant illumination at 40 or 150 μE m^{-2} s^{-1}. The photoautotrophic doubling times of wild type and ΔPsb27 cells were similar in calcium-limiting BG-11 when illuminated at 40 μE m^{-2} s^{-1}. When the illumination was increased to 150 μE m^{-2} s^{-1} ΔPsb27 cells were not able to support photoautotrophic growth (Fig. 1).

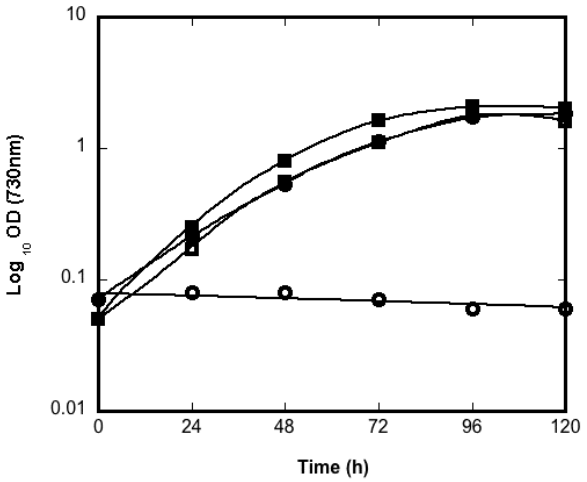

Fig. 1 Photoautotrophic growth of the wild type and the ΔPsb27 strains of *Synechocystis* sp. PCC 6803 in calcium-limiting media under continuous illumination at 40 or 150 μE $m^{-2}s^{-1}$. Wild type at 40 μE $m^{-2}s^{-1}$ (filled squares), wild type at 150 μE $m^{-2}s^{-1}$ (empty squares), ΔPsb27 at 40 μE $m^{-2}s^{-1}$ (filled circles) and ΔPsb27 at 150 μE $m^{-2}s^{-1}$ (empty circles).

No such failure to grow was observed for cultures in calcium-sufficient BG-11 under any illumination condition (data not shown).

The inability of the ΔPsb27 strain to grow under conditions of calcium limitation and moderately high illumination are consistent with Psb27 being involved in the assembly of the oxygen-evolving complex (Roose and Pakrasi, 2007) and the repair of PS II after photodamage (Chen *et al*., 2006; Bentley *et al*., 2008).

Previously the sequences of higher plant and cyanobacterial Psb27 homologues were aligned and the positions of conserved residues were mapped onto the *Synechocystis* sp. PCC 6803 Psb27 NMR structure (Mabbitt *et al*., 2009). The discovery of a second *A. thaliana* homologue by Wei and colleagues in 2010 has allowed this analysis to be extended further.

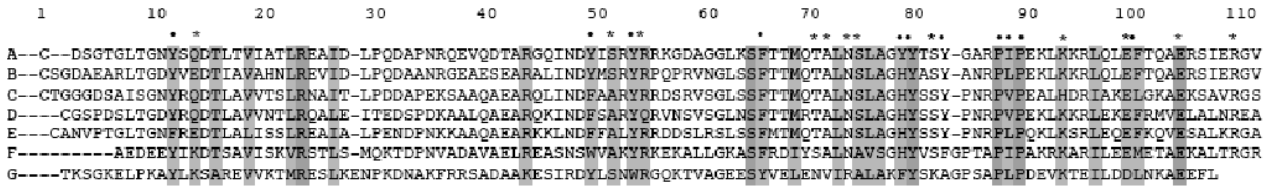

Fig. 2. Alignment of representative Psb27 sequences from cyanobacteria with those of *A. thaliana* Psb27 homologues 1 and 2. Invariant residues and conservative substitutions are highlighted in grey. Aromatic residues and the PϕP motif identified as conserved amongst cyanobacterial and higher plant Psb27-H1 homologues are indicated with dots. Similarly conserved surface residues identified in the NMR structure of Psb27 are indicated with stars (Mabbitt *et al*., 2009). Psb27 sequences (accession codes in brackets): (A) *Synechocystis* sp. PCC 6803 (P74367), (B) *Synechococcus* sp. WH8102 (Q7U5D5), (C) *Synechococus elongatus* PCC 7942 (Q31RE4), (D) *Anabaena variabilis* PCC 7937 (Q3MFN4), (E) *Thermosynechococcus elongatus* BP1 (Q8DG60), (F) *A. thaliana* Psb27-H1 (Q9LR64), and (G) *A. thaliana* Psb27-H2 (AAk4057) aligned using Clustal-W.

Fig. 2 shows a multiple sequence alignment of representative cyanobacterial Psb27 sequences with those of the two *A. thaliana* homologues. The *A. thaliana* Psb27-H1 protein shares more sequence similarities with the cyanobacterial Psb27 proteins than does the H2 homologue. However, both the *A. thaliana* H1 and H2 Psb27 homologues retain the highly conserved aromatic residues at positions 11,49,53,65,78 & 79 as well as the PϕP (where ϕ is I, L or V) motif at positions 86-88. The aromatic residues are present in the hydrophobic core of the *Synechocystis* sp. PCC 6803 NMR structures of Psb27 (Cormann *et al*., 2009; Mabbitt *et al*., 2009). The conservation of these residues suggests that the H2 homologue retains the helical-bundle fold of the cyanobacterial Psb27 but may have acquired new binding partners.

Several surface exposed residues that are highly conserved between cyanobacterial and higher plant Psb27-H1 homologues were identified in the solution structure of Psb27 (Mabbitt *et al*., 2009) (Fig. 3). These residues may be important to Psb27's function. A group of conserved, polar charged and uncharged residues on the surface of helices 3 and 4 (R54, T70, N73, S74, Y78, S81, Y82, R94, E98) may provide an interface for interaction with PS II. Of these conserved residues on helices 3 and 4 only 4 of the 9 are retained in the *A. thaliana* H2 homologue. Changes in these surface residues (Figs. 2 and 3) likely contribute to the differential functions of homologue H1 and H2 (Wei *et al.*, 2010).

We have shown that Psb27 is required for photoautotrophic growth of *Synechocystis* sp. PCC 6803 under conditions of moderate (150 μE m^2 s^{-1}) illumination and calcium limitation. This demonstrates that Psb27 could have been under strong evolutionary selection in some environments, supporting our assumption that residues conserved in Psb27 of different species are likely crucial in PS II biogenesis or repair. We have identified a number of surface exposed residues in the solution structure of Psb27 that are conserved between cyanobacteria and higher plant Psb27-H1 (Mabbitt *et al*., 2009). The majority of these residues are present on helices 3 and 4 of Psb27, and form a polar surface that potentially interacts with PS II.

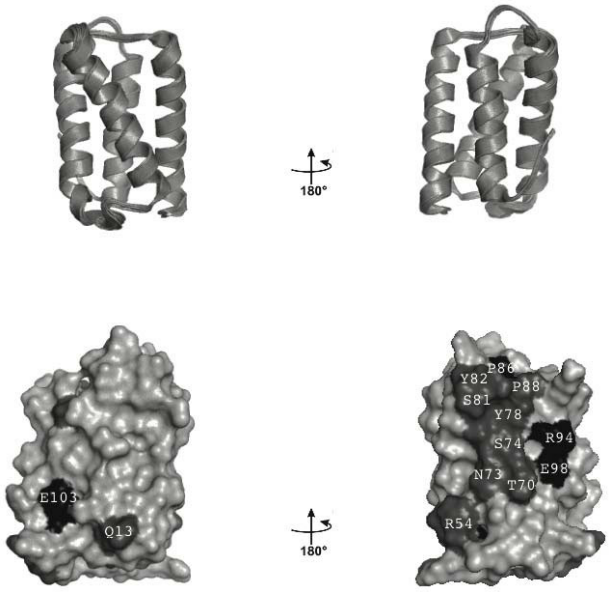

Fig. 3 Top: Ribbon diagram of the solution structure of *Synechocystis* sp. PCC 6803 Psb27. Bottom: Surface view of Psb27, residues highly conserved (dark grey) and invariant (black) amongst cyanobacteria and higher plant H1 Psb27 sequences are indicated.

Acknowledgements

This work was supported by a Marsden Grant 08-UOO-043 to JJ E-R PD M was supported by an Otago University postgraduate scholarship.

References

Bentley FK, Luo H, Dilbeck P, Burnap RL, Eaton-Rye JJ (2008) Effects of Inactivating psbM and psbT on Photodamage and Assembly of Photosystem II in Synechocystis sp. PCC 6803. Biochemistry 47: 11637-11646

Chen H, Zhang D, Guo J, Wu H, Jin M, Lu Q, Lu C, Zhang L (2006) A Psb27 Homologue in Arabidopsis Thaliana Is Required for Efficient Repair of Photodamaged Photosystem II. Plant Mol. Biol. 61: 567-575

Cormann KU, Bangert JA, Ikeuchi M, Rögner M, Stoll R, Nowaczyk MM (2009) Structure of Psb27 in Solution: Implications for Transient Binding to Photosystem II during Biogenesis and Repair. Biochemistry 48: 8768-8770

Larkin MA, Blackshields G, Brown NP, Chenna R, McGettigan PA, McWilliam H, Valentin F, Wallace IM, Wilm A, Lopez R, Thompson JD, Gibson TJ, Higgins DG (2007) Clustal W and Clustal X Version 2.0. Bioinformatics 23: 2947-2948

Mabbitt PD, Rautureau GJ, Day CL, Wilbanks SM, Eaton-Rye JJ, Hinds MG (2009) Solution Structure of Psb27 Form Cyanobacterial Photosystem II. Biochemistry 48: 8771-8773

Madan Babu M, Sankaran K (2002) DOLOP—Database of Bacterial Lipoproteins. Bioinformatics 18: 641-643

Madan Babu M, Priya ML, Selvan AT, Madera M, Gough J, Aravind L, Sankaran K (2006) A Database of Bacterial Lipoproteins (DOLOP) with Functional Assignments to Predicted Lipoproteins. J. Bacteriol. 188: 2761-2773

Nixon PJ, Michoux F, Yu J, Boehm M, Komenda J(2010) Recent Advances in Understanding the Assembly and Repair of Photosystem II. Ann, Bot. 106: 1-16

Nowaczyk MM, Hebeler R, Schlodder E, Meyer HE, Warscheid B, Rögner M (2006) Psb27, a Cyanobacterial Lipoprotein, Is Involved in the Repair Cycle of Photosystem II. Plant Cell 18: 3121-3131

Peltier JB, Emanuelsson O, Kalume DE, Ytterberg J, Friso G, Rudella A, Liberles DA, Soderberg L, Roepstorff P, von Heijne G, van Wijk KJ (2002) Central Functions of the Lumenal and Peripheral Thylakoid Proteome of Arabadopsis Determined by Experimentation and Genome-Wide Prediction. Plant Cell 14: 211-236

Roose JL, Pakrasi HB (2004) Evidence that D1 Processing Is Required for Manganese Binding and Extrinsic Protein Assembly into Photosystem II. J. Biol. Chem. 279: 45417-45422

Roose JL, Pakrasi HB (2007) The Psb27 Protein Facilitates Manganese Cluster Assembly in Photosystem II. J. Biol. Chem. 283: 4044-4050

Wei L, Guo J, Ouyang M, Sun X, Ma J, Chi W, Lu C, Zhang L (2010) LPA19, a Psb27 Homolog in Arabidopsis Thaliana, Facilitates D1 Protein Precursor Processing during PSII Biogenesis. J. Biol. Chem. 285: 21391-21398

Williams JGK (1988) Construction of Specific Mutations in the Photosystem II Photosynthetic Reaction Center by Genetic Engineering Methods in the Cyanobacterium Synechocystis 6803. Methods Enzymol. 167: 766-778

Isolation of Complete Chloroplasts from *Chromera Velia* — the Photosynthetic Relative of Parasitic Apicomplexa

Hao Pan[a], Jan Šlapeta[b], Dee Carter[c], Min Chen[a*]

[a] School of Biological Sciences, Faculty of Sciences, University of Sydney, NSW 2006, Australia;
[b] Veterinary Parasitology, Faculty of Veterinary Science, University of Sydney, NSW 2006, Australia;
[c] Discipline of Microbiology, School of Molecular Biosciences, University of Sydney, NSW 2006, Australia.
[*]Corresponding author. E-mail: m.chen@usyd.edu.au.

Abstract: The recently discovered photosynthetic alga *Chromera velia* is closely related to nonphotosynthetic apicomplexan parasites and photosynthetic dinoflagellates. Previous research has revealed features that are shared between the chloroplast of *C. velia* and the apicoplast in apicomplexan parasites. We have developed a practical method to harvest complete chloroplasts from *C. velia* to enable characterisation of their metabolic and photosynthetic capacity.

Keywords: Chloroplasts isolation; Bead beater; *Chromera velia*; Sucrose gradient

Introduction

Malaria is one of the most dangerous diseases that humans have encountered, infecting 500 million people annually (Sachs and Malaney, 2002). *Plasmodium*, the malaria parasite, together with more than 5,000 other parasites, belongs to the phylum Apicomplexa. Apicomplexan parasites contain a non-photosynthetic relic plastid termed the apicoplast (McFadden *et al*., 1996). The apicoplast is essential for various metabolic pathways, particularly fatty acid, isoprenoid, heme and iron-sulfur cluster biosynthesis (Lim and McFadden, 2010). As plastids do not occur in animals, chemicals and drugs that targeting the apicoplast can be used to kill apicomplexan parasites without interfering with the host.

A virtual metabolic map of the apicoplast of *Plasmodium* (the causative agent of malaria) has been proposed based on draft genomes of several apicomplexan species (Ralph *et al*., 2004). However, confirmation of the virtual map awaits isolation and characterisation of this minute membrane bound organelle. Although apicomplexan parasites are related to photosynthetic dinoflagellates and the plastids of both organisms are proposed to have evolved through secondary endosymbiosis (Cavalier-Smith, 1999; Janouskovec *et al*., 2010), the plastid genomes differ vastly. All genes related to photosynthesis have been lost from the apicoplast genome, while the plastid genome in dinoflagellates has been fragmented into many small mini-circles containing some of the photosynthesis genes (Zhang *et al*., 1999; Nisbet *et al*., 2008). Other genes usually located in the chloroplasts have migrated to the nucleus (Nisbet *et al*., 2008). The dinoflagellate plastid genes are so divergent that comparative studies based on their sequences inevitably yield inconsistent results.

Chromera velia is a photosynthetic alga that was recently discovered in Sydney Harbour (Moore *et al*., 2008). It is thought to be the most closely related free living organism to the parasitic apicomplexa while bearing a photosynthetically functional chloroplast (Obornik *et al*., 2009). The chloroplast of *C. velia* is surrounded by four membranes, and the cell plasma membrane is supported by cortical alveoli, which are morphological characteristics common to dinoflagellates and apicomplexans (Moore *et al*., 2008). Use of a noncanonical genetic code for tryptophan is further evidence that the *C. velia* plastid is closely related to

the apicoplast (Obornik *et al*., 2009). Sequence analysis of the nuclear-encoded plastid-targeted glyceraldehyde-3-phosphate dehydrogenase (GAPDH) gene and the small and large subunit rRNA genes likewise confirmed the affinity of the *C. velia* plastid with the apicoplast (Moore *et al*., 2008; Takishita *et al*., 2009). Finally, sequencing of the plastid genome found this contains most of the genes present in dinoflagellates plastids and apicoplasts, and also found *C. velia* plastids share form II Rubisco genes and mRNA polyuridylylation with dinoflagellates, apicomplexans and heterokont plastids (Janouskovec *et al*., 2010).

These studies indicate that understanding the properties and features of the *C. velia* plastid will help us to understand the evolutionary development of heterotrophic and photoautotrophic metabolism. However, *C. velia* cells have a thick cell wall and a cyst wall layer that impede cell disruption (Obornik *et al*., 2010). In order to study the physiological details of the *C. velia* plastid it is necessary to obtain complete and functional chloroplasts. Here we report a practical method to isolate chloroplasts from *C. velia*.

Materials and Methods

C. velia cells were grown for ~3 weeks under 20 μE white illumination (24 h light) on a slow rocking platform (100 rpm) in K+ES medium (Keller *et al*., 1987; West *et al*., 1999). An approximately 5 g pellet (from 1 L culture) was used for each preparation. Cells were harvested by centrifugation at 7,000 x g for 10 min (JA-17, Beckman), resuspended in buffer A: 50 mmol MES (pH 6.2), 2 mmol $CaCl_2$, 2 mmol $MgCl_2$ and centrifuged at 2,500 x g for 5 min (Labofuge 400R, Heraeus).

Cells were then resuspended in 2 ml enzyme mixture solution (containing 5 mg/ml cellulase (Yakult Honsha, Cat.NO.203016), 1 mg/ml macerase (Calbiochem Behring Diagnostics, Cat.NO. 441201), 1 mg/ml lysozyme (Boehringer Mannheim GmbH, Cat.NO. 107255), 0.005% Tween20 and 5 mg/ml dextran dissolved in Buffer A) and mixed on a rotating plate (~100 rpm) at room temperature in the dark for 30 min.

The cell lysis mixture was diluted with buffer A to give a total volume of 10 ml and mixed with fresh chemicals: 1 mmol PMSF and 1 mmol EDTA, 5 mmol DTT in the final mixture and an equal volume of silica beads (diameter of 0.1 mm, Biospec, Cat.No. 11079-101). Cells were further broken using a Bead-beater (Biospec) with 5 sec blending followed by a break of several minutes on ice, with the cycle repeated 20 times. The cell-bead mixture was centrifuged at 500 x g for 2 min to remove the beads, unbroken cells and large debris, and the supernatant was loaded directly onto a sucrose density gradient (density steps (w/v): 35%, 50% and 68.5% sucrose in buffer A with 0.005% Tween20). This gradient was centrifuged at 4,000 x g, 4 ^{o}C for at least 2 h to separate the cell organelles based on their size and density.

Results and Discussion

Three green bands were resolved from the sucrose density gradient after two hours centrifugation (Fig. 1a). Microscopy of the different bands indicated that band 3, located between the 50% and 68.5% sucrose layers, contained the most intact green chloroplasts (Fig. 1b).

To test the isolated chloroplasts and their properties, several experiments were undertaken, including 77 k low temperature excitation and emission fluorescence spectra (Fig. 2a) and SDS-PAGE (Fig. 2b).

To characterize the pigment protein complexes in the isolated chloroplasts, fluorescence emission spectra (excited at 435 nm) and fluorescence excitation spectra (emission at 685 nm and 710 nm respectively) of band 3 were performed in liquid nitrogen (77 k) (Fig. 2a). Two fluorescence emission peaks centred at 685 nm and 710 nm (excited at 435 nm) were seen, which originated from PSII and PSI respectively. The functional chlorophyll-binding light-harvesting protein complexes in the isolated chloroplasts were observed in excitation fluorescence spectra (a shoulder of 675 nm with emission at 685 nm and a clear 675 nm peak with emission at 710 nm). This is in good agreement with the analysis using SDS-PAGE (Fig. 2b), which found band 3 contains CP43 and CP47, PSII subunits (~ 30 kDa), and LHC subunits (~ 20–25 kDa). PSI subunits (~ 65 kDa) could not be seen, which may be due to degradation of the isolated chloroplasts during sample treatment for SDS-PAGE electrophoresis, resulting in a band of unknown proteins at ~ 17 kDa. A band was seen at the top of the SDS gel that possibly resulted from un-denatured pigment-protein complexes of PSI and PSII

supermolecules. If so, this indicates that only a fraction of the PS subunits were solubilised by the SDS denaturing treatment described above, suggesting a higher concentration of SDS or longer denaturation treatment is required.

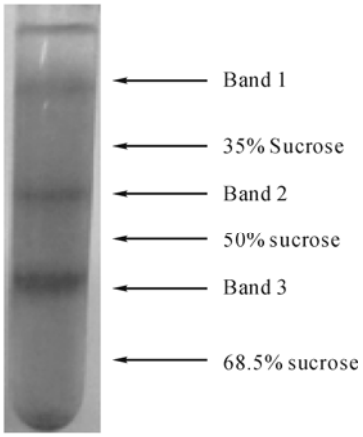

(1a)

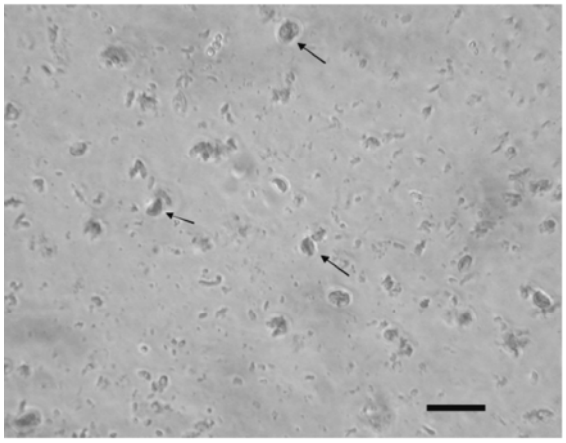

(1b)

Fig. 1 Using step sucrose density gradient to extract chloroplasts from *C. velia.*

(1a) Sucrose density gradient after centrifugation, showing three distinct bands;

(1b) Light microscopy analysis of band 3. Arrows indicate the intact green chloroplasts. Scale bar, 40 um.

In general, the results of microscopy (Fig. 1b), low temperature fluorescence spectra (Fig. 2a) and SDS-PAGE (Fig. 2b) proved that a set of photosystems (including PSI, PSII and LHCs) occur in the isolated chloroplasts that were resolved in band 3. This suggests that the method reported here is capable of isolating intact chloroplasts from *C. velia*, although more refined analyses are required, such as oxygen evolution rate measurement and improved SDS-PAGE.

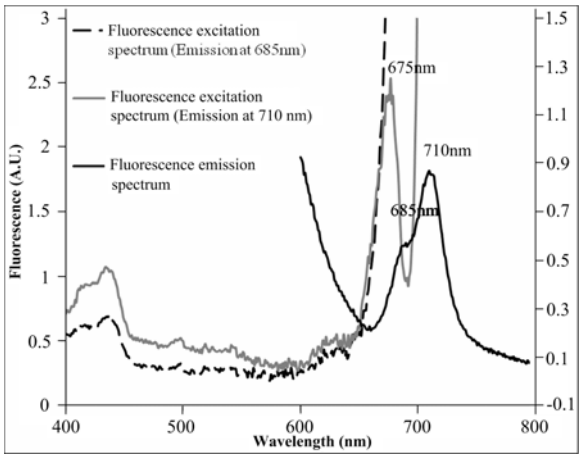

(a)

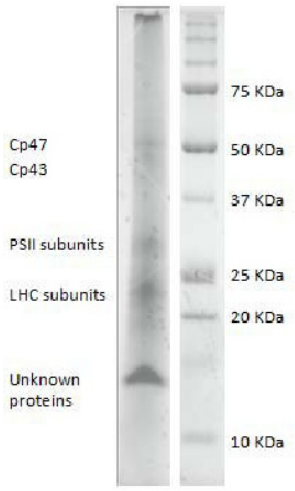

(b)

Fig. 2 Analysis of the isolated chloroplasts.

(2a) Low temperature (77k) fluorescence emission/excitation spectra of isolated chloroplasts. The fluorescence emission spectrum was excited at 435 nm (solid black line). Fluorescence excitation spectra were emitted at 685 nm (dashed line) and 710 nm (grey line);

(2b) SDS-PAGE showing proteins and complexes extracted from isolated chloroplasts of *C. velia.* Left lane, proteins from extracted band 3; Right lane, reference ladder.

Acknowledgements

MC holds an ARC QEII Fellow and thanks the Australian Research Council for support. We thank Prof. Tony Larkum for accessing the *C. velia* culture and helpful discussion throughout project. This project was partially supported by ARC Discovery Grant DP0986372 to DC and JS Thanks to Dr. Ray Ritchie for help in reviewing results and to Yuankui Lin, Yaqiong Li, Zane Duxbury and Kathie Donohoe for help provided during experiments.

References

Cavalier-Smith T (1999) Principles of Protein and Lipid Targeting in Secondary Symbiogenesis: Euglenoid, Dinoflagellate, and Sporozoan Plastid Origins and the Eukaryote Family Tree. J. Eukaryot. Microbiol. 46: 347-366

Janouskovec J, Horak A, Obornik M, Lukes J, Keeling PJ (2010) A Common Red Algal Origin of the Apicomplexan, Dinoflagellate, and Heterokont Plastids. PNAS 107: 10949-0954

Keller MD, Selvin RC, Claus W, Guillard RRL (1987) Media for the Culture of Oceanic Ultraphytoplankton. J. Phycol. 23: 633-638

Lim L, McFadden GI (2010) The Evolution, Metabolism and Functions of the Apicoplast. Philos Trans Roy Soc B 365: 749-763

McFadden GI, Reith M, Munholland J, Lang-Unnasch N (1996) Plastid in Human Parasites. Nature 381: 482

Moore RB, Obornik M, Janouskovec J, Chrudimsky T, Vancova M, Green DH, Wright SW, Davies NW, Bolch CJS, Heimann K, Slapeta J, Hoegh-Guldberg O, Logsdon JM, Carter DA (2008) A Photosynthetic Alveolate Closely Related to Apicomplexan Parasites. Nature 451: 959-963

Nisbet RER, Hiller RG, Barry ER, Skene P, Barbrook AC, Howe CJ (2008) Transcript Analysis of Dinoflagellate Plastid Gene Minicircles. Protist 159: 31-39

Obornik M, Janouskovec J, Chrudimsky T, Lukes J (2009) Evolution of the Apicoplast and Its Hosts: from Heterotrophy to Autotrophy and Back Again. Int J Parasitol. 39: 1-2

Obornik M, Vancova M, Lai DH, Janouskovec J, Keeling PJ, Lukes J (2010) Morphology and Ultrastructure of Multiple Life Cycle stages of the Photosynthetic Relative of Apicomplexa. Chromera velia. Protist 162(1): 115-30.

Ralph SA, Van Dooren GG, Waller RF, Crawford MJ, Fraunholz MJ, Forth BJ, Tonkin CJ, Roos DS, McFadden GI (2004) Tropical Infectious Diseases: Metabolic Maps and Functions of the Plasmodium Falciparum Apicoplast. Nat. Rev. Microbiol. 2(3): 203-216

Sachs J, Malaney P (2002) The Economic and Social Burden of Malaria. Nature 415(6872): 680-685

Takishita K, Yamaguchi H, Maruyama T, Inagaki Y (2009) A Hypothesis for the Evolution of Nuclear-Encoded, Plastid-Targeted Glyceraldehyde-3-Phosphate Dehydrogenase Genes in "Chromalveolate" Members. PLoS ONE. 4(3): 4737

West JA, McBride DL (1999) Long-Trm and Durnal Crpospore Dscharge Ptterns in the Ceramiaceae, Rhodomelaceae and Delesseriaceae (Rhodophyta). Hydrobiologia 298/299: 101-113

Zhang Z, Green BR, Cavalier-Smith T (1999) Single Gene Circles in Dinoflagellate Chloroplast Genomes. Nature 400: 155-159

Symposium 16

Photoprotection, Photoinhibition and Dynamics

Inhibition of Lipid Peroxidation by Plastoquinol and Other Prenyllipids

Jolanta Gruszka, Beatrycze Nowicka, Jerzy Kruk*

Department of Plant Physiology and Biochemistry, Faculty of Biochemistry, Biophysics and Biotechnology, Jagiellonian University, ul. Gronostajowa 7, 30-387 Krakow, Poland.
*Corresponding author. E-mail: jerzy.kruk@uj.edu.pl.

Abstract: Besides tocopherols, plastoquinol-9 and plastochromanol-8 are antioxidant prenyllipids whose level is increased during high light stress of plants as a response to elevated production of reactive oxygen species during the stress. Recently, it was demonstrated in several studies that these prenyllipids are effective singlet oxygen scavengers both *in vitro* and *in vivo*. These compounds are also able to inhibit lipid peroxidation – a radical chain reaction, which is responsible for destruction of membrane lipids. Here we present the comparative data on the inhibition of lipid peroxidation by plastoquinol-9, plastochromanol-8, α-tocopherol and a other prenyllipids. We observed that when lipid peroxidation was initiated within membranes, the long-chain, hydrophobic prenyllipids such as plastoquinol-9 and plastochromanol-8 were considerably more active than tocopherols in the inhibition of the peroxidation reaction, whereas lipid peroxidation was generated in the water phase, tocopherols and plastochromanol-8 were more effective than the other prenyllipids.

Keywords: Lipid peroxidation; Plastochromanol; Plastoquinol; Tocopherol

Introduction

Prenyllipids are ubiquitous compounds of different function. The first group, prenylquinones are electron and proton carriers in various electron transport chains. These compounds can be also enzyme cofactors and potent antioxidants (Nowicka and Kruk, 2010). The other group, chromanols, that includes tocopherols, are mostly known for their antioxidant properties (Munne-Bosch and Alegre, 2002). Compounds belonging to both groups are postulated to participate in regulation of gene expression and signal transduction (Munne-Bosch and Alegre, 2002; Nowicka and Kruk, 2010).

Plants are able to synthesize a wide range of prenyllipids, such as plastoquinone-9 (PQ-9), its reduced form plastoquinol-9 (PQH_2-9), ubiquinone (UQ), phylloquinone, tocopherol quinone (TQ), tocopherols (Toc), tocotrienols and plastochromanol-8 (PC-8) (Nowicka and Kruk, 2010).

Besides the function of PQ-9 as an electron carrier in photosynthetic electron transport chain, it was shown that its reduced form, PQH_2-9, is an efficient inhibitor of membrane lipid peroxidation, as well as superoxide and singlet oxygen ($^1O_2$) scavenger (Kruk and Trebst, 2008; Yadav *et al.*, 2010). Pronounced accumulation of PQH_2-9 in *Arabidopsis thaliana* exposed to high light was interpreted as a defense response to oxidative stress (Szymanska and Kruk, 2010a). The redox state of PQ-pool is thought to play a role of redox sensor in chloroplasts and participate in adaptation to changing light conditions. PQ-9 is also postulated to participate in regulation of gene expression (Nowicka and Kruk, 2010).

The antioxidant function of Tocs has been widely studied. It was shown that Tocs are able to inhibit lipid peroxidation and scavenge $^1O_2$ (Munne-Bosh and Alegre, 2002). The roles of prenyllipids in signal transduction, regulation of gene expression and carbohydrate transport require further study (Falk and Munne-Bosh, 2010).

PC-8, containing chromanol ring and a side chain longer than that of Tocs, is synthesized from PQH_2-9 by tocopherol cyclase (Szymanska and Kruk, 2010a).

It is found both in leaves and seeds, and accumulates during growth (Szymanska and Kruk, 2010a, b). However, the data concerning antioxidant function of PC-8 are sparse (Gruszka *et al.*, 2008).

Lipid peroxidation is a radical chain reaction responsible for degradation of membrane lipids containing polyunsaturated fatty acids. It can be initiated by hydroxyl or hydroperoxide radicals, that abstract hydrogen atom from a fatty acid, generating carbon centered radical. These radicals undergo further reactions leading to formation of peroxyl and alkoxyl radicals and the reaction propagates. Most of lipid soluble antioxidants act as scavengers of lipid radicals and inhibit propagation of peroxidation (James *et al*., 2004).

In the present study we have applied initiation of lipid peroxidation in plant lipid liposomes by three methods: photosensitized generation of $^1O_2$ within liposomes, by water soluble azoinitiator, 2′-azobis (2-amidinopropane) hydrochloride (AAPH) and by lipid soluble azoinitiator, 2,2'-azobis(2,4-dimethylvalero-nitrile) (AMVN). The inhibition of lipid peroxidation by different prenyllipids incorporated into liposomes was measured.

Materials and Methods

Lipid peroxidation was measured in liposomes prepared from mixture of chloroplasts lipids at proportions found for thylakoid membranes (monogalactosyldiacylglycerol: digalactosyldiacylglyce-rol: sulphoquinovosyldiacylglycerol: phosphatidylglyce-rol, 50:25: 12.5:12.5, mol/mol, respectively).

In experiments where lipid peroxidation was initiated with $^1O_2$, ethanol solutions of prenyllipids and plant lipids was mixed with zinc tetraphenylporphine dissolved in tetrahydrofuran. The samples were evaporated and rehydrated with distilled water, following addition of the fluorescent probe, diphenylhexatriene (DPH). Suspension of liposomes containing 0.5 mmol chloroplast lipids, 1 μM porphyrin, 25 μM prenyllipid and 2 μM DPH was incubated on magnetic stirrer for 15 h in the dark followed by exposition to white light (100 μmol/m^2/s) for 2 h. In the case of liposomes containing PQH_2-9, all the manipulations were performed under stream of nitrogen to prevent oxidation of the prenyllipid. For measurements of DPH fluorescence, samples were extracted with tetrahydrofuran and measured in the same solvent using λ_{ex} = 355 nm and emission range of 370–550 nm. Analysis of lipid peroxides was performed using HPLC on C_{18} column in acetonitrile: methanol : water (72:8:1, v/v), flow rate of 1.5 ml/min and absorbance detection at 234 nm. For the analysis, liposomes were extracted with ethyl acetate, the extract was evaporated and dissolved in the HPLC solvent.

In experiments where lipid peroxidation was initiated with AAPH, ethanol solutions of plant lipids and a prenyllipid were mixed and injected into 25 mmol MES buffer (pH 6.5). AAPH solution was then added. The final concentration of plant lipids was 0.5 mmol and that of AAPH was 10 mmol. Progress of the peroxidation reaction was followed by measurement of oxygen consumption using Clark electrode. All the measurements were carried out at 37 °C.

In experiments where lipid peroxidation was initiated with AMVN, ethanol solutions of plant lipids, a prenyllipid and AMVN were mixed. Then the mixture was injected into 25 mmol MES buffer (pH 6.5). The final concentrations of plant lipids was 0.5 mmol and that of AMVN was 100 μM. The preparation and incubation of liposome suspensions was carried out at 37 °C. During incubation for 5 h, samples for analysis were taken every 30 min, extracted with ethyl acetate and analyzed by HPLC. Lipid peroxides were measured as described before. Prenyllipid were analyzed using fluorescence detection (λ_{ex} = 290 nm, λ_{em} = 330 nm). In case of liposomes containing PC-8, the analysis was performed in methanol : hexane (340:20, v/v).

Results and Discussion

Lipid peroxidation initiated by $^1O_2$ was followed by DPH fluorescence that was found to decay during the reaction as a result of DPH breakdown by lipid radicals. Direct oxidation of DPH by $^1O_2$ was negligible (data not shown). Among the investigated prenyllipids, PC-8 and PQH_2-9 were the most effective in inhibition of lipid peroxidation after 2 h of the reaction (Fig. 1). On the other hand, α-Toc showed rather prooxidant effect. This unexpected observation might be due to the fact that in chloroplats tocopheroxyl radicals formed during scavenging of lipid radicals are reduced by ascorbate, that enables regeneration of α-Toc.

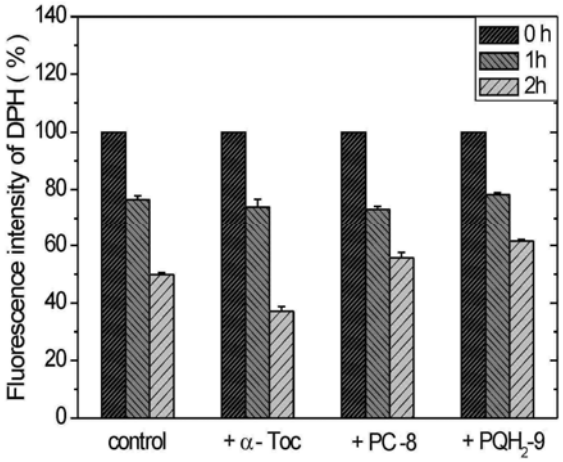

Fig. 1 DPH fluorescence in extracts of plant lipid liposomes with the incorporated photosensitizer in the course of illumination and the effect of prenyllipids on the reaction.

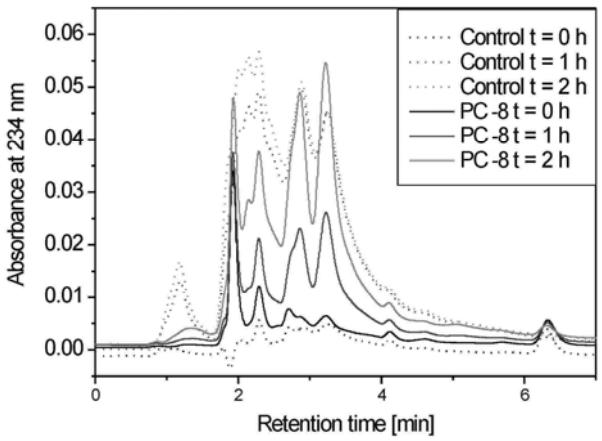

Fig. 2 Lipid peroxidation of plant lipid liposomes followed by HPLC, initiated by photosensitized singlet oxygen production in the absence and presence of PC-8.

HPLC analysis of membrane lipids demonstrates that PC-8 inhibited pronouncedly formation of lipid peroxides (Fig. 2).

In experiments where lipid peroxidation was initiation by AAPH, the reaction was followed by O_2 consumption. In the case of control samples, O_2 concentration dropped instantly, whereas for samples

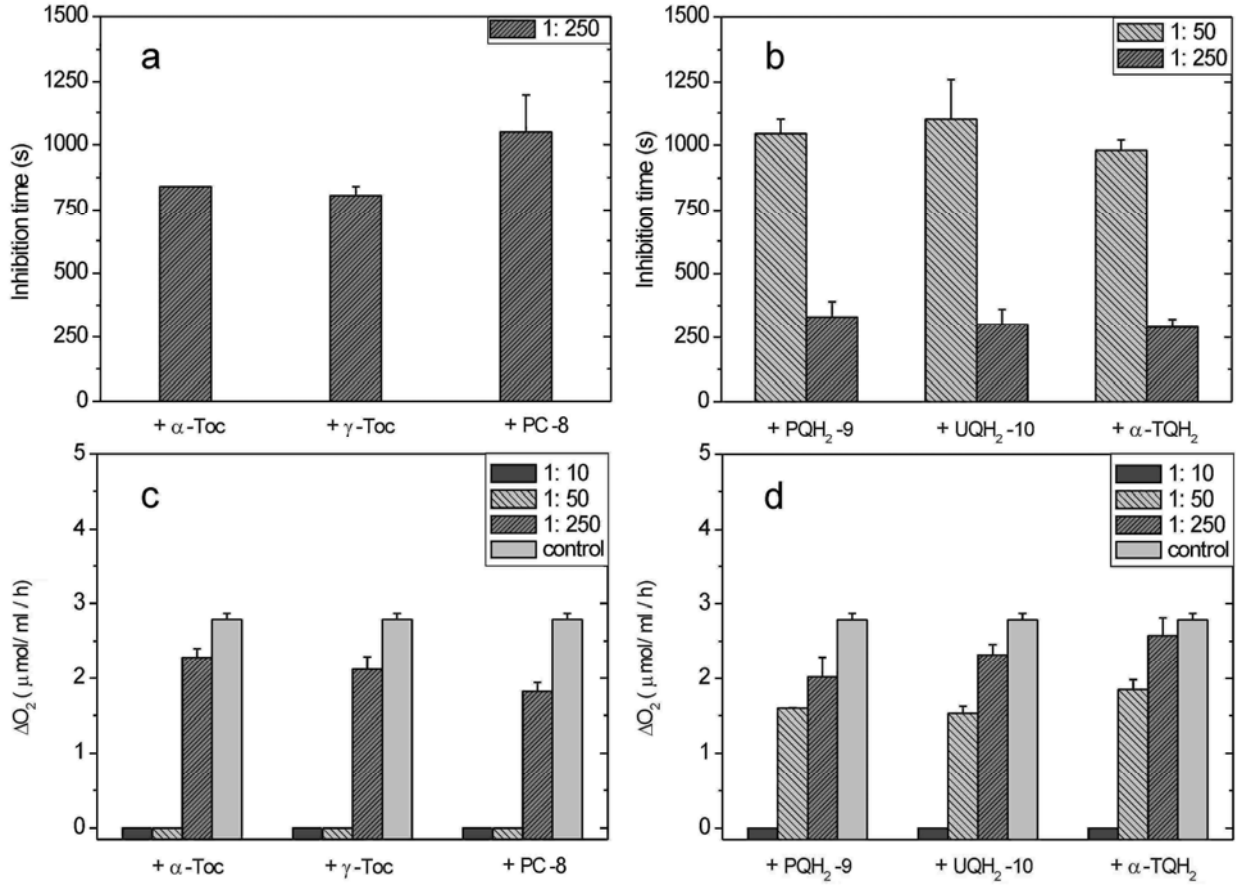

Fig. 3 (a) and (b) The effect of prenyllipids on inhibition time of lipid peroxidation during AAPH-initiated peroxidation of plant lipid liposomes, in the absence of prenyllipids the time was 0 s; (c) and (d) The effect of prenyllipids on oxygen uptake rates at time > t_h. The numbers indicate molar prenyllipid/membrane lipid proportion.

containing a prenyllipid, oxygen consumption was delayed. The time required for beginning of rapid decrease of O_2 concentration is the inhibition time and it reflects the ability of a prenyllipid to inhibit lipid peroxidation. It was found that both Tocs and PC-8 were highly, and to the similar extent, effective in the inhibition of the reaction (Figs. 3a and 3c). In the case of the reduced prenyllipids, higher concentrations of the prenyllipids were required to obtain the similar extent of inhibition (Figs. 3b and 3d).

When the reaction of lipid peroxidation was initiated by lipid soluble AMVN (Fig. 4), the reaction was followed by concentration of lipid peroxides in liposomes. Formation of the peroxides was inhibited to the highest extent by PQH_2-9, followed by PC-8. γ-Toc inhibited the reaction only at the lower content, whereas α-Toc was ineffective in the inhibition of lipid peroxidation and it stimulated the reaction.

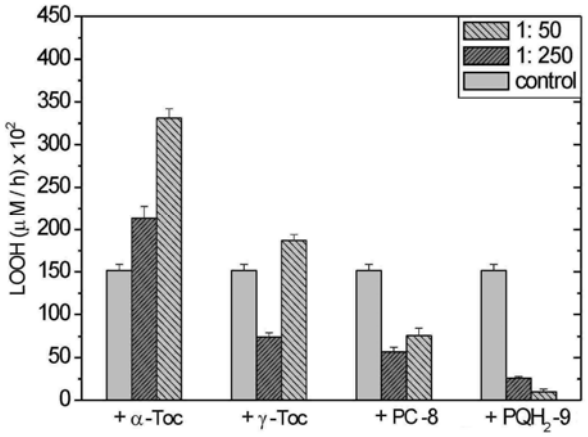

Fig. 4 The effect of different prenyllipids on rates of lipid peroxidation in plant lipid liposomes initiated by AMVN. The numbers indicate molar ratio of prenyllipid/membrane lipid.

The obtained results indicate that effectiveness of inhibition of lipid peroxidation by the investigated prenyllipids depends on the site of initiation reaction.

When lipid peroxidation was generated by singlet oxygen in liposomes, long-chain prenyllipids, like PC-8 and PQH_2-9 were more active than α-Toc in the inhibition of the reaction. When lipid peroxidation was initiated in the water phase by AAPH, more active were chromanols (Tocs and PC-8) than the reduced prenyllipids in the inhibition of peroxidation. When lipid peroxidation was initiated in the lipid phase of liposomes by AMVN, the long-chain, hydrophobic PC-8 and PQH_2-9 were only effective, while the more hydrophilic Tocs were not or poorly active in the inhibition of the reaction.

The results obtained indicate that long-chain, hydrophobic prenyllipids (PC-8 and PQH_2-9) are considerably more active antioxidants than Tocs when lipid peroxidation is initiated within membranes ($^1O_2$, AMVN), while Tocs and PC-8 are more effective than the other prenyllipids when lipid peroxidation is generated in the polar, water phase.

References

Falk J, Munne-Bosch S (2010) Tocochromanol Functions in Plants: Antioxidation and Beyond. J Exp. Bot. 61: 1549-1566

Gruszka J, Pawlak A, Kruk J (2008) Tocochromanols, Plastoquinol and Other Biological Prenyllipids as Singlet Oxygen Quenchers – Determination of Singlet Oxygen Quenching Rate Constants and Oxidation Products. Free Radical Biol. Med. 45: 920-928

James AM, Smith RAJ, Murphya MP (2004) Antioxidant and Prooxidant Properties of Mitochondrial Coenzyme Q. Arch. Biochem. Biophys. 423:47-56

Kruk J, Trebst A (2008) Plastoquinol as a Singlet Oxygen Scavenger in Photosystem II. Biochim. Biophys. Acta 1777: 154-162

Munne-Bosch S, Alegre L (2002) The Function of Tocopherols and Tocotrienols in Plants. Crit. Rev. Plant Sci. 21: 31-57

Nowicka B, Kruk J (2010) Occurrence, Biosynthesis and Function of Isoprenoid Quinones. Biochim. Biophys. Acta 1797: 1587-1605

Szymańska R, Kruk J (2010a) Plastoquinol Is the Main Prenyllipid Synthesized during Acclimation to High Light Conditions in Arabidopsis and Is Converted to Plastochromanol by Tocopherol Cyclase. Plant Cell Physiol. 51: 537-545

Szymańska R, Kruk J (2010b) Identification of Hydroxy-Plastochromanol in Arabidopsis Leaves. Acta Biochim. Pol. 57: 105-108

Yadav DK, Kruk J, Sinha RK, Pospisil P (2010) Singlet Oxygen Scavenging Activity of Plastoquinol in Photosystem II of Higher Plants: Electron Paramagnetic Resonance Spin-Trapping Study. Biochim. Biophys. Acta. 1797: 1807-1811

Tenuazonic Acid, a Novel Natural PSII Inhibitor, Impacts on Photosynthetic Activity by Occupying the Q_B-Binding Site and Inhibiting Forward Electron Flow

Shiguo Chen[a], Reto J Strasser[a, §], Sheng Qiang[a, *], Govindjee[b]

[a]Weed Research Laboratory, Nanjing Agricultural University, Nanjing 210095, China;
[b]Department of Plant Biology, University of Illinois at Urbana-Champaign, Urbana, IL 61801, USA.
[*]Corresponding author. Tel. No. 86 25 84395117; Fax No. 86 25 84395117; E-mail: wrl@njau.edu.cn.
[§] Chair Professor of Weed Research Laboratory, Nanjing Agricultural University, China;
Emeritus Professor of Bioenergetics Laboratory, University of Geneva, Switzerland.

Abstract: Tenuazonic acid (TeA), a member of representative natural tetramic acids, is a phytotoxin produced by the fungus *Alternaria alternata* isolated from diseased Croftonweed (*Eupatorium adenophorum*). TeA strongly inhibits photosynthesis, especially photosystem II (PSII) activity. Evidence from fast chlorophyll fluorescence induction transients of host plant shows that the most important action site of TeA is that it interrupts electron transport beyond Q_A, on the acceptor side of PSII, and this is due to its binding at the Q_B-site. On the basis of competition experiments with [^{14}C]atrazine, it is further confirmed that TeA does not share the same binding environment as atrazine, despite their common action target: the Q_B-site.

Keywords: Tenuazonic acid; Chl *a* fluorescence induction transients; JIP-test; PSII inhibitor; Reaction center

Introduction

Tetramic acid (pyrrolidine-2,4-diones ring system) is a recurrent motif among natural products originating from a variety of marine and terrestrial species. Tenuazonic acid (TeA) is a member of representative natural tetramic acids.

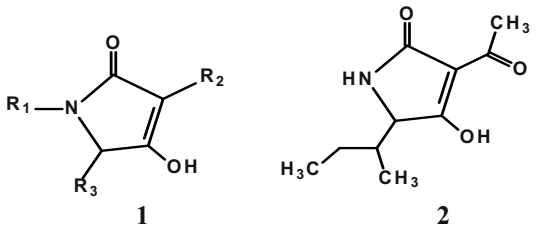

1 **2**

Fig. 1 The structure of tetramic acid **1**, tenuazonic acid **2**.

Based on evidence from the model organism *Chlamydomonas reinhardtii*, TeA is a novel photosynthesis inhibitor, which mainly interrupts forward electron transport beyond Q_A by competing with Q_B for the Q_B-niche of the D1 protein (Chen *et al*., 2007). However, for a group of new potential herbicidal natural chemicals, understanding its mechanism of action is critical and this includes not just identifying the target site in an isolated model system but knowing all aspects of interaction with the whole plant, especially the host plant and the target weed. Fast Chl *a* fluorescence transient kinetics, a non-invasive spectroscopic technique, has become an excellent tool to probe the mode of action of photosynthetic inhibitors. Combined with photoaffinity labeling with radioactive technique, we have focused here on the effect of TeA on PSII activity by determining Chl *a* fluorescence transients of the host plant.

Materials and Methods

Plant materials and chemicals

Croftonweed (*E. adenophorum*) was grown for 3 months by rooting in soil at 20–25 ºC under approximately 300 μmol photons m^{-2} s^{-1} of white light (day/night, 12/12 h) and relative humidity (about 70%) in a glasshouse.

TeA was isolated and purified from a culture of *A.*

alternata isolate 501 (Chen *et al*., 2007). [^{14}C]Atrazine was purchased from Moravek Biochemicals Inc. (Specific activity is 9.3 mCi/mmol).

Chl a fluorescence transients and the JIP-test

Croftonweed plants were placed in darkness for about 3 h before TeA treatment at room temperature (25 ^{o}C), and then pairs of the second top leaves (without detaching them from the plant) were put in trays filled with 10 mL of TeA solution (1mmol TeA, distilled water). After treatment for the indicated time, leaves (still not detached and in darkness) were removed from the TeA solution and wiped to avoid possible effects of anaerobiosis.

Detached Croftonweed leaves (the second top leaf pair) were arranged in Petri dishes between two layers of filter paper with the lower surface upwards. TeA solution or water was added to cover the paper. The samples were left for incubation for a period of 12 h in complete darkness at 25 ^{o}C.

Chl *a* fluorescence transients were measured at room temperature with a fluorometer (Handy-PEA, Hansatech Instruments Ltd., UK). Raw fluorescence OJIP transients were analysed with the JIP-test (Strasser *et al*., 2004). The initial fluorescence F_O is measured at 20 μs —at this time all reaction centers (RCs) are open; fluorescence intensity at 300 μs (K-step), 2 ms (J-step), 30ms (I-step) is denoted as F_K, F_J and F_I, respectively. The maximal fluorescence intensity F_M is equal to F_P.

The probability ψ_{Eo} that a trapped exciton moves an electron into the electron transport chain beyond Q_A^- is given as: $\psi_{Eo} = PSI_0 = ET_0/TR_0 = 1–V_J$. The maximum quantum yield of primary photochemistry, φ_{Po}, is defined as: $\varphi_{Po} = PHI(Po) = TRo/ABS = 1–F_O/F_M$. The maximum yield of electron transport (φ_{Eo}) has the following expression: $\varphi_{Eo} = PHI(Eo) = ET_0/ABS = (1–F_O/F_M)(1–V_J)$.

The amount of Q_A reducing centers = $(RC/RC_{ref.})(ABS/ABS_{ref.}) = [(RC/CS)_{treated}/(RC/CS)_{control}][(ABS/CS)_{treated}/(ABS/CS)_{control}]$. Non-$Q_A$ reducing centers (%) = 100–Q_A reducing centers.

Q_B reducing centers was calculated according to the protocol used for the so called double hit experiments (Appenroth *et al*., 2001). Dark adapted leaves were exposed twice for 1 s with saturating light at an interval of 10 s dark. The fraction of Q_B reducing centers can be calculated as follows: Q_B reducing centers = $(1–F_O/F_M)_{(second\ exposure)}/(1–F_O/F_M)_{(first\ exposure)}$. Non-$Q_B$ reducing centers = ΔV_0 = 100%–Q_B reducing centers.

An estimate of Oxygen Evolving Complexes (OEC) can be made by utilizing the value of V_K (= $(F_K–F_O)/(F_M–F_O)$) and V_J (= $(F_J–F_O)/(F_M–F_O)$). The fraction of OEC is calculated in comparison with the control sample as: Fraction of OEC = $[1–(V_K/V_J)]_{treated}/[1–(V_K/V_J)]_{control}$.

The ratio S_m/t_{Fmax} expresses the average fraction of open RCs: $S_m/t_{Fmax} = [RC_{open}/(RC_{close}+RC_{open}]av$, where $S_m = (Area/(F_M–F_O))$ is the working integral of the energy needed to close all reaction centers.

Competitive experiments of [^{14}C]atrazine bound to D1 protein

Displacement experiments were carried out using the method of Chen *et al*. (2007). The amount of bound [^{14}C]atrazine to Q_B-site was calculated from the total radioactivity added to the thylakoid suspension and the amount of free [^{14}C]atrazine in the supernatant after centrifugation.

Results and Discussion

TeA blocked PSII electron flow beyond Q_A

The following is observed from fluorescence transient OJIP curves of leaves in vivo (Figs. 2A and 2B): (1) the fluorescence rise transients, obtained from control leaves, show a typical OJIP shape; (2) with an

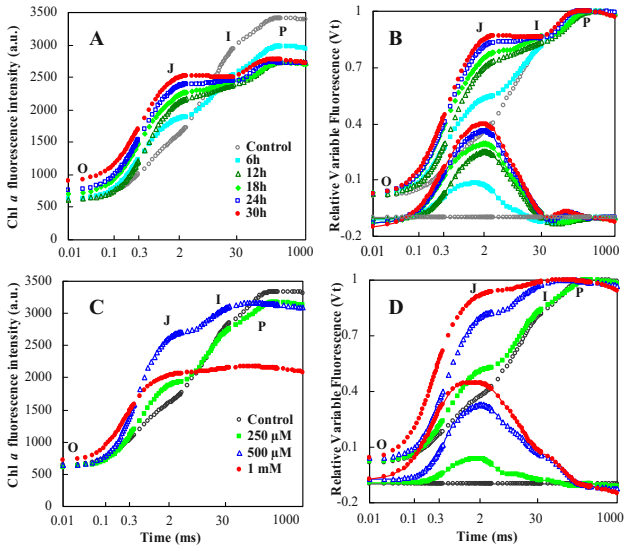

Fig. 2 Effect of TeA on Chl *a* fluorescence transients plotted on logarithmic time scale of Croftonweed leaves in vivo (A, B) or detached-intact leaves (C, D). Figs. A and C show raw curves without any normalization; in Figs. B and D the top figures show curves normalized by F_O and F_M, the bottom figures shows delta V (gain 1) full symbol curves minus control.

increase of the treatment time with TeA, the major changes are treatment-time dependent increase in the J level. Figs. 2C and 2D show that fluorescence transients OJIP of various concentrations of TeA treated detached-intact leaves. A clear rise in the J-step is observed with the penetration of TeA into the leaf. Moreover, with increasing of concentration of TeA, the J level became closer to the P level and then the IP phase began to disappear. An increase of the J step is usually interpreted as evidence for a large accumulation of Q_A^- due to a slowdown of electron transport beyond Q_A (Strasser and Govindjee, 1992).

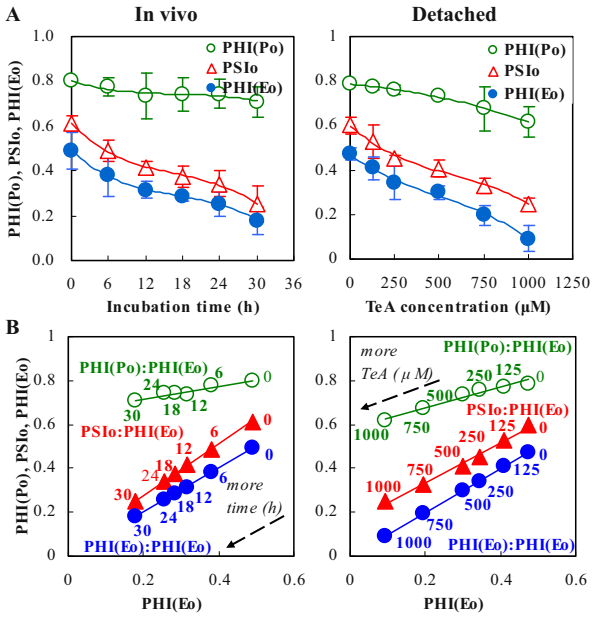

Fig. 3 Panel A: Effect of TeA on the maximum quantum yield of primary photochemistry (PHI(P_0)), the probability that an electron is going further than Q_A into the electron transport chain (PSI$_0$), the maximum quantum yield of electron transport (PHI(E_0)). Panel B: Analysis of the correlation for PHI(P_0), PSI$_0$ and PHI(E_0) versus PHI(E_0) of Croftonweed leaves treated with TeA.

In order to further demonstrate the effect of TeA on PSII, some functional parameters were used to quantify the PSII behavior and its activity. As shown in Fig. 3A, the maximum yield of primary photochemical (PHI(Po) = φ_{Po}) values do not change much. They remain in a narrow range. In contrast to φ_{Po}, the probability that a trapped exciton moves an electron into the electron transport chain beyond Q_A (PSI$_0$ = ψ_0) and the quantum yield for electron transport (PHI(Eo) = φ_{Eo}) decreased strongly as a function of the incubation time or concentration with TeA. The three parameters can be plotted as φ_{Eo}: φ_{Po}, ψ_0 and φ_{Eo} versus φ_{Eo} (Fig. 3B). By increasing the time and concentration of TeA treatment, the values of ψ_0 and φ_{Eo} declined approximately linearly with φ_{Eo}, with φ_{Po} being inactive kept constant. These results indicate that TeA reacts like DCMU: it does not inhibit the primary light reaction but the redox reaction after Q_A due to interruption of electron flow beyond Q_A.

TeA resulted in inactive of PSII reaction centers

A large accumulation of Q_A^- must lead to inactive PSII RCs. With increased time and concentration of TeA treatment, the ratio S_m/t_{Fmax} values decreased further (Fig. 4A), which means that TeA caused severe closure of PSII RCs. In order to further check the influence of TeA on PSII RCs, three types of PSII RCs, non-Q_A reducing RCs, Q_A reducing RCs including non-Q_B reducing RCs and Q_B reducing RCs, were calculated by fluorescence transients (Figs. 4B and 4C). During TeA treatment, an approximately linearly sharp increase of non-Q_A reducing RCs was observed. In contrast, amount of Q_A reducing RCs showed an approximately linear decrease. Amount of Q_B binding centers containing Q_B reducing RCs (active) and non-Q_B

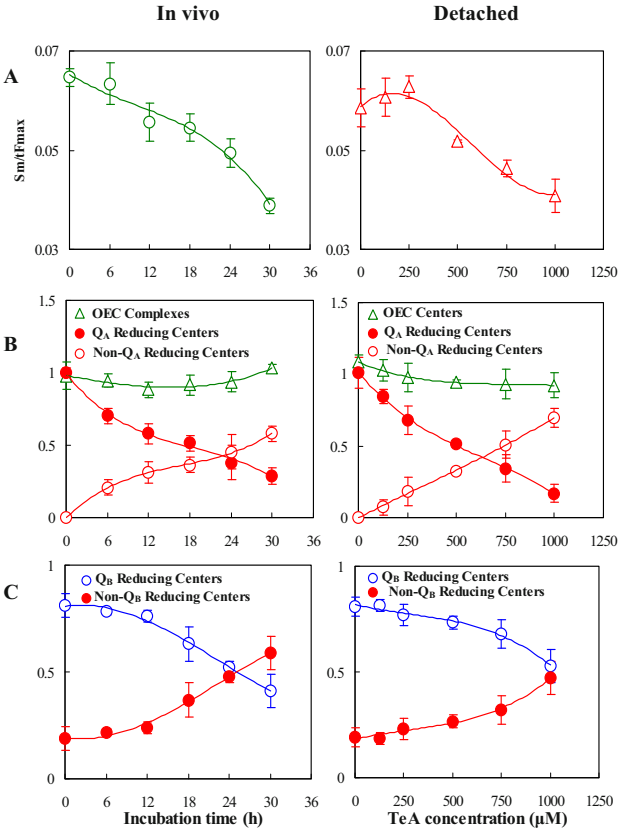

Fig. 4 Time and concentration dependent effect of TeA on (A) average fraction of open RCs (Sm/t_{Fmax}) in the time interval from 0 to t_{Fmax}; (B) fraction of Oxygen Evolving Centers (OEC) centers, Q_A-reducing RCs and non-Q_A-reducing RCs; (C) fraction of Q_B-reducing RCs and non-Q_B reducing RCs.

reducing RCs (inactive) is presented in Fig. 4C. Approximately 19% Q_B binding centers were inactive in control samples, which is equal to 19% non-Q_B reducing RCs. However, TeA treatment inactivated further the number of Q_B binding centers, which would lead to a significant increase in the amount of non-Q_B reducing RCs and a clear decrease of fraction of Q_B reducing RCs. After 30 h of 1 mmol TeA incubation of leaves in vivo, there were about 59% non-Q_B reducing RCs and 41% Q_B reducing RCs. Detached-intact leaves showed a similar change in amount of Q_B reducing RCs. However, TeA treatment had no distinct effect on OEC centers. Thus, it is concluded that TeA causes inactivity of PSII RCs by blocking electron transport of PSII acceptor side due to an increase of non-Q_B reducing RCs attributed to the binding of TeA to the Q_B site.

TeA bound to the Q_B-site

Although TeA is similar to the classical PSII herbicides (*e.g.* DCMU and atrazine) in binding to Q_B reaction centers, which does not necessarily mean that they act at the same binding site. As can be seen from the Fig. 5A, the amount of free [^{14}C]atrazine in the reaction mixture of the competition experiment increased in proportion to the addition of non-labeled TeA. This means that [^{14}C]atrazine binding to thylakoids of Croftonweed was affected by the presence of non-labeled TeA. Double-reciprocal plots of 1/μM free atrazine versus mg Chl/nmol bound atrazine were made for control thylakoids (no TeA) and in the presence of six concentrations of TeA (Fig. 5B),

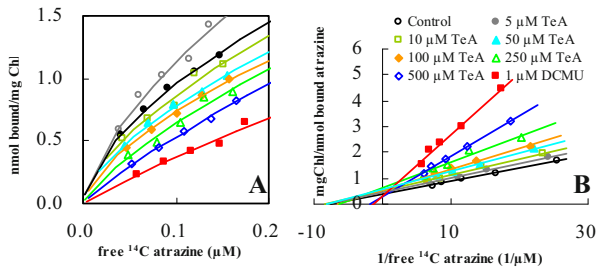

Fig. 5 Competitive experiments of [^{14}C]atrazine bound to thylakoid membranes of Crofton weed by non-labeled TeA and DCMU. (A) [^{14}C]atrazine binding curves. (B) Double-reciprocal plot of the concentration of free [^{14}C]atrazine vs. the amount of bound [^{14}C]atrazine.

which reveal a non-competitive displacement because there is not an identical ordinate intersect in various TeA concentrations. This demonstrates that TeA displaces atrazine-like inhibitors in a non-competitive manner. Hence, TeA has a different binding behavior within the Q_B-niche than by other PSII inhibitors.

Acknowledgements

The work was partially supported by the National Natural Science Foundation of China (31000834), Ph.D. Programs Foundation of Ministry of Education of China (200803071004) and 111 Project (B07030).

References

Appenroth KJ, Stöckel J, Srivastava A, Strasser RJ (2001) Multiple Effects of Chromate on the Photosynthetic Apparatus of Spirodela Polyrhiza as Probed by OJIP Chlorophyll a Fluorescence Measurements. Environ. Pollut. 115: 49-64

Chen SG, Xu XM, Dai XB, Yang CL, Qiang S (2007) Identification of Tenuazonic Acid as a Novel Type of Natural Photosystem II Inhibitor Binding in Q_B-Site of Chlamydomonas Reinhardtii. Biochim. Biophys. Acta 1767: 306-318

Strasser RJ, Govindjee (1992) The Fo and the O-J-I-P Fluorescence Rise in Higher Plants and Algae. In: Argyroudi-Akoyunoglou JH (ed.), Regulation of Chloroplast Biogenesis. Plenum Press: New York, pp. 423-426

Strasser RJ, Tsimilli-Michael M, Srivastava A (2004) Analysis of the Chlorophyll a Fluorescence Transient. In: Papageorgiou GC, Govindjee (eds.), Chlorophyll Fluorescence: a Signature of Photosynthesis. Kluwer Academic Publishers Press: Netherlands, pp. 321-362

Xiong J, Subramaniam S, Govindjee (1996) Modeling of the D1/D2 Proteins and Cofactors of the Photosystem II Reaction Center: Implications for Herbicide and Bicarbonate Binding. Protein Sci. 5: 2054-2073

Yellow Vine Syndrome of American Cranberry: a Mechanistic Assessment

Lien-Yang Chou[a], Wanshu He[a], Xuejing Hou[a], Joy Patel[a], Aaron Rasposo[a], Harvey JM Hou[a,*]

[a]Department of Chemistry and Biochemistry, University of Massachusetts Dartmouth, North Dartmouth, massachusetts 02747, USA.
[*]Corresponding authors. Tel. No. +01 508 999 8234; Fax No. +01 508 999 9167; E-mail: hhou@umassd.edu.

Abstract: American cranberry (*Vaccinium macrocapron Ait*) is an important agricultural food crop due to its abundant of antioxidants. Yellow vine syndrome of cranberry, interveinal chlorosis moving from older to younger leaves, has been observed in cranberry bogs. The reason for the development of the syndrome is unknown. Our goal is to investigate the mechanisms underlying yellow vine syndrome in cranberry plants and as a result develop a strategy to solve the problem. Recent spectrometric analysis revealed that the yellow vine leaves showed a 22%–24% loss in chlorophyll compared to normal leaves. An in vivo chlorophyll fluorescence analysis indicated that the yellow vine leaves showed substantial loss in the maximum quantum efficiency of PS II. We propose that photoprotection deficiency is a possible mechanism for the formation of yellow vine syndrome in cranberry plants in additional to nutritional imbalance and water stress. Possible limitations and future efforts are sumarized and discussed.

Keywords: Cranberry; Photosystem II; Photoinhibition; Nutritional imbalance; Water stress; HPLC; Chlorophyll fluorescence

Introduction

American cranberry (*Vaccinium macrocapron Ait*) is an important agricultural food crop. The crop size is approximately 500 million pounds annually in USA. In Massachusetts, Cranberry production in Massachusetts accounts for 23% of the national crop, with a farm-gate value of $ 47.4 million (National Agricultural Statics Service, 2006). Some medical effects were found in cranberry. Most famous one is that the cranberry juice as a remedy to treat women's urinary tract infections (UTIs) in North America (Howell *et al*., 1998). Some studies also imply that cranberry juice extracts have potential to prevent heart disease and suggested to exhibit anticancer effects (Bomser *et al*., 1996).

Yellow vine syndrome of cranberry, interveinal chlorosis moving from older to younger leaves, has been observed in cranberry bogs (Fig. 1). The symptom often becomes severe around fruit set of cranberry growth cycle. At the beginning, the cranberry leaves change from green to lime-yellow and then to bright yellow. Affected plants gradually decline. In some cases, immature plants may not turn yellow but wilt and dcollapse. Almost every year numberous reports of yellow vine syndrome of cranberry are received from the cranberry growers (Demoranville, 2009). It is becoming an increasing problem in Massachusetts (DeMoranville and Lampinen, 1999). The syndrome may affect production and quality of cranberries.

The reason for the development of the syndrome is poorly understood. We intend to investigate the mechanisms underlying yellow vine syndrome in cranberry plants and as a result to develop a strategy to solve the problem. A complete nutrition analysis suggests that a nutrition imbalance might be associated with yellow vine development in cranberry. Additionally, the yellow vine syndrome often worsens in bogs with drainage problems, indicating that water stress may be another factor in the formation of yellow vine in cranberries. In this paper, we present our recent data and summerize the advances in probing the mechanism of yellow vine formation in cranberry plants.

Fig. 1 American cranberry leaves without (a) and with (b) yellow vine syndrome.

Materials and Methods

Cranberry sampling and chlorophyll analysis

Leaves of cranberry cultivar Stevens were collected from State bog in East Wareham, Massachusetts. Three sets of samples were harvested and extracted with methanol to proper concentration before measurement. The spectrometric analysis of cranberry extract was measured with Hewlett Packard 8452A diode array spectrophotometer. The concentration of chlorophyll a (Chl a), and chlorophyll b (Chl b) was determined according to the published procedures (Porra *et al*., 1989; Wei, 2010). The methanol extract solution was analyzed to dentermine the chlorophyll content by HPLC according to the method described elsewhere (De las Rivas *et al*., 1989).

Chlorophyll fluorescence analysis

The chlorophyll fluorescence parameters of cranberry leaves in the bogs were determined with Pocket PEA Chlorophyll Fluorimeters (Hansatech Instruments Ltd, England). Four types of sample leaves in the bogs, including normal, yellow vine, normal under shade, and yellow vine under shade, were chosen randomly for chlorophyll fluorescence measurements.

Results and Discussion

Spectrometric, HPLC, and Chlorophyll Fluorescence Analysis of Yellow Vine Samples

The spectrometric and HPLC analytical data are listed in Table 1. Yellow vine leaves showed a 22%–24% loss in chlorophyll compared to normal leaves. However, it is interesting that the ratio of chlorophyll a and chlorophyll b is almost the same in normal and yellow vine leaves. The results infer that yellow vine syndrome could result from the decreasing of both PS II reaction center and light harvest complex per chloroplast. We propose that the organization of photosynthetic mechiney in yellow vine cranberry plants may not be affected. The decrease of chlorophyll in content implies the decrease in the numbers of photosynthetic reaction centers.

Chlorophyll fluorescence provides an invasive method to probe photosynthetic reaction in cyanobacteria, algae, and green plants. It is widely used to monitor the response of cells to the environemental stress (Baker, 2008; Strasser *et al*., 2004). The accessible photosynthetic parameters include (1) PS II maximum quantum yield (F_V/F_M), which is the ratio of variable fluorescence (F_V) to maximum fluorescence (F_M), (2) the size of the PS II quinone pool expressed as "Area," which the measurement of fluorescence area above the transient, and (3) photosynthetic performance index "PI," which is defined as the a driving force of the primary photosynthetic reaction (Strasser *et al*., 2004).

Table 2 lists the PS II maximum quantum yield, quinone pool size, and photosynthetic performance index of yellow vine leaves and normal samples. The PS II maximum quantum yield was decreased by ~20%, which is agreeable to the chlorophyll analysis within error. This supports the numbers of PS II reaction center may be reduced by ~20%. Similar behavior of decrease in F_V/F_M was observed in camellia leaves under stress conditions (Kruger *et al*., 1997; Oukarroum *et al*., 2009).

In contrast, the quinone pool size and photosynthetic performance index were dramatically reduced by ~80%. The discrepancy between these numbers and F_V/F_M may occur because the distribution of PS II in yellow vine leave is not optimized. In particular, the much smaller size of quinone pool will imply the vulnerable and sensitive of yellow vine syndrome to other environmental stress factors. This is supported by the observation that water stress often worsens the yellow vine symptom in cranberry bog (Demoranville, 2006). The additional reason may due to the sampling variation. This is especially true for the yellow vine samples as the measurable error is much larger than those the normal leaves (data not shown).

To further confirm our hypothesis, we also conducted the chlorophyll fluorescence analysis on the yellow vine leaves over the period of one day and of one month, respectively. The experimental data support our conclusion and indicated that the photosynthetic parameters of the yellow vine samples are substantially lower that those of the normal cranberry leaves (data not shown).

Table 1 Analytical results of chlorophyll (Chl) a, Chl b, and the Chl a/Chl b ratio in the methanol extracts of yellow vine and normal cranberry leaves by Spectrometric (a) and HPLC analysis (b). The average of three measurements was used to calculate the std.

(a)	Normal leaves	Yellow Vine leaves	Change (%)
Chl a (mg/g)	1.30±0.09	0.99±0.10	–23.8
Chl b (mg/g)	0.93±0.06	0.72±0.09	–22.6
Chls a/Chl b	1.40	1.38	–1.43

(b)	Normal leaves	Yellow vine leaves	Change (%)
Chl a area ratio (%)	56.4±5.0	42.9±4.0	–23.9
Chl b area ratio (%)	35.1±3.0	27.5±3.0	–21.7
Chl a / Chl b	1.61	1.56	–3.1

Table 2 PS II maximum quantum yield (Fv/Fm), quinone pool size (area), and photosynthetic performance index (PI) of yellow vine and normal cranberry leaves determined by chlorophyll fluorescence analysis. The average of three measurements was used to calculate the std.

	Fv/Fm	Area($\times 10^5$ unit)	PI
Normal leaves	0.82±0.01	3.34±0.42	21.3±3.9
Yellow Vine leaves	0.68±0.06	0.76±0.18	3.14±1.1
Change (%)	−17.1	−77.2	−85.3

Mechanisms of Yellow Vine Syndrome Formation

Yellow vine syndrome of cranberry is likely due to the nutritional imbalances in the cranberry plants (Demoranville, 2009). A complete nutritional analysis revealed the abnormal content of manganese and pattasium. However the fertilizer management seems not effective to reduce the symptom. Additionally, yellow vine syndrome often worses in bogs with drainage problems, indicating that water stress may be another factor in the formation of yellow vine in cranberry.

Recently we found that shading of yellow vine cranberry plants appeared to reduce the syndrome and increased the chlorophyll content by 14 ± 2% (Zi *et al*., 2010). The effect of shade treatment on yellow vine syndrome in cranberry bogs revealed that the shading of cranberry plants appears to reduce the syndrome by improving the photosynthetic activity and increasing the chlorophyll content. The yellow vine leaves were associated with 11 ± 5% and 14 ± 5% increase in Chl a/Chl b ratio after shading, respectively. The electron transport efficiency in PSII and the size of the quinone pool are increased. These results suggest that the shade effect will increase the numbers of PS II in the cells of yellow vine cranberry leaves. As PS II is the main target of photoinhibition, we speculate a possible role of photoinhibition is associated with the yellow vine syndrome in cranberry plants.

We summarize the three hypotheses for the yellow vine development in cranberry plants in Fig. 2. Three possible mechanisms including nutritional imbalance, water stress, and photodameg, may induce the formation of yellow vine of cranberry. Leaves exhibiting the yellow vine syndrome contain less numbers of photosynthetic reaction centers per chloroplast than the normal leaves.

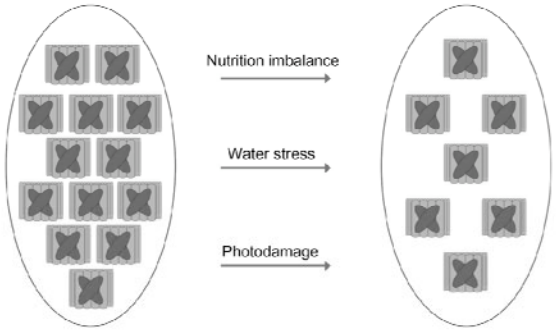

Fig. 2 A model of yellow vine formation in cranberry plants. Photoprotection deficiency a possible novel mechanism causes the decreasement of PS II reaction center and light harvest complex as well as nutritional imbalance and water stress.

Since photoprotection could be a novel important mechanism, the formation of yellow vine syndrome of cranberry may be due to the abnormality of xanthophylls, which are the yellow carotenoid pigments in plants. The xanthophyll cycle involves the enzymatic removal of epoxy groups from xanthophylls (*e.g.* violaxanthin, antheraxanthin, diadinoxanthin) to create so-called de-epoxidised xanthophylls (*e.g.* diatoxanthin, zeaxanthin). These enzymatic cycles is one of the most efficient photoprotection mechanisms in plants and can reduce the excess of light energy to reach the photosynthetic

reaction centers. We intend to apply reversed phase C-30 HPLC column to quantitatively determine the content of xanthophylls as well as detect the regulation of xanthophylls cycle in cranberry with yellow vine syndrome under high light conditions.

The recovery experiments may provide novel insights into the mechanisms of yellow vine syndrome development in cranberry bogs and offer an opportunity to solve the problem. Recent recovery of photoinhibited plant leaves was examined, and PS II mobility in thylakoid membranes may play a key role (Oguchi *et al*., 2008). We plan to conduct experiments on the recovery from the syndrome under optimized experimental conditions.

Recently some evidence showed that the use of specific herbicide such as Casoron may significantly magnify the case (Demoranville, 2009). It might be interesting to test the effects of a variety of herbicides on the development of yellow vine symptom. The low level of chlorophyll may be due to the negative regulation of chlorophyll biosynthesis and positive regulation of chlorophyll degradation. It is worthy to examine the profiles of chlorophyll degradation and biosynthesis in yellow vine samples. As there might be yellow vine genes in cranberry plants, 454 cDNA sequencing may possibly identify the yellow vine genes. Whether there are microbes involved in the yellow vine formation is not known. Althouth we have some clues and evidence for the formation of yellow vine, there is still a long way to solve the problem.

Acknowledgements

We thank Professor DeMoranville and Jeranyama at University of Massachusetts Cranberry Station for fruitful collaboration and support. We also thank Fan Zhang, Zi Wei, Nid Geh, Robert Mulkern, Sean Cederlund for participating part of the work and discussions. This work is supported in part by funding from USDA CSREES, UMD Chancellor's Resraech Fund, and UMD Cranberry Research Program.

References

National Agricultural Statics Service, 2006

Baker, N.R. (2008) Chlorophyll Fluorescence: a Probe of Photosynthesis in Vivo. Annu. Rev. Plant Biol. 59: 89-113

Bomser J, DL Madhavi, K Singletary, MAL Smith (1996) In Vitro Anticancer Activity of Fruit Extracts from Vaccinium Species. Planta Medica. 62: 212-216

De las Rivas J, A Abadia, J Abadia (1989) A New Reversed-Phase HPLC Method Resolving all Major Higher Plant Photosynthetic Pigments. Plant Physiol. 91: 190-192

Demoranville C (2006) Cranbery Best Management Practice Adoption and Conservation Farm Planning in Massachusetts. Hort. Tech. 16: 393-397

Demoranville C, DeMoranville C, B Lampinen (2009) UMass Extension's Cranberry Station Newsletter: 1-2

DeMoranville C, B Lampinen (1999) UMass Extension's Cranberry Station Newsletter: 2-3

Howell A, N Vorsa, A Der-Petrossian, L Foo(1998) New Engl. J. Med. 339: 1085-1086

Kruger GHJ, M Tsimilli-Michael, RJ Strasser (1997) Light Stress Provokes Plastic and Elastic Modifications in Structure and Function of Photosystem II in Camellia Leaves. Physiol. Plant. 101: 265-277

Oukarroum A, G Schansker, RJ Strasser (2009) Drought Stress Effects on Photosystem I Content and Photosystem II Thermotolerance Analyzed Using Chl a Fluorescence Kinetics in Barley Varieties Differing in Their Drought Tolerance. Physiol. Plant. 137: 188-199

Porra RJ, WA Thompson, PE Kriedemann (1989) Determination of Accurate Extinction Coefficients and Simultaneous Equations for Assaying Chlorophylls a and b Extracted with Four Different Solvents: Verification of the Concentration of Chlorophyll Standards by Atomic Absorption Spectroscopy. Biochim. Biophys. Acta. 975: 384-394

Strasser RJ, M Tsimilli-Michael, A Srivastava (2004) Analysis of the Chlorophyll a Fluorescence Transient. Adv. Photosynth. Respir. 19: 321-362

Wei Z, Jeranyama P, Zhang F, DeMoranville C, HJM Hou (2010) Probing the Mechanisms of the Yellow Vine Syndrome Development in Cranberry: Shade Effect, HortScience. 45: 1345-1348

Light Acclimation of Triple Inactivation Strain of Group 2 Sigma Factors in *Synechocystis* sp. Strain PCC 6803

Susanne Rantamäki, Taina Tyystjärvi*

Molecular Plant Biology, Department of Biochemistry and Food Chemistry, University of Turku, 20014 Turku, Finland.
*Corresponding author. Tel. No. +358 2 3335797; Fax No. +358 2 3335549; E-mail: taityy@utu.fi.

Abstract: The cyanobacterium *Synechocystis* sp. PCC 6803 encodes nine σ factors, all belonging to the σ^{70} family. We inactivated three out of the four group 2 σ factors of *Synechocystis* simultaneously in all possible combinations and found that all triple inactivation strains grow well under standard conditions but show defects in light acclimation. *In vivo* absorption spectra measurements indicate similar relative absorption of chlorophyll *a* and phycobilisomes in all strains but high carotenoid content in the ΔsigCDE strain. All triple inactivation strains are characterized by high PSII fluorescence in 77 K emission spectra. The ΔsigBCD, ΔsigBDE, and ΔsigCDE strains showed state 1 transition upon illumination with blue light, but the ΔsigBCE strain was locked to state 1. The strains missing both SigB and SigD factors simultaneously (ΔsigBCD and ΔsigBDE) were not able to grow faster when light was doubled from the PPFD of 40 μmol m^{-2} s^{-1} to the PPFD of 80 μmol m^{-2} s^{-1}. Furthermore, all triple inactivation strains grew slowly in dim light.

Keywords: Cyanobacteria; Sigma factor; 77 K fluorescence; Absorption spectrum; State transition

Introduction

Cyanobacteria are oxygen-evolving photosynthetic eubacteria and they are responsible for almost one-half of the net primary production (Field *et al*., 1998). The photosynthetic apparatuses of present day cyanobacteria and plants are similar, and ancient cyanobacteria are considered to be the ancestors of plant chloroplasts. *Synechocystis* sp. strain PCC 6803 (hereafter *Synechocystis*) is a unicellular, non-toxic, non-nitrogen-fixing, naturally competent fresh-water cyanobacterium commonly used as a model organism (Ikeuchi and Tabata, 2001).

Acclimation to environmental stress conditions requires many changes in gene expression. In cyanobacteria, the regulation of transcription initiation has a key role in acclimation processes. Cyanobacteria contain only one type of RNA polymerase that transcribes all rRNAs, tRNAs and mRNAs. The RNA polymerase core ($\alpha_2\beta\beta'\gamma\omega$) is able to perform the polymerization reaction but an additional subunit is required for transcription initiation. The σ subunit of the RNA polymerase holoenzyme is responsible for the specific recognition of promoter sequences and it is required for transcription initiation.

Synechocystis encode for nine sigma factors, one group 1 σ factor, four group 2 σ factors and four group 3 σ factors, which are all belong to the σ^{70} family (for a review see Osanai *et al*., 2008). The essential group 1 σ factor is SigA. Group 2 σ factors (SigB, SigC, SigD and SigE) show high sequence and structural similarity to Sig A but they are not essential (Imamura *et al*., 2003b; Pollari *et al*., 2008). Group 2 σ factors are important for acclimation to different kinds of stress conditions. One of the most important environmental factors is light and the expression of all group 2 sigma factors seems to be light regulated (Tuominen *et al*., 2003). The SigD factor together with the SigB and SigE factors has been shown to be involved in light acclimation and regulation of other genes both in light-dark transitions and upon light intensity changes (Imamura e*t al.*, 2003a; Yoshimura *et al*., 2007; Pollari *et al*., 2008, 2009, 2011).

In the present study we investigated the growth of triple inactivation strains ΔsigBCD, ΔsigBCE, ΔsigBDE and ΔsigCDE at different light conditions

and examined their ability to state transition.

Materials and Methods

The glucose tolerant strain *Synechocystis* sp. PCC 6803 (Williams, 1988) was used as control strain (CS). The triple inactivation strains of group 2 sigma factors named as ΔsigBCD, ΔsigBCE, ΔsigBDE and ΔsigCDE were constructed as described previously (Pollari *et al*., 2011).

Growth medium for S*ynechocystis* was BG-11 supplemented with 20 mmol HEPES-NaOH pH 7.5. The growth plates of the mutants were supplemented with kanamycin (50 μg/ml), streptomycin (20 μg/ml), spectinomycin (10 μg/ml), and chloramphenicol (10 μg/ml) but antibiotics were not added to short-time liquid cultures. Continuous photosynthetic photon flux density (PPFD) was 40 μmol m^{-1} s^{-1}, temperature 32 °C, and the cells were grown in ambient CO_2. Liquid cultures were shaken at 90 rpm.

Doubling times were measured at the PPFDs of 20, 40 and 80 μmol m^{-2} s^{-1}. The A_{730} of liquid cultures was set to 0.1. The 30 ml cell cultures were grown in 100 ml Erlenmeyr flasks and growth of the cells was monitored by measuring A_{730}.

77 K fluorescence spectrums were measured with an Ocean Optics S2000 spectrometer. Cells (50 μg chlorophyll/ml; 50 μl samples) were frozen directly from growth conditions, and for induction of state transitions cells were illuminated with blue light (450 nm Corion low-pass filter) of 40 μmol photons m^{-2} s^{-1} for 5 min and then frozen with liquid nitrogen. Orange excitation light was from a slide projector trough a 580 nm narrow-band filter (Corion). The spectra were corrected by subtracting a low background signal, smoothed with a moving median using a 2 nm window, and normalized by dividing by the peak value of PSI emission at 723 nm.

In vivo absorption spectra were measured with UV-3000 spectrophotometer (Shimadzu, Japan) from 350 nm to 800 nm.

Results and Discussion

The triple inactivation strains grow as well as the control strains under our standard growth conditions (Pollari *et al*., 2011). The *in vivo* absorption spectra of all triple inactivation strains were fairly similar to that of the control strain (Fig. 1). The phycobilin to chlorophyll ratio was 0.9 in all strains when calculated by divining the phycobilin peak at 625 nm with the chlorophyll peak at 678 nm. The carotenoid peak at 490 nm was slightly higher in the ΔsigCDE strain than in the other strains.

Synechocystis can balance energy distribution between photosystem I (PSI) and photosystem II (PSII) according to light quality. The major light harvesting antennae of PSII, phycobilisomes, efficiently collect orange light while the chl *a* antenna of PSI harvests mainly blue and red light. State transitions balance energy distribution between the photosystems: illumination with orange PSII-light leads to state 2 in which energy is transferred more efficiently to PSI, and treatment with PSI-light (blue light) leads to compensatory energy flow to PSII (state 1) (van Thor *et al*., 1998).

We measured the 77 K fluorescence emission spectra from the cells taken directly from growth conditions and also after 5 min of blue light illumination (Fig. 2).

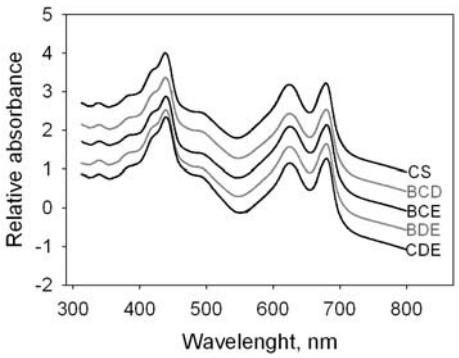

Fig. 1 The *in vivo* absorption spectra of the control and all triple inactivation strains. The cells were grown under standard growth conditions for 2 days.

Typically *Synechocystis* is in the low PSII fluorescence state (state 2) under our growth conditions, and illumination of the cells with blue light induces transition to the high fluorescence state (state 1). The state transition was obvious in the control strain when cells were illuminated with blue light (Fig. 2). The ΔsigBCD, ΔsigBDE, and ΔsigCDE strains showed state 1 transition upon illumination with blue light, although the difference in fluorescence states was not so prominent in the ΔsigBCD strain. Furthermore, all triple inactivation strains had higher PSII fluorescence peaks at 685 and 695 nm than the control strain when samples were taken from the standard growth conditions (Fig. 2). In the ΔsigCDE strain the ratio of the 695 nm peak/ the

685 nm peak was higher than in the other strains, and ΔsigCDE was the only strain that had clear changes in the phycobilisome peak after the blue light illumination. Unlike the other strains, the ΔsigBCE strain did not show state transition upon blue light illumination. This strain grows slowly in blue light (Pollari *et al*., 2011).

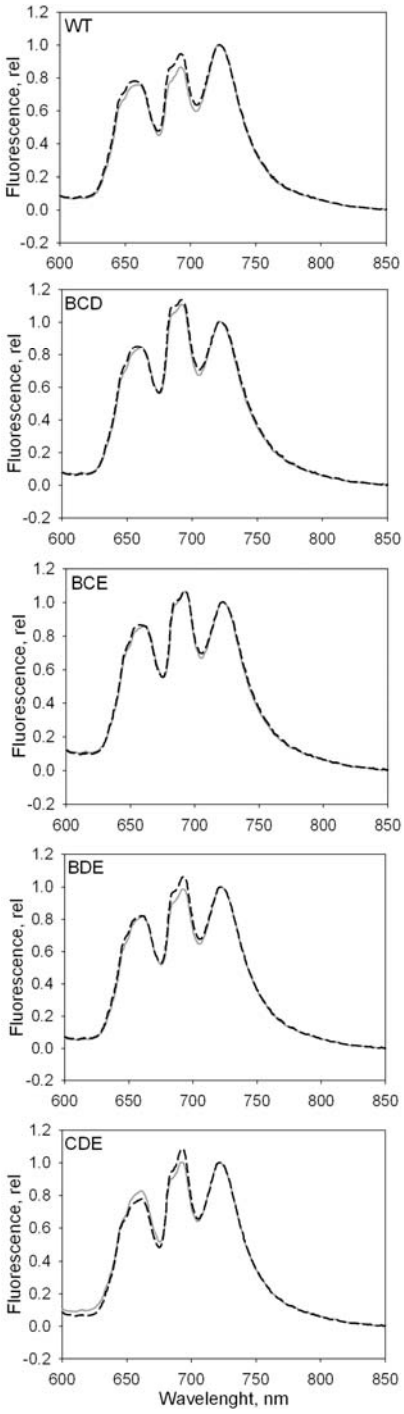

Fig. 2 State transitions in the control and triple inactivation strains. Fluorescence was measured at 77 K with orange excitation light from cells taken directly from growth conditions (grey line) or after 5 min illumination with blue light (black dashed line). The data were normalized by dividing by the height of the PSI emission peak at 723 nm.

The capacity of the triple inactivation strains to acclimate to different light conditions was tested by measuring the doubling times of the control and triple inactivation strains at the PPFDs of 20, 40 and 80 μmol m^{-2} s^{-1} during the first 24 h of growth. Low light intensity limits growth in our standard growth conditions, and doubling the light intensity enhanced the growth of the control strain (Fig. 3). The ΔsigBCD and ΔsigBDE strains, however, were not able grow faster when light was doubled from the PPFD of 40 to the PPFD of 80 μmol m^{-2} s^{-1}. These strains are missing both the SigB and SigD factors. We have previously shown that the double inactivation strain ΔsigBD cannot take full advantage of the double light intensity (Pollari *et al*., 2009). In dim light (20 μmol m^{-2} s^{-1}) all triple inactivation strains grew more slowly than the control strain (Fig. 3), the doubling time for the control strain was 15 h and for the triple inactivation strains it was from 16.5 to 17 h.

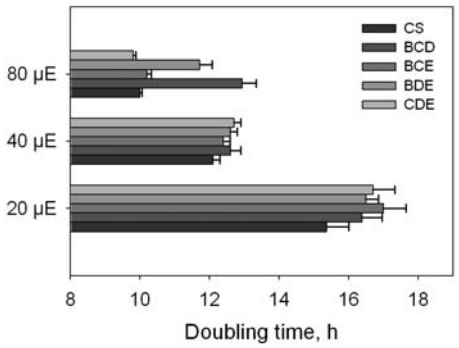

Fig. 3 Doubling times of the control and triple inactivation strains in continuous dim light at PPFD of 20 μmol m^{-2} s^{-1}, normal light at the PPFD of 40 μmol m^{-2} s^{-1} and in high light at the PPFD of 80 μmol m^{-2} s^{-1}. Each data point represents the mean of six replicates. The error bars denote SE.

It has been previously shown that single and double inactivation strains of group 2 sigma factors lacking the SigD factor grow slowly in double light intensity on agar plates (Pollari *et al*., 2008), and the ΔsigBD double inactivation strain grows slowly in liquid cultures at 80 μmol m^{-2} s^{-1}. Our new results show that the strains having either the SigB factor (the ΔsigCDE strain) or the SigD factor (the ΔsigBCE strain) as the only remaining group 2 sigma factor are able to utilize double light intensity as efficiently as the control strain while strains missing both the SigB and SigD factors (the ΔsigBCD and ΔsigBDE strains) cannot use high light efficiently. It is also known that the ΔsigBD strain has troubles to acclimate the light-harvesting system normally at higher light intensities

(Pollari *et al*., 2009). Previous results have shown that strains ΔsigBD, ΔsigBCD, ΔsigBCE and ΔsigBDE are more sensitive to photoinhibition (Pollari *et al*., 2009, 2011) because the PSII repair cycle does not function as efficiently as it should due to low induction of *psbA2* and *psbA3* genes (Pollari *et al*., 2011). The SigB and SigD factors show higher similarity with each other than any other pair of group 2 sigma factors (Pollari *et al*., 2008) and although they show clear redundancy in the regulation of light acclimation it seems that the SigD factor is more important for antenna adjustments and the SigB factor for proper function of the PSII repair cycle.

Acknowledgement

This work was financially supported by the Academy of Finland.

References

Field CB, Behrenfeld MJ, Randerson JT, Falkowski P (1998) Primary Production of Biosphere: Integrating Terrestrial and Oceanic Components. Science 281: 237-240

Ikeuchi M, Tabata S (2001) Synechocystis sp. PCC 6803 - a Useful Tool in the Study of Genetics of Cyanobacteria. Photosynth. Res. 70: 73-83

Imamura S, Asayma M, Takahashi H, Tanaka K, Shirai M (2003a) Antagonistic Dark/Light-Induced SigB/SigD, Group 2 Sigma Factors, Expression Through Redox Potential and Their Roles in Cyanobacteria. FEBS Lett. 554: 357-362

Imamura S, Yoshihara S, Nakano S, Shiozaki N, Yamada A, Tanaka K, Takahashi H, Asayama M, Shirai M (2003b) Purification, Characterization, and Gene Expression of all Sigma Factors of RNA Polymerase in a Cyanobacterium. J. Mol. Biol. 325: 857-872

Osanai T, Kanesaki Y, Nakano T, Takahashi H, Asayama M, Shirai M, Kanehisa M, Suzuki I, Murata N, Tanaka K (2005) Positive Regulation of Sugar Catabolic Pathways in the Cyanobacterium Synechocystis sp. PCC 6803 by the Group 2 σ Factor SigE. J. Biol. Chem. 280: 30653-30659

Osanai T, Ikeuchi M, Tanaka K (2008) Group 2 Sigma Factors in Cyanobacteria. Physiol. Plant. 133: 490-506

Pollari M, Gunnelius L, Tuominen I, Ruotsalainen V, Tyystjärvi E, Salminen T, Tyystjärvi T (2008) Characterization of Single and Double Inactivation Strains Reveals New Physiological Roles for Group 2 σ Factors in the Cyanobacterium Synechocystis sp. PCC 6803. Plant Physiol. 147: 1994-2005

Pollari M, Rantamäki S, Huokko T, Kårlund-Marttila A, Virjamo V, Tyystjärvi E, Tyystjärvi T (2011) Effects of Deficiency and Overdose of Group 2 Sigma Factors in Triple Inactivation Strains of Synechocystis sp. Strain PCC 6803. J. Bacteriol. 193: 265-273

Pollari M, Ruotsalainen V, Rantamäki S, Tyystjärvi E, Tyystjärvi T (2009) Simultaneous Inactivation of Sigma Factors B and D Interferes with Light Acclimation of the Cyanobacterium Synechocystis sp. Strain PCC 6803. J. Bacteriol. 191: 3992-4001

Tuominen I, Tyystjärvi E, Tyystjärvi T (2003) Expression of Primary Sigma Factor (PSF) and PSF-Like Sigma Factors in the Cyanobacterium Synechocystis sp. Strain PCC 6803. J. Bacteriol. 185: 1116-1119

van Thor JJ, Mullineaux CW, Matthijs HCP (1998) Light Harvesting and State Transitions in Cyanobacteria. Botanica Acta 111: 430-443

Williams JGK (1988) Construction of Specific Mutations in Photosystem II Photosynthetic Reaction Center by Genetic Engineering Methods in Synechocystis 6803. Methods Enzymol. 167: 766-778

Yoshimura T, Imamura S, Tanaka K, Shirai M, Asayama M (2007) Cooperation of Group 2 σ Factors, SigD and SigE for Light-Induced Transcription in the Cyanobacterium Synechocystis sp. PCC 6803. FEBS Lett. 581: 1495-1500

Gradients of Photoinhibition in the Interior of a Leaf Induced by Photoinhibition Lights of Different Colors

Riichi Oguchi[a,b,*], Peter Douwstra[a,c], Takashi Fujita[a], Wah Soon Chow[b], Ichiro Terashima[a]

[a]Department of Biological Sciences, The University of Tokyo, Tokyo, Japan;
[b]Research School of Biology, The Australian National University, Canberra, Australia;
[c]Department of Plant Sciences, Wageningen University, Wageningen, Netherlands.
[*]Corresponding author. Tel. No. +81 22 795 7732; Fax No. +81 22 795 7732; E-mail: riichi@biology.tohoku.ac.jp.

Abstract: Gradients of photoinhibition within a leaf caused by different color lights were studied to get more insight into the controversy whether photon absorption by chlorophyll or Mn is the primary cause of photoinhibition, suggested by the excess-energy hypothesis or the Mn (two-step) hypothesis, respectively. We photoinhibited lincomycin-treated leaf-discs with white, blue, green or red light. A combination of a micro-fiber fluorometer, a fiber-thinning technique and a micro-manipulator enabled us to measure the chlorophyll fluorescence signals within a leaf. Gradients of photoinhibition were also compared with results from various conventional fluorometers to estimate their depth of signal detection. The photoinhibition was more severe in the descending order of blue, red and green light near the adaxial surface, and in the descending order of blue, green and red light in the deeper tissue, which is correlated with the absorption spectrum of chlorophyll and Mn, respectively. These results cannot be explained by either hypothesis alone and strongly suggest that both mechanisms occur in photoinhibition. F_v/F_m values of photoinhibited leaves estimated with the conventional fluorometers were different from the whole tissue. This is because the depths, in which these systems detect fluorescence signals, differ depending on the wavelengths of measuring beam and detector.

Keywords: Chlorophyll fluorescence; Excess-energy hypothesis; Fluorometers; P700 redox kinetics; Photoinhibition action spectra; Mn hypothesis

Introduction

There is a marked light gradient across the leaf, analogous to the vertical light gradients in forests or herbaceous stands (Terashima and Saeki, 1983). Strong light often causes photoinactivation of photosystem II, also known as photoinhibition. The damage becomes more severe with increase in light intensity. Thus, the intra-leaf light gradient should cause a gradient of photoinhibition (Schreiber *et al*., 1996), which is usually neglected in research using chlorophyll fluorescence techniques.

Chlorophyll fluorescence instruments such as a Pulse Amplitude Modulation fluorometer (PAM) usually collect fluorescence signals from only the adaxial side of leaves, which gives little information about the depth of signal detection. However, there should be a photoinhibition gradient inside a leaf. Thus, depending on the depth of signal detection, the photoinhibition estimated by the fluorometers could be an over-estimation or under-estimation. Therefore it is very important to evaluate the difference between the extent of photoinhibition in the whole tissue and the extent of photoinhibition measured with various conventional fluorometers.

When we deal with light, its spectral composition and absorption spectra of the leaf pigments also need to be taken into account. Green light is less absorbed by chlorophyll than blue or red light; therefore, green light penetrates much better than blue and red light (Vogelmann and Han, 2000; Vogelmann and Evans, 2002). Then a question arises: How do different color

light gradients cause gradients of photoinhibition within a leaf?

In studies of the mechanism of the photoinhibition there are two conflicting hypotheses at present. One hypothesis, termed the excess-energy hypothesis, is that excess-energy received by chlorophylls, being neither utilized by photosynthesis nor dissipated harmlessly in non-photochemical quenching, causes the photoinactivation (Ögren *et al*., 1984; Demmig and Björkman, 1987). The other hypothesis is termed the Mn hypothesis (or the two-step hypothesis). It suggests that excitation of Mn by photons and loss of the Mn from oxygen evolving complex is the primary cause (Hakala *et al*., 2005; Ohnishi *et al*., 2005). Because the absorbance spectra of chlorophyll and Mn are significantly different (Fig. 1), we thought that photoinhibition experiments with different color lights would allow us to test both hypotheses.

The objectives are (1) to show the different intra-leaf photoinhibition gradients inside the leaves that were photoinhibited by different color light sources, (2) to discuss the possibility of the involvement of dual mechanisms in photoinhibition in leaves, which was suggested in our previous study (Oguchi *et al*., 2009) and (3) to evaluate the difference between the extent of photoinhibition in the whole tissue and the values measured with conventional fluorometers.

Materials and Methods

We used capsicum (*Capsicum annuum* L. 'Newtown No. 3') and spinach (*Spinacia oleracea* L. 'Try') leaves for the photoinhibition measurements. Capsicum plants were grown at 20 ºC with an 8 h photoperiod (130 μmol m^{-2} s^{-1} for a total of 7 h and 660 μmol m^{-2} s^{-1} for 1 h in mid-photoperiod) in 1.5 liter pots filled with vermiculite. Nutrients were supplemented weekly by a commercial nutrient solution (1/1000 strength of the Powder Hyponex N:P:K = 13:12:38, Hyponex Japan, Osaka, Japan). Spinach plants were grown hydroponically at 23 ºC with an 8 h photoperiod (350 μmol m^{-2} s^{-1}) with the Hoagland nutrient solution containing 4 mmol KNO_3, 4 mmol $Ca(NO_3)_2$, 0.05 mmol KH_2PO_4 and microelements. The hydroponic culture solution was renewed weekly.

In the photoinhibition treatments, lincomycin treated leaf-discs of capsicum and spinach were photoinactivated for 1 h, by white (400–700 nm), blue (400–500 nm), green (500–600 nm) or red (600–700 nm) light at 1,000 μmol m^{-2} s^{-1}. Leaf-discs floating on a lincomycin solution (1 mmol) were illuminated from the adaxial side.

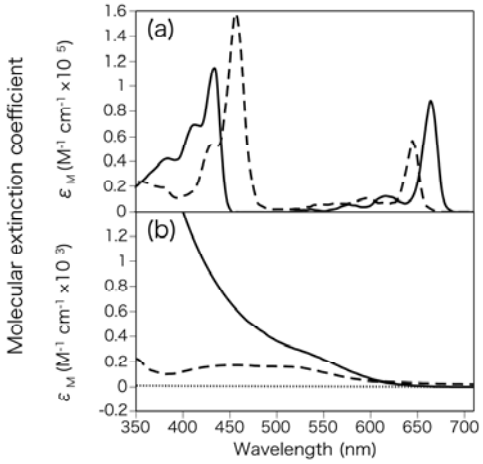

Fig. 1 (a) Molecular extinction coefficient of chlorophyll *a* (solid-line) and chlorophyll *b* (broken-line) in diethyl ether, adapted from Ohashi *et al*. (2008); (b), molecular extinction coefficient of model compounds, Mn (II) gluconate (dotted-line), Mn (III) gluconate (broken-line) and Mn (IV) gluconate (solid-line), adapted from Bodini *et al*. (1976). (Redrawn from (Oguchi *et al*., 2011); with permission from Oguchi *et al*.).

For the photoinhibition measurements, we compared 3 different measurements of PSII activity. The first method is a chlorophyll fluorescence measurement inside a leaf with a fiber PAM system. The combination of a micro-fiber PAM system (Microfiber PAM, Walz, Effeltrich, Germany), a fiber thinning technique and a micro-manipulator system (WR-60, Narishige Scientific Lab., Tokyo, Japan) made it possible to accurately measure chlorophyll fluorescence signals inside the leaf. The light source for the measuring light and the saturating flash was a standard blue LED (peak emission 470 nm). A short-pass filter ($\lambda < 600$ nm) was used for the light source and a long-pass filter ($\lambda > 640$ nm) for the detector. The end of the micro-fiber probe (diameter 140 μm) was tapered (diameter 30 μm) using a burner and a weight, for inserting into leaf-discs. The leaf-disc was sandwiched by a holder having a hole of diameter 2.5 mm for the insertion. The position of the fiber tip with respect to the leaf surface was adjusted under a microscope.

A second method was a common chlorophyll fluorescence measurement with a conventional fluorometer (PAM101, 102 and 103, Walz) with red LED measuring light (101-ED, Walz).

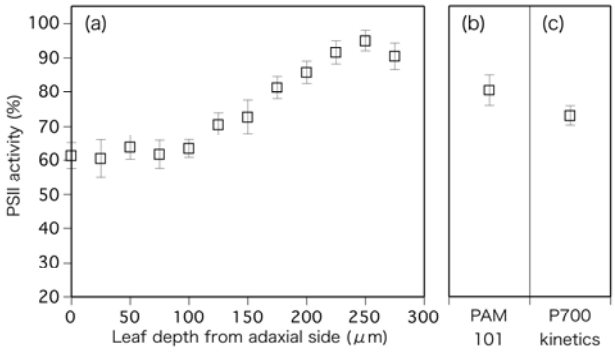

Fig. 2 The gradient of PSII activity (%) compared to non-photoinhibited leaves (a) inside photoinhibited capsicum leaves, measured by tapered fiber tips with the micro-fiber PAM system. Values are compared with those measured by PAM 101 with red LED light source (b) and P700 redox kinetics (c). Leaf-discs were photoinhibited with white light (400-700 nm, open symbols). In (a) and (b), PSII activity (%) was calculated as (F_v/F_m of photoinhibited leaves ÷F_v/F_m of non-photoinhibited leaves) × 100. Averages of 3–5 measurements for control and of 3 measurements for white-light photoinhibition are shown. Error bars indicate standard errors. (Redrawn from (Oguchi *et al*., 2011); with permission from Oguchi *et al*.).

A third method was a whole-tissue PSII activity measurement with P700 redox kinetics, which has shown a good correlation with PSII activity measured by oxygen-evolution per single-turnover saturating flash (Losciale *et al*., 2008). The redox change of P700 was measured with a dual-wavelength (820/870 nm) unit (ED-P700DW) attached to a PAM fluorometer (Walz) and used in the reflectance mode (Chow and Hope, 2004). To obtain redox changes as the result of a flash superimposed on continuous far-red light, a steady-state was sought by illumination with far-red light (12 μmol photons m^{-2} s^{-1}, 102-FR, Walz) for ≥ 20 sec. Then a single-turnover saturating flash (Fiber Strobo FS-1J10, Nissin Electronic Co., Tokyo, Japan, or XST 103 xenon flash only for Fig. 4, Walz) was applied to the adaxial side of the leaf-disc. Immediately after the flash, P700 was fully oxidized, followed by reduction by electron flow from PSII induced by the same flash. Reduced P700 was then re-oxidized by far-red light back to the steady-state concentration. In this procedure, the area between the steady-state concentration of $P700^+$ and the $P700^+$ redox kinetics curve (P700 redox kinetics area) should be correlated with the cumulative electron flow from PSII to $P700^+$ after a single-turnover flash. See Losciale *et al*. (2008) for procedure details.

Statistical analyses were performed with R statistical software (version 2.10.1; The R Foundation for Statistical Computing). The one way ANOVA with the Bonferroni-Holm method as the post-hoc tests was used to test pairwise differences among different colors.

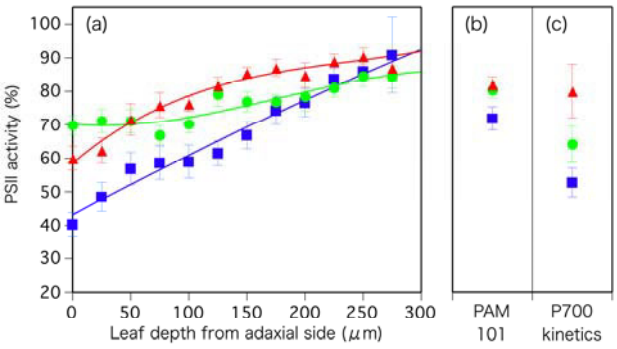

Fig. 3 The gradient of PSII activity (%) compared to non-photoinhibited leaves (a) inside photoinhibited capsicum leaves, measured by tapered fiber tips with the micro-fiber PAM system. Values are compared with those measured by PAM 101 with red LED light source (b) and P700 redox kinetics (c). Leaf-discs were photoinhibited by blue light (400–500 nm, squares), green light (500–600 nm, circles) and red light (600–700 nm, triangles). In (a) and (b), PSII activity (%) was calculated as (F_v/F_m of photoinhibited leaves) / (F_v/F_m of non-photoinhibited leaves) × 100. Averages of 4–9 measurements are shown. Error bars indicate standard errors. Third-order polynomials were used for the regressions. (Redrawn from (Oguchi *et al*., 2011); with permission from Oguchi *et al*.).

Results and Discussion

The F_v/F_m measurements inside leaves using a tapered fiber PAM system clearly showed a gradient of photoinhibition across a leaf in capsicum (Fig. 2a) and spinach (data not shown). Because of the light gradient across a leaf, shallower tissue showed the greater photoinhibition and deeper tissue showed the smaller photoinhibition. We compared this result with the result of PAM 101 and P700 redox kinetics measurement from the adaxial side of leaves (Fig. 2b, c). The value of PAM 101 was similar to the value of deeper tissue (closest to the results of 175 μm in capsicum and 200 μm in spinach). P700 redox kinetics, which represents the whole tissue PSII activity (Losciale *et al*., 2008), was lower than the value of PAM 101 and was closest to the results of the tapered fiber in the depth of 75 μm in capsicum.

When we compared the intra-leaf photoinhibition gradients among leaves that had been photoinhibited with different color lights, significantly different gradients were observed in both capsicum (Fig. 3) and spinach (data not shown). The gradient of

photoinhibition was steeper in blue- and red-light than in green-light, indicating that the blue- and red-lights were absorbed strongly near the adaxial surface, but that green-light penetrated deeper in leaf tissue because the absorbance spectrum of chlorophyll has peaks at blue and red wavelengths (Fig. 1a). This was supported by previous studies that measured the light intensity gradient inside a leaf via the chlorophyll fluorescence intensity emitted from leaf cross sections (Koizumi *et al*., 1998; Brodersen and Vogelmann, 2010). In addition, Terashima *et al*. (2009) showed that the differential quantum yield of green light in strong background white-light was higher than that of red-light.

Table 1 The F_v/F_m at the most adaxial side (Depth: 0 μm), middle (Depth: 150 μm for capsicum, 200 μm for spinach) and most abaxial side (Depth: 275 μm for capsicum, 400 μm for spinach) of leaves. F_v/F_m values were averages of both measurements from the adaxial and from the abaxial side of leaves. Lower case letters indicate significance at $P < 0.05$ with a one-way ANOVA with the Bonferroni-Holm method as the post-hoc tests for pairwise differences among different colors. The averages ± standard errors of 9–13 measurements are shown.

	Depth	Blue	Green	Red
Capsicum	0	0.278±0.025a	0.494±0.021c	0.414±0.024b
	150	0.470±0.029a	0.540±0.020ab	0.601±0.014b
	275	0.664±0.082a	0.600±0.022a	0.620±0.027a
Spinach	0	0.343±0.037a	0.571±0.027c	0.484±0.022b
	200	0.514±0.022a	0.645±0.018b	0.699±0.015b
	400	0.699±0.007a	0.678±0.018a	0.734±0.013a

On the most adaxial side (0 μm) of leaf inhibited with different color lights, the extent of photoinhibition was in the decreasing order of blue, red and green light (Table 1, Fig. 3a for capsicum), which is correlated to the chlorophyll absorption spectrum. Chlorophylls absorb blue and red much better than green light; therefore, the decrease of F_v/F_m was larger in blue and red than in green light. However, Mn absorbs green better than red light (Bodini *et al*., 1976, Fig. 2b); therefore, the Mn mechanism cannot explain the greater photoinhibition in red than in green light. On the other hand, in the deeper tissue (150 μm for capsicum, 200 μm for spinach), photoinhibition was in the decreasing order of blue, green and red light (Table 1, Fig. 3a for capsicum), which corresponded to the Mn absorbance spectrum. This result cannot be explained by the excess-energy hypothesis. Accordingly, these data strongly suggest that both the excess-energy mechanism and the Mn mechanism are involved in photoinhibition, confirming our earlier suggestion (Oguchi *et al*., 2009).

We also investigated the relationship between the PSII activity measured by the P700 redox kinetics and the F_v/F_m values measured with 5 conventional fluorometers (Fig. 4). The estimation of PSII activity from P700 redox kinetics gave a good one to one correlation with O_2/flash for the whole leaf tissue (Losciale *et al*., 2008), which indicates that both methods measure PSII activity of the whole leaf tissue. On the other hand, F_v/F_m measured by typical fluorometers showed curvilinear relationships with the value of P700 redox kinetics (Figs. 4a and 4b). The measurements with red measuring light (red symbols) showed convex curve relationships and the values were usually higher than the values of P700 redox kinetics. The measurements with blue measuring light (blue symbols) showed concave curve relationships and the values were usually lower than the values of P700 redox kinetics. This means the fluoromenter with red measuring light underestimated the extent of photoinhibition, and fluorometers with blue measuring light overestimated the extent of photoinhibition in the whole tissue.

This difference should be caused by the difference in the color of measuring light and the difference in the wavelength range of detecting fluorescence. The ordinary PAM system (PAM 101) uses a red (peak at 650 nm) or a blue (peak at 470 nm) LED light as the measuring light. In the case of red measuring light, the fluorescence is selected by a long-pass filter transmitting above about 710 nm. Therefore, the fluorescence from 710 to 800 nm is used as signal, which is not readily re-absorbed by chlorophylls, and the signals should be able to emerge from deeper tissue. On the other hand, in the case of blue measuring light, the fluorescence through either of the long-pass filters (Filter 1, $\lambda > 710$ nm; Filter 2, 710 nm $> \lambda >$ 660 nm; or Filter 3, $\lambda >$ 660 nm) is detected. Because the fluorescence between 660 and 700 nm is readily re-absorbed by chlorophylls (Agati *et al*., 1993), this fluorescence should be derived from very shallow, therefore strongly-photoinhibited, tissue. Supporting this hypothesis is that measurements with Filter 2 (triangles in Fig. 4) gave the lowest F_v/F_m, indicating that the shallowest tissue was sampled.

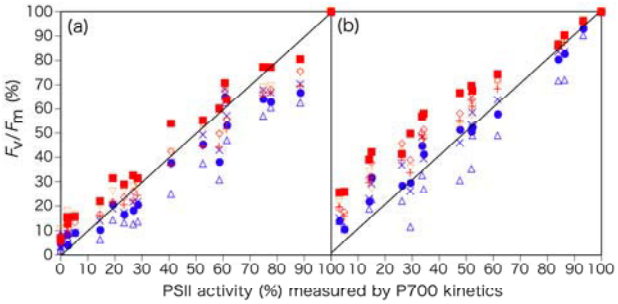

Fig. 4 The relationship between PSII activity (%) measured by P700 redox kinetics area and F_v/F_m (%) measured with 5 PAM instruments in capsicum (a) and in spinach (b). Red symbols represent instruments using red LED light as measuring light (squares, PAM 101, Walz; diamonds, miniPAM, Walz; inverted triangles, PEA meter, Hansatech, King's Lynn, UK; and crosses, PAM 100, Walz). Blue symbols represent PAM 101 using blue LED light source (beveled crosses, filter1, $\lambda > 710$ nm; triangles, filter 2, 710 nm > λ > 660 nm; and circles, filter 3, $\lambda >$ 660 nm). Control F_v/F_m values of squares, diamonds, inverted triangles, crosses, beveled crosses, triangles and circles were 0.790, 0.785, 0.791, 0.796, 0.783, 0.81 and 0.804 for capsicum and 0.817, 0.812, 0.821, 0.824, 0.799, 0.816 and 0.811 for spinach. (Redrawn from (Oguchi *et al*., 2011); with permission from Oguchi *et al*.).

Besides, red light (at 650 nm) penetrates leaves better than blue light (at 450 nm, Vogelmann and Han 2000), thus red measuring light (620–650 nm) reaches the deeper tissue, which is not strongly photoinhibited, than blue measuring light (460–470 nm). Accordingly, the different fluorometers measure different depths of leaf tissue. Because there is a photoinhibition gradient inside a leaf, this difference in depth of signal detection yields different results in F_v/F_m and photoinhibition extents.

The depth of signal detection using a given fluorometer may vary with the extent of photoinhibition. Usually, photoinhibition decreases F_m, thereby lowering F_v/F_m (= $1-F_o/F_m$) in photoinhibited leaves (Oguchi *et al*., 2009). This means that the fluorescence emitted from photoinhibited chloroplasts is decreased. Therefore, when photoinhibition is more severe, the fluorescence from chloroplasts near the photoinhibitory illuminated side decreases, and the relative contribution of fluorescence from deeper tissue increases. This should increase the depth of signal detection by the fluorometer from the photoinhibitory illumination side of leaves. Therefore, in the case of photoinhibited leaves, the fluorometers with red measuring light detect deeper tissue than the average of the whole tissue. However, in the case of non-photoinhibited leaves, the fluorometers with red measuring light measures shallower tissue than the representative depth of the average electron transfer rate of the whole tissue. It was observed that the electron transfer rate measured with a fluorometer using red measuring light was lower than the rate measured with gas-exchange measurement (Tsuyama *et al*., 2003). This is because the electron transfer rate is calculated from φPSII, the quantum yield of PSII averaged over closed and open PSII traps assayed with chlorophyll fluorescence. It should be noted that $\varphi_{PSII} = q_P \times F_v'/F_m'$, where q_P is a measure of the oxidation state of the primary quinone acceptor in PSII. Both q_P and F_v'/F_m' in the shallower tissue are expected to be lower than the average of the whole tissue due to the effect of light gradient inside a leaf (see Terashima *et al*., 2009 for F_v'/F_m').

We conclude (1) different photoinhibition gradients were observed under the different colored lights, which supports our proposal that both the excess-energy mechanism and the Mn mechanism are involved in photoinhibition, and (2) depending on the instruments, the conventional PAM fluorometers measured different depths in leaf tissue. Because of the photoinhibition gradient, fluorometers using the red measuring light tend to underestimate the extent of photoinhibition, and fluorometers with the blue measuring light tend to overestimate the extent of photoinhibition of herbaceous plants. We should not ignore the intra-leaf photoinhibition gradient, and bear in mind the fact that depth from which we are collecting fluorescence signals differs depending on the instruments and materials.

Acknowledgements

We thank H Abe for his generous offer of instruments, S Syu for his supporting plants growth, R Nakane for his experimental support and advice, Y Wang for her experimental support and Jan for her helpful comments on the manuscript. This work was supported by JSPS Research Fellowship for Young Scientists (18-8553 to R O); JSPS Postdoctoral Fellowships for Research Abroad (21-674 to R O); an Australian Research Council (DP1093827 to W S C); and Grant-in-Aid for Challenging Exploratory Research (21657007 to I T).

The original version of the present paper was published in New Phytologist (Oguchi *et al*., 2011).

References

Agati G, Fusi F, Mazzinghi P, Dipaolo ML (1993) A Simple Approach to the Evaluation of the Reabsorption of Chlorophyll Fluorescence-Spectra in Intact Leaves. J. Photochem. Photobiol. B-Biol. 17: 163-171

Bodini ME, Willis LA, Riechel TL, Sawyer DT (1976) Electrochemical and Spectroscopic Studies of Manganese (II), Manganese (III), and Manganese (IV) Gluconate Complexes I. Formulas and Oxidation-Reduction Stoichiometry. Inorg. Chem. 15: 1538-1543

Brodersen CR, Vogelmann TC (2010) Do Changes in Light Direction Affect Absorption Profiles in Leaves? Funct. Plant Biol. 37: 403-412

Chow WS, Hope AB (2004) Electron Fluxes through Photosystem I in Cucumber Leaf Discs Probed by Far-Red Light. Photosynth. Res. 81: 77-89

Demmig B, Björkman O (1987) Comparison of the Effect of Excessive Light on Chlorophyll Fluorescence (77K) and Photon Yield of O_2 Evolution in Leaves of Higher-Plants. Planta 171: 171-184

Hakala M, Tuominen I, Keränen M, Tyystjärvi T, Tyystjärvi E (2005) Evidence for the Role of the Oxygen-Evolving Manganese Complex in Photoinhibition of Photosystem II. Biochim. Biophys. Acta 1706: 68-80

Koizumi M, Takahashi K, Mineuchi K, Nakamura T, Kano H (1998) Light Gradients and the Transverse Distribution of Chlorophyll Fluorescence in Mangrove and Camellia Leaves. Ann. Bot. 81: 527-533

Losciale P, Oguchi R, Hendrickson L, Hope AB, Corelli-Grappadelli L, Chow WS (2008) A Rapid, Whole-Tissue Determination of the Functional Fraction of PSII after Photoinhibition of Leaves Based on Flash-Induced P700 Redox Kinetics. Physiol. Plant. 132: 23-32

Ögren E, Öquist G, Hallgren JE (1984) Photoinhibition of Photosynthesis in Lemna-Gibba as Induced by the Interaction between Light and Temperature I Photosynthesis in Vivo. Physiol. Plant. 62: 181-186

Oguchi R, Douwstra P, Fujita T, Chow WS, Terashima I (2011) Intra-Leaf Gradients of Photoinhibition Induced by Different Color Lights: Implications for the Dual Mechanisms of Photoinhibition and for the Application of Conventional Chlorophyll Fluorometers. New Phytol. 191: 146-159

Oguchi R, Terashima I, Chow WS (2009) The Involvement of Dual Mechanisms of Photoinactivation of Photosystem II in Capsicum Annuum L. Plants. Plant Cell Physiol. 50: 1815-1825

Ohashi S, Miyashita H, Okada N, Iemura T, Watanabe T, Kobayashi M (2008) Unique Photosystems in Acaryochloris Marina. Photosynth. Res. 98: 141-149

Ohnishi N, Allakhverdiev SI, Takahashi S, Higashi S, Watanabe M, Nishiyama Y, Murata N (2005) Two-Step Mechanism of Photodamage to Photosystem II: Step I Occurs at the Oxygen-Evolving Complex and Step II Occurs at the Photochemical Reaction Center. Biochemistry 44: 8494-8499

Schreiber U, Kuhl M, Klimant I, Reising H (1996) Measurement of Chlorophyll Fluorescence within Leaves Using a Modified PAM Fluorometer with a Fiber-Optic Microprobe. Photosynth. Res. 47: 103-109

Terashima I, Fujita T, Inoue T, Chow WS, Oguchi R (2009) Green Light Drives Leaf Photosynthesis more Efficiently than Red Light in Strong White Light: Revisiting the Enigmatic Question of Why Leaves Are Green. Plant Cell Physiol. 50: 684-697

Terashima I, Saeki T (1983) Light Environment within a Leaf I. Optical Properties of Paradermal Sections of Camellia Leaves with Special Reference to Differences in the Optical Properties of Palisade and Spongy Tissues. Plant Cell Physiol. 24: 1493-1501

Tsuyama M, Shibata M, Kobayashi Y (2003) Leaf Factors Affecting the Relationship between Cchlorophyll Fluorescence and the Rate of Photosynthetic Electron Transport as Determined from CO_2 Uptake. J. Plant Physiol. 160: 1131-1139

Vogelmann TC, Han T (2000) Measurement of Gradients of Absorbed Light in Spinach Leaves from Chlorophyll Fluorescence Profiles. Plant Cell Environ. 23: 1303-1311

Vogelmann TC, Evans JR (2002) Profiles of Light Absorption and Chlorophyll within Spinach Leaves from Chlorophyll Fluorescence. Plant Cell Environ. 25: 1313-1323

Time-Resolved Fluorescence of Photosystem I *in Vivo*: Global and Target Analysis

VV Chukhutsina†, L Tian†, G Ajlani *, H van Amerongen†§

†Laboratory of Biophysics and §MicroSpectroscopy Centre, Wageningen University, Wageningen, The Netherlands; *Institut de Biologie et de Technologies de Saclay, Centre National de la Recherche Scientifique, Commissariat à l'Energie Atomique, 91191 Gif-sur-Yvette, France

Abstract: Photosystem I (PSI) is a multi-pigment-protein complex that co-operates with photosystem II (PSII) and uses light energy to transfer electrons from plastocyanin or cytochrome to ferredoxin and eventually to NADP+. Cyanobacterial BE mutant cells that lack PSII and light-harvesting phycobilisomes, provided us with the possibility to study the picosecond fluorescence kinetics of PSI *in vivo* and the results were analyzed using global and target analysis. The obtained components (5.4 ± 0.14 ps spectral equilibration and 27.8 ± 0.09 ps excitation trapping) are very similar to those found before for isolated PSI. The rate of energy transfer from red-shifted chlorophyll *a* (Chl *a*) molecules to bulk Chls *a* occurs with a rate constant of (7.4−10.4 ps)$^{-1}$ whereas the reverse process occurs with a rate constant of (19.3−29.8 ps)$^{-1}$ according to the target analysis, whereas trapping from bulk Chls *a* occurs with rate (16.8−25.0 ps)$^{-1}$.

Keywords: Cyanobacteria; BE mutant; Target analysis; Streak camera

Introduction

Photosystem I (PSI) is one of the two photosystems that are present in oxygenic photosynthetic organisms, like cyanobacteria, green algae, and higher plants. It is a large multi-pigment-protein complex that catalyzes light-driven electron transfer from plastocyanin or cytochrome to ferredoxin across the thylakoid membrane. The BE mutant cells, lacking photosystem II and light-harvesting complexes (Krumova *et al*., 2010), provide an attractive system for studying PSI *in vivo*. Most of the research efforts were done on isolated PSI complexes from a variety of species and in different aggregation states (Gobets *et al*., 2003; Gobets *et al*., 2001; Melozernov *et al*., 2000; Setif *et al*., 1992; Holzwarth *et al*., 1991). Recently, the picosecond fluorescence kinetics of PSI were studied for the first time *in vivo,* using BE mutant cells of *Synechosystic sp*. PCC 6803 (Krumova *et al*., 2010). Here a continuation of that work is presented, including also target analysis of the kinetics obtained with a streak-camera setup.

Materials and Methods

Preparation and growing conditions of the BE mutant

BE mutant cells of *Synechosystic sp.* PCC 6803 were prepared as before (Krumova *et al*., 2010). They were grown at 30 ºC in dim light.

Time-resolved fluorescence measurements

For the fluorescence measurements the sample was diluted to an OD400 of 0.2/cm in BG11 medium. Time-resolved emission spectra were recorded using a synchroscan streak-camera system as described in (van Oort *et al*., 2008; van Oort *et al*., 2009). Before analysis the images were corrected for background signal and detector sensitivity, sliced up into traces of 3 nm. The average of 100 images each measured for 10 s was used. The time window was 800 ps. The laser power was typically 30 W, spot size 100 m, and repetition rate 250 kHz.

The streak images were analyzed using the TIMP package for R language (Mullen and van Stokkum, 2007) and Glotaran, a graphical user interface for the R-package TIMP (glotaran.org). A Gaussian-shaped instrument response function was used for the analysis

and its width was a free fitting parameter. The synchroscan period (13.16 ns) results in a back and forth sweeping of long lived components and leads to some signal before time zero in the streak-camera images (van Stokkum *et al*., 2006). This is used for long-lived component estimation. The fit quality was judged by singular value decomposition of the residuals matrix (Mullen and van Stokkum, 2007).

All the experiments were performed at room temperature (293 K).

Results and Discussion

To study the ps fluorescence kinetics of PSI *in vivo*, use was made of the BE mutant. Global and target analysis were performed on streak-camera data, obtained after 400 nm excitation. The input system vector j(t) at time zero (excitation distribution over the different pigment pools at time zero) was calculated assuming the presence of 96 Chls *a* per monomeric PSI, *i.e.* 90 Chls in the core antenna and 6 in the reaction center (RC) (Jordan *et al*., 2001). The number of red-shifted Chl *a* states in *Synechocystis sp.* PCC 6803 depends on the oligomerisation state: monomers possess a red absorption band with an oscillator strength of ~3 Chls *a* and for trimers it corresponds to 4–5 molecules. Because in BE mutants PSI is properly assembled (Krumova *et al.*, 2010) a number of 4 molecules was used for our calculations.

Global analysis

The decay-associated spectra (DAS) that result from the global analysis of the ps measurements on BE cells are presented in Fig. 1.

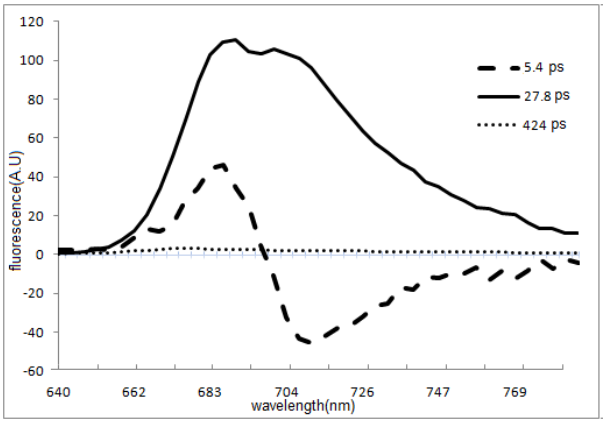

Fig. 1 DAS of BE mutants upon excitation at 400 nm. The corresponding lifetimes are given in the figure.

The kinetics are dominated by two components with lifetimes 5.4 ± 0.14 ps and 27.8 ± 0.09 ps, whereas the contribution of a $\sim 400 \pm 9$ ps component is almost negligible (~2%). The bipolar 5.4 ps component, which is positive at relatively short wavelengths and negative in the red region, reflects excitation energy transfer between bulk (blue-shifted) and red Chl *a* pools in the PSI antenna. The 27.8 ps component reflects the excitation trapping process due to charge separation in the RC. A small decay component with a lifetime around 0.4 ns has a minor contribution and can be assigned to a fraction of Chls that are unconnected to the PSI RC. The peak is around 676 nm and corresponds to free Chl and/or Chl bound to $cytb_6f$ (Krumova *et al.*, 2010; Peterman *et al.*, 1998).

Target analysis

The data were further analyzed by target analysis, using the model shown in Fig. 2A. Only one red-shifted pool was needed in the target analysis model. A fit with two pools (Gobets *et al.*, 2001) failed and a second equilibration process (9–15 ps) could not be observed.

The model contains three compartments, representing bulk Chl *a* (Bulk), red-shifted Chl *a* (Red) and a pool of Chls that are not connected to PSI (Free). The contribution of the latter component was around 2% and it was kept constant at this value during the target analysis calculations (*i.e.* j(3) = 0.02, see also Fig. 2A).

The following rate constants were included: (1) Uphill and downhill energy transfer between the red-shifted compartments and bulk Chl *a* with rate constants k_{RB} and k_{BR}, (2) Trapping from red-shifted compartment with rate k_{TR} and from bulk compartment with rate k_{TB}, (3) Decay of "Free compartment" with rate k_F.

The fitting results consist of the emission spectra (SAES) of the different compartments (which were required to be all-positive) and the rate constants that were introduced as free fitting parameters. During the fitting the ratios k_{TR}/k_{RB} and k_{BR}/k_{TB} were used as fixed parameters for each fit run. A number of runs was performed with the ratios varying from either 0 or the first point at which all compartments showed all positive emission spectra to the last point where all SAES were still all-positive. After the optimal fitting had been obtained for a certain combination of ratios k_{TR}/k_{RB} and k_{BR}/k_{TB}, the ratios were varied in a

systematic way and for all combinations the quality of the fits was compared. In Fig. 2B it is shown that different combinations of the ratios lead to fits of virtually identical quality, in other words, there is no unique best fit but all points on the curve fit the data equally well.

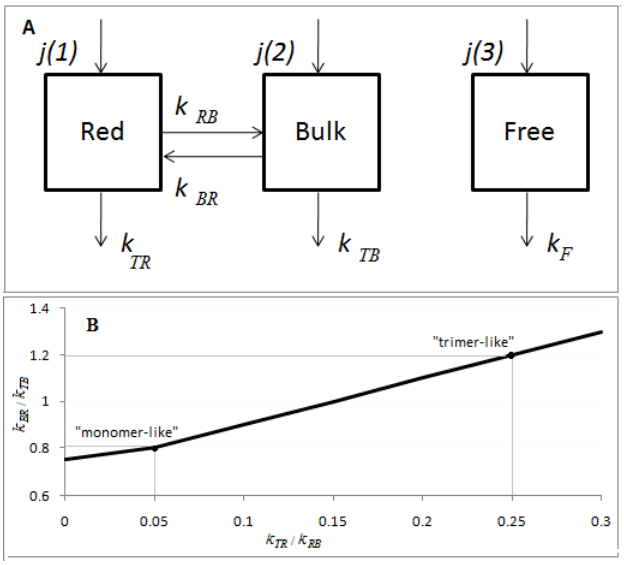

Fig. 2 Target analysis of BE mutant. (A) Compartmental model of PS I in vivo (excitation -400 nm) (B) The relation between k_{TR}/k_{RB}, k_{BR}/k_{TB} ratios and optimal solution. "trimer-like", "monomer-like" points –the solutions with lifetimes close to the ones reported for monomers and trimers *in vitro* (Gobets *et al.*, 2001) are also included.

Table 1 Lifetimes from target analysis (ps).

	τ_{RB}	τ_{BR}	τ_{TB}	τ_{TR}
min	7.4	19.3	16.8	0
max	10.4	29.8	25.0	$5*10^3$
mean	8.9	23	20.9	

Although it is impossible to get a unique solution of the model (Fig. 2A), we can at least estimate the range of possible values. In Table 1 the range of reciprocal rate values (lifetimes) are presented together with their mean values.

The mean values show good agreement with the results obtained on isolated monomers and trimers (Gobets *et al.*, 2001). The τ_{TR} reported for monomers is 170 ps while for trimers 38 ps component was found. For isolated PSI a value of τ_{RB} = 8.6 ps was found for monomers and τ_{RB} = 8.9 ps for trimers (Gobets *et al.*, 2001) whereas τ_{BR} was 31 ps for monomers and 18 ps for trimers. And τ_{TB} was 18 ps in their study.

The results indicate that there is good agreement between the kinetics found *in vitro* and *in vivo* but that without making additional assumptions, no unique solutions can be obtained for the various parameters.

In order to investigate to which extent different (optimal) combinations of the ratios k_{TR}/k_{RB} and k_{BR}/k_{TB}, lead to differences in the SAES two different combinations were used – one close to the values that were reported for trimers, another close to the reported values for monomers *in vitro* (Gobets *et al.*, 2001) and the resulting spectra are shown in Fig. 3.

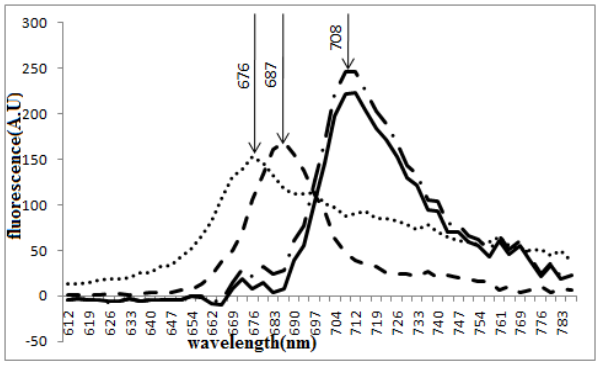

Fig. 3 SAES of two solutions on the line in Fig. 2B (one – close to reported values for trimers *in vitro*, the other –close to values reported for monomers) obtained by target analysis of fluorescence decay upon 400 nm excitation. dashed, dotted line –spectra are equal for both solutions, solid line – result for "trimer-like" fit, chain-dot – result for "monomer-like" fit.

The compartment of the free Chls for any point on the optimal solutions line also shows an identical spectrum (dotted line) with the maximum value around 676 nm and a long red shoulder extending beyond the window of observation. The maximum is characteristic for monomeric Chl *a* in solution (Hoff and Amesz, 1991), although the values in the red tail region remain higher than reported (Hoff and Amesz, 1991; Gobets *et al.*, 2001). Alternatively, the spectrum may correspond to Chl *a* in $Cytb_6f$ (Krumova *et al.*, 2010; Peterman *et al.*, 1998).

For all optimal solutions along the line in Fig. 2B the emission spectrum of the bulk Chls is identical (dashed line) with a maximum around 687 and a long red tail.

The shape of the SAES of the red-shifted Chls (solid and chain-dot lines) also remains the same as well as the peak position (708 nm). Only the intensity differs to some extent. In conclusion, our data can be described equally well with the rate constants that were reported for isolated monomeric PSI and for isolated trimeric PSI.

Acknowledgements

We would like to thank Rob Koehorst and Arie van Hoek for initial help with the streak-camera measurements, Cor Wolfs and Sashka Krumova for initial help with the cell growth and Sergey Laptenok, Joris Snellenburg and Ivo van Stokkum for seminal contributions to the data analysis. This work was supported by HARVEST Marie Curie Research Training Network (PITN-GA-2009-238017) and the European Union Sixth Framework Programme grant MRTN-CT-2005-019481 to HvA and VVC.

LT received a fellowship from the Graduate School Experimental Plant Sciences (EPS), Wageningen, The Netherlands.

References

Gobets B, van Stokkum IHM, van Mourik F, Dekker JP, van Grondelle R (2003) Excitation Wavelength Dependence of the Fluorescence Kinetics in Photosystem I Particles from Synechocystis PCC 6803 and Synechococcus Elongates. Biophys. J. 85: 3883-3998

Gobets B, van Stokkum IHM, Rögner M, Kruip J, Schlodder E, Karapetyan NV, Dekker JP, van Grondelle R (2001) Time-Resolved Fluorescence Emission Measurements of Photosystem I Particles of Various Cyanobacteria: a Unified Compartmental Model. Biophys. J. 81: 407-424

Hoff AJ, Amesz J (1991) Visible Absorption Spectroscopy of Chlorophylls. In: H Scheer (ed.), Chlorophylls. CRC Press: Boca Raton, FL, pp. 723-738

Holzwarth AR (1991) In: H Scheer (ed.), Chlorophylls. CRC Press: Boca Raton, FL, pp. 1126-1151

Jordan P, Fromme P, Witt HT, Klukas O, Saenger W, Krauss N (2001) Three-Dimensional Structure of Cyanobacterial Photosystem I at 2.5 Resolution. Nature 411: 909-917

Krumova SB, Laptenok SP, Borst JW, Ughy B, Gombos Z, Ajlani G, van Amerongen H (2010) Monitoring Photosynthesis in Individual Cells of Synechocystis sp. PCC 6803 on a Picosecond Timescale. Biophys. J. 99: 2006-2015

Melkozernov AN, Lin S, Blankenship RE (2000) Femtosecond Transient Spectroscopy and Excitonic Interactions in Photosystem I. J. Phys. Chem. B. 104: 1651-1656

Mullen KM, van Stokkum IHM (2007) TIMP: an R Package for Modeling Multi-Way Spectroscopic Measurements. J. Stat. Softw. 18(3): 1-47

Peterman EJ, Wenk SO, Pullerits T, Pâlsson LO, van Grondelle R, Dekker JP, Rögner M, van Amerongen H (1998) Fluorescence and Absorption Spectroscopy of the Weakly Fluorescent Chlorophyll a in Cytochrome b6f of Synechocystis PCC6803. Biophys. J. 75: 389-398

Sétif P (1992) Topics in Photosynthesis 11. In: J Barber (ed.), The Photosystems: Structure, Function and Molecular Biology. Elsevier Science Publishers: Amsterdam, pp. 471-499

Van Oort B, Amunts A, Croce R (2008) Picosecond Fluorescence of Intact and Dissolved PSI-LHCI Crystals. Biophys. J. 95: 5851-5861

Van Oort B, Murali S, van Amerongen H (2009) Ultrafast Resonance Energy Transfer from a Site-sSpecifically Attached Fluorescent Chromophore Reveals the Folding of the N-Terminal Domain of CP29. Chem. Phys. 357: 113-119

Van Stokkum IHM, Gobets B, Gensch T, van Mourik F, Hellingwerf KJ, Grondelle R, Kennis JTM (2006) (Sub)-Picosecond Spectral Evolution of Fluorescence in Photoactive Proteins Studied with a Synchroscan Streak Camera System. Photochem. Photobiol. 82: 380-388

Estimation of the Relative Sizes of the Two NPQ-Associated Dissipations in Rice

Satoshi Ishida[a], Fumihiko Sato[a], Tsuyoshi Endo[a*]

[a]Division of Integrated Life Sciences, Graduate School of Biostudies, Kyoto University, Kyoto 606-8502, Japan.
[*]Corresponding author. Tel. No. +81 75 753 6381; Fax No. +81 75 753 6398; E-mail: tuendo@kais.kyoto-u.ac.jp.

Abstract: In photosystem II (PSII), light energy absorbed in chlorophyll a is de-excited not only through electron transport but through basal dissipation and non-photochemical quenching (NPQ)-associated dissipation. NPQ consists of energy-dependent quenching (qE) and the other unknown quenching (designated as qU). Whereas the quantum yields of electron transport, basal dissipation and NPQ-associated dissipation have been estimated with the pulse amplitude modulation (PAM) fluorometer by several groups, the exact ratio of two NPQ-associated dissipations, qE-associated and qU-associated dissipations, have not been estimated yet. Here, we estimated the relative rate constant for qU associated dissipation (k_{qU}) in PsbS-silenced lines (qE knockdown) of rice from the fraction of NPQ, based on the lake model of energy transduction in PSII. The relative k_U in the PsbS-silenced lines showed light-dependent increase. In the wild type, the relative rate constant of qE-associated dissipation was approximately three (in low light condition) and six (in high light condition) times as much as that of qU-associated dissipation. It is concluded that the qU-associtaed dissipation is light-inducible process and that the qE-associated dissipation is a major process of NPQ-associated dissipation in rice.

Keywords: Energy allocation in PSII; Non-photochemical quenching; Photosystem II; PsbS; Rice

Introduction

In oxygenic photosynthesis, absorbed light energy at photosystem II (PSII) excites chlorophyll a and the excited energy is used for electron transport. Besides, the capacity of electron transport is limited in various conditions, and the excess energy of excited chlorophyll a is dissipated through either basal dissipation or non-photochemical quenching (NPQ)-associated dissipation. NPQ-associated dissipation consists of several components (Quick and Stitt, 1989; Adams *et al*., 1990; Johnson *et al*., 2009; Nilkens *et al*., 2010). While molecular mechanisms involved in some of the components have been obscure yet, the major component of NPQ-associated dissipation is identified as the dissipation associated with energy-dependent quenching (qE) in higher plants (Li *et al*., 2000). qE-associated dissipation converts the energy of excited chlorophyll a to heat via either zeaxanthin-dependent or zeaxanthin-independent process. The zeaxanthin-dependent dissipation is regulated by an enzymatic deepoxidation of the epoxy-xanthophyll violaxanthin to zeaxanthin (Demming-Adams *et al*., 1990). The zeaxanthin-independent dissipation relates to lutein (Pogson *et al*., 1998; Dall'Osto *et al*., 2006; Johnson *et al*., 2009). PsbS is thought to be involved in the both of the two qE-associated dissipations. PsbS is activated by an increase of a proton gradient across the thylakoid membrane (pH) (Li *et al*., 2004), as the two qE-associated dissipations are (Wraight and Crofts, 1970; Briantais *et al*., 1979). *npq4*, a PsbS deficient arabidopsis mutant, showed drastically reduced NPQ (Li *et al*., 2000). Moreover, the two qE-associated dissipations were enhanced by overexpression of PsbS (Li *et al*., 2002; Crouchman *et al*., 2006). These data suggest that PsbS is essential for both of the two qE-associated dissipations, whereas the mechanisms to dissipate the energy of excited chlorophyll a as heat is unclear. The rate constant of qE-associated dissipation is strictly controlled by light. qE-associated dissipation is regulated by an increase of pH (Wraight and Crofts, 1970). The deepoxidation of violaxanthin is activated by the pH (Yamamoto, 1979; Pfundel *et al.*, 1994).

Moreover, qE-associated dissipation disappears in several second after the transition from light to darkness, where the ΔpH is not generated by photosynthesis (Walters and Horton, 1991). qE-associated dissipation protects PSII from photo-oxidative light stress and confers plant fitness under the fields condition. The levels of photoprotection (estimated by Fv/Fm) in Arabidopsis mutants defective in qE-associated dissipation were lower than the wild type either under short-term high light or under long-term fluctuating light (Havaux and Kloppstech, 2001; Külheim *et al*., 2002; Li *et al*., 2002). However, the mutants grew as did the wild type in the laboratory under constant light (Havaux and Niyogi, 1999). These results suggest qE-independent dissipation plays an important role in photoprotection in higher plants. However, the capacities for both qE-dependent dissipation and qE-independent dissipation have not been estimated. Here, we estimated the exact relative rate constants of both qE-associated dissipation and the other NPQ (unknown quenching, designed as qU)-associated dissipation of rice in various light conditions.

According to Stern-Volmer relationship, the reduced chlorophyll a fluorescence intensity reflects a rate constant of a quenching. Based on the relationship, Kramer *et al*. (2004) and Hendrickson *et al*. (2004) estimated quantum yields of quenchings by measuring chlorophyll fluorescence. They divided quenchers in photosynthesis to three components, photosynthesis, basal dissipation and NPQ-associated dissipation. Moreover, Kasajima *et al*. (2009) divided NPQ-associated dissipation to two components, dissipation associated with a fast-relaxing NPQ and that with a slowly-relaxing NPQ. The quantum yields of the two components of NPQ-associated dissipation are estimated by the difference of the lifetime of each quenching. They assumed that the fast-relaxing NPQ includes qE. Moreover, they proposed the procedure to estimate relative rate constants of each component. In this study, we estimated the exact relative rate constants of qE-associated dissipation and qU-associated dissipations, using qE defective rice lines.

Materials and Methods

Plants

PsbS-silenced rice lines were generated, as described in Ishida *et al*. (in preparation). Rice plants were cultivated from May to October in a greenhouse in Kyoto, in which the temperature was maintained below 40 ºC.

Chlorophyll Fluorescence

Chlorophyll fluorescence parameters were measured using a PAM2000 chlorophyll fluorometer (Waltz, Effeltrich, Germany). The minimum fluorescence at the open PSII centers (Fo) was determined by measuring light. The steady-state chlorophyll fluorescence level (Fs) was recorded during actinic light illumination. Fm (maximum fluorescence yield at closed PSII centers) and Fm' (maximum fluorescence yield during illumination) were measured by the application of a 1-s pulse of saturating white light. The relative rate constant of NPQ (= k_{NPQ} / k_{Si}) was calculated as k_{NPQ} / k_{Si} = (Fo/Fm'–Fo/Fm), according to Kasajima *et al*. (2009).

Results and Discussion

Estimation of relative velocities of the rate constants of the two qE-associated dissipations

To estimate the relative rate constant of qU-associated dissipation (k_{qU}), chlorophyll fluorescence of either PsbS-silenced or wild type rice plants was measured under various light conditions. Then, the relative velocities of the rate constant of NPQ-associated dissipation (k_{NPQ}) to those of the sum of chlorophyll a de-excitation of dark-adapted plants (k_{si}) in each light intensity condition was calculated from the measured intensities of chlorophyll fluorescence, based on Kasajima *et al*. (2009). Because NPQ in the PsbS-silenced lines did not include qE (Ishida et al. in preparation), we estimated the relative velocities of k_{NPQ} of the PsbS-silenced lines as the relative velocities of k_{qU}. We hypothesized that k_{qU} of the PsbS-silenced lines would be similar to k_{qU} of the wild type under the similar light conditions, and calculated the relative velocities of the rate constant of qE-associated dissipation (k_{qE}) to those of k_{si} as follow:

$$\text{relative } k_{qE\ (\text{in the wild type})} = \text{relative } k_{NPQ\ (\text{in the wild type})} - \text{relative } k_{qU\ (\text{in the PsbS-silenced lines})}$$

qU-associated dissipation was increased with light intensity (Fig. 1a), as well as qE-associated dissipation (Fig. 1b). qU-associated dissipation in the wild type

was estimated approximately 30% of NPQ-associated dissipation in low light condition (approximately 80 μmol m^{-2} s^{-1}), whereas that under higher light conditions (more than 200 μmol m^{-2} s^{-1}) was reduced to half (approximately 15% of NPQ-associated dissipation) (Fig. 1c).

Two-stage kinetic of k_{qE} in light

qE-associated dissipation was induced even under low light conditions (Fig. 1b). In low light condition (approximately 100 μmol m^{-2} s^{-1}), the deepoxidation of violaxanthin is not activated and zeaxanthin is not produced (Finazzi *et al*., 2004). Considering that lutein is produced in dark (Finazzi *et al*., 2004), the major components of qE-associated dissipation in low light conditions might be zeaxanthin-independent dissipation. In high light conditions, zeaxanthin-dependent dissipation is major component of qE-associated dissipation, as previous reported (Niyogi *et al*., 1998). It was consistent with the two-stage curve of relative k_{qE} (Fig. 1b). Zeaxanthin-independent dissipation might compensate zeaxanthin-dependent dissipation until zeaxanthin is produced.

qU consisted of more than two components.

The relation of k_{qU} to light intensity was not linear (Fig. 1a). It suggests that qU consists of at least two components. Indeed, Quick and Stitt (1989) assumed that the components of the slowly-relaxing quenching, which does not include qE, consists of state-transition and photoinhibition. Considering that photoinhibition occurs more likely under high light conditions than under low light conditions, a major component of qE under low light conditions might be state-transition or other unknown component. The efficiencies of light dependent induction of qU were more than those of qE under low light conditions (less than 150 μmol m^{-2} s^{-1}) (Figs. 1a, 1b and 1c). The result suggests that qU-associated dissipation might play an important role to dissipate excess energy at PSII under low light conditions.

Validity of the estimation of k_{qU} and k_{qE} in the wild type

In this study, we estimated both k_{pE} and k_{qU} in wild type, referring to k_{qU} in the PsbS-silenced lines under corresponding light conditions. The validity of this was examined in two results. First result, the much lower relative velocities of k_{qU} in the PsbS-silenced lines than those of k_{NPQ} in the wild type over a wide range of light intensities (Figs. 1a and 1b) suggests that the relative velocity of qU-associated dissipation might not compensate for the loss of qE-associated dissipation in PsbS-silenced lines. Secondly, the similar quantum yields of the electron transport in PsbS-silenced lines to those in the wild type under any light conditions (Ishida *et al*., in preparation) suggests that the condition for qU-associated dissipation induction (*e.g.*, the increase of amounts of ΔpH, ATP or NADPH) in PsbS-silenced lines would be similar to that in the wild type under the same light intensity. Thus, we concluded our estimation of the relative velocities of k_{pE} and k_{qU} using PsbS-silenced lines would be valid.

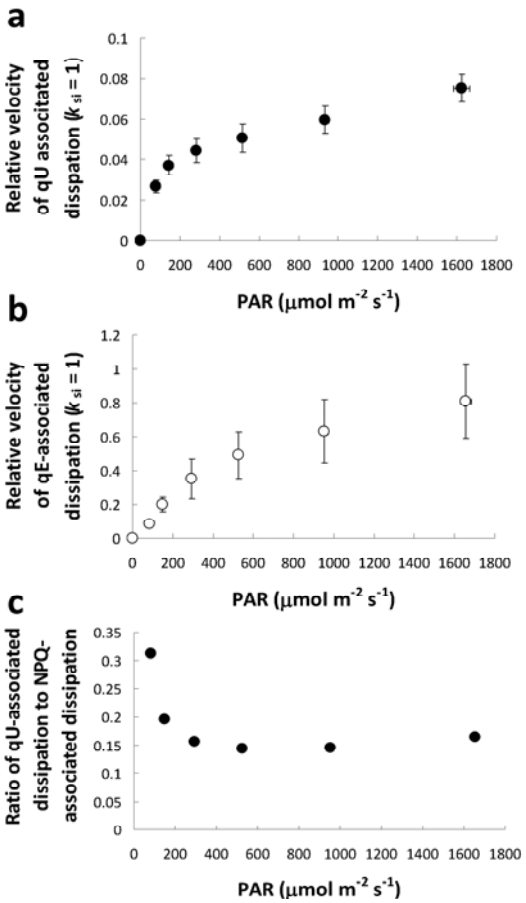

Fig. 1 Light dependencies of two NPQ-associated dissipations (a), Relative velocities of the rate constant of qU-associated dissipation, k_{qU}, to those of the sum of chlorophyll a de-excitation of dark-adapted plants, k_{si}, in the PsbS RNAi lines (n = 4). The relative velocities of k_{qU} were estimated under various light conditions, based on the Kasajima *et al*. (2009). (b), Relative velocities of the rate constant of qE-associated dissipation, k_{qE}, to those of k_{si} in the wild type (n = 4). The relative velocities of k_{qE} were calculated, based on the estimated k_{qU} in the PsbS RNAi lines. (c), Ratio of qU-associated dissipation to NPQ-associated dissipation in the wild type under various light conditions. The ratio calculated from the values of Fig. 1a and Fig. 1b.

Acknowledgements

This work was supported in part by project "Functional analysis of genes relevant to agricultural important traits in rice genome" of Agriculture and Fishery Ministry of Japan.

References

Adams WW, Demmig-Adams B, Winter K (1990) Relative Contributions of Zeaxanthin-Related and Zeaxanthin-Unrelated Types of 'High-Energystate' Quenching of Chlorophyll Fluorescence in Spinach Leaves Exposed to Various Environmental Conditions. Plant Physiol. 92: 302-309

Crouchman S, Ruban AV, Horton P (2006) PsbS Enhances Non-Photochemical Quenching in the Absence of Zeaxanthin. FEBS Lett. 580: 2053-2058

Dall'Osto L, Lico C, Alric J, Giuliano G, Havaux M, Bassi R (2006) Lutein Is Needed for Efficient Chlorophyll Triplet Quenching in the Major LHCII Antenna Complex of Higher Plants and Effective Photoprotection in Vivo under Strong Light. BMC Plant. Biology 6: 32

Finazzi G, Johnson GN, Dall'Osto L, Joliot P, Wollman FA, Bassi R (2004) A Zeaxanthin-Independent Nonphotochemical Quenching Mechanism Localized within the Photosystem II Core Complex. Proc. Natl. Acad. Sci. USA 101: 12375-12380

Havaux M, Kloppstech K (2001) The Protective Functions of Carotenoid and Flavonoid Pigments against Excess Visible Radiation at Chilling Temperature Investigated in Arabidopsis npq and tt Mutants. Planta 213: 953-966

Hendrickson L, Furbank RT, Chow WS (2004) A Simple Alternative Approach to Assessing the Fate of Absorbed Light Energy Using Chlorophyll Fluorescence. Photosynth. Res. 82: 73-81

Johnson MP, Pérez-Bueno ML, Zia A, Horton P, Ruban AV (2009) The Zeaxanthin-Independent and Zeaxanthin-Dependent qE Components of Non-Photochemical Quenching Involve Common Conformational Changes within the Photosystem II Antenna in Arabidopsis Thaliana. Plant Physiol. 149: 1061-1075

Kasajima I, Takahara K, Kawai-Yamada M, Uchimiya H (2009) Estimation of the Relative Sizes of Rate Constants for Chlorophyll De-Excitation Processes through Comparison of Inverse Fluorescence Intensities. Plant Cell Physiol. 50: 1600-1616

Kramer DM, Johnson G, Kiirats O, Edwards GE (2004) New Fluorescence Parameters for the Determination of Q_A Redox State and Excitationenergy Fluxes. Photosynth. Res. 79: 209-218

Külheim C, Ågren J, Jansson S (2002) Rapid Regulation of Light Harvesting Is Crucial for Plant Fitness in the Field. Science 297: 91-93

Li XP, Bj rkman O, Shih C, Grossman AR, Rosenquist M, Jansson S, Niyogi KK (2000) A Pigment Binding Protein Essential for Regulation of Photosynthetic Light Harvesting. Nature 403: 391-395

Li XP, Gilmore AM, Caffari S, Bassi R, Golan T, Kramer D, Niyogi KK (2004) Regulation of Light Harvesting Involves Intrathylakoid Lumen pH Sensing by the PsbS Protein. J. Biol. Chem. 279: 22866-22874

Li XP, Muller-Moule P, Gilmore AM, Niyogi KK (2002) PsbS-Dependent Enhancement of Feedback De-Excitation Protects Photosystem II from Photoinhibition. Proc. Natl. Acad. Sci. USA 99: 15222-15227

Nilkens M, Kress E, Lambrev P, Miloslavina Y, Muller M, Holzwarth AR, Jahns P (2010) Identification of a Slowly Inducible Zeaxanthin-Dependent Component of Non-Photochemical Quenching of Chlorophyll Fluorescence Generated under Steady-State Conditions in Arabidopsis. Biochim. Biophys. Acta 1797: 466-75

Niyogi KK, Grossman A, Björkman O (1998) Arabidopsis Mutants Define a Central Role for the Xanthophyll Cycle in Regulation of Photosynthetic Energy Conversion. Plant Cell 10: 1121-1134

Pfundel EE, Renganathan M, Gilmore AM, Yamamoto HY, Dilley RA (1994) Intrathylakoid pH in Isolated Pea Chloroplasts as Probed by Violaxanthin Deepoxidation. Plant Physiol. 106: 1647-1658

Pogson B, Niyogi KK, Björkman O, DellaPenna D. (1998) Altered Xanthophyll Compositions Adversely Affect Chlorophyll Accumulation and Nonphotochemical Quenching in. Arabidopsis mutants. Proc. Natl. Acad. Sci. USA 95: 13324-13329

Quick WP, Stitt M (1989) An Examination of the Factors Contributing to Non-Photochemical Quenching of Chlorophyll Fluorescence in Barley Leaves. Biochim. Biophys. Acta 977: 287-296

Walters RG, Horton P (1991) Resolution of Components of Non-Photochemical Chlorophyll Fluorescence Quenching in Barley Leaves. Photosynth Res. 27: 121-133

Wraight CA, Crofts AR (1970) Energy-Dependent Quenching of Chlorophyll Alpha Fluorescence in Isolated Chloroplasts. Eur. J. Biochem. 17: 319-327

Yamamoto HY (1979) Biochemistry of the Xanthophyll Cycle in Higher Plants. Pure Appl. Chem. 51: 639-648

Molecular Characterization of Thylakoid Membrane-Bound Ascorbate Peroxidase in *Oryza Sativa* (Rice)

Suqin Zhu, Yanhong Chen, Rong Zhou, Benhua Ji*

School of Life Sciences, Nantong University, Nantong, China.
*Corresponding author. Tel. No. +81 513 85012828; E-mail: jibenhua@ntu.edu.cn.

Abstract: A comparative kinetic analysis and enzymic inactivation in ascorbate depleted medium between thylakoid membrane-bound ascorbate peroxidase (tAPx) and cytosolic isoform of APx (cAPx1 and cAPx2) purified from rice (*Oryza sativa* L.) leaves, were performed. The three APxs follow the peroxidase ping-pong mechanism to catalyze the oxidation of ascorbate, with different k_m^{ASc} and $k_m^{H_2O_2}$ values. They share similarly enzymatic properties so far, with the exception that tAPx was more inactivation in ascorbate depleted medium than cAPxs. Three dimensional structural analysis and alignment of amino acid sequence deduced from cloned cDNA show that thylakoid-bound and cytosol APxs share the same active site composed of two substrate-binding sites: the distal histidine site where H_2O_2 binds and the γ-heme edge site where the ascorbate binds. Noteworthyly, an additional loop structure composed of 16 amino acid residues was found only in tAPx. The rapid inactivation of tAPX might be due to the additional loop structure, which forms an access channel connecting the molecular surface of tAPX to the γ-edge of heme, named γ-channel.

Keywords: Ascorbate; Ascorbate peroxidase (APx); *Oryza sativa*; Thylakoid membrane

Introduction

Thylakoid membrane-bound ascorbate peroxidase (tAPX) and stroma ascorbate peroxidase (sAPX) are both involved in the water-water cycle, where O_2^- is reduced to water in a two-step reaction catalyzed by superoxide dismutase and APx. O_2^- is produced at the PS I site by the Mehler reaction, which is one of several mechanisms for dissipating excess excitation energy. So the water-water cycle contributes to maintaining a proper ATP/NADPH ratio and to alleviating the over-reduction of photosystems when plants are exposed to photoinhibitory conditions. The *tAPx* transcript levels are weakly responsive to external oxidative stress (Panchuk *et al*., 2002). This implies that tAPx is involved in direct detoxification of H_2O_2 but not in protection from excess ROS produced under environmental stress. The tAPx was considerably more sensitive to inactivation than cAPx (Amako and Asada, 1994). The sensitivity of tAPx might reflect the rather high level of ascorbate (up to 50 mmol) normally found in the chloroplast (Salin, 1987), which protects the enzyme. In this study, a comparative kinetic analysis and sensitivity to inactivation of tAPx and cAPxs, purified from rice thylakoid membrane and cytosol, resipectively, was performed. Protein 3D structural comparison were carried out to explore the mechanism of different sensitivity to inactivation between tAPx and cAPxs.

Materials and Methods

APx activity was determined by measuring the decrease in absorbance of ascorbate (ε_{290}＝2.8 $mmol^{-1}$ cm^{-1}).

Purification of tAPx was carried out by the method of Miyake (1993). Rice cv. Ning jing-1 (*Oryza sativa*, *japonica*) leaves (1.2 kg) were homogenized with 2 liters of 50 mmol potassium

phosphate (pH 7.5)/0.1 mmol EDTA/1 mmol PMSF (phenylmethyl sulfonate)/5 mmol ascorbate. In addition, cAPxs were purified by the method of Sharma (2004). Two different peaks showing cAPX activity were obtained when DEAE-Sephacel column was eluted with buffer containing 0.15 mol NaCl and 0.25 mol NaCl. The two isoforms were designated cAPx 1 and cAPx 2 in order of their elution.

SDS-PAGE of the purified enzyme was performed in 6%–26% gradient polyacrylamide gels.

The fulllength cDNAs encoding tAPx, cAPx1 and cAPx2 were cloned using a PCR approach with primer pairs: (forward) 5' CTCACTCGACTCGAGC GCG 3', (reverse) 5' CACGCAAATCTTAGCACAG GC 3'; (forward) 5' GGTAACTTTGAAACTCCACA G 3', (reverse) 5' CGCAATACCGCATTTCATACC 3'; (forward) 5' GTAAGAAGATCTCATCCCTCC 3', (reverse) 5' GGTAACTTTGAAACTCCACAG 3', respectively, based on the known *APx* genes from gene bank.

Three-dimensional structure of APxs was constructed using DeepView Swiss Pdb Viewer. The experimental structures used for construction of 3-D structure of tAPx and cAPx-2 were chloroplastic ascorbate peroxidase (PDB: 1iyn Chain: A) from tobacco and cytosolic ascorbate peroxidase (PDB: 2ghcX) from soybean, respectively.

Results and Discussion

Inactivation of tAPx and cAPxs in ascorbate depleted medium

The APxs (5 μl, 0.1 μM) in the assay medium containing 1 mmol ascorbate were diluted with 1 ml of 50 mmol potassium phosphate, pH 7.0, 25 °C. At the indicated times after the dilution, 0.5 mmol ascorbate was added, and the APx activity was assayed by the addition of 0.1 mmol H_2O_2. In control (+ASc), the dilution was done with the buffer containing 0.5 mmol ascorbate. The residual enzymic activities were determined as the activity remaining compared to the initial activity at the beginning of the experiment and expressed as a percentage. When the tAPx was diluted with the ascorbate-depleted medium, the peroxidase activity was lost with a half time of 15.3 s. However cAPx2 and cAPx1 had high residual enzymic activity untill 180 min after the dilution (Fig. 1, cAPx1 omitted). The results above showed that tAPx was more senstive to inactivation in ascorbate depleted medium than cAPxs.

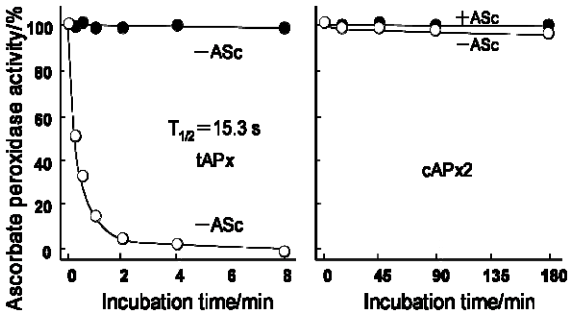

Fig. 1 Inactivation of thylakoid-bound (tAPx) and cytosol (cAPx2) ascorbate peroxidases from rice in ascorbate depleted medium.

APxs catalyze the oxidation of ascorbate by the ping-pong mechanism

The initial rates of oxidation of ascorbate were measured in the presence of H_2O_2 at various concentrations (1, 2.5, 5, 10, 25, 50, 100, 200, 400 μM)) at a range of concentrations (10, 25, 50, 100, 200, 400 μM) of ascorbate. The reciprocal of the initial rate of oxidation of ascorbate (v^{-1}), catalyzed by APxs, versus the reciprocal of the concentration of H_2O_2 (1.0–50.0 μM*)* were linearly related. When reciprocal values of the initial rate of oxidation of ascorbate were plotted against those of H_2O_2, parallel straight lines were obtained (Fig. 2). These results indicate that APxs catalyze the oxidation of ascorbate by the ping-pong mechanism. From the slopes of straight lines and the intercepts, the k_m^{ASc} value*s* of tAPx, cAPx1, cAPx2 for ascorbate were calculated to be 490, 379, 222 μM and $k_m^{H_2O_2}$ values for H_2O_2 were 95, 33, 79 μM, respectively. In the range of concentrations (10–400 μM) of ascorbate tested, the initial rates of oxidation of ascorbate of tAPx, cAPx1 and cAPx2 decreased at higher concentrations of H_2O_2 than 50, 100 and 100 μM, respectively, indicating the inactivation of APxs by H_2O_2. The lower was the concentration of ascorbate, the higher was the extent of the inactivation of APxs by H_2O_2. The present results showed that rice tAPx and the cAPxs share similarly enzymatic properties, with the exception of different degree of stability under ascorbate-deleted medium.

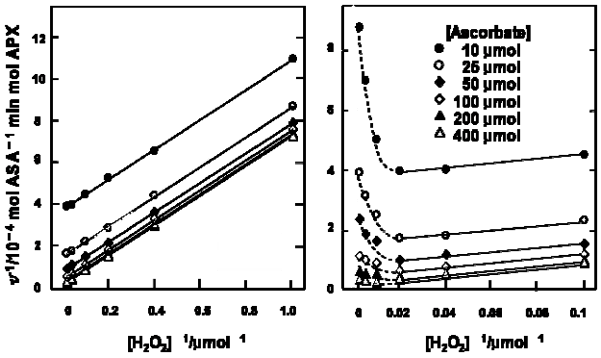

Fig. 2 Double-reciprocal plots of the initial velocity of the reaction catalyzed by tAPx from rice thylakoid membrane against the concentration of H_2O_2 (left, 1.0–50 μM; right, 10–500 μM) at the indicated concentrations of ascorbate. (Figure about cAPx1 and cAPx2 omitted).

Amino acid sequence of tAPx and cAPxs

The complete sequence of cDNA encoding tAPx consists of 1530 nt with an open reading frame coding for 478 amino acid residues. A transit peptide consisting of 76 residues is obtained by ChloroP, leaving, in this case, a mature tAPx protein consisting of 402 residues. In addition, a membrane-spanning segment, residues 381–402, was predicted by TopPred. Also the amino acid sequences of cAPx1 and cAPx2 were deduced by cDNA cloned in this experiment. Amino acid sequence alignment showed the conserved residues in Fig. 3: A1 and A2 are proximal and distal histidine, respectively. B1-B6 are the conserved residues found in the vicinity of the putative active site of all plant ascorbate peroxidases. C1 and C2 are residues forming additional hydrogen bonds with ascorbate, respectively.

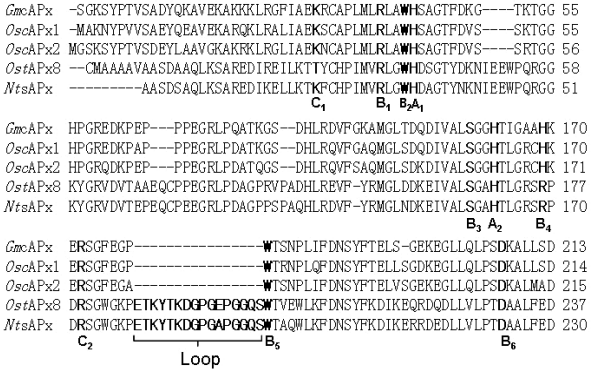

Fig. 3 Amino acid sequence alignment between thylakoid-bound and cytosol ascorbate peroxidases.

Structural comparison of tAPx and cAPx

The catalytic domain of APxs of 241–273 residues folded into characteristic 16 α-helices. In addition, there were 30 and 22 turns in tAPx and cAPx2, respectively. Heme cavity architecture, secondary structure elements, the relative locations of the heme group and key active-site residues in APxs from rice cv. NJ-1 were shown in Fig. 4. The active site is composed of two substrate-binding sites: the distal

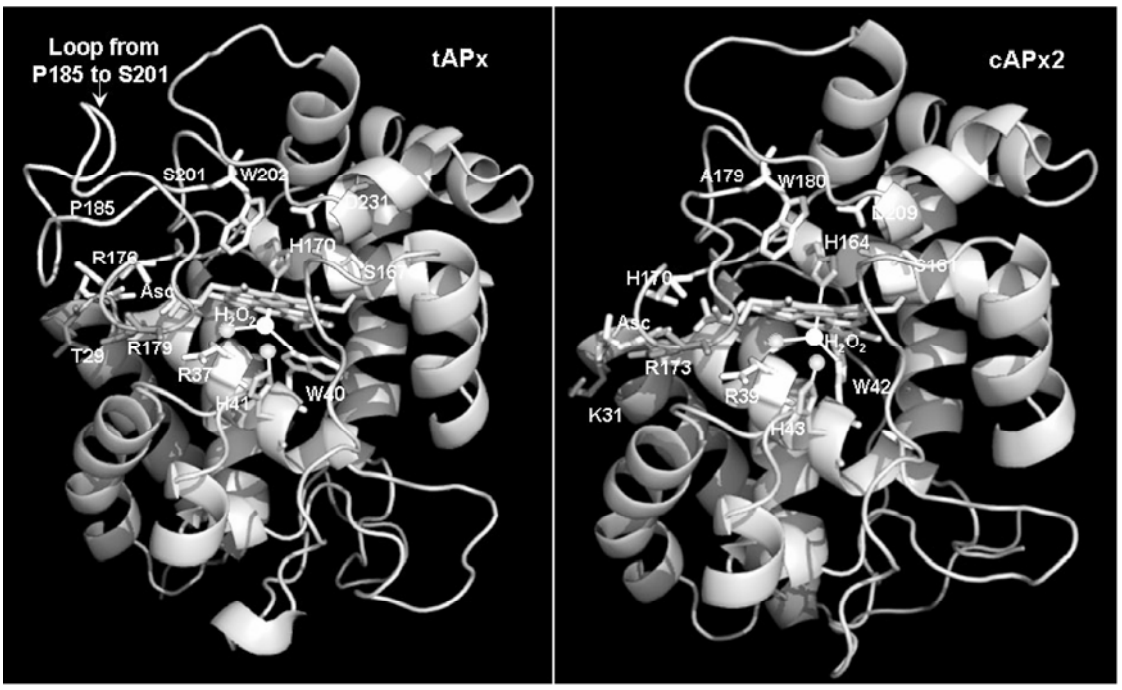

Fig. 4 Structural comparison of thylakoid-bound ascorbate peroxidase and cytosolic ascorbate peroxidase-2 from cv. NJ-1, *Oryza sativa japonica* subspecies.

histidine site where H_2O_2 binds and the γ-heme edge site where the ascorbate binds. Firstly, H170/H164 (tAPx/cAPx2) and H41/H43 are the proximal and distal histidine, respectively. The proximal H170/H164 is an axial ligand. Two residues, R37/R39 and H41/H43, in the distal heme pocket have been implicated in acid-base catalysis and cleavage of the peroxide O-O bond during compound I formation, His41/H43 as a base acceptor in this process. The distal residue R37/R39 enhances the efficiency of the reaction and the binding affinity for ligands. (Smith and Veitcht, 1998). R37/R39, W40/W42, R176/R170, S167/S161, W202/W180, D231/D209 are the conserved residues found in the vicinity of the putative active site (where H_2O_2 binds) of all plant APxs. They play an essential role in cooperation with proximal and distal histidine in access to reduction of H_2O_2. Secondly, in γ-heme edge site where the ascorbate binds, some residues forming additional hydrogen bonds with sunbstrate ascorbate. Fig. 5 showed ascorbate bound at the γ-heme edge through hydrogen bonds to T29/K31, R179/R173 (also Gig 4) and the heme 6-propionate. The substrate binding position showed that electron delivery to the heme was through the heme propionate. (Gumiero *et al*., 2010). The T29 in tAPx was replaced with K31 in cAPx2. In addition, there is an additional loop structure composed of residues P185 to S201 (Figs. 3 and 4) in tAPx, but virtually no structural information comes from homology in cAPx2 and cAPx1. According to the crystal structure of chloroplastic ascorbate peroxidase from tobacco (Wada *et al*., 2003), the additional loop structure forms a channel that connects the molecular surface of tAPx to the γ-edge of heme, named γ-channel. The overall structure of tAPx was similar to those of cAPxs from rice (cAPx2, cAPx1) and soybean (GmcAPx), with a substantial difference in a loop structure located in the vicinity of the heme (Fig. 4). The side chain of R176 in tAPX corresponding to R169 in sAPX in tobacco (NtsAPx) and H170 in cAPx2 (Fig. 3) extended in the opposite direction from the heme (Fig. 4). The rapid inactivation of tAPX might be due to the characteristic conformation of R176 owing to the loop structure of tAPX.

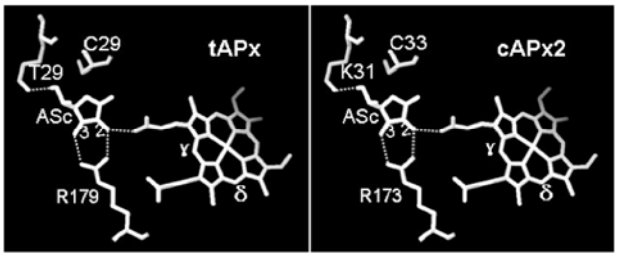

Fig. 5 The structure of the APx-ascorbate complex, showing the position of the ascobate (ASc) bound. The 2-OH group of ascorbate, is directly hydrogen bonded to the heme propionate and there are additional hydrogen bond interactions between R179/R173 (tAPx/cAPx2) and T29/K31 amino acids.

References

Amako K, Chen G, Asada K (1994) Separate Assays Specific for Ascorbate Peroxidase and Guaiacol Peroxidase and for the Chloroplastic and Cytosolic Isozymes of Ascorbate Peroxidase in Plants. Plant Cell Physiol. *35*: 497-504

Gumiero A, Murphy EJ, Metcalfe CL, Moody PCE, Raven EL (2010) An Analysis of Substrate Binding Interactions in the Heme Peroxidase Enzymes: A Structural Perspective. Archives of Biochem. Biophyis. 500: 13-20

Miyake C, Cao WH, Asada K (1993) Purification and Molecular Properties of the Thylakoid-Bound Ascorbate Peroxidase in Spinach Chloroplasts. Plant and Cell Physi. 34: 881-889

Panchuk II, Volkov RA, Schöffl F (2002) Heat Stress- and Heat Shock Transcription Factor-Dependent Expression and Activity of Ascorbate Peroxidase in Arabidopsis. Plant Physiol. 129: 838-853

Salin ML (1987) Toxic Oxygen Species and Protective Systems in the Chloroplast. Physiol. Plant. 72: 681-689

Sharma P, Dubey RS (2004) Ascorbate Peroxidase from Rice Seedlings: Properties of Enzyme Isoforms, Effects of Stresses and Protective Roles of Osmolytes. Plant Sci. 167: 541-550

Smith AT, Veitcht NC (1998) Substrate Binding and Catalysis in Heme Peroxidases. Curr. Opinion Chem. Biol. 2: 269-278

Wada K, Tada T, Nakamura Y, Ishikawa T, Yabuta Y, Yoshimura K, Shigeoka S, Nishimura K (2003) Crystal Structure of Chloroplastic Ascorbate Peroxidase from Tobacco Plants and Structural Insights into Its Instability. J Biochem. 134: 239-244

Effect of Lipids on Violaxanthin and Diadinoxanthin De-Epoxidation

Dariusz Latowski[1], Susann Schaller[2], Joanna Grzyb[1], Reimund Goss[2], Kazimierz Strzałka[1,*]

[1]Department of Plant Physiology and Biochemistry, Jagiellonian University, Kraków, Poland;
[2]Institute of Biology I, University of Leipzig School of Botany, Leipzig, Germany.
[*]Corresponding author. Tel. No. + 48 12 664 65 09; Fax No. (48-12) 664-69-02; E-mail: kazimierzstrzalka@gmail.com.

Abstract: Violaxanthin (Vx) and diadinoxanthin (Ddx) de-epoxidation are light dependent steps in one of the most important photoprotecting processes called respectively violaxanthin and diadinoxanthin cycle. Violaxanthin cycle operates in vascular plants and many groups of algae while diadinoxanthin cycle is present in diatoms.
In this study the influence of lipids on de-epoxidation of Vx and Ddx was investigated. In particular, the dependence between conversion of Vx into antheraxanthin and zeaxanthin as well as Ddx to diatoxanthin and the molecular dynamics of hydrophobic fraction of aggregates formed by inverted micelles, which are necessary for de-epoxidation, was studied. Thickness of the hydrophobic fraction of the aggregates, size of the inverted micelles, suggested by mathematical description of these structures and solubility of Vx and Ddx in various kind of lipids were the other tested parameters. Obtained results show that the rate of de-epoxidation is strongly dependent on physical/chemical properties of lipids. The key role for violaxanthin or diadinoxanthin de-epoxidase activation play non-bilayer lipids and the parameters of inverted micelles created by them, such as thickness, diameter and molecular dynamics of their hydrophobic core.

Keywords: Xanthophyll cycle; De-epoxidation; Non-lamellar lipids

Introduction

Violaxanthin (Vx) de-epoxidation and diadinoxanthin (Ddx) de-epoxidation are light dependent steps in the most important photoprotecting processes called respectively violaxanthin and diadinoxanthin cycle. So far, three different xanthophyll cycles have been described. The violaxanthin cycle operates in all higher plants, ferns, mosses and several groups of algae and involves interconversion between: Vx, antheraxanthin (Ax) and zeaxanthin (Zx) (Yamamoto *et al*., 1962; Hager, 1966; Sapozhnikov, 1967). The second kind of xanthophyll cycle is the diadinoxanthin (Ddx) cycle, in which interconversion between Ddx and diatoxanthin (Dtx) occurs (Stransky and Hager, 1970). This type of the cycle is present in the algal classes *Bacillariophyceae*, *Chrysophyceae*, *Xanthophyceae*, *Haptophyceae* and *Dinophyceae.* Another cycle called the lutein epoxide cycle was detected in a number of vascular plants and involves interconversion between lutein and epoxy-lutein (Garcia-Plazaola *et al*., 2002; Matsubara *et al*., 2003). In all these xanthophyll cycles two types of enzymes are engaged: de-epoxidases, catalyzing conversion of epoxy-xanthophylls into non-epoxy pigments under strong light conditions, and epoxidases, carrying out the backward reactions of the cycles in low light or darkness (Grzyb *et al*., 2006).

In Vx cycle these reactions are catalyzed by violaxanthin de-epoxidase (VDE) and zeaxanthin epoxidase while in Ddx cycle the enzymes engaged are diadinoxanthin de-epoxidase (DDE) and diatoxanthin epoxidase. The de-epoxidising enzymes are located in the thylakoid lumen and are activated by a decreasing lumenal pH due to light-driven photosynthetic electron transport, whereas location of the epoxidising enzymes is postulated on the stromal side of the thylakoid membrane and their pH optimum is about 7.5 (Bouvier *et al*., 1996). It is already known that both types of the xanthophyll cycle are similar on molecular level: ascorbate is the reducing agent and, as we showed previously, reverse hexagonal phase forming

lipids (monogalactosyldiacylglycerol—MGDG or phosphatidylethanolamine - PE) are necessary for de-epoxidation, while bilayer forming lipids (digalactosyldiacylglycerol - DGDG, phosphatidylcholine - PC) cannot sustain it (Yamamoto and Higashi, 1978; Latowski *et al*., 2002, 2004; Goss *et al*., 2005).

Materials and Methods

VDE was isolated from 7-day old wheat plants and Vx was extracted from daffodil petals. DDE and Ddx were prepared from thylakoid membranes of *Cyclotella meneghiniana*.

For determination of Vx and Ddx solubility by absorption spectroscopy pigments (0.4 μM each) were mixed with ethanol and a lipid: MGDG, DGDG, PE, or PC respectively. The pigment/lipid mixture was then injected into the reaction medium at pH 5.2 at 30 °C. Absorption spectra of Vx and Ddx were recorded in a wavelength range between 300 and 750 nm with a band-pass setting of 1 nm.

Reaction assay for VDE activity contained 0.33 μM Vx or Ddx, different concentration of lipids, 30 mmol sodium ascorbate and 5% ethanol (v/v) in 40 mmol MES pH 5.2 with 10 mmol KCl and 5 mmol $MgCl_2$. Reaction was started by ascorbate addition and samples were collected at 0, 2, 5 and 10 min. Reaction was stopped by mixing 700 ml of the assay mixture with 50 ml of 1 mol KOH, then centrifuged. Pellets, containing pigments, were analyzed by reverse phase HPLC column (Nucleosil C-18). Molecular dynamics of hydrophobic fraction of aggregates of inverted micelles composed of one of the following lipids: MGDG, PE from eggs, 1,2-dioleoyl-snglycero-3-phosphatidylethanolamine (PE1) or 1,2-dilinoleoyl-sn-glycero-3-phosphatidylethanolamine (PE2) or 1,2-dilinoleinoyl-sn-glycero-3-phosphatidylethanolamine (PE3) was assessed by measuring steady-state fluorescence polarization of diphenylhexatriene (DPH) with lipid:DPH ratio of 500 (final lipid concentration was 0.5 mmol), emission and excitation wavelengths 425 nm and 355 nm respectively.

Results and Discussion

In the present studies influence of lipids on de-epoxidation of Vx and Ddx was investigated. The lipids used in the studies on xanthophyll de-epoxidation by VDE and DDE were selected according to two criteria. One of them was the chemical character of the lipid molecules, and the other concerned the type of structures formed by the lipids in water environment (Sen and Hui, 1988). With respect to the chemical composition, two groups of lipids were chosen: neutral lipids containing a sugar moiety in their headgroup (galactolipids) and charged lipids without sugar residues (phospholipids). Among galactolipids and phospholipids, those producing bilayers and those forming inverted hexagonal structures were additionally selected. Studies on the solubility of Vx and Ddx in the lipids exhibiting the molecular specifications described above were performed.

Non-bilayer lipids were found to be much more effective than bilayer lipids in dissolving both Vx and Ddx (Tab. 1).

Table 1 Lipid concentration at which total solubilization of xanthophylls was achieved.

lipids	lipid concentration [μM] for:	
	Vx	Ddx
MGDG	11.6	2.0
DGDG	11.6	2.0
PE	38.7	38.7
PC	38.7	38.7

Complete solubilization of these xanthophylls was achieved at the non-bilayer lipid: pigment ratio of 5 for Ddx and 29 for Vx, whereas in the case of bilayer lipids this ratio for both pigments was almost 100. The effect of lipid concentration on the Vx and Ddx de-epoxidation rate was also studied. Ddx de-epoxidation by DDE was saturated at an MGDG or PE concentration of 2 μM. This corresponds well with the complete solubilization of Ddx. Further increase in lipid concentration did not enhance the Ddx de-epoxidation rate. On the contrary, at the MGDG concentration of 11.6 μM a slight reduction in the Ddx de-epoxidation rate was observed. On the other hand, 11.6 μM of MGDG or PE is the optimal concentration for Vx de-epoxidation by VDE. Quite a different situation was observed for the bilayer lipids. Ddx and Vx de-epoxidation was strongly suppressed even in the presence of high concentrations of PC and DGDG (38.7 μM) at which both xanthophyll cycle pigments are completely solubilized.

This indicates that xanthophyll solubilization is not the only factor that controls de-epoxidation,

although it may play an important role to provide the monomer forms of Ddx and Vx as the substrates for VDE and DDE.

The dependence between the conversion of Vx into Ax and Zx as well as Ddx to Dtx and the molecular dynamics of hydrophobic fraction of aggregates formed by inverted micelles, which are necessary for de-epoxidation, was also studied (Fig. 1). The highest activity was observed in PE1, PE2 and MGDG for VDE and DDE, respectively, although molecular dynamics of tested structures in case of these lipids was relatively low (Fig. 1).

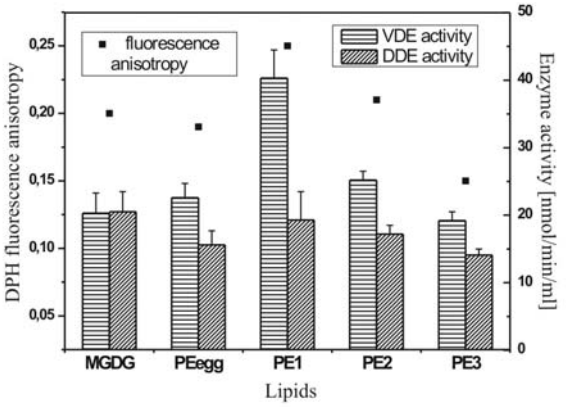

Fig. 1 Effect of molecular dynamics of hydrophobic fraction of inverted micelles composed of different types of lipids on VDE and DDE activity. Molecular dynamics was estimated by measuring DPH fluorescence anisotropy. The lower anisotropy the higher molecular dynamic.

Thickness of the hydrophobic fraction of the aggregates was another tested parameter. In this experiment two types of PE esterified with fatty acids having one double bond but differing in length were used. One of them was PE1 and the second was 1,2-dipalmitoyloleoyl-sn-glycero-3- sphosphatidylethanolamine (PE-C16). PE1 is about 600 pm longer than PE-C16 (Fig. 2). DDE activity was about 25% lower in PE-C16 than in PE1 micelles, whereas activity of VDE was 50% lower in system composed with PE-C16.

Size of the inverted micelles, suggested by mathematical description of the structures, was the last tested parameter. Diameters of the micelles varied from 7 to 9 nm, when they were created by MGDG, about 15 nm and from 20 to 21 nm when mixtures of MGDG and DGDG (50:50 and 85:15, respectively) were used (Figs. 3 and 4) (Sprague and Staehelin, 1984).

Total concentrations of MGDG, Vx or Ddx were constant and set to 0.33 μM for Vx or Ddx and 12.9 μM for MGDG.

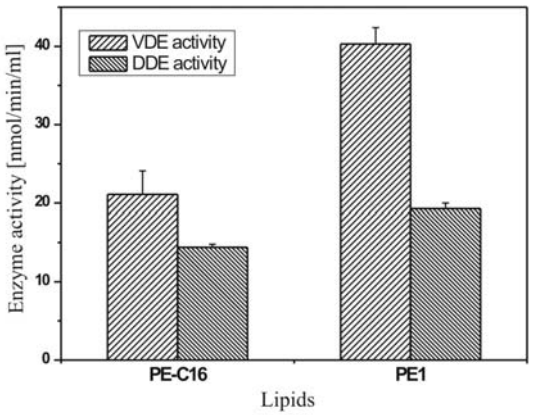

Fig. 2 Effect of the thickness of the hydrophobic fraction of inverted hexagonal structures on VDE and DDE activity. Hydrophobic fraction of the inverted hexagonal structures composed by PE1 is about 600 pm broader than hydrophobic structures created by PE-C16.

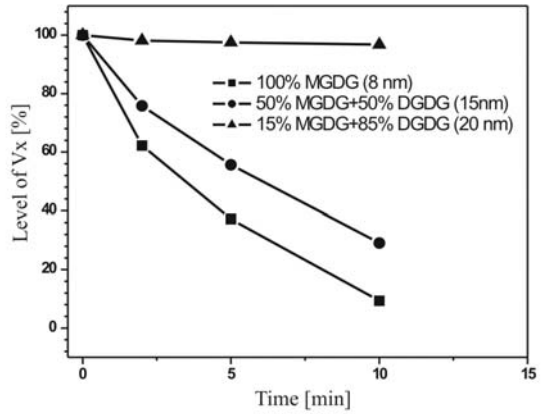

Fig. 3 Effect of diameter of inverted hexagonal structure micelles on Vx de-epoxidation.

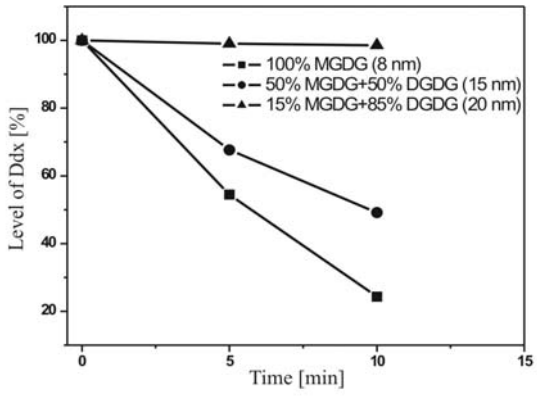

Fig. 4 Effect of diameter of inverted hexagonal structure micelles on Ddx de-epoxidation.

Obtained results show that the activity of de-epoxidation is strongly dependent on physicochemical parameters of inverted micelles such as thickness, molecular dynamics of hydrophobic core and their diameter. Mutual orientation of enzymes and

substrates or dilution of pigments by lipids are postulated as main mechanisms to explain the results.

Acknowledgements

This work was supported by the Polish Ministry of Science and Higher Education (project No. 50/N-DFG/2007/0).

References

Yamamoto HY, Nakayama TOM, Chichetser CO (1962) Studies on the Light and Dark Interconversions of Leaf Xanthophylls Arch. Biochem. 97: 168-173

Hager A (1966) Die Zusammenhange zwischen Lich-tinnduzierten Xanthophyll-Umwandlungen und Hill-Reaktion. Ber. Dtsch. Bot. Ges. 79: 94-107

Sapozhnikov DI (1967) Chemical Structure of Carotenoids and Their Conversion in the Plant Cell. Usp Sovrem Biol. 64(2): 248-267

Stransky H, Hager A (1970) The Carotenoid Pattern and the Occurrence of the Light-Induced Xanthophyll Cycle in Various Classes of Algae. VI. Chemosystematic Study. Arch Mikrobiol. 73(4): 315-23

Garcia-Plazaola JI, Hernandez A, Errasti A, Becerril JM (2002) Occurrence and Operation of the Lutein Epoxide Cycle in Quercus Species. Functional Plant Biology. 29: 1075-1080

Matsubara S, Morosinotto T, Bassi R, Christian AL, Fischer-Schliebs E, Lüttge U, Orthen B, Franco A, Scarano F, Förster B (2003) Occurrence of the Lutein-Epoxide Cycle in Mistletoes of the Loranthaceae and Viscaceae. Planta 217: 868-879.

Grzyb J, Latowski D, Strzałka K (2006) Lipocalins - a Family Portrait. J.Plant Physiol. 163: 895-915

Bouvier F, d'Harlingues A, Hugueney P, Marin E, Marion-Poll A, Camara B (1996) Xanthophyll Biosynthesis: Cloning, Expression, Functional Reconstitution, and Regulation of -Cycloxenyl Carotenoid Epoxidase from Pepper (Capsicum Annum). J. Biol. Chem.271: 28861-28867

Yamamoto HY, Higashi RM (1978) Violaxanthin De-epoxidase. Lipid Composition and Substrate Specificity. Arch Biochem Biophys. 190(2): 514-522

Latowski D, Kruk J, Burda K, Skrzynecka-Jaskier M, Kostecka-Gugała M, Strzałka K (2002) Kinetics of Violaxanthin De-Epoxidation by Violaxanthin De-Epoxidase, a Xanthophyll Cycle Enzyme, Is Regulated by Membrane Fluidity in Model Lipid Bilayers. Eur. J. Biochem. 269: 4656-4665

Latowski D, Akerlund HE, Strzałka K (2004) Violaxanthin De-Epoxidase, the Xanthophyll Cycle Enzyme, Requires Lipid Inverted Hexagonal Structures for Its Activity. Biochemistry 43: 4417-4420

Goss R, Lohr M, Latowski D, Grzyb J, Vieler A, Wilhelm C, Strzałka K (2005) Role of Hexagonal Structure-Forming Lipids in Diadinoxanthin and Violaxanthin Solubilization and De-Epoxidation. Biochemistry 44: 4028-4036

Sen A, Hui SW (1988) Direct Measurement of Headgroup Hydration of Polar Lipids in Inverted Micelles. Chem. Phys. Lipids 49: 179-184

Sprague GS, Staehelin LA (1984) Effect of Reconstitution Method on the Structural Organization of Isolated Chloroplast Membrane Lipids. Biochim. Biophys. Acta 777: 306-322

The Electron Transport in psbS-Silenced Rice

Ken-ichi Morita[a], Satoshi Ishida[a], Ko Shimamoto[b], Fumihiko Sato[a], Tsuyoshi Endo[a,*]

[a]Graduate School of Biostudies, Kyoto University, Kyoto 606-8502, Japan;
[b]Laboratory of Plant Molecular Genetics, Nara Institute of Science and Technology, Takayama 8916-5, Ikoma, Nara630-0192 Japan.
[*]Corresponding author. Tel. No. +81 75 753 6381; Fax No. +81 75 753 6398; E-mail: tuendo@kais.kyoto-u.ac.jp.

Abstract: A part of light energy absorbed in photosystem II (PSII) is used for photosynthetic electron transport and the rest is dissipated as heat and fluorescence. While there are methods to estimate the allocation of the absorbed light energy by chlorophyll fluorescence (for example, Dermming-Adams *et al*., 1996; Kramer *et al*., 2004; Hendrickson *et al*., 2004), none of them have become experimentally approved. For this purpose we generated lines of psbS knockdown rice in which both of psbS genes were efficiently silenced.

The silencing of *psb*S genes resulted in a decrease in the allocation of the absorbed light energy in PSII to TD in antenna (*D*), and an increase in that to TD in closed PSII centers, designated as excess (*E*), in wide range of light intensities, whereas energy allocation to the electron transport (*P*) did not change, suggesting that the main site of dissipation was shifted from antenna to PSII centers in PsbS-silenced lines. This also means that the rate-limiting step of photosynthetic electron transport was not at the light absorption even under low light but at acceptor side of PSII in the electron transport.

Keywords: Absorbed energy allocation; Chlorophyll fluorescence; Photosystem II; PsbS; Rice

Introduction

Since the proposal of Genty *et al*. (1989) that F_{II} can be estimated by a simple fluorescence parameter (Fm'–Fs)/Fm', this parameter, which can be easily measured by the fluorescence analysis with the pulse-modulated fluorometry (Schreiber *et al*., 1986), has been examined and justified in extensive physiological studies. On the basis of this proposal, Demming-Adams et al. further proposed that the parameter Fv'/Fm'(= (Fm'–Fo')/Fm'), that represents portion of absorbed light energy reached to the PSII centers can be divided to two categories, *Photosynthesis* ($F_P = F_{II}$) and *Excess* (F_E = (Fs–Fo')/Fm'). They defined remaining portion of absorbed light energy as *Dissipation* (F_D = Fo'/Fm'), which represents energy dissipation as heat most likely in PSII antenna.

Employing their energy allocation model, we estimated contribution of PsbS-dependent TD in total energy distribution in PSII by the comparison of the chlorophyll fluorescence of the wild type and *psb*S-silenced rice. As a result, the dissipation fraction ($F_D$was turned out to be an alternative and quantitative indicator of NPQ-TD, which can be determined without measuring Fm in the dark. We demonstrated the importance of energy dissipation in the antenna and the core, molecular mechanisms of which have not been elucidated, as well as NPQ dependent TD in rice.

Knockout of *psb*S gene(s) in rice has been reported by Koo *et al*. (2003), but the genetic background of this mutant has not been clearly shown. Therefore, we have produced new transformants in which expressions of both of two *psb*S genes in rice are down regulated.

Materials and methods

Plants

Seedling-derived calli of Japonica rice cv. Nipponbare (*Oryza sativa* L.) was transformed by

Agrobacterium with the methods of Hiei *et al*. (1994). Regenerated transgenic plants were cultivated from May to October in a greenhouse, in which temperature was maintained below 40 °C.

Chlorophyll Fluorescence

Chlorophyll fluorescence parameters were measured using a PAM2000 chlorophyll fluorometer (Waltz, Effeltrich, Germany). The minimum fluorescence at the open PSII centers was determined by measuring light. The steady state of the chlorophyll fluorescence level (Fs) was recorded during actinic light illumination. Fm (maximum fluorescence yield at closed PSII centers) and Fm' maximum fluorescence yield during illumination) were measured by application of a 1-s pulse of saturating white light. Fo and Fo' level was determined under far-red light.

The quantum yield of photochemistry in PSII during steady state photosynthesis (Φ_{II}) was calculated as (Fm'–Fs)/Fm'. NPQ was calculated as (Fm–Fm')/Fm'. The quantum yields of thermal dissipation from PSII antenna (*Dissipation*, *D*) and excess energy dissipated at PSII centers (*Excess*, *E*) were calculated as Φ_D = Fo'/Fm' and Φ_E = (Fs-Fo')/Fm', respectively, as reported in Demming-Adams *et al.* (1996).

Results

Establishment of RNAi lines

Two *psb*S genes were found in rice genome by BLASTN in NCBI data base (http://www.ncbi.nlm.nih.gov/) based on the sequence of *psb*S of *Aabidopsis thalinana*. In this study we call the gene located on chromosome 1 *psb*S1 (Accession No. NM_190784) and the other on chromosome 4 *psb*S2 (Accession No. D84392).

RNAi-mediated genes silencing using *psb*S1-specific sequences resulted in transgenic lines, Δ1&2-1, and Δ1&2-2, respectively. Both of these gene fragments showed 87% sequence identity with *psb*S2, therefore, silencing of both genes were expected in these transgenic lines. A 151 bp-*psb*S2-specific fragment on the UTR was also used in RNAi construct to generate transgenic line Δ2 in which silencing of *psb*S2 only was expected. Genomic PCR demonstrated the presence of the transgene in all the regenerated plants (data not shown). The same genomic PCR in T_1 generation showed 3:1 or 15:1 separation, in terms of transgene possession, showing that T_0 plants contained one or two copies of the transgene. In the experiments shown below, we used T_1 or T_2 plants which contained at least one copy of the transgene.

Quantitative RT-PCR analysis revealed that the amounts of both *psb*S1 and *psb*S2 transcripts were significantly reduced in Δ1&2-1 and Δ1&2-2 lines. Whereas, *psb*Ss expression in Δ2 line was not distinguishable to that of wild-type, suggesting that gene silencing of psbS2 in Δ2 line is incomplete. Immunobot analysis using anti-PsbS antibody showed that accumulation of PsbS protein were not detected in Δ1&2-1 and Δ1&2-2 lines. Two isoproteins derivied from each of the homolog genes could not be distinguished in the electrophoresis. These results indicate that the expression of *psb*Ss in Δ1&2-1 and Δ1&2-2 lines was successfully silenced by RNAi.

Photosynthetic Electron Transports in psbS RNAi Lines

Quantification of Xanthophyll cycle pigments, zeaxanthine, violaxanthine and anthorazanthine, in Δ1&2-1 and Δ1&2-2 showed that light-induced deepoxidation of violarhanthine occurred normally in these transformants, which is the same phenotype reported in the knockout mutant of *psb*S in Arabidopsis (Li *et al*., 2000).

Suppression of NPQ was found in the transgenic lines Δ1&2-1 and Δ1&2-2, in which both genes were silenced. While, in Δ2 line, which showed no clear suppression of gene expression, NPQ formation was comparable to the wild type plants. No correlation between NPQ and (Φ_{II}) was found, suggesting that suppression of thermal dissipation associated with NPQ (NPQ-TD), did not increase allocation of absorbed light energy to the photosynthetic electron trasnsport as in the case of PsbS-deficient mutant of Arabidopsis (Li *et al*., 2000) or in *npq1* Arabidopsis mutant which had no functional violaxanthin deepoxidase (Havaux and Niyogi, 1999).

Allocation of Absorbed Light Energy in PSII

Allocation of absorbed light energy to photosynthesis (P), dissipation (D) and excess (E) was estimated (Fig. 1) according to Demmig-Adams *et al*. (1996). The transgenic lines Δ1&2-1 and Δ1&2-2, that showed low NPQ, also showed low Φ_D. Thus, major portion of Φ_D is closely associated with NPQ-related thermal dissipation (NPQ-TD).

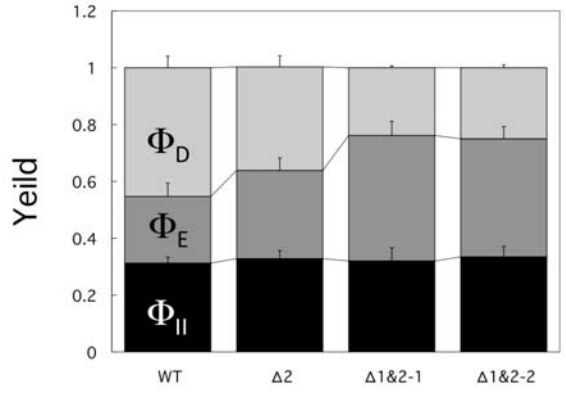

Fig. 1 Allocation of absorbed light energy to *P* (photosynthesis), *D* (dissipation) and *E* (excess) in wild type and psbS-silenced rice leaves (n = 7). Actinic white light (400 μmol m^{-2} s^{-1}) for 3 min was illuminated to leaves of 15 week-old rice, after which a saturation pulse of white light was applied to determine Fm'. Then the actinic light was turned off and Fo' was recorded under far red light.

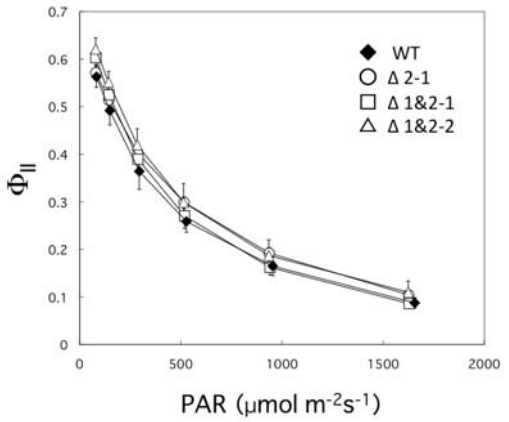

Fig. 2 Light response curves of the quantum yield of electron transport Φ_{II} in the wild type and three psbS mutants of rice. Varying intensities of white light (80–1,600 μmol m^{-2} s^{-1}) for 3 min each were illuminated to leaves of 12 week-old rice to determine chlorophyll fluorescence parameters (n = 3).

In transgenic lines Δ1&2-1 and Δ1&2-2, decrease in Φ_D and increase in Φ_E, as compared with the wild type and Δ2, were found, while Φ_{II} was in the same level in all lines. This means that the decrease in the NPQ-TD, in the transgenic plants with little PsbS, resulted in the increase in energy loss in the PSII core.

No clear correlation of Φ_{II} and Φ_D was found, while evident inverse relation is seen between Φ_E and Φ_D. Thus, decrease in NPQ-DT in PsbS-deficient mutants simply increase energy loss in the core but did not result in increases in photosynthetic electron transport. From these findings, it is concluded that increasing input pressure at the entrance of energy transduction in PSII core did not increase the output as the electron transport rate, but increases energy loss at the core. This also means that the rate-limiting step in the whole electron transport system is not light energy harvesting, but in the intersystem chain even under non-saturating light (400 μmol PAR m^{-2} s^{-1}).

Light Intensity Dependent Changes in the wild type and the RNAi lines

The light-saturation curves of the wild type and psbS-silenced RNAi lines were compared (Fig. 2). The suppression of NPQ did not affect over the wide range of light intensities, supporting the above hypothesis that the rate-limiting step in the whole electron transport system is not light energy harvesting even in light-limiting conditions.

Discussion

We adopted simple puddle model to define Φ_D and Φ_E after Demmig-Adams *et al*. (1996) because Φ_D and Φ_E in this definition may be useful to distinguish whether antenna or PSII center is responsible for dissipation. In the lake model shown above does not provide any information as for localization of each dissipation process.

This research demonstrated that the energy allocation model by Demming-Adams *et al*. (1996) could be successfully applied to elucidate the nature of *D* and *E* of the wild type and PsbS-deficient rice. Especially, the intrinsic relation of *qE-TD* and *D* was experimentally shown for the first time using PsbS-deficient transformants of rice. Further, the drastic shift of the site of thermal dissipation from antenna to PSII centers in the absence of PsbS could be visualized. Thus, this model can be a useful tool to elucidate the fate of absorbed light energy in PSII. However, this model needs further verification by experiments because the model is based on several assumptions, which have not been generally approved yet.

The most important problem is that molecular nature of *E* and *D* needs elucidation with experiments. For example, we have mentioned the relation of antenna and PSII centers, without clear definition of the antenna and the center. Although both can be conveniently distinguished by the fluorescence measurements based on the allocation model, molecular base of antenna and the PSII centers

remains obscure. Mutants of the antenna and PSII centers might be the most suited materials to verify and sophisticate the present model.

The rate of electron transport in PSII estimated from Φ_{II} value of chlorophyll fluorescence in the wide ranges of light intensity was identical in transgenic lines Δ1&2-1, Δ1&2-2, and the wild type (see Fig. 2). Thus, the increase in the input pressure in PSII did not increase the rate of electron transport even in light-limiting conditions. Higher reduction level of Q_A in the psbS-deficient lines (see Fig. 1B) suggested that the rate-limiting step is in the intersystem chain or further down stream of electron transport. One probable barrier is pH gradient across the thylakoid membranes, which may prevent electron flow in the plastoquinone pool, even under low light. This means that very low rate of the electron transport can down-regulates the further electron transport.

Acknowledgements

This work was supported in part by a project "Functional analysis of genes relevant to agriculturally important traits in rice genome" of Agriculture and Fishery Ministry of Japan.

References

Demmig-Adams B, Adams III WW, Baker DH, Logan BA, Bowling DR, Verhoeven AS (1996) Using Chlorophyll Fluorescence to Assess the Fraction of Absorbed Light Allocated to Thermal Dissipation of Excess Excitation. Physiol Plant 98: 253-264

Genty B, Briantais JM, Baker NR (1989) The Relationship between the Quantum Yield of Photosynthetic Electron Transportr and Quenching of Chlorophyll Fluorescence. Biochim biophys Acta 990: 87-92

Harvaux M, Niyogi KK (1999) The Violaxanthin Cycle Prptects Plants from Photooxidative Damage by More than One Mechanism. Proc Natl Acad Sci USA 96: 8762-8767

Hendrickson L, Furbank RT, Chow WS (2004) A Simple Alternative Approach to Assessing the Fate of Absorbed Light Energy Using Chlorophyll Fluorescence. Photosynth Res 82: 73-81

Hiei Y, Ohta S, Komari T, Kumashiro T (1994) Efficient Transformation of Rice (Oryza Sativa L.) Mediated by Agrobacterium and Sequence Analysis of the Boundaries of the T-DNA. Plant J 6: 271-282

Koo HY, Zulfugarov IS, Oh MH, Moon YH, Jansson S, An G, Lee CH (2004) The Function of the PsbS Protein in Relation to Nonphotochemical Energy Dependent Quenching in Rice Plants. In: A van der Est, D Bruce (eds.), Photosynthesis: Fundamental Aspects to Global Perspectives. Montreal, pp. 527-530

Kramer DM, Johnson G, Kiirats, Edwards GE (2004) New Fluorescence Parameters for the Determination of QA Redox State amd Excotatopm Energy Fluxes. Photosynth Res 79: 209-218

Li XP, Björkman O, Shih C, Grossman AR, Rosenquist M, Jansson, Niyogi KK (2000) A Pigment-Binding Protein Essential for Regulation of Photosynthetic Light Harvesting. Nature 403: 391-395

Schreiber U, Schliwa U, Bilger W (1986) Continuous Recording of Photochemical and Non-Photochemical Chlorophyll Quenching with a New Type of Modulation Fluorometer. Photosynth Res 10: 51-62

Photoprotective Function of Foliar Betacyanin in Leaves of *Amaranthus Cruentus* under Drought Stress

T Nakashima[a*], T Araki[b], O Ueno[c]

[a]Graduate school of Bioresource and Bioenvironmental Sciences, Kyushu University , Fukuoka, Japan;
[b]Faculty of Agriculture, Ehime University, Ehime, Japan;
[c]Faculty of Agriculture, Kyushu University, Fukuoka, Japan.
*Corresponding author. E-mail: tnak005@agr.kyushu-u.ac.jp.

Abstract: The function of foliar betacyanin as a photoprotective mechanism in water stressed *Amaranthus cruentus* plants was examined by comparing leaves of two strains differing significantly in betacyanin accumulation. Drought treatment was imposed by withholding irrigation for 2 days and at 0, 1, and 2 days after treatment onset, leaves were subjected to high light (HL) treatment to assess their tolerability to photoinhibition. The drought treatment reduced relative water content and gas exchange rate to similar extent in both strains. As drought developed, the extent of photoinhibition after HL treatment increased in both strains, however, it was significantly greater in acyanic than in betacyanic strains, indicating higher tolerance of betacyanic leaves to photoinhibition. The betacyanic leaves also exhibited higher values for quantum yield of PSII (Φ_{PSII}) and photochemical quenching (qP) during drought treatment despite the non-photochemical quenching (qN) did not differ between strains. These results may be partially explained by light screening effect of foliar betacyanin. Moreover, the increased betacyanin and decreased chlorophyll contents in betacyanic leaves were thought to have enhanced effectiveness of photoprotection provided by betacyanin during the drought period. Our results demonstrated the potential protective function of foliar betacyanin against photoinhibition in *A. cruentus* under drought conditions.

Keywords: *Amaranthus cruentus*; Foliar betacyanin; Maximum quantum yield of PSII; Photoinhibition, water-stress

Introduction

Accumulation of red pigments in leaves at certain developmental stages or in response to particular environmental stimuli is a well-conserved physiological trait across the plant kingdom, although its functional significance has long been a considerable debate. Betacyanins are alternative forms of non-photosynthetic red pigments which replace anthocyanins in nine families of Caryophyllales (Solovchenko and Merzlyak, 2008). The extensive studies on foliar anthocyanins thus far have provided a number of evidences supporting its protective function against photoinhibition induced by various abiotic stresses (*e.g.* Burger and Edwards, 1996; Hughes *et al*., 2005). Since betacyanins are known to possess similar chemical properties, they are also considered to fulfill these functions of anthocyanins (Solovchenko and Merzlyak, 2008), however, the photoprotective function of foliar betacyanins in drought stressed plants have not been well studied. Here we examined the photoprotective potential of foliar betacyanin in water-stressed *A. cruentus* plants by comparing two strains with and without significant betacyanin accumulation for their tolerability to drought-induced photoinhibition.

Materials and Methods

Two strains of *A. cruentus* L. differing in leaf coloration, namely the betacyanin-deficient (acyanic)

Tohoku 1 and the betacyanin-depositing (betacyanic) Tohoku 3, were germinated on nursery boxes. Four weeks old seedlings were transplanted to 5 L pots containing sandy loam soil and grown outdoors for 4 weeks with adequate irrigation twice a day. Drought treatment was then imposed by terminating irrigation for two consecutive clear days. At 0, 1 and 2 days after treatment onset (DAT), overnight dark-adapted leaves were subjected to high light (HL) treatment consisting of exposure to photoinhibitory illumination for 1h under the following conditions: PPFD, 1,500 μmol m^{-2} s^{-1}; chamber temperature, 30 °C; relative humidity, 60%; [CO_2], 399 ± 14 μmol mol^{-1}; [O_2], 21%. Leaves were dark-adapted for 20 min thereafter.

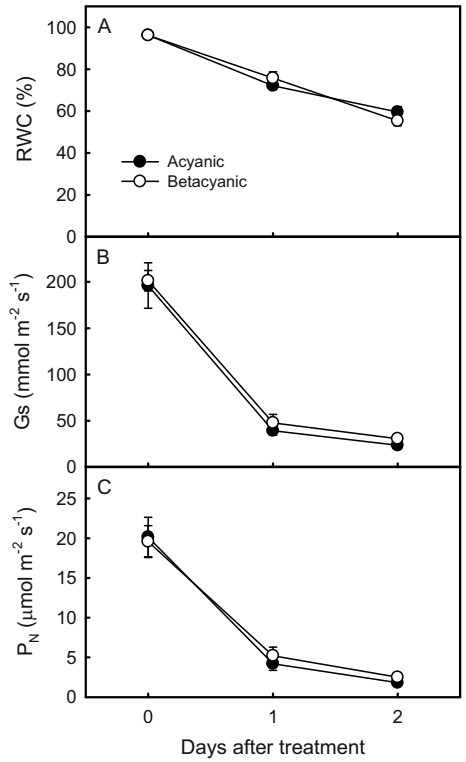

Fig. 1 Changes in leaf relative water content (RWC, A), stomatal conductance (Gs, B) and net photosynthetic rate (P_N, C) in acyanic and betacyanic leaves of *Amaranthus cruentus* during drought treatment.

At pre- and post- HL treatment, chlorophyll (Chl) fluorescence in dark-adapted state was measured to determine the maximum quantum yield of PSII (Fv/Fm, van Kooten and Snel, 1990), from which the percentage inhibition of Fv/Fm ($PI_{Fv/Fm}$) was calculated as $PI_{Fv/Fm}$ (%) = [1–(post-illumination Fv/Fm/pre-illumination Fv/Fm)] × 100. During the illumination, the quantum yield of PSII (Φ_{PSII}), photochemical quenching (qP) and non-photochemical quenching (qN) of fluorescence were measured simultaneously with gas exchange on fully light adapted leaves following the method of Genty *et al*. (1989). The stomatal conductance (Gs) and net photosynthetic rate (P_N) were calculated according to Long and Hallgren (1985). At the end of the measurements, leaves were sampled for determination of the leaf relative water content (RWC) and Chl and betacyanin quantification.

The data are expressed as means ± SE of 5–6 replicates and the statistical significance of interstrainal differences was determined by Student *t*-test.

Results and discussion

The microscopic observation of leaf cross-sections revealed the histological distribution of betacyanin within a leaf. The significant betacyanin accumulation was observed in upper and lower epidermis as well as palisade and spongy mesophyll cells of betacyanic leaves, whereas it was apparently absent from any tissues of acyanic leaves (Photos not shown).

Upon withholding irrigation, RWC in both strains fell approximately 80% of pre-stressed values at 1 DAT and below 60% at 2 DAT (Fig. 2A). Compared to relatively slow decline of RWC, Gs and P_N in both strains dropped drastically to 21%–25% of the pre-stressed values at 1 DAT, followed by further slow reduction by 35%–40% of 1 DAT at 2 DAT (Figs. 2B and 2C). These results suggested that the severity of water stress on both leaves was at a similar level and thereby a major energy sink was equally diminished under the drought condition, leading an increased risk of photoinhibition.

The Chl content as well as Chl a/b ratio decreased gradually after imposition of drought stress in both strains (Figs. 2A and 2B). This reduction of Chl contents was considered as an early avoidance response of leaves to excess incident light which has potentially harmful effects on photosynthetic apparatus (Munné Bosch and Alegre, 2000). Moreover, the rate and extent of reduction in both parameters was comparable between the strains throughout the experimental period, implying that the light capturing capacity did not differ between the strains. In contrast, betacyanin content in betacyanic leaves was remarkably higher than that in acyanic leaves and increased during drought period (Fig. 2C).

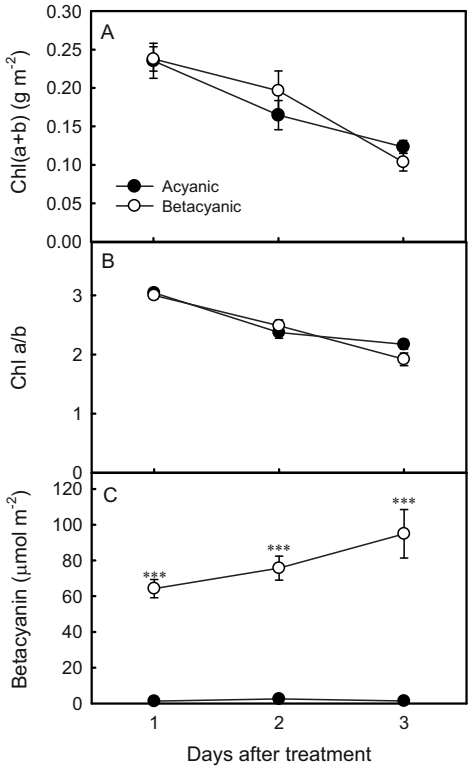

Fig. 2 Changes in total chlorophyll content (A), chlorophyll a/b ratio (B), betacyanin content (C) in acyanic and betacyanic leaves of *Amaranthus cruentus* during drought treatment
*** denotes the presence of significant differences between the two strains by Student t-test at $P < 0.001$.

With regard to equally diminished capacities of carbon fixation and Chl contents, the balance between energy acquisition and utilization was considered similar between the strains and therefore potential risk of photoinhibition was also considered to be equivalent for the strains.

The Φ_{PSII} and qP measured during HL treatment substantially decreased in both strains after the onset of drought treatment with similar trend to gas exchange parameters, however, betacyanic leaves maintained both parameters at significantly higher levels during drought period. Since these parameters reflect the efficiency of PSII electron transport and redox state of Q_A, a primary quinone acceptor of electron transport chain, respectively, (Krause and Weis, 1991), betacyanic leaves were considered capable of maintaining PSII activity either by increasing dissipation of excess energy via xanthophyll dependent heat dissipation or by reducing excitation pressure on PSII. The former possibility was discontinued since qN were almost identical between the strains throughout the experimental period (Fig. 3C). Therefore, increased betacyanin content in betacyanic leaves may have protected chloroplasts from excess incident light which causes over-excitation of PSII. Moreover, reduced Chl contents may have pronounced the effect of light attenuation by increasing the ratio of betacyanin per Chl molecule. As the result of these changes in pigment composition during the drought period, betacyanic leaves showed significantly lower extent of photoinhibition than acyanic leaves as indicated by significantly higher $PI_{Fv/Fm}$ at 1 and 2 DAT (Fig. 3D).

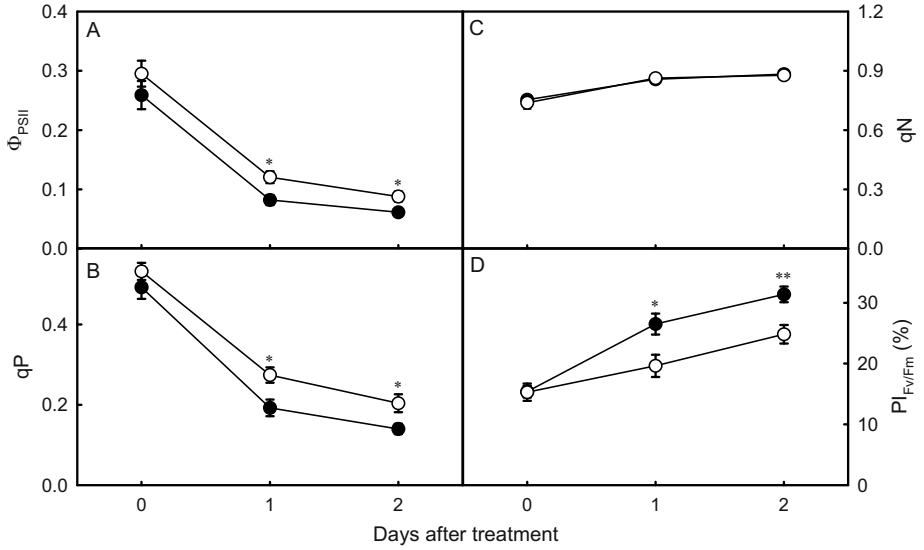

Fig. 3 Effective quantum yield of PSII (Φ_{PSII}, A), photochemical quenching of fluorescence (qP, B), non-photochemical quenching (qN, C) and percentage inhibition of Fv/Fm ($PI_{Fv/Fm}$, D) in acyanic and betacyanic leaves of *Amaranthu cruentus* during drought treatment.
* and ** denote the presence of significant differences between the two strains by Student t-test at $P < 0.05$ and 0.01, respectively.

In summary, our results demonstrated the potential photoprotective function of foliar beatacyanin in *Amaranthus* plant under drought stress. Foliar betacyanin deposited in epidermal and mesophyll tissues of betacyanic leaves was thought to attenuate excess incident light and hence reduce excitation pressure on PSII in a similar manner to anthocyanins (Steyn *et al*., 2002)., although, the alternative function of betacyanin an antioxidant suggested by several studies on foliar anthocyanins as well as betacyanins (*e.g.* Neill and Gould, 2003; Wang *et al*., 2006) still remains possible.

Acknowledgements

We would like to thank Dr. Masumi Katsuta (National Institute of Crop Science, National Agriculture and Food Research Organization, Tsukuba, Japan) for kindly providing seeds of *A. cruentus* used in this study.

References

Burger J, Edwards GE (1996) Photosynthetic Efficiency, and Photodamage by UV and Visible Radiation, in Red Versus Green Leaf Coleus Varieties. Plant Cell Physiol. 37: 395-399.

Genty B, Briantais JM and Baker NR (1989) The Relationship between the Quantum Yield of Photosynthetic Electron Transport and Quenching of Chlorophyll Fluorescence. Biochim. Biophys. Acta 990: 87-92

Hughes NM, Neufield HS, Burkey KO (2005) Functional Role of Anthocyanins in High-Light Winter Leaves of the Evergreen Herb Galax Urceolata. New Phytol. 168: 575-587

Krause GH, Weis E (1991) Chlorophyll Fluorescence and Photosynthesis: the Basics. Annu. Rev. Plant Physiol. Plant Mol. Biol. 42: 313-349

Long SP, Hallgren JE (1985) Measurements of CO_2 Assimilation by Plants in the Field and the Laboratory. In: J Coombs, DO Hall, SP Long, JMO Scurlock (eds.), Techniques in Bioproductivity and Photosynthesis. Pregamon Press: Oxford, pp. 62-94

Munné-Bosch S, Alegre L (2004) Die and Let Live: Leaf Senescence Contributes to Plant Survival under Drought Stress. Funct. Plant Biol. 31: 203-216

Neill SO, Gould KS (2003) Anthocyanins in Leaves: Light Attenuators or Antioxidants? Funct. Plant Biol. 30: 865-873

Solovchenko AE, Merzlyak MN (2008) Screening of Visible and UV Radiation as a Photoprptective Mechanism in Plant. Russ. J. Plant Physiol. 55: 803-822

Steyn WJ, Wand SJE, Holcroft DM, Jacobs G (2002) Anthoc. Yanins in Vegetative Tissues: a Proposed Unified Function in Photoprotection. New Phytol. 155: 349-361

Van Kooten O, Snel JFH (1990) The Use of Chlorophyll Fluorescence Nomenclature in Plant Stress Physiology. Photosynth. Res. 25: 147-150

Wang CQ, Liu T (2007) Involvement of Betacyanin in Chilling-Induced Photoinhibition in Leaves of Suaeda Salsa. Photosynthetica 45: 182-188

Presence of Flexible Non-Photochemical Quenching in Cryptophytes (*Rhodomonas Salina*)

Radek Kaňa[a*], Eva Kotabová[a], Ondřej Prášil[a]

[a]Institute of Microbiology, Czech Academy of Sciences, Třeboň, Czech Republic.
[*]Corresponding author. Tel. No. +420 384340436; Fax No. +420 384340415; E-mail: kana@alga.cz.

Abstract: Photosynthesis uses light as a source of energy but its excess can result in damage of photosynthetic apparatus. The protective mechanism of non-photochemical quenching (NPQ) can safely dissipate excess of light to heat. Presence and mechanism of NPQ regulation differs between photothrophs. Here we show presence of non-photochemical quenching in cryptophyte alga (*Rhodomonas salina*), that represents unique clade of chromalveolates. Cryptophytes are exceptional among photosynthetic chromalveolates (that include also diatoms and other Chl c containing algae) because beside membrane-bound chlorophyll a/c proteins they also contain lumenal phycobiliproteins. We have shown that NPQ in *R. salina* is stimulated by light absorbed by chlorophyll (orange light – 620 nm) and phycoerythrin (green light – 520 nm) to the same extent with the same maximal value around 1.6. Kinetic pattern of NPQ stimulation in high light and its recovery in dark resemble flexible energetic quenching, qE. It indicates different regulation of NPQ in cryptophytes in comparison to the same process known in diatoms because there recovery from quenching state is usually less flexible.

Keywords: Non-photochemical quenching (NPQ); Light stress; Cryptophytes; *Rhodomonas salina*; Chromalveolates; Diatoms

Introduction

There are several protective mechanisms against excessive irradiation in photothrophs. One of them is a non-photochemical quenching (NPQ) that represents a feed-back regulatory mechanism allowing safe dissipation of excessive irradiation to heat (reviewed in Horton and Ruban, 2005; Horton *et al.*, 2008). As NPQ is connected with de-excitation of chlorophyll exited state, it can be detected by analysis of chlorophyll fluorescence (Muller *et al.*, 2001) that is much easier method than direct detection of heating (Kaňa *et al.*, 2008).

Mechanism of NPQ involves several processes with various kinetics. Therefore it is usually divided based on its kinetics of stimulation and recovery into: (1) fast energetic quenching (qE) that forms as a result of lumen acidification on light; (2) slower state-transition quenching (qT); and (3) photoinhibitory quenching (qI) that represents less flexible reaction of photosynthetic apparatus to excessive irradiation (Ruban and Horton, 1995). However, in all cases NPQ acts mostly on the level of Photosystem II (PSII) light-harvesting antennae (see *e.g.* Horton and Ruban, 2005 for review). So far it has been established that light harvesting antennae of PS II are usually triggered into the dissipative mode by lumen acidification and that process is modulated by xanthophylls (Gilmore *et al.*, 1997; Horton *et al.*, 2008). There are also some proteins including PsbS in higher plants (Li *et al*., 2000) or LI818 in diatoms (Zhu and Green, 2010) that play a key role in NPQ. However, precise mechanism of the process differs between various organisms (compare NPQ in diatoms, *e.g.* in Grouneva *et al*. (2009) and in higher plants in Horton *et al*. (2008)) thus a species dependent approach is necessary.

Here we describe non-photochemical quenching in cryptophytes (*Rhodomonas salina*) and show that its kinetics differs from their evolutionary relatives, from diatoms.

Materials and Methods

The cryptophyte alga *Rhodomonas salina* (strain CCAP 978/27) was grown in artificial seawater medium with f/2 nutrient addition at t = 18 °C. Light was provided by dimmable fluorescence tubes with intensity 30 μmol m^{-2} s^{-1} (day-night cycle 12/12 h) and continually bubbled with air. Samples were taken during exponential phase of growing.

Absorption spectra were recorded with the Unicam UV 500 spectrometer (Thermo Spectronic, UK). Cells were collected on acetate filters (pore diameter 0.6 μm; Pragochema, Prague, Czech Republic), and absorption spectrum was measured in the integrating sphere with 4 nm detection bandwidth.

Quenching analysis has been done using the FL-3000 fluorometer (PSI, Brno, Czech Republic) with a typical protocol. Kinetics of variable chlorophyll a fluorescence was detected in the spectral range 690–710 nm, samples were dark adapted for 20 minutes before measurements. Fluorescence of the dark adapted sample (minimal fluorescence – F_O) has been measured before actinic light irradiation applying low intensity measuring light (2 μmol m^{-2} s^{-1}, 622 nm). Actinic irradiation and saturating flashes were provided by multicolor diodes.

Value of maximal fluorescence for the dark (F_M) and light adapted sample (F_M') has been measured during 200 ms multiple turnover actinic flashes. Parameter of non-photochemical quenching has been calculated based on Stern-Volmer formalism as NPQ = (F_M–F_M')/F_M. Maximal efficiency of photosystem II photochemistry F_V/F_M was calculated as (F_M–F_O)/F_M where F_M and F_O represent maximal and minimal fluorescence of dark adapted sample. Genty parameter, ϕ_{PSII} has been calculated as ratio (F_M'–F_t)/F_M' where F_t (F_M') is steady state (maximal) fluorescence after 120 s of irradiance.

Results and Discussion

Cryptophytes represent an unique algae from chromalveolate supergroup that includes also diatoms, brown algae or dinoflagelates. Cryptophytes possess a specific composition of light harvesting complexes that consist of membrane-integral chlorophyll a,/c-binding proteins and lumenal proteins homologous to red algal phycobiliproteins (see *e.g.* MacPherson and Hiller (2003) for review).

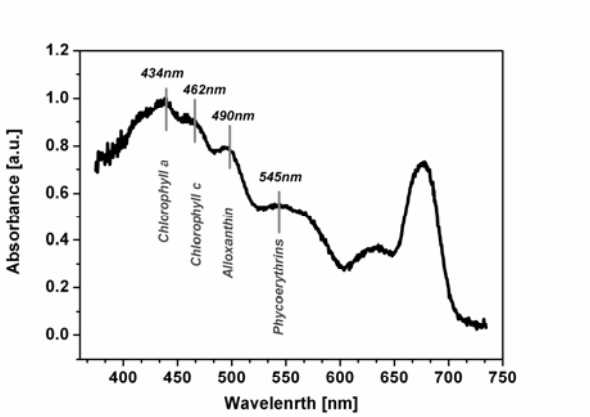

Fig. 1 Typical absorption spectrum of *Rhodomonas salina.* The main pigments are marked together with their maxima of absorption.

These two main light harvesting systems can be distinguished also in the absorption spectrum of *Rhodomonas salina* (Fig. 1). Presence of chlorophyll a and chlorophyll c in thylakoid membrane antennae caused typical absorption at 434 nm and 462 nm (Fig. 1). There is also the main absorption peak of the carotenoid alloxanthin (at 490 nm) that is typical for all cryptophytes. The broad absorption at 545 nm (Fig. 1) is caused by phycoerythrin proteins that are firmly embedded inside of the thylakoid lumen (Kaňa *et al.*, 2009).

Only a little is known about the response of the unique two component light-harvesting apparatus of cryptophytes to excessive irradiation. Therefore, we have carried out basic quenching analysis (Fig. 2). *R. salina* cells were exposed to two types of actinic light – orange (620 nm) and green (520 nm). The orange light is preferentially absorbed by the chlorophyll a/c antennae in the thylakoid membrane (Fig. 1). On the other hand, green light is absorbed by phycoerythrins (see maximum at 545 nm). Maximal efficiency of photosystem II photochemistry - F_V/F_M was similar for green and orange light (see legend of Fig. 2). This indicates efficient utilization of light absorbed in both antennae systems (in phycoerythrins and in chlorophyll a/c antennae) in photosystem II. This is also in line with the known high efficiency of energy transfer observed in phycoerythrins (van der Weij *et al.*, 2006).

The exposure of *R. salina* cells to high light induced fast quenching of maximal fluorescence (see decrease in F_M' in Fig. 2) that shows presence of non-photochemical quenching (NPQ) in *R. salina*. Maximal value of NPQ obtained in *R. salina* was usually between 1.3–1.6 in dependence on growth

conditions (data not shown). The similar values can be seen for green and orange light (see Fig. 2) that are absorbed by different antennae systems. It could indicate that NPQ proceeds in phycoerythrins and in chlorophyll a/c antennae independently. However, the more probable explanation could be that irradiation absorbed in phycoerythrins is efficiently transferred to chlorophyll a/c where it can be quenched.

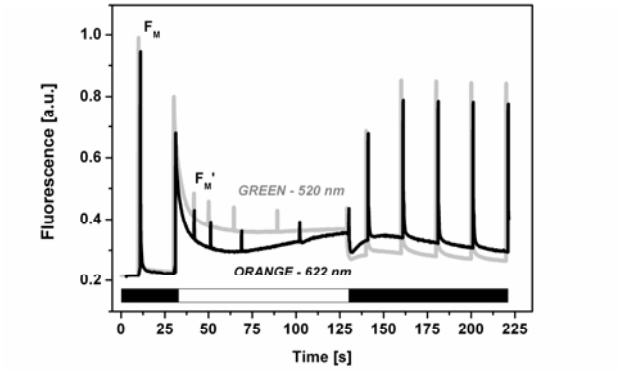

Fig. 2 Fluorescence quenching analysis measured with *Rhodomonas salina.* Two types of actinic lights with the same intensity (600 μmol m^{-2} s^{-1}) were used: (1) Excitation to chlorophylls (at 620 nm–black line); (2) Excitation to phycoerythrins (at 520 nm–grey line). White and black bars represent periods with and without actinic light, respectively. Maximal efficiency of photosystem II - F_V/F_M for green and orange light were 0.78 and 0.77, respectively.

We have also studied the kinetic of NPQ stimulation (Fig. 3). During irradiation by saturating light (300 μmol m^{-2} s^{-1}), a fast increase in NPQ can be seen with maximum at 40 seconds after onset of irradiation. On the other hand, low light (60 μmol m^{-2} s^{-1}) that represents double of growth irradiance is rather efficiently used in photochemistry as it can be deduced from the parameter ϕ_{PSII} that indicates efficiency of PSII photochemistry in light. Φ_{PSII} was below 0.2 at high light and around 0.5 at low light (see legend of Fig. 3). The fast stimulation of NPQ by actinic light was also accompanied by its fast recovery in the dark (Fig. 3). The fast reversibility of NPQ in the dark indicates fast reversibility of the quenching that resembles the typical kinetics of energetic quenching (qE) observed in other organisms (see *e.g.* Horton *et al.* (2008) for review).

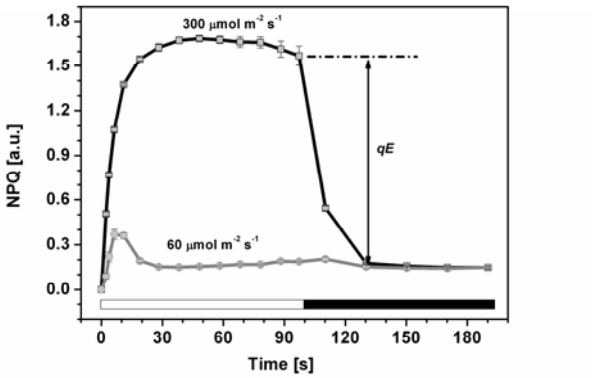

Fig. 3 Kinetics of non-photochemical quenching on blue light The PSII efficiency in the light (ϕ_{PSII}) has been estimated to be 0.5 and 0.15 for the irradiance 60 and 300 μmol m^{-2} s^{-1}, respectively. White and black bars represent periods with and without actinic light, respectively.

In conclusion, our results indicate the presence of flexible non-photochemical quenching in the cryptophyte alga *Rhodomonas salina*. In comparison to diatoms (see *e.g.* Grouneva *et al.*, 2009; Zhu and Green, 2010), the observed quenching is more flexible and resembles mostly energetic quenching that is controlled by lumen acidification. At this stage of knowledge, we can only speculate about the localization of NPQ in light-harvesting antennae of cryptophytes. These antennae consist of the so-called Cac proteins (Durnford *et al.*, 1999), that originated from separate clades in comparison to FCP proteins (Fucoxanthin Chlorophyll a/c-binding protein) in diatoms (Neilson and Durford, 2010). We have shown that similarly to diatoms (Miloslavina *et al.*, 2009), also cryptophytes are able to quench excessive irradiance by NPQ (Figs. 1 and 2). Therefore, the future task would be to compare regulation of NPQ in these two organisms on the protein level.

Acknowledgements

The project has been supported by GAČR 206/09/094 and by Institutional Research Concepts AV0Z50200510, MSM6007665808 and by project Algatech (CZ.1.05/2.1.00/03.0110). We thank Schola Ludus students (Anna Krejčí a Petr Jirásko) for preliminary measurements.

References

Horton P, Ruban A (2005) Molecular Design of the Photosystem II Light-Harvesting Antenna: Photosynthesis and Photoprotection. J. Exp. Bot. 56: 365-373

Horton P, Johnson MP, Perez-Bueno ML, Kiss AZ, Ruban AV (2008) Photosynthetic Acclimation: Does the Dynamic Structure and Macro-organisation of Photosystem II in Higher Plant Grana Membranes Regulate Light Harvesting States? FEBS J. 275: 1069-1079

Durnford DG, Deane JA, Tan S, McFadden GI, Gantt E, Green BR (1999) A Phylogenetic Assessment of the Eukaryotic Light-Harvesting Antenna Proteins, with Implications for Plastid Evolution. J. Mol. Evol. 48: 59-68

Gilmore AM (1997) Mechanistic Aspects of Xanthophyll Cycle-Dependent Photoprotection in Higher Plant Chloroplasts and Leaves. Physiol. Plant. 99: 197-209

Grouneva I, Jakob T, Wilhelm C, Goss R (2009) The Regulation of Xanthophyll Cycle Activity and of Non-Photochemical Fluorescence Quenching by Two Alternative Electron Flows in the Diatoms Phaeodactylum Tricornutum and Cyclotella Meneghiniana. Biochim. Biophys. Acta-Bioenergetics 1787: 929-938

Kaňa R, Vass I (2008) Thermoimaging as a Tool for Studying Light-Induced Heating of Leaves Correlation of Heat Dissipation with the Efficiency of Photosystem II Photochemistry and Non-Photochemical Quenching. Env. Exp. Bot. 64: 90-96

Kaňa R, Prašil O, Mullineaux CW (2009) Immobility of Phycobilins in the Thylakoid Lumen of a Cryptophyte Suggests that Protein Diffusion in the Lumen Is Very Restricted. FEBS Lett. 583: 670-674

Li XP, Bjorkman O, Shih C, Grossman AR, Rosenquist M, Jansson S, Niyogi KK (2000) A Pigment-Binding Protein Essential for Regulation of Photosynthetic Light Harvesting. Nature 403: 391-395

MacPherson AN, Hiller RG (2003) Algae with Chlorophyll c. In: BR Green, WW Parson (eds.), Light-harvesting Antennae in Photosynthesis. Kluwer Academic Publishers: Dordrecht, pp. 323-352

Miloslavina Y, Grouneva I, Lambrev PH, Lepetit B, Goss R, Wilhelm C, Holzwarth AR (2009) Ultrafast Fluorescence Study on the Location and Mechanism of Non-Photochemical Quenching in Diatoms. Biochim. Biophys. Acta-Bioenergetics 1787: 1189-1197

Muller P, Li XP, Niyogi KK (2001) Non-Photochemical Quenching. A Response to Excess Light Energy. Plant Physiol. 125: 1558-1566

Neilson Durford (2010) Structural and Functional Diversification of the Light-Harvesting Complexes in Photosynthetic Eukaryotes. Photosynth. Res. DOI 10.1007/s11120-010-9576-2

Ruban AV, Horton P (1995) An Investigation of the Sustained Component of Nonphotochemical Quenching of Chlorophyll Fluorescence in Isolated-Chloroplasts and Leaves of Spinach. Plant Physiol. 108: 721-726

Zhu SH, Green BR (2010) Photoprotection in the Diatom Thalassiosira Pseudonana: Role of LI818-Like Proteins in Response to High Light Stress. Biochim. Biophys. Acta-Bioenergetics 1797: 1449-1457

Van der Weij-De W, Doust AB, van Stokkum IHM, Dekker JP, Wilk KE, Curmi PMG, Scholes GD, van Grondelle R (2006) How Energy Funnels from the Phycoerythrin Antenna Complex to Photosystem I and Photosystem II in Cryptophyte Rhodomonas CS24 Cells. J. Phys. Chem. B 110: 25066-25073

The Slow S to M Fluorescence Rise is Missing in the RpaC Mutant of *Synechocystis sp.* (PCC 6803)

Radek Kaňa[a,b*], Ondřej Komárek[a], Eva Kotabová[a], George C Papageorgiou[c], Govindjee[d], Ondřej Prášil[a,b]

[a]Institute of Microbiology, Czech Academy of Sciences, Třeboň, Czech Republic;
[b]Institute of Physical Biology and Faculty of Biology, University of South Bohemia in České Budějovice, Czech Republic;
[b]National Center for Scientific Research Demokritos, Institute of Biology, Athens, 153 10- Greece;
[c]Department of Plant Biology, University of Illinois at Urbana-Champaign, Urbana, IL 61801-3707, USA.
[*]Corresponding author. Tel. No. +420 384340436; Fax No. +420 384340415; E-mail: kana@alga.cz.

Abstract: Transfer of phycobilisome-containing cyanobacteria from darkness to continuous light results in a typical chlorophyll a fluorescence induction that follows a pattern labeled as OJIPSMT. This pattern of fluorescence induction (FI) reflects changes in both photochemical and non-photochemical processes. We have focused on the slow S to M fluorescence rise that is dominant in cyanobacteria. We clearly observe the S-to-M fluorescence rise in the wild type (WT*)* cells of *Synechocystis sp.* (PCC 6803) in the presence of 1, 1'-dimethyl-3(3'4'-dichloro)-phenylurea (DCMU). This rise is fully suppressed by hyperosmotic glycine betaine that prevents the mobility of extramembrane phycobilisomes. The contribution of the State 2-to-State 1 transition in the S-to-M rise of WT cells was proven by changes in the 77 K emission spectra: the spectra at point O of FI (*i.e.*, in State 2, with lower ratio of F685/F726) were characteristically different from those at point M (*i.e.*, in State 1, with higher ratio of F685/F726). The S-M rise was totally missing in RpaC– mutant of *Synechocystis sp.* (PCC 6803) that is locked in the high-fluorescence State 1 and thus is unable to do state transitions. Moreover, RpaC- mutant showed quenching of phycobilin fluorescence during the S-M rise period. Taken together, these data suggest that the State 2 to State 1 transition is the dominant cause of the S to M fluorescence rise in cyanobacteria.

Keywords: PH–related fluorescence quenching; Cyanobacteria; Fluorescence induction; S to M fluorescence rise; State changes

Introduction

Kinetics of chlorophyll a fluorescence in photosynthetic organisms follows a typical pattern after irradiation: O-J-I-P-S-M-T transition (O—initial, J and I—inflections, P—peak, S—semi-steady state, M—maximum, T—the terminal steady state fluorescence). The fast part of the fluorescence induction curve (during the first second of actinic irradiance) is dominant in higher plants but rather shallow in cyanobacteria. On the contrary, the slower fluorescence increase (in tens of seconds) from the S-plateau to the M peak (Papageorgiou and Govindjee 1968) is dominant in cyanobacteria (Papageorgiou *et al*., 2007). Since cyanobacteria tend to stay in the low fluorescence State 2 during dark and are transformed into the high fluorescent State 1 during irradiation (Stamatakis *et al.*, 2007), the S to M fluorescence rise has been assigned mostly to an increase in PBS (phycobilisome) → PS II excitation transfer (Papageorgiou *et al*., 2007). The higher PBS → PS II excitation transfer accompanied by stimulation of S to M rise can be also seen in a case of inhibition in PBS → PS I excitations transfer (Papageorgiou *et al.*, 2007; Stamatakis *et al.*, 2007). Such a redistribution in energy transfer from PBS is possibly allowed either by phycobilisomes mobility (Joshua and Mullineaux, 2004) or by some other energy re-distribution mechanism (McConnell *et al*., 2002). As the S to M rise can be observed also in the presence of DCMU

(Papageorgiou and Govindjee, 1968), it rules out an involvement of electron transport between Q_B to PQ-pool (Tsimilli-Michael *et al.*, 2009). This phenomenology suggests that the S to M rise reflects regulatory distribution of PBS excitation to PSII and PSI. Here, we have further investigated the validity of this hypothesis by comparing the FI patterns of chlorophyll *a* fluorescence measured with wild type (WT) and with state-transition mutant (RpaC–) of *Synechocystis sp.* PCC6803 cells (Emlyn-Jones *et al*., 1999). Thus, we demonstrate here that the S-to-M fluorescence rise is related to State 2 to State 1 transition.

Materials and Methods

Synechococystis sp. (PCC 6803) cells were cultivated in BG 11 medium in an orbital shaking incubator at 28 °C at continual irradiance of 14 μmol (photons) m^{-2} s^{-1}. Fluorescence induction at Chl a fluorescence maximum was measured between 690–710 nm with a double modulated fluorimeter FL-100 (PSI, Czech rep.). The fluorescence spectra during FI was detected by Spectrally Resolved Fluorescence Induction (SRFI) method (see *e.g.* Kaňa *et al.*, 2009) at actinic irradiation (orange light 590 nm, ~300 μmol (photons) m^{-2} s^{-1}) and during saturating flash (590 nm, 1,500 μmol (photons) $m^{-2}s^{-1}$). The spectra were detected by a diode array spectrophotometer SM-9000 every 100 ms (PSI, Brno, Czech Republic). The low temperature (77 K) fluorescence emission spectra were detected at liquid nitrogen by spectrophotometer SM-9000 (PSI, Brno, Czech Republic).

Results and Discussion

We have observed a typical kinetic fluorescence pattern during dark-light transition in wild type (WT) *Synechocystis sp.* (PCC 6803) cells that showed both the fast OJIP transient and the slower S-M transition (see Fig. 1A). However, in *Synechocystis sp.,* the S-M rise was less pronounced (Fig. 1) than in *Synechococcus sp.* (Kaňa *et al.*, 2009). In fact, it was clearly visible with presence of DCMU (see the DCMU curve in Fig. 1A) in agreement with the previous results (Papageorgiou and Govindjee, 1968). As the S to M rise is clearly visible in the presence of DCMU (Fig. 1), it must be somehow controlled by the redox state of the PQ pool. It may mean that when PSII reaction center is closed by DCMU, PQ pool become mostly oxidized upon illumination and this may result in PBS redistribution in favor of PBS → PS II excitation transfer – and, thus, we see strong S-M fluorescence rise (Fig. 1).

We have further studied properties of the S-M rise in *Synechocystis sp.* and found that it is abolished by hyperosmotic glycine betaine (Fig. 1A). It is known that hyper-osmotic conditions in general block the SM rise in PBS-containing cyanobacteria reversibly, without blocking the OJIPS phase (Stamatakis *et al.*, 2007). It seems that glycine betaine blocks PBS redistribution from PS I to PS II during irradiation. This result can be either due to blocking of phycobilisome diffusion mobility (Li *et al.*, 2004) or due to an inhibition of some other mechanism affecting PBS → photosystem energy transfer. Such a regulatory re-distribution of PBS excitation is known as State 2-to-State 1 transition (see *e.g.* McConnell *et al.*, 2001; Mullineaux and Emlyn-Jones, 2005).

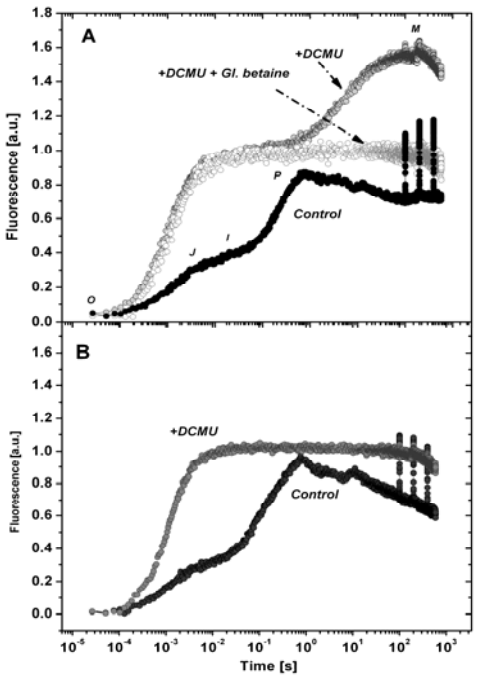

Fig. 1 Time course of chlorophyll a fluorescence induction (FI) of wild type cyanobacterium *Synechocystis sp.* (panel A) and its mutant without RpaC protein (panel B). Cells were dark adapted and exposed to orange excitation light (590 nm, 300 μmol (photons) m^{-2} s^{-1}). All curves are from the same sample before and after addition of inhibitors. First, the control curve was obtained ("Control") that was followed by the addition of 10 μM DCMU ("DCMU") and finally 520 mmol glycine betaine was added ("Gl. betaine"). Data are normalized to the maximal fluorescence before measurements. Characteristic peaks during fluorescence transient (OJIPM) are marked.

The connection between S-M fluorescence rise and State 2 to State 1 transition was shown by measurements with state-transition mutant (RpaC–) of *Synechocystis sp.* (Joshua and Mullineaux, 2005) that is unable to carry out state transition changes. Indeed, in the case of RpaC– mutant, there is no fluorescence rise even after addition of DCMU (Fig. 1B). This confirms that state transition changes are crucial for S-M fluorescence rise in *Synechocystis sp.*

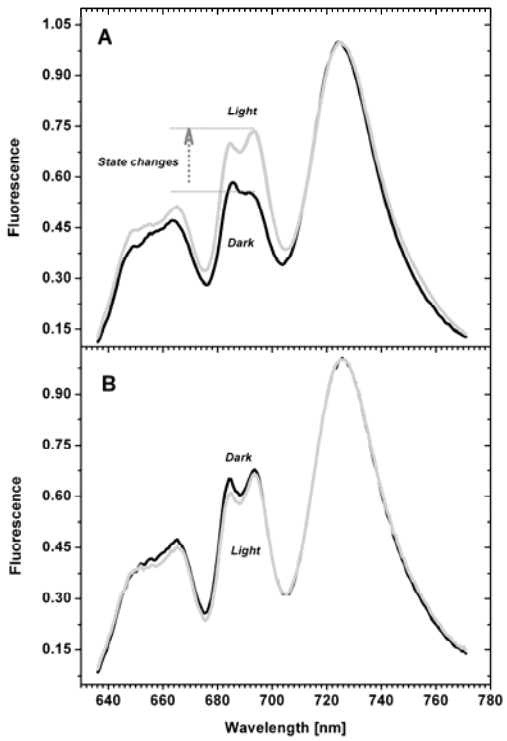

Fig. 2 Low temperature (77 K) fluorescence emission spectra measured with WT (panel A) and RpaC- mutant (panel B) of *Synechocystis sp*. Data were obtained after 20 min of dark, see "Dark" curves or after 200s long irradiation with orange light (590 nm, 300 μmol (photons) m^{-2} s^{-1}) - see "Light" curves. Fluorescence was exited at 530 nm. DCMU (10 μM) was added before measurements. Fluorescence increase due to State 2 to State 1 transition on light is marked. Data are normalized to fluorescence at 726 nm.

We have further explored the connection between state changes and the S-M fluorescence rise by low temperature (77 K) fluorescence spectroscopy. It is well known that PBS redistribution from PSI to PSII causes relative increase in PSII fluorescence (between 685–695 nm) in comparison to PSI fluorescence (with maximum at 726 nm). Indeed, such a stimulation of PSII fluorescence at 685–695 nm was visible after irradiation of WT cells of *Synechocystis sp.* treated with DCMU (Fig. 2A). On the contrary, there was no increase in fluorescence of PSII after irradiation in RpaC- mutant (Fig. 2B). Since the RpaC– mutant cells are locked in the high-fluorescence State 1 any redistribution of PBS is blocked during irradiation and thus there is no S-M fluorescence rise in RpaC– mutant of *Synechocystis sp*. (Fig. 1B). All the above mentioned data, taken together, suggest that the State 2 to State 1 transition is the dominant cause of the S to M fluorescence rise in cyanobacteria.

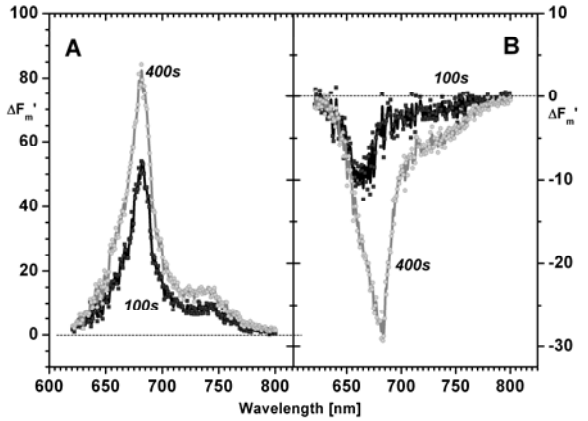

Fig. 3 Typical difference fluorescence emission spectra measured with saturated light pulses (spectra of maximal fluorescence - F_m). The ΔF_m' spectra represent the difference, F_m'- F_m, where F_m is maximal fluorescence measured in the dark and F_m' is maximal fluorescence measured after a particular time of irradiation (black line – 100 s; grey line – 400 s). Panel A represents difference fluorescence spectra of WT, and the panel B shows data obtained with RpaC- mutant. The curves shown were obtained from raw data measured by Spectrally Resolved Fluorescence Induction – SRFI method (see Materials, Methods, Kaňa *et al*., 2009).

We have also briefly explored the effect of high irradiance during the period of S-M rise in the RpaC- mutant that is incapable of PBS redistribution between photosystems, and is permanently locked in State 1 (Fig. 2B). We have measured room temperature spectra of maximal fluorescence for dark adapted sample at saturating flash (F_m spectra) and compared them with the spectra measured after 100 s and 400 s of light – the $\Delta Fm' = F_m - F_m'$ difference spectra are presented in Fig. 3. We observe (Fig. 3 A) that the irradiation of WT cells caused increases in maximal fluorescence that reflect State 2 to State 1 transition as already shown in Fig. 1 and Fig. 2. However, in the case of RpaC- mutant of *Synechocystis sp.* there decreases in maximal fluorescence after irradiation (see difference spectra ΔF_m' in Fig. 3B) due to some non-photochemical

processes because ΔF_m' was measured at saturating flashes, when reaction centers are closed. Thus, we can conclude that the inability of state transition in RpaC- mutant results in non-photochemical quenching of fluorescence.

Acknowledgements

This research project was supported by GAČR 206/09/094 and by Institutional Research Concepts AV0Z50200510, MSM6007665808 and by project Algatech (CZ.1.05/2.1.00/03.0110). We would like to thank Prof. Conrad Mullineaux for providing us RpaC- mutant of *Synechocystis sp.* (PCC6803).

References

Emlyn-Jones D, Ashby MK, Mullineaux CW (1999) A Gene Required for the Regulation of Photosynthetic Light Harvesting in the Cyanobacterium Synechocystis 6803. Molecular. Microbiol. 33: 1050-1058

Joshua S, Mullineaux CW (2004) Phycobilisome Diffusion Is Required for Light-State Transitions in Cyanobacterial. Plant. Physiol. 135: 2112-2119

Kaňa R, Prášil O, Komárek O, Papageorgiou GC, Govindjee (2009) Spectral Characteristic of Fluorescence Induction in a Model Cyanobacterium, Synechococcus sp (PCC 7942). Biochim. Biophys. Acta-Bioenergetics 1787: 1170-1178

Li DH, Xie J, Zhao JQ, Xia AD, Li DH, Gong YD (2004) Light-Induced Excitation Energy Redistribution in Spirulina Platensis Cells: "Spillover" or "Mobile PBSs"? Biochim. Biophys. Acta-Bioenergetics 1608: 114-121

McConnell MD, Koop R, Vasil'ev S, Bruce D (2002) Regulation of the Distribution of Chlorophyll and Phycobilin-Absorbed Excitation Energy in Cyanobacteria. A Structure-Based Model for the Light State Transition. Plant. Physiol. 130: 1201-1212

Mullineaux CW, Emlyn-Jones D (2005) State Transitions: an Example of Acclimation to Low-Light Stress. Journal of Experimental Botany 56: 389-393

Papageorgiou G, Govindje (1968) Light-Induced Changes in Fluorescence Yield of Chlorophyll Alpha in Vivo .I. Anacystis Nidulans. Biophys. J. 8: 1299-1315

Papageorgiou GC, Tsimilli-Michael M, Stamatakis K (2007) The Fast and Slow Kinetics of Chlorophyll a Fluorescence Induction in Plants, Algae and Cyanobacteria: a Viewpoint. Photosynth. Res. 94: 275-290

Stamatakis K, Tsimilli-Michael M, Papageorgiou GC (2007) Fluorescence Induction in the Phycobilisome-containing Cyanobacterium Synechococcus sp PCC 7942: Analysis of the Slow Fluorescence Transient. Biochim. Biophys. Acta-Bioenergetics 1767: 766-772

Tsimilli-Michael M, Stamatakis K, Papageorgiou GC (2009) Dark-to-Light Transition in Synechococcus sp PCC 7942 Cells Studied by Fluorescence Kinetics Assesses Plastoquinone Redox Poise in the Dark and Photosystem II Fluorescence Component and Dynamics during State 2 to State I Transition. Photosynth. Res. 99: 243-255

Significance of Protein Ordering in Grana Thylakoids for Light-Harvesting by Photosystem II and Protein Mobility

Stefanie Tietz[a], Chris Kinzel[a], Robert Yarbrough[a], Helmut Kirchhoff[a,*]

[a]Institute of Biological Chemistry, Washington State University, WA, USA.
[*]Corresponding author. Tel. No. +1 509 335 3304; E-mail: kirchhh@wsu.edu.

Abstract: Controlled by environmental factors, proteins in the grana thylakoid subcompartment in chloroplasts can rearrange into highly ordered semicrystalline arrays. The functional implications of these arrays are analyzed by using an *Arabidopsis* fatty acid desaturase (*fad5*) mutant as a model system, which constitutively forms these crystalline structures in thylakoid membranes. Stoichiometric analysis of the *fad5* thylakoid membranes reveal the existence of two membrane domains in grana (domains with PSII crystals and LHCII-enriched domains). Probing the light-harvesting of PSII by chlorophyll fluorescence induction indicates a very efficient energy transfer between these domains in the mutant probably by transversal energy transfer across the aqueous stromal partition gap between adjacent grana discs. Furthermore, the protein mobility in *fad5* measured by fluorescence recovery after photobleaching is higher compared to WT plants. This gives evidence for a high protein mobility in LHCII-enriched grana regions.

Keywords: Exciton energy transfer; *Fad5* mutant; Fluorescence induction; FRAP; Photosystem II; Protein order

Introduction

It is long known that proteins in grana thylakoids of higher plants can be organized in highly ordered semicrystalline arrays (*e.g.* Simpson, 1978). These structures are occasionally seen in non-stressed plants (Daum *et al*., 2010) and become more abundant under unfavorable environmental conditions (Dekker and Boekema, 2005). Although these observations indicate that semicrystalline array formation in grana thylakoids represent a physiological relevant state of the photosynthetic machinery, our knowledge about how they are formed and more importantly what the functional consequences are is rather low. From electronmicroscopic analysis, it is clear that the arrays are formed by the well-established dimeric light-harvesting II (LHCII)-photosystem II (PSII) supercomplex (Dekker and Boekema, 2005; Daum *et al*., 2010). Furthermore, from PSII electron transport measurements, it is evident that PSII in plants with a high abundance of protein arrays is fully functional (Kunst *et al*., 1989), *i.e.* semicrystalline protein arrays in grana do not represent a storage space for inactivated photosystems.

In this study we analyze the impact of semicrystalline array formation in grana on light-harvesting of PSII and the mobility of grana-hosted chlorophyll-protein complexes. The approach is a comparison between WT *Arabidopsis* plants with the fatty acid desaturase 5 (*fad5*) mutant (Kunst *et al*., 1989). This mutant is defective in producing highly unsaturated C16 fatty acids in thylakoid membranes. Thus, they accumulate mainly C16:0 fatty acids. It is established that this change causes a reorganization of the proteins in grana into semicrystalline arrays (Tsvetkova *et al*., 1994) and therefore makes *fad5* a potential model plant for studying semicrystalline array formation.

Materials and Methods

Plant material and membrane preparations

Arabidopsis thaliana wild type and *fad5* plants were grown at 120 μE m^{-2} s^{-1} and 9 h daylight.

Thylakoids were isolated from intact chloroplasts by grinding in 330 mmol sorbitol, 50 mmol HEPES, 1 mmol EDTA, 15 mmol NaCl, 5 mmol $MgCl_2$ and 5 mmol $CaCl_2$, centrifugation at 3,000 x g pelleted chloroplasts. Chloroplasts were shocked in 50 mmol HEPES, 150 mmol NaCl and 5 mmol $MgCl_2$ for 2 min and intact chloroplasts were pelleted at 200 x g for 1 min. The supernatant was pelleted at 3,000 x g for 10 min and washed in 0.1 mol sorbitol, 50 mmol HEPES, 15 mmol NaCl and 10 mmol $MgCl_2$ (washing buffer).

Grana were isolated by adding digitonin to 2% (w/v) in 2 mL to a thylakoid solution with a chlorophyll concentration of 200 μg/mL. The solutions was stirred for 15 min at room temperature, unsolubilized thylakoids were pelleted 1,000 x g for 5 min. Supernatant with grana membranes was pelleted at 11,000 x g for 15 min and grana were washed in the washing buffer mentioned above.

Protoplasts

Protoplasts of wild type and *fad5* were prepared in an enzymatic solution containing 0.5 mol mannitol, 20 mmol MES (pH = 5.7), 10 mmol $CaCl_2$ and 10 mmol KCl, 1% cellulose and maceroenzyme, respectively. Protoplasts and debris solution was filtered through 70 μm mesh, washed in buffer without enzymes and protoplasts were pelleted at 150 x g for 10 min.

Fluorescence induction

Wild type and *fad5* leaves were vacuum-infiltrated with 0.15 mol sorbitol solution, addition of 50 μM (3,4-dichlorophenyl)-1,1-dimethylurea (DCMU) blocks the plastoquinone binding site of photosystem II. Excitation wavelength was 530 nm, fluorescence was detected above 750 nm. Mathematical analysis was performed with SigmaPlot 11 software.

Fluorescence Recovery after Photobleaching (FRAP)

Isolated protoplasts were labeled with 10 μM of the lipophilic fluorophore 4,4-difluoro-5,7-dimethyl-4-bora-3a,4a-diaza-s-indacene-3-dodecanoid acid (BODIPY FL C-12) to verify the intactness of protoplast cytoplasma and endogenous membrane systems. FRAP measurements were then carried out by a Leica TCS SP5 laser-scanning confocal microscope. The 488 nm Argon laser line was selected for excitation of BODIPY FL C-12 (emission detected 510–560 nm) and chlorophyll (650–720 nm). For FRAP, total and line bleaches across the sample were performed. The total bleaches detect the recovery of bleached pigments and were substracted from the line bleach data to visualize only diffusion based fluorescence recovery. Data was analyzed through SigmaPlot 11.

Results and Discussion

The formation of semicrystalline PSII arrays in the *fad5* mutant was verified by scanning electron microscopy (SEM) on isolated grana thylakoids from the mutant showing extend particle arrays in *fad5* (not shown). In contrast, SEM images of WT plants show a non-crystalline organization. A biochemical characterization of WT and mutant membranes is summarized in Table 1. In accordance with previous results (Kunst *et al*., 1989), the data reveals that the composition of *fad5* grana membranes is almost identical to WT membranes. This makes the mutant an adequate model system for analyzing the impact of PSII array formation for the functionality of photosynthetic energy conversion because it seems that only the arrangement of proteins is altered.

Table 1 Composition of intact thylakoid membranes and grana thylakoids isolated from WT or *fad5* mutant plants.

Chl.a/b (thylakoids)	3.1±0.1	3.2±0.1
Chl.a/b (grana)	2.5±0.1	2.6±0.1
Lipid/protein (grana)	0.15	0.16
Chl./cytochrome b_{559} (grana)	269±22	255±022
LHCII-trimer/PSII (grana)	4.9	4.6

Total lipids and proteins were analyzed by thin-layer chromatography and biochemical protein determination as described (Kirchhoff *et al*., 2002). Cytochrome b_{559} content was measured form (reduced-oxidized) absorption difference spectra between 540 and 580 nm (Kirchhoff *et al*., 2002). The LHCII/PSII ratio was calculated from the chl./cytochrome b_{559} data assuming that each trimeric LHCII binds 42 chl. and each monomeric PSII (without LHCII-trimer) binds 63 chl.

A consequence of the high (WT-level) LHCII-trimer/PSII ratio in *fad5* grana (Table 1) is that at least two distinct protein domains are expected to exist in stacked membrane regions in the mutant. One contains the PSII arrays whereas the other must be enriched in trimeric LHCII. This follows the fact that the LHCII-trimer/reaction center ratio in dimeric

LHCII-PSII supercomplexes in the arrays is 1 and that the protein packing in arrays is too high to allow the placing of additional trimeric LHCII complexes in these domains (Daum *et al*., 2010). From the LHCII-trimer/PSII ratio of 1 in the arrays and the overall stoichiometry of 4.6 of these complexes in grana (Table 1) it is possible to estimate the LHCII/PSII ratio in non-arrayed regions in the mutant. For example, if 50% of PSII are localized in arrays and 50% in non-arrayed regions the latter would have a LHCII-trimer to PSII ratio of about 8 ([4.6–0.5]/0.5). If 75% of granal PSII are in arrays it is expected that the LHII/PSII stoichiometry in non-crystalline region is about 15 ([4.6–0.75]/0.25). Since the ultrastructural images show extended semicrystalline protein fields in *fad5* grana, it is likely that LHCII-enriched domains are large too. An extreme possibility would be that entire grana discs are heterogeneous, *i.e.* one type of disc contains only PSII arrays and the other type is concentrated in trimeric LHCII. At this point, we cannot discriminate between the two possibilities.

Grana protein arrays and light harvesting by PSII

Next, we examined whether the organization of granal proteins into highly ordered protein arrays accompanied by the formation of distinct protein domains (see above) effects light-harvesting by PSII. Therefore, chlorophyll fluorescence induction curves were measured on dark-adapted WT and *fad5* leaves. The normalized variable fluorescence curves are significantly faster and less sigmoid in *fad5* compared to WT plants (Fig. 1, left).

Normalized variable fluorescence kinetics (right) and connectivity plot (Fv *versus* reduction level of the primary quinone acceptor of PSII, QA) are shown.

The faster induction kinetics is indicative for a larger functional PSII antenna size. From the half time of the area growth of the normalized Fv in Fig. 1 (left), we estimate an increase in the apparent PSII antenna size of 30% in *fad5* mutants compared to the WT. This result is supported by the 20% increase in the ϕII parameter (photochemical quantum efficiency of PSII) in *fad5* under light limiting conditions (135 mmol quanta m^{-2} s^{-1}). The less sigmoid fluorescence rise can be explained by a lower excitonic connectivity between PSII centers in grana. This is clearly seen in the connectivity plot in Fig. 1, right. The degree of unlinearity in these plots reflects the excitonic connectivity. Obviously, the connectivity in *fad5* is lower compared to WT leaves.

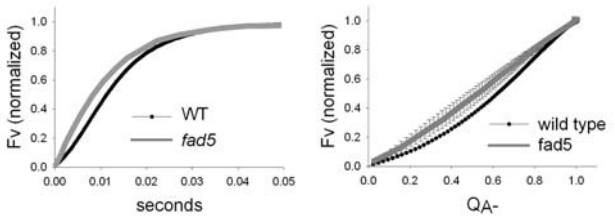

Fig. 1 Chlorophyll fluorescence induction in WT and *fad5* leaves.

Whether the faster fluorescence induction kinetics in the mutant represents a true increase in antenna size or a better functional interaction between LHCII and PSII must be clarified in further studies. However, the data indicate that the exciton energy transfer from LHCII-enriched domains to the PSII arrays must be very efficient. On a supramolecular level two possibilities exists how an efficient intermolecular energy transfer can be realized: (i) by lateral transport within grana discs from LHCII-enriched domains to PSII arrays, (ii) by transversal energy transfer over the aqueous stromal partition gap from one LHCII-enriched grana disc to an adjacent disc containing semicrystalline PSII arrays. We favor the second possibility because the large size of semicrystalline arrays requires a long-range lateral energy transfer (> 100 nm) between many LHCII-trimers, which is unlikely to be efficient. From singlet-singlet annihilation experiments on isolated LHCII-trimers, it was concluded that the mean radius of an electronic excited state is about 65 nm (Barzda *et al*., 1996). Although we found evidence that the transversal energy transfer is less efficient than the lateral transfer in isolated grana membranes of spinach (Kirchhoff *et al*., 2004), we can show recently that the width of the partition gap is flexible (manuscript in preparation). This opens the interesting possibility of a switch between lateral and transversal energy transfer controlled by the partition gap. Since the *Förster* energy transfer rate is very sensitive on the separation distance of pigments, (chlorophylls) it is expected that small alterations in the partition gap could induce significant changes in the partition between lateral and transversal energy transfer. Further studies are required to address this question.

Protein mobility in grana with semicrystalline PSII arrays

Protein mobility in WT and *fad5* protoplasts were measured by FRAP using natural chlorophyll fluorescence. Since most of the room temperature

fluorescence (> 95%) of thylakoid membranes is emitted from PSII and most of PSII (> 80%) is localized in grana thylakoid, this measurement mainly probes the grana subcompartment.

From FRAP analysis, the fraction of mobile protein complexes were deduced (Fig. 2). The data shows a clear shift in protein mobility in the *fad5* mutant.

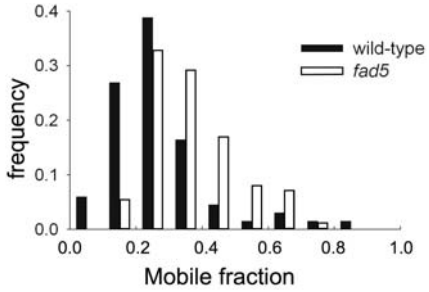

Fig. 2 Analysis of FRAP measurements in protoplasts from WT and *fad5* plants.

The mean mobile fraction in *fad5* (36%) is significantly larger ($P < 0.001$) compared to WT protoplasts (28% mobile). The higher protein mobility in the mutant cannot be explained by a fast diffusion in semicrystalline arrays since the lipidic gaps between the rows in arrays is too small (< 2 nm) to allow the passage of PSII or LHCII-trimers (Daum *et al*., 2010). Therefore, it is likely that a high mobility in LHCII-enriched grana regions explains the overall increase in protein mobility in the mutant. The fact that protein mobility is higher in *fad5* implies that the mobility of proteins in LHCII-enriched areas must be significant higher than in WT grana (assuming that proteins in semicrystalline arrays are immobile, *i.e.* they do not contribute to the mobile fraction). In consequence, PSII array formation induces a pronounced heterogeneity in membrane protein mobility. An advantage of this organization is that structural rearrangements of the main part of trimeric LHCII (about 3.6 out of 4.6) localized in LHCII-enriched membrane domains could be facilitated. This points to a potential role in state transitions, *i.e.* the phosphorylation-dependent lateral migration of LHCII from grana to PSI in distant unstacked thylakoid regions (Minagawa, 2011). Interestingly we also observed that in low-light grown plants, where it is expected that state transitions play an important role, PSII arrays are more frequent than in plants grown under normal light intensities (Kirchhoff *et al*., 2007).

Conclusions

The Arabidopsis fad5 mutant is an adequate model system for studying semicrystalline protein formation in grana thylakoids.

Semicrystalline PSII array formation induces protein domain formation (domains with PSII arrays and domains enriched in LHCII).

Excition energy transfer between the two domains is very efficient, probably by transversal transfer between adjacent grana discs.

The lower connectivity between PSII in fad5 can be explained by excitonic energy transfer only within the rows but not between rows in protein arrays (one dimension instead of two-dimension connectivity).

The higher mobility of chlorophyll-protein complexes in fad5 indicates that proteins in LHCII-enriched grana domains are very mobile.

Acknowledgement

Financial support form Washington State University (WA, USA) is acknowledged.

References

Barzda V, Garab G, Gulbinas V, Valkunas L (1996) Evidence for Long-Range Excittion Energy Migration in Macroaggregates of the Chlorophyll a/b Light-Harvesting Antenna Complexes. Biochim. Biophys. Acta 1273: 231-236

Daum B, Nicastro D, Ausin J 2nd, McIntosh JR, Kühlbrandt W (2010) Arrangement of Photosystem II and ATP Synthase in Chloroplast Membranes of Spinach an Pea. Plant Cell 22: 1299-1312

Dekker JP, Boekema EJ (2005) Supramolecular Organization of Thylakoid Membrane Proteins in Green Plants. Biochim. Biophys. Acta 1706: 12-39

Kirchhoff H, Mukherjee U, Galla HJ (2002) Molecular Architecture of the Thylakoid Membrane: Lipid Diffusion Space for Plastoquinone. Biochem. 41: 4872-4882

Kirchhoff H, Borinski M, Lenhert S, Chi L, Büchel C (2004) Transveral and Lateral Exciton Energy Transfer in Grana Thylakoids of Spinach. Biochem. 43: 14508-14516

Kirchhoff H, Haase W, Wegner S, Danielsson R, Ackermann R, Albertsson PA (2007) Low-light-induced formation of semicrystalline photosystem II arrays in higher plant chloroplast. Biochem. 46: 11169-11176

Kunst L, Browse J, Somerville C (1989) Enhanced thermal tolerance in a mutant of Arabidopsis deficient in palmitic acid unsaturation. Plant Physiol. 91: 401-408

Minagawa J (2011) State transistion – The molecular remodeling of photosynthetic supercomplexes that controls energy flow in the chloroplast. Biochim. Biophys. Acta in press

Simpson DJ (1978) Freeze-fracture studies on barley plastid membranes II: Wild-type chloroplasts. Carlsb. Res. Commun. 43: 365-389

Tsvetkova NM, Brain APR, Quinn PJ (1994) Structural characteristics of thylakoid membranes of Arabidopsis mutants deficient in lipid fatty acid desaturation. Biochim. Biophys. Acta 1192: 263-271

Moderate Heat Pretreatment Alleviates the Inhibition of Photosystem II Activity Caused by the Response of Cyanobacterial Cells to High Red Light

Zhongxian Lv[a], Lanzhen Wei[a], Quanxi Wang[a], Hualing Mi[b], Weimin Ma[a,*]

[a]College of Life and Environment Sciences, Shanghai Normal University, 100 Guilin Road, Shanghai 200234, China;
[b]Institute of Plant Physiology and Ecology, Shanghai Institutes for Biological Sciences, Chinese Academy of Sciences, 300 Fenglin Road, Shanghai 200032, China.
[*]Corresponding author. Tel. No. +86 21 64321617; Fax No. +86 21 64322931; E-mail: wma@shnu.edu.cn.

Abstract: Pre-exposure of plants to one form of stress can impact tolerance to other forms of stress. This is called cross-tolerance. However, little is known about whether this type of cross-tolerance also occurs in cyanobacteria. Here, our results clearly indicated that short-time moderate heat pretreatment considerably alleviates the inhibitory effect of high red light but not blue light on the activity of photosystem II in the unicellular cyanobacterium, *Synechocystis* sp. strain PCC 6803, as determined by a chlorophyll fluorescence parameter, Φ_{PSII}. We therefore conclude that a similar cross-tolerance strategy as identified in higher plants also occurs in cyanobacteria.

Keywords: High light; Moderate heat; Photosystem II; Cross-tolerance; Cyanobacteria

Introduction

In natural environments, the photosynthetic apparatus frequently encounters moderate heat and strong light stresses. Of the components of photosynthetic apparatus, photosystem II (PSII) is most sensitive to these stresses. To protect PSII from these stresses, plants have developed the strategy of cross-tolerance (Allen, 1995; Pastori and Foyer, 2002). Pre-exposure of plants to one form of stress can impact tolerance to other forms of stresses. For example, short-time pretreatment with moderate heat enhances the tolerance of PSII to strong light (Havaux, 1993; Kreslavski *et al*., 2008), whereas short-time pre-exposure to strong light increases the thermostability of PSII (Havaux and Tardy, 1996). In cyanobacteria, however, little is known about whether short-time moderate heat pretreatment can alleviate the inhibitory effect of strong light on PSII activity.

The aim of this study was to investigate the effect of moderate heat pretreatment on the inhibition of high light on PSII activity. Comparison of chlorophyll (Chl) fluorescence parameter, Φ_{PSII}, in moderate heat-pretreated and non-pretreated cells of the uncelulliar cyanobacterium *Synechocystis* sp. strain PCC 6803 (hereafter referred to as *Synechocystis* 6803) enabled us to reveal the alleviation of inhibitory effect of high light on PSII activity by moderate heat pretreatment.

Materials and Methods

Culture conditions

Synechocystis 6803 cells were cultured at 30 °C in BG-11 medium (Allen, 1968), buffered with 20 mmol Tes-KOH (pH 8.0) and bubbled with 2% (*v*/*v*) CO_2 in air. Continuous illumination was provided by fluorescent lamps, generating photosynthetically active radiation of 40 μmol of photons m^{-2} s^{-1}.

Heat treatments

Cells cultured for two days (A_{730} = 0.4–0.6), which showed the highest photosynthetic activity (Ma and Mi, 2005), were harvested by centrifugation (5,000 x *g* for 5 min at 25 °C), washed, and then resuspended in fresh BG-11 medium buffered with Tes-KOH

(20 mmol, pH 8.0) at a Chl *a* concentration of 20 μg mL^{-1}. Immediately after incubation at 45 °C for 10 min, the samples were subjected to the measurements of Chl fluorescence parameter.

Determination of Chl fluorescence parameter

The actual efficiency of PSII, Φ_{PSII}, was measured at room temperature (25 °C) using a Dual-PAM-100 measuring system (Walz, Effeltrich, Germany) with an ED-101US/MD unit. Immediately after moderate heat-pretreated and non-pretreated cells of *Synechocystis* 6803 were dark-adapted for 40 s and exposed to 40 or 800 μE m^{-2} s^{-1} of red light (RL, 620 nm) or 800 μE m^{-2} s^{-1} of blue light (BL; 460 nm) for 3 min, a 0.6 s *p*ulse of *s*aturating light (SP; 10,000 μE m^{-2} s^{-1}) was applied to obtain the maximum fluorescence level in the light-adapted state, F_m', and then the stable value of fluorescence, F_s, was recorded. The actual efficiency of PSII, Φ_{PSII}, were calculated as $(F_m'–F_s)/F_m'$ (Genty *et al*., 1989; Maxwell and Johnson, 2000).

Results and Discussion

Φ_{PSII}, a Chl fluorescence parameter used to evaluate the actual efficiency of PSII (Genty *et al*., 1989; Maxwell and Johnson, 2000), was considerably lower in the cyanobacterium *Synechocystis* 6803 cells illuminated by red light (RL; 620 nm) at about 800 μEm^{-2} s^{-1} than in the cells illuminated by RL at about 40 μEm^{-2} s^{-1} (Fig. 1A). Therefore, the activity of PSII as indicated by the Φ_{PSII} value was significantly inhibited under the high RL.

Moderate heat pretreatment (incubation at 45 °C for 10 min) considerably alleviated the inhibitory effect of high RL (Fig. 1B). The alleviation was more significant in the cyanobacterial cells illuminated with higher intensities of RL and did not occur at intensities below 175 μE m^{-2} s^{-1} (data not shown).

Our results further showed that such alleviation by moderate heat pretreatment was not observed under the high blue light (BL; 460 nm) (Fig. 2). It appears that the alleviation is specific to high RL. Moderate heat pretreatment did also not alleviate the inhibitory effect of high RL in Δ*ndh*B (M55) mutant (data not shown), which impairs cyclic electron transport around photosystem I (PSI; Ogawa, 1991; Mi *et al*., 1995). Therefore, it seems likely that the NADPH dehydrogenase (NDH-1)-dependent cyclic electron transport around PSI is responsible for the alleviation by moderate heat pretreatment.

The strategy of cross-tolerance for protecting PSII against stresses has been extensively studied in higher plants (Havaux, 1993; Allen, 1995; Havaux and Tardy, 1996; Pastori and Foyer, 2002; Allakhverdiev *et al*., 2008; Kreslavski *et al*., 2008). Our results demonstrated the presence of a similar strategy in the unicellular cyanobacterium *Synechocystis* 6803, namely, that moderate heat pretreatment considerably alleviates the inhibitory effect of high RL on the activity of PSII (Fig. 1). Such alleviation did not occur under a prolonged exposure to high RL (> 20 min; data not shown).

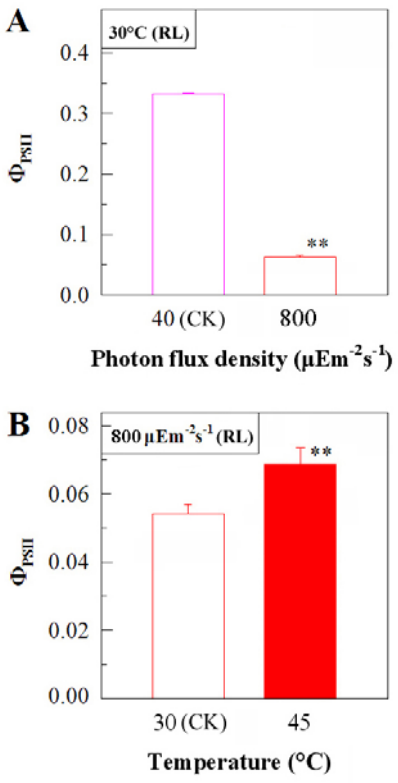

Fig. 1 The effect of moderate heat pretreatment on alleviation of the inhibitory effect of high RL on PSII activity in *Synechocystis* 6803 cells. (A) Effect of RL intensity on PSII activity. (B) Effect of moderate heat pretreatment (45 °C, 10 min) on PSII activity in cells exposed to RL at 800 μE m^{-2} s^{-1}. In each experiment, RL was irradiated for 3 min, and then Φ_{PSII} was determined. The vertical bars indicate standard errors calculated from at least 10 independent experiments and double asterisks represent significant differences compared with the control (CK) (**$p < 0.01$).

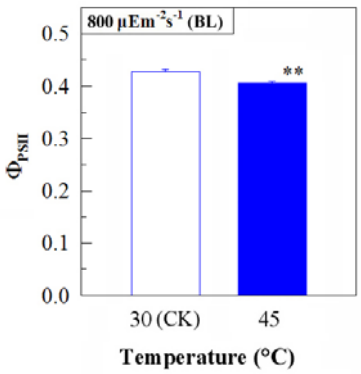

Fig. 2 Inhibition of PSII activity by high BL and alleviation of the inhibition by moderate heat pretreatment. *Synechocystis* 6803 cells were incubated at 30 °C (CK) and 45 °C (moderate heat) for 10 min, illuminated by BL (800 $\mu Em^{-2}s^{-1}$) for 3 min, and the Φ_{PSII} was measured. The vertical bars represent the average standard errors from at least 6 independent experiments, and double asterisks represent significant differences when compared with CK cells (**$P < 0.01$).

The present study performed using a unicellular cyanobacterium increased our knowledge on the cross-tolerance; it was found that short-time moderate heat pretreatment considerably alleviates the inhibitory effect of high RL on PSII activity in this cyanobacterium. Although the underlying mechanism remains unknown, to our knowledge, this is the first study to reveal the presence of the cross-tolerance strategy in cyanobacteria.

Acknowledgements

This work was supported by the National Natural Science Foundation of China (No. 30770175), the National Basic Research Program of China (No. 2009CB118500), the Key Project of Chinese Ministry of Education (No. 209045), and the Leading Academic Discipline Project of Shanghai Normal University (No. DZL808).

References

Allakhverdiev SI, Kreslavski VD, Klimov VV, Los DA, Carpentier R, Mohanty P (2008) Heat Stress: an Overview of Molecular Responses in Photosynthesis. Photosynth. Res. 98: 541-550

Allen MM (1968) Simple Conditions for Growth of Unicellular Blue-Green Algae on Plates. J. Phycol. 4: 1-4

Allen RD (1995) Dissection of Oxidative Stress Tolerance Using Transgenic Plants. Plant Physiol. 107: 1049-1054

Genty B, Briantais JM, Baker NR (1989) The Relationship between the Quantum Yield of Photosynthetic Electron Transport and Quenching of Chlorophyll Fluorescence. Biochim. Biophys. Acta 990: 87-92

Havaux M (1993) Rapid Photosynthetic Adaptation to Heat Stress Triggered in Potato Leaves by Moderately Elevated Temperatures. Plant Cell Environ. 16: 461-467

Havaux M, Tardy F (1996) Temperature-Dependent Adjustment of the Thermal Stability of Photosystem II in Vivo: Possible Involvement of Xanthophyll-Cycle Pigments. Planta 198: 324-333

Kreslavski V, Tatarinzev N, Shabnova N, Semenova G, Kosobrukhov A (2008) Characterization of the Nature of Photosynthetic Recovery of Wheat Seedlings from Short-Time Dark Heat Exposures and Analysis of the Mode of Acclimation to Different Light Intensities. J. Plant Physiol. 165: 1592-1600

Ma W, Mi H (2005) Expression and Activity of Type-I NAD(P)H Dehydrogenase at Different Growth Phases of Cyanobacterium, Synechocystis PCC 6803. Physiol. Plant. 125: 135-140

Maxwell K, Johnson GN (2000) Chlorophyll Fluorescence — a Practical Guide. J. Exp. Bot. 51: 659-668

Mi H, Endo T, Ogawa T, Asada K (1995) Thylakoid Membrane-Bound Pyridine Nucleotide Dehydrogenase Complex Mediates Cyclic Electron Transport in the Cyanobacteria Synechocystis PCC 6803. Plant Cell Physiol. 36: 661-668

Ogawa T (1991) A Gene Homologous to the Subunit-2 Gene of NADH Dehydrogenase Is Essential to Inorganic Carbon Transport of Synechocystis PCC 6803. Proc. Natl. Acad. Sci. USA 88: 4275-4279

Pastori GM, Foyer CH (2002) Common Components, Networks, and Pathways of Cross-Tolerance to Stress. The Central Role of "Redox" and Abscisic Acid-Mediated Controls. Plant Physiol. 129: 460-468

Ascorbate Alleviates Donor-Side Induced Photoinhibition by Acting as Alternative Electron Donor to Photosystem II

Szilvia Z Tóth*, Valéria Nagy, Jos Thomas Puthur[1], László Kovács, Győző Garab

Institute of Plant Biology, Biological Research Center, Hungarian Academy of Sciences, H–6701 Szeged, Hungary;
[1]Present address: Department of Botany, Calicut University, C.U. Campus P.O. Kerala-673635, India.
*Corresponding author. Tel. No. +36 66 433 591; Fax No. +36 743 744; E-mail: sztoth@brc.hu.

Abstract: Previously, we showed that ascorbate (Asc), by donating electrons to photosystem II (PSII), supports a sustained electron transport activity in heat-treated leaves. In this study, by using wild-type, Asc-overproducing and -deficient *Arabidopsis thaliana* mutants (*miox4* and *vtc2-3*, respectively), we investigated the physiological role of Asc as PSII electron donor in heat-stressed leaves (40 °C, 15 min). Chl *a* fluorescence transients show that PSII reaction centers became gradually inactivated upon illumination following heat stress, a process which was initiated by a dramatic deceleration of the electron transfer from Tyr_Z to $P680^+$ and was followed by the complete loss of charge separation activity. These processes strongly depended on the Asc content of leaves: at 300 μmol photons m^{-2} s^{-1} they occurred with halftimes of 1.2 and 10 min, 2.8 and 23 min, and 4.1 and 51 min in *vtc2-3*, the wild type and *miox4*, respectively. Photoinactivation was slowed down by diphenylcarbazide, an artificial PSII electron donor. Western blot analysis shows that in addition to D1, CP43 and PsbO are also degraded. Our data provide strong evidence for the alleviation of donor-side induced photoinhibition by ascorbate by acting as alternative electron donor to PSII.

Keywords: Ascorbate; Chl *a* fluorescence; Heat stress; Photoinhibition

Introduction

Exposure of plants to elevated temperatures results in the inactivation of the oxygen-evolving complex (OEC) of PSII, including the removal of the extrinsic proteins as well as the release of Ca- and Mn-ions from their binding sites (Nash *et al*., 1985; Barra *et al*., 2005).

Under natural conditions heat stress mostly occurs together with light stress. Though the effects of both stresses have been studied extensively, there are only a few studies where the mechanism of damage caused by combination of these two stress factors was investigated. Photosystem II preparations and leaves with chemically inactivated OECs are very sensitivity to light. The impaired electron donation from the OEC results in accumulation of highly oxidizing radicals, $P680^+$, Tyr_Z^+ and superoxide (Chen *et al*., 1995) or hydroxyl radicals (Spetea *et al*., 1997), and leads to a rapid inactivation of PSII reaction centers (Callahan *et al*., 1986; Jegerschöld and Styring, 1996). This type of photodamage is called donor-side-induced photoinhibition.

In this paper we provide experimental evidence that ascorbate (Asc) plays a protective role in photoinhibition in heat-stressed leaves. Ascorbate is present in the chloroplast, and in the absence of active OEC serves as a relatively rapid electron donor to PSII ($t_{1/2}$ approximately 25 ms; Tóth *et al*., 2009), and thus it might be capable of protecting PSII by supplying electrons to the reaction center. To test this hypothesis, we subjected intact leaves of wild-type (WT), Asc-overproducing (*miox4*, Lorence *et al*., 2004) and -deficient mutant (*vtc2-3*, Conklin *et al*., 2000) Arabidopsis plants to heat stress (40 °C, 15 min) and investigated the time course and mechanism of photoinactivation of PSII.

Materials and Methods

Plant material

Wild-type Arabidopsis (Col-0), Asc-deficient (*vtc2-3*) and Asc-overproducing mutant (*miox4*) plants

were grown in a growth chamber between 20 °C to 24 °C under short-day conditions (8 h light, 16 h dark), at 150 µmol photons m^{-2} s^{-1} in the light period.

Heat treatment

Detached leaves were submerged in a water bath of 40 °C for 15 min in the dark.

Light treatments

Heat-treated leaves were illuminated at 300 µmol photons m^{-2} s^{-1} for 4 h.

DPC treatment

vtc2-3 leaves were incubated in 1 mmol 1,5-diphenylcarbazide (DPC) for 2 h in the light (~50 µmol photons m^{-2} s^{-1}).

DCMU treatment

Whole leaves were incubated in 0.2 mmol DCMU solution for 2 h in complete darkness after the heat+light treatment.

Fast chl a fluorescence (OJIP) measurements

Fluorescence measurements were carried out with a special version of the Handy-PEA instrument that allows reducing the length of the measurement to 300 µs.

Western blot analysis

Leaf discs cut from Arabidopsis leaves were frozen in liquid nitrogen and stored until use. Western blot analysis was carried out according to Damkjær *et al*. (2009).

Results and Discussion

Electron donation rates from Asc to PSII in Arabidopsis genotypes with different Asc contents

Detached leaves of WT, Asc-overproducing (*miox4*) and Asc-deficient (*vtc2-3*) Arabidopsis plants were subjected to heat stress at 40 °C for 15 min in a water bath in the dark that totally inhibited oxygen evolution (data not shown). The Chl *a* fluorescence (OJIP) transients of untreated Asc-overproducing, Asc-deficient and WT Arabidopsis plants were essentially the same, with identical F_V/F_M values (data not shown). In leaves containing PSII reaction centers with inactive OEC the K peak appears at around 300 µs with a concomitant disappearance of the J and I steps (Fig. 1). The K peak represents approximately one stable charge separation, with Tyr_Z as the electron donor (Srivastava *et al*., 1997; Tóth *et al*., 2007). After the K peak fluorescence intensity decreases due to the reoxidation of Q_A^- by Q_B. In leaves a second peak appears at around 1 s (Fig. 1) that is due to electron donation by Asc to PSII leading to a partial reduction of the electron transport chain (Tóth *et al*., 2009). In heat-stressed (40 °C, 15 min) Asc-deficient plants this second phase was considerably smaller than in the WT and it was somewhat retarded, whereas in the Asc-overproducing mutant its intensity was somewhat higher than in the WT (Fig. 1). This is in agreement with our previous finding that the intensity of this peak depends on the Asc content of the leaves (Tóth *et al*., 2009).

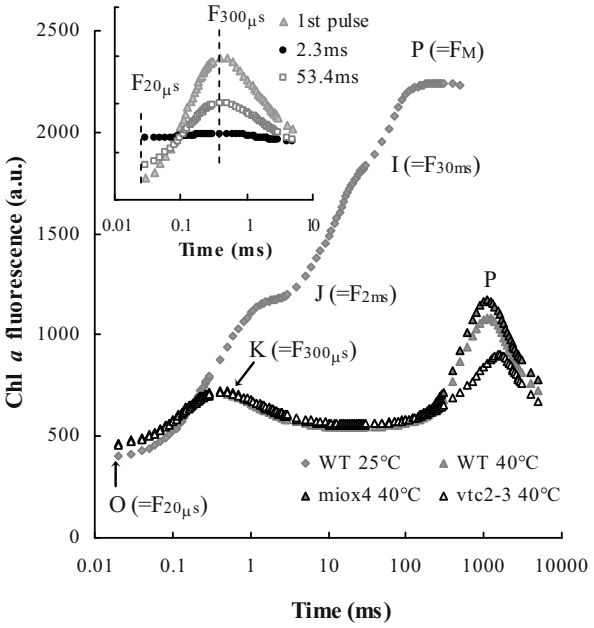

Fig. 1 Fast Chl *a* fluorescence transients in untreated and heat-stressed (40 °C, 15 min) WT, Asc-overproducing (*miox4*) and -deficient (*vtc2-3*) Arabidopsis plants. Inset: Fluorescence transients recorded on heat-stressed leaves during two 5 ms pulses that were spaced 2.3 and 53.4 ms apart (Tóth *et al*., in press; with permission from Tóth *et al*.).

The $t_{1/2}$ of electron donation from Asc to Tyr_Z^+ can be determined in samples with fully inactivated oxygen evolution by using two short (5 ms) light pulses and by varying the dark interval between them (Tóth *et al*., 2009). During the 5 ms light pulse one charge separation and the re-oxidation of Q_A^- by Q_B takes place. The inset of Fig. 1 shows that after a 2.3 ms dark interval following the first light pulse there is no variable fluorescence, which is due to the full inactivation of oxygen evolution. However, with

longer dark intervals, the K peak recovers following single exponential kinetics and the $t_{1/2}$ of the regeneration of the K peak can be used as the half-time of the rereduction of Tyr_Z^+ by Asc (Tóth *et al*., 2009). The $t_{1/2}$ was approximately 30 ms in WT and *miox4* leaves, whereas in the Asc-deficient mutant the electron donation was much slower, the $t_{1/2}$ was approximately 50 ms (Table 1).

Table 1 Half-times of electron donation to PSII from Asc and from Asc+DPC, and the half-time of the decrease of the amplitude of the K peak in heat+light-treated WT and *vtc2-3* Arabidopsis plants (Tóth *et al*., in press; with permission from Tóth *et al*.).

	wild type	*vtc2-3*	*vtc2-3* +1 mmol DPC
Half-time of electron donation to PSII	30.5±1.3 ms	49.7±3.6 ms	30.4±2.5 ms
Half-time of the decrease of the K peak in the light	2.8±0.5 ms	1.4±0.1 ms	2.5±0.3 ms

Inactivation of PSII reaction centers in heat-stressed leaves exposed to continuous illumination

Exposure of heat-stressed leaves (40 °C, 15 min) to continuous illumination (300 µmol photons m^{-2} s^{-1}) resulted in relatively fast and gradual diminishment of the K peak (Fig. 2A). Its rate of diminishment followed exponential kinetics and depended strongly on the Asc content of leaves: in the WT it exhibited a $t_{1/2}$ of 2.8 min, whereas the *vtc2-3* and *miox4* $t_{1/2}$ values were 1.2 min and 4.1 min, respectively (Fig. 2B).

To examine the relative amount of active PSII reaction centers, leaves were incubated in the dark for 2 h in DCMU solution after the heat+light treatment (Fig. 2C) in order to ensure that all PSII reaction centers are closed during the fluorescence measurement. Upon light treatment of heat-stressed samples, the fluorescence intensity gradually decreased and after 4 h the F_M value almost equaled F_0. Again, the decrease in the amplitude was significantly faster in the Asc-deficient mutant than in the WT and especially in the Asc-overproducing mutant (apparent $t_{1/2}$ 10 min, 23 and 51 min, respectively, Fig. 4D). Very similar rates were obtained in the presence of lincomycin, showing that in 4 h, no significant recovery occurred (data not shown). We also note that in the light-treated leaves the fluorescence rise was strongly decelerated: in the WT, the $t_{1/2}$ increased from 0.3 ms to 2.3 ms in 1 h; deceleration was even stronger in *vtc2-3* (from 0.3 ms to 3 ms).

The fast decrease in the amplitude of the K peak and the slowdown of the fluorescence rise determined in the presence of DCMU suggest that the first step of photoinactivation is the slowdown of the Tyr_Z-$P680^+$ and this is followed by a complete inactivation of the charge separation activity of PSII. Our data also show that the rate of PSII inactivation depends strongly on the Asc content of the leaves.

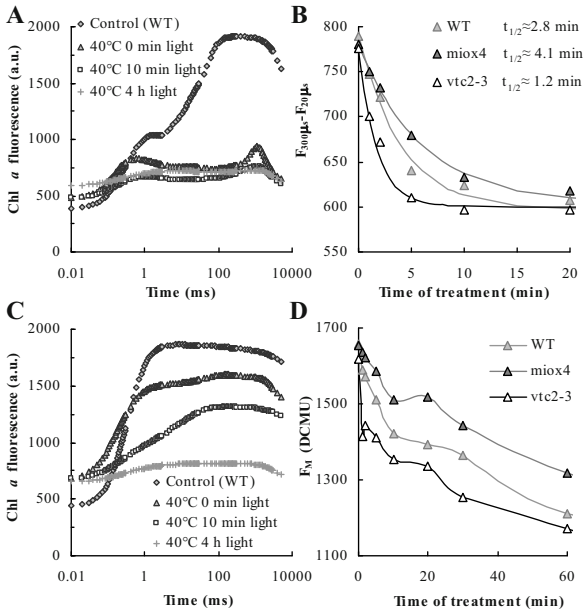

Fig. 2 Chl *a* fluorescence transients (A and C) and the time course of the decrease of the K peak calculated as $F_{300\mu s}$-$F_{20\mu s}$ (B) and of the F_M value in the presence of DCMU (D) on heat-stressed WT, Asc-overproducing (*miox4*) and -deficient (*vtc2-3*) Arabidopsis leaves exposed to white light of 300 µmol photons m^{-2} s^{-1} (Tóth *et al*., in press; with permission from Tóth *et al*.).

Asc is not only an alternative electron donor to PSII but also a direct scavenger of reactive oxygen species (ROS) produced during donor-side-induced photoinhibition (Chen *et al*., 1995; Spetea *et al*., 1997). In order to ascertain that the Asc-dependence correlates with the ability of Asc to act as a PSII electron donor, we incubated intact *vtc2-3* leaves in diphenylcarbazide solution (DPC is an artificial electron donor of PSII, with no ROS-scavenging properties) before the heat treatment. In DPC-treated *vtc2-3* leaves the $t_{1/2}$ of electron donation to PSII became similar to that in the WT (about 30 ms, Table 1). In DPC-incubated leaves exposed to light, the K peak diminished more slowly than in untreated leaves ($t_{1/2}$s of 2.5 min and 1.4 min, respectively), at a rate similar to that found in WT-leaves (2.8 min, see also Fig. 2B).

This is strong indication that Asc slows down the inactivation of the PSII reaction centers by acting as PSII electron donor and not only as a scavenger of ROS.

Light-induced degradation of PSII proteins in heat-stressed leaves

In order to investigate if the complete loss of charge separation activity of PSII in heat-stressed leaves is accompanied by protein degradation, Western blot analyses were performed, using WT leaves.

Data in Fig. 3 show that upon the heat stress about 20% of D1 protein was lost, which is in agreement with earlier results (Yoshioka *et al*., 2006) and light-treatment on heat-stressed leaves resulted in further degradation of D1: after 4 h approximately 65% of the D1 protein was lost. These data are in good agreement with data obtained with Chl *a* fluorescence measurements in the presence of DCMU (Fig. 2C). We also observed significant losses in the amount of CP43 and the PsbO protein; by the 4th h of the light treatment of heat-treated leaves, 70% and 80% of CP43 and PsbO were lost, respectively. These data suggest that there was a complete disassembly of PSII reaction centers upon the light treatment of heat-stressed leaves.

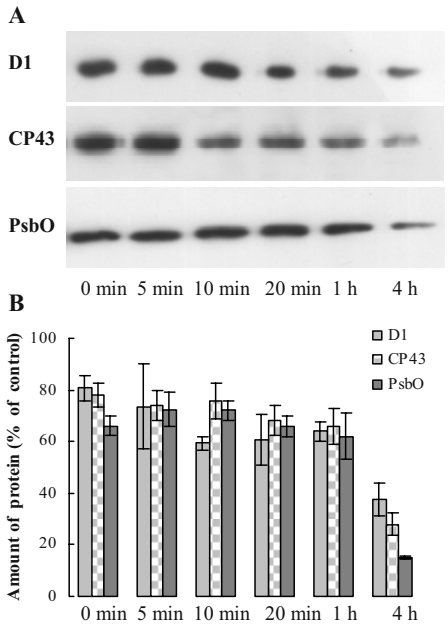

Fig. 3 Dependence of the amounts of D1, CP43 and PsbO, determined by Western blot analyses in heat (40 °C, 15 min) and heat+light-treated wild-type Arabidopsis plants as a function of illumination time (white light of 300 µmol photons m^{-2} s^{-1}). A, typical blots and B, averages determined by densitometry from 4–5 blots, as expressed in percentage of the untreated control [1] (Tóth *et al*., in press; with permission from Tóth *et al*.).

Conclusions

This study shows that Asc retards photoinactivation of PSII in heat-stressed leaves by acting as a PSII donor. We also show that photoinhibition in heat-stressed leaves occurs with a similar mechanism as described for samples with chemically inactivated OECs (Jegerschöld and Styring, 1996) that is most probably accompanied by a complete disassembly of PSII.

Acknowledgements

This work was supported by the Hungarian Research Foundation (OTKA, grant No. PD433591 and CNK80345 to S.Z.T. and G.G., respectively), by the Bolyai János Research Foundation of the Hungarian Academy of Sciences (research scholarship to S.Z.T.) and by the Department of Science and Technology, Government of India (BOYSCAST fellowship to J.T.P.). We thank Dr. Argelia Lorence and Prof. Craig L Nessler (Arkansas State University) for the *miox4* mutant and Prof. Patricia Conklin (State University of New York College at Cortland) for the *vtc2* mutants.

References

Barra M, Haumann M, Dau H (2005) Specific Loss of the Extrinsic 18 kDa Protein from Photosystem II upon Heating to 47 °C Causes Inactivation of Oxygen Evolution Likely Due to Ca Release from the Mn-Complex. Photosynth Res 84: 231-237

Callahan FE, Becker DW, Cheniae GM (1986) Studies on the Photoactivation of the Water-Oxidizing Enzyme. II. Characterization of Weak Light Photoinhibition of PSII and Its Light-Induced Recovery. Plant Physiol 82: 261-269

Chen GX, Blubaugh DJ, Homann PH, Golbeck JH, Cheniae GM (1995) Superoxide Contributes to the Rapid Inactivation of Specific Secondary Donors of the Photosystem-II Reaction-Center during Photodamage of Manganese-Depleted Photosystem-II Membranes. Biochemistry 34: 2317-2332

Conklin PL, Saracco SA, Norris SR, Last RL (2000) Identification of Ascorbic Acid-Deficient Arabidopsis Thaliana Mutants. Genetics 154: 847-856

Damkjær JT, Kereiche S, Johnson MP, Kovács L, Kiss AZ, Boekema E J, Ruban AV, Horton P, Jansson

S (2009) The Photosystem II Light-Harvesting Protein Lhcb3 Affects the Macrostructure of Photosystem II and the Rate of State Transitions in Arabidopsis. Plant Cell 21: 3245-3256

Jegerschöld C, Styring S (1996) Spectroscopic Characterization of Intermediate Steps Involved in Donor-Side-Induced Photoinhibition of Photosystem II. Biochemistry 35: 7794-7801

Lorence A, Chevone BI, Mendes P, Nessler CL (2004) Myo-Inositol Oxygenase Offers a Possible Entry Point into Plant Ascorbate Biosynthesis. Plant Physiol 134: 1200-1205

Nash D, Miyao M, Murata N (1985) Heat Inactivation of Oxygen Evolution in Photosystem II Particles and Its Acceleration by Chloride Depletion and Exogenous Manganese. Biochim Biophys Acta 807: 127-133

Spetea C, Hideg E, Vass I (1997) Low pH Accelerates Light-Induced Damage of Photosystem II by Enhancing the Probability of the Donor-Side Mechanism of Photoinhibition. Biochim Biophys Acta 1318: 275-283

Srivastava A, Guissé B, Greppin H, Strasser RJ (1997) Regulation of Antenna Structure and Electron Transport in Photosystem II of Pisum Sativum under Elevated Temperature Probed by the Fast Polyphasic Chlorophyll-a Fluorescence Transient: OKJIP. Biochim Biophys Acta 1320: 95-106

Tóth SZ, Schansker G, Garab G, Strasser RJ (2007) Photosynthetic Electron Transport Activity in Heat-Treated Barley Leaves: The Role of Internal Alternative Electron Donors to Photosystem II. Biochim Biophys Acta 1767: 295-305

Tóth SZ, Puthur JT, Nagy V, Garab G (2009) Experimental Evidence for Ascorbate-Dependent Electron Transport in Leaves with Inactive Oxygen-Evolving Complexes. Plant Physiol. 149: 1568-1578

Tóth SZ, Nagy V, Puthur JT, Kovács L, Garab G The Physiological Role of Ascorbate as Photosystem II Electron Donor: Protection against Photoinactivation in Heat-Stressed Leaves. Plant Physiol (in press)

Yoshioka M, Uchida S, Mori H, Komayama K, Ohira S, Morita N, Nakanishi T, Yamamoto Y (2006) Quality Control of Photosystem II: Cleavage of Reaction Center D1 Protein in Spinach Thylakoids by FtsH Protease under Moderate Heat Stress. J Biol Chem 281: 21660-21669

Involvement of Chlorophyll *a* Fluorescence Analyses for Identification of Sensitiveness of the Photosynthetic Apparatus to High Temperature in Selected Wheat Genotypes

Marian Brestic, Marek Zivcak*, Katarina Olsovska, Jana Repkova

Department of Plant Physiology, Slovak Agricultural University, Nitra, Slovakia.
*Corresponding author. Tel. No. +421 37 6414 821; E-mail: marek.zivcak@uniag.sk.

Abstract: The aim of our work was to evaluate the sensitivity of testing procedure and different parameters derived from the basic parameters of chlorophyll *a* fluorescence as well as from fluorescence kinetics analysis for their application in screening of wheat genotypes. In several testing cycles during vegetation period we examined a set of 31 wheat (*Triticum aestivum* L.) genotypes and local landraces of different provenances cultivated in the field trials of the RICP Piestany, Slovak Republic. In all tests we used procedure of heating of detached leaf segments closed in glass tubes for 1 hour immersed in the thermostated water bath (40 °C) in the dark. Before and after the heat treatment, the chlorophyll *a* fluorescence in a fast phase was used. To compare the leaf samples we used the maximum quantum yield of PSII photochemistry F_V/F_M and, relative variable fluorescence at 0.3 ms (W_K). The results showed considerable differences in heat sensitivity among wheat genotypes, and offered a potential to identify more tolerant or susceptible genotypes. The termostability increased and genotypic differences decreased across the vegetation period. Parameter derived from the fluorescence kinetics (W_K) was generally more sensitive and hence more useful than the basic chlorophyll fluorescence parameter (F_V/F_M).

Keywords: Heat stress; Chlorophyll a fluorescence; Photosynthetic thermostability; Wheat

Introduction

High temperature is important environmental factor affecting plant photosynthesis temporarily and reversibly by inhibition of carboxylation processes (Feller *et al.*, 1998). It copes often with other stress co-factors on irreversible impairment of the photosynthetic apparatus, especially in plant species originating from moderate climatic conditions (including world widely used agricultural crops). Among them a different level of heat susceptibility can be found. It is well known that chlorophyll *a* fluorescence represents a reliable tool for monitoring the heat effects as the high temperature affects directly primary photosynthetic processes (Bilger *et al*., 1984). Besides basic fluorescence parameters, there is group of parameters divided from analysis of fluorescence kinetics that is very sensitive to stresses caused by environmental conditions, especially to high temperature (Srivastava *et al.*, 1997). The aim of our work was to evaluate the sensitivity of testing procedure and to compare parameters derived from the basic parameters of chlorophyll *a* fluorescence as well as from fluorescence kinetics analysis for their possible application in screening of wheat genotypes.

Materials and Methods

In several testing cycles during vegetation period we examined a set of 31 wheat (*Triticum aestivum* L.) genotypes and local landraces of different provenances (Tab. 1) cultivated in the field trials of the Research Institute of Crop Production in Piestany, Slovak Republic. In all tests we used procedure of heating of detached leaf segments closed in glass tubes for 1 h immersed in the thermostated water bath in the dark. We used unified testing temperature 40 °C. Before and after the heat treatment, the chlorophyll *a* fluorescence in a fast phase was used (HandyPEA, Hansatech, GB) with saturation pulse 3,500 μmol m^{-2} s^{-1} for 1 second. To compare the leaf samples we used the maximum quantum yield of PSII photochemistry F_V/F_M and relative variable

Table 1 List of genotypes with their origin.

Geographic area	Country of origin	Genotypes
Central Europe	Slovakia	Malvina, Venistar, Torysa, Vanda, Astella, Viglasska*, Radosinska*, Vrakunska*, Kosutska*, Vendur**
	Austria	Komfort
	Switzerland	Tamaro
	Hungary	GK Forras
	Poland	Gedania
Western Europe	Great Britain	Griffen
	Germany	Biscay
Mediterran.	Italy	Verna, Mottin
	Turkey	Bbyo, Dagdas, Pehlivan
Eastern Europe and Central Asia	Russia	Echo
	Kazakhstan	Steklovidnaja
Eastern Asia	China	Shaan 8007-7, Chua-bej
	Japan	Hokushin, Nanbu Komugi
Central America	Mexico	Piopio-4, Shark-4

*historical genotypes, ***Triticum durum*

fluorescence at 0.3 ms (W_K) derived from fast chlorphyll fluorescence kinetics (1),

$$W_K = \frac{F_{0.3ms} - F_0}{F_{2ms} - F_0} \quad (1)$$

where $F_{0.3ms}$ and F_{2ms} are value of chlorophyll fluorescence in time 0.3 and 2 ms respectively, F_0 represents basal fluorescence measured in time 50 μs. Comparison of means was made with using ANOVA with F-test. Results were considered significant at the $P \leq 0.05$ level.

Results and Discussion

The average results from all performed measurements show considerable differences in heat sensitivity among the studied wheat genotypes in both observed parameters (Fig. 1). Average values of F_V/F_M before exposition ranged between 0.81 and 0.83 in all genotypes

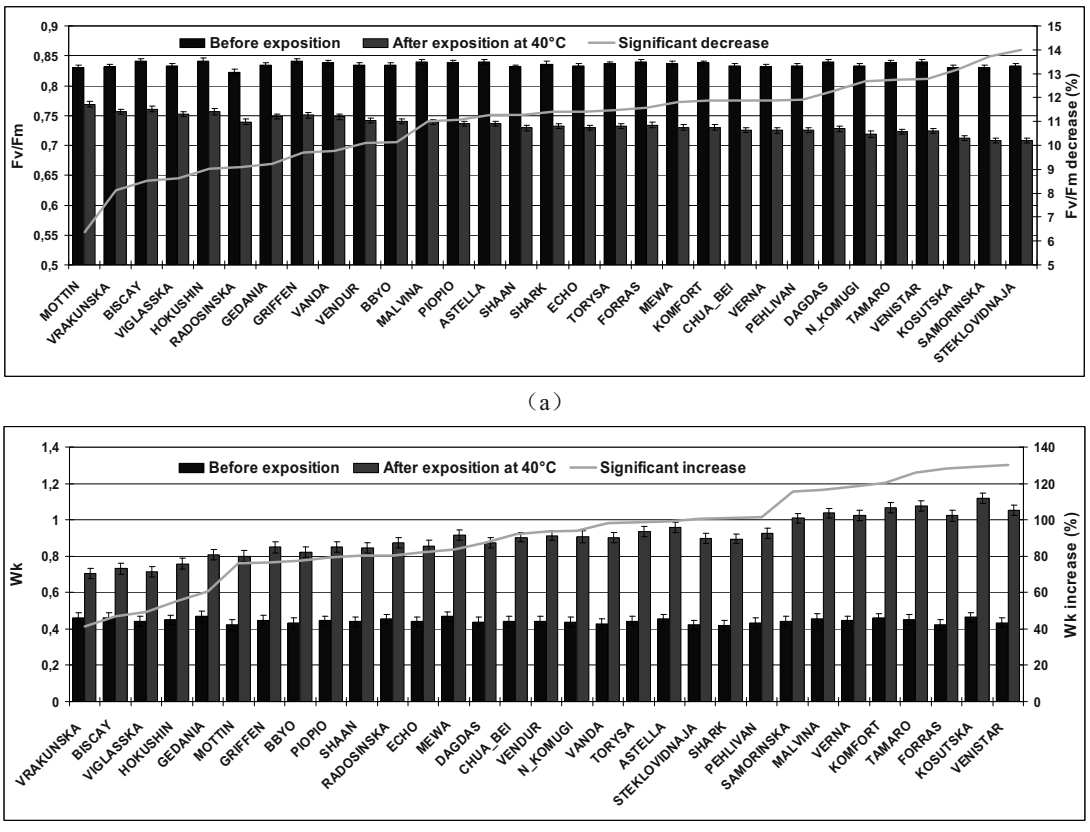

Fig. 1 Average values of maximum quantum yield of PSII photochemistry - F_V/F_M (a) and relative variable fluorescence in time 0.3 ms – W_K (b), recorded in 31 wheat genotypes before (dark columns) and after exposition to 40 °C (grey columns). Data represent mean values for several subsequent measurements done from April to June on leaves of wheat. Data were compared using ANOVA with F-test ($\alpha = 0.05$, $p < 0.001$), vertical bars represent standard error. Genotypes are ranked according to least significant difference between the values before and after exposition shown as grey line in graph (expressed as % of mean value before exposition).

indicating photosynthetic apparatus non-affected by any stress. Heat exposition at 40 °C caused decrease of F_V/F_M, the statistically significant decrease varied from 6% in most tolerant genotypes to 14% in the most susceptible.

Average values of W_K parameter in non-stressed leaves were also almost constant and ranged between 0.41 and 0.46 without considerable differences among genotypes. Exposition to heat caused appearance of K-step with peak in 0.3 ms reflected to increase of W_K values.

The appearance of K-step in OJIP fluorescence transient is typical symptom of impairment of oxygen evolving complex (OEC) functions (Lu and Zhang, 1999). We recorded significant increase of W_K from 40% in less sensitive to 120% in the most susceptible genotypes.

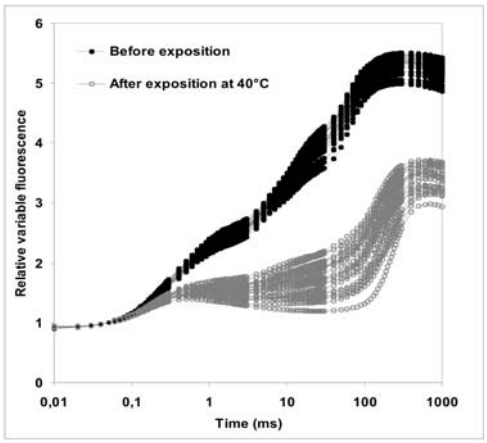

a)

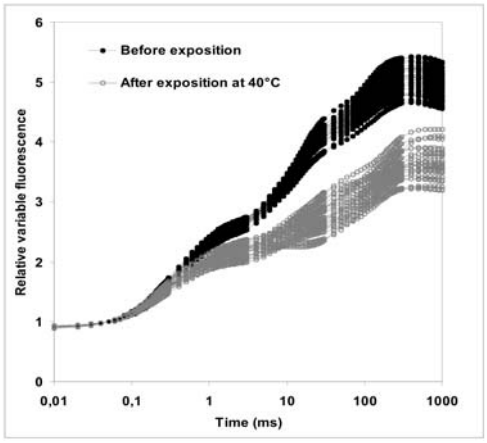

b)

Fig. 2 Values of relative variable fluorescence (OJIP-transient) displayed on logarithmic time scale for collection of 31 wheat genotypes of different provenance. Each curve represents average transient for one genotype, where black color show average curves before exposition and grey color after exposition to 40 °C. Measurements were recorded at the beginning of phenological phase of spiking (a) and at the top of the grain filling period (b).

Parameter W_K derived from the fluorescence kinetics was generally more sensitive than the basic chlorophyll fluorescence parameter F_V/F_M, for the practical use, the W_K parameter was found as more favorable, because its values before heat treatment were relatively stable; moreover, it has a clear physiological meaning and in most cases it is not sensitive to any other common co-occurring stress factors except high temperature.

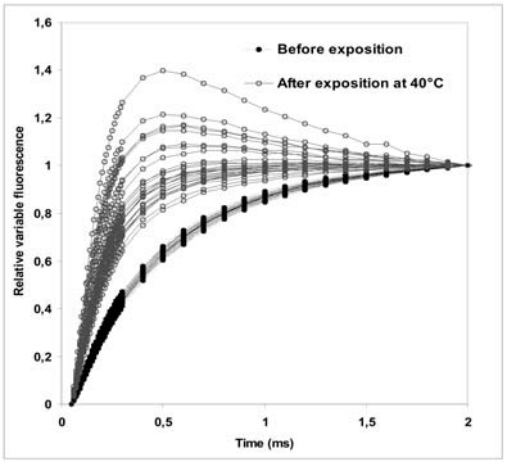

a)

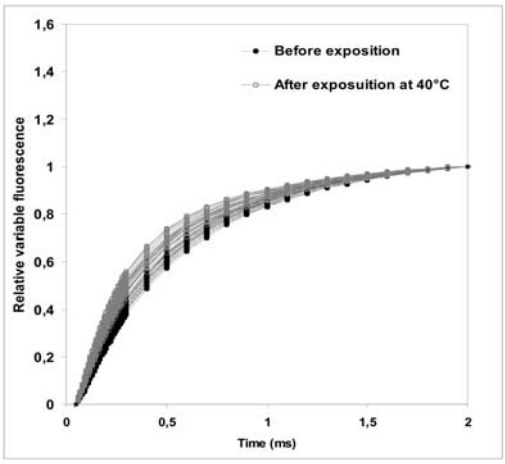

b)

Fig. 3 Values of normalized data of J-phase (0–2 ms) highlighting the K-step of fluorescence induction for collection of 31 wheat genotypes of different provenance. Each curve represents average transient for one genotype, where black color show average curves before exposition and grey color after exposition to 40 °C. Measurements were recorded at the beginning of phenological phase of spiking (a) and at the top of the grain filling period (b).

Subsequent measurements during vegetation period show trend of thermostability increase. It is obvious if we compare fluorescence OJIP curves recorded at the beginning of phenological phase of spiking (Fig. 2a) and at the top of the grain filling

period (Fig. 2b). Our analyses show that at the late growing phases temperature 40 °C does not induce obvious increase of relative variable fluorescence (K-step) as it was in early growth stages (Fig. 3).

Many studies report increase of thermostability caused by co-occurring stresses like drought stress (Havaux, 1992; Epron, 1997), salinity stress (Wen *et al.*, 2005) but also by supraoptimal ambient temperature (Daas *et al.*, 2008). The increase of thermostability goes probably mainly through synthesis of protective proteins that stabilize main function membrane complexes in plant cells (Kotak *et al.*, 2007).

Decrease of overall thermostability was accompanied by lower genotypic differences (Fig. 4). It suggests that for testing in latter growth stages, the testing temperature of 40 °C is not sufficient.

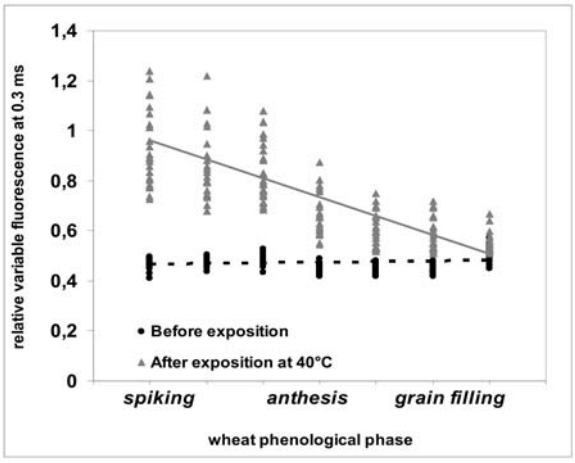

Fig. 4 Average values of relative variable fluorescence in 0.3 ms (K-step, W_K value) for collection of 31 observed wheat genotypes of different provenance. Each point represents average value for one genotype calculated from the values measured in individual measurements during vegetation period. The black color shows average values before exposition, grey color indicates values after exposition at 40 °C. The fitted lines represents linear trend of measured value across spring wheat ontogenesis (black dashed line – before exposition, grey – after exposition).

The results obtained from repeated measurements across the main season show that the determination of the photosynthetic thermostability by techniques of chlorophyll fluorescence represents an expeditive method useful for identification of more heat tolerant crops or various crop genetic resources. Use of fast fluorescence kinetics recorded within the same one-second-lasting measurement of F_V/F_M can bring additional information about heat effects and about level photosynthetic thermostability.

Acknowledgements

The work was supported by the project of the Agency for research and development support of the Slovak republic No. APVV-0770-07 and the project VEGA No. 1/0807/09.

References

Bilger HW, Schreiber U, Lange OL (1984) Determination of Leaf Heat Resistance: Comparative Investigation of Chlorophyll Fluorescence Change and Tissue Necrosis Methods. Oecologia 63: 256-262

Daas C, Montpied P, Hanchi B, Dreyer E (2008) Responses of Photosynthesis to High Temperatures in Oak Saplings Assessed by Chlorophyll-a Fluorescence: Inter-Specific Diversity and Temperature-Induced Plasticity. Ann. For. Sci. 65: 305-312

Epron D (1997) Effects of Drought on Photosynthesis and on the Thermotolerance of Photosystem II in Seedlings of Cedar (Cedrus Atlantica and C. Libani). J. Exp. Botany 48: 1835-1841

Feller U, Crafts-Brandner SJ, Salvucci ME (1998) Moderately High Temperatures Inhibit Rubisco Activase-Mediated Activation of Rubisco. Plant Physiol. 116: 539-546

Havaux M (1992) Stress Tolerance of Photosystem II in Vivo. Plant Physiol. 100: 424-432

Kotak S, Larkindale J, Lee U, Von Koskull-Döring P, Vierling E, Scharf KD (2007) Complexity of the Heat Stress Response in Plants. Current Opinion in Plant Biology 10 (3): 310-326

Lu C, Zhang J (1999) Effects of Water Stress on Photosystem II Photochemistry and Its Thermostability in Wheat Plants. J. Exp. Botany 336 (50): 1199-1206

Srivastava A, Guisse B, Greppin H, Strasser RJ (1997) Regulation of Antenna Structural and Electron Transport in Photosystem II of Pisum Sativum under Elevated Temperature Probed by the Fast Polyphasic Chlorophyll a Fluorescence Transient: OKJIP. Biochim. Biophys. Acta 1320: 95-106

Wen X, Qiu N, Lu Q, Lu C (2005) Enhanced Thermotolerance of Photosystem II in Salt Adapted Plants of Halophyte Artemisia Anethifolia. Planta 220: 486-497

Lichens Assist the Drought-Induced Fluorescence Quenching of Their Photobiont Green Algae Through Arabitol

Makiko Kosugi[1], Akihisa Miyake[3], Yasuhiro Kasino[2], Yutaka Shibata[3], Kazuhiko Satoh[2] , Shigeru Itoh[3]

[1]Division of Biosciences, Graduate School of Natural Science and Technology, Okayama University, Okayama 700-8530, Japan;
[2]Department of Life Science, School of Life Science, University of Hyogo, Harima Science Garden City, Hyogo 678-1297, Japan;
[3]Division of Material Science (Physics), Graduate School of Science, Nagoya University, Furocho, Chikusa, Nagoya 464-8602, Japan.

Abstract: In order to clarify the role of symbiotic association in drought tolerance of photosynthetic partners in lichens, responses to air-drying treatments in a green-algal lichen (*Ramalina yasudae* Rasänen) and its green algal photobiont (*Trebouxia* sp.) were studied. Responses to dehydration in the isolated *Trebouxia* sp. were different from those in the lichen. *R. yasudae.* Dehydration induced quenching of PS II fluorescence (d-NPQ) was less in the isolated *Trebouxia* sp. compared with that in *R. yasudae,* suggesting that a substance(s) or a mechanism(s) to dissipate absorbed light energy to heat was lost by the isolation of the photobiont, and the air-dried isolated *Trebouxia* sp. showed a higher sensitivity to photoinhibition than *R. yasudae.* We assayed the effects of various substances extracted from *R. yasudae* thalli on the fluorescence of *Trebouxia* sp. And we found the d-NPQ-type fluorescence quenching in the *Trebouxia* sp. was accelerated if they were dried with arabitol which was the main component of the water extract of *R. yasudae*. These results support the idea that arbitol triggered the photoprotection mechanism under drought conditions of the photobiont symbiotic with the mycobionts.

Keywords: Drought tolerance; Photoinhibition; Non-photochemical quenching; Symbiosis; Lichens

Introduction

Lichens and other poikilohydric photosynthetic organisms are known to have strong drought tolerance even to almost total loss of water from their cells. Nonphotochemical fluorescence quenching (NPQ) has been known to function to dissipate excess light energy under the high light conditions in plants and cyanobacteria. Because when photosynthesis is inhibited (due to the increased viscosity of the cytosol, increased concentrations of metal ions and/or lack of an electron donor to PSII), photochemically active PSII will generate strong reductants or oxidants, which will destroy the cells. At present three type of NPQ mechanisms are known to operate; a NPQ induced by Xanthophyll cycle, aggregation of Chl a/b antenna protein and the drought–induced NPQ in some species of cyanobacteria, green algae and lichens (Horton *et al*., 1996; Demmig-Adams, 1990; Ruban *et al*., 1994; Niyogi, 1999; Ruban and Horton, 1999; Barzda *et al*., 1999; Heber *et al*., 2006; Kopecky *et al*., 2005). The mechanism of third type of d-NPQ is not clear yet. Recently the ultra-fast decay in the antenna Chls and emit fluorescence around 740 nm were reported in lichens (Veerman *et al*., 2007; Komura *et al*., 2010). And the 740 nm component is predicted the special quencher that operates only under drought conditions. *Trebouxia* cells isolated from lichens didn't show the d-NPQ phenomena and became easily damaged of photoinhibition even under the drought stress (Kosugi *et al*., 2009) so that some specific unknown interactions between the drought-tolerant lichens and photobiont cells have been assumed for the action of the d-NPQ. In this study, we assumed that some substances removed from *Trebouxia* cells in the process of isolation from *R. yasudae,* so we extracted the components from lichen thalli and tested the

effects of various extracts to the d-NPQ responses of algal cells.

Materials and Methods

Ramalina yasudae was collected around the Harima Science Garden City Campus of University of Hyogo, Hyogo Prefecture, Japan (134.5°E, 35′N). The samples were washed with tap water and air-dried at 60% relative humidity for 1 day in the dark, and then, the dehydrated samples were stored at about –15 °C until use.

Isolation of *Trebouxia* sp. cells from thalli of *R. yasudae* was performed according to Millbank and Kershaw (1969) with some modifications (Kosugi *et al*., 2009).

For the air-drying treatment, the lichens and isolated *Trebouxia* cells were dried at 25 °C in the dark at 60% relative humidity. In the case of *Trebouxia*, air-drying treatments were done on the clear film and directly used to measurements. For the arabitol treatments, the hydrated cells were suspended in the 0.5 mol arabitol solution, and were incubated in the dark more than one hour before dehydration. For the rehydration experiments, cells air-dried in the dark were re-wet with distilled water for 1 h, in the dark.

Measurement of integrated fluorescence emission spectra calculated from picosecond time-resolved fluorescence spectra were measured with a streak camera spectrophotometer system as reported previously (Komura *et al*., 2010).

The water soluble components were extracted from lichens by grinding thalli of *R. yasudae*, which was rewetted with NANOpure water (NANOpure; Barnstead, Thermo Fisher Scientific, Waltham, MA, USA), with mortar and pestle on ice, and then, passed through a nylon mesh (pore size of 150 μm). The supernatant was desiccated by freeze-drying and stored below −15 °C. The yield of this fraction was 9.0% (W/W) of dry-thalli. We named this fraction "WE".

Picosecond time-resolved fluorescence spectra were measured with a streak camera spectrophotometer system as reported previously (Komura *et al*., 2010). The excitation light was obtained from a Ti:Sapphire laser (Mai Tai; Spectra-Physics in Newport Corporation, Irvine, CA). The frequency-doubled light at 440 nm was generated by a type-I BBO crystal from an 880 nm laser pulse with a pulse duration of 150 fs and a repetition rate of 80 MHz. The laser pulse was passed through a 440 nm interference filter and focused onto the surface of the lichen thalli. The fluorescence emitted from the sample was focused by two lenses onto the entrance slit of the monochromator (50 cm Chromex 2501-S, 100 g/mm; Hamamatsu Photonics, Hamamatsu, Japan) with a slit width of 40 μm through a long-pass filter (Y-46; Toshiba, Tokyo) to eliminate the excitation laser. The spectral resolution of the system was 3.3 nm. The wavelength-dispersed fluorescence was focused onto the entrance of the streak camera (Hamamatsu 4334; Hamamatsu Photonics Inc., Hamamatsu, Japan) and then displaced as for the arriving time under a rapidly scanning electric field. The streak camera system was operated in the photon-counting mode to give 640 (wavelength) ×480 (time)-pixel 2D images. The signal was accumulated for approximately 1 h in each measurement.

Results and discussion

The main component of water soluble extracts of R. yasudae was arabitol

We extracted water soluble components and run analysis of components by using a NMR, ESI-TOF MS, HPLC and GLC to identify the effective substances.

The H^1-NMR spectra of water extracts (WE) dissolved in D_2O showed a large amount of sugar alcohols. It became clear that sugar aldoses were little contained in WE, because there was no signal of α-hydrogens. For the extraction of the sugar alcohol and for the measurements of the mass spectrum, we acetylated WE and extracted with CH_2Cl_2 and were subjected to Mass spectrum measurement with an electrospray ionization-time of flight (ESI-TOF) mass spectrometer (Accu TOF, JEOL, JMS-T100LC). The mother peak of acetylated WE appeared at 385.04 in the positive ion mode. This mother peak corresponded to a full acetylated a pentitol ($C_5H_7(OCH_3CO)_5$ = 362.12 m/z). We referred a NMR spectrum of a commercial pentitol to the WE's NMR spectrum and finally determined the pentitol to be D-arabitol.

Time resolved fluorescence spectral analysis of the photobionts under wet and dry conditions

We measured the picosecond time-wavelength-2D image of the fluorescence kinetics using the streak camera system at 4 K as described in Materials and methods to detect the fluorescence quenching induced

by the drying. Figs. 1A, 1B, 1C and 1D represent the 2D images obtained in wet and dry arabitol-treated *Trebouxia* cells, wet and dry *Trebouxia* cells, respectively, induced by the excitation with a 150 fs laser pulse at 440 nm. The widths of the fluorescence spectra in these image along the horizontal axes are similar each other indicating that the fluorescence emitting Chls are almost the same in these samples. It is natural because all these fluorescence come from the cells of *Trebouxia.* However, the decay kinetics of fluorescence, which can be seen from the tail lengths along the vertical axes, were very different among samples indicating the different situations of excitation energy transfer processes in these cells. Arabitol-treated *Trebouxia* showed fast decay (short tail along the vertical axis) of fluorescence at 680–700 nm in the dry state suggesting the operation of fluorescence quenching phenomenon (Figs. 1A and 1B). However, the isolated *Trebouxia* cells showed the long vertical tails indicating the long lifetimes of PSII fluorescence both under the wet and dry conditions indicating no operation of fluorescence quenching (Figs. 1C and 1D). The images clearly indicate that the isolated *Trebouxia* cells do not show d-NPQ, it means that they lost the quenching mechanism induced by drought stress. And their d-NPQ appears by drying with arabitol .

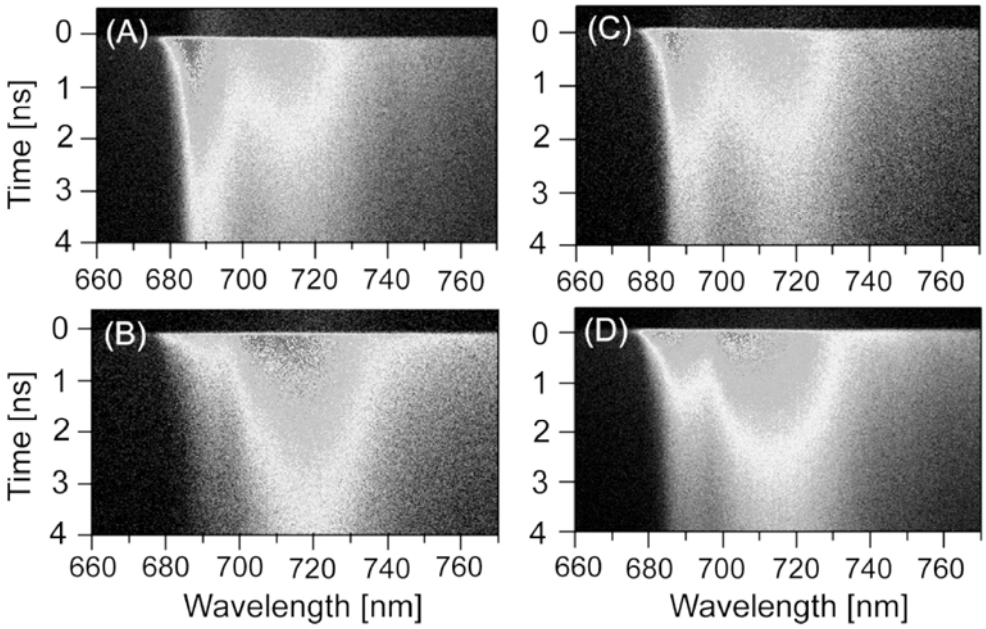

Fig. 1 Time-wavelength 2D images of arabitol-treated *Trebouxia* sp. under wet (A) and dry (B), and non-treated *Trebouxia* sp. under wet (C) and dry (D) conditions at 4 K. See Materials and methods for the details of the measuring conditions.

In conclusion, it was suggested that accumulated arabitol in lichen thalli accelerates a photoprotection mechanism of photobionts. It was reported that arabitol was synthesized by mycobionts (fungi) from ribitol which synthesized by photobionts and transferred to mycobionts (Richardson and Smith, 1968). In addition, when photobionts isolate and culture in medium, they stop to synthesize of ribitol (Hill and Ahmadjian, 1972). The accelerated mechanism of d-NPQ by arabitol is still not clear but it is highly possible that arabitol has a critical role for symbiotic relation ship between mycobionts and photobionts.

Acknowledgements

This work was partly supported by Global COE (Centers of Excellence) Program from the Ministry of Education, Culture, Sports, Science and Technology, Japan.

References

Barzda V, Jennings RC, Zucchelli G, Garab G (1999) Kinetic Analysis of the Lightinduced Fluorescence Quenching in Light-Harvesting Chlorophyll a/b

Pigment–Protein Complex of Photosystem II. Photochem. Photobiol. 70: 751-759

Demmig-Adams B (1990) Carotenoids and Photoprotection in Plants: a Role for the Xanthophyll Zeaxanthin. Biochim. Biophys. Acta 1020: 1-24

Heber U, Lange OL, Shuvalov VA (2006) Conservation and Dissipation of Light Energy as Complementary Processes: Homoiohydric and Poikilohydric Autotrophs. J. Exp. Bot. 57: 1211-1223

Hill DJ, Ahmadjian V (1972) Relationship between Carbohydrate Movement and the Symbiosis in Lichens with Green Algae. Planta (Berl.) 103: 267-277

Horton P, Ruban AV, Walters RG (1996) Regulation of Light Harvesting in Green Plants. Annu. Rev. Plant Mol. Biol. 47: 655-684

Komura M, Yamagishi A, Shibata Y, Iwasaki I, Itoh S (2008) Mechanism of Strong Quenching of Photosystem II Chlorophyll Fluorescence under Drought Stress in a Lichen, Physciella Melanchla, Studied by Subpicosecond Fluorescence Spectroscopy. Biochim. Biophys. Acta 1797: 331-338

Kopecky J, Azarkovich M, Pfündel EE, Shuvalov VA, Heber U (2005) Thermal Dissipation of Light Energy Is Regulated Differently and by Different Mechanisms in Lichens and Higher Plants. Plant Biol. 7: 156-167

Kosugi M, Arita M, Shizuma R, Moriyama Y, Kashino Y. Koike H, Satho K (2009) Responses to Desiccation Stress in Lichens Are Different from Those in Their Photobionts. Plant Cell Physiol. 50: 879-888

Millbank JW, Kershaw KA (1969) Nitrogen Metabolism in Lichens. I. Nitrogen Fixation in the Cephalodia of Peltigera Aphethosa. New phytol. 68: 721-729

Niyogi KK (1999) Photoprotection Revisited: Genetic and Molecular Approaches. Annu. Rev. Plant Physiol. Plant Mol. Biol. 50: 333-359

Richardson DHS, Smith DC (1968) Lichen Physiology. IX. Carbohydrate Movement from the Trebouxia Symbiont of Xanthoria Aureola to the Fungus. New Phytol. 67: 61-68

Ruban AV, Young AJ, Horton P (1994) Modulation of Chlorophyll Fluorescence Quenching in Isolated Light Harvesting Complex of Photosystem II. Biochim. Biophys. Acta 1186: 123-127

Ruban AV, Horton P (1999) The Xanthophyll Cycle Modulates the Kinetics of Nonphotochemical Energy Dissipation in Isolated Light-Harvesting Complexes, Intact Chloroplasts, and Leaves of Spinach. Plant Physiol. 119: 531-542

Veerman J, Vasil'ev S, Paton GD, Ramanauskas J, Bruce D (2007) Photoprotection in the Lichen Parmelia Salcata: the Origins of Desiccation-Induced Fluorescence Quenching. Plant Physiol. 145: 997-1005

FLIM (Fluorescence Lifetime Imaging Microscopy) of Avocado Leaves during Slow Fluorescence Transient (the P to S Decline and the S to M Rise)

Yichun Chen[a], Shizue Matsubara[b,*], Rosanna Caliandro[b], Govindjee[c], Robert M Clegg[a,d,e]

[a]Bioengineering Department, University of Illinois at Urbana-Champaign (UIUC), Urbana, IL 61801, USA;
[b]IBG-2: Pflanzenwissenschaften, Forschungszentrum Jülich, 52425 Jülich, Germany;
[c]Department of Plant Biology, [d] Center for Biophysics and Computational Biology, UIUC , Urbana, IL 61801, USA ;
[e]Department of Physics, UIUC, Urbana, IL 61801, USA;
*Corresponding author. E-mail: ycchen.christine@gmail.com

Abstract: Fluorescence lifetime imaging measurements were made on intact avocado leaves (*Persea americana* Mill.) during the slow part of chlorophyll (Chl) *a* fluorescence transient, the P to S and the S to M phase. Contributions of lutein-epoxide and violaxanthin cycles operating in parallel on the ΔpH-dependent (transthylakoid H^+ concentration gradient) thermal energy dissipation (qE) and slowly reversible ΔpH-independent fluorescence quenching (qI) were studied. A polar plot analysis of the lifetime data revealed three major chlorophyll *a* fluorescence lifetime pools for photosystem II. The longest lifetime pool (centered at 2 ns) was observed when linear electron transport and the resulting ΔpH build-up were inhibited in leaves. The other two lifetime pools (1.5 and 0.5 ns) were observed during ΔpH build-up under illumination. Interconversion between these two lifetime pools took place during the slow part of the chlorophyll *a* fluorescence transient. Formation of the 0.5 ns pool upon illumination was correlated with dark-retention of antheraxanthin and photo-converted lutein in leaves. In the absence of ΔpH, neither the intensity nor the lifetimes of fluorescence were affected by the presence of antheraxanthin and photo-converted lutein. We conclude that both antheraxanthin and photo-converted lutein are able to enhance ΔpH-dependent qE processes associated with the 0.5 ns lifetime pool.

Keywords: Chlorophyll *a* fluorescence transient; Fluorescence lifetime imaging microscopy; Lutein epoxide cycle; Non-photochemical quenching; Violaxanthin cycle

Introduction

There are several different non-photochemical quenching (NPQ) pathways in Photosystem II (PSII) complex (Müller, 2001). They operate in tandem to regulate the efficiency of light energy absorption, and play a role in photoprotection of chloroplasts. One of the NPQ pathways is ΔpH-dependent (transthylakoid H^+ concentration gradient) thermal energy dissipation (qE), which involves the violaxanthin (V) cycle during light-driven acidification in thylakoid lumen (Demmig-Adams and Adams III, 1996; Müller *et al*., 2001). Violaxanthin is de-epoxidized to antheraxanthin (A) and zeaxanthin (Z) by the enzyme V de-epoxidase at low lumen pH, while the reverse reactions are catalyzed by Z epoxidase on the stromal side of the thylakoid and become detectable when V de-epoxidase is inactive at high lumen pH. Some higher plants have an additional xanthophyll cycle: lutein epoxide (Lx) cycle (García-Plazaola *et al*., 2007) which involves Lx and lutein (L). Lx is de-epoxidized to lutein in a similar way as the conversion from V to A and Z. However, the epoxidation from L to Lx is at a much slower rate than the V cycle. Pogson *et al*. (1998), Pogson and Rissler (2000) and Li *et al*. (2009) have suggested that L is related also to thermal energy dissipation in *Arabidopsis thaliana*, a plant without the Lx cycle to modulate L levels via xanthophyll cycling; however, the physiological functions of the Lx cycle operation and the

consequences of the slow post-illumination Lx restoration (*i.e.* prolonged retention of photo-converted L) are still under discussion (García-Plazaola *et al*., 2003; Matsubara *et al*., 2008; Förster *et al*., 2009).

In order to study the NPQ effects of the V cycle and the Lx cycle operating in parallel, we measured the fluorescence lifetime of chlorophyll (Chl) *a* during the slow part of fluorescence transient, the P (peak) to S (semi-steady state) decline and the S to M (maximum) rise (Govindjee, 1995; Papageorgiou *et al*., 2007) in real time. As the two xanthophyll cycles have different epoxidation rates, a time-course of fluorescence lifetime measurement protocol was designed. Fluorescence lifetime can reveal the state of Chl *a* undergoing dynamic quenching. Together with the fluorescence intensity data, the fractional contribution of Chl *a* at different de-epoxidation states (DPS) in the two xanthophyll cycles, and the dynamic interconversion between those states were analyzed on "polar plots" (Clayton, 2004; Redford and Clegg, 2005; Chen and Clegg, 2009). The species fraction of the observed lifetime pools was also compared with the DPS of the two xanthophyll cycles in the samples. Details of our results and their interpretations are published in Matsubara *et al*. (2011). We present here some highlights of this research.

Materials and Methods

The fluorescence lifetime measurements of avocado leaves were made by full-field frequency-domain fluorescence lifetime imaging microscopy (FLIM) (Schneider and Clegg, 1997). The frequency-domain fluorescence lifetime parameters, M and φ, were measured at every pixel. These parameters are related to a single lifetime as follows:

$$M = 1 / \sqrt{1 + (\omega\tau)^2} \quad (1)$$

$$\varphi = \tan^{-1}(\omega\tau) \quad (2)$$

where, ω is the modulation frequency of the instrument, and τ is the fluorescence lifetime of the fluorophore. FLIM images were obtained from the adaxial surface of the leaf. The excitation light (488 nm, ~50 μmol photons m^{-2} s^{-1} at the leaf surface) was obtained from a laser; PSII fluorescence emission was collected between 670 nm to 725 nm (Chen and Clegg, 2009). The fluorescence lifetime data were presented and analyzed on "polar plots" (Clayton, 2004; Redford and Clegg, 2005; Chen and Clegg, 2009). The x- and y-axes of the polar plot are defined as:

$$x = M\cos(\varphi) \quad (3)$$

$$y = M\sin(\varphi) \quad (4)$$

The advantage of a polar plot is that it provides immediate visualization and characterization of multiple lifetime data without *a priori* assuming a model.

In order to understand the mechanism of changes in the observed fluorescence lifetimes and intensities, a two-lifetime model (as in Holub *et al*., 2007) was simulated to compare with our data. Lifetime parameters used in the simulation were obtained from the polar plot analysis of our data. In the two-lifetime model, the fluorescence intensity change is due to the interconversion of the same fluorophore between two lifetime states. This simulation is able to distinguish between changes in concentration of fluorophores (related to changes in absorption cross section caused by the so-called 'state changes', chloroplast movement or chlorophyll bleaching) and changes in rate constants of de-excitation pathways (*e.g.*, excitation energy transfer, heat loss).

The protocol of the time-course of FLIM experiment is shown in Fig. 1. For FLIM measurement we took three replicate leaf discs (50 mm^2) from different leaves. The leaf disc labeled '*control*-morning' was measured at 8:30 AM in a dark-adapted state, without any prior light treatment. Other leaf discs were exposed to 20 min room light (~5 μmol photons m^{-1} s^{-1}, labeled as *'control*-treatment') or halogen lamp (400 to 500 μmol photons m^{-1} s^{-1}, labeled as '*light*-treatment') followed by different dark adaptation times: 10 min, 60 min, 180 min, and 360 min. Twenty consecutive FLIM measurements were made on each dark-adapted leaf disc. After 5 min dark-adaptation of the sample, the last (21^{st}) measurement was made. Finally, leaf discs were dark-adapted for another 5 min and frozen in liquid nitrogen for HPLC pigment analysis. Each FLIM measurement took ~15 seconds; thus, 20 continuous FLIM measurements took 5 minutes.

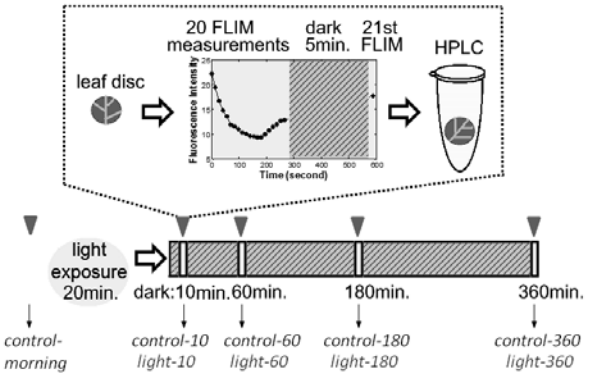

Fig. 1 The experimental protocol of the time-course of FLIM measurements used in our studies on Avocado leaves (see text, and Matsubara *et al*., 2011; with permission from Matsubara).

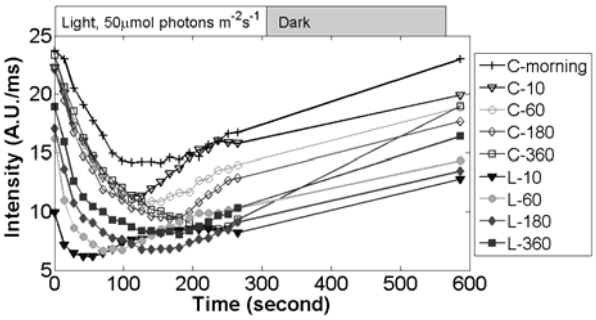

Fig. 2 Chl fluorescence intensity transients during the continuous FLIM measurements on Avocado leaves (average of three experiments). '*Control*-morning': crosses (+); other '*control*-samples': open symbols; '*light*-samples': filled (closed) symbols. Different dark adaptation time after light treatment is indicated as the number following "C" (for control) and "L" (for light). (See Matsubara *et al*., 2011; with permission from Matsubara).

Results and Discussions

Chl *a* fluorescence intensity during 20 continuous FLIM measurements under laser illumination and a subsequent 21st measurement after 5 min of dark adaptation is shown in Fig. 2. The fluorescence intensity decreases first (during the P to S phase) and then increases (during the S to the M phase) in all the samples. The '*control*-samples' start at higher intensity levels than the '*light*-samples', showing the effect of light treatment on these samples. The decreasing part of the fluorescence transient (the P to S) for the '*control*-samples' (open symbols) is essentially independent of the dark-adaptation times used (10, 60, 180, 360 min). However, the '*light*-samples' (solid symbols) vary with the same different dark adaptation times: here, the P level is lowest for the 10 min dark curve, increasing with longer dark adaptation times; even the 360 min (*light*-360) curve is still lower than the '*control*-samples'. The rising part of the fluorescence transient (the S to M phase) has slower onset time with longer dark adaptation in both the *control*- and the *light*-samples. Except for '*light*-10', the 21st measurement has the intensity level of about 80% to 90% of the 1st measurement, indicating that irreversible photoinhibition effect is not significant in our data. In '*light*-10', the 21st data has higher intensity level than that of the 1st measurement.

The fluorescence lifetime data from one of the three leaves is shown in Fig. 3. Lifetime data on the polar plot are all inside of the semicircle, indicating that there are multiple lifetimes in the sample.

As the data (Fig. 3) showed a correlation between the change in fluorescence intensity and the lifetime, we fitted them with a linear least-squares regression on the polar plot, which gives 1.5 ns and 0.5 ns values for two fluorescence lifetime pools. The two lifetimes were then used in the two-lifetime model calculation. The simulated steady-state fluorescence intensity is plotted as a function of the intensity contribution from the 0.5 ns lifetime (Fig. 3B). As the data are very close to the two-lifetime model simulation, we suggest that a reversible interconversion between the 1.5 and 0.5 ns lifetime pools is responsible for the fluorescence intensity change. The fluorescence intensity change was less affected by difference in the concentration of Chl a (*e.g.* state transitions).

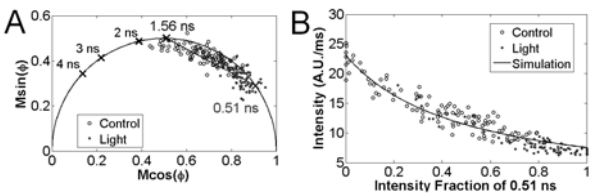

Fig. 3 Chl fluorescence lifetime data from one of the three replicates of Avocado leaves. *'Control*-samples": open circles; '*light*-samples': filled (closed) circles. (A) Polar plot representation. (B) Steady state fluorescence intensity plotted against the intensity fraction of the 0.5 ns lifetime pool. Simulation from the two-lifetime model is also shown by drawn line (Matsubara *et al*., 2011; with permission from Matsubara).

The species fraction of the short (0.5-ns) lifetime pool was also compared with the (DPS) of the two

xanthophyll cycles determined by HPLC pigment analysis.

The DPS of the V cycle is defined as ([A]+[Z])/([V]+[A]+[Z]), where [V], [A] and [Z] are the measured mmol amounts of V, A and Z per mol of Chl *a*. As Z was not detected in any of the sample, the 0.5 ns fraction was compared with [A]/([V]+[A]), as shown in Figs. 4A, 4B, and 4C. Likewise, the DPS of Lx cycle is defined as [L]/([Lx]+[L]), and the correlation with the 0.5 ns lifetime is plotted in Figs. 4D, 4E and 4F). The 0.5 ns species fraction was also compared with a combined DPS of the two cycles, ([A]+[L])/([V]+[A]+[Lx]+[L]) (shown in Figs. 4G, 4H and 4I). Linear regression lines were fitted to the data, and all of them show positive correlation. The highest R^2 values are seen between the 0.5-ns lifetime component and the DPS of the two xanthophyll cycles combined, suggesting the involvement of both the xanthophyll cycles in the interconversion between the 1.5 and 0.5 ns lifetime pools.

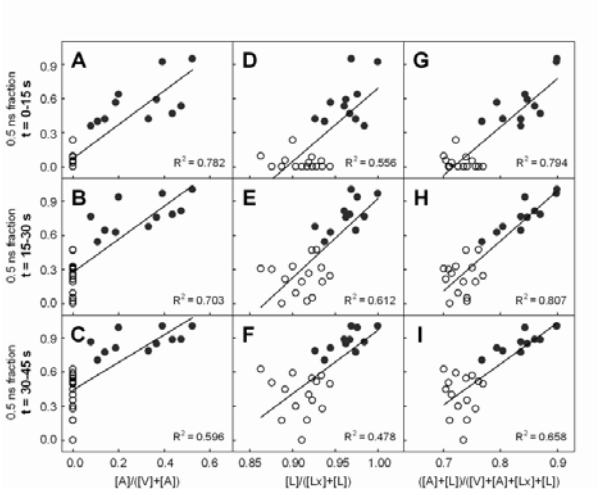

Fig. 4 Correlation between the de-epoxidation state (DPS) of the two xanthophyll cycles and the species fraction of the 0.5-ns lifetime of Avocado leaves. The 1st (t = 0 – 15 s; A, D, and G), 2nd (t = 15 – 30 s; B, E, and H), and 3rd (t = 30 – 45 s; C, F, and I) of the 21 FLIM measurements were used. '*Control*-samples': open circles; '*light*-samples': filled circles (Matsubara *et al*., 2011; with permission from Matsubara).

The linear electron flow was inhibited by 3-(3,4-dichlorophenyl)-1,1-dimethylurea (DCMU) in order to study the effects of ΔpH build-up on fluorescence lifetimes and intensity. Leaf discs were incubated in 1.2 mmol DCMU for 360 min after room light ('DCMU-*control'*) or halogen lamp light ('DCMU-*light'*) treatment. As shown in Fig. 5, the fluorescence intensity and the lifetime parameters remained nearly unchanged during laser illumination. The 'DCMU-*control'* and the 'DCMU-*light'* samples have very similar lifetime and intensity values. The least-squared fit of lifetime data on the polar plot gives 2.2 ns and 0.7 ns lifetime values, and the corresponding two-lifetime model simulation is shown in Fig. 5B. Interconversion between the two lifetime pools was not observed in the DCMU incubated samples.

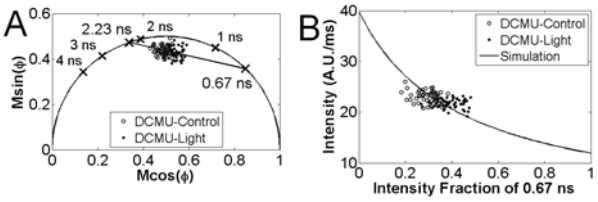

Fig. 5 When ΔpH build-up was inhibited by DCMU, the fluorescence lifetime and intensity remained constant. 'DCMU-*control'*: open circles; 'DCMU-*light'*: filled (closed) circles. (A) Polar plot representation. (B) Steady state fluorescence intensity plotted against the fractional contribution of the 0.7 ns lifetime pool. Simulation from the two-lifetime model is also shown here (Matsubara *et al*., 2011; with permission from Matsubara).

Conclusions

The fast data acquisition of FLIM enabled us to obtain real-time measurements of Chl *a* lifetimes during the slow part of fluorescence transient (the P to S; and S to M phase) in Avocado leaves. Formation of the 0.5 ns pool upon illumination could be correlated with the DPS of the two xanthophyll cycles due to dark-retention of antheraxanthin and photo-converted lutein in leaves. Data suggest that the presence of ΔpH is required for the quenching of fluorescence by antheraxanthin and photo-converted lutein. We show here the importance of both the V and Lx cycles in thermal energy dissipation processes in Avocado leaves.

References

Chen YC, Clegg RM (2009) Fluorescence Lifetime-Resolved Imaging. Photosynth. Res. 102: 143-155

Clayton AHA, Hanley QS, Verveer PJ (2004) Graphical Representation and Multicomponent Analysis of Single-Frequency Fluorescence Lifetime Imaging Microscopy Data. J. Microsc. 213: 1-5

Demmig-Adams B, Adams III WW (1996) The Role of Xanthophyll Cycle Carotenoids in the Protection

of Photosynthesis. Trends Plant. Sci. 1: 21-26

Förster B, Osmond CB, Pogson BJ (2009) De Novo Synthesis and Degradation of Lx and V Cycle Pigments during Shade and Sun Acclimation in Avocado Leaves. Plant Physiol. 149: 1179-1195

García-Plazaola JI, Hernández A, Olano JM, Becerril JM (2003) The Operation of the Lutein Epoxide Cycle Correlates with Energy Dissipation. Funct. Plant Biol. 30: 319-324

García-Plazaola JI, Matsubara S, Osmond CB (2007) The Lutein Epoxide Cycle in Higher Plants: Its Relationships to Other Xanthophyll Cycles and Possible Functions. Funct. Plant Biol. 34: 759-773

Govindjee (1995) Sixty-Three Years since Kautsky: Chlorophyll a Fluorescence. Aust. J. Plant Physiol. 22: 131-160

Holub O, Seufferheld MJ, Gohlke C, Govindjee, Heiss GJ, Clegg RM (2007) Fluorescenc Lifetime Imaging Microscopy of Chlamydomonas Reinhardtii: Non-Photochemical Quenching Mutants and the Effect of Photosynthetic Inhibitors on the Slow Chlorophyll Fluorescence Transients. J. Microsc. 226: 90-120

Li Z, Ahn TK, Avenson TJ, Ballottari M, Cruz JA, Kramer DM, Bassi R, Fleming GR, Keasling JD, Niyogi KK (2009) Lutein Accumulation in the Absence of Zeaxanthin Restores Nonphotochemical Quenching in the Arabidopsis Thaliana npq1 mutant. Plant Cell 21: 1798-1812

Matsubara S, Krause GH, Seltmann M, Virgo A, Kursar TM, Jahns P, Winter K (2008) Lutein Epoxide Cycle, Light Harvesting and Photoprotection in Species of the Tropical Tree Genus Inga. Plant Cell Environ. 31: 548-561

Matsubara S, Chen YC, Caliandro R, Govindjee, Clegg RM (2011) Photosystem II Fluorescence Lifetime Imaging in Avocado Leaves: Contributions of the Lutein-Epoxide and Violaxanthin Cycles to Fluorescence Quenching. doi:10.1016/j.jphotobiol. 2011.01.003

Müller P, Li XP, Niyogi KK (2001) Non-Photochemical Quenching: A Response to Excess Light Energy. Plant Physiol. 125: 1558-1566

Papageorgiou GC, Tsimilli-Michael M, Stamatakis K (2007) The Fast and Slow Kinetics of Chlorophyll a Fluorescence Induction in Plants, Algae and Cyanobacteria: a Viewpoint. Photosynth. Res. 94: 275-290

Pogson BJ, Niyogi KK, Björkman O, DellaPenna D (1998) Altered Xanthophyll Compositions Adversely Affect Chlorophyll Accumulation and Nonphotochemical Quenching in Arabidopsis Mutants. Proc. Natl. Acad. Sci. USA 95: 13324-13329

Pogson BJ, Rissler HM (2000) Genetic Manipulation of Carotenoids Biosynthesis and Photoprotection. Phil. Trans. R. Soc. Lond. B. 355: 1395-1403

Redford GI, Clegg RM (2005) Polar Plot Representation for Frequency-Domain Analysis of Fluorescence lifetimes. J. Fluoresc. 15: 805-815

Schneider PC, Clegg RM (1997) Rapid Acquisition, Analysis, and Display of Fluorescence Lifetime-Resolved Images for Real-Time Applications. Rev. Sci. Instrum. 68: 4107-4119

Improving the Photosynthetic Productivity and Light Utilization in Algal Biofuel Systems: Metabolic and Physiological Characterization of a Potentially Advantageous Mutant of *Chlamydomonas Reinhardtii*

Y Zhou[a], LC Schideman[a], Govindjee[b], SI Rupassara[c], MJ Seufferheld[d]

[a]Department of Agricultural and Biological Engineering, University of Illinois at Urbana Champaign, Urbana, IL 61801, USA;
[b]Departments of Biochemistry and Plant Biology, University of Illinois at Urbana Champaign;
[c]Department of Animal Sciences, University of Illinois at Urbana Champaign;
[d]Department of Crop Sciences, University of Illinois at Urbana Champaign.

Abstract: In this study, we report initial biophysical and biochemical characterization of a spontaneous 'mutant' (referred to as 'IM') of the green alga *Chlamydomonas reinhardtii* with several unique attributes that has potential for improving photosynthetic productivity, light utilization efficiency, and, perhaps, even protection against environmental stress. Growth rate experiments showed that under low light intensity (10 μmol photons m^{-2} s^{-1}), IM showed 36% higher cell density and 25% higher dry cell weight than the wild type cells (WT), while at higher light intensity (640 μmol photons m^{-2} s^{-1}), the IM did not show any advantage. Chlorophyll *a* fluorescence transient measurements and subsequent analysis indicated that IM cells grown at a light intensity of 20 μmol photons m^{-2} s^{-1} had a higher light utilization efficiency in comparison to the WT cells. Interestingly, metabolite profiling analysis showed that during the exponential growth phase with both low and high light intensities (10 and 640 μmol photons m^{-2} s^{-1}), the IM cells had higher concentrations than WT cells for several important metabolites that have been previously shown to help protect against environmental stress.

Keywords: *Chlamydomonas reinhardtii*; Mutant; Growth; Metabolite profiling; Fluorescence transient

Introduction

Fossil fuels have been widely recognized as unsustainable over the long-term, and algae offer some of the best potential for a sustainable supply of renewable biofuels (Chisti, 2007). Algae have several key advantages including: higher growth rates than plants, the ability to grow on marginal areas or in low quality water sources and ability to consume excess nutrients in eutrophic waters; further, high oil content can be achieved with certain species. Despite these significant advantages, the promise of algal biofuels remains largely unfulfilled because of several practical bottlenecks in the process. A spontaneous 'mutant' of the green alga *Chlamydomonas reinhardtii* (referred to as 'IM') showed several unique attributes that have potential for improving algal biofuel production in terms of biomass productivity, light utilization efficiency, and, perhaps, even protection against environmental stress. Thus, elucidating these distinctive characteristics of the mutant could help accelerate development of practical biofuel production processes to meet global fuel demands.

Materials and Methods

Strains and culture conditions

The 'immortal mutant' (IM) algal strain used in this study descended from the previously described ptx2 mutant of *Chlamydomonas reinhardtii* that was

constructed by insertional mutagenesis to be lacking in light-induced flagellar currents, which resulted in defects in both phototaxis and photoshock responses (Pazour *et al*., 1995). Wild type (WT) and 'immortal mutant' (IM) cultures of *Chlamydomonas reinhardtii* were maintained under room light and temperature in Tris–acetate–phosphate (TAP) agar culture medium plates (20 mmol Tris; 17.4 mmol acetate; 7 mmol NH_4Cl; 0.4 mmol $MgSO_4$; 0.3 mmol $CaCl_2$; 1 mmol phosphate buffer; 1 ml/L Hutner's trace metal solution; 15 g/L Bacto agar). Prior to each experiment, an inoculum of these cultures was grown in 250 ml Erlenmeyer flasks containing 50 ml liquid TAP medium (without Bacto agar) on an orbital shaker at 24 °C and under 20 μmol photons $m^{-2} s^{-1}$ photosynthetically active radiation (PAR) provided by fluorescent lamps.

Growth rate experiments

WT and IM cells were cultured in TAP medium at two different light intensities. For lower light intensity (10 ± 1 μmol photons $m^{-2} s^{-1}$) experiments, the light was from two linear fluorescence lamps, placed on top of the shaker; its intensity was measured at 9 evenly distributed points on the surface of the shaker. For higher light intensity experiments (average 640 ± 5 μmol photons $m^{-2} s^{-1}$), 6 compact fluorescence lamps were used to provide light for 6 culture flasks individually, and the light intensity was measured at 10 points on the surface of the flasks. The maximum was 1270 ± 35 μmol photons $m^{-2} s^{-1}$ in the center, and the minimum was 285 ± 20 μmol photons $m^{-2} s^{-1}$ on the edge. The initial cell density was 10,000 cells/ml. Duplicates of each of the algal strains were cultivated and the growth data was averaged to determine the growth curve of each strain.

Cell growth was determined by cell density and dry cell weight. Cell counting was conducted using Neubauer hemacytometer and repeated twice for each replicate to determine an average value. Dry cell weight was determined as total suspended solids according to standard methods (Clesceri *et al*., 1999).

Chlorophyll a fluorescence transient analysis

Chlorophyll *a* fluorescence transients were measured at ambient temperature (20−22 ºC) for 3 s with a portable fluorimeter (PEA, Plant Efficiency Analyzer, Hansatech Inst., UK) with excitation light (620 nm) intensity of 3,000 μmol photons $m^{-2} s^{-1}$ after cells were dark adapted for 6 min. The algal cultures used in these tests were taken from the exponential phase of growth under a light intensity of 20 μmol photons $m^{-2} s^{-1}$ (48 h after inoculation), and the cells were diluted (or concentrated) to a chlorophyll concentration of 15 μg/ml. Before the measurement began, the cell suspension was placed in flasks with stirring under room illumination. Three separate cultures of each of the strains were used for measurement, and triplicate measurements were conducted for each culture replicate (n = 9). Analysis of these data was carried out according to the JIP test procedure as previously described by Strasser *et al*. (2004) and reviewed by Stirbet and Govindjee (2011).

Metabolite profiling

Metabolite profiling of the IM and WT algal cells, both in the exponential growth phase and stationary growth phase, was conducted using GC-MS (Gas Chromatography-Mass Spectroscopy) as described previously by Rupassara (2008) with the following modifications. In the methanol extraction step, the samples were vortex-mixed and incubated at 65 °C instead of 70 °C. After the initial methanol extraction, pellets were further extracted using methanol: chloroform: 0.1mol HCl in water (5:2:3) instead of water: methanol (1:3). The GC-MS interface temperature was 310 °C, and the ion source was kept at 220 °C.

Results and Discussion

Growth rate experiments

After 337 hours of cultivation at light intensity of 10 μmol photons $m^{-2} s^{-1}$, the dry weight of IM cells (370 mg/L) was 25% higher than the WT cells grown under the same conditions (See Fig. 1, panel A), and the density of the IM cells ($1.41 \pm 0.46 * 10^7$ cells/ml) was 36% higher than WT cells ($1.03 \pm 0.40 * 10^7$ cells/ml). At a higher light intensity of 640 μmol photons $m^{-2} s^{-1}$, IM and WT cells showed very similar biomass production as shown in panel B of Fig. 1, but IM cells did have a noticeably lower cell density ($0.93 \pm 0.39 * 10^7$ cells/ml) than the WT cells ($1.47 \pm 0.39 * 10^7$ cells/ml).

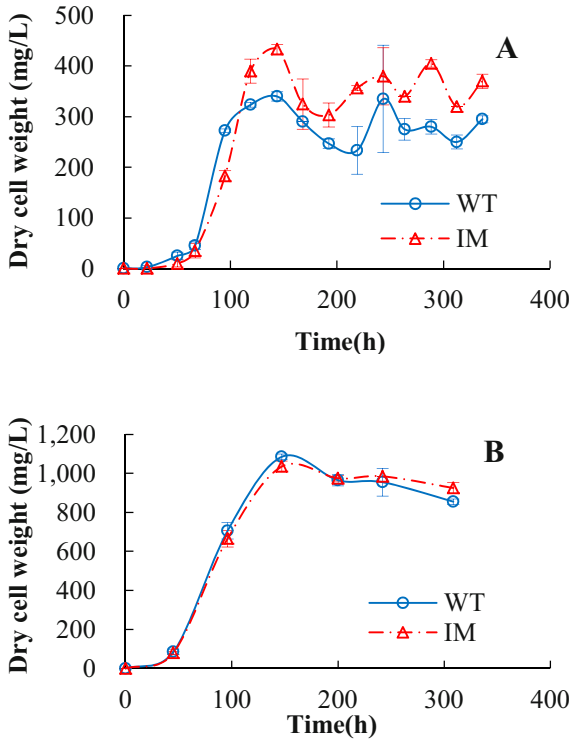

Fig. 1 Dry cell weight of wild type (WT) and 'immortal mutant' (IM) cells at two different light intensities.(**A**) At light intensity of 10 μmol photons m^{-2} s^{-1}; (**B**) At light intensity of 640 μmol photons m^{-2} s^{-1} .

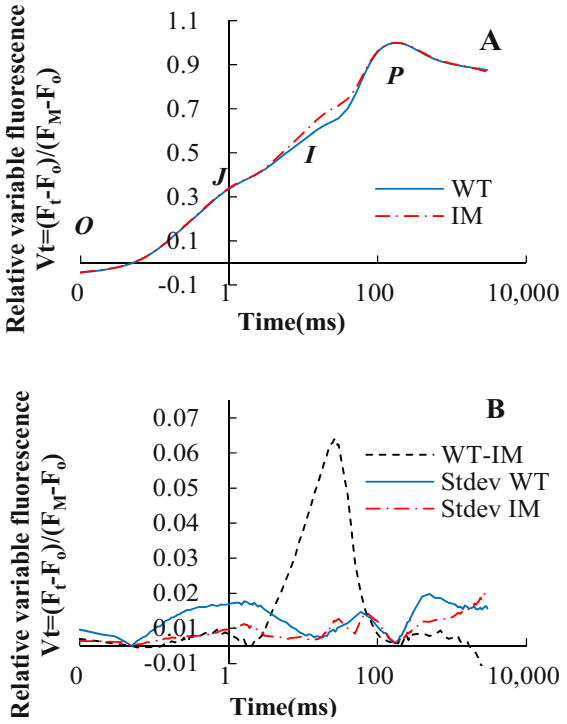

Fig. 2 (**A**) Chlorophyll *a* fluorescence transients for wild type (WT) and 'immortal mutant' (IM) cells after double normalization. O stands for origin, J and I for inflection points, and P for peak. Each curve was obtained from the average of nine independent experiments. (**B**) The difference between the relative variable fluorescence of 'immortal mutant' cells and wild type cells (IM-WT) and the standard deviation for the relative variable fluorescence of wild type cells (Stdev WT) and 'immortal mutant' cells (Stdev IM) over nine experimental replicates.

Chlorophyll a fluorescence transient analysis

Chlorophyll *a* fluorescence transients were measured and analyzed to characterize Photosystem II activity. The fluorescence transient curves were double normalized to get relative variable fluorescence, which allows for a comparison of transients measured on different samples (Strasser *et al*., 2004). As shown in panel A of Fig. 2, a small difference in the relative variable fluorescence intensity (~5%−10%) at the 'I' level was observed between IM and WT cells during the exponential growth phase at light intensity of 20 μmol photons m^{-2} s^{-1}. Similar differences were also observed during the stationary phase. In order to better highlight the difference at the 'I' level, we subtracted the relative variable fluorescence intensity of WT cells from that of IM cells as shown in panel B of Fig. 2. This difference was consistent in all of the nine replicate samples, and it was much larger than the standard deviations of the nine replicates for both the WT and IM cells, which are also shown in panel B of Fig. 2. Thus, this relatively small difference at the 'I' level indicates that there are some real differences in the Photosystem II activity of the IM cells.

The fluorescence transient data was analyzed using the JIP test method as previously reviewed (Strasser *et al*., 2004; Stirbet and Govindjee, 2011), and selected parameters are shown in Table 1. This analysis revealed that the IM cells had ~9% higher variable fluorescence ratio F_v/F_o, which is an indicator of higher capacity for photosynthetic quantum conversion and CO_2 fixation (Lichtenthaler and Babani, 2004). The IM cells also showed ~9% higher efficiency in primary photochemistry, $\varphi_{Po}/(1-\varphi_{Po})$, and a ~7% lower dissipation of energy per reaction center, DI_o/RC. These two values reflect that after the photons are absorbed by the antenna pigments, less excitation energy is lost to heat dissipation or fluorescence in the IM cells as compared to the WT cells. Thus, more excitation energy is channeled to the reaction centers and further converted to redox energy, which ultimately leads to CO_2 fixation. The performance index on an absorption basis PI(ABS), which reflects the energy conservation from photons

absorbed by the antenna to the reduction of Q_B, is also higher (~10%) in the IM cells than in WT cells. This indicates a stronger overall photosynthetic driving force. These differences could help explain the higher IM biomass yields under low light shown previously in Fig. 1.

Table 1 Selected fluorescence parameters.

	WT	IM	Difference (IM-WT)/WT
F_v/F_o	3.04	3.31	8.7%
$\varphi_{Po}/(1-\varphi_{Po})$	3.04	3.31	8.7%
DI_o/RC	0.64	0.59	7.0%
PI(ABS)	18.31	20.10	9.8%

F_v/F_o: variable fluorescence ratio
$\varphi_{Po}/(1-\varphi_{Po})$: efficiency in primary photochemistry
DI_o/RC: dissipation of energy per reaction center
PI(ABS): performance index on absorption basis

Metabolite profiling

Metabolite profiling also revealed some potentially advantageous differences of IM cells over WT cells under certain conditions. During the exponential growth phase (Fig. 3, panel A), the IM cells had higher concentrations than WT cells of several potentially important metabolites, such as total tocopherols, which has been previously shown to help protect against various environmental stress conditions (Paul, 2007; Maeda and Della, 2007). During stationary growth (Fig. 3, panel B), IM cells had higher levels of tocopherols and α-tocopherolhydroquinone than WT cells, but only under low light conditions (10 μmol photons m^{-2} s^{-1}). Trehalose and inositol were lower in the IM cells during the stationary phase. Overall, the IM cells had better production of protectant compounds during exponential growth but showed poorer production during the stationary phase.

Conclusion

In this study, a spontaneous mutant of the green alga *Chlamydomonas reinhardtii* exhibited certain unique biophysical and biochemical characteristics including higher biomass production, light utilization efficiency, and production of protective compounds under certain conditions. These unique attributes are potentially advantageous for enhancing algal biofuel production capabilities. Future research should be directed at a more detailed characterization of the IM cells including direct measurement of photosynthesis rate, non-photochemical quenching measurements and its resistance to other environmental stress conditions. Ultimately, gene sequencing could be used to identify the specific genes associated with desirable photosynthetic differences and then transfer of those genes to other algae species (or other strains of Chlamydomonas) could be pursued.

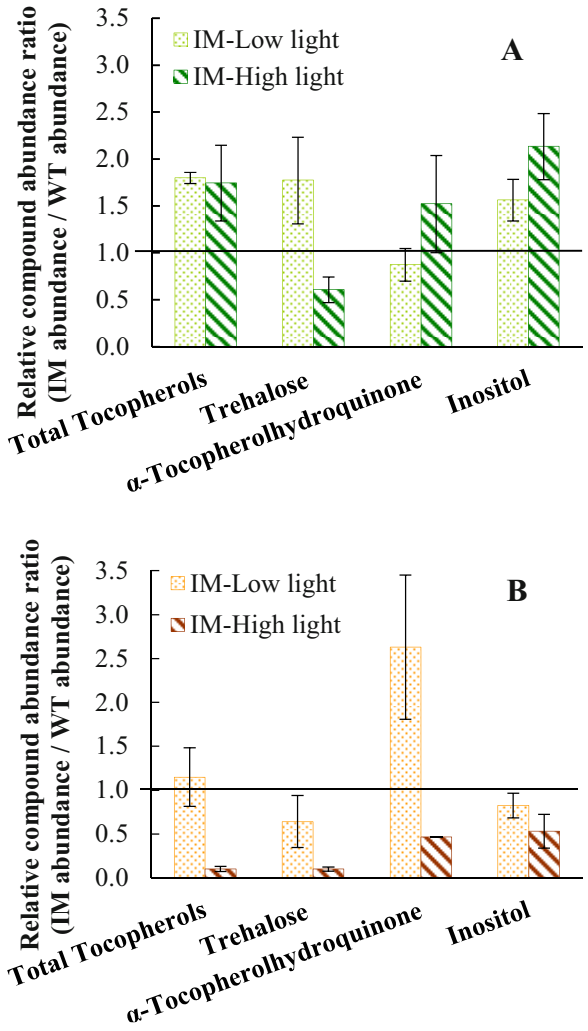

Fig. 3 Metabolite profiling data for 'immortal mutant' (IM) cells grown at low and high light intensity (20 and 640 μmol photons m^{-2} s^{-1}, respectively). All IM values have been normalized by dividing by the respective values for wild type cells indicated by the lines at value '1'. (**A**) Results for exponential growth phase cells. (**B**) Results with stationary growth phase cells.

Acknowledgements

We thank Reto Strasser, who provided us the Handy PEA instrument and the Biolyzer software, as

well as his support for the fluorescence transient data analysis.

References

Chisti Y (2007) Biodiesel from Microalgae. Biotechnol Adv 25: 294-306

Clesceri LS, Greenberg AE, Andrew DE (1999) Standard Methods for the Examination of Water and Wastewater. American Public Health Association, New York

Fiehn O, Kopka J, Trethewey R, Willmitzer L (2000) Identification of Uncommon Plant Metabolites Based on Calculation of Elemental Compositions Using Gas Chromatography and Quadrupole Mass Spectrometry. Anal Chem 72: 3573-3580

Lichtenthaler HK, Babani F (2004) Light Adaptation and Senescence of the Photosynthetic Apparatus. Analysis of the Chlorophyll a Fluorescence Transient. In: Papageorgiou GC, Govindjee (eds.), Chlorophyll a Fluorescence: a Signature of Photosynthesis. Springer: The Netherlands, pp. 713-736

Lisec J, Schauer N, Kopka J, Willmitzer L, Fernie A (2006) Gas Chromatography Mass Spectrometry-based Metabolite Profiling in Plants. Nature protocols 1: 387-396

Maeda H, Della D (2007) Tocopherol Functions in Photosynthetic Organisms. Curr Opin Plant Biol 10: 260-265

Paul M (2007) Trehallose 6-Phosphate. Curr Opin Plant Biol 10: 303-309

Pazour G, Sineshchekov O, Witman G (1995) Mutational Analysis of the Phototransduction Pathway of Chlamydomonas-Reinhardtii. J Cell Biol 131: 427-440

Rupassara SI (2008) Metabolite Profiling of Leaves and Vascular Exudates of Soybean Grown under Free-Air Concentration Enrichment. Ph.D. Thesis, University of Illinois at Urbana Champaign, USA

Strasser RJ, Tsimilli-Michael M, Srivastava A (2004) Analysis of the Chlorophyll a Fluorescence Transient. In: Papageorgiou GC, Govindjee (eds.), Chlorophyll a Fluorescence: a Signature of Photosynthesis. Springer: The Netherlands, pp. 321-362

Stirbet A, Govindjee (2011) On the Relation between the Kautsky Effect (Chlorophyll a Fluorescence Induction) and Photosystem II: Basics and Applications of the OJIP Fluorescence Transient. J Photochem Photobiol B., In Press: DOI:10.1016/J.JPHOTOBIOL.2010.12.010

Symposium 17

Perception of Environmental Stress and Acclimation

Characterization of Energy Transfer Processes and Flash Oxygen Yields of Thylakoid Membranes Isolated from Resurrection Plant *Haberlea Rhodopensis* Subjected to Different Extent of Desiccation

M Velitchkova[a*], D Lazarova[a], G Mihailova[b], D Stanoeva[a], V Dolchinkova[c], K Georgieva[b]

[a]Institute of Biophysics and Biomedical Engeneering, Bulgarian Academy of Sciences, Acad. G. Bonchev str. Bl. 21, 1113 Sofia, Bulgaria;
[b]Institute of Plant Physiology and Genetics Bulgarian Academy of Sciences, Acad. G. Bonchev str. Bl. 21, 1113 Sofia, Bulgaria;
[c] Faculty of Biology, Sofia University "St. K. Ohridski", 8 Dragan Tsankov Blvd., 1164 Sofia, Bulgaria.
[*]Corresponding author. Tel. No. +359 2 979 2655; Fax No. +359 2 971 2493; E-mail: mayav@bio21.bas.bg.

Abstract: The resurrection plants are unique with their extra desiccation tolerance. The physico-chemical properties of photosynthetic apparatus are of crucial importance for survival of plants upon water stress. In present work the effect of different extent of desiccation on the energy transfer properties and oxygen evolving capacity of isolated thylakoid membranes from resurrection plant *Haberlea Rhodopensis* are investigated. The plants from different habitats in Bulgaria are compared. Energy distribution and spillover between both photosystems are studied by means of 77 K chlorophyll fluorescence. The dependence of fluorescence ratio F735/F685 on the degree of desiccation of plants is also followed. Functionality of PSII and especially of oxygen-evolving apparatus under water deficit is estimated by flash oxygen yields and initial oxygen burst of thylakoid membranes isolated from plants desiccated up to 50% and 8% relative water content (RWC). Population of S_i states as well as the misses and the double hits are calculated according non-cooperative Kok's model and compared for plants from different habitats and different RWC. The results are discussed in terms of involvement of "fast" and "slow" centers from grana and stroma regions in oxygen evolution and alteration of their contribution as a result of desiccation.

Keywords: Desiccation; Energy transfer; Flash oxygen yields; *Haberlea Rhodopensi;,* Resurrection plants

Introduction

One of the more severe environmental factors that damages higher plants growth and productivity is drought. Most of the plants could not survive under desiccation up to air-dried state. A limited number of plants representing so called resurrection plants exhibit a remarkable tolerance to water deficit and under rehydration restore their functions (Moore *et al.*, 2009). The most sensitive part of photosynthetic apparatus to stress factor is oxygen evolving complex and photosystem II (Canaani *et al.*, 1986; Giardi *et al.*, 1996). On the other hand the effect of desiccation on thylakoid membranes and on granal structure is also of interest in order to understand the mechanism of resurrection plant tolerance to severe desiccation and the possibility to restore after rehydration.

In the present paper we studied the oxygen evolution activity of thylakoid membranes isolated from *Haberlea rhodopensis* plants from different habitats. In order to characterize the energy interaction between both photosystems 77 K fluorescence was studied of thylakoids from control and desiccated plants. Fluorescence emission at 77 K demonstrated the alterations in the overall distribution of excitation energy between PSII and PSI as well as stress-induced changes in energy interaction between pigment-protein complexes (Krause and Weis, 1991). The changes of oxygen-evolving capacity of isolated thylakoid membranes are characterized by flash induced oxygen yields (Kok *et al.*, 1970; Zeinalov, 1982). The changes of fluorescence emission and oxygen yields are discussed in terms of possible involvement of desiccation-induced structural reorganization of thylakoids and lateral rearrangement of pigment-protein complexes of PSI, PSII, LHCI and LHCII.

Materials and Methods

Thylakoid membranes were isolated according to method described by Georgieva *et al.* (2009). Well-hydrated and naturally dried Haberlea rhodopensis plants growing on rocks below trees in deep shade (Bachkovo region) or sun exposed but briefly shaded by neighboring trees (Sitovo region) were used. Low temperature (77 K) fluorescence emission and excitation spectra were registered by a Jobin Yvon JY3 spectrofluorometer, equipped with a red sensitive photomultiplier (Hamamatsu 928) and a low temperature device. Chlorophyll concentration was 10 mg chl/ml. Data were digitised and transferred to an online IBM-compatible computer for further retrieval and analysis.

Determination of oxygen flash yields and initial oxygen burst was performed using home-constructed equipment, described in details in Zeinalov, 2002, containing a fast oxygen rate electrode. For measuring of flash oxygen yields thylakoid membranes were illuminated with short (10 μs) saturating (4 J) flashes with a dark period of 0.466 s between flashes. For continuous illumination measurements, a cold light supplier (LED LXHL-LW3C, Philips Lumileds Lighting Company, San Jose, U.S.A.) providing irradiation on the surface of sample 420 μmol m^{-2} s^{-1} was used. The Si state populations, misses (a) and double hits (b), were calculated by software based on fitting the theoretically calculated oxygen burst yields to the experimentally obtained values, according to non-cooperative Kok's model (Kok *et al.*, 1970). Chlorophyll concentration was 150 mg chl/ml. The electrophoretic mobility (EPM) measurements were performed using the particle electrophoresis technique with the OPTON cytopherometer (Feintechnik Ges, m.b.H., Wien, Austria). Thylakoids were suspended at a chlorophyll concentration of 1−2 mg/ml. The thylakoids were observed under a light microscope connected to a Sony video camera providing 800 times magnification and images were recorded on a Sony video recorder RDR-GX700/S. Thylakoid membranes with approximately the equal sizes of 3–5 μm were measured. The zeta potential ζ was calculated from the electrophoretic mobility, u, using Helmholtz-Smoluchowski equation. The surface charge density (σ) was estimated according to (Chow *et al.*, 1991).

Results and Discussion

At Fig. 1 data about surface charge density of thylakoid membranes from Bachkovo and Sitovo subjected to different extent of desiccation are presented.

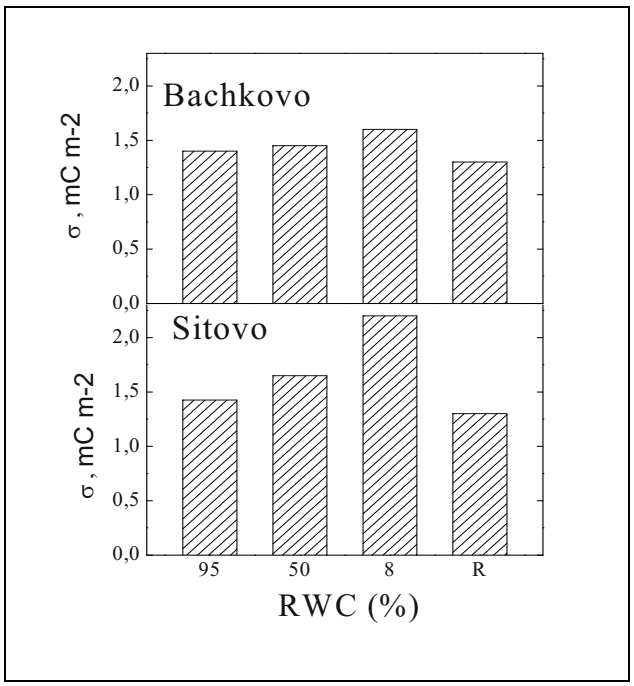

Fig. 1 Effect of desiccation on surface charge density of thylakoid membranes isolated from both habitats.

Lowernig of RWC led to an increase of σ more pronounced for membranes from Sitovo. The increase of σ is related to the exposure of more negatively charged groups from protein complexes on the membrane surface that could avoid possible aggregation upon desiccation. Rehydration of plants resulted in restoration of initial values of surface charge density. 77 K fluorescence emission spectra of thylakoid membranes isolated from plants from both habitats are recored upon excitation with 436 nm (preferential excitation of chl*a*) and 472 nm (preferential excitation of chl*b*). In addition, excitation spectra of fluorescence emitted at 735 nm (PSI) and 685 nm (PSII) are recorded in the "red" and the "blue" regions. Data about fluorescence ratios (F735/F685, E480/436 and E680/E650, reflecting energy distribution between both photosystems and involvement of chl*a* and chl*b* in energy supply of PSI and PSII) are presented at Table 1.

Table 1 Values for fluorescence emission (F735/F685 and F685/F695) ratios and excitation (E680/E650, E480/E436) ratios for control and desiccated to different degree thylakoid membranes isolated from plants from Bachkovo and Sitovo habitats. All spectra are normalized at 685 nm.

Sample habitat	RWC	Excitation with 436 nm		Excitation with 472 nm		Emision at 735 nm	Emision at 735 nm	Emision at 685 nm
		F735/F685	F685/F695	F735/F685	F685/F695	E680/E650	E480/E436	E480/E436
Bachkovo	control	1.32	1.14	1.15	1.14	1.75	2.31	3.27
	50%,	1.33	1.10	1.09	1.14	2.12	2.54	5.89
	8%	1.41	1.13	1.30	1.14	2.13	2.07	3.80
Sitovo	control	1.18	1.29	1.04	1.23	1.77	2.74	3.08
	50%	1.17	1.06	0.93	1.10	1.85	3.14	5.13
	8%	0.98	1.27	0.81	1.34	2.14	1.74	3.10

Desiccation of plants up to 50% did not result in changes of F735/F685, however a decrease of the ratio F685/F695 is observed. At 8% RWC a slight increase of F735/F685 is observed for samples form Bachkovo. The changes of the relative intensity of the peaks at 685 nm and 695 nm as well as the red shift of the maximum at 695 point out changes in the organization of the components of PSII complex as the fluorescence at 685 nm and 695 nm in 77 K spectra is emitted from CP43 and CP47, respectively (Stroch *et al.*, 2004). Emission from PSI (at 735 nm) showed an increase of the relative involvement of chl*a* in comparison with chl*b*. Contrary, emission at 685 nm (PSII) showed an increase of participation of chl*b* molecules in energy supply of PSII with the increasing of extent of desiccation. For examination of functionality of PSII and especially of oxygen-evolving complexes under desiccation flash-induced oxygen yields are studied.

At Fig. 2A the the dependence of oxygen yields on the number of flash is presented. The traces followed the well known periodicy of oxygen yields. Membranes from Bachkovo habitat showed higher oxygen yields in comparison with that from Sitovo.

We studied also the kinetic of initial oxygen burs upon continous illumination for thylakoid membranes from planst subjected different extent of desiccation (Fig. 2B). On the basis of flash oxygen yields the populations of S_0 and S_1 states are calculated as well as the misses (α) and double hits (β). Data are presented at Table 2. Desiccation led to a decrease of the number of centers in S_0 state and this decrease is proportional of the extent of desiccation and is more pronounced for membranes from Sitovo habitat. More probably this decrease is related to the reduced electron transport activity and hindered deactivation of oxidized states of oxygen evolving centers. It should be noted that at 8% RWC no oxygen yields are observed for the membranes from plants from Bachkovo.

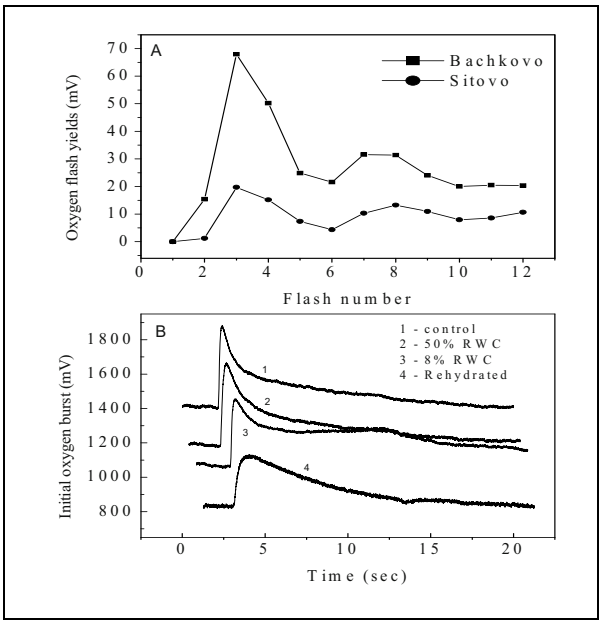

Fig. 2 Flash oxygen yields of membranes from Bachkovo and Sitovo (A) and initial oxygen burst for membranes from Bachkovo at different extent of desiccation (B).

Table 2 Values for S_0 and S_1 population and misses (α) and double hits (β) for thylakoid membranes isolated from plants from both habitats under different extent of desiccation.

Sample	S_0	S_1	α	β
Bachkovo –control	27.20	72.80	0.177	0.039
RWC - 50%	18.56	81.39	0.143	0.034
RWC - 8%	-	-	-	-
Rehydrated	8.27	91.73	0.150	0.043
Sitovo-control	39	61.00	0.077	0.082
RWC - 50%	12.9	87.10	0,220	0.027
RWC- 8%	4.02	95.98	0.240	0.031

Under rehydration flash oxygen yields are restored to 9%–8%. The typical curves of initial oxygen burst showed second order exponential decay, due to the functioning of two types of oxygen evolving centers. $PSII_\beta$ centers from stroma regions evolve oxygen by so called cooperative mechanism - by cooperation of oxygen precursors from different centers (Diner, 1974; Lavorel, 1976) while $PSII_\alpha$ centers from grana evolve oxygen by non-cooperative mechanism (Kok *et al*., 1970). The later operate more rapidly ("fast centers") and the stroma-situated centers turn more slowly ("slow center"). The contribution of both types of centers in the total oxygen production can be determined by parameters of both kinetic component of second order exponential decay. Data about amplitude and time constant of fast and slow component for membranes are presented at Table 3.

Table 3 Amplitudes A_1 and A_2 and time constant t_1 and t_2 of fast and slow components, respectively of exponential decay of initial oxygen burst for membranes from plants from Bachkovo and Sitovo.

Sample	A_1	A_2	t_1	t_2
Bachkovo	248	225	0.56	7.72
Sitovo	32	469	1.78	12.79

The amplitude of "fast" component is considerably lower for membranes from Sitovo habitat which correspond with the lower flash oxygen yields. In addition, both components of thylakoids from Sitovo plants exhibit slow time constant that those from Bachkovo. Data presented showed that the main functions of photosynthetic apparatus are concerned by desiccation but its effect depends on the conditions of growing of plants. Both habitats are characterized by different light conditions, Sitovo being more illuminated during the sunny days. Physico-chemical properties of thylakoid membranes and energy interaction between both photosystems are changed also by desiccation. The intensities of bands at 685 nm and 735 changed with the decrease of RWC. Data about F685/F695 showed that the complex LHCII-PSII is affected more pronounced for membranes from plants from Sitovo habitat. On the other hand, flash oxygen yields are lower for membranes from Sitovo, thus indicating a lower population of (or less active) PSII centers in grana regions. Recently, structurally and functionally different populations of PSII centers have been isolated from stroma and grana regions of thylakoid membranes (Danielsson *et al*., 2004). It can be supposed that centers form grana and stroma regions showed different sensibility to desiccation.

Acknowledgement

This work is supported by National Science Fund of Bulgaria under Research project ДО02-208/2008.

References

Canaani C, Havaux M, MalkinS (1986) Hydroxylamine, Hydrazine and Methylamine Donate Electrons to the Photooxidising Side of PSII in Leaves Inhibited in Oxygen Evolution Due to Water Stress. BBA 851: 151-155

Chow WS, Miller C, Anderson JM (1991)Surface Charges, the Heterogeneous Lateral Distribution of the Two Photosystems, and Thylakoid Stacking. BBA 1057: 69-77

Danielsson R, Albertsson PA, Mamedov F, Styring S (2004) Quantification of Photosystem I and Photosystem II in Different Parts of the Thylakoid Membrane from Spinach. BBA 1608: 53-61

Diner B (1974) Cooperativity between Photosystem II Centers at the Level of Primary Electron Transfer. BBA 368: 371-385

Georgieva K, Roding A, Buchel C (2009) Changes of Some Thylakoid Membrane Proteins and Pigments upon Desiccation of the Resurrection Plant Haberlea Rhodopensis. J. Plant. Physiol. 166: 1520-1528

Giardi MT, Cona A, Geiken B, Kucera T, Masojidek J, Matoo AK (1996) Long-Term Drought Stress Induced Structural and Functional Reorganization of Photosystem II. Planta 199: 118-125

Kok B, Forbush B, McGloin M (1970) Co-Operation of Charges in Photosynthetic O_2 Evolution. I. A Linear Four Step Mechanism. Photochem. Photobiol. 11: 457-475

Krause GH, Weis E (1991) Chlorophyll Fluorescence and Photosynthesis. The Basis. Annu. Rev. Plant. Physiol. Plant Mol. Biol. 42: 313-339

Lavorel J (1976) An Alternative to Kok's Model for the Oxygen-Evolving System in Photosynthesis. FEBS Lett. 66: 164-167

Moore JP, Le NT, Brandt WF, Driouich A, Farrant JM (2009) Towards a System-Based Understanding of

Plant Desiccation Tolerance. Trends Plant Sci. 14: 110-117

M Stroch, V Spunda, I Kurasova (2004) Non-radiative Dissipation of Absorbed Excitation Energy within Photosynthetic Apparatus of Higher Plants. Photosynthetica 42: 323-337

Zeinalov Y (1982) Existence of Two Different Ways for Oxygen Evolution in Photosynthesis and Photosynthetic Unit Concept. Photosynthetica 16: 27-35

Zeinalov Y (2002) An Equipment for Investigations of Photosynthetic Oxygen Production Reactions. Bulg. J. Plant Physiol. 28: 57-67

Effect of Light on the Photosynthetic Activity during Desiccation of the Resurrection Plant *Haberlea Rhodopensis*

Katya Georgieva*, Snejana Doncheva, Gergana Mihailova, Snejana Petkova

Institute of Plant Physiology and Genetics, Bulgarian Academy of Sciences, Acad. G. Bonchev Str., Bl. 21, 1113 Sofia, Bulgaria.
*Corresponding author. Tel. No. +35929792611; Fax No. +35928739952; E-mail: katya@bio21.bas.bg.

Abstract: The effect of light during desiccation of the resurrection plant *Haberlea rhodopensis* on the photosynthetic activity and some morphological parameters was evaluated using plants growing at low or high irradiance in natural habitat. Chlorophyll content was not only lower in sun plants compared to shade plants, but it declined to a higher extent when desiccation was carried out at high light irradiance. Regardless of lower chlorophyll content in sun plants their photosynthetic activity (P_N) was about 30% higher compared to shade plants. However, during dehydration P_N declined more rapidly in sun plants. The mean leaf thickness of fully hydrated leaves from sun plants was larger when compared with shade plants, which was due to higher thickness of the mesophyll. Following rehydration plants rapidly recovered and P_N was higher by about 70% in sun than in shade plants. The results showed that the sun-exposed *Haberlea* plants exhibited good adaptation to desiccation under high irradiance.

Keywords: Desiccation; Leaf thickness; Photosynthesis; Resurrection plant

Introduction

Haberlea rhodopensis belongs to a small group of angiosperms, referred to as "resurrection plants" because they are capable of tolerating extremes of desiccation. It prefers shaded, northern, chiefly limestone slopes but can be found also on the sun-exposed rocks. Our previous investigations have shown that detached *Haberlea* leaves as well as whole plants were able to survive desiccation in the dark or at low irradiance (about 30 μmol m^{-2} s^{-1}) to water content below 10% with photosynthetic activity fully recovered after rehydration (Georgieva *et al*., 2005, 2007). However, it was found that these plants were very sensitive to photoinhibition (Georgieva and Maslenkova, 2006). Desiccation of shade-adapted plants at irradiance of 350 μmol m^{-2} s^{-1} PPFD induced irreversible changes in the photosynthetic apparatus, and leaves (except the youngest ones) did not recover after rehydration (Georgieva *et al*., 2008). The aim of the present study was to evaluate the effect of light during desiccation of *Haberlea* using plants growing at low or high irradiance in natural habitat. Changes in the photosynthetic activity and some morphological parameters were studied at different degrees of desiccation as well as after rehydration of plants.

Materials and Methods

Well-hydrated and naturally dried *Haberlea rhodopensis* plants growing on rocks below trees in deep shade (Bachkovo region) or sun exposed but briefly shaded by neighboring trees (Sitovo region) were studied. Adult rosettes of similar size and appearance were selected for the experiments. All measurements were conducted on fully expanded mature leaves from control (90% RWC), moderately (50% RWC), severely dehydrated plants (25% RWC) and dried leaves (8% RWC) as well as after 5 days of rehydration of dry plants. The RWC was determined gravimetrically by weighing *Haberlea* leaves before and after oven drying at 80 °C to a constant mass and expressed as the percentage of water content in

dehydrated tissue compared to water-saturated tissues, using the equation:

$$RWC\ (\%) = (m_{fresh} - m_{dry}) \times 100/(m_{saturated} - m_{dry})$$

The net photosynthetic rate (P_N) was measured at 500 μmol m^{-2} s^{-1} PPFD using a portable photosynthesis system LC*pro*+ (ADC BioScientific Ltd., Hertfordshire, UK). CO_2 assimilation (μmol CO_2 m^{-2} s^{-1}) and stomatal conductance (mmol m^{-2} s^{-1} PPFD) were calculated according to von Caemmerer and Farquhar (1981). Chlorophyll (Chl) *a*, chlorophyll *b* and total carotenoids were extracted from leaf disks with 80% acetone. The pigment content was determined spectrophotometrically according to Lichtenthaler (1987) and the data were calculated on a dry weight basis (80 °C for 48 h). Control and water stress treatments were statistically compared. Comparison of means from six measurements from different plants was done by the Student's *t* – test.

For ligh microscopy samples of the middle portion of fully hydrated and dehydrated leaves were fixed, dehydrated and embedded in Durcupan (Doncheva *et al*., 2009). Semithin sections (1 to 2 μm) were stained with fuchsine and methylene blue and examined under a light microscope Nikon Eclipse 50 (Tokyo, Japan) eqquiped with a video camera. Thickness of the leaf and mesophyll were measured in the 5 representative semithin cross sections. Thickness data were done using the ImageJ software (http://rsb.info.nih.gov/ij/)

Results and Discussion

Chlorophyll content slightly decreased upon desiccation of shade *Haberlea* plants and it was 20% lower in dried leaves (Fig. 1A). Chl content was not only lower in sun plants compared to shade plants, but it declined to a higher extent when desiccation was carried out at high light irradiance. Following rehydration Chl content recovered reaching the control values. The content of carotenoids decreased during dehydration of both shade and sun-adapted plants but recovered after rehydration (Fig. 1B).

Regardless of lower Chl content (13%, $p < 0.05$) in sunplants their photosynthetic activity (P_N) was about 30% higher compared to shade plants (Fig. 2A). Similarly to the net photosynthetic rate, stomatal conductance (gs) was also higher in well-watered sunny leaves (Fig. 2B).

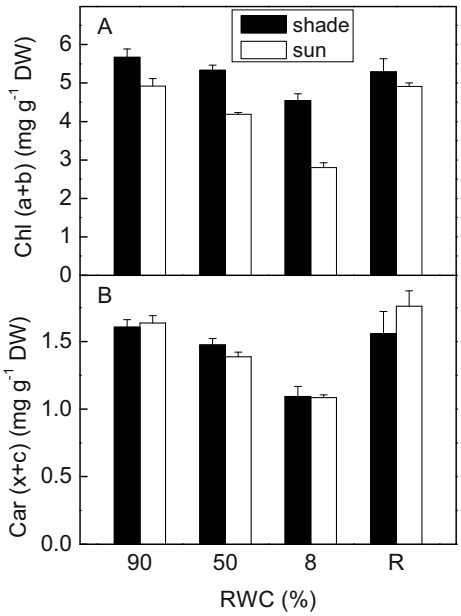

Fig. 1 Changes in chlorophyll (A) and carotenoid content (B) during dehydration and after 5 days of rehydration (R) of shade and sun *Haberlea rhodopensis*.

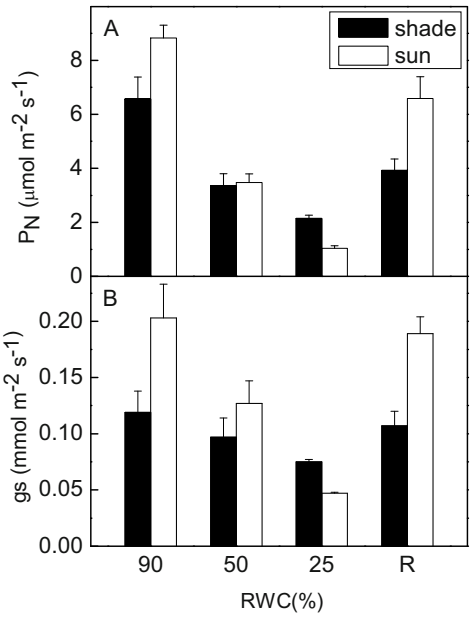

Fig. 2 Changes in CO_2 assimilation (P_N) and stomatal conductance (gs) during dehydration and after 5 days of rehydration (R) of shade and sun *Haberlea rhodopensis* plants. Mean of six measurements from different plants with standard error.

It has been shown that under high light conditions there are increases in the amounts of photosystems, electron transport, ATP synthase complexes, and enzymes of the Calvin–Benson cycle (Walters, 2005). Conversely, under low light there is an increase in the relative amounts of light-harvesting complexes and in the stacking of thylakoid membranes to form grana. It

is believed that these changes are of adaptive significance: an increase in photosynthetic capacity reduces susceptibility to photodamage, while changes in photosystem stoichiometry serve to optimize light utilization.

As a result of dehydration P_N declined more rapidly in sun plants and the values obtained were close to those in shade plants at 50% RWC (Fig. 2A). Moreover, when RWC dropped to 25%, CO_2 assimilation in sun plants was inhibited to a higher extent that in shade plants. The results showed that stomatal conductance measured in moderately desiccated plants (50% RWC) was reduced by 20% and 40% in shade and sun plants, respectively. On the other hand, gs was strongly inhibited in severely desiccated leaves (25% RWC) especially in sun plants. Stomatal control determines the rate of CO_2 assimilation and slows and minimizes the development of stress to the system over a range of RWC before metabolism is disrupted (Lawlor and Cornic, 2002). It has been shown that drought-induced decrease of leaf net CO_2 uptake observed in *Ramonda mykoni* (Schwab *et al*., 1989) and *Haberlea rhodopensis* (Peeva and Cornic, 2008) when RWC decline to 40% was strictly diffusion limited both by stomatal closure and a decrease in mesophyll conductance. The diffusion pathway through intercellular airspaces can be influenced by leaf thickness, cell shape, and packing relative to the position of stomata (Evans *et al*., 2009).

The mean leaf thickness of fully hydrated leaves from sun plants was larger when compared with shade plants (Fig. 3A), which was due to higher thickness of the mesophyll layer (Fig. 3B). The higher photosynthetic activity of well-watered sun plants could be due to the higher thickness of the mesophyll layer. C_3 leaves should have sufficient mesophyll surfaces occupied by chloroplasts to secure the area for CO_2 dissolution and transport because the affinity of Rubisco for CO_2 is low. To increase the mesophyll surface area, the leaf can either be thicker or have smaller cells (Terashima *et al*., 2006). Both leaf and mesophyll thickness decreased during desiccation (Fig. 3).

Following rehydration plants rapidly recovered and P_N was higher by about 70% in sun than in shade plants (Fig. 2A). The stomatal conductance also showed better recovery after rehydration of sun plants. The results showed that the sun-exposed *Haberlea* plants exhibited good adaptation to desiccation under high irradiance.

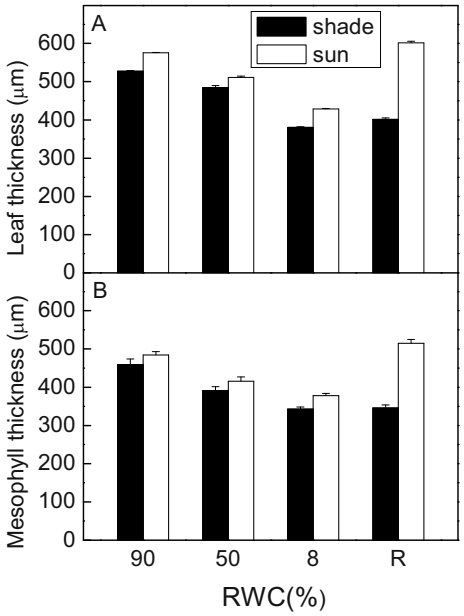

Fig. 3 Changes in leaf thickness (A) and mesophyll thickness (B) during dehydration as well as after 5 days of rehydration (R) of shade and sun *Haberlea rhodopensis* plants.

Acknowledgement

This work is supported by National Science Fund of Bulgaria under research project DO02-208/2008.

References

Doncheva S, Poschenrieder Ch, Stoyanova Z, Georgieva K, Velichkova M, Barceló J (2009) Silicon Ameliorates Manganese Toxicity in Mn-Sensitive Maize, but Is Not Responsible for Tolerance in a Mn-Tolerant Maize Genotype. Env. Exp. Bot. 65: 189-197

Evans JR, Kaldenhoff R, Genty B, Terashima I (2009) Resistances along the CO_2 Diffusion Pathway Inside Leaves. J. Exp. Bot. 60: 2235-2248

Georgieva K, Lenk S, Buschmann C (2008) Responses of the Resurrection Plant Haberlea Rhodopensis to High Irradiance. Photosynthetica 46: 208-215

Georgieva K, Maslenkova L (2006) Thermostability and Photostability of Photosystem II of the Resurrection Plant Haberlea Rhodopensis Studied by Chlorophyll Fluorescence. Z. Naturforsh. C. 61: 234-240

Georgieva K, Maslenkova L, Peeva P, Markovska Y, Stefanov D, Tuba Z (2005) Comparative Study on

the Changes in Photosynthetic Activity of the Homoiochlorophyllous Desiccation-Tolerant Haberlea Rhodopensis and Desiccation-Sensitive Spinach Leaves during Desiccation and Rehydration. Photosynth. Res. 85: 191-203

Georgieva K, Szigeti Z, Sarvari E, Gaspar L, Maslenkova L, Peva V, Peli E, Tuba Z (2007) Photosynthetic Activity of Homoiochlorophyllous Desiccation Tolerant Plant Haberlea Rhodopensis during Desiccation and Rehydration. Planta 225: 955-996

Lawlor DW, Cornic G (2002) Photosynthetic Carbon Assimilation and Associated Metabolism in Relation to Water Deficits in Higher Plants. Plant Cell Environ. 25: 275-294

Lichtenthaler KH (1987) Chlorophylls and Carotenoids: Pigments of Photosynthetic Biomembranes. Methods Enzymol. 148: 350-382

Peeva V, Cornic G (2009) Leaf Photosynthesis of Haberlea Rhodopensis before and during Drought. Environ. Exp. Bot. 65: 310-318

Schwab KB, Schreiber U, Heber U (1989) Response of Photosynthesis and Respiration of Resurrection Plants to Desiccation and Rehydration. Planta 177: 217-227

Terashima I, Hanba YT, Tazoe Y, Vyas P, Yano S (2006) Irradiance and Phenotype: Comparative Eco-Development of Sun and Shade Leaves in Relation to Photosynthetic CO_2 Diffusion. J. Exp. Bot. 57: 343-354

von Caemmerer S, Farquhar GD (1981) Some Relationships between the Biochemistry of Photosynthesis and the Gas Exchange of Leaves. Planta 153: 376-387

Walters RG (2005) Towards an Understanding of Photosynthetic Acclimation. J. Exp. Bot. 56: 435-447

Effect of Desiccation of the Resurrection Plant *Haberlea Rhodopensis* at High Temperature on the Photochemical Activity of PSI and PSII

Gergana Mihailova*, Snejana Petkova, Detelin Stefanov, Katya Georgieva

Institute of Plant Physiology and Genetics, Bulgarian Academy of Sciences, Acad. G. Bonchev Str., Bl. 21, 1113 Sofia, Bulgaria.
*Corresponding author. Tel. No. +359 2 979 2688; Fax No. +359 2 8739952; E-mail: gkm_rw@abv.bg.

Abstract: Changes in the photochemical activity of the homoiochlorophyllous poikilohydric plant *Haberlea rhodopensis* under dehydration at high temperature was investigated. Plants, growing under low irradiance in their natural habitat, were desiccated to air-dry state at a similar light intensity (about 30 μmol m^{-2} s^{-1} PPFD) under optimal (23/20 °C) or high (38/30 °C) day/night temperature. Water deficit reduced photochemical activity of PSII and PSI. The results showed that desiccation of *Haberlea rhodopensis* at high temperature had more limiting effects than desiccation at optimal temperature. However, the damage was limited to a level where repair was still possible and thus plants fully recovered after 7 days of rehydration.

Keywords: Chlorophyll fluorescence; Drought stress; Haberlea rhodopensis; High temperature; Photosynthesis

Introduction

Most higher plants are unable to survive desiccation to an air-dried state but a small group of angiosperms known as poikilohydric or resurrection plants can tolerate extreme dehydration and some are even able to equilibrate the leaves with air to 0% (v/v) relative humidity and then regain normal function after rehydration (Gaff, 1971). Resurrection plants may be subdivided into two groups: homoiochlorophyllous desiccation tolerant plants (HDT), which retain their chlorophyll during drying and poikilochlorophyllous desiccation tolerant plants (PDT), which lose chlorophyll on drying (Tuba, 1998). Drought stress is known to inhibit photosynthetic activity of the plants due to an imbalance between light capture and its utilization (Foyer and Noctor, 2000). Under natural conditions drought is often accompanied by high temperature, which has a strong impact on the vitality of plants. Important high temperature effects on photosynthesis are the inactivation of thylakoid membrane reactions and damage to the enzymes involved in photosynthetic carbon metabolism (Berry and Björkman, 1980). *Haberlea rhodopensis* Friv. (Gesneriaceae) is a rare resurrection plant of the northern hemisphere, originating from the Balkan Peninsula as an endemic and relict species of the Tertiary period. It is considered as a homoiochlorophyllous resurrection plant, since it preserves its chlorophyll content during dehydration. *Haberlea* grows in regions with severe water scarcity and simultaneous high temperature. The aim of the present study was to investigate the effect of high temperature during desiccation on the photochemical activity of PSI and PSII.

Materials and Methods

Well-hydrated *Haberlea rhodopensis* plants were collected from their natural habitat where they grow on rocks below trees under very low irradiance. Plants were subjected to drought stress by withholding irrigation either at 23/20 °C or 38/30 °C day/night temperature, irradiance of 30 μmol m^{-2} s^{-1} PPFD, 12 h photoperiod, and relative humidity of 60%. After desiccation to air-dry state, the plants were rehydrated. Control plants, kept at 23/20 °C or 38/30 °C were regularly watered during the experiment. The relative water content (RWC) of *Haberlea* leaves was determined gravimetrically by weighing them before and after oven drying at 80 °C to a constant mass and

expressed as the percentage of water content in dehydrated tissue compared to water-saturated tissues, using the equation:

$$RWC\ (\%) = (m_{fresh} - m_{dry}) \times 100/(m_{saturated} - m_{dry})$$

Chlorophyll fluorescence emission from the upper leaf surface was measured with a pulse amplitude modulation fluorometer (PAM 101–103, Walz, Effeltrich, Germany). Induction kinetics were registered and analyzed with a program FIP 4.3, written by Tyystjarvi and Karunen (1990). The redox state of P700 was monitored *in vivo* as 810/860 nm absorption changes. A Walz ED 700DW-E emitter/detector unit was connected to a PAM 101E main control unit (Klughammer and Schreiber, 1998). Leaf absorbance changes at 810 nm were measured as a function of increasing fluence rates of far-red light (FR) to calculate a 'saturation constant', *K*s, representing the far-red irradiance at which half of the maximum absorbance change ($\Delta A_{810max}/2$) was reached. Far-red intensities were varied in 11 steps. The value of *K*s was determined by Barth *et al.* (2001). The correlation coefficient *r* for linear regression was between 0.96 and 1.00. Control and water stress treatments were statistically compared. Comparison of means from six separate experiments, each in three replications was done by the Student *t* – test.

Results and Discussion

The maximum quantum efficiency of PSII photochemistry, estimated by the ratio F_v/F_m (Fig. 1), gradually decreased with increasing the degree of water loss and it was significantly reduced at 20% RWC ($p < 0.001$). Desiccation of *Haberlea* plants at high temperature reduced the photochemical activity of PSII more compared to dehydration at optimal temperature. Exposure of plants to 38 °C lowered the ratio F_v/F_m by 20%. However, the PSII activity quickly recovered after rehydration.

The signal difference ΔA_{810max} served as a relative measure for the photochemical capacity of PSI, in the following termed 'potential PSI activity' (Harbinson and Woodward, 1987; Weis and Lechtenberg, 1989). The P700 oxidation rose with increasing the far-red light intensities in *Haberlea* leaves dehydrated to 50% RWC and it was stronger when the dehydration was carried out at 38 °C. The PSI activity was inhibited when RWC dropped to 10% (Fig. 2).

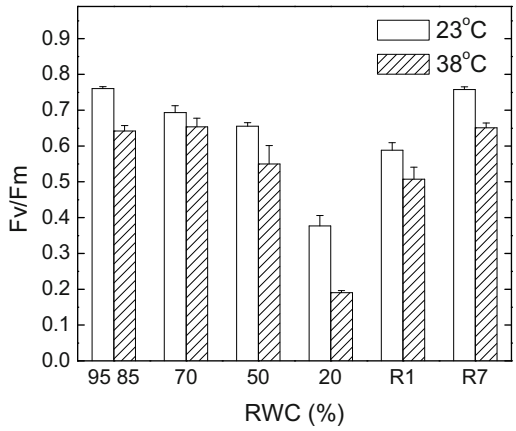

Fig. 1 Changes in maximum quantum efficiency of PSII (F_v/F_m) during dehydration and after 1 day (stage R1) and 7 days (stage R7) of rehydration of *Haberlea rhodopensis* at optimal (23 °C) and high (38 °C) temperature.

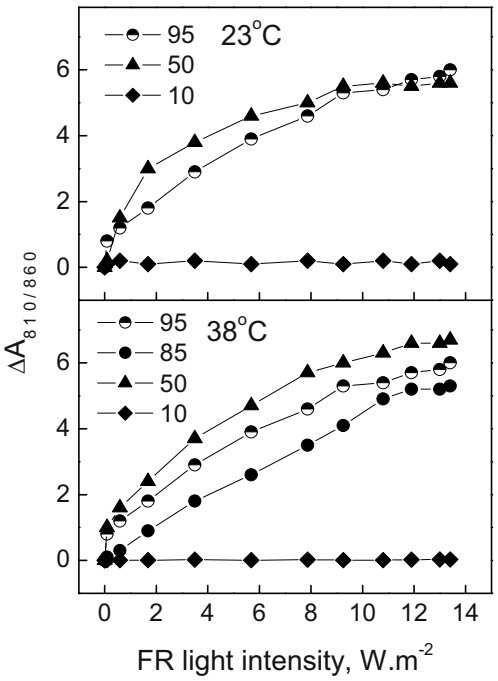

Fig. 2 Changes in the absorbtion of P700 during dehydration of *Haberlea rhodopensis* at optimal (23 °C) and high (38 °C) temperature.

High temperature treatment did not influenced significantly ΔA_{810max}, but slower enhancement to steady-state levels of A810 in light curves was observed (Fig. 2). Therefore saturation constant *Ks* was calculated from light curves of A810. The values of *Ks*, declined in the course of dehydration but they were higher in plants, treated with high temperature except the plants desiccated to 10% RWC (Fig. 3).

The decrease in *K*s observed upon desiccation indicated that lower far-red light intensity was required to oxidize P700. The significantly lower *K*s measured after desiccation could be explained by smaller LHCI cross-section and/or lower rate of charge recombination reactions between oxidized P700 and reduced acceptors (Barth *et al.*, 2001) in desiccated state. The results observed could also reflect alterations in optical properties of the desiccated leaves. The investigation of leaf absorbance in the far red region (ΔA810) excited by far red light (> 715 nm) reflected P700 oxidation because PSII was not activated by FR light and linear electron transport in thylakoid membranes of chloroplasts was not induced. Light scattering in leaves is largely determined by the intercellular air spaces (Evans *et al.*, 2004). Scattering is determined by changes in refractive index between air and cytoplasm of the cells. Leaf desiccation caused a wilting of the leaves and reduced volume of intercellular spaces that influenced the leaf absorption properties. Consequently, desiccation of leaves led to changes in the mesophyll tissues inducing a decrease in light scattering and hence a decrease in probability for light capture by P700, *i.e.*decreased far red leaf absorption.

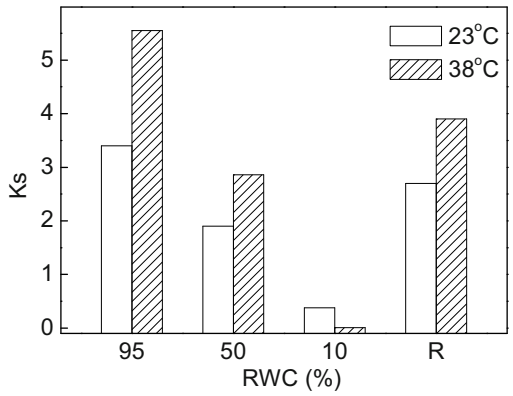

Fig. 3 Changes in the saturation constant of P700, *Ks*, during dehydration of *Haberlea* plants at optimal (23 °C) and high (38 °C) temperature.

On the other hand, higher values of *Ks* in high temperature treated plants reflected accelerated PSI activity at such conditions.

The decline in PSII and PSI activity in severely desiccated leaves could represent a protective mechanism from toxic oxygen production in order to maintain the membrane integrity and to ensure protoplast survival (Havaux and Davaud, 1994; Di Blasi *et al*., 1998). Additionally, the decline observed in F_v/F_m can be rather a regulatory adjustment to limiting carbon availability, imposed by water stress (Saccardy *et al*., 1998).

The results showed that desiccation of *Haberlea rhodopensis* at high temperature had more limiting effects than desiccation at optimal temperature. However, the damage was limited to a level where repair was still possible and thus plants fully recovered after rehydration.

Acknowledgement

This work is supported by National Science Fund of Bulgaria under research project DO02-208/2008.

References

Barth C, Krause G, Winter K (2001) Responses of Photosystem I Compared with Photosystem II to High-Light Stress in Tropical Shade and Sun Leaves. Plant, Cell and Environ. 24: 163-176

Berry JA, Björkman O (1980) Photosynthetic Response and Adaptation to Temperature in Higher Plants. Annu. Rev. Plant Physiol. 31: 491-543

Di Blasi S, Puliga S, Losi L, Vazzana C (1998) S. Stapfianus and E. Curvula cv. Consol in Vivo Photosynthesis, PSII Activity and ABA Content during Dehydration. Plant Growth Regul. 25: 97-104

Evans J, Vogelmann T, Williams W, Gorton H (2005) Sunlight Capture; Chloroplast to Leaf. In: Smith W, Vogelman T, Critchley C (eds.), Photosynthetic Adaptation: Chloroplast to Landscape. Springer, pp. 15-41

Gaff DF (1971) Desiccation Tolerant Flowering Plants in Southern Africa. Science 174: 1033-1034

Harbinson J, Woodward F (1987) The Use of Light-Induced Absorbance Changes at 820 nm to Monitor the Oxidation State of P-700 in Leaves. Plant, Cell & Environ. 10: 131-140

Havaux M, Davaud A (1994) Photoinhibition of Photosynthesis in Chilled Potato Leaves Is Not Correlated with a Loss of Photosystem-II Activity. Photosynth. Res. 40: 75-92

Klughammer C, Schreiber U (1998) Measuring P700 Absorbance Changes in the Near Infrared Spectral

Region with a Dual Wavelength Pulse Modulation System. In: G Garab (ed.), Photosynthesis: Mechanisms and Effects. v. V, pp. 4357-4360

Noctor G, Foyer CH (1998) Ascorbate and Glutathione: Keeping Active Oxygen under Control. Annu Rev. Plant Physiol. Plant Mol. Biol. 49: 249-279

Saccardy K, Pineau B, Roche O, Cornic G (1998) Photochemical Effiency of Photosystem II and Xanthophyll Cycle Components in Zea Mays Leaves Exposed to Water Stress and High Light. Photosynth. Res. 56: 57-66

Tuba Z (1998) Ecophysiological Responses of Homoiochlorophyllous and Poikilochlorophyllous Desiccation Tolerant Plants: a Comparison and an Ecological Perspective. Plant Growth Regul. 24: 211-217

Tyystjarvi E, Karunen J (1990) A Microcomputer Program and Fast Analog to Digital Converter Card for the Analysis of Fluorescence Induction Transients. Photosynth. Res. 26: 27-132

Weis E, Lechtenberg D (1989) Fluorescence Analysis during Steady-State Photosynthesis. Philosophical Transactions of the Royal Society, London B 323: 253-268

Chloroplast Structure under High Light Conditions

Radosław Mazur[a], Łucja Rudowska[b], Borys Kierdaszuk[c], Agnieszka Mostowska[b], Maciej Garstka[a*]

[a]Department of Metabolic Regulation, [b]Department of Plant Anatomy and Cytology, Faculty of Biology, University of Warsaw, Miecznikowa 1, PL-02-096 Warsaw, Poland;
[c]Department of Biophysics, Faculty of Physics, University of Warsaw, Zwirki i Wigury 93, PL-02-089 Warsaw, Poland.
[*]Corresponding author. Tel. No. +48 22 5543215; Fax No. +48 22 5543223; E-mail: garstka@biol.uw.edu.pl.

Abstract: Changes of entire chloroplast structure under high light intensity in pea (*Pisum sativum*) and bean (*Phaseolus vulgaris*) plants were investigated. These two plant species were chosen because they have different chlorophyll-protein (CP) complexes organization within thylakoid membranes which determines distinct chloroplast structure. Thylakoid membranes organization was revealed by confocal laser scanning microscopy (CLSM) and transmission electron microscopy (TEM). Arrangement of CP complexes was analyzed by low temperature (120 K) fluorescence emission spectra of thylakoid membranes. Experiments showed that high light induced reorganization of the chloroplast structure was similar in pea and bean but different rearrangements of CP complexes was observed.

Keywords: Bean; Chloroplast structure; Confocal Laser Scanning Microscopy; High light; Pea

Introduction

Thylakoids, chloroplasts inner membrane system, are divided into two main structural domains: appressed regions, called grana, composed of stacks of membranes and non-appressed ones, called stroma thylakoids, which are interconnected with grana. This type of spatial organization is achieved by separation of main photosynthetic chlorophyll-protein (CP) complexes between these two areas. PSII and LHCII are present mainly in grana whereas PSI and LHCI in non-appressed membranes (Dekker and Boekema, 2005).

CP complexes are ordered into higher level structures which enable dynamic reorganization of photosynthetic membranes during acclimation of plants to variable light conditions (Chuartzman *et al*., 2008) or abiotic stress (Garstka *et al.*, 2005; Garstka *et al.*, 2007). These rearrangements of chlorophyll-protein complexes, which lead to changes in overall chloroplast structure, are crucial for maintaining optimal photosynthetic capacity.

In present work we examined changes in chloroplasts structure of two plant species: pea and bean grown under high light intensity.

Materials and Methods

Plants were grown in a perlite-containing pots in a controlled environment at 22/20 °C day/night during a 16 h photoperiod at a photosynthetic active radiation of 200 (medium light, ML) or 800 (high light, HL) μmol photons m^{-2} s^{-1}. Fully expanded leaves of 20 days old pea (*Pisum sativum*) and 10 days old bean (*Phaseolus vulgaris*) were used in all experiments.

Isolated intact chloroplasts (Rumak *et al.*, 2010) were placed on a poly-L-lysine layer and immobilized on a microscopic glass. Samples were imaged using Zeiss LSM 510 confocal laser scanning fluorescence microscope equipped with a PlanApo 63 x, NA 1.4 objective lens. Excitation was performed at 543 nm and fluorescence emission was collected through a 560 nm long pass filter. Z-series of 1024 × 1024 pixels and 8 bit images were collected and data stacks were

deconvolved using AutoQuant X2 software (Media Cybernetics, U.S.A.). Leaves for transmission electron microscopy (TEM) were fixed in glutaraldehyde and post-fixated in osmium tetroxide (OsO_4), prepared in cacodylate buffer. Tissue was dehydrated in growing concentrations of acetone and embedded in a low viscosity epoxy resin. Sections stained with uranyl acetate and lead citrate were examined with a JEM1400 (Jeol Co. Japan) electron microscope. Fluorescence emission spectra of isolated thylakoids at 120 K were determined as previously described (Rumak *et al*., 2010). In order to determine the differences in relative contribution of specific chlorophyll-protein complexes in pea and bean thylakoids, fluorescence emmission spectra of the thylakoids were normalized to the same area (100) under the spectrum (Andreeva *et al.*, 2003).

Results and Discussion

Effect of high light on structure of pea and bean chloroplast revealed by CLSM and TEM

Numerous bright fluorescent spots of ~500 nm diameter separated by dark spaces (Fig. 1a) were revealed by CLSM in pea chloroplasts cultivated in medium light conditions. These fluorescent regions correspond mainly to appressed domains of thylakoid membranes. In bean chloroplasts (Fig. 1b) smaller and not so clearly separated from each other fluorescence areas can be observed. Under high light conditions chloroplast structure of both examined species has dramatically changed (Figs. 1c and 1d). It is still possible to distinguish regions corresponding to separate grana structures but recorded fluorescence signals are blurred and three dimensional network of thylakoid membranes is highly disturbed by large irregular dark spaces (Figs. 1c and 1d). Moreover, pea and bean chloroplasts from high light cultivation are smaller than chloroplasts isolated from plants grown under medium light intensity.

For better characterization of changes in chloroplast structure under high light intensity transmission electron microscopy (TEM) analysis was performed. TEM images of pea chloroplasts from ML conditions showed large grana stacks which are clearly separated from one another and connected by stroma thylakoids (Fig. 2a). In bean grana structures are smaller and less stacked (Fig. 2b) and bean chloroplasts contain considerably more stroma thylakoids and plastoglobules structures than pea ones. TEM pictures of chloroplasts of pea (Fig. 2c) and bean (Fig. 2d) plants taken from HL conditions show large starch grains, corresponding to large dark regions at CLSM pictures (cf. Fig. 1), which occupy most of space inside chloroplasts and push aside thylakoid membranes. Observed grana structures are twisted and oriented in different plains (Figs. 2c and 2d), whereas in medium light they are ordered paralelly to one another (Figs. 2a and 2b). High light induce also appearance of large and electron dense plastoglobules, especially in pea chloroplasts (Fig. 2c).

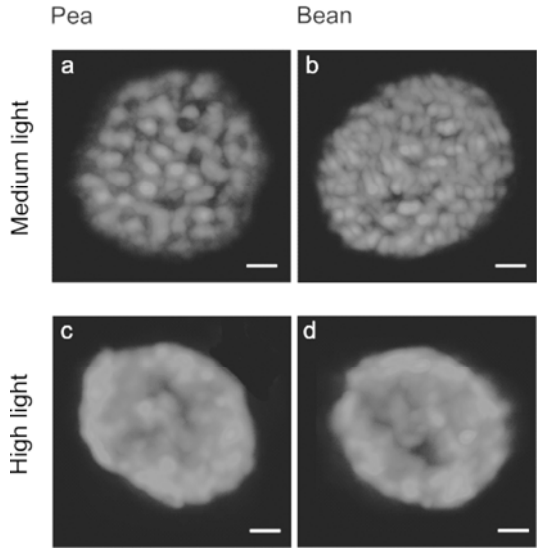

Fig. 1 Chlorophyll fluorescence of intact pea (a, c) and bean (b, d) chloroplasts from plants grown under medium (a, b) and high (c, d) light intensities revealed by CLSM microscopy. Bar = 2 μm.

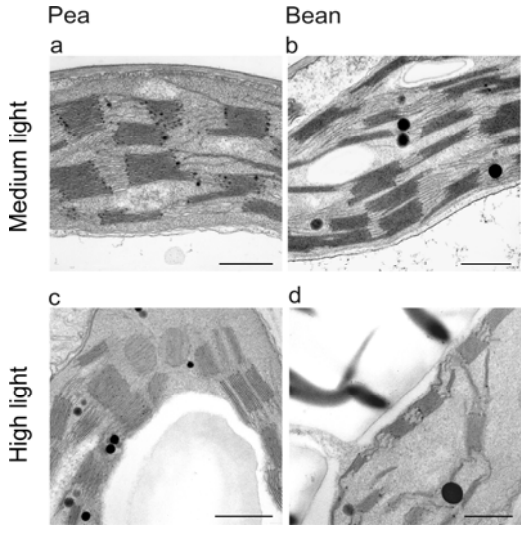

Fig. 2 Images of chloroplast from mesophyll cells of pea (a, c) and bean (b, d) from plants grown under medium (a, b) and high (c, d) light intensity revealed by TEM microscopy. Bar = 500 nm.

Effect of high light cultivation on relative contribution of specific CP complexes to an overall fluorescence pattern at 120 K of isolated pea and bean thylakoids

For investigation how high light inducing dis-organization of pea and bean thylakoid membranes is related to composition of CP complexes low temperature (120 K) steady-state fluorescence emission spectra were recorded. This method enables the detection of the relative contribution of individual CP complexes to the chlorophyll (Chl) fluorescence in thylakoid membranes.

Fluorescence emission spectra of pea thylakoids isolated from ML and HL leaves exhibited fluorescence maxima at similar wavelengths (682 and 733 nm) related to LHCII-PSII and LHCI-PSI complexes, respectively (Fig. 3a). Spectra calculated as a difference between normalized spectra of thylakoids from HL leaves and those obtained from ML leaves exhibited small positive band at 676 and significant negative band at 685 nm (Fig. 3b). These data suggested that there is a blue shift of Chl species and the decrease in the relative abundance of external antennas in HL thylakoids. Emission spectra of thylakoids isolated from bean ML and HL leaves showed fluorescence maxima at the same wavelength (683 and 737 nm) (Fig. 3c). However, the difference

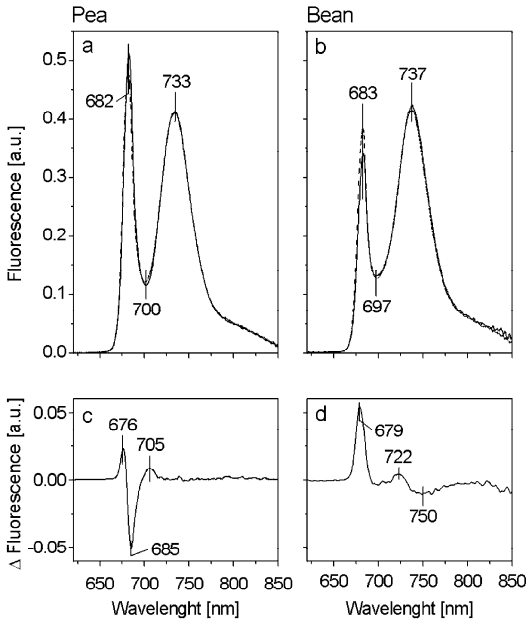

Fig. 3 120 K fluorescence emission spectra excitated at 470 nm of isolated pea (a) and bean (b) thylakoids from ML leaves (solid lines) and HL leaves (dashed lines). Fluorescence emission-difference spectra for thylakoids from HL leaves relative to that of ML leaves for pea (c) and bean (d). Samples were excited at 470 nm.

spectrum exhibited positive band at 681 nm and slight negative shoulder around 750 nm (Fig. 3d). These data suggested that relatively more Chl *b*-rich external antennae are associated with PSII in HL than in ML bean thylakoids. Moreover, the bean cultivation at high light induced a certain shift of Chl fluorescence from LHCI-PSI (F750) to LHCII-PSII (F681).

Fluorescence analysis indicated opposing effect of high light conditions on arrangement of chlorophyll-protein complexes in pea and bean thylakoids. The decrease of LHCII-PSII complexes in pea versus the increase of abundance of LHCII-PSII and LHCII complexes in bean probably indicate different protective mechanisms against excess of a light in these two species. However, those different spectral observations are related to the same changes in thylakoid structure inside chloroplasts. It means that reorganization of thylakoid network induced by high light is determined by more factors.

Acknowledgements

This work is supported by Polish Ministry of Science and Higher Education Grant N N303 4185 33.

TEM images were performed in the Laboratory of Electron Microscopy, Nencki Institute of Experimental Biology on JEM 1400 (JEOL Co. Japan) electron microscope. This equipment was installed within the project sponsored by the EU Structural Funds: Centre of Advanced Technology BIM – Equipment purchase for the Laboratory of Biological and Medical Imaging.

References

Andreeva A, Stoitchkova K, Busheva M, Apostolova E (2003) Changes in the Energy Distribution between Chlorophyll-Protein Complexes of Thylakoid Mem-Branes from Pea Mutants with Modified Pigment Content. I. Changes Due to the Modified Pigment Content. J Photochem Photobiol B 70: 153-162

Chuartzman SG, Nevo R, Shimoni E, Charuvi D, Kiss V, Ohad I, Brumenfeld V, Reich Z (2008) Thylakoid Membrane Remodeling during State Transitions in Arabidopsis. Plant Cell 20: 1029-1039

Dekker JP, Boekema EJ (2005) Supramolecular

Organization of Thylakoid Membrane Proteins in Green Plants. Biochim Biophys Acta 1706: 12-39

Garstka M, Drożak A, Rosiak M, Venema JH, Kierdaszuk B, Simeonova E, van Hasselt PR, Dobrucki J, Mostowska A (2005) Light-Dependent Reversal of Dark-Chilling Induced Changes in Chloroplast Structure and Arrangement of Chlorophyll-Protein Complexes in Bean Thylakoid Membranes. Biochim Biophys Acta 1710: 13-23

Garstka M, Venema JH, Rumak I, Gieczewska K, Rosiak M,·Kozioł-Lipińska J, Kierdaszuk B,·Vredenberg WJ, Mostowska A (2007) Contrasting Effect of Dark-Chilling on Chloroplast Structure and Arrangement of Chlorophyll-Protein Complexes in Pea and Tomato: Plants with a Different Susceptibility to Non-Freezing Temperature. Planta 226: 1165-1181

Rumak I, Gieczewska K, Kierdaszuk B, Gruszecki WI, Mostowska A, Mazur R, Garstka M (2010) 3-D Modelling of Chloroplast Structure under (Mg2+) Magnesium Ion Treatment. Relationship between Thylakoid Membrane Arrangement and Stacking. Biochim Biophys Acta 1797: 1736-1748

Effect of Salinity on Chlorophill Content and Activity of Photosystems of Wheat Genotypes

Ibrahim Azizov, Mayaxanum Khanisheva, Ulker Ibrahimova

Institute of Botany of Azerbaijan Naional Academy of Sciences, Patamdar shosse,40, Baku, Azerbaijan, AZ 1073.
E-mail: i.azizov@rambler.ru.

Abstract: The genotypes of wheat were grown in field conditions of Apsheron Peninsula and Akhsu region under salinity (1.5%) soil conditions. The summary of the analysis of variance for the biometrical parameters studied during onthogenesis of wheat showed that salinity stress had adverse effects not only on the biomass yield, leaf area and other morphological parameters, but also on photosynthetic pigments and photochemical activity of chloroplasts. Salt stress reduced plant growth of all wheat genotypes, but the genotypes Barakhatli, Giymatli and Azamatli were characterized as the most salt-tolerant. Decrease in activity of PS II of genotypes Barakhatli, Azamatli-95 and Giymatli 2/17 was less than genotypes Garagilchig-2 Girmizigul-1, Ruzi-84, Nurlu-99, Alinja-84 . Salt stress led to a block of electron flow between primary and secondary electron acceptors of PS II. Our results suggest that the genotypes of wheat Barakhatli, Giymatli 2/17 and Azamatli-95 are more tolerant to salinity and they could be used as a physiological markers during the screening for salt tolerance.

Keywords: Wheat genotypes; Salinity; Chlorophyll; PSI; PSII; Tolerance

Introduction

Soil salinity is one of the major constraints responsible for low agriculture production in many regions of Azerbaijan. Out of total hectares irrigated land, 1.3 million hectares are salt affecting. The major inhibitory effect of salinity on plant growth and yield has been attributed to osmotic effect, ion toxicity and nutritional imbalance leading to reduction photosynthetic efficiency and other physiological disorders. Adverse effects of salinity on seed germination and seedling growth as well as some physiological activities of cultivated plant species have been investigated (Ali Y *et al.*, 2001; Ashraf M *et al.*, 1997; Everard JD *et al.*, 1994; Khan AN *et al.*, 1995; Lutts S *et al*., 1996). Generally, the trend and magnitude of adverse changes varied with in species and genotypes according to the level of salinity. So far little emphasis has been placed on aspects relevant to photosynthetic efficiency crop production could be increased (Aliyev JA *et al.*, 1988). The aim of the present investigation is to provide information on the effect of salinity on chlorophyll concentration and photochemical activity of chloroplasts of wheat genotypes to see if there is any correlation between these variables.

Materials and Methods

The study was conducted during the years 2006–2009 in naturally salinized privately owned farm of Akhsu region of Azerbaijan. The experimental material comprised of twenty genotypes of wheat, which was also grown in normal soil, simultaneously. Chlorophyll (a, b and total) concentration of leaves were determined according to Arnon (Arnon DJ, 1949). The isolation medium for chloroplasts contained 400 mmol sucroze, 1 mmol EDTA, 5 mmol $MgCl_2$, 10 mmol NaCl and 50 mmol tris-HCl buffer, pH 7.8. Photochemical activity of chloroplasts were measured by monitoring oxygen evolving activity at 25 ^{o}C with a Clark type oxygen electrode in presence of 0.5 mmol potassium ferrycianide as acceptor of electrons from PS II (Aliyev JA *et al.*, 1988; Lu CM *et al.*, 1996). Uncoupled PSI driven electron transport was assayed with 5 mmol ascorbate using 50 mmol DCPIP as

electron donor in the presence of 10 mmol DCMU, 200 mmol MV as electron acceptor, 1 mmol NaN_3 and 5 mmol NH_4Cl.

Results and Discussion

Leaf dry weight, leaf area and yield per plant decreased significantly in response to salinity in all wheat genotypes. The biosynthesis of green pigments (chlorophyll a, b and carotenoids) also was affected with salinity stress (Table1).

The genotypes of wheat Qirmizi-gul, Pirshahin, Vugar-80, Shiraslan—23 and Dagdash showed maximum percent reduction over control for chlorophyll total concentration and were graded as sensitive to salinity stress. The genotypes of wheat Qiymatly 2/17, Nurlu, Qobustan, Saratovskaya-29, Akinchy 84, Azamatly and Qirmizi bugda showed minimum reduction in chlorophyll concentration and were graded as salt tolerant. Decrease in activity of PS II of genotypes Barakhatli, Azamatli-95 and Giymatli 2/17 was less than genotypes Garagilchig-2 Girmizigul-1, Ruzi-84, Nurlu-99, Alinja-84 . Salt stress led to a block of electron flow between primary and secondary electron acceptors of PS II (Table 2). The cyclic electron flow around PS I enhanced during salt stress in all genotypes of wheat. The observed increase in PS I activity is probably induced, according to other researchers, by the necessity to maintain ATP pool via cyclic photophosphorilation for Na extrusion from cytoplasm. Similar effects of salt stress on PS I activity have been observed in cyanobacters. Reduction of chlorophyll contetunder elevated salinity conditions were observed for some salt-sensitive plant species (Define *et al*., 1999; Ashraf *et al*., 2000; Jungkland *et al*., 2003; Lee *et al*., 2004). The decrease of chlorophyll content was dependent on the salinity level, the time of exposure to salts and the species. In contrast, Cl content in salt—tolerant plants does not decline or else rises with increasing salinity(Brugnoli and Bjorkman, 1992; Qui *et al*., 2003). According to Yeo and Flowers (1983) and Shiler B. *et al.* (2007), chlorophyll concentration can be used as a sensitive indicator of the celluar metabolic state.

Thus, our results suggest that the genotypes of wheat Barakhatli, Giymatli 2/17 and Azamatli-95 are more tolerant to salinity and they could be used as a physiological markers during the screening for salt tolerance.

Table 1 Effect of salinity on content of chlorophyll and carotenoids of different wheat genotypes, grown under normal and salinity environments (mg/g leaf).

Genotypes	Chlorophyll a		Chlorophyll b		Chlorophyll (total)		Carotenoids	
	control	salinity	control	salinity	control	salinity	control	salinity
Akinchy-84	5.4	4.4	1.8	1.5	7.2	5.9	1.8	1.9
Garagylchyg2	6.2	4.5	2.1	1.5	8.3	6.0	1.9	2.1
Vugar-80	5.6	4.1	1.9	1.1	7.5	5.2	1.7	1.9
Shiraslan-23	5.8	3.9	2.0	1.0	7.8	4.9	1.6	1.8
Barakatly	6.1	4.2	2.1	1.4	8.2	5.6	2.0	2.2
Alindje-84	5,1	3.5	1.7	1.2	6.8	4.7	1.5	1.7
Terter	6.2	3.8	2.2	1.3	8.4	5.1	1.8	2.0
Gobustan	6.3	5.6	2.1	1.8	8.4	7.4	2.1	2.2
Nurlu-99	5.9	5.5	1.9	1.8	7.8	7.3	1.9	2.1
Giymatly 2/17	6.8	6.2	2.3	2.1	9.1	8.3	2.3	2.5
Pirshahin	4.9	2.8	1.3	0.9	6.2	3.7	1.4	1.7
Gyrmyzygul	4.8	2.6	1.4	0.8	6.2	3.4	1.5	1.8
Azamatly-95	5.4	5.0	1.7	1.5	7.1	6.5	1.8	2.0
Ruzi-84	6.1	3.5	2.0	1.1	8.1	4.6	1.7	1.9
Taleh-38	6.0	3.3	2.0	1.2	8.0	4.5	1.5	1.7
Saratovskaya-29	5.1	4.9	1.7	1.6	6.8	6.5	1.4	1.5
Dagdash	5.4	2.7	1.8	0.9	7.2	3.6	1.7	2.0
Sharg	6.3	2.9	2.1	0.9	8.4	3.8	1.8	2.1
Gyrmyzy bugda	5.4	5.0	1.7	1.6	7.1	6.6	1.9	2.1
FEFWSN-4thNo ^{16}	4.6	3.5	1.8	1.1	6.4	4.6	1.2	2.0

Table 2 Effect of salinity on activity of PS II and PS I of chloroplasts, isolated from wheat genotypes grown under normal and saline environment (mkmol O_2/mg chl h).

Genotypes	PS II activity		PS I activity	
	control	salinity	control	salinity
Akinchy-84	85±2.1	79±1.2	125±5.4	119±3.2
Garagiltshig	92±4.3	80±3.1	136±6.2	115±2.6
Vugar-80	89±3.2	75±2.2	129±4.5	110±3.4
Shiraslan-23	95±5.4	76±1.4	141±7.2	112±4.6
Barakatly	98±4.5	79±1.1	152±6.6	125±4.5
Alindje-84	82±1.3	70±1.5	123±5.7	99±3.2
Terter	77±2.1	50±1.0	115±6.1	90±2.6
Gobustan	91±3.3	85±2.1	130±5.8	125±5.4
Nurlu-99	94±4.4	83±1.9	129±4.6	120±4.3
Giymatly 2/17	99±5.6	85±1.7	133±3.5	126±6.2
Pirshahin	87±2.7	60±2.1	109±2.9	90±3.4
Girmizigul	81±1.2	59±1.8	95±3.4	70±5.6
Azamatly-95	105± 3.9	95±1.5	150±5.5	130±6.4
Ruzi-84	93±2.2	70±2.2	110±4.2	95±3.2
Taleh-38	87±1.5	60±0.8	95±4.3	70±2.1
Saratovskaya-29	96±4.1	90±1.6	121±3.5	109± 6.1
Dagdash	87±2.4	60±1.9	98±2.8	71±2.3
Sharg	102± 4.1	85±2.2	135±5.4	95± 3.4
Girmizi bugda	105± 6.2	90±3.1	131±5.1	120±5.6
FEFWSNth№16	98±4.3	70±2.5	116± 4.4	100±4.2

References

Aliyev JA, Azizov IV, Khazibekova EG (1988) Photosynthetic Ability and Development of Chloroplast in Ontogenesis of Wheat. Elm Baku 115

Ali Y, Aslam Z, Ashraf MY, Tahir GR (2004) Effect of Salinity on Chlorophyll Concentration, Leaf Area, Yield and Yield Components of Rice Genotypes Grown under Saline Environment. International Journal of Environmental Science & Technology 3: 221-225

Arnon DJ (1949) Copper Enzyme in Isolated Chloroplasts.I.Poliphenoloxidaze in Beta Vulgaris Plant Physiology 24: 1-15

Ashraf M, Khanum A (1997) Relationship between Ion Accumulation and Growth in Two-Spring Wheat Line Differing in Salt Tolerance of Different Grow Stages. J. Agron. Crop. Sci.178: 39-50

Ashraf M, Karim F, E Rasul (2000) Interacive Effects of Gibberlik Acid (GA_3) and Salt Stress on Growth, Ion Accumulation and Photometric Capacity of Two Spring Wheat (Triticum Aestivum L.) Cultivars Differing in Salt Tolerance. Plant Growth Regulation 36: 49-59

Brugnoli E, O Björkman (1992) Growth of Cotton under Continuous Salinity Stress: Influence on Allocation Pattern, Stomatal and Non-Stomatal Components of Photosynthesis and Dissipation of Excess Light Energy.

Delfine S, Alvino A, Zacchini M, F Loreto (1999) Consequences of Salt Stress on Conductance to CO_2 Diffusion, Rubisco Characteristics and Anatomy of Spinach Leaves Australian Journal of Plant Physiology 25: 395-402

Everard JD, Gucci R, Khann SC, Flure IM, Wayne HL (1994) Gas Exchange and Carbon Partitioning in the Leaves at Various Levels of Root Zone Salinity. Plant. Physiology 106: 281-292

Khan AH, Ashraf M, Naqvi SM, Khavzada B, Ali M (1995) Growth Ion and Solute Contents of Sorghum Grown under NaCl and Na_2SO_4 Salinity Stress. Acta Physiol. Plant. 17: 261-268

Lu CM, Qin NW, Wang BS, Kuang TY (2002) Does Salt Stress Lead to Increased Susceptibility of Photosystem II , to Photoinhibition and Changes in Photosynthetic Pigment Composition in Halophyte Suaeda Salsa Grown Out Doors. Plant Sci. 3: 1063-1068

Lutts S, Kinet JM, Bouharmont J (1996) NaCl-Induced Senescence in Leaves of Rice Cultivars

Differing in Salinity Resistance. Ann.Bot. 78: 389-398

Lee G, Carrow RN, RR Duncan (2004) Photosynthetic Responses to Salinity Stress of Halophytic Seashore Paspalum Ecotypes. Plant Science 166: 1417-1425

Junklang J, Usui K, H Matsumoto (2003) Differences in the Physiological Responses to NaCl between Salt Tolerant Sesbania Rostrata and Non- Tolerant Phaseolus Vulgaris Weed Biology Management 3: 21-27

Shiler B, Danijela M, Biljana F, Zorica P, Tijana C Mijovic A. (2007) Effects of Salinity on in Vitro Growth and Phonosynthesis of Common Centuary (Centaurium Erithraea Rafn.) Arch.Biol.Sci. 59: 129-134

Yeo A, R Flowers (1983) Varietal Differences in the Toxicity of Sodium Ions in Rice Leaves. Physiologia Plantarum 59: 189-195

Identification of Dreb 1 Genes Involved in Drought Tolerance in Wheat (*Triticum* L.)

Irada M Huseynova*, Samira M Rustamova, Alamdar Ch Mammadov

Institute of Botany, Azerbaijan National Academy of Sciences, Baku, Azerbaijan.
*Corresponding author. Tel. No. +994 12 438 1164; Fax No. +994 12 510 2433; E-mail: huseynova-i@botany-az.org.

Abstract: Present research is aimed to identify a Dreb1 gene in different wheat *Triticum* L. genotypes using functional markers. A total of 12 wheat genotypes: 3 tetraploid (*Triticum durum* L., AABB, 2n = 4x = 28) and 9 hexaploid cultivars (*Triticum aestivum* L., AABBDD, 2n = 6x = 42) including tolerant, semi-tolerant and non-tolerant to drought were used. Five pairs of genome-specific primers designed for the wheat Dreb 1 genes using the Primer Premier 5.0 software was used for DNA amplification. P21F/P21R and P25F/PR were designed to amplify downstream regions of the Dreb-A1 in A genome. The P18F/P18R primers were designed as a B genome-specific primer pair. Similarly, P22F/PR and P20F/P20R was selected to amplify sequences from D genome. PCR products excised from agarose gels found out that Dreb 1 gene was located on chromosome 3A in all genotypes, including drought-resistant and drought-sensitive ones, excepting one semi-tolerant genotype Tale-38. In comparison with other genotypes, a 717 bp PCR product of Dreb-B1 gene was located on B genome in drought-tolerant sample Barakatli-95. Primers P22F/PR and P20F/P20R amplified 596- and 1193-bp fragments, respectively, from D genome, which is characteristic for hexaploid *Triticum aestivum* L. genotypes, did not revealed positive results.

Keywords: Wheat genotypes; Dreb genes; Functional markers; Genome; PCR analysis

Introduction

Drought is one of the prime abiotic stresses in the world. Crop yield losses due to drought stress are considerable. Wheat, which is one of the important staple food crops of the world, is adversely affected by drought. In view of a projection by Rajaram (2001) more than 50% of the 237 million ha area in the world under wheat cultivation is affected by periodic drought. To develop crop plants with enhanced tolerance of drought stress, a basic understanding of physiological, biochemical and gene regulatory networks is essential (Zhao *et al.*, 2008). Genetic engineering of plants for tolerance to extreme abiotic stresses could be achieved by the regulated expression of stress-induced transcription factors, which in turn would regulate the expression of a large number of relevant downstream genes. Thus, transcription factors are powerful tools for genetic engineering as their overexpression can lead to the up-regulation of a whole array of genes under their control. Dehydration-responsive element binding (DREB) proteins constitute a large family of transcription factors that are induced by abiotic stresses. They regulate a large number of functional genes related to drought, high-salinity and low temperature. The DREB transcription factors could be dichotomized as DREB1 and DREB2, which are involved in two separate signal transduction pathways (Agarwal *et al.*, 2006). To date, full-length sequences of DREB genes have been cloned from wheat (Shen *et al.*, 2003a), rice (Chen *et al.*, 2003), corn (Qin *et al.*, 2003), Arabidopsis (Liu *et al.*, 1998), and the halophyte *Atriplex hortensis* (Shen *et al.*, 2003b).

Marker-assisted selection (MAS) provides a strategy for accelerating the process of wheat breeding. Through marker-assisted breeding (MAB) it is now possible to examine the usefulness of thousands of genomic regions of a crop germplasm under water limited regimes, which was, in fact, previously not

possible (Ashraf, 2010). However, conventional markers, such as restriction fragment length polymorphisms (RFLPs), random amplified polymorphic DNAs (RAPDs), amplified fragment length polymorphisms (AFLPs) and simple sequence repeats (SSRs), used in common wheat, are usually not developed from the genes themselves because the cloning of genes in wheat is complicated by its allohexaploid (2n = 6x = 42) nature and large genome size. In contrast, functional markers (FMs) are usually designed from polymorphisms within transcribed regions of functional genes. Such markers are completely correlated with gene function. Therefore, FMs can dramatically facilitate accurate selection of target genes.

The aim of this study was to identify of Dreb1 genes in various wheat (*Triticum* L.) genotypes using functional markers.

Materials and Methods

A total of 12 wheat genotypes: 3 tetraploid (*Triticum durum* L., AABB, 2n = 4x = 28) and 9 hexaploid cultivars (*Triticum aestivum* L., AABBDD, 2n = 6x = 42) including tolerant, semi-tolerant and non-tolerant to drought were used (Table 1). Different sensitivities of these cultivars to drought had been determined during a few years in different regions of Azerbaijan based on grain yield (Aliev, 1998; Aliev, 2001). The plants were provided by Experimental Station of the Research Institute of Agriculture.

DNA was extracted from leaves using CTAB method (Murry and Thompson, 1980) with some modifications. DNA was quantified by taking the optical density (OD) at λ = 260 with a spectrophotometer ULTROSPEC 3300 PRO ("AMERSHAM", USA). The purity of genomic DNA was determined by the A260/A280 absorbance ratio. The quality was also examined by running the extracted DNA samples on 0.8% agarose gel stained with 10 mg/ml ethidium bromide in 1xTBE (Tris base, Boric acid, EDTA) buffer. The gel was visualized and photographed under UV light. PCR was carried out essentially, as described by Wei *et al*. (2009). Five pairs of genome-specific primers designed for the wheat Dreb 1 genes using the Primer Premier 5.0 software (http://www.premierbiosoft.com) were used for DNA amplification (Table 2). Genome-specific PCR was performed in a total volume of 20 μl containing 80 ng of genomic DNA, 1 x PCR reaction buffer, 0.25 μM of each primer, 0.45 mmol of each deoxyribonucleotide, 4.0 mmol $MgCl_2$ and 1.6 U of Taq DNA polymerase (Sigma, USA). The PCR was carried out using *Applied Biosystems 2720 Thermal Cycler* as follows: initial

Table 1 Wheat genotypes and their drought tolerance status.

No	Genotype name	Ploidity level and genomes	Reaction to drought
	Triticum durum L.		
1	Barakatli-95	Tetraploid (AABB)	Tolerant
2	Garagylchyg-2		Sensitive
3	Gyrmyzy bugda		Tolerant
	Triticum aestivum L.		
4	Azamatli-95	Hexaploid (AABBDD)	Tolerant
5	Giymatly-2/17		Semi-tolerant
6	Gobustan		Tolerant
7	Gyrmyzy gul		Semi-tolerant
8	Tale -38		Semi-tolerant
9	Ruzi-84		Tolerant
10	12 nd FAWWON No 97 (130/21)		Sensitive
11	4 tn FEFWSN No 50 (130/32)		Semi-tolerant
12	Saratovskaya		Tolerant

Table 2 Genome-specific primers of the wheat Dreb 1 genes used for PCR reactions.

Primers	Sequences (5′ ⟶ 3′)	Chromo some location	Expected size (bp)	Ann. temp. (˚C)
P18F	CCCAACCCAAGTGATAATAATCT	3B	717	50
P18R	TTGTGCTCCTCATGGGTACTT			
P20F	TCGTCCCTCTTCTCGCTCCAT	3D	1193	63
P20R	GCGGTTGCCCCATTAGACATAG			
P21F	CGGAACCACTCCCTCCATCTC	3A	1113	63
P21R	CGGTTGCCCCATTAGACGTAA			
P22F	CTGGCACCTCCATTGCCGCT	3D	596	63
P25F	CTGGCACCTCCATTGCTGCC	3A	596	57
PRa *	AGTACATGAACTCAACGCACAGGACAAC			

* a PR is a public primer matched with P22F and P25F, respectively.

denaturation at 94 °C for 3 min; 34 cycles of 94 °C for 1 min, an annealing step at variable annealing temperatures depending on the primer pairs for 1 min, 72 °C for 1.5 min; and a final extension at 72 °C for 10 min and then held at 4 °C prior to analysis. The PCR products were electrophoresed on 2.5% agarose gels, stained with ethidium bromide and visualized under UV light by *Gel Documentation System UVITEK*.

Results and Discussion

PCR analysis was carried out to identify Dreb 1 genes, which responsive for drought tolerance in 12 wheat genotypes (*Triticum* L.) with different level of resistance to drought (Table 1). For this purpose functional markers for Dreb 1 genes, specially synthesized for A, B and D wheat genomes, were used. P25F/PR was designed to amplify a 596-bp DNA fragment downstream of Dreb-A1 in the A genome. P21F/P21R was selected to amplify an upstream region (1113-bp DNA fragment) of the same gene. Similarly, P22F/PR and P20F/P20R were designed to amplify sequences from the D genome, with the amplifications resulting in 596 and 1193-bp DNA fragments, respectively. The P18F/P18R primers, which amplify a 717-bp DNA fragment, were designed as a B genome-specific primer pair (Table 2).

Fig. 1 demonstrates gel electrophoresis of PCR profiles of amplified DNA from *Triticum* L. using primer pair P21F/P21R. As shown in Fig. 1, fragment amplified with this marker in 1113-bp region of high drought tolerant durum wheat genotype Barakatli-95 is seemingly indicated. Excepting semi-tolerant bread wheat genotype Tale-38 in all other genotypes both drought tolerant and drought sensitive the presence of Dreb 1-responsive fragment could be obtained. This indicates that in these genotypes Dreb 1 gene responsive for the tolerance to drought as well as other abiotic stresses is in the third chromosome of A genome. 596-bp fragment that amplify by P25F/PR primer for Dreb 1 gene in A genome were not synthesized in selected genotypes. Absence of these fragments can be explained by some mutations that, probably, took place in Dreb 1 gene region, complementary to this primer. Since presence of Dreb 1 gene in A genome is proved by PCR results using primer pair P21F/P21R.

Results obtained using primer pair P18F/P18R, specific for Dreb 1 gene in B genome, are shown in Fig. 2. As it seemed from Fig. 2 fragment pair 717–789 bp reveals only in Barakatli-95. This shows that Dreb 1 gene is also occurred in Barakatli-95 B genome. It should be noted that in our experiments this genotype also shows its high drought tolerance in other parameters (Aliev, 1998; Aliev, 2001). As to the absence of this pair of fragments in other wheat genotypes it can be explained from the literature data that the DREB1 proteins showed the most specific variations in the B genome, including three single amino acid mutations (amino acids 46, 140 and 200) and a deletion of 24 amino acids in a region rich in *Ser* and *Thr* in the orthologous A and D genomes (Wei *et al.*, 2009). PCR analysis with P22F/PR and P20F/P20R primers specific for D genome was also carried out. As it is known D genome occurs in

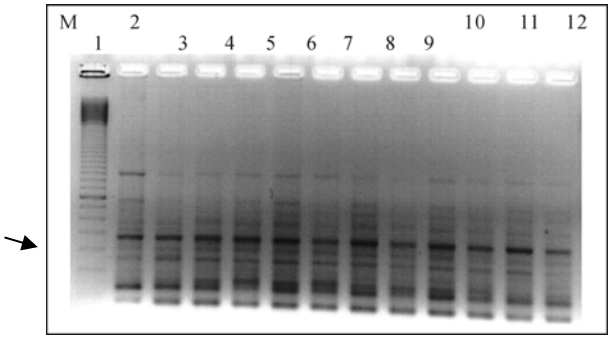

Fig. 1 PCR amplification profiles of wheat genotypes *Triticum* L. using an A genome-specific primer pair P21F/P21R. The arrow shows 1113 bp DNA fragments. M – DNA ladder 100. 1 - Barakatli-95, 2 - Garagylchyg-2, 3 - Gyrmyzy bugda, 4 - Azamatli-95, 5 - Giymatli-2/17, 6 - Gobustan, 7 - Gyrmyzy gul, 8 - Tale-38, 9 - Ruzi-84, 10 - 12nd FAWWON No 97 (130/21), 11 - 4tn FEFWSN No 50 (130/32), 12 - Saratovskaya.

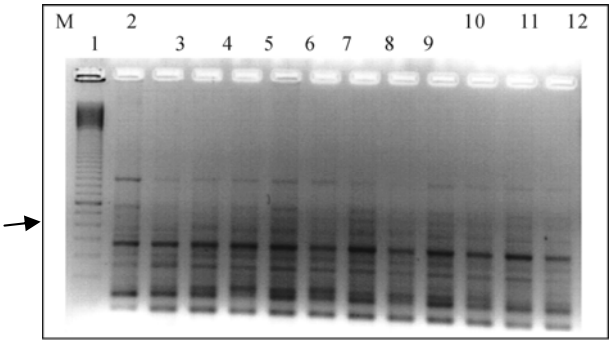

Fig. 1 PCR amplification profiles of wheat genotypes *Triticum* L. using a B genom-specific primer pair P18F/P18R. The arrow shows 717-789 bp DNA fragment. M – DNA ladder 100. 1 - Barakatli-95, 2 - Garagylchyg-2, 3 - Gyrmyzy bugda, 4 - Azamatli-95, 5 - Giymatli-2/17, 6 - Gobustan, 7 - Gyrmyzy gul, 8 - Tale-38, 9 - Ruzi-84, 10 - 12nd FAWWON No 97 (130/21), 11 - 4tn FEFWSN No 50 (130/32), 12 - Saratovskaya.

hexaploid genotypes *Triticum aestivum* L. In our experiments there were not any appropriate fragments responsive to these markers. This allows us to suppose that used hexaploid wheat varieties, possibly, were nulliosomics, *i.e.* chromosome pair which has a Dreb 1 gene is absent in their D genomes.

Understanding of the functions of these stress-inducible genes helps to unravel the possible mechanisms of stress tolerance. Marker-assisted selection was also employed to improve the staygreen trait involved in drought tolerance of wheat. The obtained results open an excellent opportunity to develop stress tolerant crops in future.

References

Agarwal PK, Agarwal P, Reddy MK, Sopory SK (2006) Role of DREB Transcription Factors in Abiotic and Biotic Stress Tolerance in Plants. Plant Cell Rep. 25: 1263-1274

Aliev JA (1998) Importance of Photosynthesis of Various Organs in Protein Synthesis in Grain of Wheat Genotypes under Water Stress. Proceedings of the XIth International Congress on Photosynthesis, Budapest, Hungary, 1998. In: G Garab (ed.), Photosynthesis: Mechanisms and Effects, Vol 5. Kluwer Academic Publishers: Dordrecht/Boston/London, pp. 3829-3832

Aliev JA (2001) Physiological Bases of Wheat Breeding Tolerant to Water Stress. Proceedings of the 6th International Wheat Conference, Budapest, Hungary, 2000. In: Z Bedo, L Lang (eds.), Wheat in a Global Environment, Vol. 9. Kluwer Academic Publishers: Dordrecht/Boston/London, pp. 693-698

Ashraf M (2010) Inducing Drought Tolerance in Plants: Recent Advances. Biotechnology Advances 28: 169

Chen JQ, Dong Y, Wang YJ, Liu Q, Zhang JS, Chen SY (2003) An AP2/EREBP-Type Transcription-factor Gene from Rice Is Cold-Inducible and Encodes a Nuclear-Localized Protein. Theor. Appl. Genet. 107: 972-979

Liu Q, Kasuga M, Sakuma Y, Abe H, Miura S, Yamaguchi-Shinozaki K (1998) Two Transcription Factors, DREB1 and DREB2, with an EREBP/AP2 DNA Binding Domain Separate Two Cellular Signal Transduction Pathways in Drought-and Low-Temperature Responsive Gene Expression, Respectively in Arabidopsis. Plant Cell 10: 1391-1406

Murray MG, Thompson WF (1980) Rapid Isolation of High Molecular Weight DNA. Nucleic Acids Res. 8: 4321-4325

Qin F, Li J, Zhang GY, Zhao J, Chen SY, Liu Q (2003) Isolation and Structural Analysis of DRE-Binding Transcription Factor from Maize (Zea Mays L.).Acta Bot. Sin. 45: 331-339

Rajaram S (2001) Prospects and Promise of Wheat Breeding in the 21st Century. Euphytica 119: 3-11

Shen YG, Zhang WK, He SJ, Zhang JS, Liu Q, Chen SY (2003a) An EREBP/AP2-Type Protein in Triticum Aestivum Was a DRE-Binding Transcription Factor Induced by Cold, Dehydration and ABA Stress. Theor. Appl. Genet. 106: 923-930

Shen YG, Zhang WK, Yan DQ, Du BX, Zhang JS, Liu Q (2003b) Characterization of a DRE-Binding Transcription Factor from a Halophyte Atriplex Hortensis. Theor. Appl. Genet. 107: 155-161

Wei B, Jing R, Wang C, Chen J, Mao X, Chang X, Jia J (2009) Dreb1 Genes in Wheat (Triticum Aestivum L.): Development of Functional Markers and Gene Mapping Based on SNPs. Mol. Breeding 23: 13-22

Zhao CX, Guo LY, Cheruth AJ, Shao HB, Yang HB (2008) Prospectives for Applying Molecular and Genetic Methodology to Improve Wheat Cultivars in Drought Environments. C. R. Biologies 31: 579-586

Detection of Tomato Yellow Leaf Curl Virus in Azerbaijan and Partial Characterization of Biochemical Properties of Naturally Infected Plants

Irada Huseynova, Alamdar Mammadov*, Nargiz Sultanova

Institute of Botany, Azerbaijan National Academy of Sciences, Azerbaijan.
*Corresponding author. Tel. No. +99412 438 1164; Fax No. +99412 510 2433; E-mail: amamedov_ib@yahoo.co.uk.

Abstract: In order to detect the presence of virus during summer and autumn 2009 tomatoes with leaf curling and yellowing symptoms were collected by us from fields and greenhouses located in the main tomato production provinces of Azerbaijan. The viral DNA was amplified by Rolling Circle Amplification (RCA) using TempliPhi Amplification Kit. Restriction fragment length polymorphism (RFLP) analysis of viral DNA revealed products with close homology to the TYLCV. At the same time, some biochemical responses to viral diseases of symptomatic plants were also studied. It was found out that the activities of antioxidant enzymes, including glutathione reductase (GR) and catalase (CAT) significantly increased in all symptomatic samples compared to non-infected plants. Dynamics of ascorbate peroxidase (APX) and superoxide dismutase (SOD) activities differed from those of CAT and GR. APX activity slightly increased in stressed samples. And SOD activity did not seem to be affected by viral stress. Total protein and chlorophyll content decreased during degradation in pathogenesis. Significant decrease was also observed in Fv/Fm ratio (0.56) of symptomatic tomatoes as compared with control (0.72). Obtained results showed that photochemical activity of PS I and PS II decreased under viral disease.

Keywords: Geminivirus; RCA; TYLCV; Antioxidant enzymes; Tomato

Introduction

Nowadays crop plants more frequently suffer from various biotic and abiotic stresses. And one of the most global constraints to the crop growth and development, as well as production and yield stability, as compared with other biotic agents is viral diseases (Abdallah NA *et al.*, 2002).

There are several factors limiting tomato productivity among which geminiviruses have been unified as very important biotic constraints for tomato cultivation in many tropical and subtropical countries of the world. Geminiviruses are a group of plant pathogens that have circular single-stranded DNA (sscDNA) genomes encapsidated within twinned particles (Abou-Jawdah Y *et al.*, 2006). Whitefly-transmitted geminiviruses with mono- or bipartite- sscDNA comprise the genus of *Begomovirus* of the family *Geminiviridae*. Tomato yellow leaf curl virus (TYLCV) is a monopartite begomovirus which exhibits a range of symptoms and causes a serious damage to tomato plants with a greater yield loss and quality reduction (Eybishtz A *et al.*, 2009). Like all geminiviruses, TYLCV has a characteristic particle of twinned morphology of approximately 20–30 nm in size (Czosnek H, 1997). The virus capsid containing a total of 22 capsomeres each containing five units of a 260-amino-acid coat protein. TYLCV has a single 2787 nt (total m.w. 980 kDa) covalently closed-genomic circular ssDNA.

Material and Methods

The aim of the present study was to detect TYLCV in tomato and characterize some biochemical properties of the virus-infected plants. In order to detect the presence of virus during summer and autumn of 2009 tomatoes with leaf curling and yellowing symptoms (Fig. 1) were collected by us from fields and greenhouses located in the main

tomato production provinces of Azerbaijan.

DNA was extracted from the fresh leaves of plants according to Edwards *et al*. (1991) with slight modifications (Edwards K *et al.*, 1991). DNA extracts were frozen at –20 p°C. Geminiviruses possess small circular single-stranded DNAs that are easily multiplied *in vitro* by rolling circle amplification using bacteriophage Phi 29 polymerase. With the reaction products, different geminiviruses can be discriminated using restriction fragment length polymorphism (RFLP), making the combination of RCA and RFLP an easy-tohandle diagnostic tool (Kheyr-Pour A *et al.*, 1992).

The circular genomic DNA was amplified by RCA using the TempliPhi Amplification Kit (GE Health Care, UK). Amplification products (10 µl) were analyzed by 1.5% agarose gel electrophoresis in 1x TAE buffer and stained with ethidium bromide with 1 kbp DNA ladder as a size marker. DNA bands visualized using a UV transilluminator.

Fig. 1 Tomato plants collected from fields associated with virus infestation showing virus like symptoms such as leaf curling and yellowing, and abnormal fruit.

RFLP is used in combination with RCA to identify differences between viruses based on the presence or absence of restriction enzyme-recognition sites. After RCA amplification, the amplicon is digested with restriction enzymes XbaI, HindIII (Sigma) according to the manufacturer´ s instructions and the fragment sizes analysed by gel electrophoresis. RFLP is a method that can be used to differentiate isolates of viruses without the expenses of cloning and sequencing. The restrictions fragments, together with the 1 kb-plus DNA size marker (Invitrogen), were separated by 2% agarose gel electrophoresis in 1x TAE buffer, stained with ethidium bromide and visualized under UV.

At the same time, some biochemical responses to viral diseases of symptomatic plants were also studied. Leaves were homogenized with a Waring blender at full speed four times for 20 s each in an ice-cold grinding chloroplast isolation medium (1:6 w/v) containing 0,4 mol sucrose, 20 mmol Tris, 10 mmol NaCl, 1 mmol EDTA, 5 mmol sodium ascorbate, and 0.1% polyethylene glycol, pH 7.8. Photochemical activities of chloroplasts isolated from control and viral-stressed plants were followed polarographically (Aliyev J *et al.*, 1992) as O_2 evolution or uptake at 20 ºC using a water-jacketed Clark type oxygen electrode chamber under illumination with saturating white actinic light (850 µE m^{-2} s^{-1}). The following electron transport activities were assayed in µmol O_2 mg^{-1} Chl h^{-1}.

The content of chlorophyll extract was determined spectrophotometrically in 80% acetone (Mc-Kinney G, 1941; Wettstein D, 1957). Measurements of photoinduced changes of fluorescence yield from F_o level to F_{max} were carried out at room temperature using laboratory-built set-up. Potential quantum yield of PSII was estimated according to the formula:

$$F_p = F_v/F_m = (F_m - F_o)/F_m$$

The activity of catalase was determined as a decrease in absorbance at 240 nm for 1 min following the decomposition of H_2O_2. The reaction mixture contained 50 mmol phosphate buffer (pH 7.0) and 15 mmol H_2O_2 and reaction was initiated by adding enzyme extract.

The activity of ascorbate peroxidase was measured as a decrease in absorbance at 290 nm for 30 sec.

Superoxide dismutase activity was estimated by using SOD Assay Kit-WST (Sigma-Aldrich). The absorbance was recorded at 450 nm and one enzyme unit of SOD activity was defined as the amount of enzime recuired to cause 50% inhibition of the rate of NBT reduction.

Glutathione reductase activity was determined at 340 nm for 10 min in 1 ml of reaction mixture containing 100 mmol potassium phosphate buffer (pH 7.8), 1 mmol EDTA, 0.2 mmol NADPH and 0.5 mmol GSSG (Gustavo G, Yannarelli *et al.*, 2007).

Protein content was determined by using bovine serum albumin as a standard (Sedmak J *et al.*, 1977).

Results and Discussions

Field observations showed that the major virus

symptoms were leaflets with cupped, curling shapes, reduction in leaf size, leaf rolling and vein banding. In addition heavy infestations of whiteflies were observed and associated with VLS that resemble geminivirus symptoms. Recently, the bacteriophage phi29 DNA polymerase has been used for the efficient amplification of circular DNA viral genomes without the need of specific primers by rolling-circle amplification (RCA) mechanism. RCA/RFLP diagnosis will become popular for practical geminivirology in the near future because of its simplicity, low costs, and robustness. Restriction fragment length polymorphism (RFLP) analysis of viral DNA revealed products with close homology to the *Tomato Yellow Leaf Cruel Virus* (TYLCV) (Fig. 2).

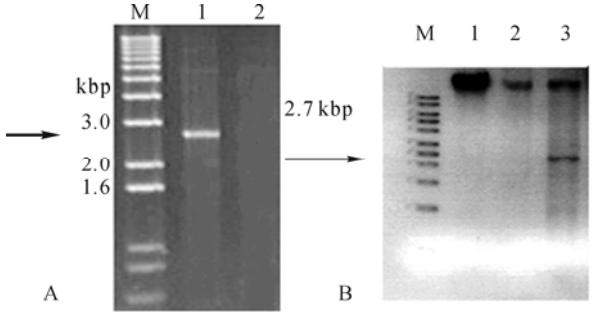

Fig. 2 Electropherogram of RCA and RFLP in 1.5% agarose gel. A. RCA products digested with restriction enzyme xBaI. Lane M- 1 kb - plus DNA size marker, Lane1- Infected tomato, Lane2 - Healthy tomato. B. RCA products digested with restriction enzyme HindIII. Lane M -1 kb-plus DNA size marker (Invitrogen), Lane1 - RCA product of infected tomato, Lane2 - genomic DNA of infected tomato, Lane3 - RCA products digested with restriction enzyme HindIII.

At the same time, some biochemical responses to viral diseases of symptomatic plants were also studied. Therefore, in plants and in other aerobic organisms antioxidant systems have evolved and different ROS are used as signalling molecules in basic cellular processes. Ascorbate and glutathione are also used as cofactors in reactions catalyzed by peroxidases (APX and GPX) to reduce H_2O_2 to water. Superoxide dismutases convert $O_2^{-\bullet}$ to H_2O_2 and thus form a crucial part of the cellular antioxidant response system. It was found out that the activities of antioxidant enzymes, including glutathione reductase (GR) and catalase (CAT) significantly increased in all symptomatic samples compared to non-infected plants. Dynamics of ascorbate peroxidase (APX) and superoxide dismutase (SOD) activities differed from those of CAT and GR. APX activity slightly increased in stressed samples. And SOD activity did not seem to be affected by viral stress.

Total protein and chlorophyll content decreased during degradation in pathogenesis.

A reduction in the total chlorophyll content and Chl a/b ratio occurred during viral stress.

Fv/Fm ratio (0.56) of symptomatic tomatoes as compared with control (0.72). Obtained results showed that photochemical activity of PS I and PS II decreased under viral disease. PS I activity (O_2 uptake rate), however, was affected much less under viral stress (Table 1). It can be caused by a higher ability of PS I to adapt to dehydration. Potential quantum yield of photochemical reactions of PSII (F_v/F_m ratio) in chloroplasts from control (non-virus stressed) plants was 0.72 and 0.56 for symptomatic tomatoes, that is typical for abnormally grown plants during pathogenesis. As it seems from *Table 1* state of PSII in dehydration process was being significantly changed.

Potential yield of photochemical reactions of PSII undergoes appreciable changes in comparison with control plants; Decreasing of a photochemical efficiency (F_v/F_m) under viral stress can be considered as a fact of damage of photosynthetic reaction centers.

TYLCV is an Old World geminivirus, first described in the Middle East (Jordan valley of Israelin) the 1960s and transmitted by *Bemisia tabaci* in a persistent manner. Biotype B is usually the form of *B. tabaci* involved which transmits with high frequency. The virus was named tomato yellow leaf curl virus (TYLCV). The virus was isolated and its genome sequenced in the late 1980s. From the early 1960s tomato cultures have been under the constant threat of TYLCV-like begomoviruses worldwide. One of the best ways to reduce TYLCV damage is to breed plants resistant to both the virus and the vector. Breeding programs for TYLCV-resistant cultivars are based on the transfer of TYLCV resistance genes from wild tomato species into cultivated tomato (Gronenborn B, 2007). Transgenic tomato plants with the capsid protein of TYLCV are resistant to the virus.

One of the most useful parameters that can be measured is the ratio of variable chlorophyll fluorescence (*Fv*) to maximum fluorescence (*Fm*). This ratio (*Fv/Fm*) is correlated to the quantum yield of photochemistry in Photosystem II it reflects the probability of the use by PSII reaction centres of the available excitation energy for photochemistry. Significant decrease was also observed in

In order to reduce the virus-associated risks high

quality diagnostics for the viruses should be developed and used in breeding programs for tolerance to virus infection. And above-mentioned data should be a promising beginning for developing such tendency in Azerbaijan.

Table 1 The Photosystem II and Photosystem I activity in chloroplasts from tomato genotypes subjected to viral stress (μmol O_2 mg^{-1} chlorophyll h^{-1}).

Genotypes	Photosystem II $H_2O \rightarrow K_3Fe(CN)_6$	in %	Photosystem I DCIP·H→MV	in %	PSI/ PS II
Tomato (control)	87 ± 4	100	242±12	100	2,80
Tomato (viral stress)	66 ± 3	43	192±9	78	3,12

References

Abdallah NA, Abo EH, Amir D, Madkour M (2002) Studying the Expression and Function of the Transgenic Tomato Plants. Symposium on Scientific Research Outlook in the Arab World: 24-27

Abou-Jawdah Y, El Mohtar C, Atamian H, Sobh H (2006) First Report of Tomato Chlorosis Virus in Lebanon. Plant Dis. 90: 378-382

Aliyev J, Suleymanov S, Guseinova I (1992) Effect of Specific Translation Inhibitors on Polypeptide Composition and Spectral Characteristics of Wheat Thylakoid Membrane. Biochem. 57: 679-686

Czosnek H, Laterrot H (1997) Tomato Yellow Curl Virus Disease, Management, Molecular Biology, Breeding for Resistance. Archives of Virology. 142: 1391-1406

Edwards K, Johnstone C, Thompson C (1991) A Simple and Rapid Method for the Preparation of Plant Genomic DNA for PCR Analysis. Nucl. Acids Res. 19: 1349-1356

Eybishtz A, Peretz Y (2009) Silencing of a Single Gen in Tomato Plants Resistant to Tomato Yellow Curl Virus Renders Them Susceptible to the Virus. Plant Plant Mol. Biol. 71: 157-171

Gronenborn B (2007) The Tomato Yellow Curl Virus, Genom and Function of Its Protein. Springer: Dordrecht, pp. 67-84

Yannarelli GG, Fernandez-Alvarez AJ (2007) Glutatione Reductase Activity and Isoforms in Leaves and Roots of Wheat Plants Subjected to Cadmium Stress. Phytochemistry 68: 505-512

Kheyr-Pour A, Gronenborn B (1992) Tomato Yellow Curl Virus from Sardinia Is a Whitefly – Transmitted Monoparlite Geminivirus. Nucl. Acid Res. 9: 6763-6769

Mc-Kinney G (1941) Absorption of Light by Chlorophyll Solution. J. Biol. Chem. 140: 315-322

Sedmak J, Grossberg E (1977) A Rapid, Sensitive, and Versatile Assay for Protein Using Coomassie Brilliant Blue G 250. Anal. Biochem.79: 544-552

Wettstein D (1957) Chlorophyll-lethal and Submicroscopic Form Changing of Plastids. Exp. Cell Res. 12: 427-506

Antioxidant Enzymes and Functional State of PS II in Plants Grown under Various Radium (^{226}Ra) Concentrations

Saftar Y Suleymanov *, Konul H Bayramova, Samira M Rustamova,
Elmira H Maharramova, Irada M Huseynova

Institute of Botany, Azerbaijan National Academy of Sciences, 40, Badamdar Shosse, Baku AZ1073, Azerbaijan.
*Corresponding author. Tel. No. (+994 12) 438 1164; Fax No. (+994 12) 510 2433; E-mail: i_guseinova@mail.ru.

Abstract: This work is devoted to study the antioxidant enzymes and functional state of photosystem (PS) II under the different concentrations of the radium in barley (*Hordeum vulgare* L.) and clover (*Trifolium pratense* L.) plants. It was determined that CAT activity increased in barley grown in the soil contaminated with low radium concentrations (29.45 ± 3.00 and 124 ± 15.00 Bq kg^{-1}) as compared with control, but decreased dramatically upon the effect of high radium concentration (242.25 ± 28 Bq kg^{-1}). CAT activity was 0.078 mmol/g min in control plants, and 0.18, 0.23 and 0.03 mmol/g min in 29.45 ± 3.00, 124 ± 15.00, 242.25 ± 28.00 Bq kg^{-1}, respectively. It was observed that in clover seedlings as the radium activity increased, CAT activity also rised, but at high concentrations, as well as in barley, enzyme activity decreased. The APX activity in barley as compared to the control decreased as a result of radium effect. APX activity in clover increased in soil with higher radium concentrations. SOD activity in barley increased at high levels of radium concentration (*i.e.* 0.5 unit/mg in the control, 0.6, 2.7 and 3 units/mg in 29.45 ± 3.00, 124 ± 15.00 and 242.25 ± 28.00 Bq kg^{-1}, respectively). In clover, changes in PS II activity decreased significantly at high ^{226}Ra concentrations.

Keywords: Radiation; Antioxidant enzymes; Photosystem I; Photosystem II; Plants

Introduction

Naturally, several types of radionuclides and heavy metals at trace amounts occur in the environment. At the background level, these components are not only harmless for living organisms but also, they are essential nutrients for plants growth. As a result of anthropogenic activity, many of these components are accumulated and create environments that contain toxic levels of the contaminants. Accordingly, at high concentrations radionuclides are passed from the soil to micro flora and fauna, plants, animals, and human via the food chain and results in toxic effects.

Currently, potential risks originated by these contaminates become the object of investigation, internationally.

Typically radioactive elements such as ^{238}U, ^{226}Ra and ^{232}Th are simultaneously presented in a polluted area. Among these radionuclides, Ra has the strongest effect. ^{226}Ra and ^{224}Ra are the members of uranium-238 and thorium-232 series, respectively. They are alpha emitter radionuclides and don't add directly gamma activity of the environment. Since both above mentioned isotopes of Ra are chemically similar to calcium, they are, therefore, absorbed from the soil by plants and are passed up through food chain to the human (Hosseini and Fathihvand, 2004). For example, after Chernobyl accident, it was determined that in acute exposure to ionizing radiation, the impact of radionuclides can be two to four times higher in the cell, due to atom decay than in external irradiation. It was determined that the biological impact of radionuclides depends on their accumulation level and localization in the organism and cells. Internal exposure in plants can increase with radionuclides accumulated in their tissues, especially in tissues with active cell division (Marĉiulionienè *et al*., 2006). At present, public concerns related to the environment

and sustainable development lead to an increase in interest for studying the effects of pollutants at the molecular, biochemical and genetic level. In plants, environmental adversity often leads to the increase in formation of highly reactive oxygen species (ROS). Under natural (non-stress) conditions ROS occur in the plant cell and, therefore, plants possess several antioxidative defense mechanisms to control the redox state of the cell which is essential for normal physiological and biochemical functioning. The defense systems are comprised of antioxidative enzymes (superoxide dismutase, peroxidase, catalase, glutathione reductase) and non-enzymatic antioxidants (*e.g.* glutathione, ascorbate) (Guseinova *et al.*, 2001). Resistance to stress factors is mainly provided by enzymes of ROS detoxification. Exposition to radionuclides (and heavy metals) may also result in direct or indirect (oxidative stress mediated) genotoxic effects. The genetic effects can be induced by ionizing radiation due to the radionuclide decay and by transmutation. Radionuclides may enter the inner cell compartments and sometimes bind to the DNA molecule (Marĉiulionienė *et al.*, 2006) Hardly any studies exist on the biological effects induced by radionuclides.

This work is devoted to study the antioxidant enzymes and functional state of photosystems in plants under radium effect.

Materials and Methods

Two test plants, barley (*Hordeum vulgare* L.) and clover (*Trifolium pratense* L.), were selected as a research object. During the experiments, we used soil contaminated with radium (^{226}Ra) concentrations of 29.45 ± 3.00, 124 ± 15.00 and 242.25 ± 28.00 Bq kg^{-1}. Before the seeds were used in the experiment, they were sterilized in the solution of 3% hydrogen-peroxide for 10 minutes, washed twice in distilled water and kept for 24 h in the dark. Then, after the seeds were ready for experiment, we grew plants in both contaminated soil (stress) and clean soil (control) in artificial climate in phytotron. Activities of antioxidant enzymes (catalase (CAT), ascorbate peroxidase (APX), superoxide dismutase (SOD)), quantum yield of PS II (F_v/F_m), and PS I and PS II activities, based on oxygen absorption and evolution, were analyzed in 20 day-old seedlings.

The activity concentration of ^{226}Ra in soil was determined using HP (Ge) gamma spectrometer.

Photoinduced changes of fluorescence yield were measured at room temperature using laboratory-built instrument as described earlier (Klimov *et al*., 1982). Potential quantum yield of PS II was estimated according to the formula:

$$F_p = F_v/F_m = (F_m - F_o)/F_m$$

where, F_0 –constant fluorescence; F_v-variable fluorescence; F_m-maximal fluorescence.

Enzyme extract was prepared by homogenizing leaf material (1 g fr wt) with a pestle in an ice-cold mortar with 0.05 mol Na_2HPO_4/NaH_2PO4 (pH 7.0) buffer. The homogenates were filtered through four layers of cheesecloth and then centrifuged at 4 °C. The supernatant were collected and used for the assays of enzymatic activities. The activity of CAT was determined as a decrease in absorbance at 240 nm for 1 min following the decomposition of H_2O_2 as described by Kumar and Knowles (1993). APX activity was assayed according to Nakano and Asada (1981). The activity was measured as a decrease in absorbance at 290 nm for 30 sec. SOD activity was estimated by using SOD Assay Kit-WST (Sigma-Aldrich, U.S.A.). The absorbance was recorded at 450 nm and one enzyme unit of SOD activity was defined as the amount of enzime recuired to cause 50% inhibition of the rate of NBT reduction. Protein content was determined according to (Sedmak and Grossberg, 1977).

Photochemical activities of chloroplasts isolated from control and drought-stressed plants were followed polarographically as O_2 evolution or uptake using a water-jacketed Clark type oxygen electrode chamber (Guseinova *et al.*, 2001). Chloropyll concentrations equivalent to 100 μg were used for all measurements. PS II activity ($H_2O \rightarrow K_3Fe(CN)_6$) was measured in a medium containing 330 mmol sorbitol, 40 mmol Hepes-NaOH, pH 7.6, 10 mmol NaCl, and 5 mmol $MgCl_2$ using 0.5 mmol $K_3Fe(CN)_6$ as terminal electron acceptor. PS I activity was assayed in the reaction mixture contained in 2 ml, 80 mmol sucrose, 30 mmol Tris-HCl, pH 8.0, 10 mmol NaCl, 10 mmol $MgCl_2$, 1 mmol sodium ascorbate, and 2 μM 3-(3-4-di-chlorophenyl)-1,1-dimethylurea (in order to block electron transport from PS II), using 0.3 mmol 2,6-dichlorophenolindophenol as electron donor and 50 μM methylviolgen as electron acceptor.

Results and Discussion

It was determined that CAT activity increased in barley grown in the soil contaminated with low radium concentrations (29.45 ± 3.00 and 124.00 ± 15.00 Bq kg^{-1}) as compared with control, but decreased dramatically upon the effect of high radium concentration (242.25 ± 28.00 Bq kg^{-1}) (Fig. 1). CAT activity was 0.078 mmol/g min in control plants, and 0.18, 0.23 and 0.03 mmol/g min in 29.45 ± 3.00, 124 ± 15.00, 242.25 ± 28.00 Bq kg^{-1}, respectively. It was observed that in clover seedlings as the radium activity increased, CAT activity also rised, but at high concentrations, as well as in barley, enzyme activity decreased. The APX activity in barley as compared to the control decreased as a result of radium effect. In clover APX activity was the same in the control and in 29.45 ± 3.00 Bq kg^{-1}, and increased in 124.00 ± 15.00 and 242.25 ± 28.00 Bq kg^{-1}. SOD activity in barley increased at high levels of radium concentration (*i.e.* 0.5 unit/mg in the control, 0.6, 2.7 and 3 units/mg in 29.45 ± 3.00, 124 ± 15.00 and 242.25 ± 28.00 Bq kg^{-1}, respectively). However, in clover SOD activity increased almost two times at low radium concentrations as compared to the control. At high ^{226}Ra concentrations it decreased close to the control SOD.

Significant difference in F_v/F_m ratio (0.8) was observed in clover at lower radium activities as compared with the control. It decreased at higher ^{226}Ra concentrations (0.7). In barley, F_v/F_m ratio slightly rised under the effect of radium and no significant changes in PS II activity were observed at lower concentrations of radium (Table 1). However, under the high concentration of radium it decreased. As mentioned Table in barley seedlings activity of the PS I and in clover seedlings activity of the PS II showed decrease as increasing activities of the radium in the soil, but at high concentration again activities increased. We did not observe any differences at the value of the PS I activities in clover among the control and the 29.45 ± 3.00, 124 ± 15.00 Bq kg^{-1}. Despite this fact, high concentrations of the radium decreased the activity of the PS I.

Table 1 Photochemical activities of the PS I and PS II based on absorption and evolution in barley and clover under the various concentrations of the radium (μmol O_2 mg^{-1} Chl h^{-1}).

Plants	Treatment (Bq kg^{-1})	PS II $H_2O \rightarrow K_3Fe(CN)_6$	PS I DCPIP· H→ MV
Barley (*Hordeum vulgare* L.)	0	60	1000
	29.45 ± 3.00	60	800
	124.00 ± 15.00	78	740
	242.25 ± 28.00	48	760
Clover (*Trifolium pratense* L.)	0	156	720
	29.45 ± 3.00	108	720
	124.00 ± 15.00	60	700
	242.25 ± 28.00	138	600

As a result of the experiment, we identified that for the barley and clover seedlings activity of the CAT decreased in high concentration of radium. In contrast, in clover, activity of APX was higher in various activities of radium. In clover, in high concentration of radium, decrease in the activity of CAT is compensated by increase in activity of APX. Peroxidase was considered to be key enzyme for the decomposition of H_2O_2 especially under CAT inactivation. APX activation in Arabidopsis subjected to oxidative stress occurred through induction of APX 1 and APX 2 gene transcription (Karpinski *et al*., 1997). Both of the plants showed loss in various photosynthetic activities under the effects of radionuclides. Accordingly, we can conclude that in barley, increase in activity of CAT under low activity of radium in soil, then decrease under its high activity, increase in activity of SOD with increase in the activity of concentration of radium, and in clover, increase in low concentrations and decrease in high concentrations of CAT, increase in activity of APX along with increase in concentration of radium in soil confirms that these enzymes protect barley and clover from the oxidative stress.

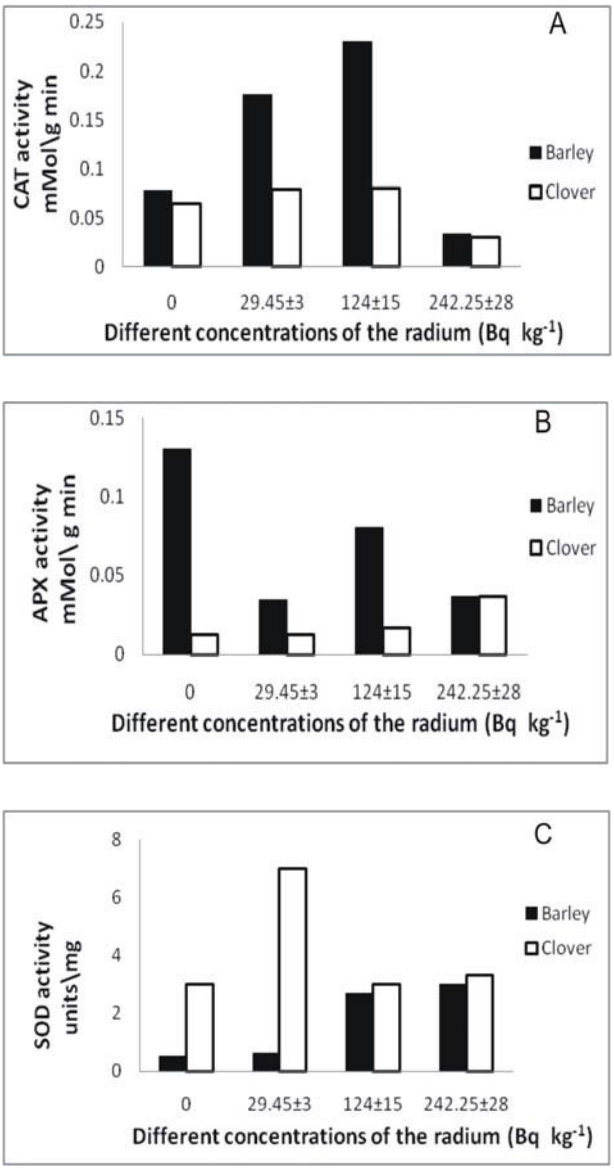

Fig. 1 Activities of catalase (A), ascorbat peroxidase (B) and superoxide dismutase (C) in barley and clover plants under the effect of radium (Bq kg^{-1}).

References

Cuypers A, Vangronsveld J, Clijsters H (2002) Peroxidases in Roots and Primary Leaves of Phaseolus Vulgaris. J. Plant Physiol 159: 869-876

Guseinova IM, Suleymanov SY, Aliyev JA (2001) Regulation of Chlorophyll-Protein Complex Formation and Assembly in Wheat Thylakoid Membrane. J. of Biochem. and Mol.Biol. 34: 496-501

Hosseini T, Fathihvand AA (2004) Radium Micro-precipitates Using Alpha Spectrometry and Total Alpha Counting Measurement. Iran. J. Radiat. Res. 2(1): 1-6

Karpinski S, Escobar C, Karpinski B, Crelissen G, Mullineaux PM (1997) Photosynthetic Electron Transport Regulates the Expression of Cytosolic Ascorbate Peroxidase Genes in Arabidopsis during Excess Light Stress. The Plant Cell 4: 627-640

Klimov VV, Allakhverdiev SI, Shuvalov VA, Krasnovsky AA (1982) Effect of Extraction and Re-Addition of Manganese on Light Reactions of Photosystem II Preparations. FEBS Lett. 148: 307-312

Kumar CN, Knowles N (1993) Changes in Lipid Peroxidation and Lipolytic and Free-Radical Scavenging Enzyme during Aging and Sprouting of Potato (Solanum Tuberosum L.) Seed-Tubers. Plant Physiol. 102: 115-124

Marĉiulionienė D, Kiponas D, Lukšienė B, Montvydienė D (2006) Low-Level ^{137}Cs Ionizing Radiation and Plants. Art Hig Rada Toksikol. 57: 3-8

Nakano Y, Asada K (1981) Hydrogen Peroxide Is Scavenged by Ascorbate Specific Peroxidase in Spinach Chloroplasts. Plant Cell Physiol. 22: 867-880

Sedmak JJ, Grossberg SE (1977) A Rapid, Sensitive, and Versatile Assay for Protein Using Coomassie Brilliant blue G250. Anal. Biochem. 79: 544-552

O-J-I-P Fluorescence Rise Kinetics Reveals Differential Cold Acclimation Capability in Sugarcane Varieties Following Exposure to Frost

Philippus DR van Heerden

South African Sugarcane Research Institute, Private Bag X02, Mount Edgecombe, 4300, South Africa.
Corresponding author. Tel. No. +27 31 508 7439; Fax No. +27 31 508 7597; E-mail: riekert.vanheerden@sugar.org.za.

Abstract: In some sugarcane-producing regions of South Africa frost occurs during winter in low-lying areas (frost pockets). There is a great demand for frost tolerant sugarcane varieties as production in these frost pockets could be more profitable. Two Louisiana (USA) varieties, known to yield high sugar even when immature (LCP 85-384 and HOCP 96-540), and two South African varieties (N21 and N36) were evaluated in a field trial for frost tolerance. Kinetic analysis of polyphasic O-J-I-P fluorescence transients, and calculation of JIP-test parameters, revealed that N36 and LCP 85-384 were capable of substantial cold acclimation following the first frost, while N21 and HOCP 96-540 lacked similar capability. Exposure to further frosts altered fluorescence rise kinetics in a variety-specific fashion, with clear recovery in N36 and LCP 85-384 towards baseline kinetics, but with further deterioration in N21 and HOCP 96-540. During the period between the first frost and harvest, N36 and LCP 85-384, which were capable of cold acclimation, increased cane quality values by 26% and 21% respectively, while N21 and HOCP 96-540, which lacked similar capability, only increased these values by 9% and 11% respectively. Sugarcane varieties capable of cold acclimation therefore show promise for use in frost pockets.

Keywords: Chlorophyll *a* fluorescence; Cold tolerance; Frost; Sugarcane

Introduction

Frost is common in the Midlands region of Kwazulu-Natal province in South Africa, especially in so-called 'frost pockets'. Cultivating sugarcane in frost-prone areas often necessitate shorter growing cycles to prevent cane deterioration (Eggleston *et al*., 2004). Annual harvesting of sugarcane in the Midlands is not profitable because the full yield potential of the crop is usually attained at 18–24 months of age. There is a need to identify frost tolerant varieties that will yield high sucrose when harvested young, to facilitate more profitable sugarcane production in frost-prone areas. The objective of this study was to evaluate the field-performance of two fast-maturing varieties (LCP 85-384 and HOCP 96-540) imported from Louisiana, USA (Dufrene and Tew, 2004), and two South African varieties (N21 and N36) under typical frost-prone growing conditions.

Materials and Methods

All varieties were bulked-up using the NovaCane® tissue culture protocol (Snyman *et al*., 2008). A field trial was planted on 18 October 2007 in a typical valley-bottom frost pocket at New Hanover in the Midlands North region of Kwazulu-Natal (South Africa). The trial consisted of five replicated plots for each variety, randomised according to soil characteristics. Trial plots were comprised of five cane rows, each 10 m long, spaced 1 m apart. Trial management proceeded as per farm practice.

Stalk samples were taken from each plot prior to frost events to determine sucrose content (%). The first light frost occurred during mid-June 2008 and was followed by heavier frosts between 26 June and 3 July 2008. The heaviest frost occurred on 11 July 2008. Cane yield (t/ha) and sucrose content (%) were subsequently determined at harvest on 23 July 2008.

For a physiological assessment of frost effects on

the varieties, fast polyphasic (O-J-I-P) fluorescence transients (Strasser and Govindjee, 1992) were recorded in the youngest fully-expanded leaves with a fluorescence meter (PEA, Hansatech Instruments Ltd, King's Lynn, Norfolk, PE 30 4NE, UK). The recorded data were used to construct difference in variable fluorescence (ΔV) curves (Strauss *et al*., 2007) and for calculating the Performance Index (PI_{ABS}) (Strasser *et al*., 2000). The PI_{ABS} is regarded as a reliable indicator of electron transport efficiency and photosynthetic capacity during low temperature stress (Strauss *et al*., 2007). Chlorophyll fluorescence measurements were started six weeks before the first frost and repeated at 2-week intervals until harvest.

Results and Discussion

Construction of ΔV curves, using the pre-frost O-J-I-P fluorescence rise kinetics (5 June 2008, black horizontal lines) for each variety as a baseline, revealed that the first frost (20 June 2008, grey curves) induced a perturbation in kinetics of very similar shape and magnitude in all four varieties (Fig. 1). However, after further mild frosts (3 July 2008, black curves) the kinetics were altered in a variety-specific fashion, with clear recovery in N36 and LCP 85-384 towards baseline kinetics (downward pointing black arrows), but with further deterioration in N21 and HOCP 96-540 (upward pointing black arrows). These results depict a typical example of stress acclimation where exposure to a light frost hardens the plants to better tolerate subsequent heavier frosts, hence enabling sustained sucrose production for longer. These results suggest that N36 and LCP 85-384 were capable of cold acclimation following the first frost, while N21 and HOCP 96-540 lacked similar capability.

Compared to the pre-frost state (05/06/2008), all varieties showed a decline in PI_{ABS} values (Fig. 2, framed areas in graphs) following the first frost (20/06/2008), however, N36 and LCP 85-384 maintained these values for at least a further two weeks, even following further frosts (03/07/2008). In varieties N21 and HOCP 96-540, on the other hand, these frosts led to a further decline in PI_{ABS} values. Ultimately, the severe frost event (18/07/2008) just prior to harvest led to high levels of damage in all varieties. Maintenance of electron transport efficiency for at least two weeks longer following the first frost indicates potential for cold acclimation in N36 and LCP 85-384, which corroborates the observed recovery in ΔV kinetics (Fig. 1). The potential for cold acclimation in plants having the C_4 photosynthetic

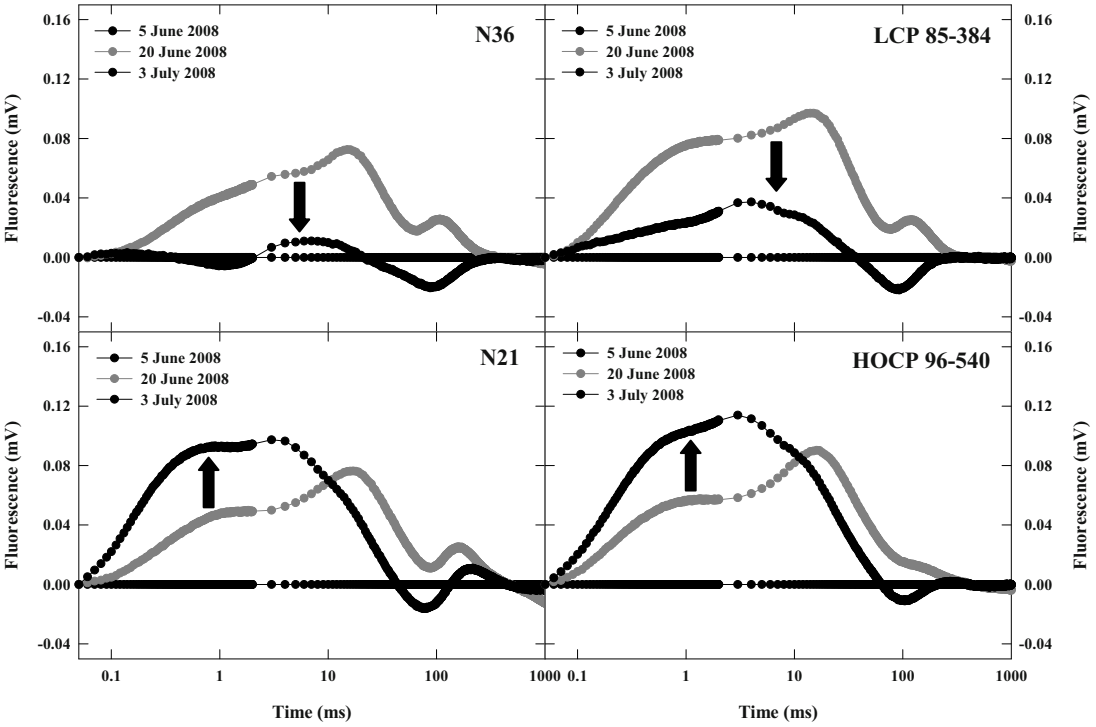

Fig. 1 Difference in variable fluorescence (ΔV) curves constructed by subtraction of normalised (O – P) fluorescence values recorded pre-frost (5 June, black horizontal baseline) from those recorded after the first frost (20 June, grey curves) or after several additional mild frosts (3 July, black curves). Each curve represents the values recorded in 15 plants.

pathway was recently demonstrated (Kakani *et al*., 2008), and in sugarcane varieties the ability to cold acclimate might be related to sensitivity of pyruvate, orthophosphate dikinase (PPDK) and NADP-malate dehydrogenase (NADP-MDH) activity (Du *et al*., 1999).

This observed cold acclimation likely enabled maintenance of higher photosynthetic potential (as indicated by the PI_{ABS} values) and stalk sucrose accumulation capacity for longer following the first frost events. Results that showed that N36 and LCP 85-384 increased cane sucrose content (%) by 26% and 21% between the pre-frost state and harvest, compared to N21 and HOCP 96-540, where the increase were only 9% and 11% (Fig. 3), support this suggestion.

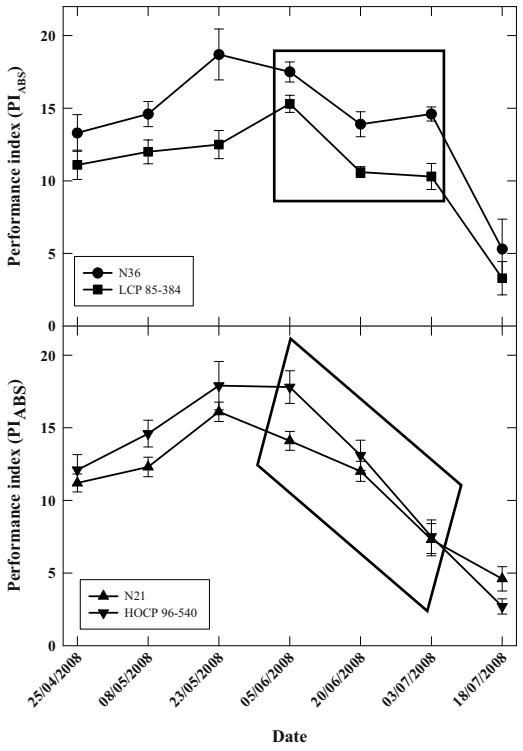

Fig. 2 Performance index (PI_{ABS}) values in the four varieties during the trial period. The framed area in each graph indicates the three time points used in Fig. 1 and discussed in the text. Data points represent the means of 15 plants ± SEM.

Although N36 and N21 had similar cane yields at harvest (results not shown), N36 had 30% higher sucrose yields (t/ha) than N21 (Fig. 4). Likewise, the reported sucrose yield advantage of HOCP 96-540 over LCP 85-384 that are observed under normal growing conditions (Dufrene and Tew, 2004) was reversed following frost.

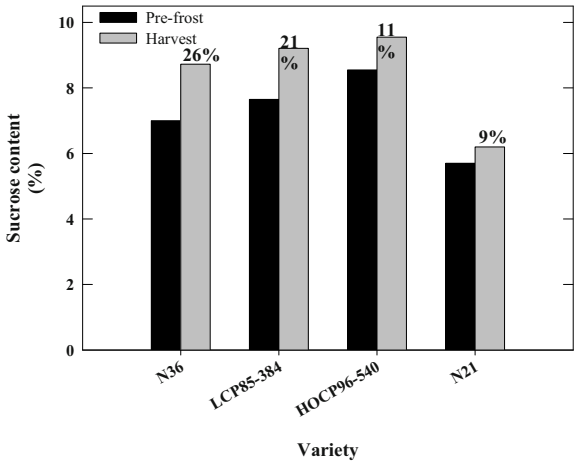

Fig. 3 Stalk sucrose content (%) in the four varieties pre-frost and at harvest. The % values indicates (per variety) how much higher the sucrose content was at harvest relative to the pre-frost state.

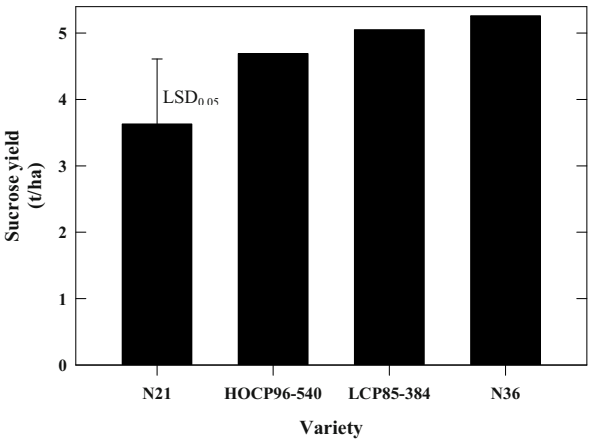

Fig. 4 Sucrose yields (t/ha) in the four varieties at harvest. The error bar indicates the least significant difference (LSD) at $p < 0.05$.

Conclusions

The ability to maintain high sucrose accumulation capacity for longer following frost due to cold acclimation could be an important factor determining sugarcane yield performance in frost-prone areas. In addition, O-J-I-P fluorescence rise kinetics show promise as a rapid screening tool for assessment of cold acclimation potential and frost tolerance in sugarcane.

References

Du YC, Nose A, Wasano K (1999) Effects of Chilling

Temperature on Photosynthetic Rates, Photosynthetic Enzyme Activities and Metabolite Levels in Leaves of Three Sugarcane Species. Plant Cell Environ. 22: 317-324

Dufrene EO, Tew TL (2004) HOCP 96-540, a Chip Off the Old Block? Am. Soc. Sug. Cane Tech. 24: 82

Eggleston G, Legendre B, Tew T (2004) Indicators of Freeze-Damaged Sugarcane Varieties Which Can Predict Processing Problems. Food Chem. 87: 119-133

Kakani VG, Boote KJ, Reddy KR, Lang DJ (2008) Response of Bahiagrass Carbon Assimilation and Photosystem Activity to Below Optimum Temperatures. Func. Plant Biol. 35: 1243-1254

Snyman SJ, Meyer GM, Banasiak M, Nicholson TL, van Antwerpen T, Naidoo P, Erasmus JD (2008) Micropropagation of Sugarcane Via NovaCane^{R}: Preliminary Steps in Commercial Application. Proc. S. Afr. Sug. Technol. Ass. 81: 513-516

Strasser RJ, Govindjee (1992) The F_0 and the O-J-I-P Fluorescence Rise in Higher Plants and Algae. In: Argyroudi-Akoyunoglou, JH (eds.), Regulation of Chloroplast Biogenesis. Plenum Press: New York, USA, pp. 423-426

Strasser RJ, Srivastava A, Tsimilli-Michael M (2000) The Fluorescence Transient As a Tool to Characterise and Screen Photosynthesic Samples. In: Yunus M, Pathre U, Mohanty P (eds.), Probing Photosynthesis: Mechanisms, Regulation and Adaptation. Taylor and Francis: London, pp. 445-450

Strauss AJ, Krüger GHJ, Strasser RJ, van Heerden PDR (2007) The Role of Low Soil Temperature in the Inhibition of Growth and PSII Function during Dark Chilling in Soybean Genotypes of Contrasting Tolerance. Physiol. Plant. 131: 89-105

Antioxidant Defence System and Chloroplasts Photochemical Characteristics of Wheat Genotypes Subjected to Water Stress

Samira M Rustamova *, Hasan H Babayev, Irada M Huseynova

Institute of Botany, Azerbaijan National Academy of Sciences, Baku, Azerbaijan.
*Corresponding author. Tel. No. +994 12 438 1164; Fax No. +994 12 510 2433; E-mail: rustamova-s@botany-az.org.

Abstract: Activities of catalase, ascorbate peroxidase, superoxide dismutase and glutathione reductase, as well as carotenoid content and photochemical activity of photosystem I and photosystem II were studied in leaves of durum and bread wheat genotypes. It was found out that dynamics of catalase and ascorbate peroxidase functioning in well-watered plants through ontogenesis practically did not change both among durum and among bread wheat cultivars. Functioning of these enzymes during ontogenesis under water deficit differed. Catalase activity increased in all stressed genotypes: in durum wheat cultivars maximal activity was observed in the milk ripeness and in bread wheat cultivars - in the end of flowering. Ascorbate peroxidase activity also increased under water deficit: in tolerant wheat genotypes maximal activity occurred in the end of flowering, in sensitive ones—in the end of ear formation. The maximum activity of glutathione reductase both as in the control, as well as in drought-subjected plants was observed in the anthesis stage. Superoxide dismutase activity was lower than the control during ontogenesis, excepting the last stages. It should be noted that PS I and PS II photochemical activity were also high in genotypes subjected to drought both in the end of ear formation and flowering stages.

Keywords: Wheat genotypes; Antioxidants; Carotenoids; PS I; PS II

Introduction

To cope with highly variable environmental stresses plants have to set a series of adaptation mechanisms ranging from cellular metabolism to physiological and developmental responses (Zaidi *et al.*, 2010). Water stress is a major constraint to wheat productivity causing substantial reduction in grain yield and quality and becoming a more devastating factor for worldwide wheat production due to global warming. Drought stress leads to increased accumulation of reactive oxygen species (ROS) in plants thus causing an oxidative stress. Various subcellular organelles such as chloroplast, mitochondrion and peroxisome are the common sites of ROS production. Increased levels of ROS cause damage to various cellular components, such as enzyme inhibition, protein degradation, DNA and RNA damage, and membrane lipid peroxidation, which ultimately culminate in cell death (Ishikawa *et al.*, 2010). To overcome it plants activate a number of evolutionary developed complex defense mechanisms. Plants have the ability to scavenge/detoxify ROS by producing different types of antioxidants. Antioxidants can be generally categorized into two different types, *i.e.*, enzymatic and non-enzymatic. Enzymatic antioxidants include superoxide dismutase (SOD), catalase (CAT), ascorbate peroxidase (APX), monodehydroascorbate reductase (MDHAR), dehydroascorbate reductase (DHAR) and glutathione reductase (GR). The commonly known non-enzymatic antioxidants are glutathione (GSH), ascorbate (AsA) (both water soluble), carotenoids and tocopherols (low molecular weight lipid soluble). Genes encoding different types of antioxidants have been engineered in different plants for achieving enhanced drought tolerance (Ashraf, 2010). Undoubtedly, engineering of genes coding for antioxidative enzymes has provided new insights into the role of these enzymes in plant cells in

counteracting stress-induced ROS. Although ROS in plants are produced under normal growth conditions and their concentration remains low (Polle, 2001). Thus, ROS are considered as cellular indicators of stresses as well as secondary messengers actively involved in the stress-response signaling pathways. Knowledge of ROS regulation and antioxidant production is necessary for generating transgenics with altered levels of antioxidant enzymes and metabolites, because enhanced antioxidant production under one kind of stress may evoke tolerance to other stresses (Ashraf, 2009).

Materials and Methods

Experiments were undertaken on the wheat genotypes differing in drought resistance—two *Triticum durum* L.: cv Barakatli-95 (drought tolerant) and cv Garagylchyg-2 (drought sensitive); two *Triticum aestivum* L.: cv Azamatli-95 (drought tolerant) and cv Giymatli-2/17 (drought sensitive). The plants were provided by Experimental Station of the Research Institute of Agriculture (Baku, Azerbaijan). Different sensitivities of these genotypes to drought had been determined during some years in different regions of Azerbaijan based on grain yield (Aliev, 1998; Aliev, 2001). All plants were grown in the field on a wide area under normal water supply and drought. Dehydration was imposed by withholding water supply. Measurements were made during the all stages of ontogenesis.

Leaves were homogenized with a Waring blender at full speed four times for 20 s each in an ice-cold grinding chloroplast isolation medium (1:6 w/v) containing 0.4 mol sucrose, 20 mmol Tris, 10 mmol NaCl, 1 mmol EDTA (sodium salt), 5 mmol sodium ascorbate, and 0.1% polyethylene glycol, pH 7.8. Samples frozen in liquid nitrogen and stored at −80 °C until required. Photochemical activities of chloroplasts isolated from control and drought-stressed plants were followed polarographically as O2 evolution or uptake at 20 °C using a water-jacketed Clark type oxygen electrode chamber under illumination with saturating white actinic light (850 μE $m^{-2}s^{-1}$), according to (Guseinova *et al.*, 2001). The following electron transport activities were assayed in μmol O_2 mg^{-1} Chl h^{-1}. The content of carotenoids was determined spectrophotometrically in 100% acetone extract (Wettstein, 1957).

Enzyme extract was prepared by homogenizing leaf material (1 g fr wt) with a pestle in an ice-cold mortar with Na_2HPO_4/NaH_2PO_4 buffer. The homogenates were filtered through four layers of cheesecloth and then centrifuged at 4 °C. The supernatant were collected and used for the assays of enzymatic activities. The activity of CAT was determined as a decrease in absorbance at 240 nm for 1 min following the decomposition of H_2O_2 as described by Kumar and Knowles (1993). The activity of ascorbate peroxidase was assayed according to Nakano and Asada (1981). The activity was measured as a decrease in absorbance at 290 nm for 30 sec. GR activity was determined at 340 nm for 10 min in reaction mixture containing 100 mmol potassium phosphate buffer (pH 7.8), 1 mmol EDTA, 0.2 mmol NADPH and 0.5 mmol GSSG (Yannarelli *et al.,* 2007). Superoxide dismutase activity was estimated by using SOD Assay Kit-WST (Sigma-Aldrich, U.S.A.). The absorbance was recorded at 450 nm and one enzyme unit of SOD activity was defined as the amount of enzime recuired to cause 50% inhibition of the rate of NBT reduction. Protein content was determined according to Sedmak and Grossberg (1977) by using bovine serum albumin as a standard.

Results and Discussion

Results showed that functioning dynamics of CAT and APX in well-watered plants through ontogenesis practically did not change both among durum and among bread wheat cultivars. In Barakatli-95 and Garagylchyg-2 both enzymes exhibited maximal activity in the end of flowering, in Azamatli-95 and Giymatli-2/17—in the end of ear formation. Functioning of these enzymes during ontogenesis under water deficit differed: CAT activity increased in all stressed genotypes as compared with control: in durum wheat cultivars maximal activity was observed in the milk ripeness and in bread wheat cultivars - in the end of flowering (Table 1).

In drought-tolerant genotypes Barakatli-95 and Azamatli-95 CAT activity increased more substantially as compared to sensitive ones. APX activity also increased under water deficit: in tolerant wheat genotypes maximal activity occurred in the end

of flowering, in sensitive ones—in the end of ear formation. The maximum activity of GR both as in the control, as well as in drought-subjected plants was observed in the anthesis stage. GR activity in drought-tolerant durum wheat Barakatli-95 and resistant bread wheat Azamatli-95 was higher than the control in all stages of ontogenesis (data not shown). SOD functioning dynamics through ontogenesis differed from CAT and APX. Interestingly, SOD activity was lower than the control during ontogenesis, excepting the last stages. In drought-tolerant Barakatli-95 and Azamatli-95 it increased against the control only at wax ripeness stage, when force of a drought was the greatest (Table 2).

Table 1 Effect of water stress at different stages of ontogenesis on CAT activity (unit/mg protein) (I - stalk emergence, II - beginning of earing, III - end of earing, IV - flowering, V - end of flowering, VI - milky ripeness, VII - wax ripeness).

Genotypes	I	II	III	IV	V	VI	VII
Barakatli-95 (control)	52	42	243	186	459	187	183
Barakatli-95 (stress)	150	131	221	242	272	471	161
Garagylchyg (control)	163	62	108	123	193	141	140
Garagylchyg (stress)	79	85	157	116	226	247	143
Azamatli-95 (control)	22	16	147	82	141	140	153
Azamatli-95 (stress)	139	65	159	121	200	166	167
Giymatli-2/17 (control)	31	58	243	205	205	93	85
Giymatli-2/17 (stress)	128	68	129	124	238	175	212

Table 2 Effect of water stress at different stages of ontogenesis on SOD activity (unit/mg protein). (I - stalk emergence, II - beginning of earing, III - end of earing, IV - flowering, V - end of flowering, VI - milky ripeness, VII - wax ripeness).

Genotypes	I	II	III	IV	V	VI	VII
Barakatli-95 (control)	6.5	3.2	1.77	5	0.9	4.4	8.5
Barakatli-95 (stress)	4	2.5	2	2.7	0.7	4	9
Garagylchyg (control)	2.8	5.5	1.3	4	1.2	2.8	10
Garagylchyg (stress)	1.8	1.8	0.9	1.8	0.3	1.8	0.3
Azamatli-95 (control)	2	1.77	11.1	1.9	0.7	2	2.9
Azamatli-95 (stress)	1.9	1.8	1.7	1.3	0.55	1.9	10
Giymatli-2/17 (control)	2.5	10	1.25	2.7	1.05	2.5	9
Giymatli-2/17 (stress)	2.7	2.5	1.8	1.77	0.35	2.75	2

Also direct correlation between APX activity and carotenoid content was observed through ontogenesis (data not shown). It should be noted that in subjected to drought genotypes PS I and PS II activities were also high both in the end of ear formation and flowering stages (Tables 3 and 4).

Table 3 Photosystem II activity in chloroplasts from wheat genotypes at different stages of ontogenesis (мmol O_2 mg^{-1} chlorophyll h^{-1}) (I - stalk emergence, II - beginning of earing, III - end of earing, IV - flowering, V - end of flowering, VI - milky ripeness, VII - wax ripeness).

Genotypes	I	II	III	IV	V	VI	VII
Barakatli-95 (control)	20	24	120	100	84	40	12
Barakatli-95 (stress)	60	60	160	92	100	45	26
Garagylchyg (control)	80	108	84	120	100	24	20
Garagylchyg (stress)	72	72	120	112	108	27	24
Azamatli-95 (control)	88	100	120	88	100	28	40
Azamatli-95 (stress)	104	72	136	120	92	16	8
Giymatli-2/17 (control)	140	72	140	112	120	20	12
Giymatli-2/17 (stress)	120	96	160	104	120	22	8

Table 4 Photosystem I activity in chloroplasts from wheat genotypes at different stages of ontogenesis (мmol O_2 mg^{-1} chlorophyll h^{-1}) (I - stalk emergence, II - beginning of earing, III - end of earing, IV - flowering, V - end of flowering, VI - milky ripeness, VII - wax ripeness).

Genotypes	I	II	III	IV	V	VI	VII
Barakatli-95 (control)	200	600	820	600	740	680	560
Barakatli-95 (stress)	540	400	840	500	520	500	280
Garagylchyg (control)	420	300	540	500	460	360	280
Garagylchyg (stress)	320	100	560	440	440	360	280
Azamatli-95 (control)	400	180	640	400	500	400	240
Azamatli-95 (stress)	400	180	640	440	520	440	160
Giymatli-2/17 (control)	400	240	740	420	440	440	120
Giymatli-2/17 (stress)	360	180	760	420	440	440	160

Obtained data can be useful in better understanding of stress-related mechanisms and selection for drought-tolerance in water-limited environments.

References

Aliev JA (1998) Importance of Photosynthesis of Various Organs in Protein Synthesis in Grain of Wheat Genotypes under Water Stress. Proceedings of the XIth International Congress on Photosynthesis, Budapest, Hungary, 1998. In: G Garab (ed.), Photosynthesis: Mechanisms and Effects, Vol. 5. Kluwer Academic Publishers: Dordrecht/Boston/ London, pp 3829-3832

Aliev JA (2001) Physiological Bases of Wheat Breeding Tolerant to Water Stress. Proceedings of the 6th International Wheat Conference, Budapest, Hungary, 2000. In: Z Bedo, L Lang (eds.), Wheat

in a Global Environment, Vol. 9. Kluwer Academic Publishers: Dordrecht/Boston/London, pp. 693-698

Ashraf M (2009) Biotechnological Approach of Improving Plant Salt Tolerance Using Antioxidants As Markers. Biotechnology Advances 27: 84-93

Ashraf M (2010) Inducing Drought Tolerance in Plants: Recent Advances. Biotechnology Advances 28: 169

Guseinova IM, Suleymanov SY, Aliyev JA (2001) Regulation of Chlorophyll-Protein Complex Formation and Assembly in Wheat Thylakoid Membrane. J. of Biochem. and Mol. Biol. 34: 496-501

Ishikawa T, Takahara K, Hirabayashi T, Matsumura H, Fujisawa S, Terauchi R, Uchimiya H, Kawai-Yamada M (2010) Metabolome Analysis of Response to Oxidative Stress in Rice Suspension Cells Overexpressing Cell Death Suppressor Bax Inhibitor-1. Plant Cell Physiol. 51(1): 9-20

Kumar CN, Knowles N (1993) Changes in Lipid Peroxidation and Lipolytic and Free-Radical Scavenging Enzyme during Aging and Sprouting of Potato (Solanum Tuberosum L.) Seed-Tubers. Plant Physiol.102: 115-124

Nacano Y, Asada K (1981) Hydrogen Peroxide Is Scavenged by Ascorbate-Specific Peroxidase in Spinach Chloroplasts. Plant Cell Physiol. 22: 867-880

Polle A (2001) Dissecting the Superoxide Dismutase–Ascorbate–Glutathione Pathway in Chloroplasts by Metabolic Modeling. Computer Simulations As a Step towards Flux Analysis. Plant Physiol. 126: 445-462

Sedmak JJ, Grossberg SE (1977). A Rapid, Sensitive, and Versatile Assay for Protein Using Coomassie Brilliant Blue G 250. Anal. Biochem. 79: 544-552

Wettstein D (1957) Chlorophyll Latale und Der Submikro-Skopische Formwechsel Der Plastiden. Exp. Cell Res.12: 427-506

Yannarelli GG, Fernandez-Alvarez AJ (2007) Glutatione Reductase Activity and Isoforms in Leaves and Roots of Wheat Plants Subjected to Cadmium Stress. Phytochemistry 68: 505-512

Zaidi I, Ebel C, Touzri M, Masmoudi K, Hanin M (2010) TMKP1 Is a Novel Wheat Stress Responsive MAP Kinase Phosphatase Localized in the Nucleus. Plant Mol Biol. 73: 325-338

Phosphorylation of PSII Proteins in Low Light Grown Maize in Response to the Pb Ions

Wasilewska Wioleta [1], Zienkiewicz Maksymilian [1], Fristedt Rikard [2],
Vener V Alexander [2], Romanowska Elzbieta [1]

[1]Department of Molecular Plant Physiology, Warsaw University, Miecznikowa 1, 02-096 Warsaw, Poland;
[2]Division of Cell Biology, Linköping University, SE-581 85 Linköping, Sweden.
Corresponding author. Tel. No. +48225543916; Fax No. +48225543910; E-mail: romanela@biol.uw.edu.pl.

Abstract: Reversible protein phosphorylation plays a crucial role in the regulation of numerous cellular functions and signal transduction pathways. In thylakoids light- and redox-induced activation or deactivation of protein phosphorylation is involved in structural changes of these membranes and in regulation of protein turnover. Photosynthesis in C4 plants involves mesophyll (M) and bundle sheath (BS) chloroplasts, which differ structurally and functionally. We studied maize plants in which lead was introduced into detached leaves with transpiration stream. Thylakoids were isolated mechanically and then proteins were analyzed. We observed that PSII activity was not affected by Pb ions in M chloroplasts, whereas in BS it was reduced. The presence of Pb ions affected only slightly photochemical efficiency of PSII (Fv/Fm ratio). Protein phosphorylation in mesophyll and bundle sheath thylakoids was analyzed using mass spectrometry and western blotting before and after lead treatment. Both methods clearly demonstrated increase in phosphorylation of the PSII proteins upon treatment with the heavy metal. We found that D1 and PsbH proteins of PSII complex were strongly phosphorylated in the presence of Pb ions. These results suggest that Pb^{2+} stimulates phosphorylation of PSII core proteins, which affects the stability of PSII complex by controlling the conversion of dimeric PSII to its monomeric form and in this way regulates the rate of D1 protein degradation. Therefore changes in phosphorylation of PSII core proteins induced by Pb ions may be a crucial regulation step in protection mechanism important for stabilization the dimeric PSII complex in stress conditions. Our results show that acclimation to Pb ions was achieved in both types of maize chloroplasts in the same way. However, these processes are obviously more complex because of different metabolic status in M and BS chloroplasts.

Keywords: Mesophyll and bundle sheath chloroplasts; Environmental stresses; Lead; Phosphorylation of PSII core proteins

Introduction

Environmental factors cause dynamic changes in thylakoid membranes which is important to sustain photosynthetic activity of plants under stress conditions. It is well known that photosynthesis is more sensitive to environmental pollutions, like heavy metals, than the other biochemical processes in higher plants (Takahashi and Murata, 2008). In C4 plants photosynthesis involves mesophyll (M) and bundle sheath (BS) chloroplasts, which differ structurally and functionally (Romanowska *et al*., 2008). Up to date little information is available about acclimation strategies of maize chloroplasts to heavy metals. One of them could be reversible protein phosphorylation, a well known mechanism that is crucial in regulation of numerous cellular functions and signal transduction pathways. This process can be modulated by environmental stresses, like irradiance. In thylakoids light- and redox-induced activation or deactivation of thylakoid protein phosphorylation is involved in structure changes and regulate protein turnover (Bellafiore *et al*., 2005; Bonardi *et al*., 2005; Fristedt *et al*., 2009).

Materials and Methods

Maize plants were grown at an irradiance 100 µmol photons m^{-2} s^{-1} (low light) in a growth chamber. Leaves were harvested from 4–5 week- old plants. Lead (5 mmol $Pb(NO_3)_2$) was introduced into the leaves with transpiration stream in weak light. Chlorophyll a fluorescence of leaves was measured at room temperature with an FMS-1 fluorometer (Hansatech). Mesophyll and bundle sheath chloroplasts were isolated mechanically (Romanowska and Parys, 2011). The isolation buffers were supplemented with 10 mmol NaF if was needed. Total chlorophyll content was determined according to the method of Arnon (1949). PSII activity was measured spectrophotometrically. SDS-PAGE was carried out on 15% gels using the procedure of Laemmli (1970). Following electrophoresis, the gels were electroblotted as described by Towbin *et al*. (1979). Polypeptides were probed with specific antibodies against PSII proteins or anti- phosphothreonine residue, and were visualized by enhanced chemiluminescence. The mapping of phosphorylation sites and the extent of PSII protein phosphorylation were analyzed by mass spectrometry (Fristedt *et al*., 2010).

Results and Discussion

The effect of lead on PSII function in maize mesophyll and bundle sheath thylakoids of plants grown under low light conditions was investigated. The presence of Pb ions did not affect photochemical efficiency of PSII (data not presented). These results are in agreement with observation that PSII activity of thylakoids isolated from mesophyll chloroplasts of maize was not affected by lead (Fig. 1). On the other hand, in bundle sheath thylakoids we observed decrease of PSII activity after lead treatment. Probably, Pb ions had inhibitory effect on the reducing site of PSII, because this reaction could be restored by using artificial electron donor (DPC, 1,5-diphenylcarbazide). We found earlier (Romanowska *et al*., 2006) that pea plants grown in low light conditions are less resistant to Pb ions than high light grown plants. Our results suggest that effect of Pb^{2+} on electron transport dependents also on the leaf structure and metal accumulation (not presented).

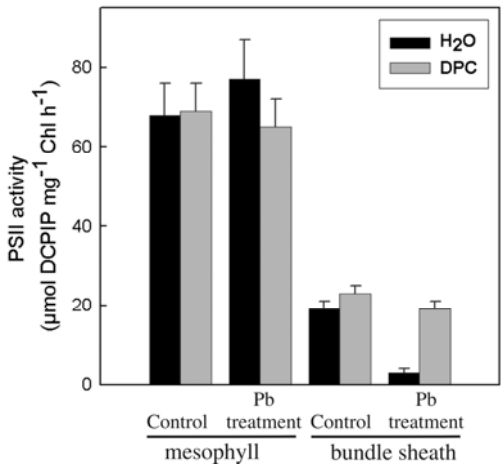

Fig. 1 PSII activity of mesophyll and bundle sheath thylakoids isolated from control and lead treated leaves (Pb).

The most interesting result of our studies was an unexpected increase in phosphorylation of the PSII proteins upon treatment with lead ions. The major proteins undergoing reversible phosphorylation in thylakoid membranes belong to photosystem II and include: D1, D2, CP43 and PsbH protein, as well as the peripheral LHCII antennae proteins (Vainonen, *et al*., 2005).

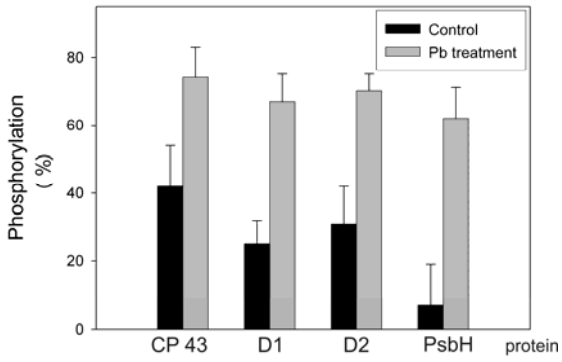

Fig. 2 *In vivo* phosphorylation stoichiometry of the PSII core proteins of maize mesophyll thylakoids isolated from the leaves after 24 h treatment with either 5 mmol $Pb(NO_3)_2$ (Pb treatment) or water (control) in weak light. Protein phosphorylation was analyzed by mass spectrometry.

The results of mass spectrometry analysis of the PSII core protein phosphorylation in maize mesophyll thylakoids isolated from control and Pb treated leaves are presented in Fig. 2. These results are in agreement with our data from western blotting (not presented). The D2 protein in phosphorylated form was found only in mesophyll membranes while the rest of the PSII core proteins were phosphorylated in both, mesophyll and bundle sheath thylakoids. Similarly to the western blotting

results the mass spectrometry analyses revealed a very poor phosphorylation of CP43 and D1 protein in control BS thylakoids what is characteristic for low light conditions. Moreover, the extent of the D1, D2 and CP43 protein phosphorylation in the mesophyll chloroplasts of the lead treated leaves was much higher than in bundle sheath thylakoids. We detected a very strong phosphorylation of PsbH protein after Pb treatment in both types of chloroplast and we believe that it is crucial for stabilization of dimeric structure of D1/D2 proteins during heavy metal stress.

We demonstrate that Pb ions affect phosphorylation of D1 protein. The western blotting analysis with anti-phosphothreonine antibody has shown that pretreatment of control maize leaves with specific electron transfer inhibitors, DCMU and DBMIB, caused decrease in the thylakoid protein phosphorylation. In the presence of Pb ions PSII core protein phosphorylation was not affected by inhibitors, while the extent of LHCII phosphorylation decreased. Also D1 protein was not dephosphorylated *in vivo* in Pb treated leaves subjected to darkness, as opposite to LHCII (data not presented). These results suggest that different kinases/phosphatases are involved in these processes and that they respond differently to Pb ions in low light conditions.

Thylakoid protein phosphorylation plays a key role in the regulation of the light- harvesting process (state transition), as well as the turnover of thylakoid proteins under various environmental conditions (Vener, 2007). By using the phosphothreonine antibody and mass spectroscopy analysis we demonstrate that heavy metal ions stimulate the phosphorylation of PSII proteins, especially of the D1 protein. Experimental data suggest that phosphorylation of PSII core proteins regulates the PSII photoinhibition-repair cycle by controlling the proteolytic degradation of photodamaged D1 protein in the thylakoid membrane (Aro *et al*., 1992). We also observed a very strong phosphorylation of PsbH protein which can indicate that it plays a significant role in the replacement of photodamaged D1 protein. The physiological role of this small, 9 kDa phosphoprotein is currently unknown, but experiments with *Chlamydomonas* have demonstrated that PsbH is needed for stable accumulation of PSII in dimeric form (Rokka *et al*., 2005).

We propose that increase in the PSII core protein phosphorylation is an adaptive response of maize to the exposure to Pb ions, which may be required to sustain photosynthesis under the heavy metal stress.

Acknowledgements

These studies were financed by the grants from the Ministry of Science and High Education of Poland NN 303 393636 and from the Swedish Research Council.

References

Arnon DI (1949) Copper Enzymes in Isolated Chloroplasts. Polyphenoloxidase in Beta Vulgaris. Plant Physiology 24: 1-15

Aro EM, Kettunen R, Tyystjärvi E (1992) ATP and Light Regulate D1 Protein Modification and Degradation. Role of D1* in Photoinhibition. FEBS Lett. 297: 29-33

Bellafiore S, Barneche F, Peltier G, Rochaix JD (2005) State Transitions and Light Adaptation Require Chloroplast Thylakoid Protein Kinase STN7. Nature 433: 892-895

Bonardi V, Pesaresi P, Becker T, Schleiff E, Wagner R, Pfannschmidt T, Jahns P, Leister D (2005) Photosystem II Core Phosphorylation and Photosynthetic Acclimation Require Two Different Protein Kinases. Nature 437: 1179-1182

Fristedt R, Willig A, Granath P, Crevecoeur M, Rochaix JD, Vener AV (2009) Phosphorylation of Photosystem II Controls Functional Macroscopic Folding of Photosynthetic Membranes in Arabidopsis. Plant Cell 21: 3950-3964

Fristedt R, Granath P, Vener AV (2010) A Protein Phosphorylation Threshold for Functional Stacking of Plant Photosynthetic Membranes. PLoS One 5: e10963

Laemmli UK (1970) Cleavage of Structural Proteins during the Assembly of the Head of Bacteriophage T4. Nature 227: 680-685

Rokka A, Suorsa M. Saleem A, Battchikova, Aro EM (2005) Synthesis and Assembly of Thylakoid Protein Complexes: Multiple Assembly Steps of Photosystem II. Biochem. J. 388: 159-168

Romanowska E, Wróblewska B, Drożak A,

Siedlecka M (2006) High Light Intensity Protects Photosynthetic Apparatus of Pea Plants Against Exposure to Lead. Plant Physiol. Biochem. 44: 384-394

Romanowska E, Kargul J, Powikrowska M, Finazzi G, Nield J, Drozak A, Pokorska B (2008) Structural Organization of Photosynthetic Apparatus in Agranal Chloroplasts of Maize. J Biol Chem 283: 26037-26046

Romanowska E, Parys E (2011) Mechanical Isolation of Bundle Sheath Cell Strands and Thylakoids from Leaves of C4 Grasses. In: Carpentier R (ed.), Methods in Molecular Biology, Photosynthesis Research Protocols. Humana Press, pp. 327-338

Takahashi S, Murata N (2008) How Do Environmental Stresses Accelerate Photoinhibition? Trends in Plant Science 13: 178-182

Towbin H, Staehelin T, Gordon J (1979) Electrophoretic Transfer of Proteins from Polyacrylamide Gels to Nitrocellulose Sheets: Procedure and Some Applications. Proc Natl Acad Sci USA 76: 4350-4354

Vainonen JP, Hansson M, Vener AV (2005) STN8 Protein Kinase in Arabidopsis Thaliana Is Specific in Phosphorylation of Photosystem II Core Proteins. J Biol Chem 280: 33679-33686

Vener AV (2007) Environmentally Modulated Phosphorylation and Dynamics of Proteins in Photosynthetic Membranes. Biochim Biophys Acta 1767: 449-457

A Potential Function for the γ2 Subunit (atpC2) of the Chloroplast ATP Synthase

Kaori Kohzuma[1, 2], Cristina Dal Bosco[3], Atsuko Kanazawa[1, 2], David M Kramer[1, 2*], Jörg Meurer[3]

[1]Plant Research Laboratory, S-222 Plant Biology Building, Michigan State University, East Lansing, MI 48824-1312;
[2]Institute of Biological Chemistry, 339 Clark Hall, Washington State University, Pullman, WA 99164-6340;
[3]Ludwig-Maximilians-Universitat, Department Biologie I, Botanik, Menzingerstrasse 67, 80638 Munchen.
[*]Corresponding author. Tel. No. +1 517-432-0072; Fax No. +1 517-432-0072; E-mail: kramed8r@msu.edu.

Abstract: Higher plants possess two, distinct genes for the ATP synthase γ subunit, atpC1 and atpC2. In *Arabidopsis*, atpC1 is the predominant form, and atpC2 is only weakly expressed in photosynthetic tissues. There is no evidence that it plays any role in energy transduction. Indeed, mutants lacking atpC1 are incapable of photoautotrophic growth, while those lacking atpC2 have no noticeable phenotype. To elucidate the possible function of these orthologs, we analyzed mutants expressing exclusively atpC1 or atpC2 in *Arabidopsis thaliana*. *In vivo* chlorophyll fluorescence and electrochromic shift (ECS) analyses demonstrated that both atpC1 and atpC2 can function in ATP synthesis, though even under a strong promoter, the activity of atpC2-containing ATP synthase was low. However, we observed a striking difference in the regulation of ATP synthase containing the two orthologs. With atpC1, the ATP synthase was inactivated in the dark, likely via oxidation of the regulatory γ subunit thiols. ATP synthase containing exclusively atpC2 showed no decrease in activity even after extensive dark adaptation. We propose that atpC2 may function to catalyze low levels of ATP-driven proton translocation in the dark, when the bulk of ATP synthase is inactivated, maintaining sufficient transthylakoid proton gradient to drive protein translocation or other processes.

Keywords: ATP synthase; γ subunit; AtpC2; *In vivo* spectroscopy

Introduction

Arabidopsis thaliana genome contains the *atpC1* (At4G04640) gene encoding the plastid ATP synthase γ subunit, and an additional gene, *atpC2* (At1G15700), encoding a homologous protein of unknown function and localization (Inohara *et al*., 1991). Knocking out atpC1 results in complete loss of photosynthesis, whereas knocking out atpC2 has little effect on photosynthetic competence under studied the conditions (Dal Bosco, 2006; Dal Bosco *et al*., 2004). Meanwhile, it has been reported that the atpC2 is localized in chloroplast from GFP fusion localization experiment using a functional targeting peptide of atpC2 (Dal Bosco, 2006). In this short paper, we analyzed an atpC2 knocked out mutant (*atpC2*) and atpC2 over-expresser mutants (C2II and C2III) in *Arabidopsis thaliana*, to reveal the possible function of two genes.

Materials and Methods

Plant Material and Growth Conditions

Wild-type Arabidopsis thaliana and mutants (*atpC2*, C2II and C2III) were grown on soil under continuous light period at 20–30 μmol photons m^{-2} s^{-1} at 22 °C for 4 weeks.

In vivo Spectroscopic Assays

Energy-dependent exciton quenching (qE) was estimated as described Kanazawa and Kramer, 2002. Steady state, light-induced *pmf* (ECSt) and the conductivity of thylakoid membrane to protons (g_{H+}), attributable to activity of the ATP synthase, was estimated from DIRK changes in absorbance associated with the electrochromic shift (ECS) at a 520 nm, described as Kanazawa and Kramer (2002), Cruz *et al*. (2005). Flash-induced relaxation kinetics (FIRK) experiments were performed on intact leaves

or infiltrated leaf disc described as Kohzaum *et al*. (2009).

Equilibrium Redox Titrations

Fully expanded detached leaves were vacuum-infiltrated with varying ratios of oxidized and reduced 20 mmol DTT solutions (Wu *et al*., 2007) for 30 min incubation in the dark. ΔA_{520} FIRK measurements were carried out described as above. The equilibrium redox potential were calculated described as Wu *et al*. (2007).

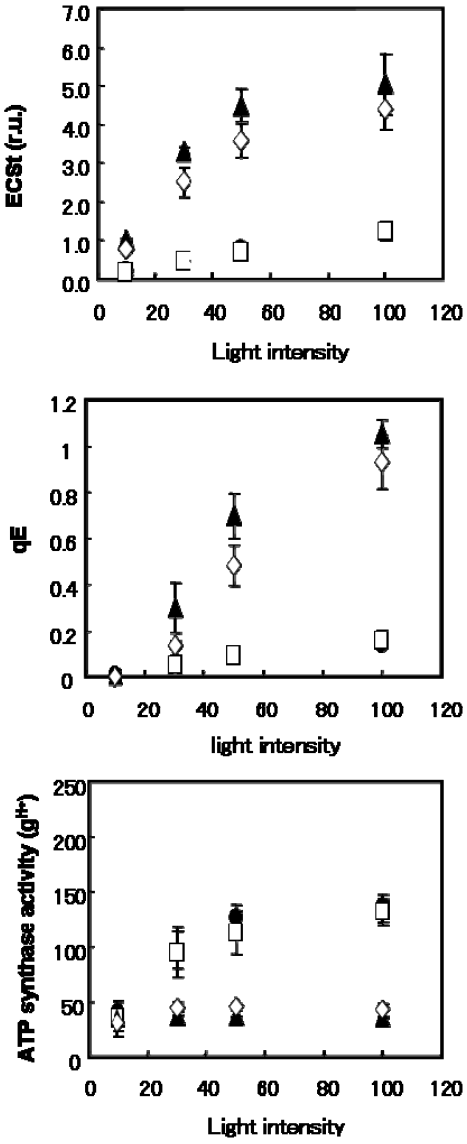

Fig. 1 WT (black circle), atpC2 (opened square), C2III (opened diamond) and C2II (closed triangle) are compared for difference in energy-dependent exciton quenching (qE), light-induced *pmf* (ECSt) and proton conductivity across the thylakoid membrane (g_{H+}) versus light intensity. These parameters were estimated by chlorophyll fluorescence yield and ECS spectroscopy analysis.

Results and Discussion

We measured chlorophyll fluorescence yields and the kinetics of the thylakoid ECS signal as probed by electron and proton transfer reactions in leaves. Estimates of proton motive force (*pmf*) as ECSt and ATP synthase activity kinetics (g_{H+}) using the electrochromic shift decay (Kanazawa and Kramer, 2002; Avenson *et al*., 2005; Cruz *et al*., 2005) and the energy-dependent exciton quenching (qE) was calculated by chlorophyll fluorescence analyses. The *pmf* and qE response of atpC2-expressed mutants increased significantly during actinit light intensity, compare to wild type and *atpC2.* The ATP synthase activity of atpC2-expressed mutants remained consistently lower than wild type and *atpC2.* These results imply that atpC2 (γ_2) dose not have a mutually complementary relationship with atpC1 (γ_1).

We found a drastic difference in the regulation of ATP synthase containing the two orthologs. The ATP synthase is usually inactivated in the dark, such as the atpC1 mainly containing wild type, likely via oxidation of the regulatory γ subunit thiols. However, the mutant containing high atpC2 (C2III) maintain activation in the dark. The atpC2 knockout mutant was slower than WT after dark adaptation. These results suggest that atpC2-ATP synthase remains high activity even after extensive dark adaptation. To further investigate the redox potential of ATP synthase containing high atpC2 mutant, we performed an equilibrium redox titration by infiltrating leaves with different proportions of oxidized and reduced DTT at a combined total concentration of 20 mmol (Fig. 2). ATP synthase with atpC2 is not modulated by redox potential over the physiological range. In wild type, the ECS decay, reflecting ATP synthase activity, was fast with reduced dithiothreitol (DTT) but slow with oxidized DTT. The ECS decay of the mutant containing high atpC2 (C2III) was independent of DTT. We conclude that the ATP synthases containing atpC2 did not regulated by thiol/disulfide switching system. The *atpC2* protein (γ_2) can functionally substitute for the atpC1 protein (γ_1). However, γ_2 appears to lack the thiol regulatory switch.

It is known that the ATP synthase is down-regulated in the dark, probably to prevent excessive ATP hydrolysis (Ort *et al*., 1990). However, some thylakoid proton gradient is maintained in the dark (Joliot and Joliot, 1989; Takizawa *et al*., 2007). In green algae, this gradient may be maintained by

chlororespiration (Bennoun, 1982), but how this operates in higher plant chloroplasts is not clear.

We propose that atpC2 may function to catalyze low levels of ATP-driven proton translocation in the dark, (*i.e.* proton pumping into the lumen driven by ATP hydrolysis) when the bulk of ATP synthase is inactivated, possibly to maintain sufficient transthylakoid proton gradient to drive protein translocation via the TAT pathway or maintain ion gradients.

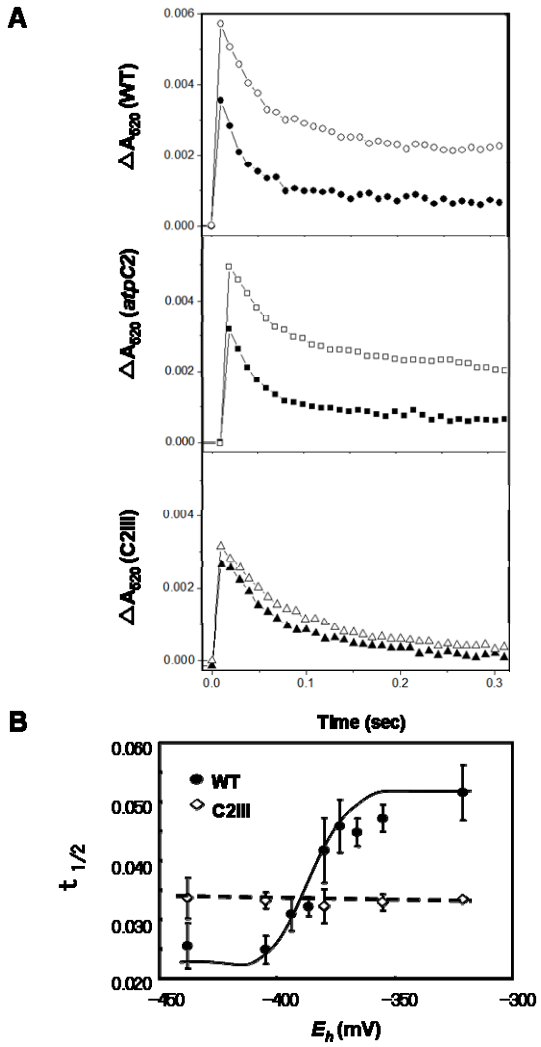

Fig. 2 A Trace of Flash induced relaxation kinetics (FIRK) in WT (circles), *atpC2* (squares) and C2III (triangles). Two kinetic measurements were traced 10 sec later (black) and 90 minutes later (white) after pre-illumination for 2 minute. **B** Equilibrium redox titration (as in Wu *et al*., 2007) of thiol/disulfide regulatory groups in the γ-subunit of the chloroplast ATP synthase. The ΔA_{520} relaxation kinetics were measured and used to calculate the halftime of the kinetics.

Acknowledgements

We are grateful to Dr. Alice Barkan (University of Oregon) for the CF_1-β antibodies. The work was supported by National Research Initiative competitive grant no. 2008-35318-04665 from the USDA National Institute of Food and Agriculture.

References

Avenson TJ, Kanazawa A, Cruz JA, Takizawa K, Ettinger WE, Kramer DM (2005) Plant Cell Environ 28: 97-109

Bennoun P (1982) Proc Natl Acad Sci 79: 4352-4356

Cruz JA, Avenson TJ, Kanazawa A, Takizawa K, Edwards GE, Kramer DM (2005) J Exp Bot 56: 395-406

Dal Bosco C, Lezhneva L, Biehl A, Leister D, Strotmann H, Wanner G, Meurer J (2004) J. Biol. Chem. 279: 1060-1069

Dal Bosco C (2006) Ph.D. Thesis, Universität München

Inohara N, Iwamoto A, Moriyama Y, Shimomura S, Maeda M, Futai M (1991) J. Biol. Chem. 266: 7333-7338

Joliot P, Joliot A (1989) Biochim. Biophys. Acta 975: 355-360

Kanazawa A, Kramer DM (2002) Proc Natl Acad Sci USA 99: 12789-12794

Kohzuma K, Cruz JA, Akashi K, Hoshiyasu S, MunekageYN, Yokota A, Kramer DM (2009) Plant. Cell and Enviroment 32: 209-219

Ort DR, Grandoni P, Ortiz-Lopez A, Hangarter RP (1990) Perspectives in Biochemical and Genetic Regulation of Photosynthesis, pp. 159-173

Takizawa K, Kanazawa A, Cruz JA, Kramer DM (2007) Biochim Biophys Acta 1767: 1233-1244

Wu G, Ortiz-Flores G, Ortiz-Lopez A, Ort DR (2007) J. Biol. Chem. 282: 36782-36789

The Role of *sll1558* and *sll1496* Genes under Acid Stress Conditions in the Cyanobacterium *Synechocystis* sp. PCC 6803

Mamoru Sambe[a], Shuichi Kitayama[a], Atsushi Moriyama[a], Junji Uchiyama[b], Hisataka Ohta[a, b, *]

[a]Department of biology, Faculty of Science, Tokyo University of Science, Shinjyuku, Tokyo 162-8601, Japan;
[b]Research center for RNA science, RIST, Tokyo University of Science, Noda, Chiba 278-8510, Japan.
[*]Corresponding author. Fax No. +81(3)5228 8374; E-mail: ohta@rs.noda.tus.ac.jp.

Abstract: The molecular mechanisms underlying plant sensitivity to acid stress are still unclear. Therefore, we intend to elucidate the mechanism of acid stress acclimation. The *sll1558* gene in *Synechocystis* sp. PCC 6803 was identified as an up-regulated gene by DNA microarray analysis in a short-time acid treatment (Ohta *et al*., 2005). This gene encodes mannose-1-phosphate guanylyltransferase, which catalyzes the reaction to GDP-D-mannose involved in N-glycan biosynthesis. The *sll1496* gene encodes the same enzyme. In this study, deletion mutants of these genes were constructed and phenotypes were analyzed. Both genes were found to be dispensable under normal growth conditions at pH 8.0. However, the *sll1558* deletion mutant was highly sensitive to acid stress conditions at pH 6.0. In contrast, the *sll1496* gene was found to be dispensable, as the *sll1496* deletion mutant was slightly sensitive to acid stress. Furthermore, the *At2g39770* (*cyt1*) gene in *Arabidopsis thaliana* has an orthologous relationship with *sll1558*. The *cyt1* mutant was more sensitive to acid stress conditions when compared with wild-type (WT) cells in the roots. The results of this study indicate that N-glycan biosynthesis contributes to acid stress and that only the *sll1558* gene plays an important role in acid stress in *Synechocystis*.

Keywords: Acid stress; Cyanobacteria; Mannose-1-phosphate guanylyltransferase; N-glycan

Introduction

Acid rain is a serious environmental problem that can have harmful effects on plants and animals through the processes of wet and soil deposition. In particular, plants, being unable to escape from harmful environments, are prone to acid stress-induced growth inhibition. In soil acidified by acid rain, toxicity induced by elution of aluminum ions has a negative influence on the growth of crops. Therefore, plants capable of growing under acid stress conditions would be expected to grow all over the world. However, the molecular mechanisms underlying plant sensitivity to acid stress are still unclear. Therefore, we intend to elucidate the mechanism of acid stress acclimation in plants.

In a previous study, we surveyed time-dependent gene expression in the unicellular cyanobacterium *Synechocystis* sp. PCC 6803 as affected by transfer acid conditions. This organism is well suited for such study because the entire genomic sequence has been determined (Kaneko *et al*., 1996), and DNA microarrays representing all open reading frames (ORFs) are now available. In the previous study, we found that the expression of the *sll1558* gene was up-regulated within 1 hour after being shifted to acid conditions. The *sll1558* gene encodes mannose-1-phosphate guanylyltransferase (EC 2.7.7.13), which catalyzes the reaction to GDP-D-mannose involved in N-glycan biosynthesis. The *sll1496* gene encodes the same enzyme.

In this study, to understand the effect of *sll1558* and s*ll1496* on acid stress, we performed quantitative real-time RT-PCR (qRT-PCR) analysis of the transcripts of the 2 genes. In addition, we examined the physiological function of cyanobacteria genes using mutant cells in which each gene was disrupted by a kanamycin and chloramphenicol resistance gene

cassette (*Km*^{r} and *Cm*^{r}). Based on phenotypes, the effect of acid stress on *sll1558* and *sll1496* deletion mutants was compared with that on WT cells. Furthermore, growth analyses were performed under acid stress conditions using the *cyt1* mutant in *Arabidopsis*, because the *cyt1* gene in *Arabidopsis thaliana* has an orthologous relationship with *sll1558*.

Materials and Methods

Strains and culture conditions

A glucose-tolerant WT strain of *Synechocystis* sp. PCC 6803 and disrupted mutants of the *sll1558* and *sll1496* genes prepared by inserting *Km*^{r} and *Cm*^{r}, were grown at 30 °C in BG-11 medium (Stanier *et al*., 1971) with 10 mmol TES–NaOH (pH 8.0) under continuous illumination provided by fluorescent lamps. Cells were grown in volumes of 50 ml in test tubes and bubbled with 3% CO_2-containing air. Cell density was measured at 730 nm using a spectrophotometer (Ultrospec 4,000 UV/Visible Spectrophotometer; Amersham Pharmacia Biotech, Uppsala, Sweden). Acid condition experiments were performed by transferring cells at the exponential growth phase (OD_{730} = 0.1–0.2) to acid condition BG-11 plates with 10 mmol MES-NaOH (pH 6.0).

Construction of mutants

A standard mutagenesis protocol for *Synechocystis* was used. The coding sequences of *sll1558* and *sll1496* were substituted into the antibiotic resistance genes *Km*^{r} and *Cm*^{r}, respectively, by homologous recombination. First, the *Cm*^{r} sequences and the *sll1558*/*sll1496* neighboring sequences were amplified by PCR. Approximately 2 or 3 kb of PCR products were cloned into pUC19 (Toyobo, Osaka, Japan). The primers for amplification were designed using the complete genome sequence of *Synechocystis*. Sequences that contained appropriate restriction sites were selected to improve cloning of fragments. The *Km*^{r} isolated from plasmid pUC4K (Amersham Pharmacia Biotech, Uppsala, Sweden) was inserted into unique restriction sites of the encoding sequences. Transformants were initially selected on a medium containing 10 μg mL^{-1} kanamycin (Km) and chloramphenicol (Cm) (Wako Pure Chemical, Osaka, Japan), whereas the segregation of clones was performed by restreaking (at least 3 transfers) of primary clones on plates supplemented with 50 μg mL^{-1} Km and 30 μg mL^{-1} Cm. During the cultivation of mutants, Km and Cm were added to the liquid media.

RNA isolation and quantitative real-time RT-PCR

Total RNA was isolated using the RNeasy Mini kit (Qiagen, Hilden, Germany), as described by (Hihar *et al*., 2001). For the reverse transcriptase (RT) reaction, 100 ng RNA was incubated with a mixture of PCR reverse primers for 10 min at 70 °C before addition of 100 U Superscript II RT (Gibco-BRL, Carlsbad, CA, USA). The RT reaction was performed at 42 °C for 1 h and terminated by incubating the cells at 72 °C for 10 min. A Perfect Real Time kit (Takara Bio, Shiga, Japan) was used according to the manufacturer's instructions.

Plant materials and growth condition of Arabidopsis

The plant materials used in this study included WT *A. thaliana* (Col-0 ecotypes) and genetic mutants derived from Col-0 ecotype. Seed germination and seedling growth were accomplished through the use of modified MS (Murashige-Skoog) media. The media was supplemented with 0.5% (w/v) sucrose and 20 mmol MES-KOH, adjusted to pH 5.7, and solidified with 1.5% purified agar (Nacalai Tesque Inc, Kyoto, Japan). In the acid condition experiments, we used the MS media with 20 mmol CH_3COONa–CH_3COOH (pH 4.5). *Arabidopsis* growth occurred in a controlled environment incubator (EYELATRON FLI-160; Eyela, Tokyo, Japan), preset with a 16-h light/8-h dark photoperiod, light intensity of 3,000 Lux, and a constant temperature of 22 °C. These growth conditions are referred to in Qin *et al*. (2008).

Results and Discussion

Characterization of the sll1558 and sll1496 deletion mutants

We first investigated mRNA levels of the genes in detail. The *sll1558* and *sll1496* expressions were analyzed using qRT-PCR to estimate the changes in transcript amounts in cells grown under acid stress conditions (pH 3.0). The *sll1558* gene showed clearly increased transcript levels. However, in the case of *sll1496,* we were not able to confirm a significant increase (data not shown). Next, we constructed the deletion mutants. The WT *Synechocystis* was transformed with *sll1558* and *sll1496* that had been interrupted with a gene cassette conferring the *Km*^{r}

and *Cm*^{r}. To examine the *segregation* of these genes within the *Synechocystis* genome, we performed PCR analysis using DNA obtained from WT, *Δsll1558*, *Δsll1496*, and double mutant cells. PCR with the chromosomal DNA of WT cells as a template was used to amplify respective DNA fragments for *sll1558* and *Δsll1496*, whereas PCR with DNA from *Δsll1558*, *Δsll1496,* and the double mutant cells yielded a fragment of resistance-cassette length (Fig. 1). This result indicated that the *sll1558* and *sll1496* genes in *Δsll1558*, *Δsll1496,* and the double mutant cells had been disrupted by the substitution of the *Km*^{r} and *Cm*^{r} genes. Subsequently, we performed phenotype analyses to identify the role of *sll1558* and *sll1496*. In normal BG-11 medium at pH 8.0, all strains exhibited a similar photoautotrophic doubling time, suggesting that deletion of these genes did not affect their growth under normal conditions (Fig. 2A). In contrast, in the acid stress conditions at pH 6.0, the growth of all mutant cells was slightly or significantly inhibited compared with that of WT cells. The *Δsll1558* and double mutants (*Δsll1558* and *Δsll1496*) were more sensitive to acid stress than the *Δsll1496* cells (Fig. 2B). Interestingly, *sll1558* and *sll1496* encode an enzyme with the same function. However, this result indicated that *sll1558* was involved more strongly in acid tolerance of *Synechocystis* cells as compared with *sll1496*.

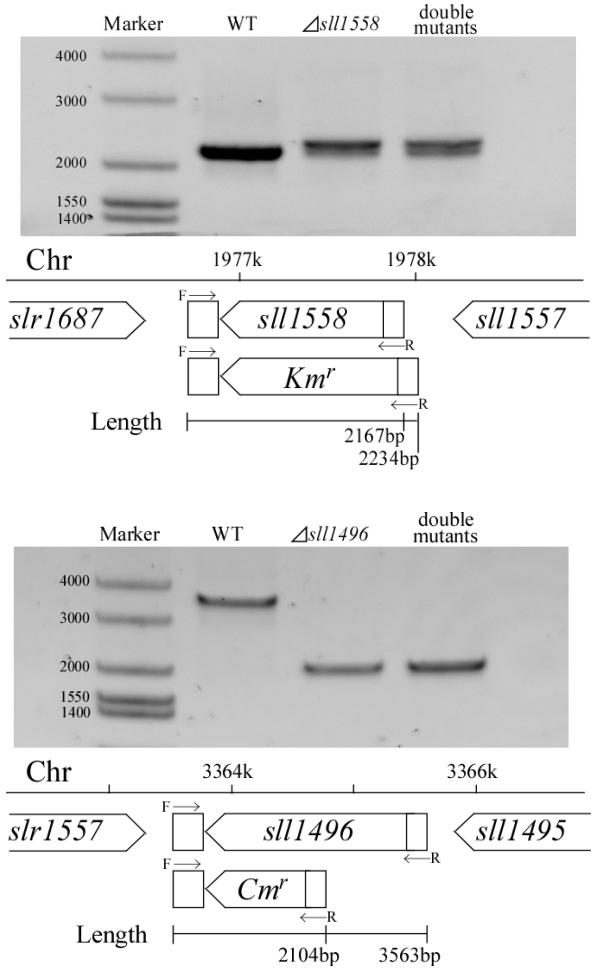

Fig. 1 Deficit confirmation of the *sll1558* and *sll1496.* Schematic drawing showed the gene organization of the chromosomal site where the *sll1558* and *sll1496* coding region and the *Km*^{r} and *Cm*^{r} were inserted. The PCR analyses using chromosomal DNA of the WT and the mutant (*Δsll1558*, *Δsll1496* and the double mutant) as a template. The primers used of specific for the *sll1558* and *sll1496* genes in order to verify disruption in the chromosomal DNA of the mutant. The marker used of Wide-Range (TaKaRa Bio, Shiga, Japan).

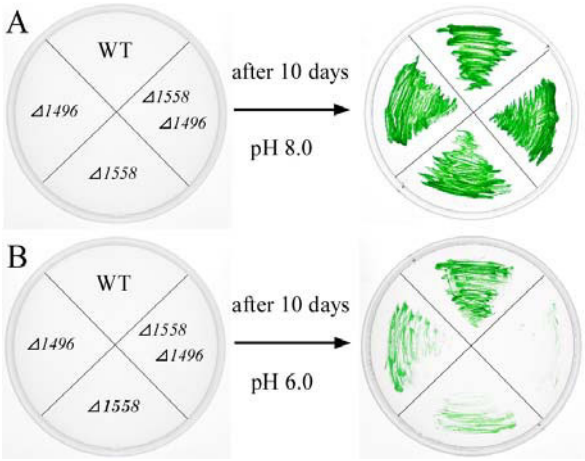

Fig. 2 Phenotypical confirmation of deletion mutants in *Cyanobacteria.*
Saturated dilutions of cultures of WT cells and deletion mutants (*Δsll1496*, *Δsll1558,* and double mutant) were streaked onto BG-11 plate (A: buffered with 10 mmol TES-NaOH [pH 8.0], B: buffered with 10 mmol MES-NaOH [pH 6.0]) and cultured for 10 days at 30 °C under 3,000 Lux of continuous cool white fluorescent light.

Morphological characterization of cyt1 mutant in Arabidopsis

To test the importance of N-glycan biosynthesis in plant growth under acid stress conditions, the level of growth in *Arabidopsis cyt1* mutant was analyzed under acid stress conditions (pH 4.5). The growth of both WT cells and *cyt1* mutants reduced under acid stress conditions as compared with normal conditions. Moreover, the level of growth retardation of *cyt1* mutants, in both aerial and root organs, also increased under acid stress conditions (Fig. 3). These results suggest that N-glycan biosynthesis contributes to the acid stress tolerance of *Synechocystis* and *Arabidopsis*.

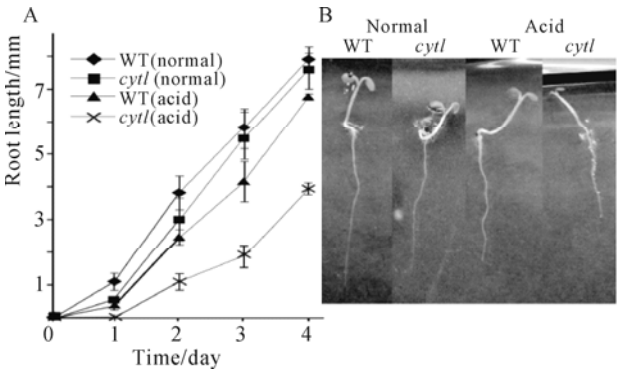

Fig. 3 Phenotypes of *cyt1* mutants in *Arabidopsis*.A: Root lengths on each of 4 days (WT-normal is a closed diamond, WT-acid is a closed square, *cyt1* mutants-normal is a closed triangle, and *cyt1* mutants-acid is a cross). B: The state of the roots 4 days after germination. The WT and *cyt1* mutants were seeded on 1/2 MS plates with 20 mmol MES-KOH adjusted to pH 5.7 (normal). In the acid condition experiments, we used MS media with 20 mmol CH_3COONa–CH_3COOH adjusted to pH 4.5 (acid).

Conclusion

We found significant differences between *sll1558* and *sll1496*, including their transcript level under acid stress conditions and sensitivity to deletion mutants. These results suggest that *sll1558* is more strongly involved in acid tolerance of *Synechocystis* cells than is *sll1496.* In addition, a positive regulation may act on only *sll1558* under acid stress conditions. To further elucidate the important differences between *sll1558* and *sll1496* under acid stress conditions, it is necessary to investigate the mechanism underlying transcriptional control.

Furthermore, our results suggest that N-glycan biosynthesis contributes to acid stress tolerance of *Synechocystis* and *Arabidopsis*. This may be the cause of the damage to the cell outer layer, such as the cell wall when sensitivity to acid stress is increased, because N-glycan is important for cell wall biosynthesis. Therefore, it is important to determine the factors that cause damage to the cell outer layer of WT cells and mutants. We are currently researching this subject through electron microscopy and analysis of the extracellular polysaccharide and cell outer layer of WT cells and mutants.

References

Ohta H, Shibata Y, Haseyama Y, Yoshino Y, Suzuki T, Kagasawa T, Kamei A, Ikeuchi M, Enami I (2005) Identification of Genes Expressed in Response to Acid Stress in Synechocystis sp. PCC 6803 Using DNA Microarrays. Photosynth. Res. 84: 225-230

Kaneko T, Sato S, Kotani H, Tanaka A, Asamizu E, Nakamura Y, Miyajima N, Hirosawa M, Sugiura M, Sasamoto S, Kimura T, Hosouchi T, Matsuno A, Akiko Muraki A, Nakazaki N, Naruo K, Okumura S, Shimpo S, Takeuchi C, Wada T, Watanabe A, Yamada M, Yasuda M, Tabata S (1996) Sequence Analysis of the Genome of the Unicellular Cyanobacterium Synechocystis sp. Strain PCC 6803. II. Sequence Determination of the Entire Genome and Assignment of Potential Protein-coding Regions. DNA Res. 3 (3): 109-136

Stanier RY, Kunisawa R, Mandel M, Cohen Bazire G (1971) Purification and Properties of Unicellular Blue-Green Alga (Order Chroococcales). Bacteriol. Rev. 35: 171-205

Hihara Y, Kamei A, Kanehisa M, Kaplan A, Ikeuchi M (2001) DNA Microarray Analysis of Cyanobacterial Gene Expression during Acclimation to High Light. Plant Cell 13: 793-806

Qin C, Qian W, Wang W, Wu Y, Yu C, Jiang X, Wang D, Wu P (2008) GDP-Mannose Pyrophosphorylase Is a Genetic Determinant of Ammonium Sensitivity in Arabidopsis Thaliana. Proc. Natl. Acad. Sci. USA 105 (47): 18308-18313

Comparative Photosynthetic Analyses of Three Widely Used *Arabidopsis* Ecotypes

Lan Yin[a], Rikard Fristedt[b], Alexander V Vener[b], Cornelia Spetea[a,*]

[a]Department of Physics, Chemistry and Biology, and [b]Department of Clinical and Experimental Medicine, Linköping University, Linköping, Sweden.
[*]Corresponding author. Tel. No. +46 13 282681; Fax No. +46 13 282817; E-mail: corsp@ifm.liu.se.

Abstract: There are over 1000 *Arabidopsis* ecotypes distributed around the world. In this study we have selected three ecotypes which are commonly used for generation of mutant lines, have distinct geographic distribution and plant morphology, namely Columbia Col-0 (Columbia USA), Landsberg erecta Ler-0 (Germany) and Wassilewskija Ws-4 (Belarus). Similar levels of photosynthetic pigment protein complexes were determined in the three ecotypes. Nevertheless, as compared to Col-0 and Ler-0, Ws-4 displayed 50% lower levels of phosphorylation for the photosystem II D1 and D2 proteins in thylakoids isolated from dark-adapted, growth light- or high-light-treated plants. These results were obtained using western blotting with phosphothreonine antibodies, and confirmed by quantitative mass spectrometry. Furthermore, photosystem II was more susceptible to high light treatment, and the D1 protein was faster degraded in Ws-4 leaves. Our results provide important information for understanding the mechanism underlying natural variation of high light acclimation in *Arabidopsis*.

Keywords: *Arabidopsis*; Ecotype; High light stress; Photosystem II; Protein phosphorylation; Thylakoid membrane

Introduction

Naturally occurring genetic variation is extensively studied in *Arabidopsis* (for a review, see Koornneef *et al.*, 2004). To identify the responsible gene or single nucleotide polymorphism for a specific trait using quantitative trait locus is a difficult task, requiring a combination of genetic and functional genomics tools. Such studies could provide insights into networks of gene regulation.

Here we study in detail three natural accessions (ecotypes) of *Arabidopsis,* which are widely used as background for generation of mutant lines, have distinct geographic distribution and plant morphology. Columbia Col-0 (Columbia, USA) was used as background for generation of T-DNA insertion mutant lines (SALK) at TAIR (Jose *et al.*, 2003). Landsberg erecta Ler-0 (Germany) was used as background for the Ds transposon (FGT) collection at the John Innes Centre (Sundaresan *et al.*, 1995). Finally, Wassilewskija Ws-4 (Belarus) was used as background for generation of T-DNA insertion lines (FLAG) at Institut National de la Recherche Agronomique (http://dbsgap.versailles.inra.fr/portail/index.jsp/).

This study focuses on variation in phosphorylation of photosystem II (PSII) proteins and its impact on the repair cycle of this complex. The gained information could be used in the careful selection of a specific background for mutant characterization, but also to learn about natural variation affecting photosynthesis.

Materials and Methods

Plant material: the Wassilewskija Ws-4 ecotype was obtained from PublicLines at INRA (http://dbsgap.versailles.inra.fr/publiclines/). Columbia Col-0 and Landsberg erecta (Ler-0) were ordered at the Salk SIGnAL T-DNA express Arabidopsis Gene mapping tool (http://www.signal.salk.edu/cgi-bin/tdnaexpress). The three ecotypes showed anatomy identical with

those displayed at TAIR site (http://www.arabidopsis.org/abrc/). The three ecotypes were grown hydroponically at 120 μmol photons m^{-2} s^{-1} at 22 °C with 8 h light/16 h dark cycles, and relative humidity 70%. For high light stress experiments, six week old plants were treated at 950 μmol photons m^{-2} s^{-1} for 3 h.

Thylakoid preparation: thylakoid membranes were isolated from 16 h dark-adapted plants and purified as described (Yin *et al.*, 2010). In some experiments aimed at studying the steady-state level of phosphorylation of PSII proteins, thylakoid membranes were isolated from leaves in the presence of 10 mmol NaF, a general inhibitor of protein phosphatases.

Quantitative analysis of PSII protein phosphorylation by mass spectrometry: thylakoid membranes isolated in the presence of NaF were treated with trypsin, in order to proteolytically shave the surface-exposed phosphorylated protein domains extending out of the membrane, and thus releasing both the phosphorylated and the nonphosphorylated parts of a protein.To make a quantitative estimation of the PSII phosphorylation between the ecotypes, we used the recently described normalization method (Fristedt *et al*., 2010).

Short-term light treatment: in experiments aimed to study the effect of inhibition of chloroplast protein synthesis, detached leaves pre-treated with 2 mmol lincomycin were exposed to 950 μmol photons m^{-2} s^{-1} for 3 h at 22 °C. Chl fluorescence was measured in leaves after 5 min of dark adaptation. The D1 protein levels were determined in Western blots loaded with thylakoids isolated from the treated leaves.

SDS-PAGE and Western blotting: thylakoid proteins were separated by gel electrophoresis (SDS-PAGE) using 14% (w/v) acrylamide gels with 6 mol urea. Following electrophoresis and electroblotting, proteins were immunodetected using specific antibodies and ECL-Plus detection system (GE Healthcare). The antibody against the D1 subunit of PSII was purchased from Agrisera (Umeå, Sweden). Where indicated, anti-phosphothreonine antibodies from Cell Signaling and Zymed were used.

Results and Discussion

The three employed *Arabidopsis* ecotypes display distinct phenotype in terms of rosette and individual leaves shape, as described in TAIR. Western blot analysis was performed using antibodies directed against various marker proteins of the four photosynthetic complexes. Based on visual inspection of the western blots, no differences in the levels of analyzed proteins were apparent in the three ecotypes (data not shown).

Reversible phosphorylation of PSII proteins regulates the repair cycle of the complex following high light stress (Aro *et al.*, 2005). Intact plants were illuminated for 3 h with 950 μmol photons m^{-2} s^{-1}, thylakoids were isolated in the presence of 10 mmol NaF, and subjected to Western blotting with two different anti-phosphothreonine antibodies. The representative pictures shown in Fig. 1 demonstrate that both antibodies, from Zymed (left panel) and from Cell Signaling (right panel) revealed the same pattern of *in vivo* phosphorylation of PSII proteins in the three ecotypes, namely phospho-CP43, D2, D1 and LHCII protein. Nevertheless, the levels of D1 and D2 phosphorylation were drastically reduced in Ws-4. The phosphrylation levels of D1 and D2 proteins were also found reduced in dark-adapted plants or illuminated for 3 h with 120 μmol photons m^{-2} s^{-1} (data not shown). Control Western blots indicated similar levels of PSII core proteins, implying that the observed immunodetected pattern in Fig. 1 must be attributed to differences in the extent of phosphorylation. Phosphorylated LHCII was detected only by the Cell Signaling antibody, and did not differ among the three ecotypes.

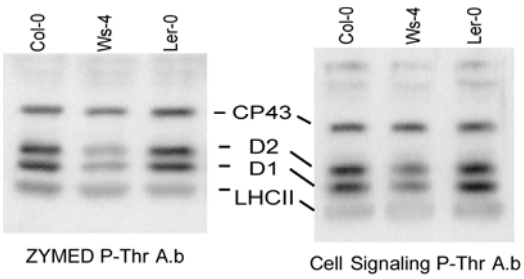

Fig. 1 Representative Western blot of endogenous protein phosphorylation in thylakoids isolated from plants treated for 3 h at an irradiance of 950 μmol photons m^{-2} s^{-1} with two different anti-phosphothreonine antibodies. The gels were loaded with 0.25 μg Chl/lane. The positions of detected phosphorylated proteins are indicated.

For quantification of changes in levels of phosphorylation of D1 and D2 proteins we used liquid chromatography combined with mass spectrometry. The amounts of phospho-D1 and D2 but not phospho-CP43 were reduced by 50% in Ws-4 as compared to the levels in Col-0 and Ler-0 (Table 1).

Table 1 Quantitative LC-MS of PSII core protein phosphorylation of Wassilewskija (Ws), Columbia (Col-0) and Landsberg erecta Ler-0 ecotypes plants grown at an irradiance of 120 μmol photons m^{-2} s^{-1} and treated for 3 h at an irradiance of 950 μmol photons m^{-2} s^{-1}.

Protein	Col-0	Ws-4	Ler-0
P-CP43	100%	100 ± 7%	100 ± 14%
P-D1	100%	50 ± 12%*	100 ± 15%
P-D2	100%	48 ± 8%*	98 ± 8%

Data represent an average of 4 independent preparations and are expressed as means ±SD. *=significantly different to Col-0 and Ler-0 (Student's t-test $p < 0.05$).

To investigate the impact of the observed difference in phosphorylation of D1 and D2 protein on the turnover of the D1 protein, detached leaves pre-treated with lincomycin, were illuminated for 3 h at 950 μmol photons m^{-2} s^{-1}, followed by measurements of F_v/F_m parameter and of the D1 protein level. The increased susceptibility of PSII to photoinhibition in Ws-4 is indicated by the significantly lower F_v/F_m parameter. In the presence of lincomycin, only the degradation phase of D1 turnover takes place, thus PSII inactivation is faster under these conditions. The reduced amounts of remaining D1 protein in thylakoid membranes isolated from Ws-4 as compared to Col-0 and Ler-o indicated a faster degradation of this protein most likely in an un-controlled manner (Fig. 2).

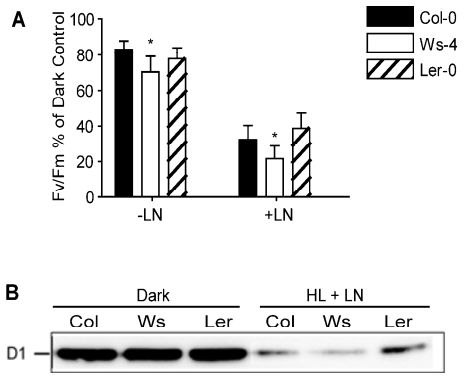

Fig. 2 High light-induced inactivation of PSII complex and D1 protein degradation (A) The F_v/F_m parameter was determined from detached leaves treated for 3 h at an irradiance of 950 μmol photons m^{-2} s^{-1} (HL) in the absence or presence of lincomycin (LN). The plot shows the F_v/F_m levels expressed as percentage of the corresponding values determined in 16 h dark-adapted leaves. Data are expressed as means ± SD. *= significantly different to Col-0 and Ler-0 (Student's t-test $p < 0.05$). (B) Western blot with anti-D1 antibody of thylakoids isolated from leaves, which were 16 h dark-adapted or treated with HL in the presence of lincomycin. The gels were loaded with 0.25 μg Chl/lane.

Although the mechanism behind the significant reduction in the PSII D1 and D2 protein phosphorylation in Ws-4 requires further investigation, the importance of protein phsophorylation for a highly regulated PSII repair cycle is obvious.

Acknowledgements

This work was supported by the Swedish Research Council and the Swedish Research Council for Environment, Agriculture, and Space Planning (C.S. and A.V.V,). LY was a recipient of a travel grant from Helge A:xon Johnson foundation.

References

Aro EM, Suorsa M, Rokka A, Allahverdiyeva Y, Paakkarinen V, Saleem A, Battchikova N, Rintamäki E (2005) Dynamics of Photosystem II: a Proteomic Approach to Thylakoid Protein Complexes. J Exp Bot. 56: 347-356

Fristedt R, Willig A, Granath P, Crèvecoeur M, Rochaix JD, Vener AV (2009) Phosphorylation of Photosystem II Controls Functional Macroscopic Folding of Photosynthetic Membranes in Arabidopsis. Plant Cell 21: 3950-3964

Jose M, *et al*. (2003) Genome-Wide Insertional Mutagenesis of Arabidopsis Thaliana. Science 301: 653-657

Koornneef M, Alonso-Blanco C, Vreugdenhil D (2004) Naturally Occurring Genetic Variation in Arabidopsis Thaliana. Annu. Rev. Plant Biol. 55: 141-172

Sundaresan V, Springer P, Volpe T, Haward S, Jones JD, Dean C, Ma H, Martienssen R (1995) Patterns of Gene Action in Plant Development Revealed by Enhancer Trap and Gene Trap Transposable Elements. Genes Dev. 9: 1797-1810

Yin L, Lundin B, Bertrand M, Nurmi M, Solymosi K, Kangasjärvi S, Aro EM, Schoefs B, Spetea C (2010) Role of Thylakoid ATP/ADP Carrier in Photoinhibition and Photoprotection of Photosystem II in Arabidopsis. Plant Physiol. 153: 666-677

Thallium Induces Morphological Changes in the Photosynthetic Apparatus of *Synechocystis* sp. PCC6803

Motohide Aoki*, Hiroe Matsumoto, Tatsuya Takahashi, Kazuya Sato, Hidetoshi Kumata, Kitao Fujiwara

School of Life Sciences, Tokyo University of Pharmacy and Life Sciences, Horinouchi 1432-1, Hachio-ji, Tokyo 192-0392, Japan.
*Corresponding author. Tel. No. +81 42 676 6792; Fax No. +81 42 676 5354; E-mail: aoki@ls.toyaku.ac.jp.

Abstract: The aim of this study was to elucidate the mechanism of thallium (Tl) ion toxicity in photosynthetic organisms. The physiological and biochemical responses to Tl exposure were analyzed in the cyanobacterium *Synechocystis* sp. PCC6803, which is a widely used model to study photosynthesis. We examined the photosynthetic activities of Tl^+-exposed cells, the extent of Tl accumulation, and the properties of membrane lipids. Exposure to Tl^+ at 2.0 and 5.0 for 24 h decreased the net photosynthetic activities of cells to 92% and 34%, respectively. After exposure to 2.5 μM Tl^+, cells concentrated the Tl to 20.8 μM on a packed cell volume basis. Exposure of *Synechocystis* to 0–2.5 μM Tl^+ resulted in an approximately 9-fold concentration factor. Treatment with 2.0 μM Tl^+ for 48 h decreased the total lipid content of the cells by 38%. Further, we observed the ultrastructure of cells treated with Tl^+. The cells exposed to 5 μM Tl^+ for 24 h showed thylakoid membrane fragmentation and generated less-dense particles following osmium staining. During this time, the net photosynthetic oxygen evolution of the cells was reduced to 34%. These results suggest that the accumulation of Tl in cells affects the integrity of the photosynthetic apparatus.

Keywords: Thallium (Tl); Toxicity; Ultrastructure; Cyanobacteria; Thylakoid

Introduction

Thallium (Tl) is a heavy metal belonging to the aluminum group. Tl is anthropogenicaly produced as a byproduct of metal mining/smelting processes or coal combustion and is released into the environment (Lis *et al*., 2003; Xiao *et al*., 2004; Yang *et al*., 2005). In aquatic systems, Tl exists in 2 oxidation states: monovalent (Tl^+), which is the predominant state, and trivalent (Tl^{3+}) (Kaplan and Mattigod, 1998). Tl^+ is highly toxic to plants, animals, and humans (IPCS, 1996). To study the mechanism of Tl^+ toxicity in photosynthetic organisms, we analyzed the physiological and biochemical responses to Tl^+ exposure in cyanobacterium *Synechocystis* sp. PCC6803, a model for photosynthetic organisms. We previously reported that the half maximal inhibitory concentration (IC_{50}) of Tl^+ for growth is approximately 1.0 μM and that 72 h incubation with 2.5 μM Tl^+ decreases the concentration of chlorophyll *a* and phycobiliproteins in each cell by 71% and 94%, respectively (Aoki *et al*., 2008). In this study, we examined Tl accumulation and its effects on the photosynthetic activities and properties of the cell membrane lipids in *Synechocystis* sp. PCC6803.

Materials and Methods

Thallium mononitrate, $TlNO_3$ (Wako Pure Chemical Industries Ltd., Tokyo, Japan) was exposed to the glucose-tolerant wild-type of cyanobacterium *Synechocystis* sp. PCC6803 at various concentrations. The cyanobacterial cells were heterotrophically grown at 30 °C with constant shaking at 120 rpm in BG-11 medium described by Allen (1968); the medium was supplemented with 5 mmol glucose and buffered with 30 mmol HEPES-NaOH, pH 7.5. The cells were illuminated with 30 μmol photons m^{-2} s^{-1} using Biolux fluorescent lamps (BR-A, NEC Corp., Tokyo, Japan).

Cell growth of cells was monitored by measuring the optical density at 730 nm. The carbon dioxide-dependent photosynthetic activities of cells were measured using an Clark-type oxygen electrode (Hansatech Instruments Ltd., Norfolk, UK) under an illumination of 1,000 μmol photons m^{-2} s^{-1}. The Tl concentration of the cells was analyzed by inductively coupled plasma mass spectrometry (ICP-MS) after acid mineralization of the samples in a heating block. Lipids were extracted from the cells using the method described by Bligh and Dyer (1959). Total lipids were separated using normal-phase thin layer chromatography with chloroform ($CHCl_3$): methanol (MeOH): aqueous ammonia (NH_{3aq}) = 13:7:1 (v/v/v) as the solvent system. The separated lipids were methyl esterified with 5% hydrochloric acid (HCl) in MeOH. Subsequently, the fatty acid content of the methyl esters was determined using a gas chromatography/flame ionization detector (GC/FID). Aracidic acid methyl ester was used as the internal concentration standard. The ultrastructure of the cells was observed using a transmission electron microscope (TEM). Cells were fixed by 2% (v/v) glutaraldehyde and 1% (w/v) osmium tetraoxide (OsO_4), dehydrated with acetone series, and embedded in EPON-812 epoxy resin at 60 °C for 24 h. Samples were thin sectioned (60–90 nm) using ultramicrotome equipped with a diamond knife and stained with platinum blue (Nisshin-EM, Tokyo, Japan) and lead acetate. The sections were then examined by electron micrography.

Table 1 Photosynthetic activities of Tl-exposed *Synechocystis* sp. PCC6803 cells.
Following exposure to 0–5 μM Tl for 24 h, the carbon dioxide-dependent photosynthetic activities of the cells were measured using an oxygen electrode under an illumination of 1,000 μmol photons m^{-2} s^{-1}. Gross photosynthetic activity was obtained by adding the oxygen consumption in the dark to the net oxygen evolution. Three independent experimental data were averaged.

Thallium concentration	Net photosynthetic activity		Gross photosynthetic activity	
	Cell basis	Chlorophyll basis	Cell basis	Chlorophyll basis
[μM]	[% of control]	[% of control]	[% of control]	[% of control]
0.0	100	100	100	100
2.0	92	99	92	99
5.0	34	47	40	59

Results and Discussion

The photosynthetic activities of Tl-exposed *Synechocystis* sp. PCC6803 cells are shown in Table 1. Exposure to 2.0 and 5.0 μM Tl^+ for 24 h decreased the net photosynthetic activities of the cells to 92% and 34%, respectively. The inhibitory effects of Tl^+ on the photosynthetic activities per cell were stronger than those on oxygen evolution, as estimated on the basis of the chlorophyll content. Gross photosynthetic activities were also decreased by Tl^+ exposure, but the inhibitory effect was less than that observed on net photosynthetic activities as a result of the increase in respiratory activity in the dark. Tl^+ decreases the content of photosynthetic pigments in each cell (Aoki *et al*., 2008). However, these results suggest that there are other causes for decrease in photosynthetic activities by Tl^+ treatment; these causes cannot be explained by the decrease in photosynthetic pigments. The results also suggest that the respiratory activity of cells is not inhibited by the Tl^+ exposure conditions used.

To clarify the relation between Tl^+ treatment conditions and Tl accumulation levels in cells, Tl concentration of cells was measured. Tl uptake of cells depended on Tl concentration that the cells were exposed to. Approximately 9-fold concentration factors were constantly observed in the 0.1–2.5 μM of Tl^+ exposure conditions, suggesting that Tl is actively transported into cells. The Tl ion has a similar ionic radiuses that of the potassium ion (Tl^+, 1.49 Å; K^+, 1.33 Å). It has been shown that Tl^+ can be transported by membrane Na^+, K^+-ATPase (Landowne, 1975; Skulskii *et al*., 1978; McCall *et al*., 1985). Therefore, the mechanism of Tl uptake in *Synechocystis* could be via an active ion transport system such as membrane Na^+, K^+-ATPase.

Furthermore, to investigate the effect of Tl^+ uptake into the cell on the photosynthetic membrane, we analyzed the membrane lipid content of the cells.

Exposure to Tl decreases the membrane lipid content of the cells. Treatment with 2.0 μM Tl^+ for 48 h decreased the total lipid content of the cells by 38%. The individual polar lipid contents, determined on the basis of cell volume, decreased remarkably on exposure to 1.0–2.0 μM of Tl^+. Marked reductions were observed, especially in monogalactosyl-diacylglycerol (MGDG) and sulfoquinovosyl-diacylglycerol (SQDG) by 49% and 33%, respectively. On the other hand, no significant changes were observed in the total fatty acid composition of the cells exposed to Tl^+. MGDG is an integral constituent of different photosynthetic pigment-protein complexes (Dörmann and Hörzl, 2009), and SQDG is essential for photoautotrophic growth of *Synechocystis* (Aoki *et al*., 2004). These dynamic changes in the membrane polar lipid composition along with decreased in the photosynthetic activities due to Tl^+ exposure suggest that Tl^+ impairs the integrity of the photosynthetic apparatus of the cell.

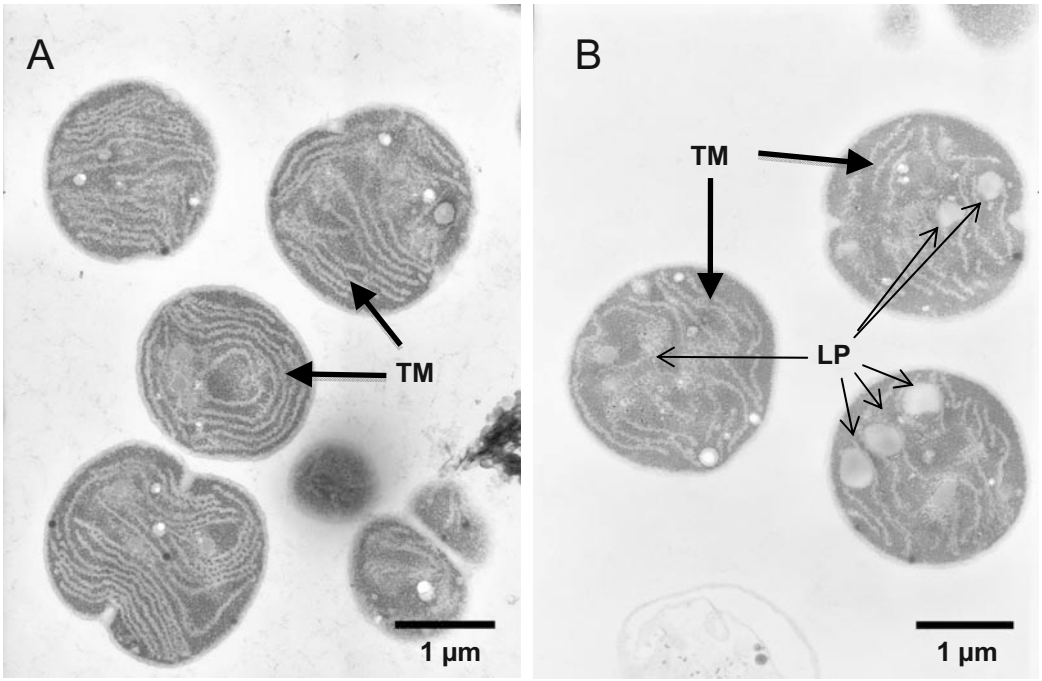

Fig. 1 Effect of Tl^+ on the ultrastructure of *Synechocystis* sp. PCC6803 cells.
The cells grown for 24 h without (A) or with 5 μM Tl^+ (B) were fixed by glutaraldehyde and osmium tetraoxide. The fixed cells were dehydrated in acetone series and embedded in epoxy resin. Samples were sectioned and observed under a transmission electron microscope. TM, thylakoid membrane; LP, low electron-dense particle.

We then observed the ultrastructure of the cells treated with Tl^+ using TEM. The control cells not exposed to Tl had cell diameters of approximately 2 μm and semi-concentrically stacked thylakoid membranes (Fig. 1A). In contrast, exposure to 5 μM Tl for 24 h induced unusual changes in the cell ultrastructure but not in the cell diameter (Fig. 1B). Exposure to Tl caused fragmentation and virtual disappearance of the thylakoid stacks in the *Synechocystis* cells (shown as TM in Fig. 1). Furthermore, several particles of approximately 100–300 nm diameters with low electron density were observed in the cells exposed to Tl^+ (shown as LP in Fig. 1B). In yeast and plant cells showing heavy metal tolerance, the vacuole is generally considered the main storage site for metals (summarized in Martinoia *et al*., 2007). Although the role of the particles produced because of Tl^+ treatment in *Synechocystis* is still unclear, these particles may play a role in easing the Tl^+ stress response. While elucidating the mechanism of Tl toxicity, the interaction between Tl accumulation and the particles in response to Tl^+ should also be considered.

Based on the experimental findings, the following mechanism is proposed for Tl toxicity in *Synechocystis* sp. PCC6803 cells, Tl from the medium is imported into the cell; Tl decreases the membrane lipid content of the cell. This decrease causes abnormalities in the cell ultrastructure, thereby leading to a decrease in the concentration of photosynthetic

pigments and photosynthetic activity. Thus, Tl inhibits cell growth.

Conclusion

Understanding the mechanism of Tl^+ toxicity in photosynthesis in the model *Synechocystis* sp. PCC6803 is important for advancing the science of heavy metal stress responses. In this study, *Synechocystis* cells exposed to Tl^+ showed thylakoid membrane fragmentation and generated less electron-dense particles, resulting in reduced net photosynthetic oxygen evolution of the cells. These results suggest that the accumulation of Tl in the cell affects the integrity of the photosynthetic apparatus.

Acknowledgements

This research was partially supported by the Ministry of Education, Science, Sports and Culture, Japan (MEXT), Grant-in-Aid for Young Scientists (B), 21710070, 2009–2011, and "Strategic Research Foundation" Project for Private Universities, S0801027, 2008–2010.

References

Allen MM (1968) Simple Conditions for Growth of Unicellular Blue-Green Algae on Plate. J. Phycol. 4: 1-4

Aoki M, Sato N, Meguro A, Tsuzuki M (2004) Differing Involvement of Sulfoquinovosyl Diacylglycerol in Photosystem II in Two Species of Unicellular Cyanobacteria. FEBS J. 271(4): 685-693

Aoki M, Suematsu H, Kumata H, Fujiwara K (2008) Physiological and Photosynthetic Toxicity of Thallium in Synechocystis sp. PCC6803. In: Allen JF, Gantt E, Golbeck JH, Osmond B (eds.), Photosynthesis Energy from the Sun: 14th International Congress on Photosynthesis. Springer: Dordrecht, The Netherlands, pp. 1399-1402

Bligh EG, Dyer WJ (1959) A Rapid Method of Total Lipid Extraction and Purification. Can. J. Biochem. Physiol. 37: 911-917

Dörmann P, Hörzl G (2009) The Role of Glycolipids in Photosynthesis. In: Wada H, Murata N (eds.), Lipids in Photosynthesis: Essential and Regulatory Functions. Springer: Dordrecht, The Netherlands, pp. 265-282

Kaplan DI, Mattigod SV (1998) Aqueous Geochemistry of Thallium. In: Nriagu JE (ed.), Thallium in the Environment. Wiley-Interscience Publication: New York, pp. 15-29

Landowne D (1975) A Comparison of Radioactive Thallium and Potassium Fluxes in the Giant Axon of the Squid. J. Physiol. (Lond) 252: 79-96

Lis J, Pasieczna A, Karbowska B, Zembrzuski W, Lukaszewski Z (2003) Thallium in Soils and Stream Sediments of a Zn−Pb Mining and Smelting Area. Environ. Sci. Technol. 37(20): 4569-4572

IPCS (1996) Thallium. World Health Organization (WHO), Geneva: International Programme on Chemical Safety (Environmental Health Criteria 182)

Martinoia1 E, Maeshima M, Neuhaus HE (2007) Vacuolar Transporters and Their Essential Role in Plant Metabolism. J. Exp. Bot. 58 (1): 83-102

McCall D, Zimmer LJ, Katz AM (1985) Kinetics of Thallium Exchange in Cultured Rat Myocardial Cells. Circulation Research 56: 370-376

Skulskii JA, Manninen J, Jarnefelt J (1978) Factors Affecting the Relative Magnitudes of the Ouabain-Sensitive and Ouabain-Insensitive Fluxes of Thallium Ion in Erythrocytes. Biochim. Biophys. Acta 506: 233-241

Xiao T, Guha J, Boyle D, Liu CQ, Chen J (2004) Environmental Concerns Related to High Thallium Levels in Soils and Thallium Uptake by Plants in Southwest Guizhou, China. Sci. Total Environ. 318: 223-244

Yang C, Chen Y, Peng P, Li C, Chang X, Xie C (2005) Distribution of Natural and Anthropogenic Thallium in the Soils in an Industrial Pyrite Slag Disposing Area. Sci. Total Environ. 341: 159-172

The Physiological Role of *Arabidopsis* Thylakoid Phosphate Transporter PHT4;1

Patrik M Karlsson[a], Sonia Irigoyen[b], Wayne K Versaw[b], Cornelia Spetea[a,*]

[a]Department of Physics, Chemistry and Biology, Linköping University, Linköping, Sweden;
[b]Department of Biology, Interdepartmental Program in Molecular and Environmental Plant Sciences, Texas A&M University, College Station, TX, USA.
[*]Corresponding author. Tel. No. +46 13 282681; Fax No. +46 13 282817; E-mail: corsp@ifm.liu.se.

Abstract: The aim of this study was to investigate the physiological role of the thylakoid phosphate transporter PHT4;1 in *Arabidopsis thaliana* through the analysis of *a pht4;1* loss-of-function mutant. Growth of the mutant was reduced in terms of rosette area and biomass to 80% of wild type (WT) values. Analysis of kinetics for slow induction of of chlorophyll fluorescence revealed a transiently higher non-photochemical quenching in the mutant leaves as compared to the WT. On the other hand, relative electron transport rates were as much as 25% lower in the mutant than in WT leaves. These results underscore the fundamental importance of thylakoid phosphate homeostasis for plant growth and modulation of stress responses.

Keywords: *Arabidopsis thaliana*; Non-photochemical quenching; Phosphate transporter; Photoprotection; Thylakoid membrane

Introduction

Phosphate (Pi) is an essential nutrient for all living organisms. As a component of nucleic acids and nucleotides, Pi is central to the genetics and energetics of life. Pi is also involved in regulation of protein phosphorylation and signal transduction. Because biological membranes are impermeable to Pi, its transport *via* specialized proteins between cells and across cell organelles is crucial for cellular homeostasis.

We have previously localized the Pi transporter ANTR1/PHT4;1 in *Arabidopsis* to the chloroplast thylakoid membrane using immunodetection (Ruiz Pavón *et al.*, 2008), and characterized its transport function in two different heterologous systems. PHT4;1 catalyzed a Na^+-dependent Pi transport when expressed and assayed in *E. coli,* and a H^+-dependent activity when expressed and assayed in yeast (Ruiz Pavón *et al.*, 2008; Guo *et al.*, 2008a). Quantitative RT-PCR revealed that the *PHT4:1* gene exhibits a circadian expression pattern with a peak of expression during the light phase of the diurnal cycle (Guo *et al*., 2008b). Most recently, several residues that are important for the Pi transport and its Na^+-dependency have been identified using homology modeling, site-directed mutagenesis and functional characterization in *E. coli* (Ruiz Pavón, Karlsson *et al.*, 2010). In this study, we have investigated the impact of PHT4;1 deficiency on plant growth, photosynthetic activity and photoprotection in *Arabidopsis*.

Materials and Methods

Plant material. *Arabidopsis* (*Arabidopsis thaliana* cv. Landsbergs erecta) plants and a *pht4;1* mutant were grown hydroponically at 120 μmol photons m^{-2} s^{-1} at 22 °C with 8-h-light/16-h-dark cycles and relative humidity 70%. The *pht4;1* mutant was obtained from from the JIC Gene Trap collection (Sundaresan *et al.*, 1995), and has a Ds transposon inserted in exon 1, 131 bp downstream of the translation start site. Thylakoid membranes from wild type (WT) and the *pht4;1* mutant were prepared by sucrose gradient centrifugation, as described in Ruiz Pavón *et al.*

(2008).

Chlorophyll fluorescence. Chlorophyll (Chl) fluorescence was measured using a PAM-210 (Walz). A rapid response curve of photosynthesis versus irradiance was measured using a standardized automatic recording developed by Walz, and described by Lundin *et al.* (2007). For determination of non-photochemical quenching (*NPQ*), slow kinetics of Chl fluorescence induction were recorded in 16 mm leaf discs vacuum infiltrated with water (control), with 5 mmol DTT or 50 μM nigericin, as described by Yin *et al.* (2010).

Protein analysis. SDS/urea/PAGE and Western blotting using an antibody against *Arabidopsis* PHT4;1 protein were performed as previously described (Ruiz Pavón *et al.*, 2008).

Results and Discussion

To investigate the physiological role of the thylakoid PHT4;1 in *Arabidopsis*, we have used a Ds transposon insertion mutant, named *pht4;1*. Western blotting using a PHT4;1-specific antibody of isolated thylakoid membranes indicated a polypeptide band of approx. 45 kDa in WT preparations, confirming previous observations (Ruiz-Pavón *et al.*, 2008). This band could not be immunodetected in corresponding preparations from the mutant, indicating that this is a knockout (Fig. 1).

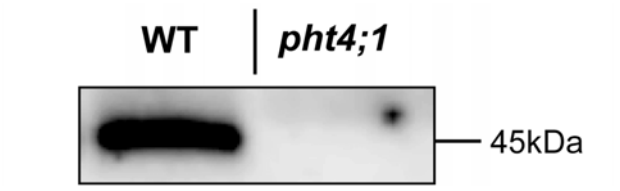

Fig. 1 Western blot with anti-PHT4;1 antibody of thylakoids isolated from wild type (WT) plants and *pht4;1* mutant (10 μg Chl/lane).

At an irradiance of 120 μmol photons m^{-2} s^{-1} and in hydroponic system, growth of the mutant was considerably slowed down (data not shown). Shoot fresh weight of the fully developed *pht4;1* mutant was 3.3 ± 0.4 g as compared to 4.1 ± 0.47 ($n = 7$), representing 80% of WT values.

To compare the light saturation of photosynthetic performance in the mutant and WT plants, we applied a rapid light curve in detached leaves. This analysis revealed that both types of plants reached saturation of the electron transport rate (ETR) in the range of 800–1300 μmol photons m^{-2} s^{-1}, and higher light intensities reduced ETR in both cases (Fig. 2). However, the mutant displayed 25% lower saturation levels of ETR than the WT.

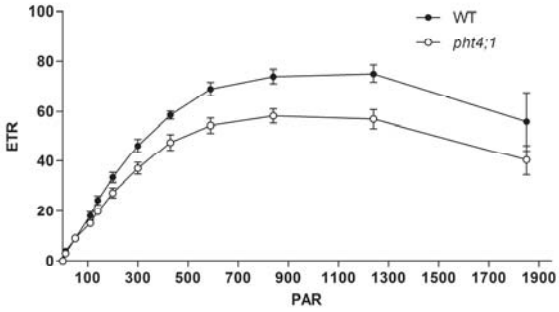

Fig. 2 Plot of relative electron transport rate (ETR) as a function of quantum flux density of the photosynthetically active radiation (PAR). The data are means ±S.D. (n=3).

Non-photochemical quenching of Chl fluorescence is an important photoprotective mechanism against excess harmfull light received by the photosynthetic apparatus (Horton *et al.*, 2008). To test if PHT4;1 deficiency affects photoprotection, the kinetics of *NPQ* formation were recorded for 20 min at 1,250 μmol photons m^{-2} s^{-1} in the *pht4;1* mutant and the WT leaves. The initial phase of *NPQ* curves reached a transient maximum faster and with higher amplitude in the mutant as compared to the WT (Fig. 3). The second phase was slow and displayed no significant differences between the WT and mutant. These results indicate that the mutant is more efficient in activating the formation of *NPQ* than the WT. These findings and the lower ETR in the mutant implies that a larger proportion of the absorbed light is dissipated than the one used for photosynthesis.

Next we have used two types of inhibitors to dissect the reasons behind the faster response of the mutant in *NPQ* formation. Nigericin and dithiothreitol (DTT) are well-known inhibitors of the trans-thylakoid pH gradient and of violaxanthin de-epoxidase, respectively, which are both important components for *NPQ* formation (Horton *et al*., 2008). As shown in Fig. 3, in the presence of nigericin the fast phase disappears, whereas the slow phase is drastically reduced, both similarly in the WT and mutant. The slow phase is also reduced, although to a lower extent, in the presence of DTT, and the kinetics of the phast phase are indistinguishable in the WT and mutant.

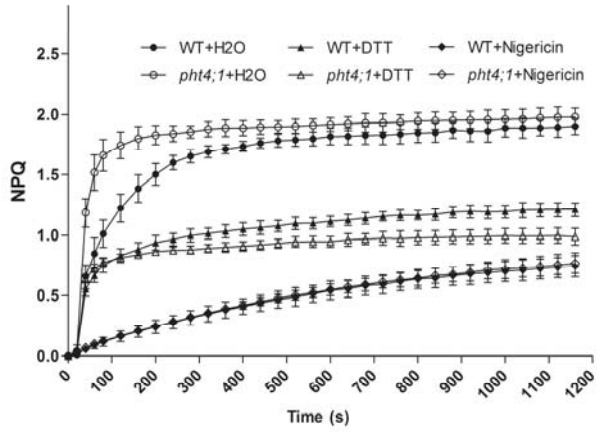

Fig. 3 Effect of nigericin and DTT on kinetics of non-photochemical quenching (*NPQ*) formation in leaves exposed for 20 min at 1,250 μmol photons m^{-2} s^{-1}. The data are means ±S.D. (n = 3).

Taken together, these results indicate that the deficiency of PHT4;1 leads to a transient acidification of the lumen in the first minutes of illumination. The acidification of the lumen more efficiently activates photoprotective xanthophyll cycle-dependent *NPQ* mechanism (Horton *et al.*, 2008). The formation of a higher H^+ gradient across mutant thylakoids could be explained if assuming that the PHT4;1 protein exports Pi from the lumen by a mechanism involving co-transport of H^+, as suggested by Guo *et al*. (2008a).

The findings of lower ETR but higher *NPQ* could explain the slower growth and reduced biomass of the *pht4;1* mutant as compared to WT plants. They underscore the fundamental importance of thylakoid Pi homeostasis for plant growth and modulation of stress responses.

Acknowledgements

This work was supported by the Swedish Research Council and the Swedish Research Council for Environment, Agriculture, and Space Planning (C.S.) and the National Science Foundation (W.K.V.). P.M.K. was a recipient of a travel grant from Helge Axon Johnson foundation.

References

Guo B, Jin Y, Wussler C, Blancaflor EB, Motes CM, Versaw WK (2008a) Functional Analysis of the Arabidopsis PHT4 Family of Intracellular Phosphate Transporters. New Phytol. 177: 889-898

Guo B, Irigoyen S, Fowler TB, Versaw WK (2008b) Differential Expression and Phylogenetic Analysis Suggest Specialization of Plastid-Localized Members of the PHT4 Phosphate Transporter Family for Photosynthetic and Heterotrophic Tissues. Plant Signal & Behavior 3: 784-790

Horton P, Johnson MP, Perez-Bueno ML, Kiss AZ, Ruban AV (2008) Photosynthetic Acclimation: Does the Dynamic Structure and Macro-Organisation of Photosystem II in Higher Plant Grana Membranes Regulate Light Harvesting States? FEBS J. 275: 1069-1079

Lundin B, Hansson M, Schoefs B, Vener AV, Spetea C (2007) The Arabidopsis PsbO2 Protein Regulates Dephosphorylation and Turnover of the Photosystem II Reaction Centre D1 Protein. Plant J. 49: 528-539

Ruiz Pavón L, Lundh F, Lundin B, Mishra A, Persson BL, Spetea C (2008) Arabidopsis ANTR1 Is a Thylakoid Na^+-Dependent Phosphate Transporter: Functional Characterization in Escherichia Coli. J. Biol. Chem. 283: 13520-13527

Ruiz Pavón L, Karlsson PM, Carlsson J, Samyn D, Persson B, Persson BL, Spetea C (2010) Functionally Important Amino Acids in the Arabidopsis Thylakoid Phosphate Transporter: Homology Modeling and Site-Directed Mutagenesis. Biochemistry 49: 6430-6439

Sundaresan V, Springer P, Volpe T, Haward S, Jones JD, Dean C, Ma H, Martienssen R (1995) Patterns of Gene Action in Plant Development Revealed by Enhancer Trap and Gene Trap Transposable Elements. Genes Dev. 9: 1797-1810

Yin L, Lundin B, Bertrand M, Nurmi M, Solymosi K, Kangasjärvi S, Aro EM, Schoefs B, Spetea C (2010) Role of Thylakoid ATP/ADP Carrier in Photoinhibition and Photoprotection of Photosystem II in Arabidopsis. Plant Physiol. 153: 666-677

Involvement of *slr0081,* a Two-Component Signal-Transduction System Response Regulator, in Acid Stress Tolerance in *Synechocystis* sp. PCC 6803

Yu Tanaka[1], Mayuko Kimura[1], Atsushi Moriyama[1], Yuko Kubo[1], Mamoru Sambe[1], Junji Uchiyama[2], Hisataka Ohta[1,2,*].

[a]Department of biology, Faculty of Science, Tokyo University of Science, Shinjyuku, Tokyo 162-8601, Japan;
[b]Research center for RNA science, RIST, Tokyo University of Science, Noda, Chiba 278-8510, Japan.
[*]Corresponding author. Fax No. +81(3)5228 8374; E-mail: ohta@rs.noda.tus.ac.jp.

Abstract: Two-component signal transduction is the primary signaling mechanism used for global regulation of cell response to changes in the environment. DNA microarray analysis identified genes up-regulated by acid stress in cyanobacteria *Synechocystis* sp. PCC 6803. Several of these altered genes are thought to be response regulators that are directly involved in this type of stress. Deletion mutants of response regulator genes were constructed and survivability was compared between the cells transfected with mutant and wild-type genes in a low-pH medium. Among these, deletion of *slr0081* affected the growth rate under conditions of acid stress (pH 6.0). We examined the genome-wide expression of genes in Δ*slr0081* mutant cells by using DNA microarray in an attempt to determine whether *slr0081* is involved in the regulation of other acid stress responsive genes. Our findings by quantitative real-time RT PCR revealed that down regulation of acid responsive genes *slr0967* and *sll0939* occurs by deletion of *slr0081.*

Keywords: Low-pH; Cyanobacteria; Stress response; Two-component system

Introduction

Plants were exposed to environmental stress such as temperature, light, salts concentration, heavy metal density and more because those have superior acclimation ability to environmental change. Recently, the acid rain is most serious environmental stress. It causes acidification of lakes and streams and contributes to damage of plants, algae, and cyanobacteria in many parts of the world. Rhizotoxicity in acid soil, which involves the action of Al^{3+} has been well investigated (Jones *et al.*, 1995). Nevertheless, little has been done to elucidate the basic set of adaptations necessary for acid tolerance in plants, algae, or cyanobacteria.

Several species of cyanobacteria serve as model organisms for elucidating both functional and regulatory aspects of photosynthesis. Above all, *Synechocystis* sp. PCC 6803 was the first photosynthetic organism for which a complete genome sequence became available (Kaneko *et al*., 1996), and DNA microarrays have been used to examine gene expression in response to various kinds of stress such as redox, oxidative, osmotic, salinity, and high light stress(Kanesaki *et al*., 2002; Hihara *et al*., 2001).

DNA microarray analysis of *Synechocystis* sp. PCC 6803 cells revealed that acid stress induced the expression of putative stress-related proteins, such as chaperones, regulatory factor, and function unknown protein (Ohta *et al.*, 2005). Gene of slr0967 and *sll0939* continuously increase 7 and 16-fold after 4 h of acid stress (Ohta *et al.*, 2005).

In this study, based on DNA microarray analysis in acid stress condition, we constructed deletion mutant cells. In acid stress condition, deletion mutants of *slr0081*, which encoded response regulator involved in phosphate limitation (Suzuki *et al.*, 2004), were weaker than wild-type cells. From analysis of quantitive real-time RT PCR, we revealed that

Slr0081 up-regulated acid responsive genes (*slr0967* and *sll0939*). Our observations suggest that Slr0081 plays an important role for *Synechocystis* to survive in acid condition.

Material and Methods

Strain and culture conditions of Cyanobacteria

Wild-type strain of *Synechocystis* sp. PCC6803 and *slr0081*-disrupted mutants, created by inserting the chlo-ramphenicol-resistance cassette, were grown at 30 °C in BG-11 medium (Stanier *et al.*, 1971) with 5 mmol TES-NaOH (pH 8.0) under continuous illumination by fluorescent lamps. Cells growing in the exponential phase were subjected to acid stress by centrifuging the cell cultures and resuspending the cell pellets in a pH-adjusted BG-11 medium. BG-11 medium was acidified using MES (pH 6.0) buffer instead of TES (pH 8.0) buffer. Cultures were streaked onto pH-adjusted BG-11 plates and cultured for 5 days. Experiments were performed in duplicates at least 3 times.

Generation of insertion mutants

Mutants with impaired expression of selected genes were generated by reverse genetic techniques. The coding and neighboring sequences as well as the chloramphenicol cassette gene were amplified by PCR. These PCR products were then cloned into pUC19 (Toyobo, Osaka, Japan). The primers for amplification were designed using the complete genome sequence of *Synechocystis* (Kaneko *et al.*, 1996), and sequences that contained appropriate restriction sites were selected to improve cloning efficiency of the fragments. Transformants were initially selected on a medium containing 10 μg CM mL^{-1} (Wako Pure Chemical, Osaka, Japan), whereas the clones were segregated by restreaking (at least 3 transfers) of primary clones on plates supplemented with 50 μg Cm mL^{-1}. During the culture of mutants, Cm was added to the liquid media.

RNA isolation and quantitative real-time RT PCR

Total RNA was isolated from *Synechocystis* cells using the RNeasy Midi kit (Qiagen) as described by Hihara *et al.* (2001). The extracted RNA was reverse-transcribed using PrimeScript^{tm} RT regent kit (Takara Bio). Real-time PCR with SYBR Green I was performed using SYBR Premix EX Taq (Perfect Real Time) (TAKARA). Each real time-PCR was performed in triplicate with *rnpB* as the internal standard.

Results and Discussion

Characterization of the slr0081 deletion mutant in acid condition

On the basis of the results of DNA microarray analysis in acid stress conditions, we constructed deletion mutant cells. Wild-type *Synechocystis* sp. PCC6803 was transformed with *slr0081* that had been interrupted with a cassette conferring resistance to chloramphenicol. Slr0081 is a reported response regulator of a two-component system that regulates the expression *phoA* gene for alkaline phosphatase under phosphate-limiting condition in *Synechocystis* (Suzuki *et al*., 2004). In normal BG-11 medium at pH 8.0, the mutant cells exhibited a similar photoautotrophic doubling time (Fig. 1), suggesting that the deletion did not affect growth in normal conditions. However, under acid stress conditions, deletion mutants of *slr0081* were weaker than the wild-type cells (Fig. 2). In addition, a growth curve showed that the growth of Δ*slr0081* mutant cells in acid stress conditions (pH 6.0) was significantly inhibited compared with that of wild-type cells (Fig. 1). These results suggest that Slr0081 plays an important role in survival of *Synechocystis* under conditions of acid stress. Slr0081 is reported to be a response regulator involved in phosphate limitation, thus *Synechocystis* in acid stress may cause phosphate limitation.

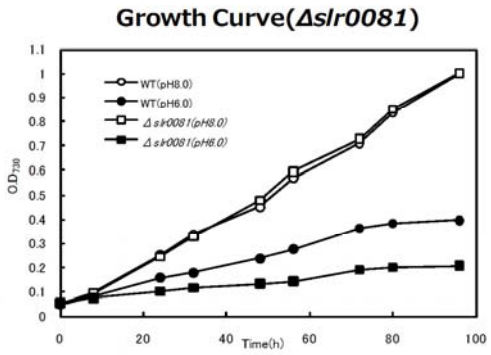

Fig. 1 Growth curves of wild type and *slr0081* deletion mutants at pH 8.0 and pH 6.0.
Cell density was measured at OD_{730}. The pH of the BG-11 medium was adjusted using 5 mmol TES-NaOH (pH 8.0) and the acid-culture used MES-NaOH (pH 6.0). This experiment was repeated 3 times.

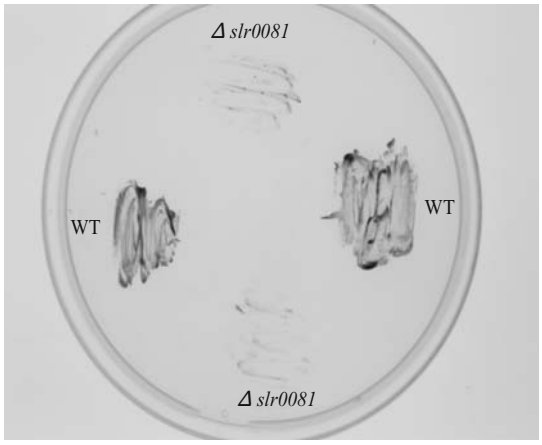

Fig. 2 Effect of WT and *slr0081* deletion on growth at pH 6.0. Wild-type and *Δslr0081* were streaked onto BG-11 plates containing MES-NaOH at pH 6.0 and cultured for 5 days. This experiment was repeated 3 times.

Quantitative real-time RT PCR analysis of slr0967 and sll0939 in slr0081 deletion mutants

To examine the effect of a deletion mutation of *slr0081* on acid tolerance of *Synechocystis* cells, we performed DNA microarray analysis of *slr0081* deletion mutant cells under acid stress conditions by culturing the mutant cells at a pH 3.0 for 30 min (data not shown). The expressions of *slr0967* and *sll0939* were induced by acid stress in wild-type, but not in *slr0081*-deleted cells. These results suggest that Slr0081 regulates transcription of *slr0967* and *sll0939*. To elucidate the relationship between *slr0081* and these genes, we performed quantitative real-time RT PCR analysis of the expression of *slr0967* and *sll0939* in *slr0081*-deleted mutants (Table 1). In the wild-type cells, the transcription level of *slr0967* and *sll0939* increased 7.78- and 33.15-fold, respectively, after acid stress treatment. In contrast, in *slr0081*-deleted cells, the expressions of these genes did not increase (1.21 and 0.64-fold, respectively) after acid stress treatment. These results indicate that Slr0081 up-regulated *slr0967* and *sll0939* genes.

Table 1 Expression levels of *slr0967* and *sll0939* after acid treatment (pH 3.0) in wild-type and *Δslr0081*, determined by *Quantitative real-time RT PCR*.

sample	*sll0939*	*slr0967*
WT(cont)	1	1
WT(acid)	7.78	33.15
Δslr0081(acid)	1.21	0.64

Wild-type and *slr0081* deletion mutants were incubated in 50 mmol Gly-HCl (pH 3.0) for 0.5 h.

References

Kaneko T, Sato S, Kotani H, Tanaka A, Asamizu E, Nakamura Y, Miyajima N, Hirosawa M, Sugiura M, Sasamoto S, Kimura T, Hosouchi T, Matsuno A, Muraki A, Nakazaki N, Naruo K, Okumura S, Shimpo S, Takeuchi C, Wada T, Watanabe A, Yamada M, Yasuda M, Tabata S (1996) Sequence Analysis of the Genome of the Unicellular Cyanobacterium Synechocystis sp. Strain PCC6803. II. Sequence Determination of the Entire Genome and Assignment of Potential Protein-Coding Regions. DNA Res. 3: 109-136

Jones DL, Kochian LV (1995) Aluminum Inhibition of the Inositol 1,4,5-Trisphosphate Signal Transduction Pathway in Wheat Roots: A Role in Aluminum Toxicity? Plant Cell. 7: 1913-1922

Ohta H, Shibata Y, Haseyama Y, Yoshino Y, Suzuki T, Kagasawa T, Kamei A, Ikeuchi M, Enami I (2005) Identification of Genes Expressed in Response to Acid Stress in Synechocystis sp. PCC 6803 Using DNA Microarrays. Photosynth Res. 84: 225-230

Hihara Y, Kamei A, Kanehisa M, Kaplan A, Ikeuchi M (2001) DNA Microarray Analysis of Cyanobacterial Gene Expression during Acclimation to High Light. Plant Cell. 13: 793-806

Suzuki S, Fejani A, Suzuki I, Murata N (2004) The SphS-SphR Two Component System Is the Exclusive Sensor for the Induction of Gene Expression in Response to Phosphate Limitation in Synechocystis. J. Biol. Chem. 279: 13234-13240

Characterization of the ABC Transporter Gene *slr1045* Involved in Acid-stress Tolerance of *Synechocystis* sp. PCC 6803

Hiroko Tahara[1], Sachiko Fukai[1], Mamoru Sambe[1], Miho Kobayashi[1], Junji Uchiyama[2], Hisataka Ohta[1, 2*]

[1]Department of biology, Faculty of Science, Tokyo University of Science, Shinjyuku, Tokyo 162-8601, Japan;
[2]Research center for RNA science, RIST, Tokyo University of Science, Noda, Chiba 278-8510, Japan.
[*]Corresponding author. Fax No. +81(3)5228 8374; E-mail: ohta@rs.noda.tus.ac.jp.

Abstract: The ATP-binding cassette (ABC) transporters form one of the largest known-protein families; these are widespread in bacteria, archaea, and eukaryotes and are encoded in the largest set of paralogous genes. In the *Synechocystis* sp. PCC6803 genome, over 50 ABC transporter-related genes have been detected by genome sequence analysis. Some of these have been identified as Na^+/H^+, iron, phosphate, polysaccharide, and CO_2 transporters. The substrates of many other ABC transporters are still unknown. To identify ABC transporters involved in acid tolerance, deletion mutants of other substrate-unknown ABC transporter genes were screened for their acid-stress sensitivities in a low-pH medium. A mutant of *slr1045* was found to be more sensitive to acid stress than wild-type cells. The abundance of expression of the genes was analyzed under various stress conditions by quantitative real time reverse transcriptase-polymerase chain reaction.

Keywords: Acid stress; Cyanobacteria; ABC transporter

Introduction

Living organisms must adapt to environmental changes. The acclimation processes of microorganisms to environmental stress are mainly regulated at the level of transcriptional activation or repression.

The pH value of soil is one of the many environmental conditions that affect the quality of plant growth. The soil pH directly affects nutrient availability. DNA microarray analysis of *Synechocystis* sp. PCC 6803 cells showed that acid stress induces the expression of putative stress-related proteins such as chaperones, regulatory factors, and proteins of unknown functions (Ohta *et al*., 2005).

ABC transporters play an important role in nutrient transport and cytoplasmic pH regulation. The ABC transporter super families constitute many different systems that are widespread among living organisms and show different functions (Higgins, 1992; Igarashi and Kashiwagi, 1999; Sangari *et al*., 2010). The general principle of ABC transport systems is the ligand translocation through a pore formed by 2 integral membrane protein domains. This is accompanied by ATP hydrolysis through 2 nucleotide-binding domains associated with the cytoplasmic side of the pore (Li *et al*., 2010). In the *Synechocystis* sp. PCC6803 genome, over 50 ABC transporter-related genes have been detected by genome sequence analysis. Some of the transporters are known as specific substrate transporters, but the functions of others are still unknown. In this study, to identify ABC transporters involved in acid tolerance, deletion mutants of ABC transporter genes whose physiological substrates are still unknown were screened for acid-stress sensitivities in a low-pH medium.

We found that a mutant of *slr1045* was more sensitive to the acid-stress condition than wild-type cells. This gene had a significant homology to *slr1344* in the *Synechocystis* sp. PCC6803. The deletion mutants of these genes were established and the acid tolerance, evaluated. These genes involved in the acid stress response were intensively investigated using quantitative real-time reverse transcriptase-polymerase

chain reaction (RT-PCR) of wild-type cells during acid-stress treatment.

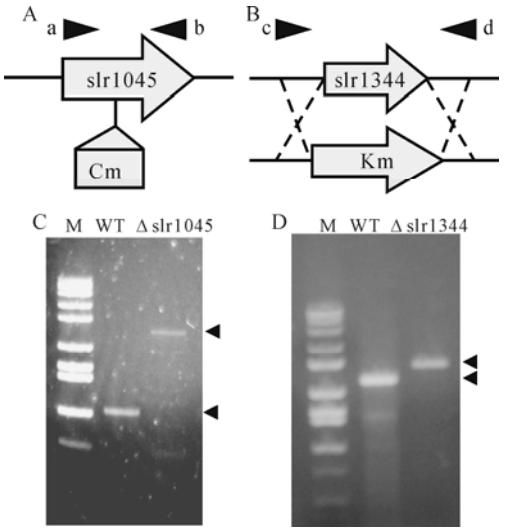

Fig. 1 Characterization of *Synechocystis slr1045* and *slr1344* mutants.
Physical maps of the *slr1045* region and *slr1344* region, respectively, of the genomes of the wild-type (WT) and the mutant cells (A and B). Correct integration of the chloramphenicol-resistance gene (Cm) was tested by PCR on genomic DNA using specific primers a and b. The results for WT and *slr1045* mutant are shown in panel C. Correct integration of the kanamycin-resistance gene (Km) was tested by PCR on genomic DNA by using specific primers c and d. The results for WT and *slr1344* mutant are shown in panel D.

Materials and Methods

Generation of insertion mutants

The mutant of *slr1045* impaired in selected genes was generated by reverse genetics. The coding sequences, *slr1045,* and the chloramphenicol cassette gene were amplified by PCR. The PCR products were cut with apposite restriction enzymes. These were ligated and subjected to homologous recombination. The upstream and downstream code of the *slr1344* gene were amplified by PCR. These PCR products were cloned into pUC19 (TOYOBO). The *aphII* gene (aminoglycoside phosphotransferase II conferring kanamycin [Km] resistance) isolated from the plasmid pUC4K (Pharmacia) was inserted into a unique restriction site of the encoding sequences. pUC19, carrying the *slr1344* neighboring sequences and the Km^r cassette gene were ligated and subjected to homologous recombination. The *slr1344* gene was rearranged by Km^r. Transformants were initially selected on a medium containing 10 μg Km ml^{-1} (Wako), while clone segregation was performed by numerous restreaking (at least 3 transfers) of the primary clones on plates supplemented with 50 μg Km ml^{-1}. During the cultivation of mutants, 50 μg Km ml^{-1} was added to the liquid media.

Growth conditions

Wild-type and mutants of *Synechocystis* sp. PCC6803 were incubated in a liquid BG-11 medium supplemented at 30 °C under continuous cool fluorescent light (3,000 lux). The pH of the BG-11 medium was maintained by addition of either 5 mmol TES-NaOH (pH 8.0) or 5 mmol MES-NaOH (pH 6.0). The cell densities of the cultures were determined by measuring the optical density at 730 nm (OD_{730}). The solid medium contained the BG-11 buffer at pH 8.0 or pH 6.0 and 1.5% agar. Cultures were streaked onto the plates and incubated for 7 days. Experiments were performed in duplicate at least 3 times.

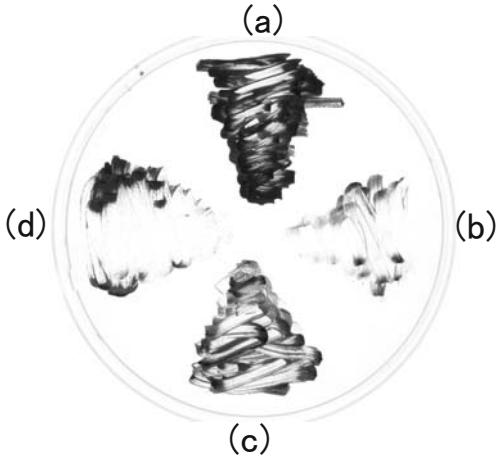

Fig. 2 Inhibition of growth of *slr1045*-mutant *Synechocystis* cells by acid stress.
Saturated dilutions of cultures of wild-type (WT) and mutants ((a) WT, (b) Δ*slr1045*, (c) Δ*slr1344*, and (d) Δ*slr1045* and the Δ*slr1344* double mutant) were streaked onto the BG-11 Plate (buffered with 5 mmol MES-NaOH (pH 6.0)) and cultured for 7 days at 30 °C under continuous cool white fluorescent light (3,000 lux).

Table 1 Relative mRNA expression.

	slr1045	*slr1344*
control	1	1
acid(1h)	7.2	19.8
acid(10h)	20.4	16.2
acid(24h)	5.1	15.2

RNA isolation and quantitative real time RT-PCR

Total RNA extraction was conducted according to a previously described protocol (Pinto *et al.*, 2009). cDNA was generated by using the PrimeScript® RT

reagent Kit (TaKaRa). After having composed the cDNA, we performed real time RT-PCR by using SYBR Premix Ex Taq ™ II, according to the manufacturer's protocol (TaKaRa).

Results and Discussion

Real-time RT-PCR analysis

We performed real-time RT-PCR for *slr1045* and *slr1344* expression in the wild-type cells under acid-stress condition in a time-dependent manner. The transcription of *slr1045* and *slr1344* had increased under the acid-stress conditions. Table 1 shows the expression profiles of *slr1045* and *slr1344* in comparison with that in the case of wild-type cells. The transcription level of *slr1045* increased steadily during the acid-stress treatment for 10 h. The RNA level of the *slr1344* gene also increased steadily during the acid-stress treatment for 1 h.

These results suggest that *slr1344* may be the rapid response gene, while *slr1045* may be the slow response gene under acid stress.

Construction of the slr1045 and slr1344 Synechocystis mutants

The deletion mutant of *slr1045* whose sensitivity had increased under the acid-stress condition was highlighted in the mutant screening processes. This gene showed significant homology to *slr1344* in the *Synechocystis* sp. PCC6803. Therefore, the deletion mutant of *slr1344* was also constructed. The deletion mutants were confirmed by PCR analysis using primer sets (Fig. 1). PCR analysis of chloramphenicol-resistant cells showed that *slr1045* was inserted by the chloramphenicol-resistance gene because of the segregation of chromosomes (Figs. 1A and 1C). Δ*slr1344* was disrupted under the background replacement with a kanamycin-resistance cassette because the PCR product was converted from 2500 bp to 2800 bp sequence (Figs. 1 B and 1D).

slr1045 mutant decreased growth under acid stress

It is shown that the growth rate of deletion mutants is similar to that in the case of wild-type cells when the mutants are cultured in the normal BG-11 liquid culture medium. This suggests that these genes are not necessary for cell viability. We, therefore, evaluated the acid tolerance of the deletion mutants on a pH-6.0 BG-11 plate. Each cell cultured on the normal BG-11 liquid medium was streaked onto the pH-6.0 plates and incubated for 7 days (Fig. 2). The growth of the deletion mutants of *slr1045* at pH 6.0 was remarkably slower than that in the case of wild-type cells. Although there was an increase in the expression of *slr1344* in wild-type cells under the acid-stress conditions in the early period, the deletion mutant of *slr1344* did not show an acid-sensitive phonotype in the pH-6.0 medium. These results suggest that the Slr1045 protein may play a role in the transport of certain factors that affect the acid-stress response and that the Slr1344 protein may have indirect functions.

References

Higgins CF (1992) ABC Transporters: from Microorganisms to Man. Annu Rev Cell Biol 8: 67-113

Igarashi K, Kashiwagi K (1999) Polyamine Transport in Bacteria and Yeast. Biochem J 344: 633-642

Li Zou, Jun Wang, Bao Huang, Ming Xie, An Li (2010) A Solute-Binding Protein for Iron Transport in Streptococcus Iniae. BMC Microbiology 10: 309

Ohta H, Shibata Y, Haseyama Y, Yoshino Y, Suzuki T, Kagasawa T, Kamei A, Ikeuchi M, Enami I (2005) Identification of Genes Expressed in Response to Acid Stress in Synechocystis sp. PCC6803 Using DNA Microarrays. Photosynth Res. 84: 225-230

Kaneko T, Pinto FL, Thapper A, Sontheim W, Lindblad P (2009) Analysis of Current and Alternative Phenol Based RNA Extraction Methodologies for Cyanobacteria. BMC Molecular Biology. 10: 79

Sangari FJ, Cayon AM, Seoane A, Garcia-Lobo JM (2010) Brucell Abortus Ure2 Region Contains an Acid-Activated Urea Transporter and a Nickel Transport System. BMC Microbiology 10: 107

Psbo Degradation by Deg Proteases under Reducing Conditions

Irma N Roberts, Helder Miranda, Lâm Xuân Tâm, Thomas Kieselbach, Christiane Funk*

Department of Chemistry and Umeå Plant Science Centre, Umeå University, SE – 901 87 Umeå, Sweden.
*Corresponding author. Tel. No. +46-90-786 7633; Fax No. +46-90-786 7655; E-mail: Christiane.Funk@chem.umu.se.

Abstract: DegP/HtrA proteases are ATP-independent serine endopeptidases widely distributed in nearly all organisms. As yet, their physiological role in oxygenic photosynthetic organisms is unclear, although it has been widely speculated that they participate in the photosystem II repair cycle. Here, we investigated the ability of Deg proteases to degrade PsbO according to its redox state. A sample of purified PsbO or photosystem II complex was incubated together with recombinant Deg proteases of *Synechocystis* sp. PCC 6803 (HhoA, HhoB or HtrA). The reducing media was conferred by the *Escherichia coli* thioredoxin/thioredoxin reductase system. The results obtained showed that HhoA is able to hydrolyze reduced PsbO while HhoB and HtrA are not. HhoA was active against free PsbO of spinach as well as PsbO of *Synechocystis* attached to photosystem II, only under reducing conditions. The finding that all three Deg proteases of *Synechocystis* co-purify with photosystem II supports the hypothesis of PsbO as a substrate for Deg proteases *in vivo*.

Keywords: Deg proteases; PsbO; Protein degradation; Thioredoxin; *Synechocystis*; Sp. PCC 6803

Introduction

DegP proteases are ATP-independent serine endopeptidases, containing a trypsin/chymotrypsin-like protease domain, and 0–3 PDZ or PDZ-like domains (Gottesman, 1996; Clausen *et al*., 2002). Initially identified in *Escherichia coli* Deg proteases were detected in nearly all organisms, including Archae, bacteria and eukaryotes.

In the genome of *Arabidopsis thaliana* 16 genes coding for DegP-like proteases have been identified (Kieselbach and Funk, 2003). Five of these proteases have been localized in the chloroplast. Deg1, 5 and 8 are localized in the thylakoid lumen whereas Deg2 and 7 are associated with the stromal side of the thylakoid membrane (Huesgen *et al*., 2009; Sun *et al*., 2010). In *Synechocystis* sp. PCC 6803 three Deg proteases have been identified (HtrA, HhoA and HhoB), showing very high homology to the lumen located plant Deg proteases (Kieselbach and Funk, 2003).

PsbO is one of the extrinsic proteins of the oxygen evolving complex (OEC) bound to the lumenal surface of photosystem II (PSII). PsbO has two conserved cysteine residues (Cys28 and Cys51 in spinach) forming a disulfide bridge between its N-terminal loop and the β1 strand (Nikitina *et al*., 2008). While PsbO has normally a long lifetime recent studies showed that in Arabidopsis it can be rapidly degraded when the disulfide bridge is reduced by thioredoxin (Hall *et al*., 2010). However, the protease activity responsible for the redox–dependent proteolysis of PsbO was not identified.

Here we demonstrate that recombinant Deg proteases of *Synechocystis* sp. PCC 6803 were able to degrade PsbO from spinach and *Synechocystis* after reduction of the disulfide bridge. In addition, we provide evidence that degradation of cyanobacterial PsbO is performed by Deg proteases *in situ*.

Materials and Methods

The constructs overexpressing Synechocystis Deg proteases were developed by Huesgen *et al*. (2007; Huesgen, Adamska, Funk, unpublished). All three

recombinant Deg proteases were purified by affinity-chromatography using His GraviTrap affinity columns (GE Healthcare) as previously described (Huesgen *et al*., 2007).

Spinach PsbO was isolated from PSII membrane fragments according to Arellano *et al*. (1994) and Irrgang *et al*. (1995). PSII from *Synechocystis* was isolated by affinity-chromatography from the HT3 strain which expresses a His-tagged CP47 as previously described (Bricker *et al*., 1998).

PsbO degradation assay was performed in a final volume of 250 µl, containing 150 µg of PsbO purified from spinach leaves or 125 µg of total protein of PSII samples purified from *Synechocystis* HT3. The reaction mix contained 50 mmol Tris-HCl buffer pH 7.5, 4 µg *E. coli* thioredoxin, 3.5 µg *E. coli* thioredoxin reductase and 1.6 mmol β-NADPH. After a pre-incubation period of 15 min at 37 ºC, 15 µg of purified recombinant HhoA, HhoB or HtrA protease were added. Samples were taken at 0, 2, 5, 7 and 10 h and analyzed by SDS-PAGE and immunoblotting.

Spinach lumen was isolated as described before (Kieselbach *et al*., 1998). PsbO degradation in this fraction was assessed by incubating a sample of lumen of 120 µg protein in the absence or presence of the reducing system as described above.

Proteins were separated on 14% SDS-PAGE and visualized by CBB R-250 or immunostained using a dilution 1:10000 (*Synechocystis* samples) or 1:20000 (spinach samples) of primary anti-PsbO antibody (Agrisera). Deg proteases were detected with a dilution 1:10000 of antibodies specific for HhoA, HhoB or HtrA. Blots were developed using a secondary antibody conjugated to HRP and the ECL Advance reagents from GE Healthcare.

Results and Discussion

The PsbO protein is known for being remarkably stable. However, it has been shown recently that both isoforms of PsbO in *A. thaliana* (PsbO1 and PsbO2) were rapidly degraded in the presence of thioredoxin (Hall *et al*., 2010). To investigate the susceptibility to degradation of the reduced PsbO protein, we isolated the thylakoid lumen from spinach leaves and incubated it for 7 h in the presence (Fig. 1, left panel) or absence (Fig. 1, right panel) of the complete *E. coli* thioredoxin system (thioredoxin, thioredoxin reductase and β-NADPH). As can be seen, PsbO degradation products were observed only under reduced conditions, in agreement with previous observations in Arabidopsis (Hall *et al*., 2010).

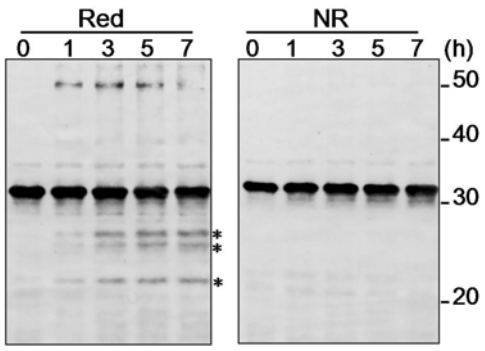

Fig. 1 PsbO degradation in the thylakoid lumen of spinach. Thylakoid lumen of spinach was isolated and incubated in reduced (Red) or non-reduced (NR) conditions. Proteins were immunostained using an antibody directed against PsbO. PsbO degradation fragments are shown with an asterisk.

Only a few proteases are known to be located in the thylakoid lumen of plants. These are the D1 processing proteases and the Deg1, Deg5 and Deg8 proteases. To investigate the role of Deg proteases in the degradation of PsbO, we performed *in vitro* experiments using recombinant Deg proteases. However, plant Deg proteases (Deg1 and Deg5) have been shown to react with reducing agents themselves. To avoid a possible redox effect in the activity of the proteases, we decided to use recombinant Deg proteases from *Synechocystis.* They are highly homologous to the luminal Deg proteases in plants and they are not subjected to redox control. Fig. 2 shows the time course of PsbO degradation in the presence of the complete thioredoxin system and the recombinant Deg proteases from *Synechocystis*, HhoA, HhoB or HtrA. A reduced sample of PsbO (upper panel) showed some residual degradation probably due to low amounts of cross-contamination by spinach proteases. Addition of HhoB or HtrA did not lead to any degradation of PsbO despite this background activity. However, addition of recombinant HhoA clearly resulted in strong degradation of PsbO under reduced conditions.

The ability of HhoA to degrade PsbO was also tested in samples of PSII of *Synechocystis* 6803 (Fig. 3a). A low PsbO degradation was observed in reduced samples after 10 h even when no external protease was added (upper panel). Addition of HhoA resulted in almost complete degradation of PsbO protein in the presence of the reducing system. By contrast, addition

of HhoB or HtrA did not enhance the degradation of reduced PsbO observed in the absence of recombinant proteases. This background activity must be due to some protease co-purified with the PSII sample. To reveal the possible presence of native cyanobacterial Deg proteases, we used specific antibodies against recombinant HhoA, HhoB or HtrA to analyze our PSII sample by western blot (Fig. 3b). Notably, all three cyanobacterial native Deg proteases, HhoA, HhoB and HtrA, co-purified with Photosystem II.

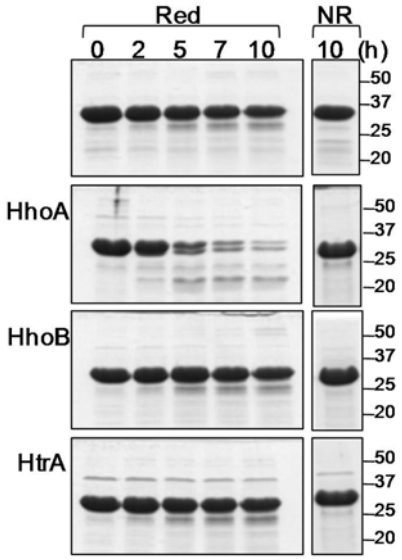

Fig. 2 PsbO degradation in the presence of recombinant Deg proteases of *Synechocystis* sp. PCC 6803.
PsbO from spinach was isolated and incubated in reduced (Red) or non-reduced (NR) conditions, alone (upper panel) or after addition of recombinant HhoA, HhoB or HtrA. Proteins were stained with CBB R-250.

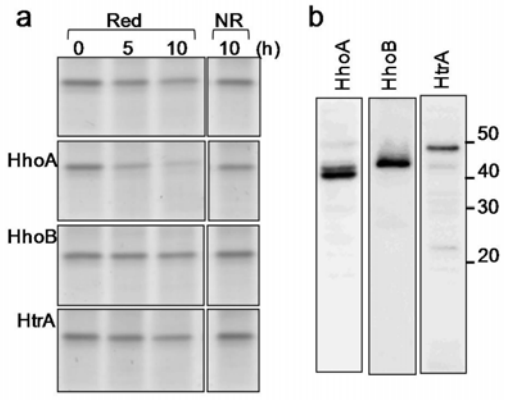

Fig. 3 a Redox-dependent degradation of PsbO in *Synechocystis* sp. PCC 6803. PSII was isolated from *Synechocystis* 6803 strain HT3 and incubated in reduced (Red) or non-reduced (NR) conditions, alone (upper panel) or after addition of recombinant HhoA, HhoB or HtrA. **b** PSII isolated from the HT3 strain was analyzed by western blot using antibodies directed against HhoA, HhoB or HtrA.

The results presented in this work demonstrate the ability of Deg proteases to degrade PsbO. Deg proteases from *Synechocystis* were able to degrade both PsbO from higher plants and cyanobacteria. While a few degradation fragments of spinach PsbO were detected, no fragments accumulated when PsbO of *Synechocystis* was used. We showed that degradation by Deg proteases clearly depends on the redox state of the PsbO protein. Normally a very stable protein in its oxidized form, it becomes highly susceptible to degradation when the disulfide bridge is reduced.

Acknowledgements

The authors thank Drs. Pitter Huesgen and Iwona Adamska for the plasmids encoding Deg proteases of *Synechocystis* sp. PCC 6803, and Dr. Terry M Bricker for the HT3 strain. We are thankful to the Royal Swedish Academy of Sciences (to CF) as well as the Lawsky foundation (to IR and LXT) for granting their positions. The work was supported by the Swedish Energy Agency (to CF), by the Carl-Trygger Foundation (to TK), and Umeå University (to CF).

References

Arellano JB, Schröder WP, Sandmann G, Chueca A, Barón M (1994) Removal of Nuclear Contaminants and of Non-Specifically Photosystem II-Bound Copper from Photosystem II Preparations. Physiol. Plant. 9: 369-374

Bricker TM, Morvant J, Masri N, Sutton HM, Frankel LK (1998) Isolation of a Highly Active Photosystem II Preparation from Synechocystis 6803 Using a Histidine-Tagged Mutant of CP 47. Biochim. Biophys. Acta, Bioenerg. 1409: 50-57

Clausen T, Southan C, Ehrmann M (2002) The HtrA Family of Proteases: Implications for Protein Composition and Cell Fate. Mol. Cell 10: 443-455

Gottesman S (1996) Proteases and Their Targets in Escherichia Coli. Annu. Rev. Genet. 30: 465-506

Hall M, Mata-Cabana A, Åkerlund HE, Florencio FJ, Schröder WP, Lindahl M, Kieselbach T (2010) Thioredoxin Targets of the Plant Chloroplast Lumen and Their Implications for Plastid Function. Proteomics 10: 987-1001

Huesgen PF, Scholz P, Adamska I (2007) The Serine

Protease HhoA from Synechocystis sp. Strain PCC 6803: Substrate Specificity and Formation of a Hexameric Complex Are Regulated by the PDZ Domain. J. Bacteriol. 189: 6611-6618

Huesgen PF, Schuhmann H, Adamska I (2009) Deg/HtrA Proteases As Components of a Network for Photosystem II Quality Control in Chloroplasts and Cyanobacteria. Res. Microbiol. 160: 726-732

Irrgang KD, Shi LX, Funk C, Schröder WP (1995) A Nuclear-Encoded Subunit of the Photosystem II Reaction Center. J. Biol. Chem. 270: 17588-17593

Kieselbach T, Funk C (2003) The Family of Deg/HtrA Proteases: from Escherichia Coli to Arabidopsis. Physiol. Plant. 119: 337-346

Kieselbach T, Hagman Å, Andersson B, Schröder WP (1998) The Thylakoid Lumen of Chloroplasts. J. Biol. Chem. 273: 6710-6716

Nikitina J, Shutova T, Melnik B, Chernyshov S, Marchenkov V, Semisotnov G, Klimov V, Samuelsson G (2008) Importance of a Single Disulfide Bond for the PsbO Protein of Photosystem II: Protein Structure Stability and Soluble Overexpression in Escherichia Coli. Photosynth. Res. 98: 391-403

Sun X, Fu T, Chen N, Guo J, Ma J, Zou M, Lu C, Zhang L (2010) The Stromal Chloroplast Deg7 Protease Participates in the Repair of Photosystem II after Photoinhibition in Arabidopsis. Plant Physiol. 152: 1263-1273

Methylmethionine (Vitamin U) Alleviates Negative Effects of Chemical Stressors on Photosynthesis of the Green Alga *Scenedesmus Opoliensis*

Laszlo Fodorpataki*, Zsolt Gy Keresztes, Csaba Bartha, Attila L Marton, Szabolcs Barna

Department of Biology, "Babes-Bolyai" University, Cluj-Napoca, Romania.
*Corresponding author: Tel. No. +40 740 507 829; Fax No. +40 264 431 858; E-mail: lfodorp@gmail.com.

Abstract: Investigation of stress tolerance in unicellular algae represents an experimental approach that contributes to elucidation of cellular events related to stress-induced metabolic and developmental reactions in plants. In this context, we investigated the interaction of methylmethionine (vitamin U) with environmental stress factors (high concentrations of heavy metals, herbicides) in photosynthetic energy conversion, net oxygen evolution and dry biomass production of the green microalga *Scenedesmus opoliensis*. Parameters of the induced chlorophyll fluorescence reveal the benefic influence of vitamin U on light use efficiency of photochemical reactions, as well as on the organization of light-harvesting pigment-protein complexes of the thylakoid membranes in algal cells exposed to micromolar concentrations of cadmium. Oxidative damage caused by the herbicide methylviologen is diminished by methylmethionine. The activities of ascorbate peroxidase and superoxide dismutase are enhanced in the algal cells exposed to the combined effect of methylviologen and vitamin U. In the absence of stress factors, vitamin U has no significant influence on the investigated physiological parameters. Further studies on the protective role of methylmethionine in the presence of stress factors may provide a better insight into the mechanisms of antistress reactions of plants grown in unfavorable environments.

Keywords: Algal photosynthesis; Antioxidants; Chlorophyll fluorescence; *Scenedesmus opoliensis*; Stress acclimation; Vitamin U

Introduction

Investigation of enhancement of stress tolerance in unicellular green algae represents an experimental approach that contributes to the elucidation of cellular events related to stress-induced metabolic and develop-mental reactions in plants. A major goal of these studies is the improvement of stress tolerance for a better development of plants in unfavorable habitats.

Different species of the *Scenedesmus* genus are green microalgae with a widespread distribution and have an important contribution to the primary biomass produc-tion and energy flow it aquatic ecosystems. Their metabolic plasticity makes them very good bioindicators of environmental stress factors that impair photo-synthesis and developmental processes (Liu *et al*., 2010). At present, the use of these algae in phytoremediation of polluted aquatic habitats proves to be a cost-effective, environmentally friendly and efficient *in situ* technology for a variety of pollutants (Dosnon-Olette *et al*., 2010). For this purpose, there is a need to apply non-invasive, highly sensitive, fast and easy to apply investigation tools in order to probe the degree of physiological injury (Prado *et al*., 2009). Furthermore, photosynthetic carbon dioxide fixation by microalgae is part of a long-term strategy in mitigating increased emission of this greenhouse gas. The biomass of microalgae, produced through photosynthetic carbon dioxide assimilation, can be converted into a variety of biofuels and chemical products of commercial interest (Ho *et al*., 2010; Hodaifa *et al*., 2010).

Several bioactive substances help survival of

plants under environmental stress conditions by interacting with harmful agents in different physiological processes. For example, salicylic acid, nitric oxide, ascorbic acid, glutathione, tocopherol and many flavonoids act as scavengers of harmful reactive oxygen species and as chemical signals for triggering defensive mechanisms, thus contributing to an enhances physiological tolerance of plant cells to unfavorable environmental factors that may impair vital functions. Among these protective substances, vitamin U (the methylated derivative of the amino acid methionine) is a natural product of the plant metabolism, and its methyl groups can be used in detoxification processes (Fodorpataki *et al*., 2009; Kovacik *et al*., 2010).

In this context, we investigated the interaction of methylmethionine (vitamin U) with environmental stress factors (high concentrations of heavy metals, herbicides) at the level of different photosynthetic and biochemical parameters of the green microalga *Scenedesmus opoliensis*. The aim of the study is to get an insight in the physiological and biochemical processes related to the interaction of vitamin U with chemical stress exerted by water pollution with a heavy metal (cadmium) and with an herbicide (methylviologen). We also proposed to identify photosynthetic and other metabolic parameters that may be good markers of stress tolerance in the green alga used as a test organism.

Materials and Methods

Axenic cultures of the freshwater green microalga *Scenedesmus opoliensis* P. Richter, strain AICB141, were grown in Bold's basal nutrient medium (BBM), at 130 μM photons m^{-2} s^{-1} 22 ºC in an algal growth chamber, on an orbital shaker with 180 rpm. The experiment consisted of 6 treatments: (1) control in BBM medium, (2) with 0.25 mmol vitamin U (methylmethionine), (3) with 0.05 mmol $CdCl_2$, (4) with 0.05 mmol $CdCl_2$ + 0.25 mmol vit. U, (5) with 0.005 mmol methylviologen (MV), and (6) with 0.005 mmol MV + 0.25 mmol vit. U. All setups had 4 replicates. Treatments were applied for 7 days.

Determination of parameters of induced chlorophyll fluorescence was performed with a PAM-FMS 2 chlorophyll fluorometer (Hansatech). Algae were collected by low pressure filtration, providing a uniform layer of cells on a 13 mm glass fiber filter. Samples were dark adapted for 10 min. The modulated light was sufficiently weak (0.04 μM m^{-2} s^{-1}) so as not to produce any significant variable fluorescence. A single saturating flash (2,000 μM m^{-2} s^{-1} for 0.5 s) was applied to reach the maximal fluorescence Fm. After the decline of the signal, the actinic light was turned on (100 μM m^{-2} s^{-1}) to start the induction kinetics. The determined parameters were initial fluorescence F_0, maximal fluorescence Fm, the Fv/Fm ratio (potential quantum efficiency of PS II), modulated maximal fluorescence Fm', steady state fluorescence Fs, and the effective quantum use efficiency (Φ) representing the ratio (Fm' – Fs)/Fm'. Net oxygen evolution of algal cell suspensions was measured with an Oxy-Lab oxymeter (Hansatech) at 20 °C, in the presence of a constant photon flux density of 110 micromole photons m^{-2} s^{-1}. Chlorophylls were extracted in dark with N,N-dimethyl-formamide, and determined spectrophotometrically. Final dry biomass was deter-mined by filtering 100 ml of each culture, and drying the cell mass at 80 ºC for 48 h, until a constant dry weight was reached (Fodorpataki *et al*., 2009; Liu *et al*., 2010).

Activity of two main antioxidative enzymes was determined spectrophotometrically. Algal cultures were centrifuged at 2,000 g for 10 minutes, then the pellets were ground in 1 g quartz sand on ice. Proteins were extracted with 1.5 ml of 0.1 mol sodium phosphate buffer (pH 7.0) and the extract was centrifuged for 20 minutes at 2,300 g and 5 ºC. Protein content (as reference for enzyme activity) was determined by the Bradford method, with bovine serum albumin as a standard. Ascorbate peroxidase (APX) activity was determined based on the absorption at 270 nm of a 5 ml final volume of reaction mixture consisting of 1 ml algal extract as enzyme source, 3.5 ml of 50 mmol sodium phosphate buffer (pH 7.5), 0.25 ml of 40 mmol sodium ascorbate and 0.25 ml of 200 mmol hydrogen peroxide. Superoxide dismutase activity was assayed by a method based on inhibition of nitroblue tetrazolium reduction. The absorbance of the illuminated reaction mixture and that of a control represented by potassium phosphate buffer was measured at 560 nm (Fodorpataki *et al*., 2009; Dosnon-Olette *et al*., 2010).

Sample means and comparison of means were made with SPSS using one-way ANOVA *post hoc* multiple comparisons with the Tukey HSD test. Differences were considered significant at the $P \leq 0.05$ level.

Results and Discussion

From among the different parameters of the conventional and pulse amplification modulated chlorophyll fluorescence, the effective quantum efficiency (Φ), the potential quantum use efficiency (Fv/Fm) and the non-modulated ground fluorescence F0) proved to be the most sensitive ones to the structural and functional disturbances caused by cadmium and methylviologen. In the case of effective quantum efficiency of the photochemical reactions that occur in photosystem II, the results showed that vitamin U significantly compensated for reduction of light use efficiency caused by the heavy metal and by the herbicide. This partial compensation was more pronounced when vitamin U was administrated simultaneously with cadmium. By itself, vitamin U did not influence significantly the value of quantum efficiency (Fig. 1).

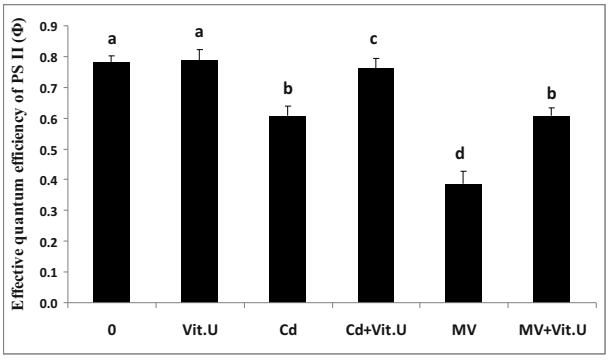

Fig. 1 Effective quantum efficiency (Φ = ΔF/Fm') of PS II in the green alga *Scenedesmus opoliensis*, treated with cadmium (Cd) and methylviologen (MV) in the absence or in the presence of vitamin U (vertical bars represent standard errors from means, n = 4, different letters indicate significant differences at $P < 0.05$).

The results suggest that vitamin U alleviates the negative effects of the applied concentrations of cadmium and methylviologen on photosystem II in the thylakoids of algal chloroplast. Variations in the functional organization of light-harvesting pigment-protein complexes and in the efficiency of energy transfer from the light-harvesting complex to the reaction centre of PS II, as reflected by the ground chlorophyll fluorescence (F0) in the dark-adapted algal samples, were measured under the influence of the applied water pollutants. As in the case of quantum efficiency, vitamin U prevented the drastical decrease of F0 caused by 0.05 mmol cadmium and by 0.005 mmol methylviologen. In other studies related to the influence of some herbicides on photosynthesis of the same alga, it was found that vitality index derived from the induced chlorophyll fluorescence was the most sensitive marker of herbicide toxicity, while quantum efficiency of PS II was decreased only by higher (millimolar) concentrations of the applied herbicides (Fodorpataki *et al*., 2009).

Under constant photon flux density and temperature, the net photosynthetic oxygen production was significantly inhibited by 0.05 mmol $CdCl_2$ and by 0.005 mmol methylviologen. The more pronounced negative effect of the herbicide may be related to its action in enhancing the Mehler reaction in the chloroplasts, resulting in overproduction of superoxide radicals and hydrogen peroxide, as reactive oxygen derivatives (Prado *et al*., 2009). Administration of 0.25 mmol methylmethionine significantly compensated for the reduction of net oxygen evolution of algal cells, caused by cadmium and methylviologen (Fig. 2). This effect may be related with protection of biomolecules against the oxidative damage, or with a more complex process of detoxification of harmful chemical agents, induced by vitamin U through an unknown mechanism.

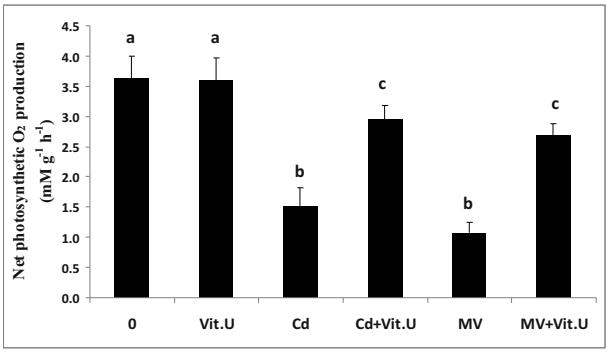

Fig. 2 Net photosynthetic oxygen production of the algal cultures under the influence of cadmium, methylviologen (MV) and vitamin U, at constant illumination and temperature (n = 4, different letters indicate significant differences at $P < 0.05$).

Because cadmium and methylviologen may induce oxidative stress that triggers the activation of antioxidative protection, the interaction of vitamin U with these stress factors was studied at the level of two important enzymatic components of the antioxidative system: superoxide dismutase (SOD) and ascorbate peroxidase (APX). These enzymes have specific isoforms in the chloroplast and contribute to the scavenging of superoxide radicals and hydrogen peroxide, respectively. Changes in the function of the two enzymes exhibited a similar pattern, but were

more pronounced in the case of ascorbate peroxidase. Cadmium caused a decrease in APX activity, while methylviologen induced an enhancement of its enzymatic activity, most probably because the increased production of hydrogen peroxide, due to the Mehler reaction, stimulates APX. Vitamin U by itself did not influence significantly APX activity, but the interaction of vitamin U with cadmium and with methylviologen increased the antioxidative activity of ascorbate peroxidase, contributing to a better protection of algal cells against oxidative damage (Fig. 3). Basicly similar results were obtained when salicylic acid was applied simultaneously with copper excess in cultures of *Scenedesmus quadricauda*, and salicylic acid was found to compensate for oxidative stress triggered by copper overdose (Kovacik *et al*., 2010). Vitamin U also compensated for the decreased chlorophyll content of algal cells exposed to cadmium and methylviologen. This effect may counteract for the reduced light use efficiency of photochemical processes (data not shown).

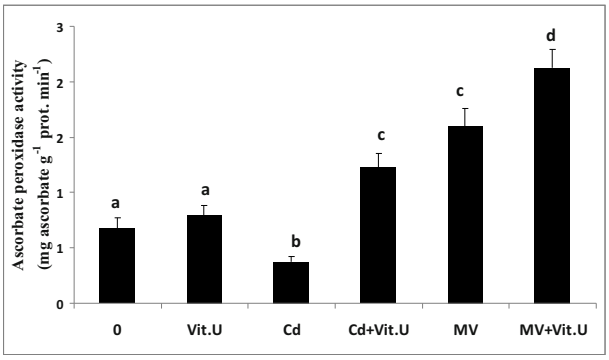

Fig. 3 Enzymatic activity of ascorbate peroxidase (APX) in cells of *Scenedesmus opoliensis* treated with 0.25 mmol vitamin U, 0.05 mmol $CdCl_2$ (Cd) and 0.005 mmol Methylviologen (MV), separately and in combination (n = 4, different letters indicate significant differences at $P < 0.05$).

Considering the overall biomass production of the algal cell cultures, the results showed that by itself vitamin U does not increase biomass, but it compensates for the net biomass reduction caused by the applied chemical stress factors (Fig. 4). This, once again, reflects its beneficial influence on overall photosynthetic production of algae exposed to certain stress factors.

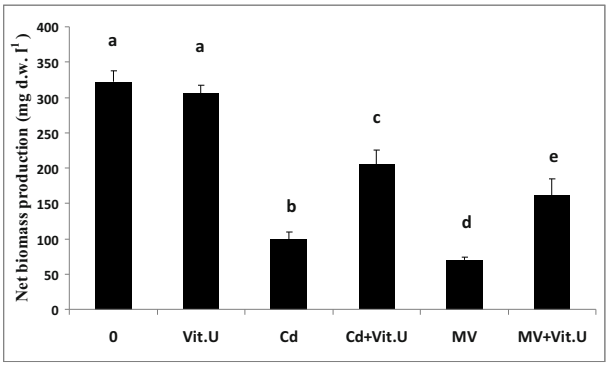

Fig. 4 Influence of 0.25 mmol vitamin U on the net dry biomass (d.w.) production of 1 week old algal cultures treated with 0.005 mmol methylviologen (MV) or 0.05 mmol Cd (vertical bars represent standard errors from means, n = 4, different letters indicate significant differences at $P < 0.05$).

Relying on the results of the above presented experiments, one can conclude that vitamin U (methyl-methionine) diminishes the negative physiological effects of heavy metals (*e.g.* Cd) and some herbicides (*e.g.* methylviologen) that induce oxidative stress. The benefic influence of vitamin U under such stress conditions may be related to detoxification of harmful products in algal cells (Dosnon-Olette *et al*., 2010). Vitamin U compensates for inhibition of photochemical light use efficiency caused by cadmium toxicity and by the herbicide methylviologen, it ensures a high chloro-phyll content and an improved oxygen production. Vitamin U reduces the negative effects of chemical stressors on components of the photosynthetic apparatus and on the activity of certain protective enzymes.

Further investigations are needed to elucidate the action site and protective mechanisms of this plant metabolite, considering that there are very few data about its role in plant metabolism and in acclimation.

Acknowledgements

The authors thank for the financial support provided from the program co-financed by the Sectorial Operational Program “Human Resources Development, Contract POSDRU 6/1.5/S/3 - Doctoral studies: through science towards society”. This work was also supported by CNCSIS-UEFISCSU project PN II-RU TE 306/2010.

References

Dosnon-Olette R, Trotel-Aziz P, Couderchet M, Eullaffroy P (2010) Fungicides and Herbicide Removal in Scenedesmus Cell Suspensions. Chemosphere 79: 117-123

Fodorpataki L, Bartha Cs, Keresztes ZsGy (2009) Stress-Physiological Reactions of the Green Alga Scenedesmus Opoliensis to Water Pollution with Herbicides. Ann. Univ. Or. 16(1): 51-56

Ho SH, Chen CY, Yeh KL, Chen WM, Lin CY, Chang JS (2010) Characterization of Photosynthetic Carbon Dioxide Fixation Ability of Indigenous Scenedesmus Obliquus Isolates. Biochem. Eng. J. 53: 57-62

Hodaifa G, Martinez ME, Sanchez S (2010) Influence of Temperature on Growth of Scenedesmus Obliquus in Diluted Olive Mill Wastewater As Culture Medium. Eng. Life Sci. 10(3): 257-264

Kovacik J, Klejdus B, Hedbavny J, Backor M (2010) Effect of Copper and Salicylic Acid on Phenolic Metabolites and Free Amino Acids in Scenedesmus Quadricauda (Chlorophyceae). Plant Sci. 178: 307-311

Liu Y, Wang W, Zhang M, Xing P, Yang Z (2010) PSII-Efficiency, Polysaccharide Production, and Phenotypic Plasticity of Scenedesmus Obliquus in Response to Changes in Metabolic Carbon Flux. Biochem. Syst. Ecol. 38: 292-299

Prado R, Garcia R, Rioboo C, Herrero C, Abalde J, Cid A (2009) Comparison of the Sensitivity of Different Toxicity Test Endpoints in a Microalga Exposed to the Herbicide Paraquat. Environ. Internatl. 35: 240-247

Effect of Ozone on Photosynthesis and Seed Yield of Sensitive (S156) and Resistant (R123) *Phaseolus Vulgaris* L. Genotypes in Open-Top Chambers

Cornelius CW Scheepers[1], Reto J Strasser[1,2], Gert HJ Krüger[1]

[1] School of Environmental Sciences, North-West University, Potchefstroom;
[2] Laboratory of Bioenergetics, University of Geneva, Switzerland.

Abstract: Rising tropospheric ozone (O_3) concentrations have been identified as a significant threat to crop production. In the present study two snap bean (*Phaseolus vulgaris* L.) genotypes with known difference in sensitivity to O_3 namely S156 (sensitive) and R123 (resistant) were compared with respect to their response to O_3 using an Open-Top chambers to throw light on the physiological and biochemical basis of O_3 effects. Seedlings were exposed to two different controlled levels of O_3 (0 and 80 nmol mol^{-1}). *Chlorophyll a* fluorescence and photosynthetic gas exchange were measured in parallel throughout the growing season. Yield data were collected at physiological maturity. The physiological O_3 induced effects were evident long before visible damage appeared in the S156 genotype. Photosynthesis was largely inhibited in the S156 genotype, mainly due to inhibition of the photosynthetic electron transport chain, resulting in decreased reduction of end electron acceptors with consequential reduced carboxylation efficiency and regeneration capacity of RuBP. The seed yield data corresponded well to the photosynthetic response of the test plants.

Keywords: *Phaseolus vulgaris*; Ozone; Open-Top chambers; Photosynthetic electron transport

Introduction

Atmospheric pollution emerged as a problem in southern Africa over the last few decades, due to a drastic increase (145%) in energy consumption (McCormick, 1997) resulting in O_3 thresholds being exceeded (van Tienhoven and Scholes, 2003). The biological effects of O_3 on plants have been studied for more than 50 years (Davison and Reiling, 1995). Open-top chamber studies have shown that seed yield production is suppressed in S156 while effects on R123 are minimal under moderate O_3 stress (Burkley and Eason, 2002). While limited photosynthesis data is available for S156, no published data for R123 is available (Heagle *et al*., 2002). We investigated the biochemical and physiological basis of the effect of O_3 on photosynthesis of sensitive (S156) and resistant (R123) bush bean genotypes. The status of the photosynthetic apparatus was assessed by CO_2 response curves (Lange *et al*., 1987) and by fast phase chlorophyll fluorescence induction kinetics (Strasser *et al*., 2004).

Materials and Methods

Experimental site and treatment

Four open-top chambers (OTCs) were used in this study. Two of the four OTCs were used as the control and were ventilated at 1.5 air replacements per minute with charcoal filtered (CF) air. The ventilating air of the two treatment chambers was enriched with O_3 (Ambient air + O_3 = AO_3) provided by an electrical O_3 generator (OLGEAR UV-20 HO) fitted inside the fan box of the blower. An average of 80 ppb O_3 were maintained in the treatment chambers (AO_3). The test plants were exposed to this elevated O_3 concentration for 9 day light hours per day for 40 days.

Photosynthetic CO_2 assimilation

Photosynthetic gas exchange was measured with an infrared gas analysis system (CIRAS-2, PP-Systems, Hertz. UK). CO_2 response curves ($A:C_i$) were created and the gas exchange parameters calculated according to Farquhar and Sharkey (1982).

Chlorophyll a fluorescence induction

Chlorophyll a fluorescence induction kinetics were measured on fully dark adapted (1 h) attached leaves using a fluorimeter (Handy-PEA, Hansatech Instruments Ltd., Kingslynn, UK). The fluorescence transients were analysed according to the JIP-test (Strasser *et al.*, 2004). A multi-parametric expression the so called photosynthetic performance index (PItotal) of the four independent functional steps of photosynthesis was introduced by Tsimili-Michael and Strasser (2008).

$$PI_{ABS,total} = \frac{\gamma_{RC}}{1-\gamma_{RC}} \bullet \frac{\varphi_{Po}}{1-\varphi_{Po}} \bullet \frac{\psi_{Eo}}{1-\psi_{Eo}} \bullet \frac{\delta_{Ro}}{1-\delta_{Ro}}$$

where $\gamma_{RC}/(1 - \gamma_{RC})$ = (RC/ABS) is the fraction of reaction centre chlorophyll (Chl_{RC}) per total chlorophyll (Chl_{RC} + $_{Antenna}$). This expression can be deconvoluted into two JIP-test parameters and estimated from the original fluorescence signals as $RC/ABS = RC/TR_0 \bullet TR_0/ABS = [(F_{2ms} - F_{50\mu s})/4(F_{300\mu s} - F_{50\mu s})] \bullet F_V/F_M$. The factor 4 is used to express the initial fluorescence rise per 1 ms. The parameter RC/ABS shows the contribution to the $PI_{ABS,total}$ due to the RC-density on a chlorophyll basis. The contribution of the light reactions for primary photochemistry is estimated according to the JIP-test as $(\varphi_{Po}/(1 - \varphi_{Po})) = TR_0/DI_0 = k_P/k_N = F_V/F_0$. The contribution of electron transport beyond Q_A is calculated as $\psi_0/(1 - \psi_0) = ET_0/(TR_0 - ET_0) = F_M - F_{2ms})/(F_{2ms} - F_{50\mu s})$. The contribution of the reduction of end reducing equivalents is calculated as $(\delta_0/(1 - \delta_0)) = RE/ABS = (1 - F_{30\mu s})/(1 - F_{2ms})$.

Extended analysis of the fluorescence transients were done by calculation of the difference in relative variable fluorescence to present so called ΔV curves (expressed as V = f(t)), *i.e.* subtracting fluorescence values of the controls of transient normalized between F_O and F_J ($V_{OJ} = (F - F_O)/(F_J - F_O)$ from the fluorescence values of their respective treatments; $\Delta V_{OJ} = V_{OJtreatment} - V_{OJcontrol}$), F_J and F_M ($V_{JM} = (F - F_J)/(F_M - F_J)$, $\Delta V_{JM} = V_{JMtreatment} - V_{JMcontrol}$), respectively.

Crop Yield

The pods were harvested at plant maturity, and dried for 24 h at 60 °C or until constant mass. Yield was determined in terms of total pods per plant, total gram per pod, total seed per plant, total gram of seed per plant, grams per 100 seed and number of seeds per pod.

Results

Growth and seed yield

A marked O_3-induced decrease in growth of S156 was evident after 35 days of fumigation. Distinctive brown-coloured lesions developed on the leaves of S156. The effect occurred to a lesser extend in R123 (Fig. 2). The visual lesions were also reflected by a decrease of 56% in seed yield of S156 and 31% in R123 (Fig. 3A).

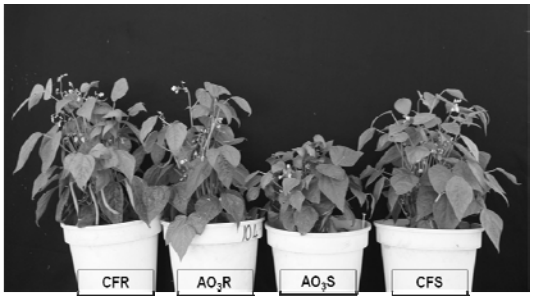

Fig. 1 Ozone resistant (R123) and sensitive (S156) *Phaseolus vulgaris* genotypes after 35 days exposure to carbon filtered air (CF) and 80 nmol mol^{-1} O_3 (AO_3) respectively. R = R123 and S = S156

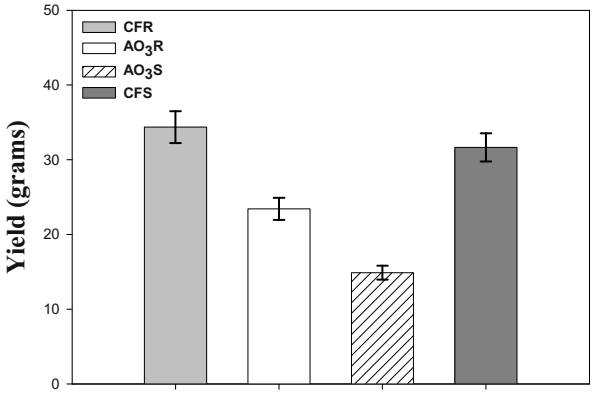

Fig. 2 Seed yield measured at maturity.

Chlorophyll a fluorescence

The photosynthetic performance index ($PI_{ABS,total}$) values of the treatments (Fig. 3B) reflected the growth and seed yield (Figs. 2 and 3A) very well. The $PI_{ABS,total}$ after 35 days in AO_3S plants decreased by 53%.

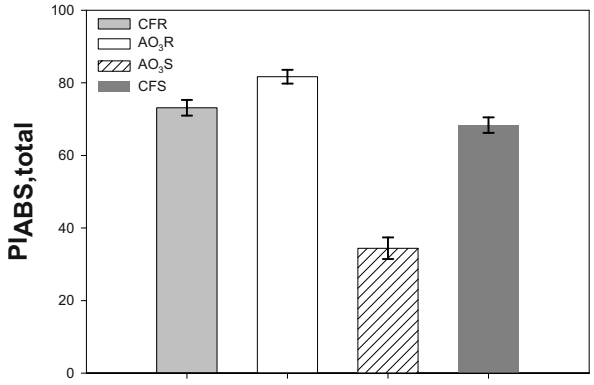

Fig. 3 Photosynthetic performance index total ($PI_{ABS,total}$) measured after 35 days fumigation.

A multi parametric presentation of the fluorescence parameters revealed that in AO_3S an O_3-induced decrease occurred in all four partial processes reflected by the $PI_{ABS,total}$ namely absorption (RC/ABS), trapping ($\varphi_{P0}/(1- \varphi_{P0})$, electron transport ($\psi_0/(1- \psi_0)$ and reduction of end electron acceptors δRo/1-δRo (Fig. 4). The major inhibition, however occurred in the reduction of end electron acceptors [δRo / (1-δRo)] and the efficiency of the conversion of trapped excitation energy to electron transport [ψ_0 / (1-ψ_0)]. The effect was also reflected by a decrease in the phenomological electron transport flux per leaf cross section (ET/CS_0) and the density of reaction centres (RC/CS). Note that the quantum efficiency of primary photochemistry, $\varphi_{P0} = F_V/F_M$ was insensitive.

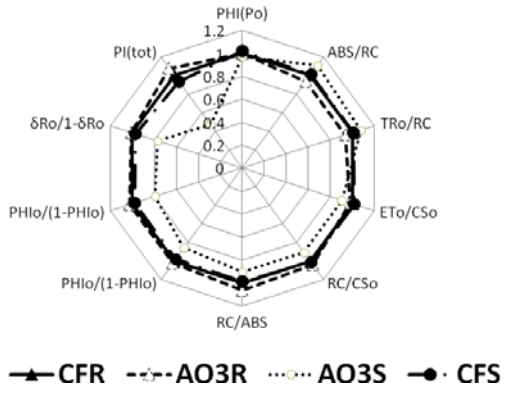

Fig. 4 Functional and structural parameters of PS II deduced by the JIP analysis of fluorescence transients. For each parameter and for both plant genotypes the values were normalized to that of the control (CFR).

Average chl *a* fluorescence transients of dark adapted leaves of *P. vulgaris* were normalized between the steps O (50 μs) and J (2 ms). This section of the transient reflects the single turnover event which includes excitation, trapping and reduction of Q_A, while the section J to P reflects the multiple turnover events, including the reduction of PQ, cytochrome, plastocyanin and PS I-driven electron transfer to the end electron acceptors on the PS I acceptor side (Strasser *et al*., 1999). The difference kinetics, ΔV_{OJ} revealed a positive ΔK-band reflecting O_3 induced inhibition of the oxygen evolving complex and/or an increase of the functional PS II antenna size in the AO_3S plants (Strasser *et al*., 2004) (Fig. 5). With the V_{JM} normalization a positive ΔI-band, pointing at inhibition of the activation state of ferredoxin $NADP^+$ reductase (FNR) and inhibition of the reduction of end electron acceptors such as $NADP^+$ and Fd.

The decrease in the maximum amplitude of the transients normalized between steps O and I pointed at an O_3 induced decrease in the pool size of end electron acceptors in AO_3S plants (Figure not shown). To compare the rate of reduction of the end electron acceptor pool, the maximum amplitude of the transients (normalized between I and P) were fixed at unity. No significant change in overall rate constant (1/half-time) was observed.

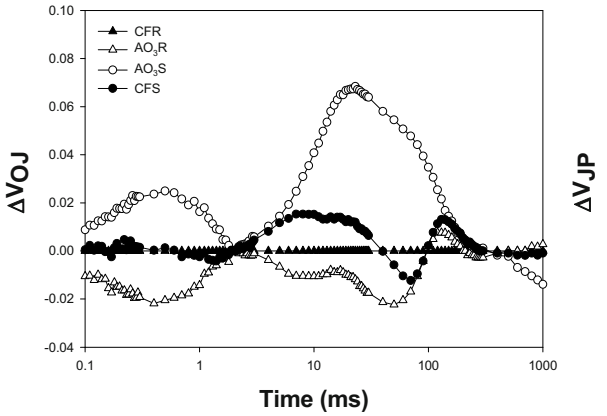

Fig. 5 Fluorescence transients, normalized between steps O and J (2ms) on the left and between J and P on the right. Both these partial transients were then plotted as difference kinetics, ΔV = V (treatment) – V (control R).

Photosynthetic CO_2 assimilation

It was deduced from the A:Ci response curves (Fig. 7) that in the AO_3S plants the carboxylation efficiency (initial slope), the assimilation rate (A_{360}) and the RuBP regeneration capacity (J_{max}) were reduced by 75%, 56% and 56%, respectively. The compensation point (Γ) increased by 49%. This strongly points at

O_3-induced mesophyll limitation. The % stomatal limitation (l) increased only moderately (8%).

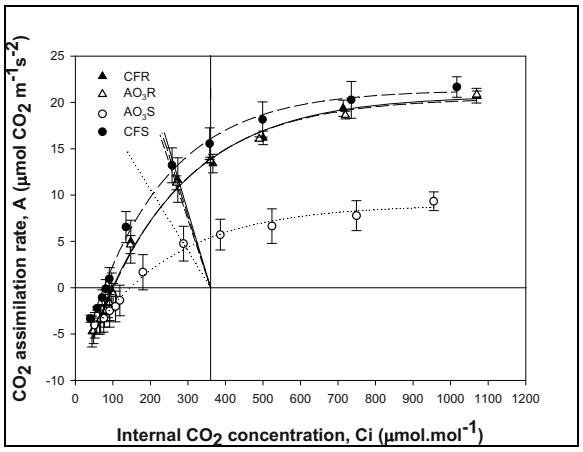

Fig. 7 Average CO_2 response curves (A:Ci) for intact leaves of R123 and S156 *P. vulgaris* genotypes after 25 days exposure to filtered air (CF) and 80 nmol mol^{-1} ozone (AO_3) respectively, measured at 1,200 µmol photons m^{-2} s^{-1} to ensure full activation of Rubisco.

Conclusion

The response of the two bean cultivars to elevated O_3 of 80 nmol mol^{-1} differed considerably. Ozone concentrations induced a more prominent visible injury on leaves of S156 genotype. Photosynthesis was largely inhibited in the S156 genotype, mainly due to inhibition of the photosynthetic electron transport resulting in decreased reduction of end electron acceptors. This was the main reason for the reduced carboxylation efficiency and regeneration capacity of RuBP. Constraints in photosynthesis of S156 genotype occurred primarily as a result of mesophyll limitation. The above limitations lead to a large reduction in seed yield in S156. Though R123 exhibited no stress symptoms with respect to fluorescence and gas exchange data, seed yield was affected. Although measured at the dark adapted state the JIP-test reflects the potential of the photosynthetic apparatus for energy supply, metabolism and eventually seed yield very well.

References

Burkley KO, Eason G (2002) Ozone Tolerance in Snap Bean Is Associated with Elevated Ascorbic Acid in the Leaf Apoplast. Physiol. Plant. 114: 387-394

Davison AW, Reiling K (1995) A Rapid Change in Ozone Resistance of Plantago Major after Summers with High Ozone Con-Centrations. New Phytologist 131: 337-344

Farquhar GD, Sharkey TS (1982) Stomatal Concuctance and Photosynthesis. Annual Review of Plant Physiology 33: 317-345

Heagle AS, Miller JE, Burkley KO, Eason G, Pursley WA (2002) Growth and Yield Responses of Snap Bean to Mixtures of Carbon Dioxide and Ozone. J. Environ. Qual. 31: 2008-2014

Lange OL, Harley PC, Beyshlag W, Tenhunen JD (1987) Gas Exchange Methods for Characterizing the Impact of Stress on Leaves. In: Tenhunen JD (ed.), Plant Response to Stress. Springer Verlag: Heidelberg, Germany, pp. 3-22

McCormick K (1997) Acid Earth – The Pollitics of Acid Pollution. 3rd ed. Earthscan Publications, London

Strasser RJ, Srivastava A, Tsimilli-Michael M (2004) Analysis of the Chlorophyll Fluorescence Transient. In: Papageorgiou G, Govindjee XUC (eds.), Chlorophyll Fluorescence a Signiture of Photosynthesis. Kluwer Academic Publishers: The Netherlands. 19: 321-362

Strasser RJ, Tsimilli-Michael M, Pêcheux M (1999) Perpetual Adaptation in a Perpetually Changing Environment As a Survival Strategy of Plants: a Case Study in Foraminifers Concerning Coral Reef Bleaching. Photosynthetica. 37(1): 71-85

Tsimilli-Michael M, Strasser RJ (2008) In Vivo Assessment of Stress Impact on Plants' Vitality: Applications in Detecting and Evaluating the Beneficial Role of Mycorhization on Host Plants. In: Varma A (ed.), Mycorrhiza: State of the Art, Genetics and Molecular Biology, Eco-Function, Biotechnology, Eco-Physiology, Structure and Systematics, 3rd ed. Springer, pp. 679-703

Van Tienhoven AM, Scholes MC (2003) Air Pollution Impacts on Vegetation in South-Africa. In: Emberson L, Ashmore M, Murray F (eds.), Air Pollution Impacts on Crops and Forests. Imperial Colledge Press: London, pp. 237-262

SO_2-Drought Interaction on Crop Yield, Photosynthesis and Symbiotic Nitrogen Fixation in Soybean (*Glycine Max*)

Heyneke E[1], Strauss AJ[1], Van Heerden PDR[1], Strasser RJ[2], Krüger GHJ[1]

[1] School of Environmental Sciences, North-West university, Potchefstroom, South Africa;
[2] Laboratory of Bioenergetics, University of Geneva, Switzerland.

Abstract: South Africa has an energy-intensive economy, resulting in substantial SO_2 pollution. Well watered and drought stressed soybean (*Glycine max*) were exposed to SO_2 in open-top chambers to study the physiology of SO_2 injury by measuring in parallel: growth, biomass accumulation, photosynthetic gas exchange, *chlorophyll a* fluorescence, *in vitro* Rubisco activity and symbiotic nitrogen fixation. A strong concentration dependent SO_2-induced inhibition was displayed in all parameters. A reduction in photosynthesis occurred without any accompanying visual injury symptoms. SO_2 exposure also resulted in large reductions in biomass and seed yield and root nodule ureide content. The *chlorophyll a* fluorescence data, pointing at impaired electron transport and formation of end electron acceptors as well as the *in vitro* Rubisco activity, supported the gas exchange data. Inhibition of photosynthesis, proved to be the main constraint imposed by SO_2. SO_2-stress was aggravated by simultaneous drought stress.

Keywords: *Glycine max*; Sulphur dioxide; Open-Top chambers; Photosynthetic electron transport

Introduction

In the heart of the South African highveld the CLRTAP critical level for forest and semi-natural vegetation was exceeded and SO_2 concentrations in this region approached the CLRTAP critical level for crops (Josipovic *et al.*, 2010). The purpose of this investigation was to examine the response of well-watered and drought-stressed soybean plants to SO_2. Crop yield, ureide content, chlorophyll fluorescence induction kinetics, photosynthetic gas exchange and *in vitro* Rubisco activity were measured in parallel, with the view to resolve the mechanism of injury by SO_2. As the photosynthetic apparatus and particularly photosystem II is known to be very sensitive to environmental stress, the emphasis of the study falls on the response of photosynthesis.

Materials and Methods

Experimental site and treatments

SO_2-fumigation was carried out in eight open-top chambers (OTCs). Plants were fumigated with SO_2 (0 ppb; 50 ppb; 150 ppb; 300 ppb) for 9 h day^{-1}; 7 days wk^{-1} from the start of the growing period until crop harvest. Each treatment was represented in two OTCs. Drought stress was induced in half of the plants of each SO_2 treatment.

Photosynthetic gas exchange (A: Ci response)

Photosynthetic gas exchange was measured with an infrared gas analysis system (CIRAS-2, PP-Systems, Hertz. U.K.). CO_2 assimilation rate (A) vs. intercellular CO_2 concentration (Ci) response curves (A:Ci curves) were generated and analysed according to Farquhar and Sharkey (1982).

Chlorophyll a fluorescence induction

Chlorophyll a fluorescence induction transients were recorded weekly on fully dark adapted (1 hour) leaves using a fluorimeter (Handy-PEA, Hansatech Instruments Ltd., Kingslynn, U.K.). The recorded fluorescence OJIP transients were analysed with the JIP-test (Strasser *et al*., 2004)

The multi-parametric expression, the photosynthetic performance index ($PI_{ABS,total}$), introduced by Tsimilli-Michael and Strasser (2008), takes into account the four independent key steps controlling photosynthesis, namely, absorption (RC/ABS), quantum efficiency of trapping ($\varphi_{Po}/(1 - \varphi_{Po})$, efficiency of converting trapped excitation energy to electron transport ($\psi_0/(1 - \psi_0)$ and efficiency of reducing PSI end electron acceptors ($\delta_0/(1 - \delta_0)$ = RE/ABS:

$$PI_{ABS,total} = \frac{\gamma_{RC}}{1-\gamma_{RC}} \bullet \frac{\varphi_{Po}}{1-\varphi_{Po}} \bullet \frac{\psi_{Eo}}{1-\psi_{Eo}} \bullet \frac{\delta_{Ro}}{1-\delta_{Ro}}$$

where $\gamma_{RC}/(1 - \gamma_{RC})$ = (RC/ABS) is the fraction of reaction centre chlorophyll (Chl_{RC}) per total chlorophyll (Chl_{RC} + $_{Antenna}$), Extended analysis of the fluorescence transients were done by calculation of the difference in relative variable fluorescence to present the so called ΔV curves, namely (i) normalized between F_O and F_J ($V_{OJ} = (F - F_O)/(F_J - F_O)$: $\Delta V_{OJ} = V_{OJ\ treatment} - V_{OJ\ control}$), (ii) normalized between F_J and F_M ($V_{JM} = (F - F_J)/(F_M - F_J)$: $\Delta V_{JM} = V_{JMtreatment} - V_{JMcontrol}$), respectively (Strasser *et al.*, 2008).

In vitro Rubisco activity

In vitro Rubisco activity was determined 28 days after fumigation on whole trifoliate leaves using the method of Keys and Parry (1990).

Biomass, crop yield and nodule ureid content

Shoots and roots were separated and dried at 60 °C for the root-to-shoot ratio to be calculated. The pods harvested at maturity, were dried at 60 °C until constant mass. Number and dry weight of immature and mature pods per plant and number and dry weight of immature and mature seeds per pod were determined. Visual symptoms were recorded weekly. Nodule ureid content after 35 days was determined according to Young and Conway, 1942.

Results

Visible foliar injury attributable to SO_2 toxicity was observed in both well watered and drought stressed plants. Only after biochemical and physiological constraints were already present. The decrease in total biomass was primarily due to a significant reduction in the shoot biomass, resulting in a reduction in shoot-to-root biomass ratio. The overall yield (seed per plant) decreased significantly by 17%, 36% and 62% for well watered plant exposed to 50, 150 and 300 ppb SO_2, respectively and by as much as 73% for drought stressed plants fumigated with 300 ppb SO_2. Drought stress caused immature pod abscission.

$PI_{ABS,total}$ values after 14 and 28 days of fumigation (Figs. 1A and 1B, inserts) supported the gas exchange data (Fig. 4). $PI_{ABS,total}$ showed an initial stimulation (19%; $p < 0.05$) for well watered plants fumigated with 50 ppb SO_2. This did not occur in drought stressed plants. $PI_{ABS,total}$ decreased significantly by 44% and 62% at 150 and 300 ppb SO_2, respectively compared to the well watered control plants.

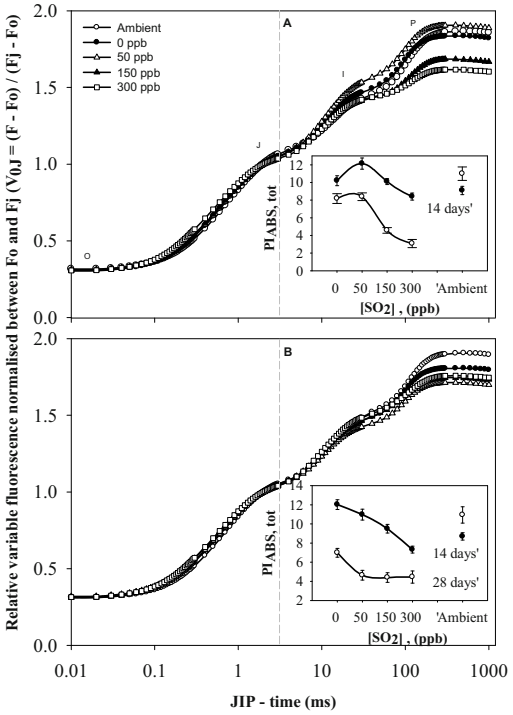

Fig. 1 *Chlorophyll a* fluorescence transients normalized between 0.05 and 2 ms for well watered (*A*) and drought stressed (*B*) *G. max* plants after 28 days' fumigation with SO_2. Insert A and B: $PI_{ABS,\ total}$ measured after 14 and 28 days.

Average OJIP fast chlorophyll fluorescence transients normalized on 50 µs (F_0) and 2 ms (F_J) indicate that concentration dependent SO_2 inhibition of photosynthesis mainly occurred in the multiple turnover events of PSII function, *i.e.* J to P (Figs. 1A and 1B), which are strongly determined by the dark reactions in the electron transport chain (Strasser *et al.*, 1999).

The ΔV plots revealed bands hidden in the J and I steps of the fluorescence kinetics which are much richer in information than the original O-J-I-P. In depth analysis of the kinetics of the relative variable fluorescence transients (Fig. 2) clearly showed an initial stimulation in the OEC (appearance of the –ΔK-band) of SO_2 exposed drought stressed plants. The +ΔK-bands that developed after 28 days of fumigation indicate that SO_2 caused uncoupling of the OEC from PSII.

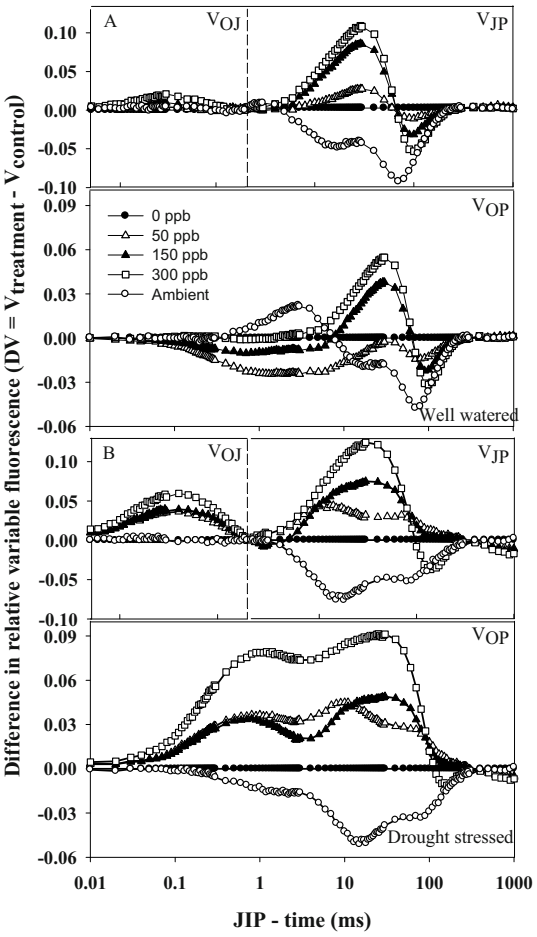

Fig. 2 Changes in difference in the relative variable *chlorophyll a* fluorescence transients recorded in well watered (*A*) and drought stressed (*B*) *G. max* plants after 28 days' fumigation with SO_2.

A SO_2 induced decrease in the probability for formation of reducing equivalents of electron transport, namely ATP and NADPH, are indicated by +ΔI-peaks occurring in the double normalized *chlorophyll a* fluorescence plots (Fig. 2). These peaks point at inhibition of electron flow further down from the reduced intersystem electron acceptors of the electron transport chain to the PSI end electron acceptors.

The A:Ci response curve were analyzed to characterize the physiological state of the photosynthetic apparatus. The demand function (initial slope) which is a measure of the apparent carboxylation efficiency (ACE) and a sensitive indicator of *in vivo* Rubisco activity decreased significantly for all treatments and were more severely affected in drought stressed plants. (Figs. 3 and 4). The *in vitro* Rubisco activity strongly corroborated this data (Fig. 3). Concomitant increases in the intercellular CO_2 concentration and in the compensation concentration (pointing at increasing mesophyll limitation), corroborated the concomitant decrease in ACE. Furthermore, the corresponding supply function (related to stomatal conductance) indicates that stomatal conductance was increasingly inhibited with increase in SO_2 concentration. Stomatal conductance in drought stressed plants decreased by up to 65% compared to the well watered control. Water use efficiency (WUE) was inhibited more in the drought stressed plants than in the well watered plants, despite the larger decrease in Gs. The calculated percentage stomatal limitation however did not increase notably, indicating that mesophyll limitations were the dominant cause of the reductions in the CO_2 assimilation rate. SO_2 fumigation in combination with drought stress aggravated the inhibition showing that drought-induced stomatal closure does not alleviate the mesophyll limitations.

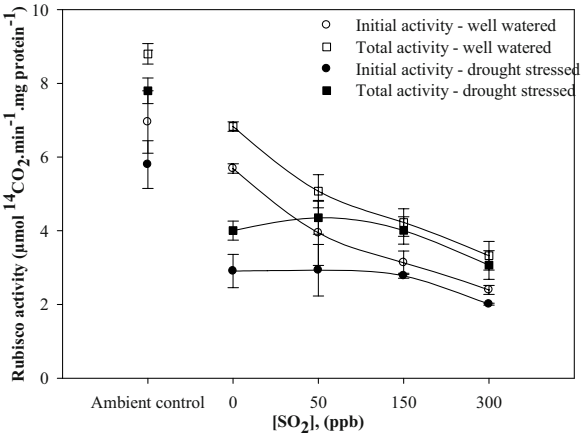

Fig. 3 Initial and total Rubisco activity measured in *G. max* after 28 days' exposure to different SO_2 concentrations.

The concentration dependent inhibition of PSII function and CO_2 assimilation was reflected in the nodule ureide content. In well-watered a reduction of up to 29% and in drought-stressed plants 66% occurred (data not shown).

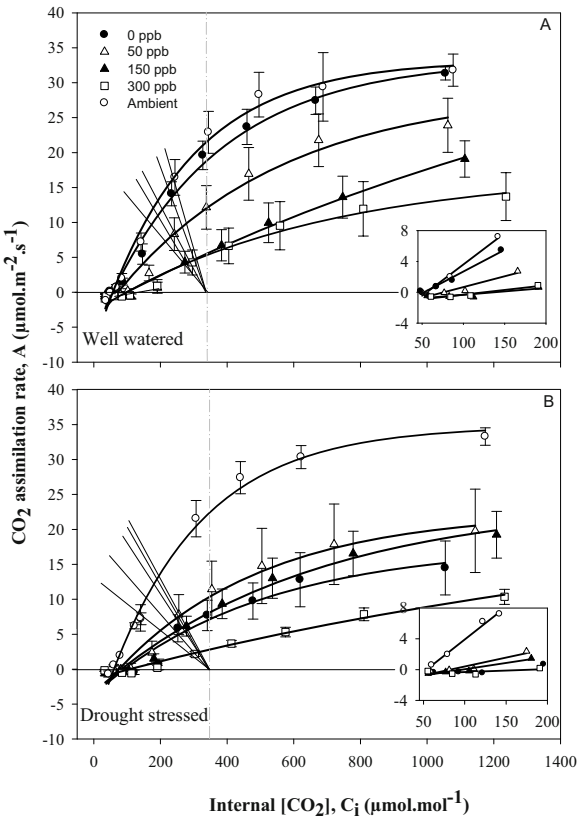

Fig. 4 Average CO_2 response curves (A:Ci) for well watered (A) and drought stressed (B) *G. max* plants after 28 days SO_2 exposure.

Conclusion

A reduction in CO_2 assimilation rate was observed at all SO_2 levels; with the reduction most severe at the highest treatment level, where a 57% reduction in yield was observed. Assimilation data showed that at the lowest treatment level permanent physiological damage occur in the absence of visible injury. Inhibition in photosynthetic rate was largely caused by mesophyll limitations. Reductions in stomatal conductance may only partially explain reductions in photosynthetic rate. Drought stressed plants showed a more severe decrease in WUE, even with decreased stomatal conductance. Decreased Rubisco activity strongly corresponds to the decrease in *vivo* Rubisco activity (CE) determined from the initial slope of the A:Ci response curve. Drought aggravated the response towards SO_2.

Although measured in the dark adapted state, the JIP test reflects the potential of the photosynthetic apparatus for energy supply, metabolism and eventually seed yield.

References

Farquhar GD, Sharkey TS (1982) Stomatal Conductance and Photosynthesis. Annual Review of Plant Physiology 33: 317-345

Josipovic M, Annegarn HJ, Kneen MA, Pienaar JJ, Piketh SJ (2010) Concentrations, Distributions and Critical Level Exceedence Assessment of SO_2, NO_2 and O_3 in South Africa. Environmental Monitoring and Assessment 171(1): 181-196

Keys AJ, Parry MAJ (1990) Ribulose Bisphosphate Carboxylase/Oxygenase and Carbonic Anhydrase. Methods in Plant Biochemistry 3: 1-15

Strasser RJ, Srivastava A, Tsimilli-Michael M (2004) Analysis of the Chlorophyll Fluorescence Transient. In: Papageorgiou G, Govindjee XUC (eds.), Chlorophyll Fluorescence a Signature of Photosynthesis. Kluwer Academic Publishers: The Netherlands. 19: 321-362

Strasser RJ, Tsimilli-MichaeI M, Dangre D, Rai M (2007) Biophysical Phenomics Functional Building Blocks of Plant System Biology: Case Study the Evaluation of Impact of Mycorrhizaton with Piriformospora Indica. In: Varma A, Oelmiiller (eds.), Advanced Techniques in Soil Microbiology. Soil Biology Springer: Germany, Chapter 21, pp. 319-341

Strasser RJ, Tsimilli-Michael M, Pêcheux M (1999) Perpetual Adaptation in a Perpetually Changing Environment As a Survival Strategy of Plants: a Case Study in Foraminifers Concerning Coral Reef Bleaching. Photosynthetica. 37(1): 71-85

Tsimilli-Michael M, Strasser RJ (2008) In Vivo Assessment of Stress Impact on Plants' Vitality: Applications in Detecting and Evaluating the Beneficial Role of Mycorrhization on Host Plants. In: Varma A (ed.), Mycorrhiza: State of the Art, Genetics and Molecular Biology, Eco-Function, Biotechnology, Eco-Physiology, Structure and Systematics, 3rd ed. Springer, pp. 679-703

Young EG, Conway CF (1942) On the Estimation of Aln by the Rimini-Shrever Reaction. Journal of Biological Chemistry 142: 839-853

UDP-Glucose Pyrophosphorylase Responsible for Sulfolipid Synthesis in a Green Alga *Chlamydomonas Reinhardtii*

Atsushi Sato, Koichi Sugimoto, Mikio Tsuzuki, Norihiro Sato*

School of Life Sciences, Tokyo University of Pharmacy and Life Sciences, Horinouchi 1432-1, Hachioji, Tokyo 192-0392, Japan.
*Corresponding author. Tel. No. +81 42 676 6716; Fax No. +81 42 676 6721; E-mail: nsato@ls.toyaku.ac.jp.

Abstract: Sulfoquinovosyl diacylglycerol (SQDG) is ubiquitous in thylakoid membranes of oxygenic photosynthetic organisms. Recently, a gene for UDP-glucose pyrophosphorylase (*UGP3*) was identified as participating specifically in SQDG synthesis in *Arabidopsis thaliana*. We here found that a mutant of *Chlamydomonas reinhardtii* disrupted in the *LPB1* gene, a homologue of *UGP3*, lacked SQDG. It was concluded that *LPB1* is the gene for UDP-glucose pyrophosphorylase involved in SQDG synthesis, based upon its responsibility for SQDG synthesis together with its similarity to the UGP3 protein in the amino acid sequence. We then examined how *LPB1* expression is regulated at the transcript level in *C. reinhardtii* under S-starved conditions where SQDG synthesis capacity is known to increase, for protection of the PSI complex, with elevation in the mRNA level of the *SQD1* gene for SQDG synthesis. Semi-quantitative analysis of transcripts by RT-PCR showed that the level of *LPB1* mRNA was remarkably increased 4 h after onset of S-starvation, thereafter the enhanced level kept for the next 20 h. The results indicated cooperative up-regulation of the transcript level of *LPB1* with that of *SQD1*, coinciding with the increase in the SQDG synthesis capacity.

Keywords: Anionic lipids; *Chlamydomonas reinhardtii*; Phosphatidylglycerol; Sulfoquinovosyl diacylglycerol; Sulfur starvation

Introduction

SQDG, an anionic lipid containing a sulfur atom, is one of lipids that construct membranes of plant plastids and their postulated ancestor, cyanobacteria. In green plants (Shimojima *et al*., 2009) and cyanobacteria (Sato and Wada, 2009), homologous genes have been identified for each of two consecutive reactions on the pathway of SQDG synthesis: *SQD1* and *sqdB* genes in plants and cyanobacteria, respectively, encode UDP-sulfoquinovose (SQ) synthase that unites UDP-glucose and sulfite whereas *SQD2* and *sqdX* genes in plants and cyanobacteria, respectively, encode SQDG synthase that transfers SQ moiety of UDP-SQ to diacylglycerol. Moreover, recent establishment of databases of genomic sequences allow us to find their homologues in red algae and the secondary symbionts. In a seed plant, *Arabidopsis thaliana*, besides genes of the above two enzymes, the *UGP3* gene was recently shown to encode UDP-glucose pyrophosphorylase that, exclusively for SQDG synthesis, forms UDP-glucose from glucose 1-phosphate and UTP (Okazaki *et al*., 2009). Despite utilization of UDP-glucose as a common substrate for SQDG synthesis for photosynthetic organisms, homologues of *UGP3* were reported to exist in green algae and seed plants, but not in cyanobacteria or red lineages, suggesting that UDP-glucose pyrophosphorylase gene for SQDG synthesis has evolved in quite a distinct manner from those of UDP-SQ and SQDG synthases.

It is known that SQDG metabolism and/or expression of genes for SQDG synthesis are regulated in cyanobacteria and green plants under some stress conditions (Sato, 2004). *A. thaliana* increases the SQDG content under phosphorus-limiting conditions concomitantly with a quantitative decrease in phosphatidylglycerol (PG), the other anionic lipid of plastid and cyanobacterial membranes. It is likely that metabolic flux of phosphorus is diverted from PG synthesis to those of some other P-compounds essential for acclimation to P-limiting conditions. The increase in SQDG would compensate for the decrease in PG, thereby keeping the negative charge of the membranes at a certain level. Similar changes as to

these two anionic lipids have been observed with cyanobacterium, *Synechocystis* sp. PCC 6803, a green alga, *C. reinhardtii*, and an anoxygenic photosynthetic bacterium, *Rhodobacter sphaeroides*. The compensation mechanism thus seems critical for photosynthetic organisms under P-limiting conditions.

Meanwhile, *Chlamydomonas reinhardtii* induces a drastic degradation of SQDG under S-starved conditions to ensure a predominant intracellular S-source for protein synthesis (Sugimoto *et al*., 2007). Simultaneously, *C. reinhardtii* up-regulates SQDG synthesis capacity by enhancing the level of *SQD1* mRNA, which allows SQDG to remain at 5% of its initial level even after S-starvation of 24 h and thereby structurally stabilizes the photosystem I complex (Sugimoto *et al*., 2010). In contrast, the PG content is up-regulated in S-starved cells of *C. reinhardtii*, which also seems to be explained by prerequisite of photosynthetic organisms for the quantitative balance of negatively charged lipids (Sugimoto *et al*., 2008).

We here examined whether or not the *LPB1* gene, a *UGP3* homolog of a green alga, *C. reinhardtii*, is involved in the synthesis of SQDG, and how *LPB1* expression is regulated at the transcript level during S-starvation.

Materials and Methods

Strains and culture conditions

C. reinhardtii CC125 or its mutant disrupted in the *LPB1* gene obtained from *Chlamydomonas* genetic center at Duke university was mixotrophically grown in a flask containing the Tris/Acetate/Phosphate (TAP) medium on a rotary shaker (120 rpm) with continuous illumination (60 μmol photons m^{-2} s^{-1}) at 30 °C. For transfer to S-starved conditions, cells grown to the midlogarithmic phase (1-5×10^6 cells mL^{-1}) were harvested by centrifugation, washed twice and then resuspended in the S-free TAP medium (TAP-S) that was prepared by replacing sulfate with chloride (Sugimoto *et al*., 2007).

Semi-quantitative analysis of transcript levels by reverse transcriptase (RT)-PCR

Total RNA was extracted and purified by phenol–chloroform extraction, as Los *et al*. described (1997), then used for cDNA synthesis by reverse-transcription with random primers, as reported by Tabei *et al*. (2007), for semi-quantitative RT-PCR. The forward (F) and reverse (R) primers used were as follows: F-ACACCGAGTTTGAGAAGCTG and R-GTCAGGTAGTCGGCCATGTT for *LPB1*, F-AGATCCACGACTCCACCAAC and R-TGCTCCGTGAACTGGTTGTA for *SQD1*, F-TGTGGACTACTCCGTCAGCA and R-GAAATCTGGGTGGAGGTGTG for *ARS1*, and F-GAGTCCAACTACGGCTACGC and R-ATGCTCTTGCTCTCCAGGTC for *CBLP*. *ARS1* encodes S-starvation-inducible arylsulfatase, whereas *CBLP* encodes the G-protein b-subunit and was used as an internal control.

Lipid analysis

Total lipids were extracted from cells, and then separated into individual lipid classes for compositional analysis of the lipids and their constituent fatty acids, as described by Sugimoto *et al*. (2008).

Results and Discussion

Identification of LPB1 as a gene encoding UDP-glucose pyrophosphorylase for SQDG synthesis

C. reinhardtii possesses the *LPB1* gene as a homologue of *UGP3* with 38% identity in the amino acid sequence. In order to examine whether or not *LPB1*, similar to *UGP3*, is involved in SQDG synthesis, we characterized the lipid composition of a disruptant of *C. reinhardtii* as to the *LPB1* gene, which had been isolated by Chang *et al*. (2005). The results showed the mutational effects only on the contents of SQDG and PG, but not on those of the other lipid classes: SQDG and PG in the wild type amounted to 6.6% and 5.7%, respectively, relative to total lipids, while the *lpb1* mutant showed a complete lack of SQDG with a content of PG increased to 13% (Table 2). This elevation in PG quantitatively compensated for the loss of SQDG, and would thus contribute to maintenance of negative charge of the membranes at an appropriate level. The lipid phenotype as to SQDG and PG is common to all mutants deficient in SQDG synthesis so far reported in some species (see Table 1 for *Chlamydomonas* mutants), definitely demonstrating that *LPB1* is responsible for SQDG synthesis. Together with its high sequence identity to that of UGP3, we concluded that the LPB1 protein functions as UDP-glucose pyrophosphorylase for SQDG synthesis.

Homologues of UGP3/LPB1 are found in genomic DNA and EST databases of green plants including seed plants and green algae, but not in those of the red lineage or cyanobacteria. Whereas the UGP3 protein is localized at stroma of chloroplasts wherein its product, UGP-glucose, can directly be utilized by SQD1 (Okazaki *et al*., 2009), other isozymes of UDP-glucose pyrophosphorylases in cytoplasm should function for sucrose and/or cellulose syntheses. Green plants thus seem to utilize the isozymes of distinct intracellular localization for separation in

space of SQDG synthesis and the other biochemical processes. Moreover, the activity of UGP3/LPB1 should be regulated to balance with that of ADP-glucose pyrophosphorylase in chloroplasts for starch synthesis in view of competition for the same substrate, glucose 1-phosphate (Deschamps *et al*., 2008). Meanwhile, red algae must supply UDP-glucose with SQD1 protein in rhodoplasts as in chloroplasts, but also with the synthetic system of starch in cytoplasm (Deschamps *et al*., 2008). As such, there are differences in metabolic flow around UDP-glucose between green and red lineages. Compared with these eukaryotic photosynthetic organisms, cyanobacteria are unique to utilize UDP-glucose for SQDG and sucrose syntheses in the same intracellular compartment, cytoplasm (Salerno and Curatti, 2003). Thus, it is undoubtful that specific systems that regulate the functioning of UDP-glucose pyrophosphorylase for SQDG synthesis exist in cyanobacteria, red algae, and green plants, respectively, and that UDP-glucose pyrophosphorylase structurally unrelated to UGP3/LPB1 proteins functions for SQDG synthesis in cyanobacteria and red algae.

Table 1 Lipid compositions of SQDG-deficient mutants isolated from *C. reimhardtii*.

Lipids	CC125	*lpb1*	*hf-2*[a]	*sqd1*[b]
MGDG	37.8	36.5	32.9	34.5
DGDG	21.2	20.0	22.0	16.3
SQDG	6.6	-	-	-
PG	5.7	13.0	11.3	12.0
DGTS	22.3	22.5	23.7	27.2
PE	5.2	6.5	7.4	7.0
PI	1.2	2.0	2.1	2.7
SQDG+PG	12.7	12.9	11.3	12.0

[a]A mutant obtained in our laboratory (Sato *et al*., 2003).
[b]A mutant obtained by Riekhof *et al*. (2003).

Expression patterns of LPB1 in response to S-starved conditions

We then examined how *LPB1* expression is regulated at the transcript level in the wild type cells of *C. reinhardtii* under S-starved conditions where SQDG synthesis capacity increases. We performed semi-quantitative analysis of the mRNA level of *LPB1* by RT-PCR (Fig. 1), owing to the level too low to be detected by Northern analysis. The results showed that the mRNA level of *LPB1*, similar to those of S-starvation inducible genes, *SQD1* and *ARS1* (arylsulfatase 1 gene), was remarkably elevated 4 h after onset of S-starvation, thereafter the elevated level kept for the next 20 h. The results indicated cooperative up-regulation of transcript levels of *LPB1* and *SQD1* genes, coinciding with the enhancement of SQDG synthesis capacity in *C. reinhardtii* under S-starved conditions.

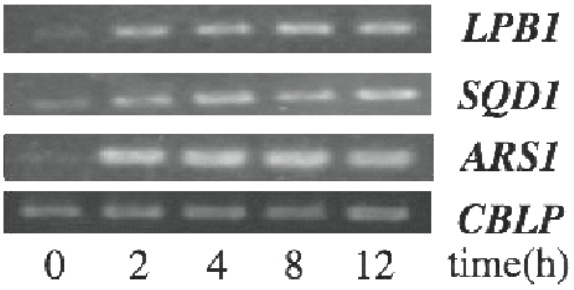

Fig. 1 Semi-quantitative analysis of *LPB1* mRNA after shift to S-starved conditions.

A. thaliana, distinct from *C. reinhardtii*, was reported to slightly decrease the transcript level of *UGP3* under S-starved conditions, compatible with only a little reduction in the SQDG content (Okazaki *et al*., 2009). The different regulation of the genes for SQDG synthesis between the two species would be explained by the role of SQDG as an internal S-source in *C. reinhardtii*, but not in *A. thaliana*, as evidenced by no remarkable induction of degradation of SQDG in *A. thaliana*. During S-starvation that induces a drastic degradation of SQDG, *C. reinhardtii* must upregulate the expression of the genes for SQDG synthesis to keep the SQDG content at a minor, but a necessary level for structural protection of the PSI complex (Sugimoto *et al*., 2010). However, the level of SQDG maintained in S-starved *Arabidopsis* plants was almost indistinguishable from that of untreated plants (Okazaki *et al*., 2009), and may thus be sufficient for the protection of the PSI complex. Vacuoles have become large enough to store a variety of compounds including sulfate in seed plants through evolution, but not yet in green algae. Seed plants cope with S-starvation stress through mobilizing sulfate in vacuoles to the synthesis of S-compounds such as proteins essential for acclimation (Blake-Kalff, 1998), and thus seemingly do not need to obtain sulfur from SQDG. Development of intracellular ultrastructure through evolution may therefore be related with the different regulatory mechanisms as to the gene expression for SQDG synthesis.

Acknowledgements

This work was supported in part by Grants-in-Aid from the Ministry of Education, Culture, Sports, Science, and Technology of Japan (MEXT), the Promotion and Mutual Aid Corporation for Private Schools of Japan, Scientific Research for Plant Graduate Students from the

Nara Institute of Science and Technology supported by MEXT, and a Sasakawa Scientific Research Grant from the Japan Science Society.

References

Blake-Kalff MMA, Harrison KR, Hawkesfold MJ, Zhao FJ, McGrath SP (1998) Distribution of Sulfur within Oilseed Rape Leaves in Response to Sulfur Deficiency during Vegetative Growth. Plant Physiol. 118: 1337-1344

Chang CW, Moseley JL, Wykoff D, Grossman AR (2005) The LPB1 Gene Is Important for Acclimation of Chlamydomonas Reinhardtii to Phosphorus and Sulfur Deprivation. Plant Physiol. 138: 319-329

Deschamps P, Colleoni C, Nakamura Y, Suzuki E, Putaux JL, Bule A, Haebel S, Ritte G, Steup M, Falco LI, Moreira D, Löffelhardt W, Raj JN, Plancke C, d'Hulst C, Dauvillee D, Ball S (2008) Metabolic Symbiosis and the Birth of the Plant Kingdom. Mol. Biol. Evol. 25: 536-548

Los DA, Ray MK, Murata N (1997) Differences in the Control of the Temperature-Dependent Expression of Four Genes for Desaturases in Synechocystis sp. PCC 6803. Mol Microbiol 25: 1167-1175

Okazaki Y, Shimojima M, Sawada, Toyooka K, Narisawa T, Mochida K, Tanaka H, Matsuda F, Hirai A, Yokota Hirai M, Ohta H, Saito K (2009) A Chloroplastic UDP-Glucose Pyrophosphorylase from Arabidopsis Is the Committed Enzyme for the First Step of Sulfolipid Biosynthesis. Plant Cell 21: 892-909

Riekhof WR, Ruckle ME, Lydic TA, Sears BB, Benning C (2003) The Sulfolipids 2'-O-Acyl-Sulfoquinovosyl Diacylglycerol and Sulfoquinovosyl Diacylglycerol Are Absent from a Chlamydomonas reinhardtii Mutant Deleted in SQD1. Plant Physiol. 133: 864-874

Sato N (2004) Roles of the Acidic Lipids Sulfoquinovosyl Diacylglycerol and Phosphati Dylglycerol in Photosynthesis: Their Specificity and Evolution. J. Plant Res. 117: 495-505

Sato N, Aoki M, Maru Y, Sonoike K, Minoda A, Tsuzuki M. (2003) Involvement of Sulfoquinovosyl Diacylglycerol in the Structural Integrity and Heat-Tolerance of Photosystem II. Planta 217: 245-251

Sato N, Wada H (2009) Lipid Biosynthesis and Its Regulation in Cyanobacteria. In: Wada H, Murata N (eds.), Lipids in Photosynthesis: Essential and Regulatory Functions. Springer, pp. 157-177

Salerno GL, Curatti L (2003) Origin of Sucrose Metabolism in Higher Plants: When, How and Why? Trends in Plant Sci. 8: 63-69

Shimojima M, Ohta H, Nakamura Y (2009) Biosynthesis and Function of Chloroplast Lipids. In: Wada H, Murata N (eds.), Lipids in Photosynthesis: Essential and Regulatory Functions.Springer, pp. 35-55

Sugimoto K, Midorikawa T, Tsuzuki M, Sato N (2008) Upregulation of PG Synthesis on Sulfur-Starvation for PS I in Chlamydomonas. Biochem. Biophys. Res. Commun. 369: 660-665

Sugimoto K, Tsuzuki M, Sato N (2009) Utilization of a Chloroplast Membrane Sulfolipid As a Major Internal Sulfur Source for Protein Synthesis in the Early Phase of Sulfur Starvation in Chlamydomonas Reinhardtii. FEBS Lett. 581: 4519-4522

Sugimoto K, Tsuzuki M, Sato N (2010) Regulation of Synthesis and Degradation of a Sulfolipid under Sulfur-Starved Conditions and Its Physiological Significance in Chlamydomonas Reinhardtii. New Phytol. 185: 676-686

Tabei Y, Okada K, Tsuzuki M (2007) Sll1330 Controls the Expression of Glycolytic Genes in Synechocystis sp. PCC 6803. Biochem. Biophys. Res. Commun. 355: 1045-1050

Essential Role of Digalactosyldiacylglycerol for Photosynthetic Growth in *Synechocystis* sp. PCC 6803 under High-Temperature Stress

Naoki Mizusawa, Shinya Sakata, Isamu Sakurai, Hisako Kubota, Naoki Sato, Hajime Wada*

Department of Life Sciences, Graduate School of Arts and Sciences, University of Tokyo, Komaba 3-8-1, Meguro-ku, Tokyo 153-8902, Japan.
*Corresponding author. Tel./Fax No. +81 3 5454 6656; E-mail: hwada@bio.c.u-tokyo.ac.jp.

Abstract: The galactolipid digalactosyldiacylglycerol (DGDG) is present in the thylakoid membranes of oxygenic photosynthetic organisms such as higher plants and cyanobacteria. Recent X-ray crystallographic analysis of protein-cofactor supercomplexes in thylakoid membranes revealed that DGDG molecules are specifically present in the photosystem II (PSII) complex (seven molecules per monomer), suggesting that DGDG molecules play important roles in folding and assembly of subunits in the PSII complex. However, the specific role of DGDG in photosynthesis has not been fully clarified. Recently, we identified the *dgdA* gene (*slr1508*) of *Synechocystis* sp. PCC 6803 that presumably encodes a DGDG synthase involved in the biosynthesis of DGDG. Disruption of the *dgdA* gene resulted in a mutant defective in DGDG synthesis. In this study, to clarify the physiological roles of DGDG in photosynthesis, we examined the effects of depletion of DGDG on growth and photosynthetic properties under high-temperature stress using the disruption mutant of *dgdA* gene.

Keywords: Digalactosyldiacylglycerol; High-temperature stress; Oxygen-evolving complex; Photosystem II; *Synechocystis* sp. PCC 6803

Introduction

In oxygenic photosynthetic organisms, thylakoid membranes are composed of uncharged lipids, monogalactosyldiacylglycerol (MGDG) and digalactosyldiacylglycerol (DGDG), as well as anionic lipids, sulfoquinovosyldiacylglycerol (SQDG) and phosphatidylglycerol (PG). DGDG is one of the major glycolipids and makes up 15%–30% of the total lipids in thylakoid membranes. Recent X-ray crystallographic analyses of photosystem (PS) II (Guskov *et al*., 2009) and PSI (Jordan *et al.*, 2001) complexes from *Thermosynechococcus elongatus*, and cytochrome b_6f from *Mastigocladus laminosus* (Kurisu *et al*., 2003) and *Chlamydomonas reinhardtii* (Stroebel *et al*., 2003) identified seven DGDG molecules per PSII monomer (Guskov *et al*., 2009); however, DGDG was not detected in PSI or cytochrome b_6f. Therefore, it is thought that DGDG is a unique component of PSII that is probably involved in the construction and stabilization of the PSII complex. However, the specific photosynthetic function of DGDG is not yet fully understood. Recently, our group (Sakurai *et al*., 2007) and Awai *et al*. (2007) identified a *dgdA* gene presumably encoding a DGDG synthase of *Synechocystis* sp. PCC 6803; this information was used to create *dgdA* disruption mutants. Because *dgdA* mutant contains no detectable amount of DGDG (Awai *et al.*, 2007; Sakurai *et al.*, 2007), it is a powerful tool to elucidate the role of DGDG in photosynthesis. Our previous studies using this mutant demonstrated that DGDG is not essential for photosynthesis in *Synechocystis* but plays an important role in the structure and function on the donor side of PSII, through the binding of extrinsic proteins required for stabilization of the oxygen-evolving complex (Sakurai *et al.*, 2007).

In this study, to understand the physiological role of DGDG in photosynthesis, we examined the effects of high-temperature stress on the growth and photosynthetic activity of *dgdA* mutant.

Materials and Methods

Organisms and growth conditions

A disruption mutant of *dgdA* gene (*slr1508*) previously generated from *Synechocystis* sp. PCC 6803 (Sakurai *et al*., 2007) is here referred to as *dgdA* mutant. Wild-type and *dgdA*-mutant cells were grown photoautotrophically at 30 °C or 38 °C in liquid BG-11 medium under continuous fluorescent white light at an intensity of 10 or 200 μmol photons m^{-2} s^{-1}. The growth of cells was monitored by assessing the optical density at 730 nm (OD_{730}).

Analysis of photosynthetic activity

Photosynthetic oxygen-evolving activity of intact cells was measured using a Clark-type oxygen electrode. Chlorophyll (Chl) concentrations were determined using the method described by Arnon *et al*. (1974). To assay the susceptibility of *dgdA* mutant cells to high-intensity light, wild-type and mutant cells that had been suspended in BG-11 medium at 10 μg Chl/ml were illuminated at 30 °C or 38 °C with white light at 2,500 μmol photons m^{-2} s^{-1} in the presence or absence of 0.1 mg/ml lincomycin.

Analysis of assembly states of PSII

To analyze the assembly states of PSII, PSII complexes isolated from the wild-type and mutant cells were analyzed by Blue native (BN)-PAGE (Kubota *et al*., 2010).

Results and Discussion

We first examined the effects of moderately high temperature (38 °C) on the photoautotrophic growth of wild-type and *dgdA* mutant cells under low light (LL; 10 μmol photons m^{-2} s^{-1}) and high light (HL; 200 μmol photons m^{-2} s^{-1}). The growth properties at 30 °C were also checked as control experiments. Wild-type cells grew normally under all conditions. At 30 °C, mutant cells grew as well as wild-type cells under LL and HL conditions. However, at 38 °C, mutant cells showed the slightly slower growth than wild-type did under LL conditions and the growth retardation in the mutant was enhanced under HL conditions. When cells were cultured in the presence to wild-type cells, even under HL conditions at 38 °C, indicating that DGDG is important for cell survival at 38 °C, especially under HL conditions.

To clarify whether growth retardation in the *dgdA* mutant at 38 °C is caused by the photoinhibition of photosynthesis, the effects of HL illumination at 30 °C or 38 °C on photosynthetic activity were compared between wild-type and *dgdA* mutant cells. Photoinhibition occurs when the rate of photodamage to the photosynthetic machinery exceeds that of repair processes (Aro *et al*., 1993; Nishiyama *et al*., 2006). It is possible to measure the rates of photodamage and repair processes separately by monitoring the time course of oxygen-evolving activity when cells are exposed to HL in the presence or absence of lincomycin, which inhibits the protein synthesis required for repair processes. At 30 °C, the wild-type cells showed a HL-induced decline in oxygen-evolving activity in the presence of lincomycin (Fig. 1A). However, this decrease was minimal in the absence of lincomycin (Fig. 1B), suggesting that the processes required to repair damaged photosynthetic machinery occurred efficiently, and thus prevented the accumulation of damage. In contrast, in mutant cells, photoinactivation occurred in both the presence and absence of lincomycin, suggesting that repair processes were inhibited in mutant cells . At 38 °C, wild-type cells showed no enhancement of photoinactivation in the absence of lincomycin compared to the degree of inactivation at 30 °C, although photoinactivation was slightly enhanced in the presence of lincomycin. In contrast, in mutant cells, photoinactivation was greatly enhanced in the presence of lincomycin and also enhanced at 38 °C in the absence of lincomycin compared to those at 30 °C (Figs. 1A and 1B). These results suggest that the enhanced photodamage to the photosynthetic machinery as well as the inhibition of repair process simultaneously occurs in mutant cells at 38 °C. Thus, the acceleration of photodamage under conditions inhibiting repair processes led to heat-induced growth retardation in *dgdA* mutant cells. Oxygen evolution was also inhibited after incubating mutant cells in the dark at 38 °C; however, wild-type cells were unaffected (Fig. 2C).

The sensitivity of the photosynthetic machinery to high temperatures in *dgdA* mutant cells was examined in more detail. Incubation in the dark for 20 min did not affect photosynthetic electron transport activity from H_2O to CO_2 (net activity) in wild-type cells, nor did it affect PSII activity, up to a temperature of 44 °C. However, in *dgdA* mutant cells, both activities began decreasing at 38 °C, as reported previously (Sakurai *et al*., 2007). The temperature-dependent inactivation

curves fit well between the net and PSII activities for any type of cell (data not shown), suggesting that PSII is the primary target site affected by incubation at high temperatures.

Our previous study demonstrated that PSII complexes isolated from *dgdA* mutant cells showed lower oxygen-evolving activity, and lacked the extrinsic proteins of PSII (PsbO, PsbU, and PsbV) required for stabilization of the manganese cluster (Sakurai *et al.*, 2007). If the extrinsic proteins of PSII stabilizing the structure of the manganese cluster are dissociated, the manganese cluster becomes more unstable upon heat treatment (Nishiyama *et al*., 1999; Kimura *et al*., 2002) or treatment with NH_2OH (Ghanotakis *et al*., 1984; Roose *et al*., 2007), and the manganese ions are easily released from the manganese cluster, leading to the inactivation of oxygen evolution. We hypothesized that the enhanced heat-induced inactivation of oxygen evolution in *dgdA* mutant *in vivo* was caused by the dissociation of extrinsic proteins from PSII. To examine this possibility, we compared the sensitivity of the manganese cluster to NH_2OH treatment in wild-type and *dgdA* mutant cells (data not shown). Upon incubation of cells with NH_2OH, the inactivation of oxygen evolution in *dgdA* mutant cells occurred at a much higher rate than in wild-type, indicating that the water-oxidation complex in *dgdA* mutant cells is more easily accessed and damaged by NH_2OH in mutant cells. Thus, it is highly likely that, in *dgdA* mutant, the extrinsic proteins are dissociated *in vivo*; as a result, the water-oxidation complex becomes highly sensitive to NH_2OH treatment.

As shown Fig. 1, in *dgdA* mutant, the repair processes of photosynthetic machinery were affected at both 30 °C and 38 °C. Among photosynthetic complexes, PSII is known to need to repair at high rates under illumination (Aro *et al*., 1993). PSII complexes are considered to exit as a dimeric form when they are active in oxygen evolution. Repair processes of damaged PSII proceed through complicated many steps including monomerization of PSII dimer, partial disassembly of the complex including detachment of CP43 and extrinsic proteins from the reaction center, degradation of D1, insertion of newly synthesized D1 to the complex, reassociation of CP43 and extrinsic proteins, assembly of the Mn cluster and dimerization of PSII. Our previous study showed that the monomer form of PSII, which has been isolated by ultracentrifugation of the crude PSII fraction on glycerol-density gradient, increases in *dgdA* mutant compared to that in wild type (Sakurai *et al*., 2007). Interestingly, in the monomer fraction, Psb27 and Psb28 proteins, which are considered to be involved in the assembly of PSII, were contained, suggesting the assembly intermediates of PSII are accumulated in *dgdA* mutant. Although there was a possibility that this monomer fraction contained additional complexes at other assembly states of PSII with similar molecular masses to the monomer, it was difficult to further separate each assembly complex by the ultracentrifugation on glycerol-density gradient. In this study, the assembly complexes of PSII in wild-type and *dgdA* mutant cells were again investigated by BN-PAGE whose method could detect CP43-retained monomer and CP43-less monomer separately (Fig. 2). In wild-type PSII, most of PSII complexes were detected as the dimer while the monomer and CP43-less monomer were little detected (Fig. 2A). In contrast, in *dgdA* mutant PSII, the monomer and CP43-less monomer significantly increased with a concomitant decrease of dimer (Fig. 2B). Since the repair processes were inhibited in *dgdA* mutant (Fig. 1A), it is highly likely that the accumulated PSII monomer and CP43-less PSII monomer are PSII assembly intermediates. Probably, such intermediates would accumulate due to the retardation of the forward assembly steps.

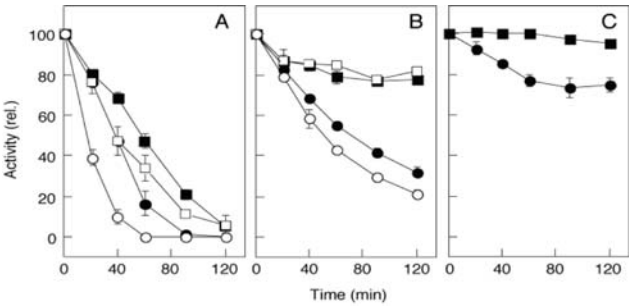

Fig. 1 Effects of high-temperature treatment under HL conditions (A and B) or darkness (C) on photosynthetic oxygen evolution in wild-type and *dgdA* mutant cells. Wild-type (squares) and *dgdA* mutant cells (circles) that cultured under illumination conditions of 40 μmol photons m^{-2} s^{-1} at 30 °C were suspended in BG-11 medium at a concentration of 10 μg Chl/ml and incubated under intense light (2,500 μmol photons m^{-2} s^{-1}) in the presence (A) or absence (B) of lincomycin at 30 °C (closed symbols) or 38 °C (open symbols). In (C), heat treatment was done under darkness at 38 °C. Error bars represent the standard deviations (SD) based on the mean values of three independent cultures.

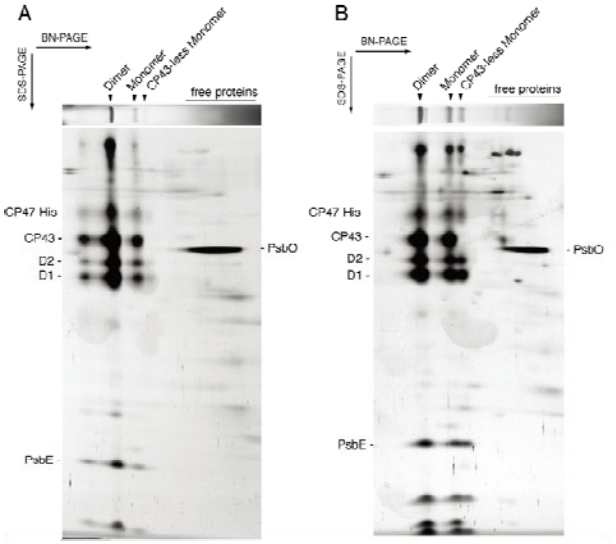

Fig. 2 Comparison of assembly states of PSII complexes isolated from wild-type (A) and *dgdA* mutant (B) cells. PSII complexes were purified by Ni-column chromatography from *Synechocystis* wild-type or mutant cells in which His-tag was attached to the C-terminus of CP47 protein. Assembly states were analyzed by 1D BN-PAGE of the purified PSII complexes. Then, protein composition of each complex was analyzed by 2D SDS-PAGE.

Recent X-ray crystallographic structure of the dimeric form of PSII from *T. elongatus* has identified seven DGDG molecules per PSII monomer (Guskov *et al*., 2009). Notably, the polar head groups of all DGDG molecules face the luminal side of PSII. Four of the DGDG molecules are located between the D1 and CP43 subunits, one molecule is located close to the D1 and PsbI subunits, another molecule is located between the D2 subunit and the α subunit of cytochrome b_{559}, and the final molecule is located between the D2 and CP43 subunits. However, no direct interaction between these DGDG molecules and the extrinsic proteins or the manganese cluster is apparent in the crystal structure (Guskov *et al*., 2009). BN-PAGE analysis showed a significant accumulation of a putative assembly intermediate of PSII, CP43-less monomer in the mutant, suggesting that the association of CP43 with the complex is interrupted by the lack of DGDG. Therefore, it is presumed that the four molecules of DGDG between D1 and CP43 identified in the crystal structure play an important role in insertion of CP43 into CP43-less PSII monomer during the repair processes. Lipid analysis of PSII from the *dgdA* mutant cells suggested that DGDG in PSII was replaced with MGDG (Sakurai *et al*., 2007). It is likely that the absence of one galactose moiety from each DGDG molecule affects interactions among the PSII proteins identified above and causes a conformational change on the luminal side of PSII that leads to the dissociation of the extrinsic proteins.

Acknowledgement

This work was supported by Grants-in-Aid for Scientific Research (no. 20608002 to N.M.) from the Ministry of Education, Culture, Sports, Science, and Technology of Japan.

References

Arnon DI, McSwain BD, Tsujimoto HY, Wada K (1974) Photochemical Activity and Components of Membrane Preparations from Blue-Green Algae. I. Coexistence of Two Photosystems in Relation to Chlorophyll a and Removal of Phycocyanin. Biochim Biophys Acta 357: 231-245

Aro EM, Virgin I, Andersson B (1993) Photoinhibition of Photosystem II. Inactivation, Protein Damage and Turnover. Biochim Biophys Acta 1143: 113-134

Awai K, Watanabe H, Benning C, Nishida I (2007) Digalactosyldiacylglycerol Is Required for Better Photosynthetic Growth of Synechocystis sp. PCC6803 under Phosphate Limitation. Plant Cell Physiol 48: 1517-1523

Ghanotakis DF, Topper JN, Yocum CF (1984) Structural Organization of the Oxidizing Side of Photosystem II. Exogenous Reductants Reduce and Destroy the Mn-Complex in Photosystem II Membranes Depleted of the 17 and 23 kDa Polypeptides. Biochim Biophys Acta 767: 524-531

Guskov A, Kern J, Gabdulkhakov A, Broser M, Zouni A, Saenger W (2009) Cyanobacterial Photosystem II at 2.9-Å Resolution and the Role of Quinones, Lipids, Channels and Chloride. Nat Struct Mol Biol 16: 334-342

Jordan P, Fromme P, Witt HT, Klukas O, Saenger W, Krauß N (2001) Three Dimensional Structure of Cyanobacterial Photosystem I at 2.5Å. Nature 411: 909-917

Kubota H, Sakurai I, Katayama K, Mizusawa N, Ohashi S, Kobayashi M, Zhang P, Aro EM, Wada

H (2010) Purification and Characterization of Photosystem I Complex from Synechocystis sp. PCC 6803 by Expressing Histidine-Tagged Subunits. Biochim Biophys Acta 1797: 98-105

Kimura A, Eaton-Rye JJ, Morita EH, Nishiyama Y, Hayashi H (2002) Protection of the Oxygen-Evolving Machinery by the Extrinsic Proteins of Photosystem II Is Essential for Development of Cellular Thermotolerance in Synechocystis sp. PCC 6803. Plant Cell Physiol 43: 932-938

Kurisu G, Zhang H, Smith JL, Cramer WA (2003) Structure of the Cytochrome b_6f Complex of Oxygenic Photosynthesis: Tuning the Cavity. Science 302: 1009-1014

Nishiyama Y, Allakhverdiev SI, Murata N (2006) A New Paradigm for the Action of Reactive Oxygen Species in the Photoinhibition of Photosystem II. Biochim Biophys Acta 1757: 742-749

Nishiyama Y, Los DA, Murata N (1999) PsbU, a Protein Associated with Photosystem II, Is Required for the Acquisition of Cellular Thermotolerance in Synechococcus Species PCC 7002. Plant Physiol 120: 301-308

Roose JL, Kashino Y, Pakrasi HB (2007) The PsbQ Protein Defines Cyanobacterial Photosystem II Complexes with Highest Activity and Stability. Proc Natl Acad Sci USA 104: 2548-2553

Sakurai I, Mizusawa N, Wada H, Sato N (2007) Digalactosyldiacylglycerol Is Required for Stabilization of the Oxygen-Evolving Complex in Photosystem II. Plant Physiol 145: 1361-1370

Stroebel D, Choquest Y, Popot JL, Picot D (2003) An Atypical Haem in the Cytochrome b_6f Complex. Nature 426: 413-418

De Novo Biosynthesis of Fatty Acids is Important for Maintenance of Photochemical Activity under Low Temperature Environments in Arabidopsis

Tsuneaki Takami[1, 3, 4, *], Masaru Shibata[2], Yoshichika Kobayashi[1], Toshiharu Shikanai[3]

[1]Graduate School of Agriculture, Kyushu University, Fukuoka, 812-8581 Japan;
[2]Department of Materials Engineering, Nagaoka National College of Technology, Nagaoka, 940-8532, Japan;
[3]Department of Botany, Graduate School of Science, Kyoto University, Kyoto 606-8502 Japan;
[4]Current address; Faculty of Sciences, Kyushu University, Fukuoka, 812-8581 Japan.
[*]Corresponding author. Tel. No. +81-92-642-3929; E-mail: takamiscb@kyushu-u.org.

Abstract: The *Arabidopsis thaliana kas3* mutant was isolated based on its hypersensitivity of photosystem (PS) II to low temperature using a chlorophyll (Chl) fluorescence imaging system. Chl content was lower in *kas3* seedlings cultured at 23 °C than in the wild type, but maximum PSII activity was only mildly affected. We also clarified that the activity and levels of photosynthetic electron transport machinery were reduced after chilling treatment. The *kas3* mutation causes an amino acid alteration in 3-ketoacyl-ACP synthase III (KasIII) which catalyzes the first decarboxy condensation step in *de novo* fatty biosynthesis in plastids. The defect in KasIII led to the partial loss of the *de novo* synthesis pathway for fatty acids in plastids. Consequently, the total fatty acid level was reduced to 75% of the wild-type level in *kas3* at 23 °C and was further reduced to 60% at 4 °C. The full activity of KasIII is required for the biogenesis of intact photosynthetic machinery in thylakoid membranes and is especially important for the process responding to low temperature.

Keywords: Chloroplast; Fatty acid; Low temperature; Photosynthesis; Photosystem II

Introduction

Photosystem (PS) II is the most light-sensitive part of the electron transport machinery in thylakoid membranes. PSII is often photoinhibited, especially under stress conditions (Murata *et al*., 2007). Photoinhibition results from an imbalance between the rate of PSII photodamage and its repair. A recent model suggests that PSII photodamage is proportional to light intensity, while environmental stresses impair the PSII repair cycle, resulting in accelerated PSII photoinhibition (Takahashi and Murata, 2008).

At low temperatures, photosynthesis is inhibited in the presence of light (Powles, 1984). Plants counteract this low-temperature photoinhibition in multiple ways, and one of their main strategies is to regulate membrane fluidity by modifying the unsaturation levels of lipids (Iba, 2002). Thylakoid membranes are mainly composed of galactolipids (Wada and Murata, 2007). In addition to their roles as membrane constituents, some lipid molecules have been identified in crystal structures of the photosynthetic machinery. These lipids contribute it structural flexibility. This flexibility may be required for the replacement of damaged D1 in the PSII repair cycle.

In this study, we characterized an *Arabidopsis thaliana* mutant (*kas3*) whose PSII is hypersensitive to low temperature. The *kas3* mutant is partially defective in the *de novo* synthesis pathway of fatty acids in plastids and exhibits pleiotropic phenotypes in chloroplast function including maintenance of photosynthetic machinery. We discuss the function of *de novo* fatty acid biosynthesis during the protective responses to low temperature.

Materials and Methods

Plant materials, growth conditions and chilling treatment

Arabidopsis thaliana (ecotype Columbia *gl1*) used in this work was grown in soil under the growth chamber

conditions (50 μmol photons m^{-2} s^{-1}, 16 h photoperiod, 23 °C). Three to four weeks after germination, plants were transferred to low temperature conditions (50 μmol photons m^{-2} s^{-1}, continuous light, 4 °C) and cultured further for one week (chilling treatment).

Analysis of Chl levels and chl fluorescence

Chlorophyll content was determined in fifth leaves using a Chl meter (SPAD-502, Konica Minolta, Tokyo, Japan) and was calculated as 0.65 x SPAD value (μg cm^{-2}). Chl fluorescence was measured using a MINI-PAM portable Chl fluorometer (Walz, Effeltrich, Germany).

Fatty acid analysis

Detached leaves were treated with 5% (v/v) HCl in methanol and 40 μM pentadecanoic acid as an internal standard at 90 °C for 1 h. The resulting methyl esters were dissolved in hexane and then analyzed by a gas chromatograph (detail in Takami *et al*., 2010).

Results and Discussion

kas3 is hypersensitive to low temperature

To study the molecular mechanisms that maintain the photosynthetic machinery at low temperatures, we screened Arabidopsis mutants exhibiting PSII photoinhibition under chilling conditions (4 °C for seven days under continuous light) using a Chl fluorescence imaging system. The Chl fluorescence parameter of *Fv*/*Fm* represents the maximum activity of PSII and can be used to monitor PSII photoinhibition. In the *kas3* mutant, *Fv*/*Fm* was significantly lower after the chilling treatment (Table 1). Before the stress, *Fv*/*Fm* was also slightly lower in *kas3* than in the wild type (Table 1). Even before the chilling treatment, the leaves of *kas3* plants were pale-green and Chl content was reduced (Table 1).

Table 1 Total Chl content and *Fv/Fm*.

	WT	*kas3*	*kas3* + *KasIII*
Total Chl (μg cm^{-2})			
23 °C	12.4 ± 0.9	9.0 ± 0.9	11.1 ± 0.9
4 °C	13.7 ± 0.6	8.4 ± 1.0	12.8 ± 0.6
Fv/*Fm*			
23 °C	0.784 ± 0.007	0.712 ± 0.019	0.784 ± 0.005
4 °C	0.744 ± 0.022	0.323 ± 0.085	0.747 ± 0.023

Table 2 Fatty acid contents in wild type and *kas3*.

	23 °C		4 °C	
	WT	*kas3*	WT	*kas3*
Total fatty acids (mg gFW^{-1})	3.46 ± 0.21	2.6 ± 0.32	3.51 ± 0.33	2.09 ± 0.09

We also characterized photochemical efficiency and photosynthetic machinery of *kas3* using mini-PAM and western blotting, respectively. *kas3* displayed the reduction low photochemical efficiency and D1 protein level (data not shown). These results suggested that chilling treatment affects photosynthetic electron transport and the levels of machinary. It is probable that the *kas3* defect pleiotropically affects the function of the photosynthetic machinery in the thylakoid membranes at low temperature.

kas3 defective in de novo synthesis of fatty acids in chloroplasts

The gene affected in *kas3* was At1g62640 coding KasIII, which is involved in *de novo* synthesis of fatty acids in plastids. The well-conserved 196th glycine (GGC) was substituted by serine (AGC) in At1g62640 of *kas3*. To verify that the *kas3* phenotype is caused by the mutation in At1g62640, a genomic fragment containing only the complete At1g62640 gene was introduced into *kas3*. The transformation fully restored the *kas3* phenotype (Table 1).

We conclude that the mutation in At1g62640 leads to the pleiotropic defects. We evaluated the *kas3* phenotype by comparing the fatty acid content between the wild type and *kas3* (Table 2). Before the chilling treatment, the level of total fatty acids (C16, C18 and C20) was reduced to 75% in *kas3* compared to the wild type. Chilling treatment did not affect total fatty acid levels in the wild type, but they were more severely affected to 60% in *kas3* after chilling treatment (Table 2). This result suggests that *de novo* synthesis of fatty acids dependent on the full activity of KasIII is required for the maintenance and high turnover rate of fatty acids during chilling treatment.

Mechanism of PSII photodamage in kas3

Consistent with this primary defect, *kas3* shows the pleiotropic phenotypes in their photosynthetic machinery at low temperature (Takami *et al*., 2010). But *kas3* was isolated based on the hypersensitivity of PSII to low temperature (Table 1).

The actual photoinhibition *in vivo* is a result of imbalance between the inactivation of D1 and its repair process. To assess which process is affected in *kas3* at low temperatures, detached leaves of wild-type and *kas3* plants were exposed to moderate light (300 µmol photons m^{-2} s^{-1}) at 4 °C and the resulting PSII photoinhibition was monitored as the decline in *Fv*/*Fm* in the presence or absence of lincomycin.

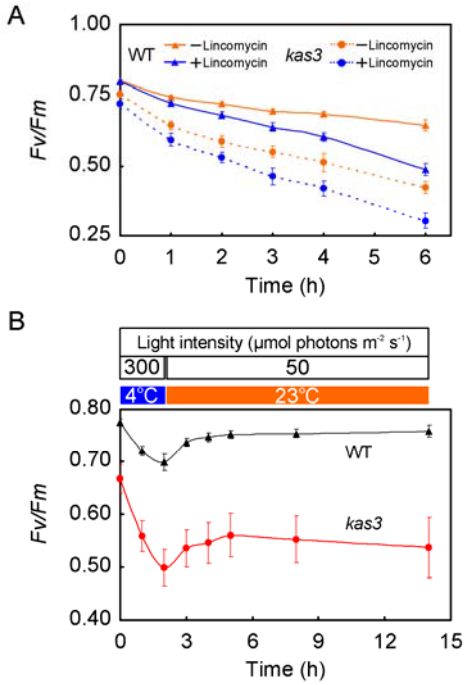

Fig. 1 Effect of the chilling treatment on PSII photoinhibition and recovery.
(A) Detached leaves of the wild type and *kas3* were infiltrated with water or 100 µg ml^{-1} lincomycin. (B) The similar experiment with (A) was performed in the absence of infiltration. After the 2-h chilling treatment *Fv*/*Fm* was measured at each time point as an indicator of photoinhibition.

In the absence of lincomycin, *Fv*/*Fm* declined more drastically in *kas3* than in wild type (Fig. 1A). Lincomycin inhibits translation in chloroplasts, allowing the rate of PSII photodamage to be evaluated independently of the repair of damaged PSII. In the presence of lincomycin, the *Fv*/*Fm* decline was faster both in *kas3* and the wild type, but it was still more drastic in *kas3* than in the wild type.

The results indicate that PSII photodamage is severer in *kas3* than in the wild type. Although PSII photodamage was faster in *kas3* than in the wild type, it was still likely that PSII repair is also affected. To test this possibility, we monitored the repair process of damaged PSII as changes in *Fv*/*Fm* after treatment (300 µmol photons m^{-2} s^{-1} at 4 °C for 2 h) in both the wild type and *kas3* in the absence of lincomycin (Fig. 1B). In the wild type, the *Fv*/*Fm* level was recovered within 1 h. Although the *Fv*/*Fm* level was slightly recovered in *kas3* with slower kinetics (within 3 h) than in the wild type, the majority of PSII activity was irreversibly impaired (Fig. 1B). The *kas3* defect is also likely to affect the repair of PSII, since the lipid environment may not be optimized for the repair cycle. This idea was supported by the results monitoring the recovery process of damaged PSII (Fig. 1B). It is likely that the hypersensitivity of PSII to low temperature in *kas3* is explained by both accelerated photodamage and an impaired PSII repair cycle.

References

Iba K (2002) Acclimative Response to Temperature Stress in Higher Plants: Approaches of Gene Engineering for Temperature Tolerance. Ann. Rev. Plant Biol. 53: 225-245

Murata N, Takahashi S, Nishiyama Y, Allakhverdiev SI (2007) Photoinhibition of Photosystem II under Environmental Stress. Biochim. Biophys. Acta 1767: 414-421

Powles SB (1984) Photoinhibition of Photosynthesis Induced by Visible Light. Ann. Rev. Plant Physiol. 35: 15-44

Takahashi S, Murata N (2008) How Do Environmental Stresses Accelerate Photoinhibition? Trends Plant Sci. 13: 178-182

Takami T, Shibata M, Kobayashi Y, Shikanai T (2010) De Novo Biosynthesis of Fatty Acids Plays Critical Roles in the Response of the Photosynthetic Machinery to Low Temperature in Arabidopsis. Plant Cell Physiol. 51: 1265-75

Wada H, Murata N (2007) The Essential Role of Phosphatidylglycerol in Photosynthesis. Photosynth. Res. 92: 205-215

Critical Temperature Derived from the Selected Chlorophyll *a* Fluorescence Parameters of Indigenous Vegetable Species of South Africa Treated with High Temperature

Marek Zivcak[a]*, Katarina Olsovska[a], Marian Brestic[a], Margaretha M Slabbert[b]

[a]Department of Plant Physiology, Slovak Agricultural University, Nitra, Slovakia;
[b]Department of Crop Science, Faculty of Science, Tshwane University of Technology, Pretoria, South Africa.
*Corresponding author. Tel./No. +421 37 6414 448; E-mail: marek.zivcak@uniag.sk.

Abstract: In our experiments we aimed at testing of photosynthetic thermostability using chlorophyll fluorescence measurements in non-stressed and in drought-stressed conditions. All measurements were realized at 6 species (*Vigna unguiculata*, *Corchorus olitorius*, *Cucurbita pepo*, *Amaranthus sp.*, *Brassica rapa*, and *Hordeum vulgare* as a reference). Plants were grown in pots in climatized growth chamber in moderate conditions. The main practice was temperature test with the chlorophyll fluorescence measurements realized after exposure at 38 °C to 50 °C in circulation water bath. We determined critical temperature values for basal fluorescence - F_0 increase, maximum quantum yield of photochemistry F_V/F_M and we identified also temperature inducing K-step appearance in rapid fluorescence kinetic indicating impairment of oxygen evolving complex (OEC). Our results show significant differences among species in critical temperature. As the most susceptible species was found *Brassica* and *Amaranthus* substantially affected by temperatures about 40 °C with almost negligible increase of critical temperature in drought-stressed conditions, moderate susceptibility in Barley with increase of thermostability caused by moderate drought and high heat tolerance in *Cucurbita*, *Vigna* and *Corchorus.* If we focus on individual florescence parameters used for testing, the K-steps appeared at temperature 1–2 °C higher than initial F_V/F_M decrease, the antennae deconnection indicated by F_0 increase appeared generally at 3–4 °C higher temperature, in some cases was not evident even at 50 °C.

Keywords: Indigenous species; Vegetable; Heat stress; Thermostability; Drought

Introduction

A serious problem of semi-arid African countries is not only availability of basic food-stuffs, but also nutritive quality of produced food, which often lacks of vitamins and other necessary compounds. Along this line a program of implementation of new untraditional indigenous vegetable species has been continuously introduced into the South African agriculture. Climatic conditions of the area of interest are characterized by frequent occurrences of dry and hot periods, which presuppose higher drought and heat tolerance of the species. A critical temperature derived from chlorophyll fluorescence measurements (Havaux, 1992; Baker and Rosenquist, 2004) is a good indicator of the PSII inactivation and may be a useful selection criterion for evaluation of plant heat susceptibility. The chlorophyll fluorescence induction analysis enables to estimate effect of heat on quantum yield of photochemistry (F_V/F_M), but can also detect heat induced deconnection of LHC from PSII shown as F_0 increase (Yamane *et al.*, 1997) and impairment of oxygen evolving complex (OEC) indicated by appearance of K-step in polyphasic fluorescence transient (Srivastava *et al.*, 1997) measured as relative variable fluorescence in 0.3 ms (W_K).

The aim of our study was to test photosynthetic thermostability of selected indigenous vegetable species and reference species grown in normal and dry conditions by means of chlorophyll *a* fluorescence method. Moreover, we compared critical temperature estimated for different parameters obtained at

fluorescence measurements and analyses of rapid fluorescence kinetics and hence we could compare an effect of heat treatment on different level of primary photochemistry.

Materials and Methods

In our experiments 6 vegetable species were studied including cowpea (*Vigna unguiculata* Walp.), tussa jute (*Corchorus olitorius* L.), pumpkin (*Cucurbita pepo* L.), tampala (*Amaranthus* sp.), common mustard (*Brassica rapa* L.), and spring barley (*Hordeum vulgare* L.) cv. Kompakt.

Plants were grown in 3 l pots with a standard peaty substrate in control growth chamber (temperature set on 23 °C, photoperiod 14/10 h, light intensity 250 μmol m^{-2} s^{-1}). Plants were tested both as well watered and dehydrated. Determination of water potential was done regularly during the whole experiment using psychrometer Psypro (Wescor, USA). High temperature of 38 °C to 50 °C was applied on the control and droughted leaf segments for 30 minutes by their exposing in water bath with a precise temperature control.

The chlorophyll *a* fluorescence in a fast phase was used with saturation pulse 3,500 μmol m^{-2} s^{-1} for 1 second. To compare the leaf samples we used the maximum quantum yield of PSII photochemistry F_V/F_M and relative variable fluorescence at 0.3 ms (W_K) derived from fast chlorophyll fluorescence kinetics (1):

$$W_K = \frac{F_{0.3ms} - F_0}{F_{2ms} - F_0} \quad (1)$$

In formula, $F_{0.3ms}$ and F_{2ms} are values of chlorophyll fluorescence in time 0.3 and 2 ms respectively, F_0 is minimal fluorescence measured in time 50 μs.

After the heat treatment a measurement of chlorophyll fluorescence kinetics (Handy PEA, Hansatech, U.K.) was realized and critical temperatures for selected chlorophyll fluorescence parameters, such as minimal fluorescence (F_0), maximum quantum yield of photochemistry (F_V/F_M) decrease as well as K-step induction within the fast fluorescence kinetics were determined as relative variable fluorescence in time 0.3 ms (W_K) as shown at Fig. 1.

Comparison of means was made with using ANOVA with F-test. Results were considered significant at the $P \leq 0.05$ level.

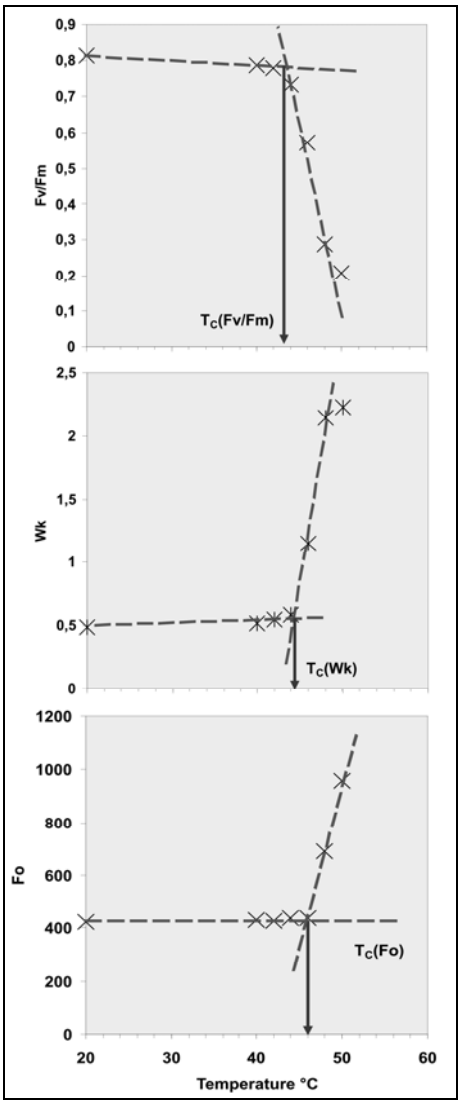

Fig. 1 Determination of critical temperature for measured and calculated fluorescence parameters F_V/F_M (upper), relative variable fluorescence in 0.3 ms, W_K (middle) and basal fluorescence, F_0(bottom). The critical temperature was estimated graphically as an intersection point of lines fitted through the points unaffected by heat and steeple increasing/decreasing points due to heat effect. An example shows determination of critical temperature in one sample of barley, the same operation was done for each sample of species.

Results and Discussion

Determination of critical temperature based on chlorophyll fluorescence measurements was introduced as an effective tool for estimation of photosynthetic thermostability in plant samples (Bilger *et al.*, 1984). There are several studies showing interspecific variability in values of critical temperature, mostly in

woody species (Epron, 1997; Dreyer *et al.*, 2001; Froux *et al.*, 2004; Daas *et al.*, 2008), with critical temperature derived from measurements of basal fluorescence F_0. Determination of critical temperature for three different fluorescence parameters shows significant differences in the critical temperatures among the studied herbal species (Fig. 2). We found two main groups of species. As more heat susceptible species were found Brassica, *Amaranthus* and *Hordeum*. Substantially higher critical temperature was found in *Cucurbita*, *Vigna* and *Corchorus*.

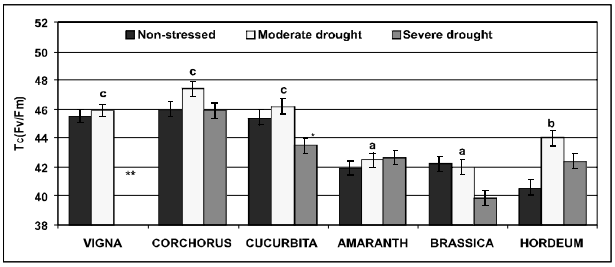

(a)

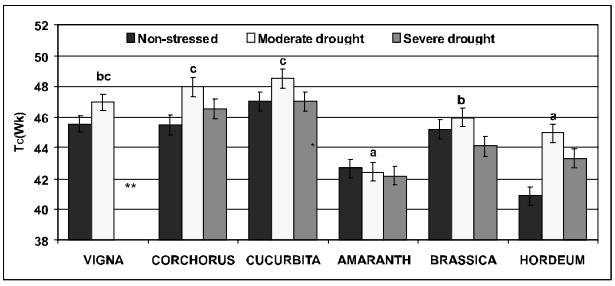

(b)

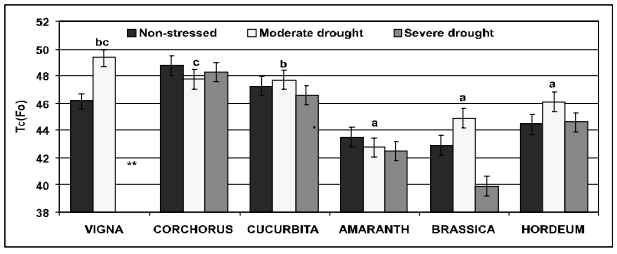

(c)

Fig. 2 Mean values of critical temperature for measured and calculated fluorescence parameters F_V/F_M (a), relative variable fluorescence in 0.3 ms W_K (b) and basal fluorescence F_0 (c). Columns left show results of measurements on leaves of non-stressed plants, middle columns show results on leaves affected by moderate drought stress (water potential $\Psi_W > -1.5$ MPa), columns right show results on severely drought-stressed leaves (Ψ_W in range −1.5 to −3 MPa; no records in *Vigna*). Data were compared using ANOVA with F-test ($\alpha = 0.05$, $p < 0.001$), vertical bars represent standard error. Comparison of species was done by Tukey HSD test ($\alpha = 0.05$), the small letters above the columns indicate statistically homogenous groups; different letters indicate statistically significant difference between species.

The increase of thermostability caused by water deficit was reported by many studies (Havaux, 1992; Epron, 1997; Lu and Zhang, 1999 etc.). In our experiments, moderate drought stress led to increase of critical temperatures in the most of cases, the highest average increase was found in *Hordeum* and *Vigna*, with increase of $T_C(W_K)$ more than 3 °C. In *Amaranthus* we found almost no evident increase caused by drought. In contrary, severe drought caused in many cases decrease of critical temperature compared to moderate drought. This effect was the most evident in *Brassica* (Fig. 2).

As the parameters that we analyzed reflect different heat effects at PS II level (antennae deconnection typical for F_0 vs. OEC inhibition for W_K vs. non-specific decrease of quantum yield for F_V/F_M), the critical temperatures recorded for these parameters were different (Figs. 2 and 3). Critical temperature estimated for an increase of K-step indicating impairment of oxygen evolving complex (OEC) showed poor correlation with the critical temperature estimated for increase of F_0 that is attributed mainly to deconnection of antennae.

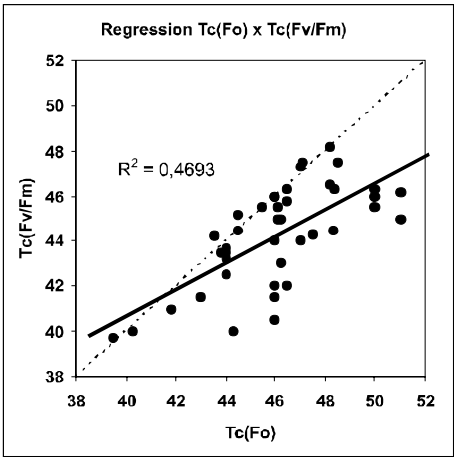

(a)

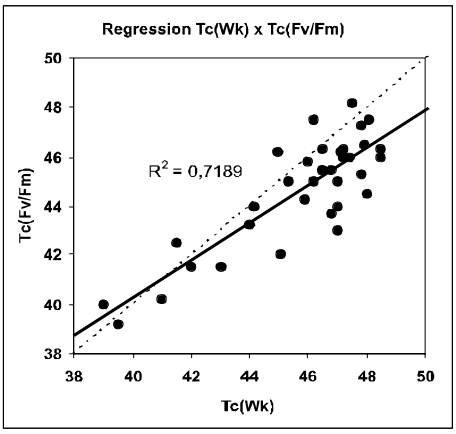

(b)

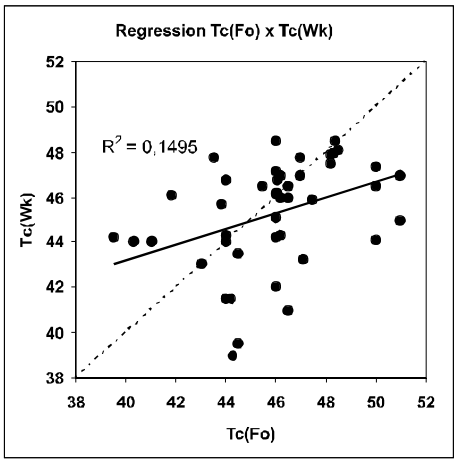

(c)

Fig. 3 Correlations between the critical temperatures $T_C(F_0)$ and $T_C(F_V/F_M)$ (a); $T_C(W_k)$ and $T_C(F_V/F_M)$ (b); $T_C(F_0)$ and $T_C(W_K)$ (c).

Our results (Fig. 4) indicate that in general, F_0 increase occurs usually at about 2 °C (in many cases 3–4 °C higher temperature, in some samples the effect of heat treatment was not evident even at 50 °C) and K-step at a 1–2 °C higher temperatures as compared to the temperature for initial F_V/F_M decrease. Although drought stress led to the increase of all critical temperatures, the intensity of the increase was not identical.

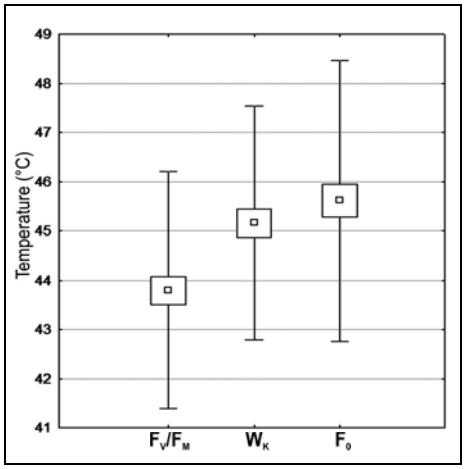

Fig. 4 Mean values of critical temperature for measured and calculated fluorescence parameters F_V/F_M, relative variable fluorescence in 0.3 ms - W_K and basal fluorescence F_0 - in summary for all measurements and observed species. Points represent mean values, boxes show mean value ± standard error, and vertical bars represent standard deviation. Data were compared by non-parametric ANOVA test ($\alpha = 0.05$, $p < 0.001$).

The results obtained from our experiments show apparent interspecific differences in photosynthetic thermostability and acclimation capacity based on measurements of chlorophyll fluorescence. Application of fast fluorescence kinetic analysis enables to recognize the site of heat impairment within PS II and hence it gives more complex information compared to simple measurements of basal fluorescence or F_V/F_M determination.

Acknowledgement

The work was supported by the VEGA project of the Ministry of Education of Slovak republic No. 1/0807/09.

References

Baker NR, Rosenquist E (2004) Applications of Chlorophyll Fluorescence Can Improve Crop Production Strategies: an Examination of Future Possibilities. J. Exp. Botany 55: 1607-1621.

Bilger HW, Schreiber U, Lange OL (1984) Determination of Leaf Heat Resistance: Comparative Investigation of Chlorophyll Fluorescence Change and Tissue Necrosis Methods. Oecologia 63: 256-262

Daas C, Montpied P, Hanchi B, Dreyer E (2008) Responses of Photosynthesis to High Temperatures in Oak Saplings Assessed by Chlorophyll-a Fluorescence: Inter-Specific Diversity and Temperature-Induced Plasticity. Ann. For. Sci. 65: 305-312

Dreyer E, Le Roux X, Montpied P, Daudet FA, Masson F (2001) Temperature Response of Leaf Photosynthetic Capacity in Seedlings from Seven Temperate tree Species. Tree Physiol. 21: 223-232

Epron D (1997) Effects of Drought on Photosynthesis and on the Thermotolerance of Photosystem II in Seedlings of Cedar (Cedrus Atlantica and C. Libani). J. Exp. Botany 48: 1835-1841

Froux F, Ducrey M, Epron D, Dreyer E (2004) Seasonal Variations and Acclimation Potential of the Thermostability of Photochemistry in Four Mediterr. conifers. Ann. For. Sci. 61: 235-241

Havaux M (1992) Stress Tolerance of Photosystem II in Vivo. Plant Physiol. 100: 424-432

Lu C, Zhang J (1999) Effects of Water Stress on Photosystem II Photochemistry and Its Thermostability in Wheat Plants. J. Exp. Botany

336 (50): 1199-1206

Srivastava A, Guisse B, Greppin H, Strasser RJ (1997) Regulation of Antenna Structural and Electron Transport in Photosystem II of Pisum Sativum under Elevated Temperature Probed by the Fast Polyphasic Chlorophyll a Fluorescence Transient: OKJIP. Biochim. Biophys. Acta 1320: 95-106

Yamane Y, Kashino Y, Koike H, Satoh K (1997) Increases in the Fluorescence F_0 Level and Reversible Inhibition of Photosystem II Reaction Center by High-Temperature Treatments in Higher Plants. Photosynthesis Research 52: 57-64

Photosynthetic Characteristics of Arctic Plants

Yameng Li, Yuxin Jiao, Qi Zhao*

Capital Normal University, 100048, Beijing, China.
*Corresponding author. Tel. No. +86-10-68901494; E-mail: zhaoqi@mail.cnu.edu.cn.

Abstract: Polar plants have to adapt to the rigorous environment, such as: chilliness, storm wind, and intense illumination. Six Arctic plants were measured by chlorophyll content, leaf area, photosynthesis characters and chlorophyll fluorescence parameters. The results showed that they appeared obvious differences by measuring chlorophyll content for 24 h. The highest chlorophyll contents of *Silene acaulis* and *Deschampsia alpina* were in the evening, and their photosynthesis were ongoing, but the highest chlorophyll contents of others were in the noon. The rapid light curve (RLC) showed that the Arctic plants have adapted to the stronger light intensity of daytime. For the photosynthetic ability of photosystem II [Y(II)], *Saxifraga hieracifolia* was the highest, *Salix polaris*, *Deschampsia alpina*, and *Silene acaulis* were intermediate; the quotient of photochemical quenching (qP) showed the photosynthetic activity of *Saxifraga hieracifolia* was the highest, and *Salix polaris* was the lowest; the quotient of non-photochemical quenching (qN) showed most Arctic plants were more adaptive to intense light than the control *Poa pratensis*, except *Silene acaulis* and *Deschampsia alpina.*

Keywords: Photosynthesis; Arctic plants; Adaptations

Introduction

With increased global warming, the polar region has become a critical and sensitive area for global climatic and environmental changes. The researches focused on the physiological mechanism of Arctic plants and provide new information on these changes. Arctic plants have to face the rigorous environment, such as chilliness, storm wind, low precipitation and high evaporation (Holzinger *et al.*, 2007; Zhao *et al.*, 2009). They have to photosynthesize 24 hours and adapt to the intense solar radiation during the daytime in summer or suffer long darkness and extremely low temperature during perpetual night in winter (Shen *et al.*, 2002; Alsos *et al.*, 2007; Holzinger *et al.*, 2007; Yeloff *et al.*, 2008).

The Svalbard Archipelago (74°–81° N, 10°–35° E) is typical of the polar climate and protecting the largely untouched, yet fragile, nature.

In this paper, the chlorophyll content, photosynthetic rate and chlorophyll fluorescence parameters of six Arctic plants from Ny-Ålesund were analyzed, in order to explore the photosynthetic characteristics and physiological mechanism of Arctic plants, and provide new data for global climate change.

Materials and Methods

The leaf area, chlorophyll content, photosynthesis characters and chlorophyll fluorescence parameters were measured at Ny-Ålesund, Svalbard. And the plants were *Dryas octopetala* L. (Fig. 1a), *Silene acaulis* (L.) Jacq. (Fig. 1b), *Deschampsia alpina* (L.) Roem. and Schult. (Fig. 1c), *Salix polaris* Wahlenb. (Fig. 1d), *Saxifraga hieracifolia* Waldst. and Kit. (Fig. 1e), *and Oxyria digyna* (L.) Hill (Fig. 1f), respectively, from Ny-Ålesund. The control plant was *Poa pratensis* L. (Fig. 1g) from the Capital Normal University, Beijing, China.

The areas of long narrow leaves were measured according to the formula:

$A = L \times W \times 0.66$; and the areas of suborbicular leaves were measured according to the formula:

$$A = L \times W.$$

Where A is the leaf area, L is the length of the leaf, W is the width of the leaf, and 0.66 is the correction coefficient of leaf area. Each number is the average of 10 repetitions.

The chlorophyll contents were measured according to Arnon (1949), with the leaves of sunny and cloudy day in Ny-Ålesund.

The chlorophyll fluorescence parameters including minimal fluorescence (Fo), maximum fluorescence yield (Fm), quantum yield of photosystem II [Y(II)], quotient of photochemical quenching (qP) and quotient of non-photochemical quenching (qN) were measured by Portable PAM-2100 Fluorometer (Heinz Walz GmbH Co.) (Schreiber, 1999; Kuang, 2003).

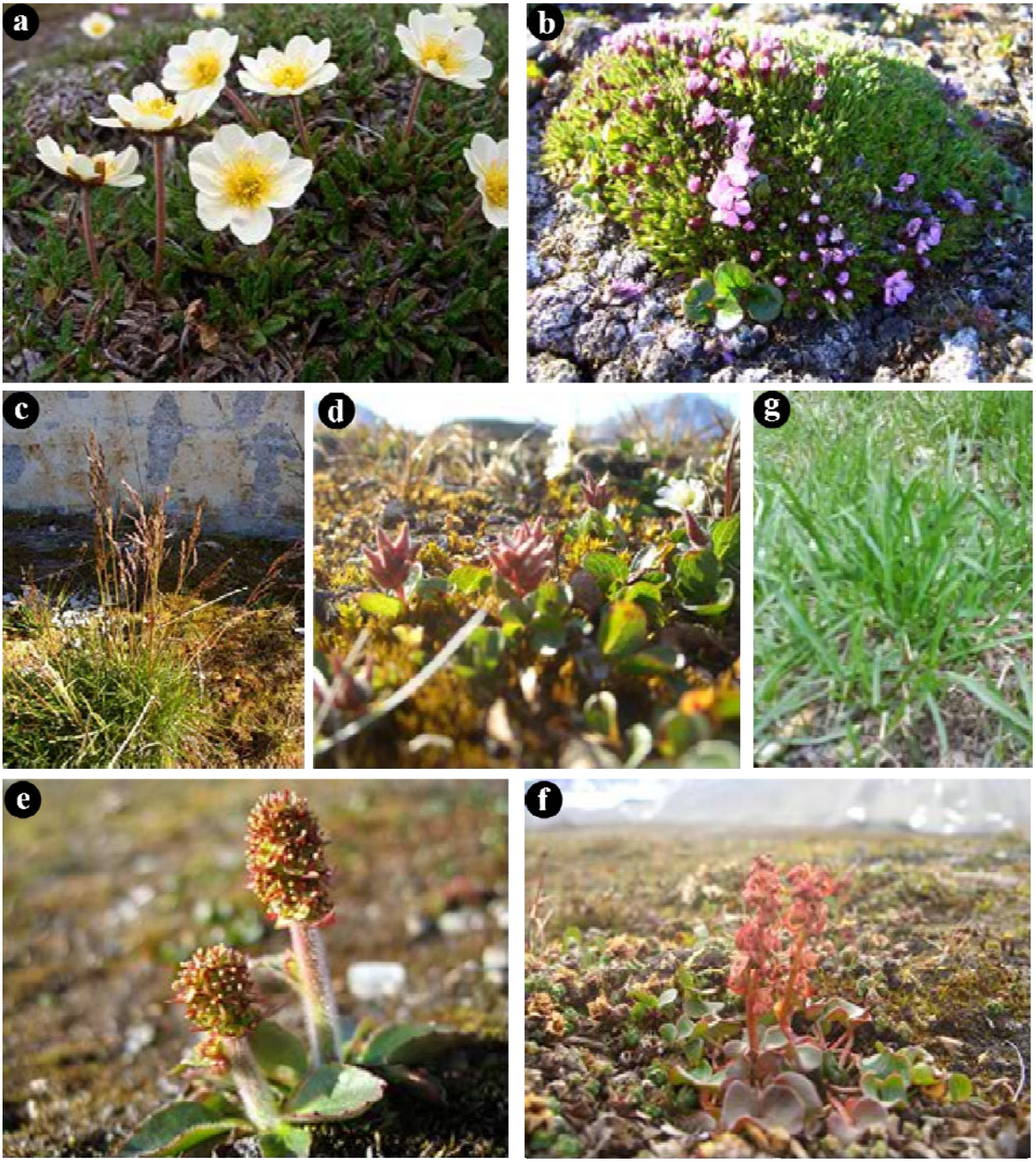

Fig. 1 The photos of the Arctic plant materials.

Results and Discussion

Leaf areas

The morphology characters of Arctic plants such as small leaf area related to the harsh extreme environment. The leaf areas of the six species, ranged from 0.17 to 1.49 cm^2 (Fig. 2), were generally smaller than their relative species of control living in warmer places, suggesting their adaptations to the cold climate and short life cycle.

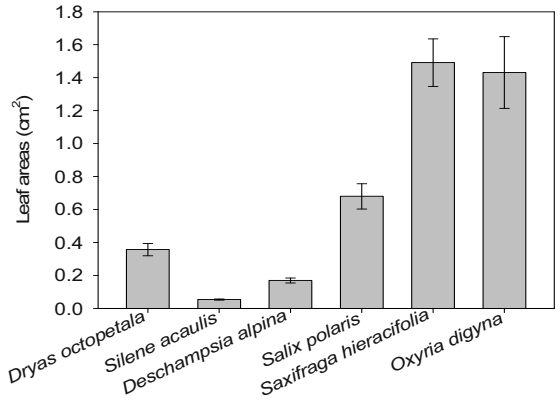

Fig. 2 The leaf areas of six Arctic plants.

Chlorophyll contents

The chlorophyll content was correlated directly with efficiency of photosynthesis. The chlorophyll contents of six Arctic plants measured on the sunny days were all higher than cloudy days, reflecting higher photosynthesis efficiency combined with higher chlorophyll content but differs in different species. The trends of chlorophyll contents of *Dryas octopetala*, *Salix polaris*, and *Oxyria digyna* during sunny and cloudy days were similar, with the highest value at 14:30. But for *Silene acaulis*, the highest value was at 20:30 on sunny days, while at 1:00 on cloudy days. For *Deschampsia alpina*, the highest value was at 20:30 both on sunny and cloudy days. For *Saxifraga hieracifolia*, the highest value was at 14:30 on sunny days, while at 1:00 on cloudy days (Fig. 3).

The chlorophyll content curves of six Arctic plants didn't show clearly changes during 24 h, and the peak values of *Dryas octopetala*, *Salix polaris*, and *Oxyria digyna* appeared at midday. But the peak values of *Deschampsia alpina* and *Silene acaulis* appeared at night. So we presume that the optimum photosynthetic condition of *D. alpina* and *S. acaulis* may be in weak brightness, and the light intensity in the midday of daytime has exceeded their light saturation point.

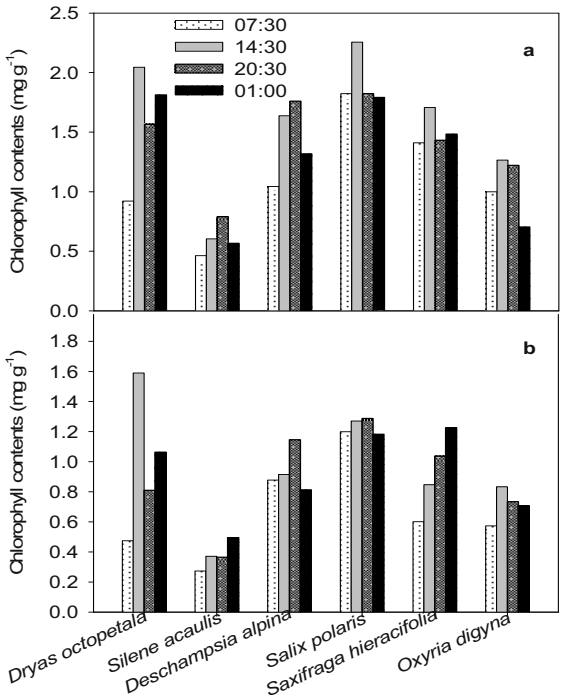

Fig. 3 The chlorophyll contents of leafs during 24 h in sunny (a) and cloudy days (b), respectively.

Chlorophyll fluorescence characters

Rapid light curve (RLC)

RLC means the photosynthetic rate under different light intensity. It is notable that the Arctic plants such as *Dryas octopetala* reached its highest photosynthetic rate when the light intensity ranged from 600 to 700 μmol m^{-2} s^{-1}, but the *Poa pratensis* from Beijing reached its highest photosynthetic rate when the light intensity ranged from 200 to 400 μmol m^{-2} s^{-1} (Fig. 4). This shows that the Arctic plants have adapted to the stronger light intensity of daytime, and all the RCL curves of Arctic plants made the same inference.

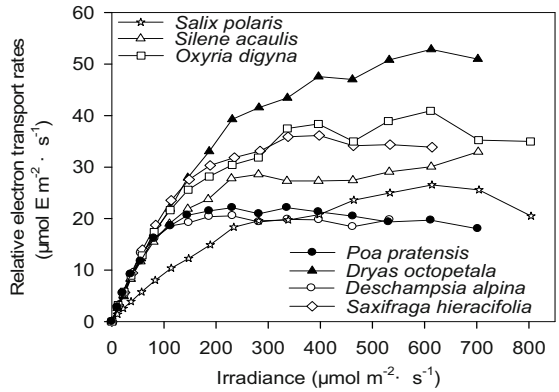

Fig. 4 Relative electron transport rates vs. irradiance curves of six Arctic plants and the control.

Quantum yield of photosystem II [Y(II)]

Y(II) means the quantum yield of PSII of any light intensity, in other words, photosynthetic capacity. When the photosynthetically active radiation (PAR) was 0 μmol m^{-2} s^{-1}, Y represents the maximum photosynthetic capacity of PSⅡ. When the PAR was 111 μmol m^{-2} s^{-1}, it represented the actual photosynthetic capacity of PSⅡ. The differences of same plant under different light intensity indicated the differences between actual photosynthetic capacity and potential photosynthetic capacity. Fig. 5 shows that their Y(II) were lower than 0.7 μmol m^{-2} s^{-1}, and the potential photosynthetic capacity of *Salix polaris*, *Deschampsia alpina* and *Silene acaulis* decreased, and they were severely stressed. In contrast, *Oxyria digyna*, *Saxifraga hieracifolia* and *Poa pratensis* still carried on photosynthesis in severe stress.

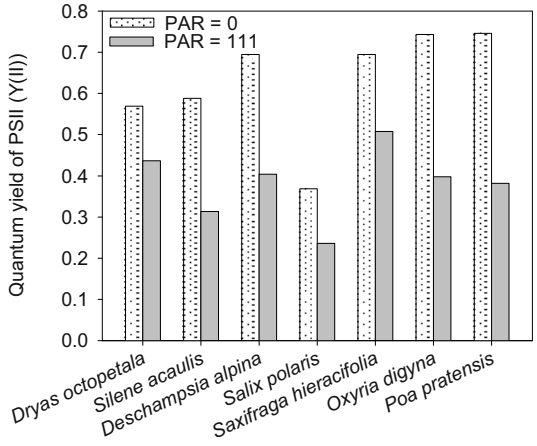

Fig. 5 Quantum yield of PSⅡ [Y(II)] of Arctic plants and the control when the photosynthetically active radiation (PAR) was 0 and 111 μmol m^{-2} s^{-1}.

Quotient of photochemical quenching (qP)

The qP value indicates the efficiency of PS Ⅱ reaction center (Larkum *et al.*, 2006). The qP of *Saxifraga hieracifolia* was the highest while *Salix polaris* was the lowest (Fig. 6). Compared with Fig. 5, *Saxifraga hieracifolia* possessed the highest photosynthetic activity and actual photosynthetic capacity. On the other hand, the photosynthetic activity of *Salix polaris* was the lowest, with lowest actual photosynthetic capacity. In short, the trends of Y(II) and qP were consistent with the ranking for each sample, this shows that the Arctic plant with more photosynthetic activity can provide more environmental adaptability .

Quotient of non-photochemical quenching (qN)

The qN value reflected the self-protection of plants from the adverse effects of photodamage (Larkum *et al.*, 2006). Plants with lower qN value can tolerate in high light intensity. The qN of control *Poa pratensis* was the highest. But the qN of Arctic plants such as *Salix polaris*, *Saxifraga hieracifolia* and *Oxyria digyna* were lower, which indicated they have higher adaptability and utilization efficiency of high light intensity during the long summer daytime (Fig. 6). The qN of *Silene acaulis* and *Deschampsia alpina* were higher than the other Arctic plants, combined with their highest chlorophyll contents occurred in night, suggested that light intensity in night was probably suitable for these two species and reflected their photosynthetic adaptability to the extreme environments in Arctic.

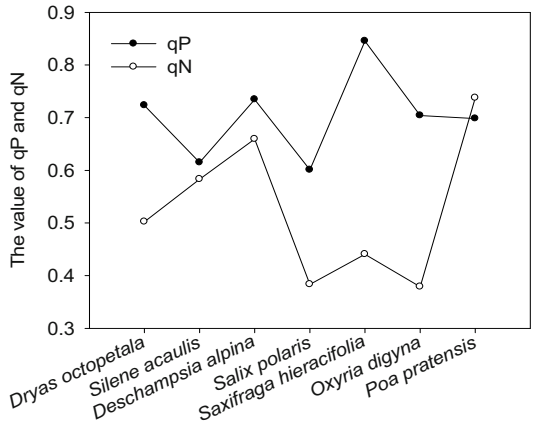

Fig. 6 The quotient of photochemical quenching (qP) and Quotient of non-photochemical quenching (qN) value of Arctic plants and the control.

In summary, Arctic plants possess more adaptability of extreme environment, and they can maintain normal photosynthetic course during the daytime in summer (Jiao *et al.*, 2008; Wang *et al.*, 2008). In addition, they appeared obvious differences by measuring chlorophyll content for 24 h, the highest chlorophyll contents of *Silene acaulis* and *Deschampsia alpina* were in the evening, but others displayed the highest chlorophyll content at noon. For the photosynthetic ability of photosystem II, *Saxifraga hieracifolia* was the highest as it accumulated chlorophyll whether sunny or cloudy night; *Salix polaris*, *Deschampsia alpina*, and *Silene acaulis* were intermediated. The qP also showed the photosynthetic activity of *Saxifraga hieracifolia* was the highest, as

its larger leaf area and chlorophyll accumulated; and *Salix polaris* was the lowest, although it accumulated most chlorophyll in the night, maybe exceeded chlorophyll endanger to photosynthesis. The qN showed they were both more adaptive to intense light than *Poa pratensis*, and most RLC of Arctic plants indicated that they could tolerate intense light till 600 to 700 μmol m^{-2} s^{-1}, but *Silene acaulis* and *Deschampsia alpina* were less adaptive to intense light. However, they revealed their ability of photoprotection through qN. There is much photosynthetic adaptability of Arctic plants waiting to be revealed.

Acknowledgement

We thank the financial assists from the State Oceanic Administration for the field work in Ny-Ålesund, Svalbard.

References

Alsos IG, Eidesen PB, Ehrich D, Skrede I, Westergaard K, Jacobsen GH, Landvik JY, Taberlet P, Brochmann C (2007) Frequent Long-Distance Plant Colonization in the Changing Arctic. Science 316: 1606-1609

Arnon DI (1949) Copper Enzymes in Isolated Chloroplasts Polyphenoloxidase in Beta Vulgaris. Plant Physiol. 24: 1-15

Holzinger A, Wasteneys GO, Lütz C (2007) Investigation Cytoskeletal Function in Chloroplast Protrusion Formation in the Arctic-Alpine Plant Oxyria Digyna. Plant Biology 9: 400-410

Jiao YX, Zhao Q, Wang XY, Xia L, Sun DL (2008) The Influence of Environmental Factors on Chloroplast Ultrastructure. Biotechnology Bulletin 2: 5-10

Kuang TY (2003) Mechanism and Regulation of Primary Energy Conversion Process in Photosynthesis. Jiangsu Science and Technology Press, Nanjing, China

Larkum AWD, Orth RJ, Duarte CM (2006) Seagrasses: Biology, Ecology, and Conservation. Kluwer Academic Pub

Schreiber U (1997) Chlorophyll Fluorescence and Photosynthetic Energy Conversion: Simple Introductory Experiments with the TEACHING-PAM Chlorophyll Fluorometer. Effeltrich, Germany: Heinz Walz GmbH

Shen FY, Liu WJ, Gao RG; Zhang WG, Zhao Q (2002) Thermodymic Analysis on Mechanism of Deep Supercooling of Tissue Water in Winter-Hardy Plants. Cryoletters 23(3): 141-150

Wang XY, Zhao Q, Jiao YX (2008) Microstructure and Ultrastructure of Four Arctic Angiosperm Plant Leaves. Acta Botanica Boreali-Occidentalia Sinica 28(10): 1989-1996

Yeloff D, Blokker P, Boelen P, Rozema J (2008) Is Pollen Morphology of Salix Polaris Affected by Enhanced UV-B Irradiation? Results from a Field Experiment in High Arctic Tundra. Arctic Antarctic and Alpine Research 40(4): 770-774

Zhao Q, *et al*. (2009) A Primary Photosynthetic Study on Polar Plants. The 10th Arctic Science Summit Week “Book of Abstracts”. page43. Mar. 22-28, Bergen, Norway

The Evolution of Far-Red Light Perception in *Acaryochloris Marina*, a Chlorophyll *d*-Containing Cyanobacterium

Zane Duxbury[a], Robert D Willows[b], Penelope M Smith[a], Min Chen[a,*]

[a]School of Biological Sciences, The University of Sydney, Sydney, NSW 2006, Australia;
[b]Department of Chemistry and Biomolecular Sciences, Macquarie University, North Ryde, 2109 Australia.
[*] Corresponding author. Tel. No. +61 2 9036 5006; Fax No. +61 2 9351 4119; E-mail: min.chen@sydney.edu.au.

Abstract: Phytochromes are photoreceptors that were first discovered in plants, but homologues have since been identified in bacteria, cyanobacteria and fungi. Phytochromes reversibly isomerise upon illumination in red or far-red light, making them uniquely adapted to regulating antenna pigments and photosystems in photosynthetic organisms. *Acaryochloris marina*, a unicellular oxygenic photosynthetic cyanobacterium, lives in infrared light enriched environments. It has adapted to these light conditions by evolving a red-shifted chlorophyll, chlorophyll *d*. Since *A. marina* has adapted to infrared light enriched light conditions, phytochrome may be an important photoreceptor for this organism. To understand red light perception in *A. marina*, the newly sequenced genome of this cyanobacterium was searched for phytochrome homologues. Interestingly, *A. marina* contains a gene for a putative red-shifted phytochrome, denoted *Amr*BphP. *Amr*BphP was included in a phylogenetic analysis of the phytochrome superfamily and found to be more closely related to bacteriophytochromes than typical cyanobacterial phytochromes. The red-shifted absorption spectrum of a bacteriophytochrome would better overlap the spectrum of Chl *d* then the spectrum of a cyanobacterial phytochrome. *A. marina* may have evolved or retained a bacteriophytochrome to adapt to the infra red light-enriched environment it inhabits.

Keywords: Bacteriophytochrome; Chromophore; Cyanobacteria; Photoreceptor; Chlorophyll *d*

Introduction

Oxygenic photosynthetic organisms utilize chlorophyll (Chl) *a* as the primary electron donor in their reaction centres to oxidize water and release oxygen. The reaction centres of anoxygenic photosynthetic organisms contain bacteriochlorophyll (Bchl), which absorbs a longer wavelength light and as a consequence is unable to generate the oxidizing potential required to oxidize water (Blankenship, 2002). *Acaryochloris marina,* a cyanobacterium that lives in environments relatively enriched in infrared light*,* is the only organism known to contain Chl *d* in its reaction centres (Kuhl *et al.*, 2005; Hu *et al.*, 1998). Chl *d* absorbs longer wavelength and lower energy light than Chl *a*, but can generate the redox potential to oxidize water (Chen *et al.*, 2005; Tomo *et al.*, 2007). Therefore, *A. marina* may represent an evolutionary intermediate between anoxygenic and oxygenic photosynthetic organisms. A key to evaluating the potential of *A. marina* as an evolutionary intermediate may be the way it regulates responses to its infrared enriched light conditions. Phytochromes are light-sensing pigment-proteins which regulate responses to red and far-red light.

Originally discovered in plants, phytochromes have since been identified in fungi and prokaryotes (Sharrock, 2008). Plant phytochromes, cyanobacterial phytochromes (Cphs) and bacterial phytochrome photoreceptors (BphPs) have different absorbance spectra depending on their attached chromophore. Chromophores bind via a conserved cysteine residue in 1 of 2 possible modular domains. Plant phytochromes and Cphs attach phytochromobilin (PΦB) and phycocyanobilin GAF (PCB), respectively, via a cysteine located in the domain (Fig. 1; Rockwell

et al., 2006); Bphs attach biliverdin (BV) via a cysteine in the PAS domain. PΦB and PCB chromophores result in relatively similar overlapping absorption spectra, while BV, in comparison, provides a red-shifted absorption spectrum (Bhoo *et al.*, 2001).

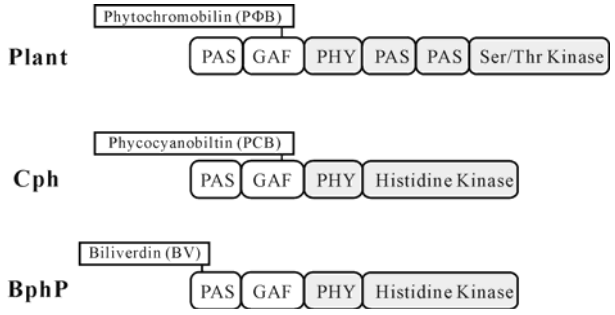

Fig. 1 Modular domains of canonical phytochromes from plants, cyanobacteria and other bacteria. Chromophores and the domain to which they attach are shown for each phytochrome.

This study aimed to identify any phytochromes utilized by *A. marina*. One phytochrome, *Amr*BphP, was discovered. A phylogenetic analysis of the phytochromes was performed to investigate the evolution of *Amr*BphP.

Materials and Methods

Phytochrome sequences, including *Amr*BphP, were identified from protein databases accessed through the NCBI (National Center of Biotechnology Information) website (www.ncbi.nlm.nih.gov) using BLAST. The GAF and PAS domains were identified from amino acid sequences using SMART (http://smart.embl-heidelberg.de/) and aligned using ClustalW. Unrooted phylogenetic trees were generated from PAS and GAF domain alignments using MrBayes (version 3.1.2). Each analysis consisted of 2 runs of 10 chains, each using the mixed amino acid model and proportion of invariable γ-distributed rates model. Convergence of runs was diagnosed with Tracer (http://tree.bio.ed.ac.uk/software/tracer) and AWTY (http://ceb.csit.fsu.edu/awty). The analysis was run for 7,000,000 generations with the first 1,691,000 generations discarded as burn-in, as graphically interpreted with the Tracer program.

Results and Discussion

BLAST searches of the genome of *A. marina* MBIC11017 genome identified only one canonical phytochrome gene containing a PAS, GAF and PHY domain. The ORF AM1_5894 is 2,544 bp long and encodes an 847 amino acid protein product (GI:158309216), with a predicted molecular weight of 94.2 kDa. The aligned GAF and PAS domain chromophore attachment regions are illustrated in Fig. 2. The translated protein contains a predicted chromophore- binding cysteine within the PAS domain, rather than the GAF domain, and therefore is likely to bind BV similarly to BphPs; the protein encoded by AM1_5894 will therefore be referred to as *Amr*BphP herein. Although some cyanobacteria utilize both a BV-BphP and a PCB-Cph, *A. marina* is the first recorded to contain only a BphP gene within its genome. The phylogenetic analysis places plant and fungal phytochromes in distinct, monophyletic clades (Fig. 3). Cphs are contained within two clades which form a single clade with cyanobacterial BV-BphPs, those cyanobacterial phytochromes that contain a predicted BV-binding cysteine within their GAF domains (Fig. 3).

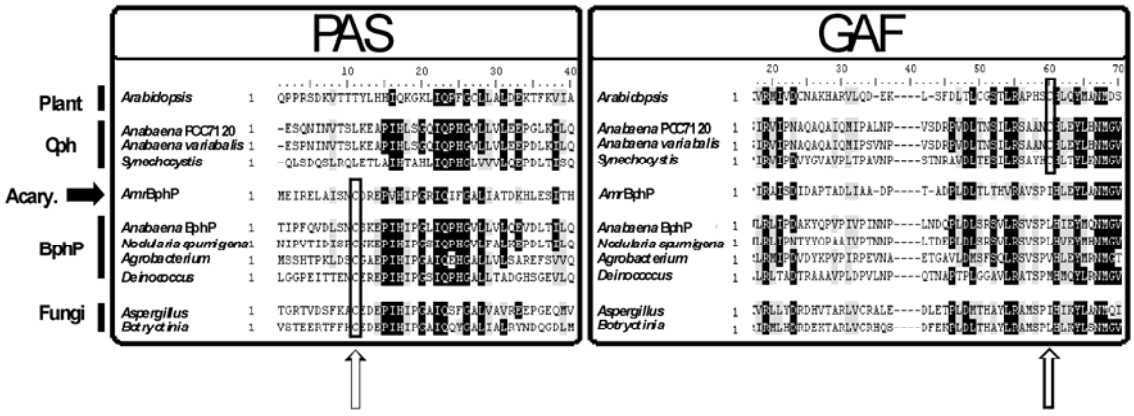

Fig. 2 Alignment of the PAS and GAF domains of representative phytochromes. Arrows indicate conserved potential chromophore-attachment sites. Conserved chromophore-binding Cys residues are highlighted.

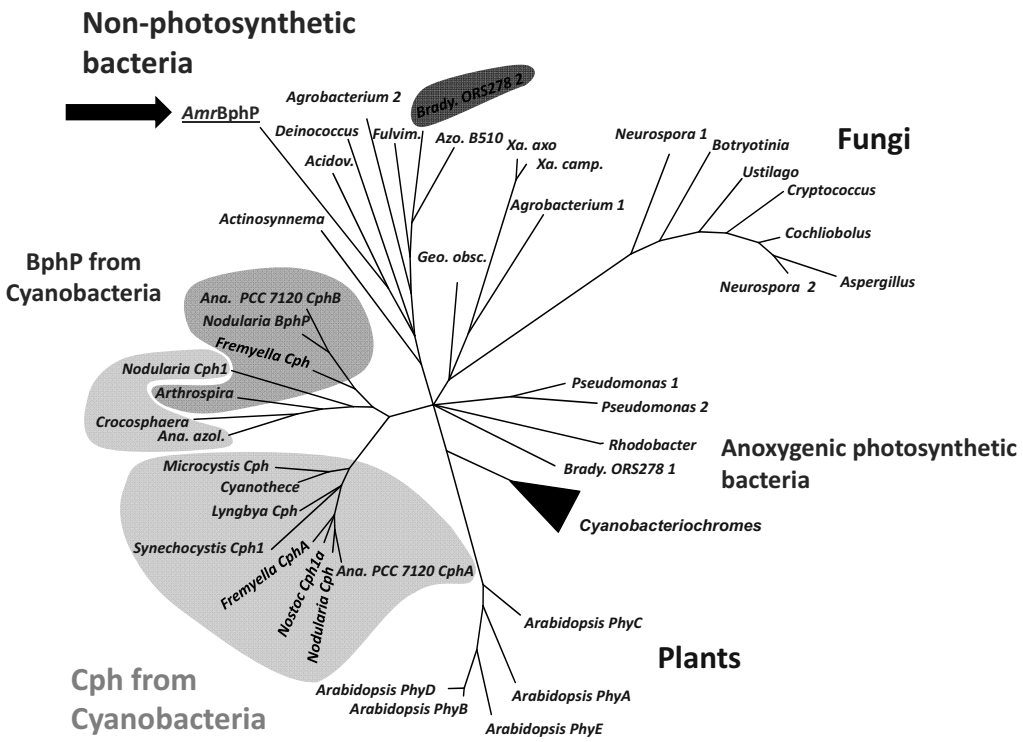

Fig. 3 Strict consensus phylogenetic tree generated by MCMC analysis using MrBayes. *Amr*BphP is underlined and indicated by an arrow. Nodes have a posterior probability greater than 50. Phytochromes from common families are labelled. The cyanobacteriochromes are a group of non-canonical phytochrome-like photoreceptors found only in cyanobacteria.

Non-photosynthetic cyanobacteria contain BV-BphPs which form three clades. *Amr*Bphp, the BphP from *A. marina*, falls within the largest of these clades and not with other cyanobacterial BphPs.

Both the predicted chromophore-binding Cys residue and the phylogenetic analysis suggest that *A. marina*, uniquely for a cyanobacterium, utilizes a BV-binding BphP. BV-binding phytochromes are red-shifted compared to PCB-binding phytochromes. The photosystems of anoxygenic photosynthetic bacteria contain Bchls, which absorb at wavelengths longer than 800 nm, thus making a red-shifted BV-BphP more suitable than PCB-Cphs for photo- regulation and shade avoidance (Bhoo *et al.*, 2001; Blankenship, 2002). The native habitat of *A. marina* is depleted in PAR utilised by Chl *a* and may have adapted to this infrared light enriched habitat by evolving the red-shifted Chl *d* (Kuhl *et al.*, 2005). A BV-binding BphP would provide *A. marina* with a red-shifted phytochrome more suitable to its natural light conditions. A free-living strain of *Acaryochloris* is unable to synthesise PCB (Chan *et al.*, 2007; Miller *et al.*, 2005). The survival of this species in this niche demonstrates the dispensability of a PCB-Cph in a red light depleted environment.

Phytochromes are active in wavelengths harvested between Chls and BChls, and are appropriate for regulating photosynthetic reactions due to overlapping absorption spectra. The regulation of photosynthesis is probably the main driver of phytochrome evolution and the switch from a red-shifted BV chromophore to PCB or PΦB was probably in response to a change in photosynthetic apparatus.

Acknowledgements

MC and RDW thank the Australian Research Council for financial support and MC holds an Australian Queen Elizabeth II Fellowship. ZD thanks Prof. Hugo Scheer, Munich University for valuable discussion.

References

Bhoo SH, Davis SJ, Walker J, Karniol B, Vierstra RD (2001) Bacteriophytochromes Are Photochromic Histidine Kinases Using a Biliverdin Chromophore. Nature 414: 776-779

Blankenship RE (2002) Molecular Mechanisms of Photosynthesis. (1st ed.). Blackwell Science Ltd,

Oxford, United Kingdom

Chan YW, Nenninger A, Clokie SJH, Mann NH, Scanlan DJ, Whitworth AL, Clokie MRJ (2007) Pigment Composition and Adaptation in Free-Living and Symbiotic Strains of Acaryochloris Marina. FEMS Microbiology Ecology. 61: 65-73

Chen M, Telfer A, Lin S, Pascal A, Larkum AWD, Barber J, Blankenship RE (2005) The Nature of the Photosystem II Reaction Centre in the Chlorophyll D-Containing Prokaryote. Acaryochloris Marina. Photochemical & Photobiological Sciences. 4: 1060-1064

Hu Q, Miyashita H, Iwasaki I, Kurano N, Miyachi S, Iwaki M, Itoh S (1998) A Photosystem I Reaction Center Driven by Chlorophyll d in Oxygenic Photosynthesis. Proc. Nat. Acad. Sci. USA 95: 13319-13323

Kuhl M, Chen M, Ralph PJ, Schreiber U, Larkum AWD (2005) A Niche for Cyanobacteria Containing Chlorophyll d. Nature 433: 820-820

Miller SR, Augustine S, Le Olson T, Blankenship RE, Selker J, Wood AM (2005) Discovery of a Free-Living Chlorophyll d-Producing Cyanobacterium with a Hybrid Proteobacterial-Cyanobacterial Small-Subunit rRNA Gene. Proceedings of the National Academy of Sciences of the United States of America. 102: 850-855

Rockwell NC, Su YS, Lagarias JC (2006) Phytochrome Structure and Signaling Mechanisms. Annual Review of Plant Biology. 57: 837-858

Sharrock RA (2008) The Phytochrome Red/Far-Red Photoreceptor Superfamily. Genome Biology 9.

Tomo T, Okubo T, Akimoto S, Yokono M, Miyashita H, Tsuchiya T, Noguchi T, Mimuro M (2007) Identification of the Special Pair of Photosystem II in a Chlorophyll d-Dominated Cyanobacterium. Proc. Nat. Acad. Sci. USA 104: 7283-7288

Effects of Ultraviolet-B Radiation on Primary Photophysical Process in Photosystem II: a Fluorescence Spectrum Analysis

Xiao Liu[a], Ming Yue[a,*], Qianrua Ji[a], Junfang He[b]

[a] Key Laboratory of Resource Biology and Biotechnology in Western China (Northwest University), Ministry of Education, Xi'an, China;
[b] State Key Laboratory of Transient Optics and Photonics; Xi'an Institute of Optics and Precision Mechanics; Chinese Academy of Sciences; Xi'an, China.
* Corresponding author. Tel. No. +86 029 88302143; Fax No.+86 029 88303534; E-mail: yueming@nwu.edu.cn.

Abstract: To clarify the effects of Ultraviolet-B (UV-B) treatment on the primary energy transfer process in photosynthesis, PSII was exposed to UV-B radiation by two different methods. beside control samples, one are PSII particles isolated from plants that were irradiated each day for 8 h by increased UV-B (on top of natural light)，second are PSII particles isolated from non-irradiated plants but exposed only to UV-B in vitro for 30 minutes directly before fluorescence spectrum was tested (the group of CK+UV-B30min). The steady-state fluorescence techniques were used, and Gaussian deconvolution analysis was employed to better identify the spectral changes resulting from UV-B radiation. The results showed that the group of CK+UV-B30min showed obviously fluorescence quenching for the degradation of some proteins in PSII, while the emission of the group of 7 day UV-B exposure was increased. The deconvolution analysis revealed that 30-min UV-B radiation changed the primary energy transfer process from Chlorophyll a (Chl a) to other pigments. However, if UV-B was added to plants for 7 day, photosystem performed overall regulation by re-arrangement of pigment-protein complexes to resist the stress, which not only altered the energy transfer process from Chl a but also Chlorophyll b (Chl b) and Carotenoid (Car).

Keywords: Energy transfer process; PSII; Steady-state fluorescence spectrum; UV-B

Introduction

The effects of ultraviolet-B (UV-B) on photosystem have attracted much interest in recent years. In photosynthetic organisms, a crucial part of the overall effect of UV-B is related to damage in the photosynthetic apparatus, which lead to decrease of total chlorophyll content, oxygen evolution, CO_2 fixation, dry weight and so on (Fiscus and Booker, 1995). It has been widely accepted that the most sensitive UV-B target is the light energy converting complex of photosystem II (PS II).

Chlorophyll fluorescence not only allows us to study the different functional levels of photosynthesis indirectly but also is a useful method to study the effects of environmental stress on plants, since photosynthesis is often reduced in plants experiencing adverse conditions, such as water deficit, nutrient deficiency, polluting agents and UV-B radiation (Baker *et al*., 2004; Hulsen *et al*., 2000). Many investigators have discussed effects of UV-B on plants by chlorophyll fluorescence, however, most of them analyze chlorophyll florescence for the purpose of elucidating the effect of UV-B on process of carbon fixation, photosynthetic electron transport chain, respiration rate and photochemical reaction of photosynthesis. Until now, little attention has been paid to primary photophysical process in photosynthesis by spectrum properties analysis with fluorescence techniques (Sprtova *et al*., 2000; Larkum *et al*., 2001; Lin *et al*., 2002; Prabha and Kulandaivelu, 2002; Liu *et al*., 2005; Szilárd, 2007; van Rensen *et al*., 2007). Moreover, most of researches employed enhanced UV-B radiation during the plant growth process, in these studies, the target of UV-B radiation

was the whole plant. Now that many investigators have reported that PSII is the target of UV-B radiation, what kinds of characters of PSII could be revealed when exposed directly to UV-B radiation? Do the characters be the same as that of exposing the whole plant to UV-B?

In this paper, PSII was exposed to UV-B radiation by two different methods. beside control samples, one are PSII particles isolated from plants that were irradiated each day for 8 hours by increased UV-B (on top of natural light) (*i.e.* PSII was exposed to UV-B indirectly), just like other reporters, second are PSII particles isolated from non-irradiated plants but exposed only to UV-B in vitro for 30 minutes directly before fluorescence spectrum was tested. Fluorescence excitation and emission spectra of PSII under these two different treatments were investigated, for the purpose of reveal the effects of UV-B irradiation on energy transfer process in PSII complex.

Materials and methods

Plant material and UV-B irradiation

Spinach seeds were obtained from the market; greenhouse experiments were carried out in Northwest University, Xi'an, China. The pretreated seeds were sown in 50 plastic pots of 31×21 cm size. After germination, unwanted seedlings were removed in order to ensure that there were 3 seedlings in each pot. To minimize the effects of microenvironment variation, the position of pots were changed weekly. When the fifth pairs of leaves fully expanded, 50 pots were divided into a control group and a treatment group, the control groups were kept under no UV-B conditions, and the treatment groups were exposed to additional UV-B radiation.

Additional UV-B radiation was supplied over 8-h centered on solar noon using Q-PANEL UV-B fluorescent lamps (40W, Qing, Baoji) mounted in metal frames suspended above the pots and filtered with 0.13 mm cellulose diacetate to remove UV-C radiation. The enhanced UV-B dose was 1.152 kJ m^{-2} d^{-1}, the radiation intensity was guaranteed by varying the distance between lamp and the plants canopy.

Isolation of PSII

Leaves of the controls and treatments were harvested for isolation of PSII particle complex, and PSII particle was prepared as described by Du (Du, 1995).

Pretreatment of PSII before spectrum measurement

Before spectrum measurement, the PSII particle sample of the control were divided into two samples, one sample was placed into a 1-cm thick quartz tube, irradiated for 30 min with hand-held UV-B lamp EB-180 (280–320 nm, center wavelength: 312 nm; Spectronics, U.S.), the irradiance reached sample surface was about 15 μw·cm^{-2}. The second sample was placed into a 1-cm thick quartz tube for measurement directly. Thus, there were three groups of PSII particle complex for spectrum measurement (see Table1).

Table 1 Three groups of different Ultraviolet-B (UV-B) treatments.

Treatment group	Interpretation
CK	*I.e.* control; PSII was separated from that grown in greenhouse and never received UV-B irradiation.
CK+UV-B_{30min}	Plants were grown in greenhouse. PSII were irradiated with UV-B lamp for 30-min before measurement.
UV-B	PSII was separated from plants that were irradiated with UV-B lamp for 7days and then conducted the measurement.

Steady-state fluorescence spectra measurement

The steady-state fluorescence emission spectra were recorded with Steady State Fluorescence Spectrometers (FLS920, Edinburgh Instruments Ltd.). The excitation source was successive light outputting by Xe 900 (Edinburgh Instrument Ltd.). The excitation wavelength was at 436, 473 and 510 nm (slit 6 nm) and the emission was between 600 and 800 nm (slit 6 nm) (M300, Edinburgh Instrument Ltd.). The fluorescence signal was detected and its characteristics were analyzed by the S900 single photon photomultiplier detection system (Edinburgh Instrument Ltd.) and F900 data analysis system (Edinburgh Instrument Ltd.). The excitation intensity was kept low (no more than 1.2×10^{12} photon/pulse) to prevent fluorescence quenching during measurements. The emission was between 600 nm 800 nm. The Chl fluorescence data were analyzed with a Gaussian deconvolution program (Origin 6.0 professional program).

Chlorophyll concentration of sample of three groups was 30 μg ml^{-1}. At the concentrations used, re-absorption of emitted Chl fluorescence was negligible (Wen *et al*., 2005). All treatments and measurements were performed in darkness.

Results

Fluorescence emission spectra

Excitation wavelengths of 436 nm (preferentially Chl *a* excited), 473 nm (mainly Chl *b* excited) and 510 nm (mainly carotenoids excited) were selected for measurements of emission spectra. The results were showed in Fig. 2. There was an obvious 680 nm emission derived from Chl *a* of reaction center (RC) in spectra of three excitation wavelength.

Fig. 1A showed emission spectra obtained with excitation at 436 nm which was absorbed mainly by Chl *a*. Upon Chl *a* excitation, three groups (CK, UV-B and CK+UV-B_{30min}) exhibited the identical characteristic emission peak at 680 nm. Yet, fluorescence yield had significant differences among the control and treaments. The tendency of signal intensity of the three groups was : UV-B>CK>CK+UV-B_{30min}. Especially, at maximum peak, the emission yield of CK+UV-B_{30min} was reduced by 75% as compared to that of UV-B (Fig. 1A). CK+UV-B_{30min} appeared obvious quenching in the region 660–690 nm, despite slightly increased at the wavelengths shorter than 640 nm. The UV-B group showed the highest emission among three groups in the whole spectrum range (600–800 nm).

Fig. 1B (excitation at 473 nm mainly stimulated the Chl *b* moleculars) showed similar fluorescence yield trend to that of Fig. 1A (Chl *a* excitation). CK+UV-B_{30min} exhibited the lowest emission among three groups at whole wavelength range distinctly. CK group was slightly higher than the others at wavelength shorter than 640 nm.

Emission properties of Car excitation (510 nm) were displayed in Fig. 1C. The fluorescence intensity tendency of the three treatments at around 680 nm keep the same with that of 436 and 473 nm excitation experiments, *i.e.*, UV-B > CK > CK + UV-B_{30min}, while, at wavelength shorter than 640 nm, the emission intensity of CK + UV-B_{30min} and UV-B samples was lower than CK. There had another prominent long-wavelength emission peak about 760 nm was observed. It was worth mentioning that the emission of 760 nm peak was equally with or even larger than that of 680 nm**.** We arranged this emission to LHCII antenna trimers. Schmid *et al.* had concluded that extreme long-wavelength chlorophylls may be present in the intact photosystem II antenna system, similarly to photosystem I. They also pointed out that the literature evidence for the far-red Chls in PSII constituents is scarce. while a tail of the absorption spectrum extending to 720 nm at room temperature has been observed in peripheral LHCII antenna trimers in a few cases, And further tailing reaching ~740 nm has been found for the bulky grana membrane fractions(Schmid *et al*., 2001; de Weerd *et al*., 2002; Pettai *et al*., 2005).

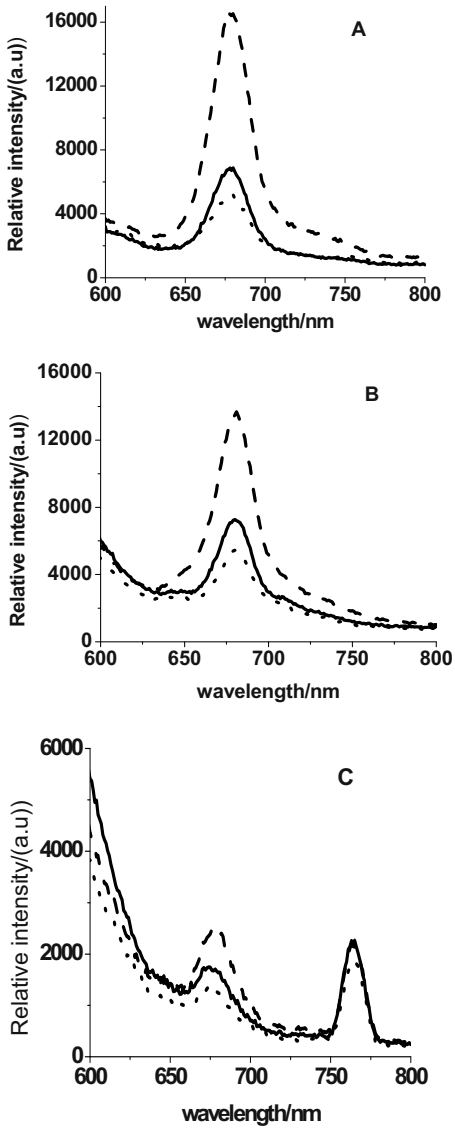

Fig. 1 Fluorescence emission spectra of three groups of PSII at room temperature with selective excitation. A:excited with 436 nm; B:excited with 473 nm; C:excited with 510 nm. CK: solid, UVB: dash, CK+UV-$B_{30min:}$ dot.

The emission spectra indicated that the pigments absorbing wavelength short than 640 nm were sensitive for UV-B radiation.

Gaussian analysis of fluorescence emission spectra

In order to reveal what parts of the photosynthetic apparatus were responsible for the changes in the related Chl fluorescence emission peaks, we fitted the

emission spectra by Gaussian components according to the assignments of emission bands to different components of the photosynthetic apparatus. For assignments of Gaussian sub-band of different photosystems, see Ref.(Garlaschi *et al*.,1994; Groot *et al*.,1999; Vasil'ev *et al*., 2001; Gopal *et al*., 2002; Liu *et al*., 2004; Mishra *et al*., 2005; Wen *et al*., 2005). We have chosen Gaussian spectral function for the curve fitting, since it provides a reasonably matching fit of the spectral data with good *F*-statistics, standard errors for peak amplitude, peak area, peak centre, and bandwidth or full width at half intensity maximum (FWHM) (Gopal *et al*., 2002; Mishra *et al*., 2005; Wen *et al*., 2005).

The results of Gaussian deconvolution at different excited wavelengths were summarized in Table 2.

Table 2 Results of Gaussian fluorescence emission spectra about photosystem II (PSII) excited with different wavelengths (436,474 and 510 nm) at room temperature.

Group	436 nm excitaion		473 nm xcitaion		510 nm excitaion	
	Center (nm)	Area (10×10^5 nm^2)	Center (nm)	Area (10×10^5 nm^2)	Center (nm)	Area (10×10^5 nm^2)
CK	594.0	1.36	582.95	3.82	592.36	2.70
	673.8	1.00	646.50	0.78	626.42	0.24
	678.1	1.10	680.02	0.99	645.55	0.16
	730.1	0.26	693.98	1.34	674.72	0.46
					710.70	0.85
					764.30	0.30
CK+ UV-B$_{30min}$	599.9	6.55	585.83	2.85	592.02	1.89
	663.2	1.37	645.63	0.64	626.05	0.15
	678.3	0.82	680.15	0.68	644.20	0.16
	754.0	0.41	695.61	1.06	675.19	0.33
					704.96	0.74
					764.66	0.25
UV-B	598.4	1.46	579.67	4.16	596.58	0.34
	658.8	0.55	671.20	2.55	609.83	1.16
	678.7	3.57	680.53	1.76	647.01	10.16
	704.3	1.84	716.44	1.11	677.57	0.54
					697.71	0.46
					764.53	0.294

Excitation at 436 and 473 nm: Table 2 showed the Gaussian deconvolution results of fluorescence emission spectra obtained with excitation at 436 and 473nm,which were absorbed main by Chl *a* and *b*. That is to say, the excitation energy was absorbed initially by Chl moleculers. All the spectra can be fitted well by 4 Gaussian sub-bands. In Fig. 3, about 600 nm emission originated from LHCII. The peaks at 674, 663 and 659 nm was suggested to be emitted by Chl in core complex of PSII. The emission at 678 nm came from Chl *a* in RC. The 704, 730 and 754 nm emissions originated from Chl moleculars in LHCII.

30-min UV-B Group: The 436 nm excitation showed that after 30 min UV-B radiation, there occurred a peak shift from 594 to 600 nm in LHCII. In core antenna, the energy was accepted by shorter wavelength pigment-protein complex, *i.e.* Chl emission peak at 674 nm in CK was replaced by peak at 663 nm. What's more, the emission areas of photosystem sub-unit was changed. For instance, the emission area of LHCII decreased from 1.36×10^5 to 6.55×10^4. Therefore, not only pathways of energy transfer from Chl *a* were altered, the proportion of energy arrangement among subunit of PSII also changed by 30-min UV-B radiation.

There were not distinctive changes of emission peak position in CK+UV-B$_{30min}$ at 473 nm excitation, the results showed that the pathway of energy transfer from Chl *b* molecules were unchanged by 30-min UV-B radiation. Nevertheless, some changes were observed about emission areas.

UV-B group: Table 2 exhibited that the peaks position and emission areas were altered by 7-day UV-B exposure. For example, a blue-shift in the spectra from 673 nm in control to 658 nm in UV-B group was showed when excited with 436 nm, and the largest fluorescence emission proportion was at 678 nm by Chl *a* in RC instead of 594 nm came from LCHII in CK. When excited with 473 nm, in UV-B group, the presence of a 671 nm component was detected while it was not found in CK group, and the 646 nm component appeared in UV-B group. Compared to CK, the largest fluorescence emission proportion happened in LHCII. The emission area of RC was increased from 1.10×10^5 to 3.57×10^5 (436 nm excitation), and from 9.88×10^4 to 1.76×10^5 (473 nm excitation).

Excitation at 510 nm: Upon exciting the Car molecules (510 nm excitation), there were six Gaussian sub-bands were fitted from emission spectra. The emission wavelength short than 647nm were assignment to LHCII. The 675 and 678 nm emission came from core complex of PSII. The band width of 764 nm emission was 12 nm, it originated from few long-wavelength Chl *b*. The band of 698–710 nm maybe derived from core complex or PSII.

CK+UV-B$_{30min}$ group: The CK+UV-B$_{30min}$ group did not show obvious changes of energy transfer pathways, the significant effect of 30-min UV-B radiation observed from emission spectra was blue-shift from 711 nm to 705 nm in LHCII.

UV-B group: In UV-B group, the fluorescence maximum was shifted to longer wavelength (677 nm). Also, a blue-shift of the fluorescence band was observed in LHCII from 626 nm (CK) to 610 nm (UV-B). Moreover, the width and height of components in LHCII became less than that of CK. Obviously, due to the reorganization of pigment-proteins in LHCII, core antenna and reaction center under 7 day UV-B condition, there was distinct changes of energy transfer pathways.

Discussion

In higher plants, algae and cyanobacteria, the absorbed energy is transferred to the reaction centers, operating in series. The photochemical reaction is the major pathway of deactivation of the excitons (more than 90% of absorbed light energy). Fluorescence and thermal dissipation are the other ways to deactivate excitons, fluorescence representing only 0.3%–3% of the absorbed light (Bissati, 2000). Fluorescence can be a probe of the process of photosynthesis.

In order to investigate the effects of different kinds of UV-B treatment on excitation energy transfer between PSII, we examined the changes in the Chl fluorescence excitation and emission spectra in spinach. In the present study, 30 min UV-B radiation had significance effect on energy transfer process from Chl *a* and Car to other pigments in LHCII and core antenna, which could be displayed from changes of emission intensity, peak position, and emission area. Also, the energy flow to RC was decreased. For instance, the fluorescence intensity of PSII showed obviously quenching at almost whole wavelength range. Emission area of RC was decreased clearly (from 1.10×10^5 to 8.20×10^4 at 436 nm excitation, 9.88×10^4 to 6.83×10^4 at 473 nm excitation, and 4.58×10^4 to 3.25×10^4 at 510 nm excitation). It was unassailable that PSII was damaged by 30 min UV-B irradiation. We believed that some proteins in RC, such as D1/D2 proteins, were degraded by 30 min UV-B light. It has been accepted that one of the main defense responses to UV-B was the repair of PSII via *de novo* synthesis of D1/D2 proteins and the reassembly of repaired PSII centers (Vass *et al*., 2002; Xu and Qiu, 2007). Moreover, a low level of visible light was required for activity recovery of D1 protein, and further metabolism of the fragment requires factor(s) that are present in intact leaves or even in whole thylakoid (Bergo *et al*., 2003). In this study, the recovery of D1 protein was restrained for several reasons. Firstly, the spectrum measurement was performed immediately after PSII exposed to UV-B radiation for 30 minutes, and the whole process of measurement were conducted in darkness (lack the visible light), therefore, the factor for D1 protein recover is lack. Otherwise, the process of newly synthesized protein to replace the damaged D1 protein might be suppressed in such a short time. Secondly, our sample is only single PSII, not intact leaves or whole thylakoid, the recover process of D1 protein was further inhibited.

Besides the damage of D1/D2 protein, some other reason should be in charge of changes of fluorescence by 30 min UV-B, such as the weakening of the pigment-proteins bonds or the structural changes of the Chl *a* and Car molecules in PSII under UV-B condition. Ségui, *et al* had pointed that Chl displacements within the PSII complex caused by $UV_{280,}$ although a period of 15 to 30 min, might have a significant influence on the PSII function (Ségui *et al*., 2000). Santabarbara et al also had reported out that near 650 nm and more prominently in the 670–675 nm interval both Chl *b* and *a* seem to be involved in energetically weakly coupled, which might play a central role in photoinhibition (Santabarbara and Jennings, 2005).

In our study, fluorescence emission intensity of PSII was increased by 7 day UV-B exposure. It seemed that PSII was unmarred at this radiation condition. This result was contrary to some investigators (Lin *et al*., 2002). The most reasonable reason was related to UV-B radiation dose, growth condition of plants (in greenhouse or field) and development phase of the plants suffered from UV-B radiation. We performed a detailed analysis for the divergence (see below).

Development phase: In most of the investigations plants were exposed under enhanced UV-B radiation at seedling stage, at this time, acclimation ability of seedling photosystem was deficient, such as synthesis and degradation of Rubisco and aggregation of LHCII. Moreover, Rubisco synthesis was significantly suppressed by supplementary UV-B radiation at the transcription step during the early leaf stages (Takeuchi *et al*., 2002). Deficiency of Rubisco and aggregate of LHCII can influence process of energy transfer in photosystem, especially the dissipation process of excess energy which would bring on

damage to RC. If damaged RC could not be recovered in time, photosynthesis will be inhibited. Nevertheless, in our study, supplementary UV-B was exposed to the mature plants, which have self-contained acclimation ability and enough time to acclimate. For this reason, fluorescence quenching was not observed in this study.

Growth condition: Some researchers have reported UV-B is an essential factor for the development of membrane stacking in chloroplasts. Yu *et al*. indicated that plant grown under visible light without supplementary UV-B radiation have poor grana development (Yu and Bjőrn, 1999), from this point, the process of photosynthesis in CK group (greenhouse, no UV-B) was influenced due to lack of well developed grana. In relative terms, grana of the UV-B group were normally developed to guarantee photosynthesis, thus the group of UV-B showed higher emission than that of CK group.

UV-B radiation dose: Another reason for fluorescence increase in our study is that more and more recent studies have illustrated that UV-B radiation cause inhibition of photosynthesis only at higher UV-B radiation levels (Shi *et al*., 2004). In our experiment, the level of UV-B radiation was lower than many other researchers (Xiong 2001; Feng *et al*., 2003), as a kind of weak stress, low level UV-B radiation stimulated the photosystem progress.

Under the condition of 7 day UV-B exposure, plant redeployed valid mode to reduce the damage to photosystem. For example, photosystem redeployed the pigments absorbing shorter wavelength to take part in the energy transfer. Besides, changes of emission intensity, peak position, and emission area at different excitation demonstrated that energy transfer pathways in photosystem were regulated full-scale to resist the UV-B stress by rearranged the position of Chl *a*, *b* and Car molecules in LHCII, core antenna and RC.

In our study, PSII had displayed different performance under two kinds of UV-B treatments. the PSII was damaged by 30 min radiation obviously, even the dose of 30 min radiation was about a third less than that of 7 day UV-B. The results demonstrated that most of enhanced UV-B radiaion was screened by mature plant to protect PSII for guarantee the process of photosynthesis. It has been widely accepted that ultraviolet absorption compounds, mainly flavonoids in leaf epidermis played a important role in this process (Staaij *et al*., 1995).

Conclusion

A lot of researches have showed that an important criteria for adaptation of the organisms is the ability to overcome damage caused by various environmental hazards such as increased UV-B radiation in sunlight. From present study, we concluded that when mature plant exposed to low radiation dose UV-B radiation, photosystem could alters energy transfer process in antenna system via reorganizes the position or distance of pigment-protein complex in units of PSII to reduce damnification to RC for guarantee the process of photosynthesis.

Acknowledgments

This study was supported by the National Nature Science Foundation of China (No. 30670366) and Innovation Foundation of Northwest University (No. 07YJC14).

References

Baker NR, Rosenqvist E (2004) Applications of Chlorophyll Fluorescence Can Improve Crop Production Strategies: an Examination of Future Possibilities. J Exp Bot. 55: 1607-1621

Bissati KE, Delphin E, Murata N, Etienne AL, Kirilovsky D (2000) Photosystem II Fluorescence Quenching in the Cyanobacterium Synechocystis PCC 6803: Involvement of Two Different Mechanisms. Biochim et Biophys Acta. 1457: 229-242

De Weerd FL, Palacios MA, Andrizhiyevskaya EG, Dekker JP, van Grondelle R (2002) Identifying the Lowest Electronic States of the Chlorophylls in the CP47 Core Antenna Protein of Photosystem II. Biochemistry 41: 15224-15233

Du LF (1995) Preparation and Storage of PS II Particles with High Oxygen-Evolution Activity. Plant Physio Commun. 31: 212-215 (in Chinese)

Feng HY, An LZ, Chen T, Qiang WY, Xu SJ, Zhang MX, Wang XL (2003) The Effect of Enhanced Ultraviolet-B Radiation on Growth, Photosynthesis and Stable Carbon Isotope Composition (δ13C) of Two Soybean Cultivars (Glycine Max) under Field Condition. Environ Exp Bot. 49: 1-8

Fiscus EL, Booker FL (1995) Is Increased UV-B a

Threat to Crop Photosynthesis and Productivity? Photosynth Res. 43: 81-92

Gopal R, Mishra KB, Zeeshan M, Prasad SM, Joshi MM (2002) Laser-Induced Chlorophyll Fluorescence Spectra of Mung Plants Growing under Nickel Stress. Curr sci. 83: 880-884

Hulsen K, Top EM, Hofte M (2000) Biodegradation of Linuron in a Phaseolus Bioassay Detected by Chlorophyll Fluorescence. New Phytol. 154: 821-829

Larkum AWD, Karge M, Reifarth F, Eckert HJ, Post A, Renger G (2001) Effect of Monochromatic UV-B Radiation on Electron Transfer Reactions of Photosystem II. Photosynth Res. 68: 49-60

Lin WX, Wu XC, Liang YY, Chen FY, Guo YC (2002) Effects of Enhanced UV-B Radiation Stress on Kinetics of Chlorophyll Fluorescence in Rice (Oryza Sativa L.). Chinese J Eco-Agr. 10: 8-12 (In Chinese, with English abstract)

Liu XL, Xu SM, Woo KC (2005) Solar UV-B Radiation on Growth, Photosynthesis and the Xanthophyll Cycle in Tropical Acacias and Eucalyptus. Environ Exp Bot. 54: 121-130

Liu Zf, Yan HC, Wang KB, Kuang TY, Zhang JP, Gui LL, An XM, Chang WR (2004) Crystal Structure of Spinach Major Lightharvestingcomplex at 2.72Å Resolution, Nature 428: 287-292

Marwood CA, Greenberg BM (1996) Effect of Supplementary UV-B Radiation on Chlorophyll Synthesis and Accumulation of Photosystems during Chloroplast Development in Spirodela Oligorrhiza. Photochem Photobiol. 64: 664-670

Mishra KB, Gopal R (2005) Study of Laser-Induced Fluorescence Signatures from Leaves of Wheat Seedlings Growing under Cadmium Stress. Gen Appl Plant Physiol. 31: 181-196

Pettai H, Oja V, Freiberg A, Laisk A (2005) The Long-Wavelength Limit of Plant Photosynthesis. FEBS Lett. 579: 4017-4019

Prabha GL, Kulandaivelu G (2002) Induced UV-B Resistance Against Photosynthesis Damage by Adaptive Mutagenesis in Synechococcus PCC 7924. Plant Sci. 162: 663-669

Santabarbara S, Jennings RC (2005) The Size of the Population of Weakly Coupled Chlorophyll Pigments Involved in Thylakoid Photoinhibition Determined by Steady-State Fluorescence Spectroscopy. Biochim et Biophys Acta. 1709: 138-149

Ségui JA, Maire V, Gabashvili IS, Fragata M (2000) Oxygen Evolution Loss and Structural Transitions in Photosystem II Induced by Low Intensity UV-B Radiation of 280 nm Wavelength. J Photoch Photobio B: Biology. 56: 39-47

Shi SB, Li WY, Hui M, Zhou DW, Han F, Zhao XQ, Tang YH (2004) Photosynthes of Saussurea Superba and Gentiana Straminea Is Not Reduced after Long-Term Enhancement of UV-B Radiation. Environ Exp Bot. 51: 75-83

Sprtova M, Nedbal L, Marek MV (2000) Effect of Enhanced UV-B Radiation on Chlorophylla Fluorescence Parameters in Norway Spruce Needles. J plant physiol. 156: 234-241

Szilárd AL, Deáka Z, Vass I (2007) The Sensitivity of Photosystem II to Damage by UV-B Radiation Depends on the Oxidation State of the Water-Splitting Complex. Biochim et Biophys Acta. 1767: 876-882

Takeuchi A, Yamaguchi T, Hidema J, Strid A, Kumagai T (2002) Changes in Synthesis and Degradation of Rubisco and LHCII with Leaf Age in Rice (Oryza Sativa L.) Growing under Supplementary UV-B Radiation. Plant Cell Environ. 25: 695-706

Van De Staaij JWM, Ernst WHO, Hakvoort HWJ, Rozema J (1995) Ultraviolet-B (280−320 nm) Absorbing Pigments in the Leaves of Silene Vulgaris: Their Role in UV-B Tolerance. J Plant physiol. 147: 75-80

Van Rensen JJS, Vredenberg WJ, Rodrigues GC (2007) Time Sequence of the Damage to the Acceptor and Donor Sides of Photosystem II by UV-B Radiation As Evaluated by Chlorophyll a Fluorescence. Photosynth Res. 94: 291-297

Vasil'ev S, Orth P, Zouni A, Owens TG, Bruce D (2001) Excited-State Dynamics in Photosystem II: Insights from the X-Ray Crystal Structure. PNAS. 98: 8602-8607

Vass I, Turcsanyi E, Touloupakis E, Ghanotakis D, Petrouleas V (2002) The Mechanism of UV-A Radiation-Induced Inhibition of Photosystem II Electron Transport Studied by EPR and Chlorophyll Fluorescence. Biochem J. 41: 10200-10208

Schmid VHR, Thomé P, Rühle W, Paulsen H, Kühlbrandt W, Rogl H (2001) Chlorophyll b Is Involved in Long-Wavelength Spectral Properties of Light-Harvesting Complexes LHC I and LHC II. FEBS Lett. 499: 27-31

Wen XG, Gong HM, Lu CM (2005) Heat Stress Induces an Inhibition of Excitation Energy

Transfer from Phycobilisomes to Photosystem II but Not to Photosystem I in a Cyanobacterium Spirulina Platensis. Plant Physiol Bioch. 43: 389-395

Xiong FS (2001) Evidence that UV-B Tolerance of the Photosynthetic Apparatus in Microalgae Is Related to the D1-Turnover Mediated Repair Cycle in Vivo. J Plant Physiol. 158: 285-294

Xu K, Qiu BS (2007) Responses of Superhigh-Yield Hybrid Rice Liangyoupeijiu to Enhancement of Ultraviolet-B Radiation. Plant Sci. 172: 139-149

Yu SG, Bjőrn LO (1999) Ultraviolet B Stimulates Grana Formation in Chloroplasts in the African Desert Plant Dimorphotheca Pluvialis. J Photochem Photobio B Biol. 49: 65-70

Shape-Changes of the Fast Chlorophyll *a* Fluorescence Transient (OJIP) and Antioxidative Enzymes in High Salt Tolerant Mangrove Trees of *Bruguiera Gymnorrhiza*

Ananth Bandhu Das[1], Reto J Strasser[2], Girish Kumar Rasineni[3], Prasanna Mohanty[1*3]

[1]Department of Agricultural Biotechnology, Orissa University of Agriculture and Technology, Bhubaneswar-751003, India, E-Mail: abdas@hotmail.com.
[1* 3]INSA Senior Scientist, Department of Agricultural Biotechnology , OUAT, Bhubaneswar-751003, India. E-Mail: photosis@rediffmail.com.
[2]Bioenergietic Laboratory, University of Geneva, CH-1254, Jussy-Geneva, Switzerland, E-Mail: Reto.Strasser@unige.ch.
[3]Department of Plant Sciences, University of Hyderabad, Hyderabad-500046, India. E-Mail : rasinenigirish@gmail.com.

Abstract: True Mangrove trees of the costal habitats are now threaten of extinction because of climate change linked to global warming, sea level raise and fluctuating salinity. The key adaptation ability of the true tree mangroves having no salt secreting gland to survive in water logged high salt and anoxic condition seems to be shedding of lower leaves. The detailed mechanism of survival from high salt stress in this sea-shore mangroves is not known. We have examined the high salt stress effect in *Bruguiera gymnorhiza* a true tree mangrove in this study. Hydroponic culture of three months old nursery raised seedlings on *B. gymnorizha* were treated in 500 mmol NaCl (high salt) for 7 and 45 days. Both fast chlorophyll transients as well as the specific activity of key antioxidative enzymes were monitored to characterize the recovery potential of this mangrove from salt stress.

Keywords: *Bruguiera gymnorhiza*; True tree mangroves; Antioxidant enzymes; OJIP-Chl Fluorescence transients

Introduction

The mangroves of costal habitats are endangered species because of a variety of anthropogenic activities. The costal mangroves possess unique abilities to tolerate high salinity as well as fluctuating salt concentration because of flooding, anoxic, varying light intensities, heavy metal ion accumulation at the root surface etc (Ball, 1986; Hogorth, 1999). In view of the rapid fluctuation of stress condition particularly like high salt in the tidal regions of the costal habitats, fluctuating light intensities, and other stress situations, these mangroves offer ideal test material for study on stress impairment and recovery. Many crop plants especially rice face similar fluctuating stress conditions (Das *et al*., 1997; Lee *et al*., 2001).

In the coastal regions of India such as the eastern coasts have mangrove forests with abundance of true mangroves and mangrove associates (Das *et al*., 1997; Mishra and Das, 2003; Parida *et al*., 2004). Six species of the Bruguiera, the typical non salt secreting true mangroves are available in these areas (Das *et al*., 1997). B. gymnorhiza has been shown to tolerate very high salt concentrations (Okinawa). The high tolerant limit of Bruguiera occurring in coastal regions of India has not been investigated fully. Fast chl *a* fluorescence transients represent a vital physiological performance of plants particularly for monitoring stress effects (Papageorgiou and Govindjee, 2004). The OJIP tests are now used for the study of salinity sensitivity and resistance of genotypes (Lange *et al*., 1987). Furthermore the changes in the specific activities of some key antioxidant enzyme like catalase, peroxidase, Superoxide dismutase (SOD) have been shown to be stress liked enzymes (Parida *et al*., 2004; Jitesh *et al*., 2006). A correlation study of fast chlorophyll *a* fluorescence changes and antioxidative enzymes in high salt stress condition as well as recovery would provide valuable information on salt tolerant strategies adopted by plants. In this study we have demonstrated that recovery from high salt stress offers a useful screening technique to estimate the upper limits of salt tolerance in plants.

Materials and Methods

Propagules of *B. gymnorrhiza* (BG) were collected from the mangrove forest of Paradeep and Bhitarkanika deltas of Orissa, India (latitude; longitude 86°45'E to 87°50'E). Seedlings were raised in a greenhouse under PAR of 677 to 1,040 µmole m^{-2} s^{-1}, and were watered with non-saline and non-brackish water (Parida *et al*., 2005). Three months old, healthy seedlings were used for hydroponics culture in full strength Hoagland's nutrient medium. These cultures were aerated continuously and were maintained in a growth chamber at 22 ± 2 °C, 80% RH, 14 h photoperiod, and a light intensity of 300 µmol m^{-2} s^{-1}. 500 mmol NaCl concentration was found to be upper limit and this concentration was chosen as upper salt concentration for investigating short-term effect of salinity. All the hydroponics cultural practice was maintained as described earlier.

SDS-PAGE protein profiles of thylakoids

Total thylakoid protein was extracted following acetone-TCA precipitation method and protein sample containing 40 µg of protein were loaded in a 12.5% gel.

Extraction and assays of antioxidative enzymes

Preparation of enzyme extract 1 g of leaf were homogenized with pre-chilled mortar and pistil with 2 ml of 50 mmol potassium phosphate buffer (pH 7.0), 1mmol EDTA, 1 mm D-isoascorbic acid, 2%(w/v) PVP (polyvinyl polypyrrolidone) and 0.05%(w/v) Triton X-100 following the procedure of Gossett *et al*. (1994). The homogenate was centrifuged at 10,000 x g for 10 min at 4 °C. The supernatant were collected and used for the assay of catalase (CAT), ascorbate peroxidase (APX) and guaicol peroxidase (GPX).

Assay of catalase (CAT) (EC 1.11.1.5) Catalase activity was determined spectrometrically by following the rate of H_2O_2 disappearance at 240 nm. A coefficien ε of 43.6 $mol^{-1}cm^{-1}$ was used at 240 nm. The reaction mixture contains 50 mmol potassium phosphate (pH 7.0), 10.5 mmol H_2O_2 and the enzyme extract containing 20 mg of protein. The reaction was run at 27 ºC for 2 min and an initial liner rate of decrease was used to calculate the activity. The reaction was started by addition of enzyme extract (Parida *et al*., 2004).

Assay of ascorbate peroxidase (APX) (EC 1.11.1.11) APX was assayed at 25 °C as described by the method of Nakano and Asada (1981). The reaction mixture contains 50 mmol potassium phosphate (pH 7), 0.2 mmol EDTA 0.5 mmol ascorbic acid and 0.25 mmol H_2O_2. The reaction was started with the addition of H_2O_2. After adding the enzyme extract containing 50 µg of protein. The decrease in absorbance at 290 nm for 1 min was recorded and the amount of Ascorbate oxidized was calculated from the extinction coefficient 2.8 mole/lit/cm (Mishra and Das, 2003).

Assay of guaiacol peroxidase (GPX) (EC. 1.11.17) GPX activity was measured spectrometrically at 25 °C. The reaction mixture (2 ml) consisted of 50 mmol potassium phosphate (pH 7.0), 2 mmol H_2O_2, and 2.7 mmol guaiacol. The reaction was started by the addition of an enzyme extract equivalent to 5 µg protein. The formation of tetra guaiacol was measured at 470 nm (ε = 26.6 mmol/cm) (Parida *et al*., 2004).

OJIP Transient and JIP-Test Chlorophyll a fluorescence induction kinetics (Strasser *et al*., 2004) were measured on fully dark adapted (1 h) attached leaves using a fluorimeter (Handy-PEA, Hansatech Instruments Ltd., Kingslynn, UK). The fluorescence transients were analysed according to the JIP-test (Strasser *et al*., 2004). A multi-parametric expression the so called photosynthetic performance index (PI total) of the four independent functional steps of photosynthesis was used (Strasser *et al.*, 2010).

Results and Discussion

Biochemical studies

Three months old *B gymnorhiza* seedlings were treated in 500 mmol NaCl for 7, 15, and 45 days. Salt treated plants were removed and kept for recovery in normal Hoagland solution for 7 days.

Earlier studies have shown that salt stress affects the levels of bio-molecules as well as total leaf and thylakoid proteins by different concentration of salt (Parida *et al*., 2004; Mishra and Das, 2003). Exploratory studies revealed that B gymnorhiza seedlings would remain healthy for more than 6 weeks in 500 mmol salt concentrations. At 600 mmol the twigs shed their leaves exhibiting signs of senescence (Data not shown). Thus 500 mmol salt concentration was considered as a maximum limit of salt concentration, unlike Okinawa mangrove species of B gymnorrhiza of Japan exhibited ocean level of salt concentration (Takamura *et al*., 2000). The Fig. 1 shows proteins in the thylakoid isolated from *B. gymnorhiza* treated with 500 mmol NaCl. A large number of coomasie stained protein bands could be seen in the gel ranging from 97 KD to 5 KD. The seven days of salt treatment

could bring out differential reduction in protein bands noticeably CP43/CP47, D1/D2 occurred. After 15 days of salt treatment the effect was further enhanced and continued till 45 days. Upon removal of high salt treatment, the leaf thylakoid exhibited substantial recovery. However the extent of recovery seem to be more for CP43/CP47 and other low molecular weight proteins.

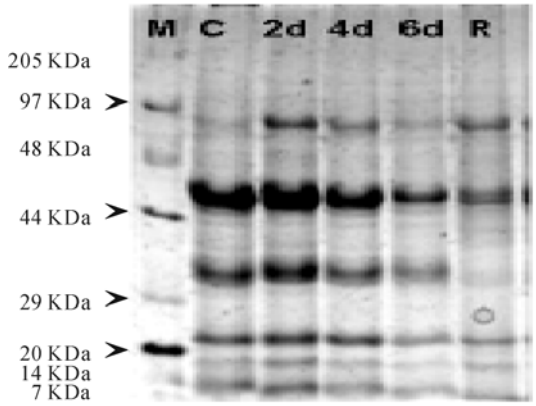

Fig. 1 Thylakoid protein profile of 500 mmol NaCl treated 3 months old *B. gymnorrhiza*; M- Molecular wt.marker, 7d, 15d, 21d, 45d treated, 15d Rerecovery.

Antioxidative enzymes are indicatives of salt stress in many glycophytes and halophytes (Lee *et al*., 2001; Jitesh *et al*., 2006). Comparative studies carried out earlier revealed that isoenzyme patterns of antioxidative enzymes such as catalase (EC 1.11.1.5), Ascorbate peroxidase (EC 1.11.1.11), guaiacol peroxidase (EC. 1.11.17) and SOD (EC 1.15.1.10) (Parida *et al*., 2004) (Figs. 2a, 2b and 2c).

Fig. 2 shows histochemical in-gel assays for four enzymes namely Ascorbate peroxidase, guaiacol peroxidate, catalase and superoxide dismutase as affected by 500 mmol salt stress for four different days. APX revealed reduction of activity level after 7 and 15 days of salt treatment but after 45 days the activity of this enzyme seems to be sustained, although the activity band of this enzyme was lower than the initial level. APX has been shown to be a good indicator of salt stress in *B. parviflora* (Parida *et al*., 2004). For the present result with *B. gymnorrhiza* we suggest that this enzyme is not a quantitative marker of salt stress (Fig. 2a).

Catalase which breaks down H_2O_2 that gets accumulated by oxidative stresses has different isoforms. In *B. gymnorrhiza* the assay of this enzyme exhibited four distinct isoforms. Among the four isoforms, isoform 3rd and 4th decreased progressively with the days of the treatment. Guaiacol peroxidase in contrast to catalase and APX exhibited enhanced activity. This enzyme contains 6 isoforms as revealed by in-gel assay, and of 6 bands 2nd and 6th showed marked increase (Fig. 2c).

SOD activity is linked to the stress mediated inhibition of PSII activity (Bjorkman and Demming, 1987). In the present study we observed that the activity of SOD showing 2 isoforms was enhanced with increasing period of 500 mmol salt treatment (Fig. 2d).

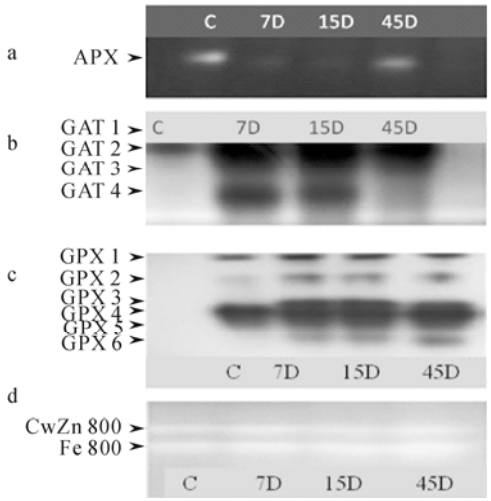

Fig. 2 Changes in antioxidant enzymes activity on different days of treatment in 500 mmol NaCl treatement.

Chl a florescence studies using Handy PEA

After prolonged treatment for 45 days the fluorescence induction curve was almost identical to that of the control suggesting high salt adaptive capacity of B. gymnorrhiza. There was no significant change in the chlorophyll content by 500 mmol NaCl.

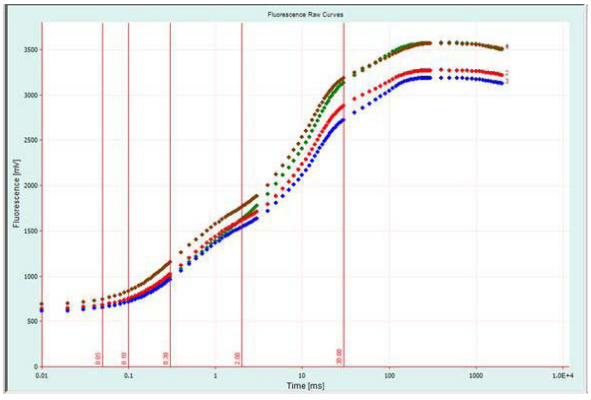

Fig. 4 NaCl shock stress effect on B. gymnorrhiza as averaged fast chl a fluorescence raw OJIP transients. Fluorescence intensities from top to bottom at I step (30 ms): control, similar to 45 days, then 7 days, then 15 days of salt treatment.

Conclusions

The 7 days of shock given hydroponically affects the shape of the OJIP transient, affecting therefore the Qa reduction seen in the O to J phase and subsequent steps J to P. Prolonged exposure to high salt appears to establish the plants function close to initial conditions. Within 7 days of salt removal the oxidative stress level gets relieved. Anti oxidative profiles showed that marker isoforms concentration change by salt shock adjustments.

Acknowledgments

The financial assistance of Council of Scientific and Industrial Research, New Delhi (38(1123)/EMR-II) to ABD and INSA to PM is thankfully acknowledged. The authors acknowledge the financial support of their granting agencies and helpful assistance and encouragement of colleagues in Hyderabad, Bhubaneswar, India. PM is grateful to CCSTDS, Chennai and Indian National Science Academy, New Delhi, India.

References

Ball MC (1986) Photosynthesis in Mangroves. Wetlands (Aust.) 6: 12-22

Björkman O, Demming B (1987) Comparison of the Effect of Excessive Light on Chlorophyll Fluorescence (77 K) and Photon Yield of O_2 Evolution in Leaves of Higher Plants. Planta 171**:** 171-184

Das P, Basak UC, Das AB (1997) Restoration of Mangrove Vegetation in Mahanadi Delta of Orissa. India, Mangroves and Salt Marshes 1: 155-161

Hernandez J, Jimenez A, Mullineaux P, Sevilla F (2000) Tolerance of Pea Plants(Pisum Sativum) to Long Term Salt Stress Is Associated with Induction of Antioxidant Defences.Plant Cell Environ 23:853-862

Hogorth PJ (1999) The Biology of Mangroves. Oxford University Press, New York

Jitesh MN, Prashanth SR, Sivaprakash KR, Parida AK (2006) Antioxidant Response Mechanism in Halophytes Their Role in Stress Defense. J. Genetics 85: 237

Lee DH, Kim YS, Lee CB (2001) The Inductive Response of the Antioxidant Enzymes by Salt Stress in the Rice (Oryza Sativa L.). J Plant Physiol. 158: 737-745

Mishra S, Das AB (2003) Effect of NaCl on Leaf Salt Secretion and Antioxidant Enzyme Level in Root of a Mangrove, Aegiceras Corniculatum. Indian J. Expt. Biol. 41: 160

Parida AK, Das AB, Mohanty P (2004) Defense Potential to NaCl in a Mangrove, Bruguiera Parviflora: Changes of Isoforms of Some Antioxidative Enzymes. J. Plant Physiol. 161: 531-542

Parida AK, Mittra B, Das AB, Das TK, Mohanty P (2005) High Salinity Reduces the Content of a Highly Abundant 23kDa Protein of the Mangrove, Bruguiera Parviflora

Papageorgiou G, Govindjee (2004) Chlorophyll a Fluorescence a Signature of Photosynthesis, Advances in Photosynthesis and Respiration, Vol. 19. Springer: Dordrecht, the Netherlands

Strasser RJ, Srivastava A, Tsimilli-Michael M (2004) Analysis of the Chlorophyll Fluorescence Transient. In: Papageorgiou G, Govindjee XUC (eds.), Chlorophyll Fluorescence a Signiture of Photosynthesis. Kluwer Press: NL , 19: 321-362

Takamura T, Hangata, N, Sugihara K, Dubinsky Z, Baba S, Karube I (2000) Physiological and Biochemical Response to Salt Stress in the Mangrove, Bruguiera Gymnorrhiza. Aqat Bot. 68: 15-28

Knock-out of Low CO_2-Induced *slr0006* Gene in *Synechocystis* sp. PCC 6803: Consequences on Growth and Proteome

Dalton Carmel, Natalia Battchikova, Maija Holmström, Paula Mulo, Eva Mari Aro*

Molecular Plant Biology, Department of Biochemisty and Food Chemistry, University of Turku, FIN-20520 Turku, Finland.
*Corresponding author. Tel. No. +358 2 333 8071; Fax No. +358 2 3338075; E-mail: evaaro@utu.fi.

Abstract: *Synechocystis* sp. PCC 6803 responds to carbon starvation by inducing several genes which are involved in the uptake of inorganic carbon (Ci). Previous transcriptomics and proteomics studies indicate that *slr0006* is one of the genes highly upregulated under air level CO_2. We describe here the construction of the Δ*slr0006* mutant and its characteristics in different environmental conditions as well as its proteome profile under air level CO_2. Although Slr0006 is strongly induced under any conditions leading to Ci starvation, the phenotype and autotrophic growth of Δ*slr0006* did not differ from those of the control strain even upon exposure of the cell to stress. Quantitative proteomics analysis revealed novel proteins encoded both by plasmids and chromosome of *Synechocystis* which might function in the same pathway as Slr0006 to sequester Ci during CO_2 limitation.

Keywords: CO_2; DIGE; NDH-1; pH; *Slr0006*; *Synechocystis* sp. PCC 6803

Introduction

The unicellular cyanobacterium *Synechocystis* sp. PCC 6803 (hereafter *Synechocystis*) is a fresh water unicellular cyanobacterium performing oxygenic photosynthesis. Like other cyanobacteria, *Synechocystis* responds to CO_2 limitations by activating carbon concentrating mechanisms (CCM) which promote accumulation of high concentration of intracellular inorganic carbon (Ci). Ci is accumulated as bicarbonate and converted into CO_2 in the carboxysomes. CO_2, in turn, is utilized in the primary CO_2 fixation reaction by RuBisCO (Ogawa andKaplan, 2003).

The comprehensive effect of Ci starvation has been well studied in *Synechocystis* at mRNA level (Wang *et al*., 2004; Eisenhut *et al*., 2007). It has been shown that the expression of the genes coding for the CCM components responds quickly to the CO_2 limitation (McGinn *et al*., 2003). Major changes include drastic upregulation of the NDH-1MS complex located in the thylakoid membrane, two bicarbonate transporters, SbtA and BCT-1 present in the plasma membrane, RuBisCO and components of the carboxysome shell. Concomitantly, the transport and assimilation of nitrogen is down-regulated in order to maintain the proper carbon-nitrogen balance.

Several genes encoding proteins with unknown functions are upregulated upon CO_2 starvation and therefore might be involved in the low CO_2 acclimation process. Among them, the *slr0006* gene demonstrates significant upregulation both at mRNA and protein levels (Battchikova *et al*., 2010b). In the present study we have constructed and characterized a knock-out mutant for *slr0006* gene. The performance of the mutant strain was similar to the control strain during normal growth and in some stress conditions including CO_2 limitation. Although the *slr0006* deletion can be compensated by other mechanisms, apparently the long term growth of the mutant cells under low CO_2 level results in the induction of several genes located in the plasmids of *Synechocystis*.

Materials and Methods

Control and mutant cells of *Synechocystis* were grown at 30 °C in BG-11 medium (Rippka, 1988) buffered either with 20 mmol HEPES-NaOH, pH 7.5, or TES-KOH, pH 8.3. Cells were grown in flasks shaken at 110 rpm, in 3% CO_2 (high-CO_2 conditions,

HC) or in air (low-CO_2 conditions, LC), under continuous light (50 µmol photons m^{-2} s^{-1}). For selection and segregation of the *slr0006* mutant, 50 µg mL^{-1} kanamycin was added to the growth medium. Growth media for the mutant strains were supplemented with appropriate antibiotics (Ohkawa *et al*., 2000; Shibata *et al*., 2002; Foleaa *et al*., 2008). However, for experiments, the cells were grown without antibiotics.

Glucose-tolerant *Synechocystis* was used to generate the *slr0006* mutant where part of the gene encoding the N-terminus of the protein was replaced by kanamycin resistance cassette (Fig. 1a). The upstream and downstream genomic regions were amplified by PCR using Phusion Hot Start DNA polymerase (Finnzymes) and primers (5'-3'): 1) ACG GTC GAA GCT TCT GTA ACT GAC TTG ATT TGC CT; 2) GTA GCC GTC GAC TGA ATT GTC CCT TGA AAC TGC CT; 3) GTA GCT GTC GAC GCA ATG CCT TTT CCC TTG GTT T; 4) TTA AGC TAT TTG TCT AGG TCT TGA . The restriction sites for HindIII (primer 1) and SalI (primers 2 and 3) are underlined. PCR was followed by restriction digestion with HindIII/SalI (the upstream fragment) and SalI/EcoRI (the downstream fragment). The digested fragments were cloned into pUC18 vector, linearised with SalI and EcoRI, by triple ligation method. Further, the kanamycin resistance cassette from pUC4Kan vector (Taylor, 1988) was inserted into the SalI site. The plasmid with the direct orientation of Km^r was used to transform *Synechocystis* cells according to (Zang *et al.*, 2007). The complete segregation of the *slr0006*: Km^r strain (hereafter Δ*slr0006*) was verified using primers 1 and 4 (Fig. 1b).

Total proteins from *Synechocystis* cells were isolated according to (Herranen *et al.*, 2004). 10 µg of total proteins were separated by using 12.5% SDS-PAGE with 6 mol urea (Laemmli, 1970). For immunoblotting, the proteins were electro-transferred to PVDF membrane (Immobilon P, Millipore) and detected by ECL™ western blotting detection kit (GE Healthcare) after probing with Slr0006 antibody (Innovagen).

For Differential in Gel electrophoresis (DIGE) quantitation, cells were continuously grown in batch culture under air level CO_2. The total protein was isolated by breaking the cells with glass beads (150–212 microns; Sigma) in the buffer containing 30 mmol Tris-HCl pH 8.8, 8 mol urea, 2 mol thiourea and 4% CHAPS. 50 µg of protein from control strain and Δ*slr0006* were labelled using CyDye DIGE Fluor minimal dyes (GE Healthcare) according to the Ettan™ 2D DIGE protocol. The pooled, labelled proteins were focused in 18-cm pH 3–11NL IPG strips using Ettan™ IPGphor™ IEF system (GE Healthcare). The focused proteins were reduced with 2% DTT in the buffer containing 50 mmol Tris-HCl pH 8.8, 6 mol urea, 30% glycerol and 10% SDS, for 15 min, and further alkylated with 2.5% iodoacetamide in the same buffer, for 15 min. SDS-PAGE in the second dimension was performed using Protean II 2D cell (Bio-Rad) and low fluorescence glass plates (Jule Inc.). Image acquisition was carried out using Geliance 1000 imaging system (Perkin Elmer) and the images were analysed using ProFINDER2D software (Perkin Elmer). Identification of proteins was performed by electrospray ionization tandem MS (ESI MS/MS) as in (Battchikova *et al*., 2005).

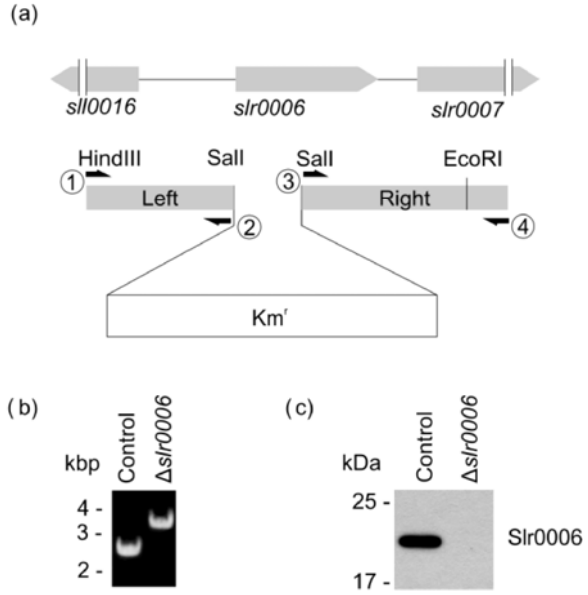

Fig. 1 Construction of deletion mutant for *slr0006* gene (a) Part of N-terminus of *slr0006* gene was replaced with kanamycin cassette (Km^r) by PCR mediated cloning method. The arrows indicate primers used to amplify left (974 bp) and right (1,196 bp) flanking regions '(b) PCR analysis of control strain and Δ*slr0006*. The primers 1 and 4 were used to verify segregation (c) The amount of Slr0006 in the control and Δ*slr0006* strains. 5 µg of total proteins were separated by SDS-PAGE and analyzed by standard western blotting using Slr0006 antibody.

Results and Discussion

To understand the functional role of the Slr0006

protein, a knock-out mutant for *slr0006* gene was constructed by replacing the part of *slr0006* ORF (coding for 132 N-terminal amino acids) with the kanamycin resistance cassette. The segregation was verified by PCR analysis of chromosomal DNA using primers 1 and 4 (Fig. 1a). Comparison of PCR products (3.4 Kbp for Δ*slr0006* and 2.5 Kbp for the control strain) confirmed that the Δ*slr0006* strain was completely segregated (Fig. 1b). Further, the absence of the Slr0006 protein in mutant was confirmed by western blotting. The Slr0006 antibody recognized a single band of ca. 20 kDa in the total protein extract of control strain while no signal could be detected in Δ*slr0006* (Fig. 1c).

To study the effect of *slr0006* inactivation on the growth of the cells upon standard (50 µmol photons m^{-2} s^{-1}) and high light (250 µmol photons m^{-2} s^{-1}) conditions under air level CO_2, the A_{750} of the cells was set to 0.1, 0.01 and 0.001, and 5 µL of cell culture was pipetted on BG-11 plates (pH 7.5). Fig. 2 shows that interruption of *slr0006* gene had no visible effect on the phenotype or on the autotrophic cell growth indicating that the *slr0006* gene is not essential for cell survival.

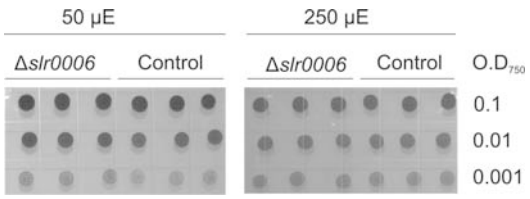

Fig. 2 BG-11 agar plates showing the effect of growth light (50 µE) and high light (250 µE) on the growth of control and Δ*slr0006* strains under low CO_2 with different cell concentration.

Induction of a specific CCM may vary in cells in response to pH of the growth medium. In aquatic systems, HCO_3^- is the major form of available Ci, particularly when pH rises. In contrast, CO_2 is the dominant form of Ci under acidic pH (Badger *et al*., 2006)**.** To test the expression of the Slr0006 protein in acidic and alkaline conditions, the control strains were grown in standard medium in 3% CO_2 until $O.D_{750}$ = 0.8–1.0, followed by centrifugation and resuspension in fresh BG-11 ($O.D_{750}$ = 0.8) buffered with either 20 mmol MES-KOH, pH 6.0, or 20 mmol CHES-KOH, pH 9.0. The growth continued at air level CO_2 for 72 hours. Western blotting demonstrated that the amount of Slr0006 was higher in cells grown in acidic condition (Fig. 3).

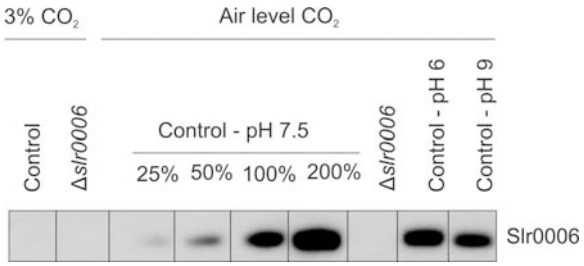

Fig. 3 Amount of Slr0006 at different pH.
Western blot analysis of total protein from the control strain and Δ*slr0006* under high CO_2 and 72 h after shift to air level CO_2 at pH 6 and pH 9.

This result suggests that Slr0006 may be involved rather in CO_2 sequestration than in bicarbonate uptake. To assess whether the source of carbon affects the growth, the control and mutant cells were continuously grown in acidic and alkaline conditions as described above at low air level CO_2 for 10 days. Fig. 4 shows that the Δ*slr0006* strain grew with the same growth rate as the control strain at both pH values.

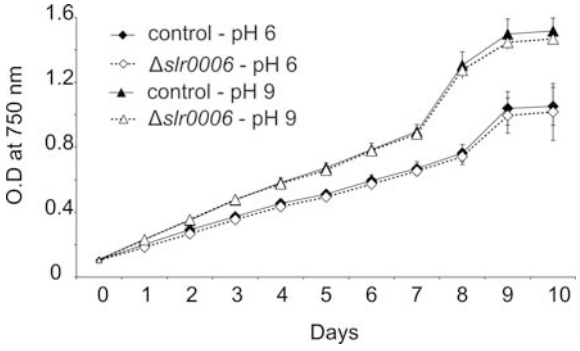

Fig. 4 Growth curve of the control strain and Δ*slr0006* at pH 6 and pH 9 under low CO_2.

Further, the availability of CO_2 is determined by the temperature: less CO_2 is available in BG-11 under high temperature than under low temperature (Tuominen *et al*., 2008). To test the expression of the Slr0006 protein at high and low temperature, the control and mutant cells were grown in standard medium in 3% CO_2 until $O.D_{750}$ = 0.8, precipitated and resuspended in fresh BG-11. The growth continued in low-CO_2 conditions either at 30 °C, 37 °C or 22 °C for 72 h. Equal amounts of cells were harvested, and total protein fractions were analysed by western blotting. Fig. 5 shows that although no distinct differences in the amount of Slr0006 could be detected between the control and high temperature-treated cells, the exposure to low temperature apparently prevents the expression of the *slr0006* gene.

These results support the hypothesis that CO_2 is the primary Ci source required for the induction of the *slr0006* gene.

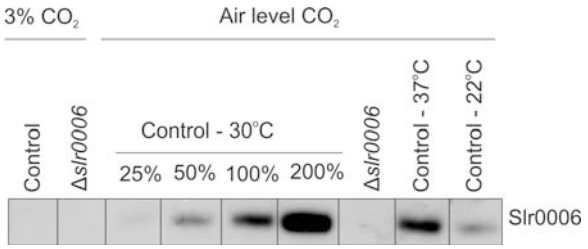

Fig. 5 Effect of high and low temperature on the expression of Slr0006.
Western blot analysis of total protein from the control strain and Δ*slr0006* under high CO_2 and air level CO_2 at temperature 37 ^{o}C and 22 ^{o}C.

To test the hypothesis that Slr0006 cooperates with some of known CCMs, we analyzed the expression of the protein in several CCM mutants. Two major CO_2 uptake systems, NDH-1MS and NDH-1MS', operate in *Synechocystis*. NDH-1MS system is induced under low CO_2 conditions, while the NDH-1MS' complex is constitutively expressed (Battchikova *et al*., 2010a). Apart from the activity and core subunits, which are shared between these complexes, the NDH-1MS complex contains NdhD3, NdhF3, CupA and CupS subunits, whereas the NDH-1MS' complex contains NdhD4, NdhF4 and CupB proteins. Further, in *Synechocystis* one of the essential components of bicarbonate transport is SbtA, which is highly upregulated under CO_2 limitation (Shibata *et al*., 2002). Western blot analysis of the *Synechocystis* Δ*ndhD3,* Δ*ndhD4,* Δ*cupA,* Δ*cupA*/Δ*cupB* and Δ*sbtA* strains revealed that the level of Slr0006 is similar between the control and mutant strains indicating that the upregulation of *slr0006* gene is not required to compensate the putatively impaired function of the studied CCM complexes (Fig. 6).

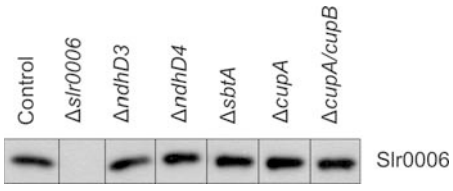

Fig. 6 Amount of the Slr0006 protein in different CCM mutants under low CO_2.
Western blot analysis shows the level of Slr0006 in different CCM mutants after 72 hours from high CO_2 to low CO_2 shift.

To understand the functional role of Slr0006, a global proteome analysis was carried out using DIGE. Solubilised proteomes of the control and Δ*slr0006* strains were labelled with Cy3 or Cy5. Cy2 was used as an internal standard to avoid gel-to-gel variations. The pooled samples were separated in 2D IEF/SDS-PAGE. The Cy3 and Cy5 images taken from each gel were virtually overlayed to study the difference between the control strain and Δ*slr0006* (Fig. 7).

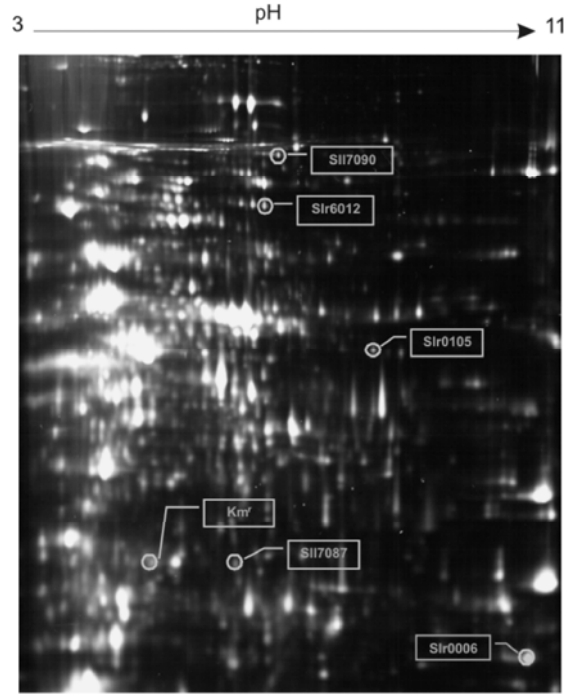

Fig. 7 The overlay image of Cy3-control and Cy5-Δ*slr0006*.
The box with ORF names indicates the differentially regulated proteins identified using mass spectromentry.

Five individual proteins were consistently down-regulated in Δ*slr0006* compared to the control strain. As expected, the Slr0006 protein was absent in the Δ*slr0006* strain (175-fold down-regulated). The level of down-regulation for other proteins (Slr0150, Sll6012, Slr7087 and Slr7090) was approximately 2-fold (Table 1). Slr0006 and Slr0150 are encoded by the *Synechocystis* chromosome, whereas the Slr7087, Slr7090 and Sll6012 are encoded by the pSYSA and pSYSX plasmids. The functions of these identified proteins are currently under study. The kanamycin resistance cassette was the only up-regulated protein detected in Δ*slr0006* as compared to the control strain.

Taken together, our results show that CO_2 might be the primary form of Ci responsible for induction of the *slr0006* gene, and that the *slr0006* gene is not essential for the cell survival. The knock-out of *slr0006* gene resulted in induction of several

uncharacterized plasmid-encoded genes. Functional characterisation of these unknown genes requires further studies.

Table 1 The down-regulated proteins in the Δ*slr0006* mutant discovered by the DIGE analysis. The fold change indicates the ratio of a protein in the Δ*slr0006* strain compared to the control strain. The value represents the average of three biological replicates.

ORF	Fold change	Location
Slr0006	-175.463	Chromosome
Slr0105	-2.372	Chromosome
Sll7087	-2.113	Plasmid - pSYSA
Sll6012	-2.342	Plasmid - pSYSA
Sll7090	-2.737	Plasmid - pSYSX

Acknowledgements

This study was financially supported by the Academy of Finland 118637 and the grant from the Maj and Tor Nessling Foundation.

References

Badger MR, Price GD, Long BM, Woodger FJ (2006) J. Exp. Bot. 57: 249-265

Battchikova N, Zhang PP, Rudd S, Ogawa T, Aro EM (2005) J. Biol. Chem. 280: 2587-2595

Battchikova N, Eisenhut M, Aro EM (2010a) Biochim. Biophys. Acta (in press)

Battchikova N, Vainonen JP, Vorontsova N, Keranen M, Carmel D, Aro EM (2010b) J. Prot. Res. 9: 5896-5912

Eisenhut M, Von Wobeser EA, Jonas L, Schubert H, Ibelings BW, Bauwe H, Matthijs HC, Hagemann M (2007) Plant Physiol. 144: 1946-1959

Foleaa M, Zhang PP, Nowaczykc MM, Ogawa T, Aro EM, Boekemaa EJ (2008) FEBS Lett. 582: 249-254

Herranen M, Battchikova N, Zhang PP, Graf A, Sirpio S, Paakkarinen V, Aro EM (2004) Plant Physiol. 134: 470-481

Laemmli UK (1970) Nature 227: 680-685

McGinn PJ, Price GD, Maleszka R, Badger MR (2003) Plant Physiol. 132: 218-229

Ohkawa H, Price GD, Badger MR, Ogawa T (2000) J. Bact. 182: 2591-2596

Ogawa T, Kaplan A (2003) Photosynth. Res. 77: 105-115

Rippka, R (1988) Methods Enzymol. 167: 3-27

Shibata M, Katoh H, Sonoda M, Ohkawa H, Shimoyama M, Fukuzawa H, Kaplan A, Ogawa T (2002) J. Biol. Chem. 277: 18658-18664

Taylor LA (1988) Nucleic Acids Res. 16 : 358

Tuominen I, Pollari M, Von Wobeser EA, Tyystjarvi E, Ibelings BW, Matthijs HC, Tyystjarvi T (2008) FEBS Lett. 582: 346-350

Wang HL, Postier BL, Burnap RL (2004) J. Biol. Chem. 279: 5739-5751

Zang X, Liu B, Liu S, Arunakumara KK, Zhang X (2007) J. Microbiol. 45: 241-245

Acid Stress Responsive Genes, *slr0967* and *sll0939*, are Directly Involved in Low-pH Tolerance of Cyanobacterium *Synechocystis* sp. PCC6803.

Hisataka Ohta[a,b,*], Yuta Kobayashi [a], Atsushi Moriyama[a], Yuko Kubo[a], Mamoru Sambe[a], Yousuke Shibata[a], Yohei Haseyama[a], Yuka Yoshino[a], Junji Uchiyama[b]

[a]Department of biology, Faculty of Science, Tokyo University of Science, Shinjyuku, Tokyo 162-8601, Japan;
[b]Research center for RNA science, RIST, Tokyo University of Science, Noda, Chiba 278-8510, Japan.
[*]Corresponding author. Fax No. +81(3)5228 8374; E-mail: ohta@rs.noda.tus.ac.jp.

Abstract: Genes expressed in response to low-pH stress in unicellular cyanobacterium *Syechosystis* sp. PCC 6803 were identified using DNA microarrays. Among these, the expression of *slr0967* and *sll0939* constantly increased during a 4 h acid stress condition [Photosynth Res. 84:225-30 (2005)]. The growth of the two genes deletion mutants on BG-11 media at pH 6.0 was significantly lower than that of wild-type cells. On the other hand, overexpression of the two genes under the control of the trc promoter caused the cells to become tolerant to short-term acid stress (pH 3.0 for 8 h). Real-time RT-PCR analysis of these mutants revealed that the expression of *sll0939* was significantly repressed in the *slr0967* deletion mutant. These results suggest that *sll0939* are directly involved in low-pH tolerance of cyanobacrerium *Syechosystis* sp. PCC6803 and *slr0967* may have been essential for induction of acid responsive genes.

Keywords: Low-pH; Cyanobacteria; Stress response

Introduction

Dating from the Precambrian era, cyanobacteria have a long history of adapting to the Earth's environment. By evolving oxygen via photosynthetic reactions similar to those of plants and green algae, these prokaryotes were essential to the evolution of the present biosphere. They continue to make a large contribution to the equilibrium of the Earth's atmosphere by producing oxygen and removing carbon dioxide. To survive in extreme or variable environments, cyanobacteria have developed specific regulatory systems, in addition to more general mechanisms equivalent to those of other prokaryotes or photosynthetic bacteria. Several species of cyanobacteria serve as model organisms for elucidating both functional and regulatory aspects of photosynthesis. Above all, *Synechocystis* sp. PCC 6803 was the first photosynthetic organism for which a complete genome sequence became available (Kaneko *et al.*, 1996), and DNA microarrays have been used to examine gene expression in response to various kinds of stress such as redox, oxidative, osmotic, salinity, and high light stress (Kanesaki *et al*., 2002; Hihara *et al*., 2001).

Acid rain is one of the most serious environmental stresses. It causes acidification of lakes and streams and contributes to damage of plants, algae, and cyanobacteria in many parts of the world. Rhizotoxicity in acid soil, which involves the action of Al^{3+} has been well investigated (Jones *et al.*, 1995). Nevertheless, little has been done to elucidate the basic set of adaptations necessary for acid tolerance in plants, algae, or cyanobacteria.

DNA microarray analysis of *Synechocystis* sp. PCC 6803 cells revealed that acid stress induced the expression of putative stress-related proteins, such as chaperones (*slr0093 [dnaJ], sll1514 [hspA]*, and *sll0170 [dnaK)]*), regulatory factors (*sll0306 [sigB] and sll2012 [sigD)]*), and proteins of unknown function (Ohta *et al*., 2005). Among the up-regulated genes with unknown function, *slr0967* and *sll0939*

continuously increase 7 and 16-fold after 4 h of acid stress(Ohta *et al*., 2005) and were up-regulated by osmotic and salt stresses(Kanesaki *et al.*, 2002). Interestingly, these two genes are located adjacently on the *Synechocystis* sp. PCC 6803 genome (Fig. 1).

In this study, we examined the physiological function of genes using mutant cells in which each gene was disrupted by a kanamycin-resistance cartridge gene. Based on phenotypes of the mutants and real-time quantitative RT-PCR analysis of the transcripts of the two genes, the expression profile of the *slr0967* deletion mutant on acid stress was compared with that of wild-type cells.

Material and Methods

Strain and culture conditions of Cyanobacteria

Wild-type strain of *Synechocystis* sp. PCC6803 and the gene of *sll0939* and *slr0967* disrupted mutants made by inserting the kanamycin resistance cassette were grown at 30 °C in BG-11 medium (Stanier *et al.*, 1971) with 5 mmol TES - NaOH (pH8.0) under continuous illumination provided by fluorescent lamps. Exponentially growing cells were acid-stressed by centrifuging the cell cultures and resuspending the cell pellets in a pH-adjusted BG-11 medium. A BG-11 medium was acidifed using MES (pH 5.5–7.0) buffer instead of a TES (pH 8.0) buffer. Cultures were streaked onto pH-adjusted BG-11 plates and cultured for 7 days. Experiments were performed in duplicated at least Three times.

Generation of insertion mutants

Mutants impaired in selected genes were generated by reverse genetics. The coding sequences and neighboring sequences were amplified by PCR. Approximately 2 kb of PCR products were cloned into pUC19 (Toyobo, Osaka, Japan). The primers for amplification were designed using the complete genome sequence of *Synechocystis* (kaneko *et al.*, 1996). Sequences that contained appropriate restriction sites were selected to improve cloning of fragments. The kanamycin (Km) resistance gene (*kmr*) isolated from plasmid pUC4K (Amersham Pharmacia) was inserted into unique restriction sites of the encoding sequences. Transformants were initially selected on a medium containing 10 μg Km mL^{-1} (Wako Pure Chemical, Osaka, Japan), whereas the segregation of clones was performed by restreaking (at least three transfers) of primary clones on plates supplemented with 50 μg Km mL^{-1}. During the cultivation of mutants, Km was added to the liquid media.

Generation of overexpressing mutants

Overexpressing mutants *trc-slr0967* and *trc-sll0939* of *Synechocystis* 6803 were generated using pTrc-*slr*0967 and pTrc-*sll*0939 plasmids. The plasmids were introduced into the *cmr* gene from pLysS (Novagen, Gibbstown, NJ, USA) *and the trc* promoter was introduced from pTrcHis B (Invitrogen, Carlsbad, CA, USA) into the upstream of the respective genes as described by Kamei *et al.*

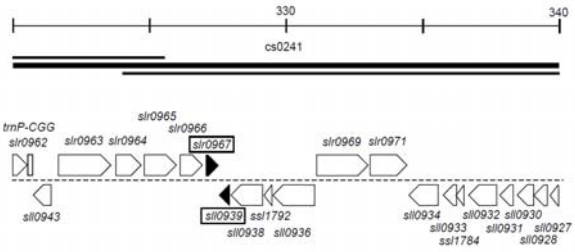

Fig. 1 Genome map of *slr0967* and *sll0939* in *Synechocystis* sp. PCC 6803.

RNA isolation and quantitative real-time RT PCR

Total RNA was isolated from *Synechocystis cells* using the RNeasy Midi kit(Qiagen) as described in Hihara *et al*. (2001). The extracted total RNAs were used to prepare cDNA samples with the SuperscritII RT(Gibco-BRL) according to the manufacture's recommendations. Real-time PCR with SYBR Green I was performed, using SYBR Premix EX Taq (Perfect Real Time) (TAKARA). Real-time PCR was carried out according to the following manufacturer's instructions.

Results and Discussion

Characterization of slr0967 and sll0939

Wild-type *Synechocystis* sp. PCC6803 was transformed with *slr0967* and *sll0939* that had been interrupted with cassette conferring resistance to kanamycin. In normal BG-11 medium at pH 8.0, all strains exhibited a similar photoautotrophic doubling time (data not shown), suggesting that deletion of these genes did not affect their growth in normal conditions. In contrast, in the acid stressed condition at pH 6.0, the growth of all mutant cells was slightly

but significantly inhibited compared with that of wild-type cells (Fig. 2). The *sll0939* and the *slr0967* and double mutants were more sensitive to acid stress than the wild-type cells (Fig. 2) indicating that *slr0967* and *sll0939* are involved in acid tolerance of *Synechocystis* cells. To test whether *sll0939* and *slr0967* genes involved in acid tolerance of Synechocystis cells, we constructed overexpressing mutants *trc-slr0967* and *trc-sll0939* of *Synechocystis* 6803.

However, overexpression of these genes failed to enhance the acid tolerance after culturing at pH 6.0 for 7 days (Fig. 2). We then characterized the expression of these two genes at the level of the transcript by quantitative RT-PCR using total RNA isolated from acid treated wild-type cells and *trc-slr0967* and *trc-sll0939* mutant cells. The relative expression of *slr0967* and *sll0939* promoted by *trc* was lower than that of wild-type cells during a 4.0 h acid stress but higher than that from non-treated wild-type cells (Table1). The relative expression level from *trc* promoter was as same as wild-type after culturing at pH 6.0 for 0.5 h. These results indicated that induction of these genes from *trc* promoter was not enough to get acid tolerance. Accordingly, viability of the mutants by acid stress treatment at pH 3.0 for 1–12 h was tested (data not shown). As a result, we found a significant difference in survival between wild-type and *trc*-mutants that were treated for 8 h. The *trc*-mutants became more tolerant to acid stress than wild-type cells.

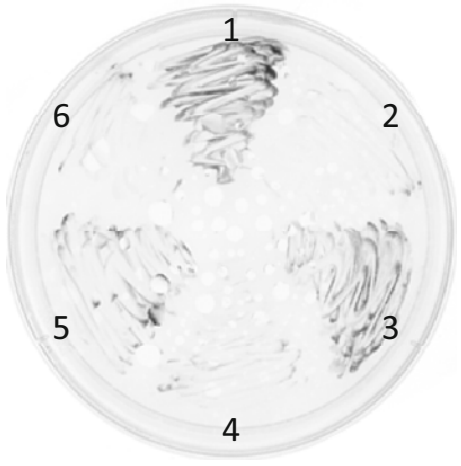

Fig. 2 Influence of acid stress on the growth of the wild-type strain and mutants.
Typical growth of the wild-type (1), Δ*slr0967* mutant (2), *trc-slr0967* mutant (3), Δ*slr0967* and Δ*sll0939* double mutants (4), *trc-sll0939* mutant (5), Δ*sll0939* mutant (6), and cultivated in solid BG11 media (pH6.0) and the plate was photographed and examined after 7 days of incubation at 30 °C. These experiments were repeated three times.

Quantitative RT-PCR analysis of slr0967 and sll0939 in deletion mutants

These two genes are located adjacent to the operon and are coded by opposite strands on the *Synechocystis* genome (Fig. 1). To examine the regulatory relationship between these two genes, the abundance of mutual genes in the deletion mutants was measured in normal growth and acid stress conditions by culturing them at pH 3.0 for 30 min (Table1). There was increased expression of *slr0967* and *sll0939* in wild-type cells by acid stress after 30 min; there was no significant alteration in *slr0967* expression evident in the Δ*sll0939* mutant. In contrast, *sll0939* expression was markedly affected by deletion of *slr0967* in both normal and acid stressed conditions. These results indicate that *slr0967* may have been essential for induction of *sll0939.*

Table1 Expression levels of *slr0967* and *sll0939 after acid stress* by QRT-PCR analysis.

Gene	Strain	Expression
slr0967	Wild-type (0 h)	1.0*
	Wild-type (0.5 h)	5.3 ±1.5
	Wild-type (4.0 h)	12.5 ± 2.1
	trc-slr0967	6.8 ± 1.3
	Δ*sll0939*	7.3 ± 2.6
sll0939	Wild-type (0 h)	1.0*
	Wild-type (0.5 h)	5.1 ± 2.4
	Wild-type (4.0 h)	25.3 ± 4.3
	trc-sll0939	4.8 ± 1.2
	Δ*slr0967*	0.5 ± 0.3

Expression levels of *slr0967* and *sll0939* after acid treatment (pH 3.0) in wild-type cells, *trc*-mutants (*trc-slr0967* and *trc-sll0939*) and deletion-mutants (Δ*slr0967* and Δ*sll0939*) by QRT-PCR analysis. These experiments were repeated three times.

References

Kaneko T, Sato S, Kotani H, Tanaka A, Asamizu E, Nakamura Y, Miyajima N, Hirosawa M, Sugiura M, Sasamoto S, Kimura T, Hosouchi T, Matsuno A, Muraki A, Nakazaki N, Naruo K, Okumura S, Shimpo S, Takeuchi C, Wada T, Watanabe A, Yamada M, Yasuda M, Tabata S (1996) Sequence Analysis of the Genome of the Unicellular Cyanobacterium Synechocystis sp. Strain PCC6803. II. Sequence Determination of the Entire Genome and Assignment of Potential Protein-Coding regions. DNA Res. 3: 109-136

Kanesaki Y, Suzuki I, Allakhverdiev SI, Mikami K, Murata N (2002) Salt Stress and Hyperosmotic

Stress Regulate the Expression of Different Sets of Genes in Synechocystis sp. PCC 6803. Biochem Biophys Res Commun. 290: 339-348

Hihara Y, Kamei A, Kanehisa M, Kaplan A, Ikeuchi M (2001) DNA Microarray Analysis of Cyanobacterial Gene Expression during Acclimation to High Light. Plant Cell. 13: 793-806

Jones DL, Kochian LV (1995) Aluminum Inhibition of the Inositol 1,4,5-Trisphosphate Signal Transduction Pathway in Wheat Roots: a Role in Aluminum Toxicity? Plant Cell. 7: 1913-1922

Ohta H, Shibata Y, Haseyama Y, Yoshino Y, Suzuki T, Kagasawa T, Kamei A, Ikeuchi M, Enami I (2005) Identification of Genes Expressed in Response to Acid Stress in Synechocystis sp. PCC 6803 Using DNA Microarrays. Photosynth Res. 84: 225-230

Stanier RY, Kunisawa R, Mandel M, Cohen-Bazire G (1971) Purification and Properties of Unicellular Blue-Green Algae (Order Chroococcales). Microbiol Mol Biol Rev. 35: 171-205

Studies on the Effects of N and P on the Competition of *Flaveria Bidentis (L.) Kunt* and *Chenopodium Album (L.) Grew*

Qing Yang, Xuemin Guan, Yanfang Liu, Aiying Guo, Ru Long, Fengjuan Zhang *

Department of life science& Technology, Hebei Normal University of Science & Technology, Hebei, China.
*Corresponding author. Tel. No. 13730336360; Fax No. 03352037936; E-mail: yangqingxy@163.com.

Abstract: In order to clarify the competition characteristics of Flaveria Bidentis, the effects of N and P on the competition of F. Bidentis were studied with C. Album as competitor. A field experiment, including nine fertilizing levels was conducted. N and P decreased Non-photochemical quenching (NPQ) and maximal fluorescence (Fm) of two kinds of plant. P increased significantly the effective quantum yield of photosystemII (Yield), electron transport rate (ETR) and Pn of F. Bidentis, so that dry weight per plant (PDW) were high (except NHPH). But P decreased Yield, ETR of C. Album. Finally, PDW and relative growth rates (RGR) of F. Bidentis in NLPLwere the highest, but these of C. Album were lower.The results showed that optimal N and P fertilizer could enhance the competition of F. Bidentis, especially for P nutrient.

Keywords: *F. Bidentis*; *C. Album*; Competition； N nutrient (N); P nutrient (P)

Introduction

Invasive alien species are known to alter species composition, structure and function of invaded ecosystems, and often cause significant environmental damage and huge economic loss worldwide (D'Antonio and Kark, 2002). Because they can compete nutrition (Wardle *et al*., 1994), water, light (Weihe and Neely, 1997) and space with native plants. For example, *Centaurea olstitialis* L. and B*rom*u *madritens* are vigorous growth by competing water and nutrition with native plant (Dyer and Rice, 1999; Meigoza and Nowak, 1990). The invasive plants possess competitive advantage in ecological habitat of higher N nutrient (Rejmanek *et al*., 1996) and fast overspread (Olson and Blicher, 2003; Bertness, 2002; Silliman and Bertness, 2004). *F. bidentis* (L.)Kunt, a compositae weed, will seriously effect crop growth when it invades farmland, so it is called ecology killer. It was found in Hengshui Province, Langfang of Hebei Province, and Tianjin since 2001 (Gao *et al*., 2004). Preventing the introduction of potentially invasive species is one of the most efficient and economical methods of controlling biological invasions. To better known competitive mechanism and control the spread of *F. bidentis*, it is necessary to study the effect of N and P on the competition of *F. bidentis*, which helps to provide theoretical basis for its alternative control.

Materials and Methods

The field experiment was conducted on the Teaching and Demonstration Farm, Hebei Normal University of Science and Technology, China from April to October 2010, including nine fertilizing levels including CK (0 kg hm^{-2}) NL (N 150 kg hm^{-2}), NH (N 300 kg hm^{-2}), P L (P_2O_5 150 kg hm^{-2}), PH (P_2O_5 300 kg hm^{-2}), NLPL (N 150 kg hm^{-2} + P_2O_5 150 kg hm^{-2}), NLPH (N 150 kg hm^{-2} + P_2O_5 300 kg hm^{-2}), NHPL (N 300 kg hm^{-2} + P_2O_5 150 kg hm^{-2}), and NHPH (N 150 kg hm^{-2} + P_2O_5 300 kg hm^{-2}). Every treatment had six replications and the pots were buried vertically to a depth of 60 cm. Every pot had two *F. Bidentis* and two *C. Albums*. The experiments were done both on 1st August and on 1st September, respectively. Photosynthetic and fluorescent parameters were determined on full expanded leaves

with a GFS3000 Portable Photosynthesis-fluorescence System (WALZ, German). Leaves, shoot and root were separated, dried and weighed, and then we measured RGR [(final dry weight – meassured initial dry weight)/measured final dry weight] , leaf area per plant(LA) and PDW on August and September, respectively.

Results and Discussion

NPQ of two kinds of plants had difference, it of *F. Bidentis* was higher in CK, NH and NHPH than other trentments (Table 1), on the contrary, it of *C. Album* was lower(Table 2). Although Fm of *F. Bidentis* had no significant difference, it of *C. Album* had highly significant differences among treatments ($P < 0.01$). Fm of *C. Album was* the higher in NLPH and CK, but it was the lowest of NLPL. These values were remarkably consistent between NPQ and Fm of *C. Album*. N and P decreased Fm of *C. Album*. P increased significantly Yield and ETR of *F. Bidentis*, but decreased that of *C. Album*. But Yield and ETR were lowest in NH than other trentments, this showed the N high lever effects light reaction of photosynthesis.

F. Bidentis and *C. Album* did not differ in Pn of on August (data not showed). Compared with *F. Bidentis*, Pn of *C. Album* was low significantly (Table 2), and Pn of fertilizer treatments remained higher than that of CK. Pn of P trentments was higher than that of no P trentments in *F. Bidentis*. Pn and Gs of NLPH was higher than other of treatments. The results showed that the responses of Gs to N and P were consistent with Pn.

Growth is one of the important traits for plants because both survival and reproduction depend on plant size and, therefore, on growth rate (Shipley, 2006). A higher growth rate may give invasive plants a competitive advantage over native plants due to its pivotal role in capturing available resources (Grotkopp and Rejmánek, 2007). In comparison with *C. Album*, *F. Bidentis* showed significantly higher value for LA, DW and RGR ($P < 0.01$), and RGR of all treatments except NHPH and PH showed higher than CK for *F. Bidentis* (Table 2). P could increase LA of *F. Bidentis*,

Table 1 Effect of N and P on September of *F. Bidentis*.
Treatments assigned different letters indicate a significant difference between the means ($P \leq 0.05$).

Treatments	NPQ	Fm	Yield	ETR	Pn (μmol CO_2 m^{-2} s^{-1})	Gs (molH_2O m^{-2} s^{-1})	Leaf area (m^2 $plant^{-1}$)	Dry weight (g $plant^{-1}$)	RGR
CK	3.44a	636bc	0.19c	82.6cd	7.35d	54.51bcd	0.11f	102.7d	7.9d
NL	3.03ab	684abc	0.24c	101.1c	9.91 bc	57.50bcd	0.32de	207.3b	11.9bc
NH	3.42ab	730.5abc	0.15c	64.2d	7.99d	32.55d	0.29e	208.7b	13.4bc
PL	2.72b	625.5c	0.42c	163.5b	13.24ab	78.32ab	0.29e	168.7c	14.1b
PH	2.67b	682.3a	0.16c	66.6d	11.17bcd	60.2bcd	0.50c	152.6c	7.9d
NLPL	2.40c	667.5bc	0.42ab	137.6b	11.16bcd	58.1bcd	0.36e	232.3a	18.3a
NLPH	2.81b	765abc	0.48a	200.1a	16.00 a	95.1a	0.65b	165.7c	10.6cd
NHPL	2.34c	778.5ab	0.36b	139.8b	9.72cd	71.1abc	0.80a	168.7c	10.9bcd
NHPH	3.34a	684.0abc	0.17c	71.1cd	9.34cd	42.2cd	0.52c	71.4e	1.0e

Table 2 Effect of N and P on September of *C. Album*.
Treatments assigned different letters indicate a significant difference between the means ($P \leq 0.05$).

Treatments	NPQ	Fm	Yield	ETR	Pn (μmol CO_2 m^{-2} s^{-1})	Gs (molH_2O m^{-2} s^{-1})	LA (m^2 $plant^{-1}$)	Dry weight (g $plant^{-1}$)	RGR
CK	3.06b	883.5a	0.24bc	89.5ab	0.50e	9.0d	0.15b	30.7bc	0.42c
NL	2.57bc	887.5a	0.32ab	87.7ab	6.09a	60.2a	0.13c	33.1bc	0.45c
NH	1.67de	660.5c	0.14cd	57.0ab	2.69bc	46.2ab	0.22a	58.6a	0.58b
PL	1.98cd	855.1ab	0.45a	130.9a	3.99bcd	51.5a	0.07d	20.4d	0.14d
PH	2.11cd	843.5 ab	0.11cd	46.5b	1.93cd	17.4d	0.15b	37.9b	0.46c
NLPL	0.94e	471.5d	0.23bc	95.0ab	3.08d	26.4bc	0.13c	25.5cd	0.48c
NLPH	4.25a	883.2a	0.08d	100.6ab	4.66b	49.4ab	0.02f	30.9cd	0.05e
NHPL	2.43bc	778.5abd	0.07d	30.0b	4.93bcd	19.5d	0.04e	33.1bc	0.48c
NHPH	1.85cd	770.0b	0.13cd	56.7ab	5.8a	58.9a	0.15b	58.6a	0.84a

whereas it decreased the above indexes of *C. Album*. For *F. Bidentis* fertilizer increased PDW except for NHPH. LA of September was lower than that of August (data not showed), probably N and P decreased Fm and NPQ, enhanced Yield, Pn and PDW, and finally increased the competitive ability of *F. Bidentis* particularly P, so that leaves of *C. Album* fell off. Finally, PDW and RGR of *F. Bidentis* in NLPL were the highest, but these of *C. Album* were lower. The results showed that optimal N and P fertilizer could enhance the competition of F. Bidentis, especially for P nutrient. These suggest that the competitive plant growth is more sensitive to P and less sensitive to N within the experimental range.

Acknowledgements

This study was funded by the Project of National Natural Science Foundation of China (31040066), Science and Technology Department Project of Hebei (10225520).

References

Davis MA, Grime JP, Thompson K (2000) Fluctuating Resources in Plant Communities, a General Theory of Invasibility. J Ecol. 88: 528-534

.D'Antonio CM, Kark S (2002) Impacts and Extent of Biotic Invasions in Terrestrial Ecosystems. Trends Ecol Evol. 17: 202-204

Dyer AR, Rice KJ (1999) Effect of Competition on Resource Availability and Growth of a California Bunchgrass. Ecology 80: 2697-2710

Grotkopp E, Rejma´nek M (2007) High Seedling Relative Growth Rate and Specific Leaf Area Are Traits of Invasive Species: Phylogenetically Independent Contrasts of Woody Angiosperms. Am J Bot. 94: 526-532

Gao XM, Tang TG, Ling Y, *et a1*. (2004) An Alert Regarding Biological Invasion by a New Exotic Plant, Flaveria Bident, and Strategies for Its Control. Biodiversity Science 12(2): 274-279

Melgoza G, Nowak RS (1990) Competition between Cheatgrass and Two Native Species after Fire: Implications from Observations and Measurements of Root Distribution. Journal of Range Management 44: 27-33

Rejmanek MRI, Chardson D M (1996) What Attributes Make Someplant Species More Invasive? Ecology 77: 1655-1661

Shipley B (2006) Net Assimilation Rate, sSpecific Leaf Area and Leaf Mass Ratio: Which Is Most Closely Correlated with Relative Growth Rate? A meta-analysis. Funct Ecol. 20: 565-574

Wardle DA, Nicholson KS, Ahmed M, Rahman (1994) Interference Effects of the Invasive Plant Carduus Nutans L.Against the Nitrogen Fixation Ability of Trifolium repens L. Plant and Soil. 163: 287-297

Weihe PE, Neely RK (1997) The Effects of Shading on Competition between Purple Loosestrife and Broadleaved Cattail. Aquatic Botany. 59: 127-138

Symposium 18

Organelle Communication

A Novel Link between Chloroplast Development and Stress Response Lessoned by Leaf-Variegated Mutant

Wataru Sakamoto, Eiko Miura, Yusuke Kato

Institute of Plant Science and Bioresources, Okayama University, Kurashiki, Okayama 710-0046, Japan.

Abstract: Recessive mutations are known to give rise to cell lineage-type leaf variegation that forms green and white sectors due to arrested chloroplast development. The *yellow variegated 2* (*var2*) mutant in *Arabidopsis thaliana* has been studied as a typical leaf-variegated mutant whose defect results from the lack of FtsH2 metalloprotease in chloroplasts. To understand physiological properties of variegated sectors, gene expression profiles were investigated between green and white sectors of *var2* leaves. Consistent with impaired thylakoid formation, a substantial number of genes related to photosynthesis and chloroplast functions were repressed in white sectors. In addition, many genes were up-regulated in white sectors. Since *var2* leaves suffer from photooxidative stress and accumulate high levels of reactive oxygen species (ROS) due to compromised Photosystem II repair, we focused ROS scavenging genes such as *Cu/Zn superoxide dismutase 2* (*CSD2*). Activation of *CSD2* was specific to white sectors and appeared to be under the control of copper availability. A lack of thylakoid membranes in white sectors perhaps leads to excess free copper and iron conditions, thus white sectors mimic a copper sufficient condition. We infer that CSD2 acts not only on ROS detoxification but also on copper buffering. Interestingly, an up-regulation of Cu/Zn SOD was commonly observed in various variegated leaves. Our findings thus highlight the crucial role for the control of oxidative stress and free metals in variegated leaf sectors.

Keywords: Leaf variegation; Chloroplast development; FtsH; photooxidative stress

Leaf variegation is a common phenomenon in many ornamental plants and crops. Recessive mutations, both in nuclear and organelle genomes, have been reported to cause leaf variegation or striping (Sakamoto, 2003). While molecular characterization of leaf-variegated mutants has confirmed that leaf variegation is caused by various redundant functions related to chloroplasts, a precise mechanism leading to such chimeric chloroplast development in the same leaf tissues is poorly understood.

We have focused on the variegated mutant *yellow variegated 2* (*var2*) in *Arabidopsis thaliana* as a model to study the formation of green/white variegated sectors. True leaves in *var2* form non-identical variegated sectors, indicating that chloroplast differentiation is defective at an early phase of leaf cell lineage (Sakamoto *et al*., 2009). The *VAR2* locus encodes FtsH2, an isoform of chloroplastic metalloprotease FtsHs (Chen *et al*., 2000; Takechi *et al.*, 2000). In chloroplasts, FtsH plays an essential role in the processive degradation of thylakoid membrane proteins along with other proteases (Sakamoto, 2006; Kato and Sakamoto, 2009). It was assumed that a level of FtsH2 below the threshold resulted in leaf variegation (Miura *et al*., 2007; Yu *et al*., 2008). Similarly to *var2*, a lack of FtsH5 results in an additional variegated mutant known as *yellow variegated 1* (*var1*) (Sakamoto *et al*., 2002). Based upon the phenotypes in *var1* and *var2*, it is proposed that FtsH is involved in both thylakoid formation and protein degradation. Besides the variegation phenotype in the mutant, FtsH protease was also shown to participate in the specific degradation of D1 protein in Photosystem II (PSII) reaction centers, as an important component of the PSII repair cycle (Bailey *et al*., 2002; Kato *et al*., 2009; Nixon *et al*., 2005). We found that as a consequence of such

photooxidative damages, *var2* leaves suffer from photooxidative stress even under normal light conditions and accumulate substantial levels of reactive oxygen species (ROS) (Kato *et al*., 2009). We assume that such a photooxidative stress reflects gene expression in green and white sectors in *var2*. Therefore, we performed a comparative microarray analysis between wild-type ecotype Columbia (Col) leaves and green and white sectors in *var2*. Our results demonstrated that a significant number of genes were either up- or down-regulated in variegated sectors. Here we focus on up-regulation of Cu/Zn superoxide dismutase (SOD) in *var2* white sectors, which may implicate relationship between impaired chloroplast development and stress response.

DNA microarray analysis was conducted to monitor gene expression profiles in variegated leaves (Miura *et al*., 2010). Total RNA was also extracted from Col wild-type leaves and all reverse-transcribed RNAs were hybridized to the Agilent *Arabidopsis* Ver. 4 DNA chip (n = 3). All genes (43,663 genes) on the array were filtered based on their flag values. A one-way ANOVA statistical test was performed with the Benjamini and Hochberg false discovery rate (BH-FDR) multiple testing correction (corrected *P*-value < 0.05) using the GeneSpring GX10 software (Agilent Technologies). As a consequence, 9,249 genes were chosen by this method and used for further analysis. Comparison between Col and *var2* white sectors showed that a substantial number of the genes were beyond the two-fold difference and showed either an increase or decrease in white sectors. The same trend was also true between *var2* green and white sectors, since Col and *var2* green sectors showed a similar expression profile. These results clearly demonstrated that many genes are responsive to the formation of white sectors.

To compare differential gene expression patterns in detail, we characterized genes that were differentially expressed between green and white sectors in *var2*. When a cutoff was made by a two-fold change, 1,304 genes were selected as up-regulated and 3,194 genes as down-regulated. To classify these genes based upon function, we performed a subsequent gene ontology (GO) analysis. As for up-regulated categories, all GO categories were principally unrelated to photosynthesis and appeared to converge in two major classes. One category was related to RNA metabolism (9 GO categories; 30%), and the other was related to several stresses (7 GO categories; 25.92%). It was notable that many of these stresses are related to oxidative stress and ROS. Thus, we considered that white sectors are highly susceptible to oxidative damage due to impaired plastid development. Since our previous investigation revealed a significant accumulation of O_2^- and H_2O_2 in chloroplasts in *var2*, we focused on up-regulated genes related to ROS (Kato *et al*., 2009). Real-time PCR and western blotting further demonstrated that ROS scavenging enzymes such as CSD2 and sAPX are up-regulated more in the white sectors than in the green sectors. Thus, we concluded that plastidic ROS scavenging enzymes, if not all isoforms, are up-regulated in *var2* white sectors.

To understand whether CSD accumulation occurs in other variegation model systems besides *Arabidopsis var2*, we characterized the expression patterns of plastidic SODs from multiple plant sources. The *Arabidopsis chloroplast mutator* (*chm*) mutant displays large white sectors due to impaired mitochondria function (Sakamoto, 2003). In this mutant, we confirmed that *chm* white sectors contained more CSD2 (Fig. 1), suggesting that the up-regulation is common in leaf variegation. We also performed immunoblot analysis using different species. Leaves from ornamental plants exhibiting leaf variegation were subjected to surgical separation into green and white sectors, and total proteins were cross-reacted with *Arabidopsis* CSD2 antibodies (Fig. 1, normalized by fresh weight). The results showed the predominant detection of one or two bands of a similar molecular mass corresponding to CSD2 (~19 kDa) in white sectors (Fig. 1). Although our results from immunoblots represent analysis from a limited number of variegated leaf models systems, these data suggest that differential expression of SODs between white and green sectors may be a common occurrence among variegated leaves. After careful consideration of these data, it does not seem plausible that the high accumulation of CSD2 directly results from the impaired PSII repair cycle as we initially hypothesized.

CSD2 expression is known to be strictly controlled by copper availability (Yamasaki *et al*., 2007; Yamasaki *et al*., 2009). Under normal growth conditions, copper is limiting (0.1 μM copper in standard MS medium) (Shikanai *et al*., 2003), and FSD1 is predominantly expressed in chloroplasts and CSD2 is repressed. However, under copper sufficient condition (5 μM copper), CSD2 expression is

enhanced and FSD1 is repressed (Yamasaki *et al*., 2007). This antagonistic expression pattern was found to be governed by a microRNA (*miR398*). *miR398* has been subsequently characterized as a key regulatory factor in copper homeostasis (Yamasaki *et al*., 2007; Yamasaki *et al*., 2009) and its target genes include *CSD1*, *CSD2*, and mitochondrial *COX5b-1* (cytochrome *c* oxidase). Thus, we were interested to characterized the activity and accumulation of plastidic SODs under different copper conditions. RNA blot analysis was subsequently performed to examine *miR398* levels and confirmed that white sectors did not accumulate any detectable levels of *miR398* regardless of copper concentration (Miura *et al*., 2010). Thus, *var2* white sectors exhibit up-regulation of plastidic SOD expression, and that this up-regulation partly results from impaired expression of *miR398*.

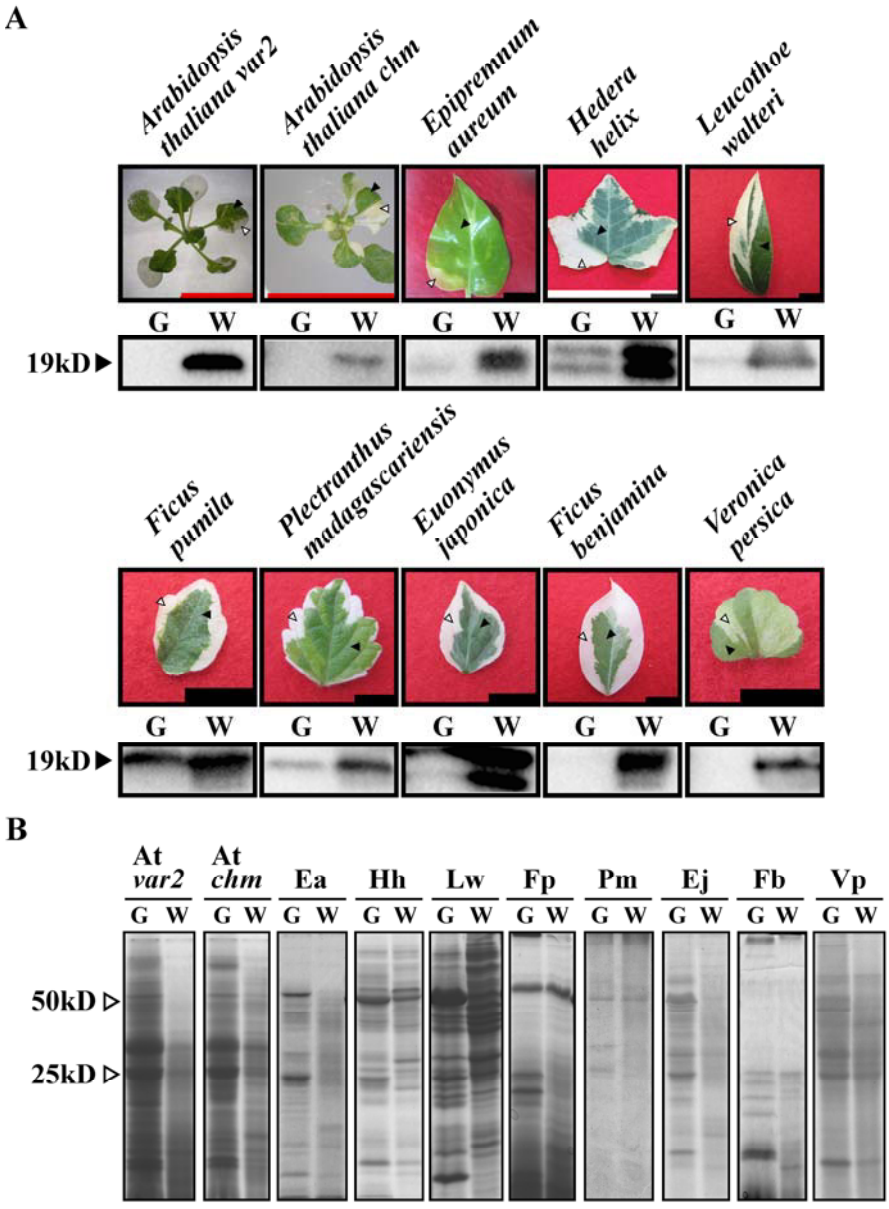

Fig. 1 Detection of Putative CSD2 Isoforms.

(A) Photographs of variegated leaves (top) and immunoblots cross-reacted with *Arabidopsis* CSD2 antibodies (bottom). G, green sector. W, white sector. Black and white arrowheads in variegated leaves corresponded to the respective green and white sectors that were used for immunoblot analysis. Bars = 1 cm. Samples were normalized by fresh weight. Immunoblot analysis and CBB staining were repeated at least two times and the representative result is shown.

(B) CBB-stained SDS-PAGE gels shown in (A). Positions of markers of known molecular mass (50 kD and 25 kD) are indicated by white arrowheads. At *var2, Arabidopsis thaliana*. At *chm, Arabidopsis thaliana*. Ea, *Epipremnum aureum*. Hh, *Hedera helix*. Lw, *Leucothoe walteri.* Fp, *Ficus pumila*. Pm, *Plectranthus madagascariensis*. Ej, *Euonymus japonica*. Fb, *Ficus benjamina*. Vp, *Veronica persica.*

Our microarray data implicate that white sectors respond to impaired plastid development and mitigate their susceptibility by activating various stress genes. We initially hypothesized that *var2* white sectors receive photooxidative stress at levels less than what green sectors experience. It should be noted, however, that CSD2 up-regulation is limited to white sectors, despite the fact that green sectors accumulate high levels of ROS. Since plastids in white sectors are almost devoid of thylakoids and photosystems, white sectors experience a different type of oxidative stress that does not result from photoinhibition of PSII. Thus, we reason that CSD2 plays an additional role in white sectors (Fig. 2). Chloroplasts are a major reservoir for copper due to the presence of plastocyanin (PC) (Shikanai *et al*., 2003). While copper functions as a necessary cofactor for PC, excess free copper simultaneously exhibits cytotoxicity. A strict regulation of copper levels in chloroplasts is orchestrated by the antagonistic expression of chloroplastic SODs, FSD and CSD (requiring iron and copper as cofactors, respectively. Under insufficient copper conditions, FSD becomes a major chloroplastic SOD which functions to save copper for PC. Conversely, sufficient copper represses FSD and CSD levels increase to keep free copper available. In addition, this copper homeostasis was recently shown to be regulated on the post-transcriptional level (Yamasaki *et al*., 2007; Yamasaki *et al*., 2009). Specifically, *miR398* targets CSD1 and CSD2 mRNAs and the levels of *miR398* decrease under low copper leading to elevated CSD accumulation (Yamasaki *et al*., 2007). Our results from immunoblot analysis, activity gels, and RNA blot analyses demonstrate that white sectors mimic copper sufficient conditions. Abnormal plastids in white sectors lack thylakoids and do not accumulate thylakoid membranes (Takechi *et al*., 2000). The up-regulation of CSD1 and CSD2 not only acts on scavenging ROS produced by oxidative stress in white sectors, but also acts as a copper carrier. We propose that in white sectors, the homeostasis of free copper, as well as the mitigation of oxidative stress, may be crucial for cell viability (Fig. 2).

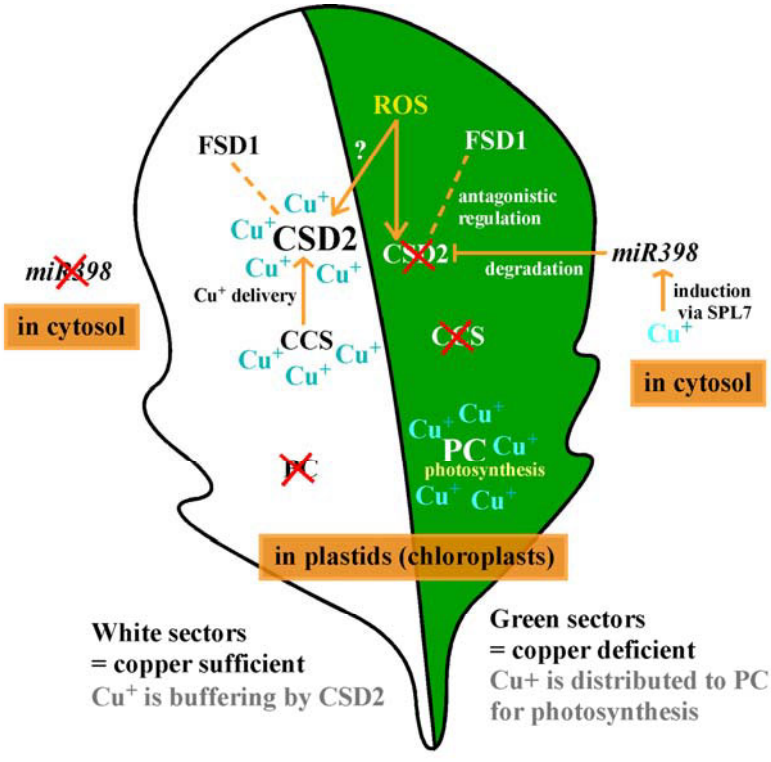

Fig. 2 Proposed Photooxidative Stress and Copper Homeostasis in *var2* Variegated Leaves.

In *var2* green sectors, chloroplasts (denoted as the interior of green sectors on this diagram) accumulate reactive oxygen species (ROS), copper ions are preferentially distributed to plastocyanin (PC) for photosynthesis, and CSD2 is degraded by *miRNA398* via SPL7-mediated regulation. This situation represents a copper deficient condition and is similar to Col leaves. In contrast, copper ions are distributed to CSD2 in white sectors due to a lack photosynthetic machinery in plastids (denoted as interior of white sectors on this diagram). CCS is responsible for copper delivery to CSD2. CSD and FSD act antagonistically against ROS.

References

Bailey S, Thompson E, Nixon PJ, Horton P, Mullineaux CW, Robinson C, Mann NH (2002) A Critical Role for the Var2 FtsH Homologue of Arabidopsis Thaliana in the Photosystem II Repair Cycle in Vivo. J. Biol. Chem. 277: 2006-2011

Chen M, Choi Y, Voytas DF, Rodermel S (2000) Mutations in the Arabidopsis VAR2 Locus Cause Leaf Variegation Due to the Loss of a Chloroplast FtsH Protease. Plant J. 22: 303-313

Kato Y, Miura E, Ido K, Ifuku K, Sakamoto W (2009) The Variegated Mutants Lacking Chloroplastic FtsHs Are Defective in D1 Degradation and Accumulate Reactive Oxygen Species. Plant Physiol. http://dx.doi.org/10.1104/pp.109.146589.

Kato Y, Sakamoto W (2009) Protein Quality Control in Chloroplasts: a Current Model of D1 Protein Degradation in the Photosystem II Repair Cycle. J. Biochem. 146: 463-469

Miura E, Kato Y, Matsushima R, Albrecht V, Laalami S, Sakamoto W (2007) The Balance between Protein Synthesis and Degradation in Chloroplasts Determines Leaf Variegation in Arabidopsis Yellow Variegated Mutants. Plant Cell 19: 1313-1328

Miura E, Kato Y, Sakamoto W (2010) Comparative Transcriptome Analysis of Green/White Sectors in Arabidopsis Yellow Variegated: Responses to Oxidative and Other Stresses in White Sectors. J. Exp. Bot. 61: 2433-2445

Nixon PJ, Barker M, Boehm M, de Vries R, Komenda J (2005) FtsH-Mediated Repair of the Photosystem II Complex in Response to Light Stress. J. Exp. Bot. 56: 357-363

Sakamoto W, Tamura T, Hanba Tomita Y, Murata M (2002) The VAR1 Locus of Arabidopsis Encodes a Chloroplastic FtsH and Is Responsible for Leaf Variegation in the Mutant Alleles. Genes. Cells 7: 769-780

Sakamoto W (2003) Leaf-Variegated Mutations and Their Responsible Genes in Arabidopsis Thaliana. Genes. Genet. Syst. 78: 1-9

Sakamoto W (2006) Protein Degradation Machineries in Plastids. Annu. Rev. Plant Biol. 57: 599-621

Sakamoto W, Uno Y, Zhang Q, Miura E, Kato Y, Sodmergen (2009) Arrested Differentiation of Proplastids into Chloroplasts in Variegated Leaves Characterized by Plastid Ultrastructure and Nucleoid Morphology. Plant Cell Physiol. 50: 2069-2083

Shikanai T, Müller-Moulé P, Munekage Y, Niyogi KK, Pilon M (2003) PAA1, a P-Type ATPase of Arabidopsis, Functions in Copper Transport in Chloroplasts. Plant Cell 15: 1333-1346

Takechi K, Sodmergen Murata M, Motoyoshi F, Sakamoto W (2000) The Yellow Variegated (VAR2) Locus Encodes a Homologue of FtsH, an ATP-Dependent Protease in Arabidopsis. Plant Cell Physiol. 41: 1334-1346

Yamasaki H, Abdel-Ghany S.E, Cohu CM, Kobayashi Y, Shikanai T, Pilon M (2007) Regulation of Copper Homeostasis by Micro-RNA in Arabidopsis. J. Biol. Chem. 282: 16369-16378

Yamasaki H, Hayashi M, Fukazawa M, Kobayashi Y, Shikanai T (2009) SQUAMOSA Promoter Binding Protein-Like Is a Central Regulator for Copper Homeostasis in Arabidopsis. Plant Cell 21: 347-361

Yu F, Liu X, Alsheikh M, Park S, Rodermel S (2008) Mutations in Suppressor of Variegation, a Factor Required for Normal Chloroplast Translation, Suppress Var2-Mediated Leaf Variegation in Arabidopsis. Plant Cell 20: 1786-1804

The Role of Plant-Specific PPR Proteins in Chloroplast RNA Editing

Kenji Okuda[a,*], Toshiharu Shikanai[b]

[a]Department of Life Science, Faculty of Science and Engineering, Chuo University, Japan; [b]Department of Botany, Graduate School of Science, Kyoto University, Japan.
[*]Corresponding author. Tel. No. +81 03 3817 1659; Fax No. +81 03 3817 1651; E-mail: okudak@kc.chuo-u.ac.jp.

Abstract: RNA editing is a post-transcriptional process that alters specific cytidine residues to uridine in the mitochondrial and chloroplast transcripts of higher plants and occurs frequently. Our analysis of mutants affected in chloroplast NAD(P)H dehydrogenase function has revealed that specific target C sites are recognized by each site-specific factors; the PLS subfamily of pentatricopeptide repeat (PPR) proteins that is specific to land plants. The PLS subfamily of PPR proteins is composed by a tandem array of PPR motifs to bind RNA and additional E and DYW motifs at the C-terminus. Based on the differences in C-terminal motifs, the PLS subfamily is classified into the E and DYW subclasses. To clarify each role of two types of site-specific factors in RNA editing, we focused on the E and DYW motifs and investigated their functions. Based on the results, we propose that the E-subclass PPR proteins recognize a specific RNA sequence motif, binds there, and recruits one or more additional proteins with the enzymatic activity through protein-protein interaction with the E motif. Moreover, our results suggests that the DYW-subclass PPR proteins might behave exactly like the E-subclass editing specificity factors despite the presence of the additional DYW motif.

Keywords: Chloroplast; PPR protein; RNA editing

Introduction

RNA editing is a post-transcriptional process that alters specific cytidine residues to uridine in the mitochondrial and chloroplast transcripts of higher plants (Chateigner-Boutin and Small, 2010). Thirty-four sites are edited in *Arabidopsis* chloroplasts, whereas more than 450 editing sites are edited in *Arabidopsis* mitochondria (Chateigner-Boutin and Small, 2010). The recognition of a specific target C site by the editing machinery requires site-specific factors that bind to the RNA upstream of the C to be edited (Chateigner-Boutin and Small, 2010). Our analysis of mutants affected in chloroplast NAD(P)H dehydrogenase function has revealed that all of these specific factors are the PLS subfamily of pentatricopeptide repeat (PPR) proteins that is specific to land plants. PPR proteins form a large protein family that is particularly prevalent in land plants and includes 450 members in *Arabidopsis thaliana* (Schmitz-Linneweber and Small, 2008). The PPR protein is composed by a tandem array of PPR motifs and the PLS subfamily contains additional motifs at the C-terminus. Based on the differences in C-terminal motifs, the PLS subfamily is further classified into the PLS, E, and DYW subclasses (Schmitz-Linneweber and Small, 2008). Two of our identified five editing specificity factors, CRR4 and CRR21 belong to the E subclass, and the others, CRR22, CRR28, and OTP82 fall into the DYW subclass (Okuda *et al*., 2007, 2008, 2010). CRR4 and CRR21, are required for the site 1 of RNA editing (ndhD-1) in the plastid *ndhD* and ndhD-2, respectively (Okuda *et al*., 2006, 2007), whereas CRR22, CRR28, and OTP82 are involved in the RNA editing of multiple plastid transcripts (Okuda *et al*., 2009).

Here we discuss how two types of editing specificity factor work in the process of RNA editing.

Materials and Methods

For the expression of CRR4 truncated in the E motif to be deleted, the wild-type genomic sequence encoding CRR4 truncated in the E motif was cloned in the pBIN19 vector. For the expression of CRR4, in which the E motif of CRR4 is replaced by that of CRR21, the nucleotide sequence encoding CRR4 truncated in the E motif was ligated to the sequence encoding the E motif of CRR21. The resultant chimeric gene was finally cloned into the pBIN19 vector. For the expression of CRR22, and CRR28 lacking their DYW motifs to be deleted, the wild-type genomic sequences encoding CRR22 and CRR28 truncated in the DYW motif were cloned into the pGWEB-NB1 binary vector. For the expression of CRR22 and CRR28 lacking their E and DYW motifs, the wild-type genomic sequences encoding CRR22 and CRR28 truncated in the E and DYW motifs were cloned into the pGWEB-NB1 binary vector. For the expression of CRR22, in which the DYW motif of CRR22 is replaced by that of CRR28, the wild-type genomic sequence encoding CRR22 truncated in the DYW motif was amplified by PCR and was ligated to the sequence encoding the DYW motif of CRR28. The resultant chimeric genes were cloned into the pGWB-NB1 binary vector. For the expression of CRR28, in which the DYW motif of CRR28 is replaced by that of CRR22, the wild-type genomic sequence encoding CRR28 truncated in the DYW motif was amplified by PCR and was ligated to the sequence encoding the DYW motif ofCRR22. The resultant chimeric genes were finally cloned into the pGWB-NB1 binary vector. These constructs were introduced into *crr4*, *crr21*, *crr22*, or *crr28* mutant plants via *Agrobacterium tumefaciens* MP90 or ASE.

For analysis of RNA editing in a series of transgenic plants, total RNA was isolated from rosette leaves using an RNeasy plant mini kit (Qiagen) and treated with DNase I (Invitrogen). DNA-free RNA (2.5 μg) was reverse transcribed with random hexamers. Sequences including the editing sites were amplified by PCR. The RT-PCR products were sequenced directly.

Results and Discussion

The tandem array of PPR motifs shows some diversity as to length and the sequence between CRR4 and CRR21. Biochemical analyses of PPR proteins have suggested that the PPR motif acts as an RNA-binding motif (Okuda *et al*., 2006). In contrast, the E motif is highly conserved (Fig. 1), suggesting that it might have a common function between CRR4 and CRR21, rather than the specific function of recognizing distinct RNA sequences. To assess this possibility, CRR4 truncated in the E motif was expressed in *crr4-3*, in which RNA editing of ndhD-1 is completely impaired (Kotera *et al*., 2005). Efficiency of ndhD-1 RNA editing was significantly reduced in the plants (7% of molecules were edited) (Table 1). It is noted that the ndhD-1 site is partially edited, even in the wild type (42%). In consistent with these observations, truncation of the E motif of CRR4 did not affect to an RNA binding activity, suggesting that the E motif is required for activity of the editing. Although CRR4 and CRR21 are involved in different editing events by recognizing distinct target RNAs for editing, conservation of the E motifs suggests a common function for these motifs. If this interpretation is true, the motif might be exchangeable between two PPR proteins. The E motif of CRR4 was therefore exchanged with that of CRR21, and the chimeric gene was introduced into the *crr4-3* allele. The introduction of the chimeric gene restored the RNA editing of ndhD-1, although the efficiency of RNA editing in transgenic plants (31%) was slightly lower than that in the wild type (42%) (Table 1). These results suggest that the E motif in CRR4 and CRR21 have a common function in RNA editing. Furthermore, truncation of the E motif did not cause complete loss of an RNA editing activity in vivo (Table 1). These observations suggest that the E motif is unlikely to be motifs that catalyze the reaction of RNA editing. Thus, we propose that the E motif of CRR4 and CRR21 might interact with an editing enzyme catalyzing C to U, which is still unclear, or another component of the editing machinery.

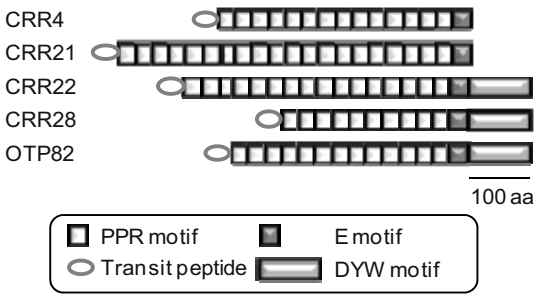

Fig. 1 Motif sturucture of editing specificity factors.

Table 1 Effect of the deletion and conservation of the E and DYW motifs in CRR4. *crr4-3+CRR4ΔE*, *crr4-3* transformed with the CRR4 truncated in the E motif; *crr4-3+CRR4-21E*, *crr4-3* transformed with the CRR4, in which the E motif was replaced by that of CRR21.

	Editing extent of ndhD-1 site (%)
Wild type	42
crr4-3	0
crr4-3+CRR4ΔE	7
crr4-3+CRR4-21E	31

Salone *et al*. (2007) proposed that PPR proteins of the DYW subclass, named for the highly conserved C-terminal DYW tripeptides (Asp, Tyr, and Trp), might carry the catalytic function required for RNA editing in plant organelles. The DYW subclass contains the characteristic DYW motif, which contains invariant Cys and His residues matching the active site of cytidine deaminases, including the human RNA editing enzyme APOBEC1 (Salone *et al*., 2007). CRR22, CRR28, and OTP82 are involved in multiple RNA editing events, which is consistent with the hypothesis that the DYW motif might be characteristic of an RNA editing enzyme (Salone *et al*., 2007). To clarify the role of the DYW subclass, we focused on the function of the DYW motifs of CRR22, CRR28, and OTP82. First, we examined whether the DYW motifs of CRR22 and CRR28 are essential for RNA editing *in vivo*. CRR22 and CRR28, in which their DYW motifs were truncated, were expressed in *crr22-1* and *crr28-1*, respectively. Both truncated genes could completely restore RNA editing at all five sites (Table 2 shows only editing of ndhB-7 site which is impaired in *crr22*). We conclude that the DYW motifs of CRR22 and CRR28 are dispensable for RNA editing *in vivo*. Next we tested whether the DYW motif could be functionally interchanged between CRR22 and CRR28. The relevant chimeric genes were introduced into *crr22-1* and *crr28-1*, respectively. Both chimeric genes could complement the function of the original gene (Table 2). Taken together, the DYW motifs of CRR22 and CRR28 have identical functions.

The DYW motif is dispensable *in vivo* for CRR22 and CRR28 (Table 2). This result is consistent with the fact that CRR4, and CRR21 lacking the DYW motif are also RNA editing factors. We showed that the E motif is essential for RNA editing and its function is common between CRR4 and CRR21 (Table 1). This motif may be involved in recruiting an unknown editing enzyme and shows high similarity among CRR4, CRR21, CRR22, CRR28, and OTP82 (Fig. 1), suggesting that the function of E motifs may also be conserved in the DYW proteins CRR22 and CRR28. To test this possibility, CRR22 and CRR28 lacking both their E and DYW motifs were expressed in *crr22-1* and *crr28-1*, respectively. The editing function of neither CRR22 nor CRR28 was complemented by the introduction of the truncated genes (Table 2). Since the deletion of the E motif is unlikely to affect RNA binding, we believe that the E motifs of CRR22 and CRR28 are essential for the RNA editing reaction.

Table 2 Effect of the deletion and conservation of the E and DYW motifs in CRR22. *crr22-1+CRR22ΔE*, *crr22-1* transformed with the CRR22 truncated in the E motif; *crr22-1+CRR22ΔE/DYW*, *crr22-1* transformed with the CRR22 truncated in the E and DYW motifs; *crr22-1+CRR22-28DYW*, *crr22-1* transformed with the CRR22, in which the DYW motif was replaced by that of CRR28.

	Editing extent of ndhB-7 site (%)
Wild type	98
crr22-1	0
crr22-1+CRR22ΔDYW	98
crr22-1+CRR22ΔE/DYW	0
crr22-1+CRR22-28DYW	99

Salone *et al*. (2007) postulated that the unknown enzyme is the DYW motif, a hypothesis at first sight reinforced by the fact that CRR22, CRR28, and OTP82 all contain DYW motifs. However, the *in vitro* assay using the recombinant DYW motif of CRR22 did not detect any cytidine deaminase activity under our assay conditions (data not shown). We demonstrated that the E motif common to almost all PLS family PPR proteins is essential for RNA editing *in vivo*, presumably via an association with an unknown RNA editing enzyme. Hence, CRR22, CRR28, and OTP82 behave exactly like the editing specificity factors CRR4, CRR21 despite the presence of the additional DYW motif. Since the DYW motif is dispensable for editing, it may have been lost in members of the E subclass, including CRR4 and CRR21.

References

Chateigner-Boutin AL, Small I (2010) Plant RNA Editing. RNA Biol. 7: 213-219

Kotera E, Tasaka M, Shikanai T (2005) A

Pentatricopeptide Repeat Protein Is Essential for RNA Editing in Chloroplasts. Nature 433: 326-330

Okuda K, Chateigner-Boutin AL, Nakamura T, Delannoy E, Sugita M, Myouga F, Motohashi R, Shinozaki K, Small I, Shikanai T (2009) Pentatricopeptide Repeat Proteins with the DYW Motif Have Distinct Molecular Function in RNA Editing and RNA Cleavage in Arabidopsis Chloroplasts. Plant Cell 21: 146-156

Okuda K, Hammani K, Tanz SK, Peng L, Fukao Y, Myouga F, Motohashi R, Shinozaki K, Small I, Shikanai T (2010) The Pentatricopeptide Repeat Protein OTP82 Is Required for RNA Editing of Plastid ndhB and ndhG Transcripts. Plant J. 61: 339-349

Okuda K, Myouga F, Motohashi R, Shinozaki K, Shikanai T (2007) Conserved Domain Structure of Pentatricopeptide Repeat Proteins Involved in Chloroplast RNA Editing. Proc. Natl. Acad. Sci. USA. 104: 8178-8183

Okuda K, Nakamura T, Sugita M, Shimizu T, Shikanai T (2006) A Pentatricopeptide Repeat Protein Is a Site Recognition Factor in Chloroplast RNA Editing. J. Biol. Chem. 281: 37661-37667

Salone V, Rüdinger M, Polsakiewicz M, Hoffmann B, Groth-Malonek M, Szurek B, Small I, Knoop V, Lurin C (2007) A Hypothesis on the Identification of the Editing Enzyme in Plant Organelles. FEBS Lett. 581: 32-38

Schmitz-Linneweber C, Small I (2008) Pentatricopeptide Repeat Poteins: a Socket Set for Organelle Gene Expression. Trends Plant Sci. 13: 663-760

Symposium 19

Marine Photosynthesis and Global Impact

The Role of tRNAs in Cyanophages

Limor-Waisberg Keren[a], Carmi Asaf[b], Scherz Avigdor[c], Pilpel Yitzhak[b], Furman Itay[b].

[a]Department of Structural Biology, [c]Department of Plant Sciences, [b]Department of Molecular Genetics.
[*]Corresponding author. E-mail: avigdor.scherz@weizmann.ac.il.

Abstract: Cyanophages, viruses infecting cyanobacteria, play key roles in the life cycle, biodiversity, evolution, and ecological modulations of their hosts. Accumulating evidence that a variety of photosynthesis-related and other host-like genes are found in genomes of cyanophages underscores the close relationship cyanophages have with the gene pools of their hosts during the infection cycle. An hypothesis follows that cyanophages are excellent mediators and innovators in lateral gene transfer and gene birth events. Cyanophages of the *Myoviridae* family appear to incorporate full-length tRNA genes into their genomes apart from host-like genes. We evaluated the possible effect of those tRNAs on the expression of cyanophages and cyanobacterial genes using the tRNA Adaptation Index, which measures the extent a given pool of tRNAs affects the translation of genes taking into account their codon usage (dos Reis, Savva *et al*., 2004). We show that, using the self-born tRNAs, myoviruses can efficiently harness the translation machinery of their hosts while maintaining genomes with considerabley lower GC-contents. In particular, the myoviral *psbA* and *psbD* genes, encoding for the D1 and D2 core proteins of the photosystem II, respectively, are seen to be better adapted to the addition of the viral tRNAs, when compared with their cyanobacterial counterparts from which they originated.

Keywords: Cyanophage; tAI; tRNA; *Myoviridae*; photosystem II

Introduction

Cyanophages, viruses infecting cyanobacteria, of the T4-like *Myoviridae* family may add to their basic and essential core genomes genes derived from their hosts (Sullivan, Coleman *et al*., 2005). Genes encoding proteins involved in photosynthesis, such as the *psbA* and, somewhat less extensively, the *psbD* genes, encoding for the D1 and D2 core photosystem II (PSII) proteins, respectively, may be found in genomes of cyanophages (Lindell, Sullivan *et al*., 2004; Millard, Clokie *et al*., 2004; Zeidner, Bielawski *et al*., 2005; Sandaa and Larsen, 2006; Sullivan, Lindell *et al*., 2006; Chenard and Suttle, 2008; Wang and Chen, 2008). With the emerging genome sequencing projects, it was soon revealed that, in addition to such host-like genes, some cyanomyoviruses bear full-length tRNA genes within their genomes (Sullivan, Coleman *et al*., 2005). Reports on the presence of tRNA genes within phage genomes date back to 1968, when they were first found in the T4 bacteriophage, which infects *E. coli* (Weiss, Hsu *et al*., 1968). The tRNAs were proposed to serve as a common integration site for genomes of temperate phage into the genomes of their hosts; their presence on the viral genome would thus be the result of an ensuing excision (Campbell, 1992; Cheetham and Katz, 1995; Canchaya, Fournous *et al*., 2004; Tan, Zhang *et al*., 2007). However, deletion of tRNAs of the T4 phage resulted in lower burst sizes and rates of protein synthesis, hence a certain fitness was proposed to be acquired for phages bearing them (Wilson, 1973). Furthermore, a significant positive association between the exact cognate tRNA distribution and codon usage was observed, leading to the hypothesis that tRNAs are selectively retained. It was suggested that some tRNAs are lost neutrally or *via* selection, leaving behind those which match codons highly used by the phage and poorly used by the bacterial host during the infection cycle (Daniel, Sarid *et al*., 1970;

Kunisawa, 1992; Kunisawa, 2000; Bailly-Bechet, Vergassola *et al*., 2007). As only some of the marine myoviruses bear tRNAs within their genomes, we decided to explore the reason and benefits of their occurrence.

In this article we suggest that a specific set of tRNAs is retained by cyanomyoviruses that infect, perhaps exclusively, hosts that are equipped with high GC-content genome and a suitable translation machinery. We then show that the cyanomyovirus set of tRNAs is among the very best sets promoting improved translation of viral genes at the expense of the translation of host genes. At last we show how host-like genes such as *psbA* and *psbD* evolve within the cyanomyoviral genome to co-adapt with the set of tRNAs embedded in the same viral genome, to ultimately act as other viral genes and outcompete the translation efficiency of the cyanobacterial counterparts.

Materials and Methods

Coding sequences and tRNA genes of cyanobacteria and cyanophages were downloaded from GenBank (http://www.ncbi.nlm.nih.gov/Genbank) or the camera (http://camera.calit2.net/) databases.

The extent to which the codon usage of a given coding sequence is adapted to the cellular tRNA abundance can be estimated using the tRNA Adaptation Index (tAI), a statistical measure that was devised in 2004 by dos Reis (dos Reis, Savva *et al*., 2004). To increase the robustness of the index, we chose a normalization scheme in which each codon weight, w_c, was normalized to the genome-wide tAI, $\mathrm{tAI(G)}=W_1^{f_1}\times W_2^{f_2}\times\cdots\times W_{61}^{f_{61}}$, such that $w_c = W_c/\mathrm{tAI(G)}$. For each bacterium-phage pair we computed two sets of tAI weights: one in which the tRNA gene copy number equals that of the bacterium genome alone, and a second set in which the copy number is the sum of the bacterium and phage copy numbers. Using this concept, we computed for each bacterial or viral gene, g, its tAI value while either accounting for the contribution of the viral tRNAs, $\mathrm{tAI}^+(g)$, or discounting that contribution, $\mathrm{tAI}(g)$. Having these two numbers, we defined for each gene the tAI difference, $\Delta\mathrm{tAI}(g)=\log\left[\mathrm{tAI}^+(g)/\mathrm{tAI}(g)\right]$. From this definition follows the definition of the separation between the bacterial and phage response to the inclusion of the viral tRNA pool:

$$\Delta\Delta\mathrm{tAI}=\frac{\mathrm{mean}\left[\Delta\mathrm{tAI}(g_{\mathrm{v}})\right]-\mathrm{mean}\left[\Delta\mathrm{tAI}(g_{\mathrm{h}})\right]}{\sqrt{\mathrm{std}^2\left[\Delta\mathrm{tAI}(g_{\mathrm{v}})\right]+\mathrm{std}^2\left[\Delta\mathrm{tAI}(g_{\mathrm{h}})\right]}}.$$

Host	Myovirus	Number of tRNAs
Synechococcus	Syn9	6
	S-PM2	24
	S-RSM4	12
	S-SM1	7
	Syn1	6
	Syn19	6
	Syn33	5
	S-SM7	5
	S-SM5	4
	S-SM2	11
	S-Shm2	1
Prochlorococcus	S-SM1	6
	P-RSM4	3
	P-SSM7	4
	P-SSM2	1
	P-SSM4	0
	P-HM2	0
	P-HM1	0

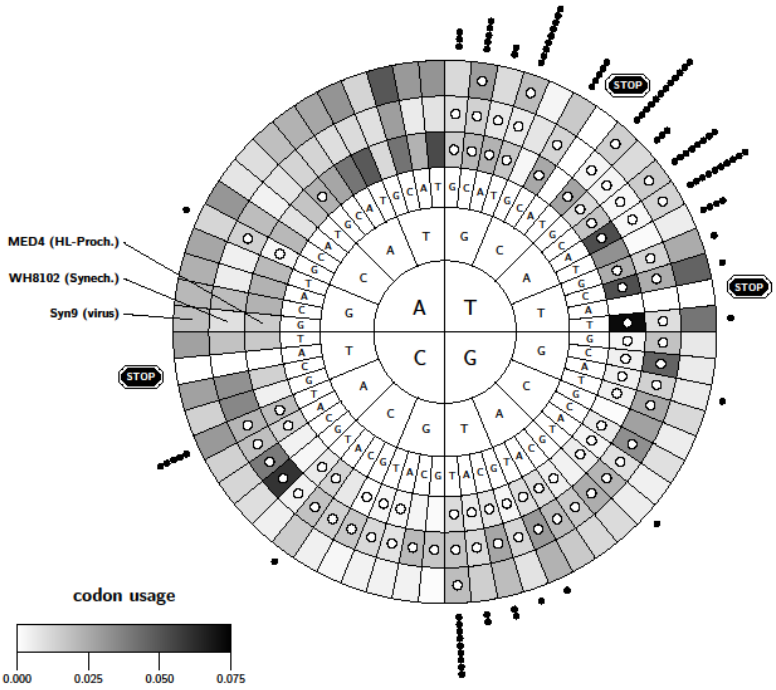

Fig. 1 Codon usage and cognate tRNA gene copy number. Codon usage of *Synechococcus* WH8102 (inner ring), HL-*Prochlorcoccus* MED4 (middle ring), and myovirus Syn9 (outer ring), is represented in grey scale (white: lowest codon usage; black: highest). The presence of a dot reflects the presence of the corresponding tRNA within the organism's genome. The presence of tRNAs in additional myoviruses listed on the left panel, is depicted with dots outside the codon usage rings.

Results and Discussion

Synechococcus, with high GC-content genomes, and *Prochlorococcus*, with low GC-content genomes, are two genera of cyanobacteria susceptible to infection by *Myoviridae* (Rocap, Distel *et al*., 2002; Dufresne, Garczarek *et al*., 2005; Kettler, Martiny *et al*., 2007; Dufresne, Ostrowski *et al*., 2008). Although all marine myoviruses have constitutive low GC-content genomes (*i.e.*, 41% GC and lower), those that were isolated in *Synechococcus* face a significantly larger gap with their host's GC-content as compared with the Myoviruses that were isolated in *Prochlorococcus*. Interestingly, myoviruses isolated from *Synechococcus* were shown to contain larger numbers of tRNA genes and Table 1. Plotting the anticodons borne by the viral tRNAs against the respective codon usage of both hosts and myoviruses reveals the preference for low GC-content anticodons (AT-richer at the wobble, Non-Watson-Crick base pairs). Based on observations in other virus-host pairs, Bailly-Bechet et al., proposed to associate this tendency with the viral low GC-content (Bailly-Bechet, Vergassola *et al*., 2007) (see also Fig. 1). A closer look at the anticodon type shows a predominance of several of the tRNAs (LeuTAA, ThrTGT, AsnGTT, ArgTCT, ValTAC and AlaTGC) out of the entire pool. Myovirus Syn9, isolated from a *Synechococcus* host, bears those six tRNAs and hence was used for further calculations. We have seen that the Syn9 pool of tRNAs mainly improves the translation of Syn9 genes when added to the *Synechococcus* pool of tRNAs, whereas it has a much lesser effect when added to the *Prochlorococcus* tRNA pool (data not shown). To evaluate how significant such influence can be, we generated 10,000 random sets of six tRNAs and calculated the effect of each set on the genomes of both the Syn9 myovirus and the *Synechococcus* host. The separation between the tAI score of the Syn9 genome and the tAI score of the *Synechococcus* genome is plotted in Fig. 2, and the separation induced by the Syn9 pool is indicated. The Syn9 pool of six tRNAs is shown to be among the very best sets of tRNAs (with only 21 out of 10,000 random sets yielding better scores) for improving the translation of viral genes at the expense of its host. Based on the fact that viral-borne tRNAs can confer a significant advantage to the virus when infecting a host with mismatching GC-content, one may naively conclude that the more tRNA the virus would bear – the better. However, roughly speaking, this is true only in the case that the tRNAs carry an anticodon with AT at the first position (AT-rich tRNA). Inspection of the tRNA repertoire of the cyanobacteria (Fig. 1) shows that it is biased towards GC-rich tRNAs (27 *vs*. 14 AT-rich tRNAs). This implies that the chance for a randomly-added tRNA to be advantageous to the virus is only 1/3, while the probability it will be advantageous to the host is about 2/3. In evolutionary terms, this means an increasingly difficult search problem for the virus: the fraction of tRNA sets that will be advantageous to the virus decreases with the increase of the number of tRNAs it will carry. Indeed, calculations of the change in translation efficiency due to viral-borne tRNAs, using random sets, reveal an increase disadvantage to the virus in parallel to a slight increase in advantage to the host, as the size of the viral-borne tRNA set increases (Fig. 3). These data support and emphasize the dynamics of tRNA acquisition and selection that ultimately leaves in genomes of viruses highly optimized sets of tRNAs.

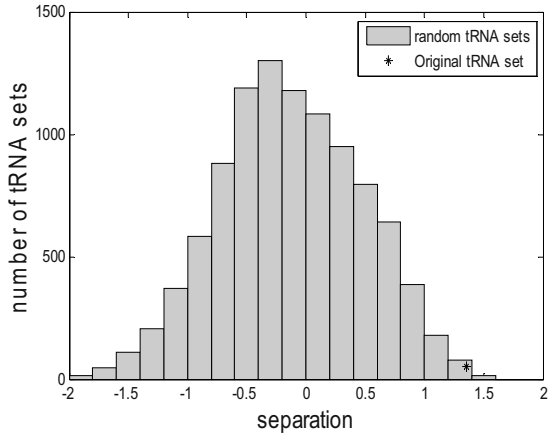

Fig. 2 The distribution of ΔΔtAI is shown for 10,000 random sets of 6 tRNAs assuming Syn9 as the virus and cyanobacterium sinechococcus as host. The position of the separation ΔΔtAI, given by the actual set of tRNA genes in Syn9 is indicated with a star.

The importance of the six tRNAs of Syn9 may be appreciated by observing their impact on the viral copies of cyanobacterial-like *psbA* and *psbD* genes. As mentioned in the introduction, *psbA* and *psbD* genes encode the D1 and D2 proteins, respectively, the two core proteins of PSII. The major role of D1 and D2 in maintenance of photosynthesis reactions and the inevitable damage those reactions cause to these

proteins require an efficient turnover mechanism replacing damaged D1 and D2 by newly synthesized copies. Acquisition and eventual expression of photosynthesis genes were suggested to raise the fitness of the phage compared to another phage devoided of such gene sets (Bragg and Chisholm, 2008). Analysis of the tAI of the cyanophage Syn9 *psbA* and *psbD* genes shows that within the higher GC content hosts translation of both cyanophage genes is boosted by the addition of its six tRNAs (Fig. 4, four right hand host); in all other hosts the effect is opposite: to lower down the translation efficiency. Moreover, in the high-GC hosts, the viral *psbA* gene becomes stronger than the host's gene. This analysis demonstrates that, despite their cyanobacterial origin, the *psbA* and *psbD* genes integrated into the cyanophage genome undergo an evolutionary process that makes them act as other viral genes and respond to the addition of the viral tRNA in a manner that outcompetes their cyanobacterial counterparts. The fitness gained by the acquisition of the photosynthesis genes keeps them within the genome, while translation constraints act to evolve a modified coding sequence, hence providing new alternatives for gene modulations.

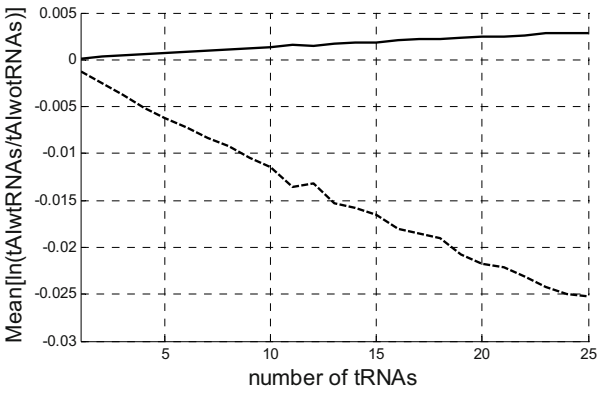

Fig. 3 Mean change of genomic tAI as function of the size of viral-borne tRNA set. The genome-wide average change in tAI, mean(ΔtAI(*g*)), is computed in Syn9 and *Synechococcus* host for 10,000 random sets of tRNAs using set size up to 25. As the size of the random tRNA sets increases, mean(ΔtAI(*g*)), increases in the *Synechococcus* host (solid line), while it sharply decreases in the phage Syn9 (doted line).

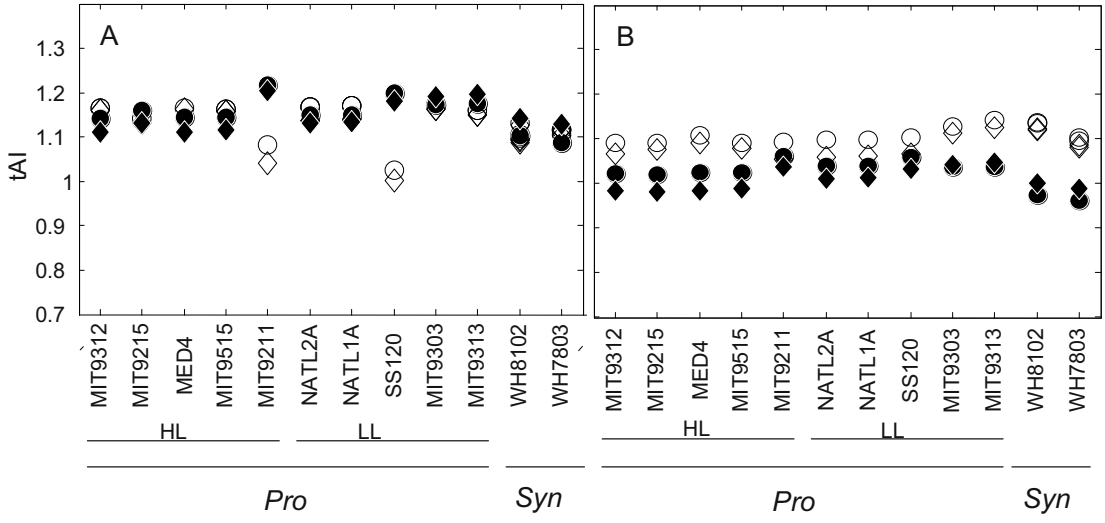

Fig. 4 The tAI values of the viral and host *psbA* (A) and *psbD* (B) genes in different cyanobacteria hosts. The values for the cyanobacteria (cyanophage) genes are represented in white (black). Diamonds (circles) depict the cases when the cyanophage tRNAs are included in (excluded from) the tRNA pool. *Prochlorococcus* (Pro) exhibit lower GC content in comparison with *Synechococcus* (Syn), with the high light (HL) clades showing the lowest GC content and low light (LL) clades intermediate values.

References

Bailly-Bechet M, M Vergassola, *et al*. (2007) Causes for the Intriguing Presence of tRNAs in Phages. Genome Research 17(10): 1486-1495

Bragg JG, SW Chisholm (2008) Modeling the Fitness Consequences of a Cyanophage-Encoded Photosynthesis Gene. PLoS ONE 3(10): e3550

Campbell AM (1992) Chromosomal Insertion Sites for Phages and Plasmids. J Bacteriol 174(23): 7495-7499

Canchaya C, G Fournous, *et al*. (2004) The Impact of Prophages on Bacterial Chromosomes. Molecular Microbiology 53(1): 9-18

Cheetham BF, ME Katz (1995) A Role for Bacteriophages in the Evolution and Transfer of Bacterial Virulence Determinants. Molecular Microbiology 18(2): 201-208

Chenard C, CA Suttle (2008) Phylogenetic Diversity of Sequences of Cyanophage Photosynthetic Gene psbA in Marine and Freshwaters. Appl Environ Microbiol 74(17): 5317-5324

Dammeyer T, SC Bagby, *et al*. (2008) Efficient Phage-Mediated Pigment Biosynthesis in Oceanic Cyanabacteria. Current Biology 18(6): 442-448

Daniel V, S Sarid, *et al*. (1970) Bacteriophage Induced Transfer RNA in Escherichia Coli. New Transfer RNA Molecules Are Synthesized on the Bacteriophage Genome. Science 167(926): 1682-1688

dos Reis M, R Savva, *et al*. (2004) Solving the Riddle of Codon Usage Preferences: a Test for Translational Selection. Nucleic Acids Research 32(17): 5036-5044

Dufresne A, L Garczarek, *et al*. (2005) Accelerated Evolution Associated with Genome Reduction in a Free-Living Prokaryote. Genome Biol 6(2): R14

Dufresne A, M Ostrowski, *et al*. (2008) Unraveling the Genomic Mosaic of a Ubiquitous Genus of Marine Cyanobacteria. Genome Biol 9(5): R90

Kettler GC, AC Martiny, *et al*. (2007) Patterns and Implications of Gene Gain and Loss in the Evolution of Prochlorococcus. Plos Genetics 3(12): 2515-2528

Kunisawa T (1992) Synonymous Codon Preferences in Bacteriophage T4: a Distinctive Use of Transfer RNAs from T4 and from Its Host Escherichia Coli. J Theor Biol 159(3): 287-298

Kunisawa T (2000) Functional Role of Mycobacteriophage Transfer RNAs. Journal of Theoretical Biology 205(1): 167-170

Lindell D, MB Sullivan, *et al*. (2004) Transfer of Photosynthesis Genes to and from Prochlorococcus Viruses. Proceedings of the National Academy of Sciences of the United States of America 101(30): 11013-11018

Millard A, MR J Clokie, *et al.* (2004) Genetic Organization of the psbAD Region in Phages Infecting Marine Synechococcus Strains. Proceedings of the National Academy of Sciences of the United States of America 101(30): 11007-11012

Ochman H, JG Lawrence, *et al.* (2000) Lateral Gene Transfer and the Nature of Bacterial Innovation. Nature 405(6784): 299-304

Rocap G, DL Distel, *et al.* (2002) Resolution of Prochlorococcus and Synechococcus Ecotypes by Using 16S-23S Ribosomal DNA Internal Transcribed Spacer Sequences. Applied and Environmental Microbiology 68(3): 1180-1191

Sandaa RA, A Larsen (2006) Seasonal Variations in Virus-Host Populations in Norwegian Coastal Waters: Focusing on the Cyanophage Community Infecting Marine Synechococcus spp. Appl Environ Microbiol 72(7): 4610-4618

Sullivan MB, ML Coleman, *et al.* (2005) Three Prochlorococcus Cyanophage Genomes: Signature Features and Ecological Interpretations. Plos Biology 3(5): 790-806

Sullivan MB, KH Huang, *et al*. Genomic Analysis of Oceanic Cyanobacterial Myoviruses Compared with T4-Like Myoviruses from Diverse Hosts and Environments. Environ Microbiol

Sullivan MB, D Lindell, *et al.* (2006) Prevalence and Evolution of Core Photosystem II Genes in Marine Cyanobacterial Viruses and Their Hosts. Plos Biology 4(8): 1344-1357

Tan YL, KB Zhang, *et al*. (2007) Whole Genome Sequencing of a Novel Temperate Bacteriophage of P-Aeruginosa: Evidence of tRNA Gene Mediating Integration of the Phage Genome into the Host Bacterial Chromosome. Cellular Microbiology 9(2): 479-491

Wang K, F Chen (2008) Prevalence of Highly Host-Specific Cyanophages in the Estuarine Environment. Environ Microbiol 10(2): 300-312

Weiss SB, WT Hsu, *et al*. (1968) Transfer Rna Coded by T4 Bacteriophage Genome. Proceedings of the National Academy of Sciences of the United States of America 61(1): 114

Wilson JH (1973) Function of Bacteriophage-T4 Transfer-Rnas. Journal of Molecular Biology 74(4): 753

Zeidner G, JP Bielawski, *et al.* (2005) Potential Photosynthesis Gene Recombination between Prochlorococcus and Synechococcus Via Viral Intermediates. Environmental Microbiology 7(10): 1505-1513

Newly Isolated Chl *d*-Containing Cyanobacteria

Yaqiong Li[1], Anthony Larkum[1], Martin Schliep[1], Michael Kühl[3], Brett Neilan[2], Min Chen[1*]

[1]School of Biological Sciences, University of Sydney, New South Wales 2006, Australia;
[2]School of Biotechnology and Biomolecular Sciences, University of New South Wales 2052, Australia;
[3] Marine Biological Laboratory, Department of Biology, University of Copenhagen, DK-3000 Helsingør, Denmark.
*Corresponding author. Tel. No. +61 2 9036 5006; Fax No. +61 2 9351 4119; E-mail: min.chen@sydney.edu.au.

Abstract: Stromatolites are sedimentary structures formed by microbial mats that are typically found in limestone- or dolostone-rich environments. Shark Bay, Australia, has abundant examples of living marine stromatolites. Although the stromatolites from Shark Bay are only about 2000–3000 years old, they are similar to fossilized evidence of life found on Earth up to 3.5 billion years ago. Using infra-red light centred at 720 nm, new chlorophyll *d*-containing microorganisms were isolated from the living stromatolites (collected from Shark Bay, Western Australia) and red algae on mangrove pneumatophores (collected from the Georges River, Sydney, Australia) and enriched in KES^+ seawater medium. Microscopic examination of the red-light enriched cultures confirmed that they are *Acaryochloris*-like cyanobacteria. Using cyanobacterial-specific 16S rRNA gene primers, we obtained almost full length sequences of 16S rDNA from the newly isolated Chl *d*-containing cyanobacteria. The sequences shared 98% identity with *Acaryochloris marina* MBIC11017. Interestingly, the strain isolated from stromatolites (designated as "*ssball1*" strain) was more similar to *Acaryochloris sp* CR111A while the strain isolated from Georges River (designated as "*Mangrove1*" strain) was more closely related to *Acaryochloris sp* CCMEE 5401, which was isolated from an inland "lake", Salton Sea in California,. Pigment composition of the newly isolated strains were determined using HPLC, However, no obvious differences were noted. Chl *d* was the major photopigment while Chl *a* was present as a minor photopigment, about 2%–3.5 % of the total chlorophyll.

Keywords: *Acaryochloris marina*; Chlorophyll *d*; Chlorophyll *d*-containing cyanobacteria; 16S rRNA classification

Introduction

Acaryochloris marina is a unicellular oxygenic photosynthetic cyanobacterium that was first discovered and isolated by Japanese scientists from a colonial ascidian in Palau (Miyashita *et al*., 1996). Instead of chlorophyll (Chl) *a* found in most oxygenic photoautotrophs, *Acaryochloris* contains Chl *d* as its major photosynthetic pigment (> 95%). Only about 3% of Chl *a* is present in its total photosynthetic pigments (Miyashita *et al*., 1997). Distribution of Chl *d*-containing cyanobacteria has been updated rapidly since we introduced infra-red light culture conditions (Kuhl *et al*., 2005; Duxbury *et al*., 2009). To date, there are three different strains reported isolated from the Great Barrier Reef region (Kuhl *et al*., 2005; Mohr *et al*., 2010; Behrendt *et al*., 2010), a strain isolated from the Salton Sea in California (Miller *et al*., 2005), besides the original strain of *Acaryochloris marina* MBIC 11017 reported in 1996 (Miyashita *et al*., 1996).

We used infra-red light to enrich Chl *d*-containing photosynthetic organisms from environmental samples. Further pigment analysis and 16S rRNA sequence comparisons showed that two new strains were isolated from a stromatolite sample and the epilithic strain from the mangrove pneumatophores. Newly isolated Chl *d*-containing cyanobacteria provide strong evidence for a more widespread occurrence of *Acaryochloris*-like cyanobacteria. Our results agree with the hypothesis that Chl *d* and phototrophs that contain it play an important role as

oxygenic primary producers in aquatic ecosystems (Kuhl *et al*., 2007; Kashiyama *et al*., 2008).

Methodology

Environmental sample collections and Culture conditions

Stromatolite and microbial mat samples from Western Australia were collected during the day from Hameiln Pool, Shark Bay, Western Australia in July, 2008 using clean and sterile instruments. The samples were stored in sterilized containers and transported on ice and in the dark to the laboratories in Sydney. Mangrove pneumatophores were collected from Salt Pan Creek Georges River, Sydney, in March, 2008.

In the laboratory the stromatolite samples were ground to a homogenate using a sterilized mortar and pestle and one gram of the homogenized sample was cultured under continuous illumination by infra-red LEDs (720 nm) as described in Chen *et al*. (2010). The epiphytic green biofilms, on the red alga, *Gelidium* sp., on mangrove pneumatophores, were selected under a microscope and cultured under the same conditions as described above.

The infra-red light enrichments were subcultured for 3–4 weeks with new media and selected for the presence of Chl *d* for several cycles under the same light-regime. To purify the Chl *d*-containing strains, we used 24-well culture plates with 2 ml KES seawater medium and 10,000 x dilution sub-inoculation per well under the same light condition for a minimum of 6 weeks (till visible green in the culture wells).

Pigment composition

Pigments were extracted in 100% methanol and analyzed using HPLC, C_{18} reverse phase (Synergi Fusion-RP 80A, 250 mm × 4.6 mm, 4 μl pore size, Phenomenex, USA) immediately. The column was equilibrated using 80% methanol and run at a flow rate of 0.8 ml/min. The running program starts with a linear gradient of solvent A (80% methanol) to solvent B (100% methanol) in 8 min, following with 100% solvent B for 30 min. Eluted pigments were detected with a photodiode array detector (SPD-M10Avp, Shimadzu, Japan) at a range of 370–800 nm. The ratio value of each pigment was calculated based on HPLC chromatogram peak area at their published absorption maxima wavelength and their extinction coefficient at this wavelength. The molar extinction coefficients (ε) of different pigments in methanol were: $\varepsilon = 77.62$ $mol^{-1}cm^{-1}$ at 696 nm for Chl *d*, $\varepsilon = 68.72$ $mol^{-1}cm^{-1}$ at 665 nm for Chl *a*, $\varepsilon = 133$ $mol^{-1}cm^{-1}$ at 452 nm for zeaxanthin, $\varepsilon = 145$ $mol^{-1}cm^{-1}$ at 448 nm for α-carotene.

Genome DNA Extraction

Cells were harvested from 1.5 ml culture by centrifugation and rinsed twice using nuclease-free water. The cell pellets were resuspended in 250 μl TE buffer (pH = 8.0) containing lysozyme (20 mg/ml). Proteinase K (0.16 mg/ml) and SDS (2%) were added to the mixture. The mixture was incubated at 50 °C for 60 min (or until cell suspension color changed from green to yellowish-brown colour). Subsequently, RNase (0.16 mg/ml) was added and incubated at 65 °C for 40 min to remove RNA. Genomic DNA was extracted by phenol-chloroform phase separation, precipitated using isopropanol and rinsed in 70 % ethanol, then stored in nuclease-free water at –20 °C.

Polymerase Chain Reaction

Nearly complete 16S rRNA gene sequence was amplified using genome DNA as template and cyanobacterial 16S rRNA specific primers **27F** (5`-AGAGTTTGATCCTG--GCTCAG-3`), **809R** (5`-GCTTCGGCACGGCT-CGGGGTCGATA-3`), **740F** (5`-GGC (TC) (AG) (AT) A (AT) CTGACACT (GC) AG GGA-3`), and **1494R** (5`-TACGGCTACCTTGTTAC GAC-3`). All PCR reactions were prepared in a volume of 20 μl using Mango Taq Polymerase PCR kit (Bioline, USA). Thermal cycling was performed with an initial denaturation step at 94 °C for 2 min, followed by 35 cycles of 94 °C for 10 s, 54 °C for 20 s and 72 °C for 60 s. An additional extension step at 72 °C for 7 min was performed after 35 cycles.

Sequencing

Amplified 16S rRNA gene fragments were separated and purified for sequencing. The complete 16S rDNA sequences were obtained by combining the two PCR products generated by primer pairs 27F/809R and 740F/1049R through 100% overlapping region between 740 site and 809 site of 16S rDNA.

Phylogenetic Analysis

Related cyanobacterial 16S rDNA sequences were downloading from NCBI. 16S 16S rDNA sequence data were aligned using the multiple sequence alignment tools (Clustal W) and modified manually

according to the 16S rDNA alignment published in Mohr *et al*. (2010). Phylogenetic relationships were inferred using the Neighbor Joining (NJ) method with a Jukes-Cantor model using Molecular Evolutionary Genetic Analysis (MEGA) software version 4.0, and the phylogenetic trees were evaluated by bootstrap replication at 1,000 times.

Table 1 Major photopigments composition of *ssball1* and *mangrovel*.

Percentage (%)	*ssball1*	*mangrove1*
zeaxanthin in total	16.10	22.90
α-carotene in total	27.30	34.70
Chl *d* / Chl *a ratio*	32.06	51.75
Chl *d*/Total Chls	96.98	98.10

Total pigments represent total chlorophylls and total carotenoids.

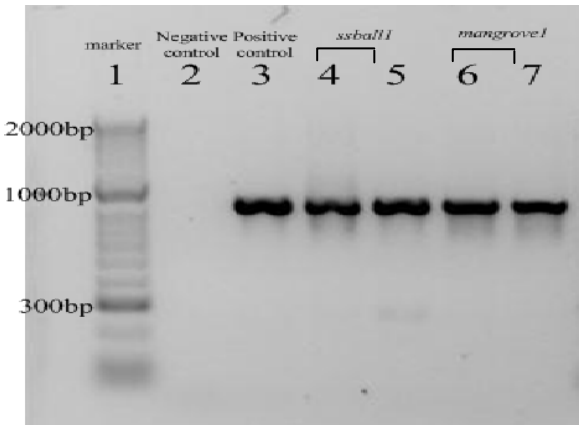

Fig. 1 PCR products of 16S rRNA gene amplified from the newly isolated photosynthetic strains *ssball1* and *mangrove1*, with 27F/809R and 740F/1409R primers. Lane 1: Marker (2 Kb); Lane 2: Negative control; Lanes 3: Positive control (*Acaryochloris* MIBC 11017 strain); Lane 4: strain *ssball1* (primers 27F/809R); Lane 5: strain *ssball1* (primers 740F/1494R); Lane 6: strain *mangrove1* (primers 27F/809R); Lane 7: strain *mangrove1* (primers 740F/1494R).

Result and Discussion

After several months of infra-red light induction, we obtained one Chl *d*-containing strain from the stromatolite sample, named as "ssball1" and one strain line from mangrove pneumatophores, named as "*mangrove1*". The pigment composition analysis showed the two new strains contain Chl *d* as their major photopigments, and are similar to those of known strains of *Acaryochloris* (Table 1).

Using specific cyanobacterial 16S rDNA primers (Jungblut *et al*., 2005; Neilan *et al*., 1997), we performed two sets of PCR amplifications and obtained around 1380 bp DNA fragments. Single PCR product band with 27F/809R primers and 740F/1494R primers, respectively, confirmed the purity of new isolates (Fig. 1).

Sequences of 27F/809R and 740F/1409R from same genomic DNA sample we aligned and converted to one sequence if there is a 100% overlap region between two PCR products. Additional primers at 27F site and 1494R site were used and confirmed as a single PCR product. Total 1,380 bp assembled PCR products were obtained from both new isolates and used for further sequence analysis.

Alignment among new isolates and known *Acaryochloris marina* strains revealed 98% identity among *ssball1, mangrove1* and *Acaryochloris sp*.

Nearly complete 16S rDNA sequences of new isolates were used for phylogenetic comparison (Fig. 2). All known strains of *Acaryochloris* formed a separated clade, mostly closed to *Cyanothece sp* PCC 7425. There are two branches resolved within *Acaryochloris* clade, the new isolate, *ssball1*, is closest to *Acaryochloris sp* CR111A, while "*mangrove1*" is closest to *Acaryochloris sp* CCMEE 5410.

16S rDNA phylogenetic tree supports the idea that new isolates belong to *Acaryochloris marina* clade genetically, although they were isolated from different geological locations and environments. Considering the special original sample collection location for *Mangrove1* strain, a set of salinity tolerance tests for Chl *d*-containing cyanobacteria is being carried out to define the optimal culture condition and understand the ecophysiology of these strains.

Acknowledgements

The authors thank Ms K Donohoe, University of Sydney, for assistance on DNA isolation and PCR reactions. MC holds an Australian Queen Elizabeth Ⅱ Fellowship and thanks ARC for financial support. MC and YL thank Prof. Hess, Freiburg University, Germany for accessing 16S rDNA alignment. Ms Y Li thanks Dr. S Murray, University of New South Wales for valuable discussion on phylogenetic analysis and Mr Y Lin for HPLC assistance.

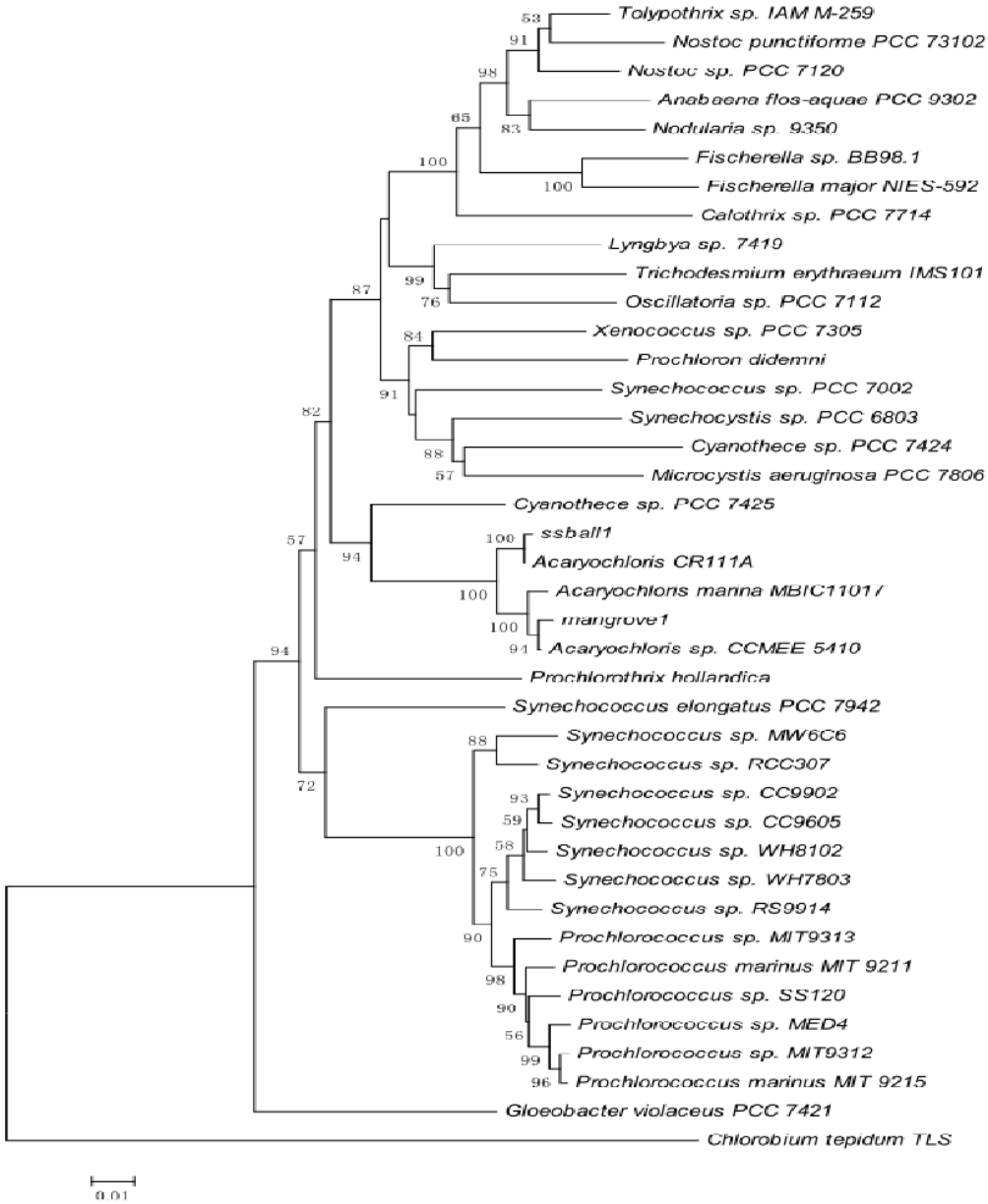

Fig. 2 Neighbour joining Phylogenetic tree analyzed based on the comparison of 1380 bp 16 S rRNA gene among new isolated photosynthetic organism *ssball1*, *mangrove1* and cyanobacterial 16S rRNA. There were 40 taxa contained in this phylogram, where green sulphur bacterium *Chlorobium tepidum* was used as the out-group. The phylogenetic relationship was constructed using the Neighbor Joining methods, where support values were calculated using molecular evolutionary genetics analysis (MEGA) software version 4.0(MEGA 4). Scale is 0.01 substitutions per nucleotide positions. Only bootstrap values > 50% of 1,000 resamplings of the data were illustrated at nodes.

References

Behrendt L, Trampe E, Larkum AWD, Norman A, Qvortrup K, Chen M, Ralph P, Sørensen SJ, Kühl M (2011) Endolithic Chlorophyll d Containing Phototrophs. ISME J (in press, doi: 10.1038/ismej.2010.195).

Chen M, Schliep M, Willows RD, Cai ZL, Neilan BA, Scheer H (2010) A Red-Shifted Chlorophyll. Science 329: 1318-1319

Duxbury Z, Schliep M, Ritchie RJ, Larkum AWD, Chen M (2009) Chromatic Photoacclimation Extends Utilisable Photosynthetically Active Radiation in the Chlorophyll d-Containing Cyanobacterium, Acaryochloris Marina. Photosynth. Res. 101: 69-75

Jungblut A, Hawes I, Mountfort D, Hitzfeld B, Dietrich DR, Burns BP, Neilan BA (2005)

Diversity within Cyanobacterial Mat Communities in Variable Salinity Meltwater Ponds of McMurdo Ice Shelf, Antarctica, Environ. Microbiol. 7: 519-529

Kashiyama Y, *et al.* (2008) Evidence for Global Chlorophyll d. Science 321: 658-658

Kühl M, Chen M, Ralph PJ, Schreiber U, Larkum AWD (2005) A Niche for Cyanobacteria Containing Chlorophyll d. Nature 433: 820-820

Kühl M, Chen M, Larkum AWD (2007) Biology of the Chlorophyll d-Containing Cyanobacterium Acaryochloris Marina. In: J Seckbach (ed.), Algae and Cyanobacteria in Extreme Environments. Springer: Berlin, pp. 101-123

Miller SR, *et al*. (2005) Discovery of a Free-Living Chlorophyll d-Producing Cyanobacterium with a Hybrid Proteobacterial/Cyanobacterial Small-Subunit rRNA Gene. Proc. Natl. Acad. Sci. USA 102: 850-855

Miyashita H, Ikemoto H, Kurano N, Adachi K, Chihara M, Miyachi S (1996) Chlorophyll d As a Major Pigment. Nature 383: 402-402

Miyashita H, Adachi K, Miyachi S, Chihara M, Ikemoto H, Kurano N (1997) Pigment Composition of a Novel Oxygenic Photosynthetic Prokaryote Containing Chlorophyll d As the Major Chlorophyll. Plant and Cell Physiology, 38: 274-281

Mohr R, Voss B, Schliep M, Kurz T, Maldener I, Adas DG, Larkum AWD, Chen M, Hess WR (2010) Niche Adaptation in a New Chlorophyll d-Containing Cyanobacterium from the Genus Acaryochloris. ISME J 4: 1456-1469

Neilan BA, Jacobs D, DelDot T, Blackall LL, Hawkins PR, Cox PT, Goodman AE (1997) rRNA Sequences and Evolutionary Relationships among Toxic and Nontoxic Cyanobacteria of the Genus Microcystis. International Journal of Systematic Bacteriology 47: 693-697

How do Enzyme Dynamics Influence Rubisco Activity?

F Grant Pearce

Biomolecular Interactions Centre and School of Biological Sciences, University of Canterbury, New Zealand.
Tel. No. +64 3 364 2987; Fax No. +64 3 364 2590; E-mail: grant.pearce@canterbury.ac.nz.

Abstract: Life on earth depends on the incorporation of inorganic carbon dioxide from the atmosphere into organic carbon in living organisms. The enzyme responsible for carrying out the primary CO_2 fixation reaction in photosynthesis is Rubisco (ribulose-bisphosphate carboxylase/oxygenase), the most abundant enzyme in the world. However, one of the great mysteries of enzymology is why, despite intense natural selection over millions of years, all forms of Rubisco are characterised by a slow catalytic rate and an enigmatic tendency to confuse the substrate CO_2 with atmospheric O_2. This ability to discriminate between CO_2 and O_2 is determined by the relative capacities of the enzyme to catalyse carboxylation or oxygenation of ribulose 1,5-bisphosphate. Despite decades of research, the reason that one of the most important and abundant enzymes on the planet should remain one of the least efficient remains unclear. Our current research seeks to shed light on this long-standing conundrum by revealing a missing piece in the evolutionary puzzle: the role of enzyme dynamics in determining enzyme efficiency. Rubisco from marine algae will be used to test the hypothesis that the peculiar lack of specificity of Rubisco enzymes is determined by protein dynamics.

Keywords: Rubisco; Enzyme dynamics; Red algae

Rubisco enzymes differ in specificity and side reactions

Among different species, Rubisco displays wide variation in kinetic parameters (Spreitzer and Salvucci, 2002). There appears to be a trade off between substrate specificity and catalytic rate, and it has been suggested that all Rubisco enzymes adapt to their environmental conditions by trading catalytic rate for specificity (Tcherkez *et al*., 2006). However, this tentative conclusion is based on a relatively small set of data, and would benefit from the study of a larger set of organisms. We have previously shown that the binding of ligands and the rate of side-reactions also correlates with the specificity and turnover rates (Table 1; Pearce, 2006). Dimeric bacterial Rubisco enzymes have low specificity, high turnover rates, and are predicted to have high flexibility compared to the hexadecameric plant and algal enzymes. Red algal enzymes, such as that from *Galdieria sulphuraria*, have low turnover rates, but high substrate specificity. Given that the structure of the active site is well conserved among species (Fig. 1), we hypothesise that differences in the kinetic parameters are due to enzyme dynamics and flexibility.

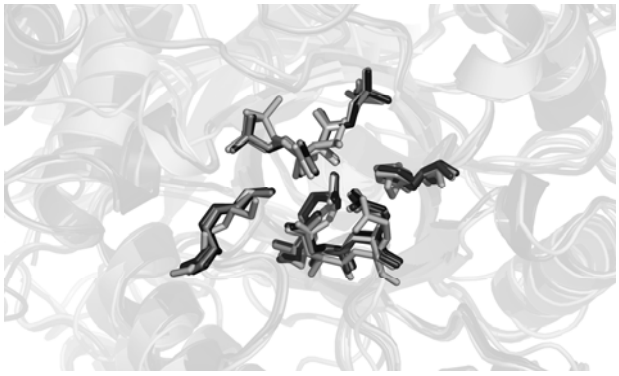

Fig. 1 Overlay of the large subunit of spinach, Synechococcus, Galdieria, Bacterosira and Rhodospirilum Rubisco. Highlighted residues include Lys201, Asp203, Glu204, Lys175 and His294.

Table 1 A comparision of kinetic parameters for different Rubisco enzymes (Table reproduced from Pearce, 2006; with permission from Pearce).

	Tobacco	*Synechococcus*	*R. rubrum*	*G. sulfuraria*
Catalytic parameters				
CO_2/O_2 specificity	82	43	12	166
V_{max} (s^{-1})	2.9 ± 0.1	13.9 ± 0.1	4.2 ± 0.1	1.2 ± 0.1
K_m (CO2) (μM)	10.7	280	67	3.3
K_m (RuBP) (μM)	58 ± 4	54 ± 4	3.9 ± 1	376 ± 42
K_i (XuBP) (μM)	4.8 ± 0.4	12.2 ± 1.0	3.1 ± 0.7	89 ± 29
Self inhibition during in vitro assays	Yes	No	No	No
Side Reactions				
XuBP production (s^{-1})	$9.2 \pm 0.03 \times 10^{-3}$	$4.9 \pm 0.1 \times 10^{-3}$	$56.9 \pm 6.5 \times 10^{-3}$	$10.5 \pm 0.08 \times 10^{-3}$
XuBP carboxylation (s^{-1})	$0.46 \pm 0.02 \times 10^{-3}$	$4.17 \pm 0.03 \times 10^{-3}$	$5.13 \pm 0.03 \times 10^{-3}$	$2.75 \pm 0.03 \times 10^{-3}$
Pyruvate synthesis (% of carboxylation)	0.68 %	0.73 %	0.68 %	1.96 %
Release from tightly bound complexes kobs (s^{-1})				
RuBP	$2.09 \pm 0.01 \times 10^{-3}$	$28.9 \pm 0.5 \times 10^{-3}$	$20.0 \pm 0.5 \times 10^{-3}$	$0.13 \pm 0.01 \times 10^{-3}$
XuBP	$0.60 \pm 0.01 \times 10^{-3}$	$29.8 \pm 0.5 \times 10^{-3}$	$19.5 \pm 0.5 \times 10^{-3}$	$0.07 \pm 0.03 \times 10^{-3}$
CA1P	$2.8 \pm 0.1 \times 10^{-3}$	$8.3 \pm 0.1 \times 10^{-3}$	$19.4 \pm 0.2 \times 10^{-3}$	$0.8 \pm 0.1 \times 10^{-3}$
CABP inhibition				
k_2 (s^{-1})	0.17 ± 0.04	0.28 ± 0.09	> 1.0	0.086 ± 0.016
k_{-2} (s^{-1})	$< 10^{-7}$	$< 10^{-7}$	4.1 ± 0.2	$< 10^{-7}$
K_i (μM)	2.3 ± 0.7	1.72 ± 1.10	> 2	220 ± 101

Red algal and diatom Rubisco enzymes have an extended small subunit

Red algal Rubisco enzymes have some of the highest recorded specificity values, and one of the key features of these Rubisco enzymes is an extended region of the small subunit (Sugawara *et al*., 1999). Our characterisation of marine Arctic algae (*Skeletonema costatum* and *Bacterosira bathyomphala*), showed that these Rubisco enzymes also have an extended C-terminal region of the small subunit, which form a beta hairpin structure that extends into the central solvent channel (Fig. 2). Our hypothesis is that the high specificity of red algal Rubisco is due to the C-terminal extensions, which act to reduce the flexibility of the enzyme.

How are enzyme dynamics involved?

In biology, a protein's function is ultimately determined by its dynamic character. The idea that proteins exist as an ensemble of fluctuating conformations has lead to an extension of the structure-function paradigm to include dynamics (Henzler-Wildman and Kern, 2007; Eisenmesser *et al*., 2005). While x-ray structures are known for a wide range of Rubisco enzymes, these static structures only provide information about an average folded state. In order to characterize the dynamics of the Rubisco enzyme, we will use a variety of techniques to probe the energy landscape. These methods have recently been used to demonstrate the increased flexibility of variants of E .coli DHDPS (Pearce *et al*., 2008; Griffin *et al*., 2008).

Small angle x-ray scattering (SAXS) is a powerful technique that provides information about the size and shape of molecules in solution. By comparing the structure in solution with the structure in the static crystal, more information can be gained about the dynamics of the enzyme. In our recent studies of the DHDPS enzyme, we used SAXS to show that a mutant of the enzyme was more flexible in solution than the wild-type enzyme, despite have an identical structure by xray crystallography. In our current research, we will use SAXS to compare the enzyme structure in solution with the crystal structure (Fig. 3).

Acknowledgements

This work was funded in part by Royal Society of New Zealand Marsden Fund, and through seed funding from the Biomolecular Interactions Centre. Travel to the Australian Synchrotron was supported by funding from the New Zealand Synchrotron Group.

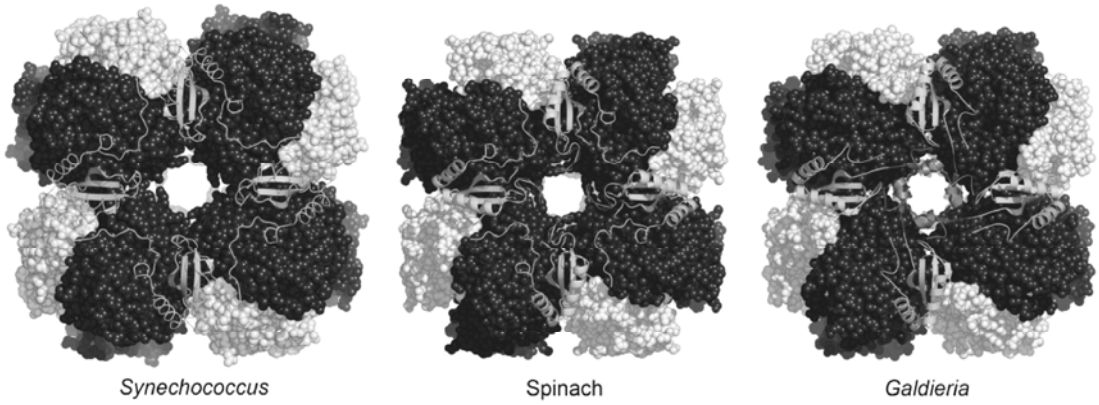

Fig. 2 Top views of Bacterosira, tobacco, and Synechococcus Rubisco, showing the large subunits (grey and blue), small subunits (green), and the extended small subunit region in red.

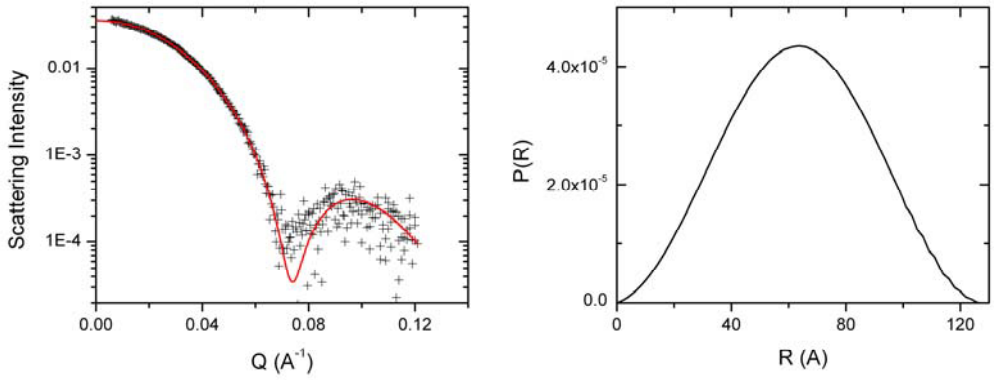

Fig. 3 Small angle x-ray scattering data of spinach Rubisco (symbols, left panel) showed good aggrement with the scattering predicted from the crystal structure (line, left panel). Scattering data was also used to calculate the size distribution of spinach Rubisco (right panel).

References

Eisenmesser EZ, *et al*. (2005) Intrinsic Dynamics of an Enzyme Underlies Catalysis. Nature 438: 117-121

Griffin MDW, *et al*. (2008) Evolution of Quaternary Structure in a Homotetrameric Enzyme. J. Mol. Biol. 380: 691-703

Henzler-Wildman K, Kern D (2007) Dynamic Personalities of Proteins. Nature 450: 964-972

Pearce FG (2006) Catalytic By-Product Formation and Ligand Binding by Ribulose Bisphosphate Carboxylases from Different Phylogenies. Biochem. J. 399: 525-543

Pearce FG, *et al*. (2008) Mutating the Tight-Dimer Interface of Dihydrodipicolinate Synthase Disrupts the Enzyme Quaternary Structure: toward a Monomeric Enzyme. Biochem. 47: 12108-12117

Spreitzer Salvucci (2002) RUBISCO: Structure, Regulatory Interactions, and Possibilities for a Better Enzyme. Annu. Rev. Plant Biol. 43: 449-475

Sugawara H, *et al*. (1999) Crystal Structure of Carboxylase Reaction-Oriented Ribulose 1, 5-Bisphosphate Carboxylase/Oxygenase from a Thermophilic Red Alga, Galdieria partita. J. Biol. Chem. 274(22): 15655-15661

Tcherkez GGB, *et al*. Despite Slow Catalysis and Confused Substrate Specificity, All Ribulose Bisphosphate Carboxylases May Be Nearly Perfectly Optimized (2006) P.N.A.S. 103: 7246-7251

Symposium 20

Crop Yield Improvement

Photosynthesis, Photorespiration and Productivity of Wheat Genotypes (*Triticum* L.)

Jalal A Aliyev

Institute of Botany, Azerbaijan National Academy of Sciences, 40 Badamdar Shosse,
Baku AZ1073, Azerbaijan. Tel. No. (994 12) 438 1164; Fax No. (994 12) 510 2433; E-mail: aliyev-j@botany-az.org.

Abstract: The results of the numerous measurements obtained during the last 40 years on gas exchange intensity using of infrared gas analyzer URAS-2T (Germany), photosynthetic carbon metabolism by exposition in $^{14}CO_2$ and activities of enzyme of primary carbon fixation, ribulose-1,5-bisphosphate carboxylase/oxygenase (RuBPC/O) in various wheat genotypes grown over a wide area in sowings and contrasting on photosynthetic traits and productivity are presented in this paper. It was established that high productive wheat genotypes with the best architectonics (7–9 t ha^{-1}) possess higher intensity of CO_2 assimilation and high values of photorespiration in leaf ontogenesis. Genotypes with moderate (4–5 t ha^{-1}) and low (3 t ha^{-1}) grain yield are characterized by relatively low intensity both of CO_2 assimilation and photorespiration. Activities of RuBP carboxylase and RuBP oxygenase were changing in a similar way in the course of the flag leaf and ear elements development. The rates of sucrose (the main transport metabolite in plants) biosynthesis and products of glycolate metabolism also correlate with the CO_2 assimilation rate and the activity of RuBP oxygenase. Hence, taking into account the versatile investigations on different aspects of photorespiration it was proved that photorespiration is one of the evolutionary developed vital metabolic processes in plants.

Keywords: Photosynthesis; Photorespiration; Productivity; *Triticum* L. genotypes; Sowing

Introduction

In plants with C_3-metabolism photosynthesis takes place simultaneously with the opposite process, which relates both to the oxygen and carbon dioxide gas exchange. This process occurs only in the light and is associated with photosynthetic metabolism, and therefore was named photorespiration. Photorespiration was discovered in 1955 by I. Decker (1955). Photosynthesis and photorespiration are closely linked processes catalyzed by the key photosynthetic enzyme—ribulose-1,5-bisphosphate carboxylase (Rubisco, EC 4.1.1.39) with the dual catalytic activity. The process of photorespiration relates to oxygenase activity of Rubisco, whose function is to fix carbon dioxide (Lorimer and Andrews, 1973). CO_2 adhesion to this enzyme substrate results in formation of two molecules of 3-phosphoglycerate. Rubisco has affinity not only for CO_2, but also for molecular oxygen, that results in formation of one molecule of 3-phosphoglycerate (integrated into the Calvin cycle) and one molecule of 2-phosphoglycolate (starting molecule of photorespiratory glycolate cycle) instead of two molecules of 3-phosphoglycerate (Orgen and Bowes, 1971). During photorespiratory metabolism oxygen is fixed and carbon dioxide is released. Photorespiratory carbon metabolism requires the integration of biochemical pathways in three separate leaf cell organelles: chloroplasts, peroxisomes and mitochondria.

For a long period of time the intensity of photorespiration was considered as a negative factor in determining the dependence of plant productivity on photosynthesis. While evaluating photorespiration magnitude many researches supposed that carbon losses in photorespiration occurs through the use of newly formed products, and this process considered to be a wasteful. Hence, it was proposed to search the ways for elimination or decreasing photorespiration by biochemical or genetic assay with the purpose of

increasing the crop productivity. However, screening for species with low level of photorespiration and high productivity was not successful. Any intervention in the plant functions led to decreasing of growth and productivity.

Taking into account very high rates of photorespiration comparable only to the rates of photosynthesis, it is remained unclear why such a wasteful process of energy dissipation has not disappeared during the evolution. On the contrary, there is a complex enzyme apparatus for recycling of phosphoglycolate, inevitable product of RuBP-oxygenase reactions (Tolbert, 1997).

In the present paper results of long-term experiments on the relationship of the intensity of photosynthesis, photorespiration and productivity of wheat genotypes grown in the field are given.

Materials and Methods

The rich genefund, comprising several thousands of wheat genotypes selected from both the ancient, aboriginal varieties from national selection and introduced from the world genefund, particularly, *CIMMYT, ICARDA* and other regional centers, with contrasting photosynthetic traits, productivity and tolerance to water stress was created. All these genotypes were grown in field on a wide area at the Absheron Experimental Station of the Research Institute of Agriculture at the optimal regime of mineral nutrition and water supply. Numerous winter wheat genotypes were selected as objects of investigations, most typical of them are shown in this study. The main parameters for selection of these genotypes were grain yield, plant phenotypic features (stem height, area and architectonics of the leaf surface, etc.), duration of the vegetative period and other morpho-physilogical traits, as well as drought resistance. Bread wheat (*Triticum aestivum* L.) varieties contrast in architectonics: Gyrmyzy gul and Azamatli-95 are short-stemmed (with the stem height of 85–90 and 60–75 cm, respectively) with vertically oriented small leaves, high-yielding (7–9 t ha^{-1}), Giymatli-2/17 is short-stemmed (85–95 cm), with broad drooping leaves, high-yielding (7 t ha^{-1}) and durum wheat (*Triticum durum* L.) variety Gyrmyzy bugda is long-stemmed (150–180 and 125–150 cm), extensive type, with drooping horizontal orientated leaves and grain yield of 3 t ha^{-1} were used.

The gas exchange of attached leaves was measured in an open system with a URAS-2T infrared gas analyzer (*Hartman and Braun*, Germany) set to the differential mode and by exposition in $^{14}CO_2$ (Aliev *et al.*, 1996b). Photosynthetic carbon metabolism and utilization of basic products of photosynthesis were studied radiometrically at atmospheric concentrations of carbon dioxide and oxygen (Aliev *et al.*, 1996b). Leaf assimilating area was measured using an automatic area meter AAC-400 (Japan).

RuBP carboxylase activity was determined spectrophotometrically, and RuBP oxygenase activity was performed by amperometric method (Aliev *et al.*, 1996 a, b), the rate of light-saturated electron transport was done spectrophotometrically.

Results and Discussion

During 50 years of comprehensive investigations of photosynthesis and productivity of various wheat genotypes in natural conditions of cultivation, attributes and parameters of photosynthetic activity of these genotypes in sowings most closely correlating with plant productivity, have been established. The main emphasis was put on: (1) architectonics; (2) CO_2 assimilation; (3) leaf activity within day and vegetation and others. One of the aspects of the study was photorespiration. The average results from multiple measurements are presented in the table.

The genotypes with two or three times less leaf areas than that with broad leaves produce similar or even greater grain yield. Genotype Gyrmyzy bugda with flag leaf area 28 cm^2 yields up to 3 t ha^{-1}, and those of 18–19 cm^2 yield up to 7–9 t ha^{-1}. In high productive genotypes with grain yield ~(7–9 t ha^{-1}) the flag leaf area differs almost for three times.

The studied genotypes of winter wheat exhibited significant differences in the intensity of CO_2 assimilation of flag leaf. More high values were detected in high productive genotypes Gyrmyzy gul and Azamatli-95, whereas the lowest CO_2 assimilation was characteristic for genotype Gyrmyzy bugda (Table 1).

Not all of genotypes with small leaves are high-productive and not all of genotypes with broad leaves are high or low productive. Genotypes with broad leaves and high yield require sufficient water supply.

In order to better understand the correlation between intensity of CO_2 assimilation and productivity, the consideration of basic parameters of plant architectonics is also essential. Vertically oriented small leaves creating an optimal architectonics promote a relatively high CO_2 assimilation of functioning leaves of all layers during grain formation. Obtained data indicates that genotypes with vertically oriented short and narrow leaves (20–30 cm^2), high specific leaf density (SLD)—600 mg/100 cm^2, with stable and long intensive CO_2 assimilation (30–40 mg dm^{-2} h^{-1}) and a high tolerance to water stress form up to 10 t ha^{-1} grain yield.

Table 1 Intensity of CO_2 assimilation and photorespiration, flag leaf area and grain yield of wheat genotypes.

Genotypes		Potential grain yield, t ha^{-1}	Mean flag leaf area, sm^2	Intensity [mg CO_2 dm^{-2} h^{-1}]	
				Photosynthesis	Photorespiration
Triticum aestivum L.	Azamatli-95	9	19	34.0±1.7	12.4±0.5
	Giymatli-2/17	7	47	25.2±1.4	8.1±0.4
	Gyrmyzy gul	7	18	36.5±2.1	10.9±0.6
Triticum durum L.	Gyrmyzy bugda	3	28	21.3±1.1	6.2±0.3

* Measurements were carried out at the earring phase, when photosynthesis intensity reaches its maximum, and at the end of leaf growth. The submitted data are average from numerous measurements.

The high intensity of CO_2 assimilation is not accompanied by low intensity of photorespiration. For high productive genotypes the high values of photorespiration are common. Genotypes with high grain yield of 7–9 t ha^{-1} possess high intensity both of CO_2 assimilation and photorespiration at corresponding architectonics. Genotypes with moderate (4–5 t ha^{-1}) and low (3 t ha^{-1}) grain yield have a relatively low intensity of CO_2 assimilation and photorespiration.

Gas exchange data agree closely with the measured activities of enzymes involved in CO_2 fixation. Throughout the entire period of flag leaf development, the high productive varieties, in comparison with the low productive ones, were distinguished by higher activity of RuBP carboxylase (Aliev *et al.*, 1996a, b). RuBP oxygenase activity was also higher in the high- rather than low-yielding varieties. In the course of flag leaf development, both activities changed similarly, and the ratio of RuBP carboxylase to oxygenase activity remained virtually unchanged in all the varieties studied (Aliev *et al*., 1996 a, b).

Measurement of The RuBP carboxylase and RuBP oxygenase activities in the different ear elements indicate that during grain formation these activities changed in parallel similarly as it is observed in the flag leaf.

Obtained results showed that studied genotypes also differed significantly in the level of photosynthetic carbon metabolism. Characteristics of photosynthetic carbon assimilation are calculated from the kinetics of $^{14}CO_2$ incorporation into photosynthesis. Radiocarbon was allotted to sugars (mainly sucrose), glycolate metabolites (serine-glycine), and, to a small extent, amino and organic acids, such as malate, aspartate, and alanine. These varieties hardly differed in ^{14}C incorporation into starch. Unlike sugars, starch incorporated not more than 5%–8% of the label. The rates of ^{14}C incorporation into glycolate metabolites and sucrose, as well as CO_2 assimilation rates, were higher in the high productive genotypes (Aliev *et al.*, 1996b). It is assumed that the high intensity of net photosynthesis observed in high productive genotypes despite increased intensities of photorespiration seems to be maintained due to increased photosynthesis. This position proves to be true by high values of true photosynthesis and quantity of light-induced CO_2 release in photorespiration. It is worth noting that the ratio of true photosynthesis to photorespiration in genotypes with different productivity is equal on the average to 3:1 with an insignificant increase of this relation in high yielding genotypes. A value of photorespiration constitutes 28%–35% of photosynthesis intensity in contrast genotypes.

Character of changes in biosynthesis rate and the total value of glycine-serine as well as ratio of RuBP carboxylase to oxygenase activities, CO_2 assimilation intensity predisposes to a parallel change in the intensity of true photosynthesis and photorespiration in leaf ontogenesis. It should be noted that the products of glycolate metabolism can also be used in sucrose synthesis or be transported from the leaves. Therefore, under certain conditions, the products of glycolate metabolism can contribute to active assimilate transport, thereby creating conditions for the maintenance of photosynthesis at a higher level.

So, there are high productive genotypes among

plants with C_3-photosynthesis and low productive among plants with C_4-photosynthesis. Despite the low value of photorespiration in C_4-plants (such as maize, amaranth, etc.), many plants of C_3-type with high photorespiration, including major crops (wheat, rice, peas, etc.) compete successfully with C_4-plants and have high potential productivity and biological yield.

Therefore, contrary to conception on wastefulness of photorespiration put forward in the many years by different authors, our comprehensive investigations on different aspects of photorespiration indicate that photorespiration is one of the evolutionary developed vital metabolic processes in plants. The attempts to reduce this process with the purpose of increasing the crop productivity are inconsistent (Aliev and Kazibekova, 1995; Aliev *et al.*, 1996 a, b; Aliev, 1998; Aliyev, 2001, 2004, 2007). Phosphoglycolate phosphatase, a key enzyme of photorespiration was first homogeneously purified from eukaryotic green algae *Chlamydomonas reinhardtii* with subsequent determination of complete nucleotide and deduced amino acid sequences (Mamedov *et al.*, 2001) (NCBI Nucleotide 1:AB052169). Since metabolic processes of photorespiration in the leaf in the light takes place simultaneously with photosynthesis, it is possible that released energy is used in certain reactions of photosynthesis.

Moreover, photorespiration dissipates excess photochemical energy under high light intensities, drought and salt stress, thus protecting the chloroplast from over-reduction (Kozaki and Takeba, 1996).

Investigations of primary processes of photosynthesis allowed to specify that chloroplasts from high productive genotypes were characterized by high rates of electron transport and photophosphorylation, and also to approve the availability of relationship between photosynthetic electron transport, CO_2 assimilation and productivity.

In conclusion, we emphasize the close relationship between photosynthesis and photorespiration; the optimal correlation of these two essential processes is one of the most important conditions that secure the highest plant productivity. High intensity of true photosynthesis and photorespiration, high activity of the primary photochemical processes together with favorable phenotypic traits, the optimum leaf area index and architectonics are crucial to the high productivity of wheat genotypes.

References

Aliev JA (1998) Importance of Photosynthesis of Various Organs in Protein Synthesis in Grain of Wheat Genotypes under Water Stress. Proceedings of the XIth International Congress on Photosynthesis, Budapest, Hungary, 1998. In: G Garab (ed.), Photosynthesis: Mechanisms and Effects. Kluwer Academic Publishers: Dordrecht/Boston/London 5: 3829-3832

Aliev JA, Guliev NM, Kerimov SKh, Hidayatov RB (1996a) Photosynthetic Enzymes of Wheat Genotypes Differing in Productivity. Photosynthetica 32(1): 77-85

Aliev JA, Kazibekova EG (1995) Peculiarities of Highly Productive Wheat Photosynthesis and Usage of Photosynthetic Signs in Selection. Proceedings of the Xth International Congress on Photosynthesis, Montpellier, France, 1995. In: P Mathis (eds.), Photosynthesis: from Light to Biosphere. Kluwer Academic Publishers: Dordrecht/Boston/London 5**:** 659-662

Aliev JA, Kerimov SKh, Guliev NM, Akhmedov AA (1996b) Carbon Metabolism in Wheat Genotypes with Contrasting Photosynthetic Characteristics. Russian J. Plant Physiol. 43(1): 42-48

Aliyev JA (2001) Diversity of Photosyn Thetic Activity of Organs of Wheat Genotypes and Breeding of High-Yielding Varieties Tolerant to Water Stress. Proceedings of the 12th International Congress on Photosynthesis, Brisbane, Australia, 2001. www.publish.csiro.au/ ps2001, S28-006

Aliyev JA (2004) CO_2 Assimilation, Architectonics and Productivity of Wheat Genotypes in Sowing. Proceedings of the 13th International Congress of Photosynthesis, Montreal, Canada, 2004. In: A van der Est, D Bruce (eds.), Photosynthesis: Fundamental Aspects to Global Perspectives. Alliance Communications Group: Kansas 2: 1047-1048

Aliyev JA (2007) The Intensity of CO_2 Assimilation, Photorespiration and Productivity of Wheat Genotypes Triticum L. Abstracts of the 14th International Congress of Photosynthesis, Glasgow, Scotland. In Photosyn. Res. 91(2-3): 278

Decker JP (1955) A Rapid, Postillumination Deceleration of Respiration in Green Leaves. Plant Physiol. 30: 82-84

Kozaki A, Takeba G (1996) Photorespiration Protects

C3 Plants from Photooxidation. Nature 384: 557-560

Lorimer GH, Andrews TJ (1973) Plant Photorespiration: An Inevitable Consequence of the Existence of Atmospheric Oxygen. Nature 248: 359-360

Mamedov TG, Suzuki K, Miura K, Kucho KK, Fukuzawa H (2001) Characteristics and Sequence of Phosphoglycolate Phosphatase from a Eukaryotic Green Alga Chlamydomonas Reinhardtii. Biol. Chem. 276: 45573-45579

Ogren WL, Bowes G (1971) Ribulose Disphosphate Carboxylase Regulates Soybean Photorespiration. Nat. New Biol. 230: 159-160

Tolbert NE (1977) The C_2 Oxidative Photosynthetic Carbon Cycle. Annu. Rev. Plant Physiol. Plant Mol. Biol. 48: 1-15

Response of Chlorophyll Fluorescence Parameters of *Illicium Lanceolatum* to Different Light Conditions

Yonghui Cao*[1], Benzhi Zhou[1], Rumin Zhang[2], Lianhong Gu[3]

[1.] Research Institute of Subtropical of Forestry,Chinese Academy of Forestry,Fuyang 311400, Zhejiang,China;
[2.] School of Forestry and Biotechnology,Zhejiang Forestry College,Lin'an 311300, Zhejiang,China;
[3.] Oak Ridge National Laboratory, Oak Ridge, TN 37831-6335,USA.
* Corresponding author. E-mail: fjcyh77@sina.com.

Abstract: *Illicium lanceolatum* is a unique plant in traditional Chinese medicine. The shikimic acid, extracted from *I.lanceolatum*, has functions of anti-inflammatory, analgesic and inhibiting platelet aggregation, arterial and venous thrombosis and cerebral thrombosis. It can also function as an intermediate for anti-virus and anti-cancer drugs. For example, it is a vital element of Oseltamivirphosphate for anti-Avian Influenza. Because of this, *I.lanceolatum* and other species in this genus have been given an unprecedented attention and have potential for further development and utilization. Previous studies have shown that photosynthetic efficiency restricted the biomass and limited the Shikimic acid content of *I.lanceolatum* seedlings. The primary objective of the study was to examine the physiological and biochemical foundation of growth and biomass accumulation of *I.lanceolatum* seedlings and to provide theoretical guidance for regular cultivation. The chlorophyll fluorescence kinetics technique was used in this study. The kinetics parameters of fast chlorophyll fluorescence were measured for 4-year-old *I.lanceolatum* seedlings in Zhejiang province of China, under different light shading treatments (0%, 50% and 80%) using a plant efficiency analyzer (PEA) and JIP-test. The results showed that the maximal photochemical efficiency of photosystem II(Fv/Fm) decreased as the shading level increased. The ratio of Fv/Fm for 50% and 80% shading treatments decreased by 1.34% and 2.79% respectively, comparing with the control (0% shading treatment). The density of reaction centers(RC/CS) decreased by 2.94% and 13.63% for 50% and 80% shading treatments respectively, comparing with the control, and the energy dissipation per RC (DIo /RC) increased by 2.2% and 62.9% respectively. ANOVA analysis showed that actual light use efficiency, the fraction of absorbed light in photochemistry (P), for *I.lanceolatum* leaf under 50% shading exhibited no significant difference from the control($P > 0.05$). However, for *I.lanceolatum* leaf under 80% shading, there was a significant decrease of the fraction of absorbed light in photochemistry (P) ($P < 0.01$). We concluded that *I.lanceolatum* seedlings under 50% shading could enhance the actual light use efficiency. The results obtained have physiological and biochemical implications for ways to improve biomass accumulation and content of Shikimic acid of *I.lanceolatum* plants.

Keywords: *Illicium lanceolatum*; Light condition; Chlorophyll fluorescence; Photosystem II

Introduction

Illicium lanceolatum also known as Mang Cao, belonging to Magnoliaceae Illicium,is a traditional and proper medicinal plant in China (Lin, 2001). The shikimic acid that is contained in *I. lanceolatum* has strong functions of anti-inflammatory, analgesic and inhibiting platelet aggregation, arterial and venous thrombosis and cerebral thrombosis, but also as is the intermediates for anti-virus and anti-cancer drugs. This discovery makes *I. lanceolatum* and other genuses of Illicium L. have been given the unprecedented attentions, and its prospects for the development and utilization are more great(Avula *et al*., 2009; Song *et al*., 2009; Dzamic *et al*., 2009). Although *I. lanceolatum* has broader ecological

amplitude, but its wild resources are scattered, the current predatory use and increasing scarcity of wild resources is more strong, which makes the protection and cultivation of its is increasingly urgent.

At present, *I. lanceolatum* had not yet carried out a large area Introduction and cultivation at home and abroad, only in some provinces had carried out sporadic cultivation as a landscaping plant resources, and were lacking for systematic research of wild populations ecology and artificial cultivation technology (Cao, 2008, 2009). After Introduction and large-scale cultivation of *I. lanceolatum*, its ecological adaptation, introduction and adaptation mechanisms will be the primary practice problems for developing its industries, improving the level of cultivation techniques and the content and quality of pesticide ingredients. In this experiment, the chlorophyll fluorescence parameters research of *I. lanceolatum* under different lighting conditions had been carried out to analysis the effect of light on potential photosynthetic capacity for leaf photosynthetic apparatus and its response to the light, to provide the theoretical basis for sustainable use and development of *I. lanceolatum*.

Materials and Methods

Test plots located in forest seedlings garden of Tianmu Mountains in Lin'an City, Zhejiang Province, and with geographical Location of 118°51'–119°52'E and 29°56'–30°23'N. It is in the north subtropical monsoon climate zone, warm and humid with four distinct seasons. The annual average temperature is 15.4 °C, mean temperature of January is not less than 3.2 °C, average temperature of July is 29.9 °C, the annual frost-free period of about 235a. Annual rainfall is 1250–1600 mm, annual sunshine hours is 1850–1950 h. The soil of experimental points is acidic, yellow loam soil, with the property of organic matter 23.95 g/kg, total nitrogen 0.44 g/kg, total phosphorus 10.09 g/kg, total potassium 6.31 g/kg, available nitrogen 217.62 mg/kg, available phosphorus 363.97 mg/kg, available potassium 40.51 mg/kg, pH value of 4.62.

The tested material was 4 years old cultivation seedling of *I. lanceolatum*, and seed sources was Tianmu Mountain Nature Reserve, Zhejiang Province. It was sowed in May 2005 and then transplanted from the seedbed to planting under tree canopy when it was 2 years old with the average height of 0.7 m. The planting density was 90–110 trees/mu. By planting under full light condition and tree canopy and to set the 3 different growth light intensity treatments, that were respectively the natural full sunlight (control), planting under *Acer cinnamomifolium* forest canopy for 2 years with 50% light intensity and under *A.buergerlanum* forest canopy for 2 years with 20% light intensity. In early September 2009, every three seedlings were randomly selected from 3 different light intensity treatments respectively, and five one-year-old leaves were also randomly selected from per plant. The parameters of chlorophyll fluorescence kinetics were measured for each leaf and then taken it indoors for the determination of leaf chlorophyll content.

The chlorophyll concentrations were measured by method of Arnon(Arnon, 1949).

The OJIP-test analysis of fluorescence kinetics is an important method to indicate the energy intensity producted by photosystem II (PSII). A typical fast chlorophyll fluorescence induction kinetics has four important inflection points of O, J, I, and P. O point show that PSⅡ reaction center can accept the maximum of light quantum, this point is the fluorescence intensity of 50 μs for the initial fluorescence (F_0); the fluorescence intensity of 2ms, known as the F_J; the fluorescence intensity at 30 ms as F_I, I point reflects the heterogeneity of PQ pool during the transfer process of QA-to QB (Strasser *et al*., 2000); P point is maximum fluorescence value of Fm.

According to methods of Strasser (Strasser *et al*., 2000), This experiment used the non-modulated chlorophyll fluorescence apparatus (made by Yaxinli device company) to measure chlorophyll fluorescence kinetics. After 10 min dark-adapted, the leaves were irradiated under the saturated blue flashing light of 3,000 μmol m^{-2} s^{-1} for 1 s, and then, by recording fluorescence signals in the interval of 10μs (2 ms before) and 1 ms (2 ms after), measured fast chlorophyll fluorescence kinetics Curve and its parameters, including: F0, FJ, FI, Fm, and the fluorescence at 300 μs ($F_{300\mu s}$).

The Calculation of chlorophyll fluorescence parameters referred to the method of Strasser(Strasser *et al*., 2000). Under dark-adapted the formula of maximal photochemical efficiency of PSⅡ was Fv / Fm = (Fm – F0)/Fm. The formula of the dissipation energy in the form of heat for unit reaction center was DIo/RC = ABS/RC – TRo/RC; and the formula of

reaction center number of photosynthetic organ for unit area was RC/CSo = (Fv/Fm) × (VJ/Mo) × F0.

The experimental data was using Origin 8.0 software for statistical analysis and mapping.

Table 1 Variation of the chlorophyll contents in leaves of *I. lanceolatum* under different light conditions.

Light treatment	Chla+b(mg·g^{-1} FM)	Chla (mg·g^{-1} FM)	Chlb(mg·g^{-1} FM)	Chla/Chlb
Full sunlight(ck)	2.93±0.02	2.20±0.11	0.73±0.07	3.01±0.09
In 50% shade	3.39±0.20*	2.37±0.09*	1.02±0.03**	2.32±0.14**
In 80% shade	3.58±0.10**	2.41±0.04*	1.17±0.07**	2.06±0.18**

* significant difference at $P < 0.05$ level; ** significant difference at $P < 0.01$ level.

Results and Discussion

The changes in chlorophyll content of I. lanceolatum seedling growing under different light levels

The data in the Tab.1 shows that the concentrations of total mass-based chlorophyll (chl), the chla and chlb of the *I.lanceolatum* leaf were increasing with the increase of light shading intensity. In contrast to full sunlight condition (in 0% shade, control), the chla concentration of another two light shade treatments (in 50% shade and in 80% shade) enhanced respectively 7.73% ($P < 0.05$) and 9.55% ($P < 0.05$), the variation of chla concentration between 50% and 80% shade treatments was unsignificant. Compared with the control, the chlb concentration of two shade treatments increased respectively 39.73% ($P < 0.01$) and 60.27% ($P < 0.01$), and the total chlorophyll concentration raised respectively 15.70% ($P < 0.05$) 和 22.18% ($P < 0.01$), whereas the variance between 50% and 80% shade treatments wasn't obvious. On the contrary, compared with the control, theChl a/b ratio of two light shade treatments decreased 22.92% ($P < 0.01$) and 31.56% ($P < 0.01$) respectively.

Chlorophyll is the material basis of capturing light energy for plant leaves, and the increase of its content and the decrease of Chl a/b ratio was one of the indicators to judging the using ability of low-light for plants growing under shading condition(Zhang *et al*., 2009). In this experiment, the increase of the chlorophyll content and the decrease of Chl a/b ratio of *I. lanceolatum* leaves indicated that shading treatment could enhance the ability of leaves to capture and absorb the light, and was a physiological response to low light environment. This result was consistent with that of Miyake *et al*. (2005) for research of tobacco leaves and Zhang *et al*. (2009) for *Cercis canadensis* 'Forest Pansy' leaves in shading condition.

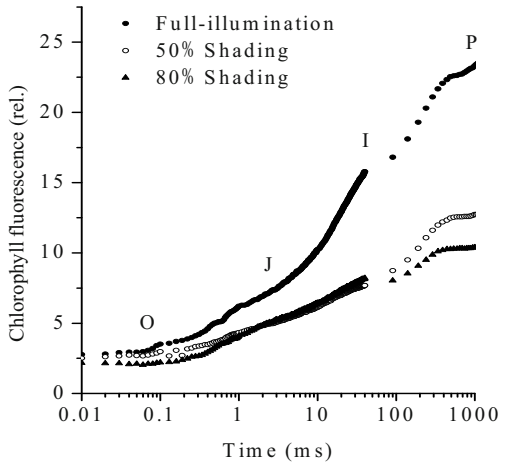

Fig. 1 Traces of the chlorophylla fluorescence transients showing the rise from the initial fluorescence level, F_0 (O), through the intermediate steps, J and I, to fluorescence maximum, F_m (P).

The impact of light intensity on the fast chlorophyll fluorescence kinetics curve of I. lanceolatum

Under different light conditions, fast chlorophyll fluorescence kinetics curve of *I. lanceolatum* leaves showed a typical O-J-I-P 4-phase type (Fig. 1). With the increase of shading level, J-I-P 3-phase showed a gradual downward trend. Compared with the natural light conditions, the maximal fluorescence relative value of leaves for plants in 50% and 80% shade treatment were decreased by 42.07% ($P < 0.01$) and 51.31% ($P < 0.01$) respectively. Whereas there was no significant difference in the maximum fluorescence value of leaf between in 50% shade and in 80% shade treatments.Under different light conditions, there was no significant difference in O-phase of initial fluorescence for *I. lanceolatum* leaves.

The impact of light intensity on the maximal photochemical efficiency of PS Ⅱ of I. lanceolatum

The result showed that under different levels of shading conditions, there was distinct difference of the maximal photochemical efficiency of photosystem

II(Fv/Fm) for current year leaves of *I. lanceolatum* (Fig. 2). The Fv/Fm values of leaves in 50% and 80% shade treatments were decreased by 1.34% and 2.79% ($P < 0.05$) respectively than the control, but there was no significant difference in Fv/Fm values of leaves between 50% and 80% shade treatments.

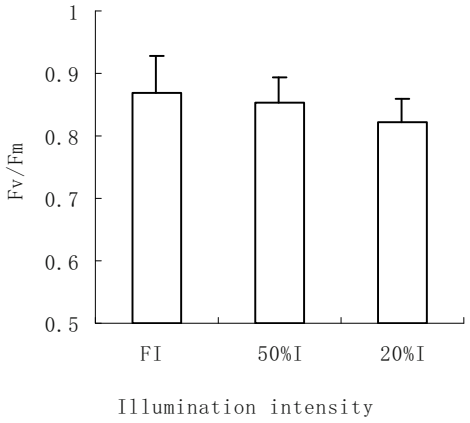

Fig. 2 Effect of different light conditions on the maximum photochemistry efficiency in PS II.

Chlorophyll fluorescence technique is seen as effective tool to discuss the damage degree of leaf photosynthetic apparatus in the case of non-destruction, and widely used in the studies of environment stress (Srivastava *et al*., 1997; Touth *et al*., 2007). The value of potential maximum quantum yield of PS II Fv/Fm reflects the maximum PS II photochemical efficiency, and has obvious decline when subjected to environmental stress. It is a good indicator and probe for indicating the level of stress.The research of Liu (Liu, 2007) found that leaf shading decreased the actual PS II photochemical efficiency (φPS), maximum photochemical efficiency (Fv/Fm) and photochemical quenching coefficient (qP), and so caused single-leaf net photosynthetic rate (Pn) decreased. So shade of vigorous period can change the physiological and biochemical characteristics of plant leaves, thus ensuring their own plants in the shade can make full use of solar energy under. In this study, the result of the decrease of Fv/Fm of *I. lanceolatum* leaves in shading conditions also indicate that the capture efficiency of excitation energy for chlorophyll molecule and the potential activity of PS II will decrease, and it may be the physical adapting of *I. lanceolatum* leaves to low-light in shade treatment. The result of the value of Fv/Fm decreased more in 80% shade treatment is similar to the result of plant leaves in 80% shade treatment with the lowest net photosynthetic rate. So fluorescence analysis of this paper reveals accurately the impact mechanism of shade on the Pn of *I. lanceolatum*.

The impact of light intensity on the distribution of energy flow in PS II reaction center of I. lanceolatum

The result showed that the DIo/RC value of PS II reaction center for *I. lanceolatum* leaves was enhancing with the increasing of light shading intensity (Fig. 3). The DIo/RC value of leaves in 80% shade treatment increased by 62. 87% ($P < 0.01$) compared with the control, and that value of leaves in 50% shade treatment increased by only 2.24% and no significant difference with the control.

The impact of light intensity on the number of PS II reaction center of I. lanceolatum

Similar to the change trend of Fv/Fm values, the number of PS II reaction center (RC/CSo) of *I. lanceolatum* leaves showed a decreasing trend with the enhancing of shading intensity (Fig. 4). Compared with the control, the value of RC/CSo for *I. lanceolatum* leaves in 50% shade treatment decreased by only 2.94% and no significant difference with the control. Whereas that of leaves in 80% shade was decreased by 13.63% ($P < 0.05$) and 12.91% ($P < 0.05$) respectively, compared with that of the control and 50% shade treatment.

In the shade, with the decline of Fv/Fm value of *I. lanceolatum* leaves, the DIo/RC value was increased and the RC/Cso value was decreased. This change may be, in the electron transfer process of PS II protein complexity, the PS II reaction center was reversible inactivation (*i.e.*, the heterogeneity of PS II) and to prevent the downstream transfer of the energy absorbed by the antenna pigments (Han *et al*., 2010), thus the change of electron flow (TRo/RC) captured by PS Ⅱ reaction center wasn't apparent and so resulted in the increased unit energy absorbed by "the active reaction center" complexity must be dissipated in the form of thermal energy. Therefore, this heterogeneity of PS II (the reversible inactivation of PS II reaction center) of *I. lanceolatum* leaves showed a adaptation mechanism of photosynthetic apparatus under high degree of shading, was also the physiological adaptation of *I. lanceolatum* leaves to low light environment.

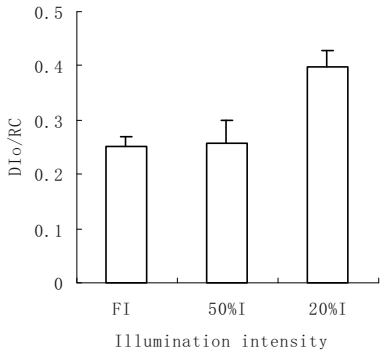

Fig. 3 Effect of different light conditions on the energy flow distribution of reaction centre in PS II.

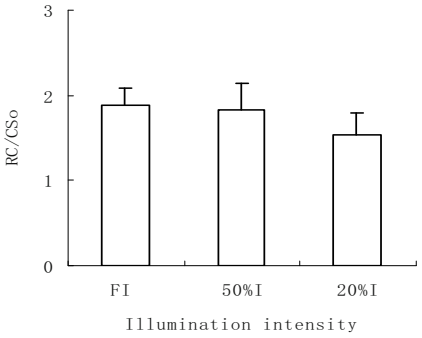

Fig. 4 Effect of different light conditions on the number of reaction centre in PS II.

Acknowledgements

This work was supported by the project about *I. lanceolatum* research and a grant from Science and Technology Department of Zhejiang Province, China.

References

Arnon DI (1949) Copper Enzymes in Isolated Chloro-Plasts, Polyphenoloxidase in Beta vulgaris. Plant Physiology 24: 1-15

Avula B, Wang YH, Smillie TJ (2009) Determination of Shikimic Acid in Fruits of Illicium Species and Various Other Plant Samples by LC–UV and LC–ESI–MS. Chromatographia.69: 307-314

Cao YH, Chen SL, Xiao JH (2008) Studies on the Interspecific Association of Illicium Lanceolatum Community in Tiantong Region, Zhejiang Province. Journal of Tropical and Subtropical Botany16(6): 100-108

Cao YH, Xiao JH, Li YC (2009) Population Structure and Spatial Patterns of Dominant Populations in Illicium Lanceolatum-Choerospondias Axliaris Community in Tiantong, Zhejiang Province. Journal of Zhejiang Forestry College 26(1): 44-51

Dzamic A, Sokovic M, Ristic MS (2009) Chemical Composition and Antifungal Activity of Illicium Verum and Eugenia Caryophyllata Essential Oils. Chemistry of Natural Compounds 45: 259-261

Han ZX, Li L, Xu XW, Lv XF (2010) Response of Chlorophyll Fluorescence Paramenters to Day-Night Temperature Difference in Two Halophytes under NaCl Treatment. Journal of Desert Research 30: 63-68

Li Q (2001) Taxonomy of the Genus Illicium Linn.Bulletin of Botanical Research. 21(2): 161-174

Liu GS, Zhao XZ, Wei FJ, Wan, Wang WJ (2007) Effects of Shading at Fast-Growing Stage and Light Intensity Transfer on Photosynthetic Efficiency in Tobacco (Nicotiana Tobacum L.) Varieties. Scientia Agricultura Sinica 40 (10): 2368-2375

Miyake C, Horiguchi S, Makino A, Shinzaki Y, Yamamoto H, Tomizawa K (2005) Effects of Light Intensity on Cyclic Electron Flow around PS I and Its Relation Ship to Non-Photochemical Quenching of Chlofluorescence in Tobacco Leaves. Plant and Cell Physiology 46(11): 1819-1830

Song TF, Zhang WD, Xia XH (2009) Two New Acorane Sesquiterpenes from Illicium Henryi. Archives of Pharmacal Research 32: 1233-1236

Srivastava A, Guisse B, Greppin H (1997) Regulation of Antenna Structure and Electron Transport in Photosystem II of Pisum Sativum under Elevated Temperature Probed by the Fast Polyphaisc Chlorophyll a Fluorescence Transient: OKJIP. Biochimica et Biophysica Acta 1320: 95-106

Strasser RJ, Tsimilli-Michael M, Srivastava A (2000) The Fluorescence Transient As a Tool to Characterise and Screen Photosynthetic Samples. YunusM, Pathre U, Mohanty E Probing Photosynthesis: Mechanisms, Regulation and Adaptation London: Taylor & Francis 25: 445-483

Touth SZ, Schansker G, Garab G (2007) Photosynthe- tic Electron Transport Activity in Heat-Treated Barley Leaves: The Role of Internal Alternative Electron Donors to Photosystem II. Biochimica et Biophysica Acta 1767: 295-305

Zhang Y, Zhuo LH, Wang CZ (2009) Effects of Shade Treatments on Net Photosynthetic Characteristics and Chlorophyll Fluorescence Parameters of Cercis Canadensis Forest Pansy. Journal of Agriucultural University of Hebei 32(6): 52-56

Effects of Elevated Root-Zone CO_2 and Root-Zone Temperature on Productivity and Photosynthesis of Aeroponically Grown Lettuce Plants

Jie He*, Lin Qin, Sing Kong Lee

National Institute of Education, Nanyang Technological University,
1 Nanyang Walk, Singapore 637 616.
*Corresponding author. Tel. No. +65 6790 3817; Fax No. +65 6896 9414; E-mail: jie.he@nie.edu.sg.

Abstract: Elevated root-zone (RZ) [CO_2] resulted in significantly higher maximal photosynthetic CO_2 assimilation rate (A) but lower stomatal conductance (g_s) in aeroponically grown temperate lettuce in the tropics. Higher midday leaf relative water content (RWC) was observed at elevated RZ [CO_2]. Grown at 20 °C-RZ temperature (RZT), all plants accumulated more biomass than at ambient (A)-RZT. The increase of biomass was greater in roots than in shoots supported by lower shoot/root ratio under elevated RZ [CO_2]. The percentage increase in biomass under elevated RZ [CO_2] was greater at A-RZT although the total biomass was higher at 20 °C-RZT. NO_3^- and total reduced N concentrations of shoot and root, total leaf soluble and Rubisco protein were significantly higher in all elevated RZ [CO_2] plants than in ambine RZ [CO_2] (360 ppm) at both RZTs. Roots, however, under each RZ [CO_2] at A-RZT had significantly higher NO_3^- and total reduced N concentration than at 20 °C-RZT. At each RZ [CO_2], total leaf soluble and Rubisco protein concentration was significant greater at 20 °C-RZT than at A-RZT.

Keywords: Elevated root-zone [CO_2]; Root-zone temperature; Photosynthesis; Total reduced N; Rubisco

Introduction

In Singapore, the temperate vegetable crops have been successfully grown in the tropics by cooling the RZ only with aeroponic systems. When grown among soil particles, plant roots normally are colonized by microorganisms and evolve more CO_2 than sterile roots. It is not unusual for CO_2 in the rhizosphere to be up to more than 10-fold higher than the atmospheric CO_2 concentration (De Jong and Schappert, 1972; Norstadt and Porter, 1984). Based on these findings, we often questioned whether the low CO_2 level in the RZ of aeroponically grown plants could regulate plant growth. Our previous study showed that elevated RZ [CO_2] reduced the negative impacts of high air temperature on growth, photosynthesis and N metabolism of lettuce plants (He *et al*., 2007, 2010). In the present study, our experimental design using aeroponically grown lettuce plants, enables us to investigate the effects of elevated RZ CO_2 and RZT not only on A and g_s but also the plant growth especially the root growth associated with the uptake and accumulation of NO_3^-. The total product of N metabolism (*i.e.*, the total reduced N), total soluble and Rubisco protein were also determined. This research may have practical significance to aeroponic vegetable production by growing plants under elevated RZ [CO_2] to enhance productivity. By studying the responses of plant growth and photosynthesis to elevated RZ [CO_2] and RZT, this not only contributes to the scientific literature but also helps the growers to improve the production of aeroponically grown vegetable crops.

Materials and Methods

Plant materials: The plant material used was Crisphead-type lettuce plants (*Lactuca sativa* L. cv. 'Wintergreen', South Pacific Seeds Ltd, New Zealand). After germination, the seedlings were transplanted to the aeroponic system. The nutrient solution used was based on full strength Netherlands Standard Composition. At full strength, the

conductivity of the nutrient solution measured 2.2 mS. The aerial parts of plants were subjected to the fluctuations of ambient temperature ranging from 23 to 38 ºC under 100% prevailing solar radiation. The maximum photosynthetic photon flux density (PPFD) on the plant canopy on sunny days was about 1,200 μmol m^{-2} s^{-1}. Relative humidity in the greenhouse was between 65% and 95%. Roots were grown in either 20 ºC-RZT or hot A-RZT. Three weeks after transplanting, four different RZ [CO_2] (ambient, 360 ppm and elevated concentrations of 2,000, 5,000, 10,000 ppm) were imposed on plants at each of the two RZTs.

Measurements of A and g_s: Two weeks after different elevated RZ [CO_2] treatments, *A* and g_s of the newly expanded leaves (the 6th leaves from the base) were measured between 0900 h to 1100 h with an open infrared gas analysis system with a 6 cm^2 chamber (LI-COR) in the greenhouse using intact plants. Readings were taken with an LED light source which supplied 1,200 μmol m^{-2} s^{-1} of PPFD. Average ambient [CO_2] and relative humidity in the chamber were 360 ±5 μmol mol^{-1} and 70% respectively. Leaf chamber temperature was set according to prevailing ambient conditions (35 °C).

Measurement of RWC: [Fresh weight (FW) – Dry weight (DW)]/(Turgid weight – DW) × 100%.

Determination of NO_3^-: It was determined using a Flow Injection Analyser (Model QuikChem 8000, Lachat Instruments Inc, Milwaukee, WI, U.S.A.) as described by He *et al*. (2010)

Determination of total soluble and Rubisco protein: Leaf discs were harvested in the middle of the photoperiod and immediately stored in liquid nitrogen. Total soluble and Rubisco protein were determined as describe by Jordan *et al*. (1992).

Statistical analysis: A two-way ANOVA was first used to test for the effect of RZ [CO_2] and RZT on all parameters. A separate ANOVA was then used to discriminate means across all treatments. All statistical analyses were carried out using MINITAB software (MINITAB, Inc., Release 15, 2007).

Results and Discussion

A, g_s and RWC

The interaction term "RZ [CO_2] x RZT" of two-way ANOVA for *A, gs* and midday leaf RWC was respectively, not significant (Table 1). Separate ANOVA analysis showed that elevated RZ [CO_2] resulted in significantly higher maximal *A* but lower g_s in all plants at both RZTs (Figs. 1A and 1B). Higher midday leaf RWC was also observed at elevated RZ [CO_2] (Fig. 1C). The degree of change in each parameter under elevated RZ [CO_2] was greater at A-RZT than at 20 °C-RZT.

Table 1 Two way analysis of variance of physiological variables, with P Values presented for each main effect and their interaction.

	RZ[CO_2]	Temperature	Interaction
A (Fig. 1A)	< 0.001	< 0.001	0.45
g_s (Fig. 1B)	< 0.001	< 0.001	0.89
RWC (Fig. 1C)	< 0.001	< 0.001	0.19
Shoot DW (Fig. 2A)	< 0.001	< 0.001	0.73
Root DW (Fig. 2B)	< 0.001	< 0.001	0.39
Shoot/root Ratio DW (Fig. 2C)	< 0.001	< 0.001	0.82
Shoot NO_3^- (Fig. 3A)	< 0.001	< 0.001	0.33
Shoot total N (Fig. 3B)	< 0.001	< 0.001	0.61
Root NO_3^- (Fig. 3C)	< 0.001	< 0.001	0.95
Root total N (Fig. 3D)	< 0.001	< 0.001	0.16
Total soluble protein (Fig. 3E)	< 0.001	< 0.001	0.21
Rubisco Protein (Fig. 3F)	< 0.001	< 0.001	0.54

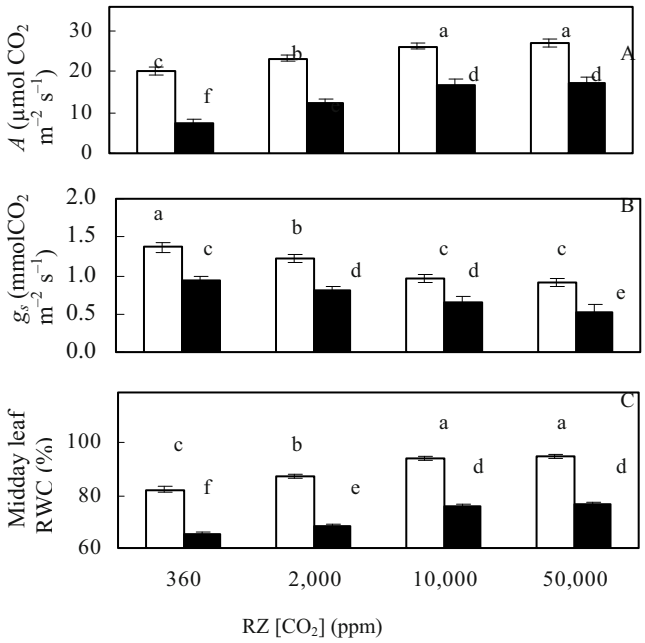

Fig. 1 *A* (A), g_s (B) and midday leaf RWC (C) of lettuce plants grown under different levels of elevated RZ [CO_2] at 20 °C-RZT (open bars) and A-RZT (closed bars) for 2 weeks. Each value is the mean of 5 measurements of 5 different leaves. Vertical bars represent the standard errors. Means with different letters above the bars are statistically different ($p < 0.001$) as determined by Tukey's multiple comparison test.

Productivity of shoot and root

"RZ [CO_2] x RZT" of two-way ANOVA for DW of shoot and root, and shoot/root ratios was respectively, not significant (Table 1). Separate ANOVA analysis showed that DW of shoot and root were significantly higher in plants at all elevated RZ [CO_2] than at ambient RZ [CO_2] (360 ppm) at both RZTs. The increase of biomass was greater in roots than in shoots supported by lower shoot/root ratio under elevated RZ [CO_2]. The percentage of increase in biomass under elevated RZ [CO_2] was greater at A-RZT than at 20 ^{o}C-RZT although the total biomass was higher at 20 ^{o}C-RZT.

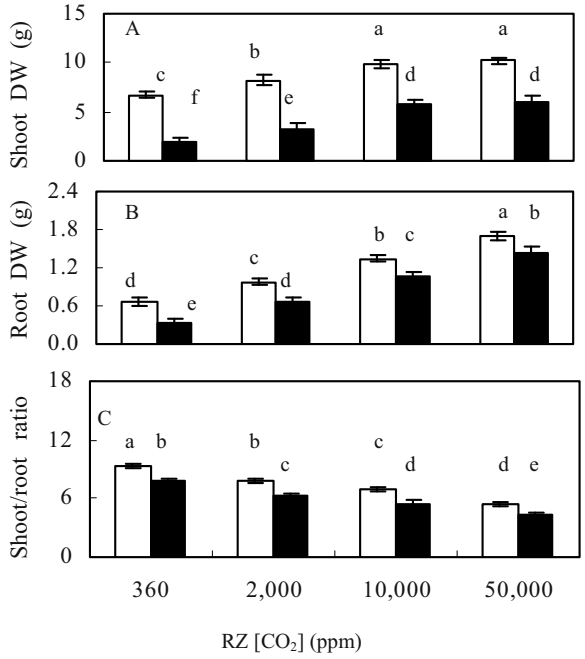

Fig. 2 DW of shoot (A) and root (B), shoot/root ratio (C) of lettuce plants grown under different levels of elevated RZ [CO2] at 20 °C-RZT (open bars) and A-RZT (closed bars) for 3 weeks. Each value is the mean of 5 measurements of 5 different leaves. Vertical bars represent the standard errors. Means with different letters above the bars are statistically different (p < 0.001) as determined by Tukey's multiple comparison test.

The above results showed that A increased with increasing RZ [CO_2] (Fig. 1A) with a RZ [CO_2] of 10,000 ppm sufficient for maximising productivity (Fig. 2). However, g_s was significantly lower at higher RZ [CO_2] than at ambient RZ [CO_2] (Fig. 1B) and therefore, the enhancement of A under elevated RZ [CO_2] was not due to an increase in g_s. Obviously, there was more internal CO_2 available to plants grown under elevated RZ [CO_2] (He *et al*., 2007, 2010) as dissolved CO_2 in the xylem sap could be carried upward in the stem when plants were transpiring (Teskey and McGuire, 2005) and fixed in green tissues (McGuire *et al*., 2009).

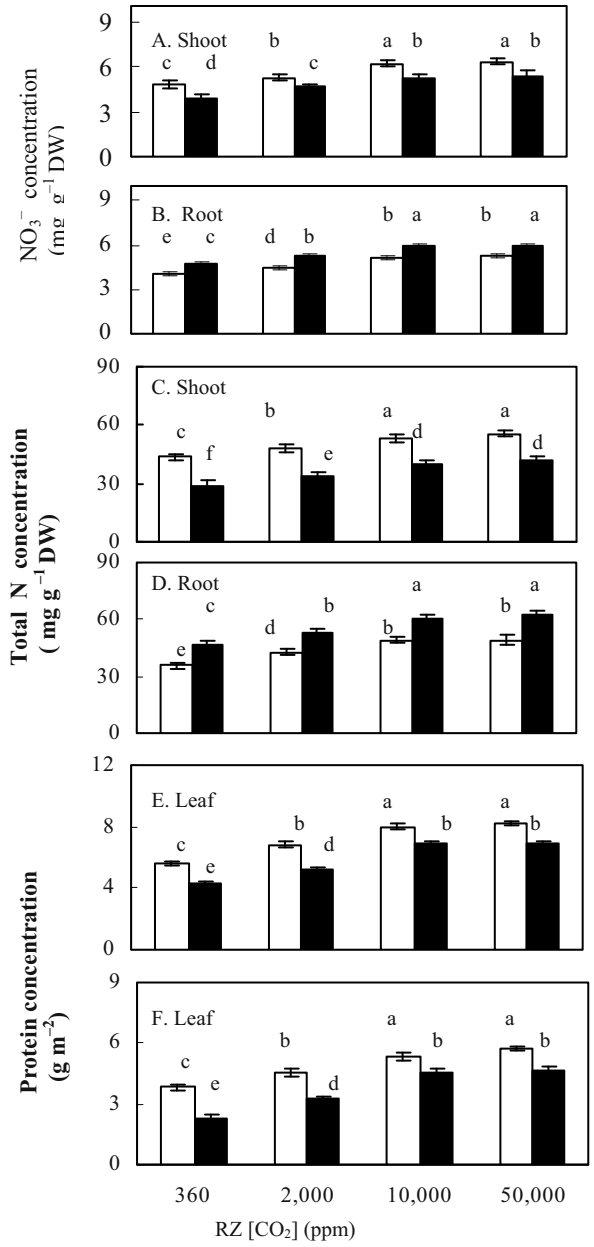

Fig. 3 NO_3^- , total reduced N concentration of shoot (A, B) and root (C, D), leaf soluble and Rubisco protein (E, F) concentrations of lettuce plants grown under different levels of elevated RZ [CO_2] at 20 °C-RZT (open bars) and A-RZT (closed bars) for three weeks. Each value is the mean of 5 measurements of 5 different plants from two different bins. Vertical bars represent the standard errors. Means with different letters above the columns are statistically different (p < 0.001) as determined by Tukey's multiple comparison test.

NO_3^-, total reduced N, soluble and Rubisco protein concentration

"RZ [CO_2] x RZT" of two-way ANOVA for NO_3^-,

total reduced N, leaf total soluble and Rubisco protein concentration was respectively not significant (Table 1). Separate ANOVA analysis indicated that NO_3^- and total reduced N concentrations of shoot and root were significantly higher in all elevated RZ [CO_2] plants than in plants grown at RZ [CO_2] of 360 ppm at both RZTs. At each RZ [CO_2], NO_3^- and total reduced N concentration of shoot were higher at 20 °C-RZT than at A-RZT. At each RZ [CO_2] NO_3^- and total reduced N concentration of shoot were higher at 20oC-RZT than at A-RZT. Roots, however, underconcentrations were also significantly higher in all elevated RZ [CO_2] plants than in plants grown at RZ [CO_2] of 360 ppm at both RZTs.

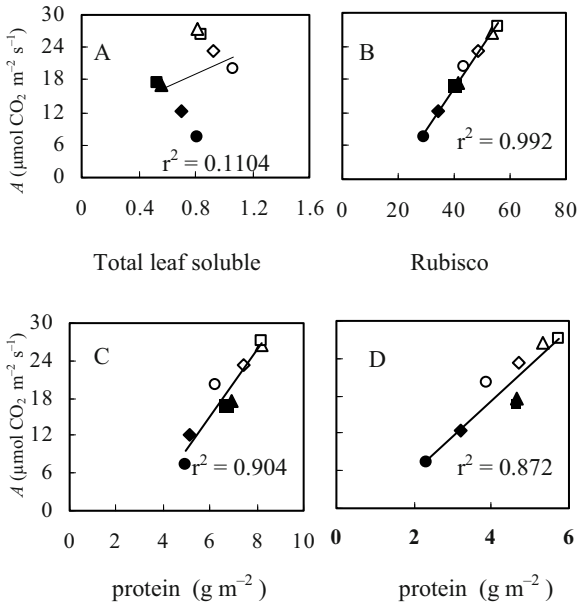

Fig. 4 Correlations between maximal *A* and maximal g_s, (A) (data derived from Fig.1) and maximal *A* and total reduced N of shoot (B), total leaf soluble (C) and Rubisco concentration (D) (data derived from Fig. 1 and Fig. 3) of lettuce plants grown under different levels of elevated RZ [CO_2] at 20$_o$C- and A-RZT for three weeks.

There was no correlation between *A* and maximal g_s (Fig. 4A, p = 0.14) but these variables were negatively correlated within each RZT. However, a close correlation between maximal *A* and total reduced N (Fig. 4B), total soluble (Fig. 4C) and Rubisco protein (Fig. 4D) concentration of shoot was established in plants grown under different RZ [CO_2], and RZTs (Figs. 4B, 4C and 4D, p < 0.001). Decreased N concentration is usually interpreted as evidence that NO_3^- uptake and assimilation have not kept pace with photosynthesis and growth in enhanced [CO_2] (Pettersson and McDonald, 1994). In this study, a larger root system under elevated RZ [CO_2] at 20 °C-RZT increased not only leaf NO_3^- but also concentration of total reduced N, leaf soluble and Rubisco protein. Plants grown under elevated RZ [CO_2] had lower g_s but higher *A* and higher productivity could also be partially due to dissolved inorganic carbon incorporation which allowed the improved incorporation of N into amino acids in the roots as a consequence of greater supplies of anaplerotic carbon for protein synthesis (Viktor and Cramer, 2003). Increases in the leaf N and Rubisco concentration result in higher *A* (Li *et al*., 2009). The increased *A* under elevated RZ [CO_2], especially at 20 °C-RZT could partially be due to higher Rubisco protein not g_s (He *et al*., 2007, 2010).

Acknowledgements

This project was supported by the Academic Research Fund (RP12/01 HJ), Ministry of Education, Singapore.

References

De Jong E, Schappert HJV (1972) Calculation of soil respiration and activity from CO_2 profile in the soil. Soil Sci. 113: 328-333

He J, Austin PT, Lee SK (2010) Effects of elevated root zone CO_2 and air temperature on photosynthetic gas exchange, nitrate uptake, and total reduced nitrogen content in aeroponically grown lettuce plants. J. Exp. Bot. 61: 3959-3969

He J, Austin PT, Nichols MA, Lee SK (2007) Elevated root-zone CO_2 protects lettuce plants from midday depression of photosynthesis. Environ. Exp. Bot. 61, 94-110

Li Y, Gao Y, Xu X, Shen Q, Guo S (2009) Light-saturated photosynthetic rate in high-nitrogen rice (Oryza sativa L.) leaves is related to chloroplastic CO_2 concentration. J. Exp. Bot. 60: 2351-2360

McGuire MA, Marshall JD, Teskey RO (2009) Assimilation of xylem-transported 13C-labelled CO_2 in leaves and branches of sycamore (Platanus occidentalis L.). J. Exp. Bot. 60: 3809-3817

Norstadt FA, Porter LK (1984) Soil gases and temperatures: a beef cattle feedlot compared to alfalfa. Soil Sci. Soc. Am J. 48: 783-789

Pettersson R, McDonald JS (1994) Effects of nitrogen

supply on the acclimation of photosynthesis to elevated CO_2. Photosyn. Res. 39: 389-400

Teskey RO, McGuire MA (2005) CO_2 transported in xylem sap affects CO2 efflux from Liquidambar styraciflua and Platanus occidentalis stems, and contributes to observed wound respiration phenomena. Trees: Structure and Function 19: 357-362

Viktor A, Cramer MD (2003) Variation in root-zone CO_2 concentration modifies isotopic fractionation of carnon and nitrogen in tomato seedlings. New Phytol. 157: 45-54

Comparative Nitrogen Allocation and Partitioning of Field-Grown *Gossypium Hirsutum* and *G. Barbadense*

Yali Zhang, Yuanyuan Hu, Honghai Luo, Wangfeng Zhang*

The Key Laboratory of Oasis Eco-agriculture, Xinjiang Production and Construction Group, Shihezi University, Shihezi, 832003, P.R. China.
* Corresponding author. E-mail: zwf_shzu@163.com.

Abstract: In our previous study, we found that though pima cotton had higher area-based total leaf nitrogen content, pima cotton had lower photosynthetic capacity than upland cotton. The principal aim of this study was to reveal underlying mechanisms contributing to the relationship between leaf nitrogen and photosynthetic capacity in pima cotton and upland cotton. Pima cotton possessed lower light-saturated photosynthetic rate, higher area-based leaf nitrogen content, and consequently lower photosynthetic nitrogen utilization efficiency. Upland cotton partitioned a higher fraction of the photosynthetic nitrogen to carboxylation and bioenergetics. The results illustrated that nitrogen allocation and partitioning were the most important factors underlying the difference in photosynthetic nitrogen utilization efficiency between upland cotton and pima cotton.

Keywords: Pima cotton; Upland cotton; Photosynthetic nitrogen utilization efficiency

Introduction

Cottons (*Gossypium* spp.) are of tropical origin, and are the most important textile fibre crops in the world. The most widely distributed commercial cotton species worldwide is upland cotton (*G. hirsutum*) which has superior yield, followed by pima cotton (*G. barbadense*) which has superior fibre properties but lower yield. In our previous study, we found that though pima cotton had higher area-based total leaf nitrogen content, pima cotton had lower photosynthetic capacity than upland cotton (Zhang *et al*., 2011). This result is paradoxical because Evans (1989) found across many species, a strong positively correlation exists between leaf nitrogen content and photosynthetic capacity. Leroux *et al*. (2001) and Feng *et al*. (2007, 2009) reported that leaf nitrogen allocation and partitioning among different photosynthetic component are important factors influence the relationship between leaf nitrogen content and photosynthesis. Thus, the principal aim of this study was to reveal underlying mechanisms contributing to the relationship between leaf nitrogen and photosynthetic capacity in pima cotton and upland cotton.

Materials and Methods

The experiment was conducted in a field of Shihezi Agricultural College, Shihezi University, Xinjiang, China (45°19′N, 86°03′E) in 2008. Upland cotton (*Gossypium. hirsutum* L. *cv.* Xinluzao 13) and pima cotton (*G. barbadense cv.* Xinhai 22) were grown under field conditions with under-mulch drip irrigation. Seeds were sown on 24 April 2008 at a plant density of 1.8×10^5 ha^{-1}. N and P_2O_5 were applied at 240 and 172.5 kg ha^{-1}, respectively. The plots were drip-irrigated and maintained well-watered throughout the growing season. Pest was controlled using pesticide, but no pesticide was applied during the measurement period. Weeds were hand-pulled periodically.

In August, cotton plants, which were at flowering and boll-setting stages, were selected at random and from each selected plant. The topmost full-expanded leaf on the main stem was chosen.

Photosynthetic responses to intercellular CO_2 concentration (C_i) and PPFD were determined on fully-expanded leaves with a LI-6400 Portable Photosynthesis System (*LI-COR Inc.*, Lincoln, NE,

U.S.A.). Illumination was provided by a 6400-02B LED light source. Under 360 μmol mol^{-1} CO_2, net photosynthetic rate (P_n) of each leaf was measured after equilibration at twelve PPFDs, in a sequence of 2,000, 1,800, 1,500, 1,200, 800, 500, 300, 200, 100, 50, 30, 0 μmol photons m^{-2} s^{-1} at leaf temperature *ca.* 33 °C. Under saturated PPFD (2000 μmol photons m^{-2} s^{-1}), P_n was measured at 50, 100, 200, 400, 600, 800 and 1,000 μmol mol^{-1} CO_2 in the reference chamber. Light-saturated photosynthesis (P_{max}) was determined from the P_n-PPFD curve. V_{cmax} and J_{max}were derived from P_n-C_i curve according to Long and Bernacchi (2003). Photosynthetic nitrogen utilization efficiency (PNUE) was calculated as the ratio of P_{max} to area-based leaf nitrogen content (N_A)

Leaf discs with a defined area were taken from each sample leaf and oven-dried at 80 °C for 48 h. leaf mass per area (LMA) was calculated as the ratio of leaf mass to area. Leaf nitrogen (N) was determined by the Kjeldahl method. The absolute chlorophyll content (C_C) was determined chemically according to Lichtenthaler and Wellburm (1983). The leaf, stem and boll (including bract) and root parts of each sample plant were harvested and were oven-dried to constant weight at 80 °C.

The fraction of the total leaf N allocated to carboxylation (P_C, g g^{-1}), bioenergetics (P_B, g g^{-1}) and light-harvesting components (P_L, g g^{-1}) of the photosynthetic apparatus were calculated as:

$$P_C=V_{cmax}/(6.25\times V_{cr}\times N_A);$$
$$P_B=J_{max}/(8.06\times J_{mc}\times N_A) \text{ and}$$
$$P_L=C_C/(N_M\times C_B);$$

where C_C was leaf chlorophyll concentration, N_M was mass-based leaf N content. V_{cr}, J_{mc} and C_B were constants (Niiements and Tenhunen, 1997). The value 6.25 was the conversion coefficient between nitrogen content and protein concentration in Rubisco and 8.06 was the conversion coefficient between cyt f and nitrogen in bioenergetics.

The fraction of leaf nitrogen allocated to total photosynthetic apparatus (P_T) was calculated as the sum of P_C, P_B and P_L.

Statistical analysis of the data was performed by one-way ANOVA and least significant differences (LSD) test at the 5% level of significance using SPSS (13.0 for windows).

Results and Discussion

Pima cotton had lower light-saturated photosynthesis (P_{max}) than upland cotton, consistent with the results of other authors (Wise *et al*., 2000; Wu *et al*., 2006). Since upland cotton had lower N_A, upland cotton had higher photosynthetic nitrogen utilization efficiency (PNUE) than pima cotton. Generally, photosynthetic capacity positively correlates with the N_A because more than about half of total nitrogen is allocated to the proteins of the Calvin cycle and thylakoids in photosynthetic apparatus (Field and Mooney, 1986; Evans, 1989; Evans and Seemann, 1989). This result was not the case in pima cotton, however. Feng *et al*. (2007, 2009) reported that a high PNUE was attributed to not only their low nitrogen content and high photosynthesis but also higher allocation of leaf nitrogen to the photosynthetic machinery. In this study, upland cotton was more efficient in photosynthetic N partitioning. Upland cotton partitioned a higher fraction of the photosynthetic N to carboxylation and bioenergetics (higher P_C and P_B). Thus, for upland cotton, the higher fraction of leaf N allocated to carboxylation and bioenergetics was the most important factor underlying the higher photosynthetic nitrogen utilization efficiency. By contrast, pima cotton partitioned a higher fraction of photosynthetic N to light-harvesting components (higher P_L). We proposed that the increased nitrogen allocation to light-harvesting components in pima cotton could compensate for the negative effect of higher leaf cupping and lower leaf diaheliotropic movement on light capture (Wise *et al*., 2000; Zhang *et al*., 2010).

There is a trade-off between nitrogen allocation to photosynthesis and to cell walls, which is mediated by leaf mass per area (LMA) (Onoda *et al*., 2004; Feng, 2008). LMA is positively associated with cell wall mass and the fraction of leaf N in cell walls, but negatively correlated with the fraction of leaf N in Rubisco (Onoda *et al*., 2004; Takashima *et al*., 2004). Upland cotton had higher P_C, P_B and P_T, meaning that upland cotton increased nitrogen allocation to photosynthesis. Nevertheless, upland cotton possessed higher LMA, indicating that upland cotton increased nitrogen allocation to cell walls as well. Thus, upland cotton in comparison with pima cotton had both higher allocation of nitrogen to photosynthesis and to cell walls, breaking the trade-off between them. Upland cotton had higher leaf thickness accompanying thicker palisade tissue, allowing an increase in

maximum photosynthetic capacity (Pachepsky and Acock, 1998; Zhang *et al*., 2011). By contrast, pima cotton was more inefficient in photosynthetic N partitioning despite its higher leaf nitrogen content. Furthermore, pima cotton allocated a large proportion of photosynthate to stem and root (Fig. 1). In addition, it is important to note that cotton species have undergone significant selection during breeding so that some aspects of current plant performance may differ from those found in other primitive species. Therefore, compared to upland cotton, much selective pressure in pima cotton is needed to suppress the residual perennial trait. Cotton breeders should in future pay attention to leaf nitrogen allocation efficiency and to the shifting of photosynthate to reproductive growth, thereby increasing photosynthetic nitrogen use efficiency and yield.

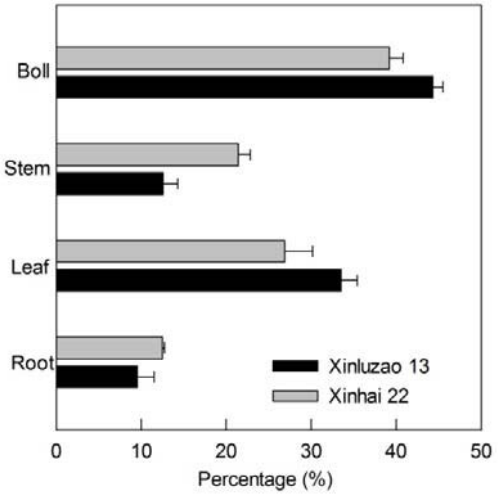

Fig. 1 Dry matter partitioning of Xinluzao 13 (upland cotton) and Xinhai 22 (pima cotton).

Acknowledgement

This study was financially supported by the National Natural Science Foundation of China (Grant No. 30460063; 30260051).

Table 1 Means and standard deviation of the variables of the Xinluzao 13 (upland cotton) and Xinhai 22 (pima cotton).

Variable	Xinhai 22	Xinluzao 13
C_C (mg dm^{-2})	5.75±0.224 a	4.95±0.014 b
N_A (g m^{-2})	2.89±0.11 a	2.58±0.13 b
LMA (g m^{-2})	76±4 b	84±6 a
P_{max} (μmol m^{-1} s^{-1})	37.8±2.1 b	43.1±0.2 a
V_{cmax} (μmol m^{-1} s^{-1})	220±23 a	230±2 a
J_{max} (μmol m^{-1} s^{-1})	271±21 a	288±11 a
PNUE (μmol g^{-1} s^{-1})	13.1±1.2 b	16.7±2.3 a
P_C (g g^{-1})	0.59±0.061 b	0.69±0.007 a
P_B (g g^{-1})	0.075±0.006 b	0.089±0.003 a
P_L (g g^{-1})	0.011±0.0001 a	0.009±0.0001 b
P_T (g g^{-1})	0.67±0.03 b	0.79±0.05 a

Different letters in the same row indicate significant differences between species.

C_C, leaf chlorophyll concentration; P_{max}, Light-saturated photosynthesis; PNUE, photosynthetic nitrogen utilization efficiency; LMA leaf mass per area, N_A, area-based leaf nitrogen content; V_{cmax}, maximum carboxylation rate; J_{max}, maximum electron transport rate; P_C, the fraction of leaf nitrogen allocated to carboxylation; P_B, the fraction of leaf nitrogen allocated to bioenergetics; P_L, the fraction of leaf nitrogen allocated to light-harvesting components; P_T, the fraction of leaf nitrogen allocated to total photosynthetic apparatus.

References

Evans JR (1989) Photosynthesis and Nitrogen Relationships in Leaves of C_3 Plants. Oecologia 78: 9-19

Evans JR, Seemann JR（1989）The Allocation of Protein Nitrogen in the Photosynthetic Apparatus: Costs, Consequences, and Control. In: Briggs WR (ed.), Photosynthesis. New York, pp. 183-205

Feng YL, Auge H, Ebeling SK (2007) Invasive Buddleja Davidii Allocates More Nitrogen to Its Photosynthetic Machinery than Five Native Woody Species. Oecologia 153: 501-510

Feng YL, Lei YB, Wang RF, Callaway RM, Valiente-Banuet A, Inderjit, Li YP, Zheng YL (2009) Evolutionary Tradeoffs for Nitrogen Allocation to Photosynthesis Versus Cell Walls in an Invasive Plant. P Natl. Acad. of Sci. USA 106: 1853-1856

Feng YL (2008) Photosynthesis, Nitrogen Allocation and Specific Leaf Area in Invasive Eupatorium Adenophorum and Native Eupatorium Japonicum Grown at Different Irradiances. Physiol. Plant 133: 318-326

Field CB, Mooney HA (1986) The Photosynthesis-Nitrogen Relationship in Wild Plants. In: Givnish TJ (ed.), On the Economy of Plant Form and Function. Cambridge University Press: Cambridge, PP. 25-55

Long SP, Bernacchi CJ (2003) Gas Exchange Measurements, What Can They Tell Us about the Underlying Limitations to Photosynthesis?

Procedures and Sources of Error. J Exp. Bot. 54: 2393-2401

Leroux X, Walcroft AS, Daudet FA, Sinoquet H, Chaves MM, Rodrigues A, Osorio L (2001) Photosynthetic Light Acclimation in Peach Leaves: Importance of Changes in Mass: Area Ratio, Nitrogen Concentration and Leaf Nitrogen Partitioning. Tree Physiol. 21: 377-386

Lichtenthaler HK, Wellburn AR (1983) Determination of Total Carotenoids and Chlorophyll a and b of Leaf Extracts in Different Solvents. Biochem. Soc. Trans. 603: 591-592

Niinumets Ü, Tenhunen JD (1997) A Model Separating Leaf Structural and Physiological Effects on Carbon Gain along Light Gradients for the Shade-Tolerant Species Acer Saccharum. Plant Cell Environ 20: 845-866

Onoda Y, Hikosaka K, Hirose T (2004) Allocation of Nitrogen to Cell Walls Decrease Photosynthetic Nitrogen-Use Efficiency. Funct Ecol. 18: 419-425

Pachepsky LB, Acock B (1998) Effect of Leaf Anatomy on Hypostomatous Leaf Gas Exchange. A Theoretical Study with the 2DLEAF Model. Biotronics 27: 1-14

Takashima T, Hikosaka K, Hirose T (2004) Photosynthesis or Persistence: Nitrogen Allocation in Leaves of Evergreen and Deciduous Quercus Species. Plant Cell Environ. 27: 1047-1054

Wise RR, Sassenrath-Cole GF, Percy RG (2000) A Comparison of Leaf Anatomy in Field-Grown Gossypium Hirsutum and G. Barbadense. Ann Bot. 86: 731-738

Wu WM, Dong HL, Wei CZ, Chen KW, Yang RB, Zhi JH (2006) Analysis of Light Flux/Effect Curves and Chlorophyll Fluorescence Characteristics of Cotton (Gossypium. Barbadense L. and Gossypium. Hirsutum L.) in South Xinjiang. Acta Bot. Boreai. Occident. Sin. 15: 141-146 (in Chinese with English abstract)

Zhang YL, Luo Y, Yao HS, Tian JS, Luo HH, Zang WF (2010) Mechanism for Photoprotection of Leaves at the Bolling Stage under Field Conditions in Gossypium Barbadense and G. Hirsutum. Chinese J Plant Ecol. 34: 1204-1212 (in Chinese with English abstract)

Zhang YL, Yao HS , Luo Y, Hu YY, Zhang WF (2011) Difference in Leaf Photosynthetic Capacity between Pima Cotton (Gossypium Barbadense) and Upland Cotton (G. Hirsutum) and Analysis of Potential Constraints. Acta Ecologica Sin. in press. (in Chinese with English Abstract)

Photosynthetic Performance of Maize Subjected to Low Temperatures

Soni S Mulakupadom[1*], Saul Otero[1], Gary Lanigan[2], Bruce Osborne[1]

[1]Plant Eco-physiology Group, School of Biology and Environmental Science, University College Dublin, Belfield, Dublin 4, Ireland;
[2] Johnstown Research Centre, Teagasc, Johnstown Castle, Wexford, Ireland.
[*]Corresponding author. E-mail: Soni.Mulakupadom@ucdconnect.ie.

Abstract: The introduction of early maturing cultivars has enabled forage maize to be grown in climatically marginal areas of Europe. The major constraint in growing maize in North-west European countries is the impact of sub-optimal temperatures during early growth and establishment. The use of plastic coverings to improve the establishment of seedlings in the field has considerable practical, economic and environmental costs, so breeders are now directing their attention at improving establishment and yield under cool-temperate conditions in the absence of plastic mulches. The objectives of the present study were to screen seedlings of nine commercial hybrids recommended for Ireland for photosynthetic performance under spring and early summer conditions. Maize seedlings subjected to sub-optimal temperatures show major variety-dependent reversible reductions in photosynthetic performance, although isotope data indicate that all have a functional C_4 pathway. Non photochemical quenching (NPQ) may be a significant factor in protecting the photosynthetic apparatus of maize seedlings subjected to sub-optimal temperatures. The patterns of variation between varieties observed during cold exposure at 15 ºC and after recovery at 20 ºC were not directly correlated. This indicates that both the traits associated with an enhanced performance under low-temperature exposure as well as those associated with recovery may need to be considered when breeding improved maize varieties for cool-temperate regions.

Keywords: Maize; Cold tolerance; Chlorophyll fluorescence; NPQ

Introduction

North West-European Countries such as Ireland, North-West U.K., The Netherlands, Belgium, Denmark and Lithuania are climatically marginal areas for maize cultivation as temperatures are often sub-optimal during the early and late growing seasons. The introduction of early maturing and cold tolerant cultivars in recent years has improved the performance of maize in climatically marginal areas of Europe, although seedling establishment is still a target for improvement. Whilst the use of plastic mulches during early growth can also markedly improve seedling performance during establishment there are environmental and economic concerns about this approach (Crowley, 1996).

The general sensitivity of maize to low temperature is thought to be due largely to an inherent susceptibility of the photosynthetic apparatus (Hayden and Baker, 1990; Baker, 1994; Fracheboud *et al*., 1999; Chenu *et al*., 2007). It has been observed, however, that there are more resistant genotypes that have the capability to form a more competent photosynthetic apparatus under cool climatic conditions (Stamp, 1984; Haldimann, 1998; Foyer *et al*., 2002). Therefore, a better understanding of the photosynthetic responses of maize seedlings to low temperature and the identification of more effective acclimation mechanisms that exists in commercial maize cultivars is a prerequisite for expanding maize cultivation to higher latitudes of Europe be it for silage or bio-fuels.

The objective of the present work was to screen nine commercial cultivars recommended for growing in Ireland, without plastic mulches, to assess the photosynthetic performance of seedlings under simulated early spring conditions and the recovery of their photosynthetic system at a higher temperature,

as would be common in late spring in the field based on gas exchange and chlorophyll fluorescence measurements which in recent years is routinely used an extremely powerful analytical tool to identify improved plant performance (Baker, 1994; Andrews *et al*., 1995; Fracheboud and Leipner, 2003).

Materials and Methods

Plant Material

Nine forage maize (Zea mays, L.) cultivars recommended by the Department of Agriculture in Ireland in 2009 for growing without plastic cover were used in the study. The certified seeds of these varieties were obtained from the Crop Variety Evaluation Division, Department of Agriculture, Fisheries and Food, Ireland. A list of the varieties used, with an assessment of their cold tolerance and maturity class characteristics are shown in Table 1.

Table 1 Maize (*Zea mays* L.) cultivars used in this study. The code is the number used as identification in this experiment for each variety. The cold tolerance assessments are based on the Early Vigor Score taken from field trials carried out at the Crop Variety Evaluation Farm, Backweston, Ireland in 2008. The maturity class is based on information provided by the seed suppliers.

Cultivar	Code	Cold Tolerance	Maturity Class
Algans	AL	Low	Early
Beethoven	BE	Low	Early
Nescio	NE	Low	Medium early
Avenir	AV	Medium	Very early
Loft	LO	Medium	Early
Tassilo	TA	Medium	Early
Andante	AN	High	Early
Fergus	FE	High	Early
Nimrod	NI	High	Early

Growth Conditions

Seeds of the nine cultivars were germinated in dark on perlite moistened with water in seed trays at 18 °C and 70% humidity. Four day old seedlings were transplanted into plastic pots (one seedling per pot) filled with John Innes No.2 compost. The seedlings were raised to the four and a half leaf stage under early spring conditions in a controlled-environment chamber (Vindon Scientific, England) with a 14:10 day:night photoperiod, 15:10 degree C day:night temperature, 75% RH and an irradiance of 300 μmol m^{-2} s^{-1}. The seedlings were watered with approximately 20 ml tap water on alternate days. There were five replicates of each variety randomly arranged in the growth chamber; pots were periodically moved to avoid any positional bias. To assess the recovery of the seedlings cultivars as temperature raises in late spring a recovery trial was used. Seedlings were raised in exactly the same way and the temperature of the controlled-environment chamber switched to a 20/15 °C (day/night) regime to simulate typical late spring/earlysummer conditions in Ireland. The seedlings were then subjected to these conditions for 10 days until they reached the ~six leaf stage before assessments were made.

Fluorescence and Gas Exchange Measurements

Leaf gas exchange and chlorophyll fluorescence measurements were made using a CIRAS-2, with a PLC6 (Universal) leaf chamber (PP Systems, Haverhill, USA). The instrument allows for automatic calculation of dark adapted and light adapted chlorophyll fluorescence parameters simultaneously with gas exchange measurements. The cuvette environment was preset with a reference CO_2 concentration of 387 μmol mol^{-1} and a relative humidity (RH) of 60%–70%, a temperature of 15 ºC for plants continuously exposed to low temperatures and 20 ºC for the recovery experiments. The maximum quantum efficiency of PSII photochemistry, F_v/F_m was measured after adapting the whole plant in a dark chamber for 15 min.

Measurements of light adapted chlorophyll fluorescence parameters: PSII operating efficiency (Φ_{PSII}), PSII efficiency factor (Q_P), non photochemical quenching at PSII (NPQ) were taken upon stabilization of the photosynthetic gas exchange in leaves exposed to an irradiance of 300 umol m^{-2} s^{-1}. The rate of transpiration (E), stomatal conductance (Gs), net photosynthesis (Pn) and internal carbon dioxide concentration (C_i) were measured simultaneously .The maximum efficiency of open PSII reaction centers (F_v'/F_m') was measured after switching off the actinic light and simultaneously applying far red light. Measurements were made by attaching the leaf chamber to the upper quarter of the third fully expanded leaf and followed a random temporal pattern to avoid any circadian cycle effects.

Carbon Isotope Discrimination Measurements

Samples of tissue from the third leaves of maize plants were collected after assessments of chlorophyll

concentration and dried in oven at 60 ºC until constant weight. Then 1 g of each sample was ground and stored until analysis following Boutton (1991) and the results were determined in ‰ of ^{13}C compared to the PDB standard.

Data Analysis

Varietal differences in the response to cold stress and recovery were estimated separately using a one-way ANOVA or Kruskal-Wallis test depending on their homoescedasticity. Bivariate correlations of selected variables for both the cold stress and recovery treatments were determined on the basis of the Pearson product-moment coefficient. All the tests were carried out using the SPSS 15 version for windows (SPSS Inc., Illinois).

Results and Discussion

The maize cultivars used in the study differed in their early vigour scores or the tolerance of their seedlings to low temperatures in the field (Table 1). Several studies have indicated that early vigor rating would be the most suitable trait to select maize genotypes with superior cold tolerance during emergence and post emergence stages, because it was the only trait for which differences among genotypes were observed in both the cold chamber and the field (Rodrígues *et al*., 1970).

The maize cultivars grown under simulated early spring cold stress in the growth chamber showed major variety-dependent depressions in photochemistry (Table 2). The recovery of their photosynthetic system at a higher temperature, under simulated late spring rise in temperature was also variety-dependent (Table 2). The patterns of variation between varieties observed during cold exposure at 15 ºC and after recovery at 20 ºC were not directly correlated.

Of the varieties examined, only Nescio showed any net carbon assimilation at sub-optimal temperatures (Fig. 1). However, assimilation was not limited by stomatal conductance or by variety-dependent disengagement of the C_4 pathway as ‰ of ^{13}C of the leaf biomass was in the range of $-13.5 \pm 1.5\%$. Photosynthetic performance seems to recover significantly in all the cultivars after exposure for 10 days at an enhanced temperature (Fig. 1). Nevertheless the early vigor rating of cold tolerance in the field of these varities was not indicative of the photosynthetic performance under simulated early spring cold stress or late spring rise in temperature.

Table 2 Statistical analyses of the differences between the photochemical parameters of the nine varieties of maize under cold stress. Each variable were compared using ANOVA or Kruskal-Wallis tests [(k)]: n.s. means non significant differences; * means $p < 0.05$; ** means $p < 0.01$ and *** means $p < 0.001$.

Photochemical parameters	Stress	Recovery
F_v / F_m	***	*
ΦPSII	***	ns
Qp	**	ns
NPQ	***	ns
$F_{v'} /F_{m'}$	n.s.	**
A	**	ns

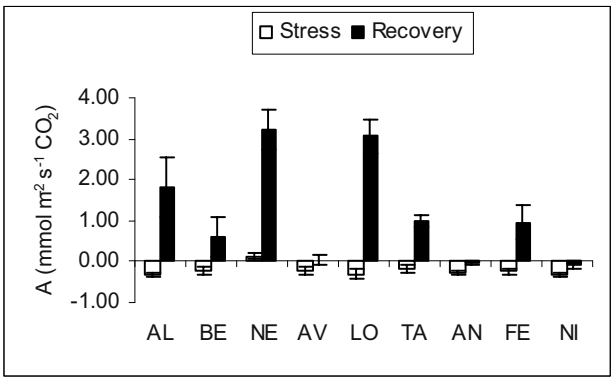

Fig. 1 Mean values for net photosynthesis of the different cultivars under cold stress and after recovery from cold stress Bars represent standard error of the mean. In the foot is the code for different varieties (Table 1).

The maximum quantum efficiency of PSII photochemistry (F_v/F_m) of maize seedlings grown under cold stress was very low (Fig. 2), as reported in several studies conducted under controlled environment conditions (Nie *et al*., 1992; Haldimann *et al*., 1996; Leipner *et al*., 1997), and in the field (Andrews *et al*., 1995; Leipner *et al*., 1999), but showed significant variation.

This inhibition of photosynthesis by the down-regulation or photodamage to PSII can take place rapidly even at moderate irradiances and is a widespread response of chilling-sensitive crops subjected to sub-optimal temperatures (Ort, 2002). Given the six fold variation in Fv/Fm there are, however, significant differences in the sensitivity to low temperatures among the group of cultivars examined (Fig. 2). The F_v/F_m of all the cultivars showed significant increases after exposure for 10 days at an enhanced temperature (Fig. 2), although in most cases the values were less than expected for

maize grown under optimal temperatures (Sowinski *et al*., 2005; Frachebound *et al*., 1999), suggesting prolonged or permanent damage. The ability in some cases for recovery to near optimal values is suggestive of an enhanced reversible flexibility of the photosynthetic apparatus to sub optimal temperatures.

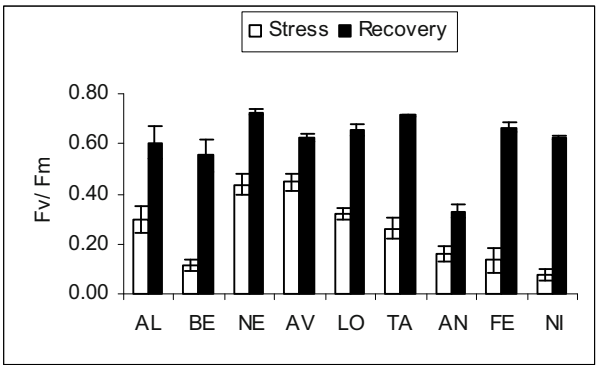

Fig. 2 Mean values for F_v/F_m of maize cultivars exposed to low temperature and after recovery from cold stress. Bars represent standard error of the mean.

The PSII operating efficiency (Φ_{PSII}) showed the same trend as seen for F_v/F_m with the low values found under low temperature exposure showing some recovery after return to more optimal conditions (Fig. 3). The PSII operating efficiency factor showed significant increases in most of the cultivars barring a few after exposure for 10 days at an enhanced temperature.

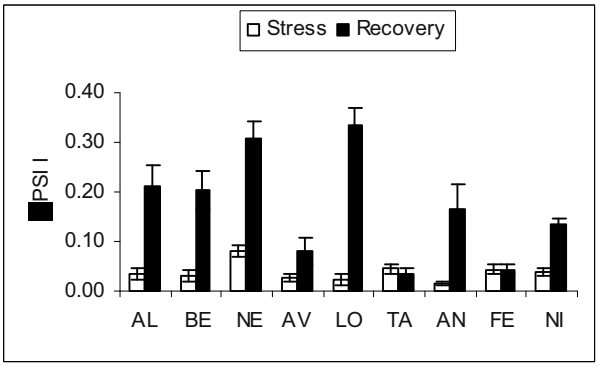

Fig. 3 Mean values for Φ_{PSII} in in maize cultivars exposed to low temperatures and after recovery. Bars represent standard error of the mean.

The augmentation of Φ_{PSII} after exposure for 10 days at an enhanced temperature in most of the varieties was concomitant to an increase in Q_p (Fig. 4) rather than F_v'/F_m'. It therefore seems that the capacity for electron flux on the reducing side of PSII is the major factor which influences the photosynthetic performance of maize than to the down-regulation of PSII by antenna quenching. Generally, reductions in temperature inhibit photosynthetic carbon metabolism (Allen and Ort, 2001; Ort, 2002) which results in a decrease in the sink for the products of electron transport (ATP and NADPH) and a decrease in Φ_{PSII} (Andrews *et al*., 1995; Fracheboud and Leipner, 2003) as found in this experiment.

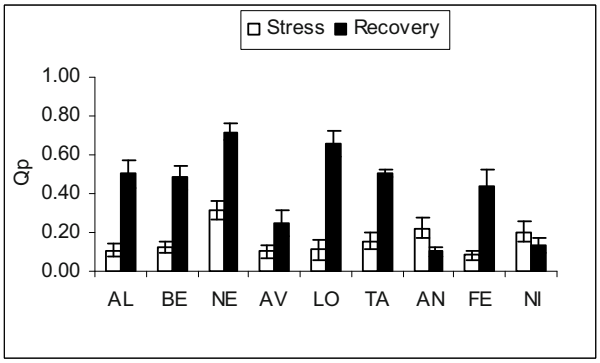

Fig. 4 Mean values for Qp in in maize cultivars exposed to low temperatures and after recovery. Bars represent standard error of the mean.

Non photochemical quenching (NPQ) is a measure of the ability of the plants to dissipate excess excitation energy through thermal processes, mainly the xanthophyll cycle pathway (Demmig-Adams and Adams, 2008; Haldimann *et al*., 1996; Leipner *et al*., 1997). Significant variations in NPQ was found with Nescio maintaining the highest value for NPQ (Fig. 5).

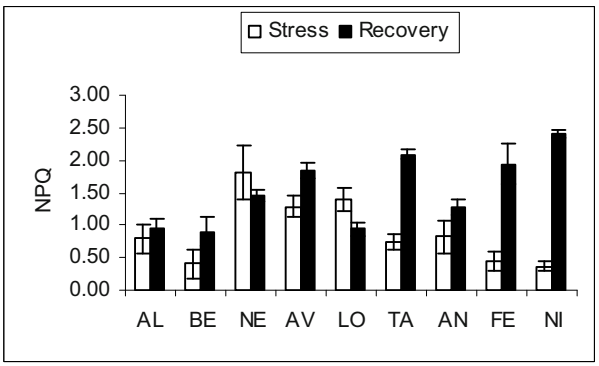

Fig. 5 Mean values for NPQ in maize cultivars subjected to low temperatures and after recovery. Bars represent the standard error of the mean.

Values for NPQ were still high in most of the cultivars after transfer to more optimal conditions however there were considerable reductions in NPQ in NE and LO, which might have contributed to the built up of a significantly higher photosynthetic activity in these cultivars than the rest of the cultivars

(Figs. 1 and 5). Interestingly, maize seedlings grown under prolonged cold stress showed a significant correlation between NPQ and F_v/F_m (Fig. 6) suggesting that the ability of the maize seedling leaves to dissipate excess energy is a significant photo protective measure under low temperatures.

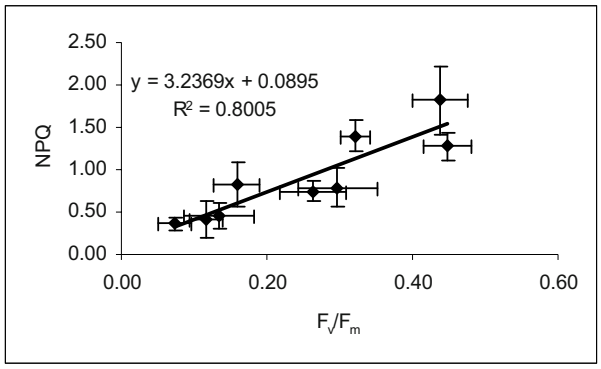

Fig. 6 Correlation between NPQ and Fv/Fm of maize cultivars during low temperature exposure.

In summary, the maize varieties showed, rather surprisingly, major variety-dependent variations in photochemistry in response to low temperatures and after recovery under near optimal conditions. Maize cultivars that maintained a higher Fv/Fm and NPQ had a more low temperature tolerant photosynthetic apparatus. Recovery of the photosynthetic performance of maize seedlings depended on an increase in ΦPSII and a general reduction in NPQ.

Photochemical traits associated with the low temperature hardiness of maize seedlings during early spring as well as those associated with recovery of the photosynthetic performance after return to more optimal conditions during late spring/earlysummer may need to be considered when breeding maize with improved early seedling performance varieties for cool-temperate regions.This study has also demonstrated that early vigour ratings based on visual clues need not necessarily depict the cold tolerance of the photosynthetic apparatus of maize seedlings but instead reflect the overall performance of seedlings under the real conditions in the field.

Acknowledgements

The project is funded as part of the Strategy for Science Technology and Innovation 2008–2013, Ireland and the Department Of Agriculture Food And Fisheries, Ireland, under grant number RSF 07501.

References

Andrews JR, Fryer MJ, Baker NR (1995) Characterization of Chilling Effects on Photosynthetic Performance of Maize Crops during Early Season Growth Using Chlorophyll Fluorescence. Journal of Experimental Botany 48: 1195-1203

Baker NR (2008) Chlorophyll Fluorescence: a Probe of Photosynthesis in Vivo. Annual Review of Plant Biology Vol. 59: 89-113

Boutton T (1991) Stable Carbon Isotope Ratios of Natural Materials I: Sample Preparation and Mass Spectrometric Analysis. In: DC Coleman, B Fry (eds.), Carbon Isotope Techniques. Academic Press Inc: San Diego, California, pp. 155-172

Chenu K, Fournier C, Andrieu B, C Giauffret C (2007) An Architectural Approach to Investigate Maize Response to Low Temperature. In: JHJ Spiertz, PC Struik, .H can Laar (eds.), Scale and Complexity in Plant Systems Research: Gene-Plant-Crop Relations. pp. 203-212

Crowley JG (1996) Growing Maize Silage under Photodegradable Polythene Film. Irish Journal of.Agricultural and Food Research 35: 90

Demmig-Adams B, Adams WW III (1996) The Role of Xanthophyll Cycle Carotenoids in the Protection of Photosynthesis. Trends in Plant Sciences 1: 21-26

Foyer CH, Vanacker H, Gómez LD, Harbinson J (2002) Regulation of Photosynthesis and Antioxidant Metabolism in Maize Leaves at Optimal and Chilling Temperatures: Review. Plant Physiol. Biochem. 40: 659-668

Fracheboud Y, Haldimann P, Leipner J, Stamp P (1999) Chlorophyll Fluorescence As a Selection Tool for Cold Tolerance of Photosynthesis in Maize (Zea Mays L.). Journal of Experimental Botany 50: 1533-1540

Haldimann P (1996) Effects of Changes in Growth Temperature on Photosynthesis and Carotenoid Composition in Zea Mays Leaves. Physiologia Plantarum 97: 554-562

Haldimann P, Fracheboud Y, Stamp P (1996) Photosynthetic Performance and Resistance to Photoinhibition of Zea Mays L. Leaves Grown at Sub-Optimal Temperature. Plant, Cell and Environment 19: 85-92

Haldimann P (1998) Low Growth Temperature-Induced Changes in Pigment Composition and

Photosynthesis in Zea Mays Genotypes Differing in Chilling Sensitivity. Plant, Cell and Environment 21: 200-208

Hayden DB, Baker NR (1990) Damage to Photosynthetic Membranes in Chilling Sensitive Plants: Maize, a Case Study. Critical Reviews in Biotechnology 9: 321-341

Leipner J, Fracheboud Y, Stamp P (1997) Acclimation by Suboptimal Growth Temperature Diminishes Photooxidative Damage in Maize Leaves. Plant, Cell and Environment 20: 366-372

Leipner J, Fracheboud Y, Stamp P (1999) Effect of Growing Season on the Photosynthetic Apparatus and Leaf Anti Oxidative Defenses in Two Maize Genotypes of Different Chilling Tolerance. Environmental and Experimental Botany 42: 129-139

Nie GY, Long SP, Baker NR (1992) The Effects of Development at Sub-Optimal Growth Temperatures on Photosynthetic Capacity and Susceptibility to Chilling-Dependent Photoinhibition in Zea Mays. Physiologia Plantarum 85: 554-560

Ort DR (2002) Chilling-Induced Limitations on Photosynthesis in Warm Climate Plants: Contrasting Mechanisms. Environmental Control in Biology 40: 7-18

Stamp P (1984) Chilling Tolerance of Young Plantsdemonstrated on the Example of Maize. Journal of Agronomy and Crop Science 7: 1-83

Sowinski P, Rudzinska-Langwald A, Adamczyk J, Kubica I, Fronke J (2005) Recovery of Maize Seedling Growth, Development and Photosynthetic Efficiency after Initial Growth at Low Temperature. Journal of Plant Physiology 162: 67-80

Rodrígues VM, Butrón A, Sandoya G, Ordás A, Revilla P (1970) Combining Maize Base Germplasm for Cold Tolerance Breeding. Crop Sci. 47: 1464-1474

Stereochemical Control of Asymmetric Reduction by Deleting an Alcohol Gehydrogenase Gene of a Cyanobacterium

Hisataka Ohta [a], Kenjro Suzuki [b], Tetsuo Takemura [b], Kaori Akiyama [b], Nobuaki Umeno [b], Yukiko Tamai [b], Kaoru Nakamura[c]

[a] Department of Biology, Faculty of Science, Tokyo University of Science, Kagurazaka 1-3, Shinjuku, Tokyo 162-8601 Japan;
[b] Department of Chemistry, Faculty of Science, Tokyo University of Science, Kagurazaka 1-3, Shinjuku, Tokyo 162-8601 Japan;
[c] Science shop, Graduate School of Human Development and Environment, Kobe University 3-11 Turukabuto, Nada, Kobe, 657-8501 Japan.
*Corresponding author. Fax No. +81(3)5228 8374; E-mail: ohta@rs.noda.tus.ac.jp.

Abstract: Cyanobacteria play important roles in carbon dioxide absorption on earth and thus the use of cyanobacteria as biocatalysts is of great significance in viewpoint of green chemistry. However, microalgae including cyanobacteria are rarely applied as biocatalysts because of luck of knowledge of controlling enantioselectivities in asymmetric reactions compared to other microbes. Here, we would like to present that knockout of an alcohol dehydrogenase gene of *Synechocystis* sp. PCC 6803 could change stereoselectivities of asymmetric reduction of ketones from the wild type microalga. Thus, asymmetric reduction of ethyl pyruvate and trifluoroacetophenone by the mutant deleting of *sll0990* and *sll1825* gene increased the enantioselectivity.

Keywords: Cyanobacteria; Knockout mutant; Dehydrogenase; Asymmetric reduction; Stereochemical control; *Synechocystis* sp. PCC6803

Introduction

Cyanobacteria belong to photosynthetic organisms and play important roles in carbon dioxide absorption on earth. Thus the use of cyanobacteria as biocatalysts for useful biotransformations is of great significance in viewpoint of green chemistry.

Microbial reductions have been widely used for synthesis of optically active alcohols, which are important starting materials for drugs and agrochemicals. However the reductions could not always afford desired alcohols in excellent enantioselectivities and several methods such as screening of microbes, modification of reaction conditions, overexpression of alcohol dehydrogenase gene in *E. coli* have been developed to increase low enantioselectivities [1].

Although the use of cyanobacteria as biocatalysts is of great significance from the viewpoint of sustainable development, algae including cyanobacteria are rarely applied as biocatalysts because of luck of knowledge of controlling enantioselectivities in asymmetric reactions compared to other microbes [2]. Previously, we have reported that the selectivity of asymmetric reduction could be controlled by illumination [3–4] and now, we would like to report a novel method for controlling the stereoselectivity of reduction with photosynthetic organisms such as cyanobacteria.

Our strategy is as follows. If a low enantioselectivity in the reduction of a ketone is due to the result of participating plural dehydrogenases which gave alcohols of different stereoselectivities each other (*R* or *S*), deletion of a gene that code a dehydrogenase which reduces the ketone will afford a mutant microbe that cannot express the corresponding dehydrogenase and will change stereoselectivity of the reduction and in the fortunate case, improve the enantioselectivity of the product alcohol.

Synechocystis sp. PCC 6803 was chosen as the microbe because all gene sequences of the microbe can be obtained from “cyanobase” [5] and we prepared several dehydrogenase-gene-deleted mutants and the effect of deletion on asymmetric reduction of ketones was investigated.

Material and Methods

Synechocystis sp. PCC 6803 Williams was used as the host microbe. Nine dehydrogenase and oxidoreductase genes, *i.e.* open reading frames (ORF's), shown in Table 1 were selected to be target genes. For example, *slr0990*was chosen as the target gene since the gene is classified as a gene for short chain alcohol dehydrogenase (ADH). It is known that several short chain ADHs could reduce artificial ketones and were used as catalysts for biotransformations [6]. Other genes, *sll1825*, *slr0315*, *slr0506*, *slr0886*, *slr0942*, *slr1192*, and *slr2124* were also chosen because these genes are categorized to dehydrogenases and reductases.

Generation of insertion mutants

Mutants impaired in selected genes were generated by reverse genetics. The encoding sequences and neighboring sequences were amplified by PCR. The approximately 2 kb PCR products were cloned into pUC19 (TOYOBO). The primers for amplification were designed using the complete genome sequence of *Synechocystis* [7]. Sequences were selected which contained appropriate restriction sites to improve cloning of the fragments. The *aphII* gene [aminoglycoside phosphotransferase II conferring kanamycin (Km) resistance] isolated from plasmid pUC4K (Pharmacia) was inserted into unique restriction sites of the encoding sequences. Transformation of *Synechocystis* has been described previously [7]. Transformants were initially selected on a medium containing 10 μg Km ml^{-1} (Wako), whilst the segregation of clones was performed by numerous restreaking (at least three transfers) of primary clones on plates supplemented with 50 μg Km ml^{-1}. During the cultivation of mutants, 50 μg Km ml^{-1} was added to the liquid media. Deletion of *slr0990* gene and other genes was checked by PCR analysis using DNA of wild-type and the mutant cells as shown in Fig. 1.

Cultivation and reaction

The mutant microbe was cultivated under 25–40 μmol photon m^{-1} s^{-2} and for biotransformation, concentrations of the microbe was set to be OD_{730} = 0.6. The mutant microbes grew almost the same rate with the original microbe. The reaction was conducted by adding 10% solution of the substrate (ethyl pyruvate(EP) or trifluoroacetophenone(TFA)) in DMSO (about 1.4 mmol) to the suspension of the microbe under 49 μmol photonm^{-1} s^{-2} of fluorescent light at 30 °C for1day. The reaction mixtures were analyzed by gas chromatography (GC); Column: Chirasil-DEX-CB, 25 m, He, 0.5 ml min^{-1}, Temp. (EP: 60 °C, TFA: 125 °C), and the results are listed in Fig. 2, Tables 1, 2 and 3.

Fig. 1 Agarose-gel electrophoresis analyses of DNA extracted from wild-type and knockout mutant cells, each right lane showing deletion of *sll0990*.

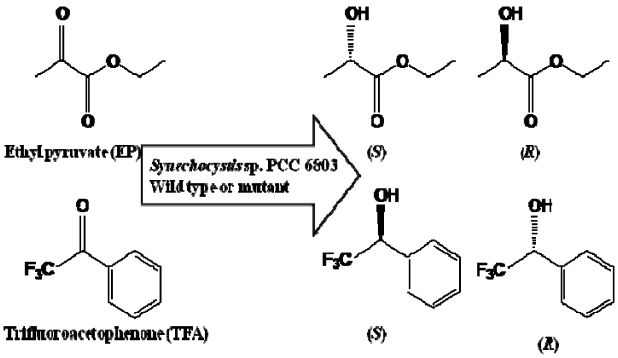

Fig. 2 Reduction of ketones with the wild type and the mutants of *Synechocystis* sp. PCC 6803.

Table 1 Target genes in *Synechocystis* sp. PCC 6803 and homology of these genes.

ORF	NN	AA	Product (Gene)
sll0990	1107	369	glutathione-dependent formaldehyde dehydrogenase
sll1825	588	196	short-chain dehydrogenase/reductase
slr0315	732	244	probable oxidoreductase
slr0506	966	322	light-dependent NADPH-protochlorophyllide oxidoreductase (*por*)
slr0886	741	247	3-oxoacyl-[acyl-carrier protein] reductase
slr0942	981	327	alcohol dehydrogenase [NADP+]
slr1192	1008	336	probable alcohol dehydrogenase
slr2124	747	249	3-oxoacyl-[acyl-carrier protein] reductase

ORF Similar dehydrogenase.

Table 2 Reduction of ethyl pyruvate (EP) with the mutants of *Synechocystis* sp. PCC 6803[a].

Strain	%ee (Config.)	% ee (Δ-WT)	% Conv.
WT	18.3 (*R*)	—	92.4
Δ-sll0990	38.8 (*R*)	20.0	92.6
Δ-sll1825	37.6 (*R*)	19.3	96.7
Δ-slr0315	30.6 (*R*)	12.3	88.9
Δ-slr0506	26.7(*R*)	8.4	92.4
Δ-slr0886	12.7(*R*)	–5.6	95.8
Δ-slr0942	26.4 (*R*)	8.1	96.0
Δ-slr1192	25.1 (*R*)	6.8	97.1
Δ-slr2124	27.1(*R*)	8.8	96.1

[a] Reaction conditions were described in the experimental section.

Table 3 Reduction of trifluoroacetophenone (TFA) with the mutants of *Synechocystis* sp. PCC 6803[b].

Strain	% ee (Config.)	% ee (Δ-WT)	% Conv.
WT	69.3 (*R*)	—	90.2
Δ-sll0990	97.2 (*R*)	27.9	89.3
Δ-sll1825	96.2 (*R*)	26.9	89.8
Δ-slr0315	71.6 (*R*)	2.3	91.1
Δ-slr0506	85.5(*R*)	19.2	87.9
Δ-slr0886	89.5(*R*)	20.2	87.5
Δ-slr0942	98.6 (*R*)	29.3	88.2
Δ-slr1192	95.5 (*R*)	26.2	90.0
Δ-slr2124	92.0 (*R*)	22.7	89.9

[b] Reaction conditions were described in the experimental section.

Results and Discussion

GC analysis of the reaction mixtures revealed that *sll0990* knockout mutant afforded the corresponding alcohol in 92.6% yield with 38.3% ee (*R*), while the wild-type microbe gave the alcohol in 92.4% yield with 18.3% ee (*R*). The other *sll1825* knockout mutant gave (*R*)-alcohol in 96.7% yield with 37.6% ee. Chemical yields of the product alcohols increased with the reaction time. The enantioselectivity, however, was not influenced by the reaction time for 24 h in each case. Another *slr0886* and *slr1192* knockout mutant gave the (*R*)-alcohol 12.7% ee and 25.1% ee, respectively. In these cases, mutation of the microbe scarcely changed the enantioselectivity of the reduction.

Thus, control of stereoselectivities was observed. Deletion of the *sll0990* and *sll1825* dehydrogenase genes from cyanobacteria increased the (*R*)-enantioselectivity while the deletion of the *slr0886* and the *slr1192* oxidoreductase gene reversed the stereochemistry to give (*S*)-alcohol with almost the similar enantioselectivities with the wild type. Thus, a novel method for stereochemical control was developed. Previously, we reported that enantioselectivities in the reduction of t-butyl acetoacetate was controlled by knockout of an alcohol dehydrogenase gene of *Synechocystis* sp. PCC 6803 [7]. The result revealed that the novel method which we present here is applied to the wide varieties of the biocatalytic reductions using photosynthetic organisms.

Recently, carbon dioxide (CO_2) concentrations have been increasing steadily in the global atmosphere and this phenomenon is thought to affect largely the life of animals and plants on earth. Then reducing the concentration of global atmospheric CO_2 is one of the most important targets for the world community as represented by 'Kyoto Protocol in 1997'. To decrease the atmospheric carbon dioxide concentrations, algae and microalgae have been considered to be one of the most suitable photosynthetic organisms. Then the use of microalgae as biocatalysts for useful biotransformations is recommended from the viewpoint of sustainable human life. The present report will open up a new field of biotransformation.

Conclusion

We have developed a novel method for microalgae-mediated asymmetric reduction of ketones. The reduction with the *Synechocystis* sp. PCC 6803 *sll0990* and *sll1825* knockout mutants increased the enantioselectivity compared to the wild-type microbe.

Since a large amount of CO_2 emitted into the atmosphere should be collected, chemical industries are forced to use CO_2 as a starting material or as a medium (*i.e.*, supercritical CO_2) for various chemical and biological reactions. Thus the novel use of CO_2 is worth investigating. Previously, we reported that enantioselectivities in asymmetric reduction of ketones with photosynthetic plant cell cultures were controlled by atmospheric carbon dioxide concentrations: the reaction in high carbon dioxide concentrations under illumination of fluorescent light afforded the corresponding L-alcohol while that in low carbon dioxide concentrations in the presence of glucose under dark conditions gave the antipode, D-alcohol [8]. The use of microalgae as biocatalysts is the another method to consume carbon dioxide and is worth to be developed.

Further research on stereochemical control using knockout mutants are under investigation in our laboratories.

References

Nakamura K, Matsuda T (2008) In: V Gotor, I Alfonsa, E Garcia-Uradiales (eds.), Asymmetric Organic Synthesis with Enzymes. Wiley–VCH Verlag GmbH & Co. KGaA:Weinheim, pp. 193-228

Nakamura K (2007) In: T Matsuda (ed.), Future Directions in Biocatalysis. Elsevier: Amsterdam, pp. 51-58

Nakamura K, Yamanaka RJ, Chem Soc, Chem Commun (2002) Light Mediated Cofactor Recycling System in Biocatalytic Asymmetric Reduction of Ketone. 1782-1783

Nakamura K, Yamanaka R (2002)Tetrahedron: Asymm. Light-Mediated Regulation of Asymmetric Reduction of Ketones by a Cyanobacterium. 13: 2529-2533

Nakamura Y, Kaneko T, Hirosawa M, Miyajima N, Tabata S (1998) CyanoBase, a Www Database Containing the Complete Nucleotide Sequence of the Genome of Synechocystis sp. strain PCC6803. Nucleic Acids Res.26: 63-67

Nie Y, Xu Y, Mu XQ, Wang HY, Yang M, Xiao R (2007) Purification, Characterization, Gene Cloning, and Expression of a Novel Alcohol Dehydrogenase with Anti-Prelog Stereospecificity from Candida Parapsilosis. Appl. Environ. Microbiol. 73: 3759-3764

Takemura T, Akiyama K, Umeno N, Tamai Y, Ohta H, Nakamura K (2009) Asymmetric Reduction of a Ketone by Knockout Mutants of a Cyanobacterium. J. Mol. Cat. B-Enzymatic 60: 93-95

Kojima H, Okada A, Takeda S, Nakamura K (2009) Effect of Carbon Dioxide Concentrations on Asymmetric Reduction of Ketones with Plant Cultured Cells. Tetrahedron Letters 50: 7079-7081

The Different Photoprotective Mechanisms of Various Green Organs in Cotton (*Gossypium Hirsutum* L.)

Yuanyuan Hu[a], Yali Zhang[a], Honghai Luo[a], Wah Soon Chow[b] , Wangfeng Zhang[a*]

[a]The Key Laboratory of Oasis Eco-agriculture, Xinjiang Production and Construction Group, Shihezi University, Shihezi, 832003, P.R. China;
[b]Division of Plant Science, Research School of Biology, College of Medicine, Biology and Environment, The Australian National University, Canberra, ACT 0200, Australia.
[*]Corresponding author. Tel. No. + 86-993-2057326; Fax No. + 86-993-2057998; E-mail: zwf_shzu@163.com.

Abstract: Photoinactivation of Photosystem II (PS II) during photosynthesis can lead to the loss of photochemical efficiency and decrease in crop yield. Plants have evolved various photoprotective strategies to ameliorate photoinactivation of PS II. Non-leaf organs of cotton also contribute to carbon gain, but it is not clear how they photoprotect themselves. This study investigated the photoprotective mechanisms in the leaf, bract, main stem and capsule wall of cotton. Our results suggested that the bract mainly relies on high activities of antioxidative enzymes and high ΔpH- and xanthophyll-regulated thermal dissipation (Φ_{NPQ}) for photoprotection. The main stem preferentially dissipated its absorbed light energy via light-regulated as well as light-independent non-photochemical quenching, aided by the moderately high activities of antioxidative enzymes. The capsule wall was less able to remove reactive oxygen species due to lower activities of antioxidative enzymes, and less able to dissipate energy via heat due to its lower Φ_{NPQ}. Its main photoprotective mechanisms seem to be (a) direct quenching of the energy by abundant carotenoids and (b) light-independent constitutive thermal dissipation via $\Phi_{f,D}$. The green organs of cotton have different ways to use or dissipate energy.

Keywords: Cotton; Non-leaf organs; Photoprotection; Carotenoid; NPQ; Antioxidant

Introduction

More than 90% of crop biomass is derived from photosynthetic products. Although many factors affect biomass production, the amount of solar radiation available and the efficiency with which solar radiation is transformed into biomass are the most important (Russell *et al.*, 1989). The quantum efficiency of electron transport decreases when photoinhibition occurs; as a consequence of the decreased efficiency of radiation use, the yield will decrease. Therefore, the ability to protect the photosynthetic apparatus from photodamage by utilizing photoprotective mechanisms is considered to be one of the physiological traits of higher yield (Horton, 2000; Zhu *et al.*, 2004).

Although leaves are traditionally considered to be the main site of photosynthesis, the reproductive structures of many plants are also able to fix substantial amounts of carbon (Aschan and Pfanz, 2003). In cotton, both the bract and capsule wall of the boll have photosynthetic function and contribute to carbon gain (Wullschleger *et al.*, 1991). However, the photoprotective mechanisms in non-leaf organs are not clear yet. This study addresses the photoprotective mechanisms in non-leaf organs.

Materials and Methods

The experiment was conducted at an experimental field of Shihezi Agricultural College, Shihezi University, Xinjiang, China (45°19′N, 86°03′E) in 2010. Cotton (*Gossypium hirsutum* L. cv. Xinluzao 13) was grown under field conditions. Seeds were sown on 24 April, 2010 in rows 12 cm apart at a plant density of 1.8×10^5 ha^{-1}. The plot was drip irrigated and maintained well-watered throughout the whole season.

Pest and weed control was carried out according to the local standard practice. The experimental design was completely randomized with three replications. Leaf, bract, main stem and capsule wall material for all the measurements were collected from the top, second or third main stem leaves at Full Bolling Stage, as well from corresponding bolls, their associated bracts, and main stem under the main stem leaves.

Analysis of photosynthetic pigment contents of all green organs

Photosynthetic pigment contents of plant organs were determinterd either from leaf, bract, capsule wall tissue dics removed by a calibrated metal borer (4 mm diameter), or main stem segments of known size. The green organs discs were extracted in 80% (v/v) acetone at for 24 h at room temperature in the dark. Absorbances of extracts were measured with a spectrophotometer (U-3900, Hitachi, Japan) and pigment contents were calculated according to Lichtenthaler, 1987).

Chlorophyll fluorescence

Chlorophyll fluorescence was measured using a saturation-pulse fluorometer Dual-PAM-100 (Walz, Effeltrich, Germany). Prior to Chl fluorescence measurement, leaves, bracts, main stems and bolls were dark-adapted sufficiently. Minimum or maximum Chl fluorescence yield (F_o, or F_m, respectively) in the dark-adapted state, and maximum photo-oxidation of P700 in weak far-red light on which was superimposed a saturating pulse (P_m) were recorded for calculation of quenching coefficients. Each leaf was illuminated at 1033 μmol m^{-2} s^{-1} for 4–5 min. F_s' (steady-state Chl fluorescence yield), F_m' and P_m', where the prime symbol refers to the light-acclimated state, were then measured, the latter two with a saturating light pulse. Then, rapid light curves were obtained with the Dual-PAM 100 using an internal program and PAR supplied by red light-emitting diodes. Nine discrete PAR steps were used (20 s each): 11, 42, 131, 344, 536, 830, 1292, 1,599, 1,957 μmol m^{-2} s^{-1}. Each light increment was followed by the measurement of F_s', and by a saturating pulse for the measurement of F_m' and P_m'. PS II quantum yield ($\Phi_{PS\ II}$) in the light was calculated as $(F_m' - F_s')/F_m'$ (Genty *et al.*, 1989). The fractions of light absorbed by the PS II antennae lost by constitutive thermal dissipation and via fluorescence ($\Phi_{f,D}$) and the fraction of light absorbed by the PS II antennae dissipated thermally via ΔpH-and xanthophylls-regulated processes (Φ_{NPQ}) were calculated as F_s'/F_m and $(F_s'/F_m') - (F_s'/F_m)$, respectively (Hendrickson *et al.*, 2004). Note that $\Phi_{PS\ II} + \Phi_{f,D} + \Phi_{NPQ} = 1$.

Antioxidative enzymes analyses

All the green organs of cotton at Full Bolling Stage were homogenized under ice-cold conditions with 5 mL of 50 mmol phosphate buffer (pH 7.0), 10 mmol sodium ascorbate and 1.0% (w/v) polyvinylpyrrolidone. The homogenate was centrifuged at 20,000 x *g* for 30 min, and the supernatant collected for enzyme assays. Key antioxidant enzymes, including SOD, APX, CAT and GR were assayed exactly as described in Pinheiron (2004). And POD activity was analyzed as the method of Polle (1994).

Results and Discussion

Excess energy may be harmful to PS II because of over-reduction of the photosynthetic electron transport chain and increased production of reactive oxygen species (ROS) in chloroplasts. Many photoprotective mechanisms have been described in higher plants, including three broad categories.

First, carotenoids (Car), consisting of carotenes and xanthopylls, protect the photosynthetic apparatus in two important ways: (i) β-carotene directly quenches both triplet chlorophyll (^{3}Chl) and singlet oxygen ($^1O_2$); (ii) The xanthophylls hinder the formation of ^{3}Chl by quenching excited singlet state of Chl (^{1}Chl). In some cases, photoprotection also arises from the reduction of light adsorption through accumulation of red carotenoids (Hormaetxe *et al.*, 2005). The total Car content of various organs were shown in Table 1. The content of Car in the capsule wall was about 3.1 fold as large as that in the leaf on an area basis. The Car/Chl ratio in bract, main stem and capsule wall was about 1.1, 1.7 and 4.7 fold of that in leaf, respectively.

Second, regulation of energy dissipation occurs through photochemical (photorespiration) and non-photochemical (xanthophyll cycle) mechanisms (Müller *et al.*, 2001). In one model (Hendrickson *et al.*, 2004), there are main three pathways of allocation of photons absorbed by the PSII antennae: photochemical conversion (Φ_{PSII}), light-dependent non-photochemical energy dissipation (Φ_{NPQ}) regulated by ΔpH- and xanthophylls, and light-independent constitutive non-

photochemical energy dissipation combined with Chl fluorescence emission ($\Phi_{f,D}$). The fate of absorbed light energy in all green organs is shown in Fig. 1. In both leaf and non-leaf green organs, $\Phi_{PS\ II}$ decreased with PAR, being highest in leaves and capsule walls, then bracts and main stem in turn. Φ_{NPQ} increased with PAR, was highest in bracts, and lowest in the capsule wall. $\Phi_{f,D}$ increased marginally at intermediate light in all green organs of cotton, and was highest in capsule walls.

Table 1 The contents of photosynthetic pigments in the leaf, bract, main stem, capsule wall of cotton grown in field.

Parameter	Structure			
	Leaf	Bract	Main Stem	Capsule Wall
Car (μmol m^{-2})	101.6 ± 4.0	38.9 ± 3.7	93.7 ± 4.5	318.0 ± 7.1
Total Chl (μmol m^{-2})	514.9 ± 17.7	194.0 ± 3.5	310.4 ± 22.2	376.5 ± 17.8
Car/total Chl	0.18 ± 0.00	0.20 ± 0.02	0.30 ± 0.01	0.84 ± 0.02

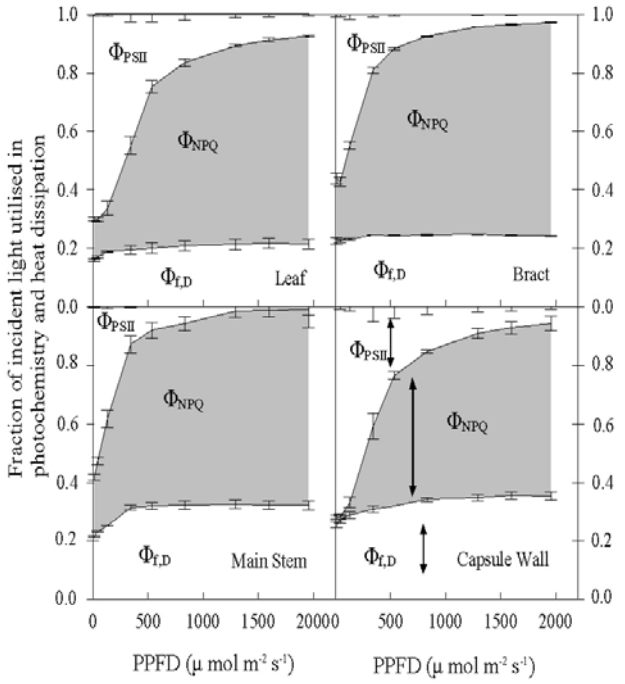

Fig. 1 Estimated fraction of absorbed irradiance consumed via PSII photochemistry (Φ_{PSII}), ΔpH- and xanthophyll-regulated thermal dissipation (Φ_{NPQ}), and the sum of fluorescence and light-independent constitutive thermal dissipation ($\Phi_{f,D}$), in leaf, bract, main stem and capsule wall of boll illuminated at varying irradiance.

Third, when the amount of excess excitation energy exceeds the capacity of thermal dissipation, the scavenging of ROS also plays a photoprotective role. Both photorespiration and the Mehler peroxidase reaction lead to an increased production of ROS such as superoxide ($O_2^{\cdot -}$) and H_2O_2. To counteract the toxicity of ROS, plants have developed a highly efficient antioxidative enzymic defence system, mainly including superoxide dismutase (SOD), ascorbate peroxidase (APX), catalase (CAT), peroxidase (POD), and glutathioe reductase (GR) (Foyer *et al.*, 1994). The activity of antioxidative enzymes, SOD, APX, POD, CAT and GR are shown in Fig. 2. On the basis of fresh weight, the activities of the enzymes in non-leaf organs were significantly lower than those in the leaf. In particular, the enzyme activities were the lowest in the capsule wall, but highest in the leaf (Fig. 2).

The activities of three antioxidative enzymes SOD, POD and GR) were relatively high in bracts, and the Car/Chl ratio, if anything, was a little higher in bracts than in the leaf. Significantly, Φ_{NPQ} was highest in bracts among all the green organs. Thus our results suggest that that the higher activity of antioxidative enzymes and higher ΔpH- and xanthophyll-regulated thermal dissipation were the main photoprotective mechanisms in bracts.

The main stem had moderate activities of antioxidative enzymes, but the Car/Chl ratio and Φ_{NPQ} were high, suggesting that it preferentially dissipated absorbed light energy via Φ_{NPQ} and $\Phi_{f,D}$. Furthermore, the moderately high antioxidative enzymes may provide another way of maintaining its photochemical efficienty.

Capsule walls appeared less able to remove ROS due to lower activities of scavenging enzymes, and less able to dissipate energy via ΔpH- and xanthophyll-regulated processes due to their lower Φ_{NPQ}. Its main photoprotective mechanisms seemed to be (a) direct quenching of energy by the abundant Car and (b) light-independent constitutive thermal dissipation via $\Phi_{f,D}$.

Taken together, our results demonstrate that the green organs of cotton have different pathways to use or dissipate the energy absorbed.

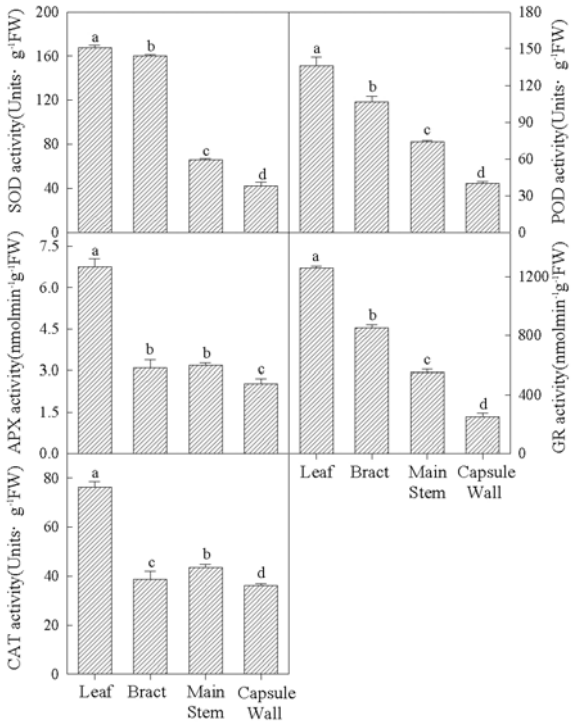

Fig. 2 The activities of superoxide dismutase (SOD), peroxidase (POD), ascorbate peroxidase(APX), glutathione reductase (GR) and catalase (CAT) in leaf, bract, main stem and capsule wall of cotton in the field. Values are means ± S.E. (n = 5). All enzyme activities are expressed on a fresh weight basis.

Acknowledgements

This study was financially supported by China Scholarship Council fellowship, the National Natural Science Foundation of China (Grant No. 31060176), by National Key Technology R&D Program of China (Grant No. 2006BAD21B02 and 2007BAD44B07) and by the Australian Research Council (DP1093827).

References

Aschan G, Pfanz H (2003) Non-Foliar Photosynthesis- a Strategy of Additional Carbon Acquisition. Flora 198: 81-97

Foyer CH, Descourvieres P, Kunert KJ (1994) Protection Against Oxygen Radicals: an Important Defence Mechanism Studied in Transgenic Plants. Plant Cell Environ. 17: 507-523

Hendrickson L, Furbank RT, Chow WS (2004) A Simple Alternative Approach to Assessing the Fate of Absorbed Light Energy Using Chlorophyll Fluorescence. Photosynth. Res. 82: 73-81

Hormaetxe K, Becerril JM, Fleck I, Pinto M, Garcia-Plazaola JI (2005) Functional Role of Red (Retro)-Carotenoids As Passive Light Filters in Theleaves of Buxus Sempervirens L.: Increased Protection of Photosynthetic Tissues? J. Exp. Bot. 56: 2629-2636

Horton P (2000) Prospects for Crop Improvement Through the Genetic Manipulation of Photosynthesis: Morphological and Biochemical Aspects of Light Capture. J. Exp. Bot.51: 475-485

Lichtenthaler HK (1987) Chlorophylls and Carotenoids: Pigments of Photosynthetic Biomembranes. Meth Enzimol 148: 350-382

Müller P, Li XP, Niyogi KK (2001) Non-Photochemical Quenching. A Response to Excess Light Energy. Plant Physiol. 125: 1558-1566

Pinheiro HA, DaMatta FM, Chaves ARM, Fontes EPB, Loureiro ME (2004) Drought Tolerance in Relation to Protection against Oxidative Stress in Clones of Coffea Canephora Subjected to Long-Term Drought. Plant Sci 167: 1307-1314

Polle A, Otter T, Seifert F (1994) Apoplastic Peroxidases and Lignification in Needles of Norway Spruce (Picea abies L.). Plant Physiol. 106: 53-60

Russell G, Jarvis PG, Monteith JL (1989) Absorption of Radiation by Canopies and Stand Growth. In: Russell G, Marshall B, Jarvis PG (eds.), Plant Canopies: Their Growth, Form and Function. Cambridge University Press: Cambridge, pp. 21-39

Wullschleger SD, Oosterhuis DM, Hurren RG, Hanson PJ (1991) Evidence for Light-Dependent Recycling of Respired Carbon Dioxide by the Cotton Fruit. Plant Physiol. 97: 574-579

Zhu XG, Ort DR, Whitmarsh J, Long SP (2004) The Slow Reversibility of Photosynstem Ⅱ Thermal Energy Dissipation on Transfer from High to Low Light May Cause Large Losses in Carbon Gain by Crop Canopies: a Theoretical Analysis. J. Exp. Bot. 55: 1167-1175

Symposium 21

Microbial Derived Biofuels

Functioning of the Bidirectional Hydrogenase in Different Unicellular Cyanobacteria

Éva Kiss[a], Péter B Kós[a], Min Chen[b], Imre Vass[a]

[a]Institute of Plant Biology, Biological Research Center, Szeged, Hungary;
[b]School of Biological Sciences, University of Sydney, NSW 2006, Australia.
[*]Corresponding author. Tel. No. +36 62 599 700; Fax No. +36 62 433 434; E-mail address: imre@brc.hu (I. Vass)

Abstract: *Synechocystis* PCC 6083 (*Synechocystis*) cells produce hydrogen in the absence of light, during oxygen deprivation. The enzyme responsible for the hydrogen production in this strain is the hox hydrogenase, which catalyses the simple $H_2 \leftrightarrow 2H^+ + 2e^-$ redox reaction. This bidirectional hydrogenase is also found in *Synechococcus elongatus* PCC 7942 (*Synechococcus*) and *Acaryochloris marina* (*Acaryochloris*). However, we could not detect *in vivo* hydrogen production neither in *Synechococcus* nor in *Acaryochloris*. In *Synechocystis*, in a dark, hypoxic environment a strongly reduced plastoquinon (PQ) pool implies that there are excess electrons and protons available for the hydrogenase, which is present in the cell in an elevated level shown by RT-PCR. Conversely, we found that the *hox* genes are suppressed in *Synechococcus* under the same conditions. In *Acaryochloris* a dark hypoxic environment induces the *hox* genes. Despite the elevated enzyme level in *Acaryochloris* H_2 production is undetectable, likely because of the shortage of reducing equivalents available for the hydrogenase that is indicated by a feeble PQ pool reduction.

Keywords: Hox hydrogenase; *Synechocystis* 6803; *Synechococcus elongatus* 7942; *Acaryochloris marina*

Introduction

Hydrogenases are widespread amongst prokaryotes, and they play a central role in microbial energy metabolism. Cyanobacterial hydrogenases are generally encoded by chromosomal genes. The peculiarity of the hydrogenase of the marine cyanobacterium *Acaryochloris* is that it is encoded in a plasmid. The hydrogenase of *Acaryochloris* is a hox hydrogenase that can reversibly oxidize hydrogen. The bidirectional hydrogenase is considered to be a heteropentameric enzyme and encoded by the *hoxEFUYH* genes (Schmitz *et al*., 2002). Of the five subunits HoxYH constitute the hydrogenase part, whereas HoxEFU constitute the diaphorase part. The regulation of this NiFe-type bidirectional enzyme is well-studied in the fresh water cyanobacterium *Synechocystis* PCC 6803. The genes of the bidirectional hydrogenase in *Synechocystis* are encoded by the *hoxEFUYH* operon under the regulation of the promoter region upstream *hoxE* (Oliveira and Lindblad, 2005; Gutekunst *et al*., 2005). The arrangement of the *hox* genes in *Acaryochloris* is very similar to that in *Synechocystis*, whereas in *Synechococcus* the *hox* genes form two separated transcriptional units, *hoxEF* and *hoxUYH* operons. Here we studied the functioning of the hox hydrogenase by investigating if the regulation of the enzyme and its intracellular environment meet a condition of hydrogen production in the above mentioned three unicellular oxygenic photoautotrophic cyanobacteria.

Materials and Methods

Synechocystis sp. PCC 6803 *Synechococcus elongatus* PCC 7942 and *Acaryochloris marina* cells were propagated under 3% CO_2 enriched atmosphere in BG-11 at 30 °C, at 40 μE m^{-2} s^{-1} and in K+ESM medium at 25 °C, under 10 μE m^{-2} s^{-1} PAR respectively. Cells in the exponential growth phase (~10 μg Chl mL^{-1}) were used. Hypoxic conditions were achieved by

incubating the cell suspension in closed conical flasks in the presence of an oxygen scavenging enzyme mix containing 5 mmol glucose, 200 U glucose oxidase and 2,000 U catalase. Under our experimental conditions the oxygen content in the cultures was below 1 μmol/L as monitored with an immersible oxygen electrode (Presens, Fibox 3).

For gene expression analysis total RNA was extracted (4), freed from DNA contamination, and reverse transcribed using H-MuLV (Fermentas) and random hexamer primers. Aliquots of the resulted cDNA were used in the RT-PCR reaction as a template. The data were normalized to the expression of rnpB gene.

The chlorophyll fluorescence (OJIP) transient was measured by a fast fluorimeter (FL 3500/F, PSI, Czech Republic) in the 10 μs to 1 s time region using a logarithmic time scale.

In vitro enzyme assay was carried out using methyl viologen (0.8 mmol) as electron donor in 0.1 mmol K Phosphate buffer (pH 8.0) at 37 °C. The reaction was started by adding sodium dithionite (up to 4 mg/ml final concentration). H_2 evolution was monitored by gas chromatography (model 6890N, Agilent Technologies).

Results and Discussion

We took samples from *Synechocystis*; *Synechococcus,* and *Acaryochloris* cultures kept at growth conditions, and from cultures in which we decreased the dissolved oxygen concentration below 1 μmol/L during dark adaptation, and measured *hox* mRNA level by quantitative RT-PCR. Oxygen deprivation in the absence of light causes *hox* gene induction in *Synechocystis* and in *Acaryochloris* cells (Figs. 1b and 1f). This was confirmed by a higher ezyme activity in hypoxic samples measured by *in vitro* assay (data not shown). However, hypoxia did not induce the hydrogenase genes in *Synechococcus* (Fig. 1d). In *Synechocystis* induction of the *hoxEF* genes is approximately 3-fold stronger compared to the *hoxUYH* genes, implying an additional regulation within the operon (É Kiss *et al*., 2009) (Fig. 1b). The arrangement of *hox* genes in *Acaryochloris* is similar to that in the *Synechocystis* genome, where the *hox* genes form one transcriptional unit. However, in Acaryochloris, the induced gene expression pattern of the five *hox* genes is similar to that measured in *Synechococcus* under growth conditions (Figs. 1f and 1c respectively). Schmitz *et al*. (2001) previously reported that in *Synechococcus* the *hox* genes are arranged into two operons, *hoxEF* and *hoxUYH*, where the later one has substantially stronger promoter. The similarity of gene induction pattern indicates that despite the gene arrangement similarity between *Synechocystis* and *Acaryochloris*, the transcriptional regulation in the later one is analogous to that in *Synechococcus.*

Besides the elevated enzyme level, the other key factor for hydrogen production is the availability of reduced equivalents that are likely accessible for the hydrogenase under highly reducing conditions, which can be monitored by measuring the redox state of the (PQ) pool.

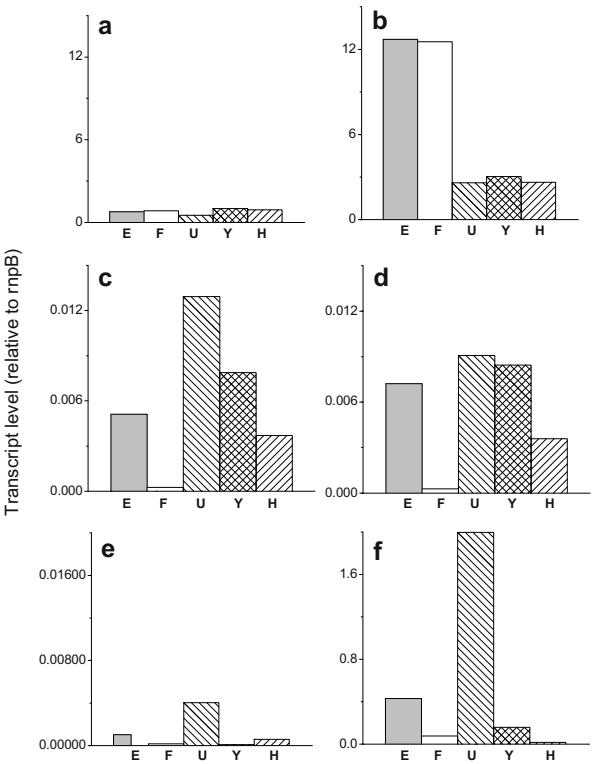

Fig. 1 Effect of oxygen deprivation in dark on *hox* transcript levels. *Synechocystis* (b), *Synechococcus* (d), and *Acaryochloris* (f) cells were made hypoxic and kept in dark for 60 min before taking samples for RNA extraction. Transcript abundance values were determined by RT-PCR for *hoxE* (light gray), *hoxF* (white), *hoxU* (left hatch), *hoxY* (cross hatch), and *hoxH* (right hatch). For comparison, relative RNA amount at growth condition are shown in *Synechocystis* (a), *Synechococcus* (c), and *Acaryochloris* (e).

After the onset of strong actinic light the increase of chlorophyll fluorescence in dark adapted photosynthetic material follows triphasic rise kinetics.

Normalizing the fluorescence curves to their variable yield shows different kinetics, and differences in the rise of the O-J phase refer to the redox state of the PQ pool (To´th *et al*., 2007). The more reduced the PQ pool was before the onset of actinic light, the higher the rise is in the level of the O-J section. In *Synechocystis* and in *Synechococcus* cells kept in a dark hypoxic environment increased amount of reducing equivalents is reflected by a higher O-J level of fluorescence kinetics (Fig. 2). However, in *Acaryochloris* under the same conditions the reduction level of the PQ pool does not increases significantly (Fig. 2).

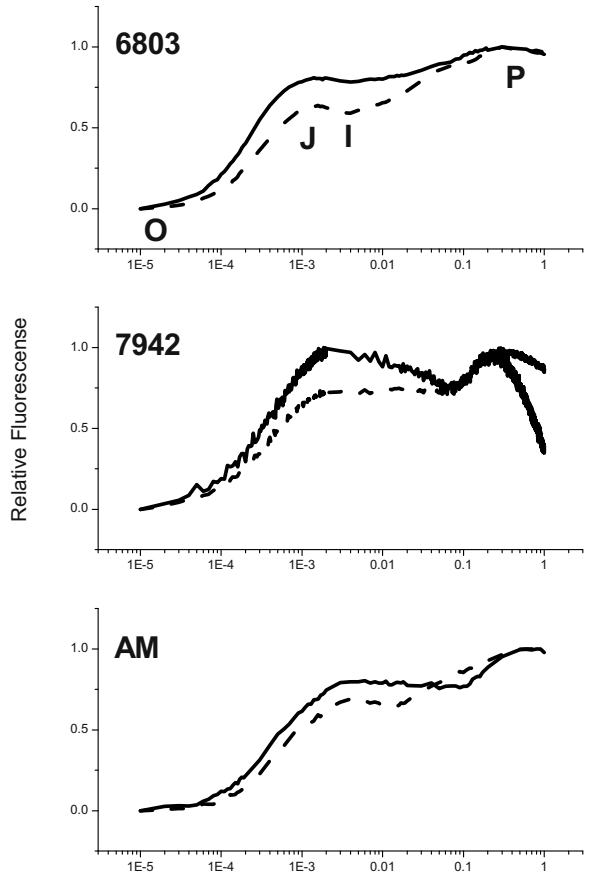

Fig. 2 Effect of dark hypoxic conditions on fluorescence induction transients. *Synechocystis* (6803), *Synechococcus* (7942), and *Acaryochloris* (AM) cells were made hypoxic by incubating in the presence of glucose, glucose oxidase and catalase, and dark adapted for 30 min (solid line) before fluorescence measurements. For comparison the fluorescence trace obtained without anaerobic treatment after 3 min dark adaptation is also shown (dashed line).

Synechocystis cells evolve hydrogen gas in an oxygen deprived environment in the dark. Under these conditions the enzyme is active, its expression is elevated and excess electrons and protons are present in the cell. In *Acaryochloris* and *Synehcococcus* cultures we could not detect emergence of hydrogen in the gas phase. Since correlation between *hox* transcript levels and enzyme activity has been shown previously (Antal *et al*., 2006), we suggest, that the inability of hydrogen production of *Synechococcus* cells is due to the suppression of transcription of the *hox* genes by dark, hypoxic conditions. In the case of *Acaryochloris* we could not detect *in vivo* hydrogen production, regardless of the elevated hox enzyme level. We suggest that *Acaryochloris* cells are unable to produce hydrogen because of the shortage of reducing equivalents available for the hydrogenase under dark hypoxic conditions, which is indicated by the feeble reduction of the PQ pool. Here we show how the regulation of the bidirectional hydrogenase is dependent on the cyanobacterial strain used. Our observations give better insight into the mechanism by which hydrogen is produced in organisms containing the bidirectional hydrogenase.

Acknowledgements

This work was supported by the EU/Energy Network project SOLAR-H2 (FP7 contract 212508), and by the Hungarian-Australian cooperation program (TET AU-1/2008. OMFB-00583/2009)

References

Antal TK, Oliveira P, Lindblad P (2006) The Bidirectional Hydrogenase in the Cyanobacterium Synechocystis sp. Strain PCC 6803. Int. J. Hydrogen Energy 31: 1439-1444

É Kiss, Péter B Kós, Imre Vass (2009) Transcriptional Regulation of the Bidirectional Hydrogenase in the Cyanobacterium Synechocystis 6803 J Biotechnol 142(1): 31-7

Gutekunst K, Phunpruch S, Schwarz C, Schuchardt S, Schulz-Friedrich R, Appel J (2005) LexA Regulates the Bidirectional Hydrogenase in the Cyanobacterium Synechocystis sp. PCC 6803 As a Transcription Activator. Mol. Microbiol. 58: 810-823

Oliveira P, Lindblad P (2005) LexA, a Transcription Regulator Binding in the Promoter Region of the Bidirectional Hydrogenase in the Cyanobacterium

Synechocystis sp. PCC 6803. FEMS Microbiol. Lett. 251: 59-66

Oliver Schmitz, Gudrun Boison, Hermann Bothe (2001) Quantitative Analysis of Expression of Two Circadian Clock-Controlled Gene Clusters Coding for the Bidirectional Hydrogenase in the Cyanobacterium Synechococcus sp. PCC 7942 Mol. Microbiol. 41(6): 1409-1417

Papageorgiou GC, Tsimilli-Michael M, Stamatakis K (2007) The Fast and Slow Kinetics of Chlorophyll a Fluorescence Induction in Plants, Algae and Cyanobacteria: a Viewpoint. Photosynth. Res. 94: 275-290

Schmitz O, Boison G, Salzmann H, Bothe H, Schütz K, Wang S, Happe T (2002) HoxE—a Subunit Specific for the Pentameric Bidirectional Hydrogenase Complex (HoxEFUYH) of Cyanobacteria. Biochim. Biophys. Acta 1554: 66-74

Szilvia Z To´th, Gert Schansker, Reto J Strasser (2007) A Non-Invasive Assay of the Plastoquinone Pool Redox State Based on the OJIP-Transient. Photosynth Res 93: 193-203

Lessons from Energy Balances for the Production Strategies of Biofuels

Christian Wilhelm[a], Torsten Jakob, Uwe Langner, Katja Stehfest, Heiko Wagner

[a] Department of Plant Physiology, University of Leipzig, Germany.
[*]Corresponding author. Tel. No. +49 341 9736874; Fax No. +49 341 9736899; E-mail: cwilhelm@rz.uni-leipzig.de.

Abstract: Energy balances from photon to biomass can help to assist the optimization of the productivity of algal photobioreactors. These balances identify those processes which decrease the efficiency of biomass production. The presented setup allows to quantify the efficiency of absorption, photochemistry, the metabolic losses and the electron partitioning into the macromolecular pools. The quantitative estimate of the metabolic losses under optimal and suboptimal conditions (*e.g.* nutrient limitation or excess light) yields the "real" value for the number of photons needed to transfer one carbon molecule from CO_2 into the biomass (P/C value). The experimentally measured values are higher than estimated from the reduction degree of the biomass, especially in the case of proteins and lipids. The reason of this finding is discussed.

Keywords: Algae; Biofuels; Carbohydrates; Lipid; Metabolic Costs; Proteins

Introduction

There is no doubt that the replacement of fossil energy by organic carbon fixed by photosynthetic processes will become crucial with respect to the so-called 2-degree limit for global warming. Therefore, there is urgent need to develop technologies which are able to produce 5–6 billion tons organic carbon in addition to the actual harvest from agricultural crops. The limited potential of crops is the main force to focus on microalgae as potential and powerful sources for biofuels. The major argument is that microalgae have a higher yield and this high productivity can be even further enhanced by metabolic engineering (Beer *et al*., 2009). The higher photosynthetic efficiency is a matter of debate. The reader can find many different figures in the scientific literature and on internet websites. Table 1 gives a more or less representative overview. The daily productivity ranges between 10 to 100 g biomass m^{-2} day^{-1}. Sometimes, the oil yield is calculated as the product of biomass yield by oil content. Also the range of the photosynthetic efficiency has a range between 2% and 15% and it is completely unclear, which is the real value under ambient conditions. In this paper we present an experimental approach to measure the photon to biomass efficiency at different steps of the energy flow through the cell and the macromolecular pools. This system allows then to identify those processes with the most important losses and thus, the targets of optimization.

Table 1

PE	BP	Yield	Oil Pr
2	20	73	19.297[1]
10	50	287	155.297[1]
-	10		12.000[2]
-	48-78	176 (30% oil)	58.700[3]
-	-	176 (70% oil)	136900[3]
	11	20	2.400[4]
-	100		200.000[5]

Legends for table:
PE; photosynthetic efficiency in %, BP, Biomass production in g m^{-2} day^{-1}, Yield in t ha^{-1} yr^{-1}, OP, Oil production in L ha^{-1} yr^{-1}.
[1] Stephens *et al*., 2010; [2] Schenk *et al*., 2009; [3] Chisti, 2007; [4] Klötze (Germany), [5] Press release from MIT.

Materials and Methods

The chemostat setup consists of a flat growth chamber which allows the quantification of the

aborbed quanta per time and cell. The suspension density is kept low (2 mg Chl L^{-1}) to largely prevent limitation by selfshading or mixing kinetics, because the task of the study is to estimate the upper most level of energy conversion efficiency as possible. The amount of absorbed energy is quantified on the basis of the spectral composition of the light source and the bio-optical features of the cells (Chl a-specific in-vivo absorption coefficient). The measurement of the operative quantum yield of PSII by PAM fluorometry allows to convert the absorbed photons into the number of electrons transported by time. The electron transport rate (ETR) is additionally measured using a clark-type electrode. The difference between fluorescence based ETR and oxygen production gives the number of electrons which are flowing back to oxygen. These electrons are designated as "alternative electrons" (alt-e). The photosynthetic quotient measured in the light allows to convert electrons into carbon molecules, whereas the respiratory quotient measured in the dark gives the amount of cabon lost during respiration. The amount of carbon per gram dry weight quantified by elemental analysis allows to convert the amount of assimilated carbon into dry weight. This calculated biomass can then be compared with the weighted dry matter. The model can be validated by the best match of both methods if no carbon is lost by excretion. In the case of good match of calculated and weighted biomass the model identifies those processes with the highest losses of photosynthetic energy and which might be a potential target for optimiziation.

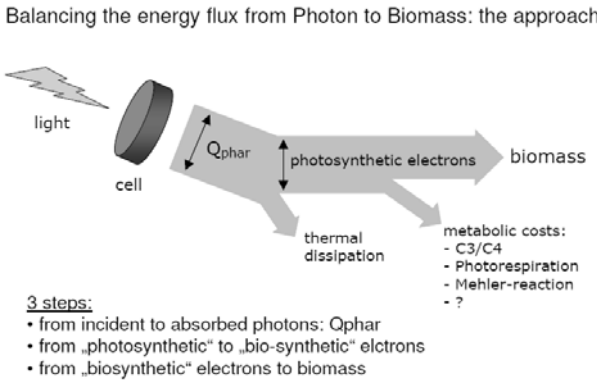

Fig. 1

The methods to measure the number of absorbed photons per cell and time (Q_{Phar}), the fluorescence and oxygen based electron transport rates (given in µmol electrons per Chl a and time), and the model how to calculate the biomass formation on the basis of these data is reported by Wagner *et al*. (2005) and by Langner *et al*. (2009).

The macromolecular composition of the biomass has been measured by FT-IR spectroscopy. Based on the IR-spectra in the fingerprint region a model was developed on the basis of calibration curves which allows to quantify the cellular amount of protein, carbohydrates and proteins. The mathematical algorithms and the instruments are described in detail in Wagner *et al*. (2010).

Results and Discussion

Fig. 2 shows the comparison of fluorescence-based electron transport rates with the oxygen yield during the time course of a simulated natural light climate.

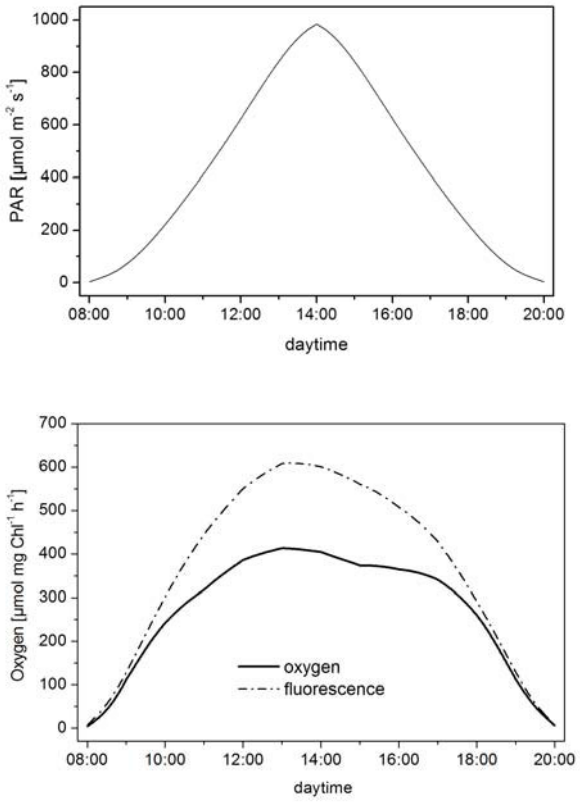

Fig. 2

It is obvious that at low light intensities the electron transport rates of PSII match perfectly the oxygen production rate, whereas at high light intensities a significant part of the electrons is lost via alternative pathways. The percentage amount of electrons lost by alternative electron pathway are highly variable as shown in Table 2.

Table 2

Alga	Condition	% of alt-e
Chlamydomonas reinhardtii	pH 6.5	44
C. acidophila	pH 2.6	38
C. acidophila	pH 6.5	53
Chlorella vulgaris	sinus light	47
C. vulgaris	oscillating light	50
Phaeodactylum tricornutum	sinus light	43
P. tricornutum	oscillating light	12

These data, taken from Langner *et al*. (2009) and Ralph *et al*. (2010), show that alternative electron rates show a variability between species and growth conditions by a factor of up to 4–5.

However, high alternative electron cycling must not be necessarily linked to low efficiency. An important secondary control step is the respiration which is linked with the "reduction degree" of the formed biomass. Langner *et al*. (2009) have shown that the acidophilic alga *C. acidophila* has a higher energy conversion rate during growth at pH 2.6 compared with a culture grown at pH 6.5 because of a reduced respiration rate in the dark. Enhanced respiration rates go along with an increased energy demand to convert carbohydrates to protein or to lipid. The electron demand to transfer one carbon from CO_2 into a carbohydrate is theoretically four, into a lipid six and into a protein between 6–8 (Kroon and Thoms, 2006). However, the real electron demand can be expected to be higher, because the so-called "entropy term" of all enzymatic reactions. That means that the total energy content of the sum of the educts is always higher than that of the products. This means that *e.g.* the reduction of sugars into lipids costs more than 2 electrons per C, because additional ATP is needed for the transport of the metabolites through the membranes, the turn-over of the lipids and the potential investment costs for the proteins needed to catalyze the biochemical reactions from sugar to lipid. The theoretical calculation is very complex, but the real values can be measured by the system setup presented above.

Fig. 3 shows the change in the biomass composition during the light phase in *C. reinhardtii* grown in a block light regime with an light intensity of about 100 µmol photons m^{-2} s^{-1} which is close to the E_k value where growth efficiency reaches its maximum.

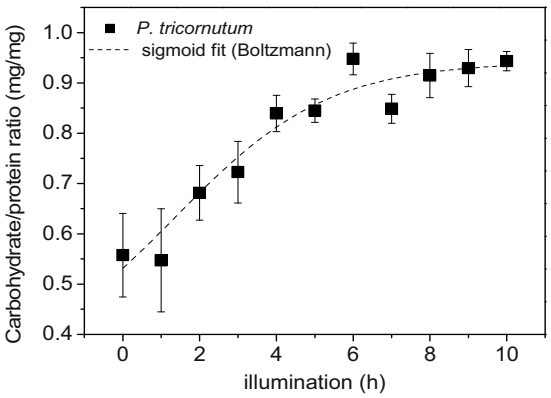

Fig. 3

It is evident that in the beginning light phase the carbohydrate/protein ratio rises because of the new synthesis of carbohydrates. However, after 5 hrs illumination the protein biosyntheses equilibrates with sugar production and the ratio is constant. These changes can be measured not only for the ratio of carbohydrates to protein, but also for the ratio of a given macromolecular pool per cell. Since the number of captured photons and the carbon assimilation number is known, it is possible to quantify the number of photons needed to transfer one carbon molecule from CO_2 into the the different macromolecular pools. These P/C values have been measured in algae with different carbohydrate/lipid/protein (Ch:L:P) ratios in their biomass.

Table 3 Photon requirement per carbon incorporated into biomass (P/C value) in *Chlamydomonas reinhardtii*.

Composition of the biomass	P/C theor	P/C real
Ch:L:P = 3:2:5	12	28
Ch:L:P = 6:1:3	10	12
Ch:L:P = 1:6:3	12	29

The data show that the real value is close to the theoretical level, if the carbon is stored as carbohydrates, whereas in the case of lipids and proteins the real values are about 2 times higher. This difference reflects the "metabolic costs" for those macromolecules which have more complex biosynthetic pathways with a higher energy investment to build up the machinery and to maintain it by turn-over.

These data clearly show that lipid enriched cells are not able to produce highly reduced carbon stores with the same quantum efficiency than carbohydrate accumulating cells. In addition, there is an unevitable conflict between carbon storage (high content in oil or starch) and growth. A decrease in protein content is

the consequence of translational control which can be induced by either nitrogen or phosphorus limitation. Under these conditions carbohydrate or lipid storage is strongly increased (Falkowski *et al*., 1989; Stehfest *et al*., 2005). This is the reason why high contents of lipids or carbohydrates can be obtained only under stress conditions when the growth rates are low. There is little chance to overcome this regulation by metabolic engineering.

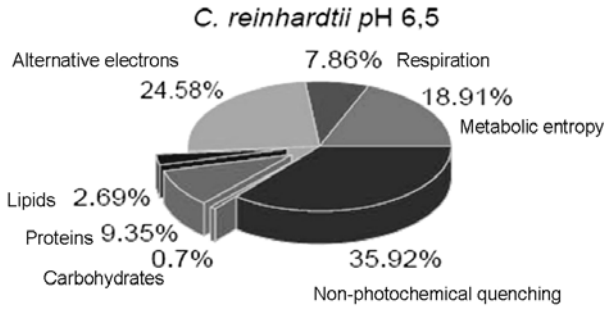

Fig. 4

Fig. 4 demonstrates that in the case of Chlamydomonas up to 13% of the energy can be stored in the biomass. Since the cell wall of this algae is composed mainly from proteins the protein/ carbohydrate ratio is unusually high. Nevertheless, under these growth optimized conditions the cells invest as much of the cellular carbon into "productive" molecules and store only a minimum. Even under those conditions, beside the well known losses by non-photochemical quenching and respiration about 50% of the metabolic costs are lost by alternative electron cycling and "metabolic entropy". Re-engineering of cells in a way that more carbon is funneled into "products" like lipids or carbohydrate will lead only to higher biomass harvest per area when the metabolic costs and the alternative electron cycling have been taken into account.

Acknowledgement

This research was funded by the DFG (Wi 874 WI 764/16-1 and Wi 764/12-2) whose support is greatly acknowledged.

References

Beer LL, Boyd ES, Peters JW (2009) Engineering Algae for Biohydrogen and Biofuel Production. Curr. Opin. Biotechnol. 20: 264-271

Chisti Y (2007) Biodiesel from Microalgae. Biotechnology Advances 2: 294-306

Falkowski P, Sukenik A, Herzig R (1989) Nitrogen Limitation in Isochrysis Galbana (Haptophycea) J. Phycol. 25: 471-478

Langner U, Jakob T, Stehfest K, Wilhelm C (2009) A Complete Energy Balance for Chlamydomonas Reinhardtii and Chlamydomonas Acidophila under Neutral and Extremely Acidic Growth Conditions. Plant Cell Environm 32: 250-258

Ralph P, Wilhelm C, Lavaud J, Jakob T, Petrou K, Kranz S (2010) Fluorescence As a Tool to Understand Changes in Photosynthetic Electroan Flow Regulation. In: D Suggett, O Prasil (eds.), Chlorophyll a Fluorescence in Aquatic Sciences: Methods and Applications. Developments in Applied Phycology 4: 75-89

Stehfest K, Toepel J, Wilhelm C (2005) The Application of Microscopy FTIR Spectroscopy to Analyse Nutrient-Stress Related Changes in Biomass Composition of Phytoplankton Algae. Plant Physiol. Biochem. 43: 717-726

Schenk PM, Skye R, Thomas-Hall, Stephens E, Marx UC, Mussgnug JH, Posten C, Kruse O, Hankamar B (2008) Second Generation Biofuels: High-Efficiency Microalgae for Biodiesel Production. Bioenerg. Res. 1: 20-43

Stephens E, Ross IL, King Z, Mussgnug JH, Kruse O, Posten C, Borowitzka MA, Hankamar B An Economic and Technical Evaluation of Microbial Biofuels. Nature Biotechnology 28: 126-128

Wagner H, Zhixin L, Langner U, Stehfest K, Wilhelm C (2010) The Use of FTIR Spectroscopy to Assess Quantitative Changes in the Biochemical Composition of Microalgae. J. Biophotonics 3: 557-566

Wagner H, Jakob T, Wilhelm C (2006) Balancing the Energy Flow from Captured Light to Biomass under Fluctuating Light Conditions. New Phytol. 169: 95-108

Improvement of Nitrogenase-Based Photobiological Hydrogen Production by Cyanobacteria by Gene Engineering — Genetic Engineering and Culture Conditions towards Improved Photobiological Hydrogen Production by Cyanobacteria

Hidehiro Sakurai[a, c,*], Masaharu Kitashima[b], Hajime Masukawa[a], Kazuhito Inoue[a, b]

[a]Research Institute for Photobiological Hydrogen Production, and [b]Department of Biological Sciences, Kanagawa University; Hiratsuka, Kanagawa 259-1293, and [c]Department of Biology, School of Education, Waseda University; Nishiwaseda, Shinjuku, Tokyo 169-8050, Japan.
*Corresponding author. Tel. No. +81-463-59-4111; Fax No. +81-463-58-9584; E-mail: sakurai@waseda.jp.

Abstract: We are proposing large-scale H_2 production on the sea surface utilizing nitrogen-fixing cyanobacteria. Their H_2 production activity is based on photosynthesis and nitrogenase activity of the cells. The mutant cells in which the hydrogenase activity had been eliminated by genetic engineering (ΔHup of *Nostoc* sp. PCC 7422) accumulated H_2 for several weeks when N_2 concentration was low. For economical H_2 production in the future, it was pointed out that the reduction of the cost of the bioreactor is very important. We are proposing a bioreactor composed of several layers of plastic film, with at least one having low permeability to H_2. We report here that cyanobacteria culture in a transparent plastic bag produced and accumulated H_2 for more than 10 days.

Keywords: Cyanobacteria; Hydrogen; Nitrogenase; Plastic bioreactor; Renewable energy; Solar energy conversion

Introduction

In order to mitigate global warming caused by increased CO_2 emission, exploitation of renewable energy source sufficiently large in quantity is essential. Photobiological production of H_2 by cyanobacteria is considered to be one of the strong candicates of renewable energy source because both the source of energy (Sun light) and the electron donor (water) are sufficiently large in quantity. We are proposing large-scale H_2 production on the sea surface utilizing nitrogen-fixing cyanobacteria (Sakurai *et al*., 2007). In our system, the enzyme of H_2 production is nitrogenase, and the presence of hydrogenase activity should be eliminated because it reabsorbs the produced H_2 (Fig. 1). We have created several hydrogenase mutants from *Nostoc* sp. PCC 7120: disrupted in uptake hydrogenase gene (*hupL*), bidirectional hydrogenase gene (*hoxH*), and the both (*hupL*/*hoxH*) (Masukawa *et al*., 2002), and from *Nostoc* sp. PCC 7422: disrupted in uptake hydrogenase gene (*hupL*) (Yoshino *et al*., 2007). The ΔHup mutant of *Nostoc* sp. PCC 7422 was able to accumulate hydrogen to 20%–30% (v/v) in 3 to 8 days, and the efficiency of light energy conversion into hydrogen was 3.7% vs visible light (calculated to be about 1.7% vs. total solar radiation).

Amos (2004) estimated the cost of H_2 produced by the green alga *Chlamydomonas*, and concluded that the reduction of the cost of the bioreactor is very important. If it cost \$100 m^{-3}, the produced H_2 will not be economically viable. We proposed the future use of bioreactors composed of several layers of plastic film, with at least one having low permeability to H_2 (Sakurai *et al*., 2010). We report here a preliminary result of H_2 accumulation in such a bag.

Materials and Methods

Nostoc sp. PCC 7422 ΔHup mutant was created by Yoshino *et al*. (2007). The determination of H_2 and

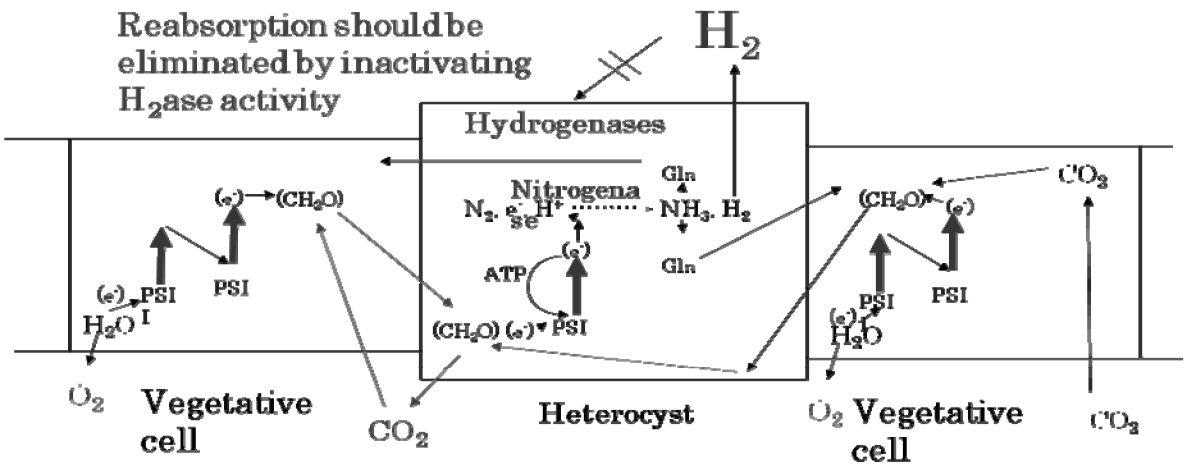

Fig. 1 itrogenase-based H_2 production by heterocyst-forming cyanobacteria.
By inactivating hydrogenase (H_2ase) activity, cyanobacteria can accumulate H_2 in the presence of O_2: $N_2 + 8\ e^- + 8\ H^+ + 16$ ATP → $H_2 + 2\ NH_3 + 16$ (ADP + Pi), and in the absence of N_2: $2\ e^- + 2\ H^+ + 4$ ATP → $H_2 + 4$ (ADP + Pi).

the methods of culture were essentially as described in (Masukawa *et al*., 2002) except that the cells were cultured under a light regime of 12 h light plus 12 h dark (12L-12D) (instead of continuous light).

Results and Discussion

Effects of N_2 concentration on H_2 accumulation

In nitrogen-fixing cyanobacteria, nitrogenase activity is induced by combined-nitrogen deficiency, and repressed by its sufficiency. When *Nostoc* sp. PCC 7422 ΔHup mutant cells were transferred from a combined-nitrogen containing medium (BG11) to a Deficient one, their H_2 production activity was induced in about 2–3 days under a light regime of 12L-12D (24–36 h under continuous light), and declined thereafter. The decline suggests that nitrogenase supplies more than enough amount of combined nitrogen than that required for cell growth, resulting in decrease in nitrogenase and H_2 production activities. When the cells were cultured under 5% CO_2 plus different concentration of N_2 in Ar, the culture of 5% N_2 accumulated higher concentrations of H_2 than those of higher N_2 (20% and 80%) concentrations (Fig. 2).

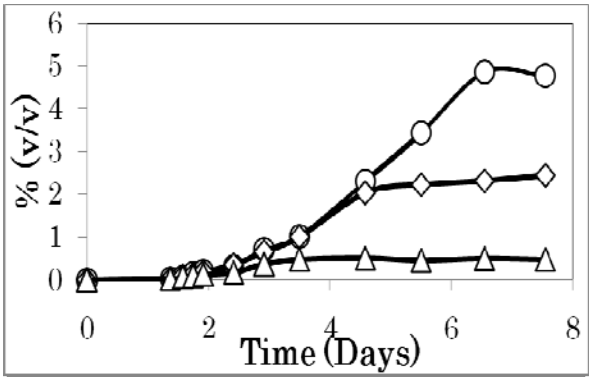

Fig. 2 Effects of different N_2 concentration in 5% CO_2 plus Ar on H_2 accumulation (ordinate). Each serum bottles (7.5 ml) contained 2.5 ml of the culture (containing 2.5 μg chlorophyll). Initial N_2 concentration; ○: 5%, ◇: 20%, Δ:80%.

Table 1 Plausible process design of marine H_2.

*Bioreactor: Large plastic bags (25×m x 200 m) floatingon the sea surface, renewal, once every two years
*Medium: renewal, twice a year
*Gas phase: 1% N_2 + 5% CO_2 in Ar
*H_2 harvesting by hose to a factory ship, every 2 months (50% H_2, v/v)
*Primary gas separation (O_2 removal) by gas-selective membranes
*H_2 purification by PSA (Pressure-swing adsorption)
*Compression to 35 MPa
*Storage in tanks
*Marine transportation to ports

Plausible process design of large-scale hydrogen production in the future utilizing mariculture-raised cyanobacteria

Although many of the element technologies are in their developing stages, a plausible process design is shown in (Table 1) (Sakurai *et al*., 2010).

Use of transparent plastic H_2 barrier film as a part of the bioreactor

Cells of the green alga *Chlamydomonas* evolve H_2

when they are transferred from a sulfur-rich to a sulfur-deficient medium. In the first medium, they photosynthetically accumulate saccharides, which are subsequently used as the electron donor for H_2 production by hydrogenase in the second medium (Ghirardi *et al*., 2006). Amos (2004) made a cost analysis of this photobiological H_2 production process, and pointed out the importance of the cost reduction of bioreactors and storage tanks. As with the *Chlamydomonas* system, the cost reduction of the bioreactors is also important with our cyanobacterial system, and we tested the use of Besela plastic film (Kureha, Tokyo). The thin layer of poly-acrylate of Besela is a barrier to several gases (H_2 permeability at 30 ^oC: 13 cm^3 m^{-2} day^{-1} atm^{-1}). The bags composed of Besela film laminated with nylon (outside) and polypropylene (inside) film was used in this study (available from GL Science, Tokyo) (Fig. 3). The cyanobacteria culture accumulated H_2 in the bag, and the volume ratio of H_2/O_2 was about 2 as expected.

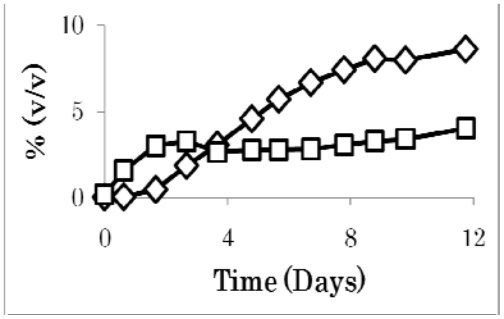

Fig. 3 Accumulation of H_2 in a plastic bag.
A 55-ml open glass bottle containing 50 ml cyanobacteria culture (70 μg chlorophyll) was put in a Besela-based plastic bag, which was heat seeled. The initial gas (about 40 ml) composition was 1% N_2 + 5% CO_2 in Ar. The H_2 (◇) and O_2 (□) in the bag were determined by gas chromatography.

Potential methods for further improvement in efficiency

For practical utilization of photobiological H_2 production by cyanobacteria, further improvement of solar energy conversion efficiency is essential. Potential methods for improvement of the outdoor energy conversion efficiency include (1) reduction of antenna size, (2) improvement of the molecular activity of nitrogenase by site-directed mutagenesis, use of V-type nitrogenase, (3) selection of promising wild-type strains followed by genetic engineering, etc.

Acknowledgements

This work was aided in part by JSPS Grant KAKENHI (B) 21380200 to HS and MEXT grant (High-Tech Research Center Project) to KI.

References

Amos WA (2004) Updated Cost Analysis of Photobiological Hydrogen Production from Chlamydomonas Reinhardtii Green Algae – Milestone Completion Report. NREL/MP-560-35593. www.nrel.gov.docs.fy04osti/35593.pdf. Accessed 27 January 2011

Ghirardi ML, Poseqitz MC, Maness PC, Dubini A, Yu J, Seibert M (2006) Hydrogenases and Hydrogen Photoproduction in Oxygenic Photosynthetic Organisms. Ann Rev Plant Biol 58: 71-91

Masukawa H, Mochimaru M, Sakurai H (2002) Disruption of Uptake Hydrogenase Gene, but Not of Bi-Directional Hydrogense Gene Leads to Enhanced Photobiological Hydrogen Production by the Nitrogenase-Fixing Cyanobacterium Anabaena sp. PCC 7120. Appl Microbiol Biotechnol 58: 618-624

Sakurai H, Masukawa H (2007) Invited Review: Promoting R & D in Photobiological Hydrogen Production Utilizing Mariculture-Raised Cyanobacteria. Mar Biotechnol 9: 128-145

Sakurai H, Masukawa H, Kitashima M, Inoue K (2010) A Feasibility Study of Large-Scale Photobiological Hydrogen Production Utilizing Mariculture-Raised Cyanobacteria. In: Hallenback PC (ed.), Recent Advances in Phototrophic Prokaryotes. Springer, pp. 291-303

Yoshino F, Ikeda H, Masukawa H, Sakurai H (2007) High Photobiological Hydrogen Production Activity of a Nostoc sp. PCC 7422 Uptake Hydrogenase-Deficient Mutant with High Nitrogenase Activity. Mar Biotechnol 9: 101-112

Phycobilisome Antenna Deletion in a Cyanobacterium does Not Improve Photosynthetic Energy Conversion Efficiency or Productivity in a Bench-Scale Photobioreactor System

Lawrence E Page, Michelle Liberton, Hanayo Sato, Himadri B Pakrasi*

Department of Biology, Washington University, St. Louis, MO 63130, USA.
*Corresponding author. Tel. No. 314 935 8133; Fax No. 314 935 6803; E-mail: pakrasi@wustl.edu.

Abstract: Light harvesting in cyanobacteria is performed by large peripheral phycobilisome antenna complexes that absorb light and transfer it to membrane integral antenna closely associated with the photosynthetic reaction center. In eukaryotic microalgae exposed to high light, truncation of the chlorophyll light harvesting antenna system results in an overall increase in cell growth and photosynthetic efficiency by reducing excess light absorption and subsequent energy dissipation on an individual cell level. In order to test this model in cyanobacteria, we used an optimized photobioreactor system for precise regulation of growth parameters and collected data over a wide range of culture conditions, including different CO_2 and light regimes. Wild-type *Synechocystis* 6803 and a PAL mutant that lacks phycobilisomes were grown in batch-mode in these bioreactors. Our data show that lack of phycobilisome antenna do not provide an advantage to *Synechocystis* 6803 cells under any of the conditions tested.

Keywords: Antenna; Phycobilisome; *Synechocystis*; PAL; Photobioreactor

Introduction

Photosynthetic microbes, including green algae and cyanobacteria, are being explored as production chassis for a variety of industrially relevant products, particularly hydrogen (Bandyopadhyay *et al.*, 2010) and oil (Weyer *et al.*, 2010) for biofuels. These organisms have an advantage over widely used industrial microbes such as *E. coli* and *S. cerevisiae* in that they can use light as a source of energy. To do this, photosynthetic microbes use antenna systems to capture light energy and transfer it to photosynthetic reaction centers where photochemistry occurs.

Antenna complexes in photosynthetic organisms are structurally diverse but functionally similar. Most cyanobacteria use a combination of membrane-peripheral phycobilisomes that contain bilin chromophores and membrane-integral chlorophyll-containing proteins. In contrast, plants and many strains of algae contain membrane-integral light harvesting complexes of the LHCII family that contain both chlorophyll *a* and *b*. No matter the structure, all light harvesting antenna serve to maximize light capture because in natural environments light energy is often the growth-limiting factor.

Modeling efforts have predicted that mitigation of the light-harvesting antenna will improve the overall biomass productivity in a bioreactor setting (Nakajima and Itayama, 2003; Ort *et al.*, 2010). This is based on the observation that photosynthetic antenna absorb considerably more light energy under conditions of high illumination than can be used for photochemistry, leading to light saturation in cells near the source of incident light. The excess photons captured must be dissipated as fluorescence or heat, resulting in an overall waste of captured light energy. Furthermore, the shading and light limitation of the more interior cells in the culture waste reaction center photochemical capacity. In fact, in cultures with truncated antenna, it has been shown that eukaryotic microalgae grow with a higher photosynthetic efficiency (Polle *et al.*, 2002; Mussgnug *et al.*, 2007; Bernat *et al.*, 2009).

In *Synechocystis* sp. PCC 6803 (hereafter *Synechocystis* 6803), phycobilisomes are composed of an allophycocyanin-containing core from which rods that contain phycocyanin radiate, and a number of linker proteins. Numerous antenna mutants have been generated in which phycobilisomes have been attenuated to varying degrees (Olive *et al.*, 1997; Ughy and Ajlani, 2004). We chose to use the PAL mutant that lacks allophycocyanin, phycocyanin, and the core-membrane linker, and is unable to assemble functional phycobilisomes (Ajlani and Vernotte, 1998).

To test whether antenna mitigation in cyanobacteria improves whole-culture productivity, *Synechocystis* 6803 wild type (WT) and the PAL mutant were grown in batch mode and high light in a 350 ml photobioreactor to stationary phase. Our data show that the PAL mutant grows slowly and does not achieve a higher density at stationary phase compared to WT cells. Furthermore, the PAL mutant accumulates less chlorophyll and demonstrates less photosystem II activity than WT when grown in constant high light.

Materials and Methods

Culture Conditions

Synechocystis 6803 was inoculated from plates into 50 ml liquid BG11 (Allen, 1968), and grown in 125 ml Erlenmeyer flasks for 5–7 days. Then, 10 ml of culture was transferred to 90 ml fresh BG11 in a 250 ml Erlenmeyer and grown for another 7 days. These cultures were then spun down at 5,000 rpm for 5 minutes at 30 °C, resuspended in 10 ml fresh BG11, and inoculated into the bioreactors. For all growth in flasks, 50 μmoles photons/m^2 s white fluorescent light was used as the sole energy source, and cultures were grown on a shaker at 150 rpm and 30 °C. The PAL mutant was treated in the same manner, except 10 μg/ml spectinomycin and chloroamphenicol were added.

In the bioreactors, no antibiotics were used to ensure the experimental conditions for both wild type and PAL were identical. Upon inoculation into the bioreactors, the cells were immediately exposed to high light and 2% CO_2. To allow the cultures adequate time to adapt to these conditions (and prevent initial lag phase), cultures were grown in turbidostat mode at OD_{735} = 0.3 for 3 days. After this time, cultures were switched to batch mode, and time point zero was recorded.

Photobioreactors and Gas Mixing

Two FMT 150 photobioreactors from Photon Systems, Inc. (Nedbal, *et al.*, 2008) were used during batch-mode growth to control light intensity, control temperature, monitor OD_{735}, and monitor pH at thirty-minute intervals. The total culture volume was 350 ml. The light source for all experiments was integrated variable intensity light emitting diodes that produce light at two wavelengths: red (630 nm) and blue (450 nm). Light intensities were set at 50 μmoles photons/m^2sec red and 100 μmoles photons/m^2sec blue throughout the experiment, as this was found to be high, but not toxic to the wild type cells (data not shown). A Mettler-Toledo Clark-type oxygen electrode, integrated into the bioreactor, was calibrated to measure dissolved oxygen concentrations at the micromolar level. This sensor allowed for precise determination of photosynthetic capacity, maximum photosynthetic capacity, and respiration (Cerveny *et al.*, 2009) on a daily basis. A gas mixing and analyzing system designed by Qubit Systems, Inc. (www.qubitsystems.com) supplied air or 2% CO_2 at 350 ml/min throughout the experiment.

Cell Counting

Cell concentration was determined daily on a Nexcelom Biosciences Auto M10 Cellometer. Counting error was determined to be less than 1% by technical replicate.

Results

Using the photobioreactor system, we were able to grow WT and PAL cultures under tightly controlled and highly reproducible conditions. Experiments were performed with bubbling of both ambient air and 2% CO_2, and OD_{735} and pH were measured (Fig. 1). With high light intensity and air bubbling, growth of PAL cells initially exceeded WT for approximately 48 hours, at which point growth of PAL declined sharply. The PAL mutant was found to be sensitive to high pH, and rapidly died at levels above ~10 (Figs. 1a and 1b). To provide a buffer against increasing pH and ensure adequate supply of carbon, 2% CO_2 was bubbled for subsequent experiments at 350 ml/min. In 2% CO_2 and high light, both WT and PAL grew to stationary

phase without a significant increase in pH (Figs. 1c and 1d).

Next, a ten-day batch-mode growth curve in high light was used to compare productivity and metabolic performance. Cell density, as measured by OD_{735}, was higher for WT than PAL during the entire experiment (Fig. 2a). Cell count, photosynthetic oxygen evolution, maximum photosynthetic capacity, and metabolic oxygen consumption were measured daily (Figs. 2b, 2c and 2d). Importantly, the PAL mutant did not demonstrate a higher capacity for photosynthetic oxygen evolution than WT as cell concentration increased, contrary to the prediction that antenna mitigation increases photosynthetic productivity. Respiration rates were higher for PAL during the first half of the growth curve (Fig. 2d), but lower at high cell densities.

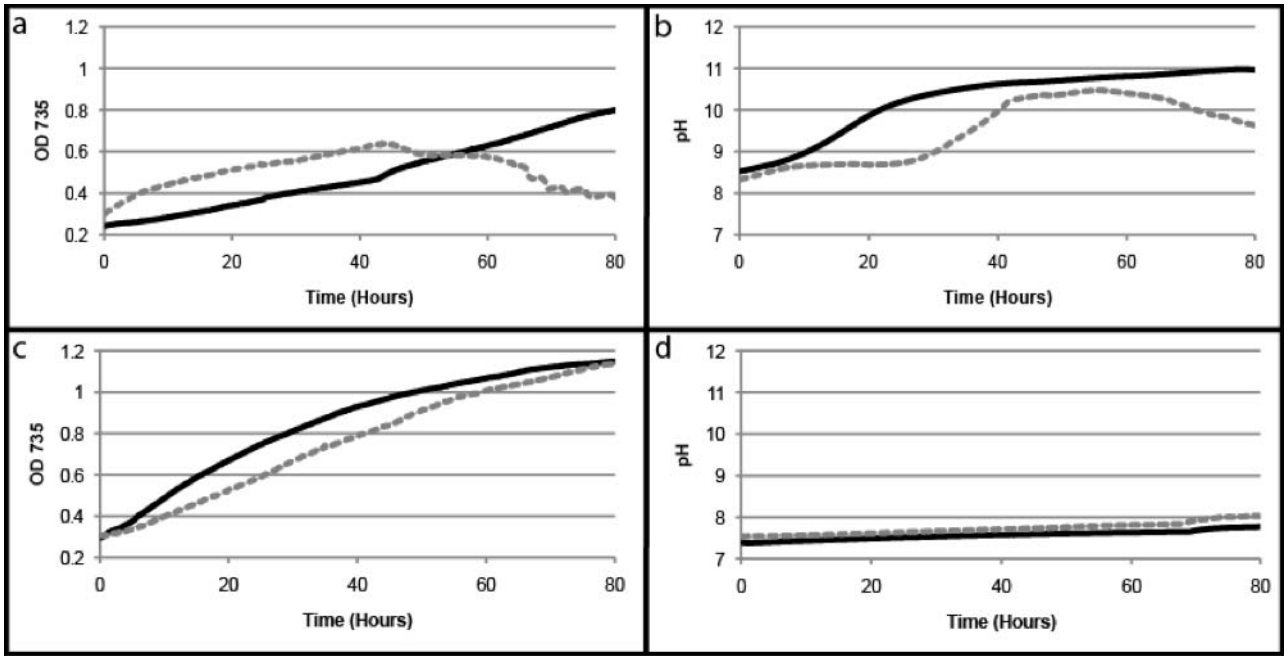

Fig. 1 WT (black) and PAL (gray) grown in high light and air (a and b) or high light and 2% CO_2 (c and d). The pH of the cultures when grown in air (b) increased with culture density. In 2% CO_2 (d), however, the pH was stabilized throughout the duration of the experiment.

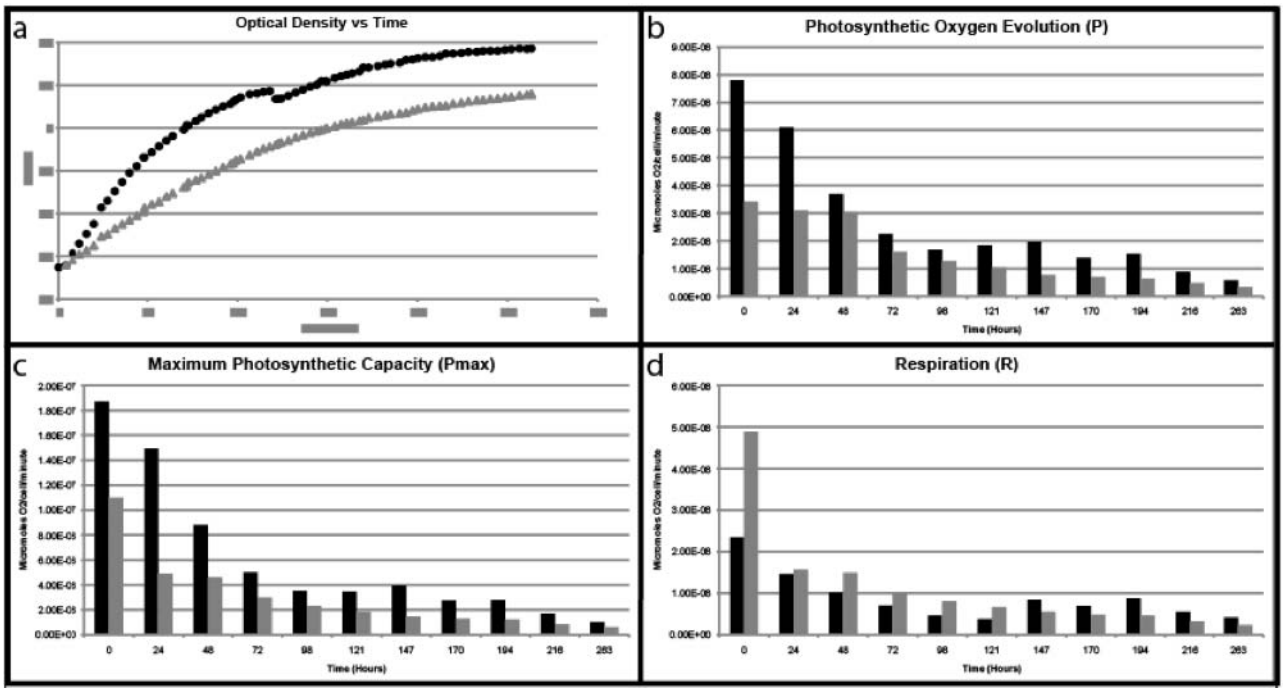

Fig. 2 Batch-mode growth dynamics of 350 ml cultures of *Synechocystis* 6803 (black) and PAL mutant (gray) in high light and 2% CO_2.

Discussion

In green algae, antenna truncation mutants have been generated and the consequences of these changes have been measured and found to provide some advantage in terms of productivity (Melis *et al.*, 1999). However, in cyanobacteria, antenna mutants have not until now been rigorously examined to determine if antenna truncation is advantageous. We have compared the PAL mutant lacking phycobilisomes to WT cells under different growth conditions, and our results indicate that there is not a substantial culture-wide advantage to minimizing the antenna systems in *Synechocystis* 6803. In air, the cultures reached a pH-limited density before they reached a light-limited stationary phase. When 2% CO_2 was bubbled at 350 ml/min., the pH limitation was alleviated, but the PAL cultures still did not demonstrate higher overall productivity. The differing results obtained from eukaryotic algae compared to cyanobacteria may be inherent to the significantly different antenna systems present in these organisms. In the future, dry biomass accumulation will be precisely measured, light-limited biomass productivity will be compared, and mutants with intermediate antenna will be studied.

Acknowledgements

We thank Ghada Ajlani for kindly providing the PAL mutant used in this study. This work was supported as part of the Photosynthetic Antenna Research Center (PARC), an Energy Frontier Research Center funded by the U.S. Department of Energy, Office of Science, Office of Basic Energy Sciences under Award Number DE-SC 0001035.

References

Ajlani G, Vernotte C (1998) Construction and Characterization of a Phycobiliprotein-Less Mutant of Synechocystis sp. PCC 6803. Plant. Mol. Biol. 37: 577-580

Allen MM (1968) Simple Conditions for Growth of Unicellular Blue-Green Algae on Plates. J. Phycol. 4:1-4

Bandyopadhyay A, Stockel J, Min H, Sherman L, Pakrasi H (2010) High Rates of Photobiological H_2 Production by a Cyanobacterium under Aerobic Conditions. Nature Communications. 1:139

Bernat G, Waschewski N, Rogner M (2009) Towards Efficient Hydrogen Production: the Impact of Antenna Size and External Factors on Electron Transport Dynamics in Synechocystis PCC 6803. Photosynth. Res. 99: 205-216

Cerveny J, Setlik I, Trtilek M, Nedbal L (2009) Photobioreactor for Cultivation and Real-Time, In-Situ Measurement of O_2 and CO_2, Exchange Rates, Growth Dynamics, and of Chlorophyll Fluorescence Emission of Photoautotrophic Microorganisms. Eng. Life Sci. 9: 247-253

Melis A, Neidhardt J, Benemann J (1999) Dunaliena Salina (Chlorophyta) with Small Chlorophyll Antenna Sizes Exhibit Higher Photosynthetic Productivities and Photon Use Efficiencies than Normally Pigmented Cells. J. Appl. Phycol. 10: 515-525

Mussgnug J, Thomas-Hall S, Rupprecht J, Foo A, Klassen V, McDowall A, Schenk P, Kruse O, Hankamer B (2007) Engineering Photosynthetic Light Capture: Impacts on Improved Solar Energy to Biomass Conversion. Plant Biotechnol. J. 5: 802-814

Nakajima Y, Itayama T (2003) Analysis of Photosynthetic Productivity of Microalgal Mass Cultures. J. Appl. Phycol. 15: 497-505

Nedbal L, Trtilek M, Cerveny J, Komarek O, Pakrasi H (2008) A Photobioreactor System for Precision Cultivation of Photoautotrophic Microorganisms and for High-Content Analysis of Suspension Dynamics. Biotechnol. and Bioeng. 100: 902-910

Olive J, Ajlani G, Astier C, Recouvreur M, Vernotte C (1997) Ultrastructure and Light Adaptation of Phycobilisome Mutants of Synechocystis PCC 6803. BBA Bioenergetics. 1319: 275-282

Ort D, Zhu X, Melis A (2010) Optimizing Antenna Size to Maximize Photosynthesis. Plant Physiol. PMID: 21078863

Polle J, Kanakagiri S, Jin E, Masuda T, Melis A (2002) Truncated Chlorophyll Antenna Size of the Photosystems-a Practical Method to Improve Microalgal Productivity and Hydrogen Production in Mass Culture. Int. J. Hyd. Energy. 27: 1257-1264

Ughy B, Ajlani G (2004) Phycobilisome Rod Mutants in Synechocystis sp. Strain PCC6803. Microbiol. 150: 4147-4156

Weyer K, Bush D, Darzins A, Willson B (2009) Theoretical Maximum Algal Oil Production. Bioenergy Rsch. 3: 204-213

Symposium 22

Photosynthesis and New Environmental Challenges

Measurement of Mesophyll Conductance in Tobacco, Arabidopsis and Wheat Leaves with Tunable Diode Laser Absorption Spectroscopy

Youshi Tazoe[a,b], Susanne von Caemmerer[b], John R. Evans[b,*]

[a]Graduate School of Biostudies, Kyoto University, Sakyo, Kyoto 606-8052, Japan;
[b]Plant Science Division, Research School of Biology, The Australian National University, Canberra, ACT 0200, Australia.
[*]Corresponding author. Tel. No. +61 2 6125 4492; Fax No. +61 2 6125 4919; E-mail: john.evans@anu.edu.au.

Abstract: In C_3 leaves, diffusion of CO_2 into leaves is restricted by stomata and subsequently by the intercellular airspaces and liquid phase into chloroplasts. This diffusion restriction within leaves has been termed mesophyll conductance, g_m, which has garnered attention because g_m limits photosynthesis at ambient CO_2. Recently, some reports have shown that g_m varies with CO_2 concentration and it may be caused by gating of aquaporins (cooporins) which are located in the plasma membrane and inner envelope of chloroplasts. However, there is still controversy about whether g_m responds to CO_2 concentration. In this study, the effects of CO_2 concentration on g_m were examined in tobacco, Arabidopsis and wheat leaves by combining gas exchange with carbon isotope discrimination measurements using tunable diode laser absorption spectroscopy. CO_2 was initially increased from 200 to 1,000 ppm and then decreased stepwise to 200 ppm and increased stepwise back to 1000 ppm. In 2% O_2, a step increase from 200 to 1,000 ppm significantly decreased g_m by 26%–40% in all three species. The CO_2 response of g_m was less in 21% O_2.

Keywords: Carbon isotope discrimination; Cooporin; Internal conductance

Introduction

For C_3 photosynthesis to occur, CO_2 has to diffuse from the atmosphere through stomata, intercellular airspace and the liquid phase into the chloroplast for fixation by Rubisco. The conductance to CO_2 diffusion from intercellular airspace to the chloroplast has been termed mesophyll conductance, g_m, which has garnered attention because g_m limits photosynthesis at ambient CO_2 concentration. Recently, some reports have shown that g_m varies with CO_2 concentration (Flexas *et al*., 2007; Vrábl *et al*., 2009). Variation in g_m may be caused by gating of CO_2 permeable aquaporins (cooporins: Terashima *et al*., 2006) located in the plasma membrane and inner envelope of chloroplasts (Uehlein *et al*., 2008). However, the effects of CO_2 concentration on the cooporins are still unknown and there is still controversy about whether g_m responds to CO_2 concentration.

Developments in tunable-diode laser absorption spectroscopy (TDLAS) have improved our ability to make rapid measurements of g_m using the carbon isotope discrimination (Δ) method. Here we describe a system that allows Δ measurements to be made over a wide range of CO_2 and O_2 concentration using TDLAS. The aims of this study were to test the short term response of g_m to step changes in CO_2 concentration and examine the reproducibility of estimates of g_m through a day. We studied responses of g_m to changes in CO_2 in two Arabidopsis genotypes (Col-0 and L*er*), tobacco and wheat, at both 2% O_2 where photorespiratory fractionations are minimized and 21% O_2.

Materials and Methods

Tobacco (*Nicotiana tabacum* cv Wisconsin) plants were grown in a growth cabinet, which was set to a 12 h photoperiod (25/20 ^oC day/night, 500 μmol quanta m^{-2} s^{-1}, 70% relative humidity). Wheat (*Triticum aestivum* L. cv.

Yecora 70) and Arabidopsis (*Arabidopsis thaliana* L. Heyhn.) Columbia-0 (Col-0) and Landsberg *erecta* (L*er*) genotypes were grown in a greenhouse under full sunlight (22/15 °C day/night) and watered daily.

Plants were transferred from the greenhouse or the growth cabinet to the laboratory (room temperature of 25 °C) in the early morning. One fully expanded leaf was placed across the 6 cm^2 leaf chamber of the LI-6400 with a red-blue LED light source (Li-Cor, Lincoln, NE, U.S.A.) and flow rate was set at 200 μmol s^{-1}. Photosynthesis was measured for approximately 40 min at irradiance of 1,500 μmol quanta m^{-2} s^{-1}, leaf temperature 25 °C, inlet CO_2 of 400 ppm, and 21% O_2. Then, O_2 was changed to 2% to reduce the carbon isotope fractionation associated with photorespiration, and the oxygen effect on infrared analysis was corrected for using the LI-6400 prompt routine based on Bunce (2002). In some instances, CO_2 responses were measured in 21% O_2 rather than 2% O_2 using tobacco and Arabidopsis. CO_2 response measurements began at 200 ppm CO_2, and then CO_2 was increased to 1000 ppm, decreased stepwise until 200 ppm and increased stepwise back to 1,000 ppm. Measurements were made over 30 min at each CO_2. After measuring the CO_2 response, the light was turned off and dark respiration (R_{dark}) was measured at both 200 and 1,000 ppm CO_2.

Gas exchange was coupled to a TDLAS (model TGA100A, Campbell Scientific, Inc., Logan, UT, USA) for on-line measurements of Δ (Bowling *et al*., 2003; Griffis *et al*., 2004). Δ was calculated from the equation presented by Evans *et al*. (1986) as:

$$\Delta = \frac{1000 \times \xi\left(\delta^{13}C_{sam} - \delta^{13}C_{ref}\right)}{1000 + \delta^{13}C_{sam} - \xi\left(\delta^{13}C_{sam} - \delta^{13}C_{ref}\right)} \quad (1)$$

where $\delta^{13}C_{sam}$ and $\delta^{13}C_{ref}$ are the carbon isotope compositions of the leaf chamber and reference gases of the LI-6400. $\xi = C_{ref}/(C_{ref} - C_{sam})$, and C_{ref} and C_{sam} are the CO_2 concentrations of dry air entering and exiting the leaf chamber, respectively, measured by the TDLAS.

An example of a typical measuring cycle is shown in Fig. 1. After measurement of N_2/O_2 gas (zero), six different CO_2 concentrations (170, 330, 490, 660, 820, 970 ppm CO_2) mixed from calibration gas #1 were measured. The gases were changed every 20 sec. Uncorrected carbon isotope values declined slightly with increasing CO_2 from −24.6‰ to −25.6‰ at 170 and 970 ppm CO_2, respectively and variability decreased with increasing CO_2. Compressed air (Cal. #2; 380 ppm CO_2) was used to adjust gain drift for the $^{12}CO_2$ signal, and then the staircase of calibration CO_2 was used to calibrate the $^{13}CO_2$ signal in each measurement cycle. The calibration was applied to the reference and sample gases to calculate $\delta^{13}C_{ref}$, $\delta^{13}C_{sam}$ and Δ for each LI-6400. Gases were measured every 4 min and the cycles were repeated 8 times at a given CO_2.

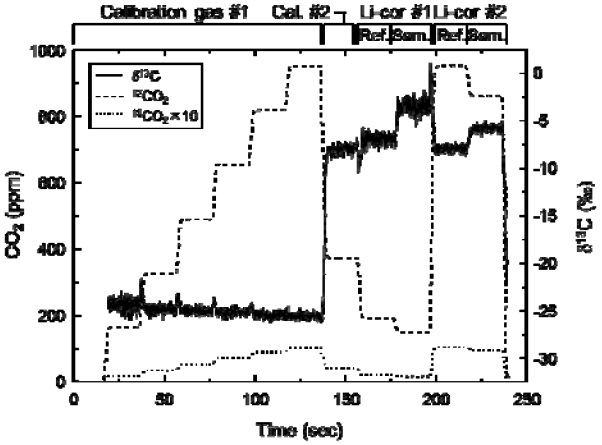

Fig. 1 Example of a typical 240 sec cycle for measurements of carbon isotope discrimination with the TDLAS.
Solid, dashed and dotted lines show uncorrected $\delta^{13}C$ values, $^{12}CO_2$ and $^{13}CO_2 \times 10$, respectively (Source: Tazoe *et al.*, 2011).

A full description of discrimination during C_3 photosynthesis was given by Evans *et al*. (1986). Due to the high boundary layer conductance in the leaf chamber, the boundary layer term was ignored, such that:

$$\Delta = a\frac{p_a - p_i}{p_a} + a_i\frac{p_i - p_c}{p_a} + b\frac{p_c}{p_a} - \frac{eR_d/k + f\Gamma^*}{p_a} \quad (2)$$

where a is fractionation factor due to diffusion through stomata (4.4‰), a_i is fractionation factor for hydration and diffusion through water (1.8‰), and b is fractionation factor for the carboxylation reaction by Rubisco and phospho*enol*pyruvate carboxylase (PEPC). In this study, b of 30‰ was used. The parameter e is associated with fractionation from day respiration, and it was assumed to be −5.1‰ (Tazoe *et al*., 2009). The parameter f (11.6‰) is the fractionation factor for photorespiration (Lanigan *et al*., 2008). p_a, p_i and p_c are the CO_2 partial pressure of the ambient, intercellular airspaces and sites of carboxylation within chloroplasts, respectively. CO_2 partial pressure equals CO_2 concentration multiplied

by atmospheric pressure, which in Canberra averages 953 mbar. Day respiration, R_d, is assumed to be the same as dark respiration (R_{dark}). Γ* is the CO_2 compensation point in the absence of R_d and we have assumed the value previously measured for tobacco (von Caemmerer *et al*., 1994) for all species, 3.68 μbar in 2% O_2 and 38.6 μbar in 21% O_2 at 25 °C. The symbol k is the carboxylation efficiency of Rubisco and $k = V_c/p_c$ where V_c is RuBP carboxylase activity per unit leaf area and $V_c = (A + R_d)/(1 - \Gamma^*/p_c)$ (von Caemmerer and Farquhar, 1981).

Mesophyll conductance, g_m is defined as $g_m = A/(p_i - p_c)$. Substituting for k and replacing p_c by $p_i - A/g_m$, Eq. 2 can be solved for g_m and

$$g_m = \frac{\left(b - a_i - \frac{eR_d}{A+R_d}\right) \times \frac{A}{p_a}}{a + \frac{(b-a)p_i}{p_a} - \Delta - \frac{eR_d(p_i - \Gamma^*)}{(A+R_d)p_a} - \frac{f\Gamma^*}{p_a}}. \quad (3)$$

Results and Discussion

We established a new gas exchange protocol to examine the short term response of g_m to a large step change in CO_2 and to a range of CO_2, also whether g_m varied over a day when measured under the same conditions. Gas exchange measurements were made over 6 hours and examples of diurnal traces from single leaves of assimilation rate, A, stomatal conductance, g_s, and g_m at different CO_2 are shown in Fig. 2. We started the measurement series with the largest step change in CO_2. When CO_2 was switched from 200 to 1,000 ppm, A in tobacco rapidly increased from 17 to 38 μmol m^{-2} s^{-1} (Fig. 2). g_s was gradually increasing in 200 ppm, and then decreased gradually following the change to 1,000 ppm. By contrast, g_m rapidly decreased when CO_2 was increased from 200 to 1,000 ppm. In 2% O_2, the initial step change in CO_2 from 200 to 1,000 ppm significantly decreased g_m by 40% in tobacco, 26% in Arabidopsis (Col-0) and 36% in wheat. For tobacco and Arabidopsis, g_m then increased as CO_2 was decreased stepwise back to 200 ppm (middle of the day) and decreased again as CO_2 was increased stepwise back to 1,000 ppm (late afternoon, Fig. 2). Wheat showed a variable response after midday, frequently having dramatic reductions in A, g_s and g_m.

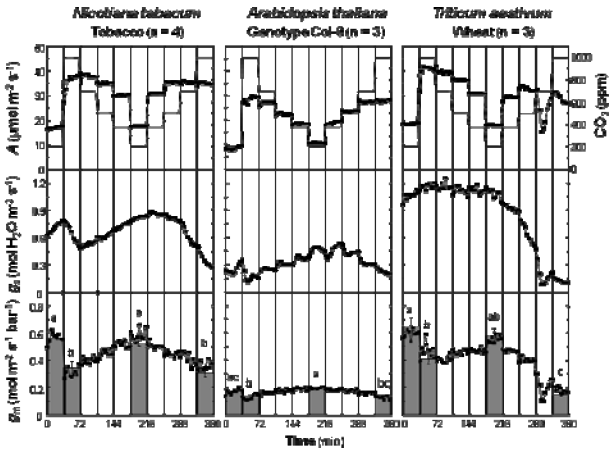

Fig. 2 Example time courses of net CO_2 assimilation rate (A), stomatal conductance to water (g_s) and mesophyll conductance to CO_2 (g_m) for individual leaves of tobacco, Arabidopsis (Col-0) and wheat. For measurement conditions, see Materials and Methods. Data bars are means ± SE for 3 or 4 different leaves, each of which was averaged over the last 12 min. To detect the differences between g_m under high and low CO_2, Tukey's multiple comparison test was applied to the data forming these means. Different letters indicate significant differences ($P < 0.05$) (Source: Tazoe *et al.*, 2011).

The relationships between the CO_2 partial pressure of the intercellular airspaces, p_i, and A, g_s, and g_m for all three species are shown in Fig. 3. For wheat, the first staircase of CO_2 change of the day was used because of the dramatic reductions in A, g_s and g_m in late afternoon (see Fig. 2). In tobacco and Arabidopsis L*er* genotype, the responses were also measured in 21% O_2. The response of A to CO_2 differed between 2% and 21% O_2 as expected due to the suppression of photorespiration at low CO_2, but g_s showed similar declines with increasing p_i. In 2% O_2, g_m decreased as p_i increased whereas it was independent of p_i in 21% O_2 (Fig. 3).

For wheat in 2% O_2, we previously found that g_m varied little with p_i between 80 μbar and 500 μbar (Tazoe *et al.*, 2009), which differed slightly from the results from Fig. 3. In this study, there was a pronounced drop in photosynthetic properties, A and g_s, later in the day (Fig. 2). Such a pronounced drop was not observed in our previous study where instead, g_s gradually declined with time irrespective of the direction of CO_2 change (data not shown). We have been unable to explain why g_s dropped later in the day. It does not appear to be associated with growing conditions or leaf/plant age but may reflect being measured in a gas exchange chamber for a longer time.

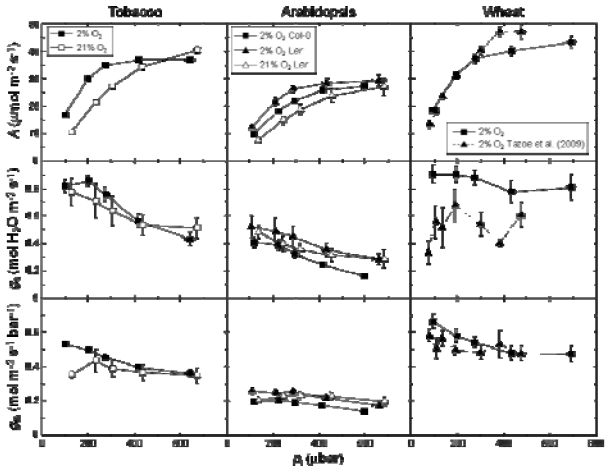

Fig. 3 CO_2 response of A, g_s and g_m in 2% (closed symbols) or 21% O_2 (open symbols). For measurement conditions, see Materials and Methods. Data points are means ± SE (n = 3 – 16). Dotted lines join our previous data for wheat (Tazoe *et al.*, 2009) (Source: Tazoe *et al.*, 2011)

We are aware of only four published studies where g_m has been compared in different CO_2 concentrations using the carbon isotope method. Loreto *et al*. (1992) measured *Quercus rubra* and *Xanthium strumarium* with the isotope method and g_m was 30% less at 750 μbar p_i than at ambient CO_2 in 21% O_2, although this was only significant for *X. strumarium*. Flexas *et al.* (2007) reported that g_m estimated by the isotope method was lower at high p_i compared to ambient CO_2 in 21% O_2 by 54% for *Nicotiana tabacum* and 34% for *Nicotiana sylvestris*. The response to CO_2 was larger in 2% O_2, increasing to 49% for *N. sylvestris*. For *Helianthus annuus*, Vrábl *et al*. (2009) found that g_m decreased by 74% as p_i increased from 200 to 800 ppm, but was also lower at 50 ppm CO_2 in 21% O_2. Given the variability in results, does the response of g_m to CO_2 differ between plant species?

To obtain unified information involving the effect of CO_2 on g_m, we measured g_m over a wide range of CO_2 and O_2 concentrations using tobacco, Arabidopsis and wheat. In 2% O_2, as p_i increased from low (92–117 μbar) to high (593–693 μbar), g_m decreased by 32% for tobacco, by 28% for Arabidopsis Col-0 and by 29% for wheat (Fig. 3). In tobacco and Arabidopsis (Col-0), the responses of g_m to CO_2 have also been measured by a chlorophyll fluorescence method in Flexas *et al.* (2007). Flexas *et al.* (2007) observed g_m decreased by 35% for tobacco and by 83% for Arabidopsis as p_i increased from low (120 μbar) to high (560 or 660 μbar) in 21% O_2. For tobacco, the response to CO_2 was similar using either isotope discrimination or chlorophyll fluorescence to calculate g_m (Flexas *et al.*, 2007). Decreases in g_m with increasing p_i have also been found for 5 species of *Banksia*, again using chlorophyll fluorescence to calculate g_m under 21% O_2 (Hassiotou *et al*., 2009).

The response of g_m to CO_2 in 21% compared to 2% O_2 is diminished either partially (Flexas *et al.*, 2007) or to a large extent (Fig. 3). It is hard to imagine that O_2 concentration could directly affect g_m. The effect of the photorespiratory fractionation factor f on Δ has been studied (Lanigan *et al*., 2008; Tcherkez, 2006; Tcherkez *et al*., 2010). The contribution by photorespiration is greater in 21% than 2% O_2 and increases at lower CO_2 concentrations. We calculated g_m using various reported values of f, but none could account for the effect of O_2 on the CO_2 dependence of g_m (Tazoe *et al*., 2011). The impact on Δ from the substrate source and the time it takes for the photorespiratory pools to turn over needs to be considered (Tcherkez *et al*., 2010). Our experiments lasted the whole day and returned to both high and low CO_2 at different times. If anything, there may have been a tendency for g_m to decrease slightly over the day, but we used both increasing and decreasing CO_2 concentrations for a given leaf and reversed the order these were applied through the day between leaves to correct for any bias this may have caused.

Acknowledgements

This work was funded by ARC Discovery grant DP0771413. YT was supported by Research Fellowship of the Young Scientists of the Japan Society for Promotion of Science (JSPS).

References

Bowling DR, Sargent SD, Tanner BD, Ehleringer JR (2003) Tunable Diode Laser Absorption Spectroscopy for Stable Isotope Studies of Ecosystem-Atmosphere CO_2 Exchange. Agricultural and Forest Meteorology 118: 1-19

Bunce JA (2002) Sensitivity of Infrared Water Vapor Analyzers to Oxygen Concentration and Errors in Stomatal Conductance. Photosynthesis Research 71: 273-276

Evans JR, Sharkey TD, Berry JA, Farquhar GD

(1986) Carbon Isotope Discrimination Measured Concurrently with Gas Exchange to Investigate CO_2 Diffusion in Leaves of Higher Plants. Australian Journal of Plant Physiology 13: 281-292

Flexas J, Diaz-Espejo A, Galmés J, Kaldenhoff R, Medrano H, Ribas-Carbo M (2007) Rapid Variations of Mesophyll Conductance in Response to Changes in CO_2 Concentration around Leaves. Plant, Cell & Environment 30: 1284-1298

Griffis TJ, Baker JM, Sargent SD, Tanner BD, Zhang J (2004) Measuring Field-Scale Isotopic CO_2 Fluxes with Tunable Diode Laser Absorption Spectroscopy and Micrometeorological Techniques. Agricultural and Forest Meteorology 124: 15-29

Hassiotou F, Ludwig M, Renton M, Veneklaas EJ, Evans JR (2009) Influence of Leaf Dry Mass Per Area, CO_2, and Irradiance on Mesophyll Conductance in Sclerophylls. Journal of Experimental Botany 60: 2303-2314

Lanigan GJ, Betson N, Griffiths H, Seibt U (2008) Carbon Isotope Fractionation during Photorespiration and Carboxylation in Senecio. Plant Physiology 148: 2013-2020

Loreto F, Harley PC, Marco GD, Sharkey TD (1992) Estimation of Mesophyll Conductance to CO_2 Flux by Three Different Methods. Plant Physiology 98: 1437-1443

Tazoe Y, von Caemmerer S, Badger MR, Evans JR (2009) Light and CO_2 Do Not Affect the Mesophyll Conductance to CO_2 Diffusion in Wheat Leaves. Journal of Experimental Botany 60: 2291-2301

Tazoe Y, von Caemmerer S, Estavillo GM, Evans JR (2011) Using Tunable Diode Laser Spectroscopy to Measure Carbon Isotope Discrimination and Mesophyll Conductance to CO_2 Diffusion Dynamically at Different CO_2 Concentrations. Plant, Cell & Environment: in press

Tcherkez G (2006) How Large Is the Carbon Isotope Fractionation of the Photorespiratory Enzyme Glycine Decarboxylase? Functional Plant Biology 33: 911-920

Tcherkez G, Schäufele R, Nogués S, Piel C, Boom A, Lanigan G, Barbaroux C, Mata C, Elhani S, Hemming D, Maguas C, Yakir D, Badeck FW, Griffiths H, Schnyder H, Ghashghaie J (2010) On the $^{13}C/^{12}C$ Isotopic Signal of Day and Night Respiration at the Mesocosm Level. Plant Cell and Environment 33: 900-913

Terashima I, Hanba YT, Tazoe Y, Vyas P, Yano S (2006) Irradiance and Phenotype: Comparative Eco-Development of Sun and Shade Leaves in Relation to Photosynthetic CO_2 Diffusion. Journal of Experimental Botany 57: 343-354

Uehlein N, Otto B, Hanson DT, Fischer M, McDowell N, Kaldenhoff R (2008) Function of Nicotiana Tabacum Aquaporins As Chloroplast Gas Pores Challenges the Concept of Membrane CO_2 Permeability. The Plant Cell 20: 648-657

von Caemmerer S, Evans JR, Hudson GS, Andrews TJ (1994) The Kinetics of Ribulose-1, 5-Bisphosphate Carboxylase/Oxygenase in Vivo Inferred from Measurements of Photosynthesis in Leaves of Transgenic Tobacco. Planta 195: 88-97

von Caemmerer S, Farquhar GD (1981) Some Relationships between the Biochemistry of Photosynthesis and the Gas Exchange of Leaves. Planta 153: 376-387

Vrábl D, Vašková M, Hronková M, Flexas J, Šantrůček J (2009) Mesophyll Conductance to CO_2 Transport Estimated by Two Independent Methods: Effect of Variable CO_2 Concentration and Abscisic Acid. Journal of Experimental Botany 60: 2315-2323

Influence of Enhanced Ultraviolet-B Radiation on Photosynthesis in Flag Leaves of a Super-High-Yield Hybrid Rice during Senescence

Meiping Zhang[a,b], Guoxiang Chen[a,*]

[a] Key Lab of Biodiversity and Biotechnology of Jiangsu Province, College of Life Sciences, Nanjing Normal University , Nanjing 210097, PR China; [b] College of Life Sciences, ShanXi Normal University, Linfen 041004, PR China.
[*]Corresponding author. Tel. No. +861 3505165673; Fax No. +86-025-85891578; E-mail: gxchen@njnu.edu.cn.

Abstract: Atmospheric pollutants resulted in a global reduction of the stratospheric ozone layer leading to an increased level of solar UV-B (280–315 nm) radiation at the surface of earth. Enhanced UV-B radiation produces deleterious effects on physiological and morphological traits of plants and thus, posing a severe threat to the existence and survival of organisms. Rice is an important food supplies crop, an kind model plant. Senescence of flag leaves of high-yield hybrid rice affect yield to improve. Aiming at enhanced UV-B, senescence of flag leaves of high-yield hybrid rice, The high-yield hybrid rice 'LiangYouPeiJiu' was studied, adopting 16 KJ/m^2 d and 40 KJ/m^2 d UV-B to treat with rice, Chlorophyll content, chlorophyll fluorescence, electron transport activities and MDA of chloroplasts were measured . Results are as follows: The chlorophyll content of flag leaves of LYPJ decreased after full expansion non-significantly, Change of UV-B treated group is higherr; Car increased after full expansion, peaked at 14 days after full expansion, and then decreased significantly, There a low peak in group UV-B treated. As the product of membrane-lipid peroxidation, MDA content increased markedly during the whole stage of leaf development after full expansion. The content of UV-B treated group is the highest. Electron transport activities increased significantly after full expansion, and then declined; Compare with CK group, group treated with low UV-B changes non-significantly, group treated with high UV-B changes significantly. With leaf senescence, F_v/F_M increased significantly after full expansion, and then declined, and peaked at 21d. UV-B and leaf senescence affect PSII performance of the photosynthesis. The study illuminates leaf senescence begin at about 21d , low UV-B stay chloroplast senescence, high UV-B accelerate chloroplast senescence.

Keywords: High-yield hybrid rice; Flag leaves; UV-B; Chloroplast senescence; photosynthesis function

Introduction

Atmospheric pollutants resulted in a global reduction of the stratospheric ozone layer leading to an increased level of solar UV radiation at the surface of earth (Zeeshan *et al.*, 2009). Ultraviolet ray in spectrum can be divided into three categories according to the differences of the organism effect: UV-C (200–280 nm), UV-B, (280–320 nm), UV-A (320 nm–400 nm). UV-A, a small part of which can be absorbed by the ozonosphere, penetrates through the ozonosphere and does little damage to human bodies; when the quantity of the UV-B is normal , O_3 of the stratosphere will take in almost all the UV-C and 90% of the UV-B. But when the O_3 density decrease, the radiation of UV-B increases, which will threaten the security of animals, plants and even human beings. It is estimated that without any control, 40% of the ozonosphere will disappear which will result in the increasing of the radiation of the reaching-earth ultraviolet ray. So, it is becoming a hot topic among scientists in the whole world (Jelte R *et al.*, 2002).

Enhanced UV-B radiation produces deleterious effects on physiological and morphological traits of plants and thus, posing a severe threat to the existence and survival of organisms.Increasing UV-B influences the organism in three aspects: individual, group and economy system (Brosche *et al.*, 2002). Moreover, the

UV-B radiation have lots of influence on cell genetics effect。It's indicated by Han Rong's reseach that the UV-B radiation brings cell excessive division (Hang Rong *et al.*, 2002).

Neduehezhan and Kalandaivelu state that UV-B radiation breaks the light system of photosynthesis, Rubiso and so on, which will decrease the photosynthesis. The stronger the UV-B radiation is, the more obvious the influence becomes (Nedunchezhian *et al.*, 1991).

Ultraviolet radiation decrease the photosynthesis rate in two ways: one way, the UV-B radiation breaks the enzyme activity of photosynthesis directly; the other way UV radiation restrains the photosynthesis indirectly. To a large extent, it decrease the rate of CO_2 conduction and stability, by restraining spiracles conduction or giving more resistence to spiracles, which will result in the decreasing of the rising rate (Prasad *et al.*, 2004 ; Wang *et al.*, 2010).

Materials and Methods

The high-yield hybrid rice "LiangYouPeiJiu" was studied, provided by the Institute of Agricultural Sciences of Jiangsu Nanjing, China. Field experiments were carried out at the experimental fields of the Institute of Agricultural Sciences of Jiangsu Nanjing. Raise the plants by using conventional fertilization. After the plants transplanted and turning green, the plants should be processed and each processing should be set three repetitions. Sampling was conducted from full expansion (22 August 2009) through advanced senescence (8 October 2009, near to harvesting time) of flag leaves on the mainculm. The sampling took place in the morning (07:30–11:30 h) on sunny days at approximately 2 weeks intervals, depending on the weather.

Processing Settings: Three groups are setted, CK group in which the high-yield hybrid rice is managed in conventional ways; L group in which the plants have been processed by using 16 kJ/m^2d doses of UV-B; H group in which the plants have been processed by using 40 kJ/m^2d doses of UV-B.

UV-B treated by using UV-B Light (QIN brand, produced in Baoji, 30 W, 297 nm), and suspend it over the plants vertically. Use 0.13 mm cellulose acetate membrane to filter out the UV under 290 nm, while use polyethylenemembrane to filter out the UV-B above 320 nm as comparision. Adjusting the distance between the UV-B Light and plants to control the intensity of UV-B radiation (Hang Rong *et al.*, 2002).

To analyze the Chl contents of the flag leaves, leaf samples were collected andimmediately frozen in liquid nitrogen. Leaf samples were extractedinice-cold 80% (v/v) acetone. The extract was centrifuged at 3,000 x g for 5min. The upper solution was measured with a UV-754 spectrophotometer (Shanghai Institute of Plant Physiology, Shanghai, China) at 645 nm and 663 nm. The Chl (a+b) were calculated as described by Arnon (1949). Malondialdehyde (MDA) was determined as anindicator of lipid peroxidation. Leaf tissue (1.0g fresh weight) was homogenized in 10ml of 5% (v: v) TCA and centrifuged at 20,000 x g for 10min. MDA in the supernatant was determined as thiobarbituric acid-reactive substances. The MDA content was expressed as nmol of MDA^{-1}g of freshweight (Zhao and Li, 1999). Activities of whole electron chain transport were measured polarographically with a Clark-type liquid-phase electrode (Chlorolab-2, Hansatech, UK) fitted with a circulating water jacket at 20 °C, similar to mean daily growth temperature during the sampling period. Actinic light from a slide projector was inserted into the side of the electrode chamber and the light intensity was 1,500 Amol m^{-2} s^{-1}. 2 ml reaction buffer (pH 7.6–7.8) contained 25 mmol Tricine, 5 mmol NaCl, 0.2 mol sucrose, 5 mmol $MgCl_2$, supplemented with 150 AM methyl viologen (MV), 2 mmol NaN_3, 0.2 mmol 2,6-dichlorophenol indophenol (DCPIP), with 2 mmol MV, 2 mmol NaN_3 and 5 mmol NH_4Cl for oxygen up take ($H_2O \rightarrow MV$, whole electron chain transport) (Chen *et al.*, 2004). Chla fluorescence measurements: Chla fluorescence transient of the flag leaf on the main culmin each plant was recorded in the morning (07:30–11:30 h) in the field with aplant efficiency analyzer (Handy PEA, Hansatech Instruments Ltd., King's Lynn, Norfolk, PE 304 NE, U.K.), having aninitial data acquisition rate of 10 ms (corresponding to a sampling rate of 100 kHz) during the first 2 ms and a sampling period of 1ms there after, with a 12 bit resolution (Strasser and Strasser, 1995). Flag leaves were dark adapted for at least 20 min before measurements and then illuminated with continuous red light (peak at 650 nm) for 1s with an intensity of 2,000 mol m^{-2} s^{-1} (sufficient excitation intensity to ensure closure of all PSII reaction centers to obtain a true fluorescence intensity of F_M) provided by an array of six light-emitting diodes focused on a circle of 5 mm diameter of the sample surface.

Statistical differences between species and between different days with respect to Chl contents, MDA content and Chl a fluorescence transient were analyzed by performing an analysis of variance (ANOVA) using the Microcal Origin (Version 7.0). Differences were considered significant at the $P < 0.05$ probability level.

Results and Discussion

Loss of chlorophyll (Chl) is an index of progress in leaf senescence (Baka and Aldesuquy, 1991). Photosynthetic pigments are important components of thylakoid membranes, the receptors of light and involved in the absorption, transmission and transformation of light during the photosynthesis. The content of photosynthetic pigment affects the photosynthetic capacity of plants directly. As Fig. 1 shown, the trends of the chlorophyll contents in CK group, L group, and H group vary consistently with each other. In CK group, after the full expansion of flag leaves of LYPJ from 0 d to 14 d the chlorophyll content remains relatively stable, and then begins to decline rapidly. In early development of the blades, the difference in the three groups is not significant ($P > 0.05$). In L group, the chlorophyll content was the highest at 21d after full expansion through senescence of flag leaves, and the difference of the three groups is significant ($P_{CK, L} = 0.014 < 0.05$; $P_{CK, H} = 0.048 < 0.05$). In H group, the content begins to decline after full expansion of flag leaves ($P_{0, 7} = 0.005 < 0.05$); the difference of the three group is significant; the trend of the content declines most rapidly. At 42d, the content in group H remains the lowest.

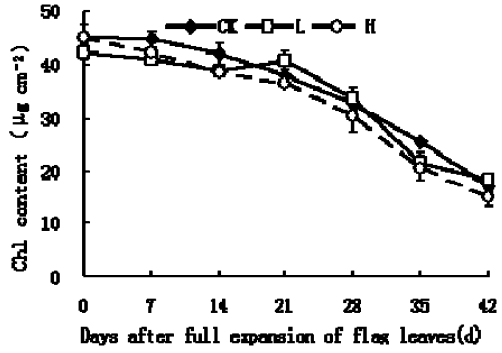

Fig. 1 Chlorophyll content versus days after emergence (DAFE) of flag leaves in a super-high-yield hybrid rice LYPJ treated UV-B in the field. Each value is the mean of three independent samples taken at the same time.Vertical bars indicate standard errors.

Malondialdehyde (MDA) content is the one of the major lipid peroxidation product and its accumulation reflects the level of lipid peroxidation (Elstner, 1982; Mascher *et al.*, 2005). Lipid peroxidation is an integral feature of membrane deterioration leading to cell death. It is evident from studies on cellular membranes that the physiological properties of membranes are deleteriously altered during senescence (Dalal and Khanna-Chopra, 1999). Fig. 2 shows that the MDA content of chloroplasts in the three treatment groups after full expansion of flag leaves is in a gradual upward trend, rising sharply at 28 d ($P < 0.05$). Throughout the process, the content in H group was the highest which indicates that with the raping of rice, free radicals in chloroplast increase and the level of membrane lipid peroxidation rises. That lipid peroxidation is exacerbated by UV-B and the exacerbation becomes serious with the increase of UV-B amount.

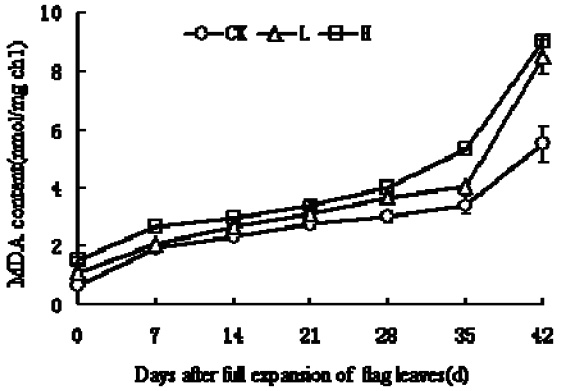

Fig. 2 MDA content versus days after emergence (DAFE) of flag leaves in a super-high-yield hybrid rice LYPJ treated UV-B in the field. Each value is the mean of three independent samples taken at the same time.Vertical bars indicate standard errors.

The photosynthetic electron transport activity of chloroplast thylakoid membrane can reflect the changes of primary photochemical reactions in the process of blades' senescence. We can see from Fig. 3 that the variation trends of the chloroplast electron transport chain in CK group, L group and H group are in consistency; whole electron chain all rise in the first half period and decline in the second half period; the trend reaches the highest at 14d and in L group the activity trend is the highest; after flag leaves full expansion, whole electron chain activity both reach the highest at 21d when PSII in CK group is the highest of all. The influences of CK and L are not very obvious ($P > 0.05$); the influences of CK and H are significant ($P < 0.05$). The PSII electron transport chain activity is in the sharpest decline.

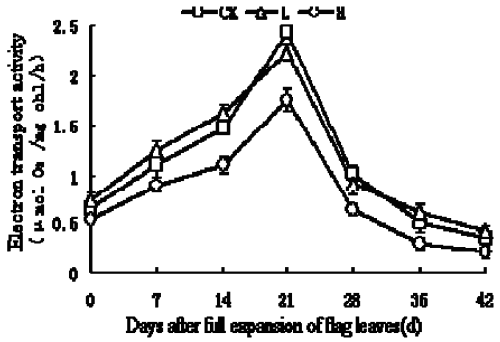

Fig. 3 Whole electron transport chain activity versus days after emergence (DAFE) of flag leaves in a super-high-yield hybrid rice LYPJ treated UV-B in the field. Each value is the mean of three independent samples taken at the same time.Vertical bars indicate standard errors.

F_V/F_M is the common characteristic index, used when plants face stress. It indicates the primary photochemical efficiency of PSII. Fig. 4 shows the trends of Fv/F_M in three groups are agreed with each other, rising at first and then declining; both the indexes in CK group and H group reach the maximum at 10 d after flag leaves full expansion, L group at 21 d when the difference with the CK group and H group is extremely significant ($P = 0.00 < 0.01$). The figure indicates that the primary photochemical efficiency of flag leaves declines at 10d after flag leaves full expansion and UV-B reduces flag leaves photochemical efficiency; the primary photochemical efficiency in H group which declines sharply at 21 d after flag leaves full expansion, can be delayed declining by low doses of UV-B which also increase the the photochemical efficiency.

F_V/F_M declines rapidly under stress, being an important index to show stress levels. The blades age from 10 d after full expansion of flag leaves, and low doses of UV-B can delay the senescence of flag leaves, UV-B increasing the Leaf senescence.

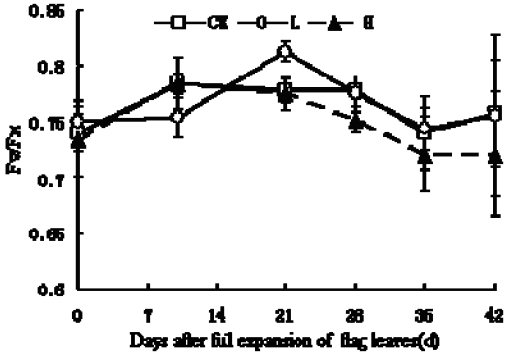

Fig. 4 Performance index F_V/F_M versus days after emergence (DAFE) of flag leaves in a super-high-yield hybrid rice LYPJ treated UV-B in the field. Each value is the mean of three independent samples taken at the same time.Vertical bars indicate standard errors.

F_M is the fluorescence when all the Q_A has been returned to Q_A the fluorescence production when PSII reaction center is fully closed. As is shown in Fig. 5, the F_M variation in CK group and L group agree with each other, rising at first, then declining and at last rising again; the trend in H group rises at the beginning and falls at last, changing slightly during the whole growth period. At 10d after flag leaves full expansion, the difference of the CK group, L group and H group is significant ($P_{CK,\ L} = 0.318 > 0.05$, $P_{CK,\ H} = 0.01 < 0.05$); at 21d after flag leaves full expansion, the difference becomes extremely significant ($P_{CK,\ L} = 0.00 < 0.01$, $P_{CK,\ H} = 0.01 < 0.01$); afterward, the F_M in CK group increasing rapidly ($P < 0.01$), reaches the maximum; in the later period, the index of CK group is higher than that of treatment group; at 42 d, the difference in the three groups was not significant. Studies show that the absorption of light declining, caused by the degradation of chlorophyll, or the inhibition of water photolysis, caused by the harm of the oxygen-evolving complex OEC, can cause the decrease of the F_M. The index in CK group declines sharply at 21 d after flag leaves full expansion, showing that the decrease of light absorption is also the stress response. In the later period, the capacity of absorption photosynthesis in CK group is higher than that in the treatment group. At 42 d flag leaves become senescent causing by the degradation of chlorophyll, the difference in the three groups is not obvious.

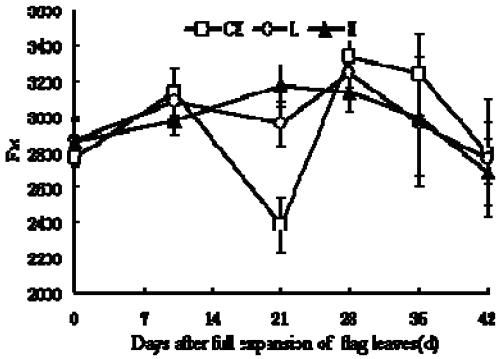

Fig. 5 Maximum fluorescence F_M versus days after emergence (DAFE) of flag leaves in a super-high-yield hybrid rice LYPJ treated UV-B in the field. Each value is the mean of three independent samples taken at the same time.Vertical bars indicate standard errors.

Initial fluorescence Fo is the fluorescent level when PSII reaction center is thoroughly open—the time that all Q_A oxidizes (Van *et al.*, 2004). Fig. 6 shows, throughout the growth period of the plant Fo

increases at first, then decreases and at last increases again; the difference amoung the three groups is not significant during flag leaves full expansion ($P_{CK,L} = 0.992 > 0.05$, $P_{CK,H} = 0.281 > 0.05$); the difference becomes significant after 10 d. Overall, the data in H group is higher than that in CK group and L group, suggesting that the process of plant senescence in H group may have been advanced. Fo has reached a small peak with the full expansion of flag leaves. With the maturatity of flag leaves and the improving of the photosynthetic function, Fo decreases, probably because in the process of maturity there are more LHCII produced in the reaction center, or probably because the the energy dissipation of PSII antenna increases.

Studies have shown that the energy dissipation exists mainly in the antenna pigment and it causes the Fo increasing, with the gradual aging flag leaves and the loss of the photosynthetic capacity. Many studies have shown that the damage or the reversible inactivation of the PSII reaction center can cause the increase of the Fo. From the Fig. 6 we can see that the structure of PSII reaction center is affected at 21 d after the flag leaves full expansion; the high doses of UV-B have great influenced PSII. Overall, the difference among H group, CK group and L group is not significant, indicating that high doses of UV-B have great influence on the photosynthetic capacity of flag leaves.

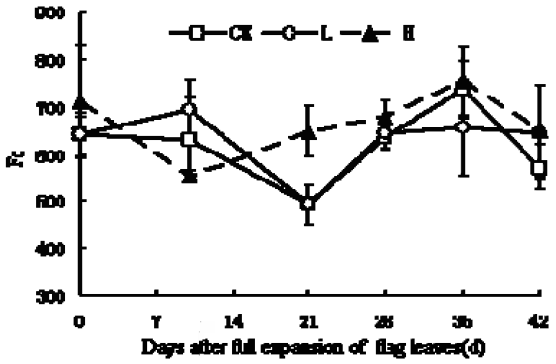

Fig. 6 Initial fluorescence versus days after emergence (DAFE) of flag leaves in a super-high-yield hybrid rice LYPJ treated UV-B in the field. Each value is the mean of three independent samples taken at the same time.Vertical bars indicate standard errors.

Discussion

In the senescence process of the plants, chloroplast senescence is the earliest change, the most direct and the most sensitive physiological event. The declining photosynthetic capacity is a major feature of flag leaves senescence which is often masured by chlorophyll degradation (Zhang MP *et al.*, 2010). The content of chlorophyll pigments is an important indicator to reflect the photosynthetic capacity of plants which changes according to the environment elements and causes the changes of photosynthetic performance (Kuo Tung Hung and Ching Huei Kao, 2004).

After the treatment of the plant "Liangyoupeijiu" in different intensity of UV-B radiation, the chlorophyll a/b in the treatment group is lower than that of the control group, indicating that the damage of the enhanced UV-B radiation on chlorophyll a is more serious than chlorophyllb. Chlorophyll b exists mainly in two main optical components of the antenna system (particularly in the antenna component of PSI), While chlorophyll a is mainly in the PSI, PSII core complex. That the core complex of the two optical systems is more sensitive to the enhanced UV-B compared with the peripheral antenna complex composition. especially in the later growth period, the senescence rate of the light-harvesting antenna in chloroplast thylakoid membrane is faster than that of the reaction center, thus affecting the absorption of light energy and resulting in the reduced photosynthesis. In addition, in the senscence process, although there is some degradation of chlorophyll a, the content of it is still higher than that of chlorophyll b, and in this process chlorophyll b can be converted to chlorophyll a, so the study indicates that in the senscence process, chlorophylla can play an important role in maintaining the consistency of the optical system structure and function.

Photosynthetic electron transport is the bond of a primary photophysical and photochemical reaction and the general biochemical reaction. In the process of flag leaves senescence, the changes of its activity have an impact on the photosynthetic oxygen evolution and photosynthetic phosphorylation activity, thereby affecting the photosynthetic capacity (Wang *et al.*, 2004).The mismatch between the electronic chain may break the original balance, causing the premature, and UV-B stress exacerbates that imbalance, increasing the chance of superoxide anion, thus accelerating the aging process. UV-B having the largest impact on the electron transport chain activity of PSII, indicates the main position that UV-B damages is PSII (Yu *et al.*, 1998).

Chlorophyll fluorescence parameters can be used as the internal probe of photosynthesis. The analysis of it can reveal the physiological state and the photosynthesis effect of plants in the process of absorption, transmission and conversion of light energy; to some extent, it can show the influence of the environmental elements on plants (for review see Strasser *et al.*, 2004). Fv/F_M is the maximum quantum yield of PSII photochemistry, reflecting the quantum when all the PSII reaction center are in the open state. PSII is directly proportional to the photochemical quantum efficiency. Studies have shown that paddy blades begin to aging from 14 d after flag leaves full expansion, and low doses of UV-B to a certain extent can slow down the aging. In the process of senescence and by the stress of high doses of UV-B, chlorophyll fluorescence parameters change significantly, such as the primary light energy conversion efficiency, specific activity parameters of photosynthetic apparatus, resulting in the decrease of the potential photosynthesis activity, the serious disruption of photosynthetic electron transport and the descent of thylakoids proton gradient, assimilation power to reduce, and ultimately affecting the conversion of light energy (Strasser, Srivastava *et al.*, 2000).

The super-high-yield hybrid rice "Liangyoupeijiu" in the aging process, its photosynthetic capacity declines. The decrease of the chlorophyll content not only is the symbol of flag leaves senscence, but also affects the chloroplasts absorption of light energy, specifically with the senescence of flag leaves chlorophyll b is more easily degraded than chlorophyll a. The light-harvesting antenna in the chloroplast thylakoid membrane is more susceptible to be injured, its aging rate faster, resulting in the decline of the light absorption capacity of the chloroplast. Chlorophyll a may protect the optical system structure and function in the aging process. On the other hand, the inactivation in parts of the PSII reaction center makes the light energy, used to dissipate hate, increase gradually, which results in the decrease of photosynthetic electron transport activity, thereby making the photosynthetic oxygen evolution and chloroplast photosynthetic phosphorylation activity decrease and the efficiency of light energy conversion decrease.The decrease of both the light energy absorption capacity of the chloroplast and the conversion efficiency has led to the decline of the photosynthetic function of flag leaves. Different intensity of UV-B results in different effects on the chloroplast, which affects the photosynthetic capacity of flag leaves (Gilbert *et al.*, 2004). PSII is the part of thylakoid membrane that is most sensitive to UV-B.

Conclusion

Studies have shown that low doses of UV-B can delay the senescence of flag leaves, playing a certain role in promoting the photosynthesis of flag leaves in the early development period; high doses of UV-B restrains the photosynthesis of the plants, exacerbate the chloroplast senscense, and therefore accelerates the rate of flag leaves senescence.

Acknowledgements

Financial support was provided by the National Natural Sciences Foundation of China (30771299), by grants from the National Basic Research Program of China (2009CB118500) and by the ShanXi Province Natural Sciences Foundation (2009021030-2). We also want to thank Lv ChuanGen provided material.

References

Arnon DI (1949) Copper Enzymes in Isolated Chloroplasts: Polyphenoloxidase in Beta Vulgaris. Plant Physiol 24: 1-15

Baka ZAM, Aldesuquy HS (1991) Changes in Ultrastructure and Hormones of the Fully Senescent Leaf of Senecio Aegyptius. Beitr Biol Pflanz 66: 271-280

Brosche M, Strid A (2003) Molecular Events Following Perception of Ultraviolet-B Radiation by Plants. Physiol Plant 117: 1-10

Chen GX, Liu SH, Zhang CJ, *et al*. (2004) Effects of Drought on Photosynthetic Characteristics of Flag Leaves of a Newly-Developed Super-High-Yield Rice Hybrid. Photosynthetica 42 (4): 573-578

Dalal M, Khanna-Chopra R (1999) Lipid Peroxidation Is an Early Event in Necrosis of Wheat Hybrid. Biochem Biophys Res Commun 262: 109-112

Elstner EF (1982) Oxygen Activation and Oxygen Toxicity. Ann Rev Plant Physiol 33: 73-96

Gilbert M, Skotnica J, Weingart I (2004) Effects of UV Irradiation on Barley and Tomato Leaves: Thermoluminescence to Screen the Impact of UV

Radiation on Crop Plants. Functional Plant Biology 31: 825-845

Hang R, Wang XL (2002) Influence of He-Ne Laser Irradiation on the Excision Repair of Cyclobutyl Pyrimidine in the Wheat DNA. Chinese Science Bulletin 47(10): 818-821

Jelte Rozema, Bas van Geel，Lars Olof Bjorn, *et al*. (2002) Toward Solving the UV Puzzle. Science 296: 1621-1622

Kuo Tung Hung, Ching Huei Kao (2004) Hydrogen Peroxide Is Necessary for Abscisic Acidinduced Senescence of Rice Leaves. J Plant Physiol. 161: 1347-1357

Mascher R, Nagy E, Lippmann B, Hornllein S, Fischer S, Scheiding W, *et al*. (2005) Improvement of to Lerance to Paraquatand Drought in Barley (Hordeum Vulgare L.) by Exogenous 2-Aminoethanol: Effects on Superoxide Dismutase Activity and Chloroplast Ultrastructure. Plant Sci. 168: 691-698

Nedunchezhian N, Kulandaivelu G (1991) Effects of UV-B Enhanced Radiation on ribulose-1, 5-Biophosphate Carboxylase in Leaves of Vigna sSinensis L. Photosynthetica 25: 431-435

Prasad SM, Zeeshan M (2004) Effect of UV-B and Monocrotophos, Singly and in Combination, on Photosynthetic Activity and Growth of Nonheterocystous Cyanobacterium Plectonema Boryanum. Environ. Exp. Bot. 52: 175-184

Strasser BJ, Strasser RJ (1995) Measuring Fast Fluorescence Transients to Address Environmental Questions: the JIP-Test. In: Mathis P (ed.), Photosynthesis: from Light to Biosphere, Vol. V. Kluwer Academic Publishers: Dordrecht, pp. 977-80

Strasser RJ, Srivastava A, Tsimilli-Michael M (2000) The Fluorescence Transient As a Tool to Characterize and Screen Photosynthetic Samples. In:Yunus M, Pathre U, Mohanty P (eds.), Probing Photosynthesis: Mechanism, Regulation and Adaptation. Taylor and Francis Press: London 25: 445-483

Van Heerden PDR，Strasser RJ, Krüger GHJ (2004) Reduction of Dark Chilling Stress in N2-Fixing Soybean by Nitrate As Indicated by Chlorophyll a Fluorescence kinetics. Physiol Plant 121: 239-249

Wang Gh, Hao Zj, Ralf H, *et al*. (2010) Effects of UV-B Radiation on Photosynthesis Activity of Wolffia Arrhiza As Probed by Chlorophyll Fluorescence Transients. Advances in Space Research 45: 839-845

Wang N, Chen GX, Lu CG (2004) Studies on Photosynthetic Characteristics of Flag Leaves in Hybrid Rice Liangyou Peijiu and its Parents. Hybrid Rice 19(1): 53-55

Yu SW, Tang ZC (1998) Plant Physiology and Molecular Biology. Beijing: Science Press. 100-105

Zeeshan M, Prasad SM (2009) Differential Response of Growth, Photosynthesis, Antioxidant Enzymes and Lipid Peroxidation to UV-B Radiation in Three Cyanobacteria. Journal of South African Botany 75: 466-474

Zhao SM, Li DQ (1999) In the Modern Experimental Directory on Plant Physiology. Science Press: Beijing, pp. 305-306

Zhang MP, Zhang CJ, Yu GH, Jiang YZ, *et al*. (2010) Changes in Chloroplast Ultrastructure, Fatty acid Components of Thylakoid Membrane and Chlorophyll a Fluorescence Transient in Flag Leaves of a Super-High-Yield Hybrid Rice and Its Parents during the Reproductive Stage. Journal of Plant Physiology 167: 277-285

Effect of Exposure to UVA Radiation on Photosynthesis and Isoprene Emission in *Populus x Euroamericana*

Emanuele Pallozzi[a], Giovanni Marino[a], Alessio Fortunati[a], Francesco Loreto[b], Mauro Centritto[a,*]

[a]Institute of Agro-environmental and Forest Biology, National Research Council, 00015 Monterotondo (RM), Italy;
[b]Institute of Plant Protection, National Research Council, 50019 Sesto Fiorentino (FI), Italy.
[*]Corresponding author. Tel. No. +39 06 90672524; Fax No. +39 06 9064492; E-mail: mauro.centritto@cnr.it.

Abstract: Isoprene, which accounts for about 40% of the global emission of biogenic volatile organic compounds, plays a dual role in the plant-environment interactions. Outside the plants, isoprene can substantially increase the amount of tropospheric ozone in the atmosphere, whereas in plants isoprene plays a protective role under different stress conditions. The magnitude of isoprene emissions may be altered by increasing UVA radiation. We examined the effects of acute UVA radiation on carbon assimilation, isoprene emission, and photochemical reflectance index (PRI) in *Populus x euroamericana* saplings. Plants were exposed to either ambient UVA (30 W m^{-2}) or enhanced UVA (60, 90 and 120 W m^{-2}) radiation until the treated leaves had shown stable values of photosynthesis. Our results show that the inhibition of photosynthesis and stomatal conductance induced by high UVA radiation was mirrored by similar reduction in PRI. In contrast, isoprene emission was strongly stimulated by increasing doses of UVA radiation, confirming that isoprene formation may have direct or indirect functions in increasing plant tolerance to stresses. These findings may be likely relevant to predict the emissions of isoprenoid in globally changing environmental condition, global atmospheric chemistry, carbon cycles and climate.

Keywords: Gas exchange; Isoprene emission; Photosynthetic reflectance index (PRI); Ultraviolet A (UVA)

Introduction

Anthropogenic climate change impact on terrestrial ecosystems is projected to increase globally (Centritto *et al*., 1999). These changes include also enhanced ultraviolet A (UVA) radiation (320–400 nm) radiation caused by stratospheric ozone depletion. UVA radiation has an extensive impact on the biosphere. Increased UVA is likely to have both direct and indirect implications on photosynthesis, as well as on the carbon emitted by many plant species in the form of isoprene and other biogenic volatile organic compounds (BVOC). These primary and secondary metabolisms are now accepted as important components of the biosphere's response to climate change (Centritto *et al*., 2011) and, consequently, there is great interest in determining their sensitivity not only to the short-wave radiation load, but also to the radiation quality. This knowledge is particularly relevant for isoprene formation which, besides having an intriguing ecological role in emitting plants (Vickers *et al*., 2009), is very reactive and influences both the atmospheric chemistry composition and physics. Consequently, any change in the potential emission of isoprene will impact on air chemistry and quality at regional and global level.

Isoprene formation occurs in the chloroplast and is closely connected to photosynthesis in non-stressed plants, because about 72%–91% of the carbon in the isoprene molecule originates from fresh photosynthates which are then the primary substrate for isoprene biosynthesis (Brilli *et al*., 2007). Thus, because UV radiation directly affects photosynthesis and stomatal conductance (Paul and Gwynn-Jones, 2003), UVA is expected to negatively impact on isoprene emission by increasing resistance to its

emission and by altering the carbon supply into its biosynthesis. However, the literature shows that BVOCs emission is not only resistant to abiotic stress but is often elicited by stress occurrence (Loreto and Schnitzler, 2010; Velikova *et al*., 2010). We specifically examined the effects of acute UVA radiation on carbon assimilation, isoprene emission, and photochemical reflectance index (PRI). In particular we address two main issues: 1) whether above-ambient levels of UVA stimulate isoprene emission, and 2) how spectral reflectance is modified when plants suffer from different levels of UVA load.

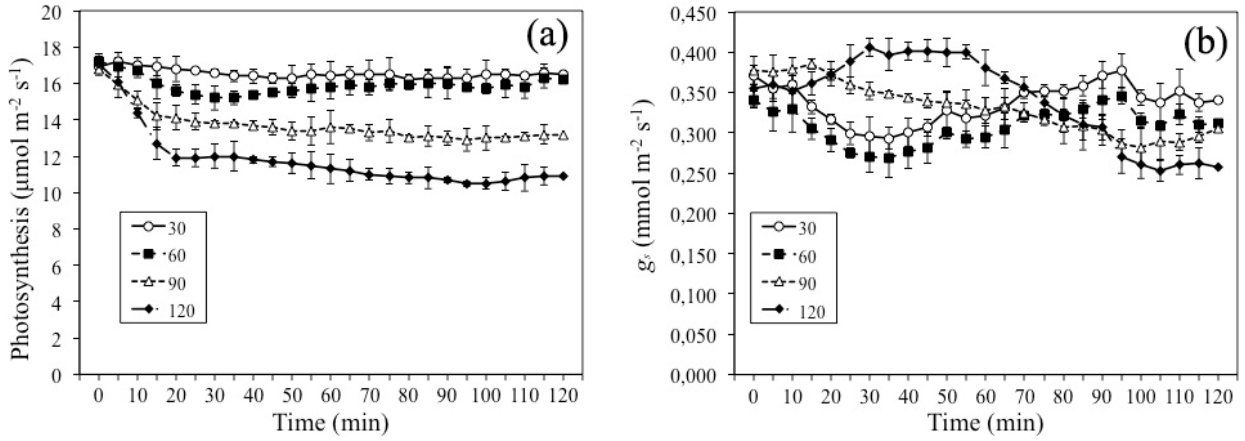

Fig. 1 Photosynthesis (a) and stomatal conductance (g_s, b) measurements in *P. euroamericana* saplings treated with increasing UVA energy intensities: 30 (O), 60 (■), 90 (Δ), and 120 (◆) W m^{-2}. Symbols represent average ± SE (n = 5).

Materials and Methods

Populus x euroamericana saplings were propagated from physiologically mature trees and potted in 1 L pots. After rooting, saplings were transplanted in 4 L pots, filled with commercial soil, and grown in a greenhouse under controlled conditions. The plants were regularly watered and fertilized with Hoagland solution once a week to supply mineral nutrients at free access rate (Centritto, 2005). The relative humidity was maintained between 50% and 60%, the light intensity was 800 μmol m^{-2} s^{-1} (12 h as a photoperiod), and the temperature was 30/25 °C day/night. UVA radiation was obtained from ENFIS 4-channel 180 W led lamps (ENFIS ltd, UK), controlled by LE Sentinel 2.2 software (ENFIS). UVA intensity was measured with a quantum-photoradiometer and thermometer DO 9721 (Delta Ohm Srl, PD, Italy) equipped with a Data-logger probe LP9021 UVA (Delta Ohm). Five plants were exposed to ambient UVA radiation (30 W m^{-2}), or enhanced UVA (60, 90 and 120 W m^{-2}) until the treated leaves had shown stable values of photosynthesis.

Photosynthesis (A), and stomatal conductance (g_s) were measured using a portable gas exchange system (LI-6400, LI-COR, Lincoln, NE, U.S.A.). Measurements were carried out at photosynthetically photon flux density (PPFD)-saturated photosynthesis (1,000 μmol m^{-2} s^{-1}). Leaf temperature was set at 30 °C, and the relative humidity in the leaf cuvette ranged between 45%–55%. Leaves were exposed to a flux of synthetic air, free of contaminants and pollutants, comprising N_2, O_2 and CO_2 in atmospheric concentrations (80%, 20% and 380 ppm, respectively). Isoprene and methanol emission was measured on-line with a proton transfer reaction-mass spectrometer (PTR-MS; Ionicon, Innsbruck, Austria) by diverting a small flux of the air flowing out of the cuvette to the instrument. The PTR-MS was set in a single ion mode to record trace of protonated isoprene (m/z 69).

The same leaves analyzed for gas-exchange and PTR-MS measurements, before and after the UVA treatments, were used to measure leaf reflectance response. Reflectance was measured by a spectrometer (ASD FieldSpec 3, Analytical Spectral Devices, Inc., Boulder, CO, U.S.A.) with a spectral range from 350 to 1,050 nm, equipped with an optic fiber probe with an angular field of view of 25°. The probe was placed at 5 cm from the adaxial leaf surface with an angle of 60°, to avoid shadow effect on the analyzed leaf surface. Reflectance measurements were calibrated with respect to a white reference measure, using a 99% reflective BaSO4 panel. Data of reflectance at 531 and 570 nm were collected for the calculation of photochemical reflectance index (PRI), which is

linked to xanthophyll pigments cycle (a component of non-photochemical de-excitation pathway) and it is sensitive to changes in photosynthetic light use efficiency (Gamon *et al*., 1997; Sun *et al*., 2008). This index is formulated as: $PRI = (R_{531} - R_{570})/(R_{531} + R_{570})$, where reflectance at 531 nm (R_{531}) corresponds to the waveband affected by the xanthophyll cycle status, and 570 nm (R_{570}) is the reference waveband that normalizes the value of the index.

Results and Discussion

To investigate the effect of UVA exposure on plant physiology, acute treatments at different and increasing UVA intensities (30, 60, 90, and 120 W m^{-2}, respectively) were performed. Exposure to 30 W m^{-2} of UVA did affect either A or g_s (Fig. 1). At 60 W m^{-2}, after an initial small decline (after *ca.* 30 min of UVA treatment), plants showed a complete recovery of photosynthesis (Fig. 1a), while g_s was not affected by UVA (Fig. 1b). Stronger effect on plant physiology of UVA radiation was observed treating poplar saplings with 90 and 120 W m^{-2} of intensity. Twenty minutes after starting the irradiation, plants showed a decline of photosynthesis of *ca.* 30% and 40%, compared to the pre-stress values, under UVA = 90 and 120 W m^{-2} (Fig. 1a), respectively. Plant exposure to very high UVA affected also g_s. Plants showed a decrease in stomatal conductance of *ca.* 25% and 35%, with respect to the control levels, after the irradiation with UVA = 90 and 120 W m^{-2}, respectively (Fig. 1b). Overall, our results confirm that the photosynthetic apparatus is rather resistant to enhanced UV radiation (Caldwell *et al*., 2003).

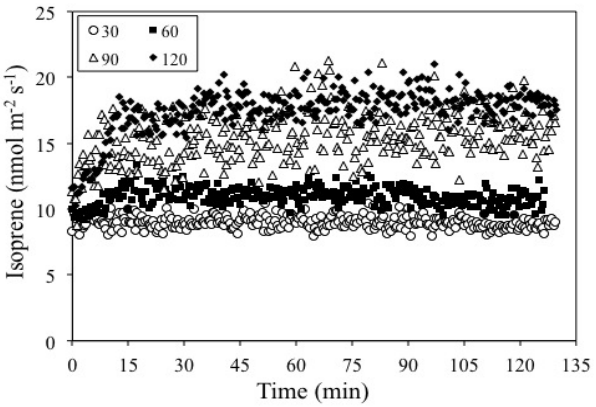

Fig. 2 Isoprene emission measurements on *P. euroamericana* saplings treated with increasing UVA energy intensities: 30 (○), 60 (■), 90 (Δ), and 120 (◆) W m^{-2}.

To study if the physiological effect of high UVA radiation doses could also affect volatile organic compound emission, isoprene release from the treated leaves was monitored on line during the experiments. Only few studies have reported on the impact of either acute or chronic UVB radiation on BVOC emission so far (Harley *et al*., 1996; Tiiva *et al*., 2007; Blande *et al*., 2009; Faubert *et al*., 2010). These studies, however, show contradictory results. It was shown by Harley *et al*. (1996) that enhanced UV-B significantly increased isoprene emission in *Quercus gambelii* but not in *Acer platanoides* and *Mucuna pruriens*. Furthermore, Tiiva *et al*. (2007) found that in subarctic fen enhanced UVB significantly increased the emission of isoprene during the warm periods of the second growing season, and at the end of the fourth growing season. Whereas in contrast, they did not detect significant UV-B effects on the emissions during the warm period in the third growing season. Recently, Faubert *et al*. (2010) showed no overall UV-B effect on the BVOC emissions, apart from toluene and 1-octene, from a subarctic peatland.

However, to our knowledge, there are no earlier data on UVA effects on isoprene emissions from broadleaf trees. Our results show that ambient UVA (30 W m^{-2}) does not affect isoprene emission, which remained stable, at *ca.* 10 nmol m^{-2} s^{-1} during the treatment (Fig. 2); while plant exposure at UVA of 60, 90 or 120 W m^{-2} progressively and dramatically increased isoprene emission (Fig. 2). The increased emissions cannot be explained by the changes in C assimilation as photosynthesis was inhibited. Plant volatiles are also recognized as important protective and signaling compounds (Vickers *et al*., 2009). We showed here, for the first time, that enhanced UVA radiation uncoupled isoprene emission from photosynthesis. This confirms that environmental stresses may increase the fraction of the photosynthetic carbon budget allocated to isoprene, or may stimulate a cross-talk with carbon sources for isoprene formation alternative to photosynthesis intermediates (Brilli *et al*., 2007). Furthermore, because environmental stresses are known to reduce chloroplastic CO_2 concentration (C_c), it may be speculated that isoprene emission enhancement under stress conditions often depends on whether leaves operate at low C_c.

The photochemical reflectance index measurement was used as a remote sensing method to assess physiological alterations occurring in poplar leaves

treated with UVA. PRI was originally developed to estimate rapid changes in the xanthophyll cycle that occurs over a minute time scale and are related to changes in photosynthetic light use efficiency (Gamon *et al*., 1992). In leaves treated with ambient UVA radiation PRI was not significantly affected (Fig. 3). Whereas PRI PRI showed a progressively, significant decrease as the intensity of UVA radiations increased from 60 to 120 W m^{-2}. This inhibition mirrored the decrease in photosynthetic rate which occurred in the high UVA-treated leaves, and is in general related to a loss of photosynthetic light use efficiency (Gamon *et al*., 1997; Sun *et al*., 2008).

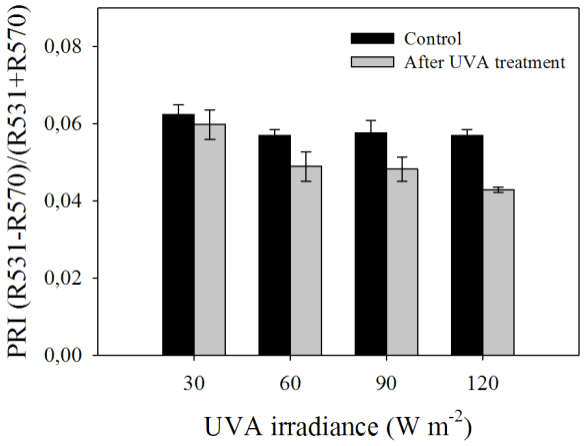

Fig. 3 Photosynthetic reflectance index (PRI) measurements on *P. euroamericana* saplings in control (black bars) and after irradiation with UVA = 30, 60, 90, and 120 W m^{-2} (gray bars). Symbols represent average ± SE (n = 5).

In conclusion, because of the increased stratospheric ozone depletion, plant responses to UV radiation have become a major area of concern. UV radiation-mediated modification in the gases exchanged by plants plays a major role in the biosphere-atmosphere interactions. Our study has provided an analysis of the components of gas exchange that undergo change when *Populus x euramericana* is exposed to a range of acute UVA doses. When taken together, the findings of this study clearly show that (1) the inhibition of photosynthesis and stomatal conductance induced by high UVA radiation was also detected by monitoring changes of the leaf spectral reflectance (namely, PRI) and this may have interesting applications for both proximal and remote sensing of UV damage; and (2) isoprene emission was strongly stimulated by enhanced UVA; this may confirm an isoprene direct protective function as well as may indicate the onset of a stress response that activates antioxidants and may feed-forward on associated plant responses against abiotic or biotic stresses. These results are important to our understanding of tree function in response to changing environmental conditions and their contribution to the BVOC emissions, which are important in the atmospheric chemistry and feedbacks on climate change.

Acknowledgement

This work has been funded by Italian National Research Council (project RSTL-DG.RSTL.010.003).

References

Blande JD, Turunen K, Holopainen JK (2009) Pine Weevil Feeding on Norway Spruce Bark Has a Stronger Impact on Needle VOC Emissions than Enhanced Ultraviolet-B Radiation. Environ. Poll. 157: 174-80

Brilli F, Barta C, Fortunati A, Lerdau M, Loreto F, Centritto M (2007) Response of Isoprene Emission and Carbon Metabolism to Drought in White Poplar (Populus Alba) Saplings. New Phytol. 175: 244-254

Caldwell MM, Ballare CL, Bornman JF, Flint SD, Bjorn LO, Teramura AH, Kulandaivelu G, Tevini M (2003) Terrestrial Ecosystems, Increased Solar Ultraviolet Radiation and Interactions with Other Climatic Change Factors. Photochem Photobiol Sci 2: 29-38

Centritto M (2005) Photosynthetic Limitations and Carbon Partitioning in Cherry in Response to Water Deficit and Elevated [CO_2]. Agric. Ecosys. Environ. 106: 233-242

Centritto M, Lee HSJ, Jarvis PG (1999) Long-Term Effects of Elevated Carbon Dioxide Concentration and Provenance on Four Clones of Sitka Spruce (Picea Sitchensis) I. Plant Growth, Allocation and Ontogeny. Tree Physiol. 19: 799-806

Centritto M, Tognetti R, Leitgeb E, Střelcová K, Cohen S (2011) Chapter 3: Above Ground Processes—Anticipating Climate Change Influences. In: Bredemeier M, Cohen S, Godbold DL, Lode E, Pichler V, Schleppi P (eds.), Forest Management and the Water Cycle: an Ecosystem-

Based Approach. Ecological Studies 212. Springer: Dordrecht, pp. 31-64

Faubert P, Tiiva P, Rinnan Å, Räsänen J, Holopainen JK, Holopainen JK, Kyrö E, Rinnan R (2010) Non-Methane Biogenic Volatile Organic Compound Emissions from a Subarctic Peatland under Enhanced UV-B Radiation. Ecosystems 13: 860-873

Gamon JA, Serrano L, Surfus JS (1997) The Photochemical Reflectance Index: an Optical Indicator of Photosynthetic Radiation Use Efficiency across Species, Functional Types, and Nutrient Levels. Oecologia 112: 492-501

Harley P, Deem G, Flint S, Caldwell M (1996) Effects of Growth under Elevated UV-B on Photosynthesis and Isoprene Emission in Quercus Gambelii and Mucuna Pruriens. Glob. Change Bio. 2: 149-154

Loreto F, Schnitzler JP (2010) Abiotic Stresses and Induced BVOCs. Trends Plant Sci. 15: 154-166

Paul ND, Gwynn-Jones D (2003) Ecological Roles of Solar UV Radiation: towards an Integrated Approach. Trends Eco. Evol. 18: 48-55

Sharkey TD, Singsaas EL (1995) Why Plants Emit Isoprene. Nature 374: 769

Sun P, Grignetti A, Liu S, Casacchia R, Salvatori R, Pietrini F, Loreto F, Centritto M (2008) Associated Changes in Physiological Parameters and Spectral Reflectance Indices in Olive (Olea Europaea L.) Leaves in Response to Different Levels of Water Stress. Int. J. Rem. Sens. 29: 1725-1743

Tiiva P, Rinnan R, Faubert P, Räsänen J, Holopainen T, Kyrö E, Holopainen JK (2007) Isoprene Emission from a Subarctic Peatland under Enhanced UV-B Radiation. New Phytol. 176: 346-55

Velikova V, Tsonev T, Loreto F, Centritto M (2010) Changes in Photosynthesis, Mesophyll Conductance to CO_2, and Isoprenoid Emissions in Popolus Nigra Plants Exposed to Excess Nickel. Environ. Poll. doi:10.1016/j.envpol.2010.10.032.

Vickers CE, Gershenzon J, Lerdau MT, Loreto F (2009) A Unified Mechanism of Action for Volatile Isoprenoids in Plant Abiotic Stress. Nature Chem. Ecol. 5: 283-291

Effects of Salt Stress on Photosystem II Efficiency and CO_2 Assimilation in Two Syrian Barley Landraces

Hazem M Kalaji [a,*], Govindjee [b], Karolina Bosa [a], Janusz Kościelniak [c], Krystyna Żuk-Gołaszewska [d]

[a] Department of Plant Physiology, Faculty of Agriculture and Biology, Warsaw University of Life Sciences SGGW, Poland;
[b] Departments of Biochemistry, and Plant Biology, University of Illinois, Urbana, Illinois-61801, USA;
[c] Department of Pomology, Faculty of Horticulture and Landscape Architecture, Warsaw University of Life Sciences SGGW, Poland;
[d] Department of Agrotechnology and Crop Production Management, University of Warmia and Mazury in Olsztyn, Poland.
* Corresponding author. Tel. No. +48 22-608079998; Fax No. +48 22 6425923; E-mail: hazem@kalaji.pl.

Abstract: Gas exchange and chlorophyll (Chl) a fluorescence measurements were made to study the effect of salinity stress (120 mmol NaCl) on the photosynthetic activity of two Syrian barley (*Hordeum vulgare* L.) landraces, Arabi (A.) Aswad and A Abiad. Our work provides important information on the detection of salt stress-induced changes in the two cultivars of barley used, since we measured, in parallel, both gas exchange and Chl fluorescence. Early reactions of the photosynthetic apparatus of barley plants must play a key role in their tolerance to salt stress. We expect extension of this research to be helpful in solving the salinity problem and other environmental challenges facing us.

Keywords: Barley; Chlorophyll fluorescence; Photosynthesis; Photosystem II

Introduction

Barley (*Hordeum vulgare* L.) is the fourth largest cereal crop in the World and, according to Jiang *et al*. (2006), it is one of the most salt tolerant crop species. However, salinity limits barley production and is one of the major abiotic stresses. The mechanisms of salt tolerance are very complex and the metabolic sites of salt influence have not been fully investigated, in particular in the photosynthetic apparatus (Kalaji and Nalborczyk, 1991; Kalaji and Pietkiewicz, 1993; Munns, 2002); thus, there are no reliable indicators of plant tolerance to salinity that could be used by plant breeders to improve salinity tolerance.

Chlorophyll *a* fluorescence kinetics is an informative tool for studying the effects of different environmental stresses on photosynthesis (see *e.g.*, Kalaji and Nalborczyk, 1991; Strasser *et al*., 2000; Fricke and Peters, 2002; Kalaji and Rutkowska, 2004; Kalaji *et al*., 2004; see chapters in Papageorgiou and Govindjee, 2004, reprinted 2010; Papageorgiou *et al*., 2007. It is important to state that the simplest and the most accepted hypothesis is that the major determinant of chlorophyll fluorescence is the redox state of Q_A, the first quinone electron acceptor of PSII: when it is in the oxidized state, fluorescence is low, and when it is in the reduced state, it is high; thus, the net concentration of Q_A^- is related to chlorophyll fluorescence yield (Duysens and Sweers, 1963; Govindjee, 1995, 2004). Further, the "O" level (or F_o) is the minimum fluorescence level when all Q_A is in the oxidized state, the reaction centers II are open; and the primary photochemistry is maximum, whereas at the "P" level (or F_{max}), fluorescence is maximum, when all Q_A is in the reduced state (Q_A^-); here, the reaction centers II are closed, and there is a traffic jam of electrons on the electron acceptor side of photosystem I and the primary photochemistry is at a minimum level (Munday and Govindjee, 1969 a, b; Govindjee, 1995, 2004).

The aim of the present study was to improve our knowledge of the responses of the barley plant photosynthetic apparatus to salinity stress through

application of the combined rapid and non-destructive fluorescence assay and gas exchange measurements. We present here some of the highlights of this research. Further details are available in Kalaji *et al*. (2010).

Abbreviations (Based on Strasser *et al*., 2000)

ABS/RC—light absorption flux (for antenna chlorophylls) per reaction center (RC),

DI_o/RC—dissipation energy flux per reaction center (RC) (at t=0),

ET_o/RC—electron transport flux (beyond Q_A^-) per reaction center (RC) (at t=0),

TR_o/RC—trapped energy flux (leading to Q_A reduction) per reaction center (RC) (at t=0),

RC/ABS—density of reaction centers per antenna chlorophyll,

Area—the area above the chlorophyll fluorescence curve (reflecting the size of the platoquinone pool),

$\Delta V/\Delta t_o$—the initial slope of the relative variable fluorescence which directly describes the trapping flux TR_o/RC,

F_o—minimum level of chlorophyll fluorescence

F_m—maximum level of chlorophyll fluorescence

F_v/F_m—a value that is related to the maximum quantum yield of PSII,

F_v/F_o—a value that is proportional to the activity of the water-splitting complex on the donor side of the PSII,

g_s—stomatal conductance,

k_N—the non-photochemical de-excitation rate constant in the excited antennae for non-photochemistry,

k_P—the photochemical de-excitation rate constant in the excited antennae of energy fluxes for photochemistry,

N—the number indicating how many times Q_A is reduced while fluorescence reaches its maximal value,

PI_{ABS}—the performance index calculated as: (RC/ABS) × (φ_{Po}/(1−φ_{Po})) × (ψ_o /(1− ψ_o)), where, RC is for reaction center; ABS is for absorption flux; φ_{Po} is for maximal quantum yield for primary photochemistry; and ψ_o is for the quantum yield for electron transport

P_N—net photosynthetic rate (measured as CO_2 uptake/ exchange),

SFI_{ABS}—an indicator of PSII 'structure and functioning', calculated as (RC/ABS) × φ_{Po} × ψ_o,

S_M—(*Area*) / (Fm-Fo), representing energy necessary for the closure of all reaction centers,

S_M/T_{FM}—the ratio representing the average redox state of Q_A in the time span from 0 to T_{FM} and, concomitantly, the average fraction of open reaction centers during the time needed to complete their closure,

SumK—the sum of photochemical rate constant k_P and non-photochemical rate constant k_N (Havaux *et al.*, 1991), where, **kn** = kh (rate constant of heat dissipation) + kf (rate constant of fluorescence emission) + kx (rate constant of energy migration to PSI),

T_{FM}—time needed to reach F_m,

Vj—relative variable fluorescence at time J (relative variable fluorescence at phase J of the fluorescence induction curve,

φ_{Do}—thermal dissipation yield,

φ_{Eo}—electron transport yield,

$\varphi_o/(1-\varphi_o)$—a 'conformation' term for primary photo-chemistry,

$\psi_o/(1-\psi_o)$—'conformation' term for thermal reactions (non-light dependent reactions).

Materials and Methods

Two barley (*Hordeum vulgare* L.) cultivars, Arabi Abiad (A. Abiad) and Arabi Aswad (A. Aswad), were grown in a computer-controlled greenhouse in 1liter dark glass pots filled with a modified Hoagland nutrient solution. The average temperature for day/night was 26/18 ^oC, relative humidity was 50%−60%, the photoperiod for the day/night cycle was 16/8 h, and the maximum photosynthetically active radiation used was ~ 1,400 μmol (photons) m^{-2} s^{-1}. After 7 days of growth, the seedlings were subjected to salinity stress. Sodium chloride was added to the nutrient solution to obtain a final concentration of 120 mmol. Plant gas exchange (net photosynthetic (CO_2) rate—P_N and stomatal conductance—g_s) and chlorophyll *a* fluorescence measurements were performed directly after stress application (24 h; 8 days after emergence) to monitor prompt reactions of photosynthetic apparatus, and 7 days after stress application (14 days after emergence) to allow observations of further stress application effects before the senescence of first, second and third leaves.

Gas exchange parameters were measured by CIRAS-2 *Photosynthesis Measurements System* (PP Systems International, Inc., Amesbury, MA, U.S.A.). Chlorophyll fluorescence parameters were measured using the *Plant Efficiency Analyzer* (HandyPEA fluorimeter, Hansatech Instruments Ltd., Pentney, King's Lynn, Norfolk, England).

Barley seedlings were pre-darkened for 45−60 minutes at room temperature. Chlorophyll *a* fluorescence induction transients were measured when leaves were exposed to a strong light pulse (3,500 μmol (photons) m^{-2} s^{-1}); these data were analyzed and the so-called JIP-test was conducted using Biolyzer v.3.0.6 software (both developed in the Laboratory of Bioenergetics, University of Geneva, Switzerland) (Strasser *et al*., 2000; for a review see Stirbet and Govindjee, 2011).

Chlorophyll fluorescence measurements and gas exchange were performed on the 1st, 2nd and 3rd leaves of barley plants. However, only the average values are shown in this paper. Measurements of chlorophyll fluorescence were made on 30 plants from each treatment and we had 3 replicates for each plant (n = 90) while the gas exchange measurements were performed on 3 plants from each treatment and we had 3 replicates for each plant (n = 9).

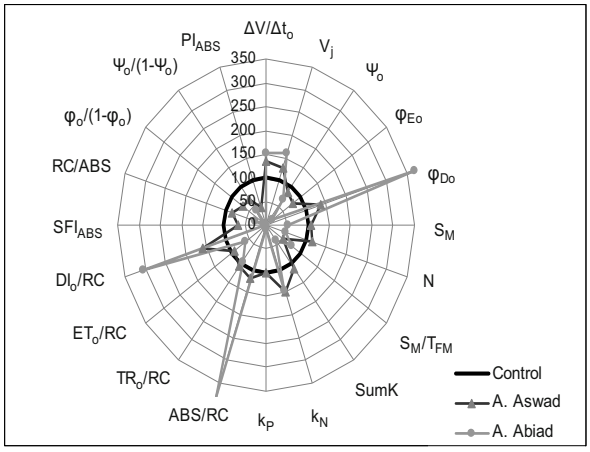

Fig. 1 A 'spider plot' of selected parameters characterizing behavior of Photosystem II of barley leaves, exposed for 7 days to 120 mmol NaCl. All values are shown as percent of control (control plants = 100).

Results and Discussion

We found that the photosynthetic apparatus of A Aswad was much more tolerant to salt treatment, compared with that of A. Abiad. Further, we found that the first stage of salinity effect on photosynthesis of barley plants is related to stomatal conductance limitation rather than to photosystem II (PSII) activity reduction (data not shown). Salinity treatment caused a decrease in both the rates of photosynthesis and PSII activity, the latter evaluated from chlorophyll (Chl) fluorescence signals. After 1 day of salt application, CO_2 uptake (photosynthetic rate - P_N) and stomatal conductance (g_s) decreased by ~20%−30% in the case of A. Abiad, whereas A. Aswad was unaffected. Surprisingly, a significant decrease of Performance Index (PI_{ABS}) was observed in A. Aswad, but less so in A. Abiad (data not shown).

The Performance Index was drastically lowered for both the cultivars after 7 days of stress application (Fig. 1). After 7 days of growth under salinity stress, time to reach F_m (T_{FM}) in A. Aswad increased significantly (ca. 200%), whereas it decreased (ca. 70%) in A. Abiad, relative to control plants (Table 1). The value of the *Area* parameter (the area above the chlorophyll fluorescence curve between F_o and F_m) of A. Aswad plants decreased to only ~ 65% of the value determined in control treatments; in contrast, the sensitive A. Abiad had a very low value (ca. 10%). Further, the maximal efficiency of PSII (calculated from F_v/F_m) decreased only slightly in A. Aswad, but drastically to ~ 25% in A. Abiad. Similarly, F_v/F_o values were reduced upon salinity treatment: A. Aswad had still a value that was ~ 70% of control; however, this value was drastically low, only ~7% of control, in A. Abiad. In agreement with the above trend, a large reduction (80%) of net photosynthetic rate and stomatal conductance was observed in A. Abiad (~20% of that in the control), but A. Aswad was tolerant; it had lost only 23% of its photosynthetic activity (the activity was 77% of control) (Table 1).

Table 1 Chlorophyll *a* fluorescence and gas exchange parameters (net photosynthetic (CO_2 exchange) rate, stomatal conductance) of two barley cultivars (Arabi Aswad and Arabi Abiad) grown under 120 mmol NaCl. Numbers are given as percentage of control after 7 days of salt application.

Parameter	A. Abiad	A. Aswad
T_{FM}	68	214
Area	9	65
F_v/F_m	25	90
F_v/F_o	7	66
P_N	21	77
g_s	35	81

In contrast to the tolerant A. Aswad, the sensitive A. Abiad showed a very high value of the initial (minimal) fluorescence (Fo) and a fluorescence transient curve that was essentially flat; this result may be due to several causes that include structural changes as well as changes in the rate constants of different dissipative processes (Fig. 2).

The Chl fluorescence parameters that were most affected, by salt treatment, in A. Abiad were: dissipation energy flux per reaction center (DIo/RC), related thermal dissipation yield (φDo) and light absorption flux per reaction center (ABS/RC) (Fig. 2).

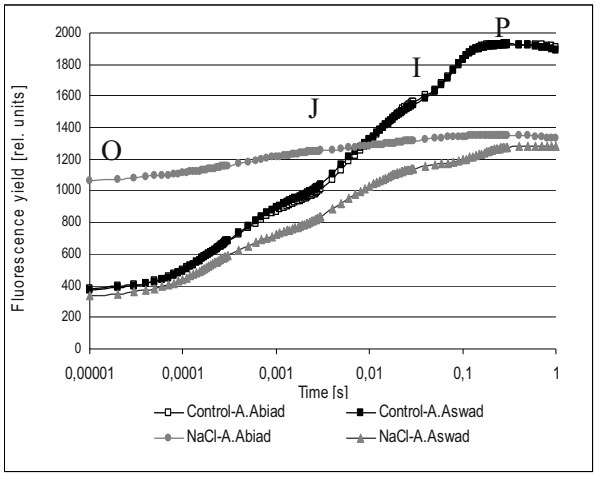

Fig. 2 Chlorophyll *a* fluorescence induction curve of barley seedlings of the two cultivars (Arabi Aswad and Arabi Abiad) grown under salinity stress (120 mmol NaCl) for 7 days.

Salinity stress negatively influenced PSII activity in barley plants, and its effect was dependent on the duration of stress application and on the cultivar used. Primary reactions of photosynthetic apparatus to salt stress of barley plants could play a key role in their tolerance to that stress.

Both the measured and the calculated values of the analyzed fluorescence parameters indicate that the photosynthetic apparatus of A. Aswad cultivar of barley is more tolerant to salinity, compared with the A. Abiad cultivar.

The results of the so-called JIP test, that analyzes quantitatively the OJIP chlorophyll fluorescence transient, has contributed to a better understanding of the responses of different barley cultivars to salinity stress, or for that matter many other plants of economic importance (see chapters in Papageorgiou and Govindjee (2004, reprinted 2010). Apart from the commonly applied fluorescence parameters, such as F_v/F_m, that measures PSII efficiency, our research, and those of many others, shows that it is also important to consider other key parameters, including the PSII performance index, oxygen evolving complex activity and the time needed to reach maximal chlorophyll fluorescence. Simultaneous measurements of chlorophyll fluorescence and plant gas exchange allowed a better understanding of the mechanism of salinity effect on photosynthetic apparatus during early stages of plant growth.

References

Duysens LNM, Sweers HE (1963) Mechanisms of Two Photochemical Reactions in Algae As Studied by Means of Fluorescence. In: Japanese Society of Plant Physiology (ed.), Studies on Microalgae and Photosynthetic Bacteria. University of Tokyo Press: Tokyo, pp. 353-372

Fricke W, Peters WS (2002) The Biophysics of Leaf Growth in Salt-Stressed Barley. A Study at the Cell Level. Plant Physiol. 129: 374-388

Govindjee (1995) Sixty-Three Years since Kautsky: Chlorophyll a Fluorescence. Aust. J. Plant Physiol. (now Funct. Plant Biol.) 22: 131-160

Govindjee (2004) (reprinted 2010) Chlorophyll a Fluorescence: A Bit of Basics and History. In: Papageorgiou G, Govindjee (eds.), Chlorophyll a Fluorescence: a Signature of Photosynthesis. Springer: Dordrecht, pp. 1-42

Havaux M, Strasser RJ, Greppin G (1991) A Theoretical and Experimental Analysis of the qP and qN Coefficients of Chlorophyll Fluorescence Quenching and Their Relation to Photochemical and Nonphotochemical Events. Photosynth. Res. 27: 41-55

Jiang Q, Roche D, Monaco TA, Durham S (2006) Gas Exchange, Chlorophyll Fluorescence Parameters and Carbon Isotope Discrimination of 14 Barley Genetic Lines in Response to Salinity. Field Crop Res. 96: 269-278

Kalaji HM, Nalborczyk E (1991) Gas Exchange of Barley Seedlings Growing under Salinity Stress. Photosynthetica 25: 197-202

Kalaji MH, Pietkiewicz S (1993) Salinity Effects on Plant Growth and Other Physiological Processes. Acta Physiol. Plant. 143: 89-124

Kalaji HM, Rutkowska A (2004) Photosynthetic Machinery Response of Maize Seedlings to Salt

Stress. Zesz. Probl. Post. Nauk Roln. 496: 545-558

Kalaji HM, Wołłejko E, Łoboda T, Pietkiewicz S, Wyszyński Z (2004) Chlorophyll Fluorescence: New Tool for Photosynthetic Performance Evaluation of Barley Plants Grown under Different Nitrogen Rates. Zesz. Probl. Post. Nauk Roln. 496: 375-383

Kalaji HM, Govindjee, Bosa K, Kościelniak J, Żuk-Gołaszewska K (2010) Effects of Salt Stress on Photosystem II Efficiency and CO_2 Assimilation of Two Syrian Barley Landraces. Environ. Exper. Botany. doi:10.1016/j.envexpbot.2010.10.009

Munday JCM Jr., Govindjee (1969a) Light-Induced Changes in the Fluorescence Yield of Chlorophyll a Fluorescence in Vivo. III. The Dip and the Peak in Fluorescence Transient of Chlorella Pyrenoidosa. Biophysic. J. 9: 1-21

Munday JCM Jr., Govindjee (1969b) Light-Induced Changes in the Fluorescence Yield of Chlorophyll a Fluorescence in Vivo. IV. The Effect of Preillumination on the Fluorescence Transient of Chlorella Pyrenoidosa. Biophysic. J. 9: 22-35

Munns R (2002) Comparative Physiology of Salt and Water Stress. Plant Cell Environ. 25 : 239-250

Strasser RJ, Srivastava A, Tsimilli-Michael M (2000) The Fluorescence Transient As a Tool to Characterize and Screen Photosynthetic Samples. In: Yunus M, Pathre U, Mohanty P (eds.), Probing Photosynthesis: Mechanisms, Regulation and Adaptation. Taylor & Francis: London, pp. 445-483

Stirbet A,Govindjee (2011) On the Relation between the Kautsky Effect (Chlorophyll a Fluorescence Induction) and Photosystem II: Basics and Applications of the OJIP Fluorescence Transient. J. Photochem. Photobiol. B: Biology, in the press: doi:10.1016/j.jphotobiol.2010.12.010.

The Effects of Antisense Suppression of δ Subunit of Chloroplast ATP Synthase on the Rates of Chloroplast Electron Transport and CO_2 Assimilation in Transgenic Tobacco

Wataru Yamori[a,b*], Shunichi Takahashi[a], Amane Makino[b], G Dean Price[a], Murray R Badger[a], Susanne von Caemmerer[a]

[a] Molecular Plant Physiology Cluster, Research School of Biology, The Australian National University, Australia;
[b] Department of Applied Plant Science, Graduate School of Agricultural Science, Tohoku University, Japan.
[*]Corresponding author. Tel. No. +81-22-717-8767; Fax No. +81-22-717-8765; E-mail: wataru.yamori@biochem.tohoku.ac.jp.

Abstract: In C_3 plants, CO_2 assimilation is limited by RuBP regeneration rate at high CO_2. RuBP regeneration rate in turn is determined by either the chloroplast electron transport capacity to generate NADPH and ATP or the activity of Calvin cycle enzymes involved in regeneration of RuBP. Here, transgenic tobacco (*Nicotianna tabacum* L. cv. W38) expressing an antisense gene directed at the transcript of either the Rieske FeS protein of the cytochrome b_6/f complex or the δ subunit of chloroplast ATP synthase have been used to investigate the effect of a reduction of these complexes on chloroplast electron transport rate. Reductions in δ subunit of ATP synthase content reduced electron transport rates. Plants with low ATP synthase content achieved higher electron transport rates per ATP synthase than wild type. In comparison, there was no difference in the electron transport rate per cytochrome b_6/f complex in plants with reduced b_6/f content and wild type. The electron transport rates decreased more drastically with reductions in cytochrome b_6/f complex than ATP synthase content. This suggests that chloroplast electron transport rate is more limited by cytochrome b_6/f than ATP synthase content and is a potential target for enhancing photosynthetic capacity in crops.

Keywords: ATP synthase; Cytochrome b_6/f complex; Electron transport; Photosynthesis; RuBP regeneration

Introduction

Plants capture light energy with their light-harvesting systems and drive photosynthetic electron transport through the thylakoid membranes of the chloroplasts. Electrons excised from water in photosystem II (PSII) are ultimately transferred to $NADP^+$ via photosystem I (PSI), resulting in production of NADPH. At the same time, the electron transport which passes through the cytochrome (Cyt) b_6/f complex generates a proton gradient across the thylakoid membrane (ΔpH). Together with the proton gradient generated by the water-splitting complex associated with PSII, these proton gradient enables ATP production by the ATP synthase complex and help to regulate non-photochemical quenching of excitation energy. (Shikanai, 2007).

ATP and NADPH generated by light reactions are utilized primarily in the Calvin cycle and photorespiratory cycle. The activity and regulation of the Cyt b_6/f complex and the ATP synthase are thus key components determining the rate of NADPH and ATP production for CO_2 fixation. Photosynthetic CO_2 assimilation rate can be viewed as being limited either by the capacity of Rubisco to consume RuBP (at lower CO_2) or by the capacity of the chloroplast electron transport to generate ATP and NADPH for RuBP regeneration (at higher CO_2) (Farquhar *et al*., 1980). However, within this framework of limitations, significant uncertainties remain in our understanding of how electron transport and ATP synthesis are coordinated and affect electron transport capacity and photosynthesis (Baker *et al*., 2007).

We used transgenic tobacco (*Nicotianna tabacum* L. cv. W38) plants expressing an antisense gene directed at the transcript of either the Rieske FeS protein of the Cyt b_6/f complex or the δ subunit of chloroplast ATP synthase to investigate the effect that

a reduction of these complexes has on chloroplast electron transport rate and CO_2 assimilation rate.

Materials and Methods

Plant materials and growth conditions

Nicotiana tabacum L. cv Wisconsin 38 plants (W38) and the progeny of several transformants of anti-Rieske FeS tobacco and anti-ATP synthase tobacco which have reduced amounts of the chloroplast Cyt b_6/f and ATP synthase were grown in controlled environmental growth cabinets (Price *et al.*, 1995; Ruuska *et al*., 2000). Plants were grown at irradiance of 60−80 μmol m^{-2} s^{-1} with a photoperiod of 20 h and ambient CO_2 concentration. The day/night air temperatures were 30/25 °C, and the relative humidity was 70%.

Gas exchange and fluorescence measurements

CO_2 gas exchange of leaves was measured with a portable gas exchange system (LI-6400, Li-COR, Lincoln, NE, USA), according to Yamori *et al*. (2005, 2009, 2010b). The CO_2 assimilation rate (A) versus intercellular CO_2 concentration (C_i) was measured at a light intensity of 1,200 μmol photons m^{-2} s^{-1}. A-C_i curves were fitted with the C_3 photosynthesis model (Farquhar *et al*., 1980), using the Rubisco kinetic constants and temperature dependencies in tobacco (Bernacchi *et al*., 2001). CO_2 assimilation rates at high CO_2 and measured rates of dark respiration (R_d) were used to calculate actual rates of chloroplast electron transport required to satisfy NADPH consumption (J_g (μmol m^{-2} s^{-1})):

$$J_g = \frac{(A + R_d)(4 + 8\Gamma^*)}{C_i - \Gamma^*},$$

where C_i (μmol mol^{-1}) is intercellular CO_2, Γ^* (μmol mol^{-1}) is the CO_2 compensation point in the absence of day respiration.

Determinations of Rieske FeS of Cytochrome b_6/f complex and δ subunit of ATP synthase

Immediately after the measurements of gas exchange, leaf discs were taken and stored at −80 °C. The frozen leaf sample was homogenized in an extraction buffer (Yamori and von Caemmerer, 2009; Yamori *et al*., 2010a). The content of Rieske FeS of Cyt b_6/f complex and δ subunit of ATP synthase was quantified by immunoblotting with anti-Rieske Fes antibody and anti-ATP synthase (δ) antibody (Agrisera, Vännäs, Sweden).

Results

CO_2 assimilation rate at 380 μmol mol^{-1} CO_2 at high light (A_{380}) was strongly decreased with reductions in the content of either the δ subunit of ATP synthase complex or the Rieske FeS subunit of the Cyt b_6/f complex (Fig. 1). However, the comparative extent of the reductions of A_{380} was greater in anti-Rieske FeS plants than in anti-ATP synthase (δ) plants.

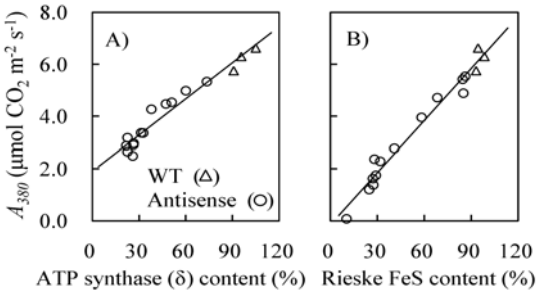

Fig. 1 CO_2 assimilation rates at 380 μL L^{-1} CO_2 concentration at 1,200 μmol photons m^{-2} s^{-1} (A_{380}) at 25 °C in antisense plants with a variety of δ subunit of chloroplast ATP synthase (A) and in antisense plants with a variety of Rieke FeS contents (B). The regression lines are shown in each figure; A) y = 0.046x + 1.906, R^2 = 0.93; B) y = 0.067x – 0.149, R^2 = 0.97. Statistical comparison of regressions showed them to be significantly different at $P < 0.000001$.

CO_2 assimilation rate (A) versus intercellular CO_2 concentration (C_i) was measured to determine RuBP regeneration and/or electron transport limited CO_2 assimilation rate at high CO_2, and these were used to calculate actual electron transport rates (J_g).

Reductions in contents either of ATP synthase (δ) or Rieske FeS led to a decrease in J_g at 25 °C (Figs. 2A and 2B). In anti-Rieske FeS plants, J_g per Rieske FeS content was constant irrespective of Rieske FeS content (Fig. 2D). However, in anti-ATP synthase (δ) plants, the J_g per ATP synthase (δ) content increased with reductions in ATP synthase (δ) content (Fig. 2C), indicating that *in vivo* ATP synthase activity of an individual ATP synthase complex was enhanced in anti-ATP synthase (δ) plants.

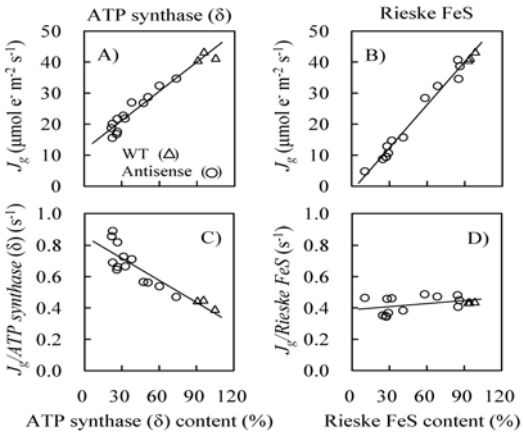

Fig. 2 The capacity of RuBP regeneration (J_g) and the J_g per ATP synthase (δ) content at 25 °C in antisense plants with a variety of δ subunit of chloroplast ATP synthase (A and C) and the capacity of RuBP regeneration (J_g) and the J_g per Rieke FeS content at 25 °C in antisense plants with a variety of Rieke FeS content (B and D). J_g was calculated from measurements of CO_2 assimilation rate at high CO_2 as described in the Materials and Methods section. The regression lines are shown in each figure. Regression coefficient (R^2); (A) R^2 = 0.95; (B) R^2 = 0.98; (C) R^2 = 0.80; (D) R^2 = 0.17. Statistical comparison of regressions shown in A) and B) showed them to be significantly different at $P < 0.00001$.

Discussion

The data presented here show that there is a strong control of chloroplast electron transport and photosynthetic capacity by the level and activity of both the Cyt *b*$_6$*f* and ATP synthase complexes. However, the manner in which each complex does this and their relative contributions is distinctly different. It was clearly evident that the Cyt *b*$_6$*f* complex exhibited much tighter control of electron transport capacity and photosynthesis than that of the ATP synthase complex (Figs. 1 and 2). A significant basis for this appears to lie in the fact that there is a strong potential for an individual ATP synthase complex to modulate its proton conductance and ATP synthesis per electron transport, while the Cyt *b*$_6$*f* complex has much less flexibility.

ATP synthase activity varies in vivo

When the ATP synthase complex content was reduced, the evidence clearly indicates that the actual chloroplast electron transport rate per ATP synthase complex increased (Fig. 2). This supports the notion that the activity of an ATP synthase complex can vary *in vivo* when ATP synthase content is reduced. This change in activity could be due to changes in substrate availability (stromal ADP, Pi and trans-thylakoid proton motive force (*pmf*)), the activation state of the complex or the proton stoichiometry per ATP.

There have been several reports about the nature of the modulation of ATP synthase activity. For example, the ATP synthase is regulated by trans-thylakoid proton motive force (*pmf*) and by reduction of γ-subunit thiols via thioredoxin (Kramer and Crofts, 1989; Ort and Oxborough, 1992; McCalluma and McCarty, 2007). It has also been suggested that ATP synthase senses the status of stromal metabolites either directly or indirectly (Kramer *et al.*, 2004) and it has been suggested that its activity can be modulated by altering Pi levels (Takizawa *et al.*, 2008).

Recent estimations of proton stoichiometry indicated that the H^+/ATP ratio is 4.66 (Baker *et al.*, 2007). Interestingly, there have been reports that the proton stoichiometry in ATPase may vary depending on environmental conditions in *Escherichia coli* (Schemidt *et al*., 1995, 1998). Thus, it may also be possible that the proton stoichiometry in ATP synthase varied between WT and anti-ATP synthase line, since their physiological states (*e.g.*, transthylakoid ΔpH) is different.

Cytochrome b$_6$*f content is rate limiting for chloroplast electron transport*

There was a strong linear relationship between chloroplast electron transport rate and Cyt *b*$_6$*f* content such that electron transport per Cyt *b*$_6$*f* content was the same for plants with a large range of Rieske FeS content (Figs. 1 and 2). The photosynthetic model of Farquhar *et al*. (1980) suggests that CO_2 assimilation in C_3 plants is limited by the rate of RuBP regeneration at high CO_2 and that RuBP regeneration rate in turn is determined by either the chloroplast electron transport capacity to generate NADPH and ATP or the activity of Calvin cycle enzymes involved in regeneration of RuBP. There have been a number of studies using transgenic plants to investigate whether Calvin enzymes limit the rate of RuBP regeneration and only SBPase has been suggested as a possible candidate for a rate limiting step (Raines, 2003).

This is the first time that the dependence of electron transport rate on Cyt *b*$_6$*f* content and ATP synthase content have been compared. Our results can be interpreted to suggest that measurements of CO_2 assimilation rate at high CO_2 can be used to infer Cyt *b*$_6$*f* content of leaves (Yamori *et al*., 2010a). The assumption that RuBP regeneration rate is limited by

chloroplast electron transport rate and Cyt b_6/f content rather than ATPase content may provide a robust mechanism for scaling carbon uptake from leaf photosynthesis to canopies, and ecosystems.

References

Baker NR, Harbinson J, Kramer DM (2007) Determining the Limitations and Regulation of Photosynthetic Energy Transduction in Leaves. Plant Cell & Environ. 30: 1107-1125

Bernacchi CJ, Singsaas EL, Pimentel C, Portis AR, Long SP (2001) Improved Temperature Response Functions for Models of Rubisco-Limited Photosynthesis. Plant Cell & Environ. 24: 253-259

Farquhar GD, Caemmerer SV, Berry JA (1980) A Biochemical Model of Photosynthetic CO_2 Assimilation in Leaves of C_3 Species. Planta 149: 78-90

Kramer DM, Avenson TJ, Edwards GE (2004) Dynamic Flexibility in the Light Reactions of Photosynthesis Governed by Both Electron and Proton Reactions. Trends in Plant Science 9: 349-357

Kramer DM, Crofts AR (1989) Activation of the Chloroplast ATPase Measured by the Electrochromic Change in Leaves of Intact Plants. Biochim. Biophys. Acta 976: 28-41

McCallum JR, McCarty RE (2007) Proton Flux through the Chloroplast ATP Synthase Is Altered by Cleavage of Its Gamma Subunit. Biochim. Biophys. Acta (Bioenergetics) 1767: 974-979

Ort DR, Oxborough K (1992) In Situ Regulation of Chloroplst Coupling Factor Activity. Ann. Rev. Plant Physiol. Plant Mol. Biol. 43: 269-291

Price GD, von Caemmerer S, Evans JR, Siebke K, Anderson JM, Badger MR (1998) Photosynthesis Is Strongly Reduced by Antisense Suppression of Chloroplastic Cytochrome b/f Complex in Transgenic Tobacco. Aust. J. Plant Physiol. 25: 445-452

Price GD, Yu JW, von Caemmerer S, Evans JR, Chow WS, Anderson JM, Hurry V, Badger MR (1995) Chloroplast Cytochrome b_6/f and ATP Synthase Complexes in Tobacco: Transformation with Antisense RNA Against Nuclear-Encoded Transcripts for the Rieske FeS and ATP Polypeptides. Aust. J. Plant Physiol. 22: 285-297

Raines CA (2003) The Calvin Cycle Revisited. Photosynth. Res. 75: 1-10

Ruuska SA, Andrews TJ, Badger MR, Price GD, von Caemmerer S (2000) The Role of Chloroplast Electron Transport and Metabolites in Modulating Rubisco Activity in Tobacco. Insights from Transgenic Plants with Reduced Amounts of Cytochrome b/f Complex or Glyceraldehyde 3-Phosphate Dehydrogenase. Plant Physiol. 122: 491-504

Schemidt RA, Hsu DKW, Deckers-Hebestreit G, Altendorf K, Brusilow WSA (1995) The Effects of an atpE Ribosome-Binding Site Mutation on the Stoichiometry of the c Subunit in the F1Fo ATPase of Escherichia Coli. Arch. Biochem. Biophys. 323: 423-428

Schemidt RA, Qu J, Williams JR, Brusilow WSA (1998) Effects of Carbon Source on Expression of Fo Genes and on the Stoichiometry of the c Subunit in the F1Fo ATPase of Escherichia coli. J. Bacteriol 180: 3205-3208

Shikanai T (2007) Cyclic Electron Transport around Photosystem I: Genetic Approaches. Ann. Rev. Plant Biol. 58: 199-217

Takizawa K, Kanazawa A, Kramer DM (2008) Depletion of Stromal P-i Induces High "Energy-Dependent" Antenna Exciton Quenching (q(E)) by Decreasing Proton Conductivity at CFO-CF1 ATP Synthase. Plant Cell & Environ. 31: 235-243

Yamori W, Noguchi K, Hikosaka K, Terashima I (2009) Cold-Tolerant Crop Species Have Greater Temperature Homeostasis of Leaf Respiration and Photosynthesis than Cold-Sensitive Species. Plant & Cell Physiol. 50: 203-215

Yamori W, Noguchi K, Hikosaka K, Terashima I (2010b) Phenotypic Plasticity in Photosynthetic Temperature Acclimation among Crop Species with Different Cold Tolerances. Plant Physiol. 152: 388-399.

Yamori W, Noguchi K, Terashima I (2005) Temperature Acclimation of Photosynthesis in Spinach Leaves: Analyses of Photosynthetic Components and Temperature Dependencies of Photosynthetic Partial Reactions. Plant Cell & Environ. 28: 536-547

Yamori W, Evans JR, von Caemmerer S (2010a) Effects of Growth and Measurement Light Intensities on Temperature Dependence of CO_2 Assimilation Rate in Tobacco Leaves. Plant Cell & Environ. 33: 332-343

Yamori W, von Caemmerer S (2009) Effect of Rubisco Activase Deficiency on the Temperature Response of CO_2 Assimilation Rate and Rubisco Activation State: Insights from Transgenic Tobacco with Reduced Amounts of Rubisco Activase. Plant Physiol. 151: 2073-2082

The Effects of Elevated CO_2 Concentration on Photosynthesis and Photosystem II Photochemistry in a Fast Growing Tree Species, *Gmelina Arborea* Roxb

Girish K Rasineni, Attipalli R Reddy*

Photosynthesis and Plant Stress Biology Laboratory, University of Hyderabad
Hyderabad 500 046, India.
* Corresponding author. Tel. No. +91-40-23134508; Fax No. +91-40-23010120; E-mail: arrsl@uohyd.ernet.in.

Abstract: Sequestering atmospheric carbon and storing it in the terrestrial biosphere is one of the options to mitigate green house gas emissions. Young fast growing tree species are believed to be major potential sinks which could absorb large quantities of CO_2 from the atmosphere. The ability of plant to capture light energy, associated with the rate of CO_2 fixation per *se,* is crucial to understand the growth dynamics under varying environmental regimes. The role of enriched CO_2 atmosphere in the kinetics of photosynthesis and *Chl a* fluorescence could be an index to understand the photosystem II photochemistry associated with carbon sequestration potential. In this study, the effects of elevated CO_2 (460 μmol mol^{-1}) on diurnal courses of net CO_2 assimilation and chlorophyll *a* fluorescence were investigated under natural high light during summer days in a fast growing tree species, *Gmelina arborea* (*Verbenaceae*). High CO_2 atmosphere led to easy recovery from the midday photosynthetic depression in the leaves. Elevated CO_2 also enhanced the utilization of captured light energy, alleviated photoinhibition and enhanced the growth of *Gmelina arborea*. Data on fluorescence induction curves and JIP-test parameters also demonstrated a positive impact of elevated CO_2 on PSII photochemical performance suggesting *Gmelina* to be a better performer for carbon sequestration even during high irradiance regimes.

Keywords: Chlorophyll *a* fluorescence ; Elevated CO2 ; *Gmelina arborea* ; Photosynthesis ; PS II efficiency

Introduction

One of the major issues of global concern today is rapidly increasing levels of CO_2 (at 2 μmol mol^{-1} $year^{-1}$) in the atmosphere and its potential to change the world climate (IPCC 2007). The rising CO_2 levels have severe implications on the functioning of physical and biological systems of the world and an increase in the size of carbon sinks can mitigate this problem. Increased biomass production through large scale tree plantings is one among the viable actions to mitigate the rising levels of CO_2 (Prentice *et al*., 2001). Fast growing tree species that can be harvested earlier in a rotation are of great interest in tropical and subtropical regions for the carbon sequestration (Swamy *et al*., 2003). The relationship between the carbon assimilation and photosynthetically active radiation is important to understand how the physical environment affects the plant growth and to identify potent photo-chemically efficient tree species for the carbon sequestration (Wang *et al*., 2003). Plants grown in tropical climates conditions experience significantly high irradiance leading to a strong midday depression of photosynthesis. The objectives of this study were to determine the dynamics of photosynthetic responses in a fast growing tree species, *Gmelina,* grown under elevated CO_2 during the peak growth season (summer), to determine the extent of midday depression of photosynthesis and the subsequent recovery in *Gmelina* grown under ambient and elevated CO_2 conditions through pattern of gas exchange and chlorophyll *a* fluorescence.

Materials and Methods

Gmelina arborea were exposed to ambient (360 μ mol mol^{-1}) and elevated (460 μmol mol^{-1}) CO_2 concentrations in two rectangular open top chambers (OTCs) which were constructed with steel frame having dimensions of 4×4×4 m covered with polycarbonate sheet (Polygal plastic industries Ltd. Israel) of 4 mm thickness and with 100% transparency. The present experiments were performed with six months-old-plants during a sequence of four summer days (May 2009). Diurnal courses of leaf gas exchange were assessed on clear days for 30 min from 06:00 to 18:00 h; measurements were made on sunlit leaves of *Gmelina* using a portable infrared CO_2/H_2O gas analyzer (IRGA) (LC Pro+, ADC Bioscientific Ltd. UK) equipped with a broad leaf chamber. Chlorophyll *a* fluorescence measurements were made with the Plant Efficiency Analyser, PEA (Hansatech instruments Ltd., King's Lynn, Norfolk, England). The translation of the measured parameters into JIP-test parameters were done through Raw fluorescence OJIP transients using WINPEA 32 software and BiolyzerP3 according to Strasser and Govindjee (1992) and Albert *et al*. (2005).

Results and Discussion

The ability to capture light energy in plant species is a character of greater importance for the magnitude of plant growth along with the rate of CO_2 fixation per *se.* In this context, concerted patterns of photosynthesis and Chl *a* fluorescence can suggest the probable role of enriched CO_2 atmosphere on the potential use of light absorbed by PSII antenna in photochemistry and in-turn in the carbon sequestration potential. During the experimental period, *Pn* increased as a result of increasing photosynthetically active radiation (PAR) (Fig. 1). There was no significant difference between ambient and elevated CO_2 grown plants during early hours (06:00 h). Photosynthetic rates reached the maximum values at 10:00 h in both ambient and elevated CO_2-grown plants *i.e.* 20 ± 1.2 and 32.5 ± 1.5 μmol m^{-2} s^{-1} respectively. Thereafter, photosynthetic rate decreased in ambient grown plants with increasing incident PAR (Fig. 1) while the photosynthetic rate in elevated CO_2 grown plants was significantly high during the peak PAR (2,000 μmol (photon) m^{-2} s^{-1}) (12:00 h). Excitation pressure in photosystem II (PS II) increases when the rate of energy absorbed by the photosystem exceeds the rate of energy used by the dark reactions of photosynthesis and this high excitation pressure may cause photooxidative damage to the thylakoid membrane (Porcar-Castell *et al*., 2008). Under high irradiance, depression of photosynthesis in plants during midday was often observed and maximum rates of CO_2 assimilation occur only during morning and late afternoon. Midday depression mainly occurs due to increased leaf temperatures and photo-inhibition (He *et al*., 2007). *Gmelina arborea*, a tropical tree species is commonly subjected to high excitation pressure during the peak summer seasons, which can limit carbon assimilation although light absorption continues. In the early morning, CO_2 assimilation in ambient and elevated CO_2- grown plants showed no statistical difference which is in a good agreement that assimilation processes were limited by the electron transport level at the low irradiance (Špunda *et al*., 2008). However, during the peak irradiance, photoinhibition was observed in ambient and elevated CO_2 grown *Gmelina* but the photosynthetic rates in *Gmelina* under elevated CO_2 atmosphere were significantly high compared to ambient grown plants. Therefore, elevated CO_2 atmosphere leads to adjusting the rate of energy absorption and the energy partitioning in the light reactions of photosynthesis to the energy demands of dark reactions.

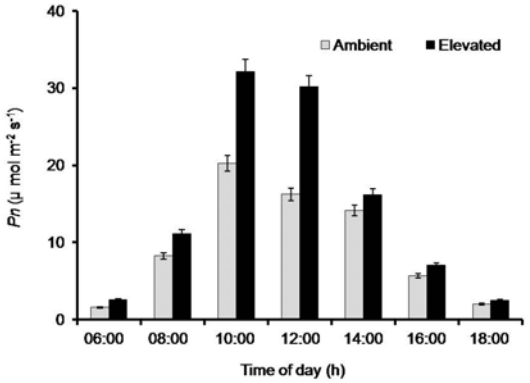

Fig. 1 Diurnal courses of photosynthetic rates (*Pn*) in *Gmelina arborea* grown under ambient and elevated CO_2 concentrations. Values are mean ± standard deviations.

Changes in F_0 and F_V/F_M are usually due to a change in the efficiency of non-photochemical

quenching. Dark-adapted values of F_V/F_M reflect the potential quantum efficiency of PSII and are used as sensitive indicator of plant photosynthetic performance (Maxwell and Johnson, 2000). Fluorescence at 50 μs depicts the stress level in leaves due to high irradiance (Fig. 2A). Chlorophyll *a* fluorescence measurements of *Gmelina,* grown under ambient and elevated CO_2 conditions, allowed us to estimate the adaptive changes induced by the growth conditions. The elevated CO_2 atmosphere had significant effect on the chlorophyll *a* fluorescence parameters and their responses to the intense incident PAR. Although the ambient and elevated CO_2-grown plants were subjected to different microclimatic conditions, predawn F_V/F_M remained very close to 0.8 (Fig. 2B) but as incident PAR irradiance increased, the F_V/F_M decreased in both the ambient and elevated CO_2 grown plants leading to their minimum values of 0.60 and 0.7 respectively. During the peak irradiance hours (12.00 h) F_V/F_M was higher in elevated CO_2 grown plants compared to ambient grown plants whereas, F_V/F_M was lower in ambient grown plants during the midday (Fig. 3). The fact that F_V/F_M was higher in elevated CO_2 grown plants under high irradiance strongly suggest that growth in elevated CO_2 increases the photochemical efficiency of PSII and in-turn photochemistry, as the reported responses to elevated CO_2 of photochemistry showed an increase in photochemical efficiency (Zhang and Dang, 2006).

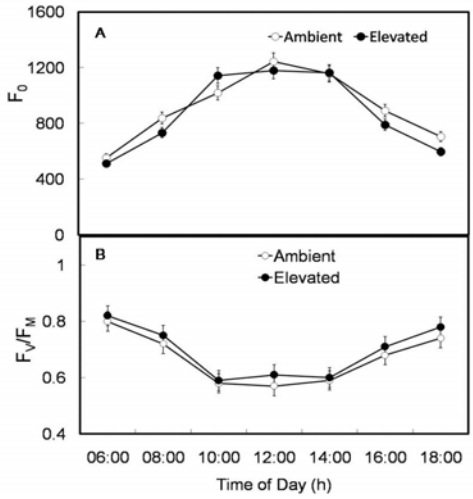

Fig. 2 Diurnal patterns of F_0 ($F_{50\mu s}$, Fluorescence at 50 μs). (A) and potential quantum yield of PSII photochemistry (F_V/F_M) (B) in *Gmelina arborea* grown under ambient and elevated CO_2 concentrations. Values are mean ± standard deviations.

The JIP-test parameters reveal information on different scales of the performance of the PSII photosynthetic machinery and have proven sensitive to detect environmental changes. They can also determine the biophysical and the biochemical performances of the photosynthetic apparatus (Clark *et al*., 2000; van Heerden *et al*., 2003; Albert *et al*., 2008). The JIP-test parameter like S_m reveals the information of photosynthetic capacity and is proportional to the amount of PSII centers capable of moving electrons from Q_A to PQ pool via Q_B (Antal *et al*., 2009). These parameters reach the highest values when electron transport between Q_A and Q_B is enhanced by elevated CO_2. Interestingly, the S_m (multiple turnover of Q_A reduction events) was also significantly ($p < 0.001$) high in elevated CO_2-grown plants when compared to ambient CO_2-grown plants. Fig. 3 shows the dynamics of S_m in elevated CO_2-grown *Gmelina* which suggests effective transfer of electrons between Q_A and PQs (S_m) and probability of effective electron transport at the acceptor side facilitating the enhancement of PSII function under elevated CO_2 atmosphere.

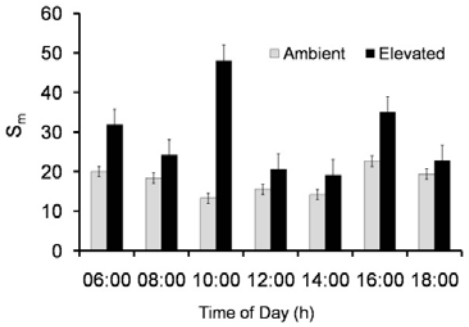

Fig. 3 Diurnal patterns of changes in the JIP-test parameter, normalized area between OJIP curve and F_P value (S_m) in *Gmelina arborea* grown under ambient and elevated CO_2 concentrations. Values are mean ± standard deviations.

The daily course of net CO_2 assimilation in *Gmelina* grown under elevated CO_2 atmosphere documented significantly higher values compared to ambient grown plants and recordings of fluorescence induction curves and calculations of JIP-test parameters clearly demonstrated a positive impact of elevated CO_2 on PS II performance. In comparison with the ambient CO_2-grown *Gmelina*, elevated CO_2 treatment led to diminution of midday depression of photosynthesis caused by the photoinhibition. Moreover, high F_V/F_M reveals the adjustment of assimilatory apparatus for the elevated CO_2 climate and the high irradiance. In conclusion, our data

demonstrate that future increases in atmospheric CO_2 may have positive effects on photochemical efficiency in fast growing tropical tree species like, *Gmelina arborea.* High CO_2 can also mitigate the photoinhibition caused due to high irradiation through enhanced electron transport rates and through efficient biochemical reactions.

Acknowledgements

We thank Department of Biotechnology, Government of India for support through research grant # BT/PR 6402/BCE/08/416/2005. We are grateful to DST-FIST and CREBB facilities during our experimentation. GKR. received SRF from CSIR, New Delhi.

References

Albert KR, Mikkelsen TN, Ro-Poulsen H (2005) Effects of Ambient Versus Reduced UV-B Radiation on High Arctic Salix Arctica Assessed by Measurements and Calculations of Chlorophyll-a-Fluorescence Parameters from Fluorescence Transients. Physiol. Plant. 124: 208-226

Albert KR, Mikkelsen TN, Ro-Poulsen H (2008) Ambient UV-B Radiation Decreases Photosynthesis in High Arctic Viccinium Uliginosum. Physiol. Plant. 133: 199-210

Antal TK, Matorin DN, Ilyash LV, Volgusheva V, Osipov IV, Konyuhov TE, Krendeleva AA, Rubin AB (2009) Probing of Photosynthetic Reactions in Four Phytoplanktonic Algae with a PEA Flourometer. Photosynth. Res. 102: 67-76

Clark AJ, Landolt W, Bucher JB, Strasser RJ (2000) Beech (Fagus Sylvatica) Responses to Ozone Exposure Assessed with a Chlorophyll a Fluorescence Performance Index. Environ. Pollut. 110: 1-7

He J, Austin PT, Nichols MA, Lee SK (2007) Elevated Root-Zone CO_2 Protects Lettuce Plants from Midday Depression of Photosynthesis. Environ. Exp. Bot. 61: 94-101

Intergovernmental Panel on Climate Change (IPCC) (2007) Climate Change 2007 Mitigation. In: Metz B, Davidson, OR, Bosch PR, Dave R, Meyer LA (eds.), Contribution of Working Group III to the Fourth Assessment Report of the Intergovernmental Panel on Climate Change. Cambridge University Press: Cambridge, United Kingdom and New York, USA

Maxwell K, Johnson GN (2000) Chlorophyll Fluorescence-a Practical Guide. J. Exp. Bot. 51: 659-668

Porcar-Castell A, Juurola E, Ensminger I, Berninger F, Hari P, Nikinmaa E (2008) Seasonal Acclimation of Photosystem II in Pinus Sylvestris. II. Using the Rate Constants of Sustained Thermal Energy Dissipation and Photochemistry to Study the Effect of the Light Environment. Tree Physiol. 28: 1483-1491

Prentice IC, Farquhar GD, Fasham MJR, Goulden ML, Heimann M, Jaramillo VJ, Kheshgi HS, LeQuere C, Scholes RJ, Wallace DWR, *et al*. (2001) The Carbon Cycle Atmospheric Carbon Dioxide. In: Houghton JT, Ding Y, Griggs DJ, Noguer M, Van der Linder PJ, Dai X, Maskell K, Johnson CA (eds.), The Scientific Basis. Contributions of Working Group I to the Third Assessment Report of the Intergovernmental Panel on Climate Change Climate Change. Cambridge University Press: New York

Špunda V, Kalian J, Urban O, Luis VC, Sibisse I, Puértolas J, Šprtova M, Marek MV (2008) Diurnal Dynamics of Photosynthetic Parameters of Norway Spruce Trees Cultivated under Ambient and Elevated CO_2: the Reasons of Midday Depression in CO_2 Assimilation. Plant Sci. 168: 1371-1381

Strasser RJ, Govindjee (1992) The Fo and O-J-I-P Fluorescence Rise in Higher Plants and Algae. In: Argyroudi-Akoyunoglou JH (ed.), Regulation of Chloroplast Biogenesis. Plenum Press: New York, pp. 423-426

Swamy SL, Puri S, Singh AK (2003) Growth, Biomass, Carbon Storage and Nutrient Distribution in Gmelina Arborea Roxb. Stands on Red Laterite Soils in Central India. Bioresource Technol. 90: 109-126

van Heerden PDR, Merope TM, Kruger GHJ, Strasser RJ (2003) Dark Chilling Effects on Soybean Genotypes during Vegetable Development: Parallel Studies of CO_2 Assimilation, Chlorophyll-a Fluorescence Kinetics O-J-I-P and Nitrogen Fixation. Physiol. Plant. 17: 476-491

Wang KY, Kellomaki S, Li C, Zha T (2003) Light and Water-Use Efficiencies of Pine Shoots Exposed to Elevated Carbon Dioxide and Temperature. Ann. Bot. 92: 53-64

Zhang SR, Dang QL (2006) Effects of Carbon Dioxide Concentration and Nutrition on Photosynthetic Functions of White Birch Seedlings. Tree Physiol. 26: 1457-1467

Influence of Elevated CO_2 Concentration on Photosynthesis and Biomass Yields in a Tree Species, *Gmelina Arborea* Roxb

Girish K Rasineni, Attipalli R Reddy*

Photosynthesis and Plant Stress Biology Laboratory, University of Hyderabad
Hyderabad 500 046, India.
* Corresponding author. Tel. No. +91-40-23134508; Fax No. +91-40-23010120; E-mail: arrsl@uohyd.ernet.in.

Abstract: The present study dissects out the CO_2 fertilization effects on photosynthetic gas exchange characteristics, key responses of photosynthetic and carbohydrate metabolizing enzymes and overall plant growth performance in a fast growing tree species, *Gmelina arborea* Roxb (*Verbenaceae*). The main objective of this investigation was to unravel and evaluate the role of elevated CO_2 on tree photosynthesis and productivity. *Gmelina* plants were grown under ambient (360 µmol mol^{-1}) and CO_2-enriched conditions (460 µmol mol^{-1}) in open top chambers for two marked growth seasons, subsequently for three years. The leaf gas exchange characteristics and associated biochemical measurements were carried out at regular intervals. *Gmelina* plants were harvested and growth parameters were measured at the end of two growth seasons for three consecutive years. *Gmelina* plants significantly responded to CO_2 enrichment. *Gmelina* plants grown under elevated CO_2 showed 52% more plant biomass compared with those grown under ambient CO_2. We conclude that fast growing tree species like *Gmelina,* exhibiting high CO_2-mediated photosynthetic up-regulation, can be used as potential tree species for efficient carbon sequestration under predicted future climate change scenario.

Keyword: Biomass yields ; Elevated CO_2 ;*Gmelina arborea*; Photosynthesis

Introduction

Atmospheric CO_2 is rising rapidly and the options for slowing the CO_2 largely require reductions in industrial CO_2 emissions or through efficient carbon sequestration. Forests cover ~43% of the earth's surface, account for some 70% of terrestrial net primary production (NPP) and are being bartered for carbon mitigation. In this scenario, it is critically important to study the impact of elevated atmospheric CO_2 on growth and productivity of forest tree species (Prentice *et al*., 2001; IPCC, 2007). The exponential increase of CO_2 in the atmosphere should theoretically stimulate photosynthesis due to enhanced rubisco carboxylation, leading to efficient CO_2 sequestration (Long *et al*., 2004). However, many plant species grown at elevated CO_2 exhibit an acclimatory down regulation associated with decreased photosynthetic potential (Davey *et al*., 2006). The objective of our study was to address the photosynthetic productivity in *Gmelina arborea,* a fast growing economically important tropical forest tree species during the marked growth seasons under CO_2-enriched atmosphere. We were specifically interested to investigate the physiological and biochemical changes associated with photosynthesis as well as to understand the role of key enzymes of photosynthetic carbon metabolism in this tree species grown under high CO_2 environment.

Materials and Methods

Gmelina plants were grown for two marked growth seasons subsequently for three years (2006 to 2008) under ambient (360 µmol mol^{-1}) and CO_2-enriched (460 µmol mol^{-1}) atmosphere in open top chambers. Leaf gas exchange characteristics and associated biochemical measurements were carried

out at regular intervals. The rate of leaf gas exchange was measured using a portable infrared CO_2/H_2O gas analyzer (IRGA) (LC Pro+, ADC Bioscientific Ltd. U.K.) equipped with a broad leaf chamber. The gas analyzer was used to measure instantaneous net photosynthetic rates (P_n; µmol m^{-2} s^{-1}), stomatal conductance to CO_2 (g_s; mol m^{-2} s^{-1}) and transpiration rates (E; mmol m^{-2} s^{-1}) periodically during each growing season between 10:00–11:00 h solar time. Instantaneous water use efficiency ($WUEi$ = P_n/E mmol CO_2 mol^{-1} H_2O) was also calculated. Extraction of RuBPcase and its activity measurements were performed according to Cheng and Fuchigami (2000). The activity of carbonic anhydrase (CA) in the leaf extracts was determined by following the time-dependent decrease in pH from 8.3 to 7.3 according to Wilbur and Anderson (1948). FBPase (Zimmerman *et al.*, 1978), SPsynthase (Huber, 1981), Hexokinase (Martinez-Barajas and Randall, 1998) and Sedheptulose 1,7 bisphosphatase (Lanzetta *et al*., 1979) activities were determined according to standard protocols. In each year, all the plants in ambient and elevated OTC's were harvested to obtain growth and yield measurements at the end of two growing seasons.

Results and Discussion

CO_2 enrichment had a profound influence on the gas exchange physiology of young *Gmelina* when compared to its counterparts grown at ambient CO_2 concentration. The P_n of *Gmelina* grown under high CO_2 atmosphere showed a significant increase in P_n ($p < 0.05$) of ~32% compared to ambient CO_2-grown plants. In anomaly to P_n, the *gs* and *E* showed a decreasing trend in the plants under high CO_2. Young *Gmelina* plants showed a significant upsurge in *Pn* in the interim enriched CO_2 exposure. Increased CO_2 concentrations can boast the rates of carboxylation sites of rubisco and concomitantly increase the *Pn* of C_3 plants. A time dependent photosynthetic down regulation under elevated CO_2 has also been observed in many plants, on account of diffusion limitation of CO_2, internal CO_2 concentration (*Ci*), availability of the light and sink capacity for photosynthates resulting in curtailment of dark reaction capacity in processing CO_2 (Norby *et al*., 2001; Oren *et al*., 2001; Ainsworth *et al*., 2004). The relationship between the P_n and *Ci* for the ambient and elevated CO_2 grown plants were shown in Fig. 1A. Elevated CO_2 atmosphere induced a positive correlation between *Pn* and *Ci* ($r^2 = 0.71$; $p < 0.001$); however, the correlation between *Pn* and *Ci* under ambient conditions was comparatively weak ($r^2 = 0.46$; $p < 0.10$). The relationship between *gs* and *Ci* showed positive correlation under ambient conditions ($r^2 = 0.41$ $p < 0.10$), where as the correlation was found to be negative in plants grown under elevated CO_2 ($r^2 = –0.65$ $p < 0.001$) (Fig. 1B). The CO_2 exchange between the plants and its atmosphere mainly occurs through the stomata and *gs* is one of the major limitations in carbon assimilation, particularly when plants are grown under elevated CO_2 (Jensen, 2000; Anderson *et al*., 2001; Beedlow *et al*., 2004; Ainsworth and Rogers, 2007). A down drop in the *gs* was observed under high CO_2 atmosphere mainly due to escalation in the *Ci* as the stomata respond to *Ci* through the guard cells (Paoletti and Grulke, 2005). The decrease in the *gs* had no effect on the *Pn* in young *Gmelina.* The subsidence in photosynthetic acclimation despite the decrement in *gs* was believed to be due to accelerated internal photosynthetic activity as the stomata were found to limit the *Pn* particularly when *Ci* is saturating (Farquhar and Sharkey, 1982; Noormets *et al*., 2001; Sage, 2002; Herrick *et al*., 2004; Paoletti and Grulke, 2005).

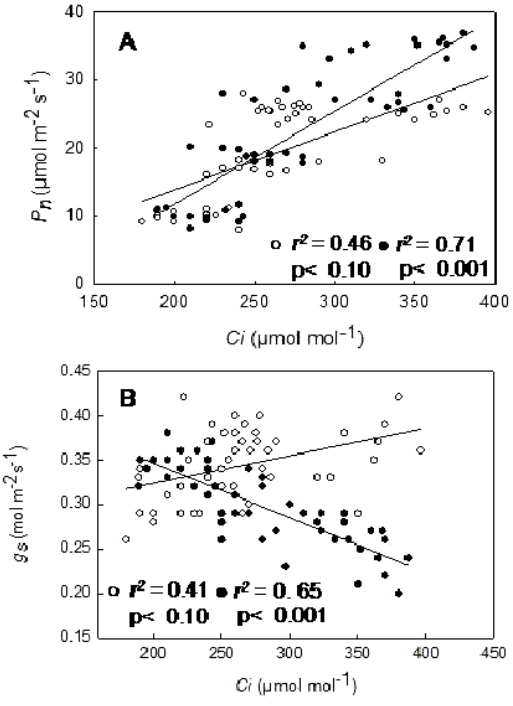

Fig. 1 Relationship between photosynthetic rates (P_n) and internal CO_2 concentration (*Ci*) (A), between stomatal conductance (*gs*) and internal CO_2 concentration (*Ci*) (B) in young *Gmelina arborea* grown under ambient and elevated CO_2 concentrations (○ ambient; ● elevated).

Changes in biochemical indices were recorded at regular intervals during 120 days of exposure to elevated CO_2. Initial and total rubisco activity of the leaf samples in *Gmelina* grown under ambient and elevated CO_2 were shown in Table 1. Initial and total rubisco activity showed a progressive enhancement during 120 days of treatment. *Gmelina* plants grown under elevated CO_2, showed ~ 48% ($p < 0.05$) and ~ 44% ($p < 0.05$) higher initial and total activity, respectively, compared to the plants grown under ambient CO_2 (Table 1). CA activity was significantly higher (61% $p < 0.05$) in plants under elevated CO_2 when compared with ambient CO_2-grown plants (Table 1). It has been proposed that enzymatic processes like modulation of rubisco activity and expression of certain other key photosynthetic enzymes probably play a important role in influencing the guard cell responses to *Ci*- saturation and prevention of down regulation of *Pn* in young tree species under high CO_2 atmosphere (Warren and Adams, 2004; Coleman, 2000; von Caemmerer and Quick, 2000; Messinger *et al*., 2006). Internal CO_2 concentrations (*Ci*) influence the rate of CO_2 fixation in the chloroplasts, where photosynthetic carbon reduction cycle is exclusively located, but the initial assimilation of CO_2 takes place in the mesophyll cells (Li *et al*., 2004). This initial assimilation of *Ci* is catalysed by the enzyme CA which plays an important role in accelerating carbon assimilation by catalyzing the reversible interconversion of CO_2 and HCO_3^- and preventing the *Ci* saturation (Coleman, 2000). In this study, *Gmelina,* grown under the high CO_2 atmosphere showed a dynamic increase in the activity of the CA. Very little is known about increases in CA activity in plants grown under elevated CO_2 (Sicher *et al.*, 1994). The increase in the *Ci* and inturn the radical increase in the activity of the CA might lead to upsurge in the rubisco activity. The rubisco activity in *Gmelina* leaves grown under enriched CO_2 was significantly high at 120 DAP followed by absonant increase in *Pn* when compared to the plants grown under ambient CO_2. The activities of key carbohydrate metabolising enzymes like FBPase, SPsynthase and hexokinase were also significantly high in the plants grown under high CO_2 atmosphere compared to those grown under ambient CO_2.

Growth and biomass of *Gmelina* grown under elevated CO_2 were significantly high compared with those grown in ambient CO_2 as evidenced by the harvest data (Table 2). Elevated CO_2 atmosphere persistently enhanced the growth in *Gmelina.* All the growth characteristics including plant height, number of branches, internodes, intermodal distance, aerial biomass and plant biomass increased significantly in the plants grown under high CO_2 suggesting that *Gmelina* plants have greater capacity for carbon accumulation.

Table 1 Effect of elevated CO_2 on key photosynthetic enzyme activities.

Enzyme	Ambient CO_2	Elevated CO_2	
RUBPcase initial activity μmol mg^{-1} protein h^{-1}	22.2±3.2	32.6±2.8	***
RUBPcase total activity μmol mg^{-1} protein h^{-1}	36.2±2.8	47.8±3.7	**
Carbonic anhydrase Units mg^{-1} protein	18.0±1.8	29.5±2.6	***
FBPase activity μmol mg^{-1} protein h^{-1}	42.3±1.7	78±3.5	***
SPsynthase activity μmol mg^{-1} protein h^{-1}	28.3±2.1	36±3.6	**
Hexokinase μmol mg^{-1} protein h^{-1}	7.4±2.3	13.5±4.7	***
Sedheptulose 1,7 bisphosphatase μmol mg^{-1} protein h^{-1}	2.8±0.9	2.7±0.7	ns

Table 2 Growth and Biomass yields of *Gmelina* grown elevated CO_2 atmosphere.

Character	**Ambient CO_2**	**Elevated CO_2**	
Plant height (cm)	209.45±2.12	359.92±2.78	***
Basal Diameter (cm)	13.21±0.59	28.40±0.80	***
Number of Branches	26.20±0.72	44.20±1.19	***
Relative plant height growth rate RHGR (g day^{-1})	2.97±0.45	4.08±0.72	**
Leaf size expansion rate	3.89±0.57	9.75±1.02	***
Root weight (kg)	3.96±0.89	5.97±0.85	**
Aerial biomass (kg)	25.67±2.32	37.67±2.98	**
Plant biomass (kg)	29.63±1.67	43.64±3.12	***

Plant height was ~82% ($p < 0.001$) more in plants grown under high CO_2 than those grown under ambient condition (Table 2). The total shoot length constituting the length of main stem and branches together was ~77% ($p < 0.001$) more in high CO_2 grown plants. CO_2 treatment had a notable effect on the aerial biomass accumulation (~41% $p < 0.05$) and in turn on the total plant biomass (~47% $p < 0.05$) (Table 2). We noticed that increased number of branches resulted in greater crown size and structure

of *Gmelina* under high CO_2 atmosphere. Profuse root growth and more number of secondary and tertiary roots in *Gmelina* under elevated CO_2 also shows the varied sink-source status of *Gmelina* plants. We demonstrate a strong and sustained photosynthetic enhancement in *Gmelina* plants grown under CO_2-enrichment and our data propound that *Gmelina* can be a potent trees species for efficient carbon sequestration corresponding to its rapid growth and high sink demand with no acclimatory responses.

Acknowledgements

We thank Department of Biotechnology, Government of India for support through research grant # BT/PR 6402/BCE/08/416/2005. We are grateful to DST-FIST and CREBB facilities during our experimentation. G.K.R. received JRF from DBT, New Delhi.

References

Ainsworth EA, Rogers A (2007) The Response of Photosynthesis and Stomatal Conductance to Rising [CO_2]: Molecular Mechanisms and Environmental Interactions. Plant Cell Environ. 30: 258-270

Ainsworth EA, Rogers A, Nelson R, Long SP (2004) Testing the "Source-Sink" Hypothesis in Elevated CO_2 in the Field with Single Gene Substitutions in Glycine Max. Agr. Forest Meteorol. 122: 85-94

Andersosn LJ, Maherali H, Johnson HB, Polley HW, Jackson RB (2001) Gas Exchange and Photosynthetic Acclimation over Sub Ambient to Elevated CO_2 in C_3-C_4 Grassland. Glob. Change Biol. 7: 693-707

Beedlow PA, Tingey DT, Phillips DL, Hogsett WE, Olszyk DM (2004) Rising Atmospheric CO_2 and Carbon Sequestration in Forests. Front. Ecol. Environ. 2: 315-322

Cheng L, Fuchigami LH (2000) Rubisco Activation State Decreases with Increasing Nitrogen Content in Apple Leaves. J. Exp. Biol. 51: 1687-1694

Coleman JR (2000) Carbonic Anhydrase and Its Role in Photosyhthesis. In: Leegood RC, Sharkey TD, von Caemmerer S (eds.), Photosynthesis: Physiology and Metabolism. Kluwer Academic: The Netherlands

Davey PA, Olcer H, Zakhleniuk O, Bernacchi CJ, Calfapietra C, Long SP, Raines CA (2006) Can Fast-Growing Plantation Trees Escape Biochemical Down-Regulation of Photosynthesis When Grown throughout Their Complete Production Cycle in the Open Air under Elevated Carbon Dioxide? Plant Cell Environ. 29: 1235-1244

Davey PA, Olcer H, Zakhleniuk O, Bernacchi CJ, Calfapietra C, Long SP, Raines CA (2006) Can Fast-Growing Plantation Trees Escape Biochemical Down-Regulation of Photosynthesis When Grown throughout Their Complete Production Cycle in the Open Air under Elevated Carbon Dioxide? Plant Cell Environ. 29: 1235-1244

Farquhar GD, Sharkey TD (1982) Stomatal Conductance and Photosynthesis. Annu. Rev. Plant Phys. 33: 317-345

Herrick JD, Maherali H, Thomas RB (2004) Reduced Stomatal Conductance in Sweetgum (Liquidambar Styraciflua) Sustained over Long-Term CO_2 Enrichment. New Phytol. 162:387-396

Huber SC (1981) Interspecific Variation in the Activity and Regulation of Leaf Sucrose Phosphate Synthase. Plant Physiol. 102: 443-450

Intergovernmental Panel on Climate Change (IPCC) (2007) Climate Change 2007 Mitigation. In: Metz B, Davidson, OR, Bosch PR, Dave R, Meyer LA (eds.), Contribution of Working Group III to the Fourth Assessment Report of the Intergovernmental Panel on Climate Change. Cambridge University Press: Cambridge, United Kingdom and New York, USA

Jensen RG (2000) Activation of Rubisco Regulates Photosynthesis at High Temperature and CO_2. Proc. Nat. Acad. Sci. USA 97: 12937-12938

Lanzetta PA, Alvarez LT, Reinach PS, Candia OA (1979) An Improved Assay for Nanomole Amounts of Inorganic Phosphate. Anal. Biochem. 100: 95-97

Li X, Hou J, Bai K, Yang X, Lin J, Li Z, Kuang T (2004) Activity and Distribution of Carbonic Anhydrase in Leaf and Ear Parts of Wheat (Triticum Aestivum L.). Plant Sci. 166: 627-632

Long SP, Ainsworth EA, Rogers A, Ort DR (2004) Rising Atmospheric Carbon Dioxide: Plants Face the Future. Annu. Rev. Plant Biol. 55: 591-628

Martinez-Barajas E, Randall DD (1998) Purification and Charcterization of Fructokinases from Developing Tomato (Lycopersicon Esculentum

Mill.) Fruits. Planta 199: 451-458

Messinger SM, Buckley TN, Mott KA (2006) Evidence for the Involvement of Photosynthetic Process in the Stomatal Responses to CO_2. Plant Physiol. 140: 771-778

Noormets A, Sôber A, Pell EJ, Dickson RE, Podila GK, Sôber J, Isebrands JG, Karnosky DF (2001) Stomatal and Non-Stomatal Limitation to Photosynthesis in Two Trembling Aspen (Populus Tremuloides Michx.) Clones Exposed to Elevated CO_2 and/or O_3. Plant Cell Environ. 24: 327 – 336

Norby RJ, Todd DE, Fults J, Johnson DW (2001) Allometric Determination of Tree Growth in a CO_2-Enriched Sweetgum Stand. New Phytol. 150: 477-487

Oren R, Ellsworth DS, Johnsen KH. et al. (2001) Soil Fertility Limits Carbon Sequestration by Forest Ecosystems in a CO_2-Enriched Atmosphere. Nature 411: 469-472

Paoletti E, Grulke NE (2005) Does Living in Elevated CO_2 Ameliorate Tree Response to Ozone? A Review on Stomatal Responses. Environ Pollut. 137: 483-493

Prentice IC, Farquhar GD, Fasham MJR, Goulden ML, Heimann M, Jaramillo VJ, Kheshgi HS, LeQuere C, Scholes RJ, Wallace DWR, *et al.* (2001) The Carbon Cycle Atmospheric Carbon Dioxide. In: Houghton JT, Ding Y, Griggs DJ, Noguer M, Van der Linder PJ, Dai X, Maskell K, Johnson CA (eds.), The Scientific Basis. Contributions of Working Group I to the Third Assessment Report of the Intergovernmental Panel on Climate Change Climate Change. Cambridge University Press: New York

Sage RF (2002) How Terrestrial Organisms Sense, Signal and Respond to Carbondioxide. Integrative and Comparative Biology 42: 469-480

Sicher RC, Kremer DF, Rodermel SR (1994) Photosynthetic Acclimation to Elevated CO_2 Occurs in Transformed Tobacco with Decreased Ribulose-1, 5-bisphosphate Carboxylase/Oxygenase Content. Plant hysiol. 104: 409-415

Solomon S, Qin D, Manning RB and others Technical summary. The Physical Science Basis. In: Solomon S, Qin D, Manning M, Chen Z, Marquis M, Averyt KB, Tignor M, Miller HL (eds.), Contribution of Working Group I to the Fourth Annual Assessment Report of the Intergovern-mental Panel on Climate Change. Cambridge University Press: Cambridge, UK/New York, NY, USA

von Caemmerer S, Quick WP (2000) Rubisco: Physiology in Vivo. In: Leegood RC, Sharkey TD, von Caemmerer S (eds.), Photosynthesis: Physiology and Metabolism. Kluwer Academic: Dordrecht, The Netherlands

Warren CR, Adams MA (2004) Evergreen Trees Do Not Maximize Instantaneous Photosynthesis. Trends Plant Sci. 9: 270-274

Wilbur KM, Anderson NG (1948) Electrometric and Colorimetric Determination of Carbonic Anhydrase. J. Biol. Chem. 176: 147-154

Zimmerman G, Kelly GE, Latzko E (1978) Purification and Properties of Spinach Leaf Cytoplasmic Fructose 1, 6-Bisphosphatase. J. Biol. Chem. 253: 5952-5956

Symposium 23

Global Photosynthesis and Climate Change

The Effect of Mineral Nutrition on Photostnthetic Activity and Saponin Content of Puncture Vine (*Tribulus Terrestris* L.)

Georgi I Georgiev[a], Liliana Maslenkova[a*], Antoaneta Ivanova[b], Luba Evstatieva[c], Albena Ivanova[a], Lozanka Popova[a]

[a]Institute of Plant Physiology and Genetics, BAS, 1113 Sofia, Bulgaria;
[b]Institute of Organic Chemistry with Centre of Phytochemistry, BAS, 1113 Sofia, Bulgaria;
[c] Institute of Botany, Bulgarian Academy of Sciences.
* Corresponding author. Tel. No. +3592 9792636; Fax No. +3592 8739952; E-mail: lili@bio21.bas.bg.

Abstract: Puncture vine (*Tribulus terrestris* L., Zygophyllaceae) is an annual prostrate medicinal plant that is widely used for treatment of sexual deficiency, as an affrodiziak. Steriodal saponins and rutin are among the basic compounds responsible for the biological activities of *T. terrestris* extracts. Efficiency of mineral nutrition (soil or foliar supply of nutrients) on the growth, dry matter and saponin content of the above ground biomass of Bulgarian variety puncture vine grown in soil as pot experiment in green house have been studied. Soil fertilization rate of 100 mgN/kg or 90 P/kg of dry soil, oppositely to the results obtained from the foliar fed plants (0.3% solution of liquid fertilizer Agroleaf^{R} (Scotts Co, U.S.A.) with formulation $N_{12}P_{52}K_5$, increased shoot total N and P without significant change of dry matter. Changes of total reducing sugars, amino acids, phenolics and flavonoids and activity of photosynthetic apparatus (thermoluminescence emission) were found to relate to the variation of individual saponin contents analysed by HPLC technique. Soil fertilized plant in contrast to the foliar fed plants showed more furostanol saponins (protodioscin, prototribestan and dioscin) than control but contained less of flavonoid glycoside rutin.

Keywords: Puncture vine (*Tribulus terrestris* L.); Mineral nutrition; Photosynthesis; Thermoluminescence; saponins; Growth

Abbreviations used: NPK- nitrogen; Phosphorus; Potassium; HPLC- high performance liquid chromatography; TL- thermoluminescence

Introduction

Puncture vine (*Tribulus terrestris* L., *Zygophyllaceae*) is a medicinal plant widely used as a drug supplier in pharmaceutical industry (Linus *et al*., 1995). Its biomass is known as a source of steroidal saponins mainly from the furostanol and spirostanol types. Extracts of plants have been used for years in traditional or modern medicine as food supplements with substantial therapeutic or health effects on humans. Irrespective to the number of investigations concerning botanic, ecological, geographical or chemo type of this plant species little is known of the relationship between growth and accumulation of saponins in its biomass. Moreover, due to extensive search of plant material for commercial purposes from different pharmaceutical companies more or less natural habitats of plant are considered as exhausted. To solve this problem it will be necessary to develop efficient methods for cultivation of this plant on arable lands. One important question of cultivated herbs is how to increase their productivity without lost of quality of the product. Regarding these considerations we have attempted to test how different forms or rate of nitrogen or phosphorus nutrition will influence the growth, dry matter and saponin content of plants grown in soil pot experiments. Accordingly, photosynthetic activity measured as chlorophyll thermoluminescence (TL) emission and the content of steriodal saponins and rutin from three different

origins of *Tribulus terrsetris* (Turkey, Hungary and Bulgaria) have been studied as well.

Material and methods

Plant material

Puncture vine plants (*Tribulus terrestris* L.) were grown under naturally lit and heated green house (day/night temperature—32/19 °C) from May to September. Ripen burrs were used for germination of plants. They were collected from the plants grown in natural habitat from the Pazardjick region, in Bulgaria. 12 randomly selected seeds were pre-sowed in the clear moist quartz sand for 3 days and then transferred to the earthen pots containing 4 kg of dry leached cinnamon meadow soil also known as Chromic Luvisols (FAO) for further growth. Soil moisture in pots was kept at 70% of full moisture capacity during the entire period of the experiment. In one set of pots, 4 weeks after the germination, the plants (budding stage of growth) were sprayed with commercial product of 0.3% solution of liquid fertilizer (Agroleaf^{R}, Scotts co, Ohio, U.S.A.) with the formulation $N_{12}P_{52}K_5$ + microelements. In another set of pots soil was amended with NH_4NO_3 to reach final concentration of soil N (soil + fertilizer N)—100 mgN/kg soil. Another set of pots was accommodated for growing plants under higher soil P fertilization. KH_2PO_4 was applied to 90 mgP/kg soil as final concentration (soil contains total 25 mg P/kg). Aerial parts of puncture vine plants were collected after 4 weeks of growth for analysis.

The study of photochemical activity and the content of saponins and rutin have been carried out with cultivated samples from different origins. They were obtained from commercial seeds of Hungary and seeds from plants, natively distributed in Turkey and Bulgaria (district Plovdiv), The plants were propagated from seedlings, sowing in the beginning of May, 2009. The seedlings were transplanted it the beginning of June on the experimental field near Sofia into plant beds. The plants were collected in full blossoming and seed formation in August, when the samples developed 100–120 cm long stems in all directions.

Biochemical analysis

Aliquots of dried material were used for analysis for free amino acids (Yemm and Cocking, 1955), reducing sugars (Dubois *et al*., 1956) and total phenols (Pfeffer *et al*., 1998) and flavonoids (Zhishen *et al.*, 1999). Elemental analysis of NPK in plant shoot was done according to Scott and Morrison (1996). Statistical analysis of the means (3–6 replicates per measurement) was performed by program Statgraphics plus (Statgraf Co, USA).

Analitical method

An HPLC system La Chrom Elite consisting of L-2130 pump equipped with gradient controller and UV detector L-2400 was used. The separation was performed on 250 × 4.6 mm i. d., 5 μm, Inertsil ODS-2 column (Tokyo, Japan) with MetaGuard Pursuit direct connect guard column from Varian was used for all separations. The mobile phase which consisted of phosphoric acid buffer with pH-3 (A) and acetonitrile (B) was used for gradient elution. The flow rate was adjusted to 1.0 ml/min, the detection wavelength was at 203 nm.

The extraction of the powdered plant material (1 g leaves and fruits, 1:1) was realized three times with 5.0 ml of 50% aqueous acetonitrile by sonication for 15 min. The standards protodioscin, prototribestin, dioscin and rutin were dissolved in 50% aqueous acetonitrile.

Thermoluminescence

Thermoluminescence (TL) measurements were carried out in darkness using a computerized setup described elsewhere (Zeinalov and Maslenkova, 1996). TL was excited by single turnover flashes (4J, 10 μs half band with 1 Hz frequency), given at 5 °C and quickly cooled in liquid nitrogen before being wormed to 60 °C with 0.6 °C /s heating rate.

Results and discussion

We have performed parallel comparative investigations of characteristics of flash-induced TL glow-curves registered from the leaves of *T. terrestris* with different origin. The pattern of TL light emission after pre-illumination with one and two consecutive light flashes is shown on Fig. 1. After a single flash (1F), which generates $S_2Q_B^-$ charge pair, TL light emission (B-band) from *Tribulus* with Bulgarian origin occurred at about 23 °C, which is typical for higher plants (Rutherford *et al*., 1984). Excised leaf pieces of *Tribulus* plants from Hungary and Turkey have considerably lower B-band temperature (16 °C and 14 °C, respectively) and amplitude (Figs. 1B and 1C).

TL signal after two pre-flashes (2F), resulting from $S_2(S_3)Q_B^-$ recombination was significantly higher than $S_2Q_B^-$ in all three investigated varieties. Similarly, different emission temperatures were registered when more than two flashes were given. According to TL theory thermoluminescence emission is a result from radiate recombination of positive and negative charges stored in Mn water-oxidising complex (S_2 and S_3 states) and on PSII acceptors, Q_A and Q_B. It is generally accepted that peak position is a measure of energetic stabilisation of separated charges, whereas the peak amplitude is a measure of the number of recombining charges. Since any changes in the redox state of electron donors and acceptors is reflected in the position of the main bands in TL glow curves we can thus study possible modifications in the components of PSII electron-transport. Illumination of the leaves with a series of single turnover flashes resulted in appearing of characteristic oscillations in B-band intensity with a period of four and maximum yield at 2 and 6 flashes which represent PSII $S_2Q_B^-$ and $S_3Q_B^-$ -state cycling (Rutherford *et al*., 1984). After normalisation of B-band intensities of different *Tribulus* plants it became obvious that TL oscillations of Hungarian and Turkey samples were significantly dampened (Fig. 1D), *i.e.* PSII reaction centers can not reach their higher oxidation states, S_3 and S_4. Considering the obtained results of TL analysis it can be concluded that photochemical activity of photosynthetic apparatus in *Tribulus* with Bulgarian origin is higher in comparison with the plants with Hungarian and Turkey origin.

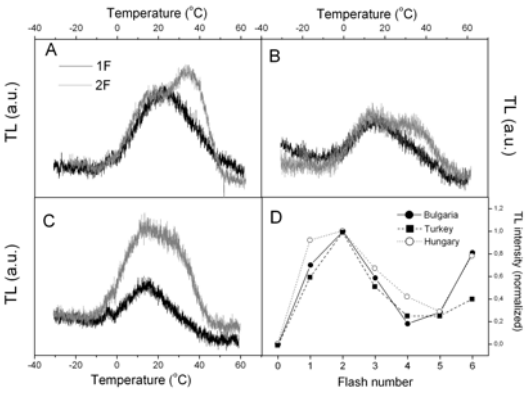

Fig. 1 TL B-band emission from the leaves of *Tribulus terrestris* with different origin: A - Bulgaria; B – Hungary; C – Turkey. D – TL oscillation pattern. The curves were registered with one and two flashes, given at 5 °C or as a function of the number of flashes, from 1 to 6, after 30 min dark adaptation of the samples.

In accordance with this observation are the obtained data from the chemical study of the investigated samples. The results show that the total concentration of the furostanol saponins (protodioscin and prototribestin) is more significant in the samples from Bulgaria (30.74 ± 0.55 mg/g) in comparison with the samples from Hungary (5.32 ± 0.1 mg/g) and Turkey (11.15 ± 0.45 mg/g)

Mineral nutrition is powerful and important tool for plant growth and productivity improvement. The experiments with Foliar fed plants from Bulgarian origin 10 days after the treatment showed slightly inhibited growth (Table 1). Decreased total biomass is related to the inhibited plant development (Table 1). In contrast, soil fertilized plants with 100 mgN/kg soil or 90 mgP/kg soil had improved growth and accumulated more dry matter (214% of control). These changes of plant productivity were related to some physiological and biochemical indexes of plants (Table 2). Leaf feeding with nitrogen decreased free amino acid content of shoot (91.7% of control) but increased the content of reducing sugars (130.3% of control). The changes of basic metabolites of primary metabolism were accompanied with increased concentrations of NPK of the leaves. Although these metabolites in soil fertilized plants were increased phenolics as representatives of secondary metabolites of plants were negatively affected. Foliar fed plants had also less flavonoids in the shoots.

HPLC analysis of saponins in shoots of treated plants showed also substantial difference from control plants (Table 3). Foliar fed plants had less prototribestan (57%) and dioscin (74.7%) but accumulated more protodioscin (120% of control). This result contrasted with a decrease of the flavonoid glycosiderutin (83.9%). In contrast to the foliar fed plants all saponin components measured in shoots of soil fertilized plants was substantially increased with the exception of rutin.

The content of protodioscin was highest in leaves under this treatment. Analysis of results indicated that the source and rate of mineral nutrition of puncture vine could be an important tool for regulation of plant and biochemical indexes of plants (Table 2). Leaf feeding with nitrogen decreased free amino acid content of shoot (91.7% of control) but increased the content of reducing sugars (130.3% of control).

Table 1 Biomass accumulation during vegetative growth of puncture vine (*Tribulus terrestris* L.) subjected to different forms and rate of mineral nutrition.

Treatments	Average length of stems, cm	Number of stems per plant	Number of leaves per plant	Number of flowers per plant	Number of burrs per plant	Fresh matter, g/plant	Dry matter, g/plant
			Foliar fertilized plants				
Control	17.12a	3.25a	27.25a	3.75a	10.52a	1.26	0.39a
0.3%Agroleaf	13.12ab	3.00a	27.54a	1.25b	6.25b	1.20	0.36ab
			Soil fertilized plants				
Control	15.45a	4.3a	30.5a	4.2a	12.13a	0.54a	0.14a
100mgN/kg	18.54b	4.9ab	34.7b	4.1a	13.80b	1.02b	0.24b
90mgP/kg	17.43c	5.1c	32.7c	4.0a	14.90c	1.41c	0.29c

Data are means of 6 replicates. Means with equal letters are not significantly different, t-test (P≤0.05).

Table 2 Effect of different forms and rate of mineral nutrition of puncture vine (*Tribulus terrestris* L) on some biochemical parameters during reproductive period of growth.

Treatments	Total free amino acids, mmol /g DW	Total reducing sugars, mg /g DW	Total soluble phenols, mg/g DW	Total soluble flavonoids, μg/gDW
		Foliar fertilized plants		
Control	4.88a	48.55a	2.85a	10.02a
0.3%Agroleaf	4.52b	63.27b	2.36b	8.30ab
		Soil fertilized plants		
Control	3.06a	81.15a	3.77a	11.24a
100mgN/kg	5.79b	71.26b	3.88a	10.89ab
90mgP/kg	5.17ab	55.41c	3.69a	11.37ab

Data are means of 3 replicates. Means with equal letters are not significantly different, t-test (P ≤ 0.05).

Table 3 Main saponins and flavonoid of shoots from puncture vine (*Tribulus terrestris* L.) plants fertilized by leaves or soil with excess of P.

HPLC analysis of main components of plant extracts, mg/g DW	Control of foliar fed plants	Foliar fed plants with 0.3% Agroleaf $N_{12}P_{52}K_5$	Control of soil fertilized plants with 90 mgP/kg	Soil fertilized plants with 90 mgP/kg
Rutin	2.98a	2.50a (83.9)	3.44a	2.23a (64.8)
Protodioscin	11.25b	13.50b (120.0)	8.29b	11.23b (135.4)
Prototribestin	16.35c	9.33c (57.0)	5.82c	8.05c (138.3)
Dioscin	1.74d	1.30d (74.7)	1.37d	1.59d (116.0)

Data are means of 3 replicates. Means with equal letters are not significantly different, t-test (P ≤ 0.05); Values in parenthesis represent % from control.

The changes of basic metabolites of primary metabolism were accompanied with increased concentrations of NPK of the leaves. Although these metabolites in soil fertilized plants were increased phenolics as representatives of secondary metabolites of plants were negatively productivity and saponin content of puncture vine grown under cultivation conditions. The presented results support evidence that the contradiction between primary and secondary metabolism can be overcome by optimizing growth conditions of plants (Zehirov and Georgiev, 2006). However, the significance of these results for *Tribulus terrestris* growth should be augmented and clarified in field trial experiments.

Acknowledgments

Authors gratefully acknowledge the financial support of the National Science Found of the Bulgarian

Ministry of Education, Youth and Science (Project DO02–246).

References

Dubois M, Gilles K, Hamilton J, Roberts P, Skith F (1956) Anal.Chem. 23-24

Linus H, W.den der Plas, Eijkelboom C, Hagendoorn JM (1995) Plant Cell, Tissue and Organ Culture. 43: 111-116

Pfeffer H, Danniel F, Romheld V (1998) Physiol. Plant. 104: 479-485

Rutherford AW, Govindjee, Inoue Y (1984) Proc. Natl. Acad. Sci USA. 81: 1107-1111

Scott, JK, SM Morrison SM (1996) Austral. J.Botany. 44: 175-190

Yemm, E, Cocking E (1955) Analyst, 80: 209-213.

Zeinalov Y, Maslenkova L (1996) Bulg. J. Plant Physiol. 22: 88-94

Zehirov G, Georgiev GI (2006) Acta Physiol. Plantarum, 28: 171-179

Zhishen Y, Mengchang T, Yianming W (1999) Food Chemistry 64: 555-559

Chlorophyll *d* Production in Crushed Algae in Aqueous Acetone

Shinya Akutsu[a], Shingo Itoh[a], Keisuke Aoki[a], Hayato Furukawa[a], Hideaki Miyashita[b], Koji Iwamoto[c], Yoshihiro Shiraiwa[c], Masaaki Okuda[a] , Masami Kobayashi[a]*

[a]Institute of Materials Science, University of Tsukuba, Japan;
[b]Graduate School of Human and Environmental Studies, Kyoto University, Japan;
[c]Institute of Biological Sciences, University of Tsukuba, Japan.
*Corresponding author. Tel. No. +81-298-53-6940; Fax No. +81-298-53-4490; E-mail: masami@ims.tsukuba.ac.jp.

Abstract: We for the first time report on the Chl *a* to Chl *d* conversion in crushed algae, *Synechocystis sp.* PCC6803, *Emiliania huxleyi*, *Gephyrocapsa oceanica*, *Isochrysis galbana*, *Helladosphaera cornifera*, *Pleurochrysis carterae, Chlorella vulgaris, Chlamydomonas acidophila,* incubated in aqueous acetone at 303 K for 2 days, where no Chl *a* was added externally to the system. The highest conversion of Chl *a* into Chl *d* was observed in *G. oceanica* (*ca.* 1.1%). The conversion yield was lower, when other algae were used: *S. sp.* PCC6803 (ca. 0.4%), *E. huxleyi* (ca. 0.3%), *C. vulgaris* (*ca.* 0.2%), *I. Galbana* (*ca.* 0.1%), *H. cornifera* (*ca.* 0.1%), *P. carterae* (*ca.* 0.06%), *C. acidophila* (*ca.* 0.04%). The well-known degradation reactions of Chl *a*, namely, pheophytinization (Chl *a* → Phe *a*) and epimerization (Chl *a* → Chl *a′*), were also observed. We should pay enough attention to the fact that Chl *d* was not detected at all in the initial algae examined here. It is interesting to note that Chl *d*, Chl *d′*, Chl *a′* and Phe *a* were also detected in processed alga food, *Chlorella* powder and dried laver. It is noteworthy that these artifacts function as key components in natural photosynthesis.

Keywords: *Acaryochloris marina*; Algae; Chl *a*; Chl *d*; Oxidase; Papain

Introduction

In 1943, Chl *d* (Fig. 1) was first discovered in some species of red algae (Manning and Strain, 1943). The molecule structure was then identified to be 3-desvinyl-3-formyl-Chl *a* (Holt and Morley, 1959; Holt, 1961). Since Chl *d* was not found in all red algae, Chl *d* had been hence thought to be an oxidative artifact of Chl *a* (Fig. 1).

A Chl *d*-dominated cyanobacterium, *Acaryochloris marina*, was accidentally discovered in 1993 (Miyashita *et al.*, 1996; Ohashi *et al.*, 2008). Chl *d* is expected to be oxidatively biosynthesized from Chl *a*, where oxidative cleavage of the C = C double bond of a vinyl group of Chl *a* at ring I (–CH = CH_2 → –CHO) is required, while the biosynthetic pathway of Chl *d* in *A. marina* has not yet been clarified. Chl *a* has many C = C bonds in the macrocycle (Fig. 1), and hence it is too difficult to oxidize only the C = C bond in the –CH = CH_2 moiety at ring I. Usually, both a special metal complex (OsO_4) and an oxidant (H_5IO_6) are needed for the selective oxidation (Mironov *et al.*, 2004).

Recently, we came across the formation of Chl *d* from Chl *a* with papain (EC 3.4.22.2) in several aqueous organic solvents (Kobayashi *et al.*, 2005; Koizumi *et al.*, 2005; Okada *et al.*, 2009; Ohashi *et al.*, 2010). The Chl *a* to Chl *d* conversion was not observed when Chl *a* was incubated with esterases (esterase EC 3.1.1.1, cholesterol esterase EC 3.1.1.13, phosphatase EC 3.1.3.2) and other proteases (α-chymotrypsin EC 3.4.21.1, subtilisin carlsberg EC 3.4.21.14, ficin EC 3.4.22.3, bromelain EC 3.4.22.4) (Koizumi *et al.*, 2005; Okada *et al.*, 2009).

Quite recently, the same conversion was observed when Chl *a* was incubated with horseradish peroxidase (Furukawa *et al.*, in this issue). Further, we found that Chl *a* was nonenzymatically converted into

Chl *d* in acetone/0.3% H_2O_2 (10/1, *v/v*) (Aoki *et al*., in this issue).

The Chl *a* into Chl *d* conversion was also observed when Chl *a* was incubated with several grated vegetables (Itoh *et al.*, 2009; in this issue). In particular, Japanese radish (root) showed higher conversion than papain.

In order to clarify the conversion mechanisms *in vitro* and the birth of Chl *d* in nature, we incubated several crushed microalgae in acetone/H_2O (5/1, *v/v*) at 303 K for 48 h in the dark, and the Chl *a* into Chl *d* conversion was seen in all crushed algae examined, even no additional Chl *a* was added to the system.

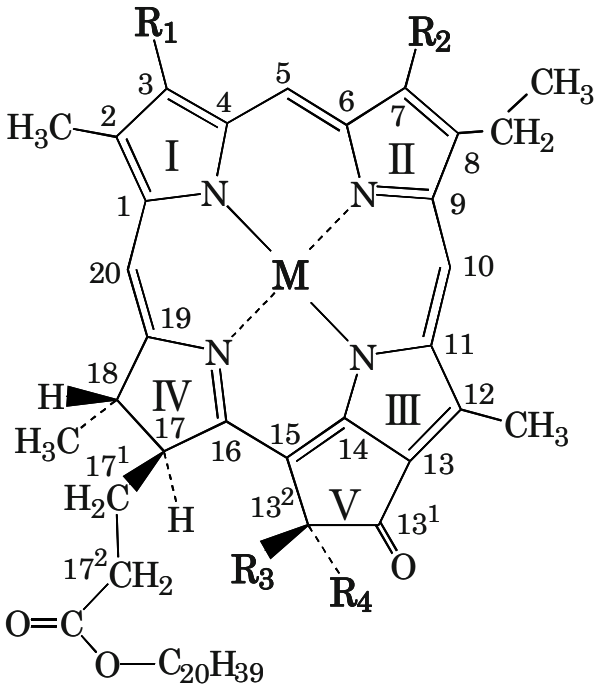

	M	R_1	R_2	R_3	R_4
Chl *a*	Mg	$CH=CH_2$	CH_3	H	$COOCH_3$
Chl *a'*	Mg	$CH=CH_2$	CH_3	$COOCH_3$	H
Phe *a*	2H	$CH=CH_2$	CH_3	H	$COOCH_3$
Chl *b*	Mg	$CH=CH_2$	CHO	H	$COOCH_3$
Chl *d*	Mg	CHO	CH_3	H	$COOCH_3$
Chl *d'*	Mg	CHO	CH_3	$COOCH_3$	H

Fig. 1 Molecular structures of chlorophylls, according to the IUPAC numbering system.

Materials and Methods

Incubation of crushed algae in aqueous acetone

Eight species of microalgae, *Synechocystis sp*. PCC6803, *Emiliania huxleyi*, *Gephyrocapsa oceanica*, *Isochrysis galbana*, *Helladosphaera cornifera*, *Pleurochrysis carterae*, *Chlorella vulgaris*, *Chlamydomonas acidophila* were sonicated in acetone/water(5/1,*v/v*) for 30 s at 277 K, and then shaken gently at 303 K in the dark.

Pigment analysis

Samples were taken periodically and filtered by poly(tetrafluoroethylene) membrane filters. The filtrate was injected into a reversed-phase Senshupak PEGASIL-ODS HPLC column (4.6 mm ID × 250 mm) cooled to 277 K in an ice-water bath. The pigments were eluted isocratically with degassed ethanol/methanol/2-propanol/water (86/13/1/3, *v/v/v/v*) at a flow rate of 0.3 mL/min, and were monitored with a JASCO Multiwavelength MD-2015 detector (λ = 300–800 nm).

In the case of commercially available processed algae, *Chlorella* powder and dried laver, they were ground in a glass mortar for 1 min at 277 K. Pigments were extracted from the ground materials by sonication in an acetone/methanol (7/3, *v/v*) mixture for 2 min in the dark at room temperature. The extract was filtered and dried *in vacuo*. The thus-obtained solid material was immediately dissolved in 10 μL of chloroform, and injected into a silica HPLC column (YMC-pack SIL, 250 × 4.6 mm ID) cooled to 277 K in an ice-water bath. The pigments were eluted isocratically with degassed hexane/2-propanol/methanol (100/0.7/0.25, *v/v/v*) at a flow rate of 0.9 mL/min, and were monitored with a JASCO UV-970 detector (λ = 700 nm) and a JASCO Multiwavelength MD-915 detector (λ = 300–800 nm) in series.

Results and Discussion

Chl d produced from Chl a in crushed algae

Typical HPLC traces for crushed algae incubated in aqueous acetone at 303 K for 2 days are shown in Fig. 2. The conversion of Chl *a* into Chl *d* was observed in all algae examined here (Figs. 2A'-H'), even though no additional Chl *a* was added to the system. The results indicate that Chl *a* present originally in these algae was directly converted to Chl *d* by the reaction with something in the algae. We should note that Chl *d* was not detected at all in the initial algae examined here (Figs. 2A-H).

The highest conversion of Chl *a* into Chl *d* was observed in *G. oceanica* (*ca.* 1.1%, Fig. 2A'). *G. oceanica* almost equals papain (*ca.* 2%, Kobayashi *et*

al., 2005; Koizumi *et al*., 2005; Okada *et al*., 2009; Ohashi *et al*., 2010) in efficiency.

The conversion yields were lower in other crushed algae: *S. sp.* PCC6803 (*ca*. 0.4%, Fig. 2F'), *E. huxleyi* (*ca.* 0.3%, Fig. 2B'), *C. vulgaris* (*ca.* 0.2%, Fig. 2G), *I. galbana* (*ca.* 0.1%, Fig. 2C'), *H. cornifera* (*ca.* 0.1%, Fig. 2D'), *P. carterae* (*ca.* 0.06%, Fig. 2E'), and *C. acidophila* (*ca*. 0.04%, Fig. 2H'), respectively.

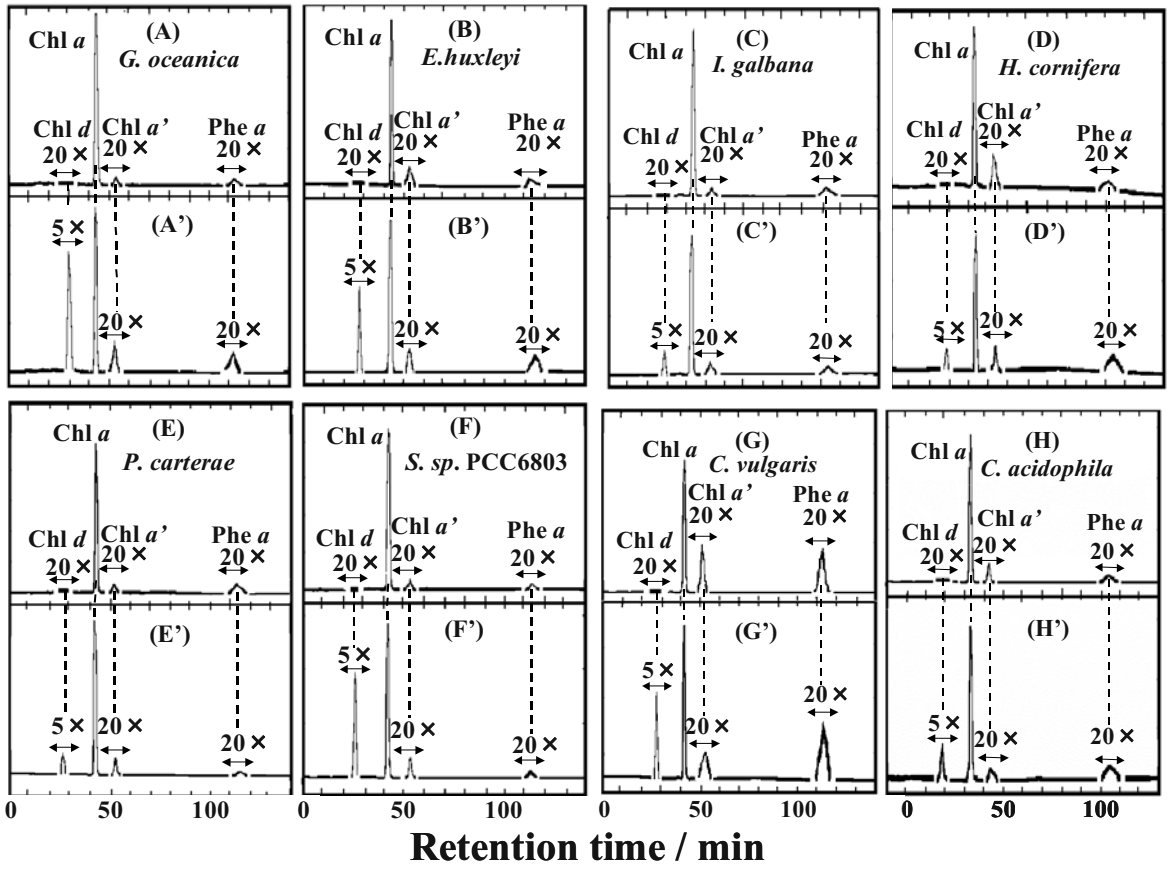

Fig. 2 Reversed-phase HPLC elution profiles for crushed algae incubated for 2 days in acetone/water(10/1, *v/v*) in the dark at 303 K. Incubation times are 0 h (A ~ H) and 48 h (A' ~ H'), respectively. Detection wavelength is 700 nm.

Phe a and Chl a' produced as artifacts of Chl a in crushed algae

In our present study, familiar degradation reactions of Chl *a*, namely, pheophytinization (Chl *a* → Phe *a*) and epimerization (Chl *a* → Chl *a'*), were also observed (Figs. 2A'–H'). In the case of *C. vulgaris* and *C. acidophila,* degradation products of Chl *b*, Phe *b* and Chl *b',* were also produced, although the corresponding peaks are not seen in Figs. 2G' and 2H', because the amount was very small and the detection wavelength was 700 nm.

Chl d detected in processed algae

In our present studies, an organic solvent, acetone, was used, but the natural world is not abundant in acetone. So we next examined the presence of Chl *d* in *Chlorella* powder and dried laver, because organic solvents including acetone are not used to make such commercially available processed alga food.

Typical HPLC traces for *Chlorella* powder and dried laver are shown in Fig. 3. In *Chlorella* powder, small amounts of Chl *d* and Phe *d* were observed (Fig. 3A). By contrast, in dried laver considerable amounts of Chl *d* and Chl *d'* were clearly detected (Fig. 3B). Pheophytinization of Chl *a* seems to have proceeded in *Chlorella* powder processing (Fig. 3A). The Chl *d*, Chl *d',* Phe *a'* and Phe *d* molecules seen in Fig. 3 are the artifacts of Chl *a* produced through processing. It is not clear whether Phe *d* seen in *Chlorella* powder had been produced from Chl *a* followed by pheophytinization or directly from Phe *a* produced by pheophytinization of Chl *a*. Anyway, it is well worth noting that Chl *d*, Chl *d'* and Phe *d* were produced from Chl *a* in the absence of acetone, meaning that organic solvents are not needed to convert Chl *a* into Chl *d*-type pigments.

Conclusion

The present findings exhibit that the Chl *a* to Chl *d* conversion is not a rare event in nature, and will provide new insight into the unsolved question as to the birth of Chl *d* in photosynthesis. We want to emphasize that Chl *a* artifacts, Phe *a*, Chl *a'*, Chl *d* and Chl *d'*, function as key components in natural photosynthesis (Fig. 4). (Akiyama *et al.*, 2001; Kobayashi *et al.*, 2005; Ohashi *et al.*, 2008, 2010).

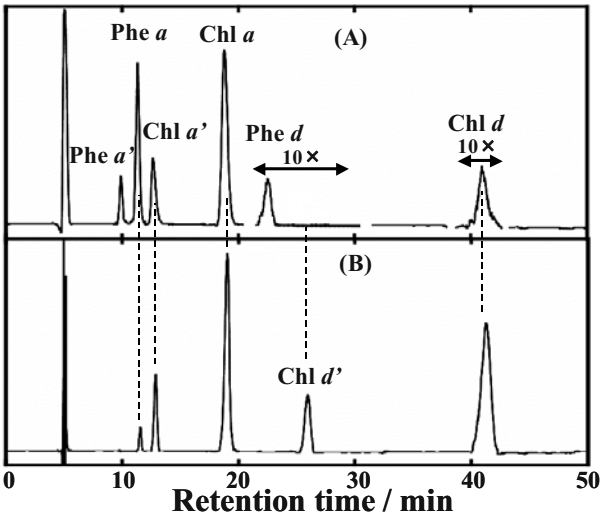

Fig. 3 Normal-phase HPLC elution profiles for (A) *Chlorella* powder and (B) dried laver. λ = 700 nm.

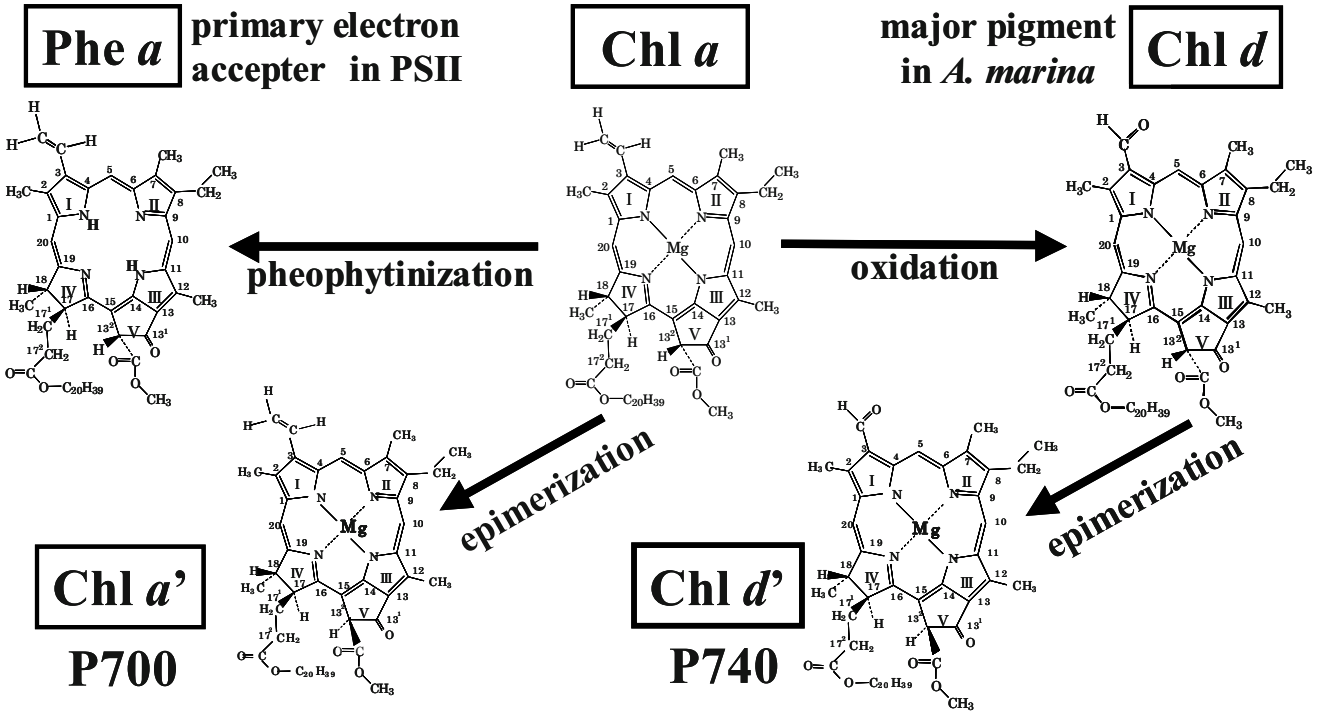

Fig. 4 Artifacts produced from Chl *a* and their function in natural photosynthesis.

References

Akiyama M, Miyashita H, Watanabe T, Kise H, Miyachi S, Kobayashi M (2001) Detection of Chlorophyll d' and Pheophytin a in a Chlorophyll d-Dominating Oxygenic Photosynthetic Prokaryote Acaryochloris Marina. Anal Sci 17: 205-208

Holt AS (1961) Further Evidence of the Relation between 2-Desvinyl-2-Formyl-Chlorophyll a and Chlorophyll d. Can. J. Botany. 39: 327-331

Holt AS, Morley HV (1959) A Proposed Structure for Chlorophyll d. Can. J. Chem. 37: 507-514

Kobayashi M, Watanabe S, Gotoh T, Koizumi H, Itoh Y, Akiyama M, Shiraiwa Y, Tsuchiya T, Miyashita

H, Mimuro M, Yamashita T, Watanabe T (2005) Minor but Key Chlorophylls in Photosystem II. Photosynth Res 84: 201-207

Koizumi H, Itoh Y, Hosoda S, Akiyama M, Hoshino T, Shiraiwa Y, Kobayashi M (2005) Serendipitous Discovery of Chl d Formation from Chl a with Papain. Sci Tech Adv Material 6: 551-557

Manning WM, Strain HH (1943) Chlorophyll d, a Green Pigment of the Red Algae. J Biol Chem 151: 1-19

Mironov AF, Ruziev RD, Lebedeva VS (2004) Synthesis and Chemical Transformations of N-Hydroxy- and N-Hydroxyalkylcycloimides of Chlorin p6. Russian J Bioorganic Chemistry 30: 466-476

Miyashita H, Ikemoto H, Kurano N, Adachi K, Chihara M, Miyachi S (1996) Chlorophyll d As a Major Pigment. Nature 383: 402

Ohashi S, Miyashita H, Okada N, T Iemura, Watanabe T, Kobayashi M (2008) Unique Photosystems in Acaryochloris Marina. Photosynth. Res. 98: 141-149

Ohashi S, Iemura T, Okada N, Itoh S, Furukawa H, Okuda M, Ohnishi-Kameyama M, Ogawa T, Miyashita H, Watanabe T, Itoh S, Oh-oka H, Inoue K, Kobayashi M (2010) An Overview on Chlorophylls and Quinones in the Photosystem I-Type Reaction Centers. Photosynth. Res. 104: 305-319

Okada N, Itoh S, Nakazato M, Miyashita H, Ohashi S, Kobayashi M (2009) Effective Hydrolysis of Chlorophyll a to Yield Chlorophyllide a by Papain in Aqueous Acetone. Current Topics in Plant Biology 10: 47-52

Conversion of Chl *a* into Chl *d* by Horseradish Peroxidase

Hayato Furukawa[a], Keisuke Aoki[a], Shingo Itoh[a], Yasuhiro Abe[a], Masataka Nakazato[b], Koji Iwamoto[c], Yoshihiro Shiraiwa[c], Hideaki Miyashita[d], Masaaki Okuda[a] , Masami Kobayashi[a]*

[a]Institute of Materials Science, University of Tsukuba, Japan;
[b]Chlorophyll Research Institute, Higashiyachiyo, Yamanashi, Japan;
[c]Institute of Biological Sciences, University of Tsukuba, Japan;
[d]Graduate School of Human and Environmental Studies, Kyoto University, Japan.
*Corresponding author. Tel. No. +81-298-53-6940; Fax No. +81-298-53-4490; E-mail: masami@ims.tsukuba.ac.jp.

Abstract: We report for the first time on the Chl *a* into Chl *d* conversion with horseradish peroxidase in aqueous acetone at room temperature in the dark, both in the presence and absence of hydrogen peroxide, H_2O_2. After 48 h incubation, the Chl *d* formation from Chl *a* catalyzed by horseradish peroxidase was observed in acetone/water (10/1, *v/v*) even in the absence of H_2O_2, where the conversion yield, 0.1%, was much lower than that observed in the case of papain, 2%. Very fast conversion occurred with the combination of horseradish peroxidase and dilute H_2O_2 (acetone/0.3% H_2O_2 = 10/1, *v/v*); the yield reached up to 1% for 2 h incubation. However, the converted Chl *d* was then gardually degraded probably due to the oxidation power of H_2O_2. In contrast, such a rapid conversion was not observed in the case of papain, where the conversion yield was, rather, depressed from 2% down to 0.2% by H_2O_2. These results suggest that chemical mechanisms for the Chl *a* into Chl *d* conversion catalyzed by papain and horseradish peroxidase are essentially different from each other, which will provide new insight into the unsolved question as to the birth of Chl *d* in nature.

Keywords: *Acaryochloris marina*; Chl *a*; Chl *d*; Horseradish peroxidase; Hydrogen peroxide(H_2O_2); Papain

Introduction

In 1943, Chl *d* (Fig. 1) was first discovered in some species of red algae (Manning and Strain, 1943). The molecule structure was then identified to be 3-desvinyl-3-formyl-Chl *a* (Holt and Morley, 1959; Holt, 1961). Since Chl *d* was not found in all red algae, Chl *d* had been hence thought to be an oxidative artifact of Chl *a*.

A Chl *d*-dominated cyanobacterium, *Acaryochloris marina*, was accidentally discovered in 1993 (Miyashita *et al.*, 1996; Ohashi *et al.*, 2008). Chl *d* is expected to be oxidatively biosynthesized from Chl *a*, where oxidative cleavage of the C = C double bond of a vinyl group of Chl *a* at ring I (–CH = CH_2 → –CHO) is required, while the biosynthetic pathway of Chl *d* in *Acaryochloris marina* has not yet been clarified. Chl *a* has many C = C bonds in the macrocycle (Fig. 1), and hence it is too difficult to oxidize only the C = C bond in the –CH = CH_2 moiety at ring I. Usually, both a special metal complex (*e.g.*, OsO_4) and an oxidant (*e.g.*, H_5IO_6) are needed for the selective oxidation (Mironov, 1996; Mironov *et al.*, 1994, 2004).

Recently, we came across the formation of Chl *d* from Chl *a* with papain(EC 3.4.22.2) in several aqueous organic solvents (Kobayashi *et al.*, 2005; Koizumi *et al.*, 2005; Okada *et al.*, 2009; Ohashi *et al.*, 2010). The Chl *a* to Chl *d* conversion was not observed when Chl *a* was incubated with esterases (esterase EC 3.1.1.1, cholesterol esterase EC 3.1.1.13, phosphatase EC 3.1.3.2) and other proteases (α-chymotrypsin EC 3.4.21.1, subtilisin carlsberg EC 3.4.21.14, ficin EC 3.4.22.3, bromelain EC 3.4.22.4) (Koizumi *et al*., 2005; Okada *et al*., 2009).

The same conversion was also observed when Chl *a* was incubated with several grated vegetables (Itoh

et al., 2009; in this issue). In particular, Japanese radish (root) showed higher conversion than papain. Japanese radish is known to be abundant in oxidase enzymes. Quite recently, we found that Chl *a* was nonenzymatically converted into Chl *d* in acetone/0.3% H_2O_2 (10/1, *v/v*) (Aoki *et al.*, in this issue).

In this study, we for the first time report on the Chl *a* into Chl *d* conversion with horseradish peroxidase even in the absence of H_2O_2.

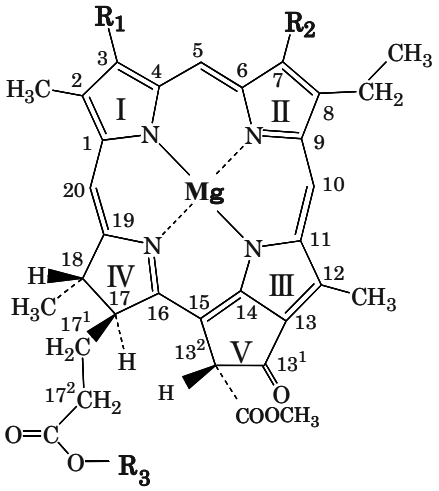

	R_1	R_2	R_3
Chl *a*	$CH=CH_2$	CH_3	$C_{20}H_{39}$
Chl *b*	$CH=CH_2$	CHO	$C_{20}H_{39}$
Chl *d*	CHO	CH_3	$C_{20}H_{39}$
Chlide *a*	$CH=CH_2$	CH_3	H

Fig. 1 Molecular structures and carbon numbering of chlorophylls, according to the IUPAC numbering system.

Materials and Methods

Pigment preparation

Chls *a* and *d* were extracted from parsley (*Petroselinum crispum*) and from *Acaryochloris marina* MBIC11017, respectively, and then they were purified by normal-phase HPLC as described previously (Akiyama, 2001).

Reaction of Chl a with enzymes

Commercially available horseradish peroxidase (EC 1.11.1.7, Wako 169-10791) and papain (EC 3.4.22.2, Calbiochem 5125) was used without further purification. The 0.5 mL of aqueous solution of enzyme (2 mg) was added to 5 mL of acetone containing Chl *a* (*ca.* 2×10^{-5} mol). The mixture was shaken gently at 303 K in the dark. In the reaction of Chl *a* with both enzyme and hydrogen peroxide, the 0.5 mL of aqueous solution containing enzyme and H_2O_2(0.03%, 0.3% and 3%) was used instead of the 0.5 mL of aqueous solution containing enzyme only.

Pigment analysis

Samples of the reaction mixture were taken periodically and filtered by poly(tetrafluoroethylene) membrane filters. The filtrate was injected into a reversed-phase Senshupak PEGASIL-ODS HPLC column (4.6 mm ID × 250 mm) cooled to 277 K in an ice-water bath. The pigments were eluted isocratically with degassed ethanol/methanol/2-propanol/water (86/13/1/3, *v/v/v/v*) at a flow rate of 0.3 mL/min, and were monitored with a JASCO Multiwavelength MD-2015 detector (λ = 300–800 nm).

Results and Discussion

Reaction of Chl a with peroxidase in the absence of H_2O_2

We have already reported that the conversion of Chl *a* into Chl *d* takes place in the presence of papain in aqueous acetone (Kobayashi *et al.*, 2005; Koizumi *et al.*, 2005; Okada *et al.*, 2009; Ohashi *et al.*, 2010), while the reaction mechanisms are not clear. The reaction is an oxidation reaction, but papain is not an oxidase but a protease. The problem involve the basic question why papain can catalyze the Chl *a* oxidation. In order to solve the question, we examined here the Chl *a* oxidation reaction catalyzed by an oxidase, horseradish peroxidase, and the same reaction was performed for the first time under the same conditions.

The Chl *a* into Chl *d* conversion was observed when Chl *a* was incubated with horseradish peroxidase in an acetone/H_2O(10/1, *v/v*) solution at 303 K in the dark (Fig. 2(right)). However, the conversion yield was unexpectedly very low (0.06% for 1 day incubation in Fig. 2(right; middle) and 0.1% for 2 day incubation in Fig. 2(right; bottom). The production yields are significantly smaller than those observed with papain (1.2% for 1-day incubation in Fig. 2(left; middle) and 2% for 2-day incubation in Fig. 2(left; bottom)).

We should note that chlorophyllide *a* (Chlide *a*, Fig. 1) was not produced when Chl *a* was incubated with horseradish peroxidase (date not shown). In the

case of papain, *ca.* 8% of Chlide *a* was observed after 2 day incubation under the same condition (Kobayashi *et al.*, 2005; Koizumi *et al.*, 2005; Okada *et al.*, 2009), which is reasonable because proteases are known to function as esterases in aqueous organic solvents (Gill *et al.*, 1996; Ooe *et al.*, 1999; Hasegawa *et al.*, 2003).

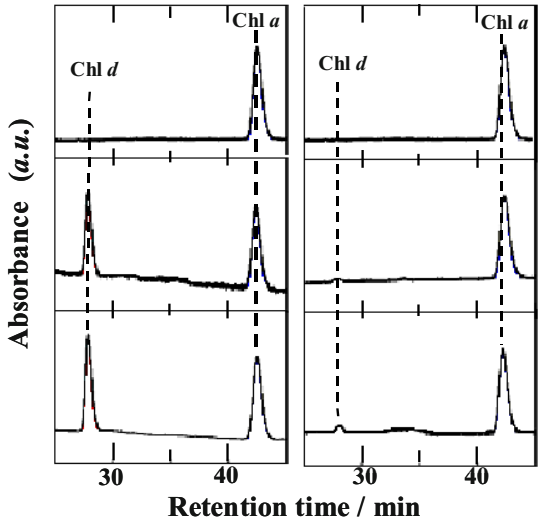

Fig. 2 Reversed-phase HPLC elution profiles for the reaction mixtures of Chl *a* with (left) papain and (right) horseradish peroxidase incubated in acetone/water(10/1, *v/v*) in the dark at 303 K. Incubation times were 0 day (top), 1 day (middle) and 2 days (bottom), respectively. Detection wavelength is 700 nm.

Reaction of Chl a with peroxidase in the presence of H_2O_2

We have shown that horseradish peroxidase is not efficient in converting Chl *a* into Chl *d* in the absence of hydrogen peroxide, H_2O_2. We then examined the conversion catalyzed by horseradish peroxidase in the presence of H_2O_2 in aqueous acetone.

An amazingly fast conversion occurred with the combination of peroxidase and H_2O_2 in an acetone/0.3% H_2O_2 (10/1, *v/v*) solution at 303 K in the dark. Approximately 1% of Chl *d* was produced within five minutes as seen in Fig. 3 (right; middle). In contrast, the conversion yield catalyzed by papain was quite low, 0.02%, in Fig. 3 (left; middle). When H_2O_2 was absent, Chl *d* was not detected for 5 min incubation with papain or horseradish peroxidase (date not shown). It is interesting to note that both production yields are significantly higher than that in the absence of H_2O_2.

However, Chl *d* could not be detected after 2-day incubation with horseradish peroxidase in the presence of 0.3% H_2O_2 (Fig. 3(right; bottom)). In contrast, the yield of Chl *d* production catalyzed by papain in the presence of 0.3% H_2O_2 incubated for 2 days were *ca.* 0.18% (Fig. 3 (left; bottom)), which is higher than that for 5 min incubation, 0.02% (Fig. 3 (left; middle)). Note that the conversion catalyzed papain for 2 day incubation was depressed by H_2O_2.

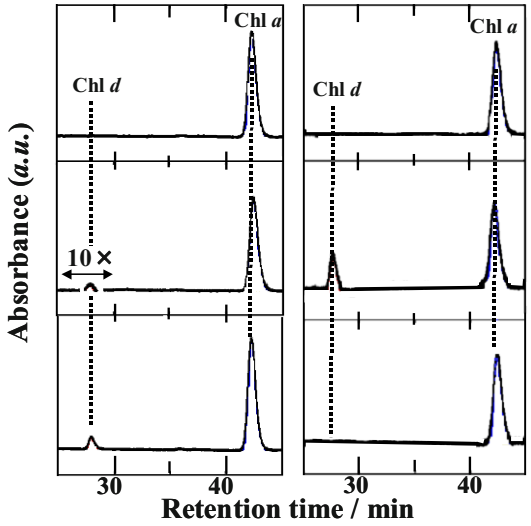

Fig. 3 Reversed-phase HPLC elution profiles for the reaction mixtures of Chl *a* with (left) papain and (right) horseradish peroxidase incubated in acetone/0.3% H_2O_2 (10/1, *v/v*) in the dark at 303 K. Incubation times were 0 min (top), 5 min (middle) and 2 days (bottom), respectively. Detection wavelength is 700 nm.

As seen in Fig. 4(B), the Chl *d* production yield reached to the maximum, *ca.* 1.4%, for 2 h incubation, when horseradish peroxidase coexisted with 0.3% H_2O_2 (□). Thereafter, the yield decreased and Chl *d* could not be detected after 2-day incubation. The converted Chl *d* seemed to be decomposed probably due to the strong oxidation power of H_2O_2. In the absence of H_2O_2, however, the Chl *d* production yield catalyzed horseradish peroxidase showed a slow increase (■).

Peroxidases have been thought to be involved in the biodegradation pathways of Chl *a* during senescence. Recently, horseradish peroxidase was reported to catalyze the hydrogen peroxide oxidation of Chl *a*, but the formation of Chl *d* was not described (Hynninen *et al.*, 2010), where the 13^2(S) and 13^2(R) diastereomers of 13^2-hydroxy-Chl *a* was characterized as major oxidation products.

In our study, however, the detection wavelength was 700 nm, and a small amount of 13^2-hydroxy-Chl *a* was under detectable level.

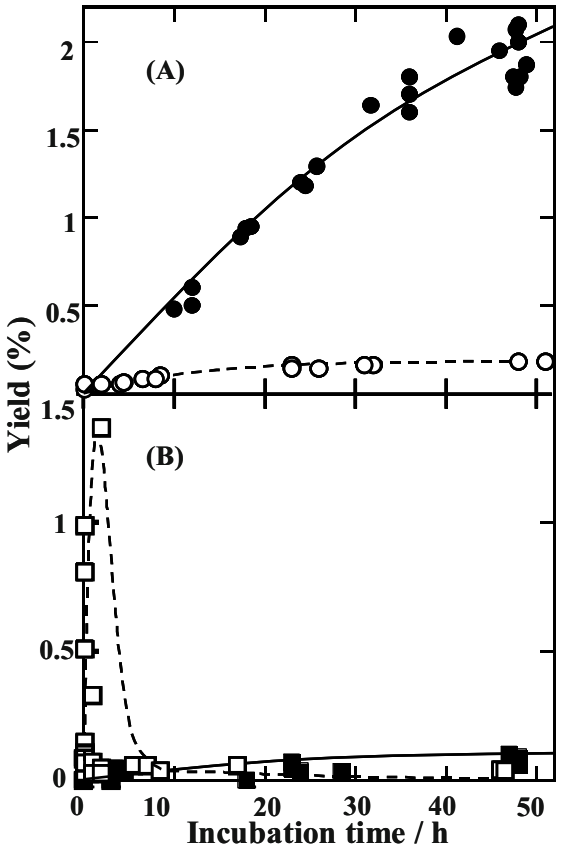

Fig. 4 Yields of Chl *d* production by the reactions of Chl *a* with (A) papain and (B) horseradish peroxidase in the absence of 0.3% H_2O_2 (● and ■) and in the presence of 0.3% H_2O_2 (○ and □) incubated in the dark at 303 K.

Reaction of Chl a with papain in the presence of H_2O_2

In contrast, such a rapid conversion from Chl *a* into Chl *d* was not observed in the case of papain even when H_2O_2 was present. The conversion catalyzed by papain was severely depressed by H_2O_2 (Fig. 4A).

These results suggest that the conversion from Chl *a* to Chl *d* catalyzed by papain and peroxidase are significantly different from each other.

Conclusion

As mentioned above, the Chl *a* into Chl *d* conversion was caused by many grated vegetables (Itoh *et al*., 2009; in this issue) as well as papain and horseradish peroxidase. It is interesting to note that the peroxidase enzymes are found widely in plants. Quite recently, we have detected Chl *d* in vegetable powder, sea vegetable powder, dried laver, green tea, and aging white radish leaves (unpublished data). Our findings suggest that the Chl *a* into Chl *d* conversion is not a rare event in nature, and will provide new insight into the unsolved question as to the birth of Chl *d* in natural photosynthesis. It is noteworthy that Chl *d*-derivatives are observed and widespread in oceanic and lacustrine environments covering a range of temperatures and salinities (Kashiyama *et al*., 2008), suggesting also that Chl *d* seems to be rather easily produced as an artifact of Chl *a* in natural environment.

References

Akiyama M, Miyashita H, Watanabe T, Kise H, Miyachi S, Kobayashi M (2001) Detection of Chlorophyll *d*′ and Pheophytin *a* in a Chlorophyll *d*-Dominating Oxygenic Photosynthetic Prokaryote Acaryochloris Marina. Anal Sci 17: 205-208

Gill I, López-Fandiño R, Jorba X, Vulfson EN (1996) Biologically Active Peptides and Enzymatic Approaches to Their Production. Enzyme Microbiol. Technol. 18: 162-183

Hasegawa M, Yamamoto S, Kobayashi M, Kise H (2003) Catalysis of Protease/Cyclodextrin Complexes in Organic Solvents Effects of Reaction Conditions and Cyclodextrin Structure on Catalytic Activity of Proteases. Enzyme Microbial Technol. 32: 356-361

Holt AS (1961) Further Evidence of the Relation between 2-Desvinyl-2-Formyl-Chlorophyll a and Chlorophyll d. Can. J. Botany. 39: 327-331

Holt AS, Morley HV (1959) A Proposed Structure for Chlorophyll d. Can. J. Chem. 37: 507-514

Hynninen PH, Kaartinen V, Kolehmainen E (2010) Horseradish Peroxidase-Catalyzed Oxidation of Chlorophyll a with Hydrogen Peroxide Characterization of the Products and Mechanism of the Reaction. Biochimica et Biophysica Acta 1797: 531-542

Itoh S, Okada N, Ohashi S, Nakazato M, Iwamoto K, Shiraiwa Y, Miyashita H, Kobayashi M (2009) Novel Conversion of Chlorophyll a into Chlorophyll d Catalyzed by Extracts of Vegetables and Fruits. Phycologia. 48(4): 49-50

Kashiyama Y, Miyashita H, Ohkubo S, Ogawa NO, Chikaraishi Y, Takano Y, Suga H, Toyofuku T, Nomaki H, Kitazato H, Nagata T, Ohkouchi N (2008) Evidence of Global Chlorophyll d. Science 321:658

Kobayashi M, Watanabe S, Gotoh T, Koizumi H, Itoh Y, Akiyama M, Shiraiwa Y, Tsuchiya T, Miyashita

H, Mimuro M, Yamashita T, Watanabe T (2005) Minor but Key Chlorophylls in Photosystem II. Photosynth Res 84: 201-207

Koizumi H, Itoh Y, Hosoda S, Akiyama M, Hoshino T, Shiraiwa Y, Kobayashi M (2005) Serendipitous Discovery of Chl d Formation from Chl a with Papain. Sci Tech Adv Material 6: 551-557

Manning WM, Strain HH (1943) Chlorophyll d, a Green Pigment of the Red Algae. J Biol Chem 151: 1-19

Mironov AF (1996) Synthesis and Properties of New Chlorin and Bacteriochlorin Photosensitizers. Proc SPIE 2625: 23-32

Mironov AF, Kozyrev AN, Perepyolkin PY (1994) New Sensitizers for Diagnosis and Photodynamic Therapy of Malignant Tissues. Proc SPIE 2078: 186-192

Mironov AF, Ruziev RD, Lebedeva VS (2004) Synthesis and Chemical Transformations of N-hydroxy- and N-hydroxyalkylcycloimides of Chlorin p6. Russian J Bioorganic Chemistry 30: 466-476

Miyashita H, Ikemoto H, Kurano N, Adachi K, Chihara M, Miyachi S (1996) Chlorophyll d As a Major Pigment. Nature 383: 402

Ohashi S, Miyashita H, Okada N, T Iemura, Watanabe T, Kobayashi M (2008) Unique Photosystems in Acaryochloris Marina. Photosynth. Res. 98: 141-149

Ohashi S , Iemura T, Okada N, Itoh S, Furukawa H, Okuda M, Ohnishi-Kameyama M, Ogawa T, Miyashita H, Watanabe T, Itoh S, Oh-oka H, Inoue K, Kobayashi M (2010) An Overview on Chlorophylls and Quinones in the Photosystem I-Type Reaction Centers. Photosynth. Res. 104: 305-319

Okada N, Itoh S, Nakazato M, Miyashita H, Ohashi S, Kobayashi M (2009) Effective Hydrolysis of Chlorophyll a to Yield Chlorophyllide a by Papain in Aqueous Acetone. Current Topics in Plant Biology 10: 47-52

Ooe Y, Yamamoto S, Kobayashi M, Kise H (1999) Increase of Catalytic Activity of α-Chymotrypsin in Organic Solvent by Co-Lyophilization with Cyclodextrins. Biotechnol. Lett. 21: 385-389

Novel Conversion of Chl *a* into Chl *d* Catalyzed by Grated Vegetables

Shingo Itoh[a], Keisuke Aoki[a], Masataka Nakazato[b], Koji Iwamoto[c],Yoshihiro Shiraiwa[c], Hideaki Miyashita[d], Masaaki Okuda[a], Masami Kobayashi[a]*

[a]Institute of Materials Science, University of Tsukuba, Japan;
[b]Chlorophyll Research Institute, Higashiyachiyo, Yamanashi, Japan;
[c]Institute of Biological Sciences, University of Tsukuba, Japan;
[d]Graduate School of Human and Environmental Studies, Kyoto University, Japan.
*Corresponding author. Tel. No. +81-298-53-6940; Fax No. +81-298-53-4490; E-mail: masami@ims.tsukuba.ac.jp.

Abstract: Novel conversion of Chl *a* to Chl *d* was observed when Chl *a* was incubated in aqueous acetone with grated papaya(skin), Japanese radish(root), wasabi(rhizome), turnip(root), broccoli(stalk), white radish(leaf), cabbage(leaf), qing-geng-cai(leaf), napa cabbage(leaf), rocket salad(leaf), scallion(leaf), garlic(bulb), green pepper(skin), garlic chives(leaf), Japanese parsley(leaf), cucumber(skin), spinach(leaf), and haricot(bean), and eggplant(skin). It is interesting to note that Chl *d* was not present in the initial vegetables. In contrast, the Chl *a* into Chl *d* conversion was not observed, when several fruits or chile pepper(bean), tomato(skin), green pea(bean), string bean(bean), ginger(roots), corn marigold(leaf) and alligator pear(skin) were used. Our finding suggests that the Chl *a* to Chl *d* conversion is not a rare event in nature, and will provide new insight into the unsolved question as to the birth of Chl *d* in natural photosynthesis.

Keywords: *Acaryochloris marina*; Chl *a*; Chl *d*; Oxidase; Papain; Vegetable

Introduction

The biosynthetic pathway of Chl *d* in *Acaryochloris marina* (Miyashita *et al*., 1996) has not yet been clarified. We serendipitously came across the formation of Chl *d* from Chl *a* with papain EC 3.4.22.2 in several aqueous organic solvents at room temperature in the dark (Kobayashi *et al*., 2005; Koizumi *et al*., 2005; Okada *et al*., 2009; Ohashi *et al*., 2010). Papain is a proteolytic and thiol protease with a relatively low selectivity which is widely used in food and medical fields. The Chl a into Chl d conversion was not observed when Chl a was incubated with esterases (esterase EC 3.1.1.1, cholesterol esterase EC 3.1.1.13, phosphatase EC 3.1.3.2) and other proteases (α-chymotrypsin EC 3.4.21.1, subtilisin carlsberg EC 3.4.21.14; ficin EC 3.4.22.3, bromelain EC 3.4.22.4) (Koizumi *et al*., 2005; Okada *et al*., 2009).

In order to clarify the conversion mechanism *in vitro* and the origin of Chl *a* to Chl *d* conversion in nature, we incubated Chl *a* with grated vegetables in acetone/H_2O (10/1, *v/v*) at 303 K for 72 h in the dark.

Materials and Methods

Pigment preparation

Chls *a* and *d* were extracted from parsley (*Petroselinum crispum*) and from *Acaryochloris marina* MBIC11017, respectively, and then they were purified by normal-phase HPLC as described previously (Akiyama, 2001).

Reaction of Chl a with grated vegetables

Commercially available fresh vegetable was cut to 0.5 cm^3(1 cm × 1 cm × 0.5 mm), and was then grated by a grater. Grated vegetable was then ground in a glass mortar for 1 min at 277 K. The ground materials was transferred in to a small glass beaker, to which 0.5 mL of water was added. The mixture was then added to 5 mL of acetone containing Chl *a* (*ca*. 2×10^{-5} mol). The reaction mixture was sonicated for 30 s at 277 K, and then shaken gently at 303 K in the dark. In the case of leaf, grating procedure was omitted.

Pigment analysis

Samples of the reaction mixture were taken

periodically and filtered by poly(tetrafluoroethylene) membrane filters. The filtrate was injected into a reversed-phase Senshupak PEGASIL-ODS HPLC column (4.6 mm ID × 250 mm) cooled to 277 K in an ice-water bath. The pigments were eluted isocratically with degassed ethanol/methanol/2-propanol/water (86/13/1/3, *v/v/v/v*) at a flow rate of 0.3 mL/min, and were monitored with a JASCO Multiwavelength MD-2015 detector (λ = 300–800 nm).

Results and Discussion

Reaction of Chl a with papain and papaya

We have already reported that the Chl *a* to Chl *d* conversion occurred in the presence of papain in aqueous organic solvents at room temperature in the dark (Kobayashi *et al*., 2005; Koizumi *et al*., 2005; Okada *et al*., 2009; Ohashi *et al*., 2010). However, some researchers complained that the reaction was not performed by papain, but was caused by some chemical impurities used for papain preparation. In order to make their complaints die down, we examined papaya.

Typical HPLC traces for the reaction mixture of Chl *a* with papain, grated mature papaya, and immature papaya incubated in an acetone/water (10/1, *v/v*) solution in the dark at 303 K for 2 days are shown in Fig. 1. The Chl *a* into Chl *d* conversion was clearly observed when Chl *a* was incubated with grated immature papaya(skin) (Fig. 1C), but the conversion did not occur when mature papaya (skin) was used (Fig. 1B). The conversion yield in the case of immature papaya(skin) was 1.8% (Fig. 1C), almost as same as that of papain (Fig. 1A). The conversion was not observed when immature papaya (flesh) was used (data not shown). The yield of Chlide *a* formation was lower (0.23%, Fig. 1C) when immature papaya (skin) was used than that when papain was used (*ca*. 2%, Fig. 1A), but immature papaya (flesh) showed a little higher yield (0.85%) than immature papaya (skin).

Reaction of Chl a with grated Japanese radish and wasabi

As seen in Fig. 1, papaya showed an effective conversion of Chl *a* to Chl *d* like papain, and we then examined grated vegetables. A typical HPLC trace for Japanese radish (root) is shown in Fig. 2A. The conversion yield was *ca*. 8%, which is remarkably higher than that incubated with papain, *ca*. 2% (Fig. 2C). As shown in Fig. 2B, wasabi (rhizome) also showed the similar conversion yield (1.6%) to that of papain. In contrast, Japanese radish (leaf) showed very low conversion yield (0.02%).

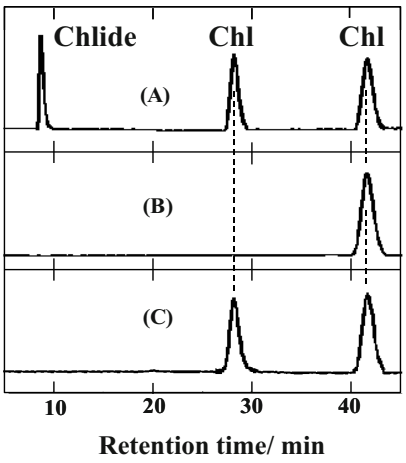

Fig. 1 Reversed-phase HPLC elution profiles for the reaction mixtures of Chl *a* incubated for 2 days in acetone/water (10/1, *v/v*) in the dark at 303 K with (A) papain, (B) grated mature papaya (skin), and (C) grated immature papaya (skin). Detection wavelength is 700 nm.

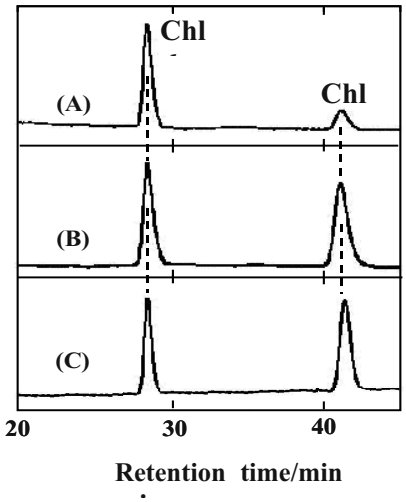

Fig. 2 Reversed-phase HPLC elution profiles for the reaction mixtures of Chl *a* with (A) grated Japanese radish (root), (B) grated wasabi (rhizome), and (C) papain for 3 day incubation in acetone/water (10/1, *v/v*) in the dark at 303 K. Detection wavelength is 700 nm.

The absorption spectrum of the pigment eluting at 28 min in Fig. 2 in an HPLC eluent was completely different from that of authentic Chl *a*, but virtually identical to that of authentic Chl *d* (Fig. 3). The pigment had the same elution time as that of authentic Chl *d* purified from *A. marina* (data not shown). We thus conclude that this pigment is Chl *d*.

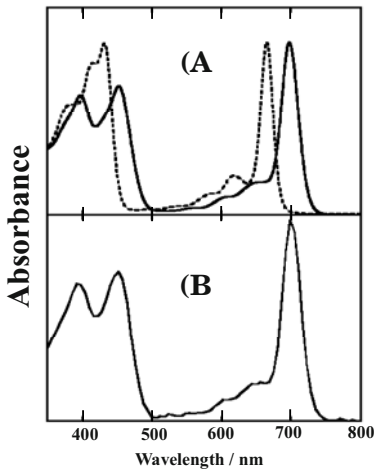

Fig. 3 Absorption spectra in an HPLC eluent of (A) authentic Chl *a* (-----) and Chl *d* (⎯), and (B) a produced pigment at the retention time of 28 min in Figs. 1, 2 and 4.

Successful vegetables

The following vegetables also exhibited the Chl *a* into Chl *d* conversion under the same conditions; turnip (root: 0.7%), broccoli (stalk: 0.5%), white radish (leaf: 0.48%), cabbage (leaf: 0.16%), qing-geng-cai (leaf: 0.1%), napa cabbage (leaf: 0.1%), rocket salad (leaf: 0.08%), scallion (leaf: 0.48%), garlic (bulb: 0.3%), garlic chives (leaf; 0.03%), cucumber (skin; 0.2%), melon (flesh: 0.2%), green pepper (skin; 0.04%), Japanese parsley (leaf; 0.05%), spinach (leaf; 0.12%), haricot (bean; 0.1%), and eggplant (skin;0.01%). We should emphasize that Chl *d* was not present at all in the initial vegetables examined here.

The yields of Chl *a* to Chl *d* as well as those of Chl *a* to Chlide *a* are summarized in Table 1. It is clearly seen that the *Brassicaceae family* showed the significantly effective Chl *a* into Chl *d* conversion. As mentioned above, the most efficient conversion was performed with Japanese radish(root); the yield was *ca*. 8%, remarkably higher than that incubated with papain, *ca*. 2%. The *Brassicaceae family*, especially Japanese radish, is known to be abundant in oxidases, and hence some oxidase enzymes in it catalyzed the Chl *a* into Chl *d* conversion in our present study.

It is noteworthy that the conversion is part-dependent. As seen in Table 1, the "leaf" of scallion caused the conversion, but the "sheath" of scallion did not. Like this, the skin of cucumber, the flesh of melon, the skin of eggplant, the skin of papaya and the bean of haricot caused the conversion, but the flesh of cucumber, the skin of melon, the flesh of eggplant, the flesh of papaya and the pod of haricot did not. The present results are most probably due to the quantity of oxidase enzymes, and further examination is needed.

Table 1 Conversion yields from Chl *a* to Chl *d* and Chlide *a* catalyzed by grated vegetables and fruits incubated in acetone/H_2O_2(10/1, *v/v*) at 303 K for 3 days in the dark.

Family	Names of Vegetables and fruits(part)	Yield(%) Chl *d*	Chlide *a*
Brassicaceae	Japanese radish(root)	7.90	0.89
	(leaf)	0.02	0.16
	wasabi(rhizome)	2.60	1.84
	Turnip(root)	0.70	7.50
	broccoli(stalk)	0.50	0.61
	white radish(leaf)	0.48	0.38
	cabbage	0.16	0.22
	qing geng cai(leaf)	0.11	1.03
	napa cabbage	0.11	9.70
	rocket-salad(leaf)	0.08	1.30
Liliaceae	scallion(leaf)	0.48	0.40
	(sheath)	0	0
	garlic	0.30	0.45
	garlic chives	0.03	0.19
Cucurbitaceae	cucumber(skin)	0.20	0.13
	(flesh)	0	0
	melon(flesh)	0.20	0.08
	(skin)	0	0.20
Solanaceae	eggplant(skin)	0.01	0.43
	(flesh)	0	0.82
	green pepper(skin)	0	0.22
	(flesh)	0	0.13
	chile pepper(bean)	0	33.09
	tomato(skin)	0	0
Caricaceae	papaya(skin)	1.93	0.25
	(flesh)	0	0.90
Apiaceae	Japanese parsley(leaf)		
Chenopodiaceae	spinach(leaf)	0.12	
Fabaceae	haricot(bean)	0.10	0.10
	(pod)	0	22.64
	green pea(bean)	0	1.35
	string bean(bean)	0	0.49
	(pod)	0	2.70
Asteraceae	corn marigold(leaf)	0	1.90
	lettuce(leaf)	0	0.06
Zingiberaceae	ginger (rhizome)	0	0.45
Malvaceae	alligator pear(skin)	0	0.97
Rutaceae	satsuma orange(peel)	0	96.35
	lime(peel)	0	53.44
	oroblanco(peel)	0	94.43
	kabosu(peel)	0	0
	yuzu(peel)	0	23.91
Actinidiaceae	kiwifruit(peel)	0	0
Moraceae	fig tree(peel)	0	3.11
Rosaceae	strawberry(flesh)	0	0.68

Unsuccessful vegetables and fruits

In contrast, the Chl *a* into Chl *d* conversion was not observed, when some vegetables, *e.g*., chile pepper(bean), tomato(skin), green pea(bean), string bean(bean), ginger(roots), corn marigold(leaf), alligator pear(skin) were used. Several fruits examined here showed no conversion of Chl *a* into Chl *d*; satsuma orange, lime, oroblanco, kabosu, yuzu, kiwi fruit, fig, strawberry, *etc*.

Effect of Solvent

The conversion of Chl *a* into Chl *d* catalyzed by

papain in aqueous or 5 ganic solution (organic solvent/ water = 10/1, *v/v*) was found to be solvent-dependent. In our previous study, acetone gave the highest yield, *ca*. 2%, followed by 2-propanol(1.1%), methanol(0.5%), ethanol(0.3%) and acetonitrile(0.3%) (Okada *et al*., 2009). In nature, ethanol seems to be the most available of all the above organic solvents. We hence examined the conversion in aqueous ethanol.

Typical HPLC traces for ground white radish(leaf) without additional Chl *a* incubated at 303 K in the dark for 2 days are shown in Fig. 4. We should note that initial leaf of white radish contained no Chl *d* at all (Fig. 4A). In aqueous acetone, the Chl *d* production yield was 0.27% (Fig. 4B), while in aqueous ethanol the yield was almost the same, 0.28% (Fig. 4C). Ethanol is produced by natural fermentation with grate ease, and aqueous ethanol condition is not a rare environment in nature.

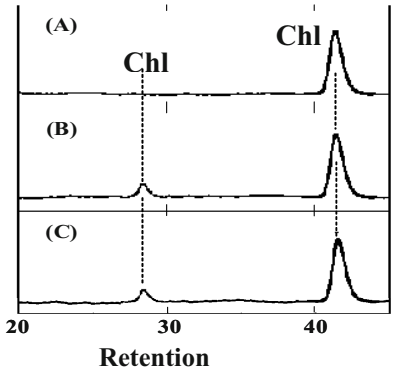

Fig. 4 Reversed-phase HPLC elution profiles for the grated white radish (leaf) incubated in (B) acetone/water (10/1, *v/v*) and (C) ethanol/water (10/1, *v/v*) at 303 K in the dark. Incubation time is (A) 0 min, and (B,C) 2 days, respectively. Detection wavelength is 700 nm.

Conclusion

In this study, novel conversion of Chl *a* into Chl *d* was performed by many grated vegetables in aqueous ethanol as well as aqueous acetone.

Quite recently, we discovered the Chl *a* into Chl *d* conversion without additional Chl *a* and organic solvent (data not shown). Chl *d* was detected, when ground leaf of white radish was incubated at 303 K in the dark for 3 h, where no organic solvent, water and Chl *a* were added (unpublished data), suggesting the new idea for the birth of Chl *d* as a degradation product of Chl *a* in aging leaves. Moreover, Chl *d* was clearly detected in processed food, *e.g*., vegetable powder, sea vegetable powder, grilled laver and green tea (unpublished data). More details will be reported elsewhere.

These findings indicate us that the Chl *a* to Chl *d* conversion is not a rare event in nature, and will provide new insight into the unsolved question as to the birth of Chl *d* in photosynthesis. It is noteworthy that Chl *d*-derivatives are observed and widespread in oceanic and lacustrine environments covering a range of temperatures and salinities (Kashiyama *et al*. 2008). Some of them seem to be produced as artifacts of Chl *a* in a natural environment.

References

Akiyama M, Miyashita H, Watanabe T, Kise H, Miyachi S, Kobayashi M (2001) Detection of Chlorophyll d' and Pheophytin a in a Chlorophyll d-Dominating Oxygenic Photosynthetic Prokaryote Acaryochloris Marina. Anal Sci 17: 205-208

Kashiyama Y, Miyashita H, Ohkubo S, Ogawa NO, Chikaraishi Y, Takano Y, Suga H, Toyofuku T, Nomaki H, Kitazato H, Nagata T, Ohkouchi N (2008) Evidence of Global Chlorophyll d. Science 321: 658

Kobayashi M, Watanabe S, Gotoh T, Koizumi H, Itoh Y, Akiyama M, Shiraiwa Y, Tsuchiya T, Miyashita H, Mimuro M, Yamashita T, Watanabe T (2005) Minor but Key Chlorophylls in Photosystem II. Photosynth Res 84: 201-207

Koizumi H, Itoh Y, Hosoda S, Akiyama M, Hoshino T, Shiraiwa Y, Kobayashi M (2005) Serendipitous Discovery of Chl d Formation from Chl a with Papain. Sci Tech Adv Material 6: 551-557

Miyashita H, Ikemoto H, Kurano N, Adachi K, Chihara M, Miyachi S (1996) Chlorophyll d As a Major Pigment. Nature 383: 402

Ohashi S, Iemura T, Okada N, Itoh S, Furukawa H, Okuda M, Ohnishi-Kameyama M, Ogawa T, Miyashita H, Watanabe T, Itoh S, Oh-oka H, Inoue K, Kobayashi M (2010) An Overview on Chlorophylls and Quinones in the Photosystem I-Type Reaction Centers. Photosynth. Res.. 104: 305-319

Okada N, Itoh S, Nakazato M, Miyashita H, Ohashi S, Kobayashi M (2009) Effective Hydrolysis of Chlorophyll a to Yield Chlorophyllide a by Papain in Aqueous Acetone. Current Topics in Plant Biology 10: 47-52

Nonenzymatic Formation of Chl *d* from Chl *a* with Hydrogen Peroxide

Keisuke Aoki[a], Shingo Itoh[a], Hayato Furukawa[a], Masataka Nakazato[b], Koji Iwamoto[c], Yoshihiro Shiraiwa[c], Hideaki Miyashita[d], Masaaki Okuda[a] ,Masami Kobayashi[a]*

[a]Institute of Materials Science, University of Tsukuba, Japan;
[b]Chlorophyll Research Institute, Higashiyachiyo, Yamanashi, Japan;
[c]Institute of Biological Sciences, University of Tsukuba, Japan;
[d]Graduate School of Human and Environmental Studies, Kyoto University, Japan.
*Corresponding author. Tel. No. +81-298-53-6940; Fax No. +81-298-53-4490; E-mail: masami@ims.tsukuba.ac.jp.

Abstract: Nonenzymatic conversion of Chl *a* to Chl *d* was performed for the first time by dilute hydrogen peroxide (H_2O_2) in aqueous acetone (acetone/dilute H_2O_2 = 10/1, *v/v*) at 303 K in the dark. The conversion was observed within five minutes incubation when 0.3% H_2O_2 was used. The Chl *d* production yield reached to the maximum, *ca.* 0.41%, at the incubation time of 5 min. The Chl *a* to Chl *d* conversion was also observed when 3% H_2O_2 and 0.03% H_2O_2 were used, but the maximum yields were much lower, 0.05% and 0.16%, respectively. The converted Chl *d* was then gradually degraded probably due to the strong oxidation power of H_2O_2. Our findings indicate that Chl *d* is apt to be produced as one of the degradation products of Chl *a* in nature.

Keywords: *Acaryochloris marina*; Chl *a*; Chl *d*; Hydrogen peroxide; Oxidation; Papain

Introduction

In 1943, Chl *d* (Fig. 1) was first discovered in some species of red algae (Manning and Strain, 1943). The molecule structure was then identified to be 3-desvinyl-3-formyl-Chl *a* (Holt and Morley, 1959; Holt, 1961). However, Chl *d* was found to be produced oxidatively from Chl *a*, and Chl *d* was not found in all red algae. Chl *d* had been hence thought to be an oxidative artifact of Chl *a*.

A Chl *d*-dominated cyanobacterium, *Acaryochloris marina*, was discovered in 1993 (Miyashita *et al.*, 1996; Ohashi *et al.*, 2008), although the biosynthetic pathway of Chl *d* in *Acaryochloris marina* has not yet been clarified.

We serendipitously came across the formation of Chl *d* from Chl *a* catalyzed by a protease, papain, in aqueous organic solvents at room temperature in the dark (Kobayashi *et al.*, 2005; Koizumi *et al.*, 2005; Okada *et al.*, 2009; Ohashi *et al.*, 2010).

Recently, we demonstrated that the same conversion proceeded when Chl *a* was incubated with several grated vegetables (Itoh *et al.*, 2009; in this issue). Especially, Japanese radish (root) abundant in oxidase enzymes showed significantly higher.

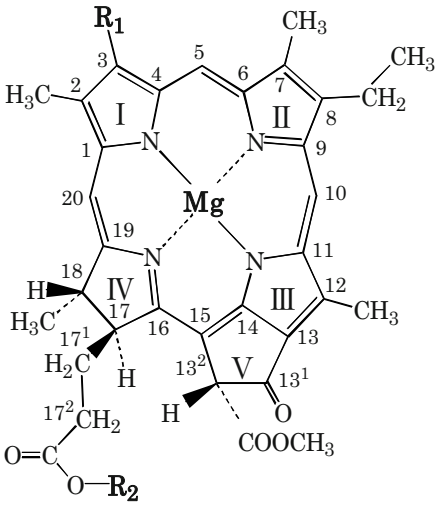

	R_1	R_2
Chl *a*	$CH=CH_2$	$C_{20}H_{39}$
Chl *d*	CHO	$C_{20}H_{39}$
Chlide *a*	$CH=CH_2$	H

Fig. 1 Molecular structures and carbon numbering of Chl *a* and *d*, according to the IUPAC numbering system conversion yield (8%) than papain (2%), indicating that some oxidase enzymes catalyzed the Chl *a* into Chl *d* conversion and that some active oxygen species were concerned in this reaction.

In the present study, we report for the first time on the nonenzymatic Chl *a* into Chl *d* conversion by hydrogen peroxide, H_2O_2, in aqueous acetone at room temperature in the dark.

Materials and Methods

Pigment preparation

Chls *a* and *d* were extracted from parsley (*Petroselinum crispum*) and from *Acaryochloris marina* MBIC11017, respectively, and then they were purified by normal-phase HPLC as described previously (Akiyama, 2001).

Reaction of Chl a with hydrogen peroxide

The 0.5 mL of aqueous solution of hydrogen peroxide (0.03, 0.3 and 3%) was added to 5 mL of acetone containing Chl *a* (*ca.* 2×10^{-5} mol). The mixture was shaken gently at 303 K in the dark.

Pigment analysis

Samples of the reaction mixture were taken periodically and filtered by poly(tetrafluoroethylene) membrane filters. The filtrate was injected into a reversed-phase Senshupak PEGASIL-ODS HPLC column (4.6 mm ID × 250 mm) cooled to 277 K in an ice-water bath. The pigments were isocratically with degassed ethanol/methanol/2-propanol/water (86/13/1/3, *v/v/v/v*) at a flow rate of 0.3 mL/min, and were monitored with a JASCO Multiwavelength MD-2015 detector (λ = 300–800 nm).

Results and Discussion

Reaction of Chl a with 0.3% hydrogen peroxide (H_2O_2)

A typical HPLC trace for Chl *a* incubated in an acetone/0.3% H_2O_2 (10/1, *v/v*) solution in the dark at 303 K for 5 min is shown in Fig. 2B. A minor and new pigment eluting at 28 min was detected. The new pigment had the same elution time as that of authentic Chl *d* purified from *A. marina* (Fig. 2C), indicating that novel formation of Chl *d* from Chl *a* occurred in aqueous acetone in the presence of dilute hydrogen peroxide at room temperature in the dark.

The absorption spectrum of this pigment in an HPLC eluent (Fig. 2E) was completely different from that of authentic Chl *a* (Fig. 2D), but virtually identical to that of authentic Chl *d* (Fig. 2F), where the Soret and Q_Y-bands were red-shifted, the Soret band was clearly split, and the Soret/Q_Y-band ratio was less than 1.0. We thus conclude that this pigment is Chl *d*.

The novel nonenzymatic conversion of Chl *a* into Chl *d* was for the first time performed by dilute H_2O_2. It is noteworthy that the conversion was observed within five minutes incubation at 303 K in the dark when 0.3% H_2O_2 was used, while the conversion yield was not so high, *ca.* 0.41% (Fig. 2B). We should note that Chl *d* formation was not observed at all for five minutes incubation in our previous studies when papain was used (Kobayashi *et al.*, 2005; Koizumi *et al.*, 2005; Okada *et al.*, 2009). We have better to emphasize also that in the absence of H_2O_2 Chl *d* was not detected at all in aqueous acetone for 3 day incubation. In contrast to papain (Kobayashi *et al.*, 2005; Koizumi *et al.*, 2005; Okada *et al.*, 2009), H_2O_2 did not produce chlorophyllide *a* (Chlide *a*, Fig. 1) from Chl *a* in the present study (data not shown).

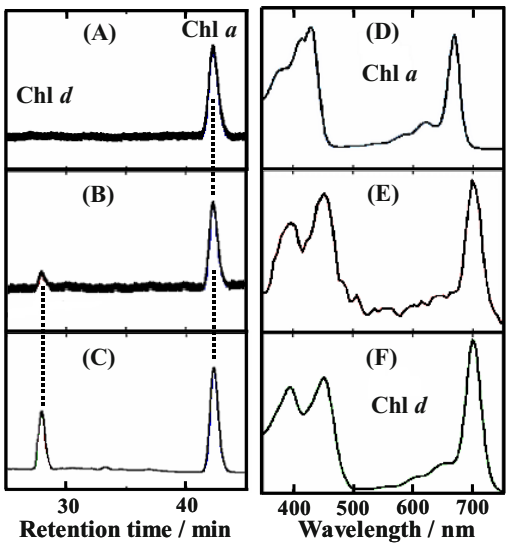

Fig. 2 (Left) Reversed-phase HPLC elution profiles for Chl *a* incubated in an acetone/0.3% H_2O_2 (10/1, *v/v*) solution at 303 K in the dark for (A) 0 min and (B) 5 min; (C) authentic Chl *a* and Chl *d*. Detection wavelength is 700 nm. (Right) Absorption spectra in an HPLC eluent of authentic (D) Chl *a*, (F) Chl *d*, and of (E) the produced pigment at the retention time of 28 min in (B).

Effect of H_2O_2 concentration on Chl d formation

The concentration of commercially available hydrogen peroxide aqueous solution is *ca.* 30%, and is a strong oxidizing agent. Oxidation power of 30% hydrogen peroxide is strong enough to degrade chlorophylls rapidly, and hence the H_2O_2 solution was diluted with water in the present study.

As mentioned above, the novel nonenzymatic conversion of Chl *a* into Chl *d* was performed only five min incubation when a 0.3% H_2O_2 solution was

used. However, the conversion yield was not so high, *ca.* 0.41% (Fig. 2B). In order to increase the conversion yield, Chl *a* was allowed to react with various concentrations of H_2O_2.

Typical HPLC traces for the reaction mixtures incubated at 303 K in the dark for 5 min are shown in Fig. 3(top). The Chl *a* into Chl *d* conversion was observed also when 3% H_2O_2 (Fig. 3A) and 0.03% H_2O_2 (Fig. 3E) were used, but the yields were much lower, 0.05% and 0.16%, than that when 0.3% H_2O_2 was used (0.41% in Fig. 3C).

In Fig. 3(bottom), typical HPLC traces for 2-day incubation are shown. Unexpectedly, the conversion yields decreased in all cases as seen in Figs. 3B, 3D and 3F, where the yields were around 0.03%.

As seen in Fig. 4, the Chl *d* production yield reached to the maximum, *ca.* 0.41%, at the incubation time of 5 min, when 0.3% H_2O_2 was used. Thereafter, the yield decreased. The results suggest that the converted Chl *d* was degraded probably due to the oxidation power of H_2O_2, even when dilute H_2O_2 was used. The reaction prefers rather mild experimental conditions, and the quest for such mild reaction conditions now goes on.

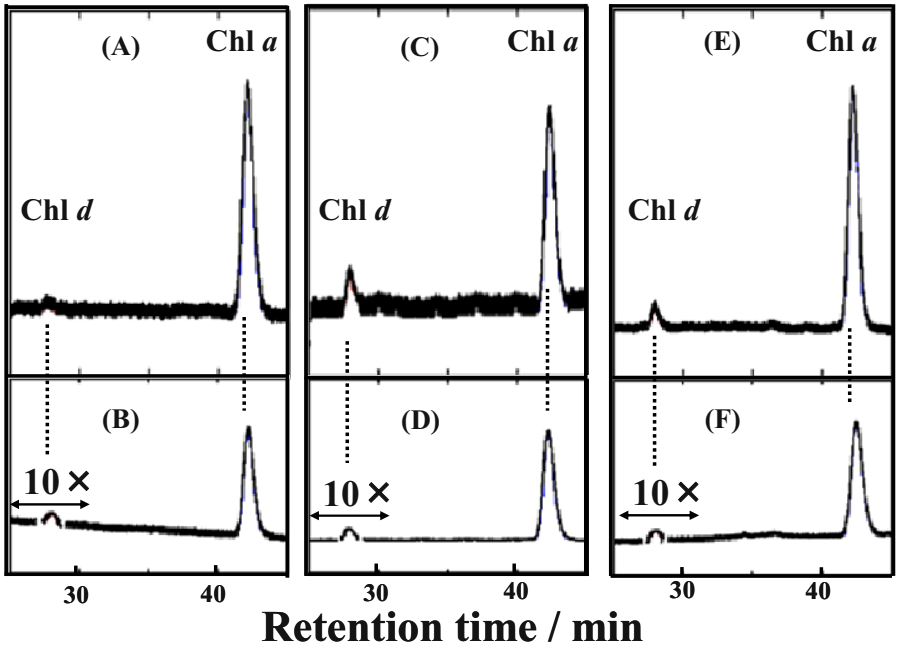

Fig. 3 Reversed-phase HPLC elution profiles for the reaction mixtures of Chl *a* with several concentrations of H_2O_2 incubated an acetone/H_2O_2 (10/1, *v/v*) solution at 303 K in the dark for (A,C,E) 5 min and (B,D,F) 48 h. Concentration of H_2O_2 was (A,B) 3%, (C,D) 0.3%, and (E,F) 0.03%, respectively. Detection wavelength is 700 nm.

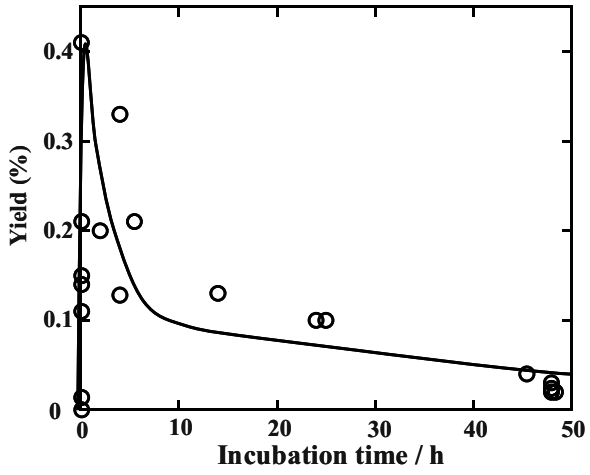

Fig. 4 Yields of the nonenzymatic Chl *d* production from Chl *a* in an acetone/0.3% H_2O_2 (10/1, *v/v*) solution at 303 K in the dark.

Conclusion

Nonenzymatic conversion of Chl *a* to Chl *d* was for the first time performed under simple reaction condition; Chl *a* was incubated for 5 min in an acetone/dilute H_2O_2 (10/1, *v/v*) solution at 303 K in the dark.

Usually, Chl *d*-derivatives are artificially synthesized from Chl *a* with a combination of a special metal complex(*e.g.*, OsO_4) and a strong oxidant (*e.g.*, H_5IO_6) (Mironov, 1996; Mironov *et al.*, 1994, 2004), or with a strong oxidant, $KMnO_4$ (Holt and Morley, 1959; Holt, 1961), but highly unlikely to occur in nature.

In contrast, H_2O_2 is an ordinary and weak oxidant, and abundant in plants and animals. The Chl *a* into Chl *d* conversion with H_2O_2 is hence likely to occur in

nature. An oxidative cleavage of a C = C double bond of the vinyl group of Chl *a* at ring I (–CH = CH_2 → –CHO) should take place during the divergent pathway to *A. marina*, resulting in the advantage of utilizing longer wavelength red light that cannot be efficiently absorbed by Chl *a*-type algae in colonial ascidians.

Recently, we found that the Chl *a* into Chl *d* conversion was caused by many grated vegetables (Itoh *et al.*, 2009, in this issue) as well as papain (Kobayashi *et al.*, 2005; Koizumi *et al.*, 2005; Okada *et al.*, 2009; Ohashi *et al.*, 2010) and horseradish peroxidase (Furukawa *et al.*, in this issue).

In the present study, the same conversion was found to occur nonenzymatically in the presence of dilute H_2O_2. Note that H_2O_2 is widely found in plants, and hence our findings suggest that the Chl *a* into Chl *d* conversion is not a rare event in nature, and will provide new insight into the unsolved question as to the birth of Chl *d* in natural photosynthesis.

It is noteworthy that Chl *d*-derivatives are observed and widespread in oceanic and lacustrine environments covering a range of temperatures and salinities (Kashiyama *et al.*, 2008). Moreover, Chl *d* was clearly detected in vegetable powder, sea vegetable powder, dried laver, green tea, and aging leaves of white radish (unpublished data). More details will be reported elsewhere. These findings indicate that Chl *d* seems to be rather easily produced as an artifact of Chl *a* on earth.

References

Akiyama M, Miyashita H, Watanabe T, Kise H, Miyachi S, Kobayashi M (2001) Detection of Chlorophyll d' and Pheophytin a in a Chlorophyll d-Dominating Oxygenic Photosynthetic Prokaryote Acaryochloris Marina. Anal Sci 17: 205-208

Hynninen PH, Kaartinen V, Kolehmainen E (2010) Horseradish Peroxidase-Catalyzed Oxidation of Chlorophyll a with Hydrogen Peroxide Characterization of the Products and Mechanism of the Reaction. Biochimica et Biophysica Acta 1797: 531-542

Holt AS (1961) Further Evidence of the Relation between 2-Desvinyl-2-Formyl-Chlorophyll a and Chlorophyll d. Can. J. Botany. 39: 327-331

Holt AS, Morley HV (1959) A Proposed Structurefor Chlorophyll d. Can. J. Chem. 37: 507-514

Kashiyama Y, Miyashita H, Ohkubo S, Ogawa NO, Chikaraishi Y, Takano Y, Suga H, Toyofuku T, Nomaki H, Kitazato H, Nagata T, Ohkouchi N (2008) Evidence of Global Chlorophyll d. Science 321: 658

Itoh S, Okada N, Ohashi S, Nakazato M, Iwamoto K, Shiraiwa Y, Miyashita H, Kobayashi M (2009) Novel Conversion of Chlorophyll a into Chlorophyll d Catalyzed by Extracts of Vegetables and Fruits. Phycologia 48: 49-50

Kobayashi M, Watanabe S, Gotoh T, Koizumi H, Itoh Y, Akiyama M, Shiraiwa Y, Tsuchiya T, Miyashita H, Mimuro M, Yamashita T, Watanabe T (2005) Minor but Key Chlorophylls in Photosystem II. Photosynth Res 84: 201-207

Koizumi H, Itoh Y, Hosoda S, Akiyama M, Hoshino T, Shiraiwa Y, Kobayashi M (2005) Serendipitous Discovery of Chl d Formation from Chl a with Papain. Sci Tech Adv Material 6: 551-557

Manning WM, Strain HH (1943) Chlorophyll d, a Green Pigment of the Red Algae. J Biol Chem 151: 1-19

Mironov AF (1996) Synthesis and Properties of New Chlorin and Bacteriochlorin Photosensitizers. Proc SPIE 2625: 23-32

Mironov AF, Kozyrev AN, Perepyolkin PY (1994) New Sensitizers for Diagnosis and Photodynamic Therapy of Malignant Tissues. Proc SPIE 2078: 186-192

Mironov AF, Ruziev RD, Lebedeva VS (2004) Synthesis and Chemical Transformations of N-Hydroxy- and N-Hydroxyalkylcycloimides of Chlorin p6. Russian J Bioorganic Chemistry 30: 466-476

Miyashita H, Ikemoto H, Kurano N, Adachi K, Chihara M, Miyachi S (1996) Chlorophyll d As a Major Pigment. Nature 383: 402

Ohashi S, Miyashita H, Okada N, Iemura T, Watanabe T, Kobayashi M (2008) Unique Photosystems in Acaryochloris Marina. Photosynth. Res. 98: 141-149

Ohashi S, Iemura T, Okada N, Itoh S, Furukawa H, Okuda M, Ohnishi-Kameyama M, Ogawa T, Miyashita H, Watanabe T, Itoh S, Oh-oka H, Inoue K, Kobayashi M (2010) An Overview on Chlorophylls and Quinones in the Photosystem I-Type Reaction Centers. Photosynth. Res. 104: 305-319

Okada N, Itoh S, Nakazato M, Miyashita H, Ohashi S, Kobayashi M (2009) Effective Hydrolysis of Chlorophyll a to Yield Chlorophyllide a by Papain in Aqueous Acetone. Current Topics in Plant Biology 10: 47-52

Winter Photosynthesis of Evergreen Broadleaf Trees from a Montane Cloud Forest in Subtropical China

Yongjiang Zhang[a,b,c], Kunfang Cao[a,*], Guillermo Goldstein[b,d]

[a] Key Laboratory of Tropical Forest Ecology, Xishuangbanna Tropical Botanical Garden, Chinese Academy of Sciences,Mengla, Yunnan 666303, China;
[b] Department of Biology, University of Miami, PO Box 249118, Coral Gables, FL 33124, USA;
[c] Graduate School of the Chinese Academy of Sciences, Beijing 100039, China;
[d] Consejo Nacional de Investigaciones Cientificas y Tecnicas (CONICET) and Laboratorio de Ecología Funcional, Departamento de Ecologia, Genetica y Evolucion, Facultad de Ciencias Exactas y Naturales, Universidad de Buenos Aires, Ciudad Universitaria, Nuñez, Buenos Aires, Argentina.
[*]Corresponding author. Tel. No. +86 691-8716732; Fax No. +86 691-8715070; E-mail: caokf@xtbg.ac.cn.

Abstract: Winter photosynthesis of trees is well studied for boreal, Mediterranean, and some temperate forests, while little is known about the forests from tropical-subtropical transition zones and subtropical areas. Evergreen broadleaf trees dominate the forests from elevation 1,000 to 2,600 m in the subtropical area of SW China, while forests in the subtropical area of SE China with similar elevations are dominated by deciduous broadleaf trees. In order to understand the winter photosynthetic performances of evergreen broadleaf trees in subtropical areas, seasonal dynamics in photosynthesis of 10 evergreen broadleaf tree species from a montane cloud forest in SW China was studied. Plant water relations and low temperature effects on photosynthetic system I and II were also studied. Although all 10 species down regulated maximum photosynthetic rate by 13% to 53% in winter, they maintained considerably high winter carbon assimilation (5.4 to 8.8 μmol m^{-2} s^{-1}) during this period. Trees did not experience water deficits in the winter/dry season, and were able to tolerate the coldest winter season in history. The considerably high winter carbon assimilation of evergreen broadleaf trees in this area may help them to establish dominance and allow these forests to sequestrate carbon during the unfavorable season.

Keywords: Winter carbon assimilation; Evergreen broadleaf forests; Carbon budget; Water deficits PSI and PSII

Introduction

Winter photosynthesis of trees is well studied for boreal, Mediterranean, and some temperate forests (Malhi *et al*., 1999). Conifer trees in boreal forests show negligible or even negative net photosynthesis in winter owing to freezing temperatures (Hanninean and Hari, 2002; Sevanto *et al*., 2006; Hari and Makela, 2003), while shrubs in Mediterranean biomes can maintain considerably high net photosynthesis in winter due to milder low temperatures (Flexas *et al*., 2001; Oliveira and Penuelas, 2004). Trees in temperate forests have different winter photosynthetic performances depending on the temperature regime and the freezing resistance of the species (Taneda and Tateno, 2005). Some tree species in temperate forests maintain high winter photosynthetic rate, while some freezing intolerant trees exhibit negative net photosynthesis (Taneda and Tateno, 2005). Trees in forests from tropical-subtropical transition zones and subtropical areas are also exposed to seasonal low temperatures, however, it is not know if they can maintain relative high photosynthetic rates during the winter period.

Water and temperature are two major limiting factors upon photosynthesis. Evergreen trees, which maintain leaves in the winter or the dry season, are prone to low temperature effects and/or water deficits. Water deficits limit photosynthesis as a consequence of low stomatal conductance (Brodribb and Holbrook,

2004; Zhang *et al*., 2009) and/or by the Calvin Cycle impairment (Flexas *et al*., 2001; Oliveira and Penuelas, 2004), while low temperatures limit photosynthesis by inducing photoinhibition (Sevanto *et al*., 2006), and impairing enzyme activities (Hammel, 1967). Subtropical zones in East Asia are subject to the influences of monsoons, resulting in strong seasonal changes in rainfall. Although there is a pronounced dry season, it is still unclear whether trees in these areas experience water deficits in the winter/dry season.

Evergreen broadleaf trees dominate the forests from 1,000 to 2,600 m in the subtropical area of SW China, while subtropical forests from SE China with similar elevations are dominated by deciduous trees. The subtropical area in SW China has milder low temperatures in winter compared to SE China as the Tibet Plateau prevents cold fronts from moving south in western China. The objectives of this study were (1) to assess winter photosynthetic performances of evergreen trees near the upper distribution limits of the subtropical zone, (2) to understand the low temperature effects in evergreen trees, and (3) to infer the importance of winter carbon assimilation for evergreen broadleaf trees, which may partially explain their dominance in subtropical montane forests of SW China.

Materials and Methods

Study site and plant materials

This research was carried out in an evergreen broadleaved forest located in a montane area (Mount Ailao) of SW China, 23°35'–24°44'N, 100°54'–101°30'E, 1100–2600 m elevation. Annual temperature of the study site is 11 °C and annual precipitation is 1,840 mm. Sunshine duration in the summer season is much lower than that in the winter season (Fig. 1).

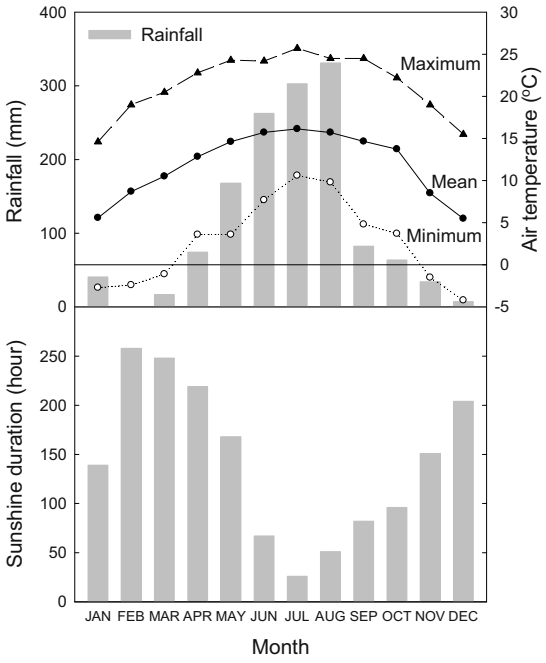

Fig. 1 Mean monthly rainfall, maximum, minimum mean temperatures, and sunshine duration in Mount Ailao for 2009 (Data from Ailaoshan Station for Subtropical Forest Ecosystem Studies; elevation 2,450 m).

The precipitation is seasonal and during 3 months of the year, the monthly precipitation is less than 20 mm (Fig. 1). The average and minimum temperature of the coldest month is 5.6 °C and –4.2 °C, respectively. The average temperature of the warmest month is 16.1 °C. Ten evergreen broadleaf tree species were selected for this study based on their dominances and feasibility in getting samples (Table 1).

Table 1 Ten evergreen broadleaf tree species selected for this study, their relative dominance in the forest, and predawn leaf water potential (Ψ_L) in the winter/dry season (January, 2009). Dominance data are from a forest survey by Yang *et al*. (2010), '-' indicates not found in the survey. Values of Ψ_L are means ± SE (n = 6).

Species	Species Code	Family	Relative dominance (%)	Predawn Ψ_L (MPa)
Lithocarpus jingdongensis YC Hsu et HJ Qian	LJ	Fagaceae	1.71	−0.07±0.01
Symplocos sumuntia D Don	SS	Symplocaceae	0.73	−0.09±0.01
Schima noronhae Reinw. ex Blume	SN	Theaceae	18.29	−0.08±0.01
Vaccinium delavayi Franch	VD	Vacciniaceae	0.02	−0.08±0.01
Manglietia insignis Blume	MI	Magonoliaceae	3.54	−0.14±0.01
Lithocarpus hypoviridis YC Hsu, BS Sun et HJ Qian	LH	Fagaceae	-	−0.12±0.02
Ternstroemia gymnanthera Sprague	TG	Theaceae	-	−0.10±0.02
Lyonia ovalifolia var. *lanceolata* Hand.-Mazz.	LO	Ericaceae	-	−0.16±0.01
Hartia sinensis Dunn	HS	Theaceae	1.63	−0.15±0.01
Illicium macranthum AC Smith	IM	Illiciaceae	2.17	−0.09±0.01

Leaf water potential and soil water potential.

Six sun-exposed fully-developed leaves from different individuals per species were collected between 06:00 and 07:00 h solar time. The samples were immediately sealed in plastic bags and kept in a cooler until balancing pressures were determined in the laboratory with a pressure chamber (PMS, Corvallis, OR, U.S.A.). Soil water potential was derived from soil water content per mass and soil moisture release curves of different soil layers in the study site (Zhang *et al*., unpublished data). Soil water content per mass was determined for different soil layers from 0 to 150 cm. Soil samples were collected from the field, transported to the laboratory immediately and the fresh weights were measured with a balance. Then the samples were oven-dried at 120 °C for 24 h, and weighed.

Gas exchange measurements

Light-saturated net CO_2 assimilation per area (A_{max}) of the ten evergreen broadleaf tree species were monitored using a portable photosynthetic system (LI-6400XT, LI-COR, Nebraska, U.S.A.), in August, October, December, January, and April. Six sun exposed mature leaves from different individuals per species were measured at a photosynthetic photon flux density of 1,500 mol m^{-2} s^{-1}, and ambient temperature and ambient CO_2 concentration. The measurements were conducted on sunny days between 08:30 and 10:30 h solar time. Some of the measurements in August were done in cloudy days because there were very few sunny days in the rainy season. The response of A_{max} to leaf temperature was analyzed, and the relationships between A_{max} and leaf temperature were fitted with second order polynomial regressions. Optimum temperatures for photosynthesis (T_{opt}; the temperature at which maximum A_{max} was achieved) were derived from the regressions.

Leaf sensitivity to low temperatures

Sensitivity of leaf photosynthetic system I and II (PSI and PSII) to low temperatures was determined in January 2010, when the trees were fully acclimated to winter temperatures. Six sun-exposed mature leaves per species from different individuals were collected in the late afternoon. After dark acclimation in black plastic bags with wet paper towels for 12 h, maximum quantum yield of PSII (F_v/F_m), and maximum P700 changes (P_m; indicating the amount of active PSI complex) were determined with a Dual PAM-100 (Walz, Germany). Leaf F_v/F_m was determined by illuminating the leaf with a saturating light pulse with photon flux density at 1,000 mol m^{-2} s^{-1} for 600 ms (Schreiber *et al*., 1994). For P_m determination, leaves were pre-illuminated with far-red light for 10 s, P_m was then measured with a saturation pulse. After measuring the control value of F_v/F_m and P_m, leaves were incubated at different temperatures in the freezer (4 °C; 0 °C; −2 °C, −5 °C, −7.5 °C, −10 °C, −12 °C, −15 °C, −17.5 °C, −20 °C, and −23 °C) for 30 min. After low temperature treatment, they were taken out from the freezer and illuminated with a weak light (200 mol $m^{-2}s^{-1}$) for 30 minutes, simulating light condition in the morning of foggy days after night freezing temperatures. After that, the leaves were allowed to thaw in the dark at room temperature (15 °C) for 12 h. Then the F_v/F_m and P_m were re-measured with the Dual PAM −100. Relative F_v/F_m or P_m was calculated as the percentage of the control values before the low temperature treatment. The relationship between relative F_v/F_m or P_m and treatment temperature was fitted with a sigmoid function, and the temperature at 50% loss of F_v/F_m or P_m was interpolated. Chlorophyll fluorescence method was widely used to assess the sensitivity of leaves to low temperatures (Boorse *et al*., 1998; Sierra-Almeida and Cavieres, 2010). The temperature at 50% loss of relative F_v/F_m or P_m was defined as the leaf lethal temperature (LT_{50}).

Results

Predawn leaf water potentials in the winter/dry season were close to zero in all the ten evergreen broadleaf tree species, ranging from −0.07 to −0.16 MPa (Table 1). Soil water potentials of different soil layers were high in the winter/dry season (> −0.5 MPa; Fig. 2), indicating that soil water was available for the plant activities.

Water potential of 0 to 20-cm-deep soil was close to zero (−0.06 MPa). Water potential of 20 to 30-cm-deep soil (0.13 MPa) was close to the predawn leaf water potential values of the trees (Table 1; Fig. 1).

All the 10 evergreen broadleaf tree species down regulated maximum photosynthetic rate by 13 to 53% in winter, depending on species (Fig. 3). However, all the trees were able to maintain considerably high winter carbon assimilation, ranging from 5.4 to 8.8 μmol m^{-2} s^{-1}, depending on species (Fig. 3). Different species showed different responses in A_{max} to leaf temperatures (Fig. 4). Leaf T_{opt} ranged from 20.7 °C to 31.4 °C, depending on species. Two species (*T. gymnanthera* and *L. ovalifolia*) did not achieve maximum A_{max} within the temperature range during measurements, and T_{opt} were not calculated for these two species.

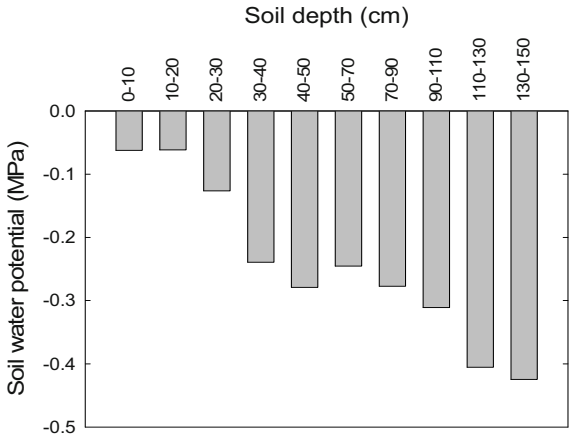

Fig. 2 Soil water potentials of different soil layers in the middle of the winter/dry season (January, 2009).

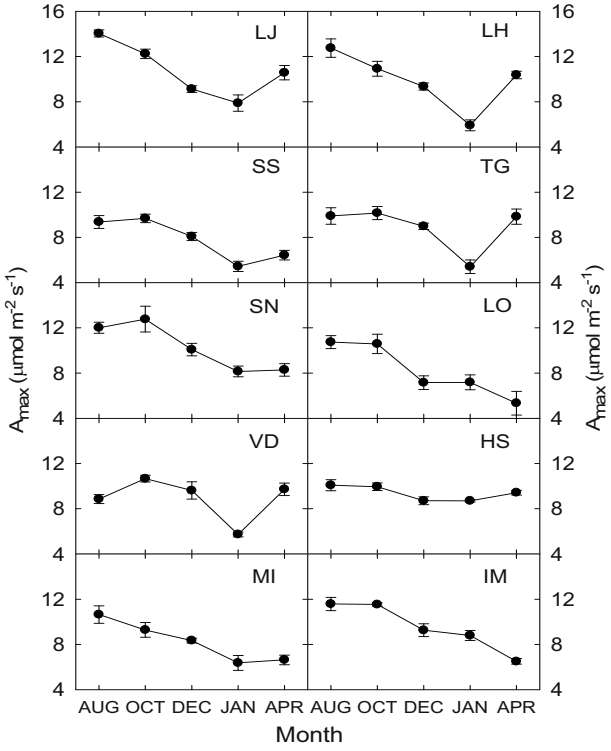

Fig. 3 Seasonal dynamics in A_{max} of ten evergreen broadleaf trees from Mount Ailao study site. Values are A_{max} averages of n = 6. Standard errors are indicated.

The freezing damage initiation temperatures (the temperature at which F_v/F_m or P_m start to decrease) in PSI and PSII of several tree species were above the minimum air temperature of the 2009–2010 winter season, and the historical minimum air temperature recorded (Fig. 5), suggesting that leaves of some tree species may experience certain degree of freezing damage in the winter. The lethal temperatures (LT_{50}) of PSII (indicated by F_v/F_m) ranged from −10.0 °C to −15.1 °C, all of which were lower than the minimum air temperature of the 2009–2010 winter season (−5.7 °C),

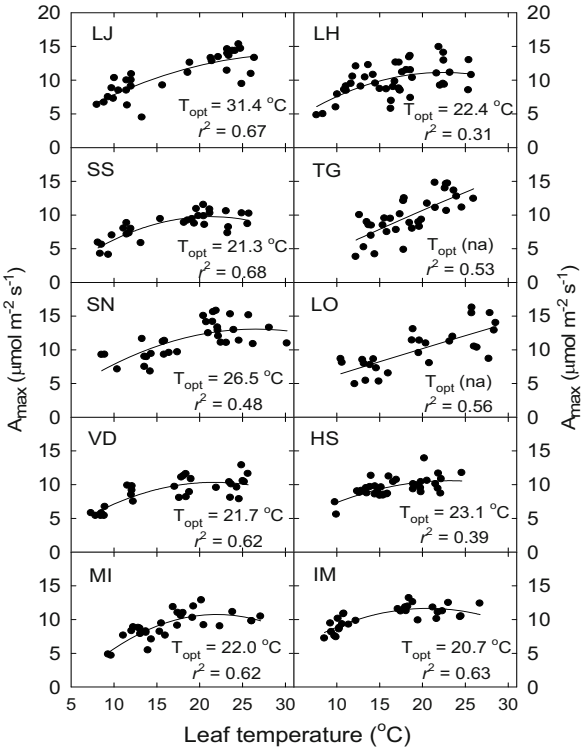

Fig. 4 Relationship between leaf maximum photosynthetic rate (A_{max}) and leaf temperature.
Second order polynomial regressions were fitted to the data and p value of all the regressions < 0.001.

and the historical minimum air temperature (−9.0 °C) (Fig. 5). Lethal temperature of PSI (indicated by P_m) ranged from −8.2 °C to −14.4 °C, which were lower than the minimum air temperature in 2009–2010 winter season (−5.7 °C). Lethal temperature of PSI in *Lyonia ovalifolia* var. *lanceolata* were higher than the historical minimum air temperature (−9.0 °C), while PSI of other species can tolerate −9.0 °C. This suggests that leaves of most evergreen broad trees in the study site will not experience unrecoverable freezing damage even in the coldest winter season (since the air temperatures records were available).

Six out of the ten tree species (*S. sumuntia, S. noronhae, V. delavayi, L. hypoviridis, T. gymnanthera, L. ovalifolia*) showed different behaviors in F_v/F_m and P_m to low temperatures. In these six species, PSI was more prone to freezing damage than PSII, and LT_{50} of PSII was 1.3 °C to 2.4 °C lower than that of PSI (Fig. 5).

Discussion

Our results revealed substantial winter photosynthetic rates in trees from a subtropical montane cloud forest at an elevation of 2,450 m. This elevation is close to

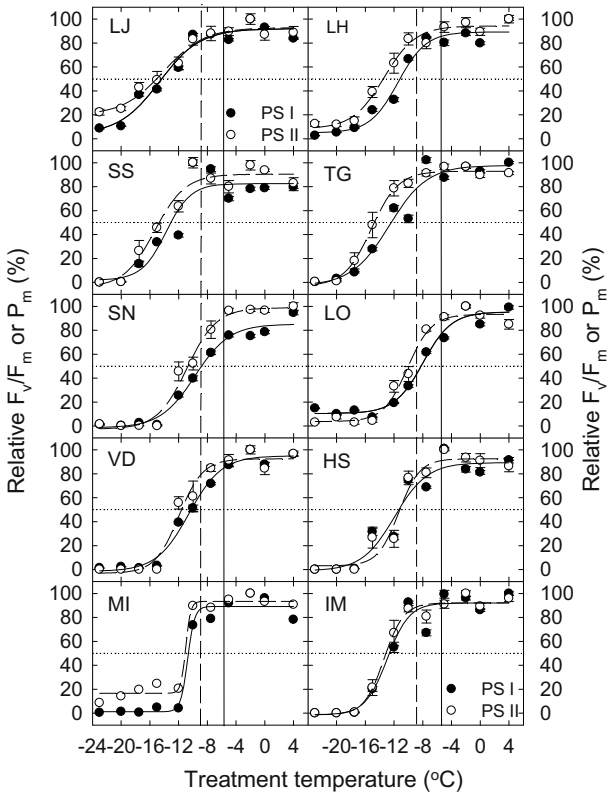

Fig. 5 Relative F_v/F_m and P_m (percentage of control values before treatment) as a function of treatment temperature. Dotted lines indicate the lethal temperature at which 50% damage occurred (LT_{50}); vertical dashed lines indicate historical minimum air temperature; solid lines indicate minimum air temperatures in January 2010. Sigmoid functions were fitted to the data, and p values of all the regressions were < 0.001.

the upper distribution limits of evergreen broadleaf trees in subtropical zones of SW China, thus winter photosynthesis of trees from lower elevations in this area will be less affected by seasonal low temperatures. The temperature regime of the study site is similar to some low elevation temperate forests (Taneda and Tateno, 2005), and the winter photosynthetic performances of trees in the study site are also similar to some low elevation temperate forests (Taneda and Tateno, 2005). Although there is a pronounced dry season according to the rainfall seasonal patterns, the trees maintained good water status in winter/dry season owing to sufficient water supply from soils. Therefore, the winter photosynthesis of evergreen broadleaf trees is not limited by water supply, but may be constrained by low temperature induced photo-inhibition or decreased enzyme activities (Hammel, 1967; Sevanto *et al*., 2006). Moreover, because there is less cloud cover and substantially higher sunshine duration in winter than in summer, the detrimental effects of low temperature on photosynthesis appears to be compensated by relatively high levels of incoming solar radiation. Rain and cloud cover in the summer/wet season may constrain CO_2 assimilation and tree growth (Graham *et al*., 2003), therefore the relative contribution of winter carbon assimilation to the whole year carbon budget may be as important as or even more important than summer carbon gain for trees in subtropical forests of SW China.

Leaves of all the evergreen broadleaf trees were able to tolerate lowest temperatures in winter without unrecoverable freezing damage. Only *Lyonia ovalifolia* var. *lanceolata*, which is a variety of a deciduous species, would experience unrecoverable damage under historical minimum temperatures. Substantial freezing tolerance found in all the tree species allows leaves to maintain positive photosynthesis in winter. Although all the tree species could tolerate freezing temperatures in winter, high variation was found in freezing tolerance and sensitivity of photosynthesis to temperature changes. Different degrees of sensitivity to freezing temperatures, and different T_{opt} in the evergreen broadleaf trees may lead to their different species-specific responses to global warming.

Sensitivities of PSI and PSII to chilling (above zero low temperatures) were different in plants (Terashima *et al*., 1994; Havaux and Davaud, 1994; Huang *et al*., 2010), while the contrasting sensitivity of PSI and PSII to freezing temperatures is unstudied. Our results suggest that the studied species behave differently: in *L. jingdongensis, H. sinensis, I. macranthum,* and *M. insignis*, PSI and PSII performed exactly the same in responding to freezing temperatures, while in *S. sumuntia, S. noronhae, V. delavayi, L. hypoviridis, T. gymnanthera*, and *L. ovalifolia*, the LT_{50} of PSII could be 2.4 °C lower than those of PSI. The damage initiation temperatures in PSI and PSII were also different in *S. noronhae*, *M. insignis*, *L. hypoviridis*, and *L. ovalifolia*.

In conclusion, our study suggested that evergreen broadleaf trees in tropical-subtropical transition zones and subtropical areas of SW China down regulated photosynthetic rates in winter, but still maintained considerably high winter CO_2 assimilation. Decrease in F_v/F_m and P_m could occur in winter, while no unrecoverable damage will happen in leaves even under extreme low temperatures for the region. The considerably high winter carbon assimilation of evergreen broadleaf trees in this area may convey advantages over deciduous trees in terms of physiological performance and help them to establish dominance as well as allow these forests to sequestrate carbon during the unfavorable season.

Acknowledgements

We would like to thank Ailaoshan Station for Subtropical Forest Ecosystem Studies for providing logistic support, and climatic data. We also would like to thank Mr. Fu Xuwei, Mr. Yang Qiuyun, Mr. Zeng Xiaodong, Mr. Ma Hong, Mr. Qi Jinhua, Mr. Luo Xin, Mr. Liu Yuhong, and Mr. Ai Ke for their assistance in the field measurements. This work was supported by a grant from the National Natural Science Foundation of China (30670320).

References

Boorse GC, Gartman TL, Meyer AC, Ewers FW, Davis SD (1998) Comparative Methods of Estimating Freezing Temperatures and Freezing Injury in Leaves of Chaparral Shrubs. International Journal of Plant Science 159: 513-521

Brodribb TJ, Holebrook NM (2004) Stomatal Protection Against Hydraulic Failure: a Comparison of Coexisting Ferns and Angiosperms. New Phytologist 162: 663-670

Flexas J, Gulias J, Jonasson S, Medrano H, Mus M (2001) Seasonal Patterns and Control of Gas Exchange in Local Populations of the Mediterranean Evergreen Shrub Pistacia Lentiscus L. Acta Oecologica 22: 33-43

Graham EA, Mulkey SS, Kitajima K, Phillips NG, Wright SJ (2003) Cloud Cover Limits Net CO_2 Uptake and Growth of a Rainforest Tree during Tropical Rainy Seasons. Proceedings of the National Academy of Sciences of the United States of America 100: 572-576

Hammel HT (1967) Freezing of Xylem Sap without Cavitation. Plant Physiology 42: 55-66

Hanninen H, Hari P (2002) Recovery of Photosynthesis of Boreal Conifers during Spring: a Comparison of Two Models. Forest Ecology Management 169, 53-64

Hari P, Makela A (2003) Annual Pattern of Photosynthesis in Scots Pine in the Boreal Zone. Tree physiology 23: 145-155

Havaux M, Davaud A (1994) Photoinhibition of Photosynthesis in Chilled Potato Leaves Is Not Correlated with a Loss of Photosystem II Activity—Preferential Inactivation of Photosystem I. Photosynthesis Research 40: 75-92

Huang W, Zhang SB, Cao KF (2010) The Different Effects of Chilling Stress under Moderate Light Intensity on Photosystem II Compared with Photosystem I and Subsequent Recovery in Tropical Tree Species I and Subsequent Recovery in Tropical Tree Species. Photosynthesis Research 103: 175-182

Malhi Y, Baldocchi DD, Jarvis PG (1999) The Carbon Balance of Tropical Temperate and Boreal Forests. Plant, Cell and Environment 22: 715-740

Oliveira G, Penuelas J (2004) Effects of Winter Cold Stress on Photosynthesis and Photochemical Efficiency of PSII of the Mediterranean Cistus Albidus L. and Quercus Ilex L. Plant Ecology 175: 179-191

Schreiber U, Bilger W, Neubauer C (1994) Chlorophyll Fluorescence As a Nonintrusive Indicator for Rapid Assessment of in Vivo Photosynthesis. In: Schulze ED, Caldwell MM (eds.), Ecophysiology of Photosynthesis. Springer: Berlin/Heidelberg/New York, pp. 49-70

Sevanto S, Suni T, Pumpanen J, Grönholm T, Kolari P, Nikinmaa E, Hari P, Vesala T (2006) Wintertime Photosynthesis and Water Uptake in a Boreal Forest. Tree Physiology 26: 749-757

Sierra-Almeida A, Cavieres LA (2010) Summer Freezing Resistance in High-Elevation Plants Exposed to Experimental Warming in the Central Chilean Andes. Oecologia 163: 267-276

Taneda H, Tateno M (2005) Hydraulic Conductivity, Photosynthesis and Leaf Water Balance in Six Evergreen Woody Species from Fall to Winter. Tree Physiology 25: 299-306

Terashima I, Funayama S, Sonoike K (1994) The Site of Photoinhibition in Leaves of Cucumis-Sativus L. at Low temperatures Is Photosystem I, Not Photosystem II. Planta 193: 300-306

Yang GP, Gong HD, Zheng Z, Zhang YP, Liu YH, Lu ZY (2010) Caloric Values and Ash Content of Six Dominant Tree Species in an Evergreen Broadleaf Forest of Ailaoshan, Yunnan Province. Journal of Zhejiang Forestry College 27: 251-258

Zhang YJ, Meinzer FC, Hao GY, Scholz FG, Bucci SJ, Takahashi FS, Villalobos-Vega R, Giraldo JP, Cao KF, Hoffmann WA, Goldstein G (2009) Size-Dependent Mortality in a Neotropical Savanna Tree: the Role of Height-Related Adjustments in Hydraulic Architecture and Carbon Allocation. Plant, Cell and Environment 32: 1456-1466

The Photosynthetic Surface Area of Apple Trees

Krzysztof Tokarz[a,*], Jan Pilarski[a,b], Maciej Kocurek[a,b]

[a] Institute of Plant Physiology PAS, Niezapominajek 21; 30-239 Krakow, Poland;
[b] The Institute of Biology, The *Jan Kochanowski* University of Humanities and Sciences, Kielce, Poland.
[*]Corresponding author. Tel. No. +48 12 425 18 34; Fax No. +48 12 425 18 44;
E-mail: K.Tokarz@ifr-pan.krakow.pl; km.tokarz@gmail.com.

Abstract: The development of stem and leaf surface areas were studied comparatively throughout a year's cycle, and the proportions of these areas within the total area of trees were calculated. Depending on the variety, the total surface areas of trees: all branches, boughs and tree trunks after winter pruning, ranged from 27 dm^2 to 118 dm^2. At the beginning of the vegetation season, the proportion of leaves in newly developed stems amounted to 90%–92%, and the proportion of these new stems was 8%–10%. Later in the vegetation season, the leaf area amounted to 83%–89%, and that of new stems 11%–17%, and there were no differences between the varieties. Towards the end of the vegetation season, total leaf area on a tree ranged from 110–120 dm^2 to 296 dm^2, whereas the area of newly grown stems ranged from 42 dm^2 to 168 dm^2.

In the course of the vegetation season, the proportion of the stem area decreased while that of leaves increased, and from August onwards the leaf area exceeded that of stems in the majority of the studied varieties. In the final part of the vegetation season, the leaf area was higher than area of stems, by over 20%–45%.

Keywords: Photosynthetic surface area; Stems; Leaf

Introduction

Leaves are the plant organs best adapted to carry on the process of photosynthesis. Both their situation and structure facilitate the easy access of solar radiation and thus, the process of photosynthesis is the most intensive. The effectiveness of chemical fixation of absorbed radiation by leaves, ranges from 1% to 5%. They provide plants with over 90% of assimilates.

Photosynthesis can also proceed either temporarily or permanently, in all non-leaf above-ground parts of the plant which contain chlorophyll. Organs such as the green perianth, or developing fruits (Weiss *et al*., 1988; Blanke and Lenz, 1989), stalks (Schaedle, 1975; Nilsen, 1995), and even the aerial roots (Benzing *et al*., 1983; Hew *et al*., 1984; Kitaya *et al*., 2002), can be active photosynthetically. Apart from these non-leaf organs where the presence of chlorophyll is visible with the naked eye, this pigment is also present in lignified parts, such as in stems which include both the leafy stems of the current-year generation, and the older, leafless, several-year old branches as well as in boughs, and in the tree trunk (Pilarski 1984; Pfanz and Aschan, 2001; Pfanz *et al*., 2002; Pilarski and Tokarz, 2006).

Most of the data available in references on the photosynthetic fixation of carbon in vascular plants concerns the leaves.

The photosynthetic production of tissues with chlorophyll, other than the foliar mesophyll, is undoubtedly partly used to cover the plant's own needs, but also positively affects the carbon balance in the whole plant. The photosynthesis of stems containing the stomata, or of elements of the perianth, functions similarly to that in leaves, whereas in the organs which are lacking stomata, *e.g.* in fruits and lignified stems, it is rather the reassimilation of the carbon dioxide released owing to the respiration of the pericarp of stems (Benzing and Pockman, 1989).

The main function of stems is to conduct water

with mineral salts from the roots and to carry assimilates from leaves (Essau, 1973; Ewers *et al*., 1991; Schultz and Matthes, 1993; Givnish, 1995; Pilarski, 1998). The presence of chlorophyll in the stems is evidence of their additional functions, which is to assimilate CO_2.

The necessary factors for the occurrence of photosynthesis include: light, photosynthetic pigments, carbon dioxide, and water. In a great number of studies, the presence of photosynthetic pigments has been discovered in lignified stems, including young ones but also those that are considerably older (several decades). This signifies the penetration of solar radiation light, confirmed in a number of studies on the distribution of radiation in tree stems where chlorophyll has been found, not only in the bark but also in the mesophyll cells of the wood, as well as in the cores of 10-year old beech stems (Dima *et al*., 2006; Pilarski, 2006; Wittmann *et al*., 2006; Tokarz, 2007). This confirms the penetration of radiation of the PAR range also into the cores of the stems. This radiation is nevertheless considerably weakened by the intensive absorption by the cork layer and spectrally changed, compared with the radiation falling on the stem (Pilarski and Tokarz, 2005; Tokarz and Pilarski, 2005).

In the studies on trees, the role of leaves are often considered without taking into consideration the surface of other above ground lignified parts, which are also the places where photosynthetic activity takes place in the plant. As shown by studies conducted in recent years, tree and shrub stems remain photosynthetically active throughout the year, and the main factor limiting their activity in winter is temperature (Pilarski, 1997, 2002). Their photosynthetic activity is measurable also during sunny winter days, and in spring the onset of their activity precedes the development of leaves. In this leafless period, the stems can be the only source of assimilates from the current production, and later in the period with developed foliage to support the photosynthetic production of leaves.

The aim of this study was to compare the development of the surface of leaves and stems and their proportions of the total surface area of the apple trees.

Material and Methods

The studies were conducted on 5-year old apple trees (Malus domestica L), grown on on M-26 stock in the experimental unit of the Agricultural University of Cracow , in Garlica Murowana near Krakow. Five trees of each of the varieties: Jonica, Szampion, Red Boskoop, Florina Novamac, and Freedom were selected for the study.

The measuring of the surface of stems was carried out in March, after winter pruning, and prior to the onset of vegetation. Because frequent pruning prevented accurate determination of the stems of older classes, the stems were therefore divided into two groups: namely: the stem of the last growth, (in this study termed the stems of the current year), and the stems of other age classes. Because of methodological problems, the growth increments in the surface stems of older annual classes—left after winter pruning, and associated with secondary growth—have not been taken into account and the value measured in March was assumed to be constant.

Each month, from June to September, in five selected trees of each variety, the surface of all newly produced stems from the current year was measured and leaves counted, and on 10 representative stems, the surface of leaves was measured with the use of a LI-COR 3000 C planimeter and the average surface of the leaf was then calculated. Based on this average, the approximate leaf surface area was calculated for each tree.

Results

The comparison of leaf areas of the trees of the five studied varieties is compiled in Fig. 1. Among the varieties analysed, the lowest total area prior to the start of vegetation occurred in Szampion (27 dm^2), whilst for the varieties Jonica and Red Boskoop it was twice the size (ca. 55 dm^2) and for the remaining varieties, Florina, Novamac and Freedom, the surface area was greater by a factor of 3 to 4 (92–118 dm^2). The proportion of the youngest stems in the total surface which was left after spring pruning was low and amounted from 5%–7% in Florina and Szampion, up to 17%–20% in Freedom and Novamac.

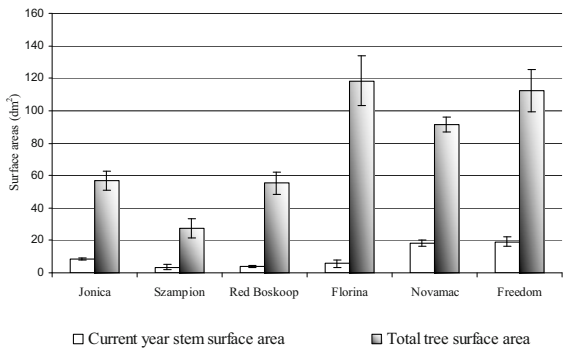

Fig. 1 Comparison of the current-year stem and total tree surface areas after winter pruning.

The analysis of growth increments of the current year's class and of the leaves in the vegetation season started at the beginning of June and ended in mid-September, when the growth increments ceased.

The dynamics of the growth increments of the current year, throughout the vegetation season is shown in Fig. 2. Also throughout the vegetation season, the lowest increment of the stem surface occurred in the Szampion variety, whereas the highest appeared in the Freedom variety, and the difference between them was almost fourfold. In all varieties, the incremental growth in the surface of current-year stems lasted till September. The majority of the varieties, except Freedom, had an uneven rate of surface increase. In the Red Boskoop and Novamac varieties, low increments of the stem's surface were observed in August, where in Jonica, Szampion and Florina it was observed in September. The intensive increment in the surface of stems observed in September in the Red Boskoop, Novamac and Freedom varieties was caused by the emergence of a high number of suckers.

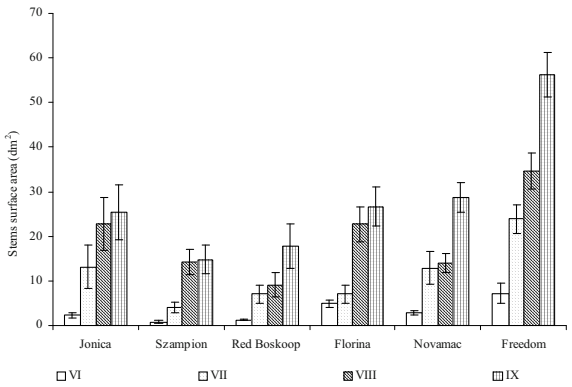

Fig. 2 The dynamics of the growth increments of the current year throughout the vegetation season.

The incremental growth in the surface of leaves throughout the vegetation season is shown in Fig. 3. The increment of the leaf surfaces lasted till September, but its course in the studied varieties varied among the studied trees and connected with the increment in the stems. In Jonica this process lasted until August, but was smaller in September, whilst in Red Boskoop the growth increment was greatest in September, as was the case in both Novamac and Freedom. In Florina, Novamac and Freedom, the very intensive incremental growth in the leaf surface occurred in July, in August the rate of increment was markedly lower, whereas in September, there was again a marked increase in the leaf surface associated with the production of suckers. In Novamac and Freedom this increase was as high as 68%.

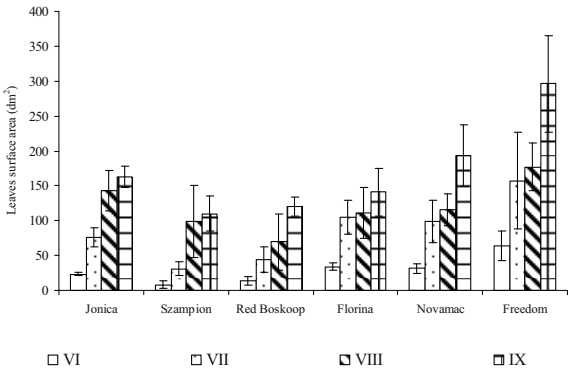

Fig. 3 The dynamics of the growth increments of the leaves throughout the vegetation season.

Among the varieties studied, the smallest leaf surface area for the whole season occurred in the Szampion and Red Boskoop varieties, and the greatest in the Freedom variety. The difference was almost threefold.

The proportions of stems and leaves in the newly-grown photosynthetic surface during the vegetation season is shown in Table 1. At the beginning of vegetation, the proportion of leaves amounted to 90%–92%, and of stems 8%–10% and only in Florina were these values lower, by 87% and 13% respectively. In the remaining portion of the vegetation season, the surface area of newly-grown leaves constituted 11%–17%, and that of leaves 83%–89% respectively, without any differences between the studied varieties. The spring pruning in orchards greatly reduces the surface area of stems, particularly those of the current year.

Table 1 Proportions of stems and leaves in the newly-grown photosynthetic surface during the vegetation season (%). L – Leaves, S – Stems.

	Jonica		Szampion		Red Boskoop		Florina		Novamac		Freedom	
	L	S	L	S	L	S	L	S	L	S	L	S
June	91,2± 3	8,8±2	92,0±6	8,0±2	91,8±2	8,2±2	86,6±2	13,4±3	92±2	8±2	90±3	10±2
July	85,4±2	14,6±4	89±3	11±3	86±3	14±3	88±2	12±1	88±3	12±3	87±4	13±3
August	85,6±3	14,4±3	87±5	13±3	88±4	12±3	83±3	17±3	89±2	11±2	84±2	16±4
September	86,3±2	13,7±4	88±4	12±4	87±3	13±4	84±2	16±2	87±2	13±3	84±2	16±3

Table 2 Comparison of the leaves and all stems surface areas (dm2) (A) and participation of the leaves' and stems' surface area in the tree total surface area (%) (B). L – Leaves, S – Stems.

A

	Jonica		Szampion		Red Boskoop		Florina		Novamac		Freedom	
	L	S	L	S	L	S	L	S	L	S	L	S
June	23,6±6	59,3±0,5	8,2±5	28,1±0,3	13,9±2	56,6±0,3	33,8±5	123,1±0,7	31,4±7	94,5±0,5	63,8±22	119,7 ± 2
July	76,4±17	70,2±5	31.0±10	31,4±1	44,3±13	62,4±4	104,7 ± 25	125,3 ± 6	98,6±31	104,6 ± 6	157,3 ± 69	136,4 ± 8
August	143,1 ± 39	80,0 ±10	98,9±52	41,7±9	69,3±29	64,5±3	111,6 ± 36	141,1 ± 4	115,6 ± 22	105,7 ± 2	176,8 ± 34	147,3 ± 14
September	163,1±13	82,6±11	110,9±24	42,3±7	120,6±15	73,2±6	141,0 ± 34	145,0 ± 4	193,0 ± 44	120,4 ± 8	296,2 ± 69	168,7±10

B

	Jonica		Szampion		Red Boskoop		Florina		Novamac		Freedom	
	L	S	L	S	L	S	L	S	L	S	L	S
June	28,4±7	71,6±1	22,5±13	77,5±1	19,7±2	80,3±4	21,5±3	78,5±3	24,9±5	75,1±2	34,8±11	65,2±1,0
July	52,1±11	47,9±3	49,7±9	50,3±2	41,5±5	58,5±4	45,5±7	54,5±3	48,5±8	51,5±3	53,5±8	46,5±1
August	64,1±7,5	35,9±4	70,4±16	29,6±6	51,8±17	48,2±2	44,2±10	55,8±1	52,2±10	47,8±3	54,6±10	45,4±4
September	63,6±8	36,4±6	72,4±15	27,6±7	62,2±11	37,8±5	49,3±2	50,7±,4	61,6±14	38,4±2	63,1±7	36,9±2

A comparison of the figures for the total surface of all stems, *i.e.* of the current year and older, is shown in Table 2. In June, the total surface area of stems was 3-times higher, on average, than the surface of leaves. In subsequent months, in line with the intensive incremental growth of the leaf surfaces, their proportion increased, and from August onwards the leaf surface area prevailed over the surface of stems. At the end of the vegetation season, the leaf surface was higher than stems by more that 20% in Red Boskoop, Novamac and Jonica, 45% in Szampion, and only in Florina were the area of stems higher than that of leaves, except in September.

Discussion

The leaves are the principal photosynthetic organs and their surface constitutes a significantly predominant portion of the overall surface area of the above-ground plant body. For this reason, in the publications concerning photosynthetic surface of plants, the leaf index (LAI) is used. This determines the proportion of the leaf surface compared to the area of occupied ground underneath it and represents an important indication of structure and productivity of the ecosystem (Chen *et al*., 1997; Scurlock *et al*., 2001; Breuer *et al*., 2003; Weiskittel and Maguire, 2006).

Other, non-leafy above-ground plant organs containing chlorophyll, however, also represent a significant portion of a plants' surface, so becoming an essential source of photosynthetic production. Among these parts, stems should be listed before any other organs.

A precise determination of the surface area of stems and trunks poses major difficulties, because of great diversity in the structure and architecture of the tree crown, even among trees of similar sizes. Therefore, because earlier studies assumed a low participation of stems in the absorption of direct radiation, in both coniferous and deciduous species (Fassnacht *et al*., 1994; Kucharik *et al*., 1998), the surface area of stems and trunks was not considered in the measurements of photosynthetic area measurements nor in the models of photosynthetic activity in trees (Weiskittel and Maguire, 2006). Later studies have proven, however, the significant participation of stems in the total respiration of trees (Bosc *et al*., 2003), and also in the retention and storage of water (Kaim, 2004) and reserve substances (Doster and James, 1998; Pierce and Grubb, 1981).

Despite these functions, the studies on the photosynthetic activity of stems, has not usually concerned the proportion of the surface area of these organs, in relation to the whole of the photosynthetic surface area of the plant (Solhaug and Hagen, 1998; Pilarski, 1999). However, in some species of CAM-type of plants, *e.g.* in *Frerea indica* (Lange and Zuber, 1977), and *Carnegiea gigantea* (Nobel and Harstock, 1986), the stems comprise almost 100% of the photosynthetic area of the plant. Similarly, the C3-type leaf-less plants found in hot and dry climates, in periods of water shortage, use their stems as a place of assimilation of CO_2. For instance, in *Eriogonum inflatum*, the surface area of stems in this period amounted to up to 80% of the total photosynthetic surface (Smith and Osmond, 1987), and in *Encelia farinosa* and *Ambroisa dumosa*– even to 100% (Comstock and Ehleringer, 1988). Also the stems of deciduous trees and bushes of the temperate zone, in the period from autumn till the following spring, represent the only photosynthetically active surface (Larcher *et al*., 1988; Kharouk *et al*., 1995; Pilarski, 1999).

In a herbaceous plant species, *Helleborus viridis*, the stems constituted some 34% of the total above-ground surface area at the beginning of the vegetation season, and at the end of summer – only 10% (Aschan *et al*., 2005). In other herbaceous plants, such as knotweed or topinambur, the proportion of stems increased throughout the vegetation season, reaching at the end of the vegetation season 8%–13% in topinambur and 15%–19% in knotweed (Kocurek, 2007).

The references offer only a small number of reports, in which the surface of above-ground lignified stems of plants is determined as a proportion of the total photosynthetic surface of plants, the former being only estimated by indirect measurement methods. The studies conducted on fir trees have shown that the total surface area of stems and trunk amounted to ca. 29% of the total surface area of the tree, with more than 82% of stems growing directly from the trunk (Weiskittel and Maguire, 2006).

In apple trees, the proportion of all stems in the total surface area of the tree which is 100% in the leafless period, decreased during the vegetation season, from ca. 75% in June to around 35% in August and September, whereas the proportion of stems from the current year increased during the season from ca. 2.7% in June to 13% in September.

In the leafless period, the stems constitute the only photosynthetically active surface, which prevent loss of the storage materials accumulated in the summer season. In the former period the only factor limiting the metabolic activity of plants is temperature. However, in sunny winter days, solar radiation absorbed by the cork layer warm up the stems and their temperature may reached even 10 ºC more than the air temperature (Sakai, 1966; Noconia, 1986; Pilarski, 1997), and the photosynthetic activity was recorded around noon in temperatures a bit below zero, in the stems *e.g.* in *Populus tremuloides* (Foote and Schaedel, 1976), and *Syrynga vulgaris* (Pilarski, 2002).

Additionally, an evident leap in the photosynthetic activity of stems occurred prior to the spring onset of vegetation. In this period, the stems are a source of necessary metabolites and energy from the current production, needed by the growing stems and leaves (Ivanov *et al*., 2006). The presence photosynthetic pigments, not only in young stems but also in the bark of the trunk *e.g.* in *Fagus sylvatica* (Pilarski, 2006), or also in the apple tree (Tokarz, 2007), indicate that the whole of the lignified surface area of trees performs the photosynthetic function, particularly in those species with minor increments in the thickness of the cork layer.

The results presented in this paper indicate the very high proportions of stems—perennial lignified organs of plants—in the total surface area of trees, which are independent of variety, and which testifies to how widespread this phenomenon might be. The stems may represent 100% of the total tree surface area in the leafless period, from mid-October till mid-April, which is roughly half a year. After the vegetation period starts, their proportion in the total surface area of trees decreases, and in most of the varieties under study it was only in July when the areas of leaves and stems are similar. In later period, the leaf surface area is higher than that of stems and at the end of vegetation season, the surface area of stems amounts to 30%–50% of the total surface area of the tree. In the newly grown stems, however, leaves represent a considerably greater surface area—ca. 85%–90%, and the proportion of stems is minor—10%–15%. Similar results were obtained in herbaceous plants (Kocurek, 2007). In *Reynutria japonica*, the surface area of stems throughout the vegetation season amounted to ca. 18%, and in *Heliantus tuberosus*—ca. 8% at the beginning of

vegetation season and in the later period of development—ca. 13% of the total surface area of the plant. The data indicates that the incremental growth of new stems progresses similarly in green and lignified plants.

Based on the results of studies obtained to-date, the quantitative assessment of the photosynthetic participation of stems in CO_2 can not be separately evaluated, but studies recent years based on the fluorescence measurement in chlorophyll a indicate the marginally less photosynthetic activity of stems compared with leaves (Wittmann *et al.*, 2006; Tokarz, 2007). Therefore, taking into account the surf in ace area of stems, it may be stated that the actual participation of stems in the photosynthesis of the apple tree in the vegetation season, could be between 10%–15% in mid-summer. The stems are the only source of assimilates helping to limit the losses, with the dark respiration of non-photosynthetic cells providing energy and carbohydrates in the period when buds and leaves emerge.

References

Aschan G, Pfanz H, Vodnik D, Batic F (2005) Photosynthetic Performance of Vegetative and Reproductive Structures of Green Hellebore (Helleborus Viridis L. Agg.) Photosynthetica 43: 55-64

Benzing DH, Friedman WE, Peterson G, Renfrow A (1983) Shootlessness, Velamentous Roots, and the Pre-Eminence of Orchidaceae in the Epiphytic Biotope. Am. J. Bot. 70: 121-133

Bosc A, Grandcourt DA, Loustau D (2003) Variability of Stem and Branch Maintenance Respiration in a Pinus Pinaster Tree. Tree Physiol. 23: 227-236

Breuer L, Eckhardt K, Frede HG (2003) Plant Parameter Values for Models in Temperate Climates. Ecol Model 169: 237-293

Blanke MM, Lenz F (1989) Fruit Photosynthesis – a Review. Plant Cell Environ. 12: 31-46

Comstock JP, Ehleringer JR (1988) Seasonal Patterns of Canopy Development and Carbon Gain in Nineteen Warm Desert Shrub Species. Oecologia 75: 327-335

Chen JM, Rich PM, Gower ST, Norman JM, Plummer S (1997) Leaf Area Index of Boreal Forests: Theory, Techniques, and Measurements. J Geophys Res 102: 29429-29443

Dima E, Manetas Y, Psaras GK (2006) Chlorophyll Distribution Pattern in Inner Stem Tissues: Evidence from Epifluorescence Mocroscopy and Reflectance Measurements in 20 Woody Species. Trees 20: 515-521

Doster RH, James DA (1998) Home Range Size and Foraging Habitat Red-Cockaded Woodpeckers in the Ouachita Mountains of Arkansas. Wilson Bull 110: 110-117

Foote KC, Schaedle M (1976) Diurnal and Seasonal Patterns of Photosynthesis and Respiration by Stems of Populus Tremuloides Michx. Plant Physiol. 58: 651-655

Hew CS, NG Y, Wong SC, Yeoh HH, Ho KK (1984) Carbon Dioxide Fixation in Orchid Aerial Roots. Physiol. Plant. 60: 154-158

Kaim RF (2004) Attenuation of Rainfall by Forest Canopies. Ph.D. Dissertation, Oregon State University: Corvallis, OR, pp. 150

Kitaya Y, Yabuki K, Kiyota M, Tani A, Hirano T, Aiga I (2002) Gas Exchange and Oxygen Concentration in Pneumatophores and Prop Roots of Four Mangrove Species. Trees 155-158

Kharouk VI, Middleton EM, Spencer SL, Rock BN, Williams DL (1995) Aspen Bark Photosynthesis and Its Significance to Remote Sensing and Carbon Budget Estimate in the Boreal Ecosystem. Water Air Soil Pollut. 82: 483-497

Kocurek M (2007) Udział Pędów Roślin Zielnych: Reynutria Japinica i Helianthus Tuberosus w Fotosyntetycznym Wiązaniu CO_2. (Participation of Stems of the Herbaceous Plants: Reynutria Japonica and Helianthus Tuberosus in Photosynthetic Assimilation of CO_2. Ph.D. Dissertation, Institute of Plant Physiology PAS, Krakow, Poland

Lange OL, Zuber M (1977) Frerea Indica, a Stem Succulent CAM Plant with Deciduous C3 Leaves. Oecologia 31: 67-72

Larcher W, Lutz C, Nagelle M, Bodner M (1988) Photosynthetic Functioning and Ultrastructure of Chloroplasts in Stem Tissues of Fagus Sylvatica. J. Plant Physiol. 132: 731-737

Nilsen ET (1995) Stem Photosynthesis Extent, Patterns and Role in Plant Carbon Economy. In: Gartner B (ed.), Plant Stems — Physiology and Functional Morphology. Academic Press: San Diego, pp. 223-240

Nobel PS, Hartsock TL (1986) Leaf and Stem CO_2

Uptake in the Three Subfamilies of the Cactaceae Plant Physiol. 80: 913-917

Pfanz H, Aschan G (2001) The Existence of Bark and Stem Photosynthesis and Its Significance for the Overall Carbon Gain. An Eco-Physiological and Ecological Approach. Progress in Botany Vol. 62: 477-510

Pfanz H, Aschan G, Langenfeld-Heyser R, Wittman C, Loose M (2002) Ecology and Ecophysiology of Tree Stems Corticular and Wood Photosynthesis. Naturwissenchaften 89: 147-162

Pilarski J (1984) Content of Chlorophyllous Pigments in Shoot Bark and Leaves in Syringa Vulgaris L. Bul. Pol. Acad. Sci. Biol. Sci. 32: 415-423

Pilarski J (1990) Photochemical Activity of Isolated Chloroplasts from the Bark and Leaves of the Lilac (Syringa Vulgaris L.). Photosynthetica 24: 186-189

Pilarski J (1997) Relations between Solar Irradiation, Temperature and the Photochemical Activity of Chloroplasts Isolated from the Bark and Leaves of Lilac Syringa Vulgaris L.). Pol. J. Environ. Stud. 6: 53-57

Pilarski J (1999) Gradient of Photosynthetic Pigments in the Bark and Leaves of Lilac (Syringa Vulgaris L.) Acta Physiol. Plant. 21: 365-373

Pilarski J (2002) Diurnal and Seasonal Changes in the Intensity of Photosynthesis in Stem of Lilac (Syringa Vulgaris L.). Acta Physiol. Plant. 24: 29-36

Pilarski J, Tokarz K (2005) Comparing the Optical Properties of Fruit Trees: the Sweet Cherry, Cherry, Pear, Common Plum and Walnut Trees. Folia Horticult. 17: 89-101

Schaedle M (1975) Tree Photosynthetsis. Annu Rev plant physiol. 26: 101-115

Scurlock JMO, Asner GP, Gower ST (2001) Worldwide Historical Estimates and Bibliography of Leaf Area Index, 1932-2000. ORNL Technical Memorandum TM-2001/268, Oak Ridge National Laboratory, Oak Ridge, Tennessee, USA

Smith SD, Osmond CB (1987) Stem Photosynthesis in a Desert Ephemeral, Eriogonum Inflatum: Morphology, Stomatal Conductance and Water-Use Efficiency in Field Populations. Oecologia 72: 533-541

Solhaug KA, Haugen J (1998) Seasonal Variation of Photoinhibition of Photosynthesis in Bark from Populus Tremula L. Photosynthetica 35: 411-417

Tokarz K, Pilarski J (2005) Optical Properties and the Content of Photosynthetic Pigments in the Stems and Leaves of the Apple-Tree. Acta Physiol. Plant. 27: 183-191

Tokarz K (2007) Fotosyntetyczna Rola Pędów Jabłoni (Malus Domestica) i Ich Udział w Bilansie Wiązania CO_2. (Photosynthetic Role of the Apple-Tree (Malus Domestica) Stems and They Participation in the Photosynthetic Assimilation of CO_2.) Ph.D. Dissertation, Institute of Plant Physiology PAS, Krakow, Poland

Weiskittel AR, Maguire AM (2006) Branch Surface Area and Its Vertical Distribution in Coastal Douglas-Fir. Trees 20: 657-667

Wittmann C, Pfanz H, Loreto F, Centritto M, Pietrini F, Alessio G (2006) Stem CO_2 Release under Illumination: Corticular Photosynthesis, Photorespiration or Inhibition of Mitochondrial Respiration. Plant, Cell and Environ. 29: 1149-1158

Weiss D, Schönfeld M, Halevy A (1988) Photosynthetic Activities in the Petunia Corolla. Plant Physiol 87: 666-670

Symposium 24

Photosynthesis Education

Evolution of the Z-Scheme of Electron Transport in Oxygenic Photosynthesis

Govindjee[a]*, Lars Olof Björn[b,c], Kärin Nickelsen[d]

[a]Biochemistry, Biophysics and Plant Biology, University of Illinois, 265 Morrill Hall, 505 South Goodwin Avenue, Urbana, IL 61801,USA;
[b]School of Life Science, South China Normal University, Guangzhou, China;
[c]Department of Biology, Lund University, Lund, Sweden;
[d]History and Philosophy of Science, Bern University, Bern, Switzerland.
*Corresponding author. Tel. No. 217-337-0627; Fax No. 217-244-7246; E-mail: gov@life.illinois.edu.

Abstract: We start with the discussion of the photosynthetic unit, based on the experiments of Emerson and Arnold (1932a, 1932b), continue with the first two-quantum proposal by Rabinowitch (1945, 1956), Emerson's *Red drop* (1943) and *Emerson Enhancement Effect* (1957) and various action spectra made for understanding the roles of the photosynthetic pigments. The experimental work of Kok (1959) and the theoretical model by Hill and Bendall (1960) were followed soon thereafter by the seminal papers of Duysens *et al*. (1961) and Duysens and Amesz (1962), in which the two photosystems were shown to be connected, in series, by cytochrome, which can be photooxidized by photo system I and photoreduced by photosystem II. Further, Witt *et al*. (1961) and others, cited in this paper, made refinement of the Z-scheme.

Keywords: Electron transport; Photosynthetic unit; Photosynthesis; Photosystem; Z-scheme

Introduction

Today, the Z-scheme of the so-called light reactions of photosynthesis is part of the common knowledge. It is published and proliferated in different degrees of detail, ranging from very rough sketches of the zig-zag pattern to detailed elaboration of the participating molecules. It was, however, a long way to get there. In this paper we provide a brief overview of the path that, eventually, led to today's two light reaction two photosystem account of the electron transport path from water to NADP in photosynthesis (See Govindjee and Björn, 2011; Nickelsen, 2010).

The Photosynthetic Unit

Emerson and Arnold (1932a, 1932b) separated and characterized the "light reaction" and the "dark reaction" of photosynthesis. They delivered very short and intense repetitive light flashes, and studied how photosynthesis in the green alga *Chlorella* changed when intensity, flash duration, and flash interval were varied. They postulated the existence of "photosynthetic units" which were activated by the light flashes, and during the intervening dark periods completed photosynthesis by carrying out the "dark reaction". They found that the maximum amount of oxygen released per flash, under optimum dark and light conditions, was one oxygen molecule per ~2,400 molecules of chlorophyll: *"We need only suppose that for every 2480 molecules of chlorophyll there is present in the cell one unit capable of reducing one molecule of carbon dioxide each time it is suitably activated by light."* However, it was in Gaffron and Wohl (1936) that the concept of the "unit", in which energy is transferred between pigment molecules, was elaborated. In later years, it became apparent that different organisms have units of different size, so that the number of 2,400 was by no means universal. Schmid and Gaffron (1968) showed that in several algae, cyanobacteria and higher plants, the number of chlorophyll molecules evolved per oxygen, under different physiological conditions, was in multiples of 300: ~300, ~600, ~1,200, ~1,800, ~2,400 and even ~4,800.

Quantum yields

The Stark-Einstein equivalence law (see Einstein, 1912) states that one photon reacts with one molecule. Until late in the 1930s, the role of light in photosynthesis was conceived of as splitting CO_2 into O_2 and activated carbon (the light reaction), which then would react with water to yield carbohydrate (the dark reaction). A simplistic application of the Stark-Einstein equivalence law to this would require one photon per CO_2 consumed or O_2 released. We now know that this theory is incorrect; the O_2 comes from water (Fig. 1).

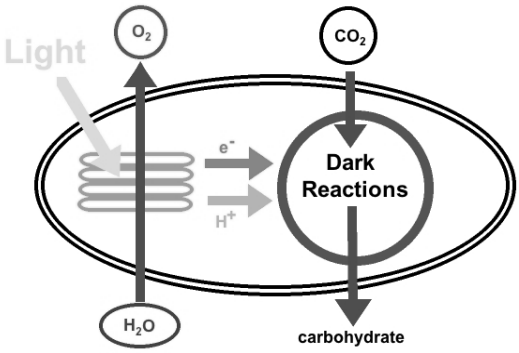

Fig. 1 A very simplified diagram of photosynthesis, showing that, in the thylakoids, light is used to convert water into molecular oxygen, electrons and protons, and, in the stroma outside the thylakoids these electrons and protons are used to make carbohydrate from carbon dioxide.

The oxidation of two water molecules to yield one oxygen molecule requires removal of 4 electrons and 4 protons, and it is natural to assume that movement of one electron or proton requires one photon. However, this was not always common sense. The experimental determination of minimum quantum requirement for photosynthesis gave, in fact, rise to one of the greatest controversies in the history of photosynthesis research. Determining this requirement was, at the time, a way to exclude certain photosynthesis theories, which were in disagreement with the energy budget. The great German biochemist Otto Warburg, who was already famous for his research on respiration enzymes, argued for a minimum quantum requirement of 4, in accordance with the one-electron-one-photon principle (Warburg and Negelein, 1923; Warburg *et al*., 1950; Warburg, 1958). He even eventually found a requirement of only 3 photons per oxygen evolved, and elaborated a theory to explain this. In contrast to this, Emerson and Lewis (1941, 1943) found a minimum quantum requirement of 10–12 photons per oxygen molecule evolved or carbon dioxide molecule absorbed. Since the experiments were highly intricate, it was far from easy to resolve this disagreement. In a final paper, Warburg *et al.* (1969) published experimental results in agreement with the value of 12 photons per oxygen, but still interpreted them, wrongly, in our opinion, as 3 photons per oxygen molecule (Govindjee, 1999). In a long series of experiments, Yuan *et al.* (1955) obtained requirements of 8.7 ± 1.0 photons per molecule of carbon dioxide assimilated, and 9.1 ± 1.1 photons per molecule of oxygen evolved. Even more importantly, Rajni Govindjee *et al*. (1968) demonstrated that the minimum quantum requirement for cultures of *Chlorella*, which were grown under conditions specified by Warburg, was 8–12.

Eugene Rabinowitch's 2-step photosynthesis scheme

In parallel to the experiments on photosynthetic quantum yields, attempts were made to spell out the biochemical (and biophysical) mechanism of photosynthesis. Eugene Rabinowitch (1945) discussed the first theory with two photochemical reactions in series in the first volume of his photosynthesis monograph. In this scheme (Fig. 2) the reaction HZ to Z corresponds to what we now call Photosystem II, and HY to Y corresponds to Photosystem I. The nature of X, Y and Z remained unknown. But already in the second volume of his monograph, Rabinowitch (1956) hinted at cytochrome as the intermediate electron carrier Y. The reason for this was the reversible oxidation of cytochrome *f* by light that had been discovered by Duysens (1955) and Lundegårdh (1954). Rabinowitch (1956) wrote:*"...photochemical transfer of electrons from reduced cytochrome to the organic acceptor (perhaps via DPN or TPN). The transfer of hydrogen (or electrons) from H_2O to the oxidized cytochrome would then require another photochemical reaction." and "The quantum requirement of the hydrogen transfer reaction as a whole would be (at least) 8, since two quanta will be needed to transfer each of the four required H atoms (or electrons), first from water to the cytochrome, and then from the cytochrome to the final acceptor."* (DPN and TPN were the acronyms used in those days for what we now call NAD and NADP.)

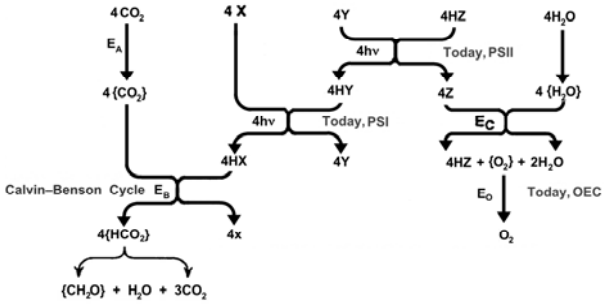

Fig. 2 A 1945 two-photoreaction scheme for photosynthesis (Rabinowitch, 1945; Modified by Govindjee; reproduced with his permission), with PSI, PSII, and OEC (oxygen evolving complex) added by the authors.

Spectral light effects: Blinks Effect and Emerson Enhancement Effect

Blinks (1957, 1960) observed strange transients in oxygen evolution, first in red algae, and later also in other algae. Even if intensities of red and green light were adjusted to give the same photosynthesis rate with each light, changes in photosynthesis rate were observed when switching from one to the other. This showed that the two kinds of light had different effects, or, in other words, were driving different reactions (while the latter was not immediately clear to Blinks); in fact, Blinks (1960) considered his effects to be due to changes in respiration.

Already in the early 1940s, Emerson and Lewis (1943) had found that the quantum yield for photosynthesis by *Chlorella* varied with wavelength. Lower yield in the blue-violet region could readily be explained by the presence of yellow pigments that did not “collect” all of its light for photosynthesis. In the yellow to red part of the spectrum the yield was higher and fairly constant up to about 680 nm, but at higher wavelengths it dropped very steeply, although the chlorophyll was still absorbing. Much later, Emerson and coworkers (Emerson *et al*., 1957; Emerson and Chalmers, 1958; cf. Emerson and Rabinowitch, 1960) discovered that a background of light of shorter wavelength could counteract this “red drop”. This became known as the “(Emerson) Enhancement Effect” of photosynthesis. Warburg *et al*. (1954) had earlier studied the effect of combining blue “catalytic” light, with red light but this experiment as well as its conclusion is not relevant to the Emerson Enhancement effect except that it might have given ideas to Emerson to use two light beams in his experiments.

Emerson and Chalmers (1958) brought forward the suggestion that there were, in fact, two light reactions in photosynthesis, while they proposed that one of them was sensitized by chlorophyll *a* and the other by chlorophyll *b* or other accessory pigments see also Myers and French (1960). However, Govindjee and Rabinowitch (1960) and R. Govindjee *et al*. (1960) showed that a short wavelength absorbing form of chlorophyll *a* was present in the same system that used chlorophyll *b* (or other accessory pigments). This agreed with the earlier observations of Duysens (1952) that all energy absorbed by chlorophyll *b* is transferred to chlorophyll *a*. Further, Govindjee *et al*. (1960) discovered a corresponding effect on chlorophyll *a* fluorescence from *Chlorella* cells: light absorbed in the “red drop” region quenched chlorophyll *a* fluorescence excited by high intensity short wavelength light. This phenomenon was thoroughly explored by Duysens and Sweers (1963) leading to an establishment of the relationship of two light reactions and two pigment systems with chlorophyll fluorescence.

The Z-scheme: Contributions of Kok, Duysens, Hill and their coworkers

Around 1960 all of the previously somewhat perplexing experimental results had a consistent explanation. Several almost simultaneous publications contributed to this: this is a clear indication of the fact that the solution was, so to speak, "in the air".

Kok (1959), in the Robert Emerson Memorial issue of Plant Physiology, showed a two-light effect (in a cyanobacterium *Anacystis nidulans*) on the redox state of a special chlorophyll which he had earlier dubbed “P700”: the pigment was oxidized when illuminated by a long wavelength light (far-red), while the oxidized P700 was reduced when a short wavelength light (orange-red) was added. Kok explicitly related these findings to the Emerson Enhancement Effect (see also Kok and Hoch, 1961 for a more detailed presentation).

Around the same time, Duysens examined the action spectra for cytochrome oxidation and $NADP^+$ reduction in different wavelengths of light, and in August1960, he presented his results at the 3rd International Congress on Photobiology at Copenhagen, Denmark. Duysens was able to show that in the red alga *Porphyridium*, green light,

absorbed by phycoerythrin, gave a low yield of cytochrome oxidation when the photosynthetic yield was high, but a high yield of cytochrome oxidation in red light, absorbed by chlorophyll a, when the photosynthetic yield was low. Based on these observations, Duysens postulated the existence of two Photosystems, 1 and 2. (At that time, he was unaware of the paper of Hill and Bendall, 1960). Duysens (1989) wrote, retrospectively, about his earlier work: *"System 1 contained the weakly fluorescent chlorophyll a, formerly said to be inactive, and oxidized cytochrome; system 2 contained the fluorescent chlorophyll a. An interaction between the two systems was shown by the different kinetics of cytochrome oxidation at different actinic wavelengths."*

The fact that there were different types of chlorophyll *a*, which had distinct functions in the photosynthetic process in *Chlorella* cells, was first brought up in Govindjee and Rabinowitch (1960) and elaborated in Rabinowitch and Govindjee (1961). French (1961) had independently come to the same conclusion. In March 1960, Rabinowitch and Govindjee stated, in view of their findings: "*the primary photochemical process in photosynthesis might consist of two steps: whereas one type of chlorophyll a was able to bring about both, the other type was restricted to one of these steps*."

The key experiment for demonstrating the existence of two light reactions was published by Duysens *et al*. (1961) (see also Duysens and Amesz, 1962): light of wavelengths attributed by the authors to system 1 (light 1) oxidized a cytochrome, while light of wavelengths attributed to system 2 (light 2) reduced it. This was the discovery of the antagonistic effect of light 1 and 2 on an intermediate that was predicted by Rabinowitch (1956) and is still the best experimental evidence for the series scheme of photosynthesis. Further, Duysens *et al*. (1961) showed that in the presence of diuron (DCMU), cytochrome can be oxidized, but not reduced.

The paper of Hill and Bendall (1960), published during this period, is a landmark in the study of the "light reactions" of photosynthesis. Hill and Bendall addressed the problem from the point of view of thermodynamics. Already in the 1950s, two plant-specific cytochromes had been found in chloroplasts (Hill and Scarisbrick, 1951; Davenport and Hill, 1952).The possibility that cytochromes might be the elements to link two photosystems and provided energy for the formation of ATP through a downhill step between the two cytochromes was clearly the novel concept in the Robert (Robin) Hill and Fay Bendall scheme—while they missed, unintentionally, we believe, citing the pioneering work of Robert Emerson, which was mentioned earlier. Due to the graphical representation of this scheme, which was adopted in later years, it became known as the "Z-scheme" of photosynthesis.

The most precise biophysical measurements of the absorption changes were by Witt, Müller and Rumberg (1961a, 1961b); they used flashing light spectroscopic methods, which greatly increased the sensitivity and the time resolution of photosynthesis studies. Based on this technique, Witt *et al*. (1961a, 1961b) found that (1) upon excitation with $light_1$ (710 nm) cytochrome *f* was oxidized and stayed in this state for seconds; (2) after excitation with $light_2$ (670 nm) an unidentified component X was oxidized to XO. From these findings, they concluded (at almost the same time as Kok and Hoch as well as Duysens and coworkers) "*that photosynthesis is triggered by two different photochemical reactions: oxidation of cytochrome by Chla-680 and reduction of XO by Chla-670".* Witt *et al*. (1961a, 1961b) additionally suggested that the reaction XO → X might be the reaction of plastoquinone to hydroquinone (see also the retrospective discussion of this work by Witt (1991)).

Losada *et al*. (1961) from Daniel Arnon's laboratory provided one of the first biochemical measurements supporting the "Z-Scheme". However, Daniel Arnon soon abandoned this scheme in favor of a 3-light reaction scheme, or a 2-light light scheme, both run by two types of Photosystem II and even a one light reaction scheme. We shall not discuss them here. By 1963, the major concepts and experiments on the two light- reaction and two-pigment scheme had been settled (see Kok and Jagendorf, 1963). The two light reaction, two pigment system scheme was further supported by the physical separation of the two photosystems (see *e.g.*, Boardman and Anderson, 1964; Anderson, 2005), by 'chemical surgery' of the entire scheme and by the use of specific inhibitors, artificial donors and acceptors of partial reactions (see *e.g.*, reviews by Vernon and Avron (1965) and Trebst (1974), and through the use of mutants that lacked specific intermediates in the electron transport chain (see *e.g.*, Gorman and Levine, 1966; see Levine, 1969, for a review).

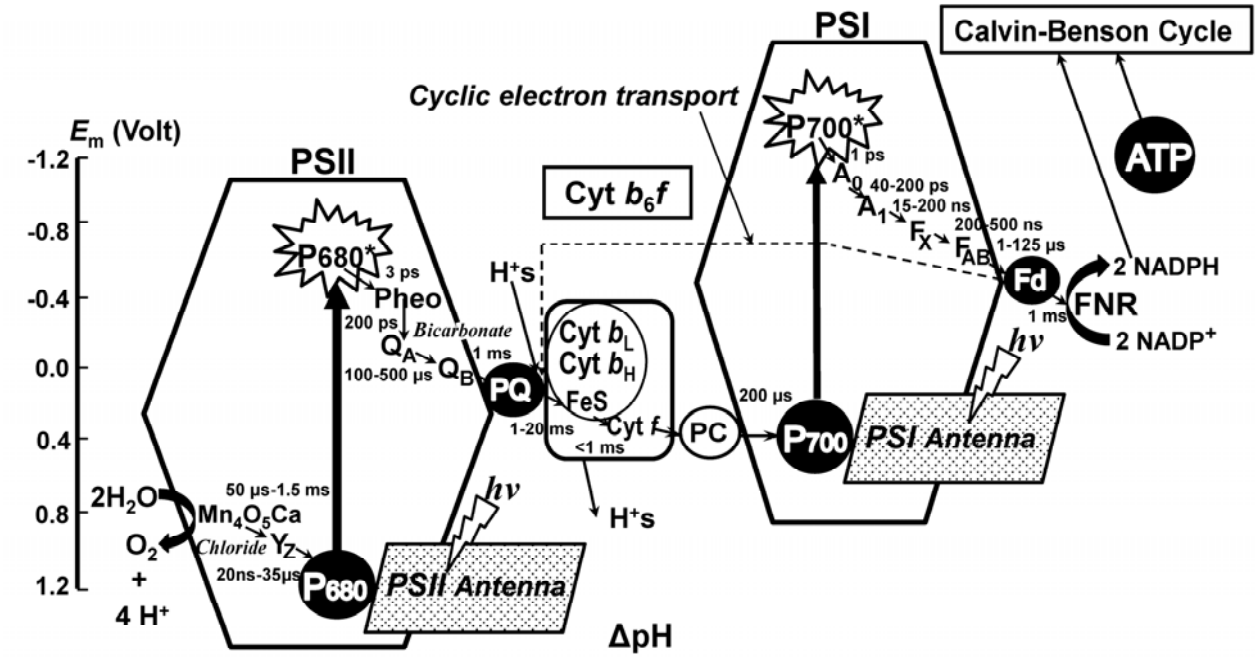

Fig. 3 A current Z-Scheme for electron transport (Stirbet and Govindjee, 2011; courtesy of Alexandrina Stirbet; Reproduced with the permission from AStirbet and Govindjee).

The current scheme

We conclude this paper by showing a selected current scheme (Fig. 3) that is used to describe the process of the photosynthetic "light reactions". Other available schemes range from a bunch of circles to a chair-like structure, from zig-zag (or Z-) shaped graphs to a slightly distorted N.

References

Anderson J (2005) Changing Concepts about the Distribution of Photosystems I and II between Grana-Appressed and Stroma-Exposed Thylakoid Membranes. In: Govindjee, Beatty JT, Gest H, Allen JF (eds.), Discoveries in Photosynthesis. Springer: Dordrecht, pp. 729-736

Blinks LR (1957) Chromatic Transient in Photosynthesis of Red Algae. In: Gaffron H, Brown AH, French CS, Livingston R, Rabinowitch EI, Strehler B, Tolbert NE (eds.), Research in Photosynthesis. Interscience Publishers: New York, pp. 444-449

Blinks LR (1960) Relation of Photosynthetic Transients to Respiration. Science 131: 1316

Boardman NK, Anderson JM (1964) Isolation from Spinach Chloroplasts of Particles Containing Different Proportions of Chlorophyll a and Chlorophyll b and Their Possible Role in Light Reactions of Photosynthesis. Nature 203: 166-167.

Davenport HE, Hill R (1952) The Preparation and Some Properties of Cytochrome f. Proc. Royal Soc. London Series B 139: 327-345

Duysens LNM (1952) Transfer of Excitation Energy in Photosynthesis. Doctoral Thesis. State University, Utrecht, The Netherlands

Duysens LNM (1955) Role of Cytochrome and Pyridine Nucleotide in Algal Photosynthesis. Science 121: 210- 211

Duysens LNM (1989) The Discovery of the Two Photosynthetic Systems: a Personal Account. Photosynth. Res. 21: 61-80

Duysens LNM, Amesz J (1962) Function and Identification of Two Photochemical Systems in Photosynthesis. Biochim. Biophys. Acta 64: 243-260

Duysens LNM, Sweers HE (1963) Mechanism of Two Photochemical Reactions in Algae As Studied by Means of Fluorescence. In: Japanese Society of Plant Physiologists (eds.), Studies on Microalgae and Photosynthetic Bacteria. University of Tokyo Press: Tokyo, pp. 353-372

Duysens LNM, Amesz J, Kamp BM (1961) Two Photochemical Systems in Photosynthesis. Nature 190: 510-511

Einstein A (1912) Thermodynamische Begründung des Photochemischen Äquivalentgesetzes. Ann. Phys. 14 (Suppl): 437-443

Emerson R, Arnold W (1932a) A Separation of the Reactions in Photosynthesis by Means of Intermittent Light. J. Gen. Physiol. 15: 391-420

Emerson R, Arnold W (1932b) The Photochemical Reaction in Photosynthesis. J Gen Physiol 16: 191-205

Emerson R, Chalmers RV (1958) Speculations Concerning the Function and Phylogenetic Significance of the Accessory Pigments of Algae. Phycol. Soc. News Bull. 11: 51-56

Emerson R, Lewis CM (1941) Carbon Dioxide Exchange and Measurement of the Quantum Yield of Photosynthesis. Am. J. Bot. 28: 789-804

Emerson R, Lewis CM (1943) The Dependence of the Quantum Yield of Chlorella Photosynthesis on Wavelength of Light. Am. J. Bot. 30: 165-178

Emerson R, Rabinowitch E (1960) Red Drop and Role of Auxiliary Pigments in Photosynthesis. Plant Physiol. 35: 477-485

Emerson R, Chalmers RV, Cederstrand CN (1957) Some Factors Influencing the Long-Wave Limit of Photo-Synthesis. Proc. Natl. Acad. Sci. USA 43: 133-143

French CS (1961) Light, Pigments and Photosynthesis. In: McElroy WD, Glass B (eds.), Light and Life.The Johns Hopkins Press: Baltimore, pp. 447-474

Gaffron H, Wohl K (1936) Zur Theorie der Assimilation. Naturwissenschaften 24: 81-90; 103-107

Gorman DS, Levine RP (1966) Photosynthetic Electron Transport Chain of Chlamydomonas Reinhardtii.VI. Electron Transport in Mutant Strains Lacking either Cyt 559 or Plastocyanin. Plant Physiol. 41: 1648-1656

Govindjee (1999) On the Requirement of Minimum Number of Four Versus Eight Quanta of Light for the Evolution of One Molecule of Oxygen in Photosynthesis. Photosynth. Res. 59: 249-254

Govindjee, Björn LO (2011) Dissecting Oxygenic Photosynthesis: the Evolution of the "Z"-Scheme for Thylakoid Reactions. In: Itoh S, Mohanty P, Guruprasad KN (eds.), Photosynthesis: Current Progress and Future Perspectives. IK Publishers: New Delhi, pp. 1-27

Govindjee, Rabinowitch E (1960) Two Forms of Chlorophyll a in Vivo with Distinct Photochemical Functions. Science 132: 159-160

Govindjee, Ichimura S, Cederstrand C, Rabinowitch E (1960) Effect of Combining Far-Red Light with Shorter Wave Light in the Excitation of Fluorescence in Chlorella. Arch. Biochem. Biophys. 89: 322-323

Govindjee R, Thomas JB, Rabinowitch E (1960) Second Emerson Effect in the Hill Reaction of Chlorella Cells with Quinone As Oxidant. Science 132: 421

Govindjee R, Rabinowitch E, Govindjee (1968) Maximum Quantum Yield and Action Spectrum of Photosynthesis and Fluorescence in Chlorella. Biochim. Biophys. Acta 162: 539-544

Hill R, Bendall F (1960) Function of the Cytochrome Components in Chloroplasts: a Working Hypothesis. Nature 186: 136-137

Hill R, Scarisbrick R (1951) The Haematin Compounds of Leaves. New Phytologist 50: 98-111

Kok B (1959) Light-Induced Absorption Changes in Photosynthetic Organisms. II. A Split-Beam Difference Spectrophotometer. Plant Physiol. 34: 184-192

Kok B, Hoch G (1961) Spectral Changes in Photosynthesis. In: WD McElroy, B Glass (eds.), Light and Life. The Johns Hopkins Press: Baltimore, Maryland, pp. 397-423

Kok B (Chairman), Jagendorf AT (Organizer) (1963) Photosynthetic Mechanisms of Green Plants. Publication #1145. National Academy of Sciences—National Research Council, Washington, DC, see 'Foreword', pp. ix

Levine RP (1969) The Analysis of Photosynthesis Using Mutant Strains of Algae and Higher Plants. Annu. Rev. Plant Physiol. 20: 523-540

Losada M, Whatley FR, Arnon DI (1961) Separation of Two Light Reactions in Non-Cyclic Photo-Phosphorylation of Green Plants. Nature 190: 606-610

Lundegårdh H (1954) On the Oxidation of Cytochrome f by Light', Physiol. Plantarum 7: 375-382

Myers J, French CS (1960) Evidences from Action Spectra for a Specific Participation of Chlorophyll b in Photosynthesis. J. Gen. Physiol. 43: 723-736

Nickelsen K (2010) Of Light and Darkness—Modelling Photosynthesis 1840-1960. Habilitationschrift-eingereicht der Phil.-nat. Fakultät der Universität Bern, Switzerland, see Chapters VI and VII

Rabinowitch E (1945) Photosynthesis and Related Processes. Vol. I. Interscience Publishers, Inc.: New York 599: 162

Rabinowitch EI (1956) Photosynthesis and Related Processes, Vol. II (Part 2). Kinetics of Photosynthesis (continued); Addenda to Vol. I and Vol. II, Part 1, pp. 1211-2088. Interscience Publishers: New York, pp. 1862

Rabinowitch EI, Govindjee (1961) Different Forms of Chlorophyll a in Vivo and Their Photochemical Function. In: McElroy WD, Glass B (eds.), A Symposium on Light and Life. The Johns Hopkins Press: Baltimore, Maryland, pp. 378-391

Schmid G H, Gaffron H (1968) Photosynthetic Units. J. Gen. Physiol. 52: 212-239

Stirbet A, Govindjee (2011) On the Relation between the Kautsky Effect (Chlorophyll a Fluorescence Induction) and Photosystem II: Basics and Applications. J. Photochem. Photobiol. B Biology in the press

Trebst A (1974) Energy Conservation in Photosynthetic Electron Transport of Chloroplasts. Annu. Rev. Plant Physiol. 25: 423-458.

Vernon LP, Avron M (1965) Photosynthesis. Annu. Rev. Biochem. 34: 269-296

Warburg O (1958) Photosynthesis. Science 128: 68-73

Warburg O, Negelein E (1923) Über den Einfluss der Wellenlänge auf den Energieumsatz bei der Kohlensäureassimilation. Z. Physik. Chem. 106: 191-218

Warburg O, Burk D, Schocken V, Hendricks SB (1950) The Quantum Efficiency of Photosynthesis. Biochim. Biophys. Acta 4: 335-348

Warburg O, Krippahl G, Schröder W, Buchholz W, Theel E (1954) Über die Wirkung sehr Schwachen Blaugrünen Lichts auf den Quantenbedarf der Photosynthese. Z. Naturforschg. 9b: 164-165

Warburg O, Krippahl G, Lehman A (1969) Chlorophyll Catalysis and Einstein's Law of Photochemical Equivalence in Photosynthesis. Am. J. Bot. 56: 961-971

Witt HT (1991) Functional Mechanism of Water Splitting Photosynthesis. Photosynth. Res. 29: 55-77

Witt HT, Müller A, Rumberg B (1961a) Experimental Evidence for the Mechanism of Photosynthesis. Nature 191: 194-195

Witt HT, Müller A, Rumberg B (1961b) Oxidized Cytochrome and Chlorophyll in Photosynthesis. Nature 192: 967-969

Yuan EL, Evans RW, Daniels F (1955) Energy Efficiency of Photosynthesis by Chlorella. Biochim. Biophys. Acta 17: 185-193

The Golden Apples of the Sun: the History of Photosynthesis—so Far

Anthony WD Larkum

School of Biological Sciences (A08), University of Sydney, NSW 2006, Australia.
Tel. No. +61 9351 2069; Fax. No. +61 9351 4419; E-mail: alark@mail.usyd.edu.au.

Abstract: This article reviews the start of life and of photosynthesis on the Earth. A pivotal evolutionary event in photosynthesis was the ability to use water as the source of hydrogen in the photosynthetic reaction, which occurred about 2.35 billion years ago. This opened up the possibility for photosynthetic organisms to live anywhere on the surface of the Earth where light and water occurred—and secondarily allowed the build-up of oxygen in the biosphere and atmosphere. The accumulation of molecular oxygen allowed the evolution of aerobic respiratory systems with much greater efficiency in output of organically-derived energy. In turn this allowed the evolution of large complex eukaryotic cells by endosymbiosis. The chloroplast was the result of one endosymbiotic development, now found in many phyla of photosynthetic protists (algae) and in land plants. The multicellular land plants, which evolved from streptophyte green algae, now account for a major part of the total bioenergy production from photosynthesis on the Earth. However, the basic mechanism of photosynthesis has changed very little in the last 2 billion years. In the future, radical changes will be necessary to make bioenergy production from algae and plants more efficient and more competitive with other methods of solar energy conversion.

Keywords: Efficiency of photosynthesis, endosymbiosis, evolution, oxygenic photosynthesis, photosynthesis, the Great Oxidation Event, Earth history

"And walk among long dappled grass,
And pluck till time and times are done
The silver apples of the moon,
The golden apples of the sun."

W B Yeats

The Earth and life before photosynthesis

The world before photosynthesis

The Earth was formed about 4.5 billion years ago (GA) at the beginning of the Solar System as the planets consolidated out of clouds of dust. Its composition was probably similar to that of all the four innermost planets, except the first, the planet Mercury, which seems to be composed of heavier elements. Over the first hundred million years or so the Earth was too hot to sustain any life as we know it. Subsequently, also, the surface of the Earth was probably too hot because of a bombardment by meteorites. This went on for another 500 million years. It had the beneficial result of bringing to the Earth three valuable cargoes: (i) organic carbon compounds, (ii) water, which doubled, at least, the liquid water on the Earth's surface, and (iii) the majority of nitrogen gas, now found in the Earth's atmosphere.

Life before photosynthesis

Approximately 3.8 billion years ago (Ga) life spread over the Earth. Prior to this time it is considered that the surface of the Earth was too hot and unstable to sustain the widespread occurrence of living cells, except in local pockets. There has been much discussion as to how life started and what form of nucleic acid formed the first replicating structures. It has recently been suggested that an early development was the evolution of organic compounds that would shield organisms from UV radiation and

that this led to the earliest processes of photosynthesis (Larkum, 1991; Mulkidjanian *et al*., 2009).

The Early Evolution of Photosynthesis

Respiration and nitrogen fixation almost certainly preceded photosynthesis because photosynthesis uses enzymes (cytochromes and chlorophyll reductases) which originate from those processes. By at least 3.5 Ga photosynthesis, *i.e.* the fixation of carbon dioxide to organic compounds powered by solar energy, was occurring (Schopf, 1993; Schidlowski, 2000). Necessarily the detailed evidence is sketchy. However by 3.0 Ga it is certain that PS eubacteria existed which could use hydrogen from a range of compounds and use it to reduce carbon dioxide to organic form (Blankenship, 1998). This general scheme was first formulated by Cornelis van Niel from his research in the 1930s and has been a cornerstone of thinking on photo-synthesis ever since (Govindjee *et al*., 2009). It defined both the oxygenic photosynthetic process where the hydrogen came from water, and the waste product was oxygen, and the anoxygenic process where the hydrogen came from other hydrogen-containing compounds, such as hydrogen sulphide and alcohols, and the wastes were oxidised products. Inspection of photosynthetic organisms existing on the Earth today shows that there are many photosynthetic bacteria which employ anoxygenic processes, whereas cyanobacteria are the only Eubacteria to have oxygenic photosynthesis [and chlorophyll *a* (Chl *a*)]. The simple conclusion from this evidence might be that cyanobacteria evolved from one or more of the ancestors of anoxygenic bacteria that exist today. However the situation is complicated by the fact that anoxygenic photosynthetic (PS) bacteria have either Photosystem I-type (FeS) or Photosystem II type (Q) photosystems. Both photosystems occur in cyanobacteria, so it might be that in evolution there was a fusion of these two types (Blankenship, 2002; Larkum, 2006). Phylogenetic evidence from gene analysis of cyanobacteria has suggested that they may have evolved from an (anoxygenic) procyanobacterium in which the photosystems evolved (Mulkijanian *et al*., 2006). It would then be possible that this ancestor gave rise also to the anoxygenic bacteria by the loss of one photosystem or the other (Larkum, 2007).

Bacteriochlorophyll has often been seen as the earliest chlorophyll pigment. And this would be consistent with the idea that anoxygenic PS bacteria with one photosystem or the other were the first comers. If, on the other hand, a procyanobacterium preceded all the other types then it is possible that chlorophyll preceded bacteriochlorophyll (Larkum, 2008).

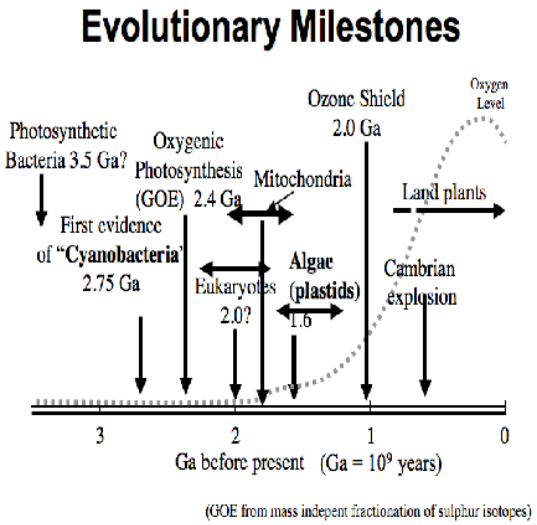

Fig. 1 Evolutionary milestones of Earth history and photosynthesis.
The scale for oxygen level is relative: the present concentration of oxygen in the atmosphere is 21%.

The evolution of oxygenic photosynthesis

Notwithstanding the origin of cyanobacteria, it has become clear over the last decade that oxygen began to appear in the biosphere rather precisely around the time of 2.38–2.35 Ga. Because this was such a pivotal event on the Earth it has become known as the great oxidation event (GOE)(Holland, 2002). The reason that the timing can be fixed so precisely is that evidence shows that at this time the discrimination of sulphur isotopes in rocks stabilised to close to its present level. It is argued convincingly that this could only have been brought about by the occurrence of molecular oxygen in the biosphere (Dekker *et al*., 2004).

Does the GOE signal the first occurrence of cyanobacteria? This has been argued (Rasmussen *et al*., 2008). However, there is evidence from fossils and tracer chemicals that cyanobacteria existed long before. Schopf and colleagues (Schopf, 1993) argued that cyanobacterial fossils could be found in rocks as old as 3.45 Ga and this was consistent with isotopic

evidence for photosynthesis (Schidlowski, 2000). However, this evidence has been contested (Brasier *et al*., 2002) and it is probably true to say that the evidence points only to photosynthetic bacteria in rocks of that age, not cyanobacteria, but possibly procyanobacteria.

So what would be the evidence for cyanobacteria or procyanobacteria? Most probably it took a relatively long time to refine the mechanism of oxygen evolution. As seen from this perspective it must have taken the concerted action of at least four proteins to do this (D1, D2, CP43, psbO manganese-stabilising protein, see, *e.g.*, Blankenship, 2002) and it is likely that the process took many millions of years to evolve to the form that we now see. How long is not known, but it is instructive that chemical markers, the 2-methyl hopanoids for cyanobacteria, have been found as far back as 2.8 Ga, (Brocks *et al*., 1999; Summons *et al*., 1999). Were these hopanoids present in early cyanobacteria or late procyanobacteria or in a form of anoxygenic PS bacterium, which later took part in the formation of cyanobacteria? At present we have no good evidence to resolve this point but the question will certainly drive further research in the future.

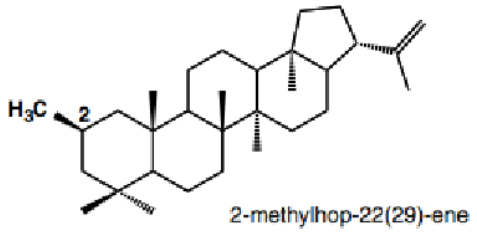

Fig. 2 Chemical formula of a 2-methyl hopanoid.

The Great Oxidation Event (GOE)

Most geologists now accept that oxygen began to spread in the biosphere at ~2.3–2.4 Ga and the most compelling reason for this is the earliest geological-scale success of cyanobacteria in splitting water in photosynthesis. There was of course no widespread oxygenation of the atmosphere at that time: cyanobacteria would have been restricted to the photic zone of the oceans, freshwater lakes and other more restricted habitats. The oceans would have remained anaerobic below the photic zone for many million of years (Poulton *et al*., 2003). Many reduced compounds in the Earth's crust would have remained unoxidised for many millions of years, and only became accessible to oxidation by tectonic movements, resulting in a gradual build-up of oxygen in the Earth's atmosphere. So we have to envisage local pockets of high oxygen in aqueous environments and a slowly rising oxygen concentration in the atmosphere up to ~1Ga.

The Rise of Eukaryotes

The release of oxygen into the biosphere from ~2.3–2.4 Ga caused a dramatic change: up to that time the Earth would have experienced only small scale release of oxygen from such processes as the hydrolysis of water by UV radiation. And the organisms of the Earth would have used an anaerobic metabolism to supply energy. While oxygen is toxic to many anaerobic organisms, ways of coping with this must have been evolved comparatively rapidly and many of the successful organisms developed further ways to utilise oxygen in respiratory process, which were many more times efficient at producing energy (ATP). Aerobic respiration became widespread in many prokaryotic organisms at this time, including cyanobacteria themselves. We do not know how all this took place but it is probable that symbiosis played an important role and that the extra energy of aerobic respiration allowed cells to become bigger. Indeed the next level of organismic complexity, the eukaryotic cell, is certainly the product of a chain of symbiotic events which gave rise to the large eukaryotc cell (Margulis, 1975), subdivided into a number of regions which specialised in such processes as information storage (the nucleus), locomotion (the flagella), katabolic energy transduction (the mitochondrion) and anabolic energy transduction (the chloroplast). By processes for which we have little evidence this gave rise to over 60 types of unicellular Eukaryotes (Protists) over the next billion years or so (2.4–1.4 Ga). The photosynthetic protists are called by the general name, "algae" and at least three evolutionary lines, the brown, the red, and the green algae, became multicellular.

Multicellularity—the rise of plants, animals and fungi

The next revolution in organismal complexity arose through multicellularity. How this happened and

why it happened in such few groups of previously unicellular, or at the most filamentous, eukaryotes is a matter for speculation. For both animals and multicellular fungi the nearest ancestor seems to be the choanoflagellates. In plants it is the streptophyte green algae. It should also be noted that in PS Protists (algae) multicellularity also occurred in two groups, the red algae and the brown algae but neither of these phyla conquered the land.

The land plants therefore derive from a group of unicellular eukaryotes that entered into symbiosis with a cyanobacterium which contained Chl *b* as well as Chl *a*, and the specific light-harvesting proteins that accompany this suite of pigments (coded by lhc genes). Whether this cyanobacterium was the same as the one giving rise to red algae and the chlorophyll *c* line (in which brown algae occur) of unicellular PS eukaryotes is still a matter of debate (Larkum *et al*., 2007; Janouškoveca *et al*., 2010)

The singular fact is that photosynthesis at the chloroplast level has changed very little from the time when oxygenic PS evolved at 2.4 Ga.

The rise of plants was mainly a land-based development. It was the conquest of the land by plants that led to an enormous boost in the productivity of the planet and allowed the rapid evolution of, mainly, land-based animals. Of course, many animals and a few plants returned to aqueous environments but the story is really about the land, since the green, the red and brown algae contribute a relatively small component to the primary production of the seas (Falkowski and Raven, 2007)

Photosynthesis in land plants—a multicellular response

Photosynthesis at the chloroplast level has remained little changed in its basic mechanisms over the last 2 Ga. However, in C4 plants two different types of chloroplasts have evolved by fine-tuning this mechanism. In mesophyll chloroplasts, the enzymes of the stroma have been modified to give rise to a carboxylation, not involving Rubisco, and the export of C4 acids. And in bundle sheath chloroplasts, photosystem II has been down-regulated and a typical Calvin-Benson cycle is provided with C4 acids brought in from the mesophyll cells and powered by PSI (Larkum, 2008).

At the cellular level, life in air rather than water has brought about very dramatic changes in anatomy and physiology: firstly of the photosynthetic lamina which eventually evolved into the plant leaf, with a stomatal system of gas control (and, where, in C4 plants, it is important to limit very strongly the loss of water). The land plant has also developed aerial stems and leaves and a subterranean part, the roots, none of which are found in the red or brown algae (Larkum, 2008).

It is this evolutionary series of events that make life on land so different from that in the sea or lakes. But it is instructive to ponder on the fact that the basic mechanism that we see in the chloroplasts of plants evolved at about 2.4 Ga ago. Liverworts and mosses came first and were succeeded by early tracheophytes with lignified stems and primitive leaves; the great carboniferous forests that laid down much of the coal measures came and went along with the dinosaurs; conifers were followed by flowering plants and insect pollination and set the world ablaze with colour. All this occurred without any great change in the basic photosynthetic machinery

Photosynthesis—the next step

Today the world is faced with the problem of increasing greenhouse gases and a shortage of liquid fuels to power motor cars, heavy transport and particularly jet aircraft. This poses a dilemma over whether to use the very great deposits of coal to produce energy for power stations in the future. By burning coal, the greenhouse gases will rise still further, bringing about still further rises in the global temperature. In these circumstances it is reasonable to ask if there is another alternative. Solar energy is just such an alternative. The global input to our planet from solar energy is some 1,000 fold the current energy consumption by Man. So it should be possible to use some of this input to offset the current use of coal in power stations. An immediate step would be to employ solar voltaic cells or solar thermal power stations. However, not so very far behind this should be the harnessing of photosynthesis through terrestrial plants to produce bioenergy for Man's use (Larkum, 2010). It is not clear at present just how this will be done. But already several countries are off-setting their fuel needs by producing bioethanol from plant products such as grains and sugar and so saving on petroleum imports. Such a resource comes with the

hazard of using agricultural land for fuel rather than agricultural produce and so has led to increasing food prices. However, many agronomists and planners are turning to marginal lands for the production of bioenergy (Larkum, 2010). Certain terrestrial crops may be used for this purpose. Furthermore, aquaculture could also be used. Microalgae can theoretically produce bioenergy more efficiently than land crops. While the latter prospect is still some way off, it is quite possible that as the push to produce liquid fuels intensifies, algal photobioreactors will become competitive (Larkum, 2010).

As will have become clear in this article, the core of the photosynthetic reactions evolved over 2 Ga ago and has changed very little since. As a result this process is inherently inefficient. Re-engineering the photosynthetic apparatus for greater efficiency would greatly improve the prospects for bioenergy production. The obvious goals for improvement would be:

(1) Change from a two photosystem in series mechanism to a single photosystem mechanism,

(2) Improve the light harvesting capacity of Chl *a* systems, especially in the green window and possibly in the infra-red region,

(3) Eliminate, as far as possible, photoinhibitory reactions, especially the xanthophyll cycle,

(4) Optimize the system to avoid unwanted pathways such as the water-water cycle and photorespiration,

(5) Enhance the output of desired natural products (Larkum, 2010).

Finally, a further step would be to produce hybrid systems employing parts of the photosynthetic apparatus, which are linked to efficient physical solar harvesting mechanisms. Hydrogen production could be an important part of this approach (Larkum, 2010).

Acknowledgements

I wish to thank all those colleagues and friends who have helped me over the years: if any one feels that I have stolen their thunder or not acknowledged their work sufficiently, I apologise. I wish to thank Prof. Govindjee for organising the Education Symposium.

References

Bekker A, Holland HD, Wang PL, Rumble D III, Stein JHJ, Hannah L, Coetzee LL, NJ Beukes (2003) Dating the Rise of Atmospheric 0xygen. Nature 427: 117-120

Blankenship RE (2002) Molecular Mechanisms of Photosynthesis. Blackwell Science, Oxford

Brasier MD, Green OR, Jephcoat AP, Kleppe AK, Van Kranendonk MJ, Lindsay JF,. Steele A, Grassineau NV (2002) Questioning the Evidence for Earth's Oldest Fossils. Nature 416: 76-81

Brocks JJ, Logan GA, Buick R, Summons RE (1999) Archean Molecular Fossils and the Early Rise of Eukaryotes. Science 1999: 1033-1036

Falkowski P, Raven J (2007) Aquatic Photosynthesis (2nd edition). Blackwell. Oxford

Govindjee, Beatty JT, Gest H (2005) Celebrating the Millenium-Historical Highlights of Photosynthesis Research, Part 2. In: Govindjee, Beatty JT, Gest H, Allen JF (eds.), Discoveries in Photosynthesis, Vol. 20, Advances in Photosynthesis and Respiration. Springer Verlag: Berlin, pp. 11-21

Holland H (2002) Volcanic Gases, Black Smokers, and the Great Oxidation Event. Geochim. Cosmochim. Acta 66: 3811-3826

Janouškoveca J, Horáka A, Oborníkb M, Lukešb J, Keeling PJ (2010) Proc. Natl. Acad. Sci. (US) 107: 10949-10954

Larkum AWD (1991) The Evolution of Chlorophylls. In: H Scheer (ed.), Chlorophylls. CRC Publ.: Boca Raton, pp. 367-383

Larkum AWD (2006) The Evolution of Chlorophylls and Photosynthesis. In: B Grimm, RJ Porra W Rudiger, H Scheer (eds.), Chlorophylls and Bacteriochlorophylls, Vol. 25, Advances in Photosynthesis and Respiration. Springer Verlag: Berlin, pp. 261-282

Larkum AWD (2008) Evolution of the Reaction Centers and Photosystems. In: G Renger (ed.), Primary Processes of Photosynthesis: Principles and Apparatus, Vol. 2. Royal Society of Chemistry: Cambridge, pp. 489-521

Larkum AWD (2010) Limitations and Prospects of Natural Photosynthesis for Bioenergy Production. Current Opinion in Biotechnology 21: 271-276

Larkum AWD, Lockhart PJ, Howe CJ (2007) Shopping for Plastids. Trends Plant Sci. 12: 189-195

Margulis L (1975) Symbiotic Theory of the Origin of Eukaryotic Organelles; Criteria for Proof. Symp. Soc. Exp. Biol. 29: 21-38

Mulkidjanian AY (2009) Hypothesis Open Access on the Origin of Life in the Zinc World: I.

Photosynthesizing, Porous Edifices Built of Hydrothermally Precipitated Zinc Sulfide As Cradles of Life on Earth. Biology Direct 4: 26 (doi:10.1186/1745-6150-4-26)

Mulkidjanian AY, Koonin EV, Kira Makarova S, Mekhedov SL, Sorokin A, Wolf YI, Dufresne A, Partensky F, Burd H, Kaznadzey D, Haselkorn R, Galperin MY (2006) The Cyanobacterial Genome Core and the Origin of Photosynthesis. Proc. Natl. Acad. Sci. (US) 1999: 13159-13164

Poulton SW, Fralick PW, Canfield DE (2003) The Transition to a Sulphidic Ocean 1.84 Billion Years Ago. Nature 431: 173-177

Rasmussen1 B, Fletcher IR, Brocks JJ, Kilburn MR (2008) Reassessing the First Appearance of Eukaryotes and Cyanobacteria. Nature 455: 1101-1104

Schidlowski M (2000) Carbon Isotopes and Microbial Sediments. In: RE Riding, SM Avramik (eds.), Microbial Sediments. Springer Verlag: Berlin, pp. 84-95

Schopf W (1993) Microfossils of the Early Archean Apex Chert: New Evidence of the Antiquity of Life. Science 260: 640-646

Summons RE, Jahnke LL, Hope JM, Logan GA (1999) 2-Methylhopanoids As Biomarkers for Cyano-bacterial Oxygenic Photosynthesis. Nature 400: 554-557

Author Index